TECHNICAL PAPERS

CICM 2015
First International Conference on
Advances in Civil Infrastructure and Construction Materials
MIST, Dhaka, Bangladesh, 14–15December 2015

SIMPLIFIED SHEAR STRENGTH PREDICTION MODEL OF FRP REINFORCED CONCRETE BEAM WITHOUT WEB REINFORCEMENT

M. A. CHOWDHURY[1], Z. I. Zahid[2] and M. M. Islam[3]

[1, 2, 3]Ahsanullah University of Science and Technology
Dhaka, Bangladesh
Email: [1]arman.chowdhury.ce@gmail.com, [2]zubayer061@gmail.com and
[3]mashfiq7777@gmail.com

Abstract. *Available codes and models generally use partially modified shear design equation, developed earlier for steel reinforced concrete, for predicting the shear capacity of FRP reinforced concrete members. Consequently, calculated shear capacity shows under or overestimation. Furthermore, in most models some parameters affecting shear strength are overlooked. In this study, a new and simplified shear capacity prediction model is proposed based on Multi-linear regression analysis considering all affecting parameters. A large database containing 157 experimental results of FRP RC beams without shear reinforcement is assembled from the published literature. A statistical analysis is performed to verify the accuracy of the proposed model. After comprehensively reviewing all previously proposed models and codes, 5 best and recent models are presented for comparison with the proposed model. Hence, it is observed that the proposed equation shows overall optimized performance compared to the presented models within the range of used experimental dataset.*

Keywords: Fiber reinforced Polymer (FRP), Shear strength, Experimental database, Multi linear Regression analysis.

1 INTRODUCTION

Corrosion of steel reinforcement is one of the major issues for the deterioration of RC Structures. Thus, it leads to the rehabilitation process of existing structures which is very costly and reduces the service life. To resolve the problem, fiber reinforced polymer (FRP) bar has been brought in as internal reinforcement in RC structures replacing conventional steel. FRP bar provides a proper combination of physical and chemical properties such as high resistance to corrosion, high strength to weight ratio and magnetically inert. Despite the advantages, FRP imparts lower modulus of elasticity and linear elastic brittle stress-strain relationship up to rupture with no yield point [7]. This may lead to an overestimated design of FRP RC beams in terms of shear strength. This is because the shear mechanisms are relatively complex, and various researchers interpret the importance of the basic mechanisms in their own ways and hence there is a dispute about which of the shear mechanisms should be focused more on, compared to the others [4].Six affecting parameters i.e. concrete compressive strength, shear span to depth ratio, effective depth, beam width, reinforcement ratio and Modulus of elasticity are found to be most liable for determining shear strength of FRP RC beams. After doing an extensive review of all the available codes and models published between the time period of 1997 to 2015, five best and recent models are selected to compare with the proposed model [2].

2 RESEARCH SIGNIFICANCE

Due to complex shear transfer mechanisms in concrete beams and various influencing parameters, understanding of shear is still relatively limited. This paper presents prediction model to predict the shear strength of FRP reinforced concrete beams without stirrups. Models are developed using a large database of 157 experimental results and the controlling parameter for shear strength measurement are also examined with respect to the model and the experimental database. The information gathered in this research and the proposed model could be very helpful in establishing design guidelines and also for future research on FRP reinforced beams.

3 EXPERIMENTAL DATABASE

In order to study the behavior of FRP-RC beams and check the performance of the proposed model a large database of 157 beams that failed in shear was compiled[2]**.**Among them, 116 data used for training the proposed multi linear regression model and another 41 data used for testing the performance of the model. The selection of training and testing data is random from the full assembled experimental database. The shear design parameter used in this study is concrete compressive strength ($f'c$), beam width (b_w), effective depth (d), beam shear span (a), shear-span to depth ratio (a/d), reinforcement ratio of longitudinal FRP bars

(ρ_f) and Modulus of Elasticity of the reinforcing bar (E_f). The shear span to depth ratio, (a/d) ranged from 1.1 to 6.5. The beam compressive strength varied from 24.1 MPa to 88.3 MPa. Beam effective depth, d varied from 141 mm to 889 mm. Longitudinal reinforcement ratio, (ρ_f) used in this study varied between 0.2% to 2.6%. In this study, Modulus of elasticity of FRP bar, (E_f) used between 4.1GPa to 145 GPa. The material and geometrical properties of the 116 members in the refined database as well as their original sources are given [2]. All specimens in the database were simply supported, tested in either two or four points loading arrangement, had no transverse reinforcement and failed in shear. The distribution of geometrical and mechanical properties of the 116 test specimens is given in Figure 1.

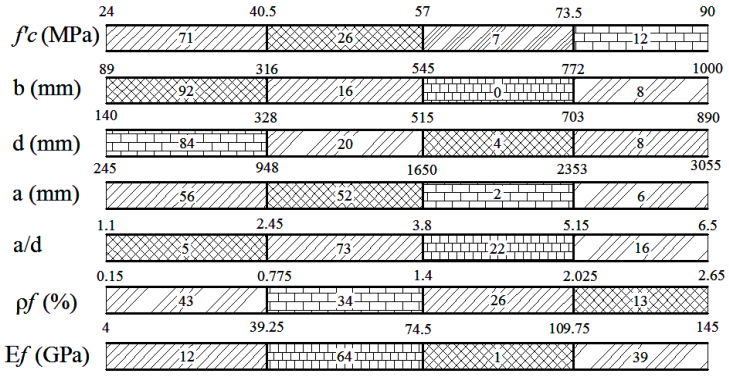

Figure 1: Data distribution of experimental parameters

4 PARAMETER AFFECTING SHEAR STRENGTH

Due to the complex behavior of FRP-RC beam in terms of shear strength, it is still a challenge to solve this problem. Substantial research effort is given to understand and predict the shear strength more accurately [3]. Because of the lacking in the current design approaches provided by different researchers, make use of FRP bar in the practical field is hindered. Based on the analysis on different influencing parameter and critical review of the available database some parameters are found to be liable for the overall contribution in shear strength. These influencing parameters are i) Shear span-to-depth ratio (a/d), ii) effective depth of beam (d), iii) reinforcement ratio, (ρ_f) iv) Modulus of elasticity of FRP bar (E_f), v) concrete tensile strength in terms of compressive strength ($f'c$) and vi) width of beam (b_w).

5 REVIEW OF CURRENT SHEAR DESIGN PROVISIONS

All available codes and models published between 1997 to 2015 are reviewed in another work of this author [2] and among them five best and recent models are

selected based on statistical parameters. These models are proposed by Mari et al. [6], Nasrollahzadeh and Basiri [8], Kara [5], Alam and Hussein [1] and Nehdi et al. [9]. Nehdi et al. [9] proposed a model based on genetic algorithm. About 168 FRP-RC beams with and without web reinforcement is used to develop the model and compared with ACI 440-1R-06, CSA S806, JSCE 1997 and ISIS 2001. Nedhi et al. [9] proposed two models for both deep and slender beams. Then a parametric analysis is done to compare the result with proposed model. This model included six parameters as used in this study.Nasrollahzadeh and Basiri[8] proposed a model based on fuzzy inference system which is exceptional with other approaches as it doesn't require priori information to analyze data and develop a model. This model also used controlling parameters as $f'c$, b_w, d, a/d, ρ_f and E_f and compared with ACI-440.1R-06, CAN/CSA, 2002. Modified compression field theory (MCFT) is used by Alam and Hussein [1] which actually proposed a modification to CSA-S806-02. Sixteen (16) experimental beams made of GFRP, CFRP and Steel is used in this study and tested under four point loading. Mari et al. [6] proposed a simple analytical model based on the principle of structural mechanics and on the experimentally observed behavior of these elements at failure. Test data from 144 experimental results was used in this study. Kara [5] used 104 experimental data among them 56 data were used for training and 28 data sets were used for testing whereas this study used 116 for training and 41 for testing. Gene Expression Programming (GAP) is used to develop this model. The only limitation of this model is the shear span to depth ratio. It can't predict the shear strength of deep beams accurately where span to depth ratio is less than 2.5.

6 MODEL DEVELOPMENT

6.1 Multi linear regression approach

In order to predict the shear strength of FRP reinforced concrete beams more accurately the experimental shear strength of FRP reinforced concrete beams was analyzed with six controlling parameters i.e. i) concrete compressive strength, ii) beam width, iii) effective depth of the beam, iv) shear span to depth ratio, v) reinforcement ratio and vi) Modulus of elasticity of FRP bar. A general pattern of multiple regression analysis as shown in equation [1] was conducted in optimizing the regression parameters i.e. $\beta_1, \beta_2, \beta_3, \beta_4, \beta_5$ and β_6.

$$V_{pred} = \beta_0 + \beta_1 f_c'^{\alpha_1} + \beta_2 b_w^{\alpha_2} + \beta_3 d^{\alpha_3} + \beta_4 E_f^{\alpha_4} + \beta_5 \rho_f^{\alpha_5} + \beta_6 \left(\frac{a}{d}\right)^{\alpha_6} \qquad [1]$$

Where, V_{pred} is the predicted shear strength in MPa, $f'c$ means concrete compressive strength, b_w is the beam width, d indicates effective depth, Modulus of elasticity defined as E_f, ρ_f is the reinforced ratio and shear span to depth ratio. The interaction between the parameters had been neglected and this can be taken as

the direction for future study. The coefficient $\alpha_1, \alpha_2, \alpha_3, \alpha_4, \alpha_5$ and α_6 are non-linear coefficients and is selected based on the proposed parameter selection network as shown in Figure 2 (b).

At first stage one parameter from each section is taken to form the initial model i.eb_w, f'_c, d, E_f^(1/3), (a/d)^(3) and ρ_f^(1/3) and it can be written as shown in equation [2].

$$V_{pred} = \beta_0 + \beta_1 f_c'^{\left(\frac{1}{2}\right)} + \beta_2 b_w^{\ 1} + \beta_3 d^1 + \beta_4 E_f^{\left(\frac{1}{3}\right)} + \beta_5 \rho_f^{\left(\frac{1}{3}\right)} + \beta_6 \left(\frac{a}{d}\right)^3 \qquad [2]$$

Then a multilinear regression is done based on 157 experimental data to find out the value of coefficients $\alpha_1, \alpha_2, \alpha_3, \alpha_4, \alpha_5, \alpha_6, \beta_1, \beta_2, \beta_3, \beta_4, \beta_5$ and β_6 which gives a final output value of V_{pred}. By this way 72 regression model is developed as equation [2] and checked with several statistical parameters. Total analysis is done by the following flow chart given in Figure 2 (a) & (b).

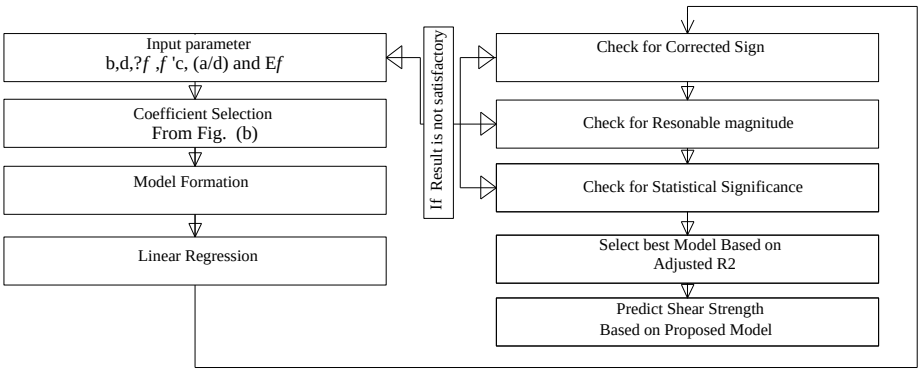

(a)

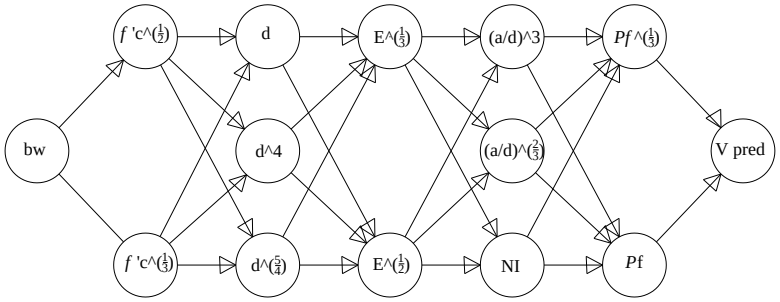

(b)

Figure 2 :(a) Algorithm to develop proposed model, (b) Network used for coefficient selection (NI means Not Included)

6.2 Proposed Model

A non-linear regression model based on experimental database collected from literature is suggested and examined with different statistical parameters such as R^2 and t test for the statistical stability of the model. This model stood well in all statistical analysis. In order to predict the shear strength of FRP-RC beams more accurately, the experimental shear strength of FRP-RC beams was analyzed with all the six parameters stated before. Finally, the proposed prediction model can be written as follows in equation [3].

$$V_{pred} = -0.223 + 0.19 \times b_w + 9.433 \times \sqrt{f_c^{'}} + (1.63 \times 10^{-10}) \times d^4 + 2.63 \times \sqrt{E_f} - 37.571 \times \left(\frac{a}{d}\right)^{\frac{2}{3}} + 12.996 \times \rho_f \quad [3]$$

Where,

$\alpha_1 = 1/2, \alpha_2 = 4, \alpha_3 = 1/2, \alpha_4 = 2/3, \alpha_5 = 1, \beta_0 = -0.223, \beta_1 = 0.19,$

$\beta_2 = 9.43, \beta_3 = 1.63 \times 10^{-10}, \beta_4 = 2.63, \beta_5 = -37.571$ and $\beta_6 = 12.996$

In reality safety factor would be employed to share capacity predictions more conservative and acceptable for design use [7].

7 TRAINING AND TESTING DATA

Verification of the proposed model is done by using a large experimental database of 157 beams. Among them, 116 beams were used for training the model and later this model is tested with 41 beams and slabs from the literature. This model showed a good prediction during the testing phase and it is shown in Fig-

ure3.This model can be used in 95% confidence level which is evident from Table 1and Table 2.

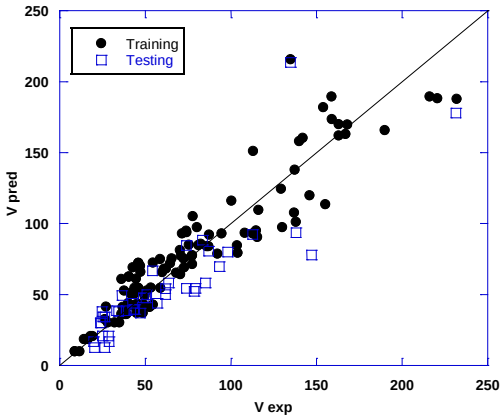

Figure 3: Training and Testing of Proposed Model

Table 1: Statistical t-test result

	Proposed model						
	β_0	β_1	β_2	β_3	β_4	β_5	β_6
t-test	-0.008	17.359	2.464	6.390	3.309	-7.294	4.00

Table 2: Confidence interval based on t-test

Confidence	**t-test**
90%	1.64
95%	1.96
99%	2.58
99.9%	3.29

8 RESULT AND DISCUSSION

For the comparison of presented models in predicting the shear strength of FRP-RC beams, a number of performance checks were used. Mean, Standard deviation, Average Absolute Error (AAE) and Coefficient of Variation (COV) indicate the overall functioning of the design algorithm. The statistical analysis of the pre-

sented models along with the proposed one is shown in Table 3. Mean of experimented and predicted values is drawn in Figure 4. (a)- (f). Root Mean Square is drawn in Figure 5. (a)- (f).The shear design equation proposed by this study had the most accurate prediction with an average of 1.03, standard deviation of 0.22, coefficient of variation (COV) of 20.9% and average absolute error (AAE) of 15.8%.Kara [5] and Mari et al. [6] has slightly more scattered results with an average of 1.05 and 1.04 respectively. In terms of COV, Kara [5] shows better results than Mari et al. [6] to 25.1%. Nedhi et al. [9] optimized the previous model and its result also shows a balanced scatter with an average of 1.14, SD of 0.24, COV of 20.8% and AAE of 17.4%. Though both Kara [5] and Nedhi[9] used Genetic Programming for predicting shear strength, Kara [5] imparts better performance. One of the latest models was proposed by Nasrollahzadeh and Basiri[8]. The model had good significance with a mean of 1.13, though SD and COV was quite larger compared to others. Besides, the model is not user friendly for its complexity.Alam and Hussein [1] used modified compression field theory which is modified from a code provided by Canadian standard association but still it overestimated the shear strength with a mean of 1.71 without considering the reduction factors. Although it gives comparatively higher accuracy at higher shear capacity but it needs improvement in COV and AAE which are 23.5% and 38.8%.

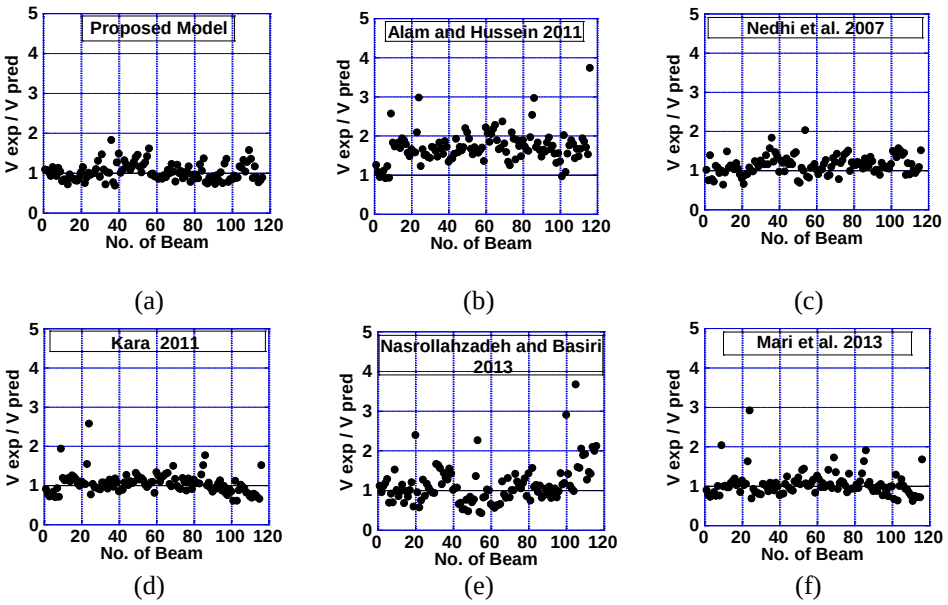

Figure 4 (a)-(f) Ratio of Predicted and Experimental shear strength

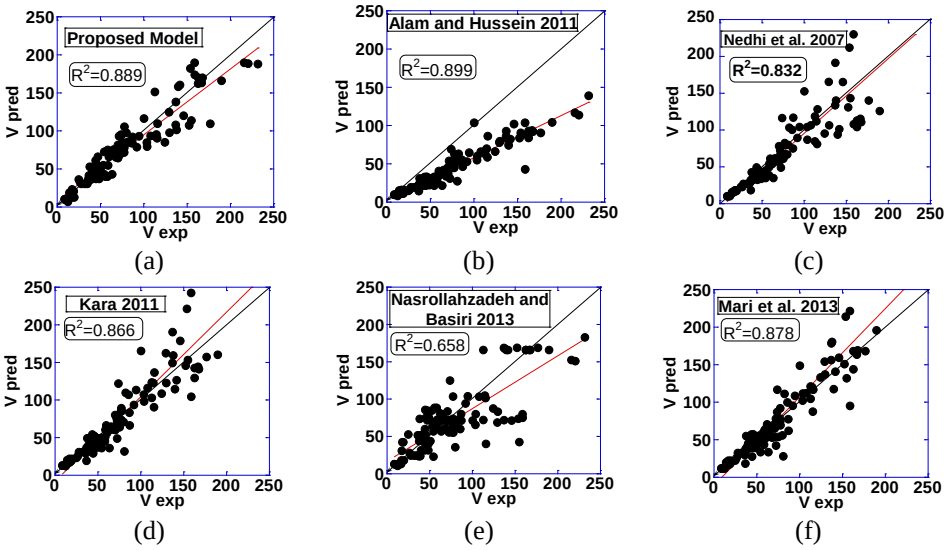

Figure 5 (a)-(f) RMS of experimental and predicted shear strength

Table 3: Analysis of Statistical Parameters

Model	Year	V exp/ Vpred				
		Mean	SD	COV (%)	AAE (%)	R^2
Proposed Model	2015	1.03	0.22	20.9	15.8	0.89
Mari et al.	2013	1.04	0.30	29.0	16.3	0.88
Nasrollahzadeh and Basiri	2013	1.13	0.48	43.0	28.0	0.66
Alam and Hussein	2011	1.71	0.40	23.5	38.8	0.90
Kara et al.	2011	1.05	0.26	25.1	16.6	0.87
Nedhi et al.	2007	1.14	0.24	20.8	17.4	0.83

9 CONCLUSIONS

This study investigated using regression approach for predicting the shear strength of FRP-RC beams without stirrups, and compared such predictions with those of the 5 available models. The following conclusion can be drawn from this study.

- The result of this research suggests that regression approach can provide a more precise and reliable alternative method for the shear design of FRP concrete beams.
- The proposed model outperformed the shear design provisions considered in this work. The proposed model used in this study developed an

average of the Vexp/Vpred ratio equal to unity, hence leading to an economic use of FRP reinforcement.

- All existing shear provisions considered in this study provided unnecessarily conservative result except Kara [5] in estimating the shear strength of FRP-RC beams without shear reinforcement. Kara 2011 showed an overall good balance In terms of scatter and standard deviation, though there is scope of improvement such as COV and AAE, which is satisfactorily reduced by our suggested model.

The proposed model is also trained and tested to predict the shear strength within the range of input variables considered. Even so, they may not demonstrate accuracy when extrapolating beyond this scope.

REFERENCES

[1] O.C. Zienkiewicz, R.C. Taylor, 1989. *The finite element method, Vol. I, 4th Edition*. McGraw Hill, p198.

[2] Alam, M. S., & Hussein, A. (2012). "Unified shear design equation for concrete members reinforced with fiber-reinforced polymer without stirrups." *Journal of Composites for Construction*, 17(5), 575-583.

[3] Chowdhury A, Islam M (2015) Shear Strength Prediction of FRP reinforced Concrete Beams: A State-of-the-Art Review of Available Models. *J Civil Environ Eng* 5: 186. doi:10.4172/2165 784X.1000186

[4] Godat, A., Labossière, P., & Neale, K. W. (2012). "Numerical investigation of the parameters influencing the behaviour of FRP shear-strengthened beams."*Construction and Building Materials*, 32, 90-98.

[5] Jung, S., & Kim, K. S. (2008)."Knowledge-based prediction of shear strength of concrete beams without shear reinforcement." *Engineering Structures*, 30(6), 1515-1525.

[6] Kara, I. F. (2011). "Prediction of shear strength of FRP-reinforced concrete beams without stirrups based on genetic programming." *Advances in Engineering Software*, 42(6), 295-304.

[7] Marí, A., Cladera, A., Oller, E., &Bairán, J. (2014). "Shear design of FRP reinforced concrete beams without transverse reinforcement." *Composites Part B: Engineering*, 57, 228-241.

[8] Machial, R., Alam, M. S., &Rteil, A. (2012). "Revisiting the shear design equations for concrete beams reinforced with FRP rebar and stirrup." *Materials and Structures*, 45(11), 1593-1612.

[9] Nasrollahzadeh, K., &Basiri, M. M. (2014). "Prediction of shear strength of FRP reinforced concrete beams using fuzzy inference system." *Expert Systems with Applications*, 41(4), 1006-1020.

[10] Nehdi, M., El Chabib, H., &Saïd, A. A. (2007). "Proposed shear design equations for FRP-reinforced concrete beams based on genetic algorithms approach." *Journal of Materials in Civil Engineering*, *19*(12), 1033-1042.

CICM 2015
First International Conference on
Advances in Civil Infrastructure and Construction Materials
MIST, Dhaka, Bangladesh, 14–15 December 2015

NONLINEAR FINITE ELEMENT ANALYSIS OFFULLY ENCASED COMPOSITE COLUMNS AND REVIEW OF CODES

Md. S. RAHMAN[1], Mahbuba Begum[2] and Raquib Ahsan[3]

[1, 2, 3]Department of Civil Engineering, BUET, Bangladesh
Email: [1]soeburrahman@gmail.com, [2]mahbuba@ce.buet.ac.bd and
[3]raquibahsan@gmail.com

Abstract. *Composite column is a structural member that uses a combination of structural steel shapes, pipes or tubes with or without reinforcing steel bars and reinforced concrete to provide adequate load carrying capacity to sustain either axial compressive loads alone or a combination of axial loads and bending moments. In a composite column both the steel and the concrete sections would resist the external loading by interacting together though bond and friction. Steel-concrete composite columns have been employed in high-rise buildings, bridges, piers, piles and earthquake resistant structures. The most usual types of composite columns are the concrete filled steel tubes and the partially or fully encased steel profiles. Fully encased composite (FEC) column provides enhanced ductility, strength, stability and stiffness. Moreover, this composite system renders better fire proofing and corrosion protection since the steel section is fully encased by concrete. This paper investigates the behaviour of axially loaded concrete encased steel composite columns experimentally as well as through numerical simulations. In the experimental investigation eleven small scale short FEC columns has been tested under concentric gravity loadings. A nonlinear 3-D finite element model has been developed to analyses the inelastic behavior of steel, concrete, and longitudinal reinforcement as well as the effect of concrete confinement in fully encased composite (FEC) columns. Attempt has been taken in this study to explore the behavior and strength of FEC columns encompassing a variety of geometry and material properties. The model has been verified against the experiments conducted in the laboratory under concentric gravity loads. It is observed that the finite element model is able to predict the experimental behaviour of FEC columns and squash load under concentric gravity loads with good accuracy. The numerical and experimental capacities were also compared with the predicted capacities according to ACI 318 (2014) and AISC-LRFD (2010) codes guidelines.*

Keywords: Composite, Columns, Experimental, Finite element, fully encased, Strength.

1 INTRODUCTION

Composite construction system first appeared in the United States 1894 but the design guidelines were established in 1930. During the past few decades, steel concrete composite structural systems have been used in many tall buildings all over the world. There are three types of composite columns commonly used in high rise building. Typical cross-section of these columns are shown in Figure 1.As shown in Figure 1(a), in FEC columns the structural steel section is fully encased by surrounding concrete where as in partially encased composite columns, as shown in Figure 1(b), the steel section is partially encased by concrete. On the other hand in concrete filled tubular composite columns, as shown in Figure 1(c) the concrete is fully confined by the surrounding steel section.

Extensive experimental investigations on FEC columns have been conducted by Sherif and Deierlein [1], Virdiand Dowling [2], Mirza and Skrabek [3], with the extensive review of most of these researches is given by Shanmugam and Lakshmi [4]. These tests were carried out on concentrically loaded and eccentrically loaded FEC columns having different slenderness ratios, different steel sections and different concrete and steel strength. Analytical and theoretical studies on concentrically loaded and eccentrically loaded FEC columns have been performed by, Tokgoz and Dundar [5], and Chen and Lin [6]. It is observed that very limited study on numerical simulation of FEC columns. Recently, Ellobody and Young [7] developed a nonlinear 3-D finite element model investigating the behaviour of axially concentric loaded FEC columns. FEC column is a relatively new system for the construction industry of Bangladesh. In the upcoming version of Bangladesh National Building Code (BNBC 2010) the design of FEC columns has been included [8]. Most of the guidelines have been adopted from AISC 2005. The applicability of these design provisions in the construction environment of Bangladesh need to be explored. Attempts have been made in this study to develop a full scale 3D FE model for FEC columns to explore the behavior and strength of FEC columns encompassing a wide variety of geometry and material properties. The model will be verified against the experiments conducted in the laboratory. It will also compared with the predicted capacities according to ACI -2014 [9] and AISC-2010 [10] codes guidelines. The validated FE model will eventually be used to explore the failure behavior of FEC columns.

2 EXPERIMENTAL INVESTIGATIONS

An experimental investigation, to determine the failure behaviour and load carrying capacity of FEC columns is presented in the study. The main variables considered in the test program were the concrete compressive strength, cross sectional dimensions and percentage of structural steel. The failure mode and experimental load-deflection behaviour of the specimens were examined in the tests.

(a) (b) (c)

Figure 1: Typical X-sections of composite columns, (a) FEC; (b) PEC; and (c) CFT

2.1 Description of Test Specimens

The test program consisted of eleven (11) numbers of FEC columns of two different sizes with varying percentages of structural steel. Six composite column specimens with square cross section (100mmx100mm, as shown in Table 1) were constructed with normal strength concrete. Another five specimens also with square section (150mmx150mm, as shown in Table 2) were constructed with high strength concrete. The concrete compressive strength (f'c) for normal and high strength concrete were 27 and 41 MPa respectively. The yield strength of reinforcement and core steel were 415 MPa. The length (L) of all FEC test columns was 900 mm respectively. The typical cross section of these columns is illustrated in Figure 2.

Table 1: Geometric properties of test specimens with normal strength concrete

Sl. No.	Specimen Designation	Steel Plate Size $b_f$xd xt_fx t_w (mm)	Reinforcement		Steel Ratio	
			Longitudinal rebar	Tie rebar (mm)	Plate (%As)	Rebar (%Asr)
1	SCN4A-1	20x20x5x5	4-φ8mm	φ6mm@50mm	3	2
2	SCN4A-2	20x20x5x5	4-φ8mm	φ6mm@50mm	3	2
3	SCN4A-3	20x20x5x5	4-φ8mm	φ6mm@50mm	3	2
4	SCN4B-1	25x25x5x5	4-φ8mm	φ6mm@50mm	3.75	2
5	SCN4B-2	25x25x5x5	4-φ8mm	φ6mm@50mm	3.75	2
6	SCN4B-3	25x25x5x5	4-φ8mm	φ6mm@50mm	3.75	2

Table 2: Geometric properties of test specimens with high strength concrete

Sl. No.	Specimen Designation	Steel Plate Size $b_f$xdxt_fxt_w (mm)	Steel Rebar		Steel Ratio	
			Longitudinal rebar	Tie rebar (mm)	Plate (%As)	Rebar (%Asr)
1	SCH6A-1	30x30x5x5	4-φ8mm	φ6mm@75mm	2	1
2	SCH6A-2	30x30x5x5	4-φ8mm	φ6mm@75mm	2	1
3	SCH6A-3	30x30x5x5	4-φ8mm	φ6mm@75mm	2	1
4	SCH6B-1	45x45x5x5	4-φ8mm	φ6mm@75mm	3	1
5	SCH6B-2	45x45x5x5	4-φ8mm	φ6mm@75mm	3	1

Axial load was applied to the composite columns specimens at the rate of 5 KN/s. The digital reading of axial load and lateral displacement were collected by using an electronic data acquisition system during testing of each specimen.

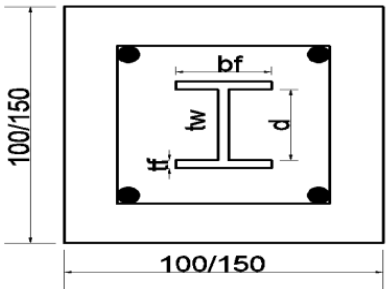

Figure 2: Typical X- section of FEC columns

Figure 3: Experimental column test setup

3 FINITE ELEMENT MODEL

A nonlinear 3D finite element model was developed in this study to investigate the behavior and strength of FEC columns encompassing a variety of geometry and material properties. Both material and geometric nonlinearities were incorporated in the FE model. ABAQUS finite element code [11] was used to develop the nonlinear FE model for FEC columns in this study. The steel section in FEC column is modeled with S4R shell element. Each node of the S4R shell element has six degrees of freedom- three translations and three rotations. The longitudinal and transverse bars were modeled using T3D2 three dimensional truss elements. The concrete of FEC column was simulated using solid C3D8R element. The load was applied using displacement control technique on the top surface of the column. The base of the column was fixed in all directions. Rik's solution strategy has been implemented to trace stable post peak behavior of the composite column up to failure.

4 MATERIAL PROPERTIES FOR FE MODEL

Steel and concrete are the main materials used in FE model for numerical investigation. Plastic properties for these materials (as shown in Table 3 and 4) were incorporated in the FE model. The subscripts $_y$, $_{sh}$ and $_u$ in the table signify the yield, onset of strain hardening and ultimate strain of the steel plates respectively. The stress strain data obtained from uniaxial tension test were converted to true stress and logarithmic plastic strain. It was calculated based on coupon test of steel plates. The value of the Poisson's ratio for steel used in the numerical analysis is 0.3.Elasto-plastic J2 material model is used to simulate the behavior of steel I section in FEC columns. The damage plasticity model in ABAQUS was used to simulate the concrete material behaviour in the composite columns. Carreira and Chu [12, 13] equations were used to generate the compression and tension stress-strain curve for concrete material in FEC columns. The ultimate strength (f'_{cu}) for concrete was obtained from standard cylinder tests performed on concrete at the test day for each test specimen.

Table 3: Material properties of test specimens

Specimen Design.	Properties of concrete				Properties of steel plate					
	f_{cu} (MPa)	E_c (MPa)	ε_c ($\mu\varepsilon$)	γ	F_y (MPa)	F_{sh} (MPa)	F_u (MPa)	ε_y (mm/mm)	ε_{sh} (mm/mm)	ε_u (mm/mm)
SCN4A SCN4B	27	24680	1900	0.18	350	355	626	0.003860	0.022320	0.129830
SCH6A SCH6B	41	30000	2000	0.18	350	355	626	0.003860	0.022320	0.129830

Table 4: Material properties of test specimens

Specimen Designation	Properties of concrete				Properties of reinforcement					
	f_{cu} (MPa)	E_c (MPa)	ε_c (με)	γ	F_y (MPa)	F_{sh} (MPa)	F_u (MPa)	ε_y (mm/mm)	ε_{sh} (mm/mm)	ε_u (mm/mm)
SCN4A SCN4B	27	24680	1900	0.18	470	471	634	0.00322	0.019170	0.13555
SCH6A SCH6B	41	30000	2000	0.18	470	471	634	0.003220	0.019170	0.13555

5 COMPARISON BETWEEN EXPERIMENTAL AND NUMERICAL RESULTS

5.1 Load Deflection Behavior

Axial compressive strength, axial shortening and failure behavior were observed and recorded for each FEC column specimens experimentally and numerically. The load-deflection behavior of column group SCN4B obtained from the FE analysis as well as from the experiments is plotted in Figure 4. It was observed that finite element model can predict the experimental behavior of FEC columns with good accuracy.

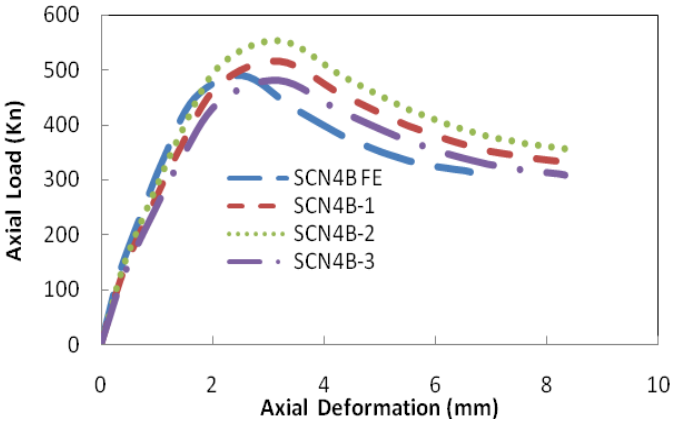

Figure 4: Comparison between experimental and numerical load

5: Failure mode of FEC test columns

The values of mean experimental and numerical peak loads, for six columns with normal strength and five columns with high strength concrete are shown in Tables 5 and 6 respectively. The mean value of experimental-to-numerical peak load ratio, P_{exp}/P_{num} and experimental-to-numerical average axial strain at peak load, $\varepsilon_{exp}/\varepsilon_{num}$, are compared for all groups of columns. It is observed that the mean value and the standard deviation of all groups of columns are reasonable.

This indicates the excellent performance of the finite element model in predicting the ultimate capacity of FEC columns with two different strength of concrete.

Table 5: Comparison of numerical and experimental results for normal strength concrete

Ser No	Specimen	Pick axial load		P_{exp}/P_{num}	Avg. axial strain at peak load		$\varepsilon_{exp}/\varepsilon_{num}$
	Designation	P_{num} (KN)	$P_{exp\ mean}$ (KN)		Num. $\varepsilon_{num\ (\mu\varepsilon)}$	Exp. $\varepsilon_{exp\ ((\mu\varepsilon)}$	
1	SCN4A	471	491	1.042	2550	2708	1.062
2	SCN4B	490	516	1.053	2541	3202	1.260
Mean				1.050			1.161
SD				0.009			0.140

Table 6: Comparison of numerical and experimental results for high strength concrete

Ser No	Specimen	Pick axial load		P_{exp}/P_{num}	Avg. axial strain at peak load		$\varepsilon_{exp}/$
	Designation	P_{num} (KN)	$P_{exp(mean)}$ (KN)		N_{um}. ε_{num} ($\mu\varepsilon$)	Exp. ε_{exp} (($\mu\varepsilon$)	ε_{num}
1	SCH6A	1181	1117	0.946	3749	4686	1.250
2	SCH6B	1238	1240	1.002	3748	4314	1.151
Mean				0.974			1.201
SD				0.039			0.070

5.2 Failure Modes

The failure modes for FEC columns were identified from the finite element analysis and compared with the failure modes observed in the test. Failure modes were captured manually for all the specimens during the test as shown in Figure 5. The local failure was prevented using FRP (2mm thick) at the top and bottom of the columns. It was observed in all cases that concrete crushing (CC) occurred before yielding of the steel plate (SY). Similar failure behavior was obtained in the nonlinear FE simulation of FEC columns under axial loads. The principle stress in concrete and steel of FEC column along 3-3 axis is shown in Figure 6.

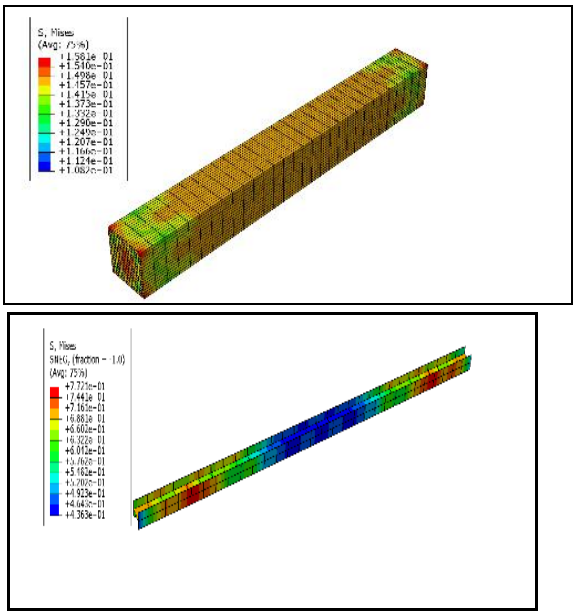

(a)

(b)

Figure 6: Deformed Shapes and stress contour at failure in a) Concrete b) Core steel of FEC columns

6 CONTRIBUTION OF STEEL AND CONCRETE IN THE CAPACITY OF FEC COLUMNS

The finite element model is able to isolate the contribution of the core steel, reinforcement and concrete in the total load carrying capacity of the FEC columns. The axial load and axial deformation of individual materials in the composite section were determined. Load carrying capacity of different elements of column group SCN4Bis shown in Figure 7. It has been observed that the contribution by steel I-section, reinforcement and concrete of the total load carrying capacity of the composite columns are 30%, 13% and 57% respectively. More over increasing the core steel ratio from 1% to 2% the axial capacity is increased by 4% for normal strength concrete of columns groups (SCN4A and SCN4B). Similarly, for high strength concrete columns groups (SCH6A and SCH6B) load carrying capacity is also increased by 5%. The effect of high strength concrete has been studied in this study. It is observed that increasing the concrete strength from 27 to 41 MPa, the capacity of columns strength is increased by 28% for SCN4B groups which is shown in Figure 8.

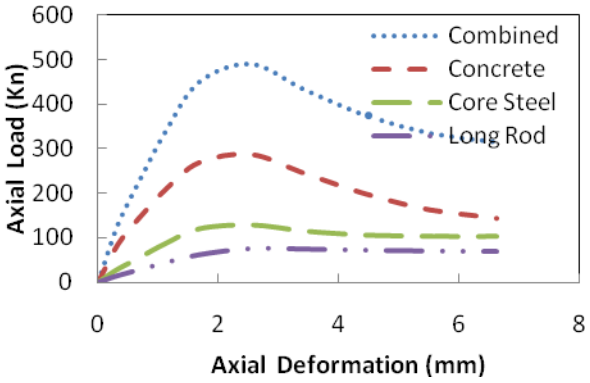

Figure 7: Contribution of steel and concrete in the ultimate capacity

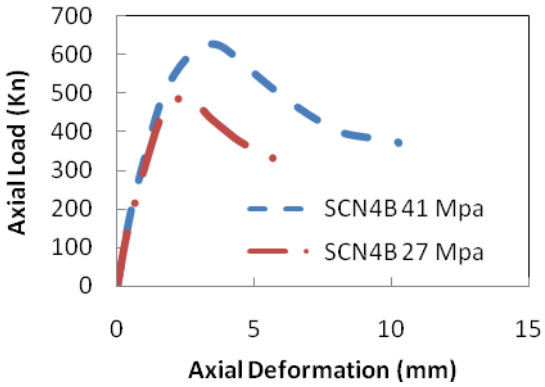

Figure 8: Effect of concrete strength on the capacity of FEC columns

7 REVIEW OF CODES

Over the last two decades, researchers have suggested analytical methods and design procedures for composite columns and design codes have been formulated. Each of these codes is written so as to reflect the design philosophies and practices in the respective countries. All the codes provided guide lineson concrete material properties, steel core requirements, transverse reinforcement requirements, longitudinal, reinforcement requirements and detailing of various structural element

7.1 ACI-318 Approach-2014 [9]

It uses the limit state design format with factors and capacity reduction factors. The strength of a composite column is computed as for reinforced concrete members. Failure is defined in terms of a 0.002 strain limit for any concrete fiber.

The expression for equation stiffness includes creep factor and cracked concrete stiffness is considered. Minimum eccentricities are specified to cover construction tolerances. It specifies maximum axial load $P_n = \phi P_0$ with $\phi = 0.85$ and equation1.

$$P_0 = 0.85 f'c\ (A_g - A_{st} - A_{ss}) + f_{yss} A_{ss} + f_y A_{st} \quad (1)$$

where, f'_c is compressive strength of concrete, A_g is gross area of column section, A_{st} is area of longitudinal reinforcement, A_{ss} is area of core steel, f_{ys}, , f_y ,yield strength of core steel and longitudinal reinforcement, respectively.

7.2 AISC-LRFD Approach-2010 [10]

The design of composite columns is based on the design equations for steel columns. The slenderness and area parameters are modified for the presence of concrete. Load transfer should be provided by direct bearing at the connections.

$$P_{no} = [0.85 f'_c A_c + f_y A_s + f_{ysr} A_{sr}] \quad (2)$$

$$P_e = \pi^2 (EI_{eff})/(KL)^2 \quad (3)$$

$$P_n = 0.75 x P_{no} x [0.658^{\frac{Pno}{Pe}}], \text{ if } \frac{Pno}{Pe} \leq 2.25 \quad (4)$$

8 COMPARISION OF COLUMN STRENGTHWITH DESIGN CODES

The strength of the concrete encased composite columns obtained using the FE and the tests are compared with the unfactored design strengths predicted using the ACI 318 [9] and AISC 2010 [10]for composite columns in Table 7. The mean values of $P_{Num}/P_{Exp,}$ P_{ACI}/P_{EXP} and P_{AISC}/P_{EXP} ratios are 0.991,0.862 and 0.805, respectively, with the corresponding cofficients of variation of 4.85,3.14 and 11.5, respectievly. It is seen that the design strength predicted by the two specifications are conservative for the test specimenses, with the AISC-2010is comparatively more conservative then ACI-318.This is due to the fact that both the codes (ACI-318 and AISC-LRFD) neglected the effects of concrete confinement on strength and ductility of FEC columns.

9 CONCLUSIONS

Experimental as well as numerical research on the behavior of square FEC column subjected to short term axial load has been presented in this paper for two different strengths of concrete different steel ratios. The complete experimental load-deflection behavior of the composite column specimens has been attained in the study. This study also conducted a nonlinear 3D finite elements analysis on FEC columns under axial load. Nonlinear material behavior for concrete has been incorporated in FE analysis.

Table 7: Comparision between experimental, numerical and code predicted capacities for FEC columns

Ser No	Specimen Designation	Concrete f'c (MPa)	Yield Strength of Steel fyt (MPa)	Yield Strength of Steel fys (MPa)	P_{Num} (KN)	$P_{Exp\ mean}$ (KN)	P_{ACI} (KN)	P_{AISC} (KN)	P_{Num}/P_{Exp}	P_{ACI}/P_{Exp}	P_{AISC}/P_{EXP}
1	SCN4A	27	470	350	471	491	413	357	0.959	0.841	0.727
2	SCN4B	27	470	350	490	516	438	374	0.950	0.849	0.725
3	SCH6A	41	470	350	1181	1117	1006	1013	1.057	0.901	0.907
4	SCH6B	41	470	350	1238	1240	1062	1069	0.998	0.856	0.862
	Mean Value								0.991	0.862	0.805
	Standard deviation								0.048	0.027	0.093
	Coefficient of Variation (%)								4.85	3.14	11.5

Geometric nonlinearities were also included in the model. The strength of the concrete encased composite columns obtained using the FE and the tests are compared with the unfactored design strengths predicted using the ACI 318 and AISC-LRFD 2010 for these composite columns.The major findings of this study can be summarized as;

a) The finite element model was found to predict the experimental behaviour of FEC columns under concentric gravity loads with good accuracy.
b) Steel carried about 30% axial load of the total capacity of FEC columns.
c) Concrete carried about 57% axial load of the total capacity FEC columns.
d) Load carrying capacity of a column increased by 28% when concrete strength is increased from 27 MPa to 41 MPa.
e) Design strength predicted by the two specifications are conservative for the test specimenses, with AISC-2010 more conservative then ACI-318.

REFERENCES

[1] E.I.Sherif, G. Deierlein, 1999. Strength and Ductility of Concrete Encased Composite Columns,*Journal of structural Engineering*, vol,125(9) pp1009-1019.

[2] K.S. Virdi, P.J. Dowling, 1973. The ultimate strength of composite columns in biaxial bending, *Proceedings of the institution of civil engineers,* Part 2, pp 251-272.

[3] S.A. Mirza, B.W. Skrabek, 1992. Statistical analysis of slender composite beam–columnStrength,*Journal of Structural Engineering, ASCE;118(5)* pp 1312–31.

[4] N.E. Shanmugam, B.Lakshmi, 2001. State of art report on steel composite columns, *Journal of constructional steel research,*vol,l57, pp 1041-80.

[5] S. Tokgoz, C. Dundar, Experimental tests on biaxial loaded concrete encased composite columns,*Journal on Steel and Composite Structure*, 8(5), 423-438, 2008.

[6] C.C. Chen, N.J. Lin, 2006. Analytical model for predicting axial capacity and behavior of concrete encased steel composite stub columns, *Journal of Constructional Steel Research*, vol62, pp 424–433.

[7] E. Ellobodya, B. Young, 2011. Numerical simulation of concrete encased steel composite columns, *Journal of Constructional Steel Research*, vol67, pp 211–222.

[8] BNBC, Bangladesh National Building Code, 1993.Housing *and Building Research Institute*, Dhaka, Bangladesh.

[9] ACI 318R, 2014. Building Code Requirements for Structural Concrete, *AmericanConcrete Institute*, ACI, Detroit.

[10] AISC-LRFD, 2010.AISCManual for Steel Construction, *American Institute for Steel Construction*, USA.

[11] Hibbitt, Karlsson and Sorensen, Inc (HKS). *ABAQUS/Explicit User's Manual*, 2010. Version 6.10.

[12] D.J. Carreira, K.H. Chu, 1984. Stress-Strain relationship for plain concrete in compression, *ACI Journal* , Technical Paper, 82-72.

[13] D.J. Carreira, K.H. Chu, 1984. Stress-Strain relationship for Reinforced concrete in Tension, *ACI Journal*, Technical Paper, 83-3.

CICM 2015
First International Conference on
Advances in Civil Infrastructure and Construction Materials
MIST, Dhaka, Bangladesh, 14–15 December 2015

PROPERTIES OF NO-CEMENT BINDER CONTAINING SLAG, FLY ASH, RICE HUSK ASH AND COCONUT FIBER WITH CHEMICAL ACTIVATOR

Md Shafiullah[1], Monjurul HASAN[2] and Md. R. Karim[3]

[1]Department of Civil Engineering, Dhaka University of Engineering and Technology, Gazipur, Bangladesh
Email: [1]engr.shafi26@gmail.com, [2]mhasan@duet.ac.bd and[3]rezaul@duet.ac.bd

Abstract. *Utilization of wastes like slag, fly ash (FA)and rice husk ash (RHA) as replacement of cement and development of no-cement binder (NCB) has been observed in many recent studies. Present study aims to investigate the mechanical characteristics of such NCB mortar containing different percentage of coconut fibers (1.0%, 1.5% and 2.0%) as a reinforcement. Mortar prisms were prepared using slag, FA, RHA with NaOH (5%, 10%, and 15%) by weight. Test results show that the compressive, flexural and tensile strength of NCB mortar (mix 3 = 50% slag, 35% FA, 13.5% RHA and 10% NaOH) without coconut fiber were found to be 12.5 MPa, 2.9 MPa and 0.8 MPa respectively. Due to addition of 1.5% coconut fiber on the same mix, these strengths were improved by 44.7%, 11.7%, and 22.41% respectively. Specific gravity of the NCB binder and mortar unit weight for the same mix (mix 3) were recoded around 2.5 and 1800 kg/m^3, while OPC and OPC mortar has shown these values as 3.15 and 2200 kg/m^3. Depending on the test results, it can be concluded that use of coconut fiber in NCB has a great potential in the production of lightweight mortar/concrete.*

Keywords: Coconut fiber, Cement, Fly ash, Flexural strength, Rice husk ash, Slag.

1 INTRODUCTION

Concrete can be addressed as the prime material to satisfy the global construction need. Every year global concrete production rate is approximately 10 cubic kilometers [1]. Despite of its popularity the environmental impact associated with the concrete production (basically for raw material preparation) has become a major concern of the environmentalists as well as the engineers. Concrete is basically a composite of cement, aggregate and water. Cement accompanies the 10 – 15 percent of the total concrete and considered as the key binding material. Global production of cement is estimated approximately 2.4 billion tons which is increasing significantly every year [2] and a large share (about 67.60% of the total) is produced in Asiatic region [3]. As the consequence of the emerging need of concrete construction, cement industries worldwide are facing growing challenges in conserving material and energy resources. Again, in a statistics, it has shown that 5 – 7 percent of the total CO_2 emission originated from the cement industries [3, 4], which catches the attention of the researchers. Thus there are numerous researches ongoing to develop new alternative binder [5 – 7] replacing cement.

Slag, fly ash (FA), rice husk ash (RHA) are the waste products of blast furnace, coal based power plant and agricultural industry respectively. Generation of these type of wastes are progressively increasing due to rapid industrialization and growth of agricultural sectors to support the growing population demand. In recent times, use of such waste materials on the production of composite cements has gained increasing interest due to various ecological, economical, technical benefits [6 – 9]. Bremner [10] reported that, 300 million tons of CO_2 can be reduced by replacing only 18.5% of cement with slag or fly ash (FA) per year globally. Natural fiber such as coconut fiber has certain physical and mechanical characteristics that can be utilized effectively to impart additional strength to the concrete [11]. To reduce the impact on the environment, use of these materials as a no-cement binder (NCB) leads to the proper disposal of these materials, resulting in reducing the impact of these materials on environment. Previously, RHA and FA have been used as partial replacement of cement in mortar [12]. Karim et al. [6] reported that 100% replacement of cement can be made with using slag, FA and RHA, where NaOH work as an activator. To the best of authors' knowledge, a full replacement of cement along with coconut fiber reinforcement is not yet investigated. Therefore, the objective of this study is to investigate different properties of a chemically activated no-cement binder containing slag, FA, RHA with coconut fibers.

2 MATERIALS AND METHODOLOGY

2.1 Materials

Ground granulated blast-furnace slag (GGBFS) is considered as slag which is basically steel industry generated waste (by-product). Annual worldwide produc-

tion of slag is about 100 million tons and from this total only 35 % (approximately) is recycled [6]. For this current research GGBFS was collected from a local company named Seven Circle (Bangladesh) Ltd. Slag was grinded using Los Angles abrasion machine before use.

Fly ash (FA) is also a by-product of the coal based power generation companies. Recent reports show that the worldwide generation of fly ash is approximately 750 million tons and Bangladesh is responsible for Bangladesh the production of 52000 metric tons. For this current research FA was collected from the same company from where the slag was collected.

Rice husk ash (RHA) is an agricultural offshoot. RHA was collected from one local rice produce mill and grinded using Los Angeles abrasion machine.

Coconut husks were first collected from local shop, then these were soaked in water for a month and further placed in 10% NaOH solution for seven days to dissolve the Lignin and Hemicelluloses to facilitate extraction of fibers. The shells were then washed properly and air dried for five days. Fibers were oven dried at 80^{o}C temperature for 5 hours and then cooled.

To activate the materials (slag, FA and RHA) and achieve the binding property of theno-cement binder (NCB) sodium hydroxide (NaOH) was used as chemical activator.

Local river sand (fine grain sand) and Sylhet sand (coarse grain sand) which passed through 4.75 mm sieve were used as fine aggregate in mortar preparation.

2.2 Methodology

2.2.1 Tests on materials

Specific gravity of the materials was determined according to BS1377 [13] testing standard. Fineness of materials was determined using the following formula calculate the percentage fineness of Slag, or FA or RHA.

$$Percentage\ of\ fineness = \frac{(W_1 - W_2)}{W_1} \times 100 \qquad (1)$$

Here, W_1 = Total weight of Slag/ FA/RHA, W_2 = Weight of residue on #200 sieve. Unit weight of the NCB composite mortar was determined according to BS EN 1015-10 [14]. Flexural and compressive strength test was performed according to BS EN 196-1 [15] testing standard.

2.2.2 Specimens Preparation

In this present research, six different mix proportions (by weight) of raw materials (water, sand, slag, FA, RHA, Coconut fiber, NaOH) were selected. The mix proportion data are summarized in Table 1.

Table 1: Mix proportion of raw materials (by weight)

Mix No.	Water / Binder	Sand / Binder	Slag (%)	FA (%)	RHA (%)	Coconut fiber (%)	Concentration of NaOH (%)
Mix 1(a)	0.50	3.0	50	35	15.0	0.0	5
Mix 1(b)	0.50	3.0	50	35	15.0	0.0	10
Mix 1(c)	0.50	3.0	50	35	15.0	0.0	15
Mix 2	0.50	3.0	50	35	14.0	1.0	10
Mix 3	0.50	3.0	50	35	13.5	1.5	10
Mix 4	0.50	3.0	50	35	13.0	2.0	10

Mortar prisms of 40 mm × 40 mm × 160 mm in size were prepared to determine the compressive strength, flexural strength, water absorption, and porosity according to corresponding testing requirements. Briquettes were prepared to determine the tensile strength of mortar. Molds of the NCB-mortars were removed after two or three days and the specimens were immersed in a clean water bath at room temperature of 25 ± 2°C for desired testing at ages of 14, 28 and 90 days. After full period of curing specimens were taken out from curing bath for the relevant testing.

3 RESULTS AND DISCUSSIONS

3.1 Physical properties

Physical properties of the materials used are summarized in Table 2. Specific gravity results show that, specific gravity of considered materials (Slag = 2.75, FA = 2.58, RHA = 1.98 and Coconut fibers = 1.18) varies in between 18 to 2.75 while specific gravity of OPC is retorted as 3.14.Thereforeobserved materials are lighter than the OPC. Fineness of considered materials are nearly same to OPC and fineness modulus of fine aggregate (sand) is 2.12.

Table 2: Physical properties of the materials

NCB Mix	Specific gravity	Fineness (% passing #200 sieve)
Ground Slag	2.75	100
FA	2.38	99.9
Ground RHA	1.98	100
OPC	3.15	100
Coconut fiber	1.18	---

3.2 Hardened properties of mortar

3.2.1 Unit weight of mortar

Unit weights and specific gravity of mortar specimens for different mix are shown in Table 2. Unit weight of mortar was calculated as the average value of the six specimens that are presented in Table 3. Highest unit weight for NCB

with coconut composite mortars is 1785 kg/m^{3}which is obtained for mix – 3 and on the other side NCB mortar without coconut fiber shows highest unit weight of 1841 kg/m^3 at 5% NaOH concentration. Besides reported value of OPC mortars is 2200 kg/m^{3}for water - binder ratio 0.5 and sand – binder ratio 3.0 [6]. Reported results show that the NCB composite with coconut fiber is the lightest among all. Thus the use of coconut fiber has great potential in the production of lightweight mortar/concrete.

Table 3: Unit weight of mortar specimens

Mix	Unit weight of mortar (kg/m3)
Mix-1(a)	1841
Mix-1(b)	1860
Mix-1(c)	1808
Mix-2	1785
Mix-3	1780
Mix-4	1775
OPC Mortar	2200

3.2.2 Compressive strength of mortar

Results of compressive strength of NCB mortar specimens with or without coconut fiber composite are presented in Fig. 1. In this present research higher compressive strength of NCB mortar was obtained 8.6 MPa for 10% of NaOH. In a previous study Karim et al. [6] reported better compressive strength for NCB mortar with 5 % NaOH. Improper grinding of the raw materials can be considered as reason for the requirement of higher amount of activator.

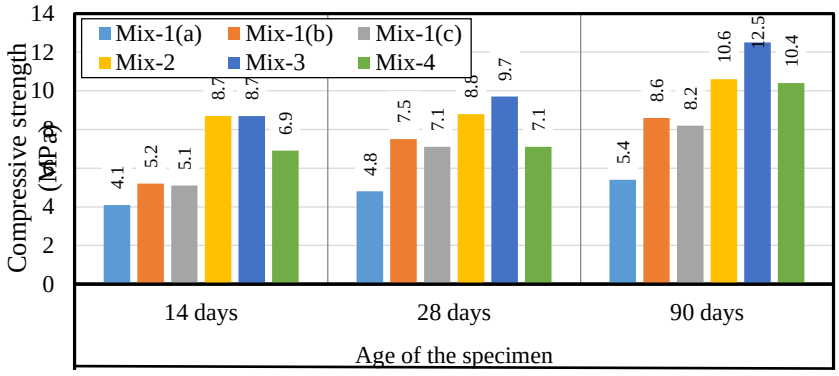

Figure 1: Compressive strength of NCB mortars specimens at different ages.

Test results show that, due to the addition of 1.5% coconut fibers with NCB, compressive strength improved by 44.7%. It is presumed that the compressive strength of NCB mortar with coconut fiber composite increases with the increase

of fiber content amount and after certain limit it starts to decrease [Fig. 2]. Optimum coconut content for NCB with coconut composite to achieve height compressive strength is 1.5 % (approximate).

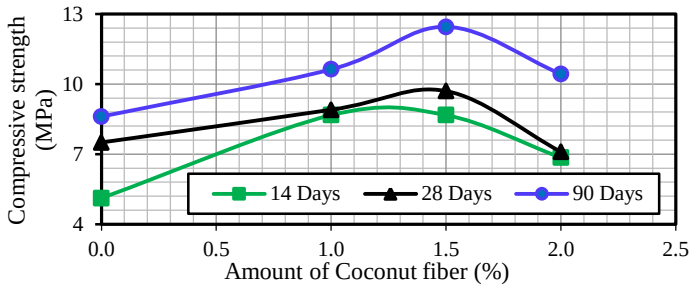

Figure 2: Compressive strength of mortar as influenced by amount of coconut fiber

3.2.3 Tensile and Flexural Strength

The overall tensile strength test results of the NCB coconut fiber composite are presented also in Fig.3. It is observed that the tensile strength of NCB mortar decreases with an increase in the fiber content on the NCB mix. Test results also point that for 1.0% and 1.5% fiber content, tensile strength of NCB composites are improved by 22.41% in comparison with NCB composite without coconut fiber. This may be due to addition of coconut fiber that acts as a reinforcing media in the mortar.

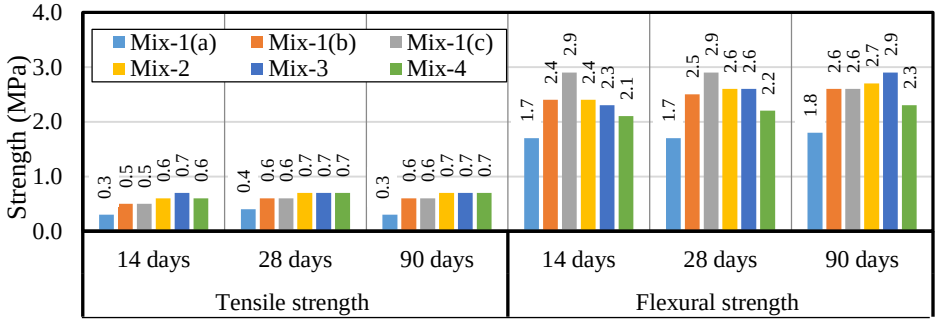

Figure 3: Tensile strength and flexural strength of mortar.

Flexural strength of NCBs increases with an increase in the fiber content up to 1.5% and after that it starts to decrease. Flexural-to-compressive strength ratio of 23.8% (maximum) is obtained for Mix-3 for this present case.

4 CONCLUSIONS

Depending on experimental results, the following conclusions can be drawn from the present study:

- Specific gravity of no-cement binder (NCB) with coconut fiber composite mortars (Slag, FA, RHA and Coconut fibers) is lower than conventional OPC mortar. Also, unit weight of NCB mortar is near about 1800 kg/m^3 and for OPC mortar this value is 2200 kg/m^3. Therefore, it can be concluded that the use of coconut fiber with NCB has great potential in the production of light-weight mortar/concrete.
- Comparing with the study of Karim et al. [6], it can be said that materials for NCB with coconut fiber composite should be processed properly maintaining high fineness. Otherwise more chemical activator (minimum 10% activator by weight of binder) must be required.
- Addition of 1.5% coconut fiber with NCB achieved best compressive and flexural strength of 12.5MPa and 2.9 MPa respectively after 90 days curing period. It shows improvement on compressive and flexural strength about 44.7 % and 11.7% respectively in comparison with NCB without coconut fiber. Therefore, 1.5 % can be declared as optimum coconut fiber content to achieve highest strength. The tensile strength of NCB was found to be 0.8 MPa at 90 days, (improved by 22.41%).

ACKNOWLEDGMENT

The authors acknowledge the financial support and necessary laboratory facilities provided by the Department of Civil Engineering of Dhaka University of Engineering & Technology (DUET), Gazipur.

REFERENCES

[1] E. Gartner, 2012. Are there any practical alternatives to the manufacture of Portland cement clinker? *Chinese Ceramic Society Journal,* **40(1)**, pp. 61 – 68.

[2] M. Schneider, M. Romer, M. Tschudin, H. Bolio, 2011. Sustainable cement production—present and future. *Cement and Concrete Research*. **41(7)**, pp. 642-650.

[3] M. B. Ali, R. Saidur, M. S. Hossain, 2011. A review on emission analysis in cement industries. *Renewable and Sustainable Energy Reviews*. **15(5)**, pp. 2252-2261.

[4] D. N. Huntzinger, T. D.Eatmon, 2009. A life-cycle assessment of Portland cement manufacturing: comparing the traditional process with alternative technologies. *Journal of Cleaner Production*. **17(7)**, pp. 668-675.

[5] S. V. Valerievna, C. A. Vasilievna, P. N. Victorovna, N. V. Viktorovna, 2013. Prospects of application of zero-cement binders of a nonhydration hardening type. *World Applied Sciences*. **25(1)**, pp. 119-123.

[6] M. R. Karim, M. F. M. Zain, M. Jamil, F. C. Lai, 2015. Development of a zero-cement binder using slag, fly ash, and rice husk ash with chemical activator. *Advances in Materials Science and Engineering*. **2015**, 14 pages.

[7] M. R. Karim, M. M. Hossain, M. N. N. Khan, M. F. M. Zain, M. Jamil, F. C. Lai, 2014. On the Utilization of Pozzolanic Wastes as an Alternative Resource of Cement. *Materials*, **7(12),** pp.7809-7827.

[8] P. Chindaprasirt, S. Rukzon, 2008. Strength, porosity and corrosion resistance of ternary blend Portland cement, rice husk ash and fly ash mortar. *Construction and Building Materials*. **22(8)**, pp. 1601-1606.

[9] Zain, M.F.M., Islam M.N., Mahmud F. & Jamil, M. 2011. Production of rice husk ash for use in concrete as a supplementary cementitious material. *Construction and Building Materials*. **25(2)**, pp.798-805.

[10] T. W. Bremner, 2001. Environmental aspects of concrete: problems and solutions. *Invited Paper for the Plenary Session of the 1st All-Russian Conference on Concrete and Reinforced Concrete*, 9-14 September, 15 pages.

[11] A. R. Agrawal, S. S. Dhase, K. S. Agrawal, 2014. Coconut fiber in concrete to enhance its strength and making lightweight concrete. *International Journal of Engineering Research and Development*. **9(8)**, pp. 64-67.

[12] A. Katroliya, A. Tiwari, 2013. The effect of rice husk ash used as supplementary cementing material on strength of mortar. *International Journal of Engineering Research and Application (IJERA)*,**3(3),** pp. 133-136.

[13] BS 1377-2:1990. Methods of test for soils for civil engineering purposes. Classification tests. *British Standards Institution*, London. UK.

[14] BS EN 1015-10:1999. Methods of test for mortar for masonry. Determination of dry bulk density of hardened mortar. *British Standards Institution*, London. UK.

[15] BS EN 196-1:2005. Methods of testing cement. Determination of strength. *British Standards Institution*, London. UK.

CICM 2015
First International Conference on
Advances in Civil Infrastructure and Construction Materials
MIST, Dhaka, Bangladesh, 14–15 December 2015

FLEXURAL RESPONSE OF CONCRETE PREPARED WITH RECYCLED GRANULATED STEEL AS PARTIAL REPLACEMENT OF NATURAL FINE AGGREGATE

Upal M. T. QUADIR[1], Kamrul Islam[2], A. H. M. Muntasir Billah[3] and M. Shahria Alam[4]

[1]Department of Civil Engineering, International University of Business, Agriculture and Technology, Dhaka, Bangladesh.
Email: towfiqz@hotmail.com

[2]Department of Civil Engineering, Military Institute of Science and Technology, Dhaka, Bangladesh.
Email: kamrul1@ualberta.ca

[3]Parsons Corporation, Burnaby, BC, Canada.
E-mail: muntasir.billah@parsons.com

[4]School of Engineering, The University of British Columbia, Canada.
Email: shahria.alam@ubc.ca

Abstract. *Recycled granulated steel (RGS) is a by-product produced in the steel re-rolling mills. Steel re-rolling mills generate significant volume of granulated steel each year. The use of RGS is new in the area of concrete research. This paper describes the influence of RGS on the flexural properties of concrete, and compared those properties with the control concrete specimens containing natural aggregates. RGS was introduced as a replacement to fine aggregates (up to 60% by weight). The tests were conducted as per ASTM standards in flexure under quasi-static loading condition. The results of the flexural properties are presented in terms of flexural stress and fracture toughness. The study shows that the flexural strength and flexural toughness increase up to 30% and 38% respectively with the increase of RGS in the concrete mixtures compared to those of control concrete. These increased flexural properties are observed mainly from 30% RGS replacement and above. Finally, this paper indicates the possible use of RGS in concrete as a replacement of fine aggregate to produce new generation concrete.*

Keywords: Recycled granulated steel, Flexural strength, Flexural toughness.

1 INTRODUCTION

The growing demand for concrete structures to mitigate the inhabitation for worldwide population consumes a higher rate of natural aggregates nowadays. This generating use of good quality natural aggregates has raised a huge concern for catalyzing the jeopardy of aggregates in near future [1]. This reason of accelerating the depletion of natural aggregate has led to a search for the feasible alternatives.

Studies show that a systematic consumption of recycled products can deplete the huge amount of industrial wastes to solve the waste disposal problem [1].The use of recycled fine and coarse aggregate in construction is comparatively a new sector of research. From a review on existing literatures it was revealed that numerous researchers are working on improvising the production of economical and environment friendly concrete using various recycled fine and coarse aggregates such as demolished structural units[1], industrial waste[2], crushedtile[3], ceramic waste[4], FRP scrap[5], grounded glass waste [6] etcMost of the researchers conducted specific experiments to investigate the regular parameters of concrete such as compressive strength, tensile strength, flexural strength, durability, modulus of elasticity, etc. These parameters are correlated with the properties of aggregate used in concrete. As recycled aggregates are obtained from different sources they possess completely different characteristics in comparison to natural aggregates. This includes a difference in gradation, shape and texture of aggregate, difference in specificgravity. Moreover,the containment of impurities due to the variation in sources is another major concern. These properties significantly influence the mechanical and durability characteristics of concrete which could not be predicted before tests [1].

Many renowned researchers are currently doing their research on the partial or full replacement of natural aggregates with the recycled ones. Studies showed that recycled concrete strength properties strongly depends on the level of replacement. Some researchers restricted the level up to 30% replacement for maintenance of standard requirements for 5% absorption capacity of aggregates[7]. It was revealed by Etxeberria et al. [7] that concrete produced with 100% recycled coarse aggregate replacement requires high amount of cement in order to lower the water/cement ratio as well as to improvise compressive strength which may exceed the economic viability of project. Same fact regarding the prohibition on 100% replacement was also supported by . Thomas et al.[8], Topcu and Canbaz [3] and Evangelisa and J. de Brito [9] in their research works.

To investigate the proper utilization of recycled material, durability of concrete is another vital criteria. Topcu and Canbaz showed that the application of crushed tile in concrete not only declined compressive strength but also posed an adverse effect on abrasion and freeze-thaw durability [3]. This issue also arose

with the utilization on the incorporation of coarse recycled concrete and ceramic aggregates which resulted in a higher chloride intrusion than conventional concrete [10]. Similar results were found by Thomas et al.[8]. Again Evangrlisa and Brito observed a linear increase in water absorption with the replacement ratio due to the porosity of fine recycled aggregate [9].

This study investigated the application of granulated steel as an alternative partial replacement of fine aggregatesinconcrete for its flexural behavior.This research work carries uniqueness without having any resemblance to previous works. At first, a pilot study was conducted to investigate the fresh and hardened properties of concrete using recycled granulated steel. The outcome of this study will pave the way for effective utilization of this industrial waste for producing commercially recognized structural concrete.A large number of steel rolling mills are currently running all over the world in order to serve the growing demand of reinforcing steel. Granulated steels are the by product left in the steel rolling mills after the production of reinforcing bars. An effective utilization of this recycled material can be beneficial for resource conservation as well as enhancement of properties of concrete against structural vulnerability.

2 OBJECTIVE OF THE RESEARCH WORK

The main objective of this research work is to investigate the flexural resistivity and behavior of recycled granulated steel replaced concrete**.**

3 MATERIALS AND METHODS

3.1 Material

The following are the details of ingredients used to prepare concrete specimens.

3.1.1 Cement

In this research work Portland Composite Cement (PCC) is used as the binding material. The cement used is fresh and without any lumps. The apparent specific gravity was found to be 3.15.

3.1.2 Natural Fine Aggregate (NFA)

Locally available well graded Sylhet sand passing through 4.75 mm sieve was used. Fineness Modulus was found to be 2.47 and apparent specific gravity was found as 2.64.

3.1.3 Natural Coarse Aggregate (NCA)

Crushed stone chips with a maximum size of19 mm were used. Fineness Modulus was found to be as 7.24 and apparent specific gravity was 2.70.

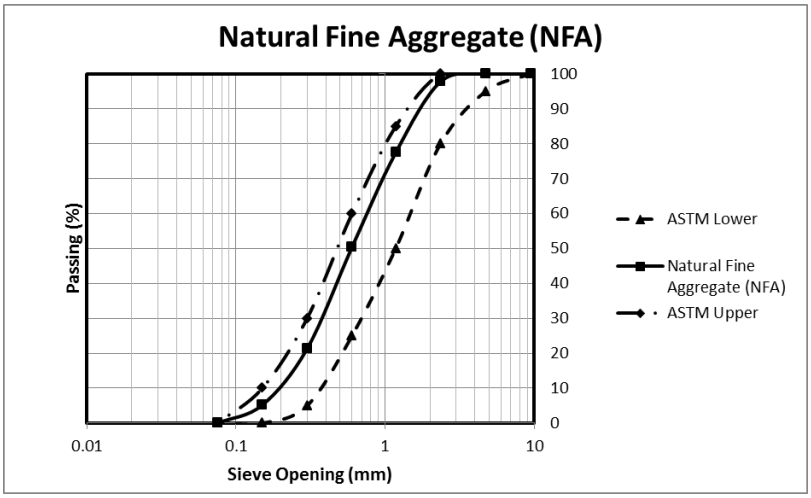

Figure.1.Gradation of natural fine aggregate (NFA)

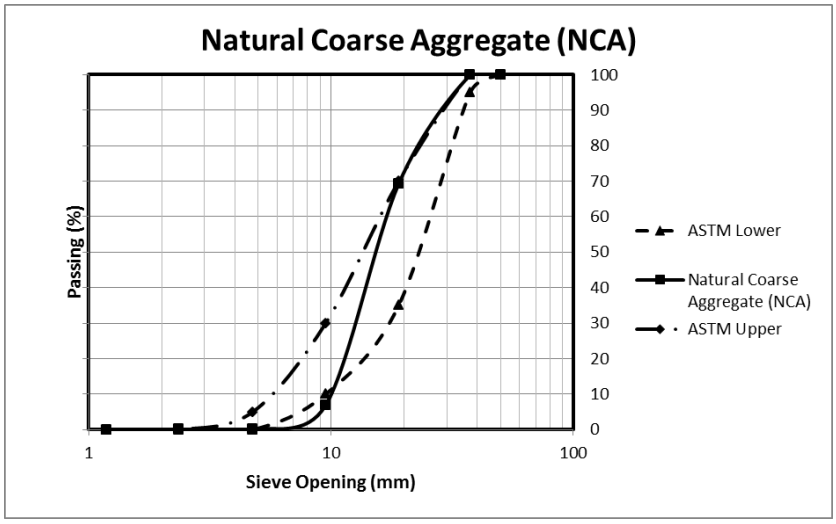

Figure.2. Gradation curve of NCA

3.1.4 Recycled granulated steel (RGS)

Recycled granulated steel is a by-product produced in the steel re-rolling mills.Texture of granulated steel aggregate was rough with more surface area than natural rounded aggregate. RGS was used as partial replacement of fine ag-

gregate on a weight basis of 10 to 60%. Fineness Modulus was determined as 3.22 and apparent specific Gravity was found as 7.90.

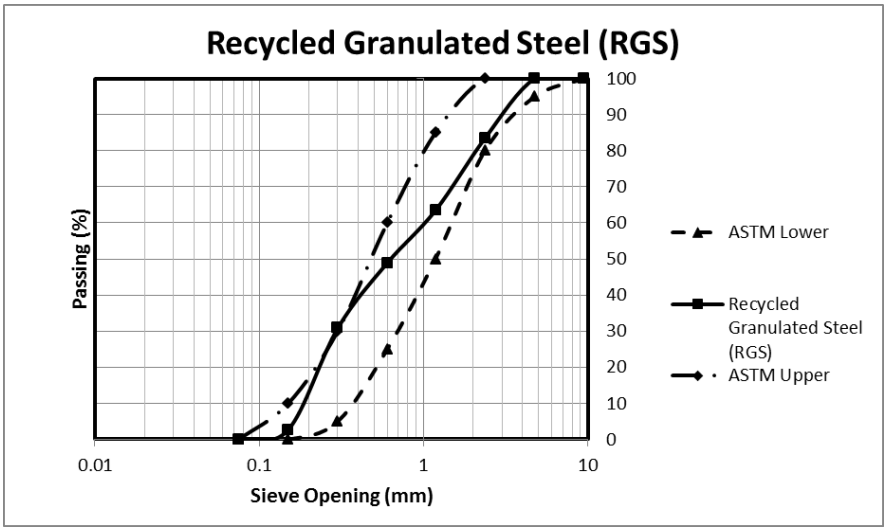

Figure.3. Gradation of recycled granulated steel (RGS)

3.2 Experimental details

3.2.1 Specimen preparing and curing

Seven distinct concrete batches comprised of 42 beams having dimensions of 100mmX100mmX350mm (effective length of 300mm) were prepared for this research work.Based on some previous researches, a weight based mix ratio of 1:2:3 was fixed and an effective water-binder ratio (w/c ratio) of 0.41 was maintained constant for all specimens [4,9]. All the types contained same cement, fine aggregate and coarse aggregate mix ratio where only the amount of granulated steel varied. Among the batches one is the control specimen and the other six batches held their identity as 10, 20, 30, 40, 50 and 60 percent partial replacement of fine NFA with RGS in weight basis.Curing period was 28 days. After this period the specimens were tested for flexural response.

3.2.2 Test setup

Thequasi static flexural test was performed in accordance with ASTM C78 [11] and ASTM C1609 [12].The concrete specimens were tested in third-point bending. A universal testing machine (UTM) with a 1,000 KN capacity was used for this test. Six beam specimens from each mix were tested via third point loading.

Load was applied with a displacement rate of 0.15 mm/min, in accordance with ASTM C78 [11].

Table 1: Quantity of ingredients for producing 1m3 concrete

Batch identity	Cement (kg)	NFA (kg)	NCA (kg)	RGS (kg)
Mix-1 (Control)	3930.82	7861.64	11792.45	N/A
Mix-2 (10% RGS)	3930.82	7075.48	11792.45	786.16
Mix-3 (20% RGS)	3930.82	6289.31	11792.45	1572.328
Mix-4 (30% RGS)	3930.82	5503.15	11792.45	2358.49
Mix-5 (40% RGS)	3930.82	4716.98	11792.45	3144.66
Mix-6 (50% RGS)	3930.82	3930.82	11792.45	3930.82
Mix-7 (60% RGS)	3930.82	3144.66	11792.45	4716.98

4 RESULT AND DISCUSSION

A summary of the quasi-static flexural properties for each batch is presented in Table 2. It is observed that concretes with RGS replacement have higher flexural strength than the control specimen. It is also seen that 30% RGS has the highest value of flexural strength (4.756 MPa). Also, concrete with40% RGS and 50% RGS shows flexural strength which is more than 4MPa. In summary, the flexural strength increased upto 31%, which indicates that RGS improves significantly the flexural property in hardened concrete.

The specimen toughness for each category is found from the respective load versus deflection relationship. According to ASTM 1609 [12], the toughness, T^{D}_{150}, indicates the total area under the load versus deflection curve up to a net deflection of L/150. All the RGS replacement specimens in this study are found to show greater toughness values than does the control specimen. The equivalent flexural strength ratio $R^{D}_{T,150}$ indicates the ratio of toughness to first peak strength of the particular category. It shows higher values for the RGS replacement specimens. This ratio is calculated as per ASTM 1609 [12] as follows:

$$R^{D}_{T,150} = \frac{150.T^{D}_{150}}{f_1.b.d^2}.100\% \qquad (1)$$

Here, $R^{D}_{T,\,150}$ is the equivalent flexural strength ratio, T^{D}_{150} is the toughness (N mm), f_1 is the first peak strength (N/mm^2) calculated from the first peak load of the load deflection curve, b is the effective width of the specimen (mm), and d is the beam depth (mm).

The post-peak energy dissipation is evaluated according to ASTM C78 [11] and JSCE-G552 [13]. The flexural toughness factor (FTF); used to evaluate the post-crack resistance; is calculated as per JSCE-G552 [13] as follows:

$$FTF = \frac{A.L}{\delta_{max} bh^2} \qquad (2)$$

Here, FTF is the flexural toughness factor (N/mm^2), A is the area under the load deflection curve up to a deflection δ_{max}, equal to L/150 (N mm), L is the beam span (mm), δ_{max} is 1 mm, b is the effective width of the specimen (mm), and h is the beam depth (mm).

Moreover, flexural toughness and equivalent flexural strength are found to increase up to 38.4% and 30%, respectively, compared to the control concrete mix.

Figure.4. Flexural strength tested beam specimen

Table 2: Summary of Flexural Response.

Properties	Control	10% RGS	20% RGS	30% RGS	40% RGS	50% RGS	60% RGS
Flexural Strength, f_p (MPa)	3.611	3.744	3.850	4.756	4.202	4.037	3.908
Flexural Toughness Factor (FTF) (KPa) (JSCE G-552)	0.657	0.806	0.839	0.774	0.68	0.809	0.910
Toughness, T^D_{150}	4381.25	5374.23	5590.78	5156.69	4532.9	5395.97	6066.21
Eqv. Flexural Strength Ratio, $R^D_{T,150}$(%)	18	21.5	22	16.5	16	20	23.5

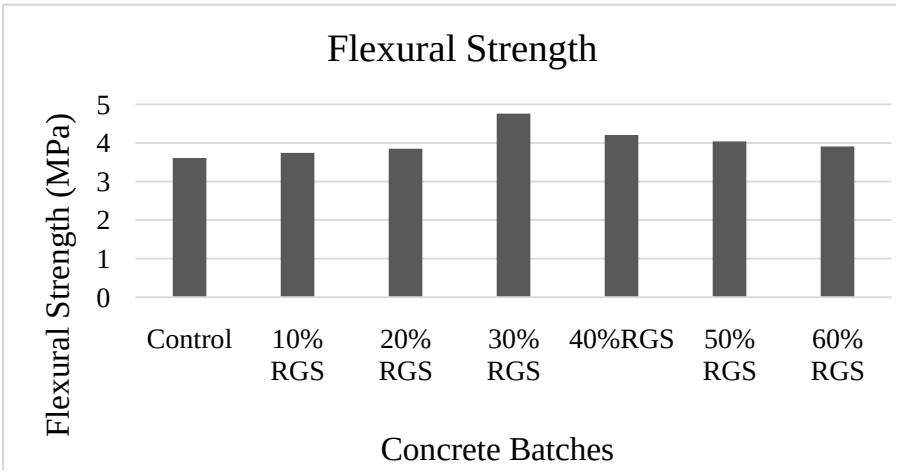

Figure.5. Variation of flexural strength with different percentage of RGS

5 CONCLUSIONS

Following conclusions can be derived from this research paper.

- The use of Recycled Granulated Steel (RGS) as a partial replacement serves an exclusive alternative of naturally available fine aggregate.All the percentages of RGS replaced concrete shows greater value of flexural strength than control concrete.
- The result analysis also shows a higher value of flexural toughness which clearly indicates the suitability of use of RGS concrete where higher flexural resistance is needed.
- The higher flexural properties of RGS concrete are resulted due to the flaky rough texture of RGS which contributes as fiber reinforcement in concrete.

Based on the results achieved in this paper, it can be concluded that tentative application of Recycled Granulated Steel (RGS) as partial replacement of Natural Fine Aggregate in concrete will be able to fulfill the flexural resistivity criteria in long run.

REFERENCES

[1] S. B. Huda and M. S. Alam, 2014, Mechanical behavior of three generations of 100% repeated recycled coarse aggregate concrete, Construction and building materials, 65, 574-582.

[2] M. Nehdi, and J. Sumner, 2003, Recycling waste latex paint in concrete, Cement and concrete research, 33, 857-863.

[3] I. B. Topcu and M.Canbaz, 2007, Utilization of crushed tile as aggregate in concrete, Iranian journal of science & technology, Transaction B, Engineering, 31(B5), 561-565.

[4] R. M. Senthamarai and P. D. Manoharan, 2005, Concrete with ceramic waste aggregate, Cement and concrete composites, 27(9–10), 910–913.

[5] M. S. Alam, E. Slater, and A. H. M. M.Billah, 2013, Green concrete made with RCA and FRP scrap aggregate: fresh and hardened properties, Journal of Materials in Civil Engineering, 25(12).

[6] V. Corinaldesi, G.Gnappi, G.Moriconi and A. Montenero, 2005, Reuse of ground waste glass as aggregate for mortar, Waste management, 25, 197-201.

[7] M. Etxeberria, E.Vázquez, A.Marí, M. Barra, 2007, Influence of amount of recycled coarse aggregates and production process on properties of recycled aggregate concrete, Cement and concrete research, 37, 735-742.

[8] C. Thomas, J. Setien, J. A. Polanco, P. Alaejos and M. S. de Juan, 2013, Durability of recycled aggregate concrete, Construction and building materials, 40, 1054–1065.

[9] L. Evangelista and J. de Brito, 2010, Durability performance of concrete made with fine recycled concrete aggregate, Cement and concrete composites, 32(1), 9–14.

[10] M. Gomes and J. de Brito, 2009, Structural concrete with incorporation of coarse recycled concrete and ceramic aggregates: durability performance, Materials and Structures, 42(5), 663-675.

[11] ASTM C78, 2010, Standard test method for flexural strength of concrete (using simple beam with third-point loading), ASTM International, West Conshohocken, PA.

[12] ASTM C1609, 2013, Standard test method for flexural performance of fiber-reinforced concrete (using beam with third-point loading), ASTM International, West Conshohocken, PA.

[13] JSCE-G 552, 1999, Test Method for Bending Strength and Bending Toughness of Steel Fiber Reinforced Concrete, Standard specification for concrete structures. Test methods and specifications, Japanese Society of Civil Engineers.

CICM 2015
First International Conference on
Advances in Civil Infrastructure and Construction Materials
MIST, Dhaka, Bangladesh, 14–15 December 2015

MECHANICAL BEHAVIOUR OF CONCRETE PREPARED WITH SAW DUST AS PARTIAL REPLACEMENT OF FINE AGGREGATE

Upal M. T. Quadir[1], Irfan Chowdhury[2], Md. M. Islam[3], Kamrul Islam[4] and A. H. M. Muntasir Billah[3]

[1] Department of Civil Engineering, International University of Business, Agriculture and Technology, Dhaka. Email: towfiqz@hotmail.com
[2, 3, 4] Department of Civil Engineering, Military Institute of Science and Technology, Dhaka. Email: [3]kamrul1@ualberta.ca
[5] Parsons Corporation, BC, Canada. E-mail: muntasir.billah@parsons.com

Abstract. *Advent of rapid urban civilization calls for the use of green concrete for sustainable development. Use of waste by product of sawmill i.e. sawdust can pave the way for a greener solution for concrete industry. This study utilizes sawdust waste as partial replacement of fine aggregate and investigates the fresh and hardened properties of sawdust concrete (SDC). 10% to 60% sand replaced SDC specimens were produced for compressive and split tensile test. The 7 and 28 days compressive and split tensile test reveals the strength of the SDC is decreasing with increasing sawdust replacement levels compared to the control specimens. Again, flexural strength measurement was also done by preparing beam specimens of SDC. Four-point bending results of these beam specimens follow a gradual drop in terms of flexural strength. However, controlling the replacement amount of fine aggregate in SDC for both criteria of acceptable compressive and flexural strength limit was achieved successfully. Apart from this, characteristics and properties of sawdust and sand were investigated as well. The FM and moisture content of saw dust differs from the sand with a considerable extent. These variations in characteristics could possibly be the reason for drop in strength of SDC concrete when the sawdust amount gets high. These findings could shed some light in building a sustainable world of concrete in the days to come.*

Keywords: Green Concrete, Mechanical behavior, Recycling, Sawdust, Sustainability.

1 INTRODUCTION

With the increasing demand of concrete structures, the use of natural aggregate is also getting significant. Almost 15 billion tons of concrete are being produced every year throughout the world [1]. To meet this demand, the quality natural aggregates sources are significantly decreasing all along the world and throughout the world 10 to 11 billion tons of aggregates are being used [2]. Specifically, in European countries, concrete of almost 2 billion tons are being used every year [3]. In a word, concrete can be considered as the second most used material after water in the world [4].

The researchers and engineers are becoming more concerned and trying to find new source of materials as replacement because of the deterioration in the global environment. So, they are going for waste materials and by products. These products also can be used in the lightweight concrete production [5]. The most used fine aggregate is natural sand for making concrete. And the non-scientific collection of this sand has become the threat to the environment and also making the scarcity of the aggregates [6]. Many developing countries are facing problems in meeting the huge demand of the concrete [7]. As there is chronic lacking in the building materials in the last decade, civil engineers are trying to replace the aggregates with the industrial wastes [8].

Improper management of sawdust can be a nuisance both for health and environment [9]. The preservatives for wood include pentachlorophenol, aromatic hydrocarbons, compounds of chrome, arsenic, copper etc. [11]. And it is a threat to the existence of a variety of the microorganisms. Moreover, sawdust accumulations and airborne sawdust present safety and health hazards [12]. So, effects can be controlled if sawdust is being utilized in making concrete. As a result, the researchers are researching on the sawdust [13].

Sawdust ash (SDA) can be suitable alternative in concrete making. With the increase of saw dust ash, the required water content also increases. For 10% sawdust ash, the bulk density, uncompact bulk density, moisture content, specific gravity and fineness modulus were found to be1436kg/cubic meter, 1435 kg/cubic meter, 3.7%, 2.67 and 2.2 respectively. The compressive tests for cylinders and cubes were done and it was found that with strength increases with increasing curing days and decreases with increasing SDA percentage. The tensile strength and flexural strength also have same conditions in case of strength. There is much availability of SDA, so it can be easily utilized. The satisfactory replaceable percentage of SDA is found to be 10% [14].

There were other numerous researches on the partial replacement of cement with sawdust and sawdust ashes in concrete. But as our main criteria were replacement of fine aggregate we didn’t bring those in our matter of concern.

2 EXPERIMENTAL INVESTIGATION

2.1 Materials

General Portland composite cement (Holcim) of a density 1441 kg/m^3 was used for the mixing. Cement component proportions are given in Table 1. In addition, Fine aggregate (Local sand) of density 1920 kg/m^3 was used. Potable water was used for the mixing purposes. Coarse aggregate with size of 19 mm was used for the test. Sand with size of 4.75mm was used. And saw dust with size of 4.75mm same as sand was used for the tests.

Table 1. Portland Composite Cement (PCC)

Ingredients used in PCC	Ratio
Clinker	65-80%
Fly Ash	21-35%
Gypsum	0-5%

2.2 Gradation

According to ASTM C136 [15], No. 100, 50, 30, 16, 8, 4, and 3/8 inch, 1.5 inch are used as the standard sieves. Gradation of an aggregate affects the properties of the hardened and fresh concrete both. And poor gradation reduces the workability or slump, can affect air content, and also can make voids in the product.

Fig 1. shows the gradation curve of fine aggregate (sand) and saw dust. We can see that there is difference in the FM values of sand and saw dust. So, this can affect the strength between controls and saw dust concrete.

2.3 Mixture proportions

The mixture proportions were followed as per the mix design of 1:2:3. The effective water-cement ratio followed was constant and the value is .45. Thus, the only variation in the batch was the amount and type of fine aggregate. The saw dust replacement was done on the basis of weight by replacing the same weight of natural fine aggregate with saw dust.

The mixture proportions have been given in the table 2. The table shows the variation in the amount of fine aggregates. Saw dust is much lighter than natural fine aggregate that’s why it will not give relevant result if replacement was done on the basis of volume.

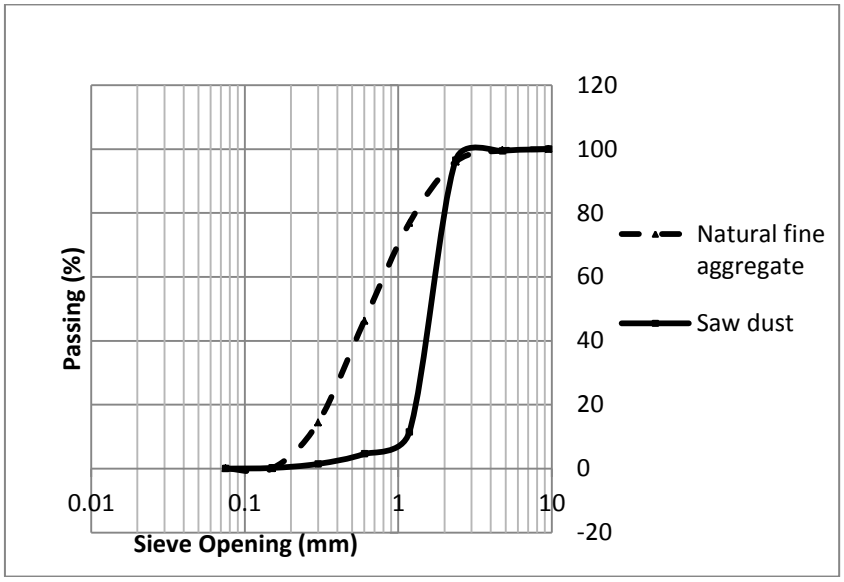

Figure 1: Gradation curve of Natural fine aggregate and Saw dust

2.4 Specimens

A total of 168 cylinders were casted, 24 for each batch that allowed the compressive and splitting tensile tests. The strength for 7 and 28 days has been done for the better accuracy. The mold size of the cylinders was 100mm diameter × 200mm height. Again, a total of 42 beams have been casted, 6 for each batch that allowed the four-point bending tests. The strength test for 28 days has been done. The mold size of the beams was 100mm×100mm×350mm.

Table 2: Proportion of Concrete Mix

Mixture	Cement (kg)	Sand (kg)	Saw Dust (kg)	Coarse Aggregate
Control	0.66	1.32	-	1.98
10% SDC	0.66	1.188	.132	1.98
20% SDC	0.66	1.056	.264	1.98
30% SDC	0.66	.924	.396	1.98
40% SDC	0.66	.792	.528	1.98
50% SDC	0.66	.66	.66	1.98
60% SDC	0.66	.528	.792	1.98

Note: SDC (Saw Dust Concrete)

2.5 Testing procedures

The cylindrical concrete specimens were used in the tests for compressive strength according to ASTM C39 [16]. Test apparatus was calibrated to execute the compressive strength test on each specimen. The load rate was 2.2-2.4kN/s.

The specified beam specimens were used in the tests for flexure according to ASTM C78 [17]. A third-point loading machine (UTM-Universal Testing Machine) was used in the flexural strength test. The load rate was .10-.15kN/s.

According to ASTM C496 [18], the splitting tensile tests were done. The load rate was $0.36 - 0.73$kN/s.

3 EXPERIMENTAL RESULTS AND DISCUSSIONS

Estimation for The mix design was done by using a mix ratio of 1:2:3 and the effective water cement ratio of 0.45%. Moreover, the saw dust used into concrete varied from 0% to 60% (at 10% increase) as a fraction (replacement) of sand weight.

3.1 Compressive Strength Response

The results from the concrete compressive strength test are shown in fig 2. It demonstrates that the 28-day compressive strength for the control concrete reached around 3909 psi (26.9 MPa). It is clear by the comparison of the strengths that; strength is reducing with the increase of the SDC percentage. At 28 days, the 10% SDC had 16% lower strength than control concrete. In case of 20% SDC the compressive strength reduces to be nearly 34.5% lesser than the control one at 28. A drastic reduction in compressive strength is observed in concrete made with 30% sawdust in replace of sand. At 28 days, it gives almost 75.8% lesser value than control mixture chalking it out to be used as load bearing component. 40%-60% SDC behaves similarly as that of 30% SDC while considering the strength gain pattern. Again, these batches show contrasting strength gain pattern with control concrete. These batches also have very low compressive strength compared to control one.

Furthermore, from the fig. 2 it is also clear that with increasing amount of sawdust in concrete there is a gradual drop in compressive strength compared to the control concrete. Several possible reasons can be attributed for lower compressive strength in SDC, which are given as follows.

The lower compressive strength of SDC concrete can be attributed to the lower Fineness Modulus (FM) of sawdust compared to that of sand. Sand's FM value is found to be 2.65 while FM of sawdust was 1.81. The higher the amount of sawdust in concrete the lower the combined FM gets, resulting in gradual increase in voids in SDC. This corresponds to the gradual drop of strength in SDC.

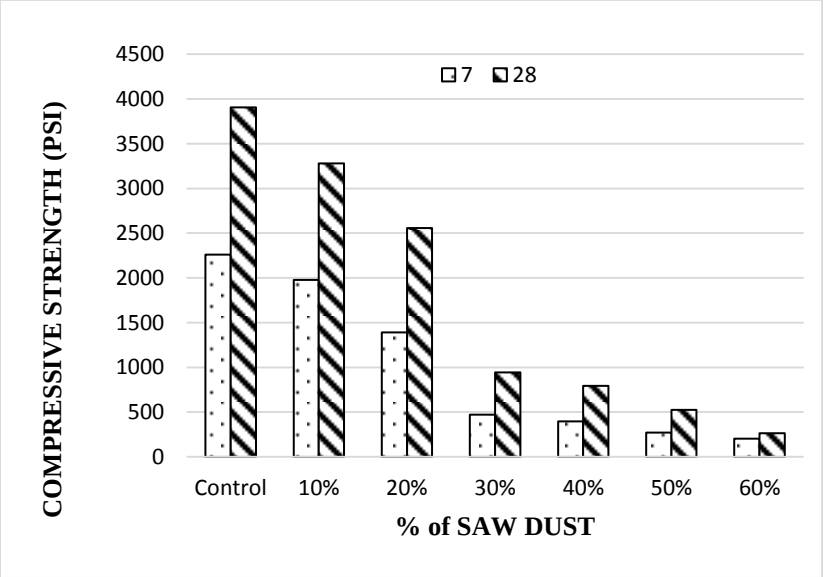

Figure 2: Variation of 7 and 28-day compressive strength of various concrete batches.

Laboratory test showed sawdust to possess very high level of absorption capacity compared to natural sand. This higher absorption of sawdust may have led to the declination of compressive strength. Due to the higher absorption even after measures being taken to use SSD condition, it was difficult to maintain such exact condition at all times in SDC. Amount of higher extent of water increases the water cement ratio and ultimately decreases strength.

Difference in chemical composition of sawdust and sand may introduce weaker bond between the mortar and aggregates. This may relate to the lesser compressive strength.

For each mix proportion, a total of 168 specimens were tested under compression, using 42 for each 7 and 28 day tests. Statistical analyses were done to determine the variation of the compressive strengths of different concrete batches. Table 3 shows such statistical parameters obtained from the hardened concrete properties based on compressive strength test data.

3.2 Tensile Response

The splitting tensile strength results for different batches are showed in fig 3. It shows that split tensile value of control cylinder reached about 363.4 Psi (2.5 MPa) at 28 days. It is also observed from the fig 3 that the behavior of SDC to

lower its strength with the increase of sawdust is maintained in case of splitting tensile strength as well.

Splitting tensile strength of 10% SDC reduced to be 2.1% less than that of control specimen at 28 days. It is evident that this reduction is quite lesser compared to flexural and compressive strength reduction. This can be attributed to the fact that when used in small amounts some fibers of sawdust may provide some tensile capacity to the concrete but in large amount this behavior is offset by the lesser FM and higher absorption capacity of FM.

Table 3: Summary of quasi-static response (Compression, Tension, Flexure)

Properties	Days	Batches	Control	10% SDC	20% SDC	30% SDC	40% SDC	50% SDC	60% SDC
Compressive Strength (psi)	7	SD	109.61	45.952	21.579	21.016	12.58	21.688	5.94
		Mean	2261	1978.8	1391.5	472.5	396.75	271.63	203
		COV	0.0485	0.0232	0.0155	0.0445	0.0317	0.0798	0.029
	28	SD	102.95	272.56	119.48	91.65	19.302	42.145	34.7
		Mean	3909	3282.1	2558.7	946.2	795.82	527.2	264.7
		COV	0.0263	0.083	0.0467	0.0969	0.0243	0.0799	0.1312
Splitting Tensile Strength (psi)	7	SD	4.4	7.8	3.78	3.7	3.5	6.17	2.9
		Mean	294.8	239.7	188.6	104.3	77.1	57.9	45.5
		COV	0.02	0.03	.02	0.04	.05	.1	.06
	28	SD	27.2	3.78	10.5	10.4	6.4	9.1	2.2
		Mean	363.4	355.7	241.4	112.3	79.7	67.9	49.4
		COV	0.08	0.02	.04	0.09	.08	.13	.05
Flexural Strength (psi)	28	SD	45.9	47.5	8.2	33.2	12.6	8.3	7.7
		Mean	755.4	547	471.9	279	243.5	176.9	123

COV	0.08	0.08	0.01	0.1	0.05	0.04	0.06

Note: SD (Standard deviation), COV (Co-efficient of variation)

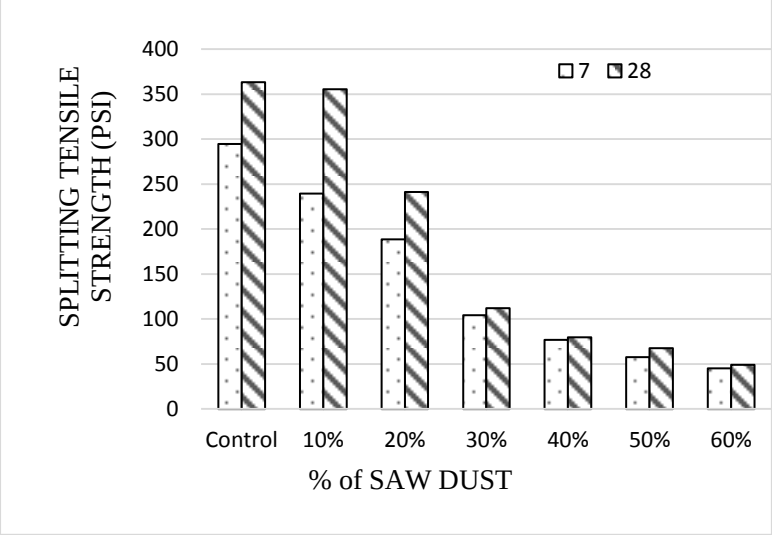

Figure 3: Variation of splitting tensile strength of control and sawdust concrete

In case of 20% SDC the value of split tensile reduces to a significant amount, this batch gives nearly 33.57% lesser value than control cylinder at 28 days. 30% SDC and onwards show declined values of split tensile. The value of split tensile strength of 30% to 60% SDC happened to be approximately 69%, 78%, 81.32% and 86.4% lesser respectively compared to the control one at 28 days' test.

Statistical parameters were determined for different batches with respect to split tensile strength and are shown in Table 3.

3.3 Flexural Response

The flexural strength test results of different concrete mixes are presented in Fig. 4 considering mean values. It shows that with the increasing amount of sawdust, the flexural strength of SDC decreased in a gradual manner. Control concrete beam reached a maximum value of 5.63MPa at 28-day. 10% SDC beam yielded a maximum flexural strength which is 26% lesser than that of control beam at the age of 28. At 28 days, mean values of 20% and 30% SDC showed 37.5% and 63% lesser flexural stress than the control beam.

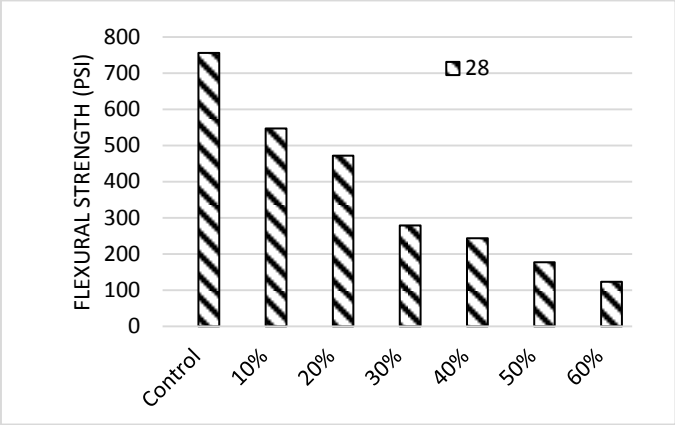

Figure 4. Variation of flexural strength of control and SDC as a function of age

Further, the reduction in flexural strength became 68% less for 40% SDC at the age of 28 days. Upon comparison of 50% and 60% SDC beam to the control one the reduction in flexural strength found at the age of 28 days were around 77% and 84% less respectively.

The failure pattern of the beams has been showed on the fig 5. All the beams were failed along the center or beside the mid axis. The fig shows also how the tests have been carried out with the UTM (Universal testing machine). The texture is getting changed with the increase of the saw dust percentage.

Figure 5: Flexural tests for different batches

Statistical parameters were found for different batches with respect to their flexural strengths. Table 3 shows the mean, SD, and co-efficient of variation (COV) obtained from different concrete batches during flexural test.

4 CONCLUSION

This study represents the fresh and hardened mechanical properties of partial fine aggregate replaced concrete made from the combination of saw dust, local sand and coarse aggregate. Throughout this project, the replaced specimens were

compared to the control specimen. All batching, testing, and mixing procedures followed ASTM standards.

The strength we are getting in compression test for 10% replacement specimen is less than the control specimen. And for 20% replacement specimen, the strength is getting less gradually. But in case of tensile test we are getting result slightly lower than the control specimen. The weight is almost 10% less for the 10% replacement specimen. The strength of the concrete reduces as the replaced saw dust increases. So, up to 10% replacement, it is feasible to use the saw dust.

Probable reasons behind the strength issues may be FM decrease in saw dust and high moisture content. We can resolve the issues, if we can get the similar FM and moisture content of sand in saw dust.

The study reveals the implementation of saw dust concrete in place of natural fine aggregate. It will thus can useful in utilizing the wastes. The study is just the initiating steps in this sector, further experiment may get much good results. A future study considering different mix ratio, water-cement ratio, use of plasticizer for better workability, other admixtures etc. can be done for better results.

5 ACKNOWLEDGMENT:

The financial contributions of Civil engineering dept. of Military Institute of Science and Technology (MIST), have been gratefully acknowledged.

6 REFERENCES:

[1] L. Barcelo, 2013, A path towards more sustainable cement. In: ACI fall convention, Phoenix, USA, 20–24 October.

[2] J. T. Simth, 2009, Recycled concrete aggregate – a viable aggregate source for concrete pavements, PhD Dissertation, Department of civil engineering, University of Waterloo, Ontario, Canada.

[3] S. W. Tabsh, A. S. Abdelfatah, 2009, Influence of recycled concrete aggregates on strength properties of concrete. Constr Build Mater ; 23(2):Page 1163–7.

[4] M. Low, 2005, Material flow analysis of concrete in the United States" Low, Manshi, Publisher; Massachusetts Institute of Technology.

[5] A. P. Adewuyi and T. Adegoke,2008, Exploratory Study of Periwinkle Shells as Coarse Aggregates in Concrete Works, Journal of Applied Sciences Research, 4 (12), Page 1678 – 1681.

[6] M. Mageswari and B. Vidivelli, 2010, The Use of Sawdust Ash as Fine Aggregate Replacement in Concrete, Journal of Environment Research and Development,3 (3),Page 720 – 726.

[7] Y. Divatar, S. Manjunath, M. U. Aswath, 2012, Experimental Investigation on Behaviour of Concrete with the Use of Granite Fines, International Journal of Advance Engineering Research, 1(4).

[8] P. Turgut, 2007, Cement Composite with Limestone Dust and Different Grades of WoodSawdust". Building and the Environment, 42, page 3801 – 3807.

[9] A. U. Elinwa and S. Abdulkadir, 2011, Characterizing Saw Dust Ash for Use as an Inhibitor for Reinforcement Corrosion, New Clues in Sciences, 1, 1 -10.

[10] V. Savie, 2010, Small-Scale Sausage Production: Sausage Casings, Food and Agriculture Organization of the United Nations, Rome.

[11] Environmental, Health, and Safety Guidelines: Sawmilling and Manufactured Wood Products, by IFC and World bank group.

[12] "Wood Dust Exposure" State Compensation Insurance Fund.

[13] wikipedia.org/wiki/Sawdust

[14] M. Mageswari and B. Vidivelli, 2009,The use of saw dust ash as fine aggregate replacement in concrete, Journal of Environmental Research and Development Vol. 3 No. 3.

[15] ASTM C136, 2014, Standard Test Method for Sieve Analysis of Fine and Coarse aggregates, ASTM International, West Conshohocken, PA.

[16] ASTM C39, 2015, Standard Test Method for Compressive Strength of Cylindrical Concrete Specimens, ASTM International, West Conshohocken, PA.

[17] ASTM C78, 2010, Standard test method for flexural strength of concrete (using simple beam with third point bending loading0, ASTM International, West Conshohocken, PA.

[18] ASTM C496, 2004, Standard Test Method for Splitting Tensile Strength of Cylindrical Concrete Specimens, ASTM International, West Conshohocken, PA.

CICM 2015
First International Conference on
Advances in Civil Infrastructure and Construction Materials
MIST, Dhaka, Bangladesh, 14–15 December 2015

DURABILITY OF CONCRETE CONTAINING RECYCLED GRANULATED STEEL AS PARTIAL REPLACEMENT OF NATURAL FINE AGGREGATE

Upal M. T. QUADIR[1], Atanu Pramanik[2], Kamrul Islam[3], M. Shahria Alam[4] and Shah M. Muniruzzaman[5]

[1] Department of Civil Engineering, International University of Business, Agriculture and Technology, Dhaka, Bangladesh.
Email: towfiqz@hotmail.com

[2, 3, 5] Department of Civil Engineering, Military Institute of Science and Technology, Dhaka, Bangladesh.
Email: 3kamrul1@ualberta.ca and [5]head@ce.mist.ac.bd

[4] School of Engineering, The University of British Columbia, Canada.
Email: shahria.alam@ubc.ca

Abstract. *This paper describes the vulnerability issue caused by sulphate exposure associated with concrete structure manufactured by Recycled Granulated Steel (RGS) derived as a waste from steel rerolling industries as a partial replacement of Natural Fine Aggregate (NFA) within the range of 0~60% in weight basis. Since durability of concrete is the critical parameter regarding sustainability, RGS needs to testify the eligibility for further utilization and so therefore, the sulphate resistance experiments were adopted for this investigation. As there are no specific ASTM codes for sulphate test of concrete, some of the guidelines were taken from ASTM C1012 and ASTM C452 which are appropriate for sulphate test of cement mortar. Basically this program emphasizes the effect of sulphate exposure on mechanical strength and physical impact of concrete specimens. This investigation reveals the fact that as being denser configuration than conventional concrete, 40% and 60% replacement of RGS specimens experienced significant amount of volume change after sulphate exposure. Notably, change in height of specimens gradually declines from the peak for 30% to 60% RGS replacement. On the contrary, the slight drop in mechanical strength of 30% to 50% RGS replacement due to sulphate exposure leads to a final remark that it is not significant amount lower to fail the ASTM guideline criteria where other percentages held a negotiable range.*

Keywords: Recycled granulated steel (RGS), Sulphate exposure, Physical degradation, Chemical attack, Compressive Strength.

1 INTRODUCTION

Concrete structures exposed to aggressive environment are prone to degradation due to capillary rise and evaporation of groundwater containing sulphate salts in the superstructure. This is due to the process of salt crystallization from a super-saturated solution in its pores. When the pores associated with concrete are disrupted by chemical hydration process, it experiences a stress generation due to expansion of volume resulting in the disturbance of bulk integrity of whole material property. The effects of physical sulphate attack leads to scaling and surface degradation where chemical exposure responses to the expansion and cracking. This expansion in concrete may occur because of ettringite formation or gypsum formation.Generation of ettringite ($C_6AS_3H_{32}$) is completed during the early stage of cement hydration process under the presence of sufficient amount of gypsum. Later this product transforms into monosulphate which results in the formation of ettrigite after some chemical reactions. Thus this continuous process leads to a devastating effect on concrete causing the intrusion of deleterious materials through the cracks. Another expansive product leading distress to concrete under sulphate attack is gypsum ($CaSO_4.2H_2O$) which requires the presence of Mg^+cation with a high pH level. Thus these two products mainly play the subversive role regarding the deterioration of concrete in harsh environment [1, 2, 3].

The study on the utilization of recycled material in concrete has acquired a high level of significance now-a-days as reported by numerous researchers. Following several earlier researches on improvising the production of economical and environment friendly concrete structure using various recycled aggregates such as demolished structural units, industrial waste, crushed scallop shells, ceramic waste, FRP scrap, grounded glass waste etc [4,5,6,7,8,9,10]**,** recycled granulated steel (RGS) in concrete was introduced by authors of current research work. Conducting some essential experiments, it was evident that utilization of recycled granulated steel (RGS) as a partial replacement of fine aggregate serves an excellent profit to refute the current demand of good quality natural fine aggregate. But as the properties of RGS are completely different from natural aggregate, it needs to fulfill the sustainability criteria of concrete for its approval on further commercial use. This current research paper will address the concern of sulphate resistance of concrete made with partial replacement of fine aggregate with RGS. Experiments were carried out to investigate the physical sulphate attack by highlighting the change in mechanical strength as well as in dimensions.

2 OBJECTIVE OF THE RESEARCH WORK

The main objective of this research work is to investigate the compatibility of recycled granulated steel as a partial replacement of fine aggregate in concrete against the aggressive environment due to sulphate exposure**.**

3 MATERIALS AND METHODS

3.1 Material

The following are the details of ingredients used to prepare concrete specimens.

3.1.1 Cement

In this research work Portland Composite Cement (PCC) was used as the binding material. The cement used was fresh and without any lumps. The specific gravity was found to be 3.15. Other properties are described in Table-1.

Table1: Properties of Cement

S.I. No.	Particulars	Experimental result	Standard Value
1.	Normal consistency	29%	25~30%
2.	Setting Time (Minutes)		
	Initial	128	Not less than 45
	Final	215	Not more than 300

3.1.2 Fine aggregate

Locally available well graded Sylhet sand passing through 4.75 mm sieve was used. Fineness Modulus was found to be 2.47 and specific gravity was found as 2.64.

3.1.3 Coarse aggregate

Crushed stone chips with a maximum size of19 mm were used. Fineness Modulus was found to be as 7.24 and Specific gravity was 2.70.

3.1.4 Recycled granulated steel (RGS)

Recycled granulated steel is a by-product produced in the steel re-rolling mills.Texture of granulated steel aggregate was rough with more surface area than natural rounded aggregate. RGS was used as partial replacement of fine aggregate on a weight basis of 10 to 60%. Fineness Modulus was determined as 3.22 and Specific Gravity was found as 7.90.

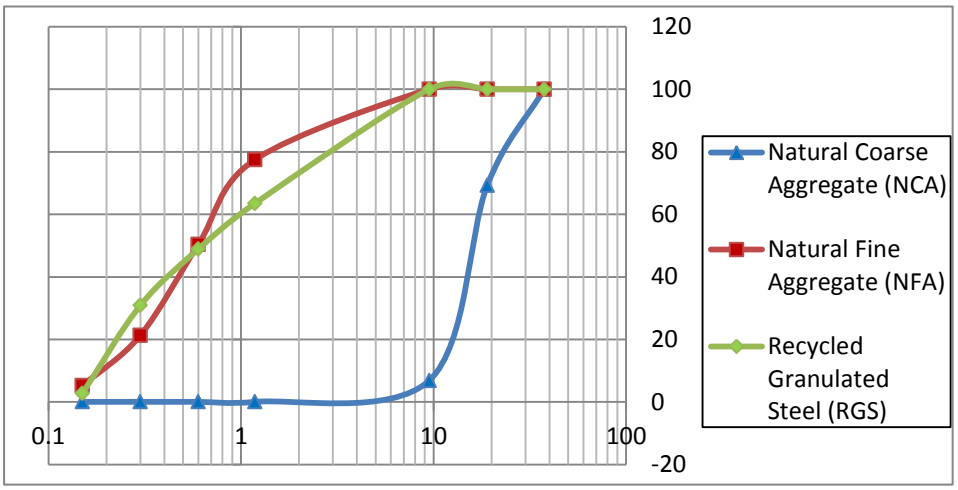

Fig 1: Gradation curves of aggregate

3.2 Experimental details

3.2.1 Mix proportion and curing

Seven distinct concrete batches comprised of 42 cylinders having dimensions of 4inch diameter and 8inch height were prepared for this research work.Based on previous studies on concrete with recycled aggregate and from practical casting work of concrete structure, the mix ratio of current program was fixed as 1:2:3 in regular weight basis of each ingredient and an effective water-binder ratio (w/c ratio) of 0.41 was maintained constant for all specimens [7,10]. All types contained same cement, fine aggregate and coarse aggregate mix ratio where only the amount of granulated steel varied. Among the batches one was the control specimen and the other six batches held their identity as 10, 20, 30, 40, 50 and 60 percent partial replacement of fine NFA with RGS in weight basis.After casting they were demolded within 24 hours to maintain a curing period of 28 days. After this period a set of 21 cylinders comprised of three cylinders from each batch were taken out from curing container, wiped with dry towels and then tested under compression according to ASTM C 39 [11].

Table 2: Quantity of ingredients for producing 1m3 concrete

Batch identity	Cement (kg)	NFA (kg)	NCA (kg)	RGS (kg)	Water (kg)
Mix-1 (Control)	3930.82	7861.64	11792.45	N/A	1611.64
Mix-2 (10% RGS)	3930.82	7075.48	11792.45	786.16	1611.64
Mix-3 (20% RGS)	3930.82	6289.31	11792.45	1572.328	1611.64
Mix-4 (30% RGS)	3930.82	5503.15	11792.45	2358.49	1611.64
Mix-5 (40% RGS)	3930.82	4716.98	11792.45	3144.66	1611.64
Mix-6 (50% RGS)	3930.82	3930.82	11792.45	3930.82	1611.64
Mix-7 (60% RGS)	3930.82	3144.66	11792.45	4716.98	1611.64

3.2.2 Preparation for sulphate test

The sulphate test was performed in accordance with ASTM C1012 [12]. But the code cannot fully represent the real behavior, since the guideline is for mortar only. So to increase the surface area and represent the real condition the performance of concrete cylinders were evaluated instead of mortar. A sulphate bath was prepared one day before the use with 5% sodium sulphate and stored at 23 ± 2^0 C. In the storage container the ratio of volume of sulphate solution to the volume of concrete cylinder was 4± 0.5. After this preparation, rest of the specimens were immersed in sulphate solution having an extension period of another 28 days to investigate the impact of sulphate exposure. During this period Sulfuric Acid was added everyday to maintain the pH of sulphate bath around 6.5 to 7. Finally after 28 days of sulphate exposure, rest of the specimens were taken out from sulphate bath to examine compression test and physical degradation.

4 RESULT AND DISCUSSION

This research work focused on the durability concern of concrete using recycled granulated steel (RGS) as a partial replacement of fine aggregate. The sulphate durability test was oriented with the mechanical strength loss as well as the change in external and internal structure of specimens. These results are categorized in the following discussion parts.

4.1 Change In Volume and Height

Dimensions of cylinders were measured before and after the sulphate test to evaluate the change. The following expressions are used for calculation.

$$\textbf{Percentage volume change, } \Delta V\ (\%) = \frac{Vt - Vi}{Vi} \times 100$$

Where Vi= Average initial volume of cylinders (cm^3) and Vt= Average volume of cylinders after a prescribed exposure period (cm^3)

$$\textbf{Percentage height change, } \Delta H\ (\%) = \frac{Ht - Hi}{Hi} \times 100$$

Where Ht= Average initial height of cylinders (cm) and Hi= Average height of cylinders after a prescribed exposure period (cm)
This change of external structure is compiled in Table-3.

Table 3: Change in dimensions of cylindrical specimens due to sulphate exposure

Condition		No. of Mix						
		1 Control)	2 10% RGS	3 20% RGS	4 30% RGS	5 40% RGS	6 50% RGS	7 60% RGS
Before Sulphate Exposure (Mean of 3 cylinders)	vol^m (cm^3)	1542	1558	1605	1514	1503	1608	1565
	height (cm)	19.9	20.1	20.03	19.93	20.06	20.06	20.2
After Sulphate Exposure (Mean of 3 cylinders)	vol^m (cm^3)	1567	1603	1635	1534	1568	1629	1621
	height (cm)	20.32	20.26	20.27	20.33	20.37	20.2	20.23
Change (%)	ΔV*	1.93	2.89	1.83	1.32	4.38	1.35	3.56
	ΔH*	2.13	1.26	1.16	2.0	1.84	0.67	.20

*ΔV indicates change in Volume and ΔH indicates change in Height of specimen

From a quick overview on this comparison table, it disclosesa clearevidence that change in volume and height did not follow any kind of sequential trend.Mix-5 observed the highest percentage of volume change whereas Mix-4 observed the lowest. Volume change is also significant for Mix-7 but other four mixes experienced close results to each other. Another important notification is that Mix-7 experienced the lowest height change but significant volume change bolsters the contention of change in peripheral area. Thus it was revealed from the data analysis that change in dimensions of specimens may occur in two dimensions.

4.2 Change In Compressive Strength

The change in compressive strength of concrete with different RGS replacement is demonstrated in Table-4. Here the table shows the range of compressive strength with average and standard deviation value. All the mixes experienced a reduction in strength except control specimens gathered a slight enhancement of about 4.49%. Here all the RGS replacements experienced a reduction of .29%, 1.46%, 15.23%, 6.87%, 15.03% and 5.92%, respectively after the sulphate exposure. The most significant point is that any of the RGS modified specimens have not failed to qualify to achieve the specified value of mechanical strength as per ASTM code after the sulphate exposure. This indicates the compatibility of RGS to be used as partial replacement of fine aggregate in concrete.

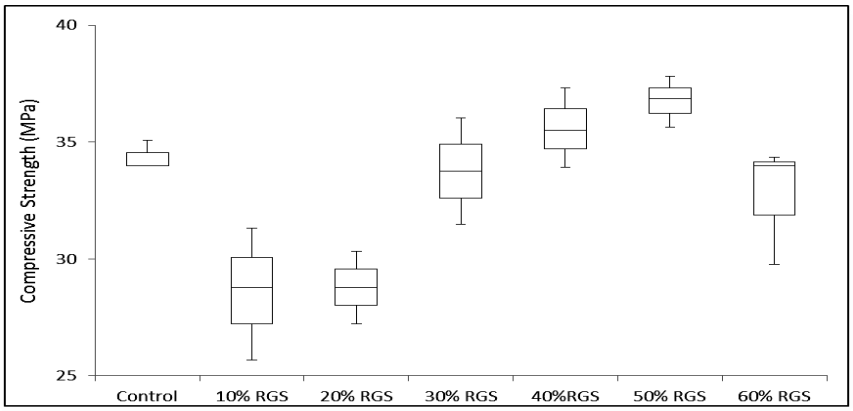

Figure 2: Compressive strength of cylindrical specimens (before sulphate exposure)

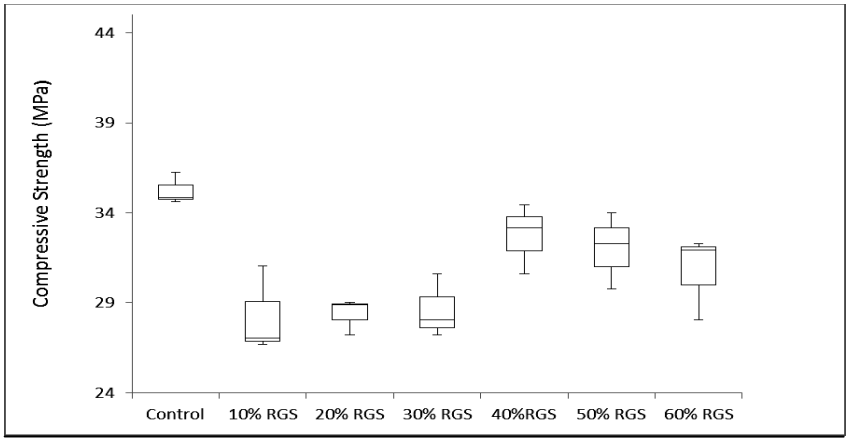

Figure 3: Compressive strength of cylindrical specimens (after sulphate exposure)

Table 4: Change in mechanical strength due to sulphate exposure

Test Condition		Mix-1 (Control)	Mix-2 (10% RGS)	Mix-3 (20% RGS)	Mix-4 (30% RGS)	Mix-5 (40% RGS)	Mix-6 (50% RGS)	Mix-7 (60% RGS)
Before Sulphate Exposure	Avg. (MPa)	33.7	28.3	28.7	33.7	35.1	37.6	32.7
	S.D. (MPa)	2.86	2.36	1.56	2.29	1.65	2.05	2.54
After Sulphate Exposure	Avg. (MPa)	35.2	28.2	28.3	28.6	32.7	32.0	30.7
	S.D. (MPa)	2.3	2.4	1.0	1.7	1.9	2.1	2.3
Remark (Increase/Decrease)		4.5%↑	.3%↓	1.5%↓	15.2%↓	6.9%↓	15.0%↓	5.9%↓

5 OUTCOME OF THE RESEARCH

The following conclusions can be derived from this research paper.

- The use of Recycled Granulated Steel (RGS) as a partial replacement serves an exclusive alternative of naturally available fine aggregate. Althoughthe compressive response proved that 30% and 50% RGS replacement experienced significant amount degradation in mechanical strength; still it is well above the guide line criteria of ASTM.

- The result analysis shown a relative higher change in volume for 40% and 60% RGS replacement due to sulphate exposure. The reason may be commented as having higher density in comparison to others resulting in expansion due to formation of ettringite in microstructure.

6 CONCLUSION

The growing demand for the rapid development of infrastructure has raised a huge concern for catalyzing the jeopardy of good quality natural aggregate. In this regard, recycled aggregate may serve an important role to stop the depletion of natural aggregate. Based on the results achieved in this paper, it can be concluded that, the tentative application of Recycled Granulated Steel (RGS) as partial replacement of Natural Fine Aggregate in concrete fulfilled the durability criteria. Therefore, Recycled Granulated Steel might be one of the best alternatives of Natural Fine Aggregate if proper utilization can be ensured in commercial and private sector.

REFERENCES

[1] Ferraris, F., C., Stutzaman, P. and Snyder, K., 2006. Sulfate Resistance of Concrete: A New Approach.

[2] Mamun, M., 2010. Loading Rate Effects and Sulphate Resistance of Fibre Reinforced Cement-based Foams, MSc. thesis Pg 38-39, University of Alberta.

[3] Suleiman, R., A., 2010. Physical Sulphate Attack on Concrete, MSc. Thesis, Pg 9-10, The University of West Ontario.

[4] Alam, S., M., Slater, E. and Billah, M.,M.,H.,A., 2013. Green Concrete Made with RCA and FRP Scrap Aggregate: Fresh and Hardened Properties. Journal of Materials in Civil Engineering, Vol. 25, No. 12, December 1, 2013.

[5] Corinaldesi, V., Gnappi, G., Moriconi, G. and Montenero, A. 2005. Reuse of ground waste glass as aggregate for mortars.

[6] Etxeberria, M., Vazquez, E., Mari, A.and Barra, M., 2007. Influence of amount of recycled coarse aggregates and production process on properties of recycled aggregate concrete.

[7] Evangelista, L., Brito, D., J., 2007. Mechanical behaviour of concrete made with fine recycled concrete aggregates.

[8] Ganjian, E.., Khorami M. and Maghsoudi, A.A., Scrap-tyre-rubber replacement for aggregate and filler in concrete.

[9] Movassaghi, R., 2006. Durability of Reinforced Concrete Incorporating Recycled Concrete as Aggregate (RCA). MASC thesis, University of Waterloo.

[10] Senthamarai, RM., Manoharan, D., P., 2005. Concrete with ceramic waste aggregate.

[11] ASTM C 39, Standard Test Method for Compressive Strength of Cylindrical Concrete Specimens, ASTM International, West Conshohocken, PA, 2015.

[12] ASTM C 1012, Standard Test Method for Length Change of Hydraulic-Cement Mortars Exposed to a Sulfate Solution, ASTM International, West Conshohocken, PA, 2015.

CICM 2015
First International Conference on
Advances in Civil Infrastructure and Construction Materials
MIST, Dhaka, Bangladesh, 14–15 December 2015

APPLICATION OF MICROBIOLOGICALLY INDUCEDPRECIPITATION PROCESS IN CEMENT AND CONCRETE RESEARCH: A REVIEW

Farzana RAHMAN[1], Sumaiya Afroz[2], Ikram H. Efaz[3], Rafid S. Huq[4] and Tanvir Manzur[5]

[1, 2, 3, 4, 5] Department of Civil Engineering, Bangladesh University of Engineering and Technology, Dhaka, Bangladesh.
Email: [1]farzanarahman022@gmail.com,[2]sumaiya0904002@gmail.com,
[3]ehe_mub@yahoo.com, [4]rafidhuq@hotmail.com and[5]tmanzur.buet@gmail.com

Abstract. *A multidisciplinary approach, Microbiologically Induced Precipitation (MICP), opens a new possibility in material engineering. This technique is also known as 'Biomineralization'. In this process, calcite is precipitated by highly urease positive bacteria like Sporosarcinapasteurii. These microorganisms decompose urea into ammonia and carbon dioxide, increasing the pH of the surrounding environment which triggers precipitation of dissolved calcium carbonate. This calcium carbonate adheres to the surface of any material and in doing so can serve as binders between particles. Moreover, such precipitation of impermeable calcium carbonate can also act as filler material within porous medium. This process has already been successfully used in soil stabilization. It has also shown potential as micro crack filler when applied externally on mortar cubes or beams. Recently, MICP has been used as a dormant self-healing agent in concrete. MICP is a biological process and pollutant free and thereby, it is generating immense attraction of researchers. However, application of MICP is still uncommon in Bangladesh. It is the responsibility of the concerned researchers of the country to find outpotentia avenue of MICP application. This article reviews the significant researches of MICP application in cement and concrete. In addition, recommendations on MICP related research are also made in context of Bangladesh.*

Keywords: Microbiologically Induced Precipitation, Biomineralization, Calcium Carbonate, Cement, Concrete.

1 INTRODUCTION

Concrete is the most widely used man made construction material in world. Among many advantages such as low cost and ability of being cast in any desirable shape, it shows some limitations too. Very low tensile strength, limited ductility and little resistance to cracking calls for further improvement in this material. Durability of concrete denotes its ability to persist for a substantial amount of time, without enduring any significant damage. For any manmade structure, the need for a durable concrete is of utter importance for both economic and structural purposes. A concrete, which is resilient to deterioration, not just makes structurally sound and stable buildings but also ensures a minimized maintenance cost. Increased durability will lead to minimization of such repair costs in the long term.When it comes to concrete, durability and permeability goes hand in hand. Other than entry through cracks, water can intrude concrete through its inherent permeable pores. An impermeable concrete is always desirable for elevated durability, since penetration of water containing dissolved salts is restricted. The pore system of concrete consists of minute capillary pores within the cement paste, used for coating aggregates and larger voids formed by improper concrete compaction. Pores without any access to fluid entry are harmless, thus doesn't affect concrete durability. However interconnected voids form a continuous passageway which facilitates water intrusion rendering the concrete more permeable, leading to poor durability. In the contemporary times, structural engineering is no longer bound within the construction scenario of concrete and steel. It has advanced in several innovative ways to adapt to the ever-changing needs of human with time. One such ground-breaking arena evolves on the incorporation of bacterial cells to induce biomineralization.

2 MICROBIOLOGICALLY INDUCED PRECIPITATION (MICP)

MICP, a multidisciplinary approach cross breeding microbiology and engineering, is a biological process by which living organisms form inorganic solids. It does not deplete any natural resources since the bacteria used can be easily reproduced by cultivation process. It is also considered as a green technology as its production does not involve greenhouse gas emission [1]. It is highly desirable because microbial activities induce the calcite precipitation which is pollution free and natural [2]. Microbially induced calcite precipitation (MICP) embodies the innovative approach to inoculate bacterial cells, for carbonate production, in cement and soil matrix. This innovative microbial technique has already been employed for improvement of engineering properties of soil and liquefaction prevention.

3 BIOMINERALIZATION IN CONCRETE

Bio-mineralization, more specifically bio-calcification in the context of cement-based-materials, is a series of biochemical reaction, followed by accumulation of calcium carbonate. The process of bio-calcification is accomplished in the presence of enzyme urease. In MICP, which is used for cement and concrete research, calcification is usually achieved by urea hydrolysis. For production of carbonate, urea hydrolysis is the most easily controlled reaction, which is likely to produce calcite within a short time [3]. There are numerous bacteria known to display urease activity. The urease-producing ability of the bacteria is commonly utilized in MICP [4, 5]. Microbes such as those the *Bacillus* species leads to the production of microbial concrete through biomineralization.

3.1 Microbial Concrete

As the names suggests such concrete is not the typical concrete which is casted on a daily basis at the construction sites. Rather this concrete derives such name from the incorporation of microbes within the cement matrix for enhancement of concrete performance. Microbial concrete, sometimes known as Bacterial concrete since urease positive bacteria is generally used, is solely produced by the biodeposition of bacterially-favored calcite production. Such concrete are produced embedding selective ureolytic bacteria within the concrete matrix.

3.2 Bacteria Strain

For the purpose of MICP the most commonly used microbe is *Sporosarcinapasteurii*, previously known as *Bacillus pasteurii*. *Sporosarcinapasteurii* is the bacterium which was frequently exploited for calcite precipitation in the very few previous researches. In research work of Whiffin [3] non-pathogenic bacteria *S. pasteurii* was employed for production of biocement at an industrial scale. The organism is a moderate alkaliphile in nature, with growth optimum pH of 9.25 [3].The utilization of bacterial mineral precipitation increases the strength and durability of concrete [6]. Other urease-producing bacteria used in MICP include *Bacillus subtilis, Bacillus sphaericus, Bacillus cohnii, Bacillus pseudofirms, Bacillus halodurans*etc [7, 8].

Sporosarcinapasteurii is facultative anaerobic. They are able to grow either aerobically or anaerobically. They prefer the presence of oxygen, however, and are metabolically active via aerobic respiration. It is therefore expected to have more calcite precipitation in areas close to surface in crack remediation [9]. *Sporosacinapasteurii* is able to endure high-alkaline environment. It is a gram positive bacterium. The extremely thick outer cell membrane enables them to remain dormant until a suitable environment is available to grow. They would become active in presence of water [10]. *B. pasteurii* produces intracellular urease that constitutes almost 1% of the dry weight of cell that contains three different subu-

nits comprising two nickel atoms in individual active sites [11]. According to Sarda et al. [12] *B. pasteurii* shows more urease production than *Bacillus lentus*and *Brevibacteriumammoniagenes.*

3.3 Urea Hydrolysisleading to Calcite precipitation

Microbially induced calcite precipitation marks the formation of calcium carbonate that eventually deposits on the surfaces of the materials used. Calcite is a carbonate mineral. Among the many other polymorphs of $CaCO_3$, calcite is the one which thermodynamically most stable [13]. In the biochemical reactions of MICP calcite is a major product that contributes to biodeposition. Bioprecipitation of $CaCO_3$ is achieved when alkaline environment prevails. The eventual chemical reactions during urea hydrolysis tend to increase the pH, thus making it alkaline.

$$Ca^{2+} + HCO_3^- + OH^- \rightarrow CaCO_3(s) + H_2O(1)$$

Urease-positive bacteria easily perform urea hydrolysis to form ammonia and carbon dioxide, which in turn aid to create alkaline conditions. With increase in alkalinity, calcite precipitation is facilitated with the availability of calcium cations in the near surrounding. Enzymatic hydrolysis of urea by bacterial enzyme urease causes an increase in pH that shifts the bicarbonate–carbonate equilibrium towards the production of more CO_3^{2-} by producing CO_2 and ammonia. The resultant precipitation is $CaCO_3$ [14, 15]. The accumulation of calcite is characterized by crystalline structure and ability to continuously grow upon itself. Possible biochemical reaction in a medium to precipitate $CaCO_3$ in the nucleation site at the cell surface are listed below: [16]

$$Ca^{2+} + Cell \rightarrow Cell\text{-}Ca^{2+}$$

$$Cl^- + HCO_3^- + NH_3 \rightarrow NH_4Cl + CO_3^{2-} \qquad (2)$$

$$Cell\text{-}Ca^{2+} + CO_3^{2-} \rightarrow Cell\text{-}CaCO_3$$

Bacterial cell wall is negatively charged that attracts calcium ions in the nutrient solution provided externally as shown in Figure 1.Dissolved inorganic carbon (DIC) and ammonium (AMM) are discharged in presence urea in the microenvironment of the bacteria Eventually calcium carbonate precipitated by a series of biochemical reactions is deposited in the bacterial nucleation sites and seals off the cracks and pores.

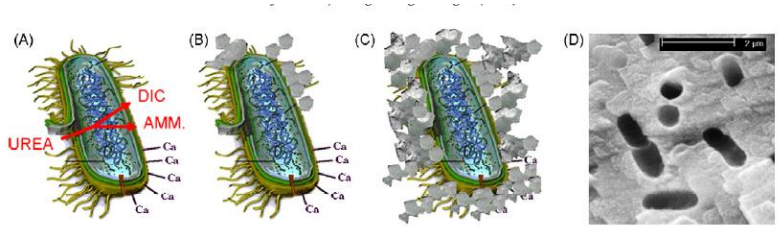

Figure 1: Simplified representation of ureolytic induced carbonate precipitation and the events occurring during the process. [14]

4 SELF HEALING CONCRETE &CRACK REMEDIATION

Micro cracks in concrete lead to structural failure. Traditional repairing system involves application of mortar on cracks. This can be time consuming and requires repeated repairing activities. It may become especially difficult to gain access to the cracks if they are underground or at a great height.

As an effective crack remediation technique self-healing in concrete is a well-known process. A biological repair technique can be used such as MICP. Dormant bacteria incorporated in concrete matrix which will contribute to the strength and durability of the concrete. Inside concrete a rather hostile environment prevails for common bacteria owing to lack of nutrients needed for growth, high internal pH, relative dryness. Specific spore forming alkaliphilic bacteria genus *Bacillus* is used commonly for MICP. Bacteria based self-healing agent comprising alkaliphilic bacteria genus *Bacillus* with a calcium-based nutrient is believed to remain hibernated within the concrete for up to 200 years [14].

Crack remediation by actuating bacteria to precipitate calcite plugs off the crack. Calcite precipitation is the fundamental process in making of a smart bacterial concrete. Bacterial concrete can be called as a "Smart Bio Material" due to its inherent ability to precipitate calcite continuously. As the name suggests this pioneering concrete is produced incorporating bacterial cells. Bacterial concrete is a biomaterial which is capable of crack remediation, induced by bacterial precipitation of calcium carbonate [9].More lately experimental study has been conducted on self-healing of cracked concrete. Dormant bacteria are embedded on concrete matrix, which is activated once external water reaches it through the cracks [7]. Once initiated, calcium carbonate is precipitated which heals the freshly formed cracks. Healing is achieved once the biodeposited calcite plugs off the cracks and inherent pores of concrete. Since it is a completely natural process, MICP is a more environmentally friendly treatment method, compared to the more commonly used conventional method of epoxy treatment as illustrated in Figure 2.

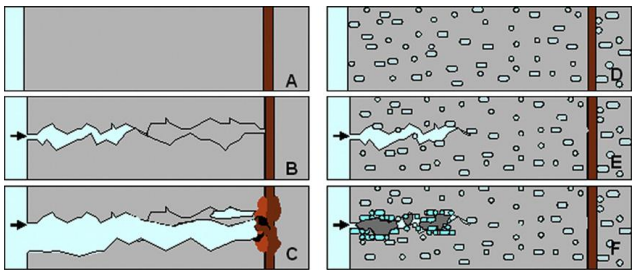

Figure **Error! No text of specified style in document.**: Schematic drawing of comparison between conventional concrete (A–C) and bacteria-based self-healing concrete (D–F). [7]

Bang et al. [17] investigated the effect of crack remediation on cement mortar cubes by *Bacillus pasteurii* immobilized in polyurethane (PU) foam and found increased strength in concrete cubes. Polyurethane (PU) foam enhanced the effectiveness of MICP method. The presence of polyurethane (PU) foam reduced crack throughout the matrices unlike other remediation processed by MICP that fills cracks close to surface. However, elastic modulus and tensile strength were not changed significantly. This led to the citation that precipitated calcite does not serve as a bonding material within the matrices and lingers as a form of precipitation only.

5 DRAWBACKS OF MICP

One of the major drawbacks of MICP is high cost. The cost based on the price of the microorganisms and the price of the nutrients could be as high as \$11–19/m^2 [14].However, most of the cost is induced from nutrients. The cost can be reduced by using any viable inexpensive alternative. In case of self-healing sustainable concrete, the nutrient must not interfere with setting time other characteristics of cement. Moreover once the process of MICP is employed in a commercial scale, the nutrient cost will be cut down drastically. The MICP method is time consuming as the production of calcium carbonate precipitate is limited by the capacity of the bacteria to produce urease [18].Though the bacteria strain is harmless, a byproduct of the process ammonia is a principal environmental pollutant. Sometimes other more harmful organisms can be induced by MICP if precautions are not taken.

6 PROSPECT OF MICP IN BANGLADESH

In the context of Bangladesh MICP is a highly intricate biotechnology which is yet to receive its due recognition. Relatively at a budding stage around the globe, MICP technique opens up a plethora of research interests. In backdrop of Bangladesh construction scenario, brick aggregates are used frequently. Brick chips

are used as coarse aggregates of concrete owing to its low costs and wide availability, against high cost and scarcity of stone aggregates. The characteristic high porosity of brick chips advocates high permeability in concrete structures. This in turn has the potential to make the embedded structural reinforcements exposed to the incoming water, leading to rusting. Eventually it could result in shorter structural service life. The innovative process of MICP can be utilized to modify the brick aggregates for concrete works by simply plugging off such water permeable pores. Preliminary experiments on this particular sector involving bacterial application on brick aggregates have yielded promising results in terms of decreasing permeability for the microbially treated bricks [19]. This is just one of the many potential aspects of MICP which is awaiting thorough research works in the related fields.

REFERENCES

[1] Isha, M., I. Afifudin, H. and MohdSaman, H., 2012.Bacillus Subtilis - and ThermusThermophilus – Derived Bioconcrete in Enhancing Concrete Compressive Strength.*International Sustainability and Civil Engineering Journal*, 1(1).

[2] Ramakrishnan, S. K., R. K. Panchalan, S. S. Bang, and R. City.,2005.Improvement of concrete durability by bacterial mineral precipitation. *In Proceedings of 11th International Conference on Fracture*, pp. 20-25.

[3] Whiffin, V. S. 2004. Microbial $CaCO_3$ precipitation for the production of biocement. *Doctoral Dissertation*, Murdoch University.

[4] Mobley, H.L.T. and Hausinger,R.P., 1989. Microbial ureases: significance, regulation, and molecular characterization. *Microbiology Reviews*, 53, pp. 85-108.

[5] Stocks-Fischer, S.,Galinat, J. K., & Bang, S. S., 1999. Microbiological precipitation of $CaCO_3$.*Soil Biology and Biochemistry*, 31(11), pp. 1563-1571

[6] Ghosh P. and Mandal S., 2006.Development of bioconcrete material using and enrichment cultureof novel thermophilic anaerobic bacteria, *Indian Journal of Experimental Biology*, 44, pp. 336-339

[7] Jonkers, H. M., &Schlangen, E., 2007. Self-healing of cracked concrete: a bacterial approach. *Proceedings of FRAMCOS6: fracture mechanics of concrete and concrete structures.* Taylor & Francis/Balkema, Leiden.

[8] Nosouhian, F., Mostofinejad, D., and Hasheminejad, H., 2015. Concrete Durability Improvement in a Sulfate Environment Using Bacteria, *Journal of Materials in Civil Engineering.*

[9] Ramakrishnan, V., Panchalan, R., & Bang, S. S., 2001.Bacterial Concrete-A Self Remediating Biomaterial. *In Proceedings of 10th International Congress on the Polymers in Concrete*, Hawaii.

[10] Jonkers, H. M. 2007. Self healing concrete: a biological approach. *Self Healing Materials*, pp 195-204.

[11] Benini, S., Rypniewski, W. R., Wilson, K. S., Miletti, S., Ciurli, S., &Mangani, S., 1999. A new proposal for urease mechanism based on the crystal structures of the native and inhibited enzyme from Bacillus pasteurii: why urea hydrolysis costs two nickels. *Structure*, 7(2), pp205-216.

[12] Sarda, D., Choonia, H. S., Sarode, D. D., &Lele, S. S., 2009. Biocalcification by Bacillus pasteurii urease: a novel application. *Journal of industrial microbiology & biotechnology*, 36(8), pp1111-1115.

[13] Kladi, A., Klepetsanis, P.G., Ostvold, T., Kontoyiannis, C.G. and Koutsoukos, P.G., 2002. Crystal Growth of Calcium Carbonate in Seawater, the effect of temperature and of the presence of Inhibitors, *Advances in Crystal growth Inhibition Technologies*, pp.85-106.

[14] De Muynck, W., De Belie, N., &Verstraete, W., 2010. Microbial carbonate precipitation in construction materials: a review. *Ecological Engineering*, 36(2),pp 118-136.

[15] Castanier, S., Le Metayer-Levrel, G., &Perthuisot, J. P., 2000. Bacterial roles in the precipitation of carbonate minerals. *Microbial Sediments*, pp. 32-39).

[16] Ramachandran, S. K., Ramakrishnan, V., & Bang, S. S., 2001. Remediation of concrete using microorganisms. *ACI Materials Journal*, 98(1).

[17] Bang, S. S., Galinat, J. K., &Ramakrishnan, V., 2001. Calcite precipitation induced by polyurethane-immobilized Bacillus pasteurii. *Enzyme and Microbial Technology*, 28(4), pp 404-409.

[18] Amidi, S., & Wang, J., 2015. Surface treatment of concrete bricks using calcium carbonate precipitation. *Construction and Building Materials*, 80, pp 273-278.

[19] Afroz, S. &Rahman, F., 2015. Influence of Biotreated Bricks on Concrete Durability. *Undergraduate Dissertation*, Bangladesh University of Engineering and Technology (BUET).

CICM 2015
First International Conference on
Advances in Civil Infrastructure and Construction Materials
MIST, Dhaka, Bangladesh, 14–15 December 2015

PERFORMANCE OF SLAG BASED GEOPOLYMER MORTAR IN ACIDIC ENVIRONMENT

O. C. DEBANATH[1], M. S. Islam[2] and M. M. Islam[3]

[1, 2, 3] Department of Civil Engineering, Chittagong University of Engineering and Technology, Chittagong, Bangladesh.
Email: [1]debnathopu60@gmail.com, [2]msislam@cuet.ac.bd and[3]mislam@cuet.ac.bd

Abstract. *This paper presents an experimental investigation conducted on the performance of geopolymer mortar subjected to acidic environment. The ground granulated blast furnace slag (GGBS) were chosen as binder material and the alkaline solution used was the combination of sodium silicate and sodium hydroxide (15M) solution to prepare AAS mortar specimens. The test specimens were 216 nos. of 50×50×50mm cube and 216 nos. of standard briquettespecimens cast using nine different mix combinations designated as AAS3-1, AAS3-1.25, AAS3-1.5, AAS5-1, AAS5-1.25, AAS5-1.5, AAS8-1, AAS8-1.25, and AAS8-1.5. The mix combinations were based on Na_2O dosage (%) and activator modulus (M_s) and the specimens cured at 40°C in a temperature controlled chamber. Performance of AAS mortar specimens in ambient as well as 5% sulfuric and hydrochloric acid solutions were evaluated periodically by monitoring visual appearance, change in weight, compressive strength, tensile strength, pH value over an exposure period of 30 and 90 days exposure. The test results indicate that the slag based geopolymer mortar has an excellent resistance against acidic attack.*

Keywords: Acidic environment, Compressive strength, Durability, Geopolymer, Tensile strength.

1 INTRODUCTION

Concrete is the most popular construction material which requires a huge amount of Portland cement as main binder. It is widely known that the production of Portland cement is associated with environmental issues and the amount of carbon dioxide released during the OPC production is around one ton for every ton of cement due to the calcination of limestone and combustion of fuel. In addition, the extent of energy required to produce OPC is only next to steel and aluminium. Geopolymer is an innovative binding material produced by the chemical action of inorganic molecules which is an excellent alternative construction material to the existing plain cement concrete.

According to Vijaya [1] the polymerization process involves a substantially fast chemical reaction under alkaline conditions on silicon-aluminum minerals that results in a three-dimensional polymeric chain and ring structure. The property of geopolymers depends on the type of activating solution and thermal activation. Since Geopolymers are novel binder that relies on alumina silicate rather than calcium silicate hydrate bonds for structurally integrity and have been reported as being acid resistance [2]. In the case of geopolymer production, the role of water is to provide workability and not involved in the chemical reaction of polymerization and instead water is expelled during heat curing and subsequent drying [3]. When the slag is used as base material and activated by using alkaline solution, the binder is called alkali activated slag (AAS) and if the fly ash is used it named as FA based geopolymer [4]. Blast furnace slag gives quick hardening behavior compared to fly ash based geopolymer which minimized the time of hardening. Higher calcium content may result in faster geopolymerisation due to the formation of semi-crystalline Ca-Al-Si gel [5].

2 MATERIALS AND METHODS

2.1 Materials

The following materials were used to conduct the experimental program to assess the performance of geopolymer mortar in acidic environment.

2.1.1 Source materials

Any material rich in silica and alumina in glassy power form is apt for acting as a source material in the geopolymeric binder. The most commonly used base materials of geopolymer binder are industrial by-product like fly ash and slag. Since the FA based binder required higher thermal activation compared to slag, so the ground granulated blast-furnace slag (GGBS) was chosen as base material to prepare AAS mortar specimen and the chemical composition is listed in table-1.

Table 1: Chemical composition of binder (GGBS)

Composition	SiO_2	Al_2O_3	Fe_2O_3	MnO	CaO	MgO	Na_2O	K_2O	LOI*
% of mass	29.27	17.07	1.76	0.49	40.07	8.35	0.61	0.23	0.06

*LOI= Loss on ignition

2.1.2 Fine aggregate

Fine sand collected from locally available source was prepared according to the guideline of ASTM C 778-02 and used to cast mortar specimens. The table 2 shows the properties of fine aggregate.

Table 2: Properties of fine aggregate

Density	2.65 kg/liter
Absorption capacity	2.3%
Moisture content	1.97%
Fineness modulus	2.00

2.1.3 Alkaline liquids

Sodium silicate (Na_2SiO_3) liquid based activator used in this study which is collected from local suppliers. The weighed quantity of sodium hydroxide (NaOH) palate is dissolved in required quantity of water to make a NaOH solution of 15 molar. Finally the measured quantity of sodium silicate was mixed with dissolved sodium hydroxide to get alkaline activator solution; the chemical composition of solution is according to table 3.

Table 3: composition of Activator

Component	Na_2SiO_3	NaOH
Na_2O	8%	29.05%
SiO_2	26%	0%
H_2O	66%	70.95%
Molarity(M)	NA	15

2.1.4 Acidic environment

Concreted H_2SO_4 having 98% purity, density 1.84 g/cm^3 and the HCl having 37% purity, density 1.2 g/cm^3 was used in this experimental program to create artificial acidic environment. To study the effects of exposure in acidic environment, specimens were immersed in diluted 5% sulfuric and hydrochloric acid solution.

2.2 Specimen Preparation and Test Methods

The mix design was performed based on absolute volume method [6] which assumed that the volume of compacted mortar is equal to the sum of the absolute volume of all the ingredients(binding materials, activator solution, fine sand, and water). The mass ratio of sand to binder was fixed at 2.75 and a water binder ratio of 0.5 was kept constant for all mix combinations. Slag was first mixed with the activator solution in a mortar mixture machine for 5 minute before sand was gradually introduced and further mixed for another 5 minutes. The mix was then transferred into 50 mm cube moulds and standard briquette moulds and compacted manually. After demoulding, the specimens were warped with polyethylene bag and stored in a temperature controlled chamber for heat curing over a period of 48 hours at 40°C to accelerate the polymerization process. At the end of curing, the specimens were allowed to cool and stored in room temperature until tested. To study the effects of acidic environment, the specimens were immersed in 5% Sulfuric acid and 5% Hydrochloric acid after 28 days age and tested after periods of 30 days and 90 days exposure. The effect of acidic environment on specimens was evaluated by visual appearance, change in weight, pH value and strength tests after the specific exposure periods.

Following variables were considered in this study:

1. Three dosage of Na_2O (%Na_2O) selected for this experiment are 3%, 5% & 8% (The ratio of Na_2O content of alkaline solution to GGBS)
2. Three activator modulus (mass ratio of SiO_2 to Na_2O) 1.0, 1.25 and 1.5 was selected for this experiment.

A total 216 nos. of 50mm cubes and 216 nos. of standard briquette specimens were prepared using nine different mix combinations. The samples were designated by corresponding dosage and activator modulus, and thus AAS 3-1.0 indicate the specimens having 3% of Na_2O dosage and an activator modulus of 1.0.

3 RESULT AND DISCUSSION

3.1 Visual appearance

The visual examination was carried out on specimens after recovering from different solutions. It has been seen that, after 30 days exposure period, the Specimen immersed in 5% sulfuric acid showed white deposition on its surface, while the specimen immersed in 5% hydrochloric acid showed a reddish deposition on the surface. After 90 days exposure, the specimen immersed in 5% sulfuric acid showed brown deposition with considerable surface deterioration, while the specimen under 5% hydrochloric acid showed a thick white gelatinous deposition

on surface with very negligible deterioration. It is noticed that no surface crack was visible and no noticeable surface degradation of specimens was observed in hydrochloric acid environment. But excessive surface erosion was visualized after 90 days exposure period of specimen in sulfuric acid solution. Photographic evidences of deteriorated specimen taken at specific stage of exposure are presented in Figure.1 and Figure.2.

30 days 90 days

Figure 1: Specimens after exposure in 5% Sulfuric acid solution

30 days 90 days

Figure 2: Specimens after exposure in 5% Hydrochloric acid solution

3.2 Change in Weight

Results of the weight changes for the AAS mortar specimens are presented in figure.3. For Specimens immersed in 5% Sulfuric Acid, a sudden loss of weight was noticed after 90 days exposure. AAS specimens with highest percentage of alkali (8% Na_2O) showed less loss of weight compared to lower percentage of Na_2O dosage. As the Na_2O content in specimens increase, weight loss decreases in both sulfuric acid and hydrochloric acid solution. However the deterioration

(weight loss) of specimens in sulfuric acid environment is much greater as compared to hydrochloric acid environment for the identical exposure periods.

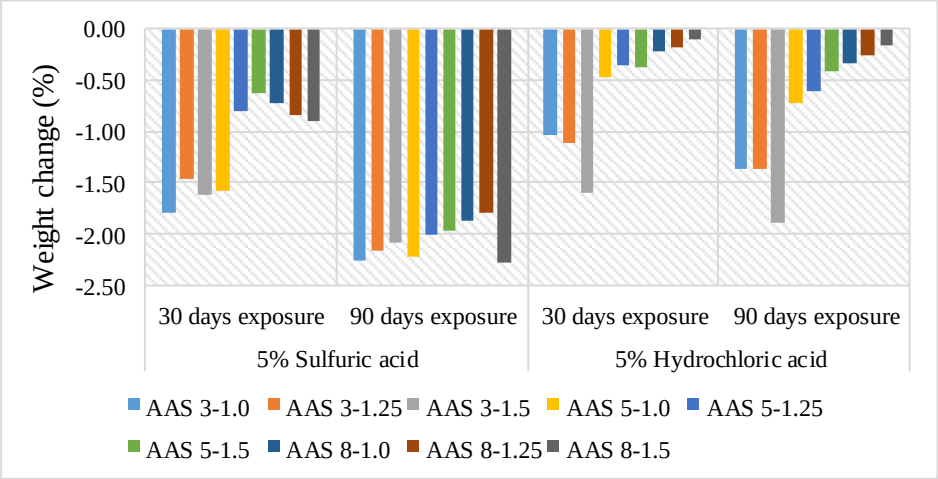

Figure 3: Weight changes of specimens in acidic environment

3.3 pH value

The pH value is an important parameter often used to assess the alkalinity condition of mortar. In this study, the pH values of specimens were determined with the help of digital pH meter and the values are found to vary within the range of 11.32 to 13.12.

3.4 Compressive Strength

Figure.4 and.5 shows the compressive strength results of AAS mortars in Sulfuric acid and Hydrochloric acid environment. Compressive strength was determined using a digital compression testing machine and the compressive strength results for normal as well as acidic environment are shown in the same graph.AAS mortar specimens of higher Na_2O dosage (5% and 8%) showed very little loss in strength in acid environment. The maximum compressive strength of AAS mortar was observed as 66.23 MPa for specimens of AAS 8-1.5 mix in normal environment at 90 days exposure. Specimens exposed to Hydrochloric acid environment showed a comparatively lesser strength loss than those in sulfuric acid. AAS mortar specimens showed substantial compressive strength, even after noticeable surface deterioration at 90 days exposure in sulfuric acid solution.

3.5 Tensile Strength

From the tensile strength data of AAS mortar specimen exposed to normal as well as acidic environment for 30 and 90 days exposure, it is seen that the gain of tensile strength shows random variation with age of specimens and mix combination. However, the maximum tensile strength was found 4.8 MPa for the mix AAS 8-1.5 in normal environment at 90 days exposure. The tensile strength of AAS mortar in normal environment lies between 1.0MPa to 4.8 MPa. The Tensile strength for the specimens exposed to sulfuric and hydrochloric acid environment are observed to lie in the range of 1.6-3.2 and 1.0-3.7 respectively.

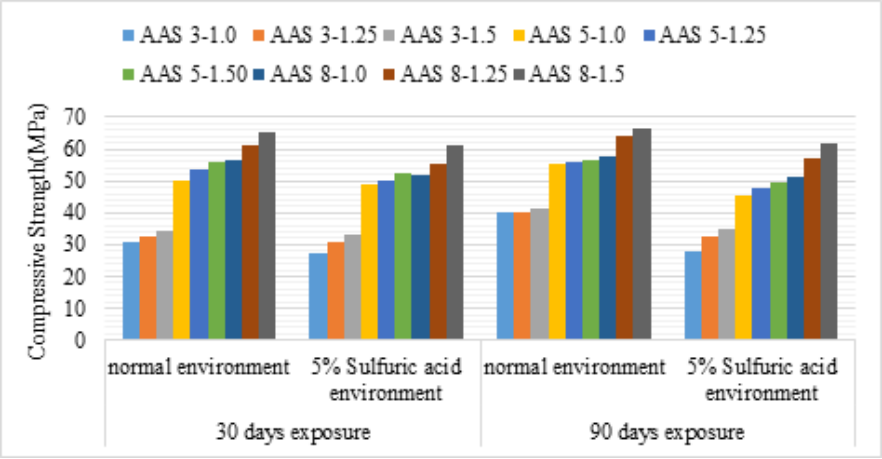

Figure 4: Compressive strength of specimens in sulfuric acid environment

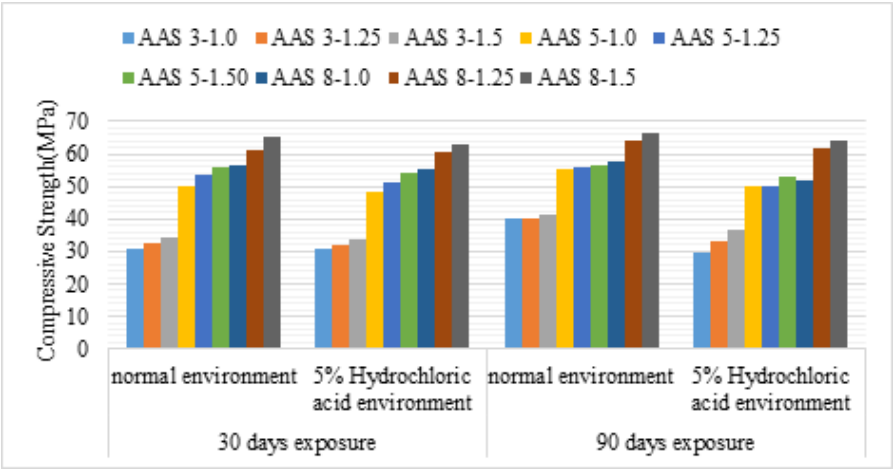

Figure 5: Compressive strength of specimens in hydrochloric acid environment

4 CONCLUSIONS

On the basis of findings of the present study, following conclusions can be drawn.

- AAS mortar specimens made from GGBS with alkaline activators remained structurally intact and did not show any noticeable change although some sample showed change in color.
- AAS 8-1.5 mix attained 62 MPa (almost 90% of 120 days) compressive strength after 7days, which indicate that geopolymer mixes having higher dosage of Na_2O can attain ultimate strength very rapidly.
- The average loss in weight of specimens is observed to be relatively higher in sulfuric acid (2.28-1.8%) as compared to hydrochloric acid (0.61-1.9%).
- Na_2O dosage and the activator modulus (M_s) has significant influence on strength properties of AAS mortar. Higher dosage of Na_2O (5% & 8%) and activator modulus (1.5) shows higher compressive strength.
- The compressive strength of AAS mortar in normal environment was found to lie in the range of 31-66.23MPa.The compressive strength values for specimens exposed to sulfuric and hydrochloric acid environment were recorded in the range of 27.14- 62.02 MPa and 29.4-63.23 MPa respectively.
- Even after having considerable surface deterioration, weight loss due to exposure in acidic environment, AAS mortar specimens still showed substantial compressive strength confirming the higher resistance of AAS mortar in acidic environment.

REFERENCES

[1] B. V. Rangon, 2008.*Low-Calcium, Fly-ash Based geopolymer concrete.* Concrete construction Engineering Handbook, Taylor and Francis Group, Boca Raton.

[2] J. davidovits, 1994. *Properties of Geopolymer Cements*. First international conference on alkaline cements and concretes, Vol. 1, pp.-131-149.

[3] S. Thokchom, P. Ghosh, S. Ghosh, 2009. *Acid Resistance of Fly ash based Geopolymer Mortars,* International journal of Recent Trends in Engineering, Vol. 1,No. 6.

[4] A.A. Adam, 2009. *Strength and durability properties of Alkali activated slag and fly ash based geopolymer concrete,* School of civil, environmental and chemical engineering, RMIT University, Melbourne, Australia.

[5] C.K. Yip, V. Deventer, J.S.J., 1501. *Effect of granulated blast furnace slag on geopolymerisation,* Proceedings of 6th world congress of chemical engineering, Melbourne, Australia.

[6] A. M. Neville, *Properties of concrete*, 1983, ISBN 0-582-40626-9.

CICM 2015
First International Conference on
Advances in Civil Infrastructure and Construction Materials
MIST, Dhaka, Bangladesh, 14–15 December 2015

COMPRESSIVE STRESS-STRAIN BEHAVIOR OF LOW GRADE STEEL FIBER REINFORCED CONCRETE MADE WITH FRESH BRICK AGGREGATES

M. S. ISLAM[1] and M. A. A. Siddique[2]

[1] Department of Civil Engineering, World University of Bangladesh, Dhaka, Bangladesh.
E-mail: shariful2@civil.wub.edu.bd

[2]Department of Civil Engineering, Bangladesh University of Engineering and Technology, Dhaka, Bangladesh.
Email: alamin@ce.buet.ac.bd

Abstract. *Plain concrete is a brittle material with a low tensile strength, limited ductility and little resistance to cracking. In order to improve the inherent tensile strength of concrete, multidirectional and closely spaced reinforcements, which can be provided in the form of randomly distributed fibers may be used. Steel fiber is one of the most commonly used fibers in fiber reinforced concrete. Short, discrete steel fibers provide discontinuous three-dimensional reinforcement that may increase load and transfer stresses at micro-crack level. This reinforcement provides tensile capacity and crack control to the concrete section prior to the establishment of visible macro cracks, thereby, enhancing ductility as well as toughness. In this paper, an experimental investigation is carried out to assess the influence of locally available low grade steel fiber reinforcements on the stress-strain behavior of concrete made with fresh brick aggregates. Hooked end steel wires with 50 mm of length and aspect ratio of 55.6 are used as fiber reinforcements in a volume fraction of 0% (control case) and 0.50%. Experimental results show that the addition of steel fiber enhances the different mechanical properties of concrete. It reveals that around 5% to 10% and 10% to 15% increase in 28 days compressive strength and tensile strength of steel fiber reinforced concrete, respectively compared to those of the control case. On the other hand, concrete strain at failure of steel fiber reinforced concrete has increased almost 30% compared to that of the control case.*

Keywords: Steel fiber, Fresh brick, Strength, Stress-strain behavior, Young's modulus.

1 INTRODUCTION

Concrete is one of the most important building material and its consumption is increasing in all countries and regions around the globe. The reasons are multiple: its components are easily available everywhere and relatively cheap, its production is also relatively simple, its application covers large variety of building and civil infrastructure works. The only disadvantage of concrete is its brittleness, i.e. relatively low tensile strength and poor resistance to crack opening and propagation [1]. Moreover, Strength and ductility are the important factors to be considered in the design of seismic resistant reinforced concrete structures. Under seismic condition, the structure may be subjected to large deformations.

Use of steel-fiber reinforced concrete has steadily increased during the last 25 years. Considerable developments have taken place in the field of steel-fiber reinforced concrete as reported by Bentur and Mindess [2].The current field of application of steel-fiber reinforced concrete includes highway and airfield pavements, hydraulic structures, tunnel linings etc. [3-5].The addition of steel-fibers significantly improves many of the engineering properties of mortar and concrete, notably impact strength and toughness. Flexural strength, fatigue strength, tensile strength and the ability to resist cracking and spalling are also enhanced. To design and analyze structures using steel-fiber reinforced concrete for compression, the stress-strain behavior of the material in compression is needed. While the compressive strength is used for the strength calculation of the structural components, the stress-strain curve is needed to evaluate the toughness of the material for consideration of ductility.

In the present study, an extensive experimental work has been carried out to study the stress-strain behavior of steel-fiber reinforced concrete with fresh brick aggregate. In addition, compressive strength, tensile strength and modulus of elasticity have also been carried out. Hooked end steel wires with 50 mm of length and aspect ratio of 55.6 are used as fiber reinforcements in a volume fraction of 0% (control case) and addition of 0.50% steel fiber.

2 EXPERIMENTAL PROGRAM

2.1 Materials

In the present study, crushed brick as coarse aggregate, locally available Sylhet and as fine aggregate (FA) and blended cement/Portland composite cement (CEM II/B-M) and low grade steel wire as steel fiber have been used.

2.1.1 Brick aggregate (BA)

Crushed brick is commonly used in Bangladesh as coarse aggregate. Collected brick samples were broken into pieces manually to have a size of 19 mm down-grade. The aggregates were then sieved to have a standard grading according to ASTM C33-93. To maintain the SSD condition, aggregates were washed properly to avoid the dust and were dried in the laboratory. The oven dry (OD) basis unit weight and saturated surface dry (SSD) basis unit weight as well as void content were determined according to the ASTM C29. Rodding method was used to calculate the unit weight. Specific gravity and absorption capacity of the brick aggregate were determined according to the ASTM standard C127.

2.1.2 Fine aggregate (FA)

Sand which was collected from the rivers in Sylhet district of Bangladesh is called "Sylhet Sand". It was collected from the local market in Dhaka city. Sand as a fine aggregate was sieving through No 4. ASTM sieve to ensure that no big particle or no rubbish were present into the samples. Table 1 shows the physical properties of aggregates i.e. BA and FA. However, Portland composite cement (CEM II/B-M) and fresh water have been used in this study for making concrete.

Table1: Physical properties of aggregate

Sl. No.	Name of Properties	Brick aggregate	Fine aggregate
1.	Bulk Specific Gravity (OD)	1.80	2.21
2.	Bulk Specific Gravity (SSD)	2.15	2.36
3.	Apparent Specific Gravity	2.38	2.56
4.	Unit Weight (OD) (kg/m^3)	1050	1583
5.	Unit Weight (SSD) (kg/m^3)	1130	1666
6.	Absorption Capacity (%)	13	5.81
7.	Void Content (%)	5	25.20
8.	Fineness modulus (FM)	5.95	2.96

2.1.3 Properties and making of steel fiber (SF)

Steel fiber having different sizes of diameter is generally found in Bangladesh. Hooked end steel fiber is used in this present study to assess the effect of fiber on both the strength and ductility of concrete as shown in figure 1.

Table 2 shows the properties of fibers that have been tested in the laboratory. In general, it is simple and easier to make different shapes fiber but it takes more

time to prepare as there is no mechanical setup. After collecting the fiber from local market, a heavy cutter was used to cut the whole bundle of wires manually. Fiber wire straightening was accomplished after cutting the bundle wires. The fiber was then cut into small pieces as the required length and it was pressed between two spikes sited on a wooden frame to make two bends at angle of 120^0. Finally, the length was checked to obtain the desired sample size of 50 mm.

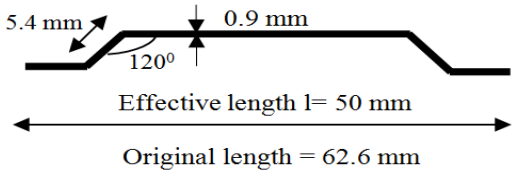

Figure 1: size and shape of the steel fiber

Table 2: Properties of steel fiber

Sl. No.	Name of Properties	Value
1.	Length L(mm)	50
2.	Diameter D(mm)	0.9
3.	Aspect Ratio (L/D)	55.56
4.	Specific Gravity	6.0
5.	Unit Weight (kg/m^3)	6000
6.	Tensile Strength (MPa)	220

2.2 Mix proportion

In the present study, two cases were considered. First, brick aggregate concrete (BAC) which is control case (0% steel fiber) and another is steel fiber reinforced brick aggregate concrete made with 0.5 % steel fiber (SFBAC 0.5%). Here, 1% fibers by volume produced unit weight of 60kg/m^3.The mixture proportions of concrete for all cases are summarized in Table 3. Water/cement (W/C) ratios of concrete were 0.44 and no admixtures were used. Cement content of concrete was 390 kg/m^{3}for all the cases. Sand to total aggregate volume ratio was 0.44. Total mixing time was 5-8 minutes that can ensure the homogeneity of mixing steel fiber. After mixing concrete, the workability of concrete was measured by slump cone test. Cylinder concrete specimens were made and demolded after one day of casting. Then the specimens were cured under water.

Table 3: Weight based mix proportion for 1 m^3 of concrete

Sl. No.	Cases	Cement (kg/m^3)	Sand (kg/m^3)	BA (kg/m^3)	SF (kg/m^3)	Water (kg/m^3)
1.	BAC	390	716.4	798	0	171.6
2.	SFBAC0.5%	390	716.4	798	30	171.6

2.3 Experimental Plan

Experimental setup has been conducted for compressive strength test, splitting tensile strength test, stress-strain behavior and modulus of elasticity of concrete.

2.3.1 Test setup

The compressive strength and splitting tensile strength of concrete was measured at 7, 14, and 28 days by using Universal Testing Machine (UTM) of loading rate 4 kN/sec over the specimens. Figure 2 shows the test setup of the present study. Compressive strength of the cylinder is determined as per ASTM C39M-03 and tensile strength of concrete is determined as per ASTM C496M-04.Non-destructive test was accomplished by the rebound hammer as per ASTM C805. The strain of concrete specimens was measured by a strain measurement setup with a dial gauges. The gauge length was 75 mm. The failure surfaces of concrete were also checked carefully after crushing of the concrete cylinders. The Young's modulus of concrete was determined from the stress-strain curves. The stress of concrete at strain level 0.0005 was used to determine the Young's modulus of concrete [6].

(a) (b) (c)

Figure 2: Test setup (a) Strain gauge (b) Compressive strength and stress-strain behavior (c) Tensile strength

3 RESULTS AND DISCUSSIONS

3.1 Fresh concrete properties

Besides the hardened concrete properties, workability as fresh concrete property has also been measured in the present study. Slump cone having a dimension of 12 inch in height, 4 inch diameter in top and 8 inch diameter in bottom, is filled with 3 layers and on each layers 25 times temping with a 5/8″ diameter rod having a weight of 1kg, are accomplished. Therefore, a total temping of 75 times for three layers are carried out, following ASTM C143.It is observed that workability of the concrete decreases with the increase of percentage of fiber addition. The value was 2.5 inch and 2 inch for BAC and SFBAC 0.5% respectively.

3.2 Hardened concrete properties

Compressive strength, splitting tensile strength, stress-strain behavior and Young's modulus have been observed as hardened concrete.

3.2.1 Compressive strength

Effect of fibers on compressive strength of concrete is tested at 7 days, 14 days, and 28 days as shown in figure 3. No significant difference is observed at 7 and 14 days compressive strength between BAC and SFBAC. However, Around 7 % strength is increased at 28 days in BAC compare to SFBAC.

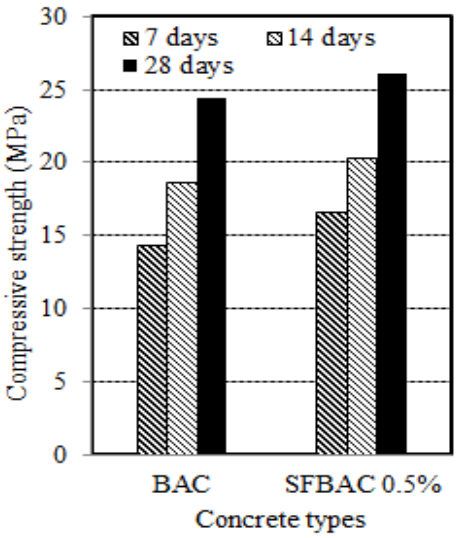

Figure 3: Compressive strength at 7, 14 and 28 days

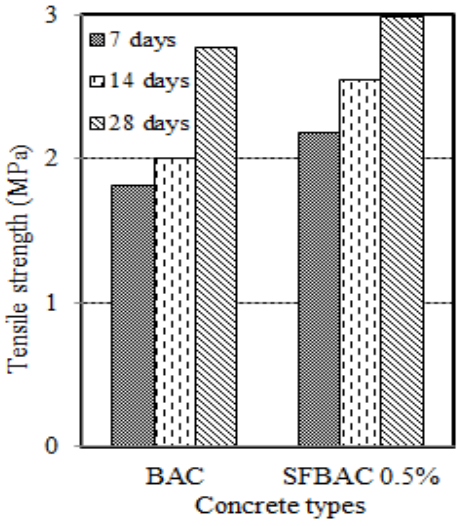

Figure 4: Tensile strength at 7, 14 and 28 days

3.2.2 Tensile strength

Effect of aggregates on tensile strength of concrete is also tested at 7, 14, and 28 days as shown in figure 4. It is seen that in all cases BAC has the lower strength than SFBAC. At 7 and 14 days the difference is 17 % and 21 % respectively. On the other hand, the strength of 28 days is not significant. A value of 8% increase in 28 days tensile strength is observed for 0.5% steel fiber addition compared to control case (0 % steel fiber addition) BAC.

3.2.3 Stress-Strain behavior

The stress-strain behavior of BAC and SFBAC has been tested for 28 days. It is observed that rupture limit of concrete with fresh brick aggregate is significantly improved for concrete with steel fiber additions. The result is around 27 % more in SFBAC compare to the control case (BAC). Since the testing machine is force controlled, the authors were unable to predict the descending branch of the stress-strain curve and are not shown in Fig.5.

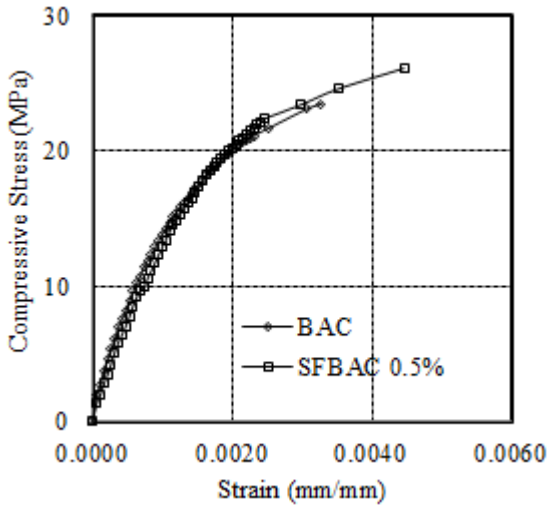

Figure 5: Stress-Strain behavior at 28 days

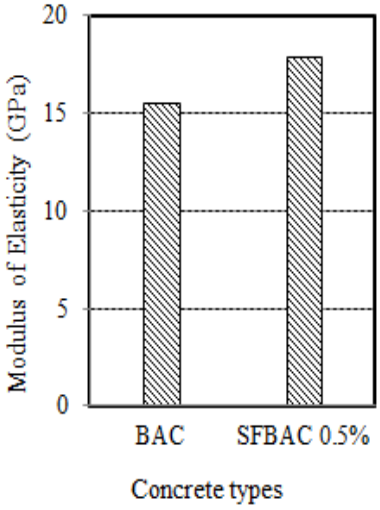

Figure 6: Modulus of elasticity 28 at days

3.2.4 Modulus of elasticity

Young's modulus of concrete for brick aggregate (BAC) is lower (about 14%) compared to the same with steel fiber reinforced brick aggregate concrete made with 0.5% addition of steel fiber at 28 days as shown in figure 6.

3.3 Failure pattern

Brittle failure is seen for the concrete made with brick aggregates (BAC). On the other hand relatively ductile failure is for the concrete made 0.5 % addition of steel fiber. Figure 7 shows the failure pattern of both concrete.

(a) (b) (c) (d)

Figure 7: Failure pattern of specimen (a) and (b) compressive and tensile strength of BAC, (c) and (d) Compressive and tensile strength of SFBAC

4 CONCLUSIONS

An experimental investigation is conducted to compare the mechanical properties of concrete made with fresh brick aggregate concrete (BAC) and concrete made with steel fiber (SFBAC). Following conclusions can be drawn from the present experimental investigation:

- Workability of steel fiber reinforced aggregate concrete (SFBAC) is relatively lower compared to that of the fresh brick aggregate concrete (BAC).
- The compressive and tensile strengths of steel fiber reinforced concrete (SFBC) at 28 days are found to be 5-10% higher than that of the fresh brick aggregate concrete (BAC).
- Modulus of elasticity of BAC (15.53 GPa) is lower in comparison to that of the SFBAC (17.92 GPa).
- Rupture strain limit of SFBAC is higher compared to that of the BAC by 25 to 30% and relatively ductile failure is seen for steel fiber reinforced concrete (SFBAC).

REFERENCES

[1] Andrzej M. Brandt, 2008.Fibre reinforced cement-based (FRC) composites after over 40 years of development in building and civil engineering, journal of composite structures, **86,** pp 3–9.

[2] Bentur A, Mindess S, 1990. Fiber reinforced cementitious composites, *Journal of Applied science*, Elsevier, UK.

[3] ACI Committee 544, 1982.State of the art report on fiber reinforced concrete. *Journal of Concrete International*.ACI 544.1R-**82**, pp 9-30.

[4] ACI Committee 544, 1993. Guide for specifying, mixing, placing and finishing steel-fiber reinforced concrete. *ACI Materials Journal*, **90(1),** pp 94-101.

[5] ACI Committee 544, 1988. Measurement of the properties of fiber reinforced concrete. *ACI Materials Journal*. **85(6),** pp 583-89.

[6]Arthur H. Nilson, David Darwin, Charles W. Dolan, 2003.*Design of Concrete Structures, 13th International Edition*, Mc Graw Hill, P 22.

CICM 2015
First International Conference on
Advances in Civil Infrastructure and Construction Materials
MIST, Dhaka, Bangladesh, 14–15 December 2015

NANOTECHNOLOGY: BRIDGING THE CRACKS BETWEEN ANCIENT AND MODERN CONCRETE TECHNOLOGY

Rishath SABRIN[1], Tanvir Manzur[2], Baishakhi Bose[3] and Rubaiya Rumman[4]

[1]Ahsanullah University of Science & Technology, Dhaka, Bangladesh.
Email: rishathsabrin@gmail.com

[2, 3, 4] Bangladesh University of Engineering & Technology, Dhaka, Bangladesh.
Email: [2]tmanzur.buet@gmail.com, [3]baishakhibose.toma@gmail.com
and[4]rubaiya.rumman@gmail.com

Abstract. *Concrete is a universal construction material in Civil Infrastructures. Versatile modern concrete technology is a challenging issue to mitigate the shortcomings of ancient concrete: low tensile strength, porosity, crack propagation with age and loading etc. Application of nanotechnology in cement-based composites creates a startling dimension in concrete technology. Decreased porosity, leading to denser microstructure and enhancement in mechanical properties create immense interest to the cement-concrete researchers. This paper reviews the effect of inclusion of carbon-nanofibers, carbon-nanotubes (CNT) in particular, on different properties of cementitious composite i.e. compressive strength, flexuralstrength, tensile strength, tensile modulus, strain, porosity, workability, and durability. The role of size, shape and dispersion of CNT on the mechanical properties of cement-based composites are also presented. It has been found that dispersion of CNT is extremely important to produce robust composites. Properly distributed CNT reinforced cementitious composites can achieve higher compressive strength as well as tensile strength as compared to plain cement mortar. This paper also sheds light on certain challenges that need to be considered while producing nanotubes reinforced cement composites.*

Keywords: Nanotechnology, Cement composites, Carbon-nanotubes, Dispersion.

1 INTRODUCTION

Structural engineering has evolved around one ubiquitous building material known as concrete. Concrete and its parent material, cement, both suffer from the same disadvantages: low tensile strength, crack propagation with age and loading. The quest to make concrete a versatile material without it being susceptible to its inherent flaws has led to the incorporation of different types of nano materials and fibers in concrete and cement paste. Utilization of different types of carbon nanotubes (CNT) has the prime focus in this regard as one of the most significant areas of research.

Carbon nanotubes can be idealized as rolled form of graphite sheets where carbon atoms are arranged in a hexagonal array. The ends are capped by a dome shaped half fullerene molecules. Normally, the elastic properties of CNT are assumed to be independent of the chirality due to the regular isotropic nature of hexagonal two-dimensional crystal. But, dislocation theory states that the strength mechanism is a function of the tube chirality [1]. Therefore, the mechanical properties of nanotubes greatly depend on the atomic arrangement of the nano structure. The atomic structure of nanotubes is defined by the tube chirality. Two limiting cases exist, i.e. ziz-zag shaped (chiral angle of 0 degree) and armchair shaped (chiral angle of 30 degrees) (Fig 1).

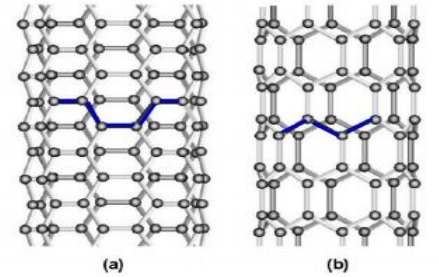

Fig 1: Illustrated atomic structure of (a) an armchair nanotube, (b) a zig-zag nanotube [2]

Carbon Nanotubes (CNT) have an average diameter ranging from <1 nm to 50 nm and an average length from 1 micron to 1 cm [3]. CNT has high aspect ratio [4], extremely high elasticity [5] and modulus [6].A single walled CNT (SWNT) looks like a single sheet rolled up into a tube, while multi-walled CNT (MWNT) looks like multiple sheets rolled into a series of tubes, one inside the other. A SWNT is typically 1-3 nm in diameter and a micrometer or more long. MWNT typically ranges in diameter from 10 to 40 nm, but has the same length as the single walled variety.

2 EFFECT OF CNT ADDITION IN CEMENTITIOUS COMPOSITES

In the 1990s, with the use of short carbon fibers in the cement mortar, an increase of 85%, 205% and 22% in flexural strength, flexural toughness and compressive strength were obtained, respectively by Chen et al. [7]. A research conducted by Li et al. [8] in 2004 showed that, the compressive and flexural strength of the cement mortar with CNT were higher than plain cement paste. Another study by the same researchers [9] in 2006 showed that the abrasive resistance of concrete improved significantly with the addition of nano-particles. The compressive and flexural strengths improved when the nano-particles content was 1% by weight of the cement. Makar et al. [10] found accelerated hydration at early age by adding SWNT. Manzur et al. [11] showed increase in compressive strength of cement mortar through addition of untreated commercial MWNT. They obtained up to 25% increase in compressive strength. A tentative optimum mix ratio for treated MWNT was proposed by them in another study in 2015[12] considering both flexural and compressive strengths of the composites. In another study, Cwirzen et al. [13] obtained 10% increment in flexural strength by MWNT reinforced cementitious composite. High early strength of cement mortar was obtained by Agullo et al. [14] through addition of MWNT in low concentration. Lelusz [15] found that compressive strength of cement composites decreased with the increase in CNT dosage. This research used different dosage rate of MWNT (0.00%; 0.06% and 0.12% by weight of cement) in powder form. Tensile strength of cement samples with CNT was found to be increased and better stress-strain relationship was observed in direct tension [16].Moreover, better tensile strength (up to 54%enhancement) was achieved through nano-fibers reinforcement. Experimental results of this research are shown in fig 2. Samples having 0.5% MWNT showed stiffer behavior, higher tensile modulus with lower strain.

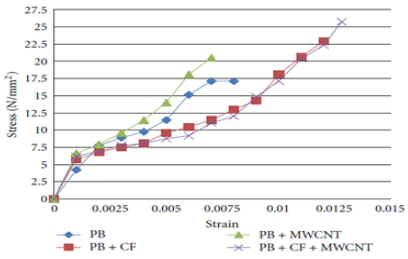

Fig 2: Stress-Strain relationship under direct tension [16].

3 EFFECT ON PHYSICAL PROPERTY OF CNT

The physical properties of CNT also have effect on behavior of CNT reinforced cement composites. The effect of various nanotubes size was investigated by Manzur et al. [17] based on compressive strengths of composites. It was found that MWNT with OD (outside diameter) 20 nm or less obtained similar compressive strengths, with the highest compressive strength being achieved by the smallest size of MWNT (OD smaller than 8nm). The fracture characteristics and early strain capacity of CNT cement composites were investigated by Metaxa et al. [18]. The results showed that the CNT of longer lengths in smaller quantities (0.025 – 0.048%) and shorter lengths in higher quantities (0.08%) could achieve good dispersions and eventually robust composites. Nano indentation results indicated that the CNT composites had higher stiffness and less porosity. This reduction of pores led to significant effect on the early strain capacity of composites.

4 EFFECT OF WATER CONTENT ON CNT-CEMENT COMPOSITES

Due to extremely high surface area, CNT tends to adhere more water and consequently decreases the workability of mixes. Therefore, water content often plays a vital role in preparing CNT-cement composites. Yazdani et al. [19] found that the 0.4 w/c ratio yielded the maximum compressive strengths for control samples. But the major difficulty associated with CNT-cement composites having lower w/c ratio was the workability. They observed that higher water cement ratio of 0.50 exhibited higher compressive as well as flexural strength for both 0.1% and 0.2% CNT reinforced mortar samples. Manzur et al.[11] also found that water cement ratio of 0.60 resulted in higher compressive strength with untreated MWNT and without any plasticizer as surfactant.

5 EFFECT ON DURABILITY

Cementitious materials are typically characterized as quasi-brittle and susceptible to cracking. Strength, ductility, creep, shrinkage, and fracture behavior of cementitious construction materials greatly depend on the micro- and nano- scale formation of the material. Considerable improvement in restricting cracks in cementitious matrices was observed by addition of CNT [20]. Due to small size of CNT, they will reduce the amount of fine pores which leads to the reduction of the capillary stresses, resulting in lower autogenous shrinkage. Hence, CNT reinforced matrix would reduce the length and width of crack in concrete and it is expected to produce significantly stronger and tougher composites than traditional reinforcing materials. Porosity of cement-composite can also be reduced by adding CNT [21, 22]. Thus, promises are being envisaged in CNT reinforced matrix for the next-generation ultra high performance and multi-

functional cement-based materials and structures [23]. Crack bridging effect can be ensured through CNT addition [12] which in turn assures lower crack widths and guarantees the load transfer across voids and cracks. Hence, it is evident that CNT has extremely high prospect as reinforcement for cement composites.

6 ROLE OF DISPERSION

Dispersion of CNT in the cement matrix possesses the major challenge when dealing with high performance cementitious composites. To achieve the desired level of reinforcement within the cement matrix, proper dispersion of CNT is required. Uniform dispersion is essential for ensuring bridging effect across cracks which can be observed by SEM images. In Fig 3,SEM images that show the crack bridging effect and uniform dispersion of CNT within cement matrix are shown. Researchers adopted different approaches for dispersing CNT and found different results. Yu et al. [24] suggested acid treated CNT are more soluble than pristine CNT; Saez et al. [25] used gum Arabic as a dispersing agent; water dispersions was done by Makar et al. [10] and Konsta et al. [26] and; Yazdanbakhsh et al. [27] and Gay et al. [28] used polycarboxylate based water reducing agent as surfactant for dispersion. Different solvents (ethanol, toluene, chloroform) were used via sonication by Li et al. [22, 29]; a polycarboxylate based super plasticizer and methylcellulose was used by Wansom et al. [30] whereas Cwirzen et al. [13] used polyacrylic acid. In all dispersion techniques ultrasonic vibration was applied since extremely high Van der Waals forces resulting from large surface area of CNT causes them to adhere together. The ultrasonication method is capable of producing required energy to break the agglomeration of CNT. Though, there is no direct measurement of quality of dispersion of CNT within cement matrix, in most cases SEM images have been used. However, SEM images require sophisticated and high cost equipment and can only provide information about a small region. A simpler technique has been suggested by Manzur et al. [31] that employs flow values of the mixes.

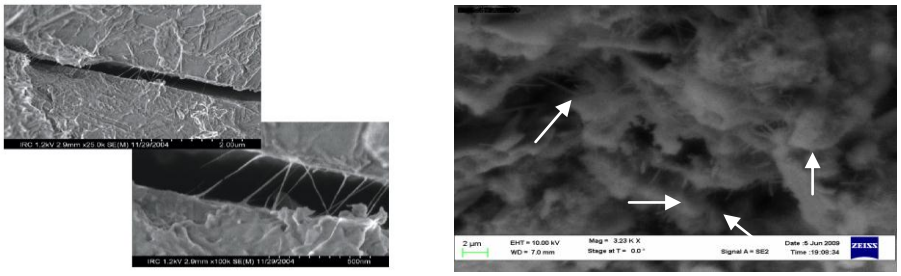

(a) (b)

Fig 3: SEM image of crack bridging effect (a) [10] and uniform dispersion of MWNT (b) [32] within nanotube reinforced cement paste

REFERENCES

[1] A. Todoroki, M. Tanaka and Y. Shimamura, 2005. "Electrical Resistance Change Method for Monitoring Delamination of CFRP laminates: Effect of Spacing between Electrodes" Compos. Sci. Technol., 65, 37-46.

[2] E. T. Thostenson, Z. F. Ren and T. W. Chou, 2001. "Advances in the science and technology of carbon nanotubes and their composites a review" Compos. Sci. Technol., 61, 1899–1912.

[3] American Society for Standard Testing and Materials (ASTM), (2011a), "Standard Test Method for Flexural Strength of Hydraulic-Cement Mortars." ASTM C348-08.

[4] Zheng, L. X., O'Connell, M. J., Doorn, S. K., Liao, X. Z., Zhao, Y. H., Akhadov, E. A., Hoffbauer, M. A., Roop, B. J., Jia, Q. X., Dye, R. C., Peterson, D. E., Huang, S. M., Liu, J. and Zhu, Y. T., 2004. "Ultra long single-wall carbon nanotubes." Nature Materials, 3, 673-676.

[5] Yu, M.F., Files, B.S., Arepaali, S., and Ruoff, R.S., 2000. "Tensile Loading of Ropes of Single Wall Carbon Nanotubes and Their Mechanical Properties." Phys. Ref. Lett., 84 (24), 5552-5555.

[6] Salvetat, J.-P., Bonard, J.-M., Thomson, N. H., Kulik, A. J., Forró, L., Benoit, W., and Zuppiroli, L., 1999. "Mechanical Properties of Carbon Nanotubes." Applied Physics A., 69, 255-260.

[7] Chen, P. W., and Chung, D. D. L., 1993. Concrete reinforced with up to 0.2% volume of short carbon fibres. Composites, 24(1), 33-52.

[8] Li, H., Xiao, H. G., Yuan, J., and Ou, J., 2004. Microstructure of cement mortar with nano-particles. Composites Part B: Engineering, 35(2), 185-189.

[9] Li, H., Zhang, M. H., and Ou, J. P., 2006. "Abrasion resistance of concrete containing nano-particles for pavement",Wear,260(11), 1262-1266.

[10] Makar, J., Margeson, J. and Luh, J., 2005. "Carbon Nanotube/Cement Composites-Early Results and Potential Application", Proceedings of the 3rd International Conference on Construction Materials: Performance, Innovations and Structural Implications, Vancouver, B.C., August 2005, 1-10.

[11] Manzur, T., and Yazdani, N., 2010. "Strength Enhancement of Cement Mortar with Carbon Nanotubes: Early Results and Potential." Journal of the Transportation Research Board, No. 2142, 102-108.

[12] Manzur, T., and Yazdani, N., 2015. "Optimum Mix Ratio for Carbon Nanotubes in Cement Mortar." KSCE Journal of Civil Engineering,19(5), 1405-1412.

[13] Cwirzen, A. Habermehl-Chirzen, K. &Penttala, V.,2008."Surface Decoration of Carbon Nanotubes and Mechanical Properties of Cement/Carbon Nanotube Composites", Adv. Cem. Res., 20 (2) 65–73.

[14] Agullo, V. J., Ligero, V. C., Rico, D. P., Casas, M. J. G., Martinez. A. G., Royo, J. M. M., and Moreno, J. G., 2009. "Mortar and Concrete Reinforced with Nanomaterials." Nanotechnology in Construction 3, 383-388.

[15] MałgorzataLelusz, 2014. "Carbon Nanotubes Influence on The Compressive Strength of Cement Composites", Technical Transactions, Civil Engineering; 1-B/2014.

[16] M. Hunashyal, Sagar, V. Tippa, S. S. Quadri and N. R. Banapurmath, 2011. "Experimental Investigation on Effect of Carbon Nanotubes and Carbon Fibres on the Behavior of Plain Cement Mortar Composite Round Bars under Direct Tension", *International Scholarly Research Network; ISRN Nanotechnology*, Volume **2011**, Article ID 856849, 6 pages.

[17] Manzur, T., Yazdani, N., andEmon, MAB., 2014. "Effect of Carbon Nanotube Size on Compressive Strengths of Nanotube Reinforced Cementitious Composites", *Journal of Materials*, Volume **2014**, Article ID 960984, 8 pages.

[18] Metaxa, Z.S., Konsta-Gdoutos, M.S. and Shah, S.P., 2009. "Carbon Nanotubes Reinforced Concrete", *ACI Special Publication 267: Nanotechnology of Concrete: The Next Big Thing is Small***SP-267-2**, 11-20.

[19] Yazdani, N., andMohanam, V.,2014. "Carbon Nano-Tube and Nano-Fiber in Cement Mortar: Effect of Dosage Rate and Water-Cement Ratio", International *Journal of Material Science (IJMSCI),***4(2),** 45-52.

[20] Z. Xia, L. Riesterb, W. A. Curtin, H. Lia, B. W. Sheldona, J. Lianga, B. Changa and J. M. Xua, 2004. "Direct observation of toughening mechanisms in carbon nanotube ceramic matrix composites" *Acta Mater.*,**52 (4),** 931-944.

[21] Nochaiya T, Chaipanich A., 2011. "Behavior of multi-walled carbon nanotubes on the porosity and microstructure of cement-based materials", *Appl Surf Sci,***257(6),** 1941–1945.

[22] G. Y. Li, P. M. Wang, and X. Zhao, 2005. "Mechanical Behavior and Microstructure of Cement Composites Incorporating Surface Treated Multi-Walled Carbon Nanotubes," *Carbon*, **43(6),** 1239–1245.

[23] S. Sasmal, B. Bhuvaneshwari and N. R. Iyer, 2013. "Can Carbon Nanotubes Make Wonders in Civil/Structural Engineering?" *Progress in Nanotechnology and Nanomaterials*,**2(4),**117-129.

[24] Yu, X., & Kwon, E. A., 2009. "Carbon Nanotube/Cement Composite withPiezoresistive Properties", *Smart Materials and Structures*, **18,** 1-5.

[25] Saez de Ibarra, Y., Gaitero, J. J. E. &Campillo, Erkizia, 2006. "Atomic Force Microscopy and Nanoindentation of Cement Pastes with Nanotube Dispersions", *Physica Status Solidi* (a),**203 (6),** 1076–1081.

[26] M.S.Konsta-Gdoutos, Z. S. Metaxa, and S. P. Shah, 2010. "Multiscale Mechanical and Fracture Characteristics and Early-Age Strain Capacity of High Performance Carbon Nanotube/Cement Nanocomposites", *Cement and Concrete Composites,* **32(2),** 110–115.

[27] Yazdanbakhsh, A., Grasley, Z., Tyson, B., and Abu Al-Rub, R. K. (2010). "Distribution of Carbon Nanofibers and Nanotubes in Cementitious Composites." *Journal of the Transportation Research Board*, No. **2142**, 89-95.

[28] Gay, C., and Sanchez, F., 2010. "Performance of Carbon Nanofiber-Cement Composites with a High-Range Water Reducer." *Journal of the Transportation Research Board*, No. **2142**, 109-113.

[29] G.Y. Li, P.M. Wang, &X. Zhao, 2007. "Pressure-Sensitive and Microstructure of Carbon Nanotube Reinforced Cement Composites", *Cem. andConcr. Comp*. **29 (5),** 377-382.

[30] Wansom, S. Kidner, N.J. Woo,L.Y. & Mason, T.O., 2006. "AC-Impedance Response of Multiwalled Carbon Nanotube/Cement Composites", *Cem. andConcr. Comp.* **28 (6),** 509–519.

[31] Manzur, T. and Yazdani, N., 2013. "Importance of Flow Values in Qualitative Evaluation of Carbon Nanotube Reinforced Cementitous Matrix." *Malaysian Journal of Civil Engineering*,**25(1),**71-80.

[32] Manzur, T., 2011. "Nano-modified cement composites and its applicability as concrete repair material"(Doctoral thesis), University of Texas at Arlington, Texas, USA.

CICM 2015
First International Conference on
Advances in Civil Infrastructure and Construction Materials
MIST, Dhaka, Bangladesh, 14–15 December 2015

APPLICATION OF POLYMER IN THE FIELD OF CONSTRUCTION: HIGH STRENGTH ACHIEVEMENT AND RETROFITTING POTENTIALITY

Atanu PRAMANIK[1], Ahmad M. Ali[2] and Alamgir Habib[3]

[1, 2, 3] Military Institute of Science and Technology, Dhaka, Bangladesh
Email: [1]pramanik.avi38@gmail.com,[2]tonmoymojtaba@gmail.com and [3]ahabib@uap-bd.edu

Abstract. *This paper will address the issue of polymer incorporation with mortar and concrete for amelioration of compressive strength. It was explored that partial replacement of Polyester polymer in conventional mortar on a weight basis of 6,8 and 10% enhanced its capacity about 1.25 times within 28 days but notably complete replacement (both epoxy and polyester) enhanced compressive strength up to about 2.25 times of conventional cement mortar within a curing period of only 3 days. Later SEM images are illustrated to represent the propagation of micro cracks in polymer mortar after application of compressive load as the external structure posed an undisturbed configuration. Polymer concrete using Epoxy as a single binder within the range of 12~25% weight basis mixture specimens surpassed the limit of compressive strength of 60 MPa within only one week of curing period. Later 20% weight basis incorporation with further modification by fly ash as micro filler established the landmark above 80 MPa within a curing period of 28 days. Therefore this investigation accentuates the utilization of Polymer in the field of retrofitting due to superior performance by rendering succinct curing period and enhancing structural strength.*

Keywords: Polymer cement mortar (PCM) and Polymer mortar (PM), Polymer concrete (PC), Microstructure analysis, Micro filler, High strength performance, Retrofitting potentiality.

1 INTRODUCTION

Polymer is a promising construction material showing its versatilities for binding and repairmen of concrete structures. Polymer materials possess some superior properties like rapid curing, high compressive strength, high specific stiffness and strength resistance to chemicals and corrosion, ability to form complex shapes, excellent vibration damping properties and so forth, Bedi et al. [3].Owing to these superior properties, polymer has become a study of interest of many researchers. Polymer modification of mortars and concrete increases the toughness, tensile and bending properties, Razl [6]. An interesting remark was concluded by Rahman and Islam [5] in their research paper showing that the addition of epoxy to cement mortars improved compressive, tensile and flexural strength while not reducing the porosity, chloride ion penetration and coefficient of thermal expansion [5]. Regarding mechanical properties, same analysis was accomplished by Aggarwal et al. [1] using epoxy and acrylic emulsion in Polymer Modified Mortars [1].

Barbuta and Harja (2008) reported that mortar incorporating with polymer show good mechanical properties required for repair works [2]. After reviewing several papers Kardon (1997), concluded that the combination of Portland Cement Concrete or mortar with polymers can result in extremely durable, tough and strong eco-friendly building material [4].

The current study will address the investigation on the mechanical properties of polymer incorporated mortar and concrete specimens facilitating the way of application of polymer to achieve high strength and retrofitting capability.

2 OBJECTIVE OF THE RESEARCH

The prime objectives of this research work are categorized as-

- To overcome the drawback factors regarding high strength gain of Portland Cement Concrete with the replacement of Polymer Concrete in construction industry.
- To emphasize on the retrofitting potentiality of Polymer incorporated mortar by evaluating the strength gain rate in comparison to conventional cement mortar.

3 EXPERIMENTAL INVESTIGATION

This session is fully decorated in details to present the undertaken investigation program of polymer associated mortar and concrete regarding mechanical strength and morphological analysis.

3.1 Materials

3.1.1 Cement

In this research work Portland Composite Cement (PCC) is used as the binding material. The cement used is fresh and without any lumps. The specific gravity is found to be 3.15.Normal Consistency is measured as30% having Initial and Final Setting time of 128 and 215 minutes.

3.1.2 Polymer and hardener

In this research program two distinct polymer naming Epoxy and Polyester resin were used. It is to be noted that Polyester was used only for mortars. Specific gravity of Epoxy and Polyester is reported to be 1.16 and 1.102 by manufacturers. Triethylenetetramine is used as hardener for both mortar and concrete associated with polymer to accelerate the setting of polymer.

3.1.3 Aggregates

For fine aggregates, two categorized locally available well graded sand with different properties passing through 4.75 mm sieve are used. On the other hand, crushed stone chips having two maximum sizes of 19mm and 12.5 mm are used for this research work. All the properties are enlisted in the Table1.
Table 1: Properties of aggregate

Type of aggregate		F.M.	Specific Gravity	Abrasion value (%)
Fine Aggregate	Sylhet sand	2.32	2.60	-
	Local Coarse sand	3.50	2.62	-
Coarse Aggregate	19 mm downgraded	8.94	2.63	22
	12.5 mm downgraded	7.59	2.58	29

3.1.4 Fly ash

In this research work, Class C fly ash of having specific gravity 2.65 was used as micro filler in polymer concrete to reduce permeability and improve mechanical strength.

3.2 Sample Preparation

3.2.1 Mortar specimens

The components of conventional cement mortar composition are mixed by a method and technique as prescribed by ASTM C305. For Polymer Cement Mor-

tar (PCM), hardener mixed with resin were added to the pre-wetted cement and sand mixture where for Polymer Mortar (PM), hardener mixed with resin were added to the calculated amount sand in absence of water. For compressive strength of mortar, specimen's size was maintained as 50.8X50.8X50.8mm cubic format. The mortar specimens were separated out from the mold after 24 hours of molding. Mortars with cement in its composition (CM and PCM) were kept in water for 3-28 days for curing and PM specimens were left to atmosphere for 28 days. It is to be noted that Ottawa Sand was used as F.A. in the preparation of Cement Mortar only.

Table 2: Ratio of ingredients used in mortar

Mortar type		Cement	F.A.*	W/C*	Resin
Portland Cement Mortar		1	2.75	.485	-
Polymer Cement Mortar		1	2.75	.40	Epoxy used as 6~10% of total weight of (Cement +F.A.)
Polymer Mortar	Polyester	-	1	-	.25
	Epoxy	-	1	-	.25

*F.A. indicates Fine Aggregate and W/C indicates Water to Cement ratio

3.2.2 Concrete specimens

The components of conventional concrete composition were mixed by a method and technique as prescribed by ASTM C305 but for Polymer Concrete (PC) a few modifications were adopted. For PC specimens, Sand and Coarse aggregate were put together in the mixing bowl and then calculated amount Epoxy resin blended with hardener were poured in the bowl and was mixed .

Table 3: Mix Ratio for Concrete

Concrete Type	Cement	F.A.*	C.A.*	W/C ratio	Epoxy Resin
Portland Cement Concrete	1	2	4	0.45	-
Polymer Concrete	-	10	20	-	12~25% weight of (F.A.+C.A)

*F.A. indicates Fine Aggregate and C.A. indicates Coarse Aggregate

For Polymer Concrete (PC) several trials were done with varying composi-tions.

Table 4: Different Trial Mixing for Polymer Concrete (PC)

Trial ID	Trial 1	Trial 2	Trial 3	Trial 4	Trial 5	Trial 6	Trial 7	Trial 8	Trial 9
Fine Aggregate.	F.M. 2.32	F.M. 2.32	F.M. 2.32	F.M. 3.50	F.M. 3.50	F.M. 3.50	F.M. 2.32	F.M. 2.32	F.M. 2.32
Coarse Aggregate	19 mm down grade	19 mm down grade	12.5 mm down grade	12.5 mm down grade	12.5 mm down grade	12.5 mm down grade	12.5 mm down grade	12.5 mm down grade	12.5 mm down grade
Polymer (Weight Basis)	12%	15%	12%	15%	20%	25%	15%	17%	20%
Fly ash (% weight of F.A.)	Nil	Nil	Nil	Nil	Nil	Nil	15 %	15%	15%

The dimension of concrete cylinders was chosen as 100mm in diameter and 200mm in height. The concrete specimens were separated out from the mold after 24 hours of molding and PCC specimens were kept in water for 7-28 days for curing while PC specimens were left to atmosphere for air drying. The dosages of resin content in Polymer Concrete reported by previous researchers lie between 12~20% in weight basis, Bedi et al. 2013[3]. So this research work sets the limit between 12~25% in weight basis.

3.3 Methods

Compressive strength of masonry mortar and concrete specimens were measured according to standard test method of ASTM C 109 and ASTM C 39.Note that, as there is no code available for polymer specimens and so ASTM general codes were applied to them.

4 RESULT AND DISCUSSION

4.1 Result Analysis of Mortar Specimens

The experimental results were analyzed on 3, 7 and 28 days curing period. The results analysis showed that Polymer Mortars (both Epoxy and Polyester) showed their superiority over other specimens. Where Polymer Cement Mortar (6, 8 and 10% weight basis epoxy) achieved 30% higher strength on an average than Conventional Cement Mortar with respect to 28 days curing period, Polymer Mortar surpassed 1.5 more times of that value within only a 3 days of curing period. This achievement ensures the pertinence of Polymer Mortar in achieving

high strength for repairmen and retrofitting possibility of RCC structures within a succinct curing period.

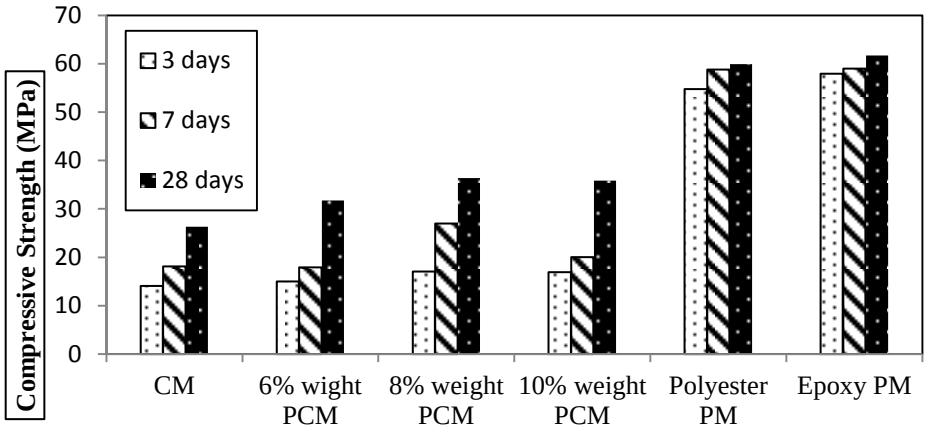

Figure 1: Comparison of compressive strength of mortar specimens

The choice of resin between Epoxy and Polyester is another issue Bedi et al. [3] reported their preference to Epoxy over Polyester because of its better mechanical properties as well as better durability when subjected to harsh environment if higher cost is not a deterrent [3]. From analysis of compressive strength presented in this paper, this preference is hard to crack as investigation on durability is missing. But based on a slight increment of strength issue, Epoxy wins over Polyester to make it a preferable choice.

4.2 Result Analysis of Concrete Specimens

The results of compressive strength were analyzed on 3,7 and 28 days for PCC specimens but for PC specimens only Trial-9 experienced the standard curing period of 28 days while others were tested on 3 and 7 days only. The results are delineated in Fig 2. A large contact area molds into a proper space filling of the gaps by smaller aggregates, Bedi et al. [3]**.** For this reason Trial-1 and Trial-2 experienced the lowest strength in comparison to others as the specimens were manufactured with 19mm downgraded aggregate which tend to be weaker in providing a compact structure.

The problems encountered with 19 mm downgraded aggregates were mitigated by using 12.5 mm downgraded aggregates and better results were achieved with Trial 3, 4, 5, 6, 7, 8 and 9. The results comparison presented that compressive strength maintained a level around 65 MPa for Polymer Concrete at Trial-3 on 7 days curing period but when Fly ash was introduced as micro filler then it boosted up to 81MPa for Trial-9 on 28 days curing period.

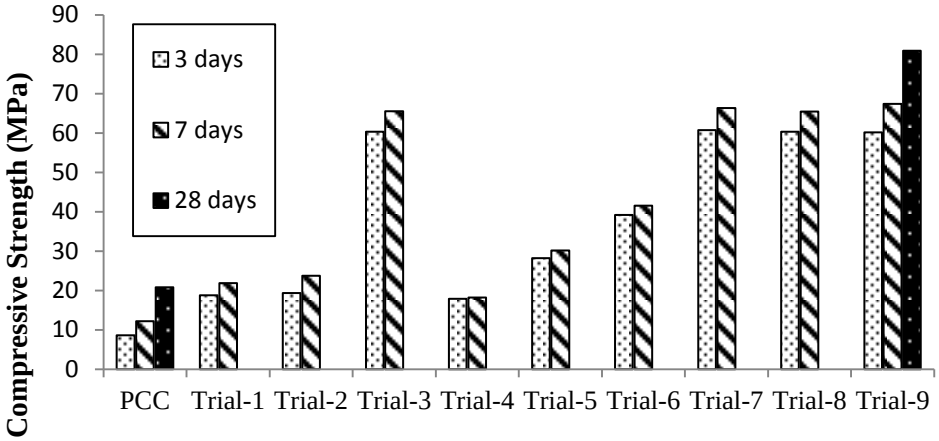

Figure 2: Comparison in compressive strength between PCC and 9 trials of PC specimens

This is because Fly ash seals the voids of porous concrete structure and provides adhesion between polymer and aggregates. Introduction of 15% Fly ash enhances 30% strength which is confirmed by Trial-7, 8 and 9 [3]. Also increase in resin content continues with higher strength with an interruption for Trial-4, 5, and 6 and this may be due to erroneous calculation or usage of fine aggregate with high F.M. which failed to provide strong interaction with coarse aggregate.

4.3 Microstructure Analysis of Polymer Mortar Specimen

Mortar samples have been cut with cutting equipment into specified size (2 mm × 2 mm) required for scanning. Figure 3 (i) demonstrates the microstructure of cut surface of Polymer Mortar specimen, prepared with 25 weight percentage epoxy resin of total weight. Cross-linked epoxy resin network is developed through curing reactions and whole products are encapsulated with the resin network. Encapsulation of matrixes with the cross-linked resin provides early strength development, filling capability and higher toughness properties to the Polymer Mortar structure.

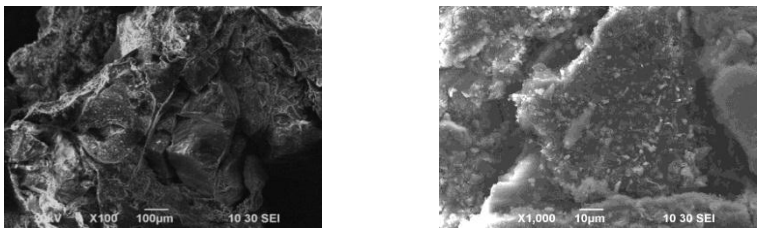

i) ii)

Figure 3: SEM images of i) Before Failure and ii) After Failure of Epoxy

Polymer Mortar Specimen

On the other hand, Figure 3 (ii) demonstrates the condition of polymer bond after failure. Though the external structure posed a certain amount settlement, the internal structure represents cracking of polymeric chain creating voids.

5 OUTCOME OF THE RESEARCH WORK

The outcomes of this research work are summarized as follows.

- For a specific composition of Polymer Concrete, the polymer content determines the strength of specimen.
- Increasing Polymer content in polymer incorporated mortars facilitates the workability but hampers the compaction.
- A large contact area seals the voids to ensure high strength and that's way 12.5 mm downgraded aggregate is preferable to 19 mm downgraded aggregate. Further modification with the use of Fly ash provided better results due to less porous compact structure.
- Initial Setting Time & Workability of Polymer Concrete are dependent on the dosages of Hardener added in concrete. Both these properties are inversely proportional to the dosages of hardener.
- Strength gain is high and rapid for polymer concrete and polymer mortar, which makes the composition suitable for rapid setting structural element as well as rapid curing. Also these features ensure retrofitting compatibility of polymer.

6 CONCLUSIONS

Polymer incorporated materials are a very promising group of new building materials. It should be used only in applications in which the higher cost can be justified by superior properties, low labor cost and energy requirements during processing and handling. The versatile applications of polymer incorporated mortar and concrete are to be explored in decades ahead. It might be the greatest development in the area of constructional rehabilitation if proper research is done.

REFERENCES

[1] Aggarwal, L. K., Thapliyal, P.C. and Karade, S. R., 2007. Properties of Polymer modified mortars using epoxy and acrylic emulsion, Journal of Construction and Building Materials.

[2] Barbuta,M., and Harja,M., 2008. Experimental Study on the Charateristics of Polymer Concrete with Epoxy Resin.

[3] Bedi, R., Chandra, R. and Singh, S.P., 2013. Mechanical Properties of Polymer Concrete.

[4] Kardon, J., B., 1997. Polymer-Modified Concrete: Review.

[5] Rahman, M., M., Islam, M., A., 2012.Effect of epoxy resin on the intrinsic properties of masonry mortars.

[6] Razl, I., Flexible Polymer-Cement Repair Materials and Their Applications.

CICM 2015
First International Conference on
Advances in Civil Infrastructure and ConstructionMaterials
MIST, Dhaka, Bangladesh, 14–15December 2015

INVESTIGATION OF SETTING BEHAVIOUR AND COMPRESSIVE STRENGTH OF MINING COAL BOTTOM ASH BLENDED CEMENT

M. R. KARIM[1], H. A. Razak[2], M. A. Rahman[3] and S. Yusoff[4]

[1, 2, 4] University of Malaya, Kualalumpur, Malaysia.
Email: [1]mrkakanda@siswa.edu.my, [2]hashim@um.edu.my, [4]sumiani@um.edu.my

[3] Shahjalal University of Science and Technology,Sylhet, Bangladesh.
Email: [3]monju_asad@yahoo.com

Abstract.*Theunused abundant generation of mining coal bottom ash (MCBA) as an industrial by-product from power plant causes the earth and environmental-pollution. The aim of this study is to analyze elemental composition, physical properties,morphology of mining coal bottom ash powder (MCBAP) and investigate the compressive strength and setting behaviour of mining coal bottom ash powder blended cement (MCBAPC).The elemental composition and morphology were observed using X-ray fluorescence (XRF) and Scanning electron microscopy (SEM) techniques, respectively. ASTM standard methods were used to observe setting time and water for normal consistency.The compressive strength of MCBAPC was explored with water to cement ratio of 0.40 and cement to sand ratio of 0.50.In this experiment, the ordinary portland cement (OPC) was replaced by MCBAP up to 60% by weight. Result found that the setting time and water demand increase, but compressive strength decreases with replacement level. Moreover, the compressive strength development rate of curing age 7 to 28 days is lower with respect of curing age 28 to 90 days. Rigorous reckoning found that the MCBAP is feasible to use in blended cement.*

Keywords: Mining coal bottom ash powder, Setting time, Blended cement, Compressive strength.

1 INTRODUCTION

Rapid industrialization and urban development lead to increase the consumption of power , and the generation of mining coal bottom ash (MCBA) waste residue has increased drastically all over the world [1]. In present practice, land filling is the only way to dispose MCBA waste that change the composition of soil and also contaminate ground water. Safe treatment and sustainable reuse of mining coal bottom ash powder (MCBAP) waste has become a society, environmental and economic problems that need to be resolved urgently.The suitability for utilization MCBAP in blended cement depends onits' chemical ,Physical, mineralogical and morphology properties [2]. The chemical composition of MCBAP is similar with fly ash of the coal burning power plant. Moreover, there has some sort of difference both in chemical and physical composition of MCBAP and fly ash. Usually, MCBAPis denser and coarser than fly ash particles [3].

The physical properties, chemical composition, mineralogy and morphology of bottom ash depends on the sources from where it is produced, burning condition, geological condition of the area where coal is generated [4]. The chemical composition of Malaysian coal bottom ash mainly SiO_2(58-67%) with Al_2O_3, Fe_2O_3 and MgO. XRD observation found that quartz and mulliteare main mineral present in coal bottom ash and amorphisityhalo present in the two theta angle in range 10-30°. The coal bottom ash haspozzolanicacitivity, but not so strong as like as fly ash. Moreover, slag and fly ash is an industrial by product which widely used for composite cement production in industrial scale [5],[6]. The coal bottom ash reduces compressive strength at an early age, but increase at later age due to formation of more C-S-H gel by pozzolanic reaction. The presence of bottom ash particle in between two active cement particle retards the hydration reaction rate. As result setting time of blended cement comparatively higher than corresponding OPC paste.The target of this work is to analyzethechemical and morphological characterization of MCBAP and suitability in term of compressive strength, setting time and water consistency to use in blended cement. This knowledge could be adventitious for utilization MCBAP in composite cement production at industrial level.

2 MATERILAS & METHODS

The MCBA(Figure 1a) was collected from a local power plant in Kuala Lumpur, Malaysia. The raw MCBA was dried and grinded for 8 hours in a ball mill of 150 rpm to achieve MCBAP (Figure 1b). The chemical composition and morphology of MCBAP were analyzed through XRF (Table 1) and SEM (Figure 2), respectively. The specific gravity, loss of ignition, specific surface area, water consistency and setting time were determined according to ASTM C118-15, ASTM C114-15,ASTM C204-14, ASTM C191-13, respectively.The type of OPC, bind-

er/sand ratio, and water/binder ratio were kept constant as CEM I 42.5 N, 0.50 and 0.40, respectively. The superplasticizer (SP) was used to maintain mortar flow 170±10 mm. The ASTM C778 standard graded sandswere used.The MCBAP based blended cements as designated in this article as MCBAP-10, MCBAP-20, MCBAP-30, MCBAP-40, MCBAP-50 and MCBAP-60, were prepared with a replacement of OPC of 10, 20, 30, 40, 50& 60% blending in a control ball mill.Blended cement and sand were mixed properly following two minutes with water and then another two minutes with SP. The mortar flow was measured according to ASTM C1437-13. Eighteen numbers of 50x50x50 mm^3 cubes were casted for each blended cement mortar. The specimens were demoulded after 24 hours and cured in water at a controlled room temperature and humidity of 27 ± 3°C and 65 ± 18%, respectively. The compressive strength of mortar was tested at the age of 1, 3, 7, 28, 56 and 90days according to ASTM C209-15.

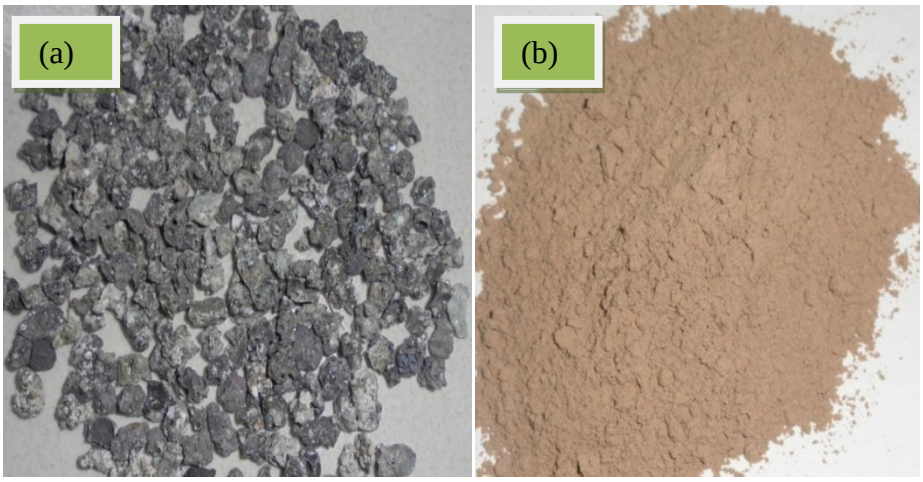

Figure 1: (a) MCBA stone(b) MCBAP collected from a power plant

3 RESULTS& DISCUSSION

3.1 Chemical and Morphological Analysis

The common physical and chemical properties of OPC and MCBAP are illustrated in the Table 1.

The SiO_2 is the main ingredient with Al_2O_3, Fe_2O_3, MgO of MCBAP. The total percentage of SiO_2, Al_2O_3 and Fe_2O_3 was 86.09 %. It is good for low calcium pozzolanic materials. The LOI of MCBAP is higher than OPC due to the incomplete burning coal in power plants. The specific gravity of MCBAP (1.87) was lower than OPC (3.15). This low value specific gravity is mainly due to hollow particle such as micro pore significantly present in MCBAP.

Table 1: Physical and Chemical Compositions of OPC and MCBAP

Parameter	OPC	MCBAP
SiO_2(%)	20.65	51.32
Al_2O_3(%)	5.10	28. 46
MgO(%)	1.47	0.30
Fe_2O_3(%)	2.29	6.31
CaO(%)	64.19	1.37
K_2O(%)	0.21	2.20
TiO_2(%)	0.11	0.69
SO_3(%)	3.48	0
Specific gravity	3.15	1.87
Fineness (m^2/kg)	404	429
LOI (%)	0.89	2.86

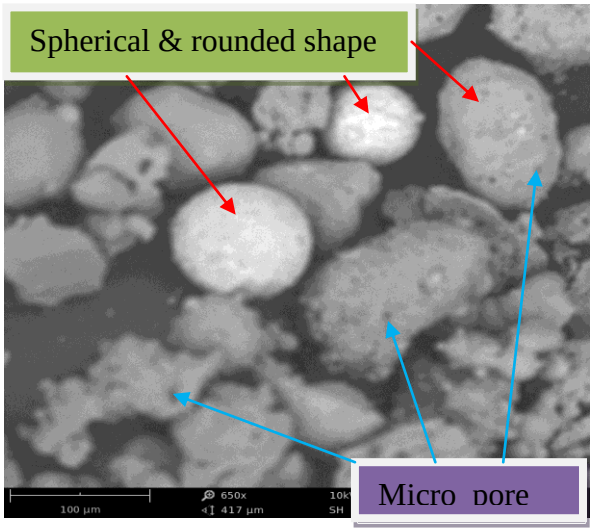

Figure 2: Micrograph of MCBAP

The SEM micrograph of MCBAP in Figure 2 shows thatboth spherical and rounded particles present [7]. The MCBAP contains micro pore. Small pore was formed in the combustion process of power plant. The black color of MCBAP is due to incomplete burning of mining coal. The chemical composition, burning condition and unburned carbon are responsible for irregular shape and porosity.

3.2 Investigation of Setting Time and Water for Normal Consistency

The rheological properties studies focused on the water demand for normal consistency. The water demand for the normal consistency of OPC and MCBAPC are represented in Figure 3. The water demand in MCBAPC increase with the

replacement level of OPC. The free bulk water is to fill interspaces among micro pore of MCBAP more compare with OPC.The initial and final setting time of OPC and MCBAPC are shown in the Figure 4. Both of the IST and FST of MCBAPC significantly increases with replacement of OPC by MCBAP.The percentage of active OPC clinker phase such as C_2S, C_3S and C_3A decrease due to dilution effect and MCBAP particle take place between two active cement particles, both of the factors are responsible to decrese the hydration reaction rate[8].

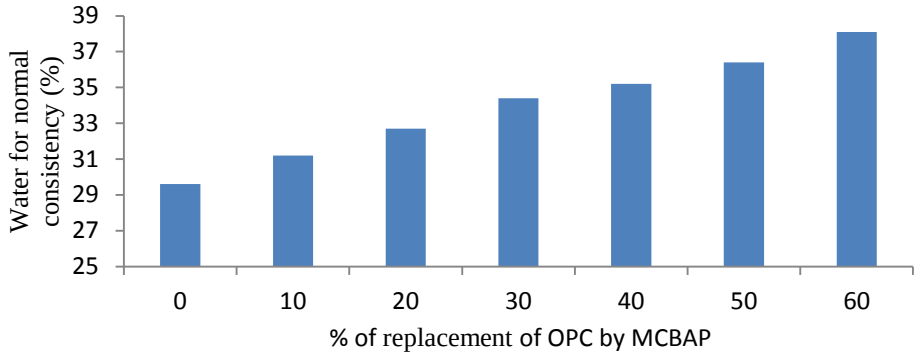

Figure 3: Water demand of MCBAPC and OPC

3.3 Effect of MCBA in Strength Development

The compressive strength of OPC and MCBAPC mortars are shown in Figure 5. From the figure, the compressive strength of the MCBAPC mortars increase with curing time, but decrease with the increment of the replacement level.

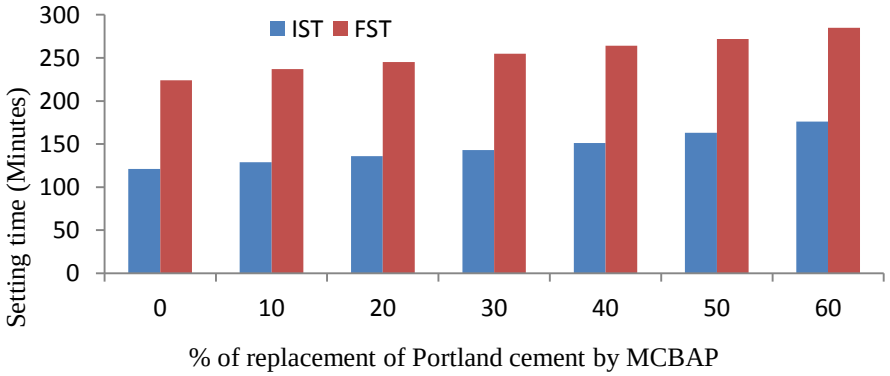

Figure 4: Setting time of OPC and MCBABC (IST-Initial setting time, FST-final setting time)

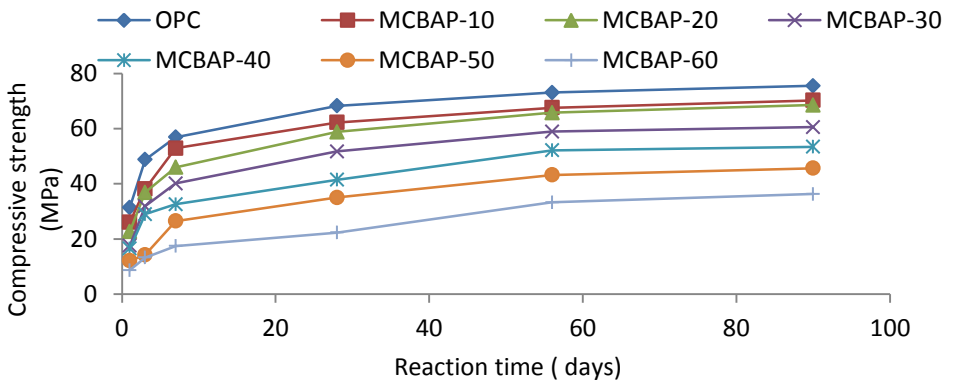

Figure 5: Variation of compressive strength with reaction time

The compressive strength developing rate of the blended cement mortar depends on factors such the hydration reaction rate, nucleation effect, packing effect and pozzolanic reaction. The compressive strengths of MCBAPC lower than OPC because of the low content active phase C_2S, C_3S and C_3A present in the MCBAPC[2]. Active phases cannot producesuficient calcium silicate hydrate (C–S–H) polymeric layer like OPC in the presence of water for strength development [6]. The compressive strength developing rate could be calculated by using the following equation stated below.

$$CSDR_{7\text{-}28} = \frac{(CS28D - CS7D)}{CS7D} \text{ X } 100 \quad (1)$$

$$CSDR_{28\text{-}90} = \frac{(CS90D - CS28D)}{CS28D} \text{ X } 100 \quad (2)$$

where, $CSDR_{7\text{-}28,}$ $CSDR_{28\text{-}90}$ indicate the rate of strength development from 7 to 28 days and 28 to 90 days, respectively. And CS7D, CS28D and CS90D denoted that the compressive strength mortar of 7, 28, 90 day, respectively. Figure 6 shows that the percentage of MCBAP addition in OPC accelerate the$CSDR_{7\text{-}28,}$ $CSDR_{28\text{-}90}$. The rate of strength development from 28 to 90days are significant. For instance, the $CSDR_{28\text{-}90}$ for MCBAP-10, MCBAP-20, MCBAP-30, MCBAP-40, MCBAP-50, MCBAP-60 are 12.81%, 16.55%, 17.02%, 28.79%, 30.33% and 42.88%, respectively. This trend of strength development may imply that SiO_2 of MCBAP reacts with $Ca(OH)_2$ at a later age[9].

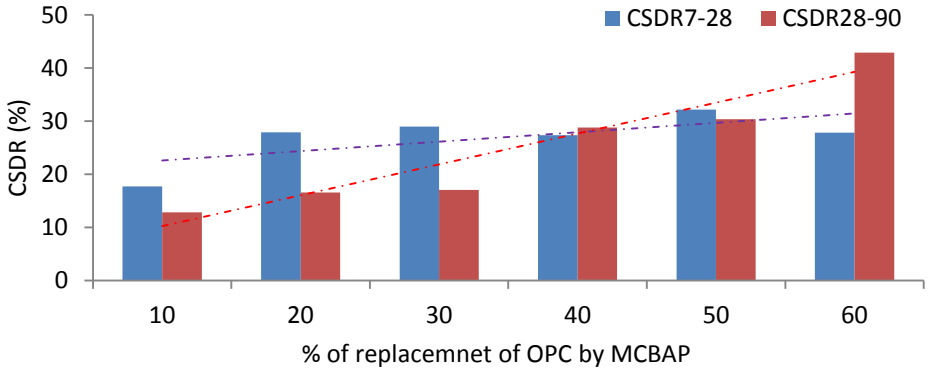

Figure 6: Compressive strength developing rate from 7 to 28days (CSDR 7-28) and from 28 to 90 days (CSDR 28-90) for mortar.

4 CONCLUSIONS

This research illustrated the influence of MCBAP on blended cement properties and setting behaviour. The conclusions are drawn as follows:

- The SiO_2 isthe main ingredient with Al_2O_3, Fe_2O_3, MgO in MCBAP. The total percentage of SiO_2, Al_2O_3 and Fe_2O_3 was 86.09 %. It is good for low calcium pozzolanic materials.
- The SEM observation found that MCBAP is porious, irregular shape, blackcolored materials.
- The water demand, IST and FST are increased with addition of MCBAP with OPC. Moreover, the addition of MCBAP with OPC weakened the micro structural properties, decrease the matrix density of mortar that lowers the compressive strength.
- Compressive strength developing rate reveal that a lower rate of strength development from 7 to 28 days compared with 28 to 90 days reaction time.

REFERENCES

[1] G. Zahedi, S. Azizi, A. Bahadori, A. Elkamel, and S. R. W. Alwi, "Electricity demand estimation using an adaptive neuro-fuzzy network: a case study from the Ontario province–Canada," Energy, vol. 49, pp. 323-328, 2013.

[2] X.-G. Li, Y. Lv, B.-G. Ma, Q.-B. Chen, X.-B. Yin, and S.-W. Jian, "Utilization of municipal solid waste incineration bottom ash in blended cement," Journal of Cleaner Production, vol. 32, pp. 96-100, 2012.

[3] B. K. Saikia, J. C. Hower, M. M. Hood, R. Baruah, H. P. Dekaboruah, R. Boruah, et al., "Petrological and biological studies on some fly and bottom ashes collected at different times from an Indian coal-based captive power plant," Fuel, vol. 158, pp. 572-581, 2015.

[4] Y. Zhang, F. He, Z. Gao, Y. You, and P. Sun, "Effects of ash-forming temperature on recycling property of bottom ashes from rice residues," Fuel, vol. 162, pp. 251-257, 2015.

[5] N. Kabay, M. M. Tufekci, A. B. Kizilkanat, and D. Oktay, "Properties of concrete with pumice powder and fly ash as cement replacement materials," Construction and Building Materials, vol. 85, pp. 1-8, 2015.

[6] K. Wu, H. Shi, L. Xu, G. Ye, and G. De Schutter, "Microstructural characterization of ITZ in blended cement concretes and its relation to transport properties," Cement and Concrete Research, 2015.

[7] Z. Yao, X. Ji, P. Sarker, J. Tang, L. Ge, M. Xia, et al., "A comprehensive review on the applications of coal fly ash," Earth-Science Reviews, vol. 141, pp. 105-121, 2015.

[8] I. Vegas, M. Cano, I. Arribas, M. Frías, and O. Rodríguez, "Physical–mechanical behavior of binary cements blended with thermally activated coal mining waste," Construction and Building Materials, vol. 99, pp. 169-174, 2015.

[9] H. Noorvand, A. A. A. Ali, R. Demirboga, H. Noorvand, and N. Farzadnia, "Physical and chemical characteristics of unground palm oil fuel ash cement mortars with nanosilica," Construction and Building Materials, vol. 48, pp. 1104-1113, 2013.

CICM 2015
First International Conference on
Advances in Civil Infrastructure and Construction Materials
MIST, Dhaka, Bangladesh, 14–15 December 2015

SOME RECENT ADVANCES IN STRUCTURAL APPLICATIONS OF ENGINEERED WOOD PRODUCTS

A. IQBAL[1]

[1] University of Northern British Columbia, Canada.
Email: Asif.Iqbal@unbc.ca

Abstract. *Wood is one of the traditional building materials and has been in use for a very long time. In recent times there have been some significant developments in technology for application in different types of structures. New wood-based materials with improved properties have been developed that can mass produced in factories. Modern design and production tools can prepare components to fit into structures. This paper highlights some of the latest developments with some examples of different types of applications across different countries.*

Keywords: Engineered wood products, Structural engineering, Seismic design.

1 INTRODUCTION

Engineered wood products involve industrial processes which combine wood of certain sizes organized and in particular orientations with adhesives to achieve desired engineering properties. Different types of engineered wood products have been developed but a few of them have been popular and widely used over the last few decades. Glue Laminated Timber, commonly known as Glulam, is widely used as a high quality material for structural members. Laminated Veneer Lumber or LVL is has high strength particularly along parallel-to-the-grain direction, ideal for beams and columns. Cross Laminated Timber (CLT) overcomes the weakness of LVL in the perpendicular-to-the-grain direction and can be produced as long panels to be used as floors and walls.

Modern engineered wood products can have strength comparable to other materials such as concrete. They can be mass produced in factories which ensure quality and brings the cost down. With modern computer aided design and manufacturing facilities the structural members can be prefabricated quickly to very precise dimensions. Because wood is significantly lighted than other materials the erection process is generally faster and less expensive. Due to all of these factors wood is a competitive material, both technically and cost-wise, for many structural applications. With ever-growing interests in sustainable development alternatives wood is becoming increasing popular as a building material. That has been ongoing in parallel to recent significant technological developments some of which are discussed here.

2 LONG-SPAN STRUCTURES

Traditional long-span structures mean wooded trusses with typical connections. With the introduction of high-strength materials and better design and production facilities these types of structures can be designed for longer spans and for much more complex geometries. The modern Computer-Aided Design software can analyze virtually any structure and detail the members and connections to minute details for production. The Computerized Numerical Controlled (CNC) machines can shape the components in precise dimensions for erection at site. The project management and construction tools can schedule the program to optimize the required time and cost. Easy availability of sophisticated construction equipment reduces the dependency on labor.

The practicality of designing long-span structures is demonstrated in the portal frames over the Aviation display hall of the Museum of Transport and Technology (MOTAT) in Auckland, New Zealand (Figure 1). The 42 m clear span frames support more than usual loads but were erected with minimum labor.

Figure 1: MOTAT Aviation Display Hall (left), during construction (right).

Figure 2: Coastland Aquatic Center (left), roof connections (right).

Figure 3: Waitomo Cave Information Center (left), joint detail (right).

Long-span roofs have been shaped in aesthetically pleasing forms with curvatures in two directions and diagonal grids (Figure 2). The technique has been extended to use composite sections and complex connections (Figure 3). Designers have managed to meet the challenges even in the very challenging conditions with irregular structures and unusual connections (Figure 4).

Figure 4: Coastland Aquatic Center (left), roof connections (right).

3 MULTI-STORIED BUILDINGS

In recent times there has been growing desire and attempts in general for more buildings with wood. The engineered materials can be produced in appropriate geometries with necessary strength to facilitate that. But few issues such as connection details and construction techniques had to be addressed. The wood industry responded through detailing and prefabrication techniques and at times worked with other materials to produce multistoried buildings including those designed for special demands e.g. seismic loading.

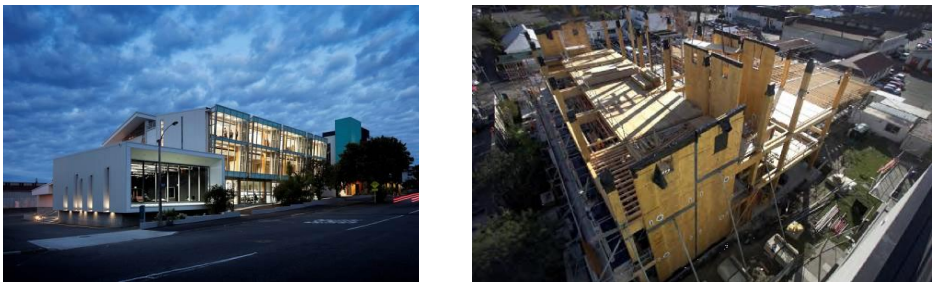

Figure 5: NMIT Arts and Media Center (left), during construction (right).

Around the middle of the last decade research on initiated in New Zealand on application of post-tensioning in structural members made of engineered wood products. The moment capacities of connections are increased due to post-tensioning, the arrangement is self-centering at removal of load. Additional replaceable ductile elements are used for seismic loading which absorbs energy during seismic events but protects the structural members from serious damage. In addition it has the same advantages as other prefabricated systems.

The first building in the world built with system is the Arts and Media Building of Nelson-Marlborough Institute of Technology in Nelson, New Zealand

(Figure 5), built around 2010. Since then the concept has been applied in a number of others have been structures in New Zealand, Europe and North America. The Trimble Navigation building in Christchurch, New Zealand (Figure 6) is a prime example of application of the idea in different types of connections. The typical frames have post-tensioning with energy dissipating elements at the beam-column joints. The columns have energy dissipaters connected to the foundation (Figure 7). The post-tensioned walls have dissipaters at the bases in addition to U-shaped Flexural Plates between them for additional energy dissipation.

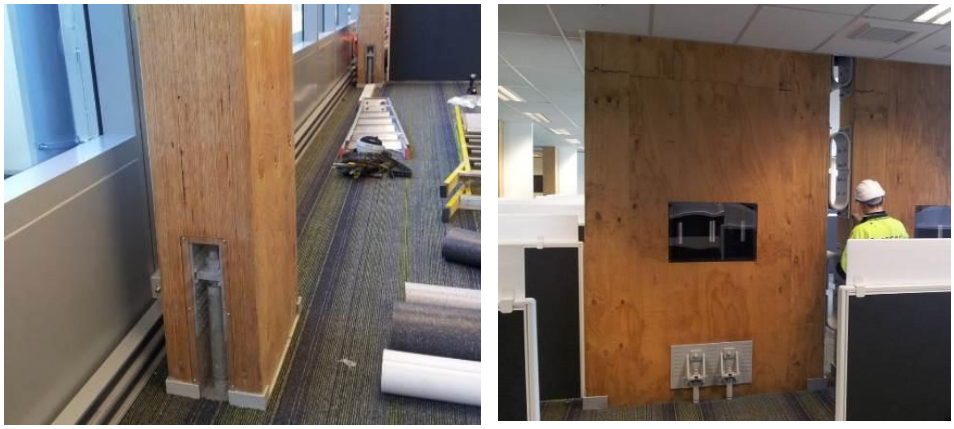

Figure 6: Column (left) and walls with post tensioning and dissipaters (right).

Figure 7: College of Creative Arts (left), post-tensioning and joint details (right).

The post-tensioned structural system with wood has been used in some variations. One of them is in a podium structure for College of Creative Arts of Massey University in Wellington, New Zealand (Figure 4). The bottom two stories of the building are of concrete and the top three are made of wood. Innovative connection details were used to overcome the weakness of LVL used in the column, wood-concrete composite system was used as floors (Figure 8).

Variations of composite systems have also been in other structures. The St Elmo court building in Christchurch, New Zealand uses concrete columns with

wooden floor and beam systems whereas in Tait Communications building, also in Christchurch, wooden frames have been used in parallel to steel braced frames and roof (Figure 5). It should be mentioned that the post-tensioned concept is applicable not only to structures made of glulam or LVL but also to those with CLT such as the Kaikoura District Council building in New Zealand (Figure 9).

Figure 8: Combination of wood with concrete (left), and steel (right).

Figure 9: Kaikoura District Council building (left), CLT shear walls (right).

Figure 10: Wooden interior with CLT stairs (left), CLT frame and roof (right).

4 HIGH-RISE STRUCTURES

CLT systems are considered well suited for wooden buildings more than five stories tall due to their strength and the potential to achieve the required fire rating. Not surprisingly, there has been a worldwide growing trend of constructing tall CLT buildings, as confirmed by the recent Forestry Innovation Investment and Binational Softwood Lumber Council survey of international tall wood buildings (Perkins+Will 2014). The 10-storied Forte Apartments (Figure 8) in Melbourne, Australia is currently the tallest building in the world but that will be soon overtaken by the 14-story tall wood apartment building in Bergen, Norway. The Wood Innovation and Design Center (WIDC) in Prince George, Canada (Figure 11) is the currently the tallest wooden building in North America. A number of others high-rise buildings are at different stages of design and approval process in United States and Canada.

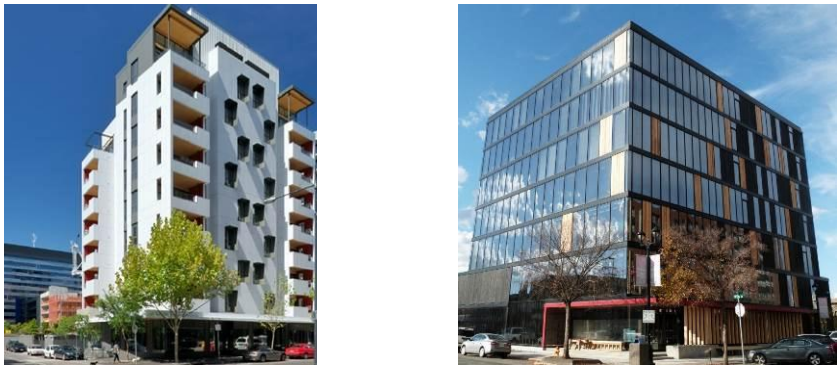

Figure 11: Forte Apartments, Melbourne (left), WIDC, Prince George, Canada (right).

Figure 12: 30-story CLT Building (MGA, left), 42-story CLT Building (SOM, right).

In parallel with the demonstration design/ prize competitions, some consultants have already designed tall buildings with CLT (Figure 12, left). Michael Green Architects (MGA) in association with Equilibrium Consultants, both from Vancouver, has designed buildings up to 30-stories tall following the "Finding Forest Through Trees (FFTT)" concept. Chicago-based consulting company Skidmore Owings and Merrill (SOM) has prepared a virtual wood design of a 42-story concrete building built in the 1960s. The design includes CLT floors and framing in combination with concrete (Figure 12, right).

5 SUMMARY

A brief overview of some advances with engineered wood products in structural applications has been presented here. The developments contribute to the increased popularity of wooden structures. The technology is still progressing and it is expected to help make wood a practical alternative for many types of structures in the near future.

ACKNOWLEDGEMENTS

Some of the research mentioned here has been financed by Structural Timber Innovation Company (STIC), a research consortium jointly funded by the New Zealand and Australian government agencies and building industry.

CICM 2015
First International Conference on
Advances in Civil Infrastructure and Construction Materials
MIST, Dhaka, Bangladesh, 14–15 December 2015

FRESH AND HARD PROPERTIES OF CONCRETE WITH POLYPROPYLENE

M. Jahidul ISLAM[1], **Sultan A. Shafian**[2] **and Navid Sarwar**[3]

[1]Department of Civil Engineering, Military Institute of Science and Technology, Dhaka, Bangladesh.
Email: jahid817@yahoo.com

[2, 3] Department of Civil and Environmental Engineering, Islamic University of Technology, Gazipur, Bangladesh.
Email: [2]shafian1@iut-dhaka.edu and [3]showmmo11@gmail.com

Abstract. *Unlike biodegradable waste non-biodegradable waste, such as plastic, remains stable for long period of time and becomes an environmental hazard. In 2013 alone, 299 million metric tons of plastic waste has been generated all over the world. Managing these large quantities of non-biodegradable waste is challenging and recycling is the best possible option for that. In this study polypropylene (PP) plastic has been recycled for coarse aggregate and fresh and hard properties of concrete with PP aggregates have been investigated. In PP concrete (PC), PP has been partially, 0%, 10%, 20% and 30% by volume, used to replace brick aggregate. Fresh values of concrete, such as workability, as well as hard values of concrete, like density, compressive strength, split tensile strength, and flexural strength have been tested and compared. Based on the results, it has been observed that PC can be used for structural purpose and concrete with 10% PC replacement has achieved higher performance compare to concrete with no replacement.*

Keywords: Concrete, Plastic aggregate, Compressive strength, Tensile strength, Density.

1 INTRODUCTION

In our day to day life, plastic becomes one of the most widely used items. More than 299 million tons of plastics were produced in 2013 alone [1]. Although it has made our life comfortable but it also create a large waste disposal problem. Because of its non-biodegradable nature it creates congestion in ground and water system. In Bangladesh 750 thousand tons of recycled plastic waste was created during 2010 – 2011 [2]. Therefore, it will be tremendous benefit to the environment if this waste plastic can be incorporated in our construction industries where a large amount of natural aggregates are used every day, and thus create a sustainable environment.

Investigations on application of plastic aggregate in concrete have been performed in recent years. Ghaly and Gill [3] replaced coarse aggregate with 5%, 10% and 15% (by mass) of polyethylene terephthalate (PET) in concrete for w/c ratio of 0.42 and found that compressive strength decreases with increasing PET content. Similar trend is also observed by several other researchers [2, 4]. Mathew et al. [5] investigated application of partial use of plastic aggregate as coarse aggregate and observed that concrete with 20% plastic aggregate had higher compressive strength. However, they also concluded that with increases in plastic aggregate compressive strength also reduces.

Based on the previous study, it is apparent that plastic aggregate replaced concrete has lower compressive strength. However, there is a potential to adopt waste plastic as a partial replacement for coarse aggregate and achieve higher strength than the regular concrete. Polypropylene (PP) is an abundant and low-cost thermoplastic with vast applications in consumer products, textiles, automotive industries and laboratory equipment. Because of its wide application it also create large amount of solid waste. Therefore, in this study waste PP has been adopted as a partial replacement (10%, 20% and 30%, by volume) of natural aggregate. Fresh and hardened properties of these concrete has been investigated and compared with the regular concrete without any PP.

2 MATERIALS AND MATERIAL PROPERTIES

2.1 Cement

Based on, ASTM C150-94, cement type I (Portland Composite Cement) were used as binding material. According to the manufacturer, it consists of 65 – 79% clinker, 21 – 35% lime stone, blast furnace slag, and fly ash.

2.2 Fine and Coarse Aggregates

Fine aggregate adopted in this study has been collected from Sylhet, Bangladesh, also known as Sylhet sand. This sand was coarser than the local river sand with a fineness modulus (FM) of 2.56. Particle size distribution of this sand has been

conducted according to the ASTM 136-05 and illustrated in Figure 1. As observed from the figure, size distribution of Sylhet sand was well within the ASTM upper and lower limits. Sylhet sand also had relatively higher specific gravity but low water absorption capacity. Properties of Sylhet sand is summarized in Table 1.

Burnt clay bricks are one of most common building materials in Bangladesh, and thus, crushed brick chips were used as the prime coarse aggregate choice for this study. First bricks with first class classification were purchased from the local market and then crushed into desired sizes. Beside, brick chips shredded polypropylene (PP) was used as coarse aggregate in this study. Preparation of PP aggregate had a process. At first, scrap plastic had been collected and washed, and then it had been melted and cooled into certain shape. Those cooled plastic bars can be shredded into specific sizes. For both coarse aggregate types, particle size distribution, specific gravity (bulk and specific) and water absorption capacity were calculated. All the test data are tabulated in Table 1. To achieve better similarity, FM for both brick chips and PP were selected as 6.54. Particle size distributions of both aggregates along with the ASTM lower and upper limits are illustrated in Figure 2 and it is close to lower bound of the ASTM requirement. However, similarities between these two aggregates end here. PP had a very low water absorption capacity then the brick chips. Furthermore, PP was lighter than the water and it had a bulk specific gravity of 0.85.

Table1: Properties of aggregate

Description	Polypropylene (PP)	Brick Chips	Sand
Maximum size	19mm	19 mm	-
Fineness modulus	6.54	6.54	2.56
Bulk specific gravity	0.85	2.30	2.25
Apparent specific gravity	-	2.80	2.43
Water absorption	0.80%	14.83%	3.40%

3 PREPARATION AND TESTS OF CONCRETE SPECIMENS

3.1 Concrete Preparation and Casting

In this work crushed brick aggregates were replaced with polypropylene (PP). Replacement ratios were 10%, 20% and 30% by volume. In order to compare the fresh and hard properties of these PP concretes a set of control of samples with no PP were also considered. For the test, two water-cement ratios were considered, like 0.45 and 0.55. For mix design of concrete volume basis were chosen.

Mix ratio for fine and coarse aggregates was 1.5:3.0. Table 2 summarizes the mix design for 1 m^3 of concrete with two water-cement ratios.

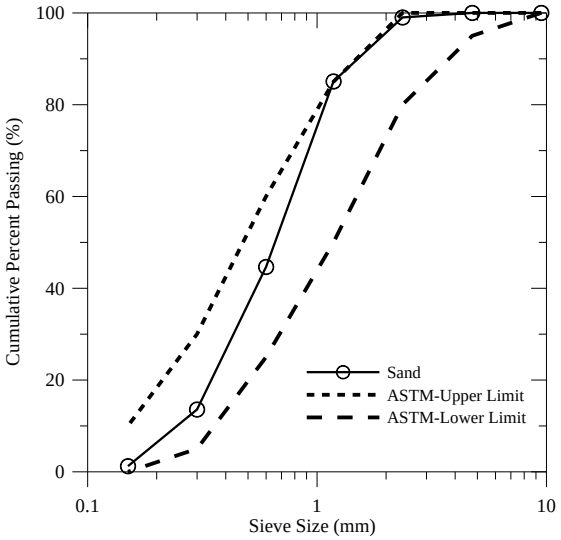

Figure 1: Grain size distribution of Sylhet sand used in the experiment along with the ASTM upper and lower limit for the fine aggregate.

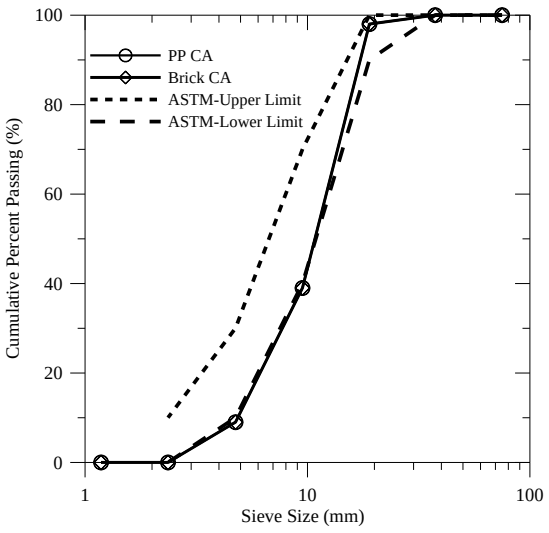

Figure 2: Grain size distribution of PP and brick coarse aggregate along with ASTM upper and lower limits for the coarse aggregate.

Compressive tests were conducted for 7, 28 and 90 days. Therefore, curing of concrete cylinders was modified as required. For example, for 28 days test concrete cylinder was moist cured for first 24 hours, and then it was submerged in water for another 26 days. On 27th day after casting, it was removed for the curing tank and air dried for 24 hours before performing the test. Similar procedure was followed for all the other tests. Prior to test the specimens were air dried for 24 hours. For compressive strength and split tensile tests, concrete cylinders with 4 in diameter and 8 in height were prepared. However, for the flexural strength tests, concrete beams with dimension 420 mm x 140 mm x 140 mm were cast.

Table 2: Mix design (for $1m^3$ of concrete)

Designation*	Water (kg)	Cement (kg)	Sand (kg)	PP (kg)	Brick Chips (kg)
Water-cement ratio = 0.45					
PC45P0	153	340	539.3	-	1102.6
PC45P1	153	340	539.3	40.5	992.3
PC45P2	153	340	539.3	81.0	882.1
PC45P3	153	340	539.3	121.6	771.8
Water-cement ratio = 0.55					
PC55P0	187	340	513.8	-	1050.4
PC55P1	187	340	513.8	38.6	945.4
PC55P2	187	340	513.8	77.2	840.3
PC55P3	187	340	513.8	115.8	735.3

*PC45P0,PC45P1,PC45P2 and PC45P3 = PP concrete with water-cement ratio of 0.45 and 0%, 10%, 20% and 30% PP replacement, respectively.PC55P0, PC55P1,PC55P2 and PC55P3 = PP concrete with water-cement ratio of 0.55 and 0%, 10%, 20% and 30% PP replacement, respectively.

3.2 Testing of Concrete

Concrete were tested for both fresh and hard properties. During the casting of concrete, slump values of the concrete mix were tested and according to ASTM C143. Slump values are indirect test for measuring the concretes workability. After concrete gain sufficient strength it becomes hard and the hard properties of concrete, like density, compressive strength, split tensile test and modulus of rupture test of concrete were conducted. Compressive and split tensile test of concrete cylinders were performed according to ASTM C 39 and C 496, respectively. On the other hand, flexural strength of concrete was executed through ASTM C 78, "Standard Test Method for Flexural Strength of Concrete (Using Simple Beam with Third-Point Loading".

4 RESULTS AND DISCUSSION

4.1 Fresh Properties of Concrete

Slump tests of fresh concretes were conducted to gain some measure of workability. Figure 3 shows the slump values (in cm) of concrete with various PP replacements and w/c ratios. Slump value of concrete depends on w/c ratios, shape and surface roughness of the aggregate and particle size distribution. PP used in the experiments had rougher surface compare to brick aggregates. Therefore, PP replaced concrete showed lower slump values compare to concrete with no PP. Figure 3 also shows the fact that the slump values are higher when the w/c ratios are higher.

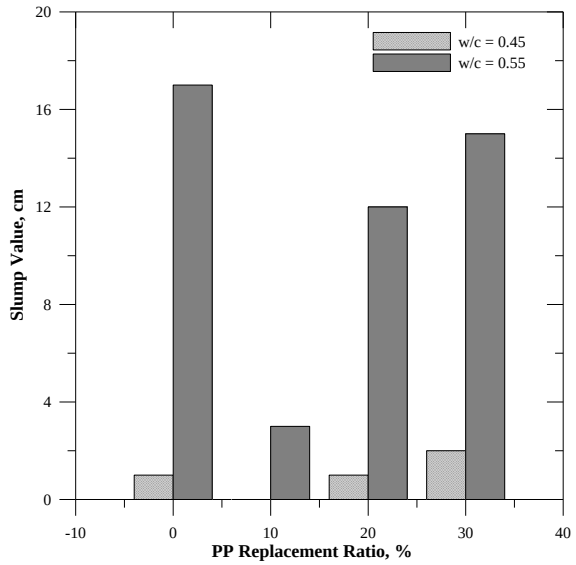

Figure 3: Comparisons of slump values with various PP replacements.

4.2 Hardened Properties of Concrete

Hardened properties of concrete include density, compressive strength, split tensile test and flexural strength test.

4.2.1 Density

Density of concrete was measured at 28^{th} days after casting. After concrete cylinder was cured for 27 days, it was air dried for 24 hours; and just before the test height, diameter and weight of the cylinders were measured. By taking ratio of weight and volume, density of the cylinder was calculated. Figure 4 describes the reduction in the concrete densities with increase in PP replacements in concrete.

Reductions in densities are as high as 8% for the 30% PP replaced concrete. However, for 10% PP replaced concrete the percentage of reduction is negligible.

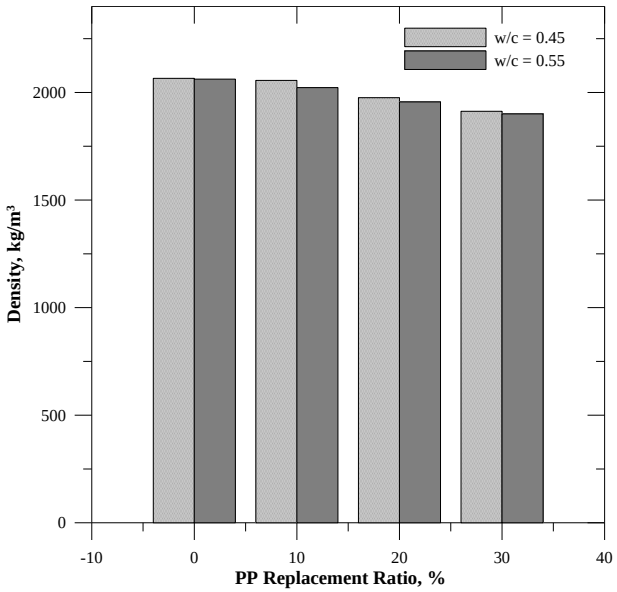

Figure 4: Change in density of concrete with two w/c ratios and various PP replacements.

4.2.2 Compressive Strength

Concrete cylinders were tested using a compression machine at 7, 28 and 90 days after casting. Figure 5 illustrates the compressive strength of concrete with various PP replacements and w/c ratios. Except for 30% PP replaced concrete, compressive strengths for w/c ratio of 0.45 is higher than the concrete with w/c ratio of 0.55. Furthermore, with increase in concrete ages compressive strength also increases. For concrete with w/c ratio of 0.55, concrete at 7 and 28 days concrete gain averages of 58% and 85% of 90 days strength, respectively. Exception of this trend is concrete with 30% replaced concrete. Similar trend is also visible for concrete with w/c ratio of 0.45 and PP replacement of 10%, 20% and 30% where compressive strength at 7 and 28 days are 46% and 89% of 90 days strength, respectively. However, for concrete without any PP shows early strength development with 7 and 28 days strength development of 60% and 97% of the 90 days strength, respectively.

Prime objective this study is to investigate the performance of concrete with PP as a replacement of coarse aggregate. As observed from Figure 5, 10% PP replaced concrete achieved better strength at 28 days compare to the concrete with no PP for both w/c ratios. It is more prominent for concrete with lower w/c

ratios. However, with the increase in PP content in concrete, compressive strength decreases and remains below the compressive strength of concrete with no PP.

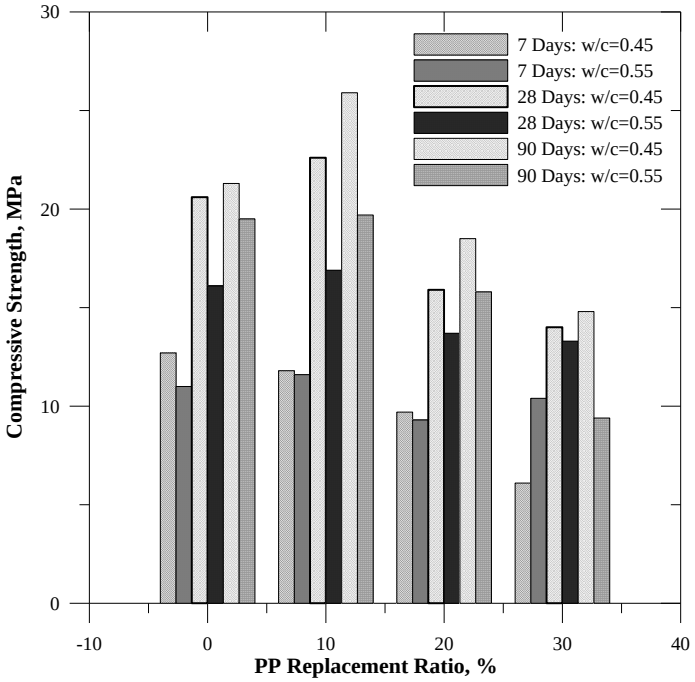

Figure 5: Comparison of compressive strength of concrete at various dates after casting with two different w/c ratios and four different PP replacements.

4.2.3 Tensile Strength

Although concrete is mostly used for its compressive strength its tensile strength is also important. Tensile strength of concrete is measured in two ways, such as split cylinder test and modulus of rupture. At 28 days split cylinders tests were conducted for tensile strength of concrete. Similarly, for flexural tensile stress concrete beams were tested at 28 days. Figure 6 describes the tensile and flexural strengths of concrete at various PP replacement condition and w/c ratios. As seen from the figure, both tensile and flexural strengths are higher for 10% replaced concrete compare to 0% PP replaced concrete at lower w/c ratio. However, at higher w/c ratio opposite trend is observed. With higher PP replaced concrete, both tensile and flexural strengths are lower compare to the 0% PP replaced concrete.

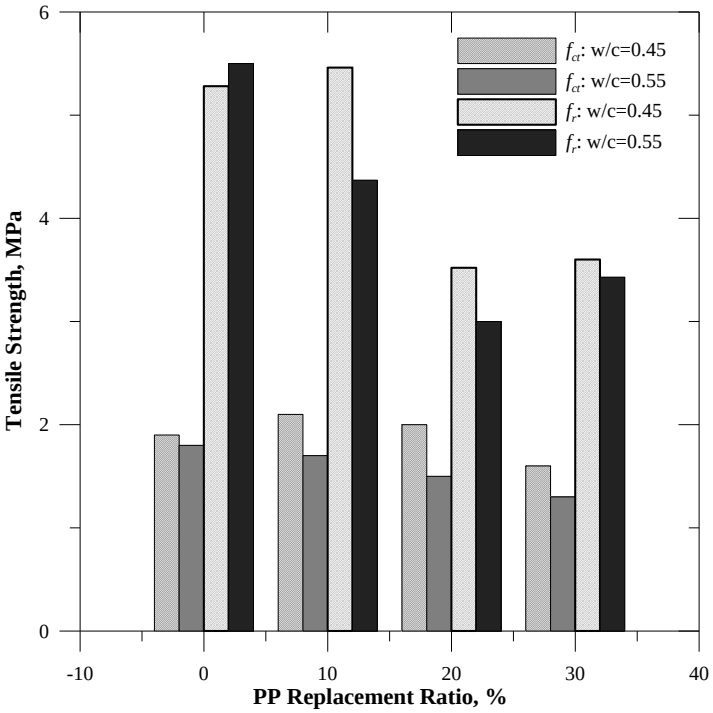

Figure 6: Tensile strengths (i) split-cylinder test (f_{ct}) and modulus of rupture (f_r) with two w/c ratios and various PP replacements.

5 CORRELATION BETWEEN TENSILE AND COMPRESSIVE STRENGTH

Although tensile and compressive strengths of PP replaced concrete do not correlate well with each other a correlation exists between the tensile strength and square root of the compressive strength.

The expression for split cylinder strength can be given as:

$$f_{ct} = 4.75 \sim 5.5\sqrt{f_c'} \qquad (1)$$

The expression for modulus of rupture can be shown as:

$$f_r = 11.4 \sim 12.3\sqrt{f_c'} \qquad (2)$$

Compare to the ACI code recommended range of tensile strengths, split cylinder strengths range are on the lower side; whereas modulus of rupture strengths are on the upper side.

6 CONCLUSIONS

Based on the experimental investigation of fresh and hardened properties of concrete without and/or with PP aggregate yield following conclusion:

- At lower w/c ratio PP replaced concrete showed very low workability. However, with higher w/c ratio workability of fresh concrete increased with increasing amount of PP in concrete.
- PP has a very low specific gravity. Hence, by adopting PP in concrete as coarse aggregate tends to reduce the self-weight of the structures. Although reduction in density for 10% PP replaced concrete was minimum it was possible to achieve 8% reduction in density for 30% PP replaced concrete.
- A distinctive rise in both compressive and tensile strengths was visible for 10% PP replaced concrete compare to the concrete without PP, especially at lower w/c ratio. However, with further increase of PP content in concrete both compressive and tensile strengths reduced gradually. At 30% PP replacement results were inconsistent.
- Considering the experimental evidences it can be concluded that 10% PP replaced concrete exhibit higher compressive and tensile strengths and lower density compare to the regular concrete without any PP. Therefore, it can be adopted in structural concrete.

REFERENCES

[1] World watch Institute, *Global Plastic Production Rises, Recycling Lags*, http://www.worldwatch.org/global-plastic-production-rises-recycling-lags-0

[2] Islam, M.J, Islam, A.K.M.R and Meherier, M.S, 2015. An Investigation on Fresh and Hardened Properties of Concrete while Using Polyethylene Terephthalate (PET) as Aggregate. In proceeding *World Academy of Science, Engineering and Technology International Journal of Civil, Structural, Construction and Architectural Engineering*, 9(5).

[3] Ghaly A. and Gill M., 2004. Compression and deformation performance of concrete containing postconsumer plastics. *Journal of Materials in Civil Engineering*, **16**, pp. 289-296.

[4] Siddique, R, Khatib, J, Kaur, I, 2008. Use of recycled plastic in concrete: A review. *Waste management*, **28(10)**, pp1835-1852.

[5] Mathew, P, Varghese, S, Pau, T and Varghese, E, 2013.Recycled Plastics as Coarse Aggregate for Structural Concrete. *International Journal of Innovative Research in Science, Engineering and Technology*, 2(3).

CICM 2015
First International Conference on
Advances in Civil Infrastructure and Construction Materials
MIST, Dhaka, Bangladesh, 14–15 December 2015

STUDY OF BOND BEHAVIOR BETWEEN STEEL BARS AND RECYCLED AGGREGATE CONCRETE

S. Moallemi POUR[1], **M. Shahria Alam**[2]

[1, 2] School of Engineering, University of British Columbia, Canada.
Email: [1]sadaf.moallemipour@alumni.ubc.ca and [2]shahria.alam@ubc.ca

Abstract. *This paper examines the behavior of deformed steel bars in different concrete mixes under direct push-out conditions. More than 48 specimens were tested where two RCA replacement percentages (i.e. 0% and 100%) and two sizes of deformed steel bars (i.e. 15M, and 20M) were used. In RCA concrete, the mode of bond failure of steel bars was found to be very similar to that of normal concrete. This paper reports in detail on the influence of various parameters that affect compressive bond strength such as diameter of the bar, concrete cover and strength. Results obtained show the role of the investigated parameters on bond stress. The bond capacity has an inverse relation with bar diameter. The slippage and bond strength increase with increasing concrete cover.*

Keywords: Recycle concrete aggregate, Push-out test, Bond strength.

1 INTRODUCTION

The growth in production and utilization of concrete in the construction sector is leading to a significant increase in consumption of natural aggregate. Therefore, environmental preservation is becoming a major concern, and usage of sustainable materials in construction is gaining popularity all over the world [1]. Using crushed concrete from demolished concrete structures as aggregate in new concrete is one of the potential solutions for the increasing construction demand within the civil engineering community. Advantages of exploiting these materials include supplementing current natural aggregate reserves and diverting construction and demolition debris from landfills [2]. An important structural property of reinforced concrete is the adhesion between reinforcing steel and surrounding concrete named bond, which leads to transfer of axial force between these two materials. This study presents part of the results of an experimental investigation of bond behaviour between recycled aggregate concrete and deformed steel bars with the variables being the diameter of the deformed steel bars and concrete cover.

2 EXPERIMENTAL PROGRAM

2.1 Materials and mix proportions

Deformed steel bars used in this research program were supplied by Okanagan Builders Ltd in the nominal diameters of 16 mm (15M) and 19.5 mm (20M). Their average yield strength was 400 MPa. Common Portland cement type GU conforming to the CSA A23.2 [3], sea sand and drinking water were used for the test specimens. Okanagan Builders Supplies Ltd provided the required RCA from demolished RC structures. Natural and recycled coarse aggregate was common crushed stone with a maximum size of 25 mm. The aggregate gradation curves of coarse aggregate combinations for all mixes met the CSA limits. Moreover, fly ash, water reducer, air entrainment and a water–cement ratio of around 0.4 was used to produce strengths of 35 MPa. Two concrete mixes with natural and recycled coarse aggregates are used in this study. The mix proportions are given in Table 2. According to CSA A23.2-4C/5C[3],the initial slump values of fresh concrete mixes were 60+/-10 mm. Air content of fresh concrete were in the range of 4-6%.

Table 1: Physical properties of NCA and RCA

Coarse aggregate	Bulk density (kg/m^3)	Apparent specific gravity	Water absorption capacity (%)	Moisture content (%)
Natural	1633	2.41	0.8	1.31
Recycled	1389	2.63	4.35	1.91

Table 2: Mix proportions of concrete (kg/m3)

Coarse aggregates	Cement (kg)	Fly Ash (kg)	Fine Aggregate (kg)	Natural Coarse Aggregate (kg)	Recycled Coarse Aggregate (kg)	Mixing Water (ml)
RCA	300	80	735	1030	0	148
NCA	300	80	735	0	1030	160

2.2 Preparation of specimens

Due to simplification and easiness of fabrication, the push-out test was used for investigating the compressive bond behavior. Push-out tests provide a simple means of comparative study of the bond behavior for various concrete mixtures and reinforcing bars [4].For comparison purpose, concrete mix with coarse aggregate replacement of 100% RCA were compared with the one with natural coarse aggregate. In order to observe the effect of the bar diameter and also cover to bar diameter ratio on bond stress, rebar with diameters of 15M and 20M rebars with embedment length to the bar diameter ratio of 5 and two different sizes of cylinders (Ø100×200 mm and Ø150×300 mm) were used in the test. Three identical specimens were cast for each category to ensure reliability of results. In order to identify the concrete compressive strength, extra cylinders were also cast. Plastic molds were used to cast the push-out specimens in a vertical position and wooden caps were used to align the rebars vertically in the center of the concrete cylinder. Also, for breaking the contact between the concrete and the embedded rebar along the debonded length, soft plastic wrap were used. The specimens were demolded after 24 hours of casting, and then they were moist cured for 28 days in the curing room. The following protocol was adopted for the sample identities: N-15M-4/8. The first numeral denotes either the control concrete mix (N) or RCA concrete mix (R). The second and third numbers denote the rebar size and the size of the cylinder in inches, respectively.

2.3 Push-out test setup

Intron stiff frame testing machine was used to apply uniform loading force which was increased gradually. The tests were completed in displacement control mode at a rate of 3 mm per min. The test initiated by applying force and pushing the embedded rebar downward through the concrete. A draw wire sensor attached to

the bottom of the rebar determines the relative displacement of reinforcement bar compared to its surrounding concrete. An NI data acquisition system captured the sensor's signal. The push-out tests were stopped after the surrounding concrete split or slippage of about 10 mm occurred.

Figure 1: Fully assembled push out testing apparatus

3 TEST RESULTS AND DISCUSSION

3.1 General Description

Splitting failure were observed in the most of the specimens. This failure mode appears when bond stress reduces dramatically due to cracking of concrete cover and splitting along the length of steel bar (see Figure 2). Specimens with normal and recycled aggregate concrete represent almost same pattern of bond slippage behavior. Figure 3ilustrates bond stress versus slip response of some of the push-out specimens. Generally, a sharp ascending happens in the first stage of bond behavior where chemical adhesion is predominant. This phase continues linearly up to peak loads for most of the specimens. Mechanical interlock seems to have more contribution in bond resistance in second stage. Also, the descending branch of the bond behavior seems to be linear for most of the specimens. The specimen with larger concrete cover to diameter ratio representlarger slippage at failiure point. On an average, the slips corresponded to the peak loads in the range of 0.011 – 1.55 mm. Studies performed by Xiao and Falkner [5] and , Prince and Singh [6] confirmed the observed results of bond stress-slip relationship in this study. Furthurmore, RCA concrete mix showed 28 days

compressive strength of 32 Mpa which is very close to the target strength while control mix had 40 Mpa strength.

Figure 2: Failure of samples

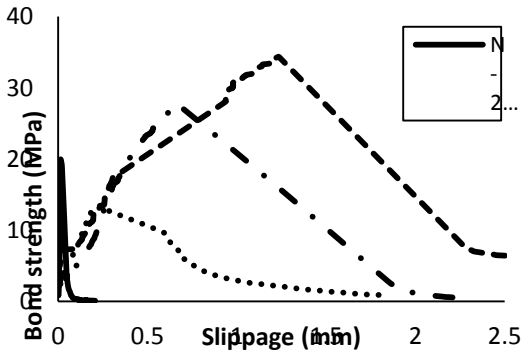

Figure 3: Bond stress versus slip response in 200 mm concrete cylinder

3.2 The Effect of Influencing Factors on Bond Strength

The average bond strength can be determined by equation (1) based on the assumption that the bond stress has uniform distribution along the embedment length of rebar in concrete:

$$\tau = P_{max}/(\pi d_b l_e) \qquad (1)$$

Where τ is the average bond strength in MPa is, P_{max} is maximum push-out load in N. $l_e$and $d_b$denote the embedded bar length and the diameter of the bar in mm, respectively.

Results show that specimens with larger bar diameter had lower bond capacityunder equivalent concrete mix proportions. When the diameter increase,

the amount of bleed water trapped between the bar surface and concrete increases. This causes increase in the voids and reduction in the contact area. Therefore, the average bond stress transferred to surrounding concrete decreases. Moreover,cylinder specimens with larger diameters demonstrate better bond resistance due to higher confinement. Regarding the test results, majority of push-out specimens show similar trend. Similar findings were reported in the literature [2], [4]. The effect of different factors on the bond behavior of concrete made of RCA is the same as conventional concrete. A previous study based on push-out tests carried out by Deeks and Su [4] presented similar factors that affect the bond strength in conventional concrete.

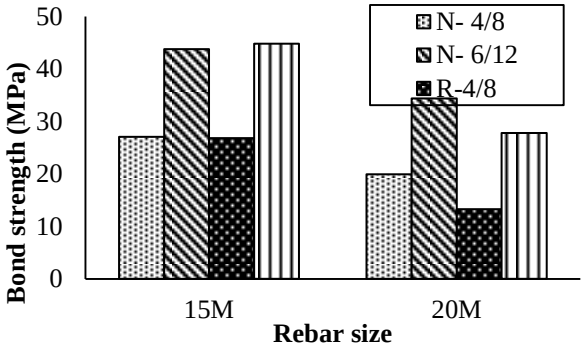

Figure 4: Relationship between bond strength and bar diameter

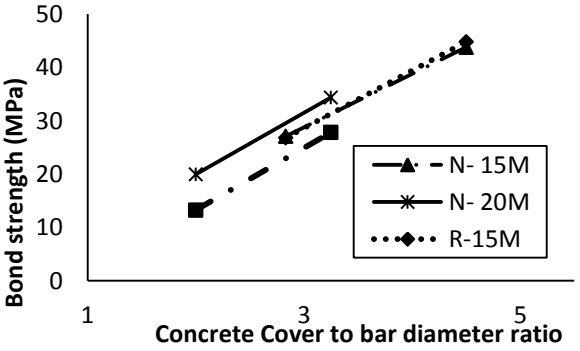

Figure 5: Relationship between bond strength and concrete cover with 30% RCA

The test results ilustrate that specimens made of concrete mixes 100% RCA replacement representthe same bond behavior in comparison with control samples. Thus, the usage of RCA will have minor effect on the bond resistance than what is expected for regular concrete. Figure 6confirms that on average,

among the specimens with the same size, the concrete mix of 100% RCA replacement have close bond capacity compared to control mix. As a concusion, the replacement of natural aggregate with recycled concrete aggregate can result in noticeable bond capacity that is comparable to regular concrete. Similar results can be foundin previous studies [6], [7].

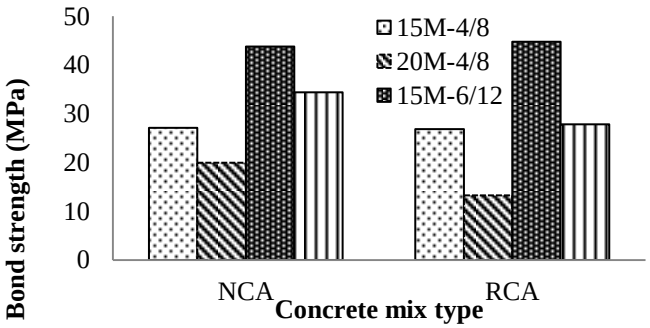

Figure 6: Relationship between bond strength and aggregate type

4 CONCLUSIONS

The major conclusions from this study can be summarized as:

- The overall bond properties including general shape of the load versus slip curve between recycled aggregate concrete and steel rebar is similar to the one for normal concrete and steel bars. Beside the acceptable compressive strength of green concrete with RCA, their bond resistances are close to normal concrete.
- Under the condition of the equivalent mix proportion and similar to that of normal concrete, the bond capacity has an inverse relation with bar diameter. The slippage and bond strength increase with increasing concrete cover.
- Similarity in overall bond capacity and behavior of concrete mixes made of RCA and normal aggregate portrays the possibility of using recycled concrete aggregates in structural application.

ACKNOWLEDGMENTS

The current study is supported by Natural Sciences and Engineering Research Council of Canada (NSERC). In addition, OK Builders Ltd. has supported our research topic and provided required materials and useful guides. We would like to thank Chungha Lee, Yongjoon Lee, and Yujia Chen who helped us during our experimental works.

REFERENCES

[1] S. B. Huda and M. S. Alam, "Mechanical behavior of three generations of 100% repeated recycled coarse aggregate concrete," Constr. Build. Mater., vol. 65, pp. 574–582, 2014.

[2] L. J. Butler, J. S. West, and S. L. Tighe, "Bond of Reinforcement in Concrete Incorporating Recycled Concrete Aggregates," J. Struct. Eng., pp. 1–12, 2014.

[3] Canadian Standards Association, "CSA Standard CAN/CSA-A23.1-14/A23.2-14. Concrete materials and methods of concrete construction/Test methods and standard practices for concrete." Mississauga, Ontario, Canada, 2014.

[4] H. Li, A. J. Deeks, and X. Su, "Experimental Study on Compressive Bond Anchorage Properties of 500 MPa Steel Bars in Concrete," J. Struct. Eng., vol. 139, p. 04013005, 2013.

[5] J. Xiao and H. Falkner, "Bond behaviour between recycled aggregate concrete and steel rebars," Constr. Build. Mater., vol. 21, pp. 395–401, 2007.

[6] M. John Robert Prince and B. Singh, "Bond behaviour of deformed steel bars embedded in recycled aggregate concrete," Constr. Build. Mater., vol. 49, pp. 852–862, Dec. 2013.

[7] S.-W. Kim and H.-D. Yun, "Evaluation of the bond behavior of steel reinforcing bars in recycled fine aggregate concrete," Cem. Concr. Compos., vol. 46, pp. 8–18, Feb. 2014.

CICM 2015
First International Conference on
Advances in Civil Infrastructure and Construction Materials
MIST, Dhaka, Bangladesh, 14–15 December 2015

EXPERIMENTAL INVESTIGATION ON MECHANICAL PROPERTIES OF LIGHTWEIGHT FOAMED CONCRETE

Washi B. W. ONNESHA[1], Mohammad A. Rahman[2], Sudarshan Sarkar[3], Habibur R. Kamal[4]

[1, 2, 3] Department of Civil Engineering, Military Institute of Science and Technology, Dhaka, Bangladesh. Email: [1]nesha11111@gmail.com, [2]ashik91surjo@gmail.com,[3]sudarshan_sarker@yahoo.com

[4] National Defense College, Dhaka, Bangladesh. Email: hrkamal@gmail.com

Abstract. *At the age of 21th century, the developments in the application of concrete technology have led to a conspicuous interest in investigation of mechanical properties of the concrete. Apart from traditional use of concrete, Lightweight concrete is now one of the popular materials in the construction field due to its lightness, versatility and its low cost potentials. Different methods are available in producing lightweight concrete, yet construction of Foam-concrete is comparatively a newer technique in the field. By reducing self-weight using foam concrete construction has enormous potentials where strength plays insignificant role. Lightweight concrete obviously means low strength. Although some researchers have been conducted research on the characteristic of foam concrete, yet much of properties and the behavior of foamed concrete are limited. This paper focuses mainly on the experimental investigation on the mechanical properties of lightweight foam concrete. The present study primarily deals with elementary analyses like the compressive strength test, water absorption test and unit weight test. The primary analysis and comparative result with traditional concrete indicate that Foam-Concrete may be used where volume not the strength is significant. Out of many fields of use, Foam concrete seemed useful and economic in respect to time and cost; examples may be filler materials, insulators, partition walls etc. However, the overall aim of this paper is to produce foam concrete and study the effect constituents, to find materials, methods of production, and application of foam concrete vis-a-vis to study properties of foam concrete including its mechanical strength.*

Keyword: Lightweight, Mechanical properties, Comparison, Absorption, unit weight.

1 INTRODUCTION

With the introduction of new technologies the construction industry is becoming extremely challenging day by day. The introduction of the use of light-weight foam concrete has added a new dimension in the construction sector. In comparison to the normal concrete the aerated concrete shows greater homogeneity due to the absence of coarse aggregates in it [1]. Based on the pore-formation process the aerated concrete can be classified as gas concrete and foamed concrete [2]. Self-weight reduction by using foam concrete has a remarkable benefit in construction work. Significant portions of loading imposed on the structures are due to the self-weight of component member. It would be highly commodious if the concrete density can be reduced [3].

The overall aim of this research the experimentally investigate the mechanical characteristic of light-weight foam concrete. The compressive strength test, water absorption test and unit weight determination tests were conducted and it was found that the ultimate strength of the material is very low and thus can be used for the non-load bearing member construction.

2 EXPERIMENTAL PLAN AND DATA ACUQUISITION

The study mainly focused on methodology for preparing the Lightweight Foamed Concrete (LFC) and later to investigate the mechanical properties and recommendation on practical implementation of lightweight foam concrete base on results. Initial preparation of investigating the mechanical properties of LFC started with preparing standard sample according to the standard codes of ASTM and as per requirements.

2.1 Sample Preparation

2.1.1 Materials

Main ingredients for constructing foam concrete we used: Cement, Polystyrene bubbles or Styrofoam, Admixture (Litho Foam) and Controlled water. As binder materials PCC (Portland Composite Cement) was used. In normal concrete aggregate which are used is replaced by Polystyrene bubbles in LFC (Figure 2). Polystyrene is an aromatic polymer of styrene which is synthetic in nature. Chemically it is a hydrocarbon of long chain where aromatic ring of benzene are attached with phenyl group $(C_8H_8)_n$. The chemical reaction is showed in Figure 1. Polystyrene is very light (density 0.96–1.04 g/cm3) and good thermal insulators (thermal conductivity 0.033 W/(m•K)). So application of this cause lighter density of concrete and make it a good insulator. Litho-Foam [4] is used as admixture which generally is a protein based foaming agent (Figure 3). Its enzymatic component reacted by diluting in water with compressed air in foam

generator and produce qualitative foam. Superfluous external material being less causes fewer disturbances in concrete. Water application is controlled by a mechanical device in the mixing machine during operation automatically.

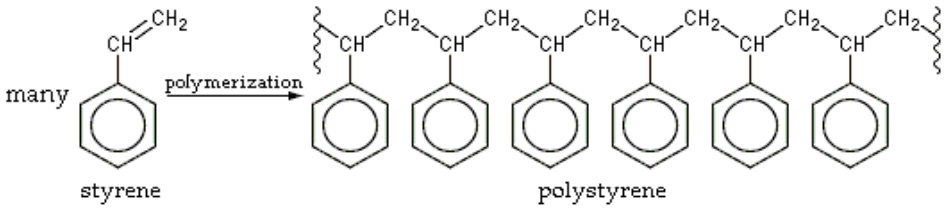

Figure 1: Chemical reaction of polystyrene (Source: Wikipedia [5])

(a) (b)

Figure 2: Polystyrene Bubble Sample (a) used in experiment [6] and (b) available in world-market.

Figure 3: Litho-Foam.

2.1.2 Mix proportion

The mix proportions for LFC depend upon the requirements for a particular job, in terms of strength, workability, and so on. Several procedures for proportioning LFC mixes are available, which emphasize the workability of the resulting mix. However, there are some considerations that are particular to LFC. The water-cement ratio was 0.5 to maintain the workability of the mixture. As no aggregate was used so the mix ratio was between polystyrene and cement of 1:16.67 and 1:23.33 was used in terms of weight for two different variations of mixture. Total 12 cylinders and 8 blocks were prepared. Admixture Litho-Foam foam was used in 1:100 ratios with water in terms of volume.

The control specimen we used is normal concrete with mix ratio 1:2:4. The water cement ration was kept 0.5.Coarse aggregate (Stone) was of 1 in passing and 3/4 in retain (50%) and 3/4 in passing and 1/2 in retain (50%). Fine aggregate had a FM of 2.65.

2.1.3 Specimen

Total 12 cylinders and 8 blocks were prepared. The cylindrical specimen were of standard size (4”dia& 6”height) and the block was of production size in the market (20"x10"x5") (Figure 4). Cylinder were prepared for mix ratio of 1:16.67 and tested at 7,14 and 28 days for compression test whereas block were prepared of both mix proportion. Aside from compression test these specimen was used for water absorption test also.

(a) (b)

Figure 4: Sample preparation (a) cylinder and (b) block.

2.1.4 Mixing Machine

A special type of mixing machine had been used during preparation of sample (Figure 5). It contains a turbine inside which rotate by external force and thus

conducting the mixing process. It has an outlet from which the mixed ingredients pumped out. In this machine water is controlled by automatic mechanical way so that required amount of water in available during mixing. The capacity of the machine is 1 m^3 and production capacity 10 m^3 per hour.

Figure 5: Mixing Machine [6].

2.1. 5 Casting & Sampling

At first water is stared to be poured in the machine and it's continued throughout the mixing time. Then the admixture is added. Other ingredients cement and poly styrene then added continuously. Then mixture drew out by pressure through an outlet pipe, which again poured in the mixture for proper mixing. When the slurry is thoroughly prepared then it is poured into the mould or used for casting.

2.2 Testing Procedure

The evaluation process for determining the mechanical properties of LFC was mainly focused on the following tests for both type of sample (cylinder and casted block) due to the choice of application of our certain type of LFC - Compressive strength test, Water Absorption test &Unit Weight of LFC.
The compressive strength is evaluated according to ASTM: C 39/C 39M – 05 [7]. Compression-testing machine and Digital universal testing machine (UTM) both were used for determining the compressive strength. Test apparatus was calibrated to execute the compressive strength test on each specimen. The load rate was 1mm/min.

For water absorption the test method ASTM C642 [8] was used where the sample was submerged in a bath tab and the weight of saturated specimen was taken. Then the oven dry weight was taken and the absorption of water is calculated.

3 EXPERIMENTAL RESULTS AND DISCUSSIONS

The strength and absorption mainly varies with water cement ratio and the mix proportion of ingredients. In our case study water cement ratio was constant so all the results vary only due to the mixing ratio. The strength of concrete is increased with increasing age of concrete. We have conducted the compression test in Compression-testing machine for determining the strength for 7 day, 14 days and 28 days.

3.1 Results for Compression Test

In foamed concrete, the polystyrene bubbles can be considered as aggregates having no resistance against loading. So, as the amount of polystyrene bubbles increases, the strength of concrete decreases. The variation of strength has been seen for the mix ratio of concrete. The control specimen that we use has a compressive strength of 3961psi. Comparing the test result with our prepared specimen it was observed to be very less as all the aggregate is replaced by the bubbles. This reduction is very excessive for 1:16.67 mix ratio and increased for 1:23.33 mix ratios. But as our main focus was to reduce self-weight, we get a better result in this parameter.

The comparison of compressive strength of control specimen and foam concrete of mix ratio 1:23.33 of 4 specimen are given in Figure 6.

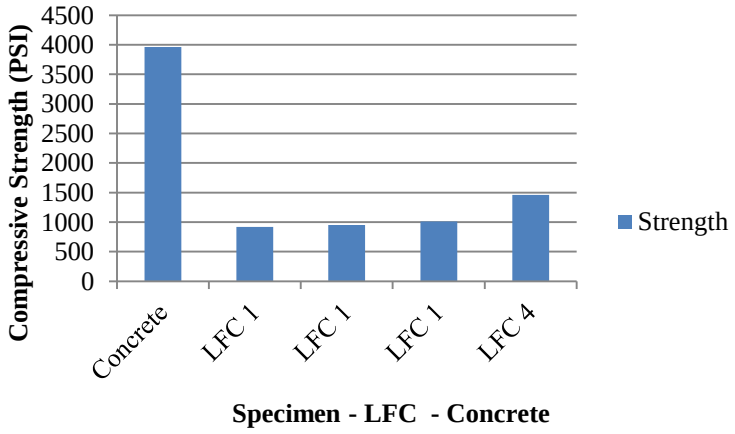

Figure 6: Compressive strength comparison of LFC and Control Specimen

Figure shows 4 specimen blocks have varying compressive strength with a reduction of strength are 76.77%, 76%, 74.5% & 63.14%. This test data shows that these specimens can't be used as structural materials. These materials can be used as non-structural member mainly partition wall. For mix ratio 1:16.67 the result is more drastic. But for being good insulator it can be used as heat insulator

in building and as filler materials. In our case for mix ratio 1:16.67 the density was very less than expected that it was floating. So this concrete can be used as floating concrete and if permeability is less the can be used in floating agriculture.

3.2 Results for Specific Strength

The ratio of a material's strength to its density is the specific strength. As polystyrene is of very low density, it decreases the concrete density with increase in proportion and that gives the structure a reduction self-weight. It is the main advantage of LFC. The specific strength at different ages is given in Figure 7. Structural efficiency improvement causes load reduction for both structure and substructure. Due to a reduction of load the size of the member and of reinforcements also reduces, that results in having more accommodation and usable space in the building and that increases the flexibility for absorbing strains and thermal properties is improved. It also minimizes the differential temperatures in building and thus results in energy conservation.

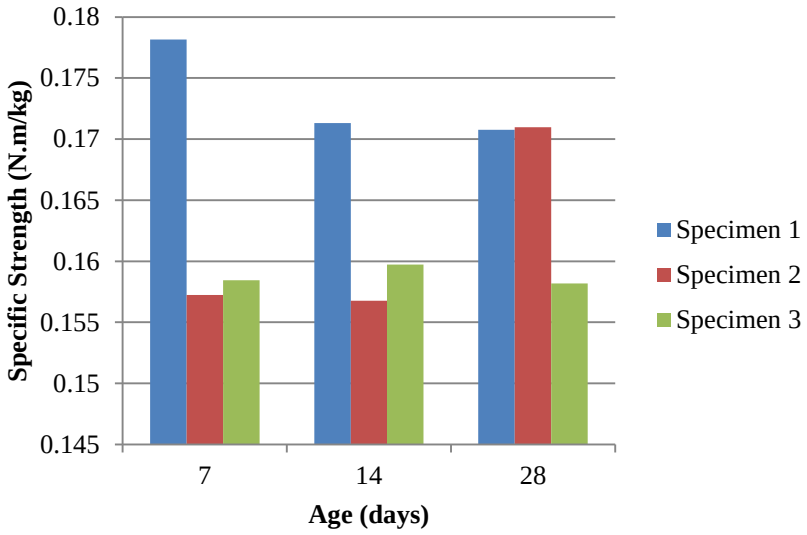

Figure 7: Specific Strength of LFC at different Ages

3.3 Results of Water Absorption

Water absorption of LFC is also less than the general concrete and brick that also give the LFC to be cracking resisting, less permeable. Thermal effect has less contribution in LFC. So it can be frequently used in areas and seasons of higher moisture content.

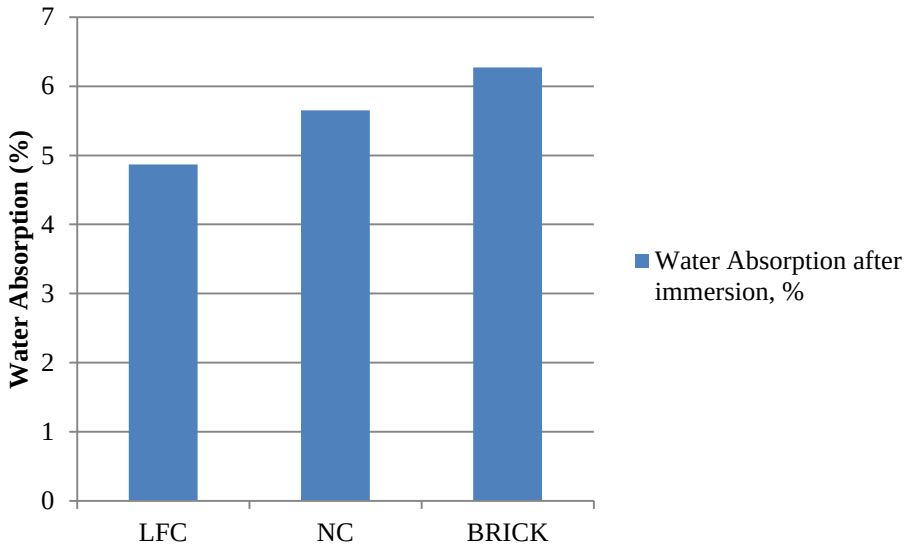

Figure 8: Water absorption of different structural materials

4 CONCLUSION

The key advantage of using foam concrete is that it is quite capable of filling void spaces with a rigid indurate formation and at the same time providing a material with lower density which will lessen the critical loading intensity. It ensures better thermal and insulation characteristics but might not be the best resolution in terms of cost consideration. This research documents an elementary research of the mechanical properties of the light-weight foam concrete.

In this study, a few parameters were selected and tested in the laboratory. It was found that the capability of foamed concrete is very low, so it cannot be used for compression member construction. But it can be very effective in case where the self-weight reduction of the structure is required. The compressive strength of the material shows a proportional increase with density, which implies with the increase of density it is more likely to take more compression. The light-weight material can be used effectively as partition wall as well as filler materials in appropriate places. The lower water absorption ensures that there will be less formation of cracking. Water absorption has inverse relation with water resistance. It indicates that lesser water absorption will make the foamed concrete structure more water resistant and as a result it can be very fecund in floating structure construction.

The findings of the study pave the way for future research activities. A permeability test can be conducted to assess the water penetrability of foam concrete.

REFERENCES

[1] Narayanan, N., and K. Ramamurthy. "Structure and properties of aerated concrete: a review." Cement and Concrete Composites 22.5 (2000): 321-329.

[2] Mohd and Samidi (1997), First Report Research Project on Lightweight Concrete, University Technology Malaysia, Skudai, Johor Bahru.

[3] Mouli, M., and H. Khelafi. "Strength of short composite rectangular hollow section columns filled with lightweight aggregate concrete." Engineering structures 29.8 (2007): 1791-1797

[4] http://www.dr-luca.com/pages/en/lithofoam_additives/index.html, December 03, 2015 at 2.25am.

[5] https://en.wikipedia.org/wiki/Polystyrene, December 03, 2015 at 2.20am

[6] PCCN Bangladesh Limited, Dhaka-1206, Bangladesh, viewed 12 August 2015,http://www.polyconcrete.com.bd/

[7] ASTM C39, 2015, Standard Test Method for Compressive Strength of Cylindrical Concrete Specimens, ASTM International, West Conshohocken, PA.

[8] ASTM C642, 2015, Standard Test Method for Density, Absorption, and Voids in Hardened Concrete, ASTM International, West Conshohocken, PA.

CICM 2015
First International Conference on
Advances in Civil Infrastructure and Construction Materials
MIST, Dhaka, Bangladesh, 14–15 December 2015

CHARACTERIZATION OF MECHANICAL PROPERTIES OF CONCRETE WITH HE CEMENT FOR CONCRETE RAILWAY SLEEPERS

Md Shamsuddoha[1], Jeremy A. McIntyre[2] and Kamrul ISLAM[3]

[1]Department of Engineering and Construction, Nelson Marlborough Institute of Technology, Nelson, New Zealand.

[2]Faculty of Engineering and Architectural Studies, Christchurch Polytechnic Institute of Technology, Christchurch, New Zealand.

[3]Department of Civil Engineering, Military Institute of Science and Technology, Dhaka, Bangladesh.

Email: [1]Md.Shamsuddoha@nmit.ac.nz, [2]mcije194@gmail.com and [3]kamrul1@ualberta.ca

Abstract. *Railway sleeper is an important component of a railway track. Sleepers maintain track performance and safety. Concrete sleepers make up the majority of sleepers around the world. Curing of concrete governs the properties of the sleepers. Due to the temperature variation in the winter and summer in Christchurch region, selection of appropriate curing method of the sleepers possesses a challenge to the manufacturers. High Early Strength (HE) cement is often used to achieve desirable strength in such unfavorable condition. The compressive, flexural and pull-out tests were carried out on the concrete specimens. The results suggest that HE cement provided average compressive strength of 83 MPa. The concrete compressive strength in the winter was found lower compared to warmer months. The pull-out tests showed that the theoretical bonding strength of the concrete according to current literature, derived from compressive strength, align with experimental bonding strength.*

Keywords: Railway sleepers, HE cement, Mechanical properties, Cold weather concreting.

1 INTRODUCTION

The railway track is made up of rails, pads, sleepers, fasteners, ballast, sub ballast and subgrade. Railway sleeper enables the structure to support trains carrying freight and/or passengers by distributing the loads onto the sub-structure. It also plays a major role in track performance and safety [1, 2]. This function can be further defined as maintaining the rails at the designed gauge length, preserving the rail and providing the rail with support [3]. Concrete sleepers now making up the majority of sleepers used around the world [4]. This type of sleeper has been adopted because concrete is strong in compression while weak in tension. Whereas steel is strong in tension. The anchoring capacity as bonding is important, to transfer the service loadings [5].

Concrete cures through the hydration of cement when added with water. Generally, a low water-cement (w/c) ratio is necessary to ensure higher strength in concrete [6]. However, the hydration process requires that there to be adequate water to hydrate the cement. If there is not enough water, the hydration process will stop leaving un-hydrated cement. Adhesion, friction and mechanical action determine the bond strength within the railway sleeper [5]. Hence, the adhesion of the concrete and steel would be affected by the curing of concrete as the cement paste makes up this adhesion. Therefore, sufficient curing should be maintained for superior performance of the sleeper.

Canterbury region in New Zealand experiences lower temperature, which affects curing of concrete. In recent years, industries in New Zealand producing railway sleepers have experienced issues in the quality of their concrete sleepers. Steam curing is considered as one of the solutions of this problem. However, autoclaving and steam curing can attract considerable cost. This led to look for using High Early Strength (HE) cement in the production of the concrete sleepers. This study investigates the compressive, flexural and bonding properties of concrete made of HE cement. A comparison of theoretical prediction pull-out strength and experimental tests is also carried out.

2 EXPERIMENTAL INVESTIGATION

The concrete mix used had a water content (w/c) of 0.323 and was made up of HE cement, Rapidcem®. Due to commercial confidentiality, composition of the cement in not provided in this article. Where the proportions of the mix were 19.2% cement, 6.2% water, 41.9% coarse aggregate and 32.7% sand by weight. *Sika ViscoCrete 2100*®, a super plasticiser was also added to this mix before the samples were poured.

The moulds for the pull-out samples were assembled from plywood and held together by screws as shown in Figure 1. These moulds were constructed so that the concrete could be poured into the moulds from the top. Each of the moulds were 400 mm by 150 mm by 150 mm with an 8 mm 7 wire strand inserted down

the middle. The steel strand extended 700 mm above the concrete and 67 mm below the concrete for allowing sufficient grip for the test fixture. 20 specimens were tested for bonding properties.

A total of 323 Compressive specimens were prepared over a duration of one year in accordance with the New Zealand Standard NZS3112: Part 2[7]. Five test samples were made up to test the flexural tensile strength of the concrete. The moulds for the samples were made up at the factory as shown in Figure 1(b). These test samples were cuboid in shape with the planned dimensions of 150 mm by 150 mm by 600 mm.

(a) (b)

Figure 1: Typical specimen preparation for (a) bonding, and (b) flexural specimens.

The data analysis of the pull-aout samples was carried out in two different ways. Firstly, pull-out loads were determined experimentally and then the theoretical pull-out load was also calculated and compared. To calculate the theoretical pull-out load, the equation found in Arel and Yazici[8] was used. This equation is given as:

$$P_t = 3 \times f_{ct28} + (f_{c28} + E_{c28} \times t + 4 \times f_{ct28} \times t)/(E_{c28} + t + 6 \times f_{ct28}) \quad (1)$$

Where f_{ct28} was the 28 day splitting tensile strength of concrete, f_{c28} was the 28 day compressive strength of concrete, E_{c28} was the 28 day modulus of elasticity and *t* was the concrete cover provide from in by the samples. The 28 day splitting tensile strength and modulus of elasticity were calculated using the following equations[9].

$$f_{ct28} = 0.56\sqrt{f_c'} \quad (2)$$

$$E_{c28} = 4700\sqrt{f_c'} \quad (3)$$

Pull-out tests were carried out using an Avery machine. The machine worked by applying a load onto the concrete part of the sample with the sample being clamped in place at the top of the steel strand. Each sample was manually loaded into the Avery machine. Each sample was then clamped into place by the steel teeth of the Avery machine and the sample was moved into the correct position for testing, as shown in Figure 2. A dial gauge measuring movement of steel was attached to the end of the steel below the concrete. This gauge was magnetic but was held in place by a U shaped clamp to provide extra support. This gauge was zeroed at the beginning of each test. Load was applied to the sample at a constant rate of increase of 15 kN/min. For a crack located in the middle third of the sample the flexural tension strength was calculated using the equation given by New Zealand Standard NZS3112: Part 2 [2]. Four-point bending test was thus carried out on the flexural specimens, which can be seen in Figure 2(b).

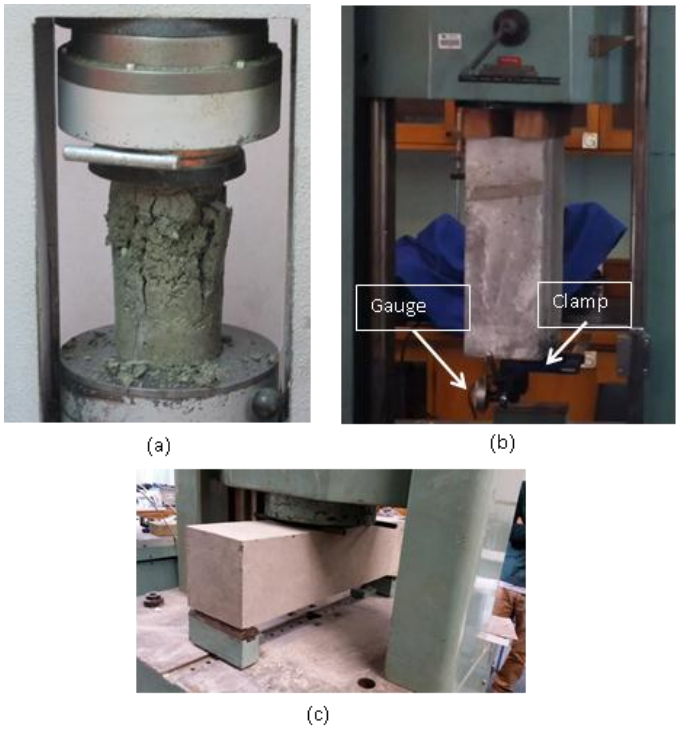

Figure 2: Testing of (a) compressive, (b) pull-out, and (c) flexural specimens

3 RESULTS AND DISCUSSION

3.1 Compressive Properties

Figure 3 shows the results for the 28 day concrete compression strengths. It shows that the majority of the compressive strengths are between 70 and 90 MPa. It also shows there are some samples which had compressive strengths either higher or lower than normal with the highest compressive strength being 113.4 MPa and the lowest being 46.1 MPa. These results showed that the overall variation between the highest and lowest compression strength was large at 67.3 MPa. The average of these samples was 82.6 MPa and he overall standard deviation was 9.29 MPa. The concrete compression strength data showed that there was a range in the compression strength over the time period. Where the majority of the results were within the expected distribution curve for the data. The deviations in the compressive strengths for some specimens, either below or above the average value, were caused by variance in the materials and mixing over a period of 12 months including winter and summer months and/or curing, hence was naturally expected. This warranted the investigation of seasonal distribution of the strength of the specimens, which is presented later in this section.

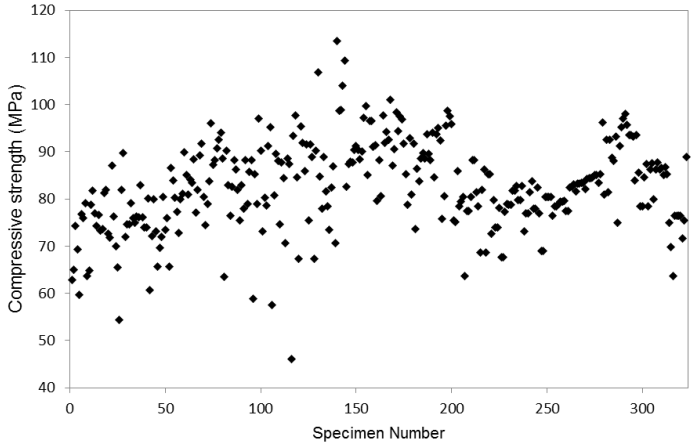

Figure 3: 28 compressive strength of the cylindrical specimens

The compression strength of concrete was further investigated to determine if there was a seasonal difference which needed to be considered in the manufacturing of the prestressed concrete sleepers. Figure 4 show the results of the compression tests when the results are separated into two sets of data, the warmer months and the colder months of the year. The first lot of data, as seen in figure 4(a) shows the compression loads of the samples which were cast over the colder 6 months of the year between 16 April and 15 October. This figure shows the

majority of test results were between 70 and 90 MPa. The average compressive strength during this period was 81 MPa with a standard deviation of 8.7 MPa. Figure 4(b) shows the compression loads of the samples which were cast over the warmer 6 months of the year between 16 October and 15 April. This data shows the majority of the compressive strength tests were between 75 and 95 MPa. The mean compressive strength during this period was 83.8 MPa with a standard deviation was 9.6 MPa.

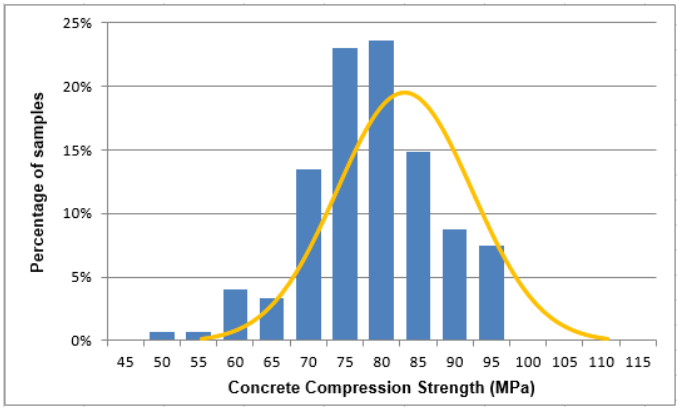

(a)

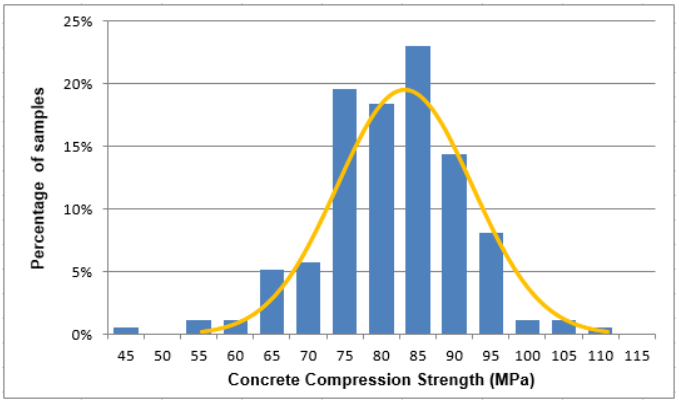

(b)

Figure 4: Distribution of compression strength with overall distribution curve superimposed for (a) winter, and (b) summer

This was seen clearly in the difference between the distributions of the summer and winter data sets where the colder months skewed lower. The results of the compression strength in the summer (warmer months) were more than those from the winter (colder) months. The difference in the compression strength be-

tween summer and winter was therefore due to temperature variations. This behavior was also found that concrete compression was affected by the variation in temperature [10].

3.2 Flexural Properties

The results of the flexural tensile strength tests are shown in Table 1. The table shows that the flexural tensile strength as tested was between 4.18 MPa and 4.51 MPa. The average strength was 4.35 MPa with a standard deviation of 0.17 MPa.

Table 1: Summary of flexural properties

Specimen ID	Flexural Strength (MPa)
1	4.18
2	4.51
3	4.35

3.3 Bond Properties

Figure 5 shows the maximum loads at which the pullout test samples failed completely. The figure shows that the maximum load achieved by any of the samples was 75.41 kN with the lowest being 45.6 kN. The average load was 54.6 with a standard deviation of 7.43 kN. Figure 5 also shows the comparison between predicted and experimental pull-out load. The prediction was carried out using an average compressive strength, 82.6 MPa of concrete, which resulted in a pull-out load of 57.8 kN. The average loads from the tests were found 54.6, which is 5.5% lower than expected. Hence, it is reasonable to consider that they agree with the previous findings [8].

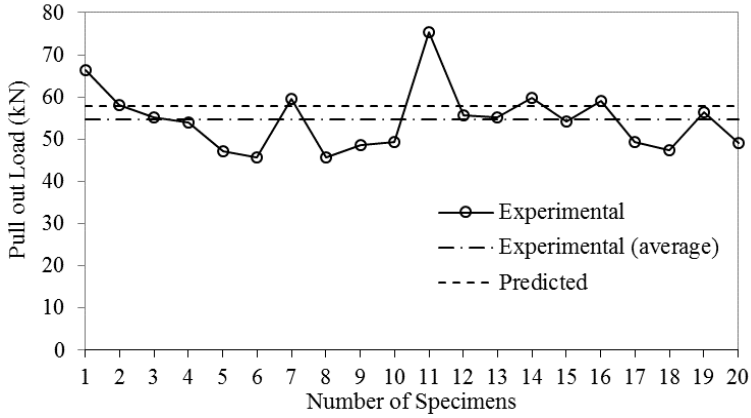

Figure 5: Comparison of experimental and predicted pull-out load.

4 CONCLUSIONS

A HE cement was used to produce concrete that can be used for railway sleepers. The compressive, flexural and pull-out tests were carried out on the specimens. The following conclusions can be drawn:

- The average compressive strength was 83 MPa with the highest value of 113 MPa.
- The compressive strength in the colder months were between 70 and 90 MPa with an average of 81 MPa, whereas the wormer months provided a strength range between 75 and 95 MPa with an average of 84 MPa.
- The average flexural strength with four point bending configuration was 4.35 MPa.
- The average load from the pull-out tests were found 54.6 kN, which was close to the predicted 57.8 kN considering the average compressive strength.

REFERENCES

[1] W. Ferdous, A. Manalo, 2014. Failures of mainline railway sleepers and suggested remedies – Review of current practice. *Engineering Failure Analysis*, 44, pp 17-35.

[2] A.M. Remennikov, M.H. Murray, S. Kaewunruen, 2012, Reliability-based conversion of a structural design code for railway prestressed concrete sleepers. *Proceedings of the Institution of Mechanical Engineers, Part F: Journal of Rail and Rapid Transit*, pp 155-73.

[3] S. Kaewunruen, A.M. Remennikov. 2008. Reliability Assessment of Railway Prestressed Concrete Sleepers. *Australasian Structural Engineering Conference (ASEC)*, Melbourne, Australia, June 26-27.

[4] M.S.J. Taherinezhad, P.A. Mendis, T. Ngo, 2013. A Review of Behaviour of Prestressed Concrete Sleepers. *Special Issue: Electronic Journal of Structural Engineering*, 13.

[5] R. Gustavson, 2002. *Structural Behaviour of Concrete Railway Sleepers*. PhD Thesis, Department of Structural Engineering. Chalmers University of Technology, Göteborg.

[6] A.M. Neville, 2012. *Properties of Concrete. 5th Edition*. Trans-Atlantic Publications Inc.

[7] NZS 3112: Part 2, 1986. *Methods of test for concrete – part 2 – tests relating to the determination of strength of concrete*. New Zealand Standard.

[8] H.Ş. Arel, Ş. Yazıcı, 2012. Concrete–reinforcement bond in different concrete classes. *Construction and Building Materials*, 36, pp 78-83.

[9] ACI 318-99, 1999. *Building Code Requirements for Structural Concrete*. American Concrete Institute, Farmington Hills, Michigan.

[10] R. Preetha, G.V.V.S.R. Kishore, C. Sundaramurthy, C.S. Pillai, A.K. Laharia, 2014. Effect of Curing Methods and Environment on Properties of Concrete. *Concrete research letters*, 5, pp 786-811.

CICM 2015
First International Conference on
Advances in Civil Infrastructure and Construction Materials
MIST, Dhaka, Bangladesh, 14–15 December 2015

REVIEW ON POSSIBLE DETRIMENTAL EFFECTS OF TANNERY WASTEWATER CONSTITUENTS ON CONCRETE

Sinha L. SULTANA[1], Samira Mahmud[2] and Tanvir Manzur[3]

[1, 2, 3] Department of CE, Bangladesh University of Engineering and Technology, Dhaka, Bangladesh.
Email:[1]sinha.lamia@hotmail.com, [2]samiramahmud528@yahoo.com and [3]tmanzur.buet@gmail.com

Abstract. *A Central Effluent Treatment Plant composed of reinforced concrete structures is being constructed in Savar. This raises the question of durability of these reinforced concrete structures against the aggressive nature of tannery wastewaters. This paper focuses on the possible detrimental effects of reactive agents which are present in tannery wastewater on the exposed concrete. Tannery wastewater is composed of sulphate, chloride, ammonium, sulfide and many other chemicals which are reactive with cementitious materials. For instance, reaction with sulphate generates expansive products which lead to spalling and disintegration. It is important to study both the individual and combined effects of all such chemicals when these are present in concentrations similar to that in tannery wastewater. It is also important to understand the long term effect of all these reactions occurring simultaneously on the concrete structures. This paper compiles information from literature which can give a guidance regarding the extent, nature, and severity of the damages caused by those chemicals which are the dominant constituents of tannery wastewater. Such information will be vital-for conducting strength and durability studies in future on concrete exposed to tannery wastewater.*

Keywords: Tannery wastewater, Chemicals, Cementitious materials, Damages, Durability.

1 INTRODUCTION

The tanneries in Hajaribag, Dhaka, process about 60,000 tons of raw hides and skins every year which are not managed in the most efficient ways. This sluggish waste management process has put the environment and human lives in serious jeopardy. The ecosystem of the Hajaribag area has already been severely blemished. With a view to terminate this cycle of environmental pollution, the Government of Bangladesh has ventured a project to relocate all tanneries from Hajaribag to Savar, along with the construction of a Central Effluent Treatment Plantin Savar for management of tannery waste. However, the treatment facility is composed of reinforced concrete structures, which poses a new question: will these structures be durable against the aggressive nature of tannery wastewaters? An average of 30–35 m^3 of wastewater is produced per ton of raw hide. Acids, alkalis, chlorides, ammonium salts, chromium salts, tannins, solvents, sulfate, sulfides, dyes, auxiliaries, and many others compounds which are used in the transformation of raw or semi-pickled skins into commercial goods, are not completely fixed by skins and remain in the effluent. [1] When these chemicals will come in contact with the concrete structures in the treatment facility, several chemical reactions will take place that may lead to degradation of the concrete. This paper focuses on the possible detrimental effects on concrete due to being exposed to four chemicals which are present in tannery wastewater, namely, sodium sulfate, ammonium nitrate, sodium chloride, and sodium sulfide.

2 SULFATE ATTACK

Cements have long been known to undergo deterioration in sulfate rich service environments. The end result of sulfate attack can be excessive expansion, surface area loss, cracking, and loss of strength [2].Sulfates are a component of tannery effluent, emanating from the use of sulfuric acid or products with a high (sodium) sulfate content. Many auxiliary chemicals contain sodium sulfate as a by-product of their manufacture. For example, chrome tanning powders contain high levels of sodium sulphate, as do many synthetic retanning agents. [3]

2.1 The Chemistry of Sulphate Attack

There are three key chemical reactions between sulfate ions and hardened cement pastes. These reactions are:

Recrystallisation of ettringite

In the presence of the calcium hydroxide formed in cement paste, when the latter comes in contact with sulfate ions, the alumina containing hydrates are converted

to the high sulfate form ettringite. It has been agreed upon that these ettringite crystals are expansive [4].

Formation of gypsum

The formation of gypsum as a result of cation exchange reactions is also capable of causing expansion but is normally linked to loss of mass and strength [4].

Decalcification of the main cementitious phase (C-S-H)

This reaction, with more gypsum formation, leads to both strength loss and expansion. Blended cements with lower initial calcium/silica (C/S) ratios in the C-S-H gel are shown to be less susceptible to this type of attack [4].

2.1 Sodium Sulfate

The alkali sulfates can react with the monosulfates to form ettringite. The calcium necessary for its formation is provided by Portlandite [$Ca(OH)_2$], or when the Portlandite is exhausted, by the C-S-H gel. As the calcium of the C-S-H gel is consumed, decreasing its CaO/SiO2 ratio, mechanical properties are adversely affected. Portlandite is dissolved and reacts with the sulfate ions to form ettringite and at higher concentrations, above 1 or 2mg/l, solid secondary gypsum [5,6].

The reactions are as follows:

$$\underset{Solid}{Ca(OH)_2} \rightarrow \underset{Solution}{Ca(OH)_2} + 2Na^+ + SO_4^{2-} \xrightarrow{(H_2O)} \underset{\substack{Solid\\Secondary\\Gypsum}}{CaSo_4.2H_2O} + \underset{Solution}{2Na^+ + 2OH^-} \cdots (1)$$

$$2SO_4^{2-} + \underset{Monosulfate}{Ca_4Al_2(OH)_{12}.SO_4.6H_2O} + 2Ca^{2+} \rightarrow \underset{\substack{Ettringite\\Expansion}}{Ca_6Al_2(OH)_{12}.(SO_4)_3.26H_2O} \ldots (2)$$

$$Ca(OH)_2 \rightarrow Ca^{2+} + 2OH^- \cdots\cdots\cdots (3)$$

The initial action of the alkali sulfates may result in increase in strength because of the filling of pores with newly formed ettringite. However, the process is physically expansive and stress is created. When the stress exceeds the tensile strength of concrete, cracking and spalling occur. A scaly surface is often produced because of the local ettringite formation or crystallization of gypsum or both. [2]

It is generally agreed [7] that the main cause of spalling under exposure to sulfate solution and wet-dry cycles is due to crystallization pressure**.** There are several theories of how crystallization pressure develops. According to Flatt [7], a crystal will grow in all directions until its surface attains a local weighted mean

curvature that is in equilibrium with the concentration of the solution. There exist large repulsive forces between the crystal and the surface of the pore. Due to this, the crystal will stop growing towards the pore surface. Scherer [8] also showed that large forces are required to overcome the surface tension and hence direct contact between the crystal and the surface of the pore is not possible. A thin film exists between the crystal and pore wall and the concentration of the thin film is not in equilibrium with the radius of the pore. As a result, the tip of crystal grows in the opposite direction of the pore and eventually causes stress within the matrix.

2.3 Sulfide Attack

The sulfide content in tannery effluent results from the use of sodium sulfide and sodium hydrosulfide, and the breakdown of hair in the unhairing process. [3]

Oxidation of sulfides in aggregates results in additional sulfate being produced that can induce formation of ettringite in the post-hardening stage [2]. The suspect aggregates have particles of pyrite or pyrrhotite, or both, that are slowly oxidized, liberating sulfate that reacts with the cement components, including any remaining calcium monosulfoaluminate, to form ettringite [2].

If the sulfide is oxidized somehow, there is a possibility of ettringite formation. The oxidation products may also react to form gypsum once the potential for ettringite formation is exceeded. Therefore, presence of sodium sulfide in tannery effluent may increase the aggressiveness of sulfate attack.

3 AMMONIUM ATTACK

Of the factors that can degrade concrete, ammonium salts are the most aggressive [9,10]. Ammonium nitrate is mostly the outcome of the deliming process, with comparatively small volumes being produced from liming and unhairing [3].Damage observed on concrete structures in contact with ammonium nitrate is of two types, depending on the environment [2]:

i) A very large increase in porosity with a weakening of mechanical properties in concrete continuously immersed in a solution of ammonium nitrate.

ii) Very notable swelling with occurrence of cracks linked to the formation of expansive crystals in concrete in contact with the air or subjected to wet-dry cycles.

3.1 Chemistry of Ammonium Nitrate Attack

Chemical attack by ammonium nitrate leads to a very soluble calcium nitrate, a slightly soluble calcium nitro aluminate, and release of ammonia gas. This process mainly induces total leaching of calcium hydroxide and rapid decalcification of C-S-H [2].

Ammonium salts are hygroscopic and highly soluble in water. They decompose in water according to:

$$NH_4NO_3 \rightarrow NH_4^+ + NO_3^- \cdots\cdots(4)$$

In a basic environment, ammonium ions (weakly acidic) are transformed to aqueous ammonia with the formation of H^+ ions according to the following equation:

$$NH_4^+ \rightarrow NH_3(aq) + H^+(aq) \cdots\cdots(5)$$

Ammonium ions react according to an exchange reaction, $2NH4^+ \rightarrow Ca^{2+}$. The calcium salt produced (calcium nitrate) is highly soluble and this leads to the progressive dissolution of the all calcium bearing cement phases. Moreover in the presence of cementitious material (pH between 12 and 13.5) the equilibrium of equation (5) is strongly moved to the right, i.e. aqueous NH_3 and H^+ ions are dominant. This release of H^+ ions decreases the pH and accelerates the successive dissolution of calcium bearing phases. Portlandite, C-S-H, and aluminates AFt ("alumina, ferric oxide, tri-sulfate")and AFm("alumina, ferric oxide, mono-sulfate")are dissolved according to the following equations [2]:

$Ca(OH)_2$:

$$Ca(OH)_2 + 2NH_4NO_3 \rightarrow Ca^{2+} + 2NO_3^- + 2(NH_3.H_2O) \text{.....(6)}$$

C-S-H:

$$C-S-H + 2xNH_4NO_3 \rightarrow C_{(1-x)} - S - H_{(1-2x)} + xCa^{2+} + 2xNO_3^- + 2x(NH_3.H_2O) \text{ .....(7)}$$

AFm:

$$3CaO.CaSO_4.Al_2O_3.12H_2O + 12NH_4NO_3 \rightarrow 4Ca^{2+} + SO_4^{2-} + 2Al^{3+} + 12NO_3^- + 12(NH_3.H_2O) + 6H_2O \text{.....(8)}$$

Aft:

$$3CaO.3CaSO_4.Al_2.O_3.32H_2O + 12NH_4NO_3 \rightarrow 6Ca^{2+} + 3SO_4^{2-} + 2Al^{3+} + 12(NH_3.H_2O) + 26H_2O \text{.....(9)}$$

Nitrate ions can react with calcium ions to form very soluble calcium nitrates. Aluminates can also react with nitrate ions to form a less soluble calcium nitro aluminate salt, $3CaO.Al_2O_3.Ca(NO_{3)2}.10H_20$ [11]. Similarly in the presence of sulfates, the possibility of the formation of a double salt $CaSO_4.(NH_4).2SO_4.2H_2O$ has also been mentioned [12].

When cementitious materials are immersed in ammonium nitrate solution, the calcium ions diffuse to the exterior without any formation of calcium salts in the material as the solubility of Portlandite increases significantly in these solutions. In this case the degradation is defined by a diffusion mechanism and its kinetics can be explained by Fick's law, relating the degraded thickness to the square root of immersion time in the aggressive solution[13].Also, the weight loss of the cement samples increases continuously with time during the leaching process [14]. If the concrete is subjected to drying, swelling related to the precipitation of salts of calcium nitro-aluminates, can be observed. In all cases, degradation reactions related to ammonium nitrate solutions are swift and severe.[15]

4 CHLORIDE ATTACK

Chlorides can attack thehydration phase of cement paste in concrete, primarily leading to lowering the alkalinity of concrete [2] and also cause other forms of concrete deterioration like corrosion of reinforcing steel pitting [16].Chloride is introduced into tannery effluents as sodium chloride usually on account of the large quantities of common salt used in hide and skin preservation or the pickling process [3].

4.1 Sodium Chloride Attack On Concrete

Sodium chloride has been shown to leach calcium hydroxide and cause chemical changes in Portland cement, leading to loss of strength, as well as attacking the steel reinforcement present in most concrete.When concrete is stored in a chloride solution, chloride ions diffuse into concrete, and the diffusion speed is dependent of the salt, in which the chloride is a part. In salts, the chloride ions diffuse much more rapidly than the metal ions so the chloride ions penetrate concrete more rapidly than the metal ions [15].

According to the "mutual diffusion theory", the hardened cement paste will lose an amount of hydroxide ions, OH^-, corresponding to how much the amount of chloride ions exceeds the equivalent amount of corresponding metal ions. This mechanism could explain the loss of calcium hydroxide in concrete, stored in a strong chloride solution [16]. Sodium chloride forms calcium chloro-aluminate hydrate and attack tetracalcium aluminate ferrite, as given in the equations below:

$$C_4AF + 4Ca(OH)_2 + 4Na^+ + 4Cl^- + 22H_2O \rightarrow C_3A.CaCl_2.12H_2O + C_3F.CaCl_2.12H_2O + 4Na^+ + 4OH^- \quad .....(10)$$

where, F stands for Fe_2O_3 (ferric oxide).

5 CONCLUSION

In this paper, the effects of those constituents of tannery effluent have been discussed which pose significant threats to concrete. The chemistry between different constituents and concrete, as described here, is of great importance for understanding the behavior of concrete under such harsh conditions.The effects of other constituents are not as detrimental as these. Both sulfates and ammonium salts have considerable adverse effects on cement paste. Sodium chloride has the effect of leaching calcium hydroxide, which could reduce the strength of concrete. The chloride may eventually attack the embedded steel reinforcement. The effect of sodium sulfide may be dependent on the oxidation of sulfide into sulfate, after which the produced sulfate can attack the cement paste. The oxidation of sulfide into sulfates may in turn depend on a number of factors, which could be explored through further studies. The exact composition and concentration of the chemicals present in tannery wastewater may vary depending on local practice, extent of treatment, sensitivity of treatment process etc.Also, there are no definitive recommendations for concrete under such conditions. Therefore, a comprehensive parametric study is required to establish guidelines for mitigation of possible damages and increase the durability of concrete exposed to tannery wastewater.

REFERENCES

[1] B.I. Islam , A.E Musa ,E.H. Ibrahim , Salma A.A Sharafa , and Babiker M. Elfaki (2014) “Evaluation and Characterization of Tannery Wastewater”, Research Article 141, Journal Of Forest Products & Industries

[2] E. Menendez, T. Matschei, F.P. Glasser (Chapter 2, Part I), Gilles Escadeillas (Chapter 5, Part I), Yuan Q, M Santhanam (Chapter 13, Part III) &A. Chatterjee, A. Goyns (Chapter 16, Part IV) (2013), Performance of Cement Based Materials in Aggressive Aqueous Environments, STAR 211-PAE, Springer.

[3] M. Bosnic, J. Buljan and R. P. Daniels (2000) “ Pollutants in tannery effluents”,9 august 2000, us/ras/92/120, Regional Programme for Pollution Control in the Tanning Industry in South-East Asia, United Nations Industrial Development Organization (UNIDO)

[4] QCL Group Technical Note, 1999. Sulphate Attack and Chloride Ion Penetration: Their Role in Concrete Durability.

[5] J. Skalny, J. Marchand, I.Odler (2002) Sulfate attack on concrete. Spon Press, Taylor & Francis Group, London
[6] P.W. Brown (1981) An evaluation of the sulfate resistance if cement in a controlled environment. Cement and Concrete Research 11(5-6): 719-727
[7] R.J. Flatt (2002) Salt Damage in Porous Materials: How High Supersaturation in Generated. Journal of Crystal Growth 242:434-454.
[8] G. Scherer (1999) Crystallization in pores. Cement and Concrete Research 29 (8): 1347-1358.
[9] F.M. Lea (1965) The action of ammonium nitrate salts on concrete, Magazine of Concrete Research 17 (52):115-116
[10] I. Biczok (1972) Concrete corrosion and concrete protection, Akademiai Kiado, Budapest
[11] V. Ukraincik, D. Bjegovic, A. Djurekovic (1978) Concrete corrosion in a nitrogen fertilizer plant. In: Proceedings of the First International Conference on the Durability of Building Materials and Components, Ottawa, Canada, 397-409
[12] A. Mohr (1925) Uber die Einwirkung von Ammoniumsalzlosungen auf Beton. Der Bauingenieur 6(8):284-293 (in German)
[13] V.H. Nguyen , H. Colina, J.M. Torrenti, C. Boulay, B. Medjar(2007) Chemo-mechanical coupling behavior of leached concrete-Part 1: Experimental results, Nuclear Engineering And Design 237 (20-21):2083-2089
[14] S.Y. Xie, J.F. Shao, N. Burlion (2008) Experimental study of mechanical behavior of cement paste under compressive stress and chemical degradation, Cement and Concrete Research 38 (12):1416-1423
[15] KejinWanga, E. Daniel, Nelsena and W. A. Nixon, "Damaging effects of deicing chemicals on concrete materials", Cement and Concrete Composites Vol. 28(2), pp 173-188
[16] Srrolczyk, G. Heinz(1968) "Chemical Reactions of Strong Chloride-Solutions with Concrete." Proceedings ofThe Fifth International Symposium on the Chemistry of Cement, Tokyo (1968).

CICM 2015
First International Conference on
Advances in Civil Infrastructure and Construction Materials
MIST, Dhaka, Bangladesh, 14–15 December 2015

EFFECT OF SPECIMEN SIZE ON COMPRESSIVE STRENGTH OF CONCRETE

Belal Hossen[1], **Md. A. Islam**[2] **and Rawson Jadid**[3]

[1]Presidency University, Dhaka, Bangladesh
Email: jabed.buet@gmail.com

[2, 3] Bangladesh University of Engineering and Technology, Dhaka, Bangladesh.
Email: [2]aziz.buet@gmail.com and [3]rowshonjadid@yahoo.com

Abstract. *It is well known that strength of any tested materials like concrete or mortar is affected by the specimen size; therefore it is important to consider the effect of specimen size when estimating the compressive strength of such materials. This study aims to assess the effect of specimen size on compressive strength of cylinder and core and establish a relationship between 150mm diameter cylinder to smaller diameter cylinder. Four different sizes of cylinder and three different sizes of cores are used with a constant mixed proportion (1:1.5:3) to obtain the conversion factors from 50mm or 100mm cylinder strength to 150 mm cylinder strength. Some best fit relationships that relate this compressive strength of different diameter are presented in this study although it cannot be generalized due to the fact that the presented results are based on limited number of test specimens with constant mix proportion and height to diameter ratio.*

Keywords: Compressive strength, Size effect, Core strength, Conversion factor.

1 INTRODUCTION

The standard specimen size for testing the compressive strength of concrete is 150mm x300mm cylinder. As the smaller specimen than the standard size save construction materials & transportation cost significantly and also smaller specimens are easy to handle, an effort has been taken to investigate the effect of smaller specimen size on compressive strength of concrete. This investigation showed that the compressive strength of concrete cylinder increases with the decrease of specimen sizes. On the other hand, 100mm x 200mm core is recommended by ASTM to measure the in-place strength of concrete. However, it is very difficult to obtain a 4 inch clear space between rebar. Also, smaller cores make the cutting operation easier and ensure greater structural safety as well. Therefore, this study adopted a test scheme to observe the effect of smaller core specimen on in-place compressive strength of concrete. It was found that the compressive strength of core specimen decreases with the decrease of core diameter.

Several researchers have compared measured strengths achieved with different sizes of cylindrical specimens for high strength concrete. For cylindrical specimens, comparisons were usually made between the compressive strength of 150x 300mm cylinders and that of 100x 200mm cylinders. Carrasquilloetal(1981) reported that the average ratio of compressive strength of150x 300mmto 100x 200 mmcylinderswas0.9regardless of strength and test age [1]. A contradiction to this finding was later reported by Carrasquilloetal (1988) in which he reported that compressive strength of 100x200 mm cylinders were 7 percent lower than those of 150x 300 mm cylinders [2]. French *et al*. (1993) observed in their study that on average 100x 200 mm cylinders tested showed6percenthigherstrengththan thatoftheircompanion150x300mmcylinders [3].Aitcin *et al.* (1994) reported that larger cylinder sizes gave rise to lower apparent compressive strength, and that compressive strength is not sensitive to cylinder size for very high strength concrete [4].

In this paper, a comparison of compressive strength of concrete for different sizes of cylinder and core strength was made and suitable conversions factors or strength factors were proposed which can be multiplied with the smaller diameter of cylinder and core specimen than the standard sizes to predict the approximate concrete strength of standard specimen. Finally, two empirical correlations were suggested to predict the strength factors for any diameter of cylindrical specimen and core respectively.

2 MATERIALS AND METHODOLOGY

2.1 Materials

The use of locally available materials from different sources in Dhaka area was emphasized in this study. For the cases where locally available materials were not attainable, commercially available materials were used. The followings are the details for the materials used in the laboratory mixes.

2.1.1 Cement

Commercially available Portland cement Type 1 conforming to ASTM C 150 specification [5] was used in this study. The Properties of the cement are shown in Table 1.

Table 1: Properties of Binding Material (Cement)

Properties	**Characteristic Values**
Specific Gravity	3.15
Normal of cement consistency	22% to 30%
Absorption, percent	0.8032%
Initial setting time	34 minutes
Final setting time	250 minutes

2.1.2 Coarse Aggregates

Locally available 20mm downgraded stone chips were used as coarse aggregates.

2.1.3 Fine Aggregates

Natural Sylhet sand was used in the overall studyits FM was 2.52. The sand was washed with water and air dried before being used to obtain Saturated Surface Dry (SSD) condition.Properties of Coarse aggregate and fine aggregate are shown in Table 2.

2.1.4 Mixing Water

Drinking tap water was used for both mixing and curing. The temperature of the used water throughout the experiment period ranged between (20~27°C)

2.2 Test Program

To study the effects of specimen size on the compressive strength of concrete, it was proposed to prepare three specimens for each size. Cylinders were casted in different sizes (50mm, 75mm, 100mm & 150mm) using steel and UPVC pipe molds according to ASTM C 192 [6]. Fresh concrete was prepared with mixing ratio 1:1.5:3 (by weight) with hand mix. The fresh concrete was placed in the mold in four layers and compacted by using 16mm (5/8") diameter and 600mm (24") in length tampering rod with hemispherical tip. In all cases, the numbers of tamping were randomly 25; 25; 18 and 12 per layer. Proper compaction was ensured over the cross-section of the mold through uniform distribution of the temping strokes. Then, the specimen was stored undisturbed for 24 hours in such a way that it prevents moisture loss and maintained the specimen within room temperature. In this study weight batching has been used for measuring the materials. After (28) days of standard curing in saturated water at (23ºC+3ºC) , specimens is then placed between the two platens of a testing machine and the load is applied at a defined rate until failure. The compressive strength tests were performed according to ASTM C 39 [7].For core strength test, a 2100mm x 250mm x 250mm column shutter was made using wooden shutter. Similar concrete was used for column casting. After 24 hours, the shutter was removed from the column and curing was started until 28 days. After completing curing for 28 days 3 NOs of 75mm diameter, 3 NOs of 50 mm diameter cores and 3 NOs of 100 mm cores were cut using core cutting machine. For making level edge, grinding machine was used.

Table 2: Physical Properties of Coarse and Fine Aggregate

Properties	Coarse Aggregate	Fine Aggregate
Fineness Modulus (FM)		2.52
Maximum Size Aggregate, mm	20	
Dry Unit Weight, lb/ft^3	100	103
Absorption, percent	0.8032%	2.6%
Bulk Specific Gravity (S.S.D)	2.74	2.64
Bulk Specific Gravity (oven-dry)	2.63	2.64

3 TEST RESULTS AND DISCUSSION

To develop a relation among different sizes of cylinder and compressive strength of concrete, four sets of cylinder were prepared in which cement content, water content, fine aggregate content and coarse aggregate content were same. The average 28-day compressive strength for 50x100 mm, 75x150mm, 100x200mm, 150x300mm are shown in the Table 3. The observed strength factors with respect to 150mm diameter cylinder are also shown in the Table 3.

Table 3: Comparison of the compressive strength of cylinder with diameter for mix ratio of 1:1.5:3

Exp. No	Dia. (mm)	Height (mm)	Load (lb)	Average Crushing strength (psi)	Strength Factor w.r.t. 150 mm dia. Strength
Exp-1	50	100	8986.80	2861.62	1.60
Exp-2	75	150	17598	2490	1.39
Exp-3	100	200	30705	2444.67	1.37
Exp-4	150	300	50550	1788.10	1

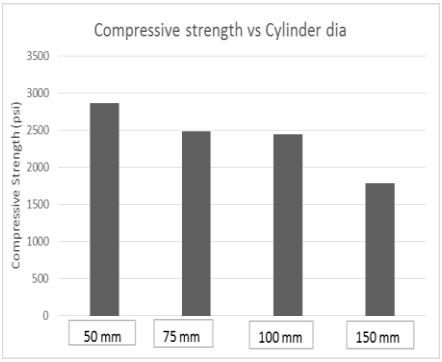

Figure 1: Decreases of compressive strength with the increase of diameter

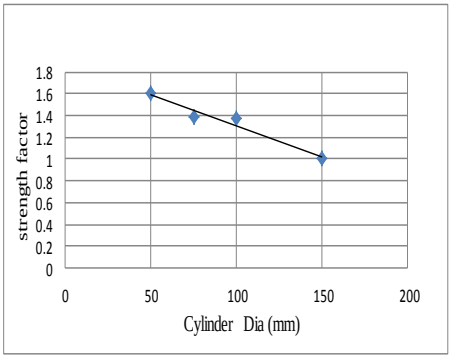

Figure 2: Strength Factor (w.r.t. 150 mm cylinder) vs cylinder diameter

From Figure 1 and Figure 2, it can be concluded that the compressive strength of concrete decreases linearly with the increase of cylinder diameter. This also confirms the presence of a size effect where the nominal compressive strength at

failure decreases with the specimen size increases [8]. From figure 2, the following empirical equation can be proposed:

$$y = -0.0057x + 1.8769 \quad (1)$$

Where, y = the ratio of the given sample strength to 150 mm cylinder strength x = the diameter (in mm) of cylinder.

For the core strength test, two cylindrical core sizes (50mm diameter x 100mm and 75mm diameter x 150mm) were cut from the casted column. The results of the compressive strength test are given in Table 4.

Table 4: Comparison of the compressive strength of core with diameter for mix ratio of 1:1.5:3

Exp. No	Dia. (mm)	Height (mm)	Load (lb)	Avg. Crushing strength (psi)	Strength Factor w.r.t.150mm dia. Strength
Exp-1 (core)	50	100	6182	1967.25	0.70
Exp-2 (core)	75	150	15511	2197.15	0.78
Exp-3 (core)	100	200	30110	2396.10	0.85
Exp-4 (cylinder)	150	300	79807	2821.30	1

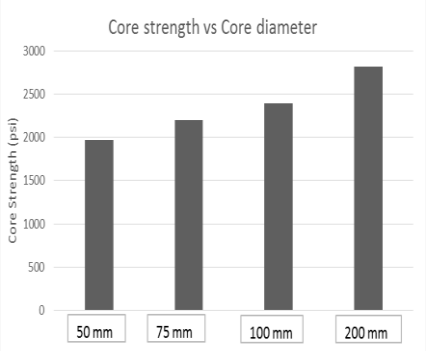

Figure 3: Variation Core strength with core diameter

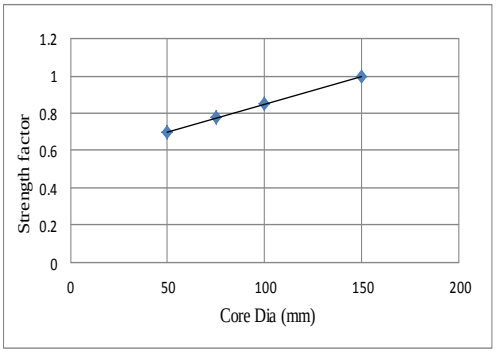

Figure 4:Strength Factor(w.r.t.100 mm core) vs core diameter

From figure 3 it is observed that core compressive strength decreases with the increase of specimen diameter. This is probably due to fact that micro crack forms during drilling operation. As small sized specimen has significant cracking effect, its compressive strength is found lower. For core strength test, the equation that relates the conversion factors or strength factors with the core diameter according to figure 4 is given below:

$$y = 0.003x + 0.5529 \qquad (2)$$

Where, y = the ratio of the given sample strength to 150 mm cylinder strength
x = the diameter (in mm) of the core sample.

4 CONCLUSION

From this investigation the following conclusion can be made:

- The strength of the cylinder specimens increases with the decrease of specimen sizes of same aspect ratio due to end frictional effect.
- The strength of the core specimen decreases with the decrease of core sizes of same aspect ratio due to formation of cracking during drilling operation.
- The reduced size of cylinder and core may be used in the test purposes with suitable conversion factors suggested by this study.

REFERENCES

[1] R. Carrasquillo, A. Nilson and F. Slate, 1981. Properties of hugh strength concrete subjectedd to short term loads. *ACI Journal,* **78(3),** pp 171-178.

[2] P.M. Carasquillo and R.L. Carrasquillo, 1988. Evaluation of the high strength concrete practice in the production of high-strength concrete. *ACI Materials Journal*,**85(1)**, pp 49-54.

[3] C.W. Frenchand A. Mokhtarzadeh, 1993. High strength concrete: effects of material, curing and test procedures on short-term compressive strength. *PCI Journal*,**38(3),** pp76-87

[4] P.C. Aitcin, W. D. Cook and D. Mitchell, 1994. Effects of size and curing on cylinder compressive strength of normal and high-strength concretes. *ACI materials Journal*,**91(4),** pp 349-354.

[5] ASTM C 150, 1997. Standard Specification for Portland Cement. Annual Book of the ASTM Standards. *American Society for Testing and Materials.*

[6] ASTM C 192, 1995. Standard Practice for Making and Curing Concrete Test Specimens in the Laboratory. Annual Book of the ASTM Standards. *American Society for Testing and Materials.*

[7] ASTM C 39, 1996. Standard Test Method for Compressive Strength of Cylindrical Concrete Specimens. Annual Book of the ASTM Standards. *American Society for Testing and Materials.*

[8] S. Sener, 1997. Size effect tests of high strength concrete. *Journal of Materials in Civil Engineering*,**9(1),**pp 46-48

CICM 2015
First International Conference on
Advances in Civil Infrastructure and Construction Materials
MIST, Dhaka, Bangladesh, 14–15 December 2015

KINETIC MODEL FOR MORTAR EXPANSION

Mohammad S. Islam[1], Abdulazziz Allessa[2], Mumtasirun NAHAR[3]

[1, 2] University of Tabuk, Tabuk, Saudi Arabia
Email: [1]shahidul92@hotmail.com

[3] Military Institute of Science and Technology, Dhaka
Email: mumtasir.mist2006@gmail.com

Abstract. *This study predicts the ultimate expansion of mortar bars (UME) due to alkali-silica reactivity (ASR). The aggregates utilized in this study were obtained from two previous studies. The experimental expansion data over the test duration of 28 days was fitted with the existing proposed decay model to predict the UME and time required to reach at 50%, 75% and 90% of UME. Finally, aggregates susceptible to alkali-silica reactivity were determined based on the existing proposed limit of ultimate mortar expansion, and were compared with the results obtained by the aggregate geology and expansion limits at the test durations of 14 and 28 days. The study showed that the ultimate mortar expansion and time required reaching various percentages of UME varied on aggregate mineralogy.*

Keywords: Alkali-silica reaction, Kinetic model, Mortar expansion, Test durations, Aggregate mineralogy, Failure limits

1 INTRODUCTION

Alkali-silica reaction (ASR) is one of the most deleterious chemical phenomena in concrete structures, and is a major concern in many countries of the world [1-4]. ASR can cause significant expansion and cracking in concrete [4-8].Among all the standard test methods to determine the ASR reactivity of an aggregate, [9-10] is the most widely used testing method due to its short test duration.

Since ASR is a kinetic type reaction, [3, 11-12] demonstrated that a kinetic model can be implemented to predict the ASR-induced expansion characteristic. Most recently, concrete at the nuclear power plants has shown to be decayed resulting a great concern for nuclear safety authorities [13]. Most recently, Islam [3] proposed the ASR decay model (ADM), shown in Eq. (1), to determine the ultimate mortar expansion (UME) and time to reach at the UME. The utilization of ASR decay model to predict the ultimate mortar expansion was very limited in the post studies. It is a vital topic that needs to be addressed.

$$\varepsilon_t = \varepsilon_0[1 - e^{(-\lambda t)}] \qquad (1)$$

Where, ε_0 is the ultimate mortar expansion; t is the test duration in days; ε_r is the residual expansion at t days; λ is the first order rate constant, which has a unit of 1/t.

2 RESEARCH SIGNIFICANCE

The utilization of ASR kinetic model (ADM) in predicting the ultimate expansion of mortar bar is a unique technique, which can widely be used by the field engineers and researchers to reduce the test duration. Finally, the ASR evaluation of the aggregates was determined using the existing limit of the ultimate mortar expansion, and was compared with the results generated from the aggregate geology and the expansion limits at the test durations of 14 and 28 days.

3 EXISTING EXPERIMENTAL DATA

The experimental data utilized in this study was compiled from the two existing research investigations, conducted by [4-5]. The raw materials utilized in this study consisted of ten aggregates (five from [4] and the remaining five from [5]. The identification and rock type of the investigated aggregate groups were shown in Table 1. The aggregate susceptibility due to the alkali-silica reaction was then determined according to the geological nomenclature, as described in the studies conducted by [2, 5, 8]. The results are also shown in Table 1. The expansion reading of mortar bar was taken at the test durations of 0, 4, 6, 10, 14, 21 and 28 days.

Table 1: Identification, rock type and ASR potential of the investigated aggregate groups

Previous Studies	Aggregate Id	Rock Type	Potential ASR Reactivity
Touma (2000)	A1-WY	Rhyolite	Innocuous
	A9-NE	Granite	Innocuous
	B4-VA	Quartz	Reactive
	C2-SD	Quartz	Reactive
	D2-IL	Dolomite	Innocuous
Islam (2010)	SN-A	Dolomite	Innocuous
	SN-C	Dolomite-Limestone	Reactive
	SN-D	Dacite	Reactive
	NN-B	Andesite	Reactive
	NN-C	Basaltic-andesite	Reactive

4 RESULTS AND DISCUSSIONS

4.1 Mortar Expansion Over the Test Duration

The development of mortar expansion of the investigated five aggregate groups, obtained from the research study conducted by [5] is shown in Fig.1. As can be seen, the mortar expansion increased with an increase in test duration, and the expansion rate was extensive and faster for the reactive aggregates as compared to that of innocuous aggregate groups.

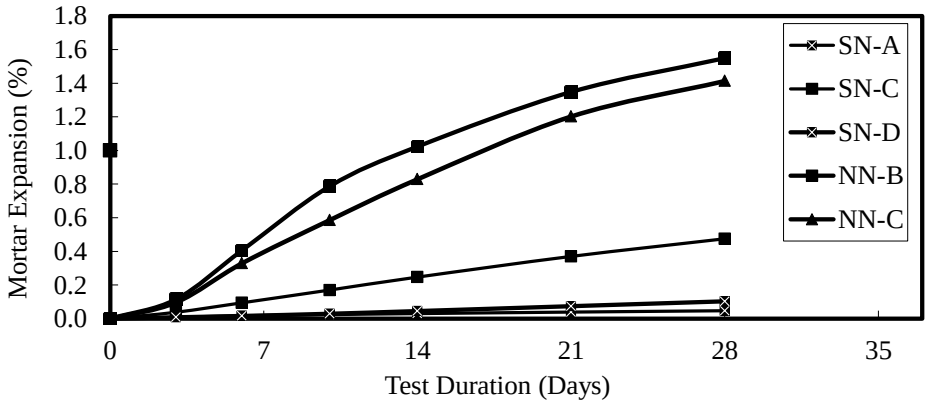

Figure 1: Progression of mortar expansions obtained the study conducted by Islam (2010)

4.2 ASR Decay Model

The mortar expansion of the aggregates over the 28-day test duration was fitted with Eq. (1), and the values of coefficient ε0 and λ, their Prob(t), Prob(F) and R^2 were determined. Finally, time needed in reaching at 50%, 75% and 90% of ultimate mortar expansions was evaluated. The results are documented in Table 2. As can be shown, a strong correlation existed with R^2values of 0.848~0.993 with an average of 0.944. Additionally, another reliable parameter for multiple regression models (R^2_{adj}) was shown very close to the R^2 values for the respective aggregate group. The Prob(t) for all regression coefficients, and Prob(F) were shown to be close proximity to 0.0000. Moreover, the standard errors of the estimate for each aggregate were shown to be very small.

Time required to reach various percentages of UME of the investigated aggregate groups is shown in Fig. 2. It can be shown, the 50%, 75% and 90% of the UME of the investigated ten aggregates occurred from 4.70 to 11.77 days with an average of 8.71 days, from 9.40 to 23.54 days with an average of 17.42 days, and from 15.61 to 39.09 days with an average of 28.93 days, respectively.

4.3 ASR Classifications of the aggregates

Table 3 shows the ASR classifications of the aggregates based on the aggregate geology and expansion limits at the ages of 14 and 28 days. Additionally, the results obtained by the failure limit of ultimate mortar bar were also evaluated, and were presented in Table 3.

Table 2: Statistical analysis of ADM model (Eq. (1)), ultimate mortar expansion (ε_0) and time required to reach 50%, 75% and 90% of ε_0

Agg. ID	Regression Coefficients (RC)		t-ratio of RC		Prob(F)	R^2	R^2_{adj}	$t_{1/2}$[a] (Days)	$t_{3/4}$[b] (Days)	$t_{9/10}$[c] (Days)
	λ	ε_0	Λ	ε_0						
A1-WY	0.0921	0.3703	-22.58	-24.41	0.0000	0.993	0.992	7.53	15.05	25.00
A9-NE	0.0781	0.4245	-8.92	-9.48	0.0007	0.957	0.947	8.88	17.75	29.48
B4-VA	0.062	0.3053	-11.14	-6.78	0.0025	0.920	0.900	11.18	22.36	37.14
C2-SD	0.0679	0.2952	-12.63	-8.20	0.0012	0.944	0.930	10.21	20.42	33.91
D2-IL	0.1475	0.0418	-8.70	-4.72	0.0092	0.848	0.810	4.70	9.40	15.61
SN-A	0.083	0.0498	-61.41	-19.41	0.0000	0.990	0.987	8.35	16.70	27.74
SN-C	0.0712	0.5475	-6.44	-8.68	0.0010	0.950	0.937	9.74	19.47	32.34
SN-D	0.0589	0.1168	-23.22	-7.27	0.0019	0.930	0.912	11.77	23.54	39.09
NN-B	0.0988	1.8678	6.20	-11.19	0.0004	0.969	0.961	7.02	14.03	23.31
NN-C	0.0897	1.7226	4.26	-8.02	0.0013	0.941	0.927	7.73	15.45	25.67

[a]Time (days) required to reach 50% of ultimate mortar expansion; [b]Time (days) required to reach 75% of ultimate mortar expansion; [c]Time (days) required to reach 90% of ultimate mortar expansion

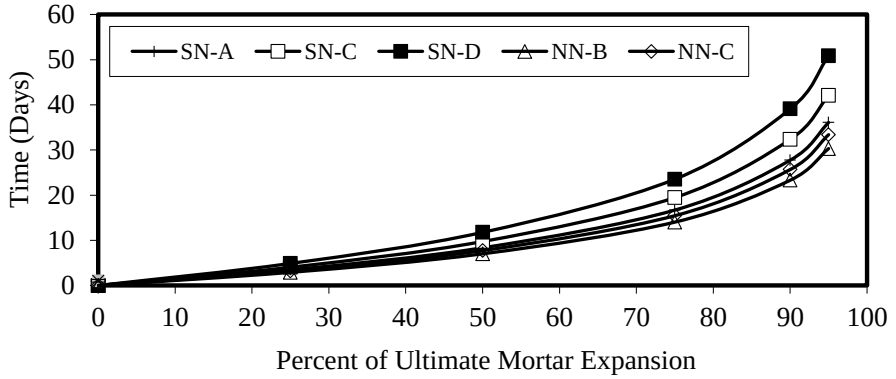

a) Islam (2010)

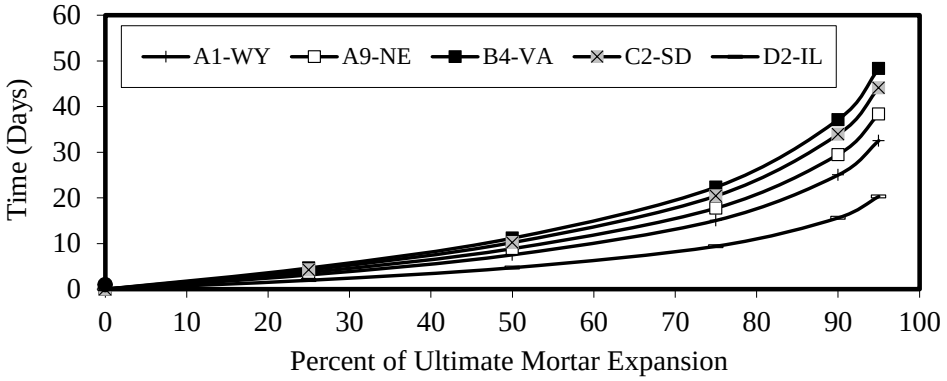

b) Touma (2000)

Figure 2: Time required reaching percent of ultimate mortar expansion

The 14-day failure criteria of the ASTM C 1260 resulted in some innocuous aggregates as reactive. As compared to the results obtained at 14 days, the limit at the extended age of 28 days showed more liable. Finally, the ultimate expansion limit underestimated some reactive aggregates as innocuous. The reason can be stated that the mortar expansion data up to the 28 testing period was not sufficient for the ADM model to predict the ultimate mortar expansion. The expansion data at the extended testing period of at least 56 days would better predict the UME of aggregates, and hence, the ASR classifications of the aggregates can be improved.

5 CONCLUSIONS

This study showed that the ASR decay model was well suited with the mortar expansion over the testing duration of 28 days. The ultimate mortar expansion (UME) and time needed in reaching at 50%, 75%, and 90% of the UME varied

mainly on the geology of the investigated aggregate group. When compared to the 14-day expansion limit, the proposed failure criteria of ultimate mortar expansion showed better correlations with the findings obtained from the previously suggested 28-day the expansion limit in evaluating alkali–silica reactivity of the investigated aggregates.

Table 3: ASR classifications based on the expansion limits of mortar bars

Agg. ID	**Aggregate Mineralogy**	**14-Day (0.10%)[a]**	**28-Day 0.28%[b]**	**UME 0.64%[c]**
A1-WY	Innocuous	0.034 (I)	0.050 (I)	0.3703 (I)
A9-NE	Innocuous	0.118 (R)	0.233 (I)	0.4245 (I)
B4-VA	Reactive	0.272 (R)	0.502 (R)	0.3053 (I)
C2-SD	Reactive	0.055 (I)	0.117 (I)	0.2952 (I)
D2-IL	Innocuous	0.044 (I)	0.067 (I)	0.0418 (I)
SN-A	Innocuous	0.465 (R)	0.620 (R)	0.0498 (I)
SN-C	Reactive	0.161 (R)	0.277 (I)	0.5475 (R)
SN-D	Innocuous	1.098 (R)	1.610 (R)	0.1168 (I)
NN-B	Reactive	0.940 (R)	1.472 (R)	1.8678 (R)
NN-C	Reactive	0.186 (R)	0.322 (R)	1.7226 (R)

I: Innocuous; R: Reactive; [a]Expansion limit suggested by ASTM C 1260 (2007)
[b]Failure limitrecommended by Islam (2010); [c]Failure limitsuggested by Islam (2015)

REFERENCES

[1] Ghafoori, N., and Islam, M. S., Time Series analysis for prediction of ASR-induced expansions. Constr Build Mater 2013; 49:194-200.

[2] Ghafoori, N., and Islam, M. S., Evaluation of alkali-silica reactivity using mineralogy of aggregates and the expansion tests, Proceedings of the 5th International Structural Engineering and Construction Conference, September 22-25, 2009, Las Vegas, pp. 467-472.

[3] Islam, M.S., and Ghafoori, N., Influence of cement alkalis on the mortar expansion of ASTM C 1260, Journal of ICE-Construction Materials, 2015 (in press)

[4] Touma, W. E., Alkali-silica reaction in Portland cement concrete: testing methods and mitigation alternatives. Doctoral Dissertation, University of Texas, 520 pp., 2000.

[5] Islam, M. S., Performance of Nevada's aggregate on alkali-aggregate reactivity of Portland cement Concrete, Doctoral Dissertation, University of Nevada, Las Vegas, 2010; 362 pp.

[6] Islam, M. S., Comparison of ASR mitigation methodologies, International Journal of Concrete Structures and Materials, 8(4), pp. 315-326, 2014.

[7] Islam, M. S., Prediction of ultimate expansion of ASTM C 1260 for various alkali solutions using the proposed decay model, Journal of Construction and Building Materials, 77, pp. 315-326, 2015.

[8] Islam, M. S., and Akhtar, S. A., Critical Assessment to the Performance of Alkali-Silica Reaction (ASR) in Concrete, Canadian Chemical Transactions, 1(4), pp. 253-266, 2013.

[9] ASTM Standard C1260, Standard Test Method for Potential Alkali Reactivity of Aggregates (Mortar-Bar Method). ASTM International, West Conshohocken, PA, 2007

[10] Golmakani, F., Possible modifications to the Accelerated Mortar Bar Test (ASTM C1260). Master's Thesis, University of Toronto 2013; 117 pp.

[11] Mukhopadhyay, A. K., Zollinger, D. G., and Shon, C. S., Evaluation of Alkali Silica Reactivity of Mineral and Aggregate Using Dilatometer Method. An Innovative Pavement Research Foundation (IPRF) Research Report, Report No. IPRF-01-G-002-02-5.1, Skokie, IL, USA, 2005, 27 pp.

[12] Ghanem, H., Zollinger, D., and Lytton, R., Predicting ASR aggregate reactivity in terms of its activation energy. Constr Build Mater 2010; 24:1101-1108

[13] MacLeod, I., Decaying concrete raising concerns at Canada's aging nuclear plants, National Post News, July 8, 2012, http://news.nationalpost.com/2012/07/08/decaying-concrete-raising-concerns-at-canadas-aging-nuclear-plants/ accessed date August 2, 2012.

CICM 2015
First International Conference on
Advances in Civil Infrastructure and Construction Materials
MIST, Dhaka, Bangladesh, 14–15 December 2015

USE OF COAL BURNT FLY ASH AS SUSTAINABLE CONSTRUCTION MATERIAL

M. ISLAM[1], M. T. Alam[2] and S. Islam[3]

[1, 2, 3] Department of Civil Engineering, Chittagong University of Engineering & Technology, Chittagong, Bangladesh.
Email: [1]moinul91@yahoo.com, [2]mtalamcuet@gmail.com and [3]msislamcuet@yahoo.com

Abstract. *In Bangladesh, there exists a rising energy demand in proportion with the growth of its population. Electrical power being the main source of energy and national economy, Bangladesh government has made a mega plan to reach a capacity 40,000MW of electricity by 2030, half of which will be generated from coal. Electricity can be generated from many sources, such as fossil fuel oil, coal and natural gas. Bangladesh has got substantial natural gas reserve and significant amount high quality coal resource. But the most hazardous waste of coal burnt power plant is fly ash, bottom ash and liquid ash which contain hazardous and radioactive metals like arsenic, lead, mercury, nickel, vanadium, beryllium, barium, cadmium, chromium, selenium and radium. Ash is found dumped in surrounding locations often polluting the environment which could be used in cement factories and brickfields. The experimental program was planned to study the effect of replacement of OPC with Bangladeshi fly ash on the strength and durability characteristics of hardened concrete. Two different grades of concrete M28 and M38 made with seven different cement replacement levels (10, 20, 30, 40, 50, 60 and 70%) with fly ash were used for the experimental program. Rapid chloride penetration resistance and compressive strength of concrete was determined up to 365 days of curing. Among all the concretes studied, the optimum amount of cement replacement is reported to be around 30 to 40%, which provides around 15% higher compressive strength and 55% higher rapid chloride penetration resistance as compared to OPC concrete.*

Keywords: Cement, Concrete, Fly ash, Rapid chloride penetration resistance, Compressive strength.

1 INTRODUCTION

Bangladesh government has launched a mega plan to reach 40,000MW capacity of electricity generation by 2030, half of which will be generated from coal. Coal is a valuable and plentiful natural global resource. Coal, a fossil fuel, is the largest source of energy for the generation of electricity, worldwide. Coal-fired power plants currently fuel 41% of global electricity. Besides natural gas, Bangladesh has significant coal reserve. Coal reserves of about 3.3 billion tons comprising 5 deposits at depths of 118-1158 meters have been discovered so far in the northwestern part of Bangladesh. The name of these deposits are-Barapukuria, Phulbari and Dighipara coal field in Dinajpur district, Khalashpir in Rangpur district and Jamalganj in Joypurhat district. Out of which 4 deposits (118-509 meters) are extractable at present. The depth of Jamalganj coal deposit is 640-1158 meter with 1053 Million Tones in-situ coal reserve where production may not be viable by present day's technology due to the huge depth of the deposits. So far, only Barapukuria coal field is under production. DinajpurBarapukuria coal fired power plant is the first coal based power plant with capacity of 250MW. Target for power generation in Bangladesh is shown in following bar diagram.

Coal is first milled to a fine powder which increases the surface area and allows it to burn more quickly. There is already a 250MW coal-based power plant at Barapukuria in Dinajpur. Coal for this power plant is supplied from Barapukuria Coal Mining Company Limited. Adjacent to the Barapukuria Power Plant, another 250MW plant of the Power Development Board is supposed to be set up. Another coal fired power plant is going to build at Matabari, Cox's Bazar. The 1200 MW power plant will be built using ultra super critical technology with the funding from both the Bangladesh government and Japan International Cooperation Agency (JICA). In addition 1320 MW coal fired power plant, **"**Maitree Super Thermal Power Project" at Rampal, Khulna is going to be established. The project is being implemented as a joint venture between India and Bangladesh. Bangladesh has recently signed a memorandum of understanding with China Huadian Hong Kong Co. Ltd for setting up a coal-fired power plant of 1320-MW capacity at Maheshkhali**i**sland in the southeastern coast of the country under a joint venture agreement. BPDB and China Huadian will set up a joint venture company soon for implementing the project on a build-own-operate (BOO) basis by 2019. Bangladesh government has planned to install one of the plants at Mawa of Munshiganj with a capacity of 522MW, while two others with the total capacity of 566MW in Khulna region, all of which are coal based.

Now in Bangladesh 250 MW coal based power plant is in running condition. Additional 5250 MW coal based power plant is going to be installed. According to the EIA report, 28.1 million tons of coal will be burnt to produce the estimated

5500 MW of electricity at the proposed power plant. Considering 10% ash generation, it will produce around 2.8 million tons of fly ash. These ashes comprising of fly ash, bottom ash and liquid ash which are extremely hazardous contain hazardous and radioactive metals like arsenic, lead, mercury, nickel, vanadium, beryllium, barium, cadmium, chromium, selenium and radium. The EIA report again becomes evasive by stating that the fly ash will be filtered before discharging through the chimney. If some ash may release to the atmosphere, it would not only fatally affect the forest, but also cause a range of lung diseases including pneumonia to the people living nearby. About managing the waste, the EIA report states that the fly ash "could" be used in cement factories and brickfields. Neither the report has an explanation of this statement, nor does the reality reflect in this view of the report. Taking Barapukuria as an example, it produces more than 300 metric tons of fly ash in one day, none of which has been ever used in cement factories and brickfields. Rather, they are found dumped in surrounding locations which is spirally affecting the environment. Depending on the location of each power plant, the unused fly ash is disposed at the ponds, lagoons or landfills. The unused fly ash and bottom ash disposed from coal combustion power plants, makes major negative environment effects such as air pollution and groundwater quality problem due to leaching of metals from the ashes, specially unused fly ash which has very small particle size [1].

Portland cement substitution by supplementary cementitious materials also called mineral admixtures or mineral additives such as natural pozzolana, slag, coal fly ash, silica fume, rice husk ash and wood fly ash is one of viable alternatives to reduce the amount of cement requirement [2]. Fly ash is one of the most common pozzolan and is being used quite extensively. Fly ash contains high amount siliceous and aluminous compounds and has high potential to be used as pozzolanic material to partially replace cement in concrete [3]**.** Through pozzolanic activity, fly ash chemically combines with water and calcium hydroxide, forming additional cementitious compounds which result in denser, higher strength concrete. The calcium hydroxide chemically combined with fly ash is not subject to leaching, thereby helping to maintain high density [4]. The conversion of soluble calcium hydroxide to cementitious compounds decreases bleed channels, capillary channels and void spaces and thereby reduces permeability [5]. With the help of these admixtures, less permeable and a denser calcium silicate hydrate (C–S–H) concrete can be obtained as compared with Portland cement. Fly ash replacement in concrete would be remarkable cement saving as well as cost minimizing steps for the construction of concrete structures without sacrificing the strength of concrete [6]. The aim of this research is to evaluate and explore the suitability of the use of Bangladeshi fly ash in structural concrete and its efficiency in enhancing concrete durability performance as well as strength characteristics through improvement of the concrete microstructure.

2 EXPERIMENTAL PROGRAM

The experimental program was planned to study the effect of replacement of cement with supplementary cementing material fly ash collected from Boropukuria Power Plant, Bangladesh, on the strength and durability characteristics of hardened concrete.

2.1 Materials used

(a) Cement: Ordinary Portland cement (ASTM Type-I) was used as binding material. Chemical compositions of OPC are given in **Table1.**

(b) Fly ash: ASTM Class F Fly ash collected from Boropukuria Power Plant, Bangladesh was used as supplementary cementitious material. Chemical analysis of the fly ash conducted using X-ray fluorescence study is shown in **Table1.**

(c) Aggregate: Locally available natural sand with fineness modulus 2.58 and specific gravity 2.61 was used as fine aggregate.The coarse aggregate was crushed stone with a maximum nominal size of 12.5 mm with fineness modulus 6.58 and specific gravity 2.70.

2.2 Mix design

Two different grades of concrete namely M38 and M28 were used in the program. Seven different mix proportions of cement fly ash (90:10, 80:20, 70:30, 60:40, 50:50, 40:60, 30:70) were used as cmentitious material. Cement fly ash mix ratio of 100:0 i.e. plain concrete specimens were also cast as reference concrete for comparing the properties of fly ash concrete. Fly ash concrete means the concrete made by using cement and fly ash as cementitious material with sand, stone chips and water. Relevant information of different concrete mixes is given in **Table2.** Concrete specimens were designated as per grade of concrete and amount of fly ash as a percentage of total cementitious material. Thus M38FA30 concrete means grade of concrete is M38 and cement fly ash mix ratio is 70:30.

2.3 Test Conducted

(a) Compressive Strength Test

Compressive strength of 100 mm cube concrete specimens was tested at the ages of 3, 7, 28, 56, 90, 180 and 365 days in accordance with the BS EN 12390-3:2009. The reported strength is taken as the average of three tests results.

Table 1: Chemical composition of OPC and FA

Composition	OPC	Fly Ash
CaO	65.18	8.6
SiO_2	20.80	59.3
Al_2O_3	5.22	23.4
Fe_2O_3	3.15	4.8
MgO	1.16	0.6
SO_3	2.19	0.1
Na_2O	--	3.2
LOI	1.70	--
IR	0.6	--

Table 2: Mix proportions of fresh concrete

Constituent	Grade	
	M28	M38
Cement (kg/m^3)	435	500
Water (kg/m^3)	218	218
Sand (kg/m^3)	545	520
Stone Chips (kg/m^3)	1150	1120
w/(c+fa)	0.50	0.44
Slump (mm)	68	60
Air content %	1.3	1.1

(b) Rapid Chloride Penetration Test

Cylindrical specimens of 100 mm diameter and 200 mm height were prepared in accordance with ASTM C39. After specific curing period they were cut into 50 mm thick slices. All specimens were epoxy coated around the cylindrical surface. At the ages of 28, 56, 90, 180 and 365 days, the prepared cut cylinders were tested using the procedures described in the ASTM C1202. The average result of three test specimens was taken as the representative data.

3 RESULTS AND DISCUSSIONS

3.1 Compressive strength

Compressive strength of OPC and fly ash concrete of two different grades M38 and M28 has been graphically presented in **Fig.1** and **Fig.2**. Relative compressive strengths are plotted in **Fig.3** and **Fig.4.** At early ages of curing, OPC concretes achieve relatively higher compressive strength as compared to fly ash concrete.

Test result shows that 7 days compressive strength for OPC concrete is around 7%, 15%, 23%, 41%, 50% and 64% higher than M28FA10, M28FA20, M28FA30, M28FA40, M28FA50 and M28FA60 concrete respectively. At initial age of curing upto 56 days, compressive strength is seen to decrease with the increase of fly ash content in concrete when compared with no fly ash concrete. For relatively longer period of curing, compressive strength of the fly ash concrete specimens up to 40% replacement level are higher than that of OPC concrete for all grade of concrete. 180 days compressive strength of OPC concrete of M28 grade is lower by around 4%, 5%, 9% and 6% respectively than M28FA10, M28FA20, M28FA30 and M28FA40 concrete. Cement normally gains its maximum strength within 28 days. During that period, lime produced from cement hydration remains within the hydration product. Generally, this lime reacts with fly ash and imparts more strength. For this reason, concrete made with fly ash will have slightly lower strength than cement concrete at early ages of curing and higher strength at the later ages of curing. At the end of 365 days of curing, 20%, 30% and 40% cement replaced fly ash concrete shows around 9%, 15% and 11% higher strength gaining as compared to OPC concrete.

Rate of strength gaining for different types of concrete is observed to vary with the grade of concrete and is higher for the higher grade of concrete. Among all the concrete studied, 365 days compressive strength is increased by about 2%, 4%, 10% and 6% for concrete M28FA10, M28FA20, M28FA30 and M28FA40 respectively as compared to OPC concrete; whereas the same value is increased by around 9%, 14%, 20% and 16% for concrete M38FA10, M38FA20, M38FA30 and M38FA40 respectively compared to the strength of no fly ash concrete. At the end of 365 days curing period, the overall strength gaining for M38 grade concrete is around 10% higher as compared to M28 grade concrete. So it can be concluded that strength gaining is relatively faster for higher grade concrete as compared to lower grade concrete.

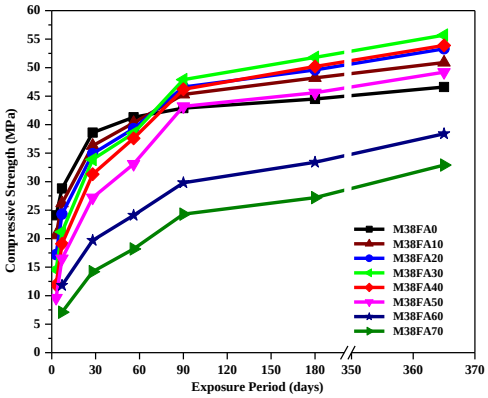

Fig.1: Compressive strength - exposure period relation for M38 fly ash concretes

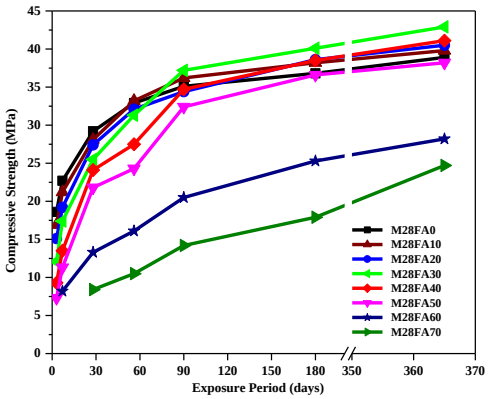

Fig.2: Compressive strength - exposure period relation for M28 fly ash concretes

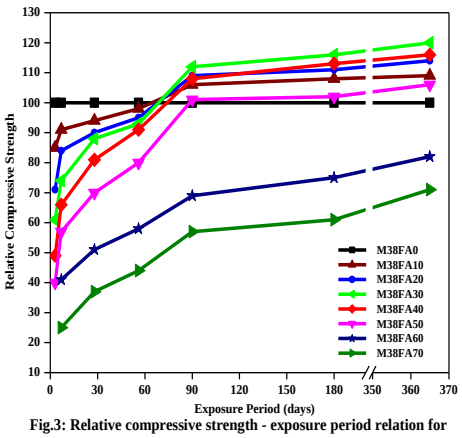

Fig.3: Relative compressive strength - exposure period relation for M38 fly ash concretes

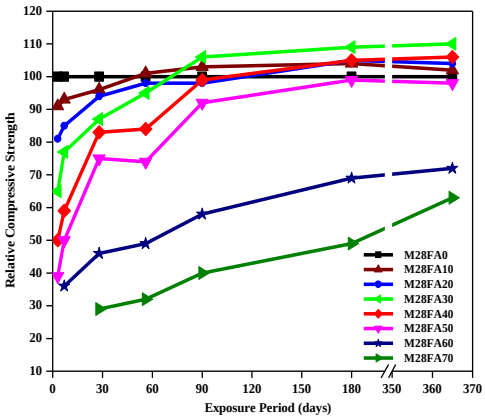

Fig.4: Relative compressive strength - exposure period relation for M28 fly ash concretes

3.2 Rapid chloride penetration

Rapid chloride penetration value for OPC and fly ash concrete at 28, 56, 90, 180 and 365 days curing period are graphically presented in **Fig.5** and **Fig.6.** At the initial age of curing RCPT values are higher for fly ash concrete compared to OPC concrete. In case of OPC concrete, amount of passing charge is observed as 4240 and 6295 coulombs for M38 and M28 grade concrete; whereas the similar value for fly ash concretes of cement replacement level of 20%, 30%, 40% and 50% are 4512, 4621, 4766 and 5280 coulombs for M38 grade concrete and 7295, 7465, 7870 and 8013 coulombs for M28 grade concrete respectively at the curing age of 28 days. But for longer age of curing, fly ash concrete shows better resistance against chloride ion penetration. After 365 days of curing, rapid chloride penetration values are respectively 31%, 27%, 23%, 18%, 15% for M38FA10, M38FA20, M38FA30, M38FA40, M38FA50 concretes and 34%, 32%, 31%, 26%, 29% for M28FA10, M28FA20, M28FA30, M28FA40 and M28FA50 concretes as compared to the 28 days RCPT values of OPC concrete of similar grade. Fly ash concrete has relatively better resistance against chloride ion penetration and hence the use of fly ash in structural concrete may inhibits the risk rebar corrosion. At the end of 365 days of curing, 20%, 30% and 40% cement replaced fly ash concrete shows around 38%, 45% and 54% lower RCPT value as compared to OPC concrete.

Relative RCPT values of fly ash concrete compared to OPC concrete are observed to vary with the grade of concrete and replacement level of fly ash with cement. At an age of 180 days of curing, RCPT values for 20%, 30%, 40%, 50% cement replaced concrete are respectively 45%, 50%, 57%, 66% lower for M38 grade concrete and 22%, 34%, 37%, 33% lower for M28 grade concrete as compared to OPC concrete of similar grade. This is happened due to high fineness of fly ash. Fly ash can react with the products liberated during hydration, forming secondary C-S-H gel that fills all the pores inside concrete and makes it more

impermeable. The study result also shows that as the amount of fly ash in concrete is increased, charge flow through the concrete specimens is decreased. It was also observed that at the end of 365 days curing period, the overall RCPT values for M38 grade concrete was around 9% lower as compared to M28 grade concrete.

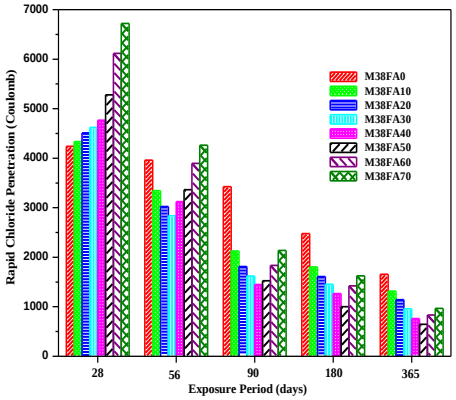

Fig.5: Rapid chloride penetration - exposure period relation for M38 fly ash Concretes

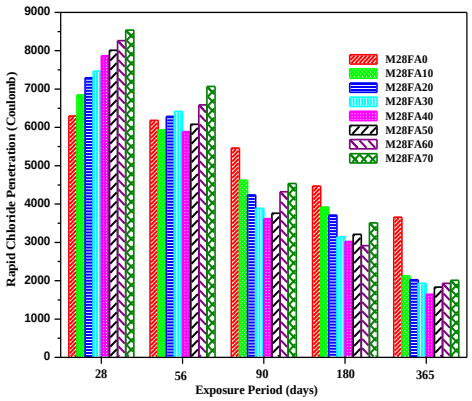

Fig.6: Rapid chloride penetration - exposure period relation for M28 fly ash Concretes

4 CONCLUSIONS

Based on the results of the investigation conducted on different fly ash concrete made with various level of cement replacement for various curing period up to 365 days, the following conclusions can be drawn:

(1) At early ages of curing, the rate of gain in compressive strength of fly ash concrete specimens is lower as compared to the corresponding OPC concrete. However, at later age of curing (after 56 days), fly ash mix concrete exhibited a higher rate of strength gain than OPC concrete.

(2) The optimum fly ash content is observed to be 30% of cement from the compressive strength point of view. Fly ash concrete with 30% cement replacement shows around 15% higher compressive strength than OPC concrete after 365 days curing.

(3) Chloride penetration resistance for fly ash concrete is observed to be improved as compared to OPC concrete. Fly ash concretes with 30% cement replacement shows around 45% lower RCPT value compared to OPC concrete.

(4) Higher grade concrete showed around 10% higher gain in strength and 9% lower RCPT value as compared to lower grade concrete.

(5) The use of fly ash in cement production will reduce CO_2 emission to the environment and the problem of its disposal, saving the valuable fertile lands.

REFERENCES

[1] B. Singh, G. Ishwarya, M. Gupta, S. Bhattacharyya, 2015. Geopolymer concrete: A review of some recent developments. *Construction and Building Materials*, 10.1016/j.conbuildmat.2015.03.036, 78-90.

[2] S. Homnuttiwong, C. Jaturapitakkul, P. Chindaprasirt, 2012. Permeability and Abrasion Resistance of Concrete Containing High Volume Fine Fly Ash and Palm Oil Fuel Ash. *Computers and Concrete*, **10**, 349-360. http://dx.doi.org/10.12989/cac.2012.10.4.349

[3] A. U. Abubakar, K. S. Baharudin, 2012. Potential use of malaysian thermal power plants coal bottom ash in construction. *Journal of Sustainable Construction Engineering & Technology*,**3(2)**, pp. 1–13.

[4] T. Xie, T. Ozbakkaloglu, 2015. Behavior of low-calcium fly and bottom ash-based geopolymer concrete cured at ambient temperature. *Ceramics International*, 10.1016/j.ceramint.2015.01.031.

[5] T. C. Madhavi, L. S. Raju, D. Mathur, 2014. Durability and Strength Properties of High Volume Fly Ash Concrete, *Journal of Civil Engineering Research,***4(2A)**, pp.71.

[6] A. Oner, S. Akyuz, R. Yildiz, 2005. An experimental study on strength development of concrete containing fly ash and optimum usage of fly ash in concrete, *Cement and Concrete Research,* **35,** pp.1165– 1171.

CICM 2015
First International Conference on
Advances in Civil Infrastructure and Construction Materials
MIST, Dhaka, Bangladesh, 14–15 December 2015

DUCTILITY PERFORMANCE OF HIGH STRENGTH LIGHTWEIGHT CONCRETE PRODUCED FROM A MIXTURE OF OIL PALM SHELL AND PALM OIL CLINKER

Md. N. HUDA[1], **Mohd Z. B.Jumaat**[2], **A.B.M. Saiful Islam**[3] **and Mahmudur R. Soeb**[4]

[1, 2, 3, 4] University of Malaya, Kuala Lumpur, Malaysia.
Email: [1]nazmulhuda.128@gmail.com, [2]zamin@um.edu.my, [3]abm.saiful@gmail.com and [4]soeb_buet@yahoo.com

Abstract. *Due to environmental issues, the use of waste materials in concrete is gaining popularity. Waste materials, such as oil palm shell (OPS) and palm oil clinker (POC) from the Malaysian palm oil industry are being used in various researches to produce lightweight concrete. Concrete containing only OPS shows more ductility and less compressive strength, while POC concrete shows less ductility but higher compressive strength. Combination of OPS and POC may exhibit improved compressive strength and ductility behaviour. In this experimental study, normal coarse aggregate is replaced by a mixture of OPS and POC aggregates in the lightweight concrete. The proportion of OPS and POC in the concrete mix varies from 40% to 70%. The results indicate that if a mixture of OPS and POC are used in producing lightweight aggregate concrete, better performance in terms of compressive strength and ductility can be achieved. Furthermore, through the utilization of waste materials, the proposed lightweight concrete helps to mitigate the negative impact on the environment.*

Keywords: Oil palm shell, Palm oil clinker, Lightweight concrete, Compressive strength, Displacement ductility.

1 INTRODUCTION

Nowadays, lightweight concrete is a popular choice in the construction industries. The use of lightweight concrete (LWC) has many advantages over normal weight concrete, such as a reduction in the size of the structural elements, increase in building height and a greater span-depth ratio for beams in pre-stressed concrete construction [1]. In designing a structural element, the compressive strength is desirable along with acceptable ductility under heavy loading to ensure adequate deflection [2]. Satisfactory ductility is a very important factor for reinforced concrete structures in high seismic areas because less ductile reinforced concrete experiences many serious complications when subjected to compression and torsion.

Currently several researchers have worked on lightweight concrete using waste materials, as recycling the solid wastes from the agricultural and manufacturing industries is long overdue [3-5]. Malaysia is the second largest palm oil producing country in the world producing more than half of the world's palm oil [6]. The residue of palm oil industry includes OPS and POC. Several investigations have shown that lightweight concrete with OPS or POC aggregate can be produced with a compressive strength ranging from 17 to 53 MPa [7, 8].LWC is still not a common material in the construction industry and there has been some reticence concerning its use in concrete structures. Even the displacement ductility of lightweight concrete has rarely been studied in the earlier literature.

The objective of this study is to produce lightweight concrete from a mixture of OPS and POC aggregates. This lightweight concrete is named as palm shell and clinker concrete (PSCC). This research also investigates the compressive strength, stress-strain curves and ductility behaviour of PSCC. The ductility characteristics have been studied by the displacement ductility index.

2 MATERIALS

2.1 Cement

In this study, ordinary Portland cement with a specific gravity of 3.14 g/cm3 and fineness of 3510 cm2/g was used as the binder material in the concrete. This cement was collected from a local Malaysian company named Tasek Corporation Berhad. The compressive strengths of the cement were 34.2 and 45.9 MPa, at 7 and 28 days, respectively.

2.2 Fine Aggregate

Local mining sand with specific gravity, fineness modulus, water absorption and maximum grain size of 2.68, 2.65, 1.17% and 4.75 mm, respectively, was selected as the fine aggregate in the concrete mix.

2.3 Coarse Aggregate

Two types of coarse aggregates were used in the concrete mix for this study, which were collected from the local palm oil factory in Malaysia as waste materials. Figure 1 shows the selected coarse aggregates for producing lightweight concrete. The OPS aggregate is shown in Figure 1 (a). After collecting the OPS from the local palm oil industry, it was washed and crushed using a stone-crushing machine in the laboratory. The flakiness of OPS decreases significantly upon crushing, which improves the performance of the coarse aggregate and yields higher compressive strength[9]. Subsequently, crushed OPS aggregate was sieved using a 5 mm-sieve to remove the aggregate less than 5 mm in size.

Fig.1. Coarse aggregate (a) OPS aggregate (b) POC aggregate

Another type of coarse aggregate, POC aggregate is presented in Fig. 1 (b). This POC was also collected from the local palm oil industry in Malaysia. In a similar fashion to OPS, the clinker was crushed and sieved using a 5 mm-sieve. As the larger size aggregate has a greater value under the abrasion test, POC retained on the 5 mm sieve was considered to be coarse aggregate.

2.4 Superplasticizer (SP)

For this experimental program, SikaViscocrete 2199, which was collected from Sika Kimia, Malaysia, was employed as the chloride free Super plasticizer, in accordance with EN 934-2, and mixed in the concrete at 2.0% of cement weight to facilitate the workability.

3 TEST METHODS

3.1 Mix Proportions

By and large, the LWAC mix design is determined by trial mixes [10]. Most of the previous studies used 480-550 kg/m^3 cement with a water cement ratio of 0.3-

0.4 to obtain concrete with a compressive strength of 30-44 MPa [11]. In this study, to obtain concrete with a compressive strength of 45 MPa, 450 kg/m^3 cement content with a water cement ratio of 0.35 was selected for the trial mix. Therefore, unlike some previous studies, this study designed the trial mixes with the less cement content to get high strength lightweight concrete (LWC) Four trial mixes were conducted in the laboratory to obtain grade 45 concrete with a moderate workability. Each and every mix had an identical water/cement ratio. To achieve workability, SP was added to all the mixes. Sieved local mining sand fills the place of fine aggregate. To attain the high strength ductile concrete, a mixture of OPS and POC was used as coarse aggregate in different proportions in the four trial mixes. In mix TM-1, the total volume of coarse aggregate was divided into two parts: 70% for the OPS and 30% for the POC. The corresponding quantities of OPS and POC in the TM-2, TM-3 and TM-4 mix were 60% & 40%; 50% & 50%; and 40% & 60%, respectively. The details of the concrete mixes with the proportions of ingredients are shown in Table 1.

Table 1: Concrete mix proportions in kg/m3

Mix ID	Cement	Water	W/C ratio	SP	Sand	OPS (% by vol.)	POC (% by vol.)	Slump (mm)
TM - 1	450	158	0.35	2%	1013	248 (70%)	141 (30%)	60
TM - 2	450	158	0.35	2%	1025	212 (60%)	187 (40%)	65
TM - 3	450	158	0.35	2%	1158	148 (50%)	195 (50%)	40
TM - 4	450	158	0.35	2%	1048	142 (40%)	**281 0%)**	70

3.2 Samples Preparation and Data Collection

During preparation of the concrete mixing procedure, cement, sand, OPS and POC were blended into a pan mixer for 5 min. Subsequently, the mixture of SP and about 80% of the water were added into the pan mixture. After 5 minutes of mixing, the remaining 20% of the water was added into the pan mixture and the mixing continued for a further 10 min. The concrete specimens were cast in steel moulds, and the specimens were compacted using the vibration table. The casting of all the specimens followed BS 1881 [12]. The specimens were remoulded after 24 hours and cured in water at 30 ± 2°C until the test days. Three specimens from each category were prepared for obtaining the average value.

Initially the slump tests were carried out for the selected mixes. The compressive strengths of the specimens were determined on the 1st, 3rd, 7th and 28th day. In addition, the modulus of elasticity was measured on the 28th day. The tests were carried out in accordance with BS 1881: Part 116 [12] using a univer-

sal compression testing machine of 3000 KN capacity with a rate of loading controller.

4 RESULTS AND DISCUSSION

4.1 Compressive Strength

Table 2 shows the 28 days compressive strength development for all the trial mixes. The test results show that if the percentage of OPS increases in the combination of coarse aggregate, the 28 days compressive strength decreases. Again, having a POC content of more than 50% also decreases the compressive strength. With the largest proportion of OPS content, TM-1 exhibits the lowest value for the 28-day compressive strength. TM-3, with a POC content of 50% in the mixture of coarse aggregate, shows the highest value for the 28-day compressive strength. In TM-4, the POC content was increased to 60%, resulting in a 9% fall in the compressive strength from TM-3. This weakening can be attributed to the round and plain surface texture of OPS, which imparts poor bondage to the concrete if its presence is excessive. On the other hand, the POC aggregate, which is rough and porous, imparts strong bonding with the cement paste. Furthermore, if OPS and POC coarse aggregate are mixed in a 50% ratio (TM-3), the 28-days compressive strength increases to 46.5 MPa, which is the maximum among all the mixes. However, POC aggregate is porous in nature, which enables some of the cementing material to enter the pores, that, eventually, decreases the overall bonding strength [13].

Table 2: Development of the compressive strength of PSCC

Mix ID	Compressive Strength (MPa)			
	1 day	3 day	7 day	28 day
TM-1	18.44	31.39	35.43	38.28
TM-2	29.46	33.7	36.01	38.57
TM-3	28.9	39.95	44.64	46.47
TM-4	30.7	36.23	40.13	42.35

4.2 Stress-Strain Behavior

Fig. 2 shows the stress-strain curves of all the tested samples containing different percentages of OPS and POC. Both vertical and lateral strains are plotted against the increase in the compressive load applied. The vertical displacement is shown in the positive X-axis and the lateral displacement in the negative X-axis in Fig. 2. The stress-strain curves of the PSCC samples softens towards a rounded peak in the post-yield stage with a very slow dropping tendency after the post yield, which is mainly because the PSCC concrete has a good interlocking [13] and bi-

linear ductile [14] stress-strain behaviour. The experimental results show that the PSCC concrete specimen can undergo larger deformation before failure, and that such a failure is ductile and gives warning of the impending failure similar to steel. For TM-3 and TM-4, the strains at maximum stress were measured in the range of 0.0028 and 0.0034, respectively showing less value than that for TM-1 and TM-2, which were 0.0035 and 0.004, respectively; this is close to the range for lightweight concrete elements [15], 0.026–0.003. With the increase in the POC aggregate in the concrete, the strain at maximum stress exhibits a lower value, and, vice versa, with an increase in OPS aggregate. It is also observed that concrete with POC aggregate only shows brittle behaviour with the maximum stress value whereas OPS concrete reveals the maximum ductile behaviour with the minimum stress value. After combining the OPS and POC in the concrete, a higher stress value is found with moderate ductile behaviour.

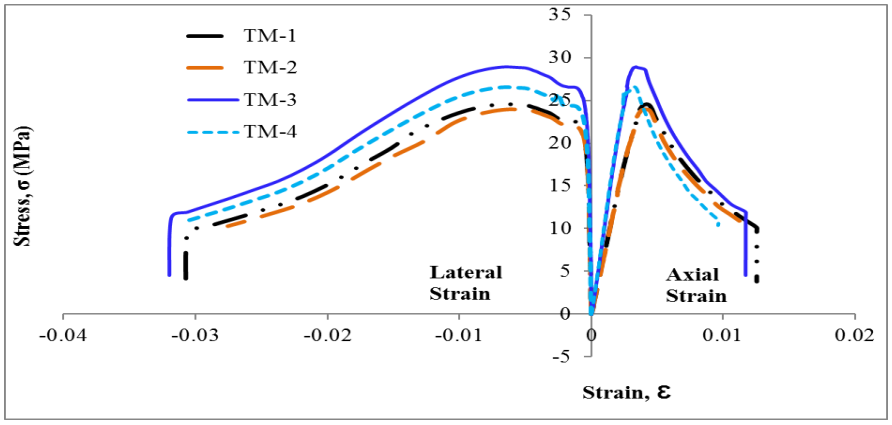

Fig.2. Stress-strain curves for vertical and lateral displacement

4.3 Displacement Ductility

The mechanical properties (compressive strength and modulus of elasticity) and ductility indices of PSCC obtained from the laboratory results are presented in Table 3. The ductility of any structural element is usually specified as 'the capacity of the structural element to undergo load still experiencing extra distortion beyond the maximum load stage' [2]. This definition is qualitative and to measure the displacement ductility of compression critical elements. The ratio of the area under the stress-strain curve up to $5\varepsilon_o$ to the area up to ε_o for displacement is defined as the ductility index (μ). The displacement ductility values stated in this study are the strain ductility of the compression-critical member. Here, ε_o is the strain at peak stress (σ_{max}) for the concrete element. The evaluation of the structural parameters of the displacement ductility index is illustrated in Table 3 for the different mix ratios. Existing literature shows that POC concrete exhibits little ductility [13]. After mixing OPS with POC in this study, all the trial mixes show

an adequate ductility index. TM-3 shows the maximum ductility among the trial mixes.

Table 3: Displacement ductility indices of PSCC for different mixture

Mix ID	Elastic modulus (GPa)	Displacement ductility		
		Stress	Strain	μ
TM - 1	6.8	24.00	0.00408	3.02
TM - 2	6.9	24.57	0.00422	2.87
TM - 3	10.16	28.92	0.00338	3.56
TM - 4	10.38	26.60	0.00324	2.96

5 CONCLUSIONS

- The PSCC samples show ductile behaviour. The ductility index decreases with the increase of porous POC aggregate content in the concrete mixes.
- The strains at maximum stress of the PSCC samples are in good agreement with the recent study of lightweight aggregate concrete.
- PSCC can be produced with a 28-day compressive strength of 46 MPa, which is higher than the structural requirement of 15MPa.
- In this study, the use of 50% OPS and 50% POC coarse aggregate seems to give the optimum mix, which produces grade 45 concrete with adequate ductility. It requires 450 kg/m3 cement to produce grade 45 concrete, which is the lowest among the recent studies.

ACKNOWLEDGEMENTS

The authors gratefully acknowledge the support given by University of Malaya (UM) for funding the study through the University of Malaya Research Grant (UMRG)RP018-2012A.

REFERENCES

[1] M. J. Shannag, "High strength concrete containing natural pozzolan and silica fume," *Cement and Concrete Composites,* vol. 22, pp. 399-406, 12// 2000.

[2] S. H. Ahmad, Y. Xie, and T. Yu, "Shear ductility of reinforced lightweight concrete beams of normal strength and high strength concrete," *Cement and Concrete Composites,* vol. 17, pp. 147-159, // 1995.

[3] H. Basri, M. Mannan, and M. Zain, "Concrete using waste oil palm shells as aggregate," *Cement and Concrete Research,* vol. 29, pp. 619-622, 1999.

[4] M. Mannan and C. Ganapathy, "Mix design for oil palm shell concrete," *Cement and concrete research,* vol. 31, pp. 1323-1325, 2001.

[5] F. O. Okafor, "Palm kernel shell as a lightweight aggregate for concrete," *Cement and Concrete Research,* vol. 18, pp. 901-910, 1988.

[6] D. C. L. Teo, M. A. Mannan, and V. J. Kurian, "Structural concrete using oil palm shell (OPS) as lightweight aggregate," *Turkish Journal of Engineering and Environmental Sciences,* vol. 30, pp. 251-257, 2006.

[7] U. Alengaram, M. Jumaat, and H. Mahmud, "Influence of cementitious materials and aggregates content on compressive strength of palm kernel shell concrete," *J Appl Sci,* vol. 8, pp. 3207-3213, 2008.

[8] P. Shafigh, M. Z. Jumaat, and H. Mahmud, "Oil palm shell as a lightweight aggregate for production high strength lightweight concrete," *Construction and Building Materials,* vol. 25, pp. 1848-1853, 2011.

[9] P. Shafigh, M. Z. Jumaat, H. B. Mahmud, and U. J. Alengaram, "A new method of producing high strength oil palm shell lightweight concrete," *Materials & Design,* vol. 32, pp. 4839-4843, 12// 2011.

[10] M. Shetty, *Concrete technology theory and practice. 1rd Multicolor illustrative revised ed*: India, 2005.

[11] ACI Committee 211.2, "Standard Practice for Selecting Proportions for Structural. Lightweight Concrete " *ACI Journal Proceedings,* vol. 64, 1998.

[12] BS, Part,116:, "Method for determination of compressive strength of concrete cubes. London: British Standard Institution," 1983.

[13] R. Ahmmad, M. Jumaat, S. Bahri, and A. S. Islam, "Ductility performance of lightweight concrete element containing massive palm shell clinker," *Construction and Building Materials,* vol. 63, pp. 234-241, 2014.

[14] P. Shafigh, H. B. Mahmud, and M. Z. Jumaat, "Oil palm shell lightweight concrete as a ductile material," *Materials & Design,* vol. 36, pp. 650-654, 2012.

[15] A. Turatsinze and M. Garros, "On the modulus of elasticity and strain capacity of self-compacting concrete incorporating rubber aggregates," *Resources, conservation and recycling,* vol. 52, pp. 1209-1215, 2008.

CICM 2015
First International Conference on
Advances in Civil Infrastructure and Construction Materials
MIST, Dhaka, Bangladesh, 14–15 December 2015

EVALUATION OF DEFLECTION OF FLEXURAL MEMBERSWITH HIGH STRENGTH REBAR

Md. I. ISLAM[1] and Ishtiaque Ahmed[2]

[1, 2] Department of Civil Engineering, Bangladesh University of Engineering and Technology, Dhaka, Bangladesh.
Email: [1]iftekharshad@gmail.com and [2]iahmed@ce.ac.bd

Abstract. *There is worldwide trend in the construction industry to use high strength steel reinforcement in concrete structures. ACI-318-14 permits use of Grade 80 steel in flexural members which are not part of special seismic structure. Advantages of using high-strength steel are manifold; besides economy, the other benefits include reduction of congestion, ease in placement of concrete, reduction of time and labor for fabrication and so forth. These advantages can deal with a number of practical problems concerning to reinforced concrete structures. Flexural members are the major component of RCC structures. The sensitive issues regarding the use of high strength steel in RCC flexural members are ductility and serviceability. Although deflection is an important serviceability criteria, but literature related to comparing experimental deflection with theoretical one using high strength reinforcement is not very common. An experimental investigation on behavior of reinforced concrete beams with Grade 80 and Grade 60 rebars has been conducted at BUET. The program involved testing of 30 half scale beams having dimensions 6" × 9.5" × 8' (150mm × 237.5mm × 2400mm). This research program is conducted to evaluate serviceability performance (deflection) at service load level. Experimental data has been compared with theoretical predictions available in the literature. It has been observed that at service load level beams with Grade 80 rebars show comparable serviceability performance with that of Grade 60 steel. The strength and ductility features of the beams with Grade 80rebars also compare favorably with those reinforced using conventional Grade 60 rebars.*

Keywords: Beam deflection, Grade 80 and 60 steel, Reinforced concrete, Effective moment of inertia.

1 INTRODUCTION

Deflection of a beam is an important criterion regarding the serviceability of RCC structures. Limited deflection is desirable not only from aesthetic point of view but also ensuring safety of nonstructural partition members. In recent ACI-318-14, it is stated in Chapter 9 that, for non prestressed beams reinforcing bar yield strength(f_y) less than or equal to 60,000 psi and not supporting or attached to partitions or other construction likely to be damaged by large deflections, overall beam depth *h* shall satisfy the limits in Table 1**,**

Table 1: Minimum depth of non prestressed beams [ACI 318-14]

Support condition	**Minimum *h***
Simply supported	ℓ/16
One end continuous	ℓ/18.5
Both ends continuous	ℓ/21
Cantilever	ℓ/8

For f_y other than 60,000 psi, the expressions in Table 1 shall be multiplied by (0.4 + f_y/100,000).The modification for f_y is approximate, but should provide conservative results for typical reinforcement ratios and for values of f_y between 40,000 and 80,000 psi [ACI-318-14].

For calculation of deflection of beams, several theories are available. A study from Kalkan [8] suggests that, the major issue associated in this case, is the calculation of in-plane bending stiffness (*EIx*) of a beam which is the product of two variables: (1) the in-plane second moment of area (the in-plane moment of inertia *Ix*), reflecting the cross-sectional resistance to loading; and (2) the modulus of elasticity (*E*), reflecting the material resistance to loading [8]. However, in concrete beams, both variables are subject to change during the course of loading (Kalkan 2013).The inelastic stress-strain behavior of concrete beyond the elastic limits causes the deviation in the modulus of elasticity with the increasing load, while on the other hand, the deviation in the moment of inertia is linked with the cracking of concrete which occurs when the tensile strains are greater than the cracking strain of concrete. Cracking of concrete declines the resistance of a RC beam to loading, leading to larger deformations in the beam while the load increment is marginal. This decrease in the second moment of area of a concrete beam throughout the course of loading is balanced by the effective moment of inertia approach. Branson (Branson 1965) proposed the following effective moment of inertia expression:

$$I_e = \left(\frac{M_{cr}}{M_a}\right).I_{ucr} + \left[1 - \left(\frac{M_{cr}}{M_a}\right)^m\right].I_{cr} \qquad (1)$$

Where, *Ma* is the Maximum moment in the beam

Cracking moment, $M_{cr} = \frac{f_r.I_g}{y_t}$ (y_t is the vertical distance of the extreme tension fibers from the neutral axis)

Modulus of rupture, $f_r = 7.5.\sqrt{f_c'}$ (f_c'' is the concrete compressive strength of 28 days cylinder specimen in psi)

Gross moment of inertia, $I_g = \frac{1}{12}.b.h^3$

Uncracked moment of inertia, $I_{ucr} = \frac{1}{12}.b.h^3 + b.h.\left(y' - \frac{h}{2}\right)^2 + (n-1).A.\left(d - y'\right)^2$

Cracked moment of inertia, $I_{cr} = \frac{1}{12}.b.c^3 + n.A_s.(d-c)^2$

(band *h* are the width and height of the beam, respectively; *y'* is the depth of the centroid of the transformed uncracked cross-section from the compression face; *n* is the modular ratio of steel to concrete; *c* is the neutral axis depth of the fully-cracked section, *As* is the total cross- sectional area of the longitudinal reinforcement; and *d* is the effective depth of the tension reinforcement)

Moreover, Al-Shaikh and Al-Zaid (Al-Shaikh and Al-Zaid 1993) showed that the value of *m* reduces with increasing reinforcement ratio (ρ). Therefore, they proposed the following equation for *m*:

$$m = 3 - 0.8\rho$$

The effective moment of inertia expression (Equation 1) proposed by Branson, which actually averages the moments of inertia of the uncracked and fully-cracked segments of a RC beam, was adopted by ACI 318 many years ago and is still part of ACI 318-14.

Another study from Bischoff (Bischoff 2005) proposed the following effective moment of inertia expression based on weighted average of the flexibilities of the uncracked and cracked portions of a RC beam:

$$\frac{1}{I_e} = \left(\frac{M_{cr}}{M_a}\right)^m . \frac{1}{I_{ucr}} + \left[1 - \left(\frac{M_{cr}}{M_a}\right)^m\right] . \frac{1}{I_{cr}} \qquad (2)$$

m=2 was proposed in Equation (2), derived from the deflection equation specified in Eurocode 2. The use of *m*=2 guarantees that the tension-stiffening contribution in the model is just dependent on the applied load level (*Ma*/*Mcr*), as explained by Bischoff (Bischoff 2005 and Bischoff 2007)thoroughly. Therefore, the tension-stiffening model turns out to be independent from the gross-to-uncracked moment of inertia ratio (*Ig*/*Icr*) and the reinforcement ratio (ρ) of the beam.

The deflection prediction in the European structural concrete code, Eurocode 2 (CEN 2002), is derived from the calculation of the curvatures and deflections of a RC beam equivalent to its uncracked and fully-cracked states. According to this code, the following equation is used for the calculation of the deflections (δ) of a RC beam loaded at cracking load level:

$$\delta = \left[1 - \beta \left(\frac{M_{cr}}{M_a}\right)^2\right] . \delta_{ll} + \beta . \left(\frac{M_{cr}}{M_a}\right)^2 . \delta_l \qquad (3)$$

Where δ_{ll} and δ_l are the deflection values equivalent to the fully cracked and uncracked states of the beam, respectively; and β is a coefficient related to the duration of loading or of repeated loading on the average strain. β is taken 1.0 for a single short-term loading (immediate deflections) and 0.5 for sustained loads (long-term deflections) or many cycles of repeated loading. β is taken 1.0 in the present study. Eurocode 2 (CEN 2002) uses the concept of averaging the flexibilities of the uncracked and cracked segments of the beam rather than averaging the stiffnesses.

2 RESEARCH SIGNIFICANCE

There is lack of studies on comparison of the actual deflection with the predicted one. The present study aims at contributing to the topic. Moreover, the deflection equations were used to predict deflections of RCC beams reinforced with Grade 60 rebars. Available equations have never been used to verify the deflection of beams with reduced steel percentages likely to be resulted for Grade 80 rebars. Other variables like reinforcement ratio, concrete compressive strength etc. were used to enhance the scope of comparison. Satisfactory deflection estimates for reinforced concrete beams was the outcome of the study.

3 EXPERIMENTAL SETUP

Thirty half scale beams having dimensions 6"X9.5"X8' (150mm X 237.5mm X 2400mm) were tested in a two point loading system. All the specimens were loaded at a constant rate by a UTM up to failure. Fig. 1 illustrates the experimental program. Eighteen of the specimens were designed with Grade 80 rebars and other twelve specimens were designed using conventional Grade 60 rebar. To ensure flexural failure, all specimens were adequately designed for shear and shear reinforcements were provided more than required.

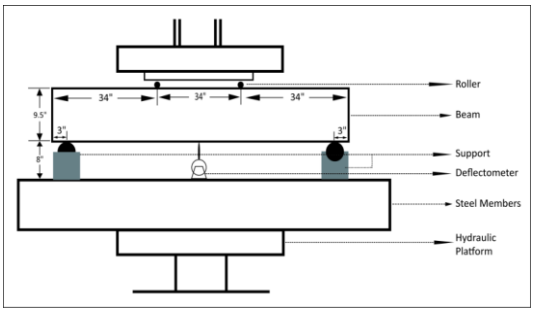

Figure 1: Experimental setup

A mechanical deflectometer was placed below the midpoint of the specimens which was used to take deflection readings and strain gauges were used on tension reinforcements to take strain data. Table 2 summarizes the details of the specimens tested.

Table 2: Details of Beam Specimens

A. Grade 80 specimens:

Specimen ID (For 80 grade)	f_c' (psi)	Bottom Reinforcement	Top Reinforcement	Effective Depth, d(in)	ρ	ρ_{max}	ρ_{min}	Modulus of Elasticity of Cocrete, E_c (k/ft2)	Modulus of rupture, f_r (k/ft2)
T- 1,2,3	3990	One #3 Two #4	Two #3	8.20	0.0102	0.0135	0.0025	518535.16	68.23
T- 4,5,6	3990	Three #3	Two #3	8.24	0.0067	0.0135	0.0025	518535.16	68.23
T- 7,8,9	3900	Two #5	Two #3	8.12	0.0126	0.0132	0.0025	512260.75	67.40
T-10,11,12	3900	Two #4	Two #3	8.18	0.0080	0.0132	0.0025	512260.75	67.40
T-13,14,15	5640	One #5 Two #5	Two #3	8.16	0.0143	0.0173	0.00282	616420.25	81.11
T-16,17,18	5640	One #4 Two #3	Two #3	8.22	0.0085	0.0173	0.00282	616420.25	81.11

B. Grade 60 specimens:

Specimen ID (For 80 grade)	f_c' (psi)	Bottom Reinforcement	Top Reinforcement	Effective Depth, d(in)	ρ	ρ_{max}	ρ_{min}	Modulus of Elasticity of Cocrete, E_c (k/ft2)	Modulus of rupture, f_r (k/ft2)
XT- 1,2,3	4120	One #4,Two #5	Two #3	8.14	0.0166	0.0185	0.0033	527104.44	69.36
XT- 4,5,6	4120	One #4 Two #3	Two #3	8.22	0.0085	0.0185	0.0033	527104.44	69.36
XT- 7,8,9	6270	Three #5	Two #3	8.12	0.0189	0.0243	0.00398	649677.59	85.48
XT- 10,11,12	6270	One #3 Two #4	Two #3	8.20	0.0102	0.0243	0.00398	649677.59	85.48

$$* \boldsymbol{\rho_{max}} = \mathbf{0.85}\boldsymbol{\beta_1}\frac{\boldsymbol{f_c'}}{\boldsymbol{f_y}}\left(\frac{\mathbf{0.003}}{\mathbf{0.003+0.005}}\right) \qquad \boldsymbol{\rho_{min}} = \frac{\mathbf{200}}{\boldsymbol{f_y}} \leq \mathbf{3}\frac{\sqrt{\boldsymbol{f_c'}}}{\boldsymbol{f_y}}$$

4 RESULTS

Deflection readings were taken for all specimens. Later they were compared with the theoretical predictions by Branson (1965), Bischoff (2005) and Eurocode 2, CEN (2002). Service load was calculated corresponding to steel stress level of 0.67 $f_{y.}$ Table 3 and Fig. 2 to Fig. 5 explain the results. Table 3 presents comparison of the observed deflection value and theoretically predicted value (Branson 1965, Bischoff 2005 and Eurocode 2, CEN 2002) at service load level for all the tests. Complete load deflection responses are compared for selected tests in Fig. 2 to Fig. 5.

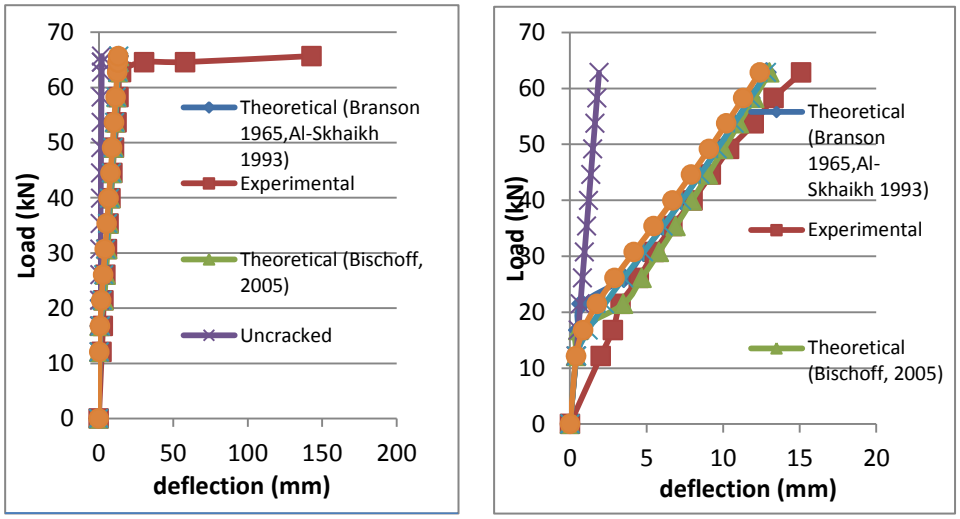

(a) Complete experimental result (b) Enlarged view

Figure 2: Comparison of the experimental and theoretical predictions of load deflection values for specimen T-6, 80 Grade sample, (ρ =0.0067), fc'=3990 psi

From Table 3, it can be seen that theoretical predictions from Branson (1965), Bischoff (2005) and Eurocode 2, CEN (2002), have estimated deflection quite satisfactorily at service load level. Fig. 2 to Fig. 5 represents the comparison of observed deflections from four experimental results and theoretically predicted deflections from the three references as mentioned above. Out of these four tests two tests represent beams with Grade 80 reinforcements and the rest two represent beams with Grade 60 reinforcements. From the figures it can be seen that beams with both the grades behaved more closely with the predictions given by Bischoff (2005). But for Grade 80 samples the predicted and observed deflections are even closer.

Table 3: Comparison of Observed and Predicted deflection at Theoretical Service Load Level

Spe. ID	$f_s=0.67f_y$ Calc. service load (kN)	$f_s=0.67f_y$ Observed deflection (mm)	$f_s=0.67f_y$ Predicted deflection (Branson 1965) (mm)	$f_s=0.67f_y$ Predicted deflection (Bischoff 2005) (mm)	$f_s=0.67f_y$ Predicted deflection (Eurocode 2, CEN ,2002) (mm)
T-1	53.03	9.8	8.95	9.05	8.71
T-2	53.03	9.25	8.95	9.05	8.71
T-3	53.03	9	8.95	9.05	8.71
T-4	36.43	6.8	6.37	7.16	5.49
T-5	36.43	6.4	6.37	7.16	5.49
T-6	36.43	6.5	6.37	7.16	5.49
T-7	61.89	9.5	10.78	10.77	10.63
T-8	61.89	9.3	10.78	10.77	10.63
T-9	61.89	9	10.78	10.77	10.63
T-10	42.32	8.3	7.61	8.07	7.62
T-11	42.32	8.7	7.61	8.07	7.62
T-12	42.32	8.9	7.61	8.07	7.62
T-13	73.87	10	9.54	9.5	9.58
T-14	73.87	10.3	9.54	9.5	9.58
T-15	73.87	9.3	9.54	9.5	9.58
T-16	46.47	6.6	6.46	6.97	6.44
T-17	46.47	8	6.46	6.97	6.44
T-18	46.47	8.3	6.46	6.97	6.44

Spe. ID	$f_s=0.67f_y$ Calc. service load (kN)	$f_s=0.67f_y$ Observed deflection (mm)	$f_s=0.67f_y$ Predicted deflection (Branson 1965) (mm)	$f_s=0.67f_y$ Predicted deflection (Bischoff 2005) (mm)	$f_s=0.67f_y$ Predicted deflection (Eurocode 2, CEN ,2002) (mm)
XT-1	62.17	8.2	7.77	7.70	7.41
XT-2	62.17	8.5	7.77	7.70	7.41
XT-3	62.17	8.3	7.77	7.70	7.41
XT-4	34.51	7.5	4.75	5.12	4.45
XT-5	34.51	5.8	4.75	5.12	4.45
XT-6	34.51	6	4.75	5.12	4.45
XT-7	73.69	9.5	7.77	7.7	5.88
XT-8	73.69	8.2	7.14	7.7	5.88
XT-9	73.69	7.5	7.14	7.7	5.88
XT-10	42.50	5	4.92	4.04	5.4
XT-11	42.50	5.7	4.92	4.04	5.4
XT-12	42.50	5.8	4.92	4.04	5.4

It can be seen from Fig. 2 to Fig. 5 that test specimens behaved similarly with theoretical predictions up to yielding. It is known that up to yielding RCC members behave almost linearly and after that they behave in nonlinear manner. The post yield behavior is beyond the scope of the theoretical predictions discussed here. For this reason, enlarged view of test results were shown to mark the differences of experimental results clearly from theoretical predictions.

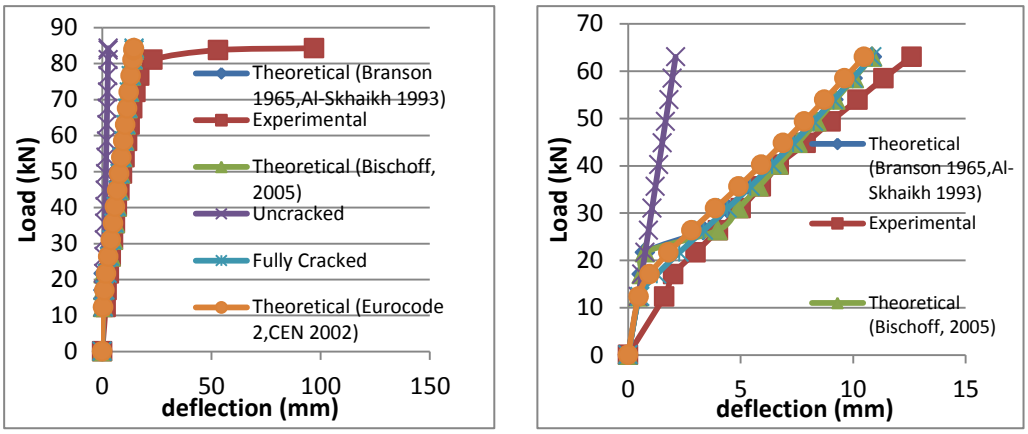

(a) Complete experimental result (b) Enlarged view

Figure 3: Comparison of the experimental and theoretical predictions of load deflection values for specimen T-3, 80 Grade sample, (ρ =0.0102), fc'=3990 psi

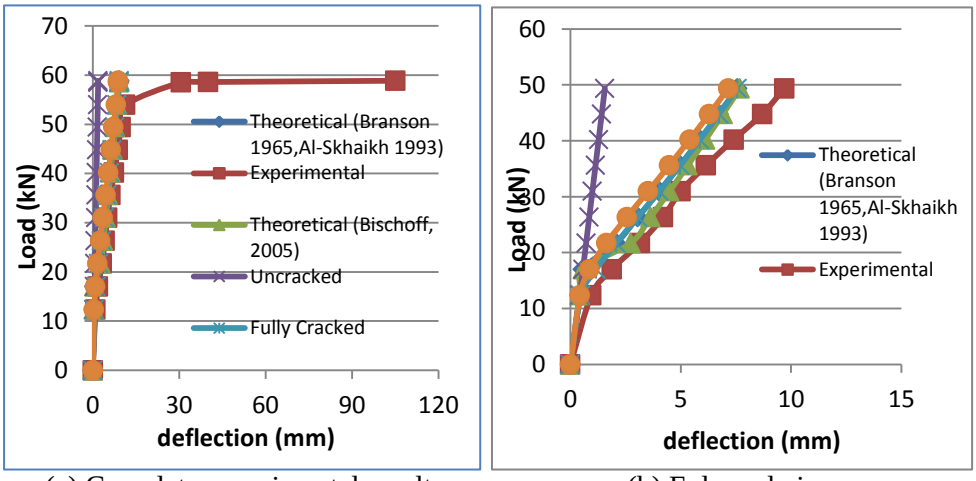

(a) Complete experimental result (b) Enlarged view

Figure 4: Comparison of the experimental and theoretical predictions of load deflection values for specimen XT-6, 60 Grade sample (ρ =0.0085), fc'=4124 psi

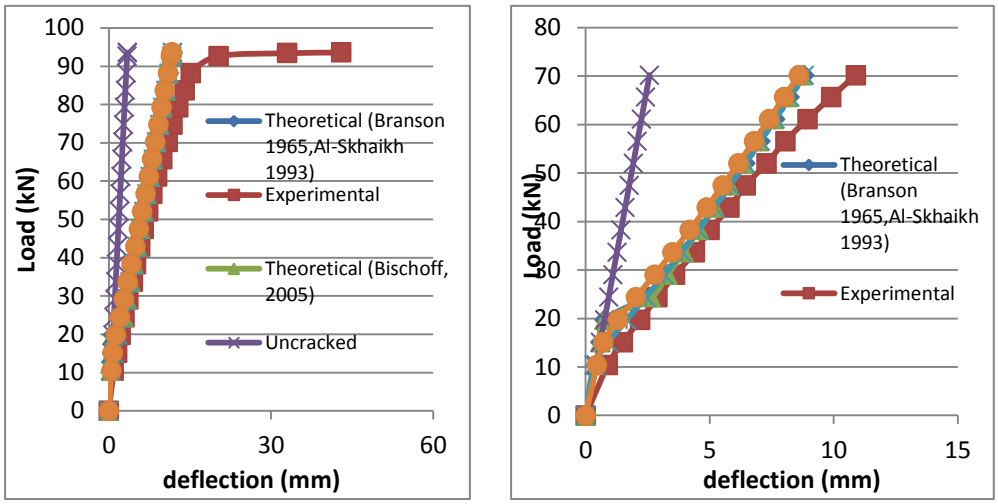

(a) Complete experimental result (b) Enlarged view

Figure 5: Comparison of the experimental and theoretical predictions of load deflection values for specimen XT-3, 60 Grade sample, (ρ =0.0166), f_c'=4124 psi.

5 CONCLUSIONS

A comparison of experimental and theoretical deflection of RCC beams reinforced with Grade 80 and Grade 60 rebars has been made in this paper. Based on the results presented, the following conclusions are drawn:

- The methods proposed by Branson (1965) and Bischoff (2005) closely estimate the load- deflection behavior of both Grade 80 and Grade 60 specimens.
- The method proposed by Bischoff (2005) provides a slightly better correlation with the actual load- deflection curves of both Grade 80 and Grade 60 specimens.
- The effective moment of inertia and the analytical load-deflection curves corresponding to it are highly dependent on the cracking moment used in the effective moment of inertia expression.
- The cracking moment estimates based on the modulus of rupture expression in Eurocode 2 (CEN 2002) are in closer agreement with the actual cracking moments of the specimens, compared to the methods given in ACI 318-14.
- Grade 80 specimens undergo higher deflections than that of Grade 60 specimens at service load level. But, it is to be noted that service load level was much higher for Grade 80 specimens.

ACKNOWLEDGEMENTS

The authors express their sincere appreciation to Bangladesh Steel Re-Rolling Mills (BSRM) for sponsoring the experimental program "Study of Flexural Strength and Ductility Characteristics of Concrete Beam Reinforced with 80 Grade Steel". The experimental data used in this paper is the outcome of the mentioned project.

REFERENCES

[1] Al-Shaikh, A. H. and Al-Zaid, R. Z. (1993), "Effect of Reinforcement Ratio on the Effective Moment of Inertia of Reinforced Concrete Beams", ACI Structural Journal, Vol. 90, No. 2, pp. 144-149.

[2] American Concrete Institute, ACI (2014), "Building Code Requirements for Structural Concrete (ACI 318-14) and Commentary (ACI R318-14)", Farmington Hills, Michigan.

[3] Bischoff, P. H. (2005), "Reevaluation of Deflection Prediction for Concrete Beams Reinforced with Steel and Fiber Reinforced Polymer Bars", Journal of Structural Engineering, ASCE, Vol. 131, No. 5, pp. 752-762.

[4] Bischoff, P. H. (2007), "Rational Model for Calculating Deflection of Reinforced Concrete Beams and Slabs", Canadian Journal of Civil Engineering, Vol. 34, No. 8, pp. 992-1002.

[5] Bischoff, P. H. and Scanlon, A. (2007), "Effective Moment of Inertia for Calculating Deflections of Concrete Members Containing Steel Reinforcement and Fiber-Reinforced Polymer Reinforcement", ACI Structural Journal, Vol. 104, No. 1, pp. 68-75.

[6] Branson, D. E. (1965), "Instantaneous and Time-Dependent Deflections of Simple and Continuous Reinforced Concrete Beams", HPR Report No. 7, Part 1, Alabama Highway Department, Bureau of Public Roads, Alabama (Department of Civil Engineering and Auburn Research Foundation, Auburn University, August 1963).

[7] European Committee for Standardization, CEN (2002), "Eurocode 2: Design of Concrete Structures - Part 1: General Rules and Rules for Buildings", Brussels, pp. 26-35 & 132.

[8] Kalkan, I., "Deflection Prediction for Reinforced Concrete Beams Through Different Effective Moment of Inertia Expressions," International Journal of Engineering Research and Development, Vol. 5, No.1, June 2013.

CICM 2015
First International Conference on
Advances in Civil Infrastructure and Construction Materials
MIST, Dhaka, Bangladesh, 14–15 December 2015

MEASUREMENT OF ULTRASONIC PULSE VELOCITY IN CONCRETE FOR ASSESSING COMPRESSIVE STRENGTH

Fatema T. JOHORA[1], Chowdhury M. T. Amin[2], S. M. Ibrahim[3], A. Haque[4], A. F. M. Saiful Amin[5]

[1, 2, 3, 4] Department of Civil Engineering, Military Institute of Science and Technology, Dhaka, Bangladesh.
E-mail: [1]fatema.mist09@gmail.com, [2]toufiq_amin@yahoo.com, [3]ibrahim4uonly@gmail.com and [4]arif6plus10@yahoo.com

[5] Department of Civil Engineering, Bangladesh University of Engineering and Technology, Dhaka, Bangladesh.
Email: samin@ce.buet.ac.bd

Abstract. *Evaluating in- place compressive strength of concrete by employing non-destructive testing method is a cardinal approach to assess concrete strength in present condition. But strength cannot be measured because non-destructive tests are relative in nature. So, indispensability arises for establishing experimental relation between the property being measured by a given test and the strength of the specimen. Concrete strength increases with time due to curing but when its use being started, environmental exposure may also deteriorate its strength. To assess the concrete strength in present condition of a structure ultrasonic pulse velocity method is used among all other non-destructive methods in order to find a correlation with concrete compressive strength. Therefore, to derive such correlation and evaluating its reliability using local material and local condition is important for judging the concrete. Finally, further observations are made on effect of concrete age and coarse aggregate which are known to be the most important parameters that affect the correlation.*

Keywords: Ultrasonic pulse velocity, compressive strength, saturation condition.

1 INTRODUCTION

For inspection, operations and monitoring of concrete structures the UPV methods have been used. UPV test is also used for the measurement as well as to control a series of basic parameters in order to ensure the quality of concrete. The matters of concern are interpretation of these test results and for that proper knowledge about the influential factors are necessary [1]. As per IS number 13311 in part one in 1992 The underlying principle of the test is the method consists of measuring the time of travel of an ultrasonic pulse passing through the concrete being tested; comparatively higher velocity is obtained when concrete quality is good in terms of density, uniformity, homogeneity etc. Concrete technologist has been working for decades in order to determine the properties of concrete using nondestructive tests. Many test methods have been proposed for laboratory test specimens using vibrational methods beginning in the 1930s. Powers, Obert, Hornibrook, and Thomson were the first to conduct extensive research using vibrational techniques such as the resonant frequency method [2].World War 2 accelerated research regarding nondestructive testing using stress wave propagation methods. The development of the pulse velocity method began in Canada and England at about the same time. In Canada, Leslie and Cheesman development an instrument called the soniscope. While in England, jones developed an instrument called the ultrasonic tester. In principle, both the soniscope and the ultrasonic tester were quite similar, with only minor differences in details. Since the 1960s, pulse velocity methods have been moved out of laboratories and to construction sites. Malhotra has compiled an extensive list of papers published on this subject. Many nations have adopted standardized procedures to measure pulse velocity in concrete [2].

2 EXPERIMENTAL DETAILS

2.1 Materials

Cubes of different grades of concrete M15, M20 and M35 were casted out of the concrete matrix during construction. To improve workability of concrete, water reducing admixture was added into each grade of concrete to control the slump and to prevent the occurrences of bleeding and segregation. Materials Used for making specimen includes cement, fine aggregate, coarse aggregate and water reducing admixture. For each type of aggregate different strength combinations were used.

Tests were conducted on different specimens. The mixture contained cement and four types of coarse aggregates such as stone, brick, recycled brick, recycled stone. Specimens with different strength and mixing ratio were casted. The specimens were allowed to gain strength on 3, 7, 14, 28, 56, 90, 107, 114, 120 days in

achieving the required strength of concrete, it is needed to specify a proper mix design with appropriate mix proportion of water, cement, fine aggregate and coarse aggregate for trial mix. Hence for the concrete in this context with strength several mix design need to be analyzed before coming up with a most suitable mix design. This is to configure the proportional content of concrete, which could also affect the ultrasonic pulse velocity.

2.2 Mix Design

Mix design was performed in accordance to BS 5328-1997 with the BRE (Building Research Establishment) concrete mix design-British method (1988) to determine the mix proportion of the materials used in casting of concrete.

Type of concrete	free water content (kg)	cement content (kg)	Total Aggregate Content (kg)	Fine Aggregate Content (kg)	Coarse Aggregate content (kg)
S10	14.41	17.84	127.67	51.06	76.60
S20	14.41	22.65	123.55	49.42	74.13
S35	15.44	30.28	114.89	42.50	72.38
B10	14.41	17.84	127.67	51.06	76.60
B20	14.41	22.65	123.55	49.42	74.13
B35	15.44	30.28	103.22	38.19	65.03
RS10	14.41	17.84	127.67	51.06	76.60
RS20	14.41	22.65	123.55	49.42	74.13
RS35	15.44	30.28	110.42	40.85	69.57
RB10	14.41	17.84	127.67	51.06	76.60
RB20	14.41	22.65	123.55	49.42	74.13
RB35	15.44	30.28	105.96	39.20	66.75

3 EXPERIMENTAL RESULTS AND DISCUSSION

3.1 Effect of Coarse Aggregate

Among different influential factors the effect coarse aggregate is most important in terms of correlation between the ultrasonic pulse velocity and concrete compressive strength. For analyzing coarse aggregate effect brick, recycled brick, stone, and recycled stone aggregate are chosen. Data are taken up to 28days.The coarse aggregate effect is shown in figure 1.

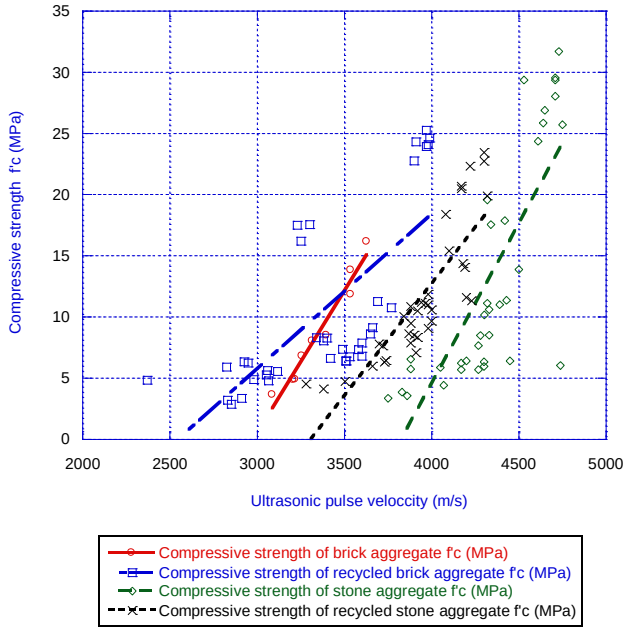

Figure 1: Compressive strength vs. ultrasonic pulse velocity (Coarse aggregate effect)

From the figure 1 it can be observed that the ultrasonic pulse velocity of recycled brick is lower than the brick. This is because the difference in density between two aggregate. Recycled brick has low density than the brick aggregate due to pores in recycled aggregate. That's why the UPV is higher in brick aggregate. Due to the similar reason the UPV in stone is higher than the UPV in recycled stone.

Table 1: Equation and co-efficient of determination for different coarse aggregate

Type of aggregate	Equations	Co-efficient of determination
Brick	y = -69.395 + 0.023268x	R^2= 0.9552
Recycled brick	y = -32.315 + 0.012657x	R^2= 0.515
Stone	y = -100.08 +0.026246x	R^2= 0.615
Recycled stone	y = -60.689 + 0.018328x	R^2= 0.697

3.2 Effect of Concrete Age

3.2.1 Correlation between Compressive Strength and UPV for Saturated Condition

Correlations between compressive strength and ultrasonic pulse for brick, recycled brick, stone and recycled stone are find out using the data up to 28 days.

Linear relation between compressive strength and ultrasonic pulse velocity for brick aggregate are shown below where continuous lines represent the linear relation between compressive strength and ultrasonic pulse velocity.

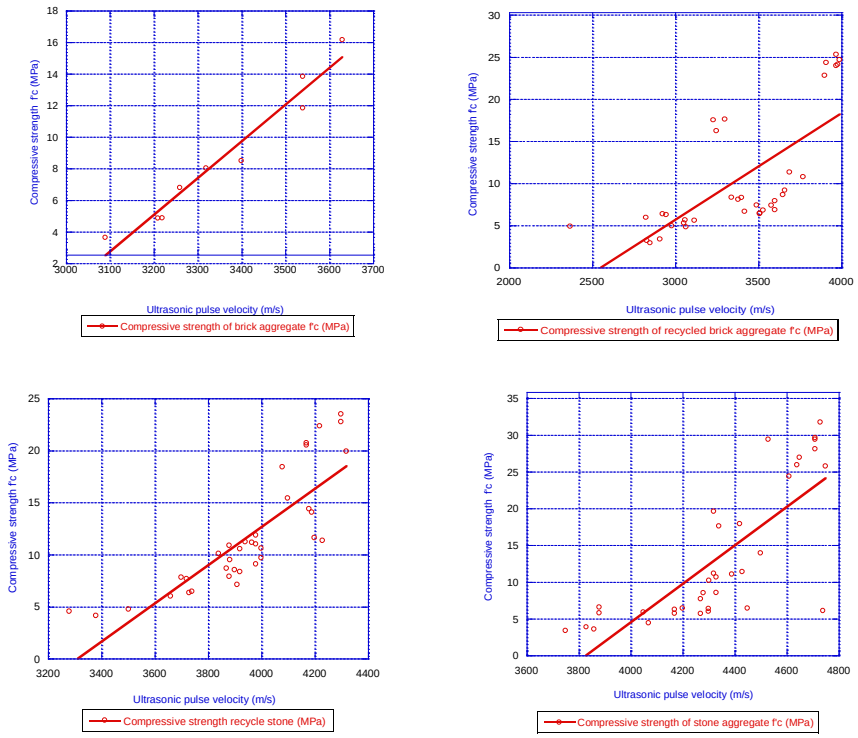

Figure 2: Correlation between compressive strength and ultrasonic pulse velocity for brick, recycled brick recycled stone, stone aggregate.

It can be inferred from the graph that with increase in ultrasonic pulse velocity compressive strength also increases. For brick aggregate the linear equation is

$$y = -69.395 + 0.023268x \quad (1)$$

$R=0.97735$, $R^2= 0.955$

Where, y= Compressive strength, x= Ultrasonic pulse velocity and the value of coefficient of determination is R^2.Similarly for recycled brick, stone and recycled stone aggregate.

Correlation between compressive strength and UPV are find out. For recycled brick, stone, recycled stone aggregate data are taken for 3, 7, 14, 28 days. Summary of results and correlation between concrete compressive strength and UPV are shown in table 2.

3.2.2 Correlation between Compressive Strength and UPV for Air Dry Condition

Correlations between compressive strength and ultrasonic pulse for brick recycled brick, stone and recycled stone are find out using the data after 28 days. For brick aggregate 35, 60 days data are taken. For recycled brick data of 90, 120, for stone 60, 90 and for recycled stone 90,107,120 days are taken. Summary of results and correlation between concrete compressive strength and UPV are shown in table 3

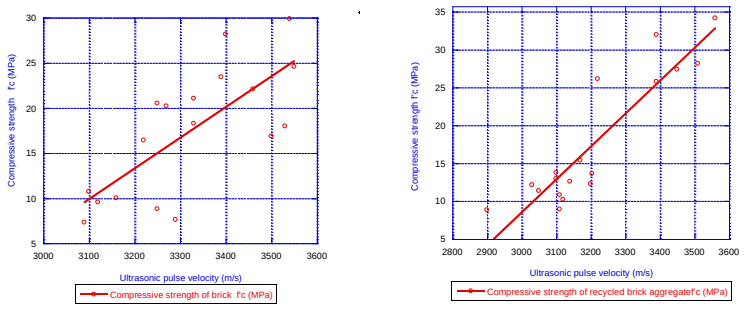

Figure 6: Correlation between compressive strength and ultrasonic pulse velocity for brick,recycle brick aggregate.

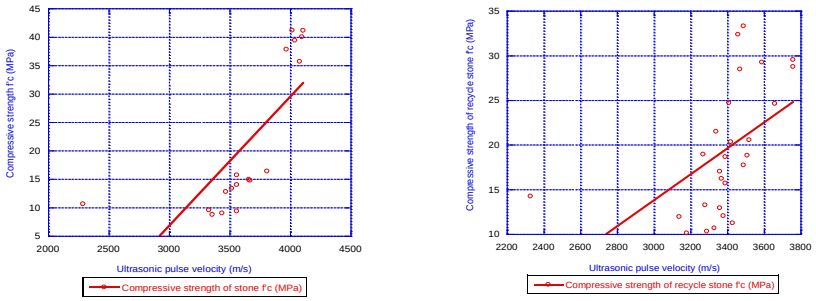

Figure 7: Correlation between compressive strength and ultrasonic pulse velocity for stone, recycle stone aggregate.

From the ACI committee report we know that at early maturities a given increase in compressive strength results in a relatively large increase in pulse velocity while at later maturity the velocity increment is smaller for the same strength increase. Analyzing the graphs and co-relations we found a concrete validity of that report.

Table 2: Summary of statistical analysis of ultrasonic pulse velocity for saturated condition

Aggregate type	Pearson coefficient (t)	Co-efficient of determination R^2	Equation	Sig-F	Correlation
Brick	0.977	R^2= 0.955	y= -69.395 + 0.023268x	0.000	Strong
Recycled brick	0.718	R^2=0.515	y= -32.315 + 0.012657x	0.000	Strong
Stone	0.783	R^2= 0.613	y= -100.09 + 0.026148x	0.000	Strong
Recycled stone	0.835	R^2= 0.697	y= -60.689 + 0.018328x	0.000	Strong

Table 3: Summary of statistical analysis of ultrasonic pulse velocity for air dry condition

Aggregate type	Pearson coefficient (t)	Co-efficient of determination, R^2	Equation	Sig-F	Correlation
Brick	0.739	R^2= 0.544	y= -95.576 + 0.034022x	0.000	Moderate
Recycled brick	0.906	R^2=0.821	y= -121.87 + 0.043461x	0.000	Strong
Stone	0.739	R^2= 0.546	y= -61.19 + 0.022659x	0.000	Moderate
Recycled stone	0.518	R^2= 0.268	y= -29.775 + 0.014517x	0.006	Moderate

4 CONCLUSION

The concrete is a heterogeneous material and the interpretation of relation between compressive strength and ultrasonic pulse velocity is complex. The attempts are made for estimating the strength and other properties of concrete for getting more reliable and dependable information of the quality of concrete without crushing. The study may contribute towards the development of a guideline to determine compressive strength using ultrasonic pulse velocity. Based on the extensive experimental works and studies, the following conclusions are drawn:

The study indicates that the variation of the age and aggregate type can generate effects those are sensible in the UPV. With the increasing age, the velocity also increases .At early age the increasing rate is rapid. Among different types of aggregates used in the study, it has been seen that for a particular strength recycled stone aggregate gives lower UPV than stone aggregate concrete and similar case is happening to recycle brick and brick aggregate. So further research works can be done based on these aggregate properties by incorporating some other important parameters like porosity, moisture content etc.

REFERENCES

[1] D. Breysse, "Quality of NDT Measurements and Accuracy of Physical *Properties," Concrete NDTCE'09, Nantes, 30 June-3 July, 2009.*

[2] HANDBOOK ON NONDESTRUCTIVE TESTING OF CONCRETE, Chapter 8.The Ultrasonic Pulse Velocity Method.

CICM 2015
First International Conference on
Advances in Civil Infrastructure and Construction Materials
MIST, Dhaka, Bangladesh, 14–15 December 2015

A COMPARATIVE STUDY OF SEISMIC RISK ASSESSMENT PROCEDURES FOR EXISTING RESIDENTIAL BUILDINGS OF DHAKA CITY

Naveel Islam[1], Kshama S. Roy[2], Kamrul Islam[3], Md. I. HOSSAIN[4] and Fatema T. Zohora[5]

[1,2] Faculty of Engineering and Applied Science, Memorial University of Newfoundland, Canada. Email: [1]ni5867@mun.ca and [2]ksr037@mun.ca.
[3, 5] Department of Civil Engineering, Military Institute of Science and Technology, Dhaka, Bangladesh. Email: [3]kamrul1@ualberta.ca and[5]fatema.mist09@gmail.com.
[4] Bangladesh University of Engineering and Technology, Dhaka, Bangladesh, E-mail: mimranhossain09@gmail.com.

.

Abstract. *Severe earthquakes in recent time have imposed tremendous threat to humanity. Seismic risk assessments of the existing buildings are gaining more attention to assess correctly the degree of risk to which such critical structures may be subjected to in the event of an earthquake. Various seismic vulnerability assessment procedures can be found in the literature based on building plan, foundation, structural system, structural and non-structural components, and structural performance. Such vulnerability assessment procedures would show realistic performance of a building if the building was built according to the proper building design code and architectural features. The assessment of the seismic vulnerability of the existing medium to low-rise Reinforced Concrete (RC) buildings of Dhaka City, which are not built according to the standard building code has gained significant attention in recent years. A detailed survey has been carried out in the Dhaka city to assess the earthquake vulnerability of existing medium to low-rise reinforced concrete buildings. Two seismic vulnerability assessment techniques, Turkish method and Japanese method are considered in the current study. The main objective of this study is to compare the two seismic risk assessment methods for existing buildings of Dhaka city. A brief discussion on the performance score and seismic performance indices predicted by the two methods is also presented in this paper. Results show that, Japanese method might provide more reliable assessment compared to the Turkish method for the existing medium to low-rise buildings of Dhaka city.*

Keywords: Japanese method, Turkish method, Seismic vulnerability assessment, Reinforced concrete building

1 INTRODUCTION

Seismic vulnerability assessment or seismic risk assessment methodologies are followed almost all over the earthquake prone countries of the world for various forms of structure. This increased awareness against earthquake aroused due to some of the severe damage caused by the recent earthquakes (Turkey, 2015; Afghanistan and Pakistan, 2015; Nepal, 2015; Japan, 2011; New Zealand, 2010 & 2011; Mexico, 2011, Indonesia, 2010 & 2011; China, 2010; Haiti, 2010). As mentioned in the field reports and documented cases, the devastations in some cases were more severe because of the tilting of the buildings, bridges, dams and similar man-made structures. Various analytical, experimental, and hypothetical models from realistic data have been developed to assess the seismic vulnerability of existing structures. Dhaka is the world's 16thbiggest city, and the capital of 8thmost populous country. According to the July, 2015 study by Demographia [1] its 15,414,000 inhabitants live within 134 square miles, giving the city a suffocating density of 115,000 inhabitants per square mile. Dhaka has been named as the worlds' densest metropolitan area by Demographia where the abrupt growth of low-to medium rise reinforced concrete (RC) buildings due to improper planning as made the city extremely vulnerable to natural disasters like earthquake. Although the city lies in the moderate earthquake zone but the movement of tectonic plates over the boundary of the country has shaken the city over a number of times in the past two decades. Moreover few incidences of major structural cracks in RC buildings were reported in the past which might lead to consequential casualties in major portions of the city. Researchers and urban planners are deeply concerned to resolve and minimize the effect to some extent adopting various methodologies. Building codes are being revised and extended portions of the cities are pre-planned to accustom the current mitigation measures. As a result, effective seismic vulnerability assessment methodologies have become a very important issue to assess the sustainability of buildings in Dhaka City.

Researchers have been trying to implement an effective seismic vulnerability methodology for Dhaka city for quite a long time. But due to the lack of a proper seismic risk assessment code except the National Building Code, almost all the studies regarding seismic vulnerability were based on methodologies and reports developed in other countries. But recent research works [2-16] shows that some of these methodologies can be directly implemented to the major cities of Bangladesh (i.e. Dhaka) in accordance to identical soil conditions, building category and earthquake movement. A brief segment of identical approaches are presented in the following sections of the paper. Authors through their previous studies [11-16] have checked the adequacy of the two prominent methodologies in various portions of Dhaka city through detailed survey procedure. In this paper, emphasis will be given to provide a brief summary of the various seismic vulnerability assessment procedures that might be applicable to Dhaka city. A detailed survey is

conducted on the existing medium to low-rise buildings located at some major portions of Dhaka city to compare two seismic vulnerability assessment procedure, Turkish method and Japanese method. This paper focuses on the major results obtained from the survey.

2 SESIMIC RISK ASSESSMENT PROCEDURES

Most of the seismic vulnerability assessment procedures found in the literature are based on screening i.e. street surveys for low- to mid-rise reinforced concrete and masonry buildings. These procedures mainly rely on the data collected through visual investigations on each building. For example, New Zealand method [17] is basically a two-stage process consisting of the initial evaluation procedure (IEP), intended as a coarse screen followed by the detailed assessment. However, the Canadian method [18] is based on identifying the main features of any building affecting risk of seismic hazards. The importance of the building is determined by its use and occupancy. The European Code [18, 22], is based on appropriate actions and possible modified safety-factors. This has been developed for smaller uncertainty with respect to dead loads, smaller existing life span and for properties of existing materials. These are used for seismic analysis of the building. Calculation is based upon both non-seismic and seismic actions for an existing building. The assessment is for the period of its intended lifetime. In case of Italian procedure [18], the detection of eleven (11) parameters, as well as the score assignment for each of them is the result of the post-earthquake surveys. In U.S. method [17], each building is assigned a basic score first. This is then modified for the building height along with the presence of any structural weaknesses, the soil type, and whether the building is designed according to a seismic code. This helps in providing a final score for the buildings. The Indian method [16] is a modification of the U.S. method and provides additional building types including four different types of unreinforced masonry (URM) buildings and modified values of related parameters. The ASCE 31 [19] standard includes procedures for Life Safety and Immediate Occupancy Performance Levels. This methodology evaluates the seismic resistance of buildings consisting of a three-tier approach. The first tier is the screening phase, the second tier is the evaluation phase, and the third tier is the detailed evaluation phase. This standard is later modified to form the ASCE 31-03 [20], which is the last step in the development of a standard for seismic evaluation of existing buildings. Major changes to this process include a reorganization of the nonstructural checklist and a rewrite of the URM special procedure. It also embodies the latest efforts in the development of performance-based analysis techniques. ASCE 41-13 [21] combines seismic evaluation and retrofit into one document and brings consistency to the process. The Tier 1 Screening is essentially the same as it was in ASCE 31-03 [20], with some reor-

ganization and technical changes to the checklists. But the specific Tier 2 analysis procedures and ASCE 31-03 m-factors were eliminated. Other seismic vulnerability assessment procedures include but not limited to the Hybrid Method [22], which consists of FEMA 154 (2002), FEMA 310 (1998), Euro Code 8, New Zealand Guidelines (NZSEE 2000, 2003) and NRC Guidelines (NRCC 1993). FEMA 154 (2002) is a relatively quick procedure in developing a list of potentially risky buildings without the expensive detailed seismic analysis of individual buildings. FEMA 310 (1998) is presented as an advanced seismic evaluation procedure for existing buildings that describes a three-tiered procedure of increasing details and reducing margin of safety for the seismic evaluation of existing buildings. NRC Guidelines (NRCC 1993) consists of both structural and nonstructural hazards, and the importance of the building is determined from the use and occupancy classes. Indexing method requires the acquisition of extensive data on building materials, site conditions and structural systems and involves vast analytical efforts. Fuzzy logic is applied to seismic vulnerability assessment procedure in case of Fuzzy Rule based modeling where it is used to integrate descriptive (linguistic) judgment and numerical data and make approximate reasoning algorithms to propagate the uncertainties[15,23].

Seismic vulnerability of unreinforced masonry walls was assessed by conducting a numerical study on the interaction of axial and lateral resistance [24]. The walls were modeled in an Abaqus environment using a plastic damage mode. Centrifuge modeling method [25] describes an investigation on the performance of shallow foundations susceptible to seismic liquefaction, considering the particular vulnerability that this type of foundation has shown in the field during past earthquakes. Ranking method [26] requires only the dimensions of structure as input and is based on defining the position of a building on a two dimensional plot using the wall and column indices. Likewise, GIS-based extension [4, 9, 27] provides users with a familiar environment to estimate and observe the probable damages and fatalities of a deterministic earthquake scenario. Statistical method [28] which is an improvement on the methodology of the National Group for Earthquakes Defense (GNDT-SSN 1994) based on the vulnerability assessment methodology is also considered for the seismic vulnerability evaluation of masonry buildings. A schematic and sequential representation of a large variety of seismic assessment methodologies can also be found in [29].

3 METHODOLGIES OF INTEREST

Due to economic availability of building raw materials; Reinforced Concrete Frame buildings are most common in Dhaka city [5]. Authors are primarily interested in two of the prominent methodologies (Turkish and Japanese) that cover reinforced concrete building frames and have been used by previous researchers for Dhaka City [5,11-16]. Both of the methodologies do not require strong exper-

tise in the field but involve works in both visual screening and structural detailing surveys.

3.1 Turkish Method of Seismic Vulnerability Assessment

According to the opinion of a German earthquake expert Dorka [31], Turkish method of seismic risk assessment can be considered for a developing country like Bangladesh, where standard building codes are not followed properly. Authors through their previous studies [11-13] checked the suitability of Turkish Method by conducting detailed Level 1 and Level 2 surveys for buildings in densely constructed portions of the city. Turkish method is a multiple-level seismic vulnerability assessment methodology for the existing reinforced concrete (RC) buildings. The Turkish method includes two-level evaluation: (i) level one – walk down evaluation and (ii) level two measurements at ground level and basement. The walk down evaluation procedure consists of taking notes of different external features of the building. Buildings are then described as belonging to 'safe', 'intermediate' or 'unsafe'. After level one survey, buildings that fall into the moderate and high risk levels can be subjected to more detailed level two survey to determine their performance scores. Once the vulnerability parameters of a building are obtained from two-level surveys and its location is determined, the seismic performance scores for survey levels 1 and 2 are then calculated [30].

A general equation for calculating the seismic performance score (PS) can be formulated as follows:

$$PS = (\text{Initial Score}) - \Sigma\,(\text{Vulnerability parameter}) \times (\text{Vulnerability Score}) \quad (1)$$

The detailed calculation for vulnerability scoring can be found atSucuoglu et al. [30] and authors' previous studies [11-13] and is not repeated here. However, a sample calculation is shown in Table 2.0.

3.2 Japanese Method of Seismic Vulnerability Assessment

The Japanese seismic vulnerability assessment is based on both site inspection and structural calculation to represent the seismic performance of existing medium and low–rise reinforced concrete buildings in terms of seismic performance index of structure, I_s. Three levels of screening procedure, namely the first, the second, and the third level screening, have been used for the seismic evaluation. Any level of the screening procedures may be used in accordance with the purpose of evaluation and the structural characteristics of the building [32]. Building inspections are conducted to check the structural characteristics of the building, which are necessary to calculate the seismic index of structure, I_s. Appropriate methods for inspection i.e. site inspection, collection of design drawings, and/or material test are selected in accordance with the screening level. In case, design drawings of the building are not available, inspections on the structural dimensions, diameters and arrangements of reinforcing bars need to be examined on

site, which are necessary for seismic evaluation of the building in accordance with the screening level [32]. The seismic performance index of structure (I_s) is evaluated by the following equation at each storey and to each direction,

$$I_s = E_0 * S_D * T \quad (2)$$

Where,

E_0= Basic seismic index of structure,

S_D= Irregularity index

and T = Time index

Seismic safety of structure is judged by the following equation,

$$I_s \geq I_{so} \quad (3)$$

Where,

I_s= Seismic index of structure and I_{so}= Seismic demand index of structure

If Equation (3) is satisfied, the building is assessed as 'Safe - the building possess the seismic capacity required against the expected earthquake motions'. Otherwise, the building is assessed as 'Uncertain' in seismic safety.

The thorough procedure can be found in the authors' previous publications [15,16] and in Otani [33], which was formulated based on the standard for seismic evaluation and guideline for seismic retrofit of existing reinforced concrete building revised from the general outline given by Umemura [34] and by Japan Building Disaster Prevention Association in 1990 [32]. The details of the calculations are not the scope of the present study. However, a sample calculation is shown in Table 2.0 for clarification.

4 SURVEY DETAILS

Four major locations: Mirpur, Mohammadpur, Dhanmondi and Jhigatola that cover parts of the major crowded portions of Dhaka City with high densities of residential buildings are chosen. Zone II where the Dhaka City lies is considered to be the most vulnerable city for a major form of earthquake. The expected intensity of earthquake for Dhaka city is around VIII (Modified Mercalli Intensity Scale) which may be assumed to correspond to a peak ground acceleration (PGA) in a range of 0.2g to 0.25g. According to current seismic zoning map of building code, for Dhaka city (Zone II) the PGA is around 0.15g on very firm soil, considering site effects it can be 0.20g or more [11, 35-36].Altogether, thirty (30) buildings with six stories from a set of sixty (60) surveyed buildings are randomly selected for the present study. The distribution of the buildings in the study areas is shown quantitatively and qualitatively in Figure 1.0 (a) and Figure 1.0 (b) respectively. Note that, detailed survey results of the sixty (60) buildings will be published in authors' future publications.

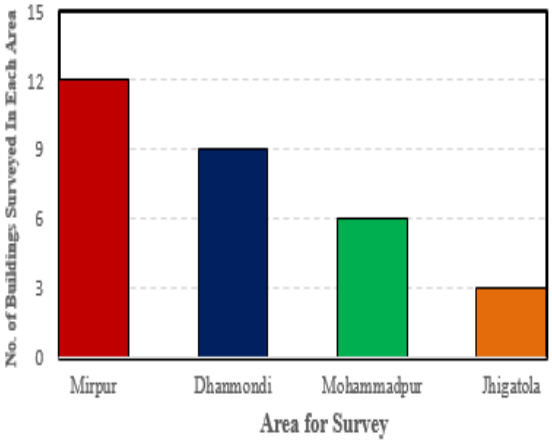

Figure 1.0 (a) Quantitative Distribution of Buildings within the study areas

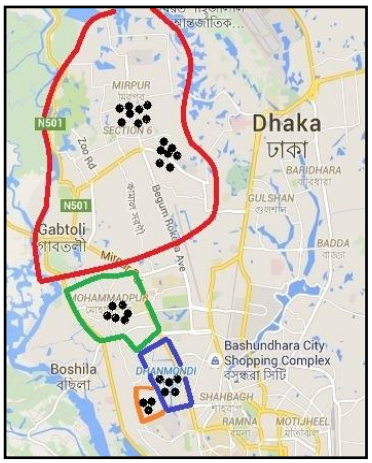

Figure 1.0 (b) Map showing the locations of the study area

5 RESULTS

Both of the methodologies are considered for the analysis of the surveyed buildings in the study areas. Figure 2.0 shows the distribution of performance score (calculated based on Equation 1) with building inventory, where the survey areas are highlighted beneath the building numbers representing the study locations. Two horizontal lines at PS (Low) and PS (High) for PS 70 and PS 50 are considered which divide the zone of PS in three segments namely, SAFE, INTERMEDIATE and UNSAFE. Depending on the sub divisions the qualitative safety assessments are shown in Figure 4.0 (a) and (b) for Level 1 and 2 respectively. Likewise, analysis is considered for the same buildings by Japanese Method of assessment, whereas the seismic indices (calculated as per equation 2) are plotted against the building inventory as shown in Figure 3.0. Equation 3.0 provides the degree of safety for Japanese Method. For the locations of Dhaka City, I_{so} is calculated as 0.68 [16, 34]. The horizontal line represents I_{so} which again subdivides the plot area into two segments SAFE and UNCERTAIN (indifferent from Turkish Method).From Figure 3.0 it can also be seen that, $I_s<I_{so}$ for only the values for I_sY where Y represents the shorter directions of the building. The qualitative safety assessment in Figure 4.0 (c) shows the zone of UNCERTAIN for the five (5) buildings out of the thirty (30) surveyed buildings in the study locations.

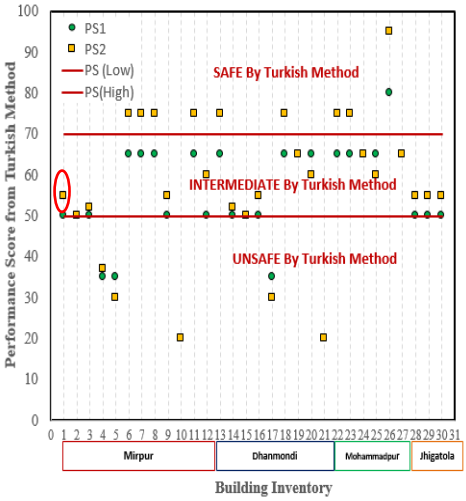

Figure 2.0 Performance Score from Turkish Method with Building Inventory

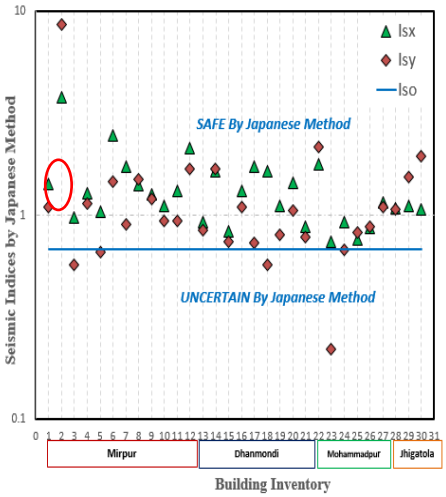

Figure 3.0 Seismic Indices by Japanese Method with Building Inventory

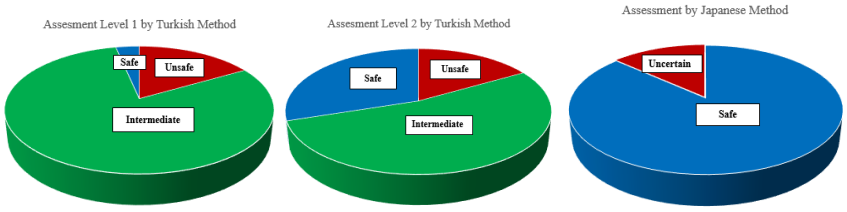

(a) (b) (c)

Figure 4.0 Qualitative safety assessment based on the survey in the study locations by (a) Level 1 Assessment by Turkish Method (b) Level 2 Assessment by Turkish Methods and (c) Japanese Method

6 COMPARISON BETWEEN THE RESULTS

The two seismic vulnerability assessment methodologies used in the present study has been used by previous researchers to provide considerable results. But substantial variations on the results may cause dilemma in providing proper judgments regarding the overall safety of the buildings. Considering Figure 2.0-4.0, it can be seen that, Japanese Method which is a more extensive and detailed method [15,32] shows less damage susceptibility in buildings compared to results obtained by Turkish Method. The overall safety assessment of the surveyed buildings can be more clearly viewed in Table 1.0. As mentioned in Table 1.0, only a single building is assessed to be completely unsafe from both the methods.

Whereas, majority lies in the zone where the level of safety is assessed to be SAFE from Japanese method, but INTERMEDIATE from Turkish method. A detailed stepwise calculation for both Turkish and Japanese methods for building number 1 (circled in Figures. 2.0 & 3.0) is presented in Table 2.0.

Table 1.0 Itinerary of the Buildings Based on Safety Assessment comprising both Turkish and Japanese Method

SAFE By Turkish Method ***SAFE By Japanese Method*** **6,7,8,11,13,22,26**	**SAFE By Turkish Method** ***UNCERTAIN By Japanese Method*** **18,23**
INTERMEDIATE By Turkish Method ***SAFE By Japanese Method*** **1,2,9,12,14,15,16,19, 20,25,27,28,29,30**	**INTERMEDIATE By Turkish Method** ***UNCERTAIN By Japanese Method*** **3,24**
UNSAFE By Turkish Method ***SAFE By Japanese Method*** **4,10,17,21**	**UNSAFE By Turkish Method** ***UNCERTAIN By Japanese Method*** **5**

7 SAMPLE CALCUATION FOR A SURVEYED BUILDING

In the following Table 2.0 the sample calculation for a surveyed building is presented for both the seismic vulnerability methods. The building is marked in both Figures 2 and 3. The details of the parameters mentioned in the calculation can be found in authors' recent publication in Islam et al. [15].

Table 2.0 Sample Calculation for Survey Building

Building Location	**Mirpur 11, Dhaka**	**Building ID**	**1 (Circled in Figs. 2 & 3)**
Number of Storey	6	**Floor Area**	1415.13 ft^2
Assessment by Turkish Method		***Assessment by Japanese Method***	
Presence of soft storey	Yes	Compressive Strength of Concrete	20 N/mm^2
Heavy Overhanging	No	Column clear height	2438.4 mm
Apparent Building Quality	Moderate	Column depth	279.4 mm
Presence of Short Columns	No	Thickness of wall	127 mm
Pounding Between Adjacent Building	No	Length of wall along longer direction	788.52 m

Topographic Effect	No	Length of wall along shorter direction	593.96 m
Plan Irregularity	No	Total Cross sectional area of storey concerned	27251.56 mm^2
Normal Redundancy Ratio	2.8513 (Redundant)	Strength Index of Walls along longer direction	126.95
Strength Ratio	1.1326 (Strong)	Strength Index of Walls along shorter direction	95.63
		Strength Index of Columns	1.209
		Strength Index of extremely short columns	2.591
Performance Score from Level 1 survey	50	Basic Seismic Index of the structure along longer direction, E_oX	21.3
Performance Score from Level 2 survey	55	Basic Seismic Index of the structure along shorter direction , E_oY	16.08
		Irregularity Index, S_D	0.8
Assessment from Level 1 survey	Intermediate	Time Index, T	1
Assessment from Level 2 survey	Intermediate	Seismic Index of the Structure for longer direction , I_sX	17.08
		Seismic Index of the Structure along shorter direction , I_sY	12.89
		Basic Seismic demand Index	0.8
		Zone Index	0.85
		Usage Index	1
		Ground Index	1
		Seismic Demand Index	0.68
		Judgement of seismic safety: **SAFE** (The building possesses the seismic capacity required against the expected earthquake motion)	

8 CONCLUSIONS

The paper aimed to introduce a generalized comparison between two seismic vulnerability assessment procedures (Turkish and Japanese methods) by conducting a detailed survey in densely populated portions of Dhaka city. Results show that Japanese method might be more applicable to Dhaka city compared to the Turkish method. Attempts were also made to introduce a number of highlighted seismic vulnerability assessment procedures that are currently being followed all over the world. This paper focuses part of a detailed survey and comparison of various seismic vulnerability assessment procedures that might be applicable to densely populated cities like Dhaka city. A detailed discussion on the comparison

and complete survey including the implementation of more vulnerability methods (along with widespread surveys) that could provide more convincing reliability parameters for existing buildings of Dhaka city and other major urban cities of Bangladesh will be shown in authors' future publications.

REFERENCES

[1] Demographia World Urban Areas Report; 11th Edition, 2015:01.

[2] M. H. Ansary, and M. A. Noor, 2004. Vulnerability assessment of existing engineered and non-engineered structures of Dhaka city using RVS and NDT Techniques. Third International Symposium on New Technologies for Urban safety of Mega Cities in Asia, Agra, India.

[3] M. Z. Ahmed, M. K. Islam, R. Ahsan, and G. Ozcebe, 2007. Seismic vulnerability assessment methods: a possible application to Bangladesh. First Bangladesh Regional Science Association (BRSA)Conference, Dhaka

[4] M. J. Alam, M. A. R. Khan, and A. Paul,2009.Seismic vulnerability assessment of existing RC buildings in GIS Environment. Earthquake Engineering Research Center (EERC), Dept. of Civil Engineering, Chittagong University of Engineering & Technology (CUET), Bangladesh.

[5] M. R. Sadat, M. S. Huq, M. A. Ansary, 2010. Seismic Vulnerability Assessment of Buildings of Dhaka city. Journal of Civil Engineering, Inst. of Engineers, Bangladesh. 38 (2), 159-172.

[6] R. P. Ishita and S. Khandaker, 2010.Application of analytical hierarchical process and GIS in Earthquake vulnerability assessment: case study of ward 37 and 69 in Dhaka City. Journal of Bangladesh Institute of Planners, 3:103-112.

[7] M. Ahmed, K. M. Khaleduzzaman, N. A. Siddique and S. Islam, 2012. Earthquake vulnerability assessment of schools and colleges of Sylhet, a North-eastern city of Bangladesh. SUST Journal of Science and Tech., 19(5): 27-34.

[8] M. A. Rahman, M. S. Ullah, 2013. Seismic vulnerability assessment of RC Structures: A Review. Asian Transactions on Eng., 02(06).

[9] M. M Ahmed, I. Jahan and M. J. Alam, 2014.Earthquake vulnerability assessment of existing buildings in Cox's -Bazar using Field Survey & GIS. International Journal of Eng. Research & Technology (IJERT), 3 (8).

[10] A. Sarraz, M. K. Ali and D. C. Das, 2015. Seismic vulnerability assessment of existing building stocks at Chandgaon in Chittagong city, Bangladesh. American Journal of Civil Engineering, 3(1): 1-8.

[11] M. Z. Ahmed, K. Islam, K. S. Roy, M. S. Arafat, and T.M. Al-Hussaini, 2010. Seismic vulnerability assessment of RCF Buildings in Dhaka City. Proceedings of the 3rd International Earthquake Symposium (IESB-3), Dhaka, Bangladesh.

[12] K. S. Roy, K. Islam and M. S. Arafat, 2010. Seismic risk assessment of existing low-rise buildings in unplanned urban regions of Dhaka City. Proceedings of the 2nd International Conference on Construction in Developing Countries (ICCIDC-2), Cairo, Egypt.

[13] K. S. Roy, K. Islam and M. S. Arafat, 2011. A novel statistical approach for investigating the significant factors that influence the Performance Score of the Turkish Method. Proceedings of International Conference on Geotechnique, Construction Materials and Environment (GEOMAT-2011), Tsu City, Mie, Japan.

[14] K. S. Roy, M. J. Hassan, K. Islam and N. Islam, 2015. Application of fuzzy set theory to seismic vulnerability assessment. Fifth International Conference on Geotechnique, Construction Materials and Environment, Osaka, Japan.

[15] N. Islam, K. S. Roy, K. Islam, M. Imran and A. Hoosain. 2015. Seismic vulnerability assessment of existing Reinforced Concrete residential buildings by Japanese Method. First International Conference in Advances in Civil Infrastructure and Construction Materials (CICM 2015), MIST, Dhaka, Bangladesh. (In Press)

[16] N. Islam, K. S. Roy, and K. Islam, 2015. Use of design of experiment in seismic vulnerability assessment for existing RC Buildings by Japanese Method. Fifth International Conference on Geotechnique, Construction Materials and Environment, Osaka, Japan.

[17] H. Mahmood and J. M. Ingham, 2011.Seismic vulnerability assessment of Pakistan unreinforced masonry buildings at a National scale. Seismological Research Letters, 82(5), 676-685.

[18] R. P. Nanda and D. R. Majhi, 2013.Review on rapid seismic vulnerability assessment for bulk of buildings. Journal of the Institution of Engineers (India), Series A, 94(3), 187-197.

[19] B. Kehoe, 2004.Standardizing seismic evaluation of existing buildings, 13th World Conf. on Earthquake Engineering, Vancouver, B.C., Canada.

[20] D. B. Hom and C. D. Poland, 2004.ASCE 31-03: Seismic Evaluation of Existing Buildings, In Structures 2004Building on the Past, Securing the Future, ASCE, 1-9.

[21] R. Pekelnickyand C. D. Poland, 2012.ASCE 41-13: Seismic Evaluation and Retrofit of Existing Buildings, SEAOC 2012 Convention Proceedings.

[22] N. Alam, M. S. Alam, and S. Tesfamariam, 2012.Building's seismic vulnerability assessment methods: a comparative study. Natural hazards 62(2), 405-424.

[23] S. Tesfamariam and M. Saatcioglu, 2010.Seismic vulnerability assessment of reinforced concrete buildings using hierarchical fuzzy rule base modelling. Earthquake Spectra, 26(1), 235-256.

[24] B. H. Al-Gohi, C. Demir, A.Ilki, M. H. Baluch and M. K. Rahman, 2014. Assessing seismic vulnerability of unreinforced masonry walls using elas-to-plastic damage model, In Seismic Evaluation and Rehabilitation of Structures, Springer, 95-114.

[25] D. S. Marques, A. S. P. De Figueiredo, P. A. L. Coelho, S.Haigh and G. Madabhushi, 2014.Centrifuge modeling of liquefaction effects on shallow foundations. In Seismic evaluation and rehabilitation of structures, Spring-er, 425-440.

[26] A. F. Hassan and M. A. Sozen, 1997.Seismic vul. Assess. of low-rise buildings in regions with infrequent earthquakes. ACI Struc. Journal, 94(1).

[27] M. Hashemi and A. A. Alesheikh, 2012.Development and implementation of a GIS-based tool for spatial modeling of seismic vulnerability of Tehran. Natural Hazards and Earth System Science, 12(12), 3659-3670.

[28] F. Neves, A. Costa, R. Vicente, C. S. Oliveira and H. Varum, 2012.Seismic vulnerability assessment and characterization of the build-ings on Faial Island, Azores, Bulletin of Earthquake Engineering, 10(1), 27-44.

[29] G. M. Calvi, R. Pinho, G. Magenes, J. J. Bommer, L. F. Restrepo-Vélez and H. Crowley, 2006. Development of seismic vulnerability assessment methodologies over the past 30 Years. ISET Journal of Earth. Technology, 43(3), 75-104.

[30] H. Sucuoglu and U. Yazgan, 2003.Simple survey procedures for seismic risk assessment in urban building stocks, Seismic Assessment and Rehabil-itation of Existing Buildings, 97-118, NATO Science Series, IV/29, Edi-tors: S.T. Wasti and G. Ozcebe, Kluwer.

[31] Dorka, U. 2005.Personal Communication.

[32] Standard for Seismic Evaluation and Guidelines for Seismic Retrofit of Existing Reinforced Concrete Buildings, 2001 (English Edition), Japan Building Disaster Prevention Association.

[33] S. Otani, 2000.Seismic vulnerability Assessment Methods for Buildings in Japan. Earthquake Engineering and Eng. Seismology, 2 (2): 47-56.

[34] H. Umemura, 1980.A guideline to evaluate seismic performance of exist-ing medium and low rise RC buildings and its application, Proc. of The 7th World Conf. on Earthquake Eng., Istanbul, Turkey, 4: 505-512.

[35] Y.M. Wu, T.L. Teng, T.C. Shin and N.C. Hsiao, 2003.Relationship be-tween Peak Ground Acc., Peak Ground Velocity and Intensity in Taiwan. Bulletin of the Seismology Society of America, 93(1), 386–396.

[36] N. Islam, M. J. Alam, A. S. M. F. Hossain. 2015. One Dimensional Ground Response Analysis at Distinctive Locations of Bangladesh. First International Conference in Advances in Civil Infrastructure and Construc-tion Materials (CICM 2015), MIST, Dhaka, Bangladesh. (In Press)

CICM 2015
First International Conference on
Advances in Civil Infrastructure and Construction Materials
MIST, Dhaka, Bangladesh, 14–15 December 2015

PERFORMANCE ASSESSMENT OF EXISTING RC GARMENT MANUFACTURING FACTORY BUILDING: CASE STUDY IN THE CONTEXT OF BANGLADESH

A. K. M. Golam Murtuz[1], Khadiza B. Jalal[2], Rifat J. Priti[3], Kamrul Islam[4] and M. Shahria Alam[5]

[1, 2, 3, 4] Department of Civil Engineering, Military Institute of Science and Technology, Dhaka, Bangladesh.
E-mail: [1]golam.murtuz.bd@gmail.com, [2]nishi_vnsc@hotmail.com, [3]rifatjabin11@gmail.com, [4]kamrul1@ualberta.ca
[5]School of Engineering, The University of British Columbia, Canada
Email: shahria.alam@ubc.ca

Abstract. *The objective of the present study is to assess the performance of the readymade garment manufacturing factory buildings under service loading and under natural hazards like earthquake, extreme wind loading etc. For this purpose, five garment manufacturing factory buildings were chosen randomly based on the availability of the design data. All the buildings were then primarily assessed by the rapid screening method to determine the vulnerability and level of vulnerability imposed by probable earthquake threats. Three rapid screening methods namely the Turkish method, Japanese method and ASCE 31-03 method were used and result shows a good correlation between Turkish and ASCE 31-03 methods. Initial assessment shows a fair to moderate level of vulnerability and hence a detailed analysis was performed later on the following five factory buildings. Static and dynamic analysis was performed to assess the seismic performance of the buildings. The performance of the buildings under service loading was investigated based on the performance of the column sections in the ground to first floor level. Five representative columns from each buildings were selected for this purpose from different locations like interior column, corner column and peripheral column. The adequacy of these column sections were then assessed using the demand data and axial load (P) and Bi-axial moment (MM) carrying capacity of the column. Analysis shows that most of the columns are not inadequate under existing gravity loading condition.*

Keywords: Performance Assessment, Rapid Screening, Nonlinear Analysis, Adequacy

1 INTRODUCTION

In the last decade, Bangladesh's economy has seen a robust expansion of Readymade Garments (RMG) sector with approximately 5600 garments factory and an estimated 4 million workers working under this sector [1]. In financial year 2012, Ready Made Garments (RMG) industry exported garment products of 19.1 billion USD, which is accounted for a total of 13% of the country's GDP [2]. Despite of this huge contributions, Garments sector are now being castigated due to the recent incident of "Rana Plaza" collapse which causes a total death of over 1138 workers [3]. This incident is considered as the most devastating accidental structural failure of the modern history based on the number of causalities. Such devastation have motivated researchers to concern themselves more with the development of suitable and sustainable technique to minimize vulnerability of structures subjected to various uncertainty like major earthquakes.

Most of the garment manufacturing factory building are reinforced concrete moment resisting frame system. Lack of supervision and corruption leads to the construction of sub-standard buildings of this sector in order to incorporate maximum profit out of this. Also the violation of the design specification to minimize the construction cost is a major concern of vulnerability for this structures. Inadequate frame section, low standard material quality and lack of quality control are the common problems for most of the garment manufacturing factory buildings and thus leads to serious accidental events like "Rana Plaza". Present study aims at to investigate the vulnerability of five garment manufacturing factory buildings in terms of factor of safety against service loads of various columns in the bottom storey.

Deadliest earthquakes of last two decades causes several damage to human lives and also pose a great threat to worlds economy by destroying important infrastructures. For instance, 2010 Haiti earthquake causes fatalities of approximately 316000 lives and also damages 250000 residences and 30000 commercial buildings [4]. 2004 Sumatra (India) earthquake and 2008 Sichuan (China) earthquake also causes a total death of 300000 lives and destruction of various RC structures [5, 6]. Almost 80000 people were died in Pakistan during the devastating earthquake of Kashmir in 2005. Approximately 400000 masonry and RC frame structures were severely damaged due to Kashmir earthquake among which 7000 were school buildings and hospitals that causes post-earthquake evacuation and rehabilitation crisis on that region [7, 8]. Beside this, major earthquakes such as 1999 Kocalei and Duzec earthquake in Turkey, 1994 Northridge, 1999 Chi-Chi, 2010 Chile, Japan 2011, New Zealand (2010, 2011), Mexico 2011, Indonesia (2010, 2011) have garnered the attention of researchers to predict the severity of damages to infrastructures as a result of natural disasters. Bangladesh is not also free from that kind of earthquake risk.

Bangladesh National Building Code (BNBC) were implemented in the year of 1993. Many factory buildings were build prior to the development of any guidelines or the current codes. Lack of seismic design criteria is a serious concern for the existing factory buildings which are built prior to the establishment of BNBC, 93. Many of the factory buildings designed as per BNBC code might not be adequate against seismic hazard due to re-evaluation of the code in its most recent version. Previously divided three seismic zone are now further divided into four parts. The seismic zone co-efficient of Zone-II (previous code) is going to be increased to 0.20 from the previous zone coefficient of 0.15. In spite of this fact, many existing factory buildings were designed as residential building and then started functioning as factory. As well as illegal vertical extension, installation of heavy machineries, deviation from the original design specification, poor construction process etc. make the factory buildings highly susceptible to extreme events.

2 DEVELOPMENT OF CASE STUDY

Five factory buildings were selected for the analysis based on different parameters like number of storey, storey height, Floor area, infill wall condition, size and distribution of frame elements, number of bays and span lengths in both the longitudinal and transverse direction, concrete compressive strength, type of reinforcing steel used for shear and longitudinal reinforcement and location of the buildings. Different types of buildings based on the parameters mentioned above are selected in order to incorporate the variation of the recent construction practices for garment factory buildings. All the buildings are located close by the Dhaka city, the capital of Bangladesh.

2.1 Description of Buildings

The different parameters of the five garment manufacturing factory buildings are summarized in Table 1. Also the plan and 3d view of FB_1 is represented in Figure 1.

2.2 Frame Sections

The column sections which will be used to evaluate the factor of safety are selected basically on two different parameters. Dimensional variation and the distribution of the column sections are taken into account as the selection criteria. Since the vulnerability of the columns are highly dependent on the section size especially for axially loaded column and axial load and bi-axial moment for bi-axially loaded column. Also the distribution of the column like center column, corner column and peripheral column influence the condition of the structure. Thus both the issues are incorporated to finally assess the safety factor of the

factory buildings. The column sections and their size for five different factory buildings are presented in Table 2.

Table 1: Different parameters of the selected factory buildings.

Parameters	FB_1	FB_2	FB_3	FB_4	FB_5
Number of storey	5	2	7	6	6
Bottom storey height (m)	5	5.4	4.7	3	3.7
Typical storey height (m)	4	5.4	3.5	3	3.2
Plan area (m^2)	335.7	7816.47	3147.31	868.72	605.29
Number of bays in X-Z plane	6	9	6	6	3
Number of bays in Y-Z plane	2	10	9	9	3
Concrete compressive strength for column section (MPa)	20.68	20.68	20.68	19.31	24.5
Long reinforcement yield strength (MPa)	413	413	413	275	420
Transverse reinforcement yield strength (MPa)	413	413	413	275	420

Table 2: Section size and reinforcement distribution of the selected columns

Building ID	Grid ID	Section Size (Depth x Width) mm x mm	Main Reinforcement	Shear Reinforcement
FB_1	A1, E1, F3	300 x 300	4-21.875mm 4-25 mm	12.5mm @ 150 mm c/c
	C2, E2	350 x 350	10-20 mm	10 mm @ 150 mm c/c
FB_2	A15	650 x 500	16-20mm	10 mm @ 125 mm c/c
	A16	650 x 500	14-20 mm	10 mm @ 125 mm c/c
	B1	500 x 500	14-15.625 mm	10 mm @ 125 mm c/c
	C1	550 x 500	16-20 mm	10 mm @ 125 mm c/c
	I5	450 x 450	10-15.625 mm	10 mm @ 100 mm c/c
FB_3	A1	450 x 450	10-20 mm	10 mm @ 150 mm c/c
	A2	450 x 450	12-20 mm	10 mm @ 150 mm c/c
	C2	600 x 600	20-20 mm	10 mm @ 150 mm c/c
	E7, M7	450 x 450	8-28.125 mm	12.5 mm @ 152.4 mm c/c
FB_4	B2, H1, G1', A4'	450 x 450	8-25 mm	10 mm @ 125-175 mm c/c
	G5	300 x 300	8-25 mm	10 mm @ 125-175 mm c/c
FB_5	A6	355.6 x 355.6	8-25 mm	10 mm @ 127 mm c/c
	A4, B6, C6, D6	381 x 381	12-25 mm	10 mm @ 127 mm c/c

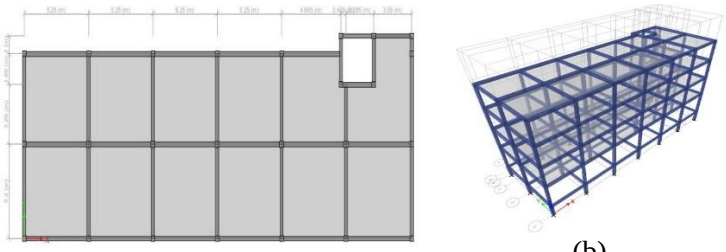

(a) (b)

Figure 1: (a) Plan View, (b) 3D model View

3 RAPID SCREENING

Tectonic framework of Bangladesh and adjoining areas indicate that Bangladesh lies well within an active seismic zone. The after effect of earthquake is more severe in an underdeveloped and a densely populated country like ours than any other developed countries. The collision of the northward moving Indian plate with the Eurasian plate is the cause of frequent earthquake in the region comprising North-East India, Nepal, Myanmar, Bhutan and Bangladesh. Earthquake occurring in any of these areas can affect Bangladesh .There is general consensus among national and international experts that Bangladesh faces significant earthquake risk. Realistic assessment of the seismic risk is, therefore, of paramount national importance, as mitigation measures will depend on the level of risk. Active fault systems capable of producing large magnitude earthquakes are located within the country or within the close neighborhood. Absence of strong earthquakes affecting Bangladesh for more than 80 years has left us all unaware of the possibility of a strong earthquake. As a natural consequence, a majority of buildings in the urban areas of Bangladesh are lacking earthquake resistant design. The effect may be further compounded by poor quality of materials and construction .Should a major earthquake occur, the densely populated cities of Bangladesh with vulnerable infrastructure may be a showcase for a massive disaster. Thus the current paper investigates the vulnerability of the buildings subjected to earthquake ground motion using three rapid screening method.

3.1 Turkish Method

The Turkish Method of seismic risk assessment [9, 10, 11] is based on the statistical analysis of observed earthquake damages of Reinforced Concrete Frame (RCF) buildings in Turkey. This is a very crude and handy method that uses very basic structural information of a building and presents a level of seismic risk in terms of performance score. This method can be used in countries like Bangladesh where standard building codes are not followed and seismic risk assessment of buildings have not been done yet. It gives a preliminary idea about

the general standard of construction with respect to seismic hazard. This method uses the Performance Scores (PS) to classify the buildings as "safe", "unsafe" and "Moderate" to seismic hazards. The buildings classified as "Safe" for PS greater than 70, "Moderate" 50 to 70 and "Unsafe" PS less than 50. The result is summarized in the following table.

3.2 Japanese Method

The Japanese method of seismic performance assessment of existing RC buildings evaluates the performance of the buildings based on ductility of the buildings, their ultimate strengths and failure modes. A basic seismic index is calculated for each story based on which the building is rated as either safe or unsafe. Following table shows summarizes the result obtained from the Japanese method.

Table 3: Risk classification of five factory buildings according to Turkish method

Building ID	PS Scores		Risk Classification	
	Level1	Level2	Level 1	Level 2
FB_1	75	72	safe	safe
FB_2	120	125	safe	safe
FB_3	75	52	safe	Moderate
FB_4	50	38	Moderate	unsafe
FB_5	90	77	safe	safe

Table 4: Seismic performance of five factory buildings according to Japanese methods

Building ID	(Is)	Floor No							Is o	Remarks
		1st	2nd	3rd	4th	5th	6th	7th		
FB_1	X	3.32	1.77	1.18	.88	1.726	1.456	1.248		Safe
	Y	5.51	3.23	2.15	1.16	0.71	1.867	1.56		Safe
FB_2	X	0.51	0.23	-	-	-	-	-		unsafe
	Y	0.39	0.17	-	-	-	-	-		unsafe
FB_3	X	2.28	1.20	0.80	0.60	0.52	-	-	0.68	Safe
	Y	3.52	2.02	1.35	1.01	0.85	-	-		Safe
FB_4	X	4.59	226	1.50	0.71	1.29	-	-		Safe
	Y	4.26	2.09	1.39	2.483	1.09	-	-		Safe
FB_5	X	2.22	1.07	0.74	0.55	0.44	-	-		Safe
	Y	2.07	1.00	0.69	0.51	0.4	-	-		Safe

3.3 ASCE 31-03 Method

Analysis of the five factory buildings using ASCE 31-03 [12] method evaluates all the buildings as "Fair" which means their performance during major seismic disturbance is anticipated to result in structural and nonstructural damage and/or falling hazards that would represent low life hazards. Buildings with this rating would be given low priority for expenditures to improve their rating as "Good". The obtained result is shown in Table 5.

Table 5: Seismic performance according to ASCE 31-03 method

Building ID	NC Items	Description of NCs	Final Assessment
FB_1	Mass	Change in effective mass more than 50% between ground floor and first floor	Fair
FB_2	Nil	Change in effective mass more than 50% between ground floor and first floor	Fair
FB_3	Mass	Change in effective mass more than 50% between ground floor and first floor	Fair
FB_4	Nil	Change in effective mass more than 50% between ground floor and first floor	Fair
FB_5	Nil	Change in effective mass more than 50% between ground floor and first floor	Fair

3.4 Comparison of Three Methods

Comparison of three rapid screening method shows a good correlation between the Turkish method and ASCE 31-03 methods. Performance of the buildings according to different methods are represented below in Table 6.

Table 6: Comparative assessment of seismic risk of factory buildings

Building ID	Turkish Method		Japanese Method	ASCE31-03	Remark
	Level-1	Level-2			
FB_1	Safe	Safe	Safe	Fair	Turkish and ASCE31 result commensurate
FB_2	Safe	Safe	unsafe	Fair	Japanese and ASCE31 result commensurate
FB_3	Safe	Moderate	Safe	Fair	Turkish and ASCE31 result commensurate
FB_4	Moderate	Unsafe	Safe	Fair	Turkish and ASCE31 result commensurate
FB_5	safe	safe	Safe	Fair	Turkish and ASCE31 result commensurate

Comparative assessment of the five factory buildings indicate a potential vulnerability of the structures under seismic loading. Hence the study is further expanded to justify the result of rapid screening method with different nonlinear analysis procedure.

4 SEISMIC SAFETY ASSESSMENT OF BUILDINGS

Seismic vulnerability of the garment buildings are assessed through the results obtained from dynamic analysis. The maximum storey drifts in each direction were compared to the code specified limits of drift demands for different performance objectives. The guidelines for the drift demands considered were Bangladesh National Building Code (BNBC) [13] guideline, ATC-40 [14, 16] and FEMA-356 [15, 16] guideline. The code specified limit state values for drift demands are summarized in the following Table 7.

Performance of the buildings according to the code specified storey drift limits are represented in the Table 8 and Table 9. Result shows different level of performance for different buildings.

Table 7: Storey drift limits value according to ATC-40, FEMA-356 and BNBC guideline.

Storey drift limit state values according to the ATC-40 guideline				
Performance Level	Immediate Occupancy	Damage Control	Life safety	Structural Stability
Storey Drift Limits	1%	1-2%	2%	7%
Storey drift limit state values according to the FEMA-356 guideline				
Performance Level	Fully Operational	Operational	Life Safe	Near Collapse
Storey Drift Limits	0.20%	0.50%	1.50%	2.50%
Storey drift limit state values according to the BNBC guideline				
Maximum Storey Drift Limits	0.015h; h is the storey height below level x			

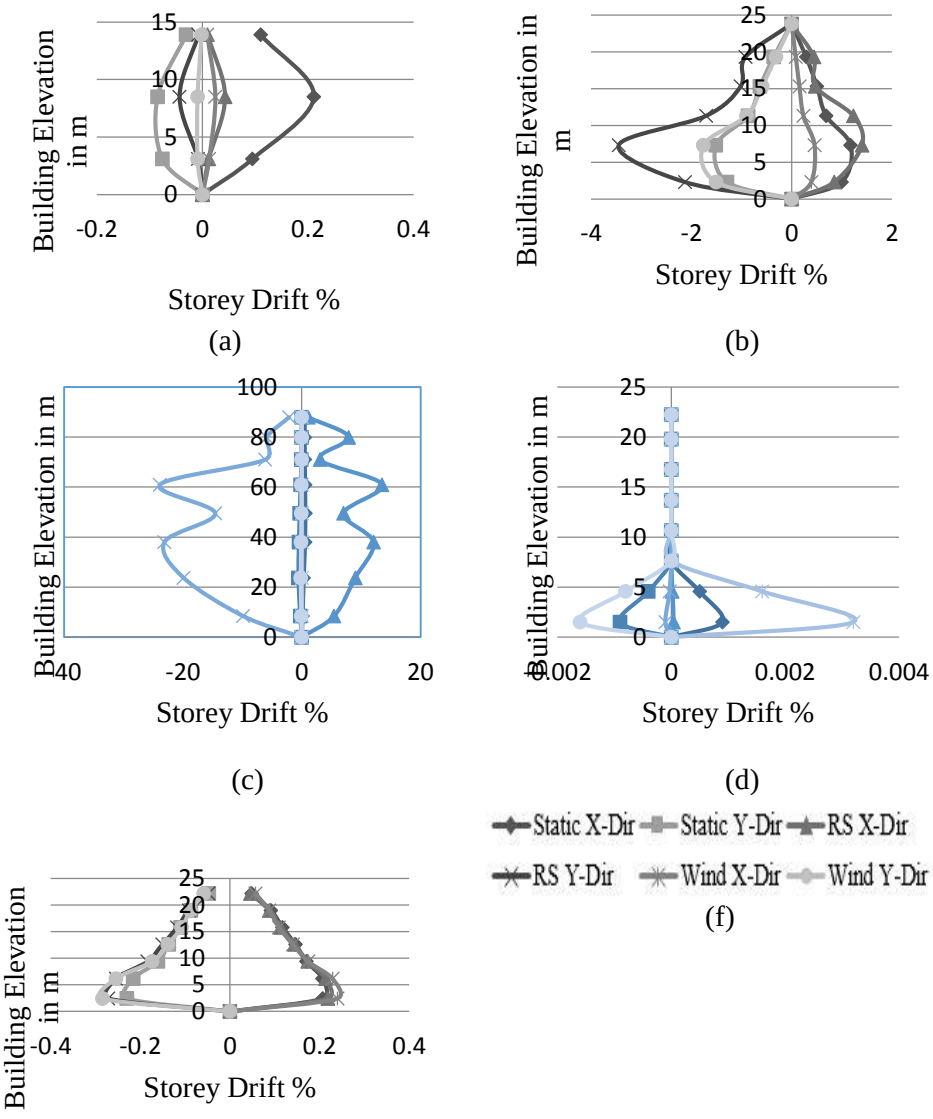

Figure 2: Building elevation storey drift plot for (a) Factory Building 1, (b) Factor Building 2, (c) Factory Building 3, (d) Factory Building 4, (e) Factory Building 5 and (f) Legends.

Table 8: Basic seismic performance of factory buildings according to FEMA-356 guideline.

Seismic performance of buildings according to FEMA-356								
Building ID	Performance Level							
	Static Analysis				Dynamic Analysis			
	Fully Operational	Operational	Life Safe	Near Collapse	Fully Operational	Operational	Life Safe	Near Collapse
FB_1			X					X
FB_2	X				X			
FB_3			X					X
FB_4	X				X			
FB_5		X				X		

Table 9: Basic seismic performance of factory buildings according to ATC-40 guidelines.

Seismic performance of buildings according to ATC-40								
Building ID	Performance Level							
	Static Analysis				Dynamic Analysis			
	Immediate Occupancy	Damage Control	Life Safety	Structural Stability	Immediate Occupancy	Damage Control	Life Safety	Structural Stability
FB_1		X						X
FB_2	X				X			
FB_3	X							X
FB_4	X				X			
FB_5	X				X			

Seismic performance of the factory buildings were assessed considering the maximum drift % in either of the x direction or in the y direction. Result shows that the FEMA-356 guideline is more conservative as compared to the ATC-40 guideline. As per, FEMA-356 guideline performance of FB_1 and FB_2 were found to be in the life safety performance level under static analysis and in the near collapse performance level for dynamic analysis. The same two buildings were found immediate occupancy category under ATC-40 guideline except the conformation of FB_3 which indicates a structural stability performance level. Observation shows that the performance level obtained from FEMA-356 guideline matches with the performance of the buildings assessed Turkish method of rapid screening procedure.

5 PERFORMANCE UNDER SERVICE LOADING

The performance of the buildings under service loading was initially attributed to the performance of the frame sections specially the load carrying capacity of the column sections. Spatial distribution of the columns are important for assessing the global performance of the buildings. Thus the current study selected five column sections from ground floor to first floor level with different spatial distribution namely center column, corner column and peripheral column. Their capacity to withstand the existing gravity loads were assessed using the column capacity ratio parameter or column PMM ratio. The axial load and biaxial moment carrying capacity of individual column sections are compared with relative demand parameter and finally the individual columns are assigned with a PMM ratio value. The numerical value of the PMM ratio varies from zero to higher values. Capacity and demand of the frame sections are perfectly matched when the PMM ratio is exactly 1 and increased value (PMM>1) of column capacity ratio indicates inadequacy of the sections under vertical loads. Result shows that almost 68% of the selected columns are overstressed for various load combinations. All the columns of three factory buildings were found overstressed and hence required to enhance their capacity under gravity loads. Figure 3 summarizes the result of the five factory buildings in a bar diagram.

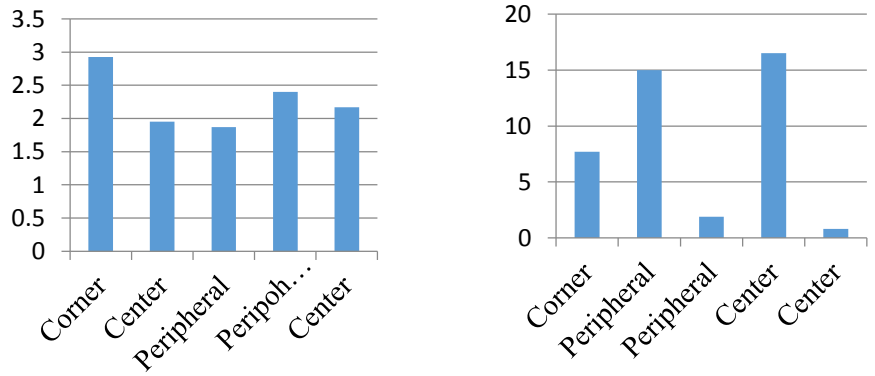

(a) (b)

Figure 3: Column capacity ratio (PMM ratio) for (a) Factory building 1, (b) Factor building 2

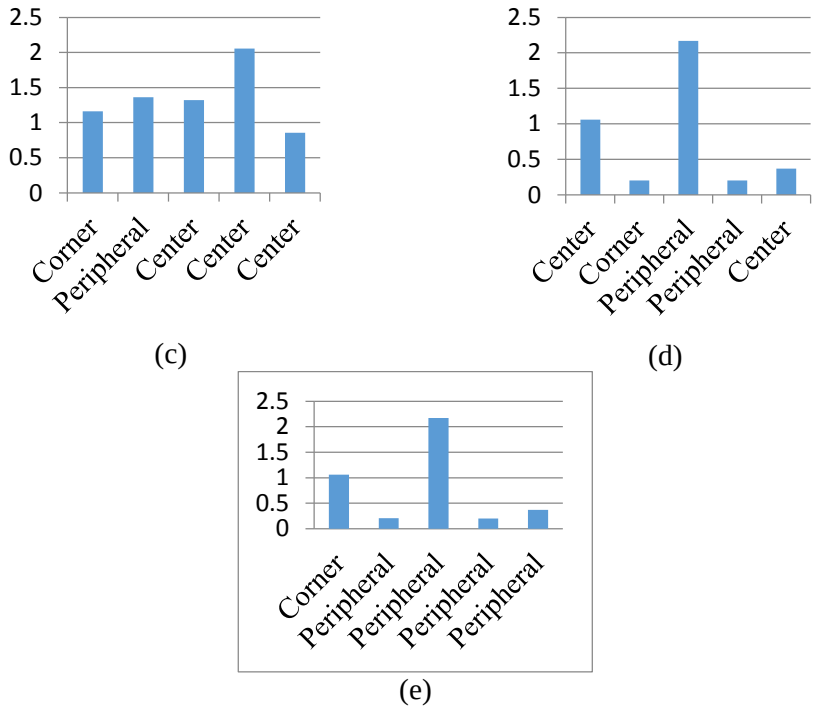

Figure 3 (continue): (c) Factory building 3, (d) Factory building 4, and (e) Factory building 5.

6 CONCLUSIONS

The performance of the buildings under service load is quite vulnerable. Most of the columns considered were overstressed under the normal service loading condition and hence prone to failure under critical circumstances like earthquake events or any increase beyond the present loading condition. The study can be summarized as follows-

- Result shows that the factor of safety against axial load is far more than 1 and hence the columns are able to carry the axial load alone when considered concentrically loaded.
- In case, when column axial load is coupled with the bi-axial moment its factor of safety goes below 1 and hence shows the vulnerability of eccentrically loaded columns.
- Building shows vulnerability under seismic loading condition in terms of storey drifts. Thus the global response of the buildings subjected to lateral loading like earthquake and wind should be investigated further to predict the level of damage after an extreme event.
- In order to get insight into the dynamic behavior of the structures it is recommended to perform more deliberate dynamic analysis like static

pushover analysis, dynamic time history analysis etc. in order to find the susceptibility to failure and predict the probable level of damage after any earthquake events.

- Columns found vulnerable can be strengthen through various retrofit like concrete jacketing, steel encasing, ECC jacketing, FRP wrapping etc.
- Further study can be carried out to find the most suitable retrofit method in the context of Bangladesh with respect to economy and technology available.

From the above discussion it is evident that most of the factory buildings are vulnerable under existing loading condition and can leads to a progressive collapse under extreme seismic events. Hence the author's suggest further investigation regarding the safety of this sector in order to ensure the satisfactory performance of garment manufacturing factory buildings under different loading conditions.

REFERENCES

[1] Bangladesh Garment Manufacturers and Exporters Association (BGMEA)
[2] World trade Report 2014.
[3] After Rana Plaza, A report into the readymade garment industry in Bangladesh. Bangladesh All Party Parliamentary Group, 2013.
[4] List of largest and deadliest EQ by year 1990-2011. United States Geological Survey (USGS).
[5] Kaushik H B and Jain S K. *Impact of Great December 26, 2004 Sumatra Earthquake and Tsunami on Structures in Port Blair*. Journal of Performance of Constructed Facilities. April, 2007, Vol. 21(2), pp. 128 – 142.
[6] Miyamoto H K, Gilani A S and Wada A. *Reconnaissance report of the 2008 Sichuan earthquake, damage survey of buildings and retrofit options*. Proceedings of the 14th World Conference on Earthquake Engineering, Beijing, China. October 12-17, 2008.
[7] Maqsood S T and Schwarz J. *Analysis of Building Damage during the 8 October 2005 Earthquake in Pakistan*. Seismological Research Letters. April 2008. Vol. 79, pp. 163-177.
[8] Maqsood S T and Schwarz J. *Seismic vulnerability of existing building stock in Pakistan*. Proceedings of the 14th World Conference on Earthquake Engineering, Beijing, China. October 12-17, 2008.
[9] GuneyOzcebe, HalukSucuoglu, M.SemihYucemen, Ahmet Yakut and Joseph Kubin, "Seismic Risk Assessment of Existing Building Stock in Istanbul, A Pilot Application in Zeytinburnu District".
[10] Tahmeed M. Al-Hussaini, "Seismic Hazard and Risk Assessment for Bangladesh"
[11] M. Z. Ahmed, K. Islam, K. S. Roy, M. S. Arafat, T. M. Al-Hussaini,"Seismic Vulnerabilty Assessment of RCF Buildings in Old Town of

Dhaka City", Proceedings, 3rd International Earthquake Symposium Bangladesh, Dhaka,March 5-6,2010.
[12] ASCE31-03 Manual.
[13] Bangladesh National Building Code (BNBC), 2014.
[14] ATC-40. Seismic evaluation and retrofit of concrete buildings. Applied Technical Council, California Seismic Safety Commission, Report No. SSC 96-01. Redwood City, California, US; 1996.
[15] FEMA356. Pre-standard and commentary for the seismic rehabilitation of buildings. Washington, DC: Federal Emergency Management Agency; 2000.
[16] Chaulagain, H., H. Rodrigues, J. Jara, E. Spacone, and H. Varum. "Seismic response of current RC buildings in Nepal: a comparative analysis of different design/construction." *Engineering Structures* 49 (2013): 284-294.

CICM 2015
First International Conference on
Advances in Civil Infrastructure and Construction Materials
MIST, Dhaka, Bangladesh, 14–15 December 2015

SEISMIC RESPONSE MODIFICATION FACTOR OF CONCRETE FRAME BUILDING REINFORCED WITH SHAPE MEMORY ALLOY (SMA) REBAR

Moniruzzaman Moni[1], Mumtasirun NAHAR[2], Kamrul Islam[3], and M. Shahria Alam[4]
[1, 4] School of Engineering, The University of British Columbia, BC, Canada.
Email: [4]shahria.alam@ubc.ca

[2, 3] Department of Civil Engineering, Military Institute of Science and Technology, Dhaka, Bangladesh.
Email: [3]kamrul1@ualberta.ca

Abstract: *In this study, an analytical approach has been carried out to investigate the effect of SMA used in beam in the concrete frame structures. Three reinforced concrete (RC) buildings of different stories (3, 6 and 8) are taken into consideration. Reinforcement detailing are different for each type of building. For 3, 6 and 8 storey all beams are reinforced as fully steel reinforcement (Steel), SMA rebar in the plastic hinge region of the beams and steel rebar in other regions (Steel-SMA), and with SMA rebar (SMA). For each case, columns are reinforced with steel rebar. Nonlinear static pushover analyses, nonlinear incremental dynamic time history analyses and linear dynamic time history analyses were performed to determine the overstrength factor (R_o), ductility reduction factor (R_d) and finally response modification factor (R) of the considered buildings. In addition, the supply and demand of ductility reduction factors are also compared. The results indicate that the code proposed response modification factors can be used for the SMA RC and Steel-SMA RC frames.*

Keywords*:* Overstrength factor, Ductility reduction factor, Response modification factor, Ductility, RC frame, Shape memory alloy.

1 INTRODUCTION

Generally, the current seismic design codes including the National Building Code of Canada [1] recommend a force-based design of structures. The technique is based on the postulation that well-detailed structures be able to withstand lateral forces in excess of their design strength and maintain large inelastic deformation without collapse [2]. The force-based approach generally considers a reduction in the elastic base shear so that the structures acquire considerable reserve strength (over-strength) and ductility. These two properties are included in the structural design through a response modification factor (R), which represents a ratio of the elastic base shear (V_e) of a structure under a specified ground motion to the design base shear (V_d). The role of the response modification factor is very important in designing the seismic load resisting structures. This factor was first introduced in 1984 by the Applied Technology Council [3], and there was no specific guideline about response modification factor. In 1995, ATC-19 and ATC-34 [4-5] provided a detailed guideline in calculating response modification factor of a structure by considering its overstrength, ductility reduction, and redundancy factor. The present Canadian code [1] accounts for ductility and overstrength to compute response modification factor. Besides NBCC [1], US codes [6-7] also accounts for reserve strength and ductility for calculating response modification factors [5].

Many earthquakes have caused devastation resulting in permanent damage and collapse of many important buildings and bridges, which were designed as per force based method. Recent earthquakes in New Zealand (2010, 2011), Haiti (2010), Chile (2010) and China (2008) highlight the vulnerability of such reinforced concrete structures due to seismic related damages and their resulting impact on the economy. Nevertheless, conventional steel RC structures experience high residual drifts during large earthquakes, which is often responsible for serviceability issues and structural collapse of a building. Recent experimental and analytical investigations have reported its potential uses in mitigating seismic induced damages of civil engineering structures [8-9]. In the plastic hinge regions of RC columns SMA bars is used [10] to reduce its permanent deformation, and less residual drift is observed in RC columns. An experimental study [11] used different reinforcement ratios ranging from 0.1% to 0.9%, and found that the residual deformation for SMA reinforced beam was only 20% to that of a steel reinforced beam. Shape memory alloys material is used for the seismic isolation of bridge [12-13] using isolation systems based on flats sliding bearing.

The current study provides a detailed view of the response modification factor (R) for SMA induced frame structures. Inelastic pushover analyses are performed to determine their overstrength factors and ductility. Linear dynamic and nonlinear incremental dynamic time history analyses are performed to determine

the ductility reduction factor. Additionally, ductility reduction factor and response modification factor demand for the investigated structures are also computed by using empirical models, which are then compared with the analytical results.

2 RESPONSE MODIFICATION FACTOR

The actual lateral capacity, V_y is usually observed by performing pushover analyses. The overstrength factor (R_o) is defined as the ratio of the actual lateral strength (V_y) to the design lateral strength (V_d).

$$R_o = \frac{V_y}{V_d} \tag{1}$$

The ductility reduction factor (R_d) is defined as the ratio of the maximum base shear for an elastic system (V_e) to the maximum base shear (V_y) for an elastic perfectly plastic system.

$$R_d = \frac{V_e}{V_y} \tag{2}$$

Finally, the response modification factor (R) is obtained by dividing the elastic strength (V_e) to the design strength (V_d) or by multiplying the ductility reduction factor (R_d) to the over-strength factor (R_o).

$$R_d = \frac{V_e}{V_y} \tag{3}$$

Quantification of the actual overstrength is important as it can be employed to reduce the forces used in the design, hence leading to more economic structures [14-15]. Figure 1 shows the actual nonlinear behavior of an RC frame in terms of base shear versus roof top displacement, which is idealized by a bilinear elastic-perfectly plastic relationship. The way to compute the elastic base shear is shown graphically in Figure 2.

3 PROPERTIES OF SHAPE MEMORY ALLOYS AND ITS MODELLING

Super-Elasticity (SE) of SMA is a special property that makes SMA unique and exclusive compared to other structural materials. SE SMA can return to its original position, even from its inelastic range, upon unloading or by heating. Among different compositions, Ni-Ti has been the most suitable SMA for structural applications because of its huge recoverable strain, super elasticity and extremely good resistance to corrosion [7]. When an SMA is subjected to a cycle of axial deformation within its super elastic strain range, it dissipates a definite quantity of energy without permanent deformation. This has resulted due to the

phase transformation between austenite and martensite during loading and unloading. Generally, civil engineering applications of SMA are associated with the use of bars and wires, so one-dimensional phenomenological models are often considered suitable. A number of finite element software, [16-17] incorporated the superelastic behaviour of SMA.

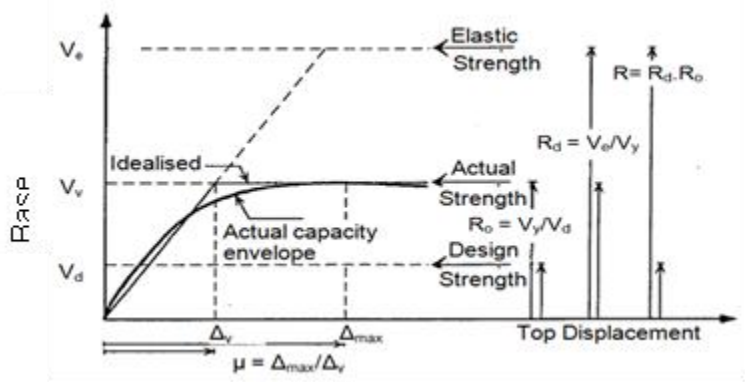

Figure 1: The relationships between force reduction factors (R), overstrength factor (R_o), ductility reduction factor (R_d), and displacement ductility (μ) (Mwafy and Elnashai, 2002 with permission).

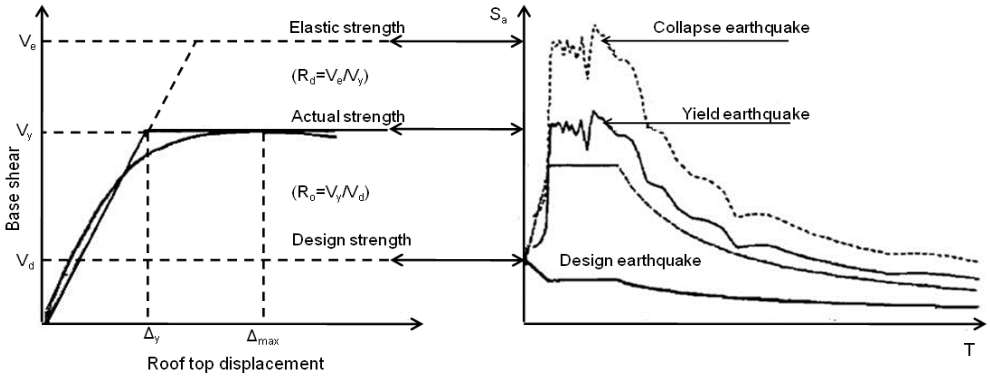

Figure 2: Comparison between the ductility reduction factor (Rμ) and the definition of Rc,ay (Mwafy and Elnashai, 2002 with permission)

4 DESIGN OF FRAME STRUCTURES

In the present study 3, 6, and 8-storey frame buildings have been considered, where each building has three different types of rebar arrangements in its beams, i.e. Steel, Steel-SMA and SMA as described in Section 1. Each building has five

bays in both directions with the same bay length of 5m each [18]. These RC buildings have been analyzed as per NBCC [1] and designed according to CSA A23.3-04 (2004) considering as ductile moment resisting frames. The buildings are considered to be located in western Canada, and the seismicity of this region is obtained from NBCC [1]. Table 1 shows the material properties used for the design and analysis of the buildings adopted from Alam et al. [19].

5 MATERIAL PROPERTIES USED IN THE FINITE ELEMENT PROGRAM

Table 1: Material properties used in the finite element program

Material	Mechanical Property	Value
Concrete	Compressive strength (MPa)	35
	Tensile strength (MPa)	3.5
	Strain at peak stress (%)	0.2
Steel	Modulus of elasticity (MPa)	200,000
	Yield strength (MPa)	400
	Strain hardening parameter	0.5
SMAs	Modulus of elasticity (MPa)	60,000
	Austenite to martensite starting stress (MPa)	400
	Austenite to martensite finishing stress (MPa)	500
	Martensite to Austenite starting stress (MPa)	300
	Martensite to Austenite finishing stress (MPa)	100
	Super elastic plateau strain length (%)	6

The plan of the investigated buildings is kept similar to each other and the storey height is 3 m for all the buildings. The reinforcement of the building has been detailed as per Canadian standards (CSA A23.3-04) and Tables 2 and 3 show the member sizes and the reinforcement detailing of columns and beams, respectively. The 20 columns located along the perimeter of the buildings are designated as C2, and the remaining interior 16 columns are designated as C1. In the case of Steel-SMA building SMA bars have been used in the plastic hinge regions of the beam, and steel reinforcements have been used in the remaining parts of the beam. The plastic hinge length of the beam is estimated using an analytical expression proposed by Paulay and Priestley (1992). In this study it is assumed that steel and SMA rebar are coupled together using mechanical anchorages/couplers [20].

Table 2: Column size and reinforcement arrangements

Storey Id	Floor level	Description	Column ID C1	Column ID C2
3-Storey	Up to roof	Size (mm x mm)	375x375	300x300
		Main reinforcement	8-15M	4-20M
6 -Storey	Up to 3rd floor	Size (mm x mm)	450x450	300x300
		Main reinforcement	8-25M	6-20M
	3rd floor to roof	Size (mm x mm)	450x450	300x300
		Main reinforcement	8-20M	4-20M
8-Storey	Up to 3rd floor	Size (mm x mm)	500x500	300x300
		Main reinforcement	8-25M	6-25M
	3rd floor to roof	Size (mm x mm)	500x500	300x300
		Main reinforcement	6-25M	6-20M

Table 3: Beam reinforcement details

Storey Id.	Beam Id.	Size (mm x mm)	Section Id.					
			Section 1-1		Section 2-2		Section 3-3	
			Top	Bottom	Top	Bottom	Top	Bottom
3-storey	B1	300x450	3-20M	3-20M	3-20M	3-20M	3-20M	3-20M
6-storey	B1	300x500	3-25M	5-20M	3-25M	5-20M	3-25M+2-20M	3-20M
	B2	300x500	3-20M	3-20M	3-20M	3-20M	3-20M	3-20M
8-storey	B1	300x500	3-25M	5-20M	3-25M	5-20M	3-25M+2-20M	3-20M
	B2	300x500	3-20M	3-20M	3-20M	3-20M	3-20M	3-20M

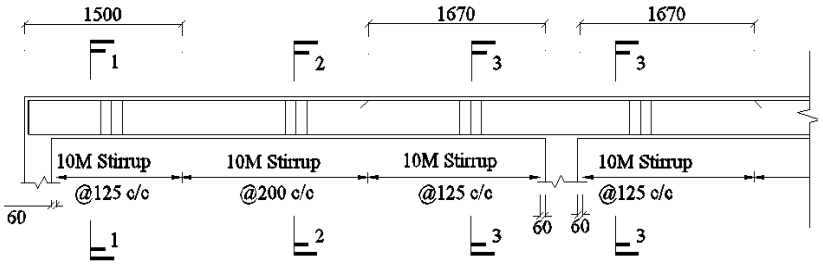

Figure 3: Typical longitudinal section of beam reinforcement.

Figure 3 shows the reinforcement detailing of a typical beam. For 3-storey building, beam B1 is used in all the storeys, where the longitudinal reinforcements for all the beams at different floor levels are similar. For both 6 and 8-storey frames, beam B1 is used for the lower first three storeys, and in the case of upper part of the building beams B2 is used. From sectional analyses moment curvature relationships have been developed for the considered beam sections to determine the effective stiffness for the SMA reinforced and steel reinforced concrete sections. The moment curvature relationships for SMA and steel reinforced sections are illustrated in Figure 4. The effective stiffness for the Steel RC section is 2.2 to 2.8 times higher than that of the SMA RC section.

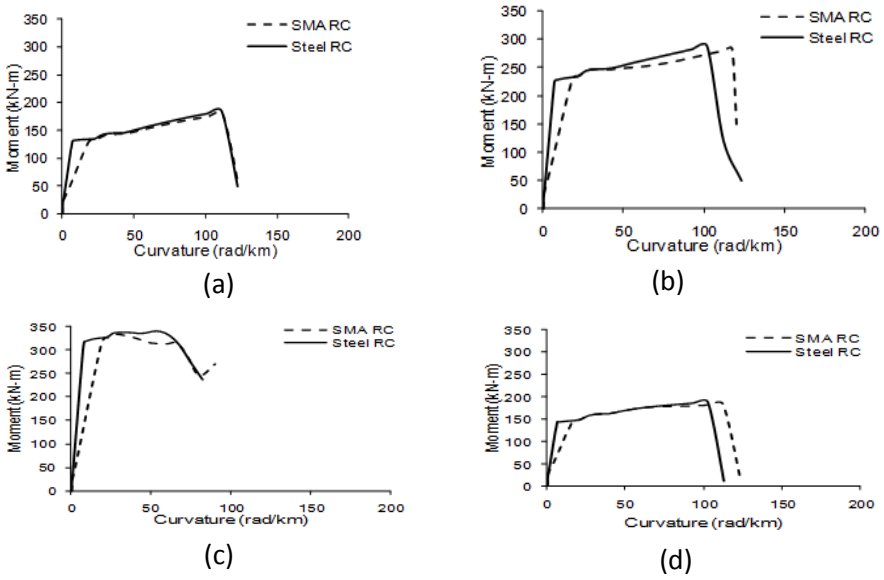

Figure 4: Moment curvature relationship for (a) B1 of 3-storey frame (b) Section 1-1 and 2-2 for Beam B1 for both 6-and 8-storey frame, (c)) Section 3-3 for Beam B1 for both 6- and 8-storey frame and (d) beam B2 for both 6 and 8-storey frame.

The lower limit is obtained for section 3-3 of beam B1 for both 6 and 8-storey frames whereas the upper limit 2.8 is obtained for the beam of 3-storey frame. This effective stiffness value is then used to determine the fundamental period of the structures using SAP 2000 (CSI 2010) [21]. Eigen value analyses were performed by considering the uncracked section and the effective stiffness method for all the frames to determine their fundamental periods (Table 4). The analyses results show that the use of SMA as reinforcement in beams increases the fundamental period of the structure compared to mild steel, because of

SMA's lower modulus of elasticity. As the stiffness decreases, the period of the structure increases.

Table 4: Fundamental period of the structure

Storey Id	Fundamental period, T_1 (sec)						
	Code prediction	Uncracked section			Effective stiffness, K_{eff}		
		Steel	SMA	Steel-SMA	Steel	SMA	Steel-SMA
3	0.39	0.26	0.26	0.26	0.39	0.42	0.41
6	0.66	0.49	0.49	0.49	0.67	0.74	0.70
8	0.81	0.68	0.68	0.68	0.86	1.00	0.93

The serviceability limits states have also been checked against deflection, which has been found satisfactory for all SMA RC elements, as well as Steel-SMA RC frames as per CSA A23.3-04. For instance, the maximum allowable deflection limit for the frame beams is 10.4 mm. From analyses it has been observed that the 8 storey SMA-RC frame experienced the maximum deflection, which is only 6.4 mm, compared to 10.4 mm, as per CSA standards.

6 ANALYTICAL MODELS

SeismoStruct (2010) [17] software has been used to perform pushover analysis, linear and nonlinear dynamic time history analyses. 3D beam-column elements have been used for modelling the beam and column where the sectional stress-strain state of the elements is obtained through the integration of nonlinear uniaxial stress-strain response of the individual fibres in which the section has been subdivided. For nonlinear, pushover and incremental dynamic time-history analyses, inelastic displacement-based frame elements have been used for beams and columns whereas elastic frame elements have been used for linear dynamic analyses. Concrete has been represented using the constitutive relationship proposed by Mander et al. (1988) and the cyclic response by Martinez-Rueda and Elnashai (1997), and a bilinear kinematic strain hardening model is used for steel. SMA has been modelled according to the model of Auricchio and Sacco (1997), and the parameters used to define the material model were discussed in the previous section. The beam and column were divided longitudinally into 8 and 4 elements, respectively, where two of the beam elements represent the plastic hinge region of the beam at each beam-column joint region. Each beam and column element was divided transversely into 200 by 200 fibre elements. In the case of the Steel-SMA frame, the beam-column joint has been represented by the model [22], to consider the slippage of SMA rebar inside the coupler.

7 PUSHOVER ANALYSES

Pushover analysis has been performed for each building using SeismoStruct (2010) considering a 2D interior frame. A triangular lateral load distribution has been considered to perform nonlinear pushover analyses. The vertex of the triangular load is considered at roof level, whereas the apex of the load is considered at the base of the building. The pushover response curves are shown in Figures 6 (a), (b) and (c) for 3, 6, and 8 storey buildings, respectively.

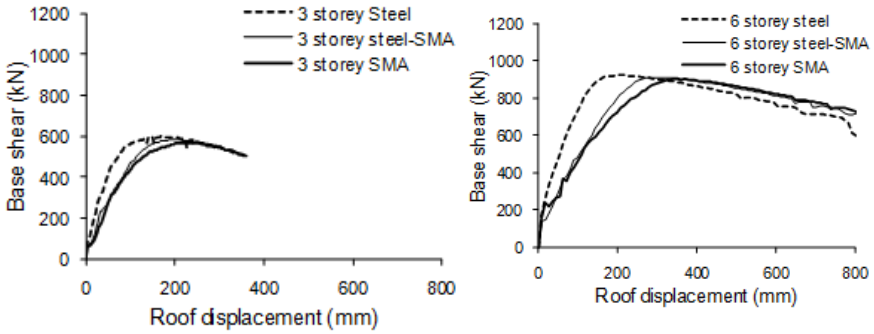

(a) (b)

Figure 6: Pushover curve for (a) 3-storey, (b) 6-storey

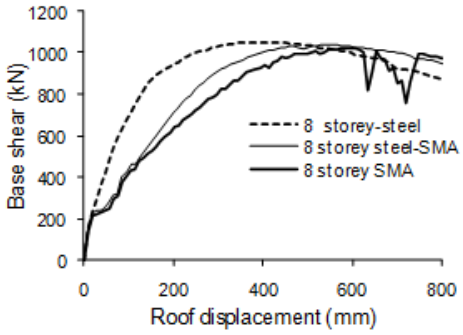

(c)

Figure 5: (c) 8-storey frame

In the case of pushover response curves for 3-storey frames (Figure 5 a), the ratio of lateral capacities (V_y) to the design base shear (V_d) for Steel, Steel-SMA and SMA RC frames are 1.45, 1.45 and 1.42. These ratio which is defined as the overstrength factor reached the capacity at a roof displacement of (169 mm), (205 mm) and (230 mm), respectively. For 6-storey frames (Figure 5 b), the capacity (V_y) is larger for SMA RC comparing to Steel, Steel-SMA frames. The ratio is 1.59 times the design base shear (V_d) which the corresponding to a roof displacement (351 mm), almost 10% higher than other two types of frames. Higher roof displacement is observed for 8-storey frames as shown in (Figure 5

c) which are (383 mm), (538 mm) and (586 mm) providing the lateral capacities 1.55, 1.61 and 1.68 times the V_d for Steel, Steel-SMA and SMA RC frames, respectively. The initial stiffness of Steel, Steel-SMA and SMA RC frames were similar for each type of frames. Before cracking SMA and Steel resist the forces but after the development of crack SMA rebar becomes effective in resisting forces, as a result reduced stiffness is observed for Steel-SMA and SMA RC frames, compared to that of Steel RC frames.

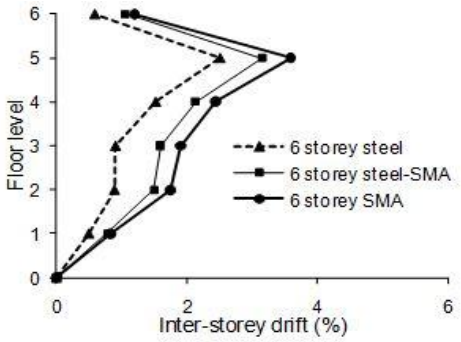

Figure 6: Inter-storey drift distribution for 6-storey

Figures 6 show the distribution of inter-storey drifts at collapse as observed from the pushover analyses over different floor levels for 6-storey frame. Other inter storey drift curve is explained in [18]. When the base shear of the frame reaches its maximum capacity the inter-storey drift of the investigated frame is calculated. Here, the inter-storey drift capacity is considered as the maximum inter-storey drift at collapse, which is the state when the beams and columns of different storeys have failed and the frames are not capable of taking any further load, i.e. the point of maximum load [19]. In all cases, Steel RC frames exhibited the highest stiffness and lowest inter-storey drift. The maximum inter-storey drift is observed as 3.1, 3.9 and 4.2 percent for the Steel, Steel-SMA and SMA RC frames, respectively [19].

8 DYNAMIC TIME-HISTORY ANALYSES

Incremental nonlinear dynamic time history analyses were performed for each frame using nine real earthquake data and an artificial earthquake ground motion data developed by Atkinson (2009) [23] for the city of Vancouver. This time history analyses were conducted to determine performance of three building in terms of Response modification factor supply, Ductility reduction factor supply. Ten different earthquake data are considered which is adopted from [19]. These accelerograms were chosen such that they represent the seismic characteristics of

the site of the structure. All earthquake data are scaled considering 5% damping spectral acceleration with respect to the NBCC [1] spectral acceleration of Vancouver.

9 RESULTS AND DISCUSSIONS

In this study the supply and demand of response modification factor (*R*) has been computed for different reinforced concrete frames.

8.1 RESPONSE MODIFICATION FACTOR (*R)* SUPPLY

Table 5 shows the elastic base shear (V_e) for the considered frames. The arithmetic average of the ten elastic base shear is used to compute the ductility reduction factor and the response modification factor. From Table 5 it can be concluded that the elastic base shear completely depends on the characteristic of the earthquake records. The elastic base shear observed for earthquake record LGP is much higher than the average values whereas for the ChiChi-longt the value is much lower compared to the average one for all types of frames. The summary for the response modification factor (*R*) supply is presented in Tale 6.

Table 5: Elastic base shear V_e

Types of RC frames	ART	ATS	BTS	ChiChi-longt	Chy-006	Chy-019E	Chy-019N	HBP	LGP	TTN	Avg.
3 SMA	3619	5328	8624	2332	6255	3013	3896	10104	28834	3822	7583
3 Steel-SMA	3619	2420	4617	2332	7216	4645	7216	3932	20710	1433	5814
3 Steel	3800	5808	8315	2332	6735	3658	6762	9782	17799	2866	6786
6 SMA	4102	10074	21222	2275	14980	4732	4690	9044	19045	8649	9881
6 Steel-SMA	5127	11230	20915	2225	10943	11603	10577	16137	25208	7842	12181
6 Steel	6896	13112	18640	2543	10943	11853	10577	6926	18467	7842	10780
8 SMA	12402	17517	13740	2596	25546	17064	10636	9670	32167	7696	14904
8 Steel-SMA	9286	10789	17114	2714	6016	5958	7305	34712	43246	17927	15507
8 Steel	11956	11071	14514	2784	23278	11153	15277	24518	36995	15780	16733

Table 6 : Response modification factor (*R*) supply

Parameters	3 storey			6 storey			8 storey		
	Steel	Steel-SMA	SMA	Steel	Steel-SMA	SMA	Steel	Steel-SMA	SMA
Overstrength factor, R_o	1.45	1.45	1.42	1.52	1.53	1.59	1.55	1.61	1.68
Ductility, μ	2.34	1.92	1.79	1.85	1.61	1.56	2.12	1.96	1.74
Ductility reduction factor, R_d	11.3	10.0	13.3	11.7	13.4	10.9	15.9	14.9	14.6
Response modification factor, R	16.4	14.5	18.9	17.8	20.5	17.4	24.7	24.1	24.6

Figure 8 (a) shows the comparison of the overstrength factor (R_o) for different types of frames considered in this study. Although NBCC [1] specifies (R_o) as 1.7 for ductile reinforced concrete buildings, the result of this study shows that the framing system offers a lower overstrength factor in all cases where it was on an average 15%, 9% and 5% lower for 3, 6 and 8 storey frames, respectively. This might be due to not considering the slab action during analysis. From Figure 7 (a) it can be observed that although SMAs have lower modulus of elasticity compared to regular steel, SMA RC frames offer almost similar overstrength factor (R_o). The overstrength factors of 6 and 8-storey SMA RC frames are slightly higher than those of the Steel and Steel-SMA RC frames, but in the case of the 3-storey frame this values is slightly lower for SMA RC frames.

The ductility reduction factor (R_d) supply obtained in this study is presented in Figure 7 (b). In this study the minimum ductility reduction factor obtained is 10.0 for the 3-storey Steel-SMA RC frame. The ductility reduction factor (R_d) supply obtained from this study is inconsistent in pattern. In the case of 3-storey frames, the SMA RC frame offers more ductility reduction factor compared to Steel-SMA and Steel RC frames. But in the case of 6 and 8-storey frames, Steel-SMA and Steel RC frames offer higher ductility reduction factor (R_d) compared to SMA RC frames. The Response modification factor (R) supply obtained in this study is illustrated in Figure 7 (c). NBCC-2005 [1] proposes response modification factor of 6.8 for ductile moment-resisting reinforced concrete buildings, but in this study the minimum response modification factor (R) supply obtained is 14.5 for the 3-storey Steel-SMA RC frame. The highest response modification supply is offered by the 8-storey Steel RC frame. In the case of 3-storey frames, the SMA RC frame offers a higher response modification factor compared to the Steel-SMA and Steel RC frames. In the case of 6-storey Steel-

SMA and 8-storey Steel RC frames, they supply a greater response modification factor compared to the other frames.

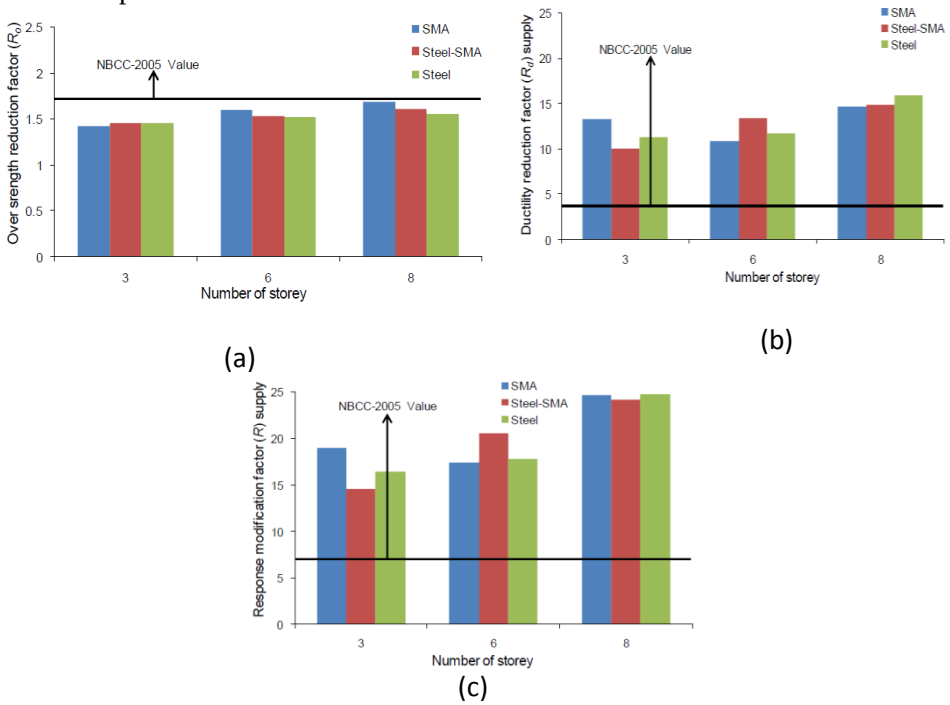

Figure 7: (a) Over-strength factor, R_o for different storeys and frame types, (b) Ductility reduction factor (R_d) supply for different storeys and frame types (c) Response modification factor (R) for different storeys and frame types.

8.2 RESPONSE MODIFICATION FACTOR (*R)* DEMAND

The ductility reduction factor (R_d) demand is calculated by using the system ductility (μ) [24] and they also proposed an equation [Eq. 4] to calculate the ductility reduction factor.

$$R_d = \frac{\mu - 1}{\phi} + 1 \qquad [1]$$

$$\phi = 1 + \frac{1}{10T - \mu T} - \frac{1}{2T} e^{-1.5(\ln(T) - 0.6)^2} \qquad [2]$$

Where T is the fundamental period of the structure, μ is the system ductility and Φ is a coefficient reflecting soil condition. The ductility reduction factor and

response modification factors are calculated by using the equation 4 and 5 as demand, which are presented in Figures 8 (a) and (b).

The results show that the ductility reduction factor demand increases with the increase of number of stories. Although NBCC [1] specifies ductility reduction factor as 4.0 for ductile moment-resisting reinforced concrete buildings, the maximum demand obtained from this study is 2.24 for the 8-storey Steel RC frame. The ductility reduction factor demand is less for the SMA RC frames, compared to the Steel-SMA and Steel RC frames for 3, 6 and 8-stories. The ductility reduction factor supply-demand ratio is presented in Figure 8 (c). The results show that the ductility reduction supply demand ratios for SMA and Steel-SMA RC frames are higher compared to that of Steel RC frames of different stories.

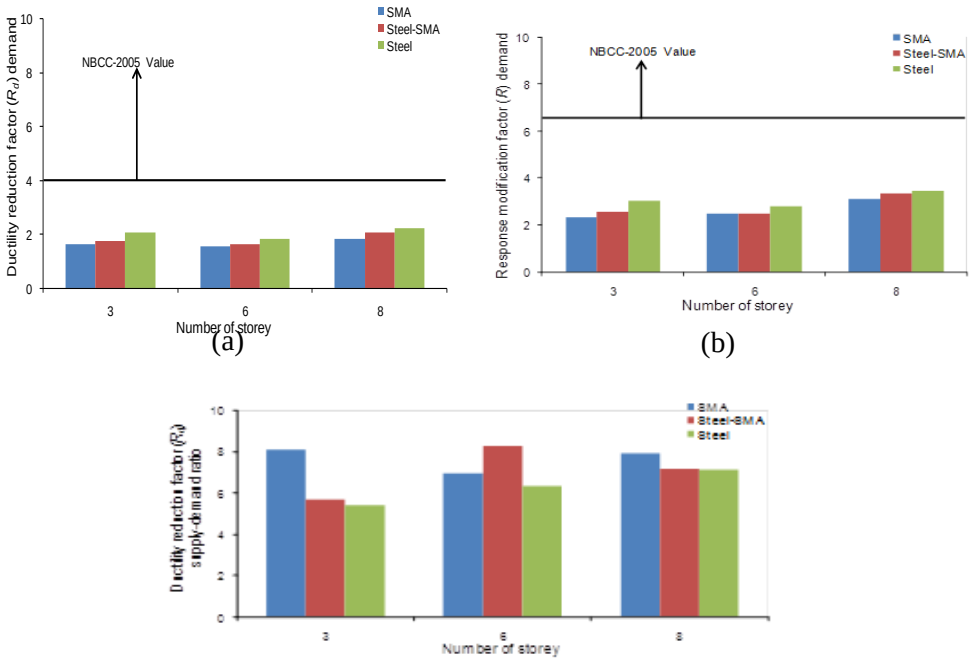

Figure 8: (a) Ductility reduction factor (R_d) demand for different storeys and frame, (b) Response modification factor (R) demand for different storeys and frame types, (c) Ductility reduction factor (R_d) supply-demand ratio for different storeys and frame types

10 CONCLUSIONS

In this study the effect of SMA as reinforcement in concrete frame structures is investigated, where three different types of reinforced concrete (RC) building of different stories (3, 6, and 8) are considered. For each type of frame, three reinforcement detailing i) only steel as RC material ii) steel-SMA, where SMA is used only in the plastic hinge region of the beam and steel in the other region and iii) SMA is used as RC in the full length of beam (SMA-RC).

1. From push over analysis, lateral base shear capacities are almost similar for all types of frames (3,6 and 8 stories) before cracks developed in the beam. But after the development of crack SMA-RC show much reduced stiffness compared to steel RC frames. The overstrength factor vary in between 1.45 to 1.52 for 3 storey frame, 1.45 to 1.61 times for 6 storey and 1.42 to 1.68 times for 8 storey frame for steel, steel-SMA and SMA RC frames respectively which is almost similar. Though the higher stiffness is observed, lower inter-storey drift is found for steel-RC frames comparing to SMA-RC frames.
2. The overstrength factor increases with increasing the number of storey, however SMA-RC possess slightly lower overstrength compared to steel RC frames. Due to the lower modulus of elasticity of SMA it experience higher flexibility and reduced stiffness which causes delay in achieving the capacity.
3. From the displacement ductility calculation, lesser ductility is observed for SMA-RC frames compared to Steel-RC frames and steel-SMA frames. For 3, 6, and 8 storey the ductility is almost 30%, 20%, 21% and 22%, 15%, 8% lesser for Steel-RC and SMA-RC frames respectively.
4. Higher ductility reduction factor (R_d) supply is found for the frames with increasing the number of storey. Though the value of ductility reduction factor (R_d) is larger in SMA-RC frame for 3 storey, but for 6 and 8-storey frame R_d is higher for steel-RC and Steel-SMA frames comparing to SMA-RC frames.
5. Response modification factor also follow the same pattern as ductility reduction factor where higher response modification factor is found for 6 and 8-storey steel-RC and steel-SMA frames compared to SMA-RC frames.
6. The ductility reduction factor is less for the SMA-RC frames compared to the steel-SMA and steel-RC frames for 3, 6, and 8 stories. From the result of ductility reduction factor supply-demand ratio it is observed that SMA-RC frames offer higher ratio comparing to steel-RC and Steel-SMA frames for 3 and 8 storey.
7. Dynamic time history analysis should also be performed to determine the inter-storey drift so that it does not exceed the code limit. Further

research is required to determine the optimum distribution of SMA rebar in different storeys, which could substantially reduce the use and cost of SMA, and at the same time could gain the benefits of recentering.

REFERENCES

[1] NBCC (2005). National Building Code of Canada, Canadian Commission on Building and Fire Codes. National Research Council of Canada, Ottawa.

[2] Kim J, Choi H (2005) Response modification factors of chevron braced frames, Eng Struct 27:285-300.

[3] ATC-3-06 (1985) Tentative Provisions for the Development of Seismic Regulations for Buildings, Applied Technology Council 555 Twin Dolphin Drive, Suite 550, Redwood City, CA 94065.

[4] ATC-19 (1995) Structural Response Modification Factors, Applied Technology Council 555 Twin Dolphin Drive, Suite 550, Redwood City, CA 94065.

[5] ATC-34 (1995) A Critical Review of Current Approaches to Earthquake-Resistant Design, Applied Technology Council 555 Twin Dolphin Drive, Suite 550, Redwood City, CA 94065.

[6] FEMA 356 (2000) NEHRP Guidelines for the seismic rehabilitation of buildings. Federal Emergency Management Agency, Washington DC.

[7] Uniform Building Code (1997), the International Conference of Building Officials (ICBO).

[8] Dolce M, Cardone D, Marnetto R, Mucciarelli M, Nigro D, Ponzo FC, Santarsiero G (2004) Experimental static and dynamic response of a real RC frame upgraded with SMA re-centering and dissipating braces. Proc. of the 13th World Conf. on Earthq Eng, Canada, Paper no. 2878.

[9] Wilde K, Gardoni P, Fujino Y (2000) Base isolation system with shape memory alloy device for elevated highway bridges. Eng Struct 22: 222–229.

[10] Saiidi MS, Wang H (2006) Exploratory study of seismic response of concrete columns with shape memory alloys reinforcement. ACI Struct J 103:435– 442.

[11] Saiidi MS, Zadeh MS, Ayoub C, Itani A (2007) Pilot study of behavior of concrete beams reinforced with shape memory alloys. J Mater Civil Eng, ASCE 19:454–461.

[12] Dolce M, Cardone D, Palermo G (2007) Seismic isolation of bridges using isolation systems based on flat sliding bearings. Bull Earthq Eng 5:491–509.

[13] Jalali A, Cardone D, Narjabadifam P (2011) Smart restorable sliding base isolation system. Bull Earthq Eng 9:657-673.

[14] Uang CM (1991) Establishing R (or R_w) and C_d factors for building seismic provisions. ASCE J Struct Eng 117:19–28

[15] Mitchell D, Paulter P (1994) Ductility and overstrength in seismic design of reinforced concrete structures. Can J Civil Eng 21:1049–1060.

[16] Auricchio F, Taylor RL, Lubliner J (1997) Shape-memory alloys: macromodelling and numerical simulations of the superelastic behaviour. Comput Method Appl M 146:281-312.

[17] SeismoStruct user Manual, (2010)Version 5.0.1. Pavia, Italy. Seismo-Soft Inc. Supporting Services

[18] Moni M., Performance of shape memory alloy reinforced concrete frames under extreme loads. Master's thesis, 2011. School of Engineering, The University of British Columbia, Kelowna, Canada; 2011.

[19] Alam, M.S., Moni, M., and Tesfamariam, S. (2012). Seismic Overstrength and Ductility of Concrete Buildings Reinforced with Superelastic Shape Memory Alloy Rebar. Engineering Structures, Elsevier Ltd, 34, 8–20.

[20] Alam MS, Youssef MA, Nehdi M (2010) Exploratory investigation on mechanical anchors for connecting SMA bars to steel or FRP bars. Mat and Struct 43(S1): 91-107.

[21] CSI. 2010. SAP 2000 integrated software for structural analysis and design. Computers and Structures Inc. (CSI), Berkeley, Calif.

[22] Alam MS, Youssef MA, Nehdi M (2008) Analytical prediction of the seismic behaviour of superelastic shape memory alloy reinforced concrete elements. Eng Struct 30:3399-3411.

[23] Atkinson GM (2009) Earthquake time histories compatible with the (2005) National building code of Canada uniform hazard spectrum. Can J Civil Eng 36: 991–1000.

[24] Miranda E, Bertero VV (I994) Evaluation of strength reduction factors for earthquake resistant design. Earthq Spectra 10:357-379.

CICM 2015
First International Conference on
Advances in Civil Infrastructure and Construction Materials
MIST, Dhaka, Bangladesh, 14–15 December 2015

EVUALUATION OF SEISMIC DESIGN RESPONSE FACTORS OF HIGH-RISE STEEL BUILDINGS UNDER VARIOUS INTERNATIONAL DESIGN CODES

Nadeem HUSSAIN[1] **and M. Shahria Alam**[2]

[1, 2] School of Engineering, The University of British Columbia, Canada.
Email: [1]n.hussain@alumni.ubc.ca and [2]shahria.alam@ubc.ca

Abstract. *Seismic response factors are used by various international standards while designing buildings under earthquake loads. These factors being empirical are still widely used to estimate the strength and deformation demands of a structure that will usually behave nonlinearly during a design earthquake. Four high-rise framed steel buildings with varying heights ranging from 8 to 20 stories are selected and designed using international seismic codes. Values of design base shears and story drifts are compared between the different referred buildings using various codes. Twenty earthquake records are considered to account for the ground motion uncertainty for the study region. Detailed fiber-based modeling approach is adopted on the reference structures to assess the seismic design response factors using large number of inelastic pushover analyses (IPAs) and incremental dynamic collapse analyses (IDCAs). The results provided sufficient safety margins indicating the possibility of increasing the design response factor values adopted in various design codes. The proposed study provides comparisons between different seismic design codes for the range of the reference buildings. The recommendations of this study may provide practical insights to the designers to achieve more cost-effective and optimistic designs on a wide range of high-rise steel buildings.*

Keywords: High-rise steel buildings, Seismic codes, Seismic design, Seismic design response factors, IDA.

1 INTRODUCTION

The design of a high-rise building is typically governed by lateral forces generated due to wind or earthquakes. International codes adopt elastic analysis using force-based design methods to design these buildings. Significant nonlinear deformations are witnessed in high-rise buildings during earthquakes causing the buildings to behave in a nonlinear way. To account for this nonlinear behavior in the code-recommended elastic design, a reduction in the seismic design load is permitted by codes based on buildings reserve strength (overstrength) and the capacity to dissipate energy (ductility). This reduction is done through response modification factor (R), which eventually amplifies the buildings deformation and helps in achieving safe design with optimized cost. Seismic response factors have a potential influence on seismic design forces in the force-based design approach. Any increase in these factors reduces the seismic design forces resulting in reduced cost of the overall structural system. These factors introduced in various seismic design codes do not provide a uniform safety margin and design optimization covering different structural systems and materials[1], since their values are empirical and based on horizontal force factors as illustrated in ATC [2]. Several developments were witnessed in international seismic codes in the recent past in these factors to represent nonlinear behavior of the structures in their respective codified design procedures. This presses the need to assess the seismic design response factors for a range of high-rise buildings considering various international design codes.

Five international seismic design codes namely, European Codes [3], International Building Code [4] with American Society for Civil Engineers code for loads [5], National Building Code of Canada [6], New Zealand Code [7] and Uniform Building Code [8] are selected in the present study to meet the study objective. Four high-rise steel buildings with varying heights are designed and detailed using three-dimensional (3D) models in accordance with the selected codes to assess the seismic design response factors. Inelastic static pushover analyses (IPAs) and incremental dynamic analyses (IDAs) are conducted in the current study. Twenty natural and artificial seismic records are employed on the detailed fiber-based simulation models to perform the extensive inelastic analyses in order to assess and verify the seismic design response factors.

2 STRUCTURAL DESIGN AND MODELING

Four regular high-rise steel buildings with varying heights are selected and conceptualized on a similar footprint representing a typical architectural layout in the study region (Dubai). The selected four buildings of 8, 12, 16 and 20 stories are laid horizontally on an equal seven grid system of 5m span each on either side, with a total measure of 30m x 30m in plan as shown in Figure 1. The total heights considered for each of the four buildings are 27.60, 40.80, 54.00 and

67.20 meters, respectively, with typical floor height of 3.3m for the upper stories and 4.50m at the ground story. The structural system selected in the current study provides higher lateral stiffness and resists the lateral loads from wind and seismic effects efficiently for the considered number of stories [9]. These buildings are designed using three dimensional (3D) structural analysis and design program ETABS [10].

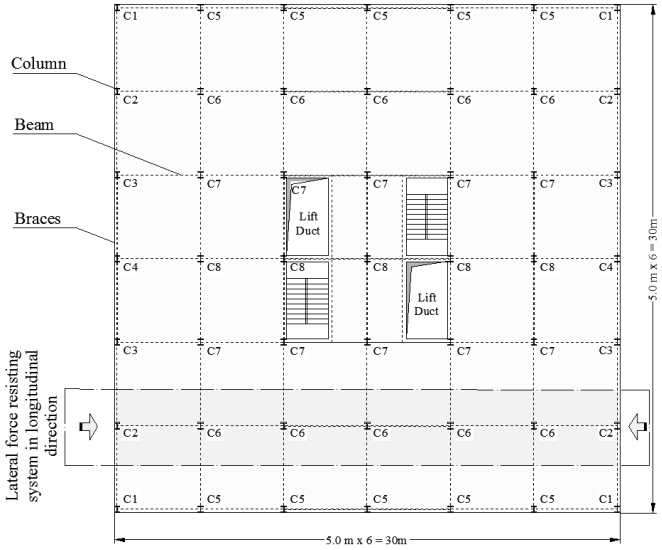

Fig (a)

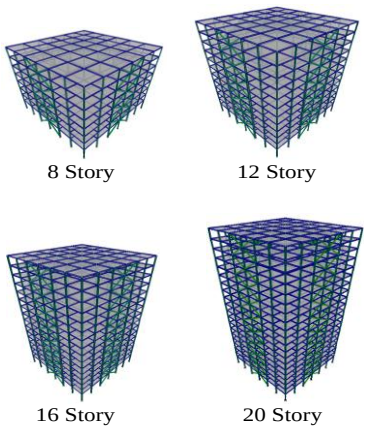

Fig (b)

Figure 1: High-rise steel buildings (a) Typical building layout (b) 3D models of 8, 12, 16 and 20 story buildings.

The selected building models are developed and designed individually with each of the five international seismic codes to resist the seismic forces in accordance with the load combinations recommended in the design provisions of the respective codes. Medium seismicity region is considered with peak ground acceleration (PGA) of 0.16g and 10% probability of exceedance in 50 years. The seismic design parameters of the selected codes are shown in Table 1.

Table 1: Summary of seismic design parameters of all selected design codes

Seismic Codes	Soil/Site Class	Seismic Design Parameters
EN, 2006	B	Ground acceleration, a_g = 0.16g Spectrum type = 2 behavior factor, q = 4 and Correction factor, λ = 1
ICC, 2012	C	Spectral accelerations, S_s = 0.80 and S_1 = 0.32 Response modification factor, R = 3.25 Importance factor, I = 1
NBCC, 2005	C	PGA = 0.24 g (value of 0.15g for 10% probability of exceedance in 50 years), F_a and F_v =1, I = 1, Higher mode factor, M_v = 1.2 $S_{0.2}$ = 0.52, $S_{0.2}$ = 0.31, $S_{1.0}$ = 0.15 and $S_{2.0}$ = 0.086 Ductility modifier, R_d = 3.0, Overstrength modifier, R_o = 1.3
NZS, 2004	C	Hazard factor, Z = 0.15g Return period = 1 and Near fault distance, D = 150 KM Structural performance factor, S_p = 0.7 and Ductility factor, μ = 3.0
UBC, 1997	S_c	Seismic zone factor, Z = 0.15, Zone classification = 2A Site coefficients, C_a = 0.18 and C_v = 0.25 Overstrength factor, R = 3.25, Importance factor, I = 1

All the four buildings are modeled using structural steel sections with a 350 MPa yield strength along the height. Columns and beams form the components of the lateral force resisting system, which are braced at the mid spans of each frame to effectively resist the lateral actions. Cast-in-situ reinforced concrete (RC) slabs of 0.16 m thick resting on the steel beam sections form the floor system that prevents undesirable failure modes. Floor slabs are designed considering the ef-

fects of lateral actions generated on the structural system due to seismic forces with the yield strength of 420 MPa for steel and compressive strength of 40 MPa for concrete. Elastic analyses are performed on the selected buildings under five seismic codes by adopting Equivalent Lateral Force Analysis (ELFA) method and Modal Response Spectrum Analysis (MRSA) method. Accordingly, the 3D elastic seismic response of the respective buildings are assessed and compared with the five seismic codes.

Inelastic analyses are performed in the current study by adopting fiber-based idealization approach employing actual material strength using ZEUS-NL [11]. Seismic performance is assessed using this approach based on the output generated from the elastic analysis on the most optimistic code-designed building from the five seismic codes on each of the four selected buildings. This approach being conservative is considered in the current study to assess the seismic response factors. The spread of yielding along the structural member length and section depth is monitored over a division of several number of cubic elasto-plastic elements. Geometric nonlinearities and material inelasticity are covered through integration of the non-linear stress-strain response in the different subdivided fibers. This approach was practiced in many previous studies on several large projects as the moment-curvature relationships is avoided[12]. Since 3D inelastic analysis is computationally demanding based on the above approach in investigating a range of selected buildings using 20 seismic records, two-dimensional (2D) idealization is adopted in the current study. Each building is assumed with five framing systems to resist seismic forces along the horizontal direction. The total mass of the building is loaded on these five frames with a 20% mass contribution from each frame as shown in Figure 1. To reduce the number of analyses and computational work, the present study focuses on the governing frame to perform non-linear analyses on the buildings in evaluating the seismic response factors.

3 ASSESSMENT OF ELASTIC SEISMIC RESPONSE

Elastic seismic response assessment is performed in the current study by analyzing and designing each of the selected building with five international seismic codes using ETABS. Design outputs of the four selected buildings are compared between the five seismic codes with respect to their elastic periods, story drifts, story shear and base shear. Building fundamental periods are controlled within their respective allowable tolerance limits to assure fair comparison between the various codes. Elastic periods at different mode shapes compared for each of the buildings with varying heights resemble similar results between all the codes, except the NBCC and UBC as shown in Table 2. This implies that the buildings with varying height designed with NBCC witnessed higher stiffness than the buildings designed with other codes. Further, buildings designed with IBC and

NZS codes witnessed higher periods and drifts making the selected buildings less stifferas the height progressed, in comparison to NBCC.

Table 2: Elastic periods of the reference buildings with various international codes

Building	**Code**	**Elastic Period, secs**					
		Mode 1	**Mode 2**	**Mode 3**	**Mode 4**	**Mode 5**	**Mode 6**
8 Story	EN	1.121	0.963	0.931	0.363	0.323	0.308
	IBC	1.115	1.044	0.958	0.368	0.349	0.323
	NBCC	0.794	0.761	0.719	0.261	0.260	0.242
	NZS	1.154	1.073	0.984	0.373	0.356	0.328
	UBC	0.880	0.841	0.754	0.299	0.287	0.260
12 Story	EN	1.534	1.308	1.271	0.524	0.459	0.444
	IBC	1.763	1.620	1.459	0.564	0.532	0.487
	NBCC	1.235	1.221	1.137	0.408	0.402	0.376
	NZS	1.785	1.644	1.478	0.568	0.536	0.490
	UBC	1.220	1.207	1.064	0.423	0.416	0.363
16 Story	EN	1.691	1.687	1.482	0.605	0.604	0.540
	IBC	2.316	2.171	1.934	0.710	0.678	0.620
	NBCC	1.660	1.574	1.476	0.573	0.520	0.495
	NZS	2.205	2.018	1.876	0.679	0.678	0.590
	UBC	1.693	1.651	1.489	0.567	0.554	0.499
20 Story	EN	2.130	2.079	1.848	0.736	0.713	0.655
	IBC	2.963	2.797	2.434	0.912	0.872	0.786
	NBCC	2.053	1.973	1.809	0.697	0.652	0.611
	NZS	2.387	2.300	2.003	0.786	0.759	0.676
	UBC	2.164	2.102	1.879	0.715	0.702	0.634

Design base shear of the buildings are compared with various codes along their governing axis as shown in Figure 2. The values of base shear coefficients reduced constantly with an increase in building height under all seismic codes. Figure 3 shows the comparison of base shear coefficient to identify the governing code in optimizing the building design with varying heights. Buildings lower than 12 stories are governed with EN and NZS codes, with EN being the most optimum. Whereas, IBC and NBCC codes govern over other codes for buildings higher than 12 stories, with IBC being the most optimum. Seismic performance is assessed using inelastic analysis on these optimized code-designed buildings from the five seismic codes for each of the respective story heights. Detailed comparisons between the various codes for buildings with varying heights are presented in the following sections.

4 SEISMIC GROUND MOTIONS

Based on previous studies, higher impact on the response of high-rise buildings was witnessed with long distance seismic events[13]. Accordingly, a set of twenty strong natural and artificial seismic ground motions representing the medium seismicity region are selected representing the long-distance events [14] as shown in the Figure 4. The records were scaled to a design PGA of 0.16g with an earthquake magnitude of 6.93 to 7.72 and epicentral distance of 95 to 160 km for 10% probability of exceedance in 50 years, which also fit the Uniform Hazard Spectrum (UHS) of Dubai. Inelastic dynamic analyses (IDAs) are performed using these records, which reduce the uncertainties arising from ground motions.

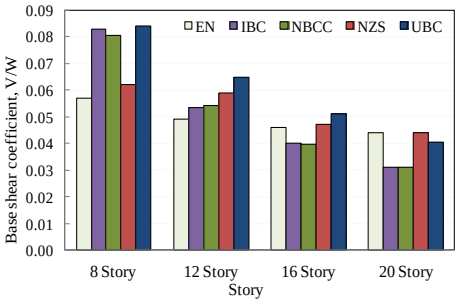

Figure 2. Elastic base shear comparison of 8, 12, 16 and 20 story buildings with various seismic codes

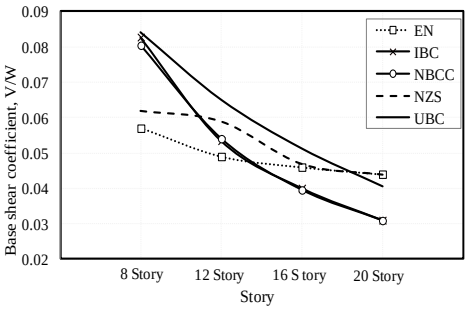

Figure 3. Comparison showing governing base shear from 8, 12, 16, 20 story buildings with various seismic codes

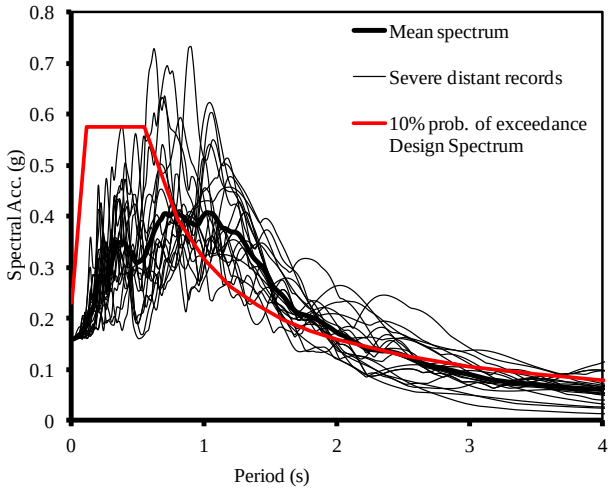

Figure 4 : Response spectra of 20 ground motions

5 ASSESSMENT METHODOLOGY ADOPTED TO VERIFY SEISMIC RESPONSE FACTORS

Buildings are designed by reducing the elastic seismic forces to the design seismic forces using the Response modification factor (R). This design seismic force is kept consistent with the first significant yielding in a structure by the seismic codes [1]. Under the effect of an earthquake, a well-designed structure witnesses the occurrence of first significant yield at strengths higher than the yield limit state, while expected collapse is higher than the elastic design spectrum. This assumption is also confirmed in the current study based on the results presented in the following sections. In the current study, the R factor is evaluated based on the equation suggested by Mwafy and Elnashai [15]:

$$R = R_{ideal} . \Omega_y = [(a_g)_c / (a_g)_y] . \Omega_y \quad (1)$$

where, R is the response modification factor, R_{ideal} is the response modification factor for ideal structure that is dependent on ground motions, $(a_g)_c$ is the PGA at collapse earthquake, $(a_g)_y$ is the PGA at first significant yield and $\Omega_y$is the first yield over strength defined as the ratio of first significant yield strength to the design strength.

To evaluate the seismic response factors, the response of the buildings at the two limit states, i.e., at first significant yielding and the first collapse indication, should be measured. Inelastic analyses are employed in the current study to determine the first significant yielding and the indication of first collapse in the structure. The indication of the first significant yield is considered when the strain of the structural steel exceeds the yield strain, whereas the collapse indication for the braced frame structures is defined when the inter-story drift ratio (IDR) exceeds 2.0% in the structure. This criterion of collapse prevention is defined in accordance with the code provisions [16].

Extensive IPAs and IDAs are performed on each of the respective governing code-designed building representing varying heights based on the results from the elastic analysis. PGA at first significant yield and collapse are determined from the governing buildings under the effect of 20 scaled seismic records till the structure reaches collapse limit to get the ground motion dependent component of the response modification factor. In order to indicate the first significant yield in the buildings, the plastic hinge formations in different structural members are screened in all the buildings under the effect of 20 seismic records.

6 EVALUATION OF SEISMIC RESPONSE FACTORS

The first yield over strength (Ω_y) of the selected buildings is evaluated using both IPAs and IDAs. IPAs are performed using both inverted triangular load distribution and uniform distribution pattern to monitor the capacity curve from its yield-

ing till collapse for each of the buildings designed with varying heights from the respective governing codes. Based on the previous studies, uniform lateral load distribution pattern can be used to obtain the conservative lateral capacity of the structure [13]. Hence, this has been adopted in the current study to evaluate the lateral capacity of the selected buildings as shown in Figure 5.

Plastic hinge formations are monitored and the first yield is witnessed in the braced members, followed by beam and the column in all the respective buildings as shown in the Figure 6. This is in good agreement with the strong column and weak beam theory. Previous studies concluded that the pushover analysis results are on the conservative side when compared with IDA results [17]. In high-rise structures, some important deformation modes may not be detected by the IPA. To overcome the shortfalls in IPAs, IDAs are considered to evaluate the seismic response factors in the current study. Accurate behavior assessment of the buildings under seismic loads covering the ground motion uncertainty can be obtained using IDA.

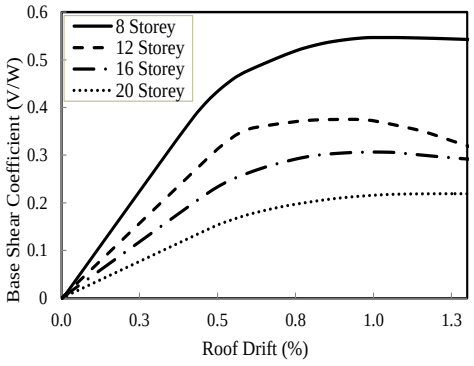

Figure 5: Capacity envelopes of buildings using IPA

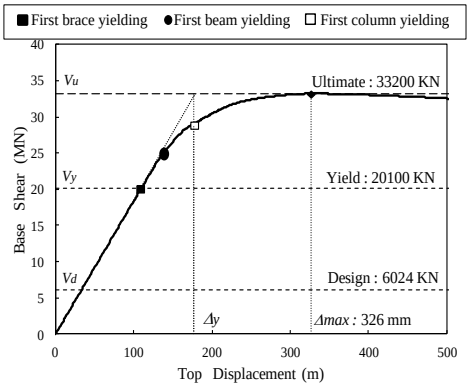

Figure6: Sample capacity curve of 8 story building showing plastic hinges

Over 1500 multiple nonlinear inelastic response history analyses are performed using a set of seismic records. All the selected 20 seismic records are incrementally scaled from a PGA of 0.08g to 1.28g using a scaling factor of 0.08g to capture the behavior of the building up to the collapse level. Plastic hinge formations at the yield point in all the structural members are monitored. First yield overstrength (Ω_y) results from the IDAs are obtained and then compared with the results of IPAs as shown in Figure 7.

The Ω_y factor results obtained from the IPA witnessed lower values than the IDA values due to the effects of higher modes in high-rise structures. However, towards a conservative approach in evaluating the R factor, the values of Ω_y factor from IPAs are adopted in the present study.

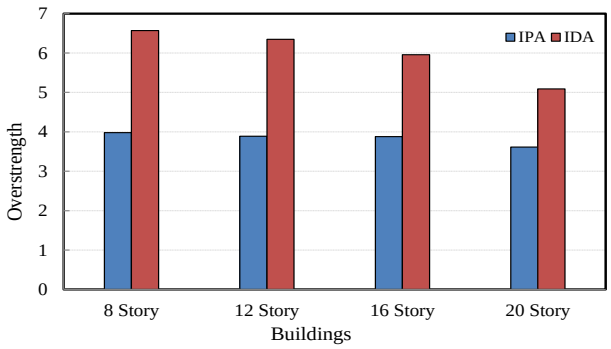

Figure7: Comparison of first yield overstrength (Ω_y) estimation of the four buildings using both IPA and IDA

To evaluate the seismic response factors of the governing code-designed buildings from each of the respective story heights, the PGAs and IDRs obtained from the IDAs at both the yield and collapse limit states results are utilized. The results covering all the seismic ground motions of each building are used in evaluating the seismic response factors. The collapse-to-yield PGAs and IDRs are summarized and presented as shown in Figure 8. Each dot in Figure 8 of the respective building represents the value obtained from one seismic record.

In order to estimate the value of the R factors, the collapse-to-yield PGA ratios are used along with the first yield overstrength (Ω_y). The collapse-to-yield PGA ratios resemble similarity in values from all buildings irrespective of the varying heights. The first significant yield and the indication of the first collapse in the lower story buildings are at a higher PGA than compared with the higher story buildings. This implies that the impact of the earthquakes increases as the story height increases for the selected structural system, resulting in decreasing the margin of safety in the buildings with increase in their respective story height.

Figure 9 summarizes the seismic response factors evaluated using twenty seismic records for each of the governing code buildings with varying heights. Median R and median collapse - yield are shown in Figure 9. Median R is obtained from the R factors derived with different seismic records. Then median collapse-yield is obtained from the median PGAs taken from Figure 8. The evaluated response modification factors of the various buildings are significantly higher than the values recommended in the respective codes, reflecting higher safety margins. These margins decreases with the increase in height of the building as shown in Figure 9 and is in good agreement with several earlier studies [18], [19].

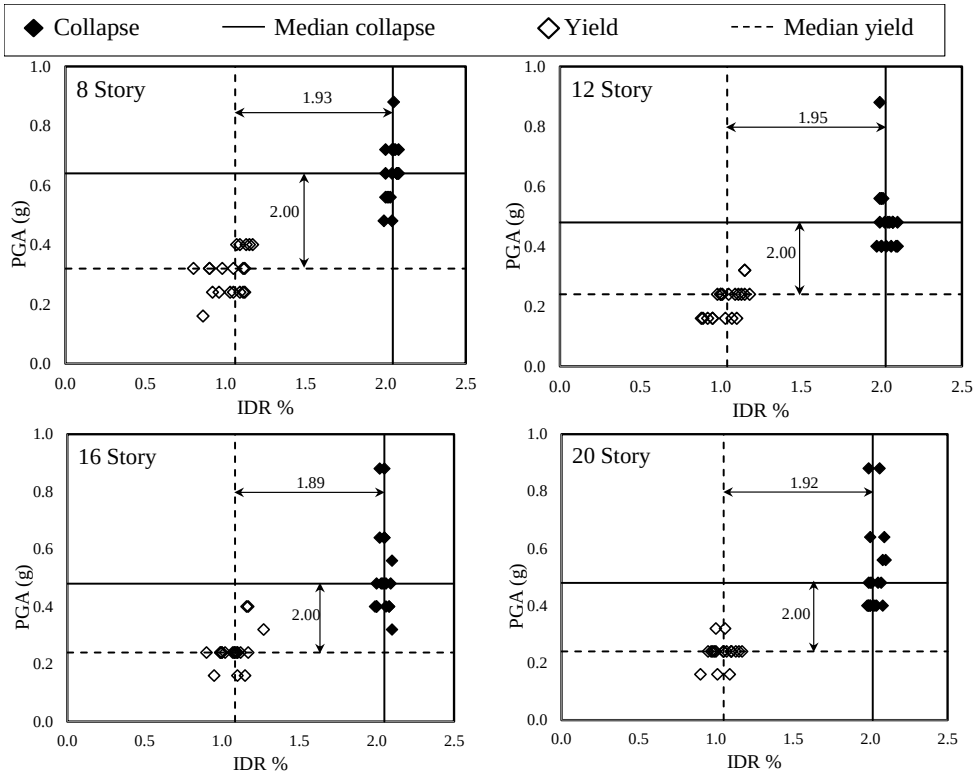

Figure 8: Yield and collapse results showing collapse-to-yield PGA and IDR ratios from 20 seismic records for different buildings

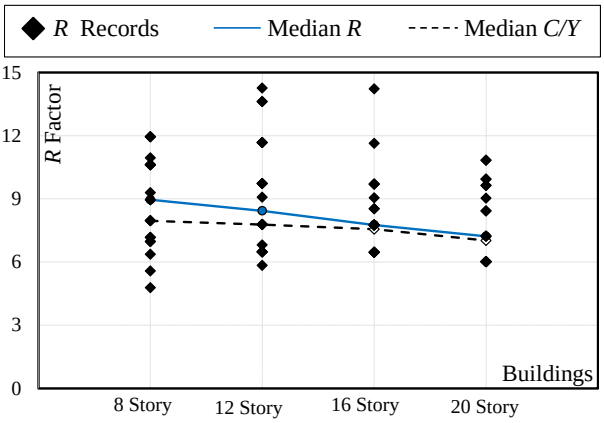

Figure9: Response modification factors of different buildings obtained from 20 seismic records

7 COMPARISON OF DESIGN SAFETY MARGINS

The designs of all the selected buildings with varying heights are compared with five international seismic codes. These building performed fairly well with a significantly higher value of R factor than the respective code recommended values. Base shear coefficient values from each building with five international codes are compared and the excess design safety margins relative to the building with the governing codes are assessed as shown in Figure10.

For the sake of comparative reference within the buildings, Eurocode is considered for 8 story and 12 story buildings, and IBC is considered for 16 and 20 story buildings based in Figure 3. Excess design margins of 47.4% and 32.6% are observed in 8 and 12 story buildings designed with UBC relative to the EN code. For 16 and 20 story buildings, design margin in excess of 27% and 42% were observed with UBC and NZS, respectively, relative to the IBC. This may contribute in the reduction of structural steel materials for those buildings designed with excess design margin with acceptable values of R factors.

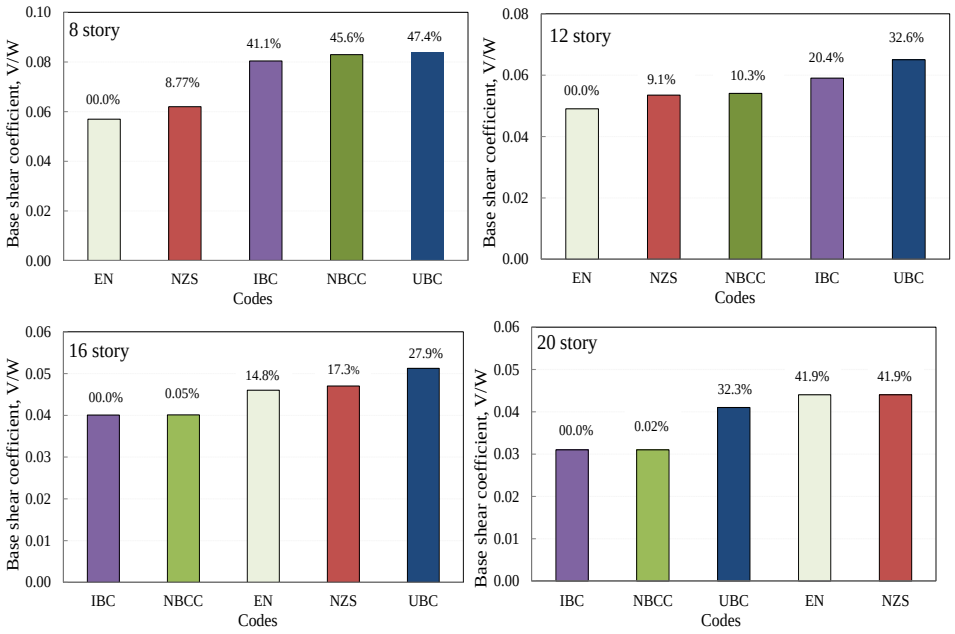

Figure10: Comparison of design safety margins relative to the governing design code buildings

8 CONCLUSION

This paper investigated the seismic design response factors of high-rise steel buildings designed with various international codes. Elastic seismic response of all buildings was assessed using various codes and inelastic analysis was performed on the optimistic governing code-designed building to evaluate the response factors. The excess design margins among the various codes were compared with the governing code for each of the selected building and the evaluated results were presented.

Eurocode governed the design for buildings 12 stories and lower, whereas IBC governed for buildings higher than 12 stories. Seismic response factors, namely, the overstrength factor and the response modification factor were evaluated using IPAs and IDAs. The governing code-designed buildings performed fairly well with significant higher safety margins of R factors than the respective code recommended values. This implies that significant amount of steel can be saved in the buildings that are designed with non-governing codes in comparison with the governing code-designed building. The median R factors evaluated for the selected buildings were significantly higher than the respective code recommended values. Higher overstrength factors in the buildings contributed mainly due to the increase in the R factors. The safety margin of the R factors increased with decrease in height of the buildings. Based on the higher safety margins of R factors in the buildings, the possibility to increase the R factors is recommended in the respective international codes to achieve more cost-effective designs for the selected systems. Further research is recommended to cover building irregularities as this study was limited to regular buildings.

ACKNOWLEDGEMENTS

This work was supported by the Natural Sciences and Engineering Research Council (NSERC) of Canada through Discover Grant.

REFERENCES

[1] FEMA P695, “Quantification of Building Seismic Performance Factors, FEMA P695,” Fed. Emerg. Manag. Agency, Washington, DC, 2009.

[2] ATC, “Applied Technology Council (ATC). (1995a). ‘“Structural response modification factors.”’ Rep. No. ATC-19, Redwood City, Calif.,” Rep No ATC-19, 1995.

[3] EN, Eurocode 8: Design of structures for earthquake resistance. 2006.

[4] ICC, “International Building Code,” Int. Code Counc. Ctry. Club Hills, IL., 2012.

[5] ASCE 7, Minimum Design Loads for Buildings and Other Structures. American Society of Civil Engineers, 2010.

[6] NBCC, "National Building Code of Canada, 2005,"

[7] NZS, NZS 1170.5:2004 Structural design actions - Earthquake actions - New Zealand. 2004.

[8] ICBO, "Uniform Building Code, 1997 Edition. International Conference of Building Officials: Whittier, CA.," 1997.

[9] M. M. Ali and K. S. Moon, "Structural developments in tall buildings: current trends and future prospects," Archit. Sci. Rev., vol. 50, no. 3, pp. 205–223, 2007.

[10] CSI, "ETABS - Integrated Building Design Software,." Computers and Structures, Inc., Berkeley, California, 2013.

[11] A. Elnashai, V. Papanikolaou, and D. Lee, "ZEUS-NL - A system for inelastic analysis of structures, user's manual, Mid-America Earthquake (MAE) Center, Department of Civil and Environmental Engineering, University of Illinois at Urbana-Champaign, Urbana, IL; 2012," 2012.

[12] S. H. Jeong, A. Mwafy, and A. Elnashai, "Probabilistic seismic performance assessment of code-compliant multi-story RC buildings," Eng. Struct., vol. 34, 527–53, 2012.

[13] A. Mwafy, A. Elnashai, R. Sigbjörnsson, and A. Salama, "Significance of severe distant and moderate close earthquakes on design and behavior of tall buildings," Struct. Des. Tall Spec. Build., vol. 15, no. 4, pp. 391–416, 2006.

[14] PEER, "Pacific Earthquake Engineering Research Center, University of California, Berkeley, California," PEER NGA Database. 2013.

[15] A. M. Mwafy and A. S. Elnashai, "CALIBRATION OF FORCE REDUCTION FACTORS OF," vol. 6, no. 2, pp. 239–273, 2002.

[16] ASCE/SEI 7-05, NEHRP recommended seismic provisions for new buildings and other structures, Part 2. 2009.

[17] A. M. Mwafy, N. Hussain, and E.-S. Khaled, "Impact of high-strength material on seismic design response factors and economics of multi-story buildings," SMAR, 2013.

[18] G. Abdollahzadeh and A. M. Kambaksh, "Height Effect on Response Modification Factor of Open Chevron Eccentrically Braced Frames," Iran. J. Energy Environ., vol. 3, no. 1, pp. 89–94, 2012.

[19] J. Kim and H. Choi, "Response modification factors of chevron-braced frames," Eng. Struct., vol. 27, no. 2, pp. 285–300, Jan. 2005.

CICM 2015
First International Conference on
Advances in Civil Infrastructure and Construction Materials
MIST, Dhaka, Bangladesh, 14–15 December 2015

SEISMIC PERFORMANCE EVALUATION OF RC GARMENT MANUFACTURING BUILDINGS RETROFITTED WITH DIFFERENT ALTERNATIVES

AKM G. MURTUZ[1], K. B. Jalal[2], R. J. Priti[3], M. Mohiuddin[4], K. Islam[5] and M. S. Alam[6]

[1, 2, 3, 4, 5] Department of Civil Engineering, Military Institute of Science and Technology, Dhaka, Bangladesh
Email: [1]golam.murtuz.bd@gmail.com,[2] nishi_vnsc@hotmail.com, [3]rifatjabin11@gmail.com, [5]kamrul1@ualberta.ca

[6]School of Engineering, The University of British Columbia, Kelowna, Canada
Email: shahria.alam@ubc.ca

Abstract. *Seismic performance assessment of Readymade Garment Manufacturing (RMG) building unveils the vulnerability of gravity load designed RMG building subjected to seismic loading. The present study aims at to investigate the suitability of three different retrofit provisions namely concrete jacketing, carbon and glass fiber reinforced polymer wrapping for strengthening seismically vulnerable RC buildings in Bangladesh. Static and dynamic nonlinear analyses have been carried out to for retrofitted and original building frames. Ground motion data matched with local response spectra have been employed to assess the seismic responses of the buildings. Results show an enhanced seismic performance of retrofitted buildings as compared to original building. Also, the relative comparison of different retrofit techniques were carried out in terms of quantifiable demand parameters i.e. ductility, interstory drift demand, maximum story displacement etc. in order to propose the best retrofitting technique for gravity load designed garment factory buildings.*

Keywords: Readymade Garment Buildings, Seismic vulnerability, Structural Strengthening, Seismic Performance.

1 INTRODUCTION:

Bangladesh is one of the most potential candidate for garment manufacturing products and the increased economic prospect of this field gained attention of several stakeholder groups thus, leading to a robust expansion of the factory buildings in the late 70's of last century. RMG industries are currently leading Bangladesh from the front to its economic growth. But it is a fact that the infrastructural development of this industry is not guided. According to Bangladesh Garment Manufacturers and Exporters Association (BGMEA) there are 4222 garment factories running at present with 4 million workers [1] and most of them are functioning in or surrounding the capital or major cities like Dhaka, Chittagong, Khulna, Sylhet etc. The recent incident of the utter structural failure of Rana Plaza gained attention of different research groups, stakeholders and government organization like Public Works Department (PWD) to ensure safety and desired performance of factory buildings under gravity and other loading conditions. Being motivated by the scope of improving the scenario, Authors conducted an investigation on five garment factory buildings to assess their performance under gravity loads and moderate earthquake loading condition [2, 3]. Results from nonlinear analysis show the vulnerability of most of the buildings subjected to earthquake loadings thus necessitating a suitable rehabilitation method to strengthen the vulnerable frames of the structure.

Various rehabilitation techniques are available for enhancing the performance of deficit buildings. Strengthening structural frame elements with reinforced concrete jacketing, steel encasing, steel bracings, Fiber reinforced polymer jacketing, Engineered Cementetious Composite (ECC) jacketing are known as structural retrofitting that can significantly increase the performance of RC buildings against seismic hazards [11]. Numerous Passive Damping Device (PDD), such as Yielding shear panel device, Friction damper incorporated within steel bracings, Fluid viscous damper can be alternatively used to reduce the earthquake induced motion and hence, to increase the energy dissipation capacity of RC structures [8]. Steel shear plates and external pre-stressing are also used as rehabilitation techniques for various RC frame structures [8]. Suitability of above mentioned rehabilitation techniques largely depend on the financial consideration, technical expertise and also social acceptability of particular methods. Present study mainly focuses on various retrofit techniques those are common in regional construction practice and are feasible based on socio-economic condition of this region.

Effect of steel bracing on RC building frames against seismic ground motion have been studied by previous researchers [10]. Analytical investigation has shown that, steel bracing can be used to significantly improve the seismic performance of RC frames [10]. But their effectiveness largely depend on the orientation of the braces. Yuksel et. al. have shown that, cross diamond braced CFRP retrofitting scheme can be effectively used to strengthen infill wall against

brittle shear failure as well as reduces the load distribution on beam-column joint [7]. Incorporation of steel bracings in the garments factory building requires adequate free space and increases the complexity during installation process. Thus, initially the steel bracing might not be a viable option for the garment factory building as a rehabilitation method against seismic hazards. Authors limited the scope of this study within different jacketing techniques and hence leaving the scope of future study on performance of garment buildings braced with steel braces.

Reinforced concrete jacketing is the most commonly considered retrofit techniques for low strength concrete frames. Both analytical and experimental investigations have shown the enhanced strength and stiffness properties of RC buildings retrofitted with concrete jacketing [11]. Larger ductility of the structural members can also be achieved by concrete jacketing in comparison with FRP jacketing or steel encasing [11]. In some cases, larger thickness of concrete jacket made this method inconvenient for structural rehabilitation of RC buildings. Relatively thin High-Performance Fiber Reinforced Polymer (FRP) can be a suitable alternative for this cases [9]. Pampanin et. al., and Eshghi and Zanjanizadeh have experimentally shown that Carbon Fiber-Reinforced Polymer (CFRP) and Glass Fiber-Reinforced Polymer (GFRP) can have satisfactory result for strengthening vulnerable structural elements with almost similar performance as compared to traditional rehabilitation techniques [5, 6].

The present study aims at to investigate the suitability of three different retrofit schemes namely the concrete jacketing, Carbon and Glass Fiber Reinforced Polymer (FRP) wrapping. Finite element analyses using freely available software SeismoSoft and Response 2000 have been carried out on a two bay four storied internal frame to investigate the suitability of three different retrofit alternatives. Result from nonlinear static and dynamic analyses were compared in terms of inter story drift percentage, maximum roof displacement and drift, different damage state, total energy dissipation capacity and ductility of the buildings. Finally, the relative performance of these retrofit schemes were compared with the performance of the original building without retrofitting and hence an educated decision were made to propose the most effective retrofit options for strengthening the RC garment manufacturing factory buildings in Bangladesh.

2 RESEARCH SIGNIFICANCE:

After the collapse of Rana plaza a preliminary structural investigation report shows that about 60 % of the factory buildings are structurally deficit [9]. These events has shown an undoubted amplified seismic risk of the existing buildings considering the geological position and present development scenario. Besides, most of these buildings ignored the seismic design provision for earthquake resistant building construction and hence are susceptible to any such events that

might strike Bangladesh in the near future. In addition, occurrence of frequent earthquake i.e. Chilmari (2015), Assam (2015), Mizoram (2015), Sikkim (2015) in recent years including the devastating Nepal (2015) earthquake in the South Asian region has made stakeholders to feel the importance of seismic performance enhancement of existing structures. Though it's unexpected but the fact is, neither the seismic performance of these garment buildings and possible extents of seismic damage are known nor there do any guideline for their strengthening measure. However, to enhance the seismic performance of existing structures to desired level, retrofit of the structure is an accepted solution in the field of civil engineering. It is technical interventions in structural system of a building that improve the resistance to earthquake by optimizing the strength, ductility and earthquake loads.

In response to the present situation structural strengthening /retrofit can take as a target solution involves adjusting features of the elements or whole building to eliminate or reduce existing risk of damage. Considering Bangladesh perspective an optimum retrofit technique needs to be adopted as solution which will ensure desirable performance of structure along with satisfying technical, economic, social and historical aspects of the issue [4]. Also appropriate knowledge, expertise, guidelines and research on retrofit methods, both in understanding design concept and construction mechanism are required to attempt successful applications in necessary circumstances. Accumulation of all these phenomena accompanied by well-planned government policy and support can offer a safer structural system with improved earthquake resistance. At present, a project is ongoing to contribute in developing capacity on some retrofitting methods which include RC jacketing, RC shear wall, RC wing wall, Steel framed bracing, Carbon fiber sheets wrapping and silt on brick standing wall under the Public Works Department (PWD), Bangladesh with the cooperation of Japan International Cooperation Agency (JICA). A properly developed design concept and construction knowledge of retrofit approaches can be used in practical cases to improve the existing performance of deficit structures. The present study will facilitate the stakeholders, construction engineers and the policy makers to make an educated decision while choosing the retrofit techniques to be adopted for enhancing the performance of vulnerable buildings to achieve the desired performance objective.

3 FRAME SECTION DETAILS:

In order to evaluate the seismic performance of garment buildings, a four storied RC factory building is considered in this study. Authors intentionally bound themselves from mentioning the name of the factory buildings considered for performance analysis in order to prevent the negative socio-economic impact that might have on the building owners. The building is typical a moment resisting RC frame structure designed as per the Bangladesh National Building Code

(BNBC'1993) guideline having a floor area of 335.7 square meters. The four storied building is regular in plan section but has vertical irregularities. For the simplicity of the study one transvers frame of the building is considered for analysis. Column sections of the frame varies over the height of the storey whereas, floor beam sections remain constant for all the stories of the building except the grade beam in the ground level. The building consists of infill brick walls only in the peripheral region thus the wall loads are applied over the peripheral beam as uniformly distributed gravity loads. Cross sectional dimension, reinforcement detailing of the column section are presented in the Figure 1 below. A two dimensional front view of the frame considered is also presented in Figure 1.

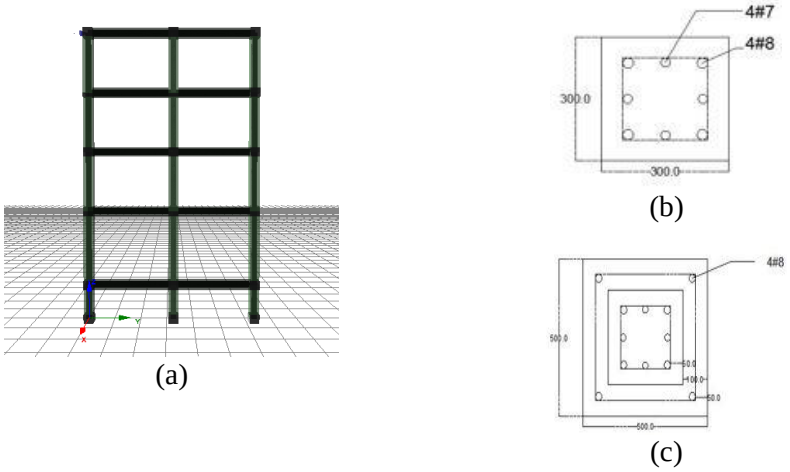

(a) (b) (c)

Figure 1: (a) Front elevation of the 2D building frame and (b) Typical concrete column cross section without retrofitting and (c) Column cross section with retrofitting.

4 RETROFITTING TECHNIQUES

Mainly two different retrofitting techniques has been considered for the current study namely the Reinforced Concrete (RC) jacketing and Fiber Reinforced Polymer (FRP) jacketing. Both the Carbon Fiber Reinforced Polymer (CFRP) and Glass Fiber Reinforced Polymer (GFRP) jacketing has been employed to assess the suitability of different FRP wrapping for strengthening vulnerable structures. The design specification and material properties for both the FRP and RC jacketing materials are described below:

4.1 RC Jackets

Reinforced Concrete (RC) jacketing is considered as the potential technique for retrofitting the vulnerable frame elements of the factory buildings. Usually a minimum jacket thickness of 100 mm is used as per the Indian Standard. For the present study we used a jacket thickness of 100 mm according to the Japanese guideline for seismic retrofitting of existing RC structures. The thickness of the jacket was considered based on several factors including minimum cover requirements for additional reinforcement in the jacketed section and space required for 135 degree hooks at the end of the stirrups. Material properties for the new concrete was similar to that of the existing column concrete properties having a concrete compressive strength of 20.68 MPa. Four number 8 bars were used for reinforcing the jacketed section of the concrete. It is to be noted that the new section of the concrete jacketed column should be well connected with the existing column concrete section following proper construction practices and guidelines to achieve the maximum benefit and enhanced performance of the retrofitted column section.

4.2 CFRP Composite Jackets

For the analytical study presented here, the CFRP jacket retrofitting technique and the material properties has been adopted from Pantelides and Gergely (2002) where the material comprised of 48,000 fibers per tow unidirectional carbon fibers [12]. The width of the carbon sheets was 457 mm and the tow numbers per 25 mm of sheet was 6.5. The CFRP composites were cured with an ambient temperature and then their properties were determined using the ASTM D 3039 specification. The design parameters for the CFRP composite materials include a maximum tensile strength of 628 MPa; modulus of elasticity of 65,000 MPa; Ultimate axial strain for unidirectional CFRP composite was 10 mm/m; initial stiffness value of 6.5×10^4 MPa; layer thickness was 1.32 mm and the fiber volume fraction was 35. The CFRP jacketing section thickness was calculated as 3.96 mm (3 layers) for 300 x 300 mm column sections and 5.28 mm (4 layers) for 350 x 350 mm column sections.

4.3 GFRP COMPOSITE JACKETS

Parghi and Alam (2015) investigated the performance of RC circular bridge columns under axial and cyclic lateral loading where they used the GFRP jacket retrofitting technique [13]. The material properties for GFRP retrofit techniques has been adopted from their study. Design parameters for the GFRP composite materials include a ultimate tensile strength of 3450 MPa; modulus of elasticity of 41,000 MPa; Ultimate axial strain was 18 mm/m; initial stiffness value of 19.13×10^3 MPa; layer thickness was 1 mm and the fiber volume fraction was 35. The GFRP jacketing section thickness was calculated as 1 mm (1 layers) for

300 x 300 mm column sections and 1 mm (1 layers) for 350 x 350 mm column sections.

5 FINITE ELEMENT MODELLING

The analytical model for the two bay four storied frame element was developed in the freely available finite element package SeismoStruct as 2-D frame elements. The Menegotto-Pinto steel model has been employed for modelling the reinforcing bars with a yield strength of 414 MPa. Similar model was adopted for reinforcing stirrups and ties in the beam and column sections. The strain hardening parameter and modulus of elasticity for the steel models were considered as 0.5% and 200 GPa. Mander et. al. nonlinear concrete model has been used for concrete material modelling with a compressive strength of 21 MPa and a maximum of 10 percent tensile strength. The strain at peak stress was considered as 0.002 m/m. Figure 1 show the retrofitted cross section of the column with proper reinforcement distribution and sectional dimensions. Tri-linear FRP model were employed for the fiber reinforced polymer materials with designed parameters mentioned earlier. Both the CFRP and GFRP materials were employed following the tri-linear constitutive model for fiber reinforced polymer materials.

All the frame sections are defined as the inelastic displacement based frame element with Rayleigh damping properties. Reinforced concrete rectangular sections were adopted for existing non-retrofitted beam column sections whereas, reinforced concrete rectangular jacketed sections were used to define the column sections retrofitted as both the RC jacketing and FRP wrapping techniques. Finally nonlinear static pushover and dynamic time history analyses have been performed to assess the performance of the retrofitted building frames and a relative comparison of different retrofit techniques were carried out for determining the most suitable retrofit measures for strengthening vulnerable factory buildings. Eigenvector analysis of retrofitted and non-retrofitted frames have been performed to observe the shift of buildings natural time period as result of different retrofit measures which is shown in Table 1.

Table 1: Time Periods for Non retrofitted and retrofitted frames

RCC Frame	Structural Time Period (s)			
	T1	T1	T1	T1
Normal	1.644	0.4876	0.27	0.1966
Concrete jacketed	1.145	0.3173	0.15	0.0821
CFRP	1.510	0.4460	0.24	0.1761
GFRP	1.609	0.4786	0.26	0.1939

6 SELECTION OF GROUND MOTION

A total of five earthquake ground motion data's has been selected for this study to perform dynamic time history analysis. The characteristics of all the earthquake data are presented in Table 1. The Peak Ground Acceleration (PGA) values for all these ground motion data's are very high starting from 0.47g to 1.07g. All these earthquake data's are matched with the local response spectra to get the resultant acceleration response spectra with a 5% damping ratio. Figure 2 shows the resultant acceleration response spectra as obtained from matching earthquake ground motion data's with BNBC'2015 response spectrum.

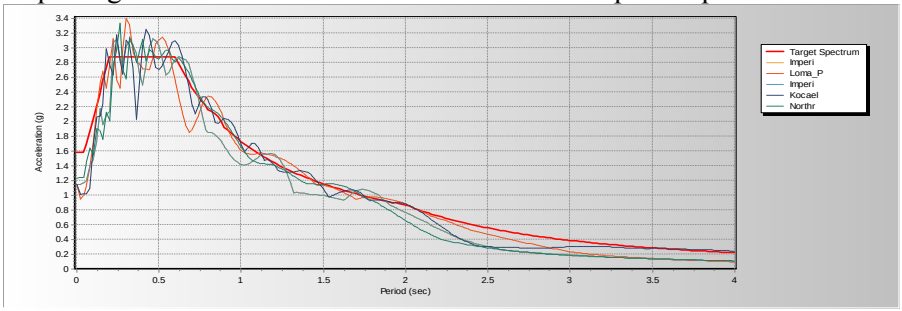

Figure 2: Resultant acceleration response spectra

7 STATIC PUSHOVER ANALYSIS

Nonlinear static pushover analysis has been performed for all the three different retrofitted frames and their relative performance has been compared in terms of capacity curve, ductility demand and maximum roof drift percentage. The load controlled pushover analysis was carried out with all gravity loadings provided as distributed loads in the frame sections. Incremental load was applied at the right top node of the frame section in the form of displacement. The maximum displacement value has been calculated considering a total of 8 percent drift that the building might experience during any extreme earthquake. From the pushover response curve, as plotted in Figure 3, it is observed that the maximum capacity has been achieved with the RC jacketing retrofit scheme. CFRP and GFRP retrofit scheme also shows an improved performance in terms of lateral capacities as compared to the normal frame structure.

Figure 4 (a) represents the global ductility values for the retrofitted frames and the original building frame. It can easily be observed that the ductility value increases for the retrofitted sections and the most ductile building frame is obtained with CFRP and GFRP retrofitted schemes. For the GFRP retrofit schemes the ductility value increases by 45% than the original ductility value. It is to be noted that the ductility of the frame is calculated using the ratio of the maximum top displacement (Displacement value corresponding to the maximum base shear value) and the yield displacement. The yield displacement is

determined through the bilinear curve approximation of the capacity curve obtained from static pushover analysis.

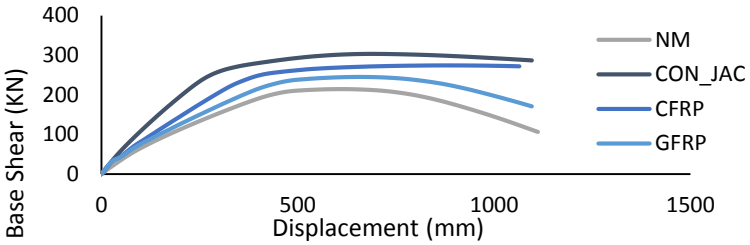

Figure 3: Capacity curve (Base Shear-Displacement) for building frame.

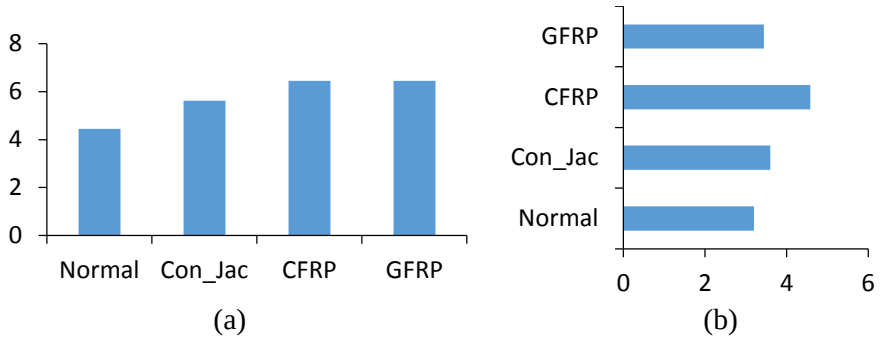

Figure 4: (a) Ductility of retrofitted building and (b) Maximum roof drift (%)

The top roof drift percentage for the building frame retrofitted with different alternatives are represented in Figure 4(b). The larger the drift (%) the higher the capacity of the retrofitted section to sustain loading before collapse and hence provide an index for choosing the best retrofit methods. Results show that the maximum drift (%) has been experienced by the CFRP retrofitted building with a drift (%) of 4.5855%. The RC jacketed and the GFRP retrofitted frames experiences a drift of 3.6 and 3.44 percentage respectively.

Different damage state has been proposed using the result obtained from the pushover analysis. In Table 2 five different performance criteria and corresponding drift limit has been selected for concrete jacketing and the original column sections whereas, three different damage states were prescribed for FRP retrofitted sections. Only the column sections are considered for representing the global damage state of the building frame and their sequence of occurring is presented in Figure 5 with numbers starting from 1 indicating the least damage state of the column sections.

Table 2: Different Performance Criteria and Drift Limit

Damage State	Drift Limit			
	Normal Frame	Concrete Jacketed	CFRP	GFRP
Concrete Crack reached	0.16%	0.32%	NA	NA
Reinforcement Yeild reached	2.96%	3.6%	4.01%	3.04%
Concrete Spalling reached	3.36%	5.44%	NA	NA
Concrete Core Crushing reached	4%	6.56%	4.51%	4.08%
Reinforcement Fracture	NA	NA	NA	NA

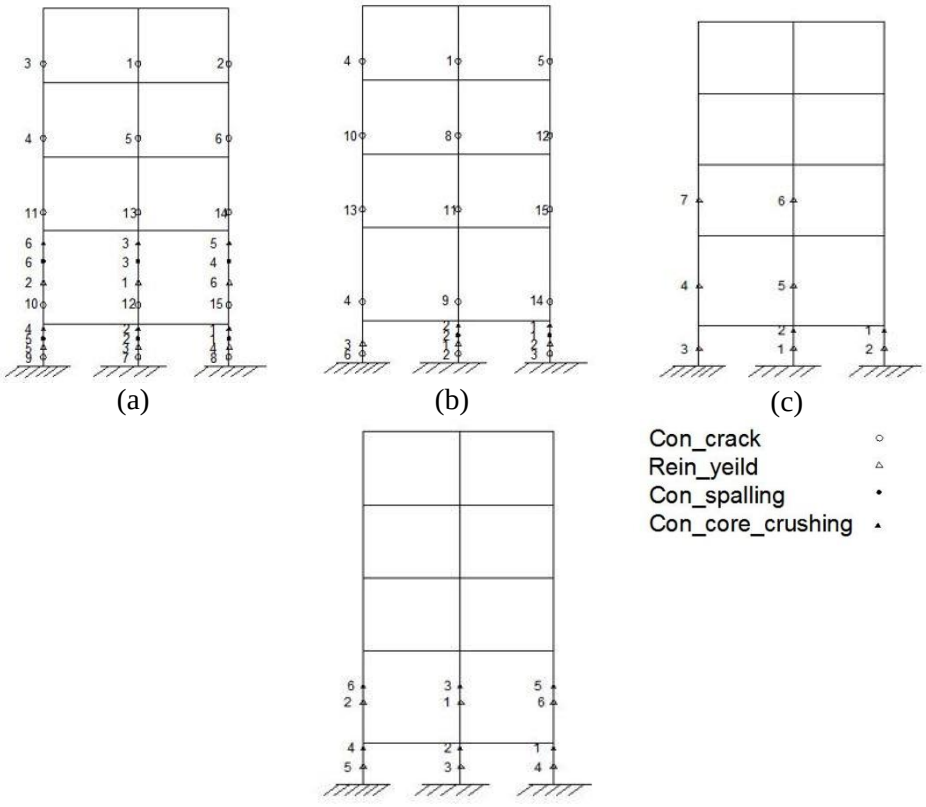

Figure 5: Damage state of the building frame for (a) Original Frame, (b) RC jacketed frame, (c) CFRP jacketed frame and (d) GFRP jacketed frame.

8 DYNAMIC TIME HISTORY ANALYSIS

Five earthquake ground motion data as described previously has been used for dynamic time history analyses. The performance of different retrofit scheme is observed in terms of top displacement and maximum interstory drift (%) demand.

The capacity of the building frame is obtained from the pushover analysis and their demand is obtained from the time history analysis. Maximum top displacement demand is observed from the displacement time histories as presented in Figure 6. Though the displacement demand for concrete jacketing was almost similar to the normal building frame but FRP wrapping significantly decreases the top displacement of the building.

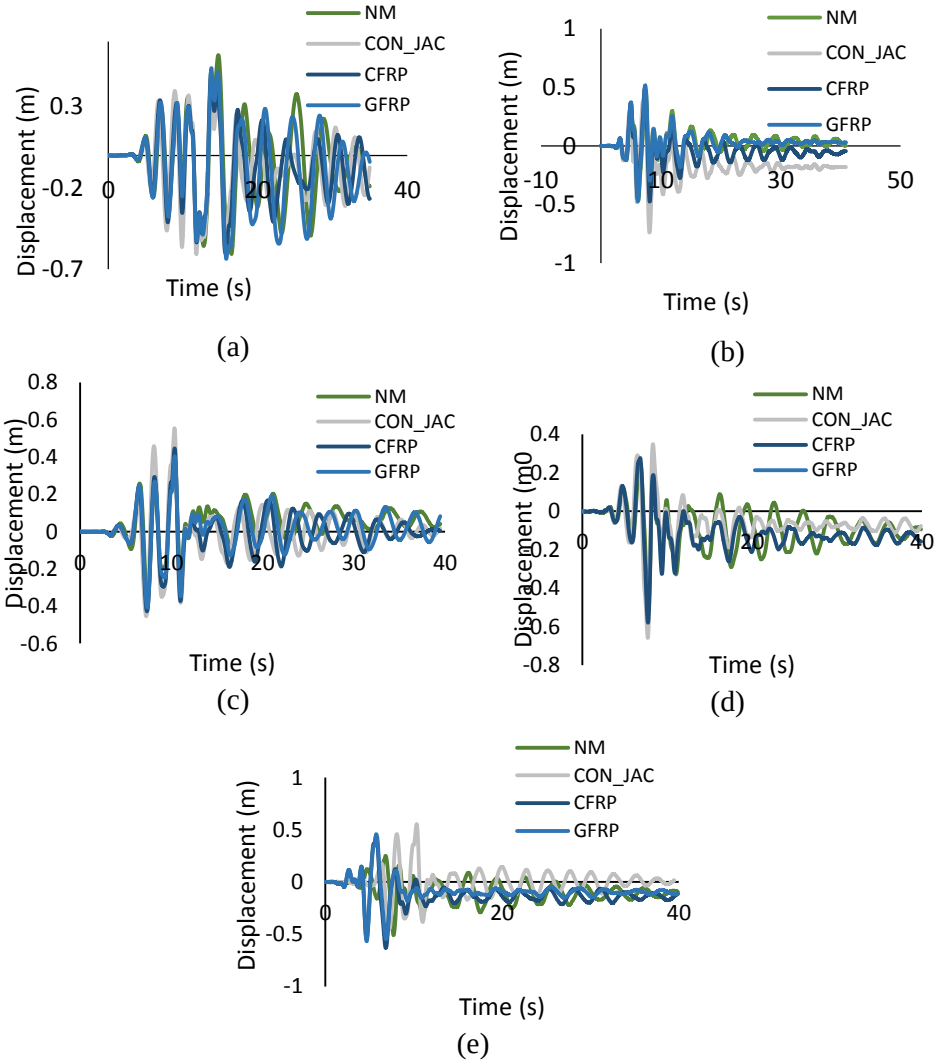

Figure 6: Displacement verses time curve for retrofitted sections under various ground motion (a) Kocaeli, (b) Kobe, (c) Imperia Valley, (d) Northridge and (e) Loma Prieta.

Maximum interstory drift of the building is shown in Figure 7 where it shows that interstory drift (%) is higher for both CFRP and GFRP jacketed frame sections. It is to be noted that the absolute interstory drift is considered for calculating the maximum value of drift demand. Drift demand of each floor is calculated individually and then the maximum of them is presented in the figure. Hence, the relative comparison of different retrofit scheme can't be made from the data available. But, the values can be attributed to the higher ductility of the retrofitted column section as obtained from pushover analysis. The improved ductility of the column enables them to undergo large displacement before collapse when subjected to different seismic loading.

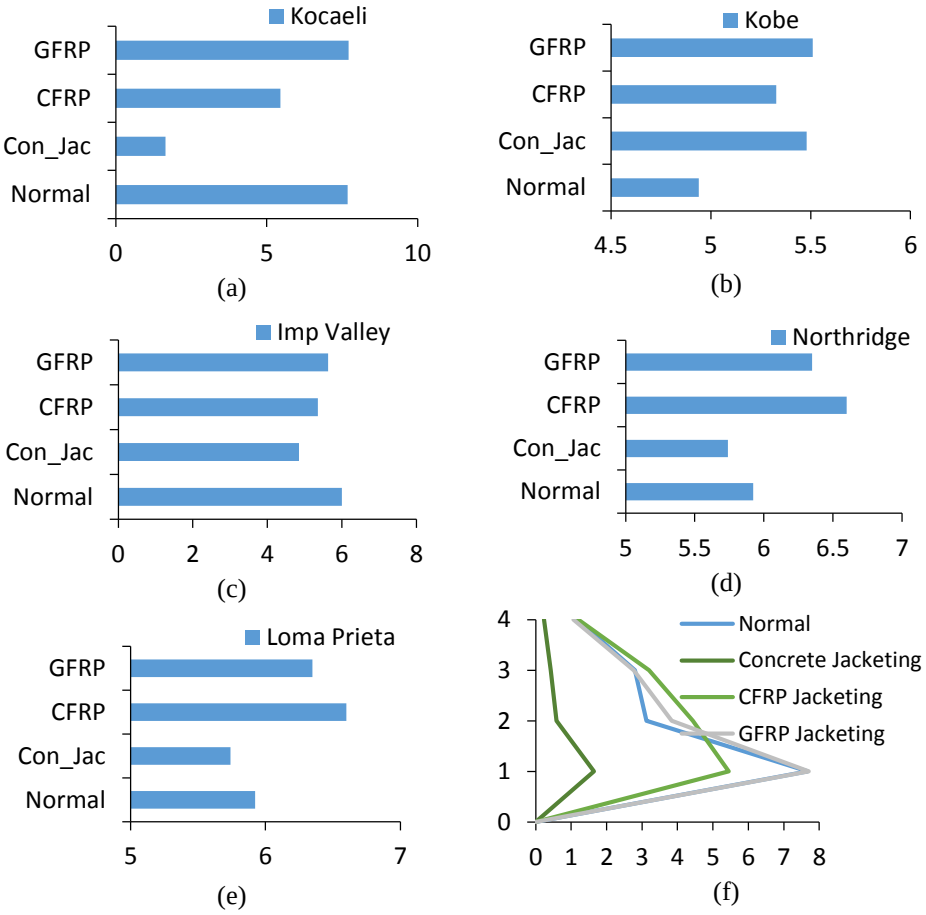

Figure 7: Maximum inter story drift of 4 storey RC frames for (a) Kocaeli, (b) Kobe (c) Imperia Valley, (d) Northridge, (e) Loma Prieta earthquake motion after incorporating Concrete Jacketing, CFRP Jacketing and GFRP Jacketing and (f) Interstory drift demand profile for the typical four storied building for Kocaeli earthquake.

9 CONCLUSION

In this study, the relative performance of different retrofit technique namely RC jacketing, CFRP and GFRP wrapping has been conducted. Result obtained from the pushover analysis of the building frame unveils the potentials of different retrofitting options for strengthening structural frame elements. Though the ductility of the concrete jacketed frame was relatively little less than the CFRP and GFRP retrofit scheme, but the capacity curve shows that concrete jacketing has the maximum base shear capacity with an inclination to brittle failure. On the other hand, damage state obtained from pushover analysis help us to conclude that the local failure of the frame element can be significantly reduced with CFRP and GFRP retrofitting techniques. Concrete jacketing also reduces the local failure but has less impact than the other two retrofitting methods. Also, the interstory drift demand profile show that concrete jacketing experiences almost similar drift as the normal building frame whereas, CFRP and GFRP shows enhanced interstory drift profile. Thus, the authors concluded that the most desired retrofit technique for strengthening vulnerable garment factory buildings is the FRP wrapping as both CFRP and GFRP shows better performance than the concrete jacketing.

REFERENCES

[1] Murtuz, A.K.M.G., Islam, K., Alam, M.S., Jalal, K.B., Priti, R.J. (2015). Performance Assessment of Existing RC Garment Manufacturing Factory Buildings: Case Study in the Context of Bangladesh. Proceedings of the First International Conference on Advances in Civil Infrastructure and Construction Materials, 14-15th December 2015, Dhaka, Bangladesh.

[2] Bangladesh Garment Manufacturers and Exporters Association (BGMEA)

[3] After Rana Plaza, A report into the readymade garment industry in Bangladesh. Bangladesh All Party Parliamentary Group, 2013.

[4] Manzur T and Noor M A. Displacement Based Fragility Curves for R.C.C. Frame Structures in Context of Dhaka, Bangladesh. Proceedings of the 6th Asia-Pacific Structural Engineering and Construction Conference (APSEC 2006), Kuala Lumpur, Malaysia, 5 – 6 September 2006.

[5] Pampanin, S., Bolognini, D., & Pavese, A. (2007). Performance-based seismic retrofit strategy for existing reinforced concrete frame systems using fiber-reinforced polymer composites. Journal of Composites for Construction, 11(2), 211-226.

[6] Eshghi, S., & Zanjanizadeh, V. (2008). Retrofit of slender square reinforced concrete columns with glass fiberreinforced polymer for seismic resistance.Iranian Journal of Science and Technology, Transaction B: Engineering,32(B5), 437-450.

[7] Yuksel, E., Ozkaynak, H., Buyukozturk, O., Yalcin, C., Dindar, A. A., Surmeli, M., & Tastan, D. (2010). Performance of alternative CFRP retrofitting schemes used in infilled RC frames. Construction and Building Materials, 24(4), 596-609.

[8] Cheung, M., Foo, S., & Granadino, J. (2000). Seismic retrofit of existing buildings: innovative alternatives. Public works and government services, Canada, 1-10.

[9] Rosignoli, D. A. R. I. O., Simonelli, F. R. A. N. C. E. S. C. A., Rosignoli, R., & Meda, A. (2012). High Performance Fiber Reinforced Concrete Jacketing in a Seismic Retrofitting Application. ICRI Bulletin-International Concrete Repair Institute, Illinois USA-Progetto, sperimentazione ed esecuzione per il rinforzo strutturale ed adeguamento sismico di edificio scolastico in Zagarolo (Roma).

[10] El-Amoury, T., & Ghobarah, A. (2005). Retrofit of RC frames using FRP jacketing or steel bracing. JSEE, 7(2), 83-94.

[11] Ismail, A. (2014). Non linear static analysis of a retrofitted reinforced concrete building. HBRC Journal, 10(1), 100-107.

[12] Pantelides, C. P., & Gergely, J. (2002). Carbon-fiber-reinforced polymer seismic retrofit of RC bridge bent: Design and in situ validation. Journal of Composites for Construction.

[13] Parghi, A., & Alam, M. S. (2015). Analysis of RC circular bridge columns retrofitted with fiber reinforced polymer under axial and lateral cyclic loading. Proceedings of CSCE 4th Annual Conference at Regina.

CICM 2015
First International Conference on
Advances in Civil Infrastructure and Construction Materials
MIST, Dhaka, Bangladesh, 14–15 December 2015

NUMERICAL INVESTIGATION ON INFLUENCES OF SLENDERNESS AND WRAPPING THICKNESS OF CFRP CONFINED CONCRETE CYLINDER

Shahana A. ESHA[1], **Sabreena Nasrin**[2] **and Zubayer I. Zahid**[3]

[1, 2, 3] Department of Civil Engineering, Ahsanullah University of Science and Technology, Dhaka, Bangladesh.
Email: [1]eshace6@gmail.com, [2]sabreena.ce@aust.edu and [3]zubayer061@gmail.com

Abstract. *External confinement of concrete cylinder with fiber reinforced polymer (FRP) sheets leads to significant improvements on the axial compressive behavior of concrete cylinders. While a comprehensive research has been conducted on the behavior of such strengthened cylinders, only a very limited amount of work has examined the slenderness effect in these cylinders. To cover up this deficiency, 3D finite element models have been developed to investigate the effect of slenderness of cylinders with varying wrap thickness under concentric load by using ABAQUS. Compressive stress and axial strain have been recorded to evaluate the stress-strain relationship, ultimate strength and ductility of the specimens. The result obtained from the simulation clearly demonstrates that composite wrapping can enhance the performance of cylinders in terms of both maximum strength and ductility. The use of CFRP wraps to allow slender columns to achieve higher strengths and to reduce lateral deflections is also demonstrated. The effects of test parameters are evidenced and compared.*

Keywords: Confinement, CFR, Axial behavior, Slenderness, Finite element model, Simulation.

1 INTRODUCTION

Recent evaluation in building construction of Bangladesh has demonstrated the need of strengthening of damaged structures. Several devastating incidents like collapse of residential building sand garments factories, cracks in bridge piers etc. have drawn the worldwide attention. So, it is a great concern to preserve and maintain those structures by strengthening and retrofitting. Compared to conventional retrofitting technique by steel materials, FRPs have many benefits like high strength to weight ratio of FRP composites which means these are very easy to handle on site and add very little weight to the structures, increase stiffness at service loads etc. In recent years, the use of fiber reinforced polymers (FRP) as an externally wrapping has achieved considerable popularity for the strengthening and repairing of concrete structures. This strengthening method is based on the phenomenon that the axial compressive strength and the strain of concrete can be substantially increased through the lateral confinement. This mechanism is easy to understand for concrete under uniform confinement in the case of circular column rather than rectangular columns. An abundance of test has established this fact on generally smaller scale specimens of unreinforced concrete cylinders [1, 2, 3, 4]. Several parameters influence the confinement effectiveness of the FRP wrap, which include concrete strength, wrap thickness or number of FRP layers, slenderness ratio etc. But, with increasing slenderness, slenderness effects can prohibit the column from attaining its maximum strength and the column may become susceptible to instability. Mirmiran et al. 2001 [5] tested ten concrete-filled fiber-reinforced polymer tubes (CFFTs) with the slenderness ratio L/D ranging from 2.1 to 18.6. The conclusion is that, when the slenderness ratio is increased from 5.5 to 18.6, the strength is dropped rapidly from about 75% of the equivalent short column to less than 30%. The influence of the slenderness and wrapping on the load carrying capacity of the column has been explained in Chaallal et al. (2006) [6]. The experiment has been conducted with varying column diameter while keeping the column length constant. But effect of slenderness with varying cylinder length keeping the diameter constant is not mentioned which is the point of interest of this study. This research is focused on the response of a 3D FE model of circular concrete cylinder confined with FRP subjected to concentric axial loading. The numerical simulation has been performed by using ABAQUS. The performance of the model has been studied by simulating experimental cylinder at Rahai et al. 2008 [4].After the validation, a parametric study has been conducted which includes slenderness and wrapping thickness.

2 FINITE ELEMENT ANALYSIS

A nonlinear FEA is performed using the general purpose FEA software ABAQUS (2010) for the simulation of CFRP-confined concrete specimens. The

models used to represent the axial behavior reported by Rahai et al. 2008 [4] have been integrated in the present FEA modeling.

2.1 Geometry

Circular concrete cylinders with a diameter (D) of 150 mm and a length (L) of 300 mm are initially considered; cylinders with other lengths are also considered in studying the effect of slenderness. In the case of CFRP, four different wrap thickness as one layer(T), two layer(TT), three layer (TTT)and four layer(TTTT) having corresponding thickness of 0.9, 1.8, 2.7, 3.6 mm with respect to the hoop direction are investigated. In this study, a 3D model of full concrete cylinder is developed for FE simulation. The 3D, eight-node linear element C3D8R in ABAQUS is utilized for modeling the both concrete and CFRP on the basis of mesh convergence study. The contact pair algorithm is used to define the bond between the concrete and the CFRP laminate to ensure no relative sliding between them.

2.2 Material Property

2.2.1Concrete

In this paper, the model used for concrete is the concrete damaged plasticity model. The concrete damaged plasticity model is suitable for the analysis of other quasi-brittle materials, such as rock, mortar and ceramics etc. Under low confining pressures, concrete behaves in a brittle manner; the main failure mechanisms are cracking in tension and crushing in compression. Here, the unconfined concrete model has a compressive strength f'_{co} of 40 MPa with a corresponding axial strain ε_{co} of 0.22 %.

2.2.2CFRP

The CFRP material is considered to be linear elastic isotropic until failure. Since the composite is unidirectional, it is obvious that the behavior is essentially orthotropic. When a composite is primarily stressed in the fiber direction, it is probable that the modulus in the fiber direction is the more important parameter. Hence, in the present studies an isotropic model was considered. The initial modulus in the fiber direction of the unidirectional CFRP material considered for the numerical simulation is 41000MPa [4]. The value of the Poisson's ratio is 0.28 and the rupture strain is taken up to 1.5% for the isotropic model.

2.3 Boundary Condition & Solution Strategy

The boundary conditions for cylinders are fixed at lower end. In order to extraction the force in the second analysis step more conveniently, the top surface nodes of the column is coupled with pre-set reference point and the

boundary condition of the top, displacement loading is applied to the reference point. The model is shown in Figure 1. Specimen is divided into four parts for better mesh quality.

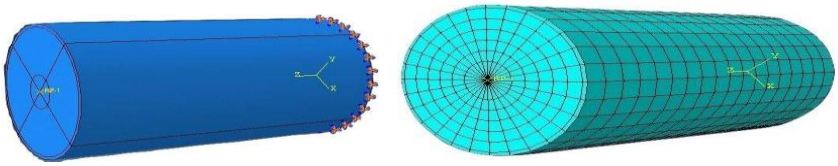

(a) (b)

Figure 1: FE Model with (a) Boundary Condition, (b) Mesh.

3 VALIDATION OF NUMERICAL MODEL

3.1 Ultimate Strength & Ultimate Strain

Unconfined concrete strength, f'_c reported in reference literature varies between 35 to 45MPa and the corresponding strain, ε_{co} varies between 0.2 to 0.25 %. The axial stress strain curves for the plain test specimens are presented in Figure 2(a). Among those the average f'_c of 40 MPa and ε_{co} of 0.22 percent were calculated. Axial stress-strain behavior of both numerically simulated and experimental unconfined concrete cylinder is shown in Figure 2(b).It shows f'_c is 39 MPa and ε_{co} is 0.18 which is very close to experimental results. This means this model can predict the experimental behavior of concrete cylinder.

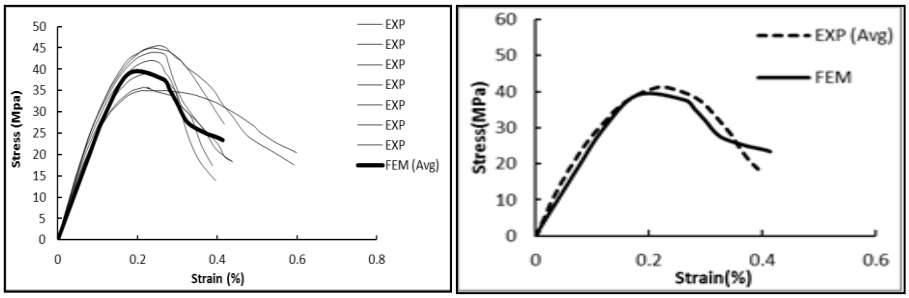

(a) (b)

Figure 2: (a) Stress-strain behavior of plain specimens (Rahai et al.), (b) Experimental and Numerical Axial Stress-Strain behavior of Unconfined Concrete Cylinder

Numerical and experimental typical axial stress-strain curves of the wrapped specimen with one layer of transverse orientation (T) are shown in figure 3(a). This shows that the experimental ultimate concrete strength, f'_{cc} is increased up to79MPa and ultimate strain of confined concrete, ε_{cc} is increased up to 0.62%.

Whereas, numerical f'_{cc} is increased up to 102MPa and ε_{cc} increased up to 1.39%. Figure 3(b) shows that, f'_{cc} for two layer wrapped specimen (TT) is increased up to 91.9MPa whereas FEM model strength increases up to 116.64MPa.The corresponding ε_{cc} for both experimental and numerical results are 0.96 and 1.29. From figure 3(c), for three layer wrapped specimen (TTT), f'_{cc} for both experimental and numerical model are 125.4 and 139.62MPa respectively. Corresponding ε_{cc} are 1.32 and 1.45%. The model predicts that its strength has been increased by 1.11times than experimental specimen. From figure 3(d), f'_{cc} of four layer wrapped specimen (TTTT) for both experimental and numerical model are 132.23 and 139.89MPa respectively. The corresponding ε_{cc} are 1.49 and 1.5%. The model predicts that its strength has been increased by 1.05 times than experimental.

The confined specimen model depicts that up to unconfined strength both wrapped and unwrapped specimens show almost the same behavior. This indicates that up to this level CFRP is ineffective. However, after reaching the unconfined strength, stress-strain curves became downward due to tension stiffening and then forms upward which means CFRP starts to be effective.

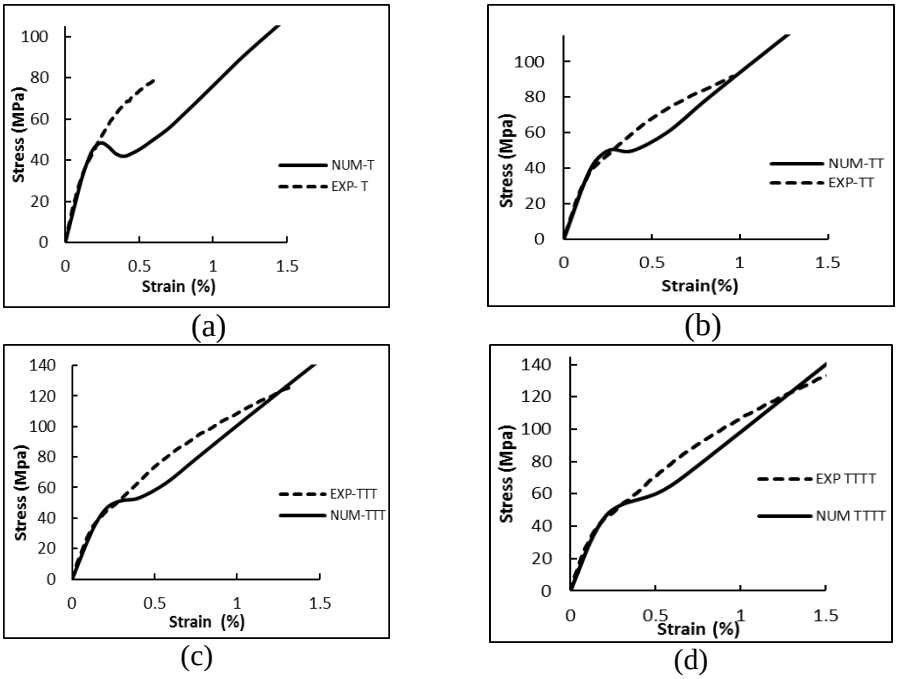

Figure 3: Axial Stress-Strain behavior of (a) one layer,(b) two layer, (c) three layer, (d) four layer wrapped specimen in hoop direction.

3.2 Results

The numerical results of four cylinder test specimen along with their experimental responses are shown in Table 1. For specimen T, the numerical analysis does not predict the experimental behavior well as in this case, numerical strain is much more than the experimental strain which could be the effect of very low wrapping thickness. Specimen TT, TTT, TTTT predicts the experimental behavior too closely. For the four models ratio of experimental to numerical ultimate strengths varies from 0.77to 0.95. The mean value of ultimate strength ratio is 0.85 with a standard deviation of 0.07, which means the quite good performance of finite element model predicting ultimate strength capacity. However, the mean ratio of the experimental to numerical average axial strain is 0.77 with a standard deviation 0.21. This relatively high value of standard deviation results is from the difference between the numerical and experimental strains for specimens T.

Table 1: Comparison of Numerical and Experimental Results of Concrete Cylinders

Specimen Designation	Ultimate Strength		σ_{exp}/σ_{nu} m	Ultimate Strain		$\varepsilon_{exp}/\varepsilon_{nu}$ m
	$\sigma_{numerical}$ (MPa)	$\sigma_{experimental}$ (MPa)		$\varepsilon_{numerical}$ (%)	$\varepsilon_{experimental}$ (%)	
T	102	79	0.77	1.39	0.62	0.43
TT	116.64	91.8	0.79	1.29	0.96	0.74
TTT	139.62	125.4	0.89	1.45	1.32	0.91
TTTT	139.89	132.23	0.95	1.5	1.49	0.99
Mean			0.85			.77
SD			0.07			.21

4 PARAMETRIC STUDY

The global stability of the cylinder is controlled by the overall slenderness ratio, which is defined as the ratio of the length of the cylinder, l, to radius of gyration of the cylinder, r_g. Three different slenderness ratios 8, 10 and 15 are employed in the parametric study to cover the range of short, intermediate and slender cylinders having same diameter of 150mm and different lengths 300mm, 375mm and 563mm respectively. These three types of cylinders, wrapped with two layers (1.8mm) and four layers (3.6mm) are then investigated with respect to confined to unconfined concrete strength ratio. Parameters were combined in a systematic

way to obtain their effect and interrelationships. Table 2 presents the resulting confined to unconfined stress ratio in terms of specimen parameters.

Table 2: Details of cylinders for parametric study

Cylinder Designation	Diameter (mm)	Length (mm)	Layer No	f'c	f'cc	f'cc/f'c
1	150	300	2	40	116.64	2.92
2	150	300	4	40	139.89	3.49
3	150	375	2	40	137.03	3.42
4	150	375	4	40	173.79	4.34
5	150	563	2	40	132.57	3.31
6	150	563	4	40	167.3	4.18

The result shows that increase in wrapping thickness associated with slenderness ratio up-to critical length increases ultimate stress (Figure 4). 17.5% to 24.2% ultimate stress increases for cylinders with slenderness 10 with respect to cylinders with slenderness 8. But further increasing the slenderness, ultimate stress starts to reduce and wrapping seems to be having no effect. Therefore, with two and four layer wrapping, the increase of slenderness at 15, results in decrease of the confined strength from 3.3% to 3.7% with respect to cylinders with slenderness 10. Increasing the wrapping layer results considerable increase in confined strength up to 3 to 4.5 times of unconfined strength.

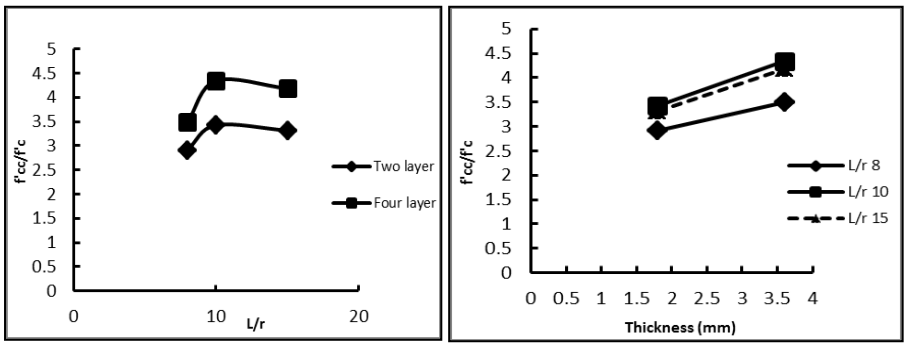

(a) (b)

Figure 4: (a) Confined to unconfined concrete strength versus L/R, (b) Confined to unconfined concrete strength ratio versus Thickness.

5 CONCLUSIONS

- In this study Finite element models were developed to investigate the axial behavior, slenderness and wrapping effect of CFRP wrapped cylinders

subjected to concentric loading. An experimental study on CFRP-wrapped cylinders in the literature was employed to validate the numerical analysis.

- The average experimental to numerical ratios of the ultimate strength was 0.85 with standard deviation of 0.07. The numerical stress versus axial strain responses for the models was in very good agreement with the experimental responses with only a few exceptions. However, the mean ratio of the experimental to numerical average axial strain was 0.77 with a standard deviation of 0.21. This relatively high value of standard deviation results from the difference between the numerical and experimental strains for first specimen.
- Based on the parametric analysis using the finite element modeling, the following conclusions can be drawn. Slenderness has a significant effect on the strength and stiffness of the cylinders. Increasing slenderness up to critical length can increase strength of cylinders and beyond the critical length strengths will be decreased. When the slenderness increases from 8to 10, stress increases from 2.92 to 4.34 times of unconfined stress. At slenderness 15, confined stress reduces from 3.3% to 3.7% of cylinders with respect to slenderness 10.
- The effect of wrapping thickness can be observed well in short and intermediate cylinder having slenderness 8 and 10 respectively. Increasing the wrap thickness can increase the strength approximately 3 to 4.5 times of unconfined cylinders.

REFERENCES

[1] Mirmiran, A., Shahawy, M., Samaan, M., and El Echary, H. (1998). "Effect of column parameters on FRP-confined concrete." *J. Compos.Constr., 24, 175–185.*

[2] Xiao, Y., and Wu, H. 2000. "Compressive behavior of concrete confined by carbon fiber jackets." *J. Mater. Civ. Eng., 122, 139–146.*

[3] Teng, J. G., and Jiang, T. (2008). "Strengthening of reinforced concrete(RC) columns with fibre-reinforced polymer (FRP) composites." *Strengthening and rehabilitation of civil infrastructures using fibrereinforced polymer (FRP) composites*, L. C. Hollaway and J. G. Teng, eds., Woodhead, Cambridge, U.K., Chap. 6.

[4] Rahai, A.R., Sadeghian, P., Ehsani, M.R., (2008). "Experimental Behavior of Concrete Cylinders Confined with CFRP Composites".*The 14th World Conference on Earthquake Engineering*. October 12-17, 2008, Beijing, China.

[5] Mirmiran A, Shahawy M, Beitleman T. Slenderness limit for hybridFRP-concrete columns. *J Compos Const* 2001;5(1):26–34.

[6] Chaallal, O.; Hassan, M.; LeBlanc, M; (2006). "Circular Columns Confined with FRP: Experimental versus Predictions of Models and Guidelines". *J.Compos. Constr., ASCE, ISSN, Vol.10, No.1*, 1090-0268.

CICM 2015
First International Conference on
Advances in Civil Infrastructure and Construction Materials
MIST, Dhaka, Bangladesh, 14–15December 2015

DETECTION OF FOUNDATION OF SOME BUILDINGS OF BUET USING ELECTRICAL RESISTIVITY TOMOGRAPHY (ERT)

B.S. P. BISWAS[1], A. Khair[2] and M.A. Ansary[3]

[1, 2] Bangladesh Network Office for Urban Safety, Bangladesh University of Engineering and Technology, Dhaka, Bangladesh.
Email: [1]akhairce08@gmail.com and [2]pushpendue.biswas@gmail.com

[3] Department of Civil Engineering And Director of Bangladesh Network Office for Urban Safety, Bangladesh University of Engineering and Technology, Dhaka, Bangladesh.
Email: ansary@ce.buet.ac.bd

Abstract. *The paper presents the application of non-pervasive Electrical Resistance Tomography (ERT) subsurface imaging surveys for the detection of foundation of three buildings of BUET, Dhaka, to assess the cross-section of the foundation and also to check the deviation of the constructed foundation structure with the designed foundation structure. The use of several high-resolution geoelectrical methods derived from the field survey techniques proved to be very effective in the Non-Destructive Testing and survey of subsurface structure. The ERT method was under-taken with several different electrode spacing. Wenner–Schlumberger array was used as electrode arrays. Primary data were processed through a 2-D inverse method, using the program RES2DINV by creating a pseudo-section of the apparent resistivity values and then two-dimensional (2-D) resistivity contour maps were created. In particular the application of a tomographical approach allowed in obtaining subsurface images of the sections of the foundation structures that clearly shows the actual exiting scenario of the building foundation.*

Keywords: Electrical resistivity tomography (ERT), Iterations, Non-destructive testing, Pseudo-section, RES2DINV.

1 INTRODUCTION

The application of geophysics to subsurface investigation dates back to the early 1950s. The rapidly evolving technology over the past 20 years has made the geophysical approach a reliable investigative and survey tools. Geophysical prospecting allows the physical parameters of the subsoil to be mapped in large-scale reconnaissance surveys. In specific cases, it can provide useful information on the depth and shape of buried structures. One of the most commonly applied techniques of geophysical surveying is the electrical resistivity tomography (ERT) that provides the measurement of the specific electrical resistance of soil [1, 2].

The objectives of the study were to assess the cross-section of the foundation of the three different buildings of the study area and to assess the deviation of the constructed foundation structure with the designed foundation structure. The methodology of the work was first to collect the data using the Electrical Resistivity Tomography (ERT) and then analyzing the collected data using the software RES2DINV and then interpreting the analyzed results.

2 LITERATURE REVIEW

Electrical resistivity is known to be highly variable among other physical properties of rock. In some cases, different in extreme values of a single rock type can differ by a factor approaching several orders of magnitude. Wide range of rock's resistivity parameter has always been the reason that makes it difficult to distinguish subsurface rock type if no information on the geological surroundings of field survey is available. Electrical current flows through the earth material under subsurface through two methods, which are electrolytic and electronic conduction [3].

For 2D resistivity imaging, it is important to have a large set of data recorded along a survey line to effectively map the complex resistivity distribution of subsurface structure. The most practical way to acquire such large amount of data is by using automated multi-electrode data acquisition system. In the interpretation of ground resistivity survey, it is important to differentiate between apparent resistivity and true resistivity. Apparent resistivity can be defined as the volumetric average of a heterogeneous half-space, except that the averaging is not done arithmetically but by a complex weighing function dependent on electrode's configurations [4].

The electrical resistivity method allows the calculation of the resistivity present in soil. The calculation of resistivity makes it possible to obtain information about the subsoil nature and structure. Applying a potential difference (ΔV) to the two poles of a conductor, in it will pass a current of intensity (I) which is related to the potential difference from Ohm's law:

$$R = \frac{\Delta V}{I} \qquad (1)$$

Where,

R= electrical resistance that depends on the nature and geometric characteristics of the conductor.
ΔV = difference of potential measured between M and N [V]
I = current injected into soil [A]
For each acquisition performed in the selected spreading, the following formula is generally applied:

$$\rho = (\frac{\Delta V}{I})K \qquad (2)$$

Where,

ρ = apparent resistivity [Ω m]
ΔV = difference of potential measured between M and N [V]
I = current injected into soil [A]
K = geometric coefficient related to the sounding being used

2.1 Electrode Array

Common array types are: (i) Wenner array: Is an attractive choice for a survey carried out in a noisy area (due to its high signal strength) and also if good vertical resolution is required; (ii) Wenner-Schlumberger array: Might be a more suitable choice if good horizontal resolution and data coverage is important; (iii) Dipole-dipole array: Is an all-round alternative if both good horizontal & vertical resolutions are needed, particularly if good signal strength is also required; (iv) Pole-dipole: It is an alternative to the dipole-dipole for IP surveys; and (v) Multiple gradient array: Relatively new array developed primarily for multi-channel resistivity meter systems. In the multiple gradient arrays, different sets of measurements are made with the potential electrodes at different locations for the same current electrodes [5].

2.2 The Software RES2DINV

RES2DINV is a computer program that will automatically determine a two-dimensional (2-D) resistivity model for the subsurface for the data obtained from electrical imaging surveys [6]. This program is designed to invert large data sets (with about 200 to 21000 data points) collected with a system with a large number of electrodes (about 25 to 16000 electrodes). The 2-D model used by the inversion program which consists of a number of rectangular blocks. A forward modeling subroutine was used to calculate the apparent resistivity values, and a non-linear least-squares optimization technique is used for the inversion routine [7, 8].

3 METHODOLOGY OF THE STUDY

The research has been conducted with the following methodology:

3.1 Study Area

Three different buildings of Bangladesh University of Engineering and Technology (BUET) were selected as the study area. Figure 1 (a), 1(b), 1(c) shows the points (red star marked) of the study area of Dhaka city and Figure 2 (a), 2(b), 2(c) shows the study buildings.

Figure 1(a): Map of Bangladesh

Figure 1(b): Map of Dhaka City

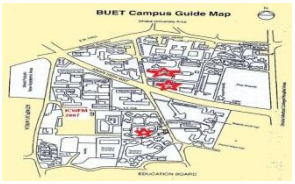

Figure 1(c): Map of BUET

Figure 2(a): Civil Engineering Building

Figure 2(b): Mechanical Engineering Building

Figure 2(c): Staff Quarter Building (No. 17)

Table1 shows the Geological and Geomorphological classification of the study area.

Table 1: List of the study buildings of BUET Campus

Sl. no	Date	Name of the point of study area	Location		City
			Latitude	Longitude	
01	05/09/2015	Civil Engineering Building, BUET	23° 43' 19" N	90° 23' 48" E	Dhaka
02	13/09/2015	Mechanical Engineering Building	23° 43' 20" N	90° 23' 47" E	Dhaka
03	14/10/2015	Staff Quater Building (No. 17), BUET	23° 42' 24" N	90° 23' 53" E	Dhaka

3.2 Data Collection

The Electrical Resistivity Tomography data have been gathered through electrodes of length equal to 50 cm, partially driven into the ground. The electrodes were then connected through multichannel cables, adopting the Wenner-Schlumberger array configuration. The details of the data collection of the points are given below:

1) Civil Engineering Building, BUET: 32 electrodes were used with electrodes saping 1 m.
2) Mechanical Engineering Building: 32 electrodes were used with electrodes saping 1 m.
3) Staff Quarter Building (No. 17): 16 electrodes were used with electrodes saping 1 m.

3.3 Data Processing and Analysis

The data collected from the survey have been analyzed with the software RES2DINV. RES2DINV is a computer program that automatically determined a two-dimensional (2-D) resistivity model of the subsurface for the data obtained from electrical imaging surveys.

4 RESULTS AND ANALYSIS

Primary data were processed through a 2-D inverse method, using the program Res2DInv. The presented figures are the results of smoothness-constrained inversion; these outputs best fit the situation observed in the sites. The validity of these results is supported by the low RMS error.

Table 2: Reference resistivity values table of various materials

Types of soil or water	Typical Resistivity (Ωm)	Usual limit (Ωm)
Sea water	2	0.1-10
clay	40	8-70
Ground well and spring water	50	10-150
Clay and sand mixtures	100	4-300
Shale, Slate, Sandstone etc.	120	10-100
Peat, Loam and Mud	150	5-250
Lake and brook water	250	100-400
Sand	2000	200-3000
Moraine gravel	3000	40-10000
Ridge gravel	15000	30-30000
Solid granite	25000	10000-50000
Ice	100000	10000-100000

4.1 Civil Engineering Building, BUET

Foundation of three columns (C1, C2, C3) of Civil Engineering Building, BUET were selected for the study and the present and past scenario has shown in the Table 3. Figure 3 shows the model resistivity of ERT at Civil Engineering Building, BUET.

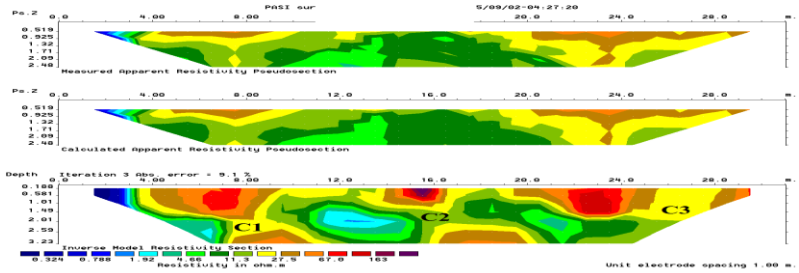

Figure 3: Model resistivity of ERT of Civil Engineering Building, BUET

Table 3: Electrical Resistivity Tomography (ERT) result of Civil Engineering Building, BUET

	Section of Footing Foundation		Resistivity Ranges (Ω m)
	ERT Results Section (Length x Depth) (in meter)	Actual Designed Constructed Section (Length X Width X Depth) (in meter)	
C1	1.6 X 1.45	1.83 X 1.83 X 1.5	67-150
C2	1.5 X 1.3		67-200
C3	1.8 X 1.5		67-163

4.2 Mechanical Engineering Building, BUET

Foundation of five columns (C1, C2, C3, C4, C5) of Mechanical Engineering Building, BUET were selected for the study and the present and past scenario has shown in the Table 4. Figure 4 shows the model resistivity of ERT at Mechanical Engineering Building, BUET.

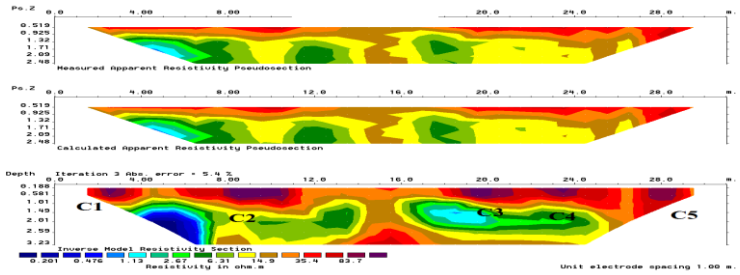

Figure 4: Model resistivity of ERT of Mechanical Engineering Building, BUET

Table 4: Electrical Resistivity Tomography (ERT) result of Mechanical Engineering Building, BUET

	Section of Footing Foundation		ResistivityRanges (Ω m)
	ERT Results Section (Length x Depth) (m)	Actual Designed Constructed Section (Length X Width X Depth) (m)	
C1	2.0 X 1.3	2.5 X 2.5 X 1.5	83.7-150
C2	2.4 X 1.4		83.7-185
C3	2.1 X 1.3		83.7-185
C4	2.0 X 1.3		83.7-185
C5	2.0 X 1.4		83.7-185

4.3 Staff Quarter Building (no.17), BUET

The Staff Quarter Building (No.17), BUET was selected for the study of masonry structure foundation and the present and past scenario has shown in the Table 5.Figure 5 shows the model resistivity of ERT Staff Quarter Building (No.17), BUET.

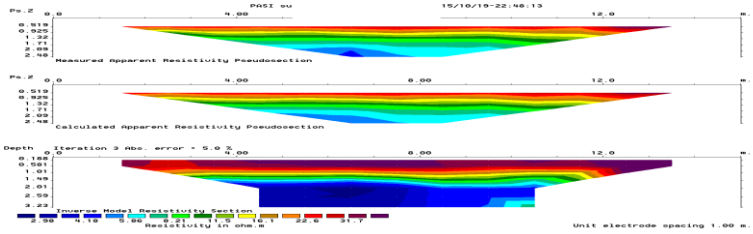

Figure 5: Model resistivity of ERT Staff Quater Building (No.17), BUET.

Table 5: Electrical Resistivity Tomography (ERT) result of Staff Quarter Building (No.17), BUET

Masonary Load BearingFoundation		ResistivityRanges (Ω m)
ERT Results (Depth, m)	Designed Constructed Depth (m)	
1.40 m	1.5 m	27-60

5 CONCLUSION

The foundations were observed from the traverse have found very much similar to the designed constructed values. In the case of Civil Engineering Building, BUET the constructed section of the foundation has a much more deviation compared to the required design where as the constructed section of the Mechanical

Engineering Building, BUET and The Staff Quarter Building (No.17), BUET shows very little deviation from the required design. The result of the investigation is therefore recommended as a useful guide for civil engineering Non-Destructive investigation of foundation structure.

6 LIMITATIONS

Though it was not possible to cover all the sides required to represent a complete section of a footing as those sides are inside of the building that's why partial section information's have represented. To overcome the problem, more research is needed to clarify the suitable data collection array method and to create more spaces for the spread of cables and electrodes and if it is not possible then the ERT is not the suitable technique for that specific site. For the testing of ERT, open space is of major issue for the spread of the electric cables. ERT is not very suitable for the soil whose surface is not pure soil i.e., if its surface layer is filled with construction and other solid rubbish in several feet's. Another major fundamental issue is, if the top soil is sand fill and very much dry then it creates real difficulties to ERT investigations.

REFERENCES

[1] Mol, L., P. Preston, 2010. The writing's in the wall: A review of new preliminary applications of electrical resistivity tomo-graphy within archaeology. Archaeometry, 52(6): 1079-1095.

[2] Tsourlos, P.I., G.N. Tsokas, 2011. Non-destructive Electrical Resistivity Tomography Survey at the South Walls of the Acropolis of Athens, Archaeol. Prospect, 18: 173-186.

[3] Loke, M.H. Tutorial, "2-D and 3-D electrical imaging surveys" (2004), pp. 13

[4] Dahlin, T. "The development of DC resistivity imaging techniques" Computer & Geosciences 27 (2001), pp. 1019 – 1029

[5] PASI Geophysics, "Geotechnical Resistivity Methods" (2010)

[6] Griffiths D.H. and Barker R.D., 1993, "Two-dimensional resistivity imaging and modelling in areas of complex geology," Journal of Applied Geophysics, 29, 211-226

[7] deGroot-Hedlin, C. and Constable, S., 1990, "Occam's inversion to generate smooth, two-dimensional models form magnetotelluric data," Geophysics, 55, 1613-1624.

[8] Loke M.H. and Barker R.D., 1996, "Rapid least-squares inversion of apparent resistivity pseudo-sections using a quasi-Newton method," Geophysical Prospecting, 44, 131-152

CICM 2015
First International Conference on
Advances in Civil Infrastructure and Construction Materials
MIST, Dhaka, Bangladesh, 14–15 December 2015

BONDING BETWEEN OLD AND NEW CONCRETE IN CONCRETE JACKETING

Md. M. H. CHOWDHURY[1], Khondaker S. Ahmed[2], MD. Moniruzzaman[3], Habibur R. Kamal[4], Washi B. W. Onnesha[5]

[1, 2, 4, 5] Department of Civil Engineering, Military Institute of Science and Technology, Dhaka, Bangladesh.Email:[1]hafizchowdhury40@gmail.com, [2]sakil0104@gmail.com, [4]hrkamal@gmail.com, [5]nesha11111@gmail.com

[3] ECLECTIC, Dhaka, Bangladesh.
Email: moniruzzaman@eclecticbd.com

Abstract. *Retrofitting of existing concrete structures has become an important issue nowadays in the construction industry. It is needed especially when a member is unable to take any loads or caused serious damage due to various reasons. In such situations, the remedy is either to demolish the existing structure and construct a new one or to retrofit the existing structure by an appropriate strengthening methodology. As Bangladesh is densely populated country and maximum buildings constructed here are without appropriate building code, so demolishing those structure are beyond imagination, that's why re-strengthening those structure are much more feasible and economical. Due to this reason Retrofitting has become very popular in Bangladesh. In this experiment we have emphasized on the connection between old and new concrete. 7 cores have been jacketed with 1.5 inch thickness of concrete and cured for 28 days. An adhesive (Nitobond SBR) has been applied on the outer surface of the core so that there is a strong bondage between old concrete and new concrete. The main purpose of this experiment is to see weather old and new concrete fail or not. The interface between concretes must assure enough shear strength as a main requirement to resist the applied actions on the structure. In this experiment a sufficient connection of concrete between contact surfaces, pattern of failure mode, and performance of a retrofitted member as a "composite" element are presented.*

Keywords: Retrofitting, interface between concretes, composite elements, bondage between old concrete and new concrete.

1 INTRODUCTION

Geographically Bangladesh is in active Earthquake zone. Bangladesh is located close to the boundary of two active plates: the Indian plate in the West and the Eurasian plate in the East and North. As a result the country is always under a potential threat to earthquake at any magnitude at any time, which might cause catastrophic death tolls in less than a minute. The recent Earthquake held in Nepal has really made a strong alarm to the Engineers. In Bangladesh old buildings are more vulnerable to Earthquake rather than new building. The buildings which were constructed before the publishing of BNBC 1993 lack the seismic provision. Those building were not constructed according to the building code. In recent years lots of Earthquake had hit our country, due to this lot of building has been damaged that's why to prevent disaster in future earthquakes the existing deficient buildings need to be strengthened and the most economical solution is retrofitting. After the incident of RANA plaza many owners have taken initiatives to retrofit their garments or buildings but the seismic strengthening normally focuses on vertical extension (Column and Walls). Strengthening of beams is usually considered as a second priority, since the structural integrity is mainly affected by the capacity of the vertical elements. There are different ways to retrofit a column but in our country concrete jacketing is the most popular method. Concrete jacketing involves placing an additional layer of concrete covering the existing column together with additional longitudinal bars. The main purpose of concrete jacketing is to increase column's ductility, shear capacity and bending capacity. It has been proved by many engineers that concrete jacketing increases column's axial load carrying capacity and it alleviates problem caused by inadequate lap splice length. Though new concrete layers are placed but there are still some unsolved issues like bonding between old and new concrete, whether they truly behave like a composite element or not and etc. Bonding between old concrete and new concrete is not guaranteed because of some uncertainties. Yet proper surface preparation, material choice, curing etc. should be ensured. However, the shear stress transfer mechanism between two concrete layers is a complex phenomenon that involves the combination of different interactions and depends on several parameters that influence the transmission process, such as the amount of reinforcement crossing the interface, the compression resistance of the weaker concrete, the roughness of the interface, the presence of cracking or the stress caused by normal forces across the interface. It is rarely possible to see/prove whether old concrete and new concrete ina retrofitted column really bonded together or really transmit shear stress as a composite element. That's why in this experiment we have retrofitted cores with concrete and shown the failure pattern and performance of the retrofitted element.

2 EXPERIMENT AND TEST SETUP

For this experiment we have collected 8 cores from different garments industries. In this experiment, cores have been jacketed by concrete and then cured for 28 days. Diameter of the core was 3 inch and its height was 6 inch. The experiment was conducted in two phase. In 1st phase, 3 cores had been jacketed and in 2nd phase, 4 cores had been jacketed. The diameter and height of the jacketed cores were 6 inch and 8 inch respectively.

Figure 1: Cores

Figure 2: Jacketed cores

The mix design ratio of concrete for 1st phase was 1:3:5 and aggregate size was 12mm downgraded. We used Sylhet sand as our fine aggregade. Details of the materials have been listed below.

Table 1: List of tests performed during the experiment

Fineness modulus of Fine aggregade	2.67
Absorbtion capacity of course aggregade	0.05%
Absorbtion capacity of fine aggregade	0.5%
P_H of Water	7.4
Temperature of water	28.7 Deg Celsius
Course aggregade size	12mm downgraded
Water/cement ratio	0.5

Before the experiment starts the outer surface of the cores were placed in water for 10 minutes, to make a better connection with new concrete. 6x12 inch cyl-

inders were used for this experiment. Initially 2 inch layer of concrete was placed in the bottom of the cylinder then the cores were placed in the center position of the cylinder after that concrete was placed until the height of the cylinder gets to 10 inch. Cement grout has been used on outer surface of the cores to make better connection with new concrete. Though cement grout has not been considered as adhesive.

Figure 3: Concrete casting

In the 2nd phase we have jacketed 4 cores but this time our mix design ratio was 1:1.5:3. Course aggregate size was 10 mm downgraded and Sylhet sand has been used as fine aggregate. W/C ration was kept to 0.5. Before the start of experiment we have roughened the cores with chisel and steel brash and then placed in the water for 10 minutes so that the connection between core and new concrete gets strong. The procedure was same like the 1st phase but this time we used NITOBOND SBR as an adhesive. As the adhesive was liquid so we place that liquid adhesive to the outer surface of the core by a brush and the placed immediately at the middle of the cylinder above 2 inch of concrete and then poured concrete until it gets to 10 inch height. After casting concrete it was dried for 24 hours and then cured for 28 days.

After 28 days of curing, we dried the jacketed cores for 24 hours and then we cut the additional layer of 2 inch concrete by concrete cutting machine. After that we crushed the jacketed cores by concrete crushing machine

Figure 4: Placing the core at the center of cylinder

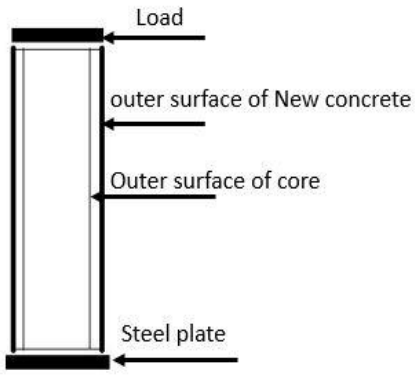

Figure 5: Elevation view of jacketed core

Figure 6: Crushing concrete in concrete testing machine

3 TEST RESULT

In our 1st phase of experiment, after crushing the jacketed core it has been observed that the old concrete (core) and new concrete didn't failed together, all the loads were taken by new concrete, core didn't take any load. It happened because of the plain outer surface and adhesive was not used. So combined failure didn't occur. In the 2nd phase of our experiment we found that the Old concrete and new concrete failed together. Both core and new concrete has taken same amount of loads, so from this point of view it can be said that the specimen with roughened surface and with the application of adhesive on the outer surface will fail combined.

Figure 7: Combine failure didn't occur

Figure 8: Combine failure occured

Table 2: Max load and Stresses of different specimen

Series	Surface preparation	Pace rate	stress		Max load	
core	plain	2.3 KN/sec	1589.613 psi		41 KN	
Jacketed core with-out adhe-sive	plain	2.3 KN/sec	Sample 1	4329.7 psi	Sample 1	541.9 KN
			Sample 2	3461.15 psi	Sample 2	433.1 KN
			Sample 3	3964.3 psi	Sample 3	496.1 KN
Jacketed core with adhesive	Rough	2.3 KN/sec	Sample 1	4406.246 psi	Sample 1	536.9 KN
			Sample 2	4720.978 psi	Sample 2	575.2 KN
			Sample 3	3994.339 psi	Sample 3	486.7 KN
			Sample 4	4388.841 psi	Sample 4	534.8 KN

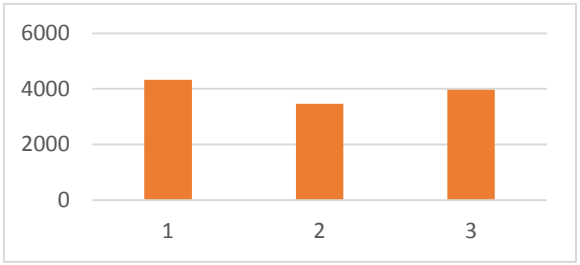

Figure-9: Failure stress of specimens in 1st phase of experiment (without adhesive)

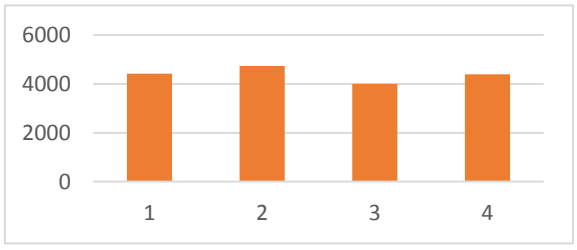

Figure-10: Failure stress of specimens in 2nd phase of experiment (with adhesive)

From the table and the charts we can observe that, the failure stress of normal core was 1589.613 psi only but after jacketing its strength goes over 4000 psi in some cases so it proves that jacketing increases the strength of the core. Though the failure stresses and maximum loads of jacketed core without adhesive and jacketed core with adhesive may be close but the main reason for combined failure was because of the rough surface and the adhesive (Nitobond SBR). Because of the rough surface and the use of adhesive in the 2nd phase of experiment the shear force has transferred properly between the outer surface of core and inner surface of new concrete. From this experiment we can say that if a column is jacketed by new concrete and if the surface is roughed enough and appropriate adhesive is used then both old and new concrete will work as a single element.

4 CONCLUSION

Strengthening or retrofitting columns by the addition of reinforced concrete layers or jackets are normal construction practices in many earthquake prone countries. However, there are many unresolved issues regarding the capacity of the strengthened elements. Engineering judgment is often necessary to solve these unresolved issues. The present study has investigated the bonding between old concrete and new concrete. To the end of this experiment the following observation can illustrated below

- Concrete with smaller course aggregate particle size (10 mm downgraded) are suitable for jacketing
- The core with roughened surface bonded stronger and performed better than core with planer surface.
- Roughening the surface with chisel and steel brush gave better rough surface
- Jacketed cores strength was almost 3 times stronger than normal core
- The adhesive (Nitobond SBR) made stronger connection between old concrete and new concrete.

ACKNOWLEDGEMENT

The author would like to thank ECLECTIC firm for their support and contribution.

REFERENCES

[1] G. Kaliyaperumal, A. K. Sengupta, 2009. Seismic retrofit of columns in buildings for flexure using concrete jacket. ISET Journal of Earthquake Technology, Paper No. 505, Vol. 46 (2), pp. 77–107.

[2] S. E. Dritsos, 2007. Seismic strengthening of columns by adding new concrete. Bulletin of the New Zealand Society for Earthquake Engineering, Vol. 40 (2), June 2007. pp. 49-68.

[3] Y.H. Chai, M.J.N. Priestley, and F. Seible, 1990. Seismic retrofit of circular bridge columns for enhanced Flexural performance. ACI Structural Journal, V. 88 (5), September-October 1991. pp. 572-584.

[4] Y.H. Chai, M.J.N. Priestley and F. Seible, 1993.Analytical model for steel-jacketed RC circular bridge columns. Journal of Structural Engineering, Vol. 120 (8), August, 1994, pp. 2358-2376.

[5] J.H. Wang, K. Kikuchi, M. Kuroki, 2005. Seismic retrofit of existing r/c rectangular columns with circular steel jackets.30th Conference on OUR WORLD IN CONCRETE & STRUCTURES: 23 - 24 August 2005, Singapore

[6] K. Yoshimura, K. Kikuchi, M. Kuroki, J. Wang and K. Ichinose, 2004. Seismic strengthening of rectangular r/c columns Confined by circular steel- and cf-jackets.13th World Conference on Earthquake Engineering, Vancouver, B.C., Canada, August 1-6, 2004, Paper No. 2036

[7] A. Teran and J. Ruiz, 1992. Reinforced concrete jacketing of existing structure. Earthquake Engineering Tenth World Conference, 1992, Balkema, Rotterdam, pp-5107-5113

[8] B. Dadasaheb, 2013. Retrofitting of existing RCC buildings by method of jacketing. IJRMEET-V. 1 (5), June 2013.

[9] AA.VV. ACI 318-02 Building Code Requirements for Structural Concrete and Commentary. Committee 318, American Concrete Institute, 2002.

CICM 2015
First International Conference on
Advances in Civil Infrastructure and Construction Materials
MIST, Dhaka, Bangladesh, 14–15 December 2015

SEISMIC VULNERABILITY ASSESSMENT OF EXISTING REINFORCED CONCRETE RESIDENTIAL BUILDINGS BY JAPANESE METHOD

Naveel ISLAM[1], **Kshama S. Roy** [2], **Kamrul Islam** [3], **Mohiuddin Imran**[4] and **Arif Hoosain**[5]

[1, 2] Faculty of Engineering and Applied Science, Memorial University of Newfoundland, Canada. Email: [1]ni5867@mun.ca;[2]ksr037@mun.ca.
[3] Department of Civil Engineering, Military Institute of Science and Technology, Dhaka, Bangladesh. Email: kamrul1@ualberta.ca.
[4, 5] Bangladesh University of Engineering and Technology, Bangladesh.
E-mail: [5]mohiuddin.imran82@gmail.com and [6]arifhoosain58@gmail.com.

Abstract. *In regions where earthquake occur in intervals measured in centuries, there is a prime need for a simple evaluation method that focuses on selection of buildings with high vulnerability rather than those with a high probability of survival. The current study focuses on the application of relatively simple but effective Japanese Method of seismic vulnerability assessment to existing medium to low-rise building of Dhaka city. A detailed survey has been carried out in the Dhaka city to assess the earthquake vulnerability of existing medium to low-rise reinforced concrete buildings. Three levels of screening have been followed for the seismic vulnerability assessment procedure. The Japanese seismic performance evaluation is based on both site inspection and structural calculation to represent the seismic performance of existing medium and low–rise reinforced concrete buildings in terms of seismic performance indices of a structure. On the basis of the seismic performance index, the building is assessed either as 'Safe - the building possess the seismic capacity required against the expected earthquake motions' or as 'Uncertain' in seismic safety. This study presents the results of the detailed survey conducted on sixty randomly selected buildings of specific areas of Dhaka city.*

Keywords: Japanese method, Seismic vulnerability assessment, Reinforced concrete building, Seismic performance index

1 INTRODUCTION

In recent years several severe earthquakes (Turkey, 2015; Afghanistan and Pakistan, 2015; Nepal, 2015; Japan, 2011; New Zealand, 2010 & 2011; Mexico,2011, Indonesia, 2010 & 2011; China, 2010; Haiti, 2010) have not only imposed inexorable threat to humanity but also posed tremendous challenges to the researchers to develop a simple but effective seismic vulnerability assessment method. To predict the potential damage caused by such natural hazards like earthquake before its occurrence is still considered as a major scientific challenge. In regions where earthquake occurs in intervals measured in centuries, there is a prime need for a simple evaluation method that focuses on selection of buildings with high vulnerability rather than those with a high probability of survival. A relatively simple but effective method of seismic vulnerability assessment is used in the present study to check its suitability and application to Dhaka city which is considered as one of the most earthquake vulnerable cities by many earthquake specialists [6-9]. Previous researchers [1-10] have used various types of seismic vulnerability methods (i.e. Rapid Visual Screening (RVS) and Non Destructive Testing (NDT) Method [1], GIS Environment [3, 5], Turkish Method [4, 6-8], Fuzzy Approach [9] and Design of Experiment Methodology [8, 10]) for the existing medium and low-rise reinforced concrete buildings of Dhaka city. A detailed comparison of the existing seismic vulnerability methods can be found in authors' other publications [6-10]. However, after reviewing the existing methods and also after recommendations of other researchers [10-12], Japanese method of seismic vulnerability assessment is found to be a relative simple but appropriate method for densely populated earthquake prone cities like Dhaka. The expected intensity for Dhaka City is around VIII (Modified Mercalli Intensity Scale) which may be assumed to correspond to peak ground acceleration (PGA) in a range of 0.2g to 0.25g. According to current seismic zoning map of building code, for Dhaka city (Zone II) the PGA is around 0.15g on very firm soil, considering site effects it can be 0.20g or more [6, 13-14].A detailed survey was carried out in four different areas of Dhaka city as a part of the present study to assess the earthquake vulnerability of existing medium to low-rise reinforced concrete buildings. Three levels of screening have been followed for the seismic vulnerability assessment procedure. Detailed discussion of the Japanese method is not the scope of the present study. However, a summary of the method will be presented in the next section followed by the summary of the survey details. The results for the survey area will be shown in terms of seismic performance index of structure. On the basis of the seismic performance index, the building is assessed either as 'Safe - the building possess the seismic capacity required against the expected earthquake motions' or as 'Uncertain' in seismic safety. A parametric study of the factors affecting the seismic performance index can be found at the later sections. Finally the results obtained from the survey will be compared with the design of experiment method which is considered as a novel statistical

approach to explain the variation of information under conditions that are hypothesized to reflect the variation.

2 JAPANESE METHOD OF SEISMIC VULNERABILITY ASSESSMENT

The Japanese seismic performance evaluation is based on both site inspection and structural calculation to represent the seismic performance of existing medium and low–rise reinforced concrete buildings in terms of seismic performance index of structure, I_s. Three levels of screening procedures, namely first, second, and third level screening, have been proposed for the seismic evaluation. Any level of the screening procedures may be used in accordance with the purpose of evaluation and the structural characteristics of the building [15].

Building inspections are conducted to check the structural characteristics of the building, which are necessary to calculate I_s. Appropriate methods for inspection are selected in accordance with the screening level; namely site inspection, collection of design drawings, and material tests. In case, design drawings of the building are not available, inspections on the structural dimensions, diameters and arrangements of reinforcing bars need to be examined on site, which are necessary for seismic evaluation of the building in accordance with the screening level [15].

The seismic performance index of structure (I_s) is evaluated based on the following equation valid for each storey and for each direction,

$$I_s = E_0 * S_D * T \quad (1)$$

Where, E_0= Basic seismic index of structure, S_D= Irregularity index and T = Time index

Basic Seismic Index, E_0 (representing the basic seismic performance of a building) is a function of the strength index (C), the ductility index (F), and the storey-shear modification factor. The strength index (C) represents the lateral strength or the lateral load carrying capacity of a member or a storey in terms of shear coefficient, namely the shear normalized by the weight of the building sustained by the storey. Ductility Index (F) signifies the deformation capacity of a structural member. Irregularity Index, S_D is considered for modifying E_0 in consideration of unbalance in stiffness distribution and/or irregularity in structural plan, elevation of a building and time Index, T for modifying E_0 in consideration of aging of a building.

The Basic Seismic Index of the Structure, $E_0$is determined based on the following equations5and 6(whichever is larger) for the direction concerned.

$$E_0 = \frac{n+1}{n+i} (C_w + \alpha_1 C_c). F_w \quad (5)$$

$$E_0 = \frac{n+1}{n+i} (C_{sc} + \alpha_2 C_w + \alpha_3 C_c). F_{sc} \quad (6)$$

Where, n = number of stories of a building, i = number of the storey for evaluation, (the first storey is numbered as 1 and the top storey as n)
Irregularity index, S_D is determined based on the factors that are mentioned in Table 1.

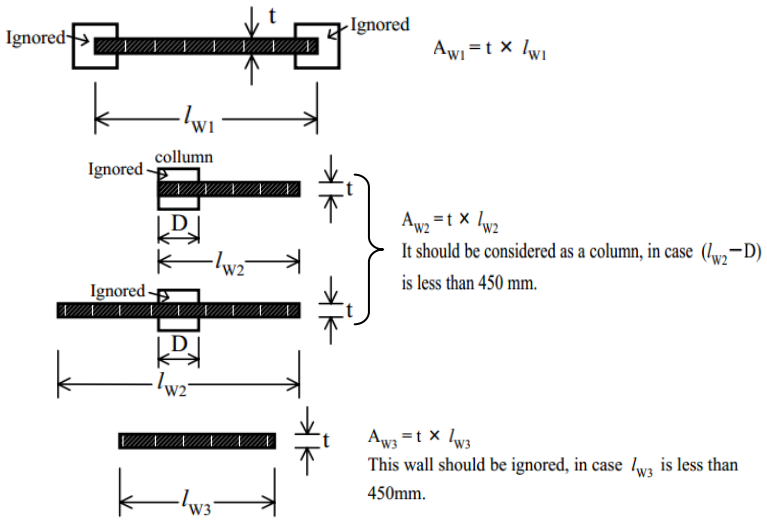

Figure 1: Definition of Cross Section Area of Wall,directly adopted from [15]

Table 1: Factors for Irregularity Index

Items to be checked	Degree	Parameters for Degree of Incidence
Horizontal Balance	Regularity	G_a&R_a
	Aspect ratio of plan [Remarks b, b= length of the long side / length of the short side]	G_b&R_b
	Narrow part	G_c&R_c
	Expansion joint (EJ) [d= clear width of the EJ / height from the base to the EJ]	G_d&R_d
	Well–style area	G_e&R_e
	Eccentric well–style area	G_f&R_f
	Underground floor	G_h&R_h
Elevation Balance	Story height uniformity	G_i&R_i
	Soft storey	G_j&R_j

Irregularity Index, $S_D = q_{1a} \times q_{1b} \times q_{1c}$-------x q_{1j} (7)
and Degree of Incidence, $q1i$ = $\{[1-(1-G_i) \times R_{1j}]$ ------$\{i$=a,b,c,d,e,f,i,j$\}$ (8)
= $[1.2-(1-G_i) \times R_{1j}]$ ------ $\{i$=h$\}$

Time Index is calculated based on the factors obtained from the degrees indicated for the items in Table 2.

Table 2: Factors for Time index

Items to be checked	Degree
Deflection	Tilting of a building or obvious uneven settlement is observed
	Landfill site or former rice field
	Deflection of beam or column is observed visually
	No correspondence to the foregoing
Cracking in walls and columns	Rain leak with rust of reinforcing bar is observed
	Inclined cracking in columns is obviously observed
	Countless cracking is observed in external wall
	Rain leak without rust of reinforcing bar is observed
	No correspondence to the foregoing
Fire experience	Trace
	Experience but traceless
	No experience
Occupation	Chemical has been used
	No correspondence to the foregoing
Age of building	30 years or older
	Age of building 20 years or older
	19 years or less
Finishing condition	Significant spalling of external finishing due to aging is observed
	Significant spalling and deterioration of internal finishing is observed
	No problem

Seismic Demand Index of Structure, I_{so} defined as the standard level of the seismic index required for a building to be safe against the earthquake hazard on the site of the building. Expressed as the product of the constraints in Table 3.

Table 3: Constraints for I_{so}

Basic Seismic Demand Index of Structure, E_s (A sub-index representing the basic seismic demand for a building)
Zone Index,Z (sub-index accounting for the expected seismic activities and seismic intensities)
Ground Index,G (A sub-index accounting for the effects of soil profiles, geological conditions, and soil-and-structure interactions)
Usage Index, U (sub-index accounting for the use of a building)

Seismic safety of structure is judged by the following equation,

$$I_s \geq I_{so} \qquad (9)$$

Where, I_s= Seismic index of structure and I_{so}= Seismic demand index of structure

If Equation (9) is satisfied, the building is assessed as 'Safe - the building possess the seismic capacity required against the expected earthquake motions'. Otherwise, the building is assessed as 'Uncertain' in seismic safety.

The thorough procedure can be found in the Standard for seismic evaluation and Guideline for Seismic Retrofit of existing Reinforced Concrete building which is revised from the general outline given by Umemura [11] and by Japan Building Disaster Prevention Association in 1990 [15]. Authors were successful in similar analysis in implementing Design of Expert Methodology (DOE) for Japanese Method of assessment [10].

3 SURVEY DETAILS

For the particular seismic vulnerability survey, four major areas (Mirpur, Mohammadpur, Dhanmondi and Jhigatola) of the Dhaka City were chosen. Figure 2.0 shows the distribution of the buildings in each surveyed area. The survey areas are also marked in the map as shown in Figure 3.0. The buildings in these areas are analogous to most of the densely populated areas which have high density of multi-storied residential buildings. Likewise the surveyed areas also reflect the unplanned constructions over the city. Sixty (60) randomly distinctive buildings were selected, of four (4) to six (6) storied levels above ground surface to conduct a detailed inspection for gathering data related to the structural dimensions of the buildings by the survey team. As per the new Bangladesh National Building Code (BNBC) 2013, provisions are now being given to higher levels of multi storied residential buildings due to the increase in the population density but still the older buildings with majorly the six stories were predicted to be the most seismically vulnerable. For this, analysis were conducted on majorly the buildings with six storied levels which sums up to forty three (43) buildings out of the sixty (60) residential buildings from the four distinguished survey areas.

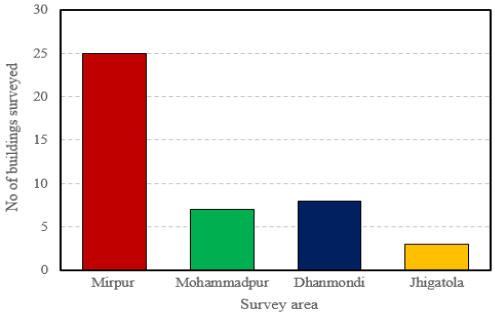

Figure 2: Distribution of Buildings in Each Survey Area

Figure 3: Map on the portion of Dhaka City showing the Survey Locations in the Study Areas

4 RESULTS

Data are analyzed in the detailed spreadsheet which is developed using the Microsoft Excel software program for calculating the seismic performance indices where Tables1.0, 2.0 and 3.0 and empirical equations2-8areconsidered. Figure 4.0 shows the distribution of the seismic index parameters with the building inventory at each of the study area. Here, E_0(X) and E_0(Y) defines the basic seismic index of the structure for the directions concerned. S_D defines the seismic index and T,as the time Index.

The study areas are marked along the axis of the building inventory for simplicity. However, Figure 5.0 shows the change in the seismic performance index of structure, I_s(X) and I_s(Y) for the direction concerned for the buildings in the study area. The seismic demand index, I_{so} is marked by the horizontal line which is calculated based on the parameters in Table 4.0. Comparison betweenFigures4.0 and 5.0 concludes that, I_s (X) and I_s(Y) are mainly dependent on E_0(X) and E_0(Y) as S_D and T are almost the same in all the study locations. This also indicates, the exterior outlook of the buildings do not affect much on the performance Index Score of the buildings.

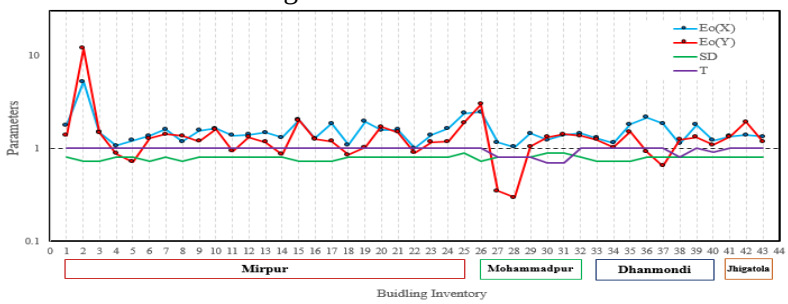

Figure 4: Variation of Seismic Index Parameters with Building Inventory

If any of the seismic performance indices, I_s(X) or I_s(Y) is less than the seismic demand index (I_{so}) for a particular building, the building is assessed to be UNCERTAIN. Figure 5.0 shows for a particular building in Mirpur area, I_s(Y) is lower than I_{so} which leads the assessment of the building to be 'UNCERTAIN'. Similarly, for Mohammadpur area two of the buildings are assessed to be UNCERTAIN which means the buildings have the high susceptibility to damage in high ground motion based on the performance score, I_s(Y). Figure 6.0 shows the qualitative vulnerability of the buildings based on the study areas. Among the forty three (43) surveyed buildings, thirty eight (38) buildings are assessed as SAFE whereas five (5) buildings are assessed as UNCERTAIN as shown in Figure. 6.0. The reason for the five (5) 'UNCERTAIN' buildings is mainly due to the I_s(Y) i.e. the shorter length of the buildings showing higher vulnerabilities.

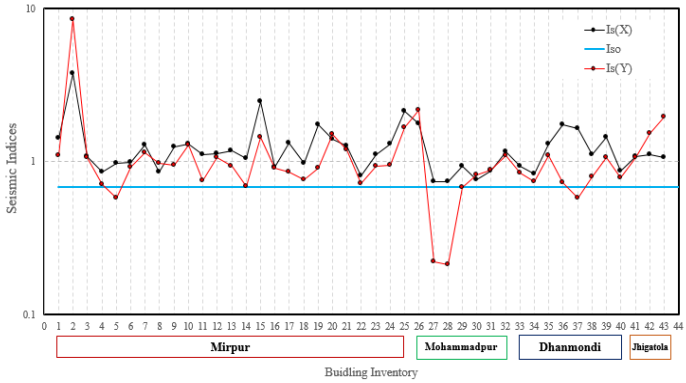

Figure 5: Variation of Seismic Indices with Building Inventory

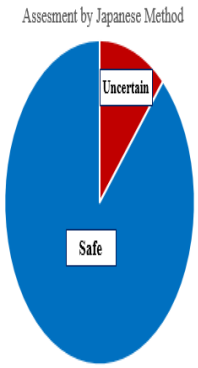

Figure 6: Qualitative Assessments on the safety of the buildings

Figure 7.0 shows the change in the seismic vulnerability Indices with the increase in the number of stories. Four (4) randomly selected six storied buildings from each of the study areas are considered. Likewise, the buildings in the prescribed study locations are indicated in the graph by the seismic index symbols. A parabolic decrease in the seismic performance indices with the increase in the number of stories can be seen for most of the study locations which indicates that the increase in the number of stories increases the susceptibility to seismic damage.

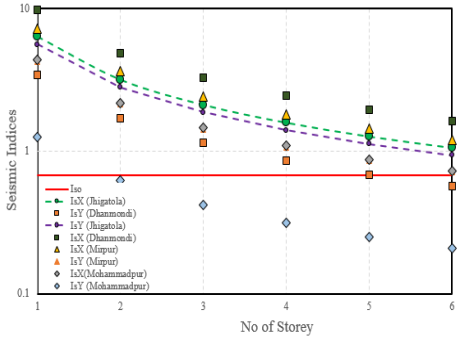

Figure 7: Variation of seismic indices with the change of number of stories for the study areas

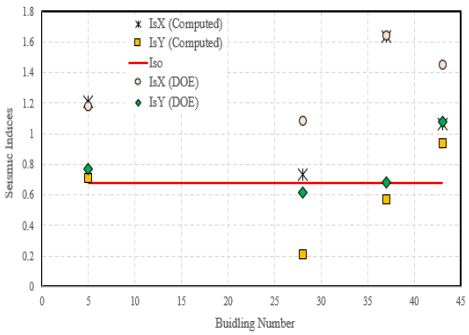

Figure 8: Comparison of DOE and Computed Seismic Indices for Randomly selected Buildings

Figure 8.0 shows the change in the computed I_s(X) and I_s(Y) in the randomly selected building numbers with the I_s(X) and I_s(Y) calculated using Design of Expert (DOE) Methodology [16-17] based on the Japanese Method as explained by the authors' previous publications [10]. For all the locations, the I_s(X) and I_s(Y) are calculated based on the regression equations shown in [10] with the significant parameters from the current survey data. Figure 8.0shows that the computed scores from the study locations are in good agreement with those determined using the DOE Methodology. Detailed discussion on this issue will be published in authors' future publications.

5 CONCLUSIONS

A relatively simple but effective Japanese method of seismic vulnerability assessment is considered in the present study.A detailed survey was carried out in four different areas (Mirpur, Mohammadpur, Dhanmondi and Jhigatola) of Dhaka city as a part of the present study to assess the earthquake vulnerability of existing medium to low-rise reinforced concrete buildings. Three levels of screening have been followed for the Japanese method of seismic vulnerability assessment. The results for the survey area are shown in terms of seismic performance index of structure. On the basis of the seismic performance index, the buildings are assessed either as 'Safe - the building possess the seismic capacity required against the expected earthquake motions' or as 'Uncertain' in seismic safety. Among the forty three (43) surveyed buildings, thirty eight (38) buildings are assessed as SAFE whereas five (5) buildings are assessed as UNCERTAIN.A parametric study of the factors affecting the seismic performance index are also performed. Finally, the results obtained from the survey are compared with the design of experiment method (DOE) and similar responses are found.

REFERENCES

[1] M. H. Ansary, and M. A. Noor, 2004. Vulnerability assessment of existing engineered and non-engineered structures of Dhaka city using RVS and NDT Techniques.*Third International Symposium on New Technologies for Urban safety of Mega Cities in Asia*, Agra, India.

[2] M. Z.Ahmed, M. K.Islam,R. Ahsan, andG. Ozcebe, 2007. Seismic vulnerability assessment methods: a possible application to Bangladesh.*First Bangladesh Regional Science Association (BRSA) Conference*, Dhaka.

[3] M. J.Alam,M. A. R. Khan, andA. Paul,2009.Seismic vulnerability assessment of existing RC buildings in GIS Environment.*Earthquake Engineering Research Center (EERC)*, Dept. of Civil Engineering, Chittagong University of Engineering & Technology (CUET), Bangladesh.

[4] M. R. Sadat,M. S. Huq, M. A. Ansary, 2010. Seismic Vulnerability Assessment of Buildings of Dhaka city. *Journal of Civil Engineering*,Inst. of Engineers, Bangladesh. 38 (2), 159-172.

[5] R. P. Ishita and S. Khandaker, 2010.Application of analytical hierarchical process and GIS in Earthquake vulnerability assessment: case study of ward 37 and 69 in Dhaka City. *Journal of Bangladesh Institute of Planners*, 3:103-112.

[6] M. Z. Ahmed, K. Islam, K. S.Roy, M. S. Arafat and T. M. Al-Hussaini, 2010. Seismic Vulnerability Assessment of RCF Buildings in Dhaka City, *Proceedings of the 3rd International Earthquake Symposium (IESB-3)*, Dhaka, Bangladesh.

[7] K. S. Roy, K. Islam and M.S Arafat, 2010. Seismic Risk Assessment of Existing Low-rise Buildings in Unplanned Urban Regions of Dhaka City, *Proceedings of the 2nd International Conference on Construction in Developing Countries (ICCIDC-2)*, Cairo, Egypt.

[8] K. S. Roy, K.Islam and M. S. Arafat, 2011. A Novel Statistical Approach for Investigating the Significant Factors that Influence the Performan*ce Score of the Turkish Method, Proceedings of International Conference on Geotechnique, Construction Materials and Environment (GEOMAT-2011),* Tsu City, Mie, Japan.

[9] K. S. Roy, M. J. Hassan, K. Islam and N. Islam, 2015. Application of Fuzzy Set Theory to Seismic Vulnerability Assessment *Fifth International Conference on Geotechnique, Construction Materials and Environment, Osaka, Japan.*

[10] N. Islam, K. S. Roy and K. Islam, 2015. Use Of Design Of Experiment In Seismic Vulnerability Assessment For Existing RC Buildings By Japanese

Method *Fifth International Conference On Geotechnique, Construction Materials And Environment, Osaka, Japan.*

[11] H. Umemura, 1980 .A Guideline to Evaluate Seismic Performance of Existing Medium and Low Rise RC Buildings and Its Application. *Proc. of The 7th World Conf. on Earthquake Eng.*, Istanbul, Turkey, 4: 505-512.

[12] S. Otani, 2000.Seismic vulnerability Assessment Methods for Buildings in Japan. *Earthquake Engineering and Eng. Seismology*, 2 (2): 47-56.

[13] Y.M. Wu, T.L. Teng, T.C. Shin and N.C. Hsiao, 2003.Relationship between Peak Ground Acc., Peak Ground Velocity and Intensity in Taiwan. *Bulletin of the Seismology Society of America*, 93(1), 386–396.

[14] N. Islam, M. J. Alam and A.S.M.F. Hossain. 2015. One Dimensional Ground Response Analysis at Distinctive Locations of Bangladesh. *First International Conference in Advances in Civil Infrastructure and Construction Materials (CICM 2015)*, MIST, Dhaka, Bangladesh. (In Press)

[15] *Standard for Seismic Evaluation and Guidelines for Seismic Retrofit of Existing Reinforced Concrete Buildings*, 2001 (English Edition), Japan Building Disaster Prevention Association.

[16] Montgomery, D.C. 2013. *Design and analysis of experiments*, 8th ed., John Wiley & Sons Incorporated, New York, NY, USA.

[17] Box, G.P., Hunter, J., Hunter W. 2005 *Statistics for experimenters design innovation and discovery*, 2nd ed. Wiley and Sons.

CICM 2015
First International Conference on
Advances in Civil Infrastructure and Construction Materials
MIST, Dhaka, Bangladesh, 14–15 December 2015

EXPERIMENTAL INVESTIGATION OF NEAR SURFACE MOUNTED RC BEAMS WITH ADVANCED STRENGTHENING MATERIALS

K. M. DARAIN[1, 2], **M. Z. Jumaat**[1], **M. Obaydullah**[1] **and Md N. Huda**[1]

[1]Department of Civil Engineering, University of Malaya, Kuala Lumpur, Malaysia.
Email: khmahfuz@gmail.com
[2]Architecture Discipline, Khulna University, Khulna, Bangladesh

Abstract. *This paper presents the flexural behavior of the Reinforced Concrete (RC) beams strengthened with Near Surface Mounted (NSM) technique. This technique is quite new and researchers generally used Fiber Reinforced Polymer (FRP) as a strengthening material. Having several attractive attributes, FRP products are less ductile, barely available and expensive. These are the major shortcomings of it to become a popular material of the current construction industry. In this perspective, steel bar is chosen in this study as an inexpensive but promising strengthening material in addition to the Carbon FRP material. The experimental study consists of seven NSM strengthened RC beams using variable bond length with different NSM strengthening material (steel and CFRP bar). The NSM strengthened RC beams showed an increment of 46% to 107% of ultimate strength compare to the control beam. Besides, NSM steel strengthened beams showed better performance in terms of crack width and stiffness, although NSM CFRP strengthened beams exhibited enhanced strength increment*.

Keywords: NSM, Load-deflection, FRP, Steel, Crack, Stiffness and flexural strength.

1 INTRODUCTION

Structural strengthening is now becoming an important branch of structural engineering which aims to improve the efficiency of underperforming structures. Externally Bonded Reinforcement (EBR) and NSM techniques are popular strengthening methods for RC structures. The EBR technique affixes the FRP plate or fabric on the beam soffit. However, premature debonding failure at plate end is a major drawback of it[1]. In NSM technique, FRP bar or strip is slotted in the groove of the concrete cover and attach with epoxy[2]. This technique offers higher level of strengthening efficacy, less prone to premature debonding failure and enhance protection against fire, mechanical damage, aging effect and vandalism acts. It also demonstrate better durability, stress sharing mechanisms and fatigue performance as the reinforcement is located inside [3].

FRP strengthened beams posed brittle failure due to its inferior ductility property. Besides, FRP materials are not readily available to most of the countries and extremely costly[4]. Rahaland Rumaih [5] explored shear strengthening performance using NSM technique with conventional steel and CFRP bar and only 7%–10% shear capacity improvement was observed for CFRP over the steel strengthened test region. Rasheed et. al.[6] investigated to detect the corrosion influence on RC beam with NSM steel wrapped with GFRP jacket which was submerged in highly concentrated deicing salt solution. The study found that NSM steel was secured by the surrounding adhesive and GFRP laminate. Darain et.al [7, 8] compared NSM steel and CFRP strengthened beams and developed an Artificial Intelligence based serviceability prediction model.

The assemblage of corrosion protective epoxy and ductile steel could be a promising NSM strengthening option. However, a few data are available on steel as a NSM strengthening material. The present study has a goal to assess and compare the flexural performance of NSM strengthened RC beam using CFRP and steel bar. Another important focus is to visualize the influence of variable embedment length on debonding failure behavior of the NSM strengthened RC beam.

2 MATERIALS AND METHODS

2.1 Test Matrix

Numerous parameters influence the flexural performance of RC beams strengthened with NSM technique. This paper focuses only on the bond length deviation (1600 mm, 1800 mm and 1900 mm) and the strengthening materials (steel and CFRP bar). A total of seven RC beams were experimented under monotonic load with four-point bending until breakdown. The test matrix is presented below in Table 1.

Table 1: Test matrix of the experimental program

Sl. No.	Notation	Description	Groove size (mm)	Total bond length (mm)
1	CB	Control RC beam (unstrengthened)	-	-
2	N1.6F	12 mm NSM CFRP bar	24×24 ($2d_b$)	1600
3	N1.6S	12 mm NSM Steel bar		1600
4	N1.8F	12 mm NSM CFRP bar		1800
5	N1.8S	12 mm NSM Steel bar		1800
6	N1.9F	12 mm NSM CFRP bar		1900
7	N1.9S	12 mm NSM Steel bar		1900

d_b = Diameter of the NSM bar

2.2 Materials

RC beam specimens were prepared in laboratory with strict supervision during steel reinforcement fabrication and casting operation. The concrete cube compressive strength at 28 days was 43.24 MPa and cylinder strength was 35.63 MPa. Flexural strength was found to be 5.01 MPa. The deformed 12 mm diameter bars for internal and NSM reinforcement were tested in the laboratory and their yield stress was 400 and 520 MPa respectively and both of their modulus of elasticity was 200 GPa. The ultimate strength and modulus of elasticity ofsand coated 12 mm diameter CFRP bars were 2400 MPa and 165 GPa respectively. The compressive, tensile and shear strengths of Sikadur® 30 epoxy adhesive were 85-95 MPa, 26-31 MPa and 16-19 MPa respectively at 7 days curing time and at 35^0 C temperature (Sikadur®-30).

2.3 Experimental Setup

The under-reinforced RC beams were 2.3 m long with effective spans of 2 m and rectangular cross-sections with dimension of 125 mm × 250 mm. The tension reinforcements consisted of two 12 mm diameter ribbed bars with two 10 mm diameter ribbed bars in the compression zone as hanger bars. These bars were omitted at the middle top portion of the compression zone to ensure flexure failure. The shear reinforcements were made with 8 mm diameter ribbed steel bars spaced 90 mm apart. Figure 1displays the details of the beam configuration.

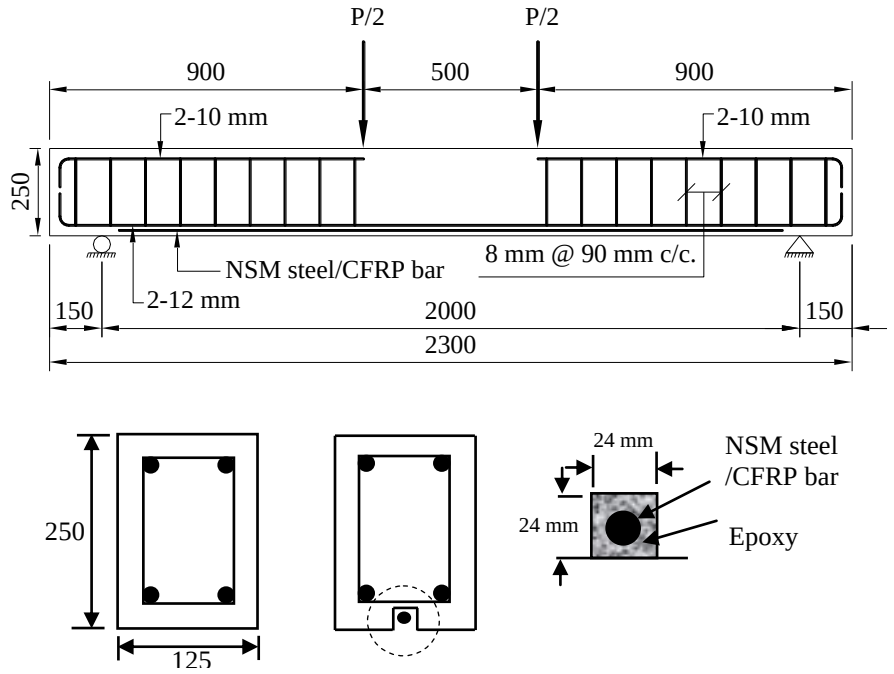

Figure 1: Reinforcement and strengthening detail of RC beam

A special concrete saw with a diamond blade was used to create the groove (24 mm × 24 mm) in the longitudinal direction on the tension side of the RC beam. The groove dimension was selected twice the NSM bar diameter ($2d_b$)based on the experimental findings of different researchers work[9, 10]with a clear cover of 6 mm. The groove was filled with epoxy adhesive to around 2/3 of the groove depth. The CFRP or steel bar was gently inserted halfway and the remaining space in the groove was filled with epoxy with proper surface levelling.

2.4 Test Setup and Instrumentation

A closed-loop Instron universal testing machine of 500kN capacity was used to apply four-point bending load on the prepared specimens. The machine was operated under load control mode with a loading rate of 5 kN/min up to yielding of the internal reinforcement and then with displacement control at a rate of 1.8 mm/min. The instrumentation of the beams is shown in Figure 2. Three vertical Linear Variable Differential Transducers (LVDT) were installed at the center, 250 mm from the center (under the spreader beam load point) and 500 mm from the center of the RC beam to measure the deflection at these different points. 5 mm length strain gauges were attached to the center of both the internal steel reinforcements and the NSM rods to measure tensile strains. 30 mm strain gauges

were placed on the top surface of the RC beam to measure concrete compressive strains. Demec discs were planted at the midspan of the beams along the depth to measure transverse strains. A Dino-Lite digital microscope was used to measure micro cracks on the surface of the beams.

Figure 2: Instrumentation and loading setup

3 RESULTS AND DISCUSSION

3.1 Load Deflection Behavior

Figure 3(a) showed the load versus mid-span deflection of control and NSM CFRP strengthened RC beam. Figure 3(b) highlighted the moment-deflection behavior with an example of N1.8F beam. Trilinear response was observed for all the CFRP strengthened RC beam which can be divided into three distinct regions. These are (a) elastic region, (b) concrete cracking to steel yielding region and (c) steel yielding to ultimate failure region.

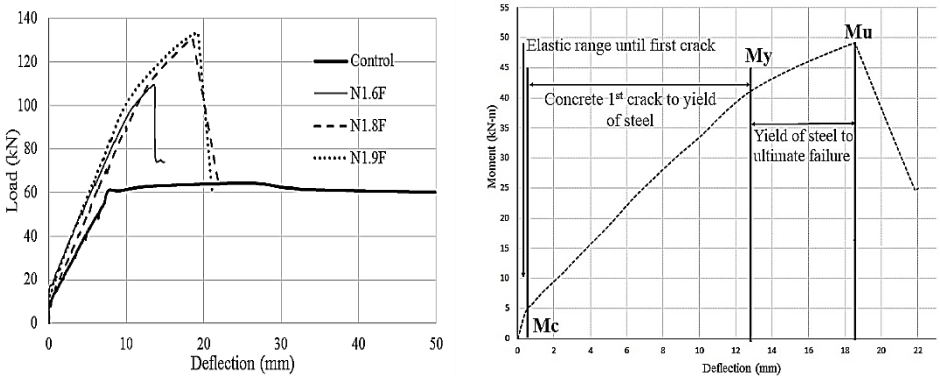

Figure 3: (a) Load – deflection diagram of control and NSM CFRP strengthened RC beam (b) explanation of moment vs. mid-span deflection for N1.8F beam

The first linear elastic region ends until the 1st cracking of concrete. After conversion to moment, it can be addressed as cracking moment, Mc in Figure 3. The 2nd phase stayed until steel yielding, where widths were getting widened in old cracks with development of new cracks. The number of cracks stabilized at yielding moment M_y. At third phase after the steel yielding, the curve slightly changed its slope from M_y to the ultimate moment Mu due to lower stiffness of the CFRP bar. The load deflection curves in Figure 4for the NSM steel strengthened beams displayed almost a bi-linear response up to the yielding stage. Beyond this region the behavior of the specimens was totally nonlinear. All the strengthened beams demonstrated superior first cracking loads compare to the control beam. In addition, from Figure 4 it can be seen that the slope of the load deflection curve for steel is steeper than CFRP due to the higher modulus of elasticity.

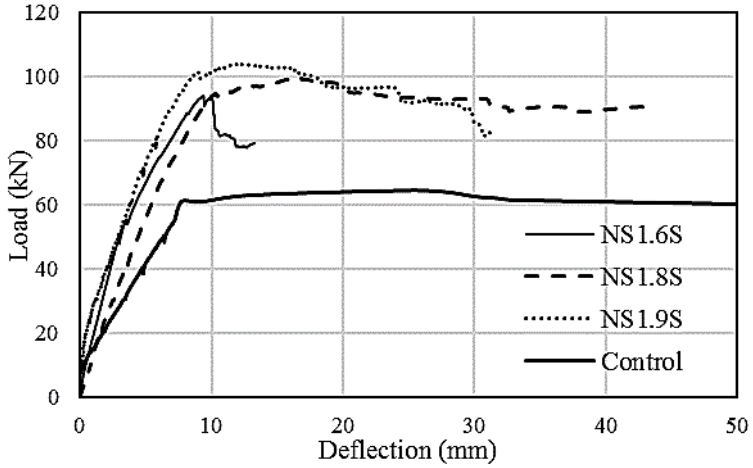

Figure 4: Load – deflection diagram of control and NSM CFRP strengthened RC beam

Table 2: Load-Defection results for different RC beams

Beam ID	Pcr (kN)	Δcr (mm)	Py (kN)	Δy (mm)	Pu (kN)	Δu (mm)	Failure mode
CB	10.6	0.3	61.0	7.7	64.4	24.7	FF
N1.9F	15.0	0.3	104.5	10.7	133.2	19.2	CCS
N1.9S	23.0	0.7	101.3	10.0	103.8	12.4	FF
N1.8F	14.0	0.6	110.6	13.0	130.8	18.6	CCS
N1.8S	15.5	1.0	94.7	10.8	99.6	16.8	FF
N1.6F	17.5	0.4	83.6	8.5	109.5	13.6	CCS
N1.6S	14.4	0.7	88.7	8.3	94.1	9.4	CCS

Here, Pcr = first crack load; Py = yield load; Pu = ultimate load; Δcr = deflection at 1st crack; Δy = deflection at yield of steel; Δmax = mid-span deflection at maximum load, FF = flexural failure (concrete crushing after steel yielding), CCS = concrete cover separation.

The effect of variable bond length (1600, 1800 and 1900 mm) irrespective of the strengthening material (CFRP or steel) is quite clear from the results of Table 2. Here, 1900 mm bond length was performed efficiently compare to others. Other researchers also supported this findings [11, 12].From Table 2, at ultimate stage of the steel NSM beam with 1900 mm bond length exhibited less deflection(12.4 mm) compare to N1.9F beam. It is the highest percentile deflection reduction (55%) within steel or CFRP material group. Besides, N1.9S beam showed a tremendous 1st crack load improvement of 117% over control beam while for N1.9F it was only 42%. However, due to the higher tensile capacity of CFRP bar, it took the lead (70% to 107%) over steel NSM beam (46% to 61%) for the ultimate capacity of the beam comparing un-strengthened beam.

3.2 Failure Modes

The control beam was failed by concrete crushing at the compression zone after the internal tensile steel yielded. All the NSM CFRP strengthened beams were failed due to premature debonding problem. Except N1.6S, the other two NSM steel strengthened beams were failed due to concrete crushing after internal steel yielding. This is the most desirable failure mode of strengthened structures that commonly termed as flexure failure. The failure mode of N1.9F and N1.9S is displayed in Figure 5 and Figure 6 which were failed due to concrete cover separation and concrete crushing respectively.

Figure 5: Failure mode of N1.9F RC beam

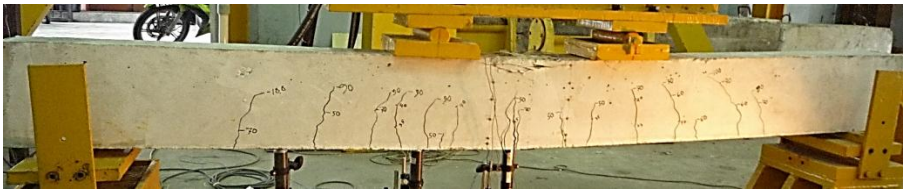

Figure 6: Failure mode of N1.9S RC beam

Failure for all CFRP strengthened beam and N1.6S beam was occurred due to concrete cover separation that initiated at the tip of NSM bar cut-off region. Several tiny shear cracks were formed after the internal steel yielding of this beam and those cracks were close to the support region. The debonding failure was occurred slowly after formation of these shears cracks. The shear crack at the end of NSM CFRP rod triggered the failure mechanism where a bending crack further aggravated the problem. Combination of these cracks further guided by horizontal cracks formed at the level of internal steel and put forward along the beam mid-span which ensued final failure.

3.3 Cracking Behavior

Serviceability is measured by considering the magnitudes of deflections, cracks, and vibrations of structures. The well-known Gergely and Lutz [13] crack width equation is modified (Equation 1-2) for FRP reinforced members[14] which is as follows:

$$w = \frac{2.2}{E_f}\beta_h k_b f_f \sqrt[3]{d_c A} \quad (1)$$

$$f_f = M_s \frac{n_f d(1-k)}{I_{cr}} \quad (2)$$

Here, k_b can be less than, equal or greater than 1 depending upon FRP bond behavior with steel; E_f = modulus of elasticity of FRP (MPa); β_h = a ratio; f_f= stress level in FRP (MPa); d_c = thickness of cover from the tension face to the center of the closest bar (mm); A = the effective tension area of concrete around the main reinforcement divided by the number of bars (mm^2).

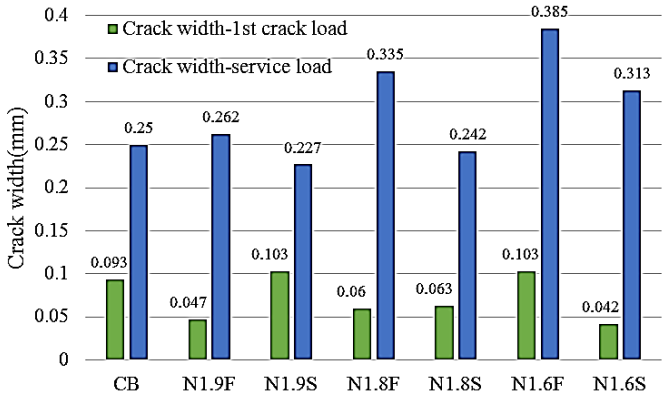

Figure 7: Crack width during 1stcrack and service load for different specimens

Figure 7 describes the different measurements of crack width at first crack and service loading. According to ACI 318-11, the service load deflection (span/480) for the beam specimens was found to be 4.17 mm. After analysis, the corresponding service load and its associated crack width was determined. During testing the crack width was measured with the help of digital crack microscope at different load. At first crack, N1.9F, N1.8F, N1.8S and N1.6S beams showed almost same width around 0.05 mm. However, during service loading, N1.9S and N1.8S showed about 0.22 mm crack width which was lesser than other beams.

3.4 Stiffness Behavior

Stiffness can be defined as the capacity to repel bending or deflection when subject to loading which is also known as flexural rigidity. According to linear elastic theory, the moment curvature relationship can be expressed as follows (Equation 3):

$$\frac{1}{r} = \frac{M}{EI} \tag{3}$$

Here, *1/r* = the curvature, *M* = the bending moment and *K* =*EI*, the flexural stiffness.

Due to the composite nature of normal or FRP strengthened RC beam, this flexural stiffness changes according to increasing moment and corresponding cracking phenomenon (Figure 8).

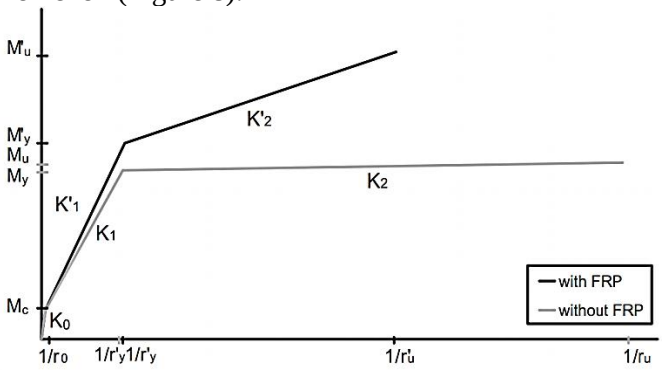

Figure 8: Moment-curvature diagram of FRP and without FRP strengthened structure

The pre-crack stiffness K_0 of all specimens were completely linear until first crack appeared and those were steeper compare to others stiffness (Table 3). From 1st crack up to the yield stage, the pre-yield stiffness K_1 was comparatively lower than K_0. However, this stiffness is significant as the service load range lies within this limit according to the most code of practice. The value of the pre-ultimate stiffness K_2 was the least among others stiffness (K_0 and K_1). At service

load level, the N1.9S beam displayed the superior pre-yield stiffness K_1 among others which was due to the better modulus of elasticity of NSM steel.

Table 3: Stiffness variation of control and strengthened RC beam

Beam ID	Pre-crack stiffness, K_0 (kN/m)	Pre-yield stiffness, K_1 (kN/m)	Pre-ultimate stiffness, K_2 (kN/m)
CB	35333	7922	2607
N1.9F	50000	9766	6938
N1.9S	32857	10130	8371
N1.8F	23333	8508	7032
N1.8S	15500	8769	5929
N1.6F	43750	9835	8051
N1.6S	20571	10687	10011

4 CONCLUSION

The aim of the present study is to evaluate the flexural performance of NSM strengthened beams using steel and CFRP material with variable bond length. Recent research concentrates on CFRP product and a lack of data is found for steel as a NSM strengthening material. This study assesses and compares the flexure behavior of both materials and the outcomes are summarized as follows:

- For both steel and CFRP strengthening materials, 1900 mm bond length performed better compare to 1800 mm and 1600 mm bond length. Even, the beams with least bond length (N1.6F and N1.6S) demonstrated enhanced ultimate capacity of 70% and 46% respectively compare to the control beam.
- Flexure failure (concrete crushing after yielding of internal steel) was occurred only in N1.9S and N1.8S beams where NSM steel was used with 1900 mm and 1800 mm bond length. This result also confirmed the full composite action of the NSM steel with RC beams. The other samples were failed due to concrete cover separation which is generally known as premature debonding failure.
- Altogether the NSM strengthened beams presented superior flexural performance compare to the control beam. Even though CFRP strengthened beams exhibited greater increase in strength, the stiffness and cracking behavior were not outstanding and even less compare to steel strengthened beams.

ACKNOWLEDGEMENTS

The authors gratefully acknowledge the support given by University of Malaya (UM) for funding the study through the University of Malaya Research Grant (UMRG) RP018-2012A.

REFERENCES

[1] A. Bilotta, F. Ceroni, M. Di Ludovico, E. Nigro, M. Pecce, and G. Manfredi, "Bond efficiency of EBR and NSM FRP systems for strengthening concrete members," Journal of Composites for Construction, vol. 15, pp. 757-772, // 2011.

[2] L. De Lorenzis and J. G. Teng, "Near-surface mounted FRP reinforcement: An emerging technique for strengthening structures," Composites Part B: Engineering, vol. 38, pp. 119-143, 3// 2007.

[3] O. Rosenboom and S. Rizkalla, "Behavior of prestressed concrete strengthened with various CFRP systems subjected to fatigue loading," Journal of Composites for Construction, vol. 10, pp. 492-502, 2006.

[4] H. V. S. GangaRao, P. V. Vijay, and N. Taly, "Frequently Asked Questions about Composite Materials," in Reinforced Concrete Design with FRP Composites, ed: CRC Press, 2006, pp. 1-18.

[5] K. N. Rahal and H. A. Rumaih, "Tests on reinforced concrete beams strengthened in shear using near surface mounted CFRP and steel bars," Engineering Structures, vol. 33, pp. 53-62, Jan 2011.

[6] H. Rasheed, A. Wuertz, A. Traplsi, H. Melhem, and T. Alkhrdaji, "Externally Bonded GFRP and NSM Steel Bars for Improved Strengthening of Rectangular Concrete Beam," ACI Special Publication, vol. 298, 2014.

[7] K. M. U. Darain, M. Z. Jumaat, M. A. Hossain, M. A. Hosen, M. Obaydullah, M. N. Huda, et al., "Automated serviceability prediction of NSM strengthened structure using a fuzzy logic expert system," Expert Systems with Applications, vol. 42, pp. 376-389, 2015.

[8] K. M. u. Darain, S. Shamshirband, M. Z. Jumaat, and M. Obaydullah, "Adaptive neuro fuzzy prediction of deflection and cracking behavior of NSM strengthened RC beams," Construction and Building Materials, vol. 98, pp. 276-285, 2015.

[9] L. De Lorenzis, "Strengthening of RC structures with near surface mounted FRP rods," PhD Thesis, Department of Innovation Engineering, University of Lecce, Italy, 2002.

[10]] R. Parretti and A. Nanni, "Strengthening of RC members using near-surface mounted FRP composites: Design overview," Advances in Structural Engineering, vol. 7, pp. 469-483, 2004.

[11] S. M. Soliman, E. El-Salakawy, and B. Benmokrane, "Flexural behaviour of concrete beams strengthened with near surface mounted fibre reinforced polymer bars," Canadian Journal of Civil Engineering, vol. 37, pp. 1371-1382, 2010.

[12] T. Hassan and S. Rizkalla, "Investigation of bond in concrete structures strengthened with near surface mounted carbon fiber reinforced polymer strips," Journal of Composites for Construction, 2003.

[13] P. Gergely and L. A. Lutz, "Maximum crack width in reinforced concrete flexural members," ACI Special Publication, vol. 20, pp. pp. 87-117, 1973.

[14] D. Gao, B. Benmokrane, and R. Masmoudi, A Calculating Method for Flexural Properties of FRP-reinforced Concrete Beam: Department of Civil Engineering, Faculty of Engineering, University of Sherbrooke, 1998.

CICM 2015
First International Conference on
Advances in Civil Infrastructure and Construction Materials
MIST, Dhaka, Bangladesh, 14–15 December 2015

DETAIL ENGINEERING ANALYSIS OF ASSESSMENT OF RETROFIT MEASURE BY CONCRETE JACKETING METHOD

Omar R. Chowdhury[1], Jaher Wasim[2], A. K. M. Hasan Julkernine[3], M. A. Habib[4], B. Shahriar[5] and M. A. B. Siddique[6]

[1, 2, 3, 4, 5, 6] Mantissa Design and Consultant, Dhaka, Bangladesh.
Email: [1]omarrashidchowdhury@gmail.com and [2]wasim@jaherwasim.com

Abstract. *Retrofit measures are important considering recent events of devastating building failures, especially in the ready-made garments sector in Bangladesh. This paper will be assessing retrofit measures on existing structures with respect to realistic case studies. According to different codes and engineering practices, retrofit measures may vary considerably. The paper will be introducing and evaluating different retrofit measures based on FEM modeling and in perspective to existing seismic conditions. To achieve this, evaluations will also be made based on Pushover and Time history analyses conducted on the structure in its present state and after retrofitting. The paper will basically focus on column jacketing retrofit technique, which is the most common practice in this field in Bangladesh. The paper shows that concrete jacketing method, in view of scenario in Bangladesh, is an effective method of retrofitting. Using time history analysis it has been seen that story drift decreases in a large manner in retrofitted frame.*

Keywords: Finite element modelling, Retrofit, Seismic Response.

1 INTRODUCTION

Retrofitting is technical interventions in structural system of a building that optimize the building capacity by strengthening beam, column , footing and other structural members. Strength of the building is generated from the structural dimensions, materials, shape and number of structural elements. Ductility of the building is generated from good detailing, materials used, degree of seismic resistance etc. Earthquake load is generated from the site seismicity, mass of the structures, important of buildings, degree of seismic resistant etc. Due to variety of structural condition of building, it is hard to develop typical rules for retrofitting. Each building has different approaches depending on the structural deficiencies. Hence, engineers are needed to prepare and design the retrofitting approaches. In the design of retrofitting approach, the engineers must comply with the building codes. The results generated by adopting retrofitting techniques must fulfill the minimum requirements on the building codes such as deformation, detailing strength etc." [1] In view of this, the paper will be assessing a case study of an existing structure located in Gazipur. It is a six storied RC structured building. The building was constructed in two phases between 2007 and 2009. A three story structure was completed in 2007 and a further three stories were constructed in 2009. This building is used mainly for light factory operations including operational offices, dining, and sewing, cutting, finishing and finished goods storage.

2 METHODOLOGIES

Several visits were made to check and collect data to assess building stability through Scanning, Rebar testing and Core cutting, on RCC column, beam and slab of different levels of the building. To assess and analyze data followed the code of BNBC [5], the guide line of Accord, Alliance and National Tripartite Plan of Action (NTPA) on structural integrity, using ACI-562 code to evaluate concrete strength from core test results. The software generated program ETABS [6] was used to analyze different types of load calculation and develop a 3D model of existing building structure. Based on the evaluation, a retrofit model was also developed.

2.1 Preliminary Assessment of the Structure

Based on visual inspection a preliminary assessment report was made including:

Item 1: Highly Stressed Columns
Item 2: Cracking above slabs around columns.
Item 3: Building documentation does not match as built structure and undocumented cantilever slabs.
Item 4: Localized areas of high loading in all building
Item 5: Unrestrained parapet at roof level

2.2 Geotechnical Investigation

This proposed land consisted of 6 bore holes were drilled up to 15 meter depth from the existing ground level (EGL). The allowable bearing capacity of soil under the bore hole 1 to bore hole 6 considered as isolated column footing (shallow foundation) in the following way : The allowable bearing capacity of footing qa is taken for BH-1, 2 & 4 as 1.30 tsf, bh-3 & 5 as 1.40 tsf and BH-6 1.20 tsf. (F.S=2.50) at a depth 8 feet from EGL.

2.3 Strength Assessment Of Concrete

To assess the strength of the concrete, we performed core test in June 2014 and March 2015. According to the core test result of the concrete strength is 11.5 MPA.

2.4 Test Of Collected Steel Sample

Rebar samples collected from the building showed 380 MPA yield strength according to laboratory test results.

2.5 Scanning Of Structural Member

To verify the reinforcement in the existing columns, beams and slabs, Ferro scanning was performed. Reinforcements were scanned at nineteen locations at different floor levels; two locations at level 1 (two beams), Five locations at level 2 (four columns and one slab), seven locations at level 3 (four columns, one slab and two beams) and five locations at level 6 (four columns one slab).

3 STRUCTURAL ANALYSIS

3.1 Structural Model

A three dimensional Finite Element (FE) analysis has been performed for this building based on as-built layout. The building has beam supported slab system (level-1, 2, 3) and edge supported slab system (level-4, 5, 6). Beams and columns were modeled with appropriate frame elements. The slab was modeled with shell elements. Fig.-1 shows the 3D model of the building and Fig.- 2 show the plan at typical floor level as modeled in the FE package ETABS 9.7.0. [2] Structural details are given in the table 1.

Table 1 : Structural Details of the Model Studied

f_c'	11.5 MPA
f_y	380 MPA
Beam	0.375mx0.25m
Column C1	0.3mx0.3m
Column C2	0.4mx0.3m
Column C3	0.45mx0.3m
Column C4	0.6mx0.3m
Slab S5	0.125m
Slab P5P5	0.175m
Slab S8	0.2m

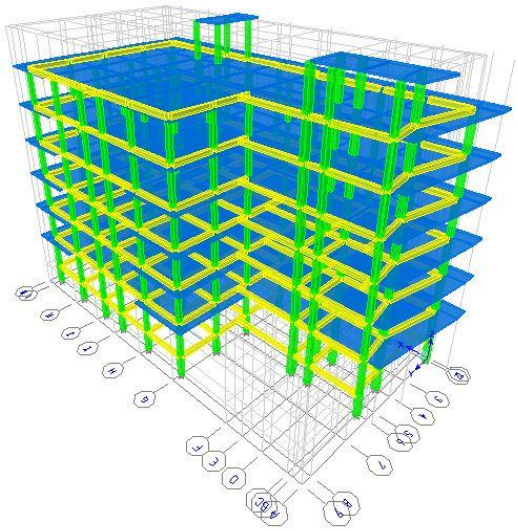

Figure 1: 3D view of the building

3.2 Boundary Condition

For a structure like this building, it is reasonable to assume that the bases of columns are fully restrained in all directions both translational and rotational. Thus, all the nodes at the bottom of each column were rendered fully restrained against all sort of displacement in the node.

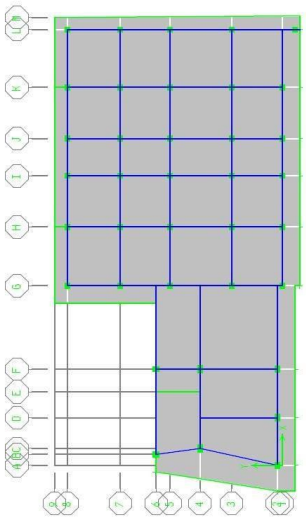

Figure 2: Plan view of the building

3.3 Retrofit Assessment

After conducting FE analysis, a great number of columns in the building were found to be inadequate. Design Load to Structural Element Capacity of Column (D/C Ratio) for columns in Level-1 are shown in Table-2. Inadequate columns are to be considered as those with D/C ratio greater than 1 and marked in red in the table.

Table 2: D/C ratio for columns in level-1.

Grid Line	A	B	C	D	E	F	G	H	I	J	K	L
1							2.18	1.91	2.37	2.34	2.33	
1C												O/S
2	1.61			1.75		1.66						
3							2.66	1.98	2.06	2.01	2.42	2.24
4			1.71			1.67						
5							2.95	2.01	1.99	1.97	2.02	2.11
6		1.36				1.64						
7							1.88	1.95	1.96	1.97	1.95	1.95
8							2.55	2.02	1.90	1.92	2.01	1.89
	N	O	P	Q	R	S	T	U	V	W	X	Y
1A							2.51	2.58				
1B	1.65			2.23		1.87						

After retrofitting the design load to structural element capacity are as follows (Table 3).

Table 3: D/C ratio for columns after retrofit in level-1.

Grid Line	A	B	C	D	E	F	G	H	I	J	K	L
1							0.44	0.38	0.39	0.36	0.33	
1C												0.32
2	0.42			0.21		0.41						
3							0.42	0.35	0.34	0.33	0.34	0.33
4			0.48			0.47						
5							0.44	0.35	0.24	0.24	0.27	0.31
6		0.43				0.43						
7							0.39	0.27	0.23	0.23	0.24	0.24
8							0.37	0.25	0.19	0.19	0.24	0.25
	N	O	P	Q	R	S	T	U	V	W	X	Y
1A							0.89	0.91				
1B	0.81			0.96		0.82						

Column jacketing method was incorporated in the structural retrofit model using SD section design process in ETABS 9.7.0 software. The column sections were increased by 5 inches on each side by reinforced concrete jacketing method. [3]

3.4 Time History Analysis

In this study, nonlinear time history analysis was performed using SAP2000 [4] in basic frame and retrofitted frame. It has seen that, in retrofitted frame, story drift was decreased by 40% with respect to the as built structure. Story drift data has shown in fig 3.

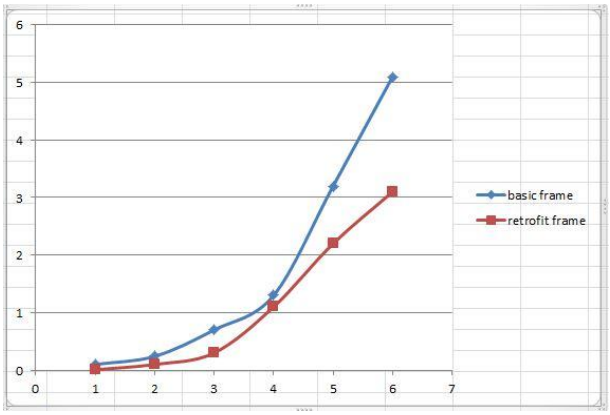

Figure 3: Story Drift in Basic Frame and Retrofit Frame

4 CONCLUSIONS

Based on the present study, the following conclusions can be drawn:

- Concrete jacketing of columns and encasing the joint region in a reinforced fillet is an effective but the most labor-intensive strengthening method due to difficulties in placing additional joint transverse reinforcement.
- Retrofitting by column jacketing decrease story drift by 40%
- It is important to obtain accurate as-built information and analytical data to perform a seismic evaluation of the existing structure and to select the appropriate retrofitting strategy
- Further research should be conducted to improve the selection of appropriate retrofit techniques using criteria based on performance, economy and constructability

REFERENCES

[1] Bhavar Dadasaheb, June 2013. Retrofitting of existing RCC buildings by method of jacketing, Volume 1, Issue 5. IJRMEET

[2] Computer and Structures Inc., ETABS Nonlinear Version 9.7, California, USA.

[3] A. Teran, J. Ruiz, 1992. Reinforced concrete jacketing of existing structures. *Earthquake Engineering, 10th World Conference (ISBN 9054100605)*, Balkema, Rotterdam.

[4] Computer and Structures Inc., SAP2000, California, USA.

[5] BNBC (2015) Bangladesh National Building Code, Housing and Building Research Institute, Mirpur, Dhaka, Bangladesh

[6] Computer and Structures Inc., ETABS Nonlinear Version 9.7, California, USA

CICM 2015
First International Conference on
Advances in Civil Infrastructure and Construction Materials
MIST, Dhaka, Bangladesh, 14–15 December 2015

FIELD EXTERIOR GIRDER ROTATION IN PLATE GIRDER BRIDGES DURING CONSTRUCTION

M. ASHIQUZZAMAN[1], **L. Hui**[2], **A. Ibrahim**[3], **W. Lindquist**[4] **and R. Hindi**[5]

[1, 2, 5] Department of Civil Engineering, Saint Louis University, Saint Louis, USA.
Email: [1]ashiquzzamanm@slu.edu, [2]huil@slu.edu and[5]rhindi@slu.edu

[3] Department of Civil Engineering, University of Idaho, Moscow, USA.
Email: aibrahim@uidaho.edu

[4] Kansas Department of Transportation, Topeka, Kansas, USA.
Email: will.lindquist@gmail.com

Abstract. *Bridge decks often overhangs past exterior girders in order to increase the width of the deck. Bridge designers typically proportion overhangs so that the same sections can be used for both the interior and exterior girders. While this leads to economical designs, the construction of these overhangs results in torsional moments due to the placement of the screed rails on the overhang form. These moments can cause excessive rotation of the exterior girders leading to thin decks, reduced concrete cover, poor rideability, instabilities during construction, and possible girder overstress. The deck overhang is usually formed by wood sheathing supported with brackets spaced over the length of the bridge. The brackets are connected to the top of the fascia girder with steel hangers and react against the girder webs. In some cases, the construction loads have resulted in bridges that were dangerously close to failures resulting from global or local instabilities. For this research, two plate girder bridges were monitored during construction to determine the exterior girder rotations due to the unbalanced construction loads. This paper presents the field maximum rotation of the exterior girder due to construction loads.*

Keywords: Plate Girder Bridge, exterior girder rotation, screed machine, Overhang deck.

1 INTRODUCTION

The decks of large plate girder steel bridges typically overhang past the fascia girders. In fact, the overhanging portion of the deck (shown in Fig. 1) is typically proportioned so the same section can be used for both the interior and exterior girders. During deck construction, loads on the overhanging portion are supported by cantilever forming steel brackets placed every 3 ft. to 6 ft. along the length of the exterior girders.

In fact, the loads from fresh concrete and screed machine as shown in Fig. 2 can make an unbalanced eccentric loading to the exterior girders. In some cases, these loads have resulted in bridges that were dangerously close to failures resulting from local and global instabilities [1]. Local instabilities are a particular concern for plate girder bridges due to the slenderness effect of the girder webs [2, 3]. There have been several studies to evaluate commercially available overhang brackets and hangers [4, 5, 6] although girder rotation continues to be a concern due primarily to difficulties with implementation and analysis.

Figure 1: Overhang deck in a typical steel girder bridge

Figure 2: Concrete pouring and finishing work using screed machine

Rotation in large plate girder bridges usually depends on the span length, symmetrical and unsymmetrical cross sections of the girder [7], and lateral bracing system or lateral support system and their connection with the main girder [8,9]. In particular, the exterior girder rotation (shown in Fig. 3**)** mostly depends on the overhang deck width, total construction load on the overhang and on the effectiveness of the bracing system used to prevent exterior girder rotation during construction. Several types of construction loads are applied to the overhang deck which is transferred to the exterior girders through steel brackets placed along the exterior girder. Typically, construction loads include the weight of fresh concrete, bridge deck finishing screed and rails, overhang formwork, weight of laborers and other construction-related live loads. It is possible to reduce the net torsional moment caused by these loads by placing the machine rails directly on the centerline of the exterior girders (zero eccentricity) rather than on the overhang formwork. The reduction in moment must be weighed against potential construction difficulties as the overhang requires hand placing and finishing. Most contractors prefer to place the screed rail on the overhang form since in this configuration, the finishing machine can reach 95% of the deck surface and the movement of the screed rails setup during placement is not necessary [10].

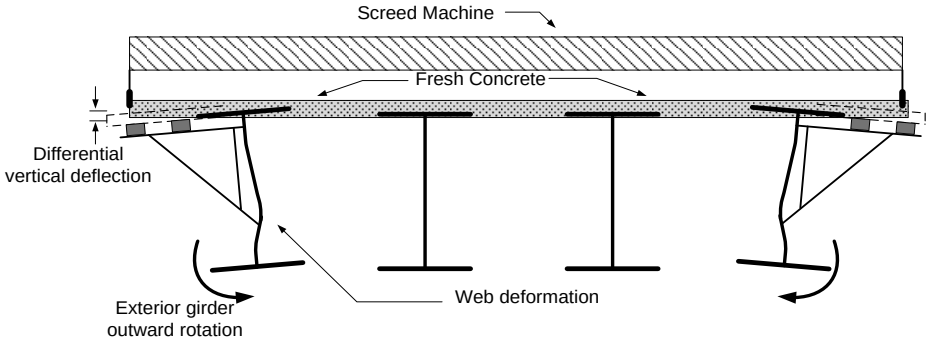

Figure 3: Exterior girder rotation due to unbalanced eccentric load on overhang deck

To prevent the exterior girder rotations due to the unbalanced loads from the overhang deck, it is essential to provide an appropriate bracing system for the girders. Commonly used bracing systems in the state of Illinois include transverse and diagonal ties; mostly transverse ties for large plate girder bridges. The transverse tie arrangement (shown in Fig. 4) is a No. 4 steel reinforcing bar connected from one exterior girder to the other exterior girder. An alternate bracing system with diagonal ties is shown in Fig. 5. In the diagonal bracing system, No. 4 bars are used as a diagonal link from the top flange of the exterior girder to the bottom flange of the first interior girder. All of these bracing bars are typically spaced at 3ft. to 4ft. along the span of the bridge. Proper tightening of the ties

plays an important role in their effectiveness. Square timber blocks (4in. × 4in.) are also used in between girders to prevent exterior girder rotations as shown in Fig.5.

Figure 4: Transverse ties

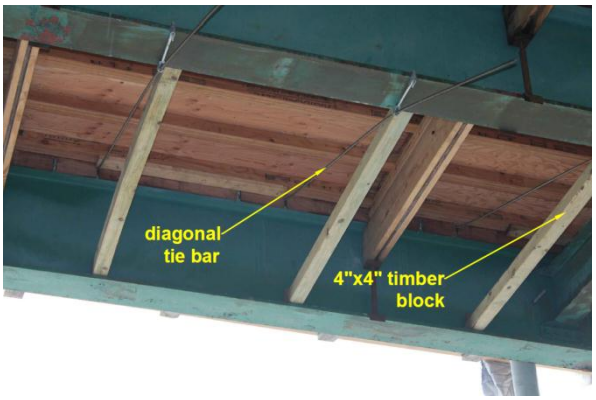

Figure 5: Diagonal ties

In this paper, two plate girder bridges (one is skewed and another is non-skewed) were monitored during construction in the field to measure the exterior girder rotation due to the overhanging portion of the deck during construction. A comparison of maximum rotation in the fascia girders is shown between these plate girder bridges.

2 BRIDGE DESCRIPTION AND INSTRUMENTATION

For this study, a skewed and a non-skewed plate girder bridge were selected to instrument in the field in the state of Illinois. The basic information for these bridges is presented in Table 1.

Table 1: Information of the bridges

	Belleville-II Bridge	Carlyle Bridge
Beam Type	64” PLG	78” PLG
Skewed?	30º	None
Staged construction?	Yes	None
No of Span	2	2
Span length	145’	200’
Concrete Poured	Up to 78’-0”	Up to 100’-0”
Overhang Width	3’-5”	3’-4”
Girder Spacing	9’-1”	6’-6”
Tie Type	Transverse	Transverse
Screed Type	Screed machine	Screed machine
Screed Location	On overhang deck	On overhang deck

2.1 Two-axis tilt sensor

CXTLA02 (2-axis: transverse and longitudinal direction) tilt sensors were used to monitor the girder rotations as shown in Fig. 6. The sensitivity of the tilt sensors was checked prior to installation. The range of tilt sensors in measuring rotation is ±20º as recommended by the manufacturer manual. Therefore, two specific locations (bottom flange and web) in any predefined girder at any section were chosen to attach the tilt sensors with some extra care during erection in every direction. All rotations were measured in degrees.

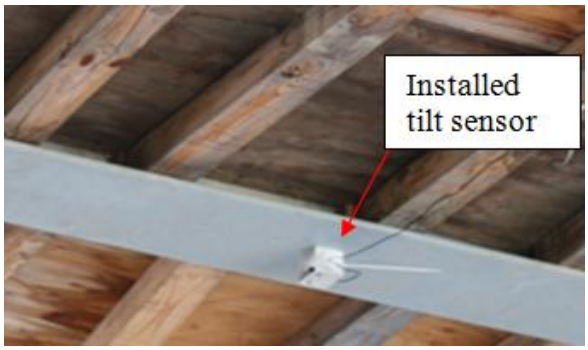

Figure 6: Installed tilt sensor in the bridge

3 FIELD DATA COLLECTION AND ANALYSIS

The middle spans were instrumented in both of the bridges to monitor the exterior girder rotations. The section of interest is the section at the point of maximum rotation for the exterior girders in the middle span, generally either located approximately at 40% or 50% of the span. Therefore, the section for instrumentation was chosen at mid-span (located between the diaphragms) of the selected span where most of the tilt sensors were placed to find the largest possible transverse rotation of the exterior girders. The tilt data was time-history data. To process the data, simple moving average (SMA) system (considering four periods) was followed to get a smooth trend line for the field data.

Figs.7 and 8 show the outward rotations during construction at mid-span in the exterior girder, respectively. In the Figs. 7 and 8**,** "maximum rotation" means the rotation of the exterior girder when all loads (fresh concrete, screed machine, work bridge, and other live loads) are placed at mid-span and "stable rotation" means the rotation of the exterior girders when there are no other loads except fresh concrete load.

The maximum rotation in Carlyle Bridge is 0.92º whereas the maximum rotation in Belleville-II Bridge is 1.03º. In case of stable rotation for all two bridges are pretty negligible.

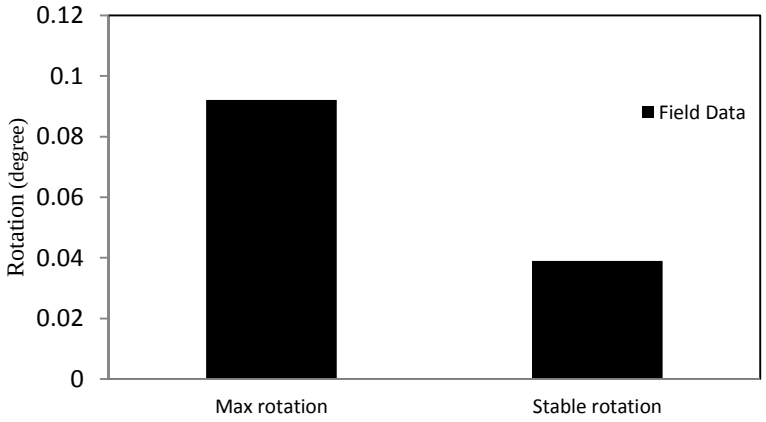

Figure 7: Exterior girder rotation in Carlyle Bridge

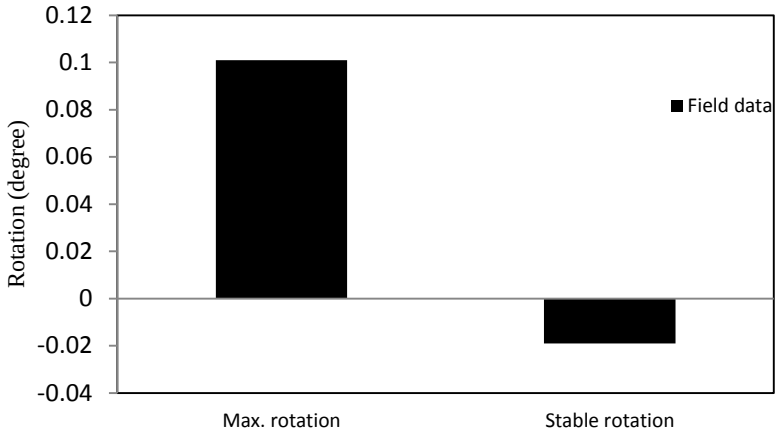

Figure 8: Exterior girder rotation in Belleville II Bridge

4 CONCLUSION

Based on the field data, it can be concluded the following points:

- The exterior girders experienced very small amount of rotation in large plate girder bridges due to unbalanced eccentric loadings from the overhang deck.
- Difference in rotation between two bridges is 10.58%, which is very small. Therefore it can be said that the rotation in large plate girder bridges does not depend on the skewness of the bridges.
- Span length of the bridges does not really affect to introduce more rotation to the exterior girder.

ACKNOWLEDGEMENTS

This project was made possible through funding from the Illinois Department of Transportation (IDOT) through the Illinois Center of Transportation (ICT); this support is very much appreciated. Also, many thanks also go to Saint Louis University (SLU) for all of the support. The authors would like to thank Mr. Darren Green, SLU, for his great help throughout this research. The opinions and findings of this paper are those of the authors.

REFERENCES

[1] Fasl, J. 2008. The influence of overhang construction on girder design (Doctoral dissertation). University of Texas at Austin.

[2] Shokouhian, M., and Shi, Y. 2015. Flexural strength of hybrid steel I-beams based on slenderness. Engineering Structures, 93, 114-128.

[3] Gupta, V. K., Okui, Y., and NAGAI, M. 2006. Development of web slenderness limits for composite I-girders accounting for initial bending moment. Structural Engineering/Earthquake Engineering, 23(2), 229S-239S.

[4] Ariyasajjakorn, D. 2006. Full scale testing of overhang falsework hangers on NCDOT modified bulb tee (MBT) girders (Master's thesis). North Carolina State University.

[5] Clifton, S. and Bayrak, O. 2008. Bridge deck overhang construction, (Rep. No. IAC 88-5DD1A003-2). Austin, Texas: Texas Department of Transportation.

[6] Grubb, M. 1990. Design for concrete deck overhang loads (Final report). AISC Marketing Inc.

[7] Schilling, C. G. 1988. Moment-rotation tests of steel bridge girders. Journal of Structural Engineering, 114(1), 134-149.

[8] Helwig, T., and Yura, J. 2012. Steel Bridge Design Handbook: Bracing System Design (No. FHWA-IF-12-052-Vol. 13).

[9] Roddis, W. K., Baghernejad, S., and Winters, E. L. 2008. Cross-Frame Diaphragm bracing of steel bridge girders (No. K-TRAN: KU-01-2). Kansas Department of Transportation.

[10] Suprenant, B. 1994, Setting screed rails for bridge deck paving, concrete construction, The Aberdeen Group.

CICM 2015
First International Conference on
Advances in Civil Infrastructure and Construction Materials
MIST, Dhaka, Bangladesh, 14–15 December 2015

REPAIR OF EARTHQUAKE DAMAGED BRIDGE DECK USING FRP BARS

M. ASHIQUZZAMAN[1], **M. T. Islam**[2], **K. J. Hong**[3]

[1] Department of Civil Engineering, Saint Louis University, Saint Louis, USA
Email: ashiquzzamanm@slu.edu

[2] Bangladesh University of Engineering and Technology, Dhaka, Bangladesh.
Email: tausif.islam25@gmail.com

[3] KookminUniversity, Seoul, Korea.
Email: kjhon.g@kookmin.ac.kr

Abstract. *A study was conducted into the flexural behavior of earthquake-damaged bridge deck repaired with fiber reinforced plastic (FRP) bars. A 20'x7'x8" bridge deck was modeled in ABAQUS environment. FRP bras was placed down below the deck at 5" spacing. Static was applied to bridge deck to see the response due to the applied load. Performance of repaired decks in terms of their response is evaluated and compared to those of the original and unretrofitted deck. The results indicate that the suggested repair system is highly effective. Both flexural strength and displacement of deck was higher than those of the original deck.*

Key word: Bridge deck, Seismic retrofitting, FRP bars, Earthquake.

1 INTRODUCTION

Nowadays near surface mounted (NSM) FRP is becoming a great technology for increase the flexural strength and shear resistance of deficient concrete bridge deck. This technology includes of employing the FRP rebars or strips into grooves pre-cut into the concrete cover in the tension section of the deck filled with high strength adhesive. NSM methods have become gradually common due to advantages over outstanding bonded reinforcement (EBR) such as a better attaching capacity of the FRP, better bonding performance and more ductility. While the structural behavior of RC members and concrete deck strengthened with NSM under normal environmental conditions is getting more and more documented [1-6] their satisfactory behavior at raised temperature.

Concrete decks are the members of the bridge that can be weakened due to the vibration of during earthquake. FRP materials are susceptible to deterioration of mechanical properties and combustion when exposed to environment. Indeed, the overall performance of the NSM FRP strengthened members depends on the properties of the FRP-adhesive and adhesive–concrete bond interfaces.

In this paper, finite element results investigating the behavior of NSM FRP strengthened deck. To evaluate the feasibility of achieving FRP system, an investigation was undertaken to find out the performance of near surface mounted (NSM) FRP strengthened concrete deck.

2 MATERIAL PROPERTIES

2.1 Concrete deck

The considered dimensions of the deck is 20’x7’x8” as shown in Fig. 1. The material properties considered for the finite element analysis is shown in Table 1a and b.

Table 1: a) Material Properties of concrete

Elastic Behavior	Young’s Modulus	1300000 psi
	Poisson’s Ratio	0.2
Damping Behavior	Structural damping	0.00323
Mass Density	--	0.00868lb/in3

2.2 Normal reinforcement bars

The material properties of steel bars are shown in Table 2.

Table 2: Material Properties of conventional steel bars

Elastic Behavior	Young’s Modulus	29000000 psi
	Poisson’s Ratio	0.3
Mass Density	--	0.2836lb/in^3

Table 1: b) Concrete Damaged Plasticity

Plasticity		Compressive Behavior		Tensile Behavior	
Dilation Angle	36.31	Yield Stress	Inelastic Strain	Yield Stress	Cracking Strain
Eccentricity	0	0.013	0	0.00029	0
fb0/fc0	0	0.0241	0.001	0.00194393	0.066185
K	0			0.00130305	0.12286
Viscosity parameter	0			0.000873463	0.173427
				0.0005855	0.22019
				0.000392472	0.264718
				0.000263082	0.308088
				0.000176349	0.35105
				0.00011821	0.394138
				7.92388E-005	0.437744
				5.31154E-005	0.482165

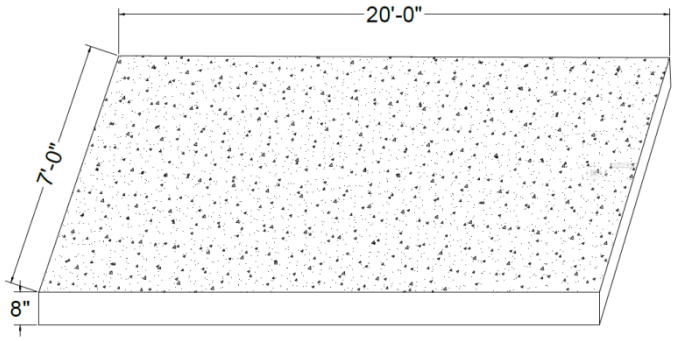

Figure 1: Concrete deck and the dimensions

2.3 NSM FRP reinforcement bars

The material properties of NSM FRP steel bars are shown in Table 3.

Table 3: Material Properties of NSM FRP bars

Area per No. 3 bar	0.1 in^2
Ultimate tensile strength	250ksi
Rupture strain	0.013 in./in.
Modulus of elasticity of FRP laminates	19230ksi

The detailing of the NSM FRP bar installation is shown below:

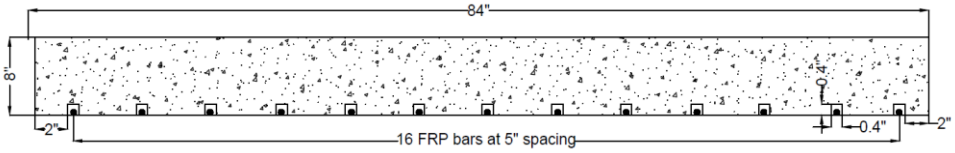

3 FINITE ELEMENT MODELING AND RESULTS

3.1 FE Modeling

The finite element model was constructed using ABAQUS 6.13 environment as shown in Fig. 2. The concrete was modeled as solid element. The steel bar and NSM FRP bars were modeled using beam element. "Embedded Region" constraint was to keep the rebars inside of the concrete. An uniformly distributed load of 5 lbs was applied at top surface of the deck.

Two different models were run to investigate the behavior of the NSM FRP bars; i) concrete deck with NSM FRP bars, ii) concrete deck without NSM FRP bras.

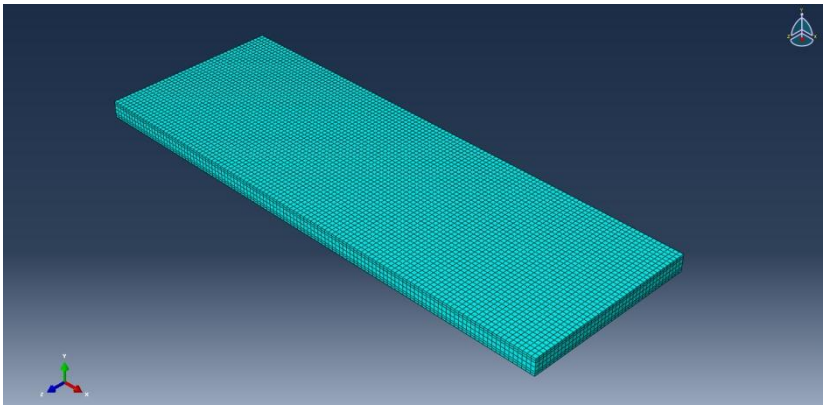

Figure 2: Finite element model for the concrete deck (meshed part)

3.2 Results

The deformed shapes of the concrete deck due to loading are shown in Fig. 4 to 5. The deflection of concrete at mid span due to loading is shown in Fig. 6 where the deflection with and without NSM FRP bars. Figure 6 and 7 show that adding of the FRP bars reduces the vertical deflection and stresses of concrete respectively.

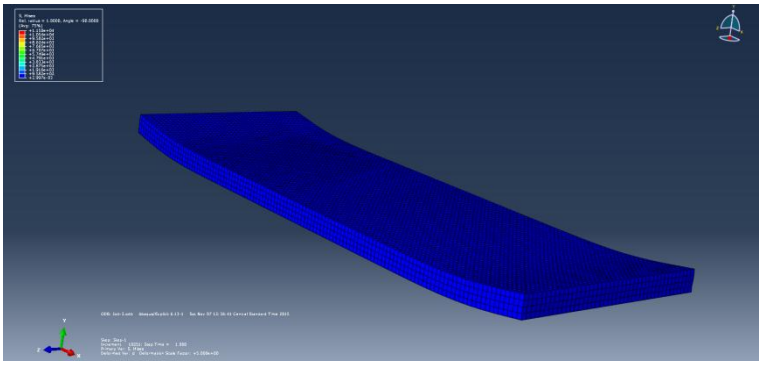

Figure 3: Deformed shape of the concrete deck

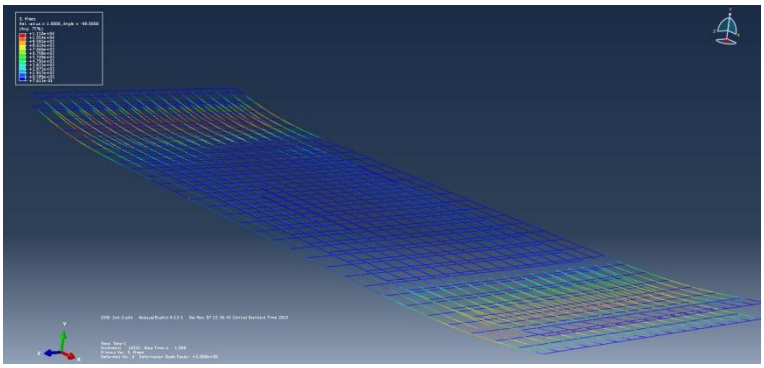

Figure 4: Deformed shape of concrete embeded normal reinforcement

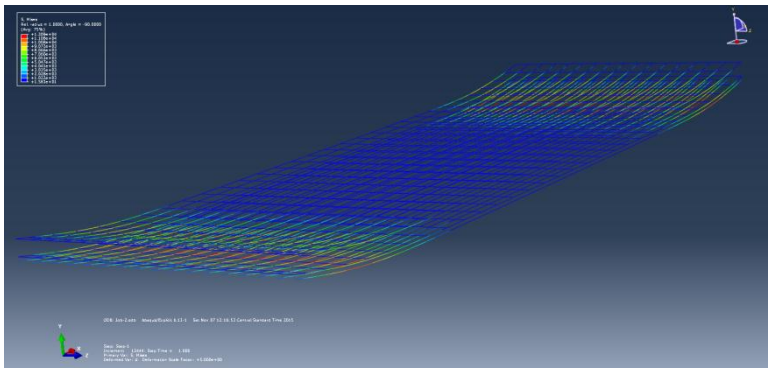

Figure 5: Deformed shape of concrete embeded normal reinforcement with NSM FRP bars

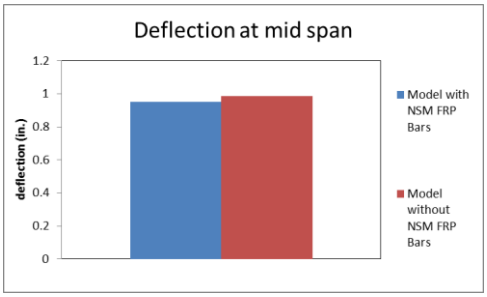

Figure 6: Deflection of concrete at mid span due to loading

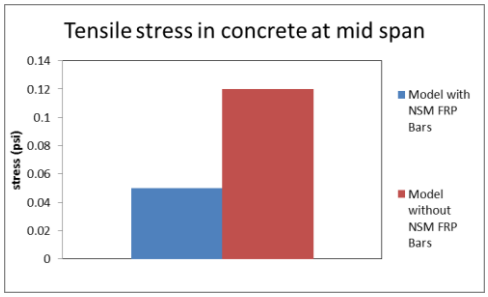

Figure 7: Tensile stress of concrete at mid span due to loading

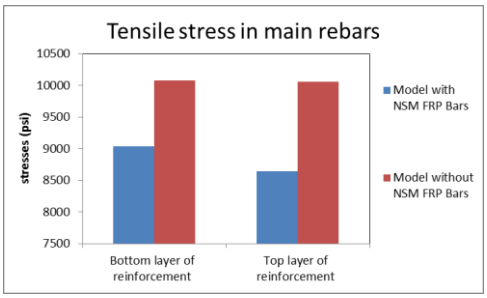

Figure 8: Tensile stresses in main rebars at support location due to loading

Figure 8 shows that adding of the FRP bars can increase the overall flexural capacity of the tensile elements.

4 CONCLUSION

Based on the field data, it can be concluded the following points:

- NSM FRP bars can increase the overall capacity of the deck during earthquake.
- Addition of FRP bars can increase the flexural strength of the deck by 10%.
- Effective deck thickness could be increased due to application of NSM FRP bars.

REFERENCES

[1] Blaschko M. Bond behaviour of CFRP strips glued into slits. In: Proceedings of FRPRCS-6, Singapore; July 2003. p. 205–14.

[2] De Lorenzis L, Lundgren K, Rizzo A. Anchorage length of near-surface mounted FRP bars for concrete strengthening – experimental investigation and numerical modeling. ACI Struct J 2004;101(2):269–78.

[3] Kotynia R. Strain efficiency of near-surface mounted CFRP-strengthened reinforced concrete beams. In: Proceedings of international conference on composites in construction, Lyon; July 2005. p. 35–42.

[4] Seracino R, Saifulnaz MRR, Oehlers DJ. Generic debonding resistance of EB and NSM plate-to-concrete joints. J Compos Constr ASCE 2007; 11(1):62–70.

[5] Palmieri A, Matthys S, Taerwe L. Strengthening with near surface mounted reinforcement: structural and fire behavior. In: Proceedings of third fib international congress 2010 (fib-2010), Washington DC; July 2010 [CD-ROM].

[6] Hawileh R. Nonlinear finite element modeling of RC beams strengthened with NSM FRP rods. Constr Build Mater 2012; 27(12):461–71.

CICM 2015
First International Conference on
Advances in Civil Infrastructure and Construction Materials
MIST, Dhaka, Bangladesh, 14–15 December 2015

PRODUCTION OF MICRO-CONCRETE USING INDIGENOUS MATERIALS

Raquib AHSAN[1], **Md R. Hassan**[2] **and Shofiq Ahmed**[3]

[1] Civil Engineering Department, Bangladesh University of Engineering and Technology, Dhaka, Bangladesh.
Email: [1]raquibahsan@ce.buet.ac.bd, [2]rakibulhassan.buet@gmail.com and [3]ashofiq@gmail.com

Abstract. *Concrete is one of the basic elements of RCC structure and also the most crucial one. In recent years, a lot of researches have been conducted to develop special types of concrete for special purposes. Micro-concrete is one of them which is mainly used for retrofitting. According to recent statistics, a large number of structures in the major cities of Bangladesh are vulnerable to collapse. Retrofitting may thus be required as a sustainable solution and for this purpose we can consider the utilization of micro-concrete. In this study we have aimed at producing micro-concrete using available local materials. Import of micro-concrete from foreign countries costs almost five to six times more than that produced using local materials. We can also reduce the production cost even more by magnifying the scale of production. This paper delineates proper mixing proportions of water, cement, aggregates and admixtures, to attain characteristics of micro-concrete using indigenous material in the context of Bangladesh.*

Keywords: Retrofitting, Vulnerable, Sustainable solution, Strength, Low cost, Indigenous material.

1 INTRODUCTION

Recently retrofitting of structures has become an important issue to get continued service of existing structures such as building, bridge and others. Owing to structural deficiencies, as in a lot of cases, columns are found inadequate under seismic or lateral loads and thereby jeopardizing stability and performance of whole structure. In these cases, columns are needed to be repaired or retrofitted. Recently, several initiatives have been taken to identify structurally deficient RMG (ready mate garments) factory buildings of the country after the tragic incident of Rana Plaza. Eventually, retrofitting of several buildings will become inevitable though such practice is not very common in Bangladesh. Use of Micro-concrete is one of the most convenient ways. Due to its high price, the practice of retrofitting using micro-concrete is not common in Bangladesh. If its price can be reduced then it might be the most effective way. By using these materials high strengthen concrete can be achieved. Not only it will enhance the load carrying capacity but also it will give us the privilege to do retrofitting in a convenient way.

2 MATERIALS & PROPERTIES

The raw materials used for laboratory tests are locally available and they are of low cost too. In this study ordinary Portland cement, locally available sylhet sand, 5 mm downgraded coarse aggregate, non-shrink water reducing admixture and potable water have been used to form concrete samples. The properties of these materials are as follows:

Table 1: Properties of raw materials

Materials	Properties
Ordinary Portland Cement	(i) Specific gravity – 1.56
Fine Aggregate (FA)	(i) Absorption capacity - 1.11% (ii) Specific gravity - 2.60 (iii) Fineness modulus- 2.83
Course Aggregate (CA)	(i) Absorption capacity- 2.17% (ii) Specific gravity - 2.48
Master Glenium JP30 Admixture	Non-shrink, water reducing
Water	Potable water

3 METHODOLOGY

As micro concrete is mainly used for retrofitting purpose, the basic objective of this study is to find a mix ratio that will provide high early (14 days) compressive strength as well as enough tensile strength (28 days); and also high flow ability

for self-compaction. After collecting materials the properties were tested. Initially the target was to achieve at least 7000 psi compressive strength and determined normal concrete mix ratio 1: 0.96:1.56 (Cement: FA: CA) for 7000 psi compressive strength. Five ratios were selected on this basis of normal concrete mix ratios. 9 cylinders were made for each ratio including 3 for 7 days compressive strength, 3 for 14 days compressive strength and 3 for tensile strength. In following table those mix ratios is shown along with the amount of admixture, w/c ratio and their cost:

Table 2: Final ratios of concrete tested for compressive strength

Trails	Cement : Sand : Coarse Aggregate	w/c ratio	Admixture (ml/kg of cement)	Material Cost (Taka/cft)
F-1	1 : 1.5 : 3	0.37	6	386
F-2	1 : 1.2 : 1.7	0.34	6	409
F-3	1 : 1.1 : 1.6	0.35	6	415
F-4	1 : 1 : 1.5	0.31	4.55	422
F-5	1 : 1.1 : 1.4	0.30	3.33	418

3.1 WORKING FLOW DIAGRAM

Total working procedure is presented below by flow diagram and sample pictures are shown in Figure 1.

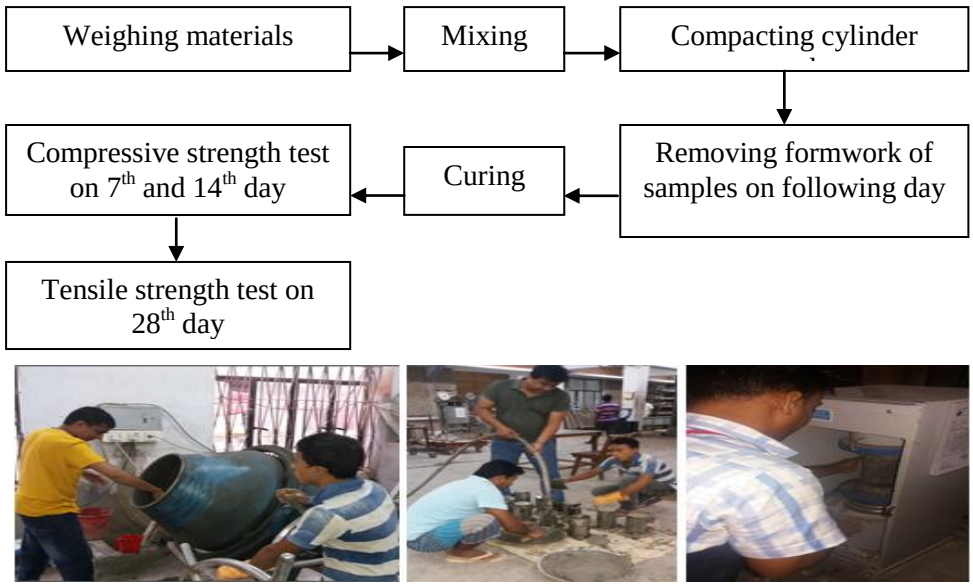

Figure 1: Working on laboratory

4 CYLINDER TESTS

4.1 COMPRESSIVE STRENGTH TEST

Compressive Strength test of the concrete specimen is most widely used test to measure its compressive strength. For this purpose two types of concrete specimen are used, Cubes & Cylinder. In this study we use cylinder test

Initial Compressive strength was measured at 7 days of casting and final compressive strength was measured at 14 days. At time of casting initial slum value and slum value after 12 minutes was also counted. The compressive strength and slum value of final mix ratios are shown in the following:

Table 3: Compressive strength and slum value of final mix ratios of concrete

Trials	Compressive strength (psi)		Slum value Initial (inch)	Slum value 12 min (inch)
	7 days	14 days		
F-1	4910	5350	3.25	2.8
F-2	6260	6830	8.5	6.45
F-3	5600	5780	8	6.4
F-4	6990	7820	9	6.9
F-5	6820	7110	8	6.5

From ASTM C 39-03"Standard test method for compressive strength of cylindrical concrete specimens" shows five different types of fracture. Such as a) cone, b) Cone and split c) Cone &shear, , d) shear, e) Columnar. Shear failure which occurs in this compressive strength test is shown in figure-4.

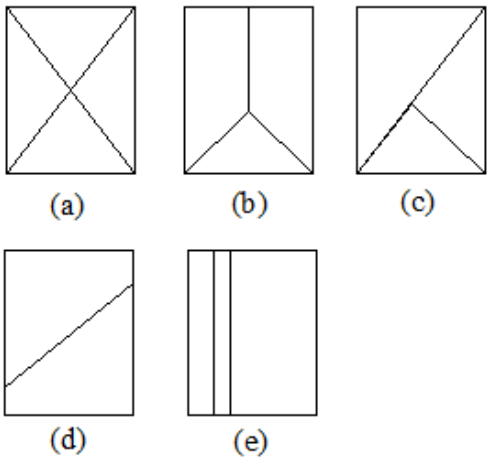

Figure 2: Compressive test

4.2 TENSILE STRENGTH TEST

Tensile strength is an important property of concrete because concrete structure is highly vulnerable to tensile cracking. Due to difficulty in applying uniaxial tension to concrete specimen, the tensile strength of concrete is determined by indirect test method: 1) split cylinder test, 2) flexure test. To determine tensile strength, here split cylinder test was done and we follow ASTM designation C 496-96. The compression load is applied to diametrically and uniformly along the length of cylinder until the failure of the cylinder along the vertical diameter.

The tensile strength test was done at 28th days of curing. Conventionally tensile strength is always approximately 10% of compressive strength. But here it was found more than 10% for all the ratios. In the following table these values of tensile strength are shown:

Table 4: Tensile strength of final mix ratios of concrete

Trails	Tensile Strength (psi) 28 days	Tensile Strength of %Compressive Strength
F-1	915	17
F-2	1270	18.6
F-3	900	15.6
F-4	1215	15.5
F-5	950	13.4

The cylinder concrete specimens of tensile strength tests were failed along the vertical diameter of cylinder and sample pictures are shown in Figure 3.

Figure 3: Tensile test

5 TEST RESULTS

A comparison between compressive strength of 14 days, tensile strength of 28 days and cost of every trial are shown by the following diagram:

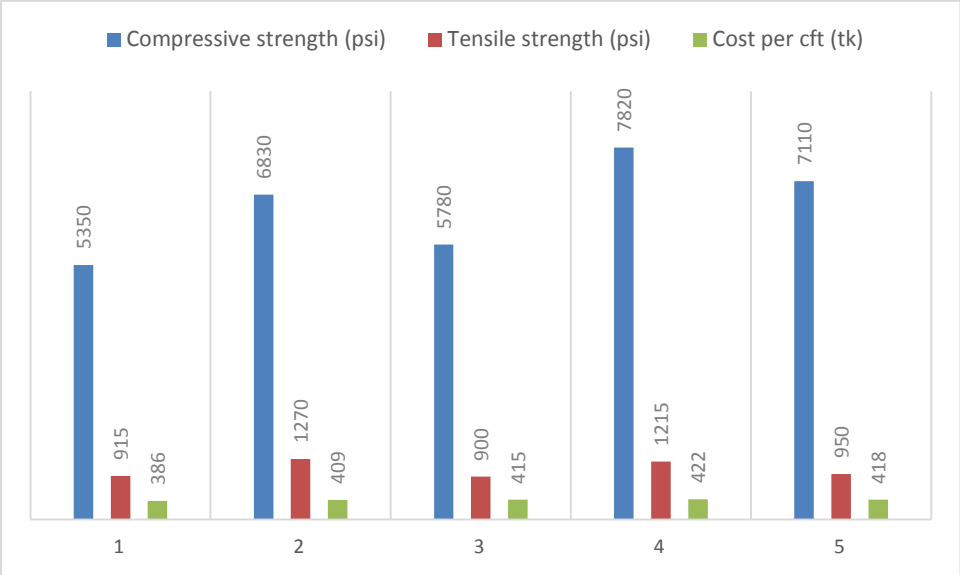

Figure 4: Comparison between compressive and tensile strength

a) For F-1 trial, cost and strength both are minimum. Because here the amount of cement is less comparing to coarse and fine aggregate's surface area and as a result presence of void is more and bonding strength becomes low. Its slum value is also comparatively low.

b) For F-4 trails maximum material cost is required but it provides maximum compressive as well as tensile strength. Here the strength is maximum because cement is more enough with respect to surface area of course and fine aggregate and so inter particular void is reduced and bonding strength is high. Its flow ability is also high enough for self-compaction.

c) Another trial F-2 shows average material cost with average compressive strength but its tensile strength is highest and tensile strength is 18.6% of compressive strength where generally we assume tensile strength is 10% of compressive strength. The trial shows initial slum value of 8.5 inch and after 12 minutes it becomes 6.45 inch which indicates high flow ability.

6 CONCLUSION

In this study various trials of concrete samples was designed using indigenous materials varying in proportion of cement, coarse aggregate, fine aggregate, admixture and w/c ratio. Highest compressive strength 7820 psi was achieved for ratio of 1:1:1.5 (cement: sand: coarse aggregate) and its corresponding tensile strength was 1215 psi which was 15.5% of compressive strength. The water cement ratio was0.31 and the amount of admixture used was 4.55 ml/kg of cement. Its initial slum value is 9 inch and after 12 minutes it was 6.9 inch which represents high flow ability. Material cost for this specimen is 422 per cft of concrete.

Hence, it can be concluded that the ratio of 1:1:1.5 can be considered as micro concrete which will have high compressive strength, higher tensile strength and higher slum value than conventional concrete.

However, depending on one's requirement other mix ratios may be selected considering the compressive strength, tensile strength and cost data of figure 4. Figure 4 may also serve as a guideline for the trend of those properties for other mix ratios.

ACKNOWLEDGEMENT

We are very thankful to the EIMS (Environmental and Infrastructure Management Solution Ltd.) for financial and raw material support.

We also grateful to the concrete lab instructors of Department of Civil Engineering Department of Bangladesh University of Engineering and Technology, Dhaka for technical support and conducting tests.

REFERENCES

[1] Concrete Technology, A.M Neville CBE, J.J Brooks "Mix design" Chapter 19, page 363-398.

[2] Mix Design as per "ACI 211.1-91"

[3] Conference paper; "effect of aspect ratio on column strengthening using frp laminates"- Md. Shajal Khan, Md. Abul Bashar Emon, Tanvir Manzur.

[4] T.Jeevetha, Dr S.Krishnamoorthi, G.S.Rampradheep "study on strength properties of self-compacting concrete with micro silica" International Journal of Innovative Research in Science, Engineering and Technology(An ISO 3297: 2007 Certified Organization) Vol. 3, Issue 4, April 2014

[5] Mudasir Hussain Pandit, Mrs. D. Renuka Parameswari "High Density Con crete Using Fly Ash, Micro Silica and Recycled Aggregate – An Experimental Study" International Journal of Engineering Trends and Technology (IJETT) – Volume 10 Number 1 - Apr 2014

[6] Laboratory manual of Materials sessional, CE 202, BUET. "determination of specific gravity absorption capacity, sieve analysis of CA & FA"

CICM 2015
First International Conference on
Advances in Civil Infrastructure and Construction Materials
MIST, Dhaka, Bangladesh, 14–15 December 2015

ASSESSMENT ON MOMENT CONCENTRATION AT SLAB-COLUMN JOINT OF RC FLAT PLATES DUE TO GRAVITY AND LATERAL LOADS

Mohammad R. ISLAM[1] and Tahsin R.Hossain[2]

[1]Department of Civil and Environmental Engineering, Shahjalal University of Science and Technology, Sylhet, Bangladesh.
Email: rafiqul-cee@sust.edu

[2]Department of Civil Engineering, Bangladesh University of Engineering and Technology, Dhaka, Bangladesh
Email: tahsin@ce.buet.ac.bd

Abstract. *Bangladesh lies in moderate to high seismic zones. Many high-rise buildings are being constructed in different cities of the country. As per BNBC 2006, flat plate structures, as a part of lateral load carrying system is not permitted in high-seismic zone. However, many flat plate building have already been constructed in high-seismic zones, i.e. in Sylhet. Also, there are many flat plate buildings which have been designed without considering the seismic loads at all. For flat plates, the region around the column is always the critical location as it transfers combined gravity and lateral loads in a relatively small shallow section. Unbalanced moments generated due to seismic action need to be transferred to column from the flat plate. These moments are large, particularly for high-rise building having large span length and pose a problem in the design of the connection. The percentage of moment transfer through different strip of slab of a ten storied flat plate structure is analysed by using Simpson's 1/3rd rule and 'ETABS' software under gravity and lateral loads and compared with percentage according to ACI code provision.*

Keywords: Flat plate structure, Percentage of moment, Gravity load, Seismic load, ETABS software.

1 INTRODUCTION

Bangladesh and the north-eastern Indian states have long been one of the seismically active regions of the world and have experienced numerous large earthquakes during the past 200 years. In geological point of view, part of Bangladesh is situated in moderate to high seismic zones. However, in the country a rapid urbanization is going on. Presently, flat plate building is popular for its advantages regarding use and constructability. However, in the design of reinforced concrete flat plates, the regions around the column always pose a critical analysis problem. When exposed to seismic loads, the performance of slab-column frames has often been less than satisfactory. Brittle punching failures of flat plates have been observed during several earthquakes as documented by AISI, (1964) and Mitchell et al. (1990). Moreover, flat plate as part of lateral load carrying system is not permitted in high seismic zone according to ACI 318, (2008) and BNBC, (2006) code provisions as slab-column connection performance are not satisfactory in carrying seismic loads. So it is important to understand the slab-column connection at critical section of flat plates. Many research efforts have been made in the past and are still being continued to establish rather restrictive rules for flat-slab systems in earthquake prone regions. It has also inspired researchers to start extensive experimental work, and to develop new ways to make the connections stronger and more ductile in order to allow more widespread use of flat slab systems in seismic zones. In the mid-seventies, Hawkins et al. (1975) were the first to research the effects of lateral loads on flat plate structure. Numerous tests (Ghali et al., 1976; Pan et al., 1989; Cao, 1993; Dilger et al., 1994) have been carried out to evaluate the behavior of slab-column connection at critical section.

In this study, consider a ten storied building having flat plate slab system. For such type of flat plate structures in regions of seismic risk, checked the percentage of moment for column strip and middle strip under gravity and lateral loads. Again recheck the percentage of moment transferred through effective width (c+3h) due to lateral load. Computer software 'ETABS' have used for three dimensional frame analysis based on elasticity.

2 GENERAL SPECIFICATIONS

In the flat plate structures, whereas the columns are cast integrally with the floor slabs and reinforced in two directions so that it brings its loads directly to supporting columns behave similar to moment resisting frames under horizontal loading. The lateral deflections of the structure are a result of simple double curvature bending of the columns and a more complex three-dimensional form of double bending in the slab. Flat plate slab systems may be designed for gravity loads by empirically based direct design method according to ACI Code provision [Code Sec. 13.6]. The direct design method is generally simpler to use, but

is restricted to very regular layouts and normal live-load-to-dead-load ratios as outlined below:

1. A minimum of three spans each way, directly supported on columns.
2. Rectangular panels with the long span not more than twice the short span.
3. Successive spans not differing by more than 1/3 of the longer span.
4. Live load not more than 3 times dead load.
5. All loads to be uniformly distributed gravity loads.
6. For panels with beams between columns on all sides the beam relative stiffness must fall within a range of 5 to 1.

Considering above all points, a typical interior frame of a ten storied flat plate building has been considered having 18 ft (5.5 m) (Short span) × 20 ft (6.1 m) (Long span) slab, supported on a 15 inch (381 mm) square column as shown in [Fig. 1] and [Fig. 2]. The thickness of the slabs is 7 inch (177.8 mm) by ensuring that punching shear failure has not occurred according to ACI 318-08 and BNBC (2006) code provisions. In this modeling the dead load with self weight was 162.5 psf (7.8 kN/m^2) and the live load was 40 psf (2 kN/m^2) as it is a residential building. Seismic zone have considered according to BNBC (2006) code provision. Zone-2 have been selected to analyze the frame considering lateral loads as the above mentioned residential building is located at Dhaka city. For the modeling of this flat plate structure, the compressive strength of concrete and yield strength of steel have been considered 4000 psi (27.6MPa) and 60 ksi (413 MPa) respectively.

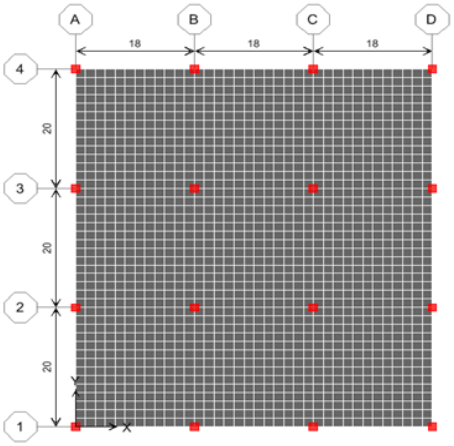

Figure 1: Plan view of flat plate slab system

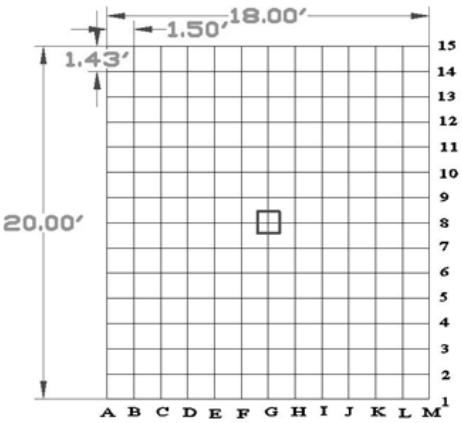

Figure 2: Plan view of interior panel

Sec. 13.6 of ACI 318-08 code provision regarding direct design method was considerably simplified by the 1983 Code revision. That removed the somewhat cumbersome earlier procedures for determining the distribution of total span moment in end spans and substituted a table of moment coefficients. This simplification allows direct determination of end-span moment distributions without the need for computation of equivalent column stiffness.

According to ACI 318 (2008) code provision, the percentages of total negative moment, total positive moment, column strip moment and middle strip moment for interior panel are as follows:

Negative factored moment ..... 65% of total factored static moment
Positive factored moment..... 35% of total factored static moment
Column strip negative moment..... 75% of negative factored moment
Middle strip negative moment..... 25% of negative factored moment
Column strip positive moment..... 60% of positive factored moment
Middle strip positive moment..... 40% of positive factored moment

In this study, an analysis has been done to check the percentage of moment transfer through column strip and middle strip of flat-plate slab system by using Simpson's 1/3rd rule and 'ETABS' software due to gravity and lateral loads. Again, recheck the amount of total moments have transferred through column strip and effective width due to lateral load.

This rule is applicable when even number of strips and odd number of ordinates.

Area=Common distance/3{1^{st} ordinate + last ordinate +2(Σ even ordinates) + 4(Σ odd ordinates)}

$$\text{Area}=\Delta x/3\{y_0 + y_n +2(y_2 + y_4 + \ldots) + 4(y_1 + y_3 + \ldots)\} \quad (1)$$

3 RESULTS AND DISCUSSIONS

The plan view of flat plate slab system and interior panel have given in figure1and figure 2 respectively. The flat plate slab or interior panel is divided by grid lines. Thirteen grid lines (A, B, C, D, E, F, G, H, I, J, K, L, M) have considered in one direction(short span) of interior panel and Fifteen grid lines (1, 2, 3, 4, 5, 6, 7, 8, 9, 10, 11, 12, 13, 14, 15) have considered in other direction(long span) of interior panel. After apply the loads and complete the analysis by using 'ETABS' software, moment at all nodal points can be determined. Total moment in the grid lines mentioned above can be calculated by using Simpson's 1/3rd rule.

A graphical representation of moments for that interior panel under gravity load is given below:

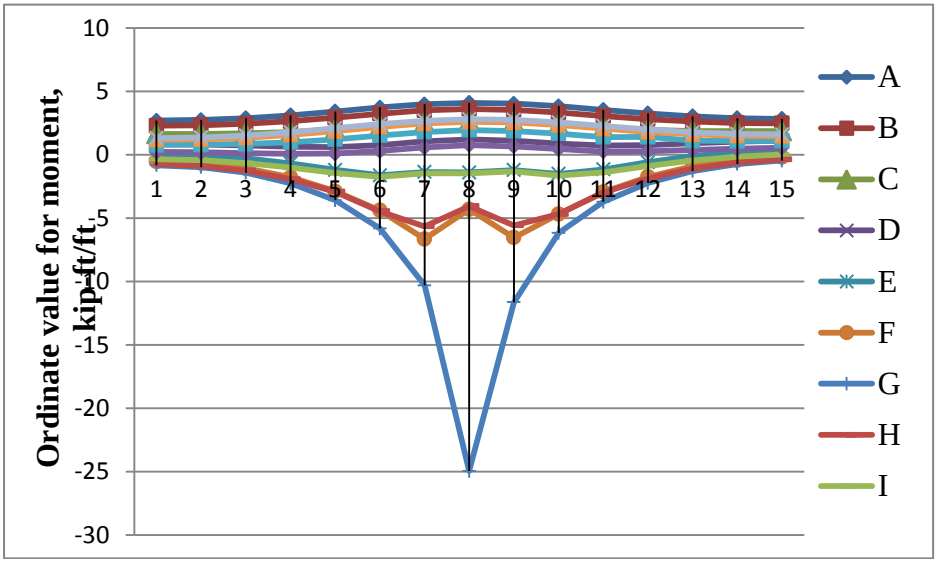

Figure 3: Ordinate value for moment in kip-ft/ft under gravity load along short span of interior panel of flat plate structure (1 kip-ft = 1.36 kN-m).

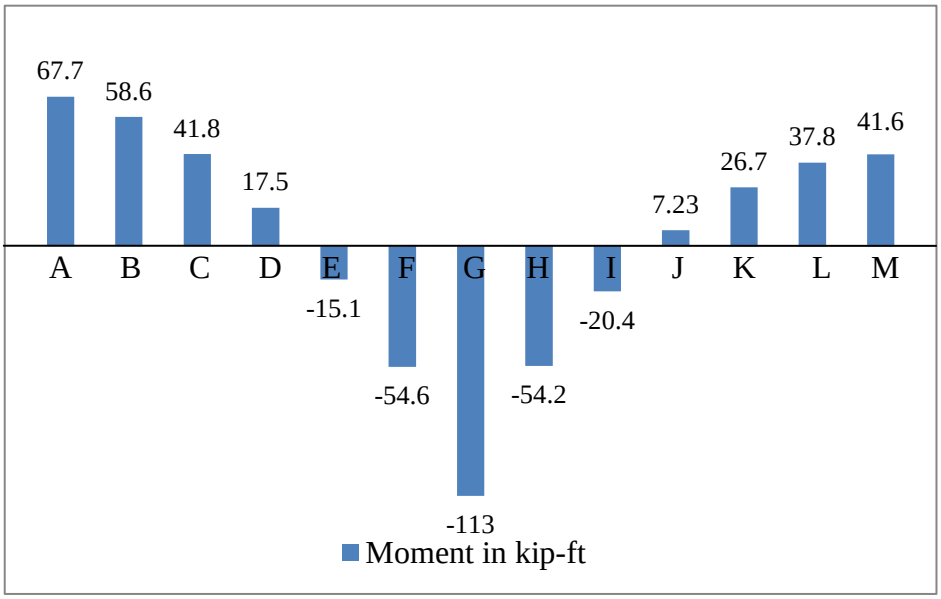

Figure 4: Moment in kip-ft under gravity load along short span of interior panel of flat plate structure (1 kip-ft = 1.36 kN-m).

Under gravity load the percentages of total negative moment, total positive moment, column strip moment and middle strip moment for that interior panel are given below:

Negative factored moment ..... 67.4% of total factored static moment
Positive factored moment..... 32.6% of total factored static moment
Column strip negative moment..... 83.7% of negative factored moment
Middle strip negative moment..... 16.3% of negative factored moment
Column strip positive moment..... 53% of positive factored moment
Middle strip positive moment..... 47% of positive factored moment

There are some differences in between the above discussed percentages of moment from Simpson's 1/3rd rule and 'ETABS' software and the percentages of moment based on direct design method according to ACI 318 (2008) code provision as discussed in Sec. 2for an interior panel.

A graphical representation of moments for that interior panel under lateral load is given below:

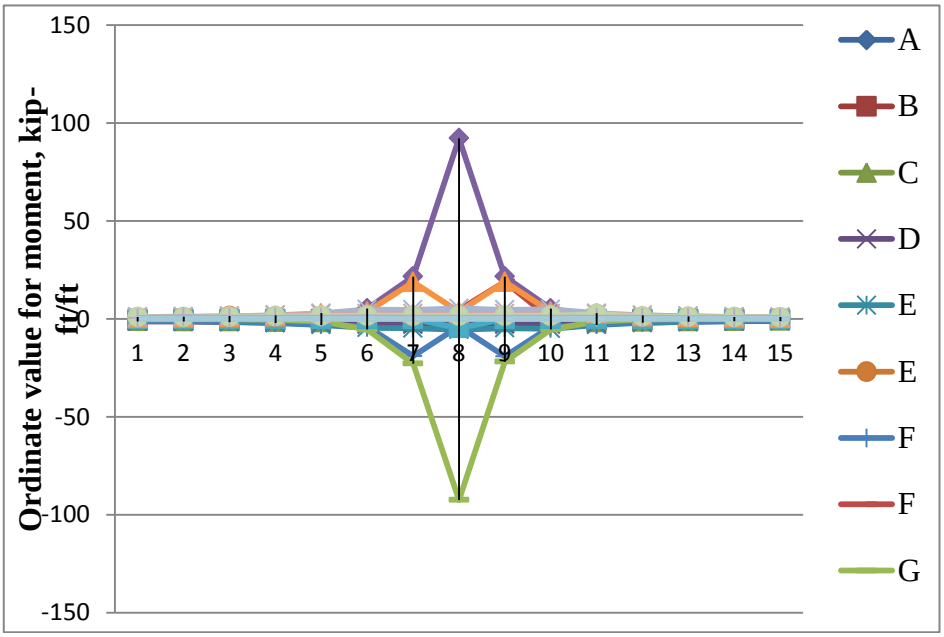

Figure 5: Ordinate value for moment in kip-ft/ft under lateral load along short span of interior panel of flat plate structure (1 kip-ft = 1.36 kN-m).

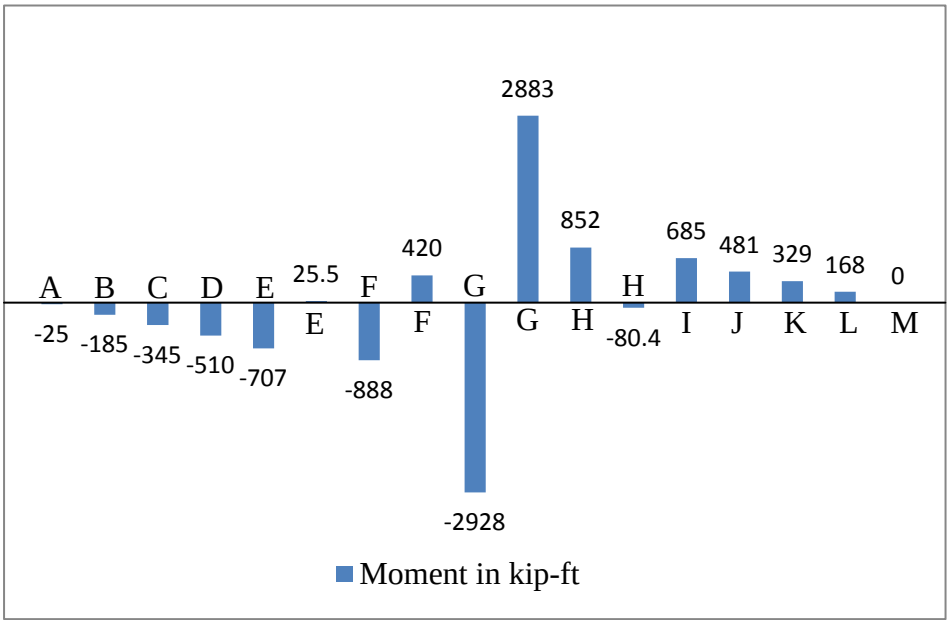

Figure 6: Moment in kip-ft under lateral load along short span of interior panel of flat plate structure (1 kip-ft = 1.36 kN-m).

Again, under lateral load the percentages of total negative moment, total positive moment, column strip moment and middle strip moment for that interior panel are given below:

Negative moment..... 100% at one side of the supporting end
Column strip negative moment..... 98.6% of negative moment
Middle strip negative moment..... 1.4% of negative moment
Positive moment..... 100% at other side of the supporting end
Column strip positive moment..... 99.1% of positive moment
Middle strip positive moment..... 0.9% of positive moment

The above discussed percentages of moment from Simpson's 1/3rd rule and 'ETABS' software in case of positive or negative moments at column strip due to lateral load, it can be decided that about 100% moment has transferred through column strip. It is also observed that in case of negative moment about 82% of column strip negative moment has transferred through effective width (c+3h) and 18% of column strip negative moment has transferred through rest of the column strip. Similarly, in case of positive moment about 82.4% of column strip positive moment has transferred through effective width (c+3h) and 17.6% of column strip positive moment has transferred through rest of column strip.

4 CONCLUSIONS

Based on limited number of model stated above, the following conclusions can be drawn. The study provides some necessary information related to percentage of moment transfer through different strip of flat plate slab system:

- It is found that the percentages of moment from Simpson's 1/3rd rule and 'ETABS' software plays on column strip and middle strip is slightly different from moment as specified by direct design method according to ACI 318 (2008) code provision under gravity load.
- In case of lateral load it is found that about 100% moment has transferred through column strip where the significant amount (82%) of column strip moment has passed through effective width(c+3h).

REFERENCES

[1] ACI 318. 2008. *Building Code Requirements for Reinforced Concrete*. American Concrete Institute, Farmington Hills, Michigan.

[2] AISI. 1964. *Anchorage and Alaska Earthquake*.

[3] Bangladesh National Building Code (BNBC). 2006. *Housing and Building Research Institute and Bangladesh Standards and Testing Institution*. Dhaka, Bangladesh.

[4] Coa, H. 1993. *Seismic Design of Slab Column Connection*. *M.Sc.* Thesis, University of Calgary, Calgary, pp. 185.

[5] Dilger, WH;Coa, H. 1994. Behavior of Slab-Column Connections under Reversed Cyclic Loading. Proc., *5th International Colloquium on Concrete, Cairo, Egypt*, pp. 595-606.

[6] Ghali, A; Elmasri, MZ; Dilger, WH. 1976. Punching of Flat Plates under Static and Dynamic Horizontal Forces. *ACI Journal, Proceedings*, V. 73, No. 10, Oct. 1976, pp. 566-572.

[7] Hawkins, NM; Mitchell, D; Hanna, SH. 1975. The Effect of Shear reinforcement on the Reversed Cyclic Loading Behavior of Flat Plate Structures. *Canadian Journal of Civil Engineering*, Vol. 2, pp. 572-582.

[8] Mitchell, D and Tinawi, R. 1990. Damage to Buildings Due to the 1989 Loma Prieta Earthquake- A Canadian Code Perspective. *Canadian Journal of Civil Engineering*, Vol. 17, No.10, Oct., pp. 813-834.

[9] Pan, A; Moehle, JP. 1989. Lateral Displacement Ductility of Reinforced Concrete Flat Plates. *ACI Structural Journal*, May-June 1989, pp. 250-258.

CICM 2015
First International Conference on
Advances in Civil Infrastructure and Construction Materials
MIST, Dhaka, Bangladesh, 14–15 December 2015

APPLICATION OF FUZZY LOGIC FOR DEFLECTION PREDICTION OF NEAR SURFACE MOUNTED RC BEAMS

K. M. DARAIN[1], **M. Altab Hossain**[2], **M. Z. Jumaat**[3] **and M. Obaydullah**[4]

[1, 3, 4] Department of Civil Engineering, University of Malaya, Kuala Lumpur, Malaysia.
Email: [1]khmahfuz@gmail.com

[2] Department of Nuclear Science and Engineering, Military Institute of Science and Technology, Dhaka, Bangladesh

Abstract. *This paper presents the deflection prediction model of Near Surface Mounted (NSM) RC beam using Fuzzy Logic Expert System (FLES) with different types of membership function. The absence of complete theoretical deflection prediction model of NSM strengthened RC beams persuades this research to develop an Artificial Intelligence based prediction model using FLES. The proposed model uses triangular and trapezoidal membership function to simulate the deflection behavior of strengthened beams. An experimental study was conducted with one control and seven NSM strengthened beams, where the study variables were the strengthening materials (steel and CFRP), and the length of NSM bars (1600mm, 1800mm and 1900 mm). In this study, two inputs (applied load and variable length) were used to predict two outputs (deflection of steel and CFRP strengthened beams). The relative error of the predicted values was found to be within the acceptable limit (5%) and the goodness of fit of the predicted values was found to be closed to 1.0.*

Keywords: Artificial intelligence, Steel, CFRP, Prediction model, Error analysis.

1 INTRODUCTION

Structural strengthening can upgrade the existing underperforming structural system to carry additional loads. Among several techniques, NSM technique is comparatively new and effective due to its better bonding arrangement with concrete substrate. In this technique, FRP bar or strip is fixed in the groove of the concrete cover with epoxy [1]. It demonstrates less possibility of premature debonding failure, and enhances protection against fire, and vandalism acts [2].

It is essential to predict the deflection behavior of a new structural technique to make it popular in the professional field. However, NSM technique does not have any complete theoretical model. To address this gap, the present study is proposing a deflection prediction model using FLES which is simple, rapid, reliable and accurate alternative method. Already a number of researchers used this technique in similar applications [3, 4]. FLES uses expert appraisals as well as a logical system closer to human reasoning rather than extensive experimental results [5, 6]

The present study develops a deflection prediction model using artificial intelligence (AI) based technique. Another aim is to assess and compare different membership function used in the FLES. It is expected that this approach could be directly applied to real application without solving complex mathematics.

2 METHODOLOGY OF THE EXPERIMENTAL PART

2.1 Test Matrix

The parameters of this study were different bond length (1600 mm, 1800 mm and 1900 mm) and strengthening materials (steel and CFRP bar). Seven RC beams were tested under four-point bending load. Table 1 showed the test matrix.

Table 1: Test matrix of the experimental program

Sl. No.	Notation	Description	Groove size (mm)	Total bond length (mm)
1	CB	Control RC beam	-	-
2	N1.6F	12 mm NSM CFRP bar	24×24	1600
3	N1.6S	12 mm NSM Steel bar		1600
4	N1.8F	12 mm NSM CFRP bar		1800
5	N1.8S	12 mm NSM Steel bar		1800
6	N1.9F	12 mm NSM CFRP bar		1900
7	N1.9S	12 mm NSM Steel bar		1900

2.2 Materials

RC beam specimens were prepared in laboratory with 28 days' cube compressive and flexural strength of 43.24 MPa and 5.01 MPa respectively. The yield stress of deformed 12 mm diameter internal and NSM reinforcement were 400 & 520 MPa respectively with a common 200 GPa modulus of elasticity. The ultimate strength and modulus of elasticity of sand coated 12 mm diameter CFRP bars were 2400 MPa and 165 GPa respectively.

2.3 Experimental Setup

The under-reinforced RC beams were 2.3 m long with an effective span of 2 m and a rectangular cross-section of 125 mm × 250 mm (Figure 1). The main bar, top hanger bar and shear reinforcement were 12mm, 10mm and 8 mm diameter respectively. Four-point bending load was applied through a 500 kN capacity universal testing machine. LVDT and strain gauges were mounted to capture the linear deflection and strain variation.

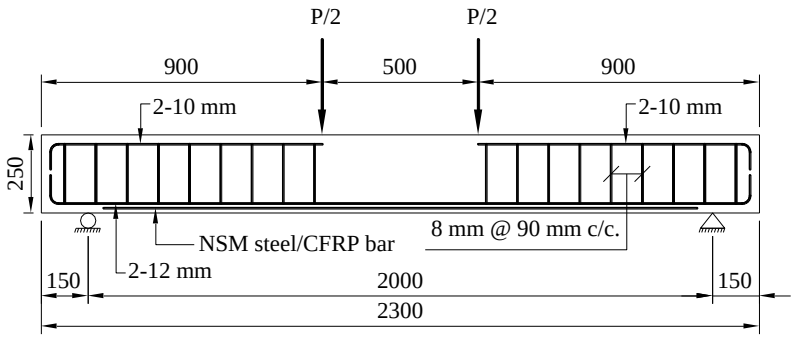

Figure 1: Reinforcement and strengthening detail of RC beam

3 FUZZY LOGIC EXPERT SYSTEM PREDICTION MODEL

3.1 Fuzzy Inference System

The basic two-dimensional Mamdani type fuzzy logic expert system (FLES) comprises of four principal components [7].They are: (1) Fuzzification – which takes crisp numeric inputs and converts them into the fuzzy form needed by the decision-making logic, (2) Rule base – which holds a set of if-then rules, that quantify the knowledge that human experts have amassed about solving a specific problem, (3) Inference – which creates the control actions according to the information provided by the fuzzification module and by applying knowledge, and (4) Defuzzification – which calculates the actual output, i.e. converts fuzzy output into a precise numerical value (crisp value).

3.2 Membership Function

Membership function (MF) describes the way that every single point in the input space is mapped to a membership value (or degree of membership) between 0 and 1. The input space is sometimes referred to as the universe of discourse, a fancy name for a simple concept [8, 9]. The membership function which represents a fuzzy set is usually denoted by μ_A. For an element x of X, the value $\mu_A(x)$ is called the membership degree of x in the fuzzy set. The Fuzzy Logic includes 11 built-in membership functions. These 11 functions are, in turn, built from several basic functions: piecewise linear functions, the Gaussian distribution function, the sigmoid curve, and quadratic and cubic polynomial curves. The membership with piecewise linear function are the simplest. Among this category triangular function are mostly used due to its simplicity and rigorousness. Basically these choice of the membership function depends on the nature of the work [10].

Figure **2** showed the triangular and trapezoidal MF which were used in this study.

A triangular MF is described by three parameters *a*,*b* and *c* given by the expressions; where the parameters *a* and *c* locate the feet of the triangle and the parameter *b* locates the peak.

$$f(x,a,b,c) = max\left\{min\left(\frac{x-a}{b-a},\frac{c-x}{c-b}\right),0\right\} \quad (1)$$

A trapezoidal MF is described by four parameters *a*, *b*, *c* and *d* given by the expressions; where the parameters *a* and *d* locate the feet of the trapezoid and *b* and *c* locate the shoulder.

$$f(x;a,b,c,d) = max\left\{min\left(\frac{x-a}{b-a},1,\frac{d-x}{d-c}\right),0\right\} \quad (2)$$

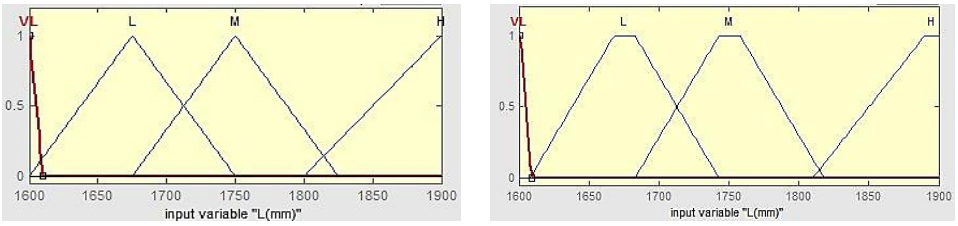

Figure 2: a) Triangular MF; b) Trapezoidal MF for input variables Length (L)

3.3 Fuzzy Logic Development

The proposed FLES model has two input parameters: applied monotonic load (F) and variable bond length (L). It was experimentally found that these two input parameters could significantly influence the two output parameters: deflection of NSM steel (DS) and FRP (DF) strengthened RC beams. The load was changed within the range from 0 to 100 kN and the bond length of NSM reinforcement

was altered between 1600 mm and 1800 mm. For fuzzification, the input variable F was given eleven possible linguistic variables: very very low (VVL), very low (VL), low (L), High low (HL), low medium (LM), medium (M), high medium (HM), medium high (MH), high (H), very high (VH), and very very high (VVH). Four linguistic variables were used for input variable L: very low (VL), low (L), medium (M), and high (H). The linguistic variables used for the output variables were Level 1 to 12 for DS and DF.

Table 2: Rules for the FLES prediction model

Rule no.	Input variables		Output variables	
	F	*L*	*DS*	*DF*
1	VVL	VL	L1	L1
7	VL	M	L2	L2
….	….	….	….	….
25	VHM	VL	L6	L9
36	H	H	L7	L9
….	….	….	….	….
44	VVH	H	L9	L10

A Mamdani max-min inference approach and the center of gravity defuzzification method were applied as these operators assured a linear interpolation of the output between the rules [5] . A total of 44 fuzzy inference rules were formed based on expert knowledge and past experience. Some of the rules were shown in Table 2. An example was illustrated in Figure 3 concerning how the output parameters were generated using the FLES rules.

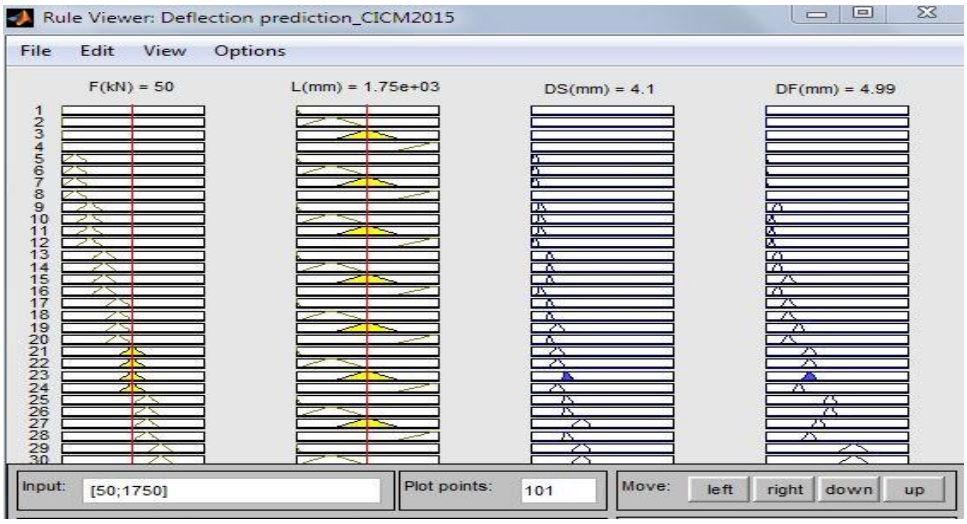

Figure 3: Rule viewer of fuzzy inference system

Explanations of these rules are described below for rule no. 1st and 36th.

- Rule 1: If applied force (F) is very very low (VVL), and bond length (L) is very low (VL) then deflection for steel bar strengthened beams (DS) is level 1 (L1), and deflection for CFRP bar strengthened beams (DF) is level 1 (L1).
- Rule 36: If applied force (F) is high (H), and bond length (L) is high (H) then deflection for steel bar strengthened beams (DS) is level 7 (L7), and deflection for CFRP bar strengthened beams (DF) is level 9 (L9).

3.4 Numerical Error Criterion

The following statistical indicators were picked to assess the efficacy of the FLES. In order to establish the relative error (ε) of the structure, the following Eq. (3) was used.

$$\varepsilon = \sum_{i=1}^{n} \left| \frac{y_i - \hat{y}_i}{y_i} \right| \frac{100\%}{n} \tag{3}$$

In addition, the goodness of fit (η) of the predictive system was calculated as follows [Eq. (4)].

$$\eta = \sqrt{1 - \frac{\sum_{i=1}^{n} \left(y_i - \hat{y}_i \right)^2}{\sum_{i=1}^{n} (y_i - \bar{y})^2}} \tag{4}$$

where n is the number of interpretations, y_i is the measured value, $\hat{y}_i$ is the predicted value, and $\bar{y}$ is the mean of measured values. The relative error provides the difference between the predicted and measured values and in a perfectly accurate system should be equal to zero. The goodness of fit provides the ability of the developed system and its highest value is 1.

4 RESULTS AND DISCUSSION

4.1 FLES Model Analysis

The FLES prediction model was developed using MATLAB® software. The simulated output of the prediction model was checked thoroughly by changing the input values. Figure 3 showed an example where the applied load (F) was 50 kN and the rod length (L) was 1750 mm, then all forty-four fuzzy rules were assessed concurrently to determine the fuzzy outputs deflection for steel bar strengthened beams (DS), and deflection for CFRP bar strengthened beams (DF) respectively. The simulated fuzzy control surfaces were depicted in Figure 5 and Figure **6**. It demonstrated about the dynamic nature of the fuzzy simulation over time which synchronized with the input and output parameters. The plots were used to verify the rules and the membership functions. It is also important to monitor the parameters which could significantly improve the output. The incremental trend of the control surface demonstrated the impact of the increasing load on both steel and CFRP strengthened RC beams.

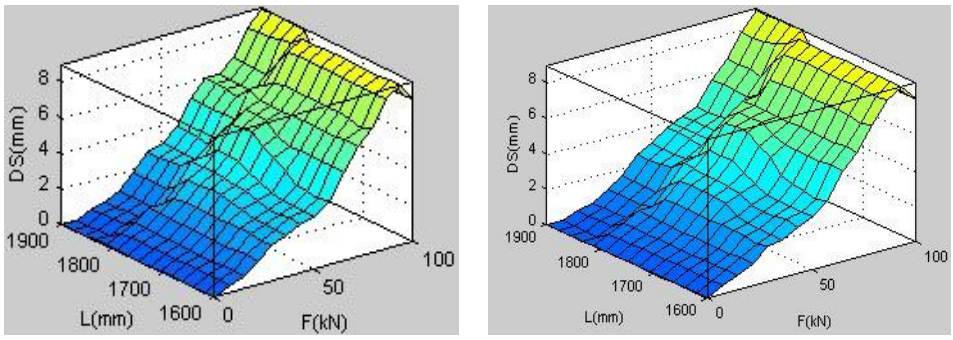

Figure 4: Control surface for deflection of NSM steel beam using (a) triangular MF, and (b) trapezoidal MF

Deflection increased slowly at first phase as applied load also increased until a certain value and reached its peak when the applied load and bar length were both at their maximum levels. The increment of deflection was less prominent at the higher levels of bar length since the stiffness of the beam became high. Consequently, deflection was less for the lower levels of applied load and bar length, which is as expected.

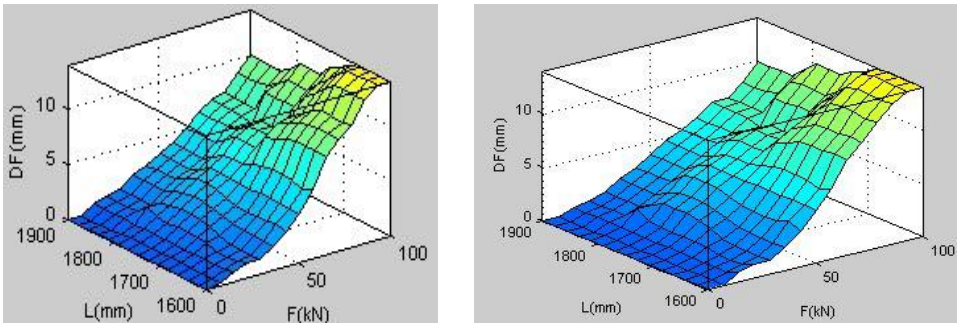

Figure 5: Control surface for deflection of NSM steel beam using (a) triangular MF, and (b) trapezoidal MF

If these control surfaces are analyzed carefully, it can be easily understood that the difference of the triangular and trapezoidal MF are negligible and their effect is also less significant. It was early mentioned that the selection of MF and its performance is actually dependent on the nature of the work and their data pattern. Some researchers also agreed that the triangular MF gave better response and the trapezoidal MF showed the identical result [10]. However, those works were involved with induction motor drive controller. So, the present study of deflection prediction model and its results also support the same hypothesis as others postulated.

4.2 Error Analysis

The difference between the experimental values and the fuzzy predicted output were verified using Eqs. 3-4. The experimental and predicted values were analyzed considering variable load and bond length. The correlations between predicted and experimental values for deflection of steel and FRP bars were depicted in Figure 6 and 7. In the case of steel bar, the correlation coefficient (R) and mean relative error between the experimental and predicted deflection values were found to be 0.9854 and 10.20% for triangular MF and 0.9924 and 8.75% for trapezoidal MF respectively (Figure 6). Whereas, in the case of CFRP bar deflection, the values were 0.9904 and 9.24% for triangular MF and 0.9893 and 8.04% for trapezoidal MF, respectively (Figure 7).

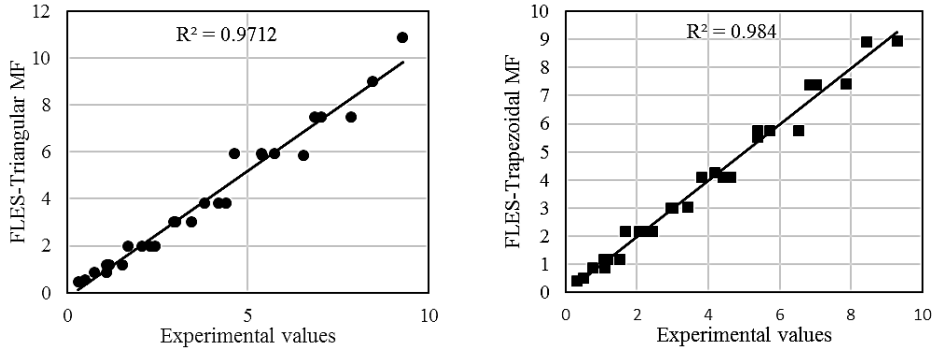

Figure 6: Correlation between experimental and fuzzy output of steel bar deflection with (a) triangular MF; (b) trapezoidal MF

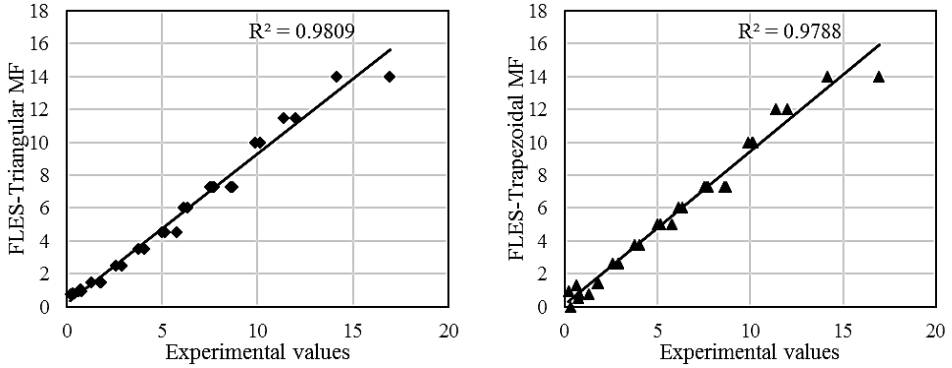

Figure 7: Correlation between experimental and fuzzy output of CFRP bar deflection with (a) triangular MF; (b) trapezoidal MF

The experimental outcomes confirmed about the good prediction accurateness of the fuzzy inference model. From Figure 6 and 7, it was observed that the correlation coefficient for both steel and CFRP NSM beam showed similar superior performance which was very close to 1. However, trapezoidal MF showed slight improved correlation over triangular MF for steel bar. This behavior was fully contrasted in case of CFRP bar where the correlation of triangular MF was improved than trapezoidal MF. The relative error of trapezoidal MF was less compare to the triangular MF for both steel and CFRP NSM beam.

5 CONCLUSION

This study developed a deflection prediction model for NSM strengthened RC beam. Static applied load and variable reinforcement length were the input parameters to obtain the deflection of NSM steel and CFRP strengthened RC beam. The triangular and trapezoidal membership function was considered for fuzzification process in this analysis. This MF was chosen deliberately to check wheth-

er there was any significant difference and impact on the fuzzification process or not. The conclusion is as follows:

- The outputs of the suggested FLES model conformed well to the experimental results. A very good correlation was found for the predicted and experimental values for deflection behavior of steel and CFRP strengthened RC beams. The relative error of the predicted values was found to be within the acceptable limit of 5% and the goodness of fit of the predicted values was very close to 1.0, confirming the superior performance of the developed model.
- No significant difference was observed for the triangular and trapezoid MF for the prediction model using FLES. The variance of the correlation coefficient and relative errors were also negligible. The slight differences in these statistical parameters would not affect the performance of the proposed model. This observation is also supported by different researchers who worked in other area of soft computing research.

ACKNOWLEDGEMENTS

The authors gratefully acknowledge the support given by University of Malaya (UM) for funding the study through the University of Malaya Research Grant (UMRG) RP018-2012A.

REFERENCES

[1] L. De Lorenzis and J. G. Teng, "Near-surface mounted FRP reinforcement: An emerging technique for strengthening structures," *Composites Part B: Engineering,* vol. 38, pp. 119-143, 2007.

[2] A. Bilotta, F. Ceroni, M. Di Ludovico, E. Nigro, M. Pecce, and G. Manfredi, "Bond efficiency of EBR and NSM FRP systems for strengthening concrete members," *Journal of Composites for Construction,* vol. 15, pp. 757-772, 2011.

[3] K. M. U. Darain, M. Z. Jumaat, M. A. Hossain, M. A. Hosen, M. Obaydullah, M. N. Huda, *et al.*, "Automated serviceability prediction of NSM strengthened structure using a fuzzy logic expert system," *Expert Systems with Applications,* vol. 42, pp. 376-389, 2015.

[4] K. M. U. Darain, S. Shamshirband, M. Z. Jumaat, and M. Obaydullah, "Adaptive neuro fuzzy prediction of deflection and cracking behavior of NSM strengthened RC beams," *Construction and Building Materials,* vol. 98, pp. 276-285, 2015.

[5] A. Hossain, A. Rahman, and A. Mohiuddin, "Fuzzy evaluation for an intelligent air-cushion tracked vehicle performance investigation," *Journal of Terramechanics*, vol. 49, pp. 73-80, 2012.

[6] A. Hossain, R. Singh, I. A. Choudhury, and A. Bakar, "Energy efficient wind turbine system based on fuzzy control approach," *Procedia Engineering*, vol. 56, pp. 637-642, 2013.

[7] K. M. Passino, S. Yurkovich, and M. Reinfrank, *Fuzzy control* vol. 42: Citeseer, 1998.

[8] L. A. Zadeh, "Fuzzy sets," *Information and control*, vol. 8, pp. 338-353, 1965.

[9] K. Shukla, "Neuro-genetic prediction of software development effort," *Information and Software Technology*, vol. 42, pp. 701-713, 2000.

[10] J. Zhao and B. K. Bose, "Evaluation of membership functions for fuzzy logic controlled induction motor drive," in *IECON 02 [Industrial Electronics Society, IEEE 2002 28th Annual Conference of the]*, 2002, pp. 229-234

CICM 2015
First International Conference on
Advances in Civil Infrastructure and Construction Materials
MIST, Dhaka, Bangladesh, 14–15 December 2015

DRIVE-BY BRIDGE DAMAGE EVALUATION USING APPARENT PROFILE

Ahmed El-Hattab[1], Nasim UDDIN[2] and Eugene Obrien[3]

[1, 2] University of Alabama at Birmingham

[3] University College Dublin, Ireland

Abstract. *Bridge structures are subjected to continuous degradation due to environmental effect and excess loading. Monitoring of bridges is a key part of any maintenance strategy as it can give an early warning if the bridge becomes unsafe. This paper theoretically assesses the ability of vehicle fitted with accelerometers to evaluate and localize the bridge damage. Damage is defined in this study as loss in structure stiffness. A two degree of freedom quarter car model is used to represent the passing vehicle. The bridge is modeled as a simply supported beam. Both car and bridge is modeled using Finite Element Analysis computer program LS-DYNA program.*

.

Keywords: Bridge structure, Degradation, Damage.

1 INTRODUCTION

In recent years there has been a move toward sensor based monitoring for bridges instead of visual inspection. However, sensor based monitoring is costly, and need maintenance. Some authors have shifted to the instrumentation of a passing vehicle, rather than the bridge for monitoring. This approach is referred to as 'drive-by' bridge inspection (Kim and Kawatani, 2009). Using this approach, bridge itself is not instrumented, and so the concept has the potential to be far more cost effective than traditional Structure Health Monitoring (SHM).

The feasibility of using an instrumented vehicle to extract the first natural frequency of the bridge has been verified in numerical studies and filed tests (Yang et al., 2004; Lin and Yang, 2005; Oshima et al., 2008). The use of drive-by method for health monitoring has been developed by Kim and Kawatani (2009), McGetrick et al. (2010) and Toshinami et al. (2010).

McGetrick et al. (2009) investigated the effect of road profile on drive-by methods for health monitoring. Results shows that the method works well in absence of road roughness, that the road roughness excites the bridge, and the axle frequency acceleration become predominate in the Power Spectral Density.

Keenahan et al. (2012) studied the use of half car four degree of freedom system (with two axles) model over rough profile. The study shows that the effect of road profile in acceleration spectra can be removed by subtracting the two axle acceleration at the same location.

This paper presents a novel alternative to acceleration signal analysis using the Apparent Profile to evaluate bridge damage. When a car passes over certain road profile without a bridge, the car starts to excite. Using the acceleration data as an input we can recalculate the profile that causes the excitation. If the car starts to pass over the same road profile over a healthy bridge, the back calculated profile will be contaminated by bridge displacement which refers to the 'Apparent Profile'. By repeating the process for the same road profile with damaged bridge we will have a damaged 'Apparent Profile'. Subtracting the damaged apparent profile from undamaged one will show the damage level of the bridge. In this paper the a set of graphs shows the change in the 'Apparent Profile' for different damage levels, and locations are calculated and referred to 'Damage Mapping' which will be used to determine the damage levels and location.

2 VEHICLE AND BRIDGE MODEL

A theoretical quarter car model (Fig. 1) is considered with two degrees of freedom, which allows for axle hop and body mass bouncing. The body mass of the car is presented by a suspension mass ms while the axle mass is presented by ma. The body mass ms is connected to the axel mass ma by a suspension spring with stiffness ks and viscous damper with damping value cs. The axel mass is connected to the road surface by spring with stiffness ka. The tire damping is ne-

glected. The body mass vertical acceleration is represented by $\ddot{u}_s$ and the axle vertical acceleration is represented by $\ddot{u}_a$

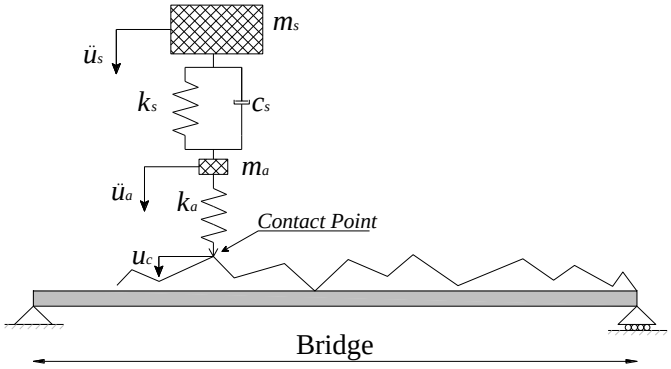

Figure 1: Theoretical quarter car model

The properties of the car are listed in Table 1 and are obtained from work by Cebon (1999) and Harrise et al. (2007)

Table 1: Properties of quarter car model

Property	Unit	Symbol	Quarter Car Model
Body Mass	kg	Ms	17300
Axel Mass	kg	Ma	700
Suspension Stiffness	N/m	Ks	4 × 105
Suspension Damping	N.s/m	Cs	10 × 103
Tire Stiffness	N/m	Ka	1.75 × 106
Body mass frequency of vibration	Hz	Fbounce	0.69
Axel mass frequency of vibration	Hz	Faxle	8.8

The paper studies a real 10 m span reinforced concrete bridge. The bridge properties are calculated from the geometry of the bridge. An Eigen value analysis was made to extract the bridges first natural frequencies. The three bridge properties are listed in Table 2.

Table 2: Properties of the Actual Bridges

Bridge(m)	First Natural Frequency (Hz)	Moment of inertia around horizontal axe (m4)
10	8.75	0.0434

An equivalent 1D Belytschko-Schwer full cross-section integration beam element issued to represent the bridge. The equivalent rectangular beam has the same moment of inertia and first natural frequency for the bridge. The Elastic Modulus is Ec=3.5 × 1010 N/m2 and the density γ=2400 kg/m3. The equivalent Bridges properties are listed in Table 3.

Table 3: Equivalent 1D bridge properties

Bridge	First Natural Frequency(Hz)	Moment of inertia around horizontal axe (m4)	Section Area(m2)
10m	8.75	0.0434	2.04

The crossing of the moving vehicle over the bridge is modeled by LS-Dyna FEA program. The quarter car model is moving with 25m/s constant speed over a 200 m approach distance to reach the steady state case for car excitation, followed by the bridge.

3 CALCULATION OF THE APPARENT PROFILE

This section describes the Apparent Profile calculation process for quarter car model. The process is divided into two main stages, both of them are used to be modeled using LS-Dyna FEA program. First to run the quarter car model over the bridge to generate the acceleration data for the body mass $\ddot{u}_s$ and the axle mass $\ddot{u}_a$. This model use to simulates the actual acceleration data that will be collected from the instrumented truck. The quarter car applies a force on the bridge which can be calculated form equation (1)

$$F = m_s.\ddot{u}_s + m_a.\ddot{u}_a + (m_s + m_a).\mathrm{g} \quad (1)$$

Where'g' is the ground acceleration. This force will be used as a data input in the second model to get the apparent profile.

The second model is for quarter car only without bridge. By applying the body mass acceleration $\ddot{u}_s$ to the body mass, the axle mass acceleration $\ddot{u}_a$ to the axle mass and the force 'F' to the contact point, thenrunning this model we should get the same profile 'u_c' which produce the acceleration data. The method is illustrated in Fig. 2

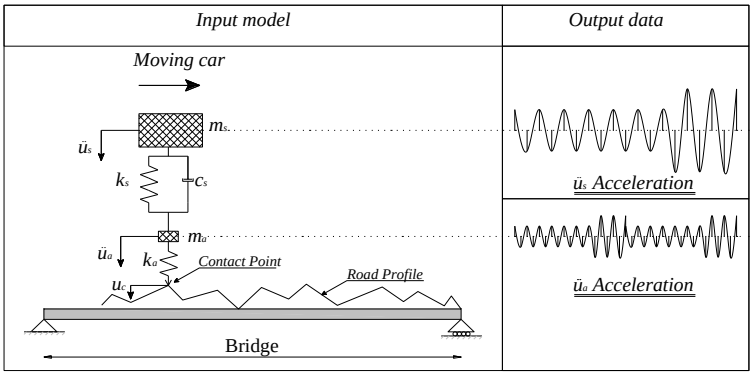

a) First Model : simulate the real life truck and the accelerometer data.

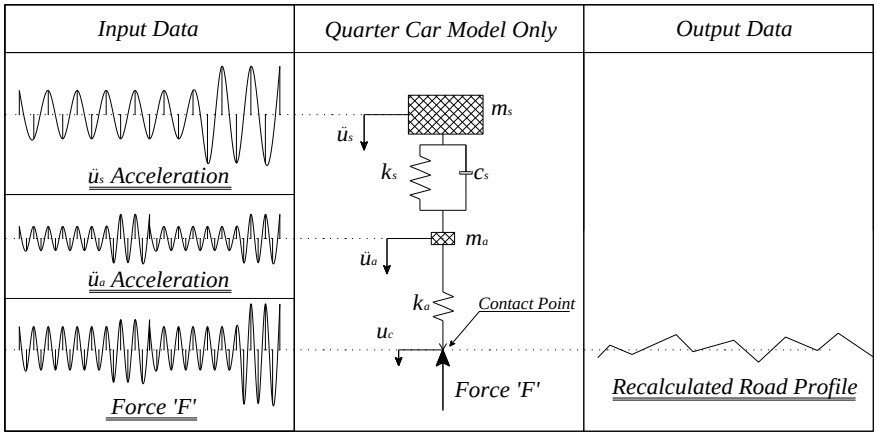

b) Second Model : recalculatingthe profile u_c

Figure 2: Apparent Profile calculation process

4 CREATE 'DAMAGE MAPPING' GRAPHS

In this section, the quarter car is simulated crossing an approach distance followed by damaged bridge without roughness to create 'Damage Mapping' graphs. The damage is represented as loss in stiffness as recommended by Shinha et al. (2002). The crack causes a loss in stiffness over a region of three times the beam depth varying linearly from maximum at the center. The damage is defined as ratio of crack depth to overall beam depth; thus, 20% damage implies that the crack depth is 20% of the beam depth.The quarter car crosses a 200 m approach distance followed by 10m simply supported bridge. The damage is located at 10% of the bridge span (1m

from the end support) .The process is repeated six times for each damage level (from 0% to 50%). Then the damage location moved to 20% of the bridge span(2m from the support) and then the process is repeated six times for each damage level(from 0% to 50%). This process is respected 9 times for different damage location along the bridge (from 1m to 9m).The damage location is shown in Fig. 3

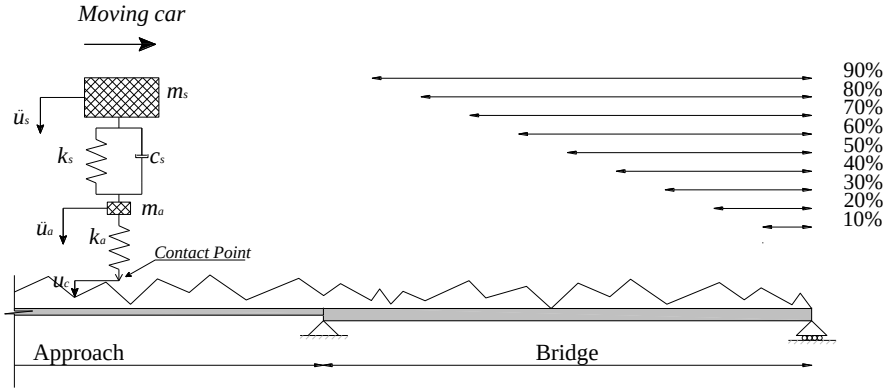

Figure 3: Damage Locations along the Bridge

The change in the Apparent Profile represents the damage level in the bridge, so damage level for 10% damage can be calculated by subtracting the Apparent Profile for 10% damage from the Apparent Profile for 0%. For 20% damage, by subtracting the Apparent Profile for 20% damage from the Apparent Profile for 0% and so on. The change in the 'Apparent Profiles' for each damage level (from 10% to 50%) is calculated for each damage location. This set of changes in 'Apparent Profiles' refers to the 'Damage Mapping' for the 10m bridge which will be used to determine the exact damage value and location for the bridge. The 'Damage Mapping' graphs are shown in Fig. 4

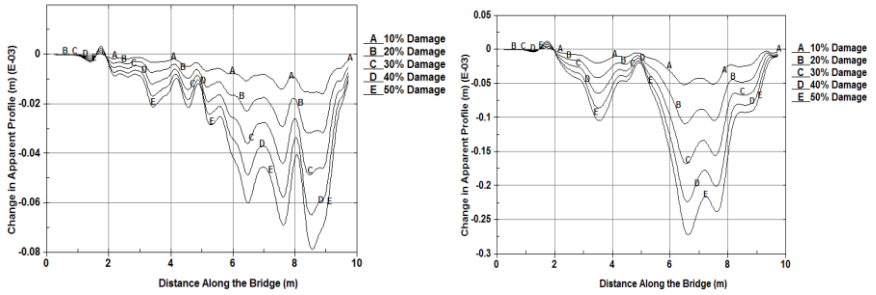

(a)Damage at 10% of bridge span (b) Damage at 20% of bridge span

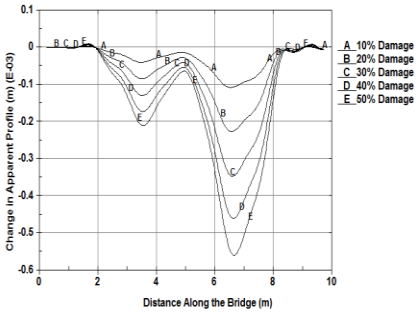

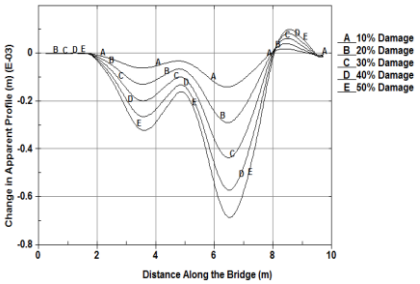

(c)Damage at 30% of bridge span (d)Damage at 40% of bridge span

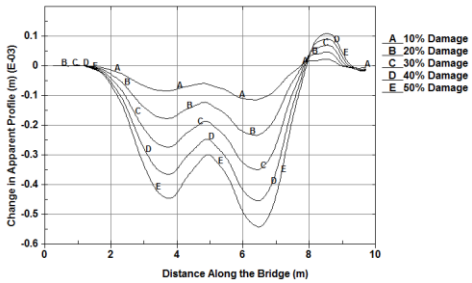

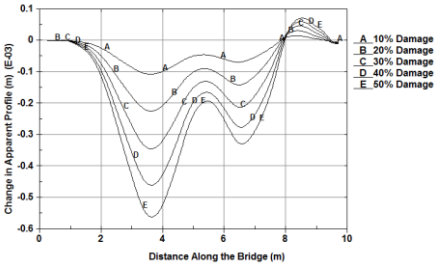

(e)Damage at 50% of bridge span (f)Damage at 60% of bridge span

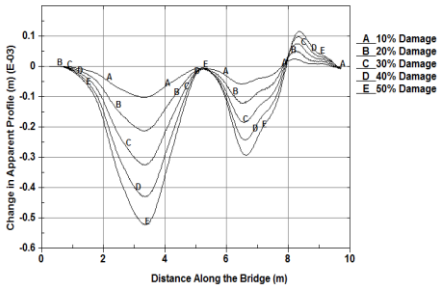

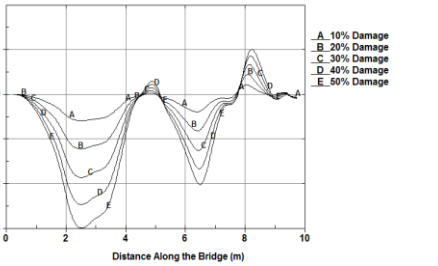

(g)Damage at 70% of bridge span (h) Damage at 80% of bridge span

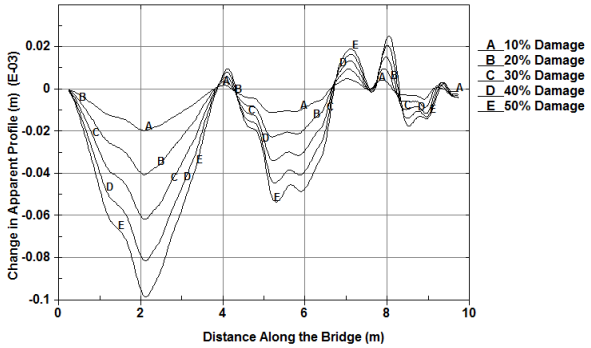

(i)Damage at 90% of bridge span

Figure 4: 'Damage Mapping' For 10m Bridge.

5 DETERMINE DAMAGE LOCATION AND VALUE FOR DAMAGED BRIDGE

In this section, the quarter car is simulated crossing an approach distance followed by the damaged bridge. The damage is predefined at certain locations with certain level, and the process seeks to determine the damage level and location. In order to study the effect of the road roughness on the process, three different road profiles are used in the simulation. The road roughness is randomly generated according to ISO (International Organization for Standardization). Road roughness Class 'A' used for a 'very good' profile (Fig. 5a), Class 'B' for 'good' profile (Fig. 5b) and Class 'C' for 'fair' profile (Fig. 5c).

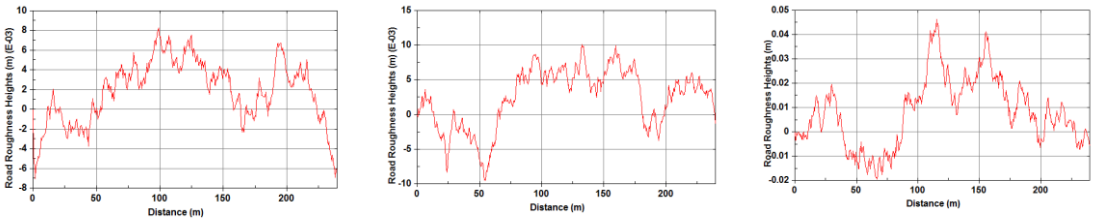

(a) Profile A (b) Profile B (c) Profile C

Figure 5: Road roughness along the car path.

The quarter cross a 200 m approach distance followed by 10m simply supported bridge with road roughness Class 'A'. This process repeated two times:

first for healthy bridge, second for damaged bridge with 30% damage level at 20% of bridge span (2m from the end support). Fig. 6 shows the recalculated damaged 'Apparent Profile' over 'Damage Mapping' graphs.

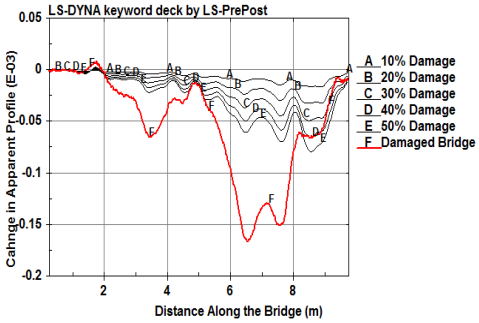

(a)Damage at 10% of bridge span

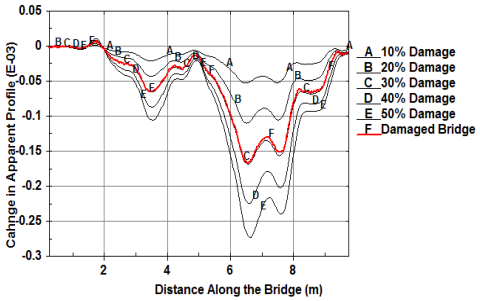

(b) Damage at 20% of bridge span

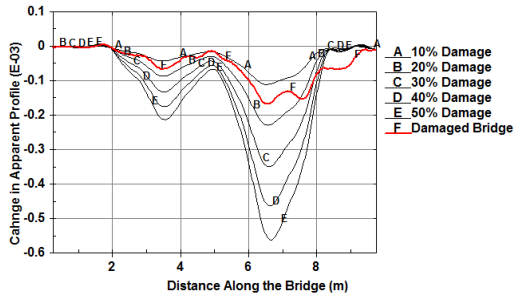

(c)Damage at 30% of bridge span

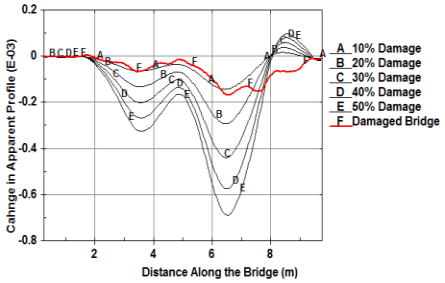

(d)Damage at 40% of bridge span

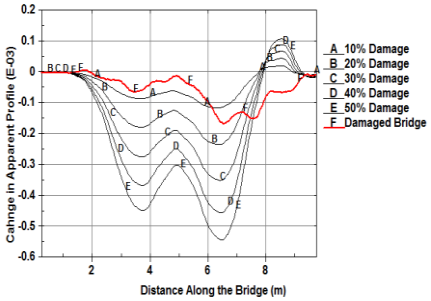

(e)Damage at 50% of bridge span

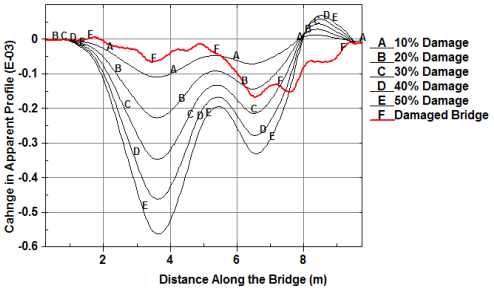

(f)Damage at 60% of bridge span

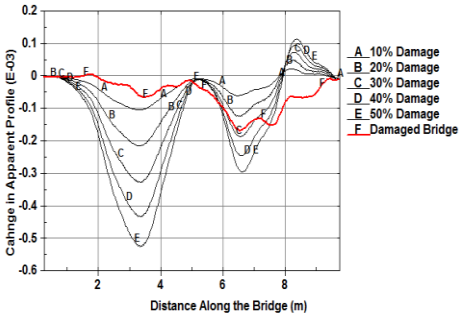

(g)Damage at 70% of bridge span

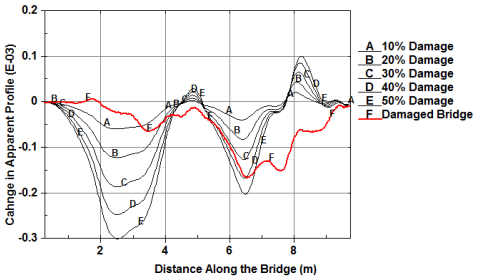

(h) Damage at 80% of bridge span

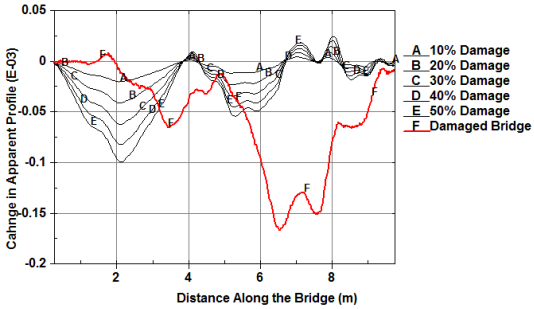

(i)Damage at 90% of bridge span

Figure 6: Damaged 'Apparent Profile' over 'Damage Mapping' For 10m Bridge.

The result shows that the 'Apparent Profile' for damaged bridge is matching only with the 'Damage Mapping' graph for damage at 20% of bridge span with 30% damage level which identical with the defined damage level and location. The process has been repeated for damaged bridge with all other damage levels at different location of the span with very similar level of success and not reported here for the sake of brevity of the paper. The process has been repeated two times for road roughness Class 'B'& Class 'C' for both damage location (20%and 50% of bridge span) with the same damage value (30% damage). A plot shows the results for 20% damage location for both road roughness Class 'B'& Class 'C' in Fig. 7. The results show that the process is not affected by the road roughness. Similar results has been obtained for other damage locations but not reported here for the sake of brevity.

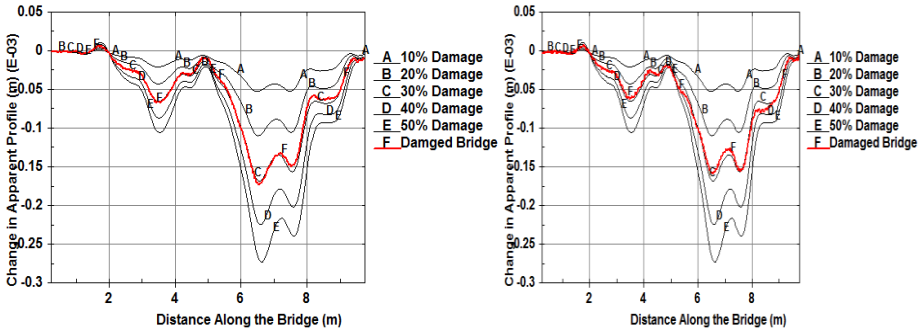

Fig. 7a Profile Class B Fig. 7b Profile Class C

Figure 7: Apparent Profile over Damage Mapping for 20% Damage location with 30% damage value

6 CONCLUSION

This paper studies the feasibility of using the 'Apparent Profile' to evaluate damage level and location. The damage evaluation process is divided in to two main steps. First to calculate the 'Damage Mapping' graphs which is a set of apparent profiles for different damage levels and locations. Second the bridge damage level is extracted from the 'Apparent Profile'. By comparing the damaged 'Apparent Profile' with the 'Damage Mapping' graphs we can determine the damage level and location. The study shows also that the process is not affected by the road roughness.

REFERENCES

[1] Kim, C.W. &Kawatani, M. Challenge for a drive-by bridge inspection. Proceedings of the 10th International Conference on Structural Safety and Reliability, ICOSSAR2009. Osaka, Japan. 2009:758-765.

[2] Yang, Y.B., Lin, C.W. &Yau, J.D., 2004. Extracting bridge frequencies from the dynamic response of a passing vehicle. Journal of Sound and Vibration, 272(3-5), pp.471–493.

[3] Lin, C.W. & Yang, Y.B., 2005. Use of a passing vehicle to scan the fundamental bridge frequencies: an experimental verification. Engineering Structures, 27(13), pp.1865–1878.

[4] Oshima, Y., Yamaguchi, T., Kobayashi, Y. &Sugiura, K., 2008. Eigenfrequency estimation for bridges using the response of a passing vehicle with excitation system. In Proceedings of the Fourth International Conference on Bridge Maintenance, Safety and Management, IABMAS2008. Seoul,

Korea: CRC Press, Taylor and Francis Group, London, UK, pp. 3030–3037.

[5] McGetrick, P.J., González, A. & O'Brien, E., 2010. Monitoring bridge dynamic behaviour using an instrumented two axle vehicle. In Bridge and Concrete Research in Ireland. Cork, Ireland.

[6] Toshinami, T., Kawatani, M. & Kim, C.W., 2010. Feasibility investigation for identifying bridge's fundamental frequencies from vehicle vibrations. In Proceedings of the Fifth International Conference on Bridge Maintenance, Safety and Management, 20 IABMAS2010. Philadelphia, USA: CRC Press, Taylor and Francis Group, London, UK, pp. 317–322.

[7] McGetrick, P.J., González, A. & OBrien, E.J., 2009. Theoretical investigation of the use of a moving vehicle to identify bridge dynamic parameters. Insight: Non-Destructive Testing & Condition Monitoring, 51, pp.433–438

[8] Keenahan J.,McGetrick P.,González, A. & OBrien, E.J., 2012. UsingInstrumentedVehicle To Detect Damage In Bridges. Proceedings of 15th International Conference on Experimental Mechanics,2934

[9] Cebon, D. Handbook of vehicle-road interaction. The Netherlands: Swets&Zeitlinger, 1999

[10] Harris, N. K., OBrien, E.J. & González, A., 2007. Reduction of bridge dynamic amplificationthrough adjustment of vehicle suspension damping. Journal of Sound and Vibration, 302: 471-485.

[11] Sinha JK, Friswell MI and Edwards S., 2002. Simplified modelsfor the location of cracks in beam structures using measuredvibration data. J Sound Vib, 251: 13–38.

CICM 2015
First International Conference on
Advances in Civil Infrastructure and Construction Materials
MIST, Dhaka, Bangladesh, 14–15 December 2015

AERODYNAMIC BEHAVIOUR OF BOX GIRDER BRIDGE DECK WITH EDGE FAIRING: EFFECTS OF NOSE LOCATION

Md. N. HAQUE[1] **and Mohammed R. Islam**[2]

[1]Department of Civil Engineering, Chittagong University of Engineering and Technology, Chittagong, Bangladesh
Email: naimulce@gmail.com

[2]Department of Civil Engineering, Military Institute of Science and Technology, Dhaka, Bangladesh
Email: ce_russel@yahoo.com

Abstract. *Edge fairings are often applied to the box-girder to improve the aerodynamic behavior of the long-span bridge deck. The effects of fairing on aerodynamic behavior should be well investigated for a better design of the long-span bridge deck and to ensure safety against wind. The present study numerically investigated the influence of nose location of edge fairing on aerodynamic behavior of box-girder bridge deck. The flow was simulated by two-dimensional Unsteady RANS simulation with k-ω-SST turbulence model. Two identical shapes of fairing one with nose-up position and another one with nose-down position were considered and their aerodynamic behaviors were compared. The mean and RMS values of force coefficients were calculated. The pressure and velocity fields were scrutinized in detail to explain and understand the influence of nose location on aerodynamic characteristics of the bridge deck. Simulations were conducted at a Reynolds number of $6.0x10^4$. The results depicted that the nose location of the fairing influences the aerodynamic response significantly and the fairing with nose-down position had a better aerodynamic behavior than the fairing with nose-up position for the considered shape of the fairing.*

Keywords: Aerodynamic response, Box girder, Fairing, Nose location, CFD, Unsteady RANS.

1 INTRODUCTION

Long-span bridges often suffer from the aero-elastic problems. Various aerodynamic countermeasures are applied to the deck to improve the aerodynamic performance of the long-span bridge. Edge fairing is one of the most common aerodynamic countermeasures that is often applied to the long-span bridge deck to improve the aerodynamic behavior by reducing the along wind load and afterbody vortex shedding activity.

For edge fairing, there are a number of important shaping parameters such as the top plate slope (θ_T), bottom plate slope (θ_B) and the nose location (h/D) as shown in Figure 1. The aerodynamic response is quite sensitive to the shape of the fairing [1, 2]. In previous studies [2 – 4] only the top (θ_T) and bottom (θ_B) plate slopes were taken into consideration and their influence on aerodynamic responses were investigated. However, along with the top (θ_T) and bottom (θ_B) plate slopes, the nose location (h/D) is also an important shaping parameter and its effects on aerodynamic responses and flow field should be known for efficient design of the long-span bridge deck.

In this study the influence of nose location (h/D) of edge fairing on the aerodynamics of a closed box girder was investigated numerically. A two-dimensional unsteady RANS simulation with *k-ω-SST* turbulence model was employed to predict the static aerodynamic response and the flow field around the bridge deck. A comparative study was made between two shapes of the edge fairing, one with nose-up position ($h/D>0.5$) and another one with nose-down position ($h/D<0.5$). The top and bottom plate slopes were kept same, yet the nose location (h/D) was altered by changing the orientation of the top and bottom plate slopes as demonstrated in Figure 1. The force coefficients and the flow fields such as the pressure and the velocity distributions were considered as parameter of interest. All the simulations were carried out at a Reynolds number (R_e) of $1.2\text{x}10^4$.

2 NUMERICAL PROCEDURE

The unsteady Reynolds-Averaged Navier-Stokes (URANS) equations were used to model the flow around the bridge deck. Flow was assumed to be two dimensional and incompressible in nature. The governing equations are as follows:

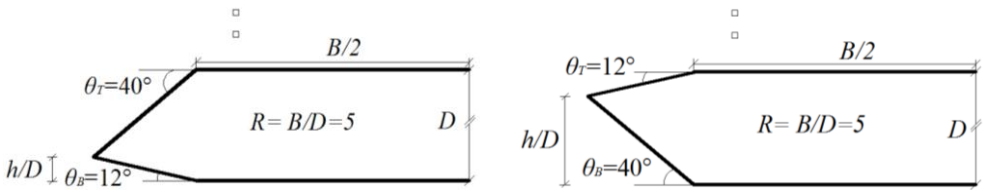

(a) Nose-down (b) Nose-up

Figure 1: Geometric configuration of the considered bridge deck

$$\frac{\partial \overline{U}_i}{\partial x_i} = 0 \tag{1}$$

$$\frac{\partial \overline{U}_i}{\partial t} + \overline{U}_j \frac{\partial \overline{U}_i}{\partial x_j} = -\frac{1}{\rho}\frac{\partial \overline{P}}{\partial x_i} + \frac{\partial}{\partial x_j}\left[\nu\left(\frac{\partial \overline{U}_i}{\partial x_j} + \frac{\partial \overline{U}_j}{\partial x_i}\right) - (\overline{u_i' u_j'})\right] \tag{2}$$

Where, $\overline{U}_i$ and x_i are the averaged velocity and position vectors respectively, t is the time, $\overline{P}$ is the averaged pressure, ρ is the air density, ν is the fluid viscosity. Due to time averaging process, the new variable $\overline{u_i' u_j'}$ appeared is known as Reynolds stress. It needs modeling to close the equation, which is known as turbulence modeling. Turbulence modeling was attained by *k-ω-SST*, a two equations turbulence model [5]. The Convective and diffusive terms in the governing equation were discredited with second order accurate central differencing schemes. For time integration second order accurate backward differentiation formulae method was utilized. PISO (Pressure implicit with splitting of operator) algorithm was utilized to solve those discredited equations. An open source code Open FOAM was used.

A two dimensional domain with 48D in the lengthwise direction and 25D in the vertical direction, where D is the height of the bridge deck section was used to conduct the simulation. The object was placed at 18D downstream of the inlet. The outlet boundary was placed at 25D downstream of the object and height of the domain was 25D. The height of the domain was justified in [6]. At the outlet, pressure boundary condition, at the top and bottom of the domain, slip boundary condition and at the body, non-slip boundary condition was implemented. The domain was discredited spatially by a non-uniform structured grid and the cell size was varied gradually with a geometric progression of 1.05 in all directions based on previously proposed strategy [6]. The first cell height away from the body was selected such a way that the normalized wall distance (y^+) remains a value near about 5. Further details and validation of the study can be found in [6, 7].

3 RESUTLS AND DISCUSSIONS

Simulation was conducted for the bridge decks as shown in Figure 1. The top (θ_T) and bottom (θ_B) plate slopes were kept unchanged, yet the orientation was altered to change the nose location (h/D) of the fairing. Table 1 summarizes the common statistics of the aerodynamic coefficients. The aerodynamic coefficients were calculated in per unit length in the span-wise direction and normalized with the width (B) of the deck.

Table 1: Aerodynamic coefficients of the considered bridge deck

	Fairing with nose-down position (θ_T40-θ_B12)	Fairing with nose-up position (θ_T12-θ_B40)
Mean drag (C_D)	0.12508	0.131131
Mean lift (C_L)	-0.34875	0.17178
Mean moment (C_M)	0.093889	-0.06161
RMS drag (C_D')	0.000619	0.001178
RMS lift (C_L')	0.020485	0.033174
RMS moment(C_M')	0.005276	0.008553

The results imply that the fairing with nose-up position has higher drag as compared to the nose-down position. The sign of the lift force and moment coefficients also alter when the nose location (*h/D*) of the fairing changes. The moment coefficient sign doesn't bear any significance, yet the sign of the lift force coefficient bears significant meaning in bridge aerodynamics field. The deck with nose-down position has better aerodynamic behavior as the lift force acts downward (negative value) increasing the cable tension and thereafter the stability of the deck against wind. The root mean square (RMS) value of the aerodynamic coefficients provides a general idea about the dynamic characteristics of the bridge deck against wind. Similar to the mean value of the aerodynamic coefficients, the bridge deck with nose-down position has smaller RMS value of aerodynamic coefficients.

The mean surface pressures are plotted in Figure 2 for detailed analysis of the flow field. The mean pressures are mainly affected in the leading edge side due to variation of the nose location (*h/D*). The magnitude and sign of the lift and moment coefficients are mainly controlled by the leading edge side pressure distribution. In case of nose-down position, there is a large negative pressure in the leading edge bottom surface and positive pressure in the leading edge top surface of the deck, as a result the bridge deck experienced negative lift force coefficient (downward) and positive moment coefficient (counterclockwise). Reverse mechanism is true for the case of nose-up position. The RMS pressures of the bridge decks are compared in Figure 3. In contrary to the mean surface pressure the RMS pressures are mainly affected at the trailing edge side and the deck with nose-up position had a little bit higher amplitude than the nose-down position.

To improve the understanding about the flow field, the time averaged velocity fields are plotted in Figure 4. The general observation that was made in the last section also reflected in Figure 4. The clear shear layer separation and reattachment can be seen in the leading edge side and after-body vortex shedding can be found. The velocity distribution at the middle of the section is plotted in Figure 5. The picture depicts that the flow moves much faster on the bottom deck surface

in case of nose-down position and creates suction on the bottom deck surface, increasing the negative lift value of the bridge deck.

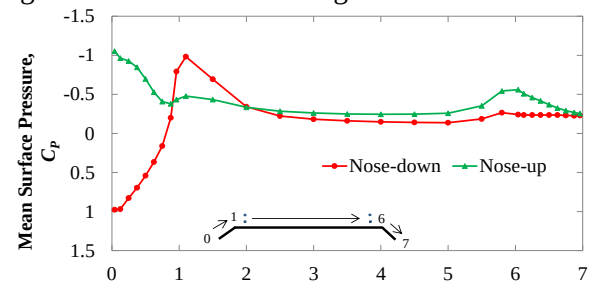

(a) Top surface pressure

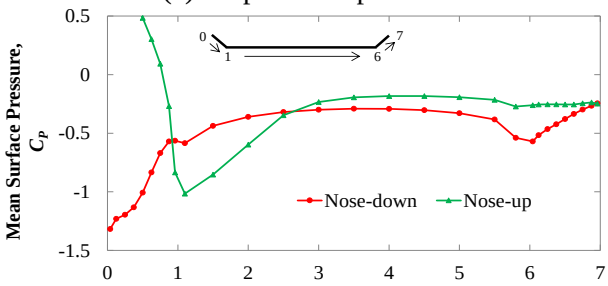

(b) Bottom surface pressure

Figure 2: Mean surface pressure distribution around the bridge deck

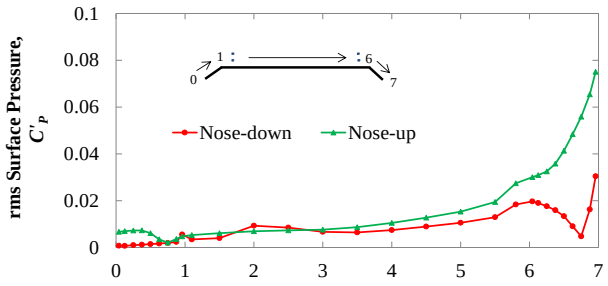

(a) Top surface pressure

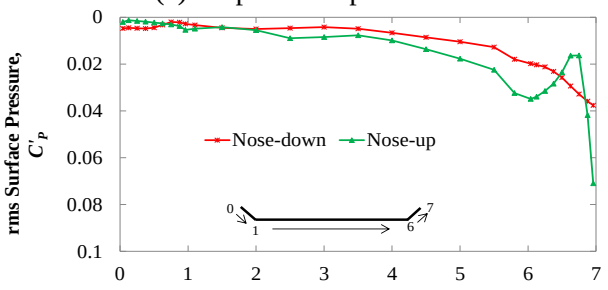

(b) Bottom surface pressure

Figure 3: RMS surface pressure distribution around the bridge deck

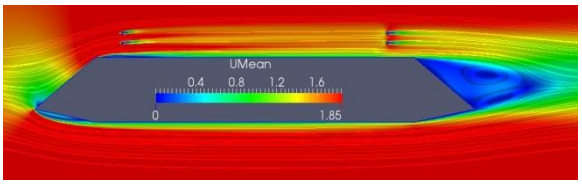

(a) Nose-down position

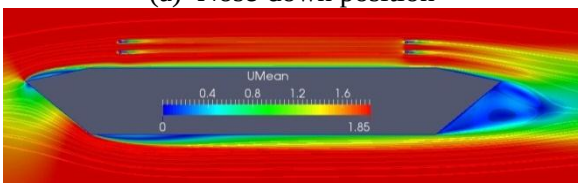

(b) Nose-up position

Figure 4: Time averaged velocity field around the bridge deck

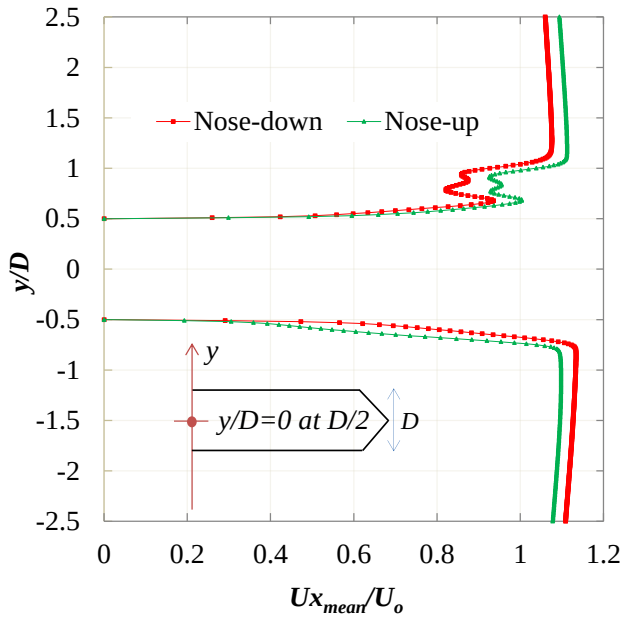

Figure 5: Velocity distribution at the mid-section of the bridge deck

4 CONCLUSIONS

The influence of nose location (*h/D*) on aerodynamic response of a box girder bridge deck with edge fairing was investigated by employing two-dimensional

unsteady RANS simulation. The magnitude of the top (θ_T) and bottom (θ_B) plate slopes were kept same, yet the orientation of the slopes were altered to change the nose location (*h/D*). For the considered shape (θ_T40-θ_B12 or θ_T12-θ_B40) of the fairing, it was found that the nose-down position of the edge fairing has better static aerodynamic performance. The deck experienced lower aerodynamic loading and less fluctuation of flow around the deck for the nose-down position of the edge fairing. However, in the present study only steady-state responses were explored and the discussion was limited for a particular shape of the fairing (θ_T40-θ_B12 or θ_T12-θ_B40).In future, detailed investigation will be carried out to explore both the static and dynamic responses of the bridge deck for a wide range of shapes of the edge fairing.

REFERENCES

[1] M. De Miranda and G. Bartoli, 2001. Aerodynamic optimization of decks of cable-stayed bridges. *Proceeding of IABSE Conference: Cable-Supported Bridges – Challenging Technical Limits*, Seoul Korea, June 12-14, pp. 34-41.

[2] F. Nagao ,H. Utsunomiya, T. Oryu and S. Manabe, 1993. Aerodynamics efficiency of triangular fairing on box Girder Bridge. *Journal of Wind Engineering and Industrial Aerodynamics*, 49, pp. 565-574.

[3] Sukamta, F. Nagao,M. Noda and K. Muneta, 2008. Aerodynamic stabilizing mechanism of a cable stayed bridge with two edge box girder. *Proceedings of 6th Int. Colloquium on Bluff Body Aerodynamics and Applications*, Milano, Italy, July 20-24, pp. 1-12.

[4] M.N. Haque, H. Katsuchi,H. Yamada, M. Nishio, 2014. Investigation of bridge deck shaping effects on aerodynamic response by RANS. *Proceeding of 6th Int. Symposium on Computational Wind Engineering*, Hamburg, Germany, June 8-12, pp1-8.

[5] F.R. Menter, 1994. Two-equation eddy-viscosity turbulence models for engineering application, *AIAA Journal*, 32, pp. 1589-1605.

[6] M.N. Haque, H. Katsuchi,H. Yamada,and M. Nishio, 2015a. Strategy to develop efficient grid system for flow analysis around two-dimensional bluff bodies. *KSCE Journal of Civil Engineering, DOI:* 10.1007/s12205-015-0696-2.

[7] M.N. Haque, H. Katsuchi, H. Yamada, and M. Nishio, 2015b. A numerical study on aerodynamics of a pentagonal shaped cable-supported bridge deck. *Journal of Structural Engineering (JSCE)*, 61A, pp. 375-387.

CICM 2015
First International Conference on
Advances in Civil Infrastructure and Construction Materials
MIST, Dhaka, Bangladesh, 14–15December 2015

NUMERICAL ANALYSIS OF CONCRETE FILLED STEEL TUBULAR (CFT) COLUMNS

Sharmin R. CHOWDHURY[1], **Khandaker M. Hasan**[2], **Md. M. Rahman**[3], **Sharif I. Ibrahim**[4] **and Sadia Mahajabin**[5]

[1, 2, 3, 4, 5]Ahsanullah University of Science and Technology, Dhaka, Bangladesh.
Email: [1]chowdhury.ce@aust.edu

Abstract. *The Concrete Filled Steel Tubular (CFT) column system has many advantages compared with the ordinary steel or the reinforced concrete system as the orientation of the steel and concrete in the cross section optimizes the strength and stiffness of the section. In this study a three dimensional linear finite element method using ANSYS 10.0, finite element software, has been employed to simulate a Concrete Filled Steel Tubular (CFT) column under axial loading and bending to investigate the capacity and load-displacements behavior of the composite sections. The dimension of the column is 5×5×113 in., slenderness ratio (l/r) is 78.29 and the thickness of the outer steel is taken 0.5 in. During analysis with ANSYS software, the CFT column model is created using 3D Solid65 element representing the linear behavior of concrete and 3D Solid45 element representing steel tube and steel plates. For the goal of this study, Concrete constitutive relation is assumed linear; steel is assumed elastic plastically perfect and perfect bonding is assumed at the concrete-steel interface. The analysis results obtained from this study are well matched with theoretical and numerical results available in literature. It is found from the study that capacity of CFT column is decreasing when eccentricity increases, and for concentric & eccentric loading, displacement increases with load increment.*

Keywords: Concrete filled steel tubular (CFT) column, Load-displacement behavior, Concentric, Eccentric, Finite element modeling.

1 INTRODUCTION

Composite steel-concrete structures are used in civil engineering projects worldwide. Applications include buildings, bridges, foundations, and special structures steel-concrete composite systems combine the advantages of a ductile steel frame with the stiffness of concrete components to control drift. Steel-concrete composite columns are among the most common type of composite structural system. There are two types of composite columns: Concrete Encased Structural Steel Columns and Concrete Filled Steel Tubes (CFTs). Concrete Filled Steel Tubular (CFT) column consists of a steel tube filled with concrete and column is simply constructed by filling a steel hollow section with concrete. Concrete Filled Steel Tubular (CFT) columns have the potential of becoming the common place structural members in both low-rise and high-rise building construction. The advantages of using Concrete Filled Steel Tubular (CFT) columns in structures are: economic designs, improved constructability, and enhanced performance. Concrete Filled Steel Tube (CFT) also has many advantages over other types of columns, including (a) The tube eliminates the column formwork during construction, (b) The tube provides longitudinal and confining reinforcement, so that usual reinforcement for concrete columns is often not used, (c) The steel pipe prevents spalling of the concrete, (d) The concrete prolongs the local buckling of pipe wall, (e) CFTs possess more strength, lateral stiffness, and ductility relative to reinforced concrete columns of similar size. Researches on Concrete Filled Steel Tube (CFT) as a composite member have been on-going for many decades. An experimental research on Circular Concrete Filled Steel Tubular (CCFT) columns published in German is cited in English by Knowles and Park [1] who described the experimental results and the other details. Malone [2] focuses on the behavior of concrete-filled tubular (CFT) columns under combined axial load and bending moment by using ANSYS finite element software. Slender columns were studied with varying amounts of load eccentricity. His results were compared to study buckling failure modes and section capacities.

This study focuses on the numerical analysis of the Concrete Filled Steel Tubular (CFT)) columns under concentric and eccentric axial loading. The study was conducted using ANSYS finite element software. With the help of Microsoft Excel, Capacity-Eccentricity, Displacement-Eccentricity, Load-Stress and Load-Displacement curves were plotted for concentric and eccentric loading condition. Eventually results are compared with the experimental and theoretical results (Malone, 2002) and understand the behavior of Concrete Filled Steel Tube (CFT) properly.

2 MODELLING APPROACH AND VALIDATION

This study discuss about the Behavior of Concrete Filled Steel Tubular (CFT) slender column. The results obtained were initially compared with available pa-

per where theoretical results as well as ANSYS results were carried out. While comparing with the software data the element type, the properties of the elements used, the steps of analysis and the analysis type were kept almost indifferent with that of available paper. The similarity of the result was encouraging enough to proceed further towards the study eliminating the need for carrying out laboratory tests reducing the time for analysis thus helping to carry out more detailed and elaborate study.

Two materials are used to develop the Concrete Filled Steel Tube (CFT) model. These two materials are designated by material 1 which stands for concrete and material 2 which stands for steel tube and steel plates. The characteristic strengths of concrete (material 1): compressive strength of 3.5 ksi and tensile strength of 0.35 ksi with an elastic modulus, E= 3372 ksi and Poisson ratio ϑ=0.2. Figure 1 shows the liner stress-strain curve of concrete.

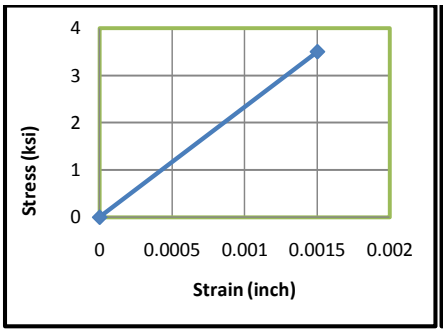

Figure1: Stress Strain Curve of Concrete for Liner Action

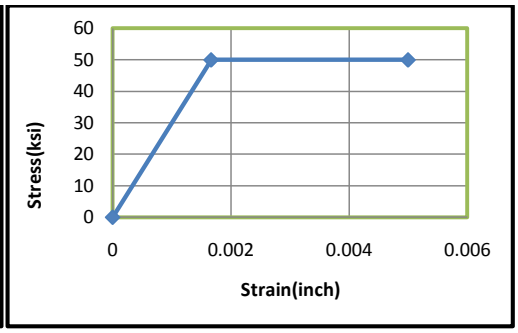

Figure 2: Stress Strain Curve of steel for Liner Action

Steel (Material 2) was assumed to be elastic plastically perfect with yield stress Fy = 50 ksi. with an elastic modulus E = 30,000 ksi. and Poisson ratio ϑ=0.3. Figure 1 shows the liner stress-strain curve of steel. Figure 2 shows the liner stress-strain curve of steel. A Concrete Filled Steel Tubular (CFT) column with concentric and eccentric loading was considered for analysis whose geometric section shown in Figure 3.

In this paper no convergence study was carried out to determine an appropriate mesh density. So an assumed mesh size was examined in ANSYS. As the mesh density becomes finer, the degree of accuracy of the results becomes higher. Therefore, 0.5 in. mesh density is selected to develop this model and the ultimate load was obtained. Results obtain from theory and ANSYS in Malone [2] paper has been used for validation. The results of Malone's [2] study supplemented experimental research which was conducted at the University of Massachusetts Structural Engineering Laboratory.

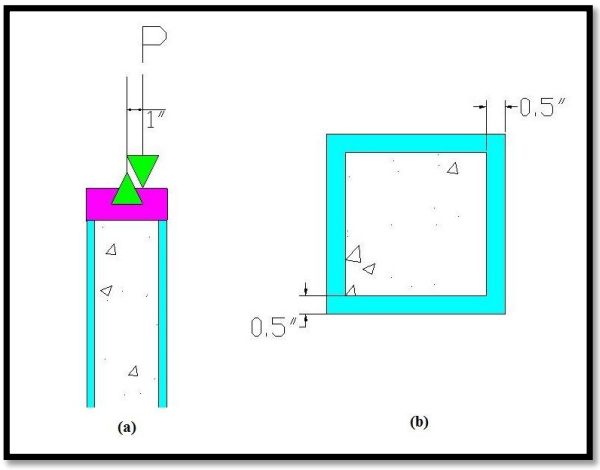

Figure 3: Specimen Geometry (a) Longitudinal Section with Steel Plates (b) Cross Section.

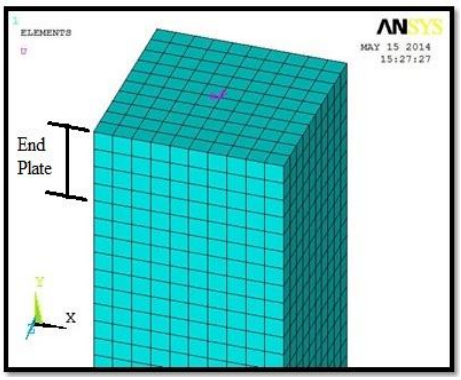

Figure 4: Boundary Condition at Top Surface.

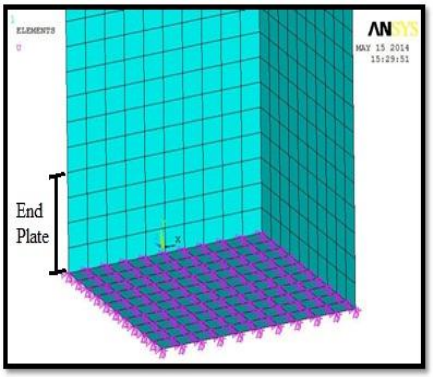

Figure 5: Boundary Condition at Bottom Surface.

The end boundary conditions for all the finite element models were chosen to simulate the actual experimental set up. The pin ended boundary condition has been modeled by restraining all the translational degrees of freedom and rotational degree of freedom of the nodes at both ends, except the translational degree of freedom in the axial direction at the top end of the column. Since the load is applied from the top of the column the translational degree of freedom has been released. Nodes other than the two ends are free to translate and rotate in X, Y and Z directions. Figure 4 and 5 show a schematic of the loading condition at the ends of each tube.

During modeling of CFT column in Malone's [2] paper, solid45 used for steel assumed elastically plastic and solid65 used for concrete which supports cracking and crushing properties of concrete. But in this study, properties of concrete are limited to linear. Loading, eccentricity and boundary conditions are kept same. The result of model created in ANSYS 10.0 shows some difference from the result of the study of Aaron W. Malone [2]. These variations take place due to linear concrete constitutive model is used in this study, whereas non-linear concrete constitutive model is used in Malone's study. The percentage of variation is 2.96% for concentric loading, 0% for 1 in eccentric loading and, 5.33% for 2 in eccentric loading Table 1 and Figure 6). Therefore, it is proven that ANSYS software is an appropriate method to analysis the model accurately and this model can be used for further study.

Table 1: Comparison of loads on CFT Results

Eccentricity (inch)	Theory(Malone,2002)	ANSYS(Malone,2002)	ANSYS (This study)
0	139	135	131
1	85	90	90
2	64	68	71

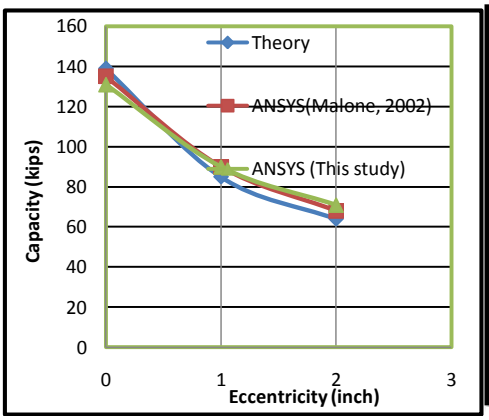

Figure 6: Comparison of Capacity-Eccentricity curve between the study of Malone[2] and this study

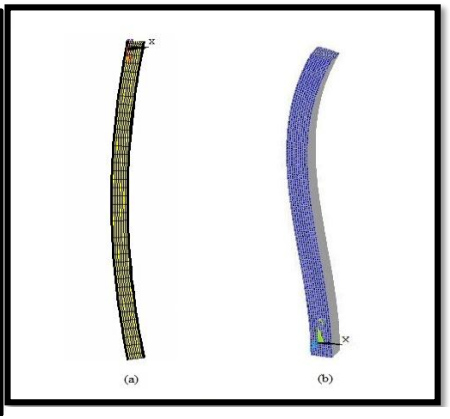

Figure 7: Buckling (a) Model Response Capture by Malone, 2002 (b) Model Response from this Study for 2 in.

From Figure 7(a) it is understood that in Malone's response failure was controlled by global instability, there was no yield observed in steel tube. But Figure

7(b) global buckling is not captured in this study due to linear steel and concrete constitutive model are used for modeling CFT column.

3 RESULTS AND DISCUSSIONS

3.1 Behavior of Concrete Steel Filled Tube (CFT) with Varying of Load

Figure 8(a) and 8(b) shows the comparison of load-stress and load-displacement respectively between three types of loading condition i.e. Case 1 (Concentric Loading), Case 2 (Eccentric Loading of 1 in.) & Case 3 (Eccentric Loading of 2 in.)

3.1.1Case 1: Concentric Loading

The model was developed in ANSYS with 0.5 in. mesh. The point load was applied concentrically on a 2 in thicken plate to distribute the load over the column. The ultimate load obtained from ANSYS is 131 kips and concrete exceed its crushing limit at the upper end of column near loading plate with the increment of further load. The stress varies linearly with loads as concrete is assumed to be linear. The maximum lateral displacement occurs at the top surface. From the curve it is seen that the lateral displacement increases linearly with the increment of loads.

3.1.2Case 2: Eccentric Loading of 1 inch

Model was analyzed under 1 in. eccentric loading. The load was applied eccentrically. The ultimate load obtained from ANSYS is 90 kips. Stress is maximum at the upper end of column near loading plate where concrete meet its crushing limit. Maximum lateral displacement occurs at 76 in from the bottom face of column.

3.1.3Case 3: Eccentric Loading of 2 inch

Model was analyzed under 2 in. eccentric loading. The load was applied eccentrically. The ultimate load obtained from ANSYS is 71 kips. Stress is maximum at the upper end of column near loading plate where concrete meet its crushing limit. Maximum lateral displacement occurs at 76 in from the bottom face of column.

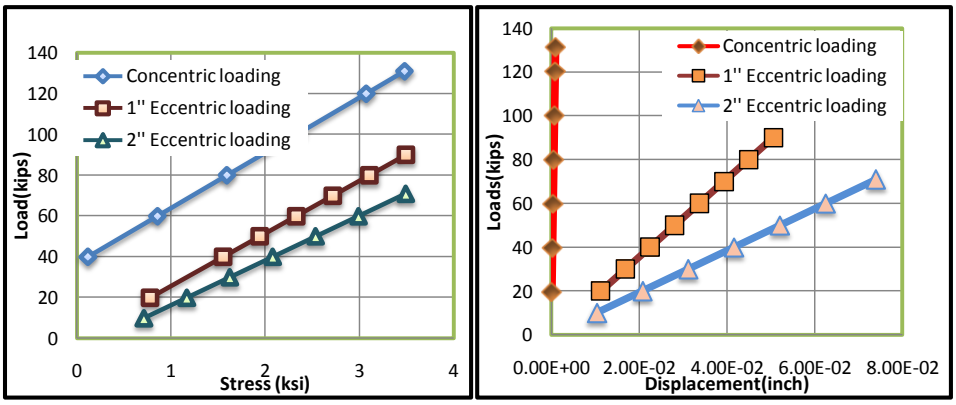

(a) (b)

Figure 8: (a)Load-Stress Comparison Graph (b) Load-Displacement Comparison Graph for Three Loading Cases.

3.2 Relation of Displacement with Eccentricity

Figure 9 shows the variation of displacement with varying eccentricity for any fixed load, i.e. 60 kips and displacement increases with the increases of point load distance from the centre point of the plate (eccentricity).

Figure 9: Displacement- Eccentricity Graph for 60kips Loads.

4 CONCLUSIONS AND RECOMMENDATIONS

Following conclusions and recommendations can be drawn on the basis of the result obtained from the analysis of Concrete Filled Tube (CFT) under concentric and eccentric loading.

- The ultimate load obtained from ANSYS in this study for Concrete Filled Steel Tube (CFT) is very close to the ultimate load measured by both theory and ANSYS performed by Aaron W. Malone [2].
- Comparing with the theory results of Malone [2], it is obtained that the percentage of variation in between the range of 5% to 11%. Comparing with the ANSYS results of Malone [2], the percentage of variation is in between the range of 0% to 5%.
- In this study the linear properties of Solid65 (concrete) are taken in consideration. It would be better if nonlinear properties are taken on account to perform the study. The results would be more precise when the mesh sensitivity are performed i.e. finer mesh provides more accurate results. The results may be less accurate due to the assumption of perfect bonding of the steel-concrete interface.
- The deterioration of load capacity with increasing load eccentricity was captured by CFT models. From load-stress relation, it is seen that stress increases with the increase of loads i.e. stress varies linearly with loads and also indicates the linear behavior.
- Non-linear analysis can be performed on various shapes (i.e. circular, rectangular etc) Concrete Filled Steel tubular (CFT) columns.
- A study on Concrete Filled Steel tube with various slenderness ratios can take place. This study could demonstrate that the behavior of concrete filled tube can be affected by slenderness ratio.
- Contact material can be used in the interface of concrete and steel to investigate the interface bond of the composite sections.
- Buckling analysis can be performed to determine critical load at which a structure becomes unstable and buckled.

REFERENCES

[1] R. B. Knowles and R. Park, 1970, Strength of Concrete-Filled Steel Tubular Columns, *J. Structures. Div. ASCE*, 95(12), 25658-2587.

[2] A. W. Malone, 2002, Concrete Filled Steel Tubular Columns, a Finite Element Study, University of Massachusetts Amherst, ASME.

[3] K. M. Hasan, M. M. Rahman, S. I. Ibrahim and S. Mahajabin, 2014,*Numerical Analysis of Concrete Filled Steel Tubular (CFT) Columns*, B.Sc Thesis, Ahsanullah University of Science and Technology (AUST)

CICM 2015
First International Conference on
Advances in Civil Infrastructure and Construction Materials
MIST, Dhaka, Bangladesh, 14–15 December 2015

GREEN ROOFS FOR RESIDENTIAL BUILDINGS IN TROPICAL CLIMATES: THE BANGLADESH PERSPECTIVE

Kamron N. LIPI[1], Bernd Möller[2] and F. M. Zahid Hossain[3]

[1]Europa-Universität Flensburg, Germany. Email: nahar_kamrun@yahoo.com

[2]Interdisciplinary Institute for Environmental Social and Human Studies, Europa-Universität Flensburg, Germany.

[3]Departmentof Civil Engineering, Military Institute of Science and Technology, Dhaka, Bangladesh. Email: zahidedu@mail.ubc.ca

Abstract. *The objective of the research is to determine how the energy efficiency of building in Bangladesh can be improved. This research introduces the concept of green roofs, which has been assessed using the PHPP software. The cooling demand of the building is modelled on the basis of the physical and behavioural aspects of the occupancy. The building configurations considered are: 1) without green roof; 2) with green roof.A cost analysis of energy efficient measure at the building is done using Microsoft excels. The study reveals in which extent the reduced cooling demand reduce utility bills. A green roof will be financially attractive if the externality is internalized. The research compares the cost of green roof and insulation systems which reduce energy consumption and energy bill with internalized externalities and the cost of present energy situation with the existing building. The findings from the study indicate that design modification related to the green roof can reduce cooling load of the case study building top floor by 37%. It can be calculated that the savings stand at about taka 40, 384Tkfor the Shapla building. It can be concluded that architects, developers, government bodies and users should be influenced and motivated to change the design practice.*

KEYWORDS: Green Roof, PHPP, Building envelop, Bangladesh National Building Code (BNBC).

1 INTRODUCTION

Bangladesh is a very densely populated country located in south Asia with one of the lowest per capita energy consumption in the world. The country has total area of 1, 47,750 km^2, out of which1, 30,168km^2 is land and13, 830km^2 is water(Bangladesh Area). Bangladesh lies between 20.420-26.38N latitude and 88.010-92.5000E longitude (Bangladesh latitude and Longitude Map). According to world population review, 160.4 million people live in Bangladesh, making it the 8th most population country in the world. The density of population in Bangladesh is 1, 033 people per kilometres; making it rank 12th of the world(Bangladesh Population 2015- World Population Review). Dhaka the capital of Bangladesh is located at Eastern longitude 90° and Northern longitude 23°45´(Worldatlas).. The current population of Dhaka city is 15.391 million. Reasons are rural-urban migration at one of the globally highest annual rates of 5% (Risks and opportunites of Urbanisation and magacities). Mirpur city is one of the conurbations in Dhaka, famous for the freedom fighter memorial. This city is also highly populated because of several garments factories. The case study building is in the Mirpur cantonment, located at 23.8042°N; 90.3667°E(Mirpur road wikipedia). It has a total area of 58.66km^2 and is situated in the north east of Dhaka. Mirpur had a population of 10,74,232 in 2011(Mirpur road wikipedia). Mirpur Cantonment is well known to be the education village of Bangladesh armed forces, a hub of knowledge for military and civil professions. The number of buildings and flat of the area, including the conditions and characters of the flat were studies. The house owners enjoy the liberty to choose and afford internal layout and energy efficient house appliances at their own expenses. The house owners are not allowed to change the wall thickness, partition wall, floor tiles and roof insulation material. The case study building is shown in the following figure

Source: (worldatlas) Source: Google Earth

2 GENERAL PROBLEM

In spite of having large natural gas resources and very small amount of oil and coal in reserve energy infrastructure in Bangladesh is poorly managed. In October 2011, the electricity generation capacity was 7, 119MW (Ahmed, 2011). Only 68% of population has access to energy and per capita availability of

electricity is 348 Wh per annum (Dhaka Tribune). Despite a high poverty rate and low energy availability, it is achieving steady economic growth with increased rateof electrification. The energy consumption rate has increased gradually due to rapidly growing population.

3 CLIMATE OF STUDY AREA

Climate refers to many elements including temperatures, precipitation, humidity, air pressure and wind. Bangladesh has a tropical climate because of its geographical location. Bangladesh has mainly six seasons. A hot humid summer from March to June; a rainy monsoon season from July to October; and dry winter from November to February. The use of appropriate climate data is essential to accurately designing an energy efficient building as it defines the boundary conditions, upon which all of the thermal modelling calculations are based. For the project, climate data were derived from the Meteonorm7 software (Meteonorm data given by Dipl.-Ing.Wulf Boie, Europa-Universität Flensburg). Latitude and longitude of the location was entered into the PHPP software. The two cases (normal case and worst case) of data are entered. PHPP requires two types of climate data set of monthly temperature and radiation in order to be able to calculate the cooling demand and heating demand. One of normal cases and one of worst cases has been shown in the following Table 1 and 2.

Table 1: Climate data normal cases of Dhaka iterate into PHPP

Dhaka Normal	Latitude:	23,7	Longitude °	90,37	Altitude m	15	Location	Dhaka Normal	ΔTSummer K	7,5	Source	Example data set: PHI	Heating load 1	Heating load 2	Cooling load 1
Ambient temp	17,4	20,9	25,1	27,7	28	28	28	28,3	27,9	26,6	23	19	15,4	27,3	29,0
North	37,0	38,0	48,0	54,0	66,0	61,0	60,0	52,0	46,0	43,0	36,0	33,0	49	44	91
East	81,0	84,0	99,0	104,0	106,0	81,0	83,0	85,0	82,0	84,0	80,0	80,0	109	49	146
South	150,0	134,0	117,0	80,0	63,0	51,0	52,0	60,0	77,0	113,0	154,0	174,0	207	48	82
West	77,0	82,0	108,0	104,0	107,0	78,0	83,0	80,0	79,0	84,0	88,0	83,0	104	48	144
Global	128,0	143,0	177,0	182,0	195,0	147,0	152,0	147,0	140,0	143,0	138,0	132,0	171	91	270
Dew point	13,2	15,3	18,8	22,4	23,8	25,1	25,2	25,4	25,1	23,8	19,3	15,2	4d	4d	2d
Sky temp	6,9	10,2	14,0	17,2	20,0	21,7	21,9	21,6	20,4	19,1	13,5	8,2	w1: 12/1	w2: 21/6	s: 20/5

*Sources: PHPP

Table 2: Climate data worst cases of Dhaka iterate into PHPP

Dhaka Worst	Latitude:	23,7	Longitude °	90,37	Altitude m	15	Location	Dhaka Worst	ΔTSummer K	6,9	Source	Example data set: PHI	Heating load 1	Heating load 2	Cooling load 1
Ambient temp	15,9	19,2	23,7	26,8	29,3	29,3	28,8	28,7	28,5	26,1	22,3	18,4	13,8	18,9	30,2
North	37,0	39,0	48,0	53,0	68,0	67,0	66,0	56,0	49,0	42,0	37,0	34,0	49	44	94
East	68,0	76,0	97,0	118,0	121,0	94,0	96,0	96,0	97,0	74,0	76,0	76,0	95	63	164
South	118,0	120,0	109,0	86,0	63,0	54,0	56,0	66,0	92,0	99,0	141,0	157,0	175	93	80
West	66,0	77,0	99,0	118,0	123,0	89,0	94,0	94,0	97,0	76,0	83,0	78,0	96	61	169
Global	111,0	132,0	167,0	205,0	225,0	171,0	173,0	170,0	167,0	128,0	130,0	123,0	155	108	308
Dew point	11,8	13,8	17,6	23,6	25,2	26,5	26,0	25,9	25,8	23,3	18,6	14,7	4d	4d	2d
Sky temp	5,9	8,7	12,9	17,8	20,8	22,7	22,3	21,6	20,2	19,0	13,0	8,0	w1: 12/1	w2: 3/1	s: 20/5

*Sources: PHPP

From the climate analysis maximum and minimum temperatures in the normal case 28.7°C in mid-July and minimum temperatures is 17.7°C in the early January. It is shown in the Figure 1 that the maximum temperature in the normal case is 29.3°C in mid-June and minimum temperature is 15.9°C in early January,

it is shown in the Table 3. Heat can enter building directly through the roof or it can heat the building shell to higher temperature than the ambient, increasing the heat transfer through the building envelope.

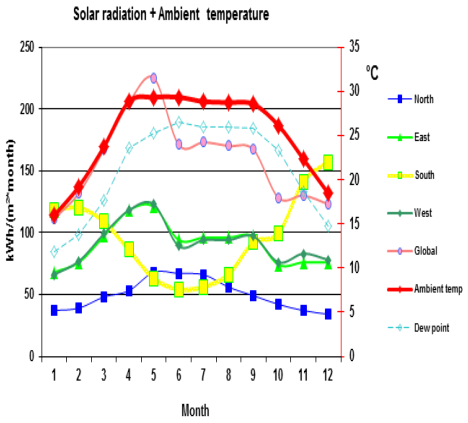

Figure 1: Ambient temperatures Worst case (Sources: Author, using PHPP).

In the case study building both cases are considered. The first analysis comprises the present situation of the building. After that, solutions for saving energy are analysed. For example, by adding insulation systems in the top floor roof. Figure 2 illustrates the maximum heat gains in the room bellow of roof. In the case study building, there is no insulation system on the roof. Therefore, the roof absorbs and gains a lot of heat. Through Figure 2 and 3 it has been shown a lot of heat gain reduce after using insulation material on the top floor roof.

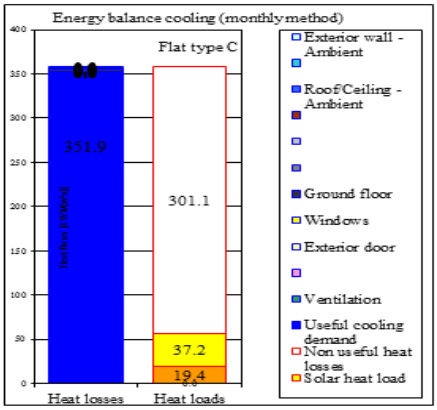

Figure 2 Energy Balance cooling without insulation

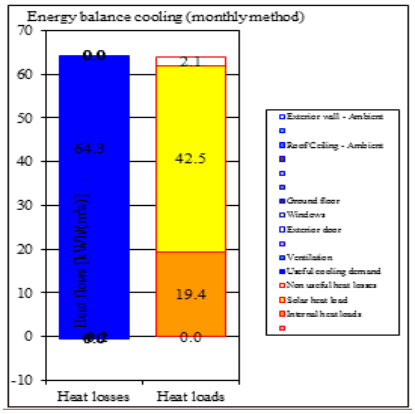

Figure 3 Energy Balance cooling with insulation

4 AN OVERVIEW OF CASE STUDY BUILDING

The name of this 14-storey residential building is Shapla; it is situated in Mirpur Cantonment in Dhaka. These types of high-rise buildings are very demanding in Bangladesh because of increasing population. Government also prefers to build high rise buildings. This case study building has 4 flats on each floor, making total of 52 flats on all 14 storeys. There are two types of flats, C and D types. All dwellings are for higher middle classes. The C type floor area is 156.06m^2 while the D type has 139.21m^2. The building design followed the USD method and BNBC. In this report, only top floor energy consumption is discussed. Figure 4 shows the Shapla building of Mirpur.

Figure 4: Elevation view of East (A), West (B), North (C), and South (D) (Source: Provided by MIST).

According to PHPP software all the components of the building envelope (the building envelope of a house consists of its roof, sub floor, exterior doors, and windows and of course the exterior wall) need to work together to keep a building cool. This building roof is flat and of 100mm thickness with cement finish on top. The house owner of the top floor pronounced that in summer it is very hot and very cold in winter. Systematic energy analysis of the energy consuming systems of the building a bottom-up approach has been chosen. This approach includes detailed analysis of principal sources of energy usage, which are celling fan and air-condition.

All flat owners want to use celling fan because celling fan is cheaper than the air-conditions.In this building, all ceiling fans are 55 inches (1397 mm), which consume 100W. According to the survey, they use ceiling fans for 15 hours during 8 months of the year and during 2 months for 5 hours daily and another 2 months for 1 hour each day. According to the interview, some time they also use the ceiling fan to dry their room. Occupants clean their rooms with water every day. The total numbers of air conditions are 8 in the top floor. The absence of insulation systems in the roof increases the need for air-conditioning. A room air condition system is used to cool rooms and they

come in many different sizes, depending on the size of the room. This type of air conditioning unit consumes 1000 W electricity. According to the survey, occupants use air condition 6 hour daily during 8 months and during 2 months it is used for 2 hours each day. In winter they do not use air condition.

5 ECONOMIC ANALYSIS

To estimate the cost for power per category the current rate of energy is taka 16.00 per kWh. The results of the demand calculation were elaborated using Microsoft Excel as a calculation tool. The service, which contributes to the thermal conditioning of the building, accounts for almost 49% of the overall power consumption. Because of the weather, the cooling demand is very high. The total energy consumption for cooling is 16,277 KWh/year, which results in costs of taka 260,432 TK per year in the building. A big amount of electricity is consumed by the top floor compared to other floors. The top floor is very hot because the rear insulation systems. Figure 5 shows the combined annual electricity consumption by different appliances in the building.

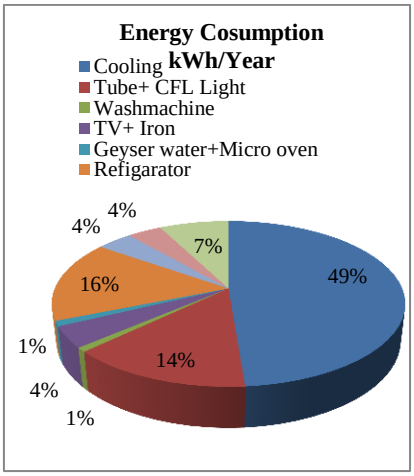

Figure 5: Percentage of energy consumption by Appliances

6 DATA USED FOR COOLING DEMAND CALCULATION

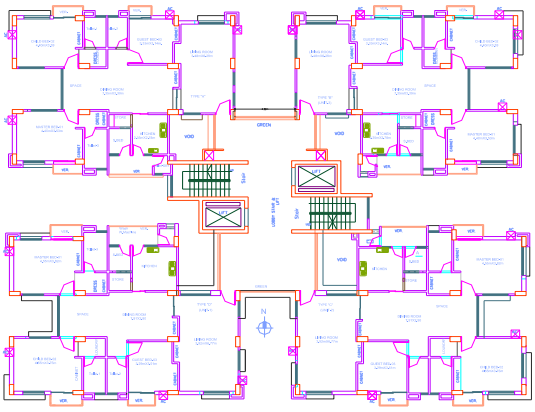

Figure 6: Top floor plan before rehabilitation (provided by architect)

PHPP only considered the thermal envelope and composition of a given space to calculate cooling demand for such space. For the present paper, only the thermal envelope of the top floor of the case study building was considered in cooling demand calculation shown in Figure 6. The dimension of the thermal envelope was taken from the architectural drawing. The composition and thickness of the thermal envelope components required for the calculation of U-values in PHPP were taken from data provided by MIST.

7 COOLING DEMAND CALCULATION WITH PHPP

The top floor of Shapla building will have a major impact on the overall energy consumption by air-conditioning. The decision to equip all rooms in the building with air condition is the major reason of the high energy consumption. The thermal conductivity value is used to calculate U-value for the various thermal envelope components, external walls, ceiling, floor, external doors chosen from the PHPP manual.

Exterior and interior heat transfer resistance of these components were taken from general literature review. Using the passive house planning package (PHPP) software tool from the Passive House Institute, the energy demand required to keep the rooms in the building of the case study at a temperature of 25°C or less in the present situation was calculated for the top floor. In the present situation the energy demand is 1301.5kWh/flat. After a green roof is installed, the top floor energy consumed for cooling is reduced to 773kWh/flat. All roof material is chosen from the green roof cross section plan.

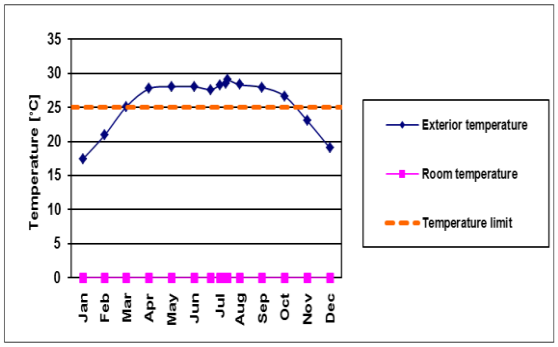

Figure 7 Temperature levels of the top floor (Source: Author using PHPP)

The calculated cooling load of 5,411 kWh/flat for insulation in the case of weather condition, and 9,110.5 kWh/flat for the case without insulation and the same weather conditions. Figure 10 illustrates the energy demand being reduced to 37% because of the insulation system. There are many proposed buildings of this kind, while several buildings are under construction.

A green roof consists of mechanisms to support the roof structure as well as components to help perform the traditional function on a roof, which is waterproofing and channelling excess water towards the drains. Figure 11 shows a cross section of a green roof. The soil and water both have the ability to store heat, and they contribute to reducing the temperatures of the roof. Regarding the urban heat island effect, experiences show that green roof surfaces absorb solar radiation and this has a positive impact on both outdoor and indoor quality. It could be a great shade for the roof. It also adds beauty to the building.

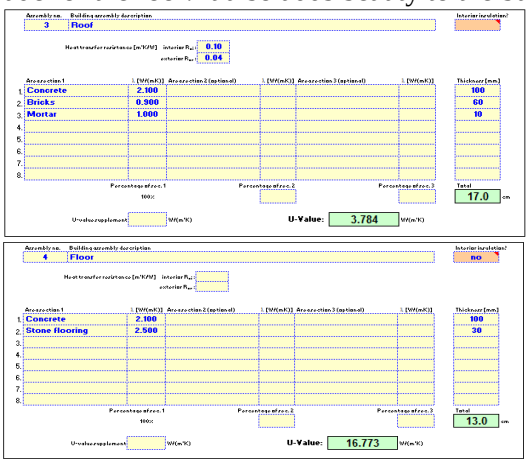

Figure 8: U-values for Roof without insulation

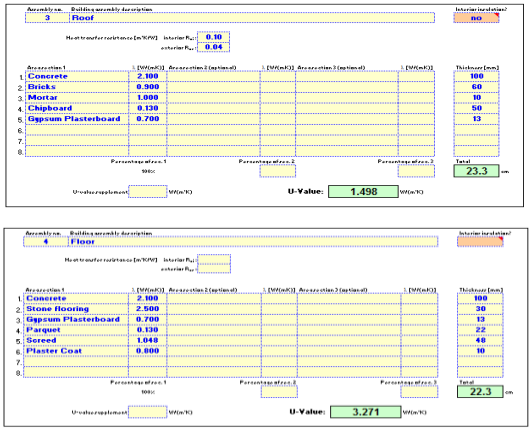

Figure 9: U-values for Roof with in insulation system

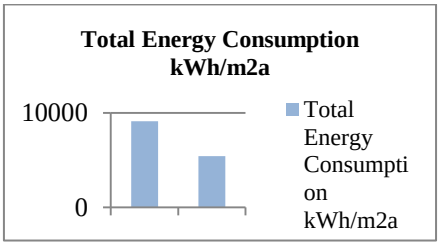

Figure 10: Comparison between present and future energy consumption kWh/Year

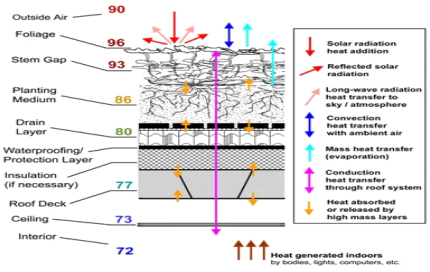

Figure 11 Cross section of Basic element of roof (Source: Christopher 2010)

8 STRUCTURE

Additional loading is the main issue of the case study building. If a green roof is part of the initial design of the building, the additional load can be

accommodated easily. However, if a green roof is installed on an existing building the design will limit the carrying capacity of the existing roof. This is a matter to be considered in Dhaka, Bangladesh, where existing roofs are typically designed for a live load of 120 kg/m2. According to British Building Code, a green roof may have a thickness of 35.6 cm (14``). In Bangladesh, there is no code for green roofs, but if the owner wishes to make a roof garden then they should consider a live load 50 kg/m^2. Therefore, the live load is not problem for green roof. This concept is very new for Bangladesh, which is a rainy country. Although the green roof will retain much of the rain that falls onto it, proper drainage must be maintained. As this is a high rise building, this green roof is to be used only for flower beds or vegetables. It may not be advisable to plant big and heavy trees. An example for a vegetable garden on a green roof is shown in Figures 12 and 13.

Figure 12: Farming on a green roof (Source: www.intercongreen.com)

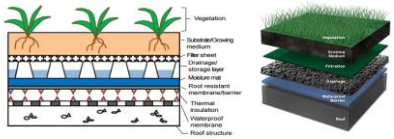

Figure 13: Cross section of the green roof for a vegetable garden

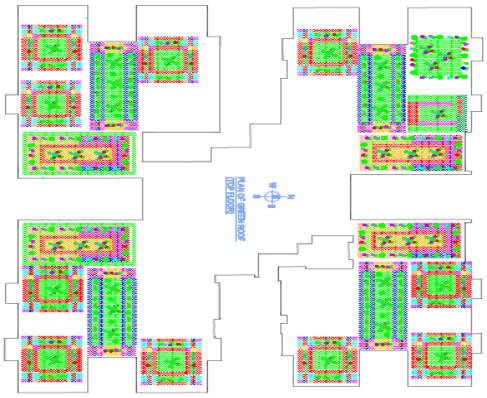

Figure 14: Green roof plan for the top floor

Table 3: Total energy consumption and cost each year

Energy consumption(kWh/year) Cooling demand both weather			
Without green roof		With green roof	
Cooling Demand kWh/year	Cost per year	Cooling Demand kWh/year	Cost per year
9,110.5	145,768	5,411	86,576

For the calculation of the economic feasibility, it was assumed that the electricity tariff of taka 16.00 /kWh and the remaining electricity consumption remain constant. The total electricity consumption for cooling in the base scenario is 9,110.5kWh/ year, which will be reduced significantly after the green roof is constructed.

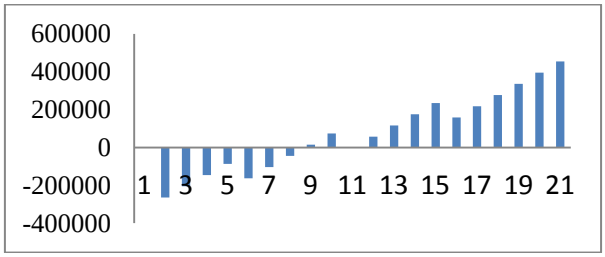

Figure 15: Cash Flow of Green Roof

9 SUGGESTION AND CONCLUSIONS

In warm climate region like Bangladesh, where temperatures are high round the year, designing for the climate means designing to reduce heat gain. Orientation and carefully planning is very important for a comfortable house.

Looking at the overall house design, the more surface area a building envelope has the more the heat gains and losses. Increasing the solar reflectivity of roof and horizontal or near horizontal surface around building and planning shade trees can yield dramatic energy savings. The benefit of trees arises both for direct shading and cooling the ambient air.

The entire feature that was analysed in this case study was the reduction of the energy demand for cooling. According to the analysis, 37% of the cooling demand of the top floor can be reduced in the Shapla building by constructing a green roof. Therefore, the study suggests influencing the developers, architects, owners, and the government to build energy efficient building. This case study building is a government residential building; therefore, if government considers the construction cost and the moderate pay-back period of 9 years, it may be possible to design energy efficient residential building all over Bangladesh.

About 50% of electricity consumed in households are relates to cooling demand. The present use of air-conditioning is not always comfortable, because there are only 8 air-conditions to cover the cooling demand, where really there is a requirement of 25 air-conditions.

The total annual energy demand of the case study building top floor has been identified as 16,277.00 kWh. per year, resulting in costs of taka 260,444.00per year according to researchers calculations based on present data.

From the financial analysis, 37% of these costs can be saved by insulation of the roof.Apart from the economic gains for the occupants, a green roof can

address many of the challenges urban cities like Dhaka are facing. Plants reduce carbon dioxide in the atmosphere and produce oxygen. Green roofs reduce the volume of rain water submitted to drainage by capturing precipitation in the vegetated surface and through evaporation from soil and the evapotranspiration of plants.

A green roof policy should be included in the BNBC. Green roofs should be mandatory for all new constructed buildings. Government may provide subsidies for a significant amount of green roof installation costs to home owners and developers.

REFERENCES

[1] A. Ahmed, (2010). An overview of Energy sector of Bangladesh. Military Institute of Science and Technology.

[2] Bangladesh Area. (n.d.). *Retrieved from* http:// www.indexmundi.com/ Bangladesh / area.html.

[3] Bangladesh latitude and Longitude Map. (n.d.). *Retrieved from* http://www.mapsofworld.com/lat_long/bangladesh-lat-long.html

[4] Bangladesh Population 2015-World Population Review. *Retrieved from* http://worldpopulationreview.com/countries/bangladesh-population/

[5] Dhaka Tribune. Retrieved from http: //www.dhakatribune.com/ bangladesh/2015/jan/04/powergeneration-capacity-doubled-6-years

[6] Mirpur road wikipedia. (n.d.). Retrieved from https:// en.wikipedia.org/ wiki/ Mirpur_Road

[7] Risks and opportunites of Urbanisation and magacities. (n.d.). Retrieved from http:// www.fig.net/ resources/ proceedings/ fig_proceedings/ athens/ papers/ps02/ps02_2_kotter.pdf

[8] Worldatlas. (n.d.). Retrieved from http:// www.worldatlas.com/ webimage/ countrys/asia/bd.htm

[9] Worldatlas. (n.d.). Retrieved from http:// www.worldatlas.com/ webimage/countrys/asia/bangladesh/bdlatlog.htm

CICM 2015
First International Conference on
Advances in Civil Infrastructure and Construction Materials
MIST, Dhaka, Bangladesh, 14–15 December 2015

EFFECT OF MASONRY INFILL WALLS ON THE SEISMIC RESPONSE OF A THREE STOREY INDUSTRIAL BUILDING IN BANGLADESH

Jaher Wasim[1]

[1] Structural Engineer, Mantissa Design and Consultant, Dhaka, Bangladesh
Email: wasim@jaherwasim.com

Abstract. *Masonry infill panels are often used as interior partitions and exterior walls in buildings. They are usually treated as non-structural elements, and their interaction with the bounding frame is often ignored in design. A three storey reinforced concrete frame structure consists of RC frames, RC floor slabs and URM infill walls are analyzed for strong ground motions to evaluate the influence of masonry infill panels on the dynamic response. Equivalent Strut method has applied on the simulation of infill walls. A detailed finite element model is constructed to carry out three-dimensional nonlinear time history analysis on the structure. The response simulations were performed for of bare frame and in filled frame.*

Keywords: Infill wall, Seismic response, Equivalent strut method, Time history analysis

1 INTRODUCTION

Reinforced concrete framed building with masonry infill walls have been widely constructed for commercial, industrial and residential buildings in seismic-prone regions worldwide. It is a structural composite system which consists of a reinforced concrete frame with masonry or concrete panels filling the planar rectangular voids between lower and upper beams and side columns. Structural engineers, during the design process of a building, typically, ignore the effects of infill masonry walls in the structural analysis. The Masonry panels which are required to build the partition and enclose the structure are generally considered as non-structural elements. Observations made after earthquake that these non-structural elements had beneficial effect on buildings seismic lateral capacity. The main objective of this paper is to bring a contribution to the knowledge of the effect of infill wall on seismic response of RC frame buildings. Fig. 1 shows lateral load transfer mechanism in bare frame and infill wall frame.

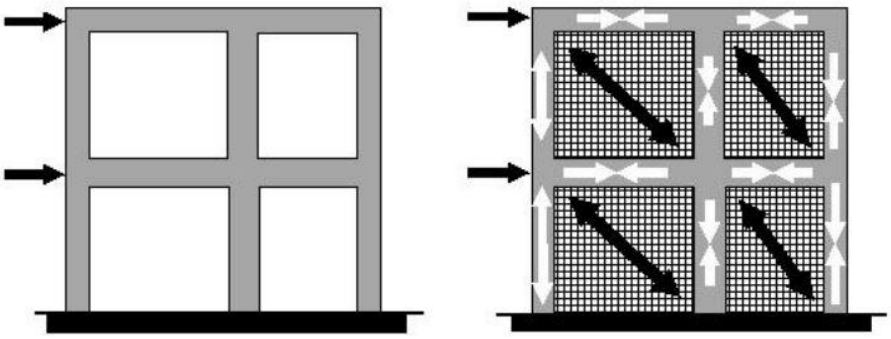

Frame action in bare frame Compression action in infill frame

Figure 1: Change in the lateral load transfer mechanism due to infill wall panels

2 EQUIVALENT STRUT METHOD

From several research paper studies it shows that Equivalent diagonal strut method is used for modeling the infill wall to easy represent the effect of inplane during lateral load and its equations for equivalent diagonal strut width for full infill wall given by various researchers are,

In 1961, Holmes [1] states that the width of equivalent strut to be one third of the diagonal length of infill.

$$w = \frac{dz}{3} \qquad (1)$$

Where d_z = diagonal length of infill panel

In 1969 Stafford smith and cater [2] proposed a theoretical relation for the width of the diagonal strut based on the relative stiffness of infill and frame.

$$w = 0.58\left(\frac{1}{H}\right)^{-0.445}.\left(\lambda_h.H_{inf}\right)^{0.335d_{inf}\left(\frac{1}{H}\right)^{0.064}} \quad (2)$$

$$\lambda_h = \sqrt[4]{\frac{E_{inf}t\sin 2\theta}{4E_cI_cH_{inf}}} \quad (3)$$

Where, t, H in f and E in f are the thickness, the height and the modulus of the infill respectively, θis the angle between diagonal of the infill and the horizontal, Ec is the modulus of elasticity of the column, $I_c$is the moment of inertia of the columns, His the total frame height, and $\lambda_h$is a dimensionless parameter.

In 1971 Mainstone [3] gave equivalent diagonal strut concept by performing tests on model frames with brick in fill's

$$w = 0.175d_z(\lambda_h H)^{-0.4} \quad (4)$$

In 1984 Liauw and Kwan [4] proposed another relationship

$$w = \frac{0.95\,H\cos\theta}{\sqrt{\lambda_h H}} \quad (5)$$

In 1992 Paulay and Preistley [5] proposed,

$$w = \frac{dz}{4} \quad (6)$$

3 RESEARCH OBJECTIVES

The main objective of this study is to investigate the contribution of hollow masonry infill panels to lateral strength and stiffness of RC frame buildings. The simulation has done by creating a 3-D analysis model by ETABS 2015 a product of Computer and Structure Inc. [7]

4 THE CASE STUDIED

4.1 General Description Of The Structure

The three story concrete structure shown in the Fig. 2 is designed according to the BNBC 1993 (Bangladesh National Building Code) [6]. From soil report it has

found the structure is built on soft soil (SD Type, SPT < 15) in zone 2 (moderate seismic intensity zone) of Bangladesh Seismic map.

This building is 64.5mx45m in plan and 4m x 3 floors in elevation. The bays are 8m center to center in X direction and 5 m center to center in Y direction with 8 bays in X direction and 9 bays in Y direction. There is an expansion joint in the middle of X direction. It has exterior infill wall panel in the all four sides of structure. To assess the influences of infill wall two structural models has been developed, one with infill wall panel (IF) another one is bare frame (BF). Infill panels with openings are not considered here, for simplification purposes.

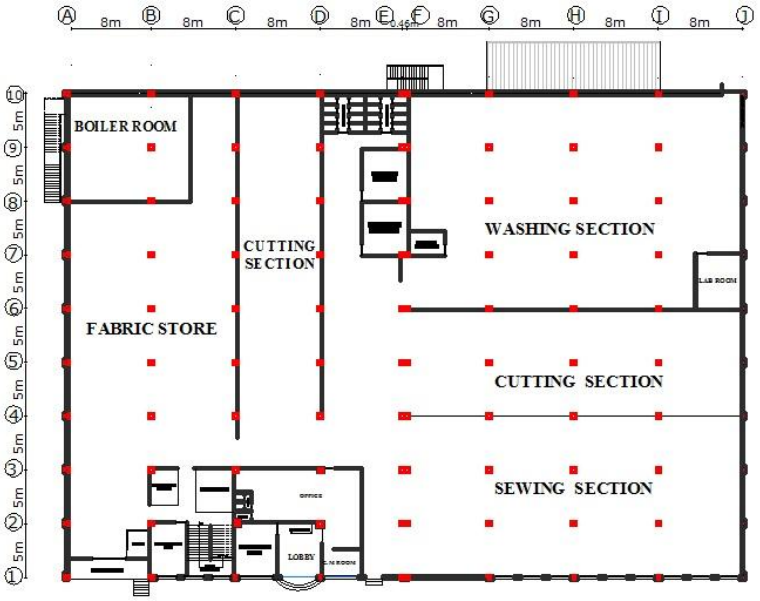

Figure 2: Typical layout plan of 3 storied industrial building

4.2 Mechanical Properties Of Materials

The compressive strength of concrete found from core test results is, f'c = 18 MPA for all the element, yield strength of the longitudinal and transverse reinforcement is $f_{y=}$ 415 MPA and the average compressive strength of masonry infill wall was 10 MPA. The modulus of elasticity of brick masonry is 8275MPA.

The geometrical parameters of the frame members are presented in the Table 1, and the properties of the materials are in the Table 2.

Table 1: Geometrical parameters of the frame members

Frame Element	Transverse Dimension (m)	Transverse Section Area (m^2)	Moment of Inertia (m^4)
Longitudinal Beams	0.38x0.76	0.29	0.0139
Transverse Beams	0.38x0.76	0.29	0.0139
Columns	0.38x0.38	0.14	0.00174

Table 2: Properties of material

Frame Element	Modulus of Elasticity (KN/m^2)	Poison Coefficient	Tension Steel , A_s (cm^2)	Compression Steel , A_s (cm^2)
Longitudinal Beams	$2.9x10^6$	0.3	17.03	8.51
Transverse Beams	$2.9x10^6$	0.3	14.19	8.51
Columns	$2.9x10^6$	0.3	34.064	34.064
Masonry	$1.2x10^6$	0.17	-	-

5 NUMERICAL METHODS

All computer models are generated and analyzed by ETABS 2015 finite element software developed by a product of Computer and Structure Inc.

Preliminary assessment, modal analysis and time history analysis has done to investigate changes in different parameter in infill wall frame with respect to bare frame.

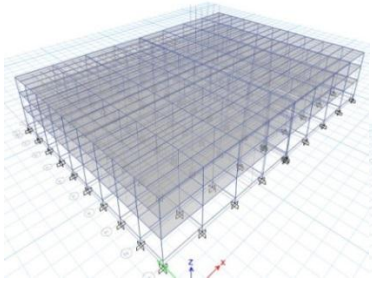

Figure 3: Bare frame 3D model

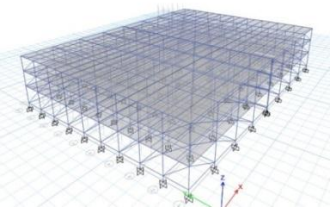

Figure 4: Infill Wall frame 3D model

6 FINDINGS AND DISCUSSION

6.1 Dynamic Responses

The response of a structure subjected to dynamic loading mostly dependent on such basic properties as the damping and fundamental period of structure. These properties are dependent on the mass, stiffness and strength of the structure affected by bay size, steel ratio, section dimension, number of storey, infill panel, concrete cracking and axial load level.

After performing a modal analysis it can be seen that the fundamental period for the bare frame is 0.476s and for infill wall frame 0.366s.

From the decreasing of fundamental period in infill wall frame it can be pointed out that infill wall contribute to increase the stiffness of the structure. In case of bare frame the time period calculated by Raleigh's method $T = 0.075H^{0.75} =$ 0.484s is close the estimated value. With regard instead of infill structure, the formula reported by BNBC 1993, $T = 0.046H^{0.9}$ = 0.431s can be assumed as a reference point.

Finally a comparison has been carried out also with respect to displacements. It is possible to observe that the presence of infill is crucial. Moreover, it is observed a reduction of about 175% of the maximum displacement in the X direction between the bare and infilled frame and 110% in the Y direction.

6.2 Time History Analysis

In this study an earthquake record obtained at Natore (Ansary, 2009) is taken as a reference which has been used to develop earthquake time history for Dhaka after appropriate scaling. The acceleration data for recent earthquake at Station ID:ALTUS S/N 2928, 06th Jan 2009 16:04:03 (GMT), Magnitude 4.0, location: Natore, Bangladesh is shown in Fig. 5.

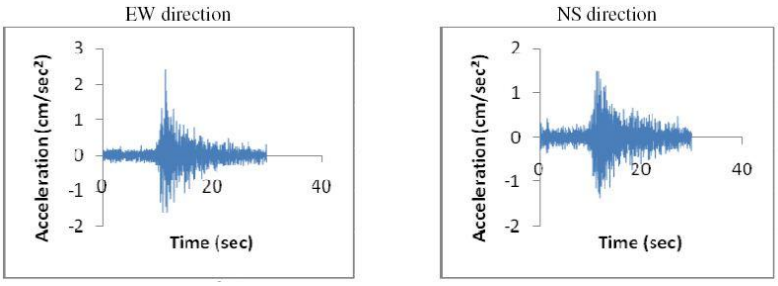

Figure 5: Earthquake Time History of Natore

Here in the Natore earthquake record the peak ground acceleration is 2.43 cm/sec^2 at 11.425 sec. but the maximum ground acceleration as per BNBC (1993)

for Dhaka is 0.15g = 147.15 cm/sec^2 resulted 61.58 times greater. So, the values have been multiplied by 61.58 and the modified Time history curves for Dhaka is shown in Fig. 6

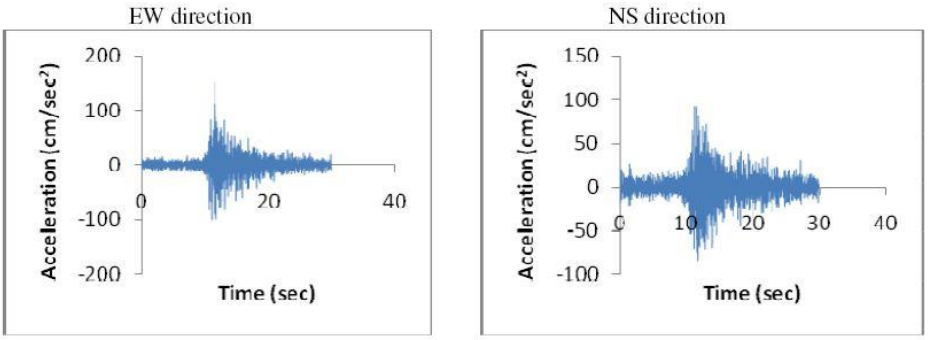

Figure 6: Modified Earthquake Time History of Dhaka

The story drift value for time history analysis is shown in Table 3.

Table 3: Storey Drift value for bare frame and infill frame

Story Level	Direction	Story Drift in mm	
		Bare Frame	Infill Frame
0	X	0	0
3		1.13	0.09
0	Y	0	0
3		1.75	0.15

7 CONCLUSIONS

Under the light of the results of the present numerical study, the following conclusions may be stated:

- The distribution of masonry infill panel throughout the story has insignificant effect on seismic response of reinforced concrete buildings.
- As compared to the bare frame the maximum roof displacement is reduced in a large extent in infill wall frame.
- The storey drift values decreases in infill frame and therefore infills increase the stiffness of RC frame
- It can be concluded that brick infill wall is to be included and carrying out seismic analysis of multistoried frame.
- This three storied RC frame arranged with symmetric pattern of infill wall panel further study can be worked out for unsymmetrical arrangement of infill wall.

8 REFERENCES

[1] M. Holmes, "Steel Frames With Brickwork and Concrete Infilling," Proceeding of the Institution of Civil Engineers, vol. 19, pp. 473-478, 1961.

[2] B. Stafford Smith and C. Carter, "A method of analysis for infill frames," Proceedings of the Institution of Civil Engineers, vol. 44, pp. 31-48, 1969.

[3] R. J. Mainstone, "On the Stiffness and strength of infilled frames," Proceeding of the Institution of Civil Engineers, Supplement IV, pp. 57-90, 1971.

[4] T. C. Liauw and K. H. Kwan, "Nonlinear Behavior of Non-Integral Infilled Frames," Computers & Structures, vol. 18, pp. 551-560, 1984.

[5] T. Paulay and M. Priestley, Seismic Design of Reinforced Concrete and Masonry Buildings. New York: Jhon Wiley & Sons, 1992.

[6] BNBC (1993) Bangladesh National Building Code, Housing and Building Research Institute, Mirpur, Dhaka, Bangladesh.

[7] Computer and Structures Inc., ETABS Nonlinear Version 15, California, USA.

CICM 2015
First International Conference on
Advances in Civil Infrastructure and Construction Materials
MIST, Dhaka, Bangladesh, 14–15 December 2015

SHEAR CONNECTIONS WITH SELF-TAPPING-SCREWS FOR CROSS-LAMINATED-TIMBER PANELS

Afrin HOSSAIN[1] **and Thomas Tannert**[2]

[1] Wood Science, UBC Vancouver, Canada
Email: afrin.hossain@alumni.ubc.ca

[2] Wood Science and Civil Engineering, UBC Vancouver, Canada.
Email: thomas.tannert@ubc.ca

Abstract: *The use of Self-tapping Screws (STS) in Cross-laminated Timber (CLT) is increasingly becoming popular in both residential and non-residential applications in North America. This paper presents the experimental results on CLT-STS shear connections of thirty quasi-static tests. Different joint types were tested in 3-ply CLT: i) Single surface spline with STS in shear, ii) Half-lap with STS in shear, iii) Half-lap with inclined STS in withdrawal, iv) Butt-joints with inclined STS in withdrawal at double angles, and v) Butt-joints with STS in shear. The performance of the connections were evaluated in terms of i) capacity; ii) yield strength; iii) stiffness; and iv) ductility. The results confirmed that ductile but less stiff connections can be achieved using STS in shear. Much stronger and stiffer connections can be achieved using STS in withdrawal; this screw configuration, however, exhibits low ductility. Using double inclined STS in butt joints leads to high capacity, high stiffness, and moderate ductility. The obtained data will provide guidance to the structural engineers, architects, and builders for designing shear connections with STS in CLT panels.*

Keywords: Cross-laminated-timber, Self-tapping-screws, Static tests.

1 INTRODUCTION

The forest industry is a key driver of the economies of several Canadian provinces and US states, and one main application of forest products is the use of solid timber and its engineered wood products (EWPs) derivatives in construction. In non-residential construction in North America, however, wood products are underutilized compared to steel and concrete. In Canada, one reason is the lack of design guidance in the National Building Code of Canada [1], and the Canadian Standard for Engineering Design in Wood [2] for novel EWPs like CLT or novel fasteners like STS.

One external driver in Canada for giving timber products more consideration in non-residential construction is Bill 9 [3], passed in 2009 by the province of British Columbia, which aims to promote a culture of living and building with wood by requiring its use as a principal material in any provincially funded building. Besides this Bill, several Canadian provinces implemented code changes that allow for wood to be used in six-storey high light-frame buildings.

Timber has been successfully used in multi-storey buildings because of its light weight, smaller carbon footprint, and the ease of prefabrication and assembly [4]. Apart from those advantages, however, there are several challenges in designing and constructing timber buildings, including the stability against wind loads, fire safety, noise, vibration, and durability. In buildings where stiff wind bracing systems are required, CLT elements can be a solution either in some part of the walls or as a whole [5-7].

An important issue of consideration is the connection between CLT panels, especially for heavily loaded walls [8]. STSs are a cost efficient timber connector appropriate for many structures as they do not require pre-drilling and are therefore faster to install than traditional lag or wood screws [9].

The objective of this study, carried out at the University of British Columbia Vancouver (UBC), was to investigate the performance of STS shear connections between CLT panels. Specifically the following characteristics are presented: i) capacity; ii) yield strength; iii) stiffness; and iv) ductility.

2 TEST SERIES OVERVIEW

A total of thirty CLT test specimens, 700mm wide, 290mm high, and 105mm 3-ply) thick, were tested. Each test specimen consisted of two CLT panels exhibiting one joint plane. The load was applied at a 14.5^0 angle to the center line of the specimen, see **Error! Reference source not found.**.Five types of joints were investigated: i) Single surface spline with STS in shear; ii) Half-lap with STS in shear, iii) Half-lap with STS in withdrawal, iv) Butt joint with STS in withdrawal, and v) Butt joint with STS in shear. Six replicates per test series were fabricated and tested. Different STS were used according to the joint configurations, leading to the use of screws with lengths of 80mm, 90mm, 140mm, and 180mm (**Error! Reference source not found.**).

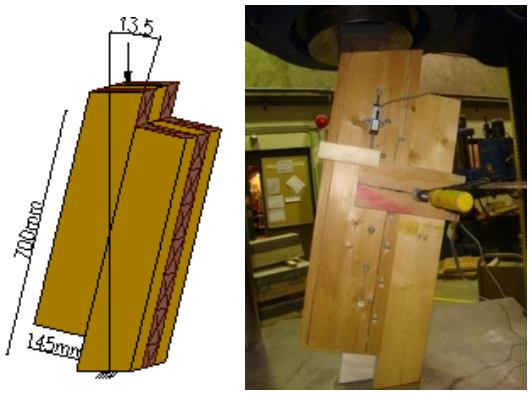

Figure 1: Test specimen (left), test setup (right)

Table 1: Test Series

Series	Joint Type	STS action	STS length [mm]	STS#
1	Surface Spline	Shear	80	8
2	Lap Joint	Shear	90	4
3		Withdrawal	140	6
4	Butt Joint	Withdrawal	180	4
5		Shear	140	8

2.1 Series 1: Surface spline with STS in shear

For the surface splines, 3/4" (3-ply) or 1" (5-ply) deep and 40mm wide slots were cut into the panels. Plywood sheets 3/4" or 1" deep and 80mm wide were used as splines.

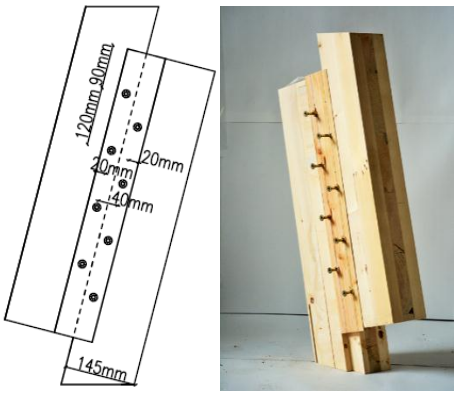

Figure 2: Surface spline joints with STS in shear (layout and specimen)

2.2 Series 2: Lap joint with STS in shear

The laps were 80mm wide and 52.5mm (3-ply) or 87.5mm (5-ply) deep (half the panel thickness).

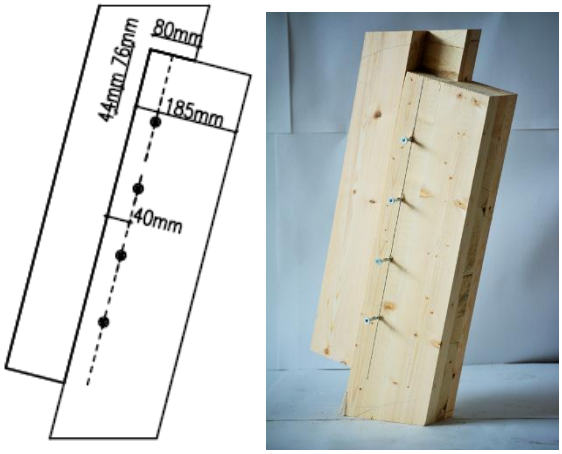

Figure 3: Half lap joints with STS in shear(layout and specimen)

2.3 Series 3: Lap joint with STS in withdrawal

The laps were cut identical to those of lap joint with STS in shear. In this joint, however, the STS were placed at an angle of 45° to load these in withdrawal.

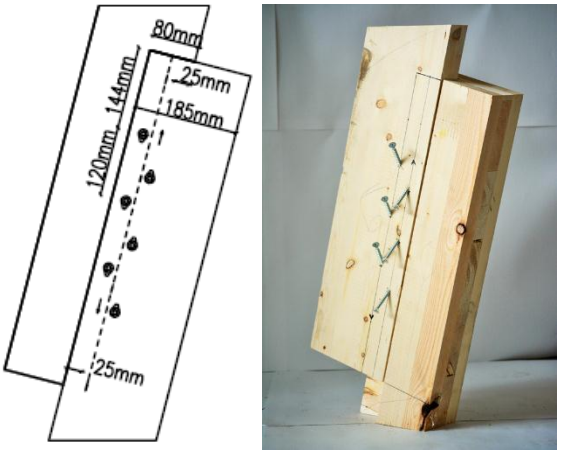

Figure 4: Half lap joints with STS in withdrawal (layout and specimen)

2.4 Series 4: Butt joint with STS in withdrawal

STS were installed at an angle of 45° to the edge of the CLT panels, and at an angle of 33° to the face of the panels. This joint was tested only for 3-ply.

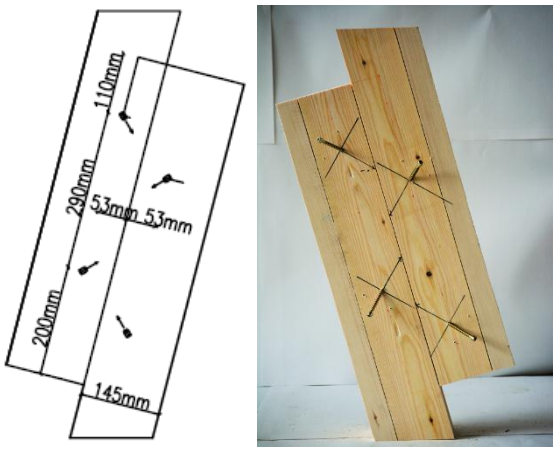

Figure 5: Butt joints with STS in withdrawal (layout and specimen)

2.5 Series 5: Butt joint with STS in shear

STS were installed at an angle of 45° to the face of the panels. This joint was tested only for 3-ply.

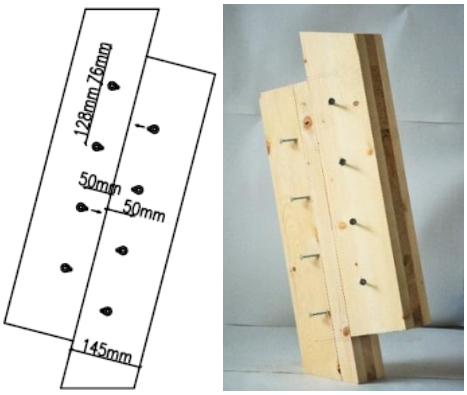

Figure 6: Butt joints with STS in shear (layout and specimen)

3 MATERIAL

CLT panels (3-ply and 5-ply) were supplied by Structurlam Products Ltd. STS were provided by MyTiCon Timber connectors Ltd. For shear action SWG

ASSY Eco with CSK head type partially threaded STS and for withdrawal action SWG ASSY VG with CSK head type or cylindrical head type fully threaded STS were used. The STS and CLT are shown in Figure 7. The screw were spaced according to the product approvals [10, 11].

Figure 7: CLT (left) and STS (right)

4 METHODS

A hydraulic actuator with a capacity of 400kN was used to apply the load to one of the CLT pieces. Two 20mm thick 100x100mm steel plates were used to distribute the load (**Error! Reference source not found.**). The other CLT piece was placed on a steel support with. The actuator load was applied according to a modified loading protocol [12]at a displacement controlled rate of 5mm/min. At first the specimen was loaded up to 40% (approx.) of estimated maximum load, then that load was hold for 30 seconds. After that the specimen was unloaded to 10% (approx.) of estimated maximum load and again the load was hold for 30 seconds. Finally the specimen was loaded to failure where failure is assumed to occur when load drops to 80% of the recorded maximum load. The actuator load and the relative vertical displacements between the two CLT panels using two transducers attached at front and back of the assembly were recorded at a sampling rate of 10 Hz.

5 RESULTS

Table 2summarizes the results and Figure 8illustrates the averages of the experimentally observed load-displacement curves of all test series using 3-ply CLT panels. Herein, the common definition of ductility (μ) as the ratio between the ultimate displacement, δ_u at maximum load, V_{max} and the effective yield displacement, $\delta_{y,eff}(\delta_{Vmax}/\delta_{y,eff})$ was applied. Stiffness was calculated for the region of the load-displacement curves between 10% and 40% of the ultimate load according to [12].

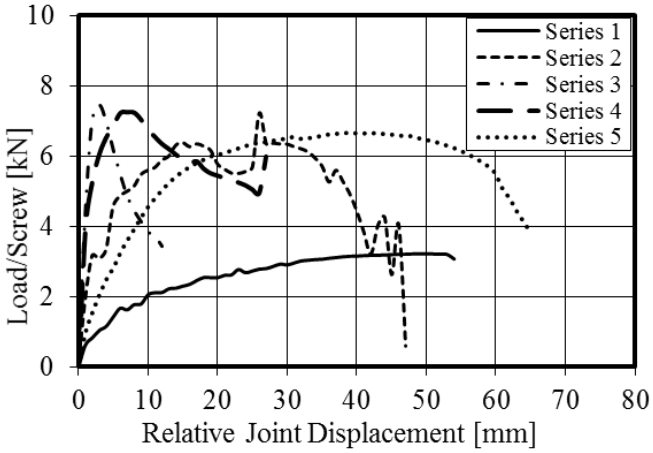

Figure 8: Load-displacement curves

Table 2: Test results summary

Series	Capacity V_{max} (kN)	Yield load V_Y (kN)	Displ.@ capaityΔ_{max} (mm)	Displ.@ yield Δ_y (mm)	Ductility μ (-)	Stiffness k (kN/mm)
1	3.42	1.46	51.00	6.62	7.71	2.57
2	7.23	4.93	18.00	3.04	5.91	5.39
3	6.44	7.16	7.00	1.66	4.21	25.84
4	7.60	6.72	4.00	1.39	2.88	19.54
5	6.67	5.96	40.00	9.46	4.23	4.77

Note: Results are averages out of 6 specimens. *All values are per screw.

6 CONCLUSIONS

This study provides experimental results on the structural performance of STS shear connections between CLT panels. Using STS in shear led to moderately ductile connections which can reach very large relative displacements between the individual panels. In that context it needs to be reminded that the measure of ductility can be misleading, as it is a relative measure for the ratio between displacement at capacity and maximum displacement. Using STS in withdrawal leads to much stronger and stiffer joints. These joints, however, exhibit much lower deformation capacity and fail at very small relative displacements. Using STS with double inclined angles in butt joints leads to high capacity, high stiffness, and moderate ductility.

REFERENCES

[1] NBCC. (2010). National Building Code of Canada. National Research Council of Canada, Ottawa, Canada.

[2] CSA O86. (2009). Engineering Design in Wood. Mississauga, Canada.

[3] Bill 9 -2009: Wood First Act 2009 Legislative Session: 1st Session, 39th Parliament.

[4] Gagnon, S., and Pirvu, C. (Canadian E.) (2011). Cross Laminated Timber (CLT) Handbook.FPInnovations, Vancouver, Canada.

[5] Blass, H.J., &Fellmoser, D. P. (2004). Design of Solid Wood Panels with Cross Layers. In WCTE-meeting. Lahti, Finland.

[6] Dujic, B., Pucelj, J., & Zarnic, R. (2004). Study of Innovative Wooden House Based on Racking Test of Solid Wall Panels. In Proceedings of the COST-E29 meeting. Florence, Italy.

[7] Moosbrugger, T., Guggenberger, W., & Bogensperger, T. (2006). Cross-Laminated Timber Segments under Homogeneous Shear – with and without Openings. In WCTE-meeting. Portland, USA.

[8] Vessby, J., Enquist, B., Petersson, H., &Alsmarker, T. (2009). Experimental Study of Cross-Laminated Timber Wall Panels. European Journal of Wood and Wood Products, 67(2), 211–218

[9] Blass, H.J., &Bejtka, I. (2004). Selbstbohrende Holzschrauben und ihre Anwendungs-möglichkeiten. HolzbauKalender, Bruderverlag Karlsruhe, ISBN 3-87104-136-X.

[10] ETA-11/0190. (2013). European Technical Approval.

[11] CCMC. (2013). "Evaluation Report CCMC 13677-R SWG ASSY® VG Plus and SWG ASSY® 3.0 Self-Tapping Wood Screws". Canadian Construction Materials Centre, Ottawa, Canada.

[12] EN-26891. (1991). Timber Structures, Joints Made with Mechanical Fasteners, General Principles for the Determination of Strength and Deformation Characteristics. CEN European Committee for Standardization, Brussels, Belgium.

CICM 2015
First International Conference on
Advances in Civil Infrastructure and Construction Materials
MIST, Dhaka, Bangladesh, 14–15 December 2015

EXPERIMENTAL AND FINITE ELEMENT ANALYSIS OF CROSS LAMINATED TIMBER (CLT) PANELS

Md Shahnewaz[1], Thomas Tannert[2], M. Shahria Alam[3] and Marjan Popovski[4]

[1, 2] UBC, Vancouver, Canada.
Email: [1]md.shahnewaz@alumni.ubc.ca and[2]thomastannert@ubc.ca

[3] Associate Professor, UBC, Kelowna, Canada.
Email: thomastannert@ubc.ca

[4] Principal Scientist, FPInnovations, Vancouver, Canada.
Email: marjanpopovski@fpinnovations.ca

Abstract. *Cross-laminated timber (CLT) is a relatively new product that is gaining popularity in residential and non-residential applications in the North American construction market. As an engineered wood product, CLT provides many benefits when compared to either light-fame wood construction or concrete and steel construction. An accurate quantification of in-plane stiffness of the CLT panels is required to design a CLT structure subjected to wind and earthquake loads. Nevertheless, till today, there are no standardized methods for determining the stiffness of CLT walls in the North American codes. Therefore, the present study aims to quantify the stiffness of CLT walls under in-plane loading. An experimental programme was conducted on CLT beams and walls at FPInnovations, Canada, to measure the load-deformation and the in-plane behavior of CLT panels. A finite element (FE) model of CLT panels was developed where the wood was modelled using orthotropic elastic material, and the glue-line between lamellas using non-linear contact elements. The FE model was verified from test results of CLT panels which showed that the FE analyses were sufficiently accurate in predicting elastic stiffness of CLT panels.*

Keywords: Cross laminated timber, Finite element analysis, Stiffness.

1 INTRODUCTION

Cross-laminated timber (CLT) is an engineered wood product categorized as "mass" timber. The use of CLT is increasingly gaining popularity because of its many benefits when compared to either light-fame wood construction or concrete and steel construction. The cross lamination provides dimensional stability, strength and rigidity. CLT has a low carbon footprint due to low embodied greenhouse gas emissions and carbon storage capacity of wood. The good thermal insulation and a fairly good behavior in case of fire are added benefits. Furthermore, it is a clean product to work with resulting in less waste and dust produced on site which is better in terms of health and safety.

CLT panels consist of several layers of boards stacked crosswise and glued together. A CLT element has usually 3 to 11 glued layers of boards placed orthogonally (90^0) to form a solid panel (Figure 1). The pre-cut wall and floor panels are assembled on the construction site using various types of screws and steel connectors to form the structural system.

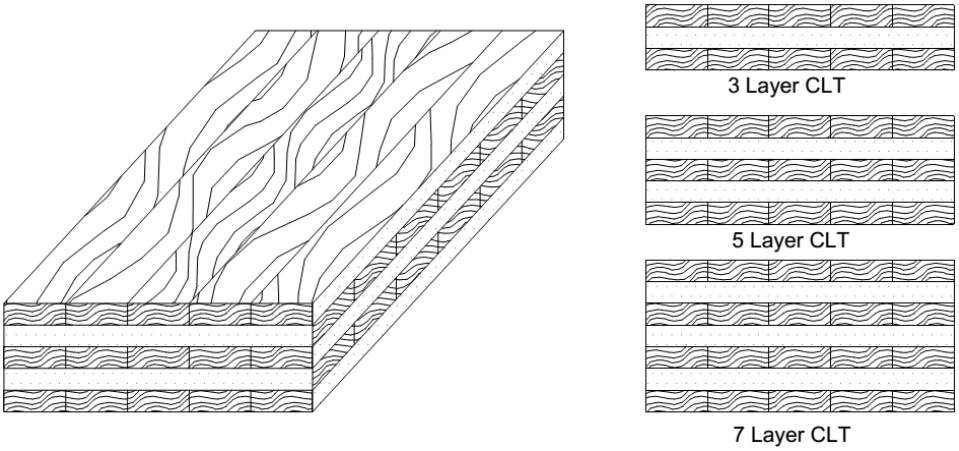

Figure 1: CLT panel configuration.

To design CLT shear walls, understanding of the mechanical properties of CLT panels and connectors connecting them is needed. Several studies have been carried out in this field and some analytical equations to predict the mechanical properties of CLT panels loaded in plane are proposed. E.g., Blass and Fellmoser [1] developed a methodology for the design of CLT panels under in-plane loading based on the composite theory. The composition factors (k-factors) were proposed to calculate the strength and stiffness of CLT panels in various directions, based on single layer properties. Moosbrugger et al. [2] proposed a mechanical model based on the regular periodic internal geometric structure of the CLT wall element, considering uniform shear loading on CLT wall boundaries. They defined the complex internal structure of CLT element with smallest unit cell called

Representative Volume Element (RVE). The RVE extends over the whole plate thickness and is sub-divided into the sub-element named as Representative Volume Sub-Element (RVSE). Bogensperger et al. [3] experimentally investigated the in-plane behavior of CLT panels and verified their results with FE analyses. The effective shear modulus was calculated and a deviation of the shear modulus of up to 26% was reported comparing tests results and FE analyses. Bogensperger et al. [4]also performed FE analysis to achieve better correlation between the experimental and analytical results and further verify the studies by Moosbrugger et al. [2]. Their FE model accurately predicted the effective shear of CLT panels. Finally, Flaig and Blass [5] developed a new methodology for shear design of CLT beams loaded in plane and proposed analytical equations for shear stress and stiffness and verified them with test results.

Nevertheless, till today, no general approach is available for the design of CLT-members loaded in plane. In fact, the strength and the stiffness properties reported in different technical approvals for verification of in plane resistance of CLT walls vary significantly [5]. Although, accurate quantification of the in-plane strength and stiffness of CLT panels and shear walls is required to design a CLT structure subjected to lateral loads,, there are no detailed analysis and design provisions for CLT buildings under lateral loads in the current North American building codes (National Building Code of Canada, ASCE7 and IBC in the US). In addition, there are no standardized methods for determining the stiffness and resistance of CLT shear walls in the respective material design standards: the CSA O86 [6] in Canada, and the NDS [6] in the US. The present study aims to calculate the in plane stiffness of CLT panels analytically to address this research need.

2 EXPERIMENTAL PROGRAMME

A four point bending test on CLT panels was performed at FPInnovations, Canada. Three series of CLT beams (2 replicates of each type) were tested with a span length of 3.5m, 5.9m, and 8.4m, see Figure 2. The beams were 1.2m high and laterally supported, where the CLT panels were made of 5-ply boards with a thickness of 175mm. CLT panels were from Canadian S-P-F and manufactured at NORDIC. The specifications of different CLT beams are shown in Table 1. The deformation was measured at mid span by LVDT under a monotonic loading from top using a hydraulic actuator. From the load-deformation behavior and the geometry of the beams, the stiffness and modulus of elasticity (MOE) of the beams were calculated (See Table 1).

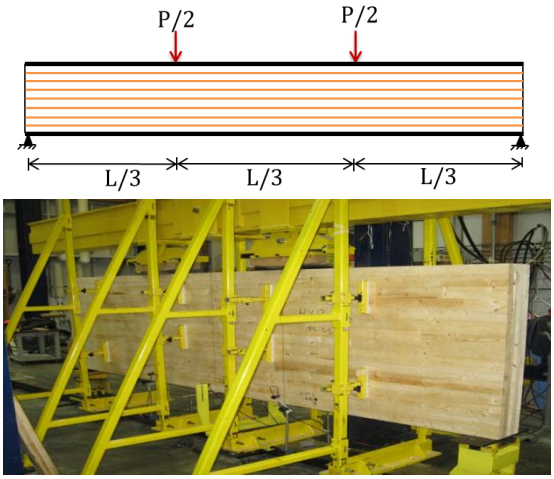

Figure 2: A schematic of CLT beam (top) and 3.5 long CLT beam specimen, A1 (bottom).

Table 1: Description of CLT beams series.

Test Series	Specimen #	Width (mm)	Depth (mm)	Span (mm)	MOE (MPa)	Stiffness K (N/mm)
A	1	175	1220	3505	1014	35139
	2	175	1220	3505	1012	35077
B	1	175	1220	5944	3122	22190
	2	175	1220	5944	3400	24165
C	1	175	1220	8382	4762	12065
	2	175	1220	8382	5075	12861

The present study also adopted monotonic test results on CLT walls at FP Innovations, Vancouver, Canada [8]. The results obtained from CLT wall test were calibrated in the FE modelling. The test walls were made of 3-ply boards with 2.3m X 2.3m panel size and thickness of 94mm (Figure 3). CLT panels were made of European spruce and manufactured at KLH. Several types of connectors (hold-downs and steel brackets) and fasteners (annular ring nails, spiral nails, screws, and timber rivets) were used for the connections.

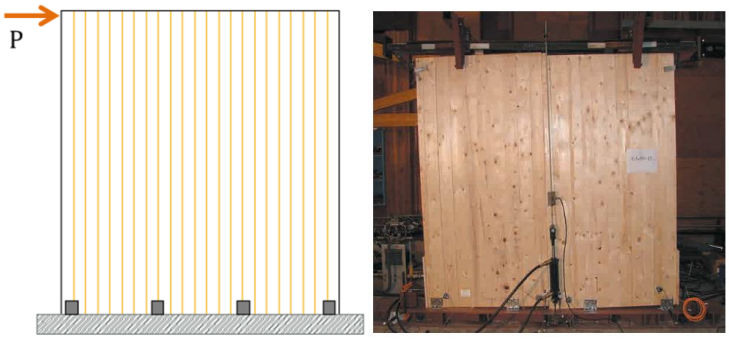

Figure 3: A schematic of CLT wall (left) and 2.3m X 2.3m wall specimen (right [8]).

3 FINITE ELEMENT ANALYSES

3.1 Model Development

A 3D FE model of CLT panel was developed in ANSYS (Figure 4). The CLT panel was modelled using 20-node SOLID186 element where each node has three degrees of freedom. Elastic material properties were assigned in each orthogonal direction of the lamella as prescribed from manufacturer's specifications. The glue-line in between panels was modelled using contact element (Conta_174 and Targe_170). A high frictional co-efficient (1.0) for the glue-line was used since the glue-line was found very stiff from the test results.The connection between the CLT wall and floor was modelled using linear COMBIN14 spring element. The stiffness properties for the connections were taken from previous research [9].

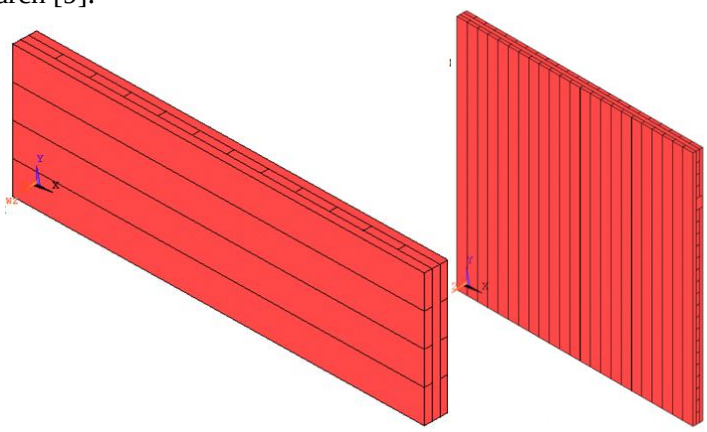

Figure 4: FE models of CLT beam (left) and wall (right).

3.2 FE Model Validation

The FE model was validated using the load-deformation curves from the test results, see Figure 5. The numerical results closely matched with the elastic part of the experimental curves. The inelastic behavior was out of scope for the present study. A deformed shape of the CLT beam and wall from FEA is presented in Figure 6.

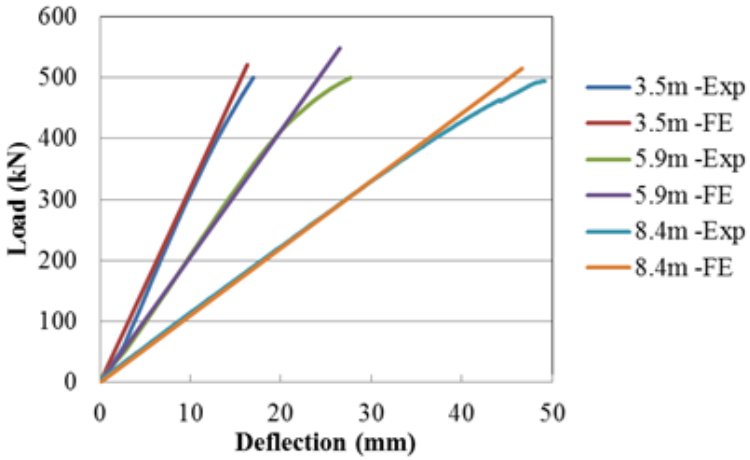

Figure 5: Experimental vs FE load-deflection curves.

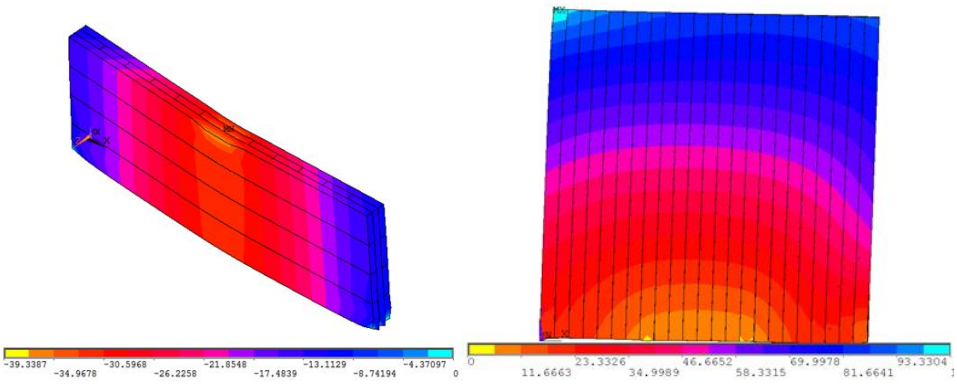

Figure 6: Deformed shape of CLT beam (left) and CLT wall (right) from FEA.

3.3 Parametric Study

A parametric study was performed with variation of the wall thickness and the wall aspect ratio. The same material properties and modelling technique was applied in the FE. The stiffness of different CLT walls was calculated and compared from the parametric study.

4 RESULT AND DISCUSSION

4.1 Walls With Various Thicknesses

The research studied the effect of thickness on in-plane stiffness of CLT panels. The panel thickness was varied from 3 to 7-layers of lamellas where each layer has a thickness of 35mm. The stiffness increased up to 24% (Table 2).

Table 2: Effect of wall thicknesses on stiffness.

CLT	Size (m)	Thickness (mm)	k (N/mm)	% Increase
3-Layer	2.3x2.3	105	3491	-
5-Layer	2.3x2.3	175	4028	15
7-Layer	2.3x2.3	245	4324	24

4.2 Walls With Various Aspect Ratios

The effect of panel aspect ratios (length vs. height) on the in-plane stiffness was also investigated. It was observed that the in-plane stiffness was increased up to 79% with a 50% increase in wall aspect ratio (Table 3).

Table 3: Effect of wall aspect ratios on stiffness.

Aspect Ratio	Size (m)	Thickness (mm)	k (N/mm)	% Increase
1:1	2.3x2.3	94	3,403	-
1.25:1	2.9x2.3	94	4,660	37
1.5:1	3.5x2.3	94	6,087	79

5 CONCLUSIONS

FE models were developed that accurately predict the in-plane stiffness of CLT panels. The experimental and analytical investigation on the CLT panels allows the following conclusions to be drawn:

- The FE model accurately predicted the load-deformation of CLT panels. The stiffness of the panels from experiment and FE model was found similar.
- It was observed that both wall thicknesses and aspect ratios are affecting the stiffness of walls.
- However, the future study should include the effect of opening on CLT wall stiffness.

ACKNOWLEDGEMENTS

The research was supported by the FPInnovations, Canada through in collaboration with Softwood Lumber Board (SLB), USA.

REFERENCES

[1] H.J. Blass, P. Fellmoser,2004. Design of solid wood panels with cross layers. *In Proceedings of the 8th World Conference on Timber Engineering*, June 14-17, 2004, Lahti, Finland, 2:543-548

[2] T. Moosbrugger, W. Guggenberger, T. Bogensperger, 2006. Cross-Laminated Timber Wall Segments under Homogenous Shear - with and without Openings. *9th World Conference on Timber Engineering*, Portland, USA.

[3] T. Bogensperger, T. Moosbrugger, G. Schickhofer, 2007. New Test Configuration for CLT-Wall-Elements under Shear Load. CIB W-18.

[4] T. Bogensperger, T. Moosbrugger, G. Silly, 2010. Verification of CLT-plates under loads in plane. *11th World Conference on Timber Engineering*.

[5] M. Flaig, H.J. Blass, 2013. Shear strength and shear stiffness of CLT-beams loaded in plane. *In Proc CIB W18*, Vancouver, Canada.

[6] CSA O86-14. Engineering design in wood, Canadian Standards Association, Mississauga, Canada, 2014.

[7] NDS 2015. American Forest & Paper Association.(AF&PA). National Design Specification for Wood Construction. Washington, DC: American Wood Council 2015.

[8] M. Popovski, J. Schneider, M. Schweinsteiger, 2010. Lateral load resistance of cross laminated wood panels. *In Proc WCTE*, Riva del Garda, Italy.

[9] J. Schneider, 2015. Conventional and novel timber steel hybrid connections: testing, performance and assessment. PhD thesis, UBC Vancouver, Canada

CICM 2015
First International Conference on
Advances in Civil Infrastructure and Construction Materials
MIST, Dhaka, Bangladesh, 14–15 December 2015

NONLINEAR SEISMIC RESPONSE OF RC STRUCTURES WITH SOFT STORIES

Iftekhar ANAM[1], **Main Uddin**[2] **and Himadree Roy**[3]

[1, 3] Department of Civil Engineering, University of Asia Pacific, Dhaka, Bangladesh.
Email: [1]iftekhar@uap-bd.edu

[2] Bangladesh Garment Manufacturer & Exporters Association (BGMEA)

Abstract. *This work presents results of numerical and experimental works performed on the seismic response of structural models with soft stories. Part of the work concentrates on the numerical work on nonlinear three-dimensional RC frames with brick infills, which show the potentially destructive effect and significant permanent deformation of structures with soft stories caused by a major earthquake. Simple 6- and 12-storied RC building frames are designed for vertical loads only, incorporating the seismic detailing provisions for major and moderate earthquakes. Relative floor deflections and curvatures (for 'Partial Infill's) demonstrate the significance of masonry infills. The experimental facilities described in the latter part of the work includes a small shake table capable of generating defined earthquake motion (scaled El Centro earthquake) using an indigenous and inexpensive approach. The soft-storied structural models used for the experiments also demonstrate the possible severe distress in the soft storied floor columns. The experimental results are found to match very well with the experimental data.*

Keywords: Equivalent diagonal strut, Nonlinear dynamics, Seismic detailing, Soft storey, Partial infill, Shake table.

1 INTRODUCTION

Reinforced Concrete (RC) frame structures constitute a common type of building structure in Bangladesh. However, due to quick growth of high-rise buildings and lack of parking facilities, most newly built buildings are designed with open ground floors supporting stories with masonry infills, which creates a 'soft' or 'weak' storey at ground floors. Structural damage patterns during earthquakes all over the world have diagnosed it as a prime reason of structural failure. But very little attention is paid to this potentially serious deficiency by architects or engineers in Bangladesh.

Therefore, it is necessary to understand the characteristics of masonry infills to better understand the structural behavior of the frame itself. Analytical and experimental works indicate the behavior of the combined infill-frame system depends on the mechanical properties and overall arrangement of infill, relative stiffness and interface behavior of frame and infill [1].

2 MODELING OF INFILLS

The in-plane behavior of infills has been studied extensively over the last several decades [e.g., 2, 3, 4, 5 among others] in attempts to develop a rational approach for design of such frames. Nonlinear dynamic analysis is performed in this work by replacing the brickwalls by an 'Equivalent Diagonal Strut' based on masonry infill model proposed by Saneinejad and Hobbs [6] and modified by Madan et al. [7]. The proposed analytical development assumes that the contribution of the masonry infill panel can be modeled by replacing the panel by a system of two diagonal masonry compression struts, which provides a lateral load resisting mechanism for opposite lateral directions of loading.

The lateral force-deformation relationship for the structural masonry infill panel is assumed to be a smooth curve bounded by a bilinear strength envelope with an initial elastic stiffness until the yield force V_y thereon a post-yield degraded stiffness until the maximum force V_m is reached. The corresponding lateral displacement values are u_y and u_m respectively. The proposed maximum lateral force V_m and corresponding displacement u_m in the infill masonry panel are

$$V_m^{\pm} \le A_d f'_m \cos\theta \le v\, tL'/[(1-0.45\tan\theta)\cos\theta] \le 0.83t1'/\cos\theta \quad (1)$$

$$u_m^{\pm} = \varepsilon'_m L_d /\cos\theta \quad (2)$$

Here, t = Thickness of the infill panel, L'= Lateral dimension of the infill panel, f'_m = Masonry compressive strength, ε'_m = Masonry compressive strain, θ = Inclination of the diagonal strut, v = Basic shear strength of masonry, A_d= Area of equivalent diagonal strut, L_d = Length of equivalent diagonal strut. These quantities can be estimated by using the formulations of [6].

Initial stiffness K_0 of the infill masonry panel may be estimated using the fol-

lowing formula [7]

$$K_0 = 2\ V_m/u_m \qquad (3)$$

3 STRUCTURAL MODEL

Figure 1 shows structural plan of both the (6- and 12-storied) buildings used in this work, with wall arrangement assuming exterior walls W_1, W_2 as 10″ walls and interior walls W_3, $W_4$to be 5″thick In this work, the stiffness K_0 for 10″ walls came out to be around 11,000 kip/ft, while those of the 5″ walls were about 5,000 k/ft. However, it must be mentioned that the walls will crack at large deformations and those with thickness $\leq L_d/40$ are not effective as diagonal struts.

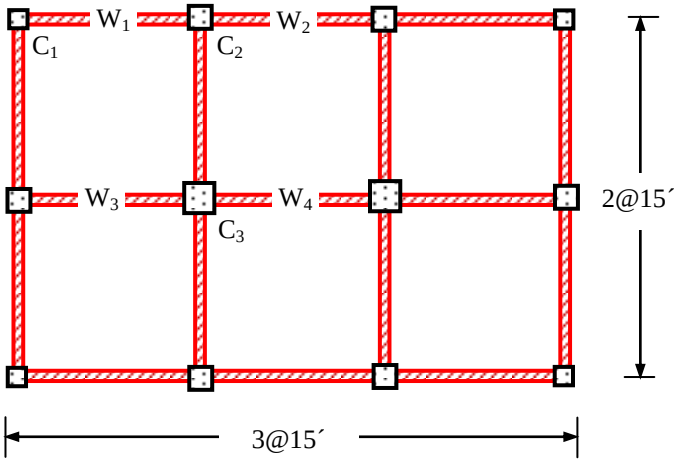

Figure 1: Building plan showing Infill Walls

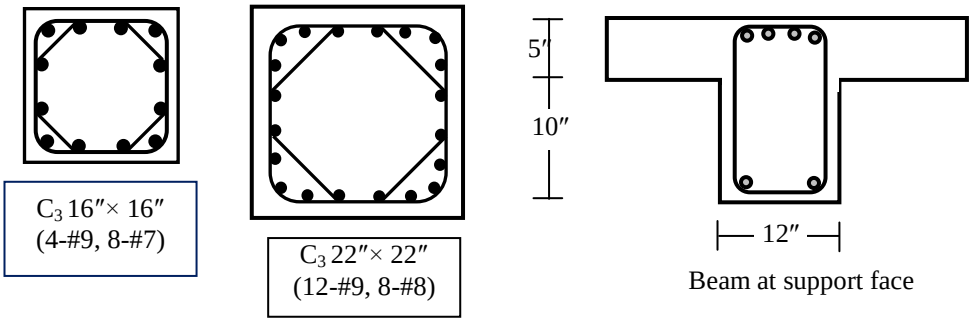

Figure 2: Cross-sections for Column C_3 (6- and 12-storied) and Beam (at support face)

The frames are analyzed and designed for vertical loads only. The column and

beam sections (with steel reinforcements) obtained are shown in Figure 2.

4 NUMERICAL ANALYSIS OF RC FRAMES

4.1 Moment-Curvature Relationships

The material properties used in this work include ultimate strength of concrete (f_c' = 3 ksi), yield strength of steel (f_y = 60 ksi), their elastic moduli as well as ultimate strains. For concrete it is obtained for unconfined and confined concrete without and with moderate and major seismic detailing [8]. The nonlinear Moment-Curvature (M-ϕ) relationships (Figure 3 and 4) based on earlier work at UAP [9] show results for sections with and without moderate and major seismic detailing. They indicate relatively weaker columns for 6-storied building (Figure 3) and beneficial effect of seismic detailing for columns (Figure 3, 4). However the strength or curvature ductility of beam section hardly improves due to seismic detailing (Figure 3).

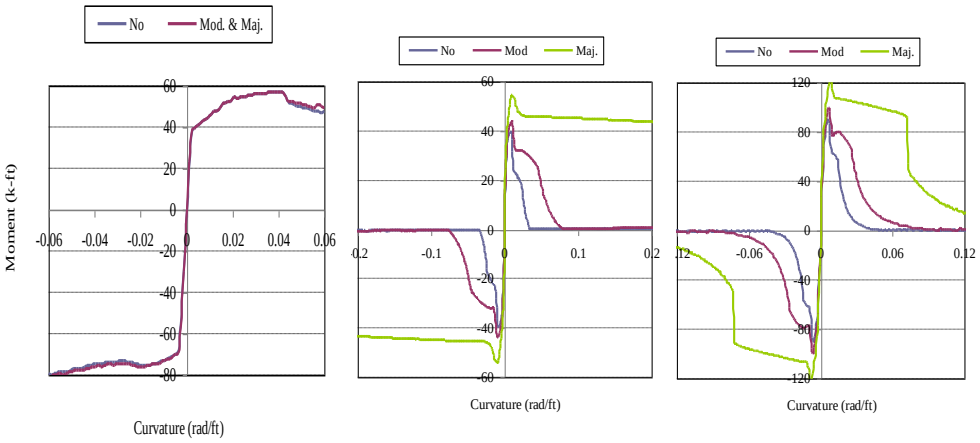

Figure 3: M-ϕ relationship for (a) Beam at support face, (b) 6-storied C_1, (c) 6-storied C_2

4.2 Relative Floor Deflections

The relative floor deflections (F0, F1, FTop indicate ground, 1st floor, top floor in Figures 5 and 6) demonstrate the significance of masonry infills by concentrating the structural stiffness and thereby inducing significant deflections in the softer stories. This is demonstrated more profoundly in results with 'Partial Infills' (Figure 6). Whereas 'No infill' option (Figure 5) may result in large permanent deformations particularly due to plastic hinges formed at weaker columns of 6-storied building, the 'Partial Infill' increases the relative deflections drastically.

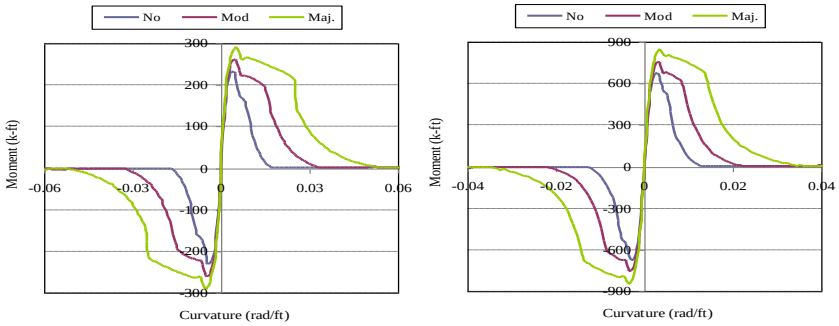

Figure 4: M-ϕ relationship for Column C_3 for (a) 6-storied, (b) 12-storied building

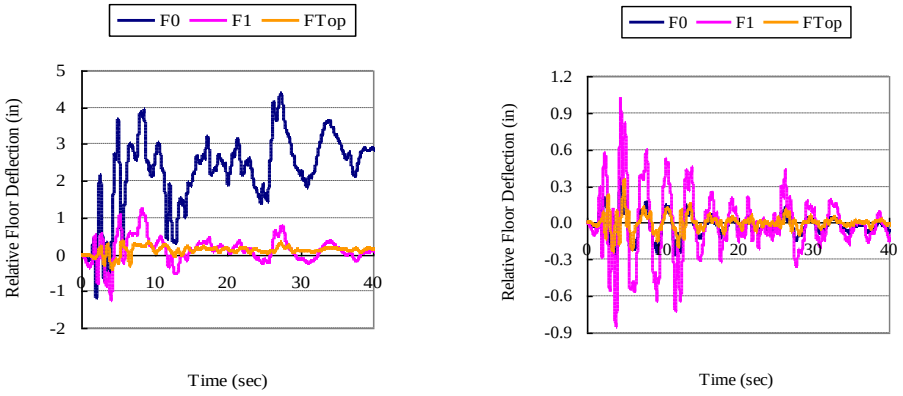

Figure 5: Relative floor deflections of (a) 6-storied, (b) 12-storied building (No Infill)

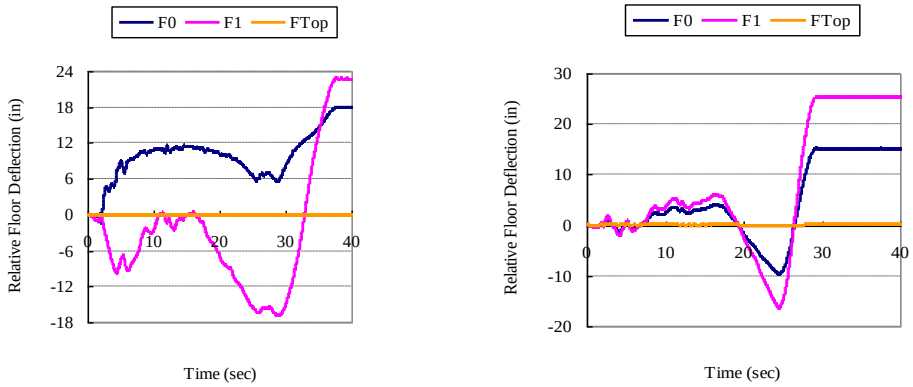

Figure 6: Relative floor deflections of (a) 6-storied, (b) 12-storied building (Partial Infill)

4.3 Member Curvatures

The curvatures induced in columns $C_3$and beams are shown in Figure7 for frames with partial infill. As with relative floor deflections, the curvatures also increase drastically for frames with partial infills. Although the beams are able to withstand these large curvatures (as shown by the beam M-ϕ graphs of Figure 4) and the relatively lightly loaded columns (of 6-storied building) may barely survive with major seismic detailing, the more heavily loaded columns (of 12-storied building) will not survive such curvature demands even with major seismic detailing, as shown by comparing Figures7(b) and 3(b).

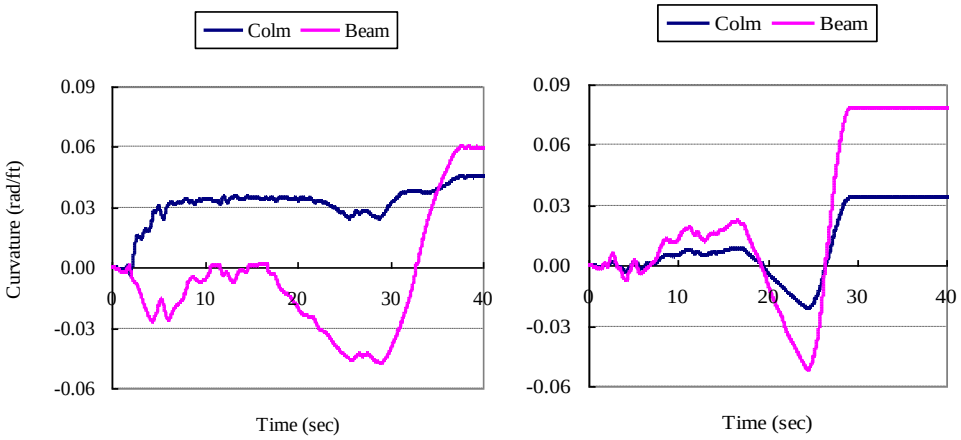

Figure 7: Curvature for 1st Floor $C_3$and Bam (a) 6-storied, (b) 12-storied (Partial Infill)

5 RESULTS FOR LABORATORY MODELS

Structural model used in the experimental works is a three-storied model structure [Figure 8(a)] in addition to the ground floor and is about 2 ft high. Each floor is composed of a 2′× 2′ timber plate (‘floor slabs’) and nine helical springs (‘columns’). The ground floor is supported on four rollers on the corner. Each floor weighs about 4 pounds with provisions for attaching extra weight. Ground motion is created by a 5 ft long plate marked by El Centro earthquake data reduced by a numerical value (3.68). Figure 8(b) shows considerable distress of soft storey ‘columns’ (reduced number of springs) during laboratory simulations. Figure 9(a) and 9(b) show a sample result demonstrating very good agreement between numerical and experimental results (peak displacements being 5.02″ numerical vs. 4.80″ experimental).

Influence of soft storey is apparent in results shown from the laboratory model. Figure 10(a) shows relative floor displacements of 1.76″ and 1.35″ in the 1st and 2nd storey of regular model (with extra weight on the top two floors). On the

other hand, Figure 10(b) shows a corresponding soft first storey results in maximum relative column deformations of 3.32″ and 1.51″, while Figure 10(c) shows these deformations to be 1.84″ and 2.59″for a soft second storey.

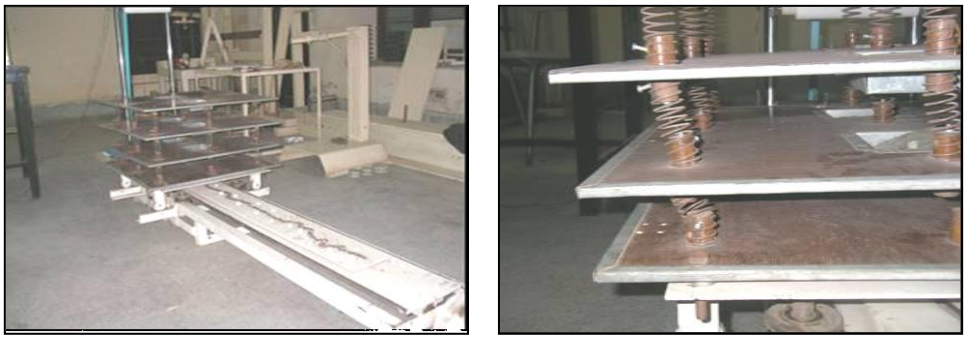

Figure 8: (a) Structural model with ground motion, (b) 'Column'distress at soft storey

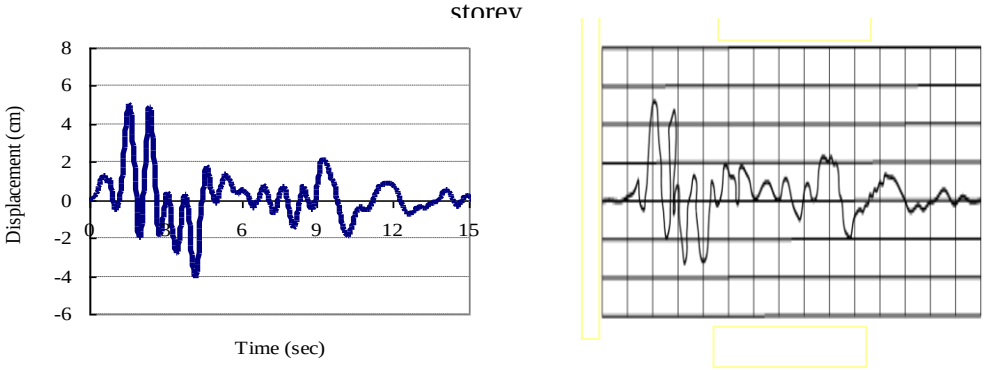

Figure9: 1st Floor Displacement (Soft Storey1) (a) Numerical, (b) Experimental

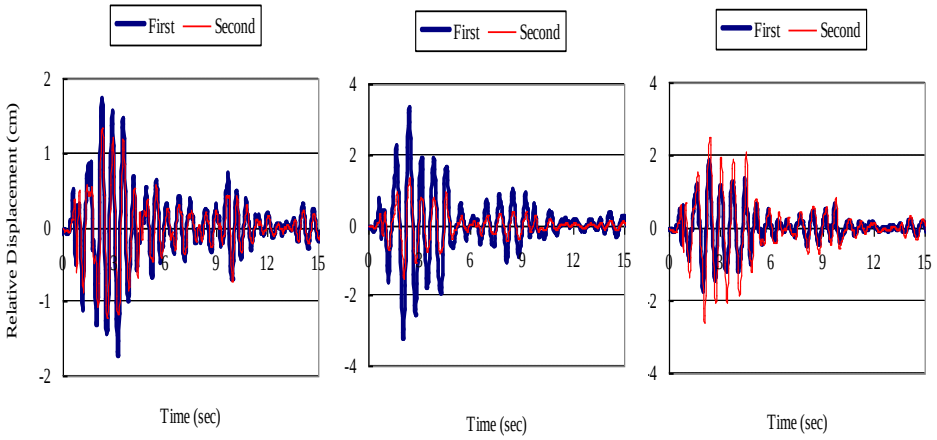

Figure10: Column Displacements (a) No Soft Storey (b) Soft Storey1, (c) Soft Storey2

6 CONCLUSIONS

Numerical results presented in this paper show that the structural behavior of RC frames changes drastically by the inclusion of infill walls (particularly when discontinued at ground floor level) in the dynamic analyses. Results also show potentially destructive effect of a major earthquake and permanent deformation of structures with soft stories, demonstrating that even if these structures do not collapse, they are unlikely to remain serviceable. In this work, relatively weaker columns of 6-storied building are rendered more vulnererable by soft stories, while collapse mechanism also transfersfrom beam to stronger columns of 12-storied buildings, whose smaller ductility would cause immediate collapse.

Experiemental results on a 3-storied model show very good agreement with numerical results and also demonstrate very large deformations and significant distress in soft-storied 'columns'.

REFERENCES

[1] S. Islam, 2006. Earthquake resistant design and retrofit of buildings: Lessons from the front lines. *1st Bangladesh Earthquake Symposium*, Dhaka, Bangladesh.

[2] A. E. Fiorato, M.A. Sozen, W.L. Gamble, 1970. An investigation of the interaction of reinforced concrete frames with masonry walls. *Civil Engg. Studies*, Str. Res. Series No. 370, Univ. of Illinois, Urbana, Illinois, USA.

[3] B.S. Smith, A. Coull, 1991. Infilled-Frame Structures. *Tall Building Structures Analysis and Design*, John Wiley & Sons Inc., pp. 168-174.

[4] M. Papia, 1998. Analysis of infilled frames using a coupled Finite Element and Boundary Element solution scheme. *International Journal of Numerical Methods in Engineering*,**26**, pp. 731-742.

[5] P.G. Asteris, 2003. Lateral stiffness of brick masonry infilled plane frames. *ASCE Journal of Structural Engineering*,**129**, pp. 1313-1323.

[6] A. Saneinejad, B. Hobbs, 1995. Inelasticdesign of infilled frames. *ASCE Journal of Structural Engineering*, **121**, pp. 634-643.

[7] A. Madan, A.M. Reinhorn, J.B. Mander, R.E, Valles, 1997. Modeling of masonry infill panels for structural analysis. *ASCE Journal of Structural Engineering*, **123**, pp. 1295-1302.

[8] C.C. Kent, R. Park, 1971. Flexural members with confined concrete. *ASCE Journal of Structural Engineering*, **97 (7)**, pp. 1969-1990.

[9] I. Anam, Z.N. Shoma, 2002. Nonlinear properties of Reinforced Concrete structures. *2nd Canadian Conference on Nonlinear Solid Mechanics*, Vancouver, Canada, **2**, pp. 657-666.

CICM 2015
First International Conference on
Advances in Civil Infrastructure and Construction Materials
MIST, Dhaka, Bangladesh, 14–15 December 2015

NUMERICAL STUDY ON DESIGN OF BLAST RESISTANT BUILDINGS

Iftekhar ANAM[1] **and Habiba Islam**[2]

[1] University of Asia Pacific, Dhaka, Bangladesh
Email: iftekhar@uap-bd.edu

[2]Chevron Bangladesh
Email: habiba.ph@gmail.com

Abstract. *The main objective of the present work is to explore the effect of blast loads on the dynamic response of RC structures. Simple RC building models of three different heights (6-, 12- and 24-storied) are analyzed as 'equivalent' SDOF systems and their 'Ductility Demands' from blast loads of various weights and stand-off distances are compared with 'Ductility Ratios' derived numerically from column moment-curvature curves.*

The study shows the drastic change in blast pressure with stand-off distance and equivalent weight of the explosive. Material stress-strain properties also change significantly with strain rate. Nonlinear dynamic response to blast loads and the 'Ductility Demand' are found to vary most significantly with resistance ratio. Seismic detailing provisions are found to increase the ductility of RC sections at slow strain rates, but their effect on 'high strength' materials at large strain rates are insignificant.

For charge weights of 100, 1000, 10000 kg, almost all the structures are found to 'fail' for stand-off distances of 3m or less, while they 'survive' most other conditions (all weights and stand-off distances 10 and 30m).

Keywords: Blast load, Nonlinear Dynamics, Charge weight, Stand-off, Ductility ratio.

1 INTRODUCTION

The abrupt and violent release of energy in blast may result in dynamic loads that are much greater than the typical design loads of most structures and can cause catastrophic damage to life and property. Efforts have been made during the past fifty years to develop methods of structural analysis and design to resist blast loads.

The problem has been relatively rare and some relevant publications are considered classified secrets therefore also not readily available. As a result, in a developing country like Bangladesh with much more common and pressing engineering challenges, the wealth of knowledge and available literature on this topic is rather thin. However, with the rise of extremist views and efforts within the region and increasing access to explosive materials, engineers should realize the impact that even one single blast may have on a nation's history and its citizens' lifestyle. The significance of this research can be justified in this context.

2 NATURE OF BLAST LOADING

2.1 Blast Pressure and Stand-off Distance:

Blast loading is a function of distance of the structure from the explosion and the charge weight. Charge Weight or weapon size (W) is expressed in weight or mass of TNT; the equivalent W of any other explosive material is based on experimentally determined factors or the ratio of its heat of detonation to that of TNT. Stand-off distance refers to the direct, unobstructed distance between a weapon and its target. It is the key parameter that determines blast pressure, so for protecting a structure is to keep the bomb as far away as possible by maximizing stand-off distance.

Blast wave parameters for conventional high explosive materials have been the focus of a number of studies during the 1950's and 1960's. The factor $Z = R/W^{1/3}$ was used by Brode [1] to estimate the peak overpressure due to blast, as

$$p_{s0} = 0.975/Z + 1.455/Z^2 + 5.85/Z^3 - 0.019 \quad (0.1 < p_{s0} < 10 \text{ bar}) \tag{1a}$$

$$p_{s0} = 6.7/Z^3 + 1 \quad (p_{s0} > 10 \text{ bar}) \tag{1b}$$

Other equations on blast pressure include [2], [3]. Comprehensive discussion for predicting blast pressures and blast durations are given by [4], [5].

As blast wave propagates through the atmosphere, the velocity of air particles, and hence the wind pressure, depends on the peak overpressure of the blast wave. This later velocity of the air is associated with the dynamic pressure, $q(t)$, whose maximum value, q_s, is given by

$$q_s = 2.5\, p_{s0}^2/(p_{s0} + 7\, p_0) \tag{2}$$

where p_0 is the atmospheric pressure.

Figure 1 shows the variation of peak dynamic blast pressure with the stand-off distance (R) and weight (W) of blast load of various explosives. The drastic change of blast dynamic pressure with the standoff distance (i.e. from 10^7 to 10^{-6} psi within 5 meters) as well as the explosive weights is to be noted.

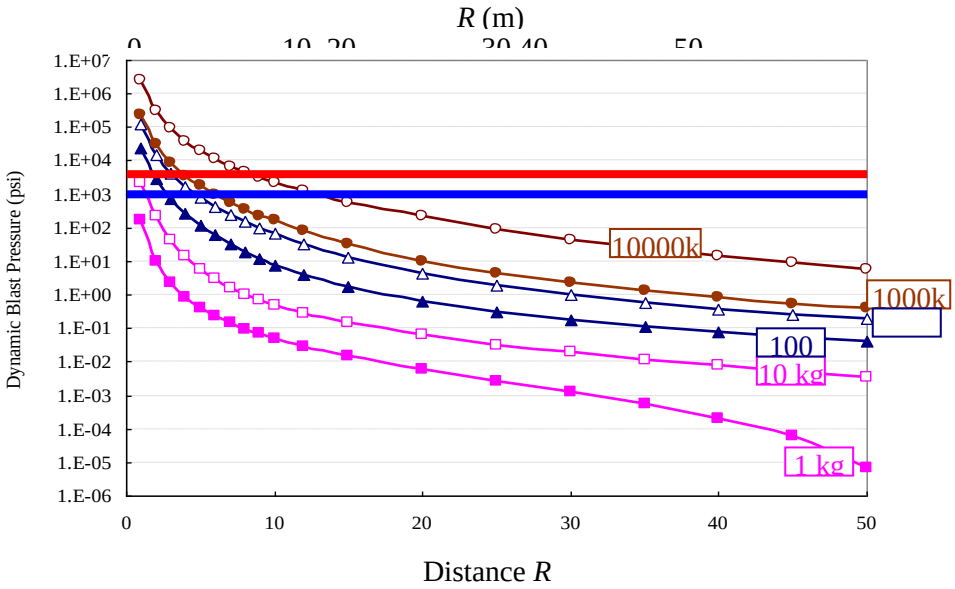

Figure 1: Peak Dynamic Blast Pressure vs. Stand-off Distance

The range of pressures between 1~10 psi is noted in Figure 1, which also relates to corresponding stand-off distances for various weights of explosives. Table 1 shows the stand-off values obtained therefrom. These pressures are chosen for their significance in causing damage and fatalities to human beings. As shown in Table 1, smaller loads (e.g. W = 1 kg hand-grenade) may cause fatalities at very close ranges (R < 2m) only, while larger loads (e.g. W = 10,000 kg truck-bomb) may cause significant fatalities up to about 50m from the source.

Table 1: Stand-off R (m) for Dynamic Pressures and TNT Equivalents

W (kg)	q_s = 1 psi	q_s = 100psi
1	3.8	1.1
100	17.4	5.3
10,000	81.0	24.4

Figure 2(a) shows the typical variation of blast pressure with time, which is represented in building codes (also in BNBC) in Figure 2(b) and more simplified in Figure 2(c), also used in this work.

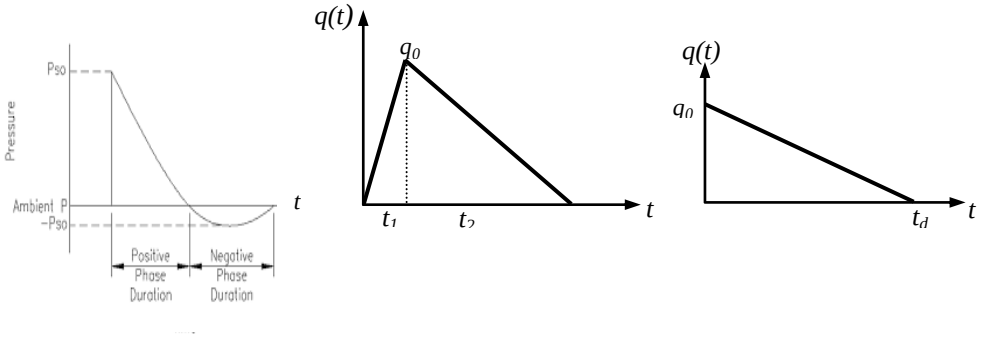

Figure 2: Dynamic Blast Loading (a) Typical, (b) Code specified, (c) Simplified

3 STRUCTURAL MODEL AND MATERIAL PROPERTIES

Structural analysis in this work uses the single-degree-of freedom (SDOF) model, since its objective is to provide an approximate first estimate of the implications of blast-loading on various structures. The SDOF model approach, commonly used to analyze individual components, is likely to produce overly conservative designs, while an accurate representation of the structural system truly requires a complex multi-degree-of-freedom (MDOF) model.

The model 6-, 12- and 24-storied buildings considered for structural analysis have the same (30′× 30′) plan and supported by RC columns at four corners. Figure 3shows the column cross-sections as well as steel reinforcements.

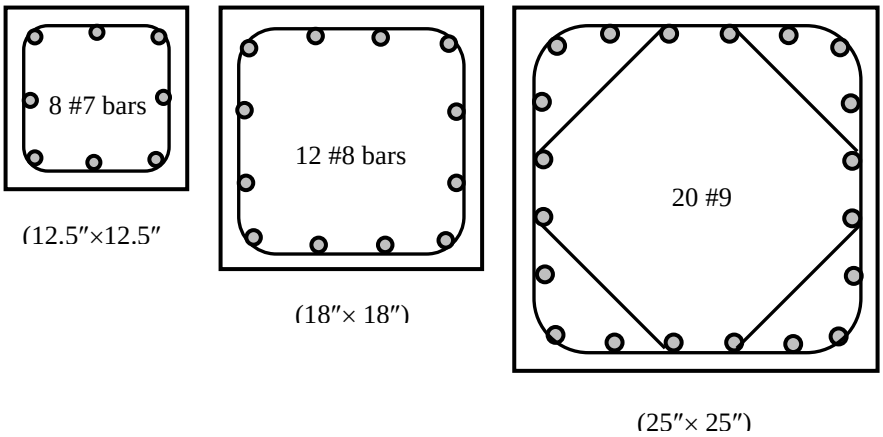

Figure 3: Column Sections of 6-, 12- and 24-storied buildings

Mechanical properties of concrete (at low strain rate) used in this work are the compressive strength f_c' = 3 ksi, modulus of elasticity $E_c = 3.15 \times 10^3$ ksi, strain at peak stress $\varepsilon_\chi = 1.80 \times 10^{-3}$, maximum strain (at failure) $\varepsilon_{max} = 3.35 \times 10^{-3}$and tensile strength f_t= 0.30 ksi. Moreover, steel of yield strength f_y = 60 ksi and maximum strain = 0.20 is also used.

However, these properties change significantly at high strain rates; i.e. the ultimate strength of concrete increases to 5.34 and 12.23 ksi at strain rates of 100/sec and 1000/sec respectively. The corresponding yield strengths of steel are 97.5 and 106.1 ksi respectively. Figure 4 shows the Dynamic Increase Factor (DIF) of the strengths of concrete and steel. Such increases are quite common in literature. In fact strength magnification factors as high as 4 in compression for strain rates in the range 100~1000/sec have been reported [6].

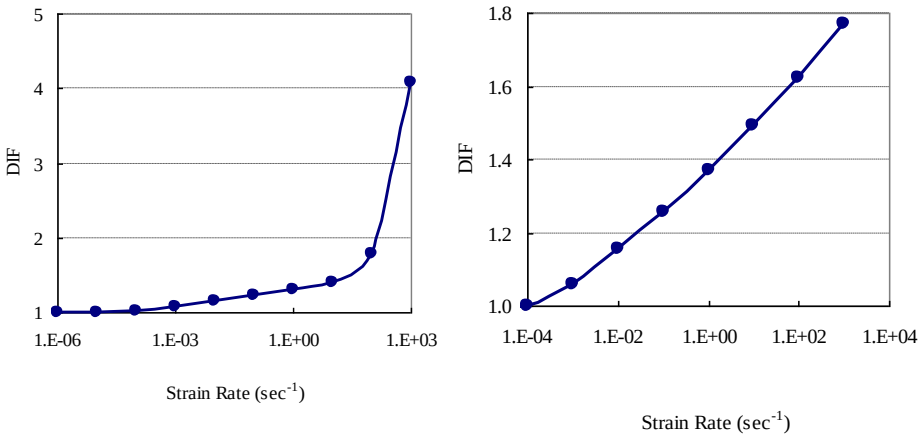

Figure 4: Dynamic Increase Factor (DIF) vs. Strain Rate (sec^{-1}) for (a) Concrete in compression, (b) Steel in Tension

4 RESULTS FROM NUMERICAL ANALYSIS

4.1 Effect of Design Parameters

Figure 5(a), (b) and (c) show the significance of the parameters (i.e., Damping Ratio DR, Resistance Ratio RR and Time Ratio TR). The 'reference' model is considered to have a DR of 0.05 (= 5%), and both the RR (i.e., ratio of the maximum internal 'spring' force within the structure to the maximum blast force) and TR (duration t_d of blast force to time period of structure) equal to 1.0.

Figure 5(a) shows the effect of structural DR, as it varies between 0, 0.05 and 0.10. Of course the structural displacement decreases with increased damping ratio, but damping also slows down the structural vibration, as shown by the longer time periods for DR of 0.05 compared to 0, and 0.10 compared to 0.05.

The effect of RR [Figure 5(b)] shows the very large increase (about 4 times) in structural displacement (as well as slowing down of vibration, as the structure shifts to a more flexible nonlinear range) for RR of 0.5 and a large decrease (about half) for RR of 2.0. Figure 5(c) shows the increase in peak displacement for larger TR (= 2.0, compared to 1.0) and decrease for TR of 0.50. However, this change is less than the value of TR, and the structure retains its original period of vibration.

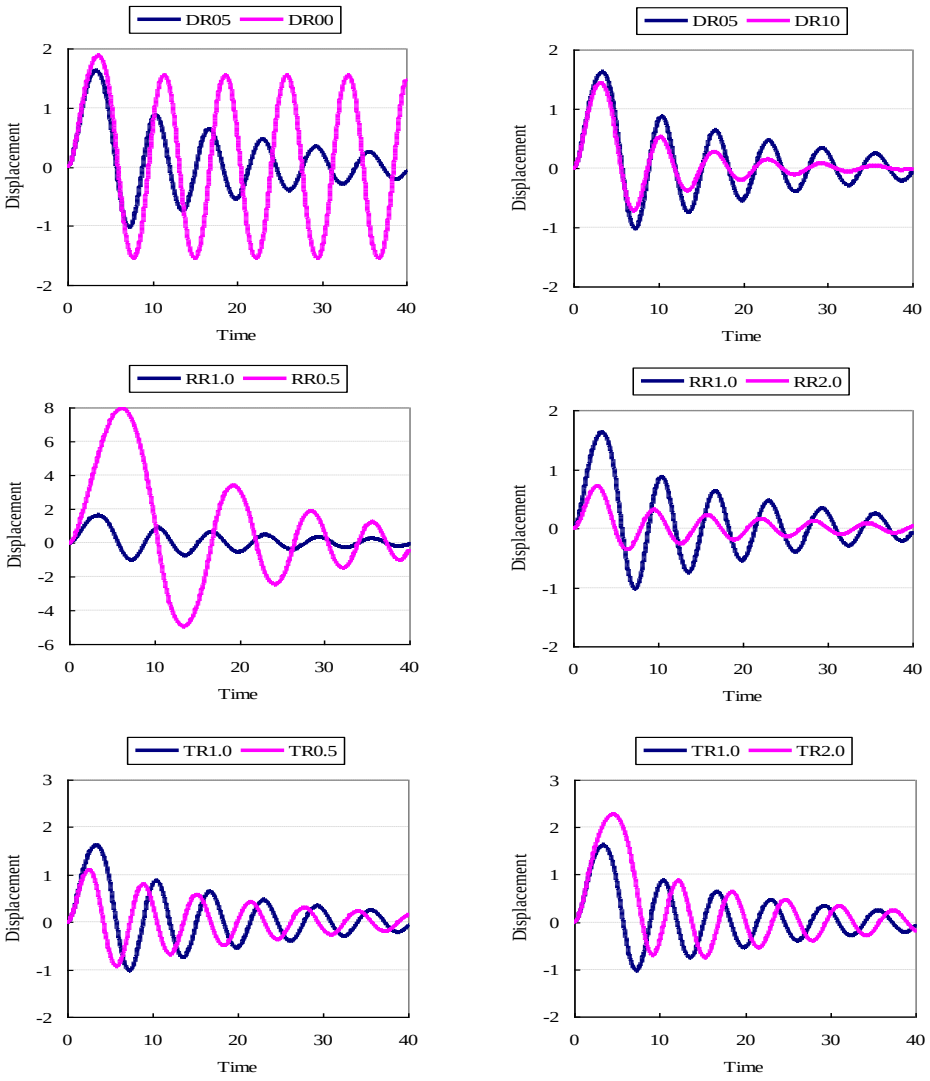

Figure 5: Effects of (a) Damping Ratio (0~10%), (b) Resistance Ratio (0.5~2.0), (c) Time Ratio (0.5~2.0) on the Blast Response of Nonlinear SDOF System

4.2 Nonlinear Moment (M) vs. Curvature (ϕ) Relationship

The nonlinear moment-curvature relationship of only the 12-storied column sections are shown in Figure 6. The strain rates are shown with the number of stories (e.g., 12-1000 indicates strain rate of 1000/sec for 12-storied buildings) and detailing provisions (N for 'No' detailing and M for 'Major' seismic detailing).

Results show that seismic detailing (often assumed to be effective in blast resistant design) is very effective particularly increasing the section's ductility at

slow strain rates [i.e. 'zero' in Figure 6(a)], but is much less effective on materials at large strain rates [i.e. 1000 sec^{-1} in Figure 6(b)].

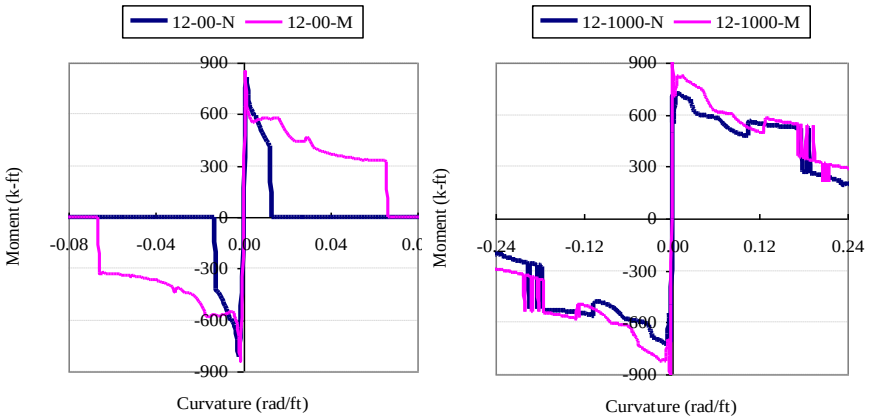

Figure 6: M-ϕ of 12-storied Building Columns for Strain Rate (a) zero, (b) 1000 sec^{-1}

Dynamic response properties of the SDOF multi-storied structures are shown in Table 2 and 3. Table 2 shows the column 'Ductility Ratios' (i.e., ratio of ultimate deformation y_u to elastic deformation y_e), while Table 3 summarizes the 'Ductility Demands' on the structures (i.e., ratio of maximum deformation y_m to the elastic deformation y_e) for different 'time ratios TR' (blast duration t_d compared to the structure's natural period of vibration T_n). Therefore, comparison between the (y_u/y_e) of Table 2 and the (y_m/y_e) of Table 3 forms the core of design conclusions.

Table 2: 'Ductility Ratios' (y_u/y_e) of Different Columns

Column	y_e(ft)	y_u (ft)	R_u (k)	y_u/y_e
6-00N	1.06E-02	0.43	15.2	40.3
6-00M	9.45E-03	3.83	12.0	406
6-1000	1.69E-02	6.14	18.7	364
12-00N	1.28E-02	0.21	28.0	16.6
12-00M	4.89E-03	1.10	21.7	225
12-1000	1.47E-02	3.24	35.7	221
24-00N	1.44E-02	0.15	43.3	10.4
24-00M	5.83E-03	0.73	35.0	124
24-1000	1.87E-02	2.10	59.0	112

Such comparison indicates that all 6-storied columns 'fail' for stand-off distances of 3m (except 100 kg with TR = 0.0125), while they survive most other

conditions. Columns of 12- and 24-storied structures can withstand larger forces (with larger RR), but they are less ductile which offsets the advantage.

Table 3: Ductility Demand (y_m/y_e) for Different Loading Conditions

W (kg)	t_d/T_n	6-Storied		12-Storied		24-Storied	
		R = 3m	R=30m	R = 3m	R=30m	R= 3m	R=30m
100	0.0125	356	0.016	153	0.008	90	0.005
	0.0500	1859	0.069	879	0.035	560	0.023
10000	0.0125	55190	6.91	27480	2.32	18266	1.34
	0.0500	245327	65.90	122519	24.08	81661	12.85

5 CONCLUSIONS

Nonlinear structural dynamic response to blast loads and the 'Ductility Demand' vary significantly with damping ratio (decreasing with higher damping), time ratio (increasing at larger time ratios), and resistance ratio. Seismic detailing provisions are found to increase the ductility of RC sections at slow strain rates, but their effect on at large strain rates are insignificant.

Stand-off and charge weights are two key factors of blast pressure. It is usually economically efficient to increase the standoff distance and keep the threat away from a facility in the first place. The columns (of model SDOF structures) studied here 'fail' in most cases at stand-off distances of 3m, while they survive all other conditions of TNT weights and stand-off distances.

REFERENCES

[1] H.L. Brode, 1955. Numerical solution of spherical blast waves.*Journal of Applied Physics*, American Institute of Physics, **26 (6)**, pp. 766-776.

[2] N.M. Newmark, R.J. Hansen, 1961. Design of blast resistant structures, *Shock and Vibration Handbook*, **3**, McGraw-Hill, New York, USA.

[3] C.A.Mills, 1987.The design of concrete structure to resist explosions and weapon effects.*1st Int. Conference on concrete for hazard protections*, Edinburgh, UK, pp. 61-73.

[4] G.C.Mays, P.D. Smith, 1995. *Blast Effects on Buildings*, Thomas Telford Publications, Heron Quay, London, UK.

[5] TM 5-1300, 1990. The Design of Structures to Resist the Effects of Accidental Explosions, *Technical Manual, US Department of the Army, Navy, and Air Force*, Washington, USA.

[6] D. Grote, S. Park, M. Zhou, 2001. Dynamic behavior of concrete at high strain rates and pressures,*Journal of Impact Engineering*, **25**, pp. 869-886.

CICM 2015
First International Conference on
Advances in Civil Infrastructure and Construction Materials
MIST, Dhaka, Bangladesh, 14–15 December 2015

FRACTURE TOUGHNESS OF PLAIN CONCRETE SPECIMENS MADE WITH INDUSTRY-BURNT BRICK AGGREGATES IN MARINE ENVIRONMENT

TAFSIROJJAMAN[1], **M. Shaheduzzaman**[2], **M. F. Rahman**[3] **and M. R. Alam**[4]

[1] Department of Civil Engineering, Sonargoan University, Dhaka, Bangladesh.
Email: tafsirojjaman@gmail.com

[2, 3, 4] Department of Civil Engineering, Chittagong University of Engineering and Technology, Chittagong, Bangladesh.
Email: [2]shaheduzzaman08@gmail.com, [3]faizur24rahman@gmail.com

Abstract. *Fracture toughness of plain concrete specimens made with industry-burnt brick aggregates cured in marine environment was determined in this study. To determine the fracture toughness value for different depth of beam having initial crack, at the mid span of beams, thirty beams made of brick chips were tested according to ASTM specifications. Range of initial crack depths were taken varied between 0.30 to 0.45 times the beam depths. The experimental failure load for each beam with crack was determined. Fracture toughness was determined from the established formula of ASTM specifications, for 4-point loading. It was observed that the fracture toughness values obtained from the experimental study in marine environment was varying between 0.445 and 0.790.The experimental investigations referred that the fracture toughness values increase with the decrease of beam widths.*

Keywords: Fracture toughness, Industry-burnt brick aggregate, Plain concrete, Initial crack, Marine environment, Four-point loading.

1 INTRODUCTION

Concrete is one of the most commonly used building materials in the world. It is utilized in different forms such as, Normal Strength Concrete (NSC), High Strength Concrete (HSC) and Ultra High Strength Concrete (UHSC), depending on the requisite design strength and the importance of the structure. However, in some countries of South East Asia, viz., Bangladesh, Myanmar, India, and others, for NSC production where stone aggregates are not easily available, industry-burnt brick aggregates are also used as an alternative to stone aggregates.

When a fracture in the form of crack develops in the structure, its load bearing capacity reduces significantly. If it develops in the major structural components such as beams/girders, columns/piers, shear wall, retaining walls, dams, etc., to a significant amount, the entire structure could be collapsed. It is also important to study the behavior of concrete with inherent flaws under static or dynamic loading. For this reason fracture toughness test of concrete is important. Fracture toughness is the resistance of a material to failure from a fracture, starting from a preexisting crack [1]. The durability of structural components also depends on their sub-critical crack growth. Recent publications have shown that fracture mechanics has now been established as a fundamental approach that can explain certain nonlinear aspects of concrete behavior, help to prevent brittle failures of the structure and be an important aid in materials engineering [2, 3]. From the discussion of applications of fracture mechanics to failure of concrete structures, it was demonstrated that experimental phenomena associated with the failure of concrete such as size effect on tensile strength and brittleness of concrete can be interpreted properly through fracture mechanics [4]. For large concrete specimens, fracture toughness increases initially as crack propagates but that a length-independent value is reached asymptotically. In addition, the failure of large size concrete elements can be predicted realistically using linear elastic fracture mechanics [5]. The naturally cracked beams (pre-cracked) yield higher failure loads and stress-intensity values than notched beams with the same crack length and the average stress intensity factors to be higher by 38%, 77% and 96% for pre-cracked beams than for notched beams, for the crack-depth ratios of 0.3, 0.5 and 0.7, respectively, where crack-depth ratios means that the ratio between initial crack depth and depth of the beam [6].

The primary chemical constituents of seawater are the ions of chloride, sodium, magnesium, calcium and potassium [7]. The concentration of major salt constituent of seawater is given in percentage such as 78% NaCl, 10.5% $MgCl_2$, 5% $MgSO_4$, 3.9% SO_4, 2.3% K_2SO_4 and 0.3% KBr [9]. It is evident from above that sodium chloride is by far the predominant salt component of seawater. NaCl and $MgCl_2$are a total 88.5% of the entire salt content [10].Alkali – aggregate reaction is a chemical reaction between certain types of aggregates and hydroxyl ions (OH^-) associated with Alkalis in the cement or concrete [7, 8]. The chemical action of seawater on concrete is mainly due to attack by magnesium sulphate

($MgSO_4$) [11]. It is equally claimed that potassium and magnesium sulphate (KS, MgS) present in salt water can cause sulphate attack in concrete since they readily react with calcium hydroxide ($Ca(OH)_2$) present in the set cement through the hydration. The effect of ocean salts on flexural strength of concrete cast and cured with salt water was observed among other things that there were varying percentage increment in strength gained after 28 days depending on the cement brand and possible sea salt (NaCl, $MgCl_2$, Na_2SO_4, or $CaCl_2$) and some chemical processes or reaction must have taken place [12]. Tensile strength properties, such as modulus of rupture and fracture toughness in marine environment, were independent of fly ash replacement, but increased with the period of accelerated testing [13].

Most of the earlier studies on fracture toughness of plain concrete specimens have used stone and brick aggregates with other ingredients (cement, sand and water) to prepare the plain concrete specimens. However, none of the earlier studies have reported on the fracture toughness of plain concrete specimens made with industry-burnt brick aggregates in marine environment. The study reported in this paper has considered the fracture toughness of normal plain concrete specimens made of brick aggregates, sand, cement and water in marine environment.

2 EXPERIMENTAL PROCEDURE

2.1 Preparation Of Test Specimens

In the preparation of concrete mix for test specimens, cement, sand and brick aggregate were mixed in a ratio of 1: 1.5: 3 (by weight). Brick aggregates used in this study were 19 mm down and 13 mm up grades. ACV (Aggregate Crushing Value) test of aggregates was carried out to check the quality of brick aggregates. Water cement ratio was taken as approximately 0.36 by weight to maintain a slump of 63.5 mm (in a slump cone test) for better workability. Aggregate was washed with water and surface dried before mixing it with sand and cement. The initial and final setting times of cement were determined before using it with other ingredients. Sieve analysis of fine aggregates was also carried out before adding it into the mixture. In order to determine the strength of mortar, compressive strength tests of cube specimens and tensile strength tests of briquette specimens were carried out in the laboratory by mixing cement and sand in the ratio of 1:1.5. Crushing strength of concrete mix used in preparing test specimen was determined by carrying out compression test of standard concrete cylinders (dia. = 15 cm and height = 30.48 cm). These cylinders were cast from the same concrete mix that was used for preparing specimens of fracture toughness test. The compression tests of concrete cylinders were carried out after 28 days of curing in water. Before carrying out the tests, each specimen was kept in a dry place for 24 hrs. The test was performed using a calibrated 100 ton hydraulic machine under displacement control condition.

Geometry of test specimen for fracture toughness test was fixed as length (L) of 0.8128 m (32 inch), width (B) of 0.152 m (6 inch) and depth (W) of 0.2032 m (8 inch) according to ASTM C 1421 – 99 standard dimensions (L = 4W, B = 0.75W)[14]. Effect of specimen widths on the fracture toughness of plain concrete was also examined in this study. For this, only the width of the beam was changed and all the other dimensions such as length and depth of the beam and crack length were kept constant. Wooden moulds were made according to the specimen dimensions. Crack was introduced during the casting of specimens, by inserting a greased 1 mm thick steel plate of width equal to the specimen width, and up to the required depth of crack in the beam. The steel plate was greased first and then fixed with wooden shutters before placing concrete. Wooden mould (shutter) was also greased properly before placing the concrete mix. The concrete was prepared in a revolving drum mixer. This concrete mix was then poured into the specimen moulds carefully and tamped properly, in three layers, for each specimen. Mixing proportion of cement, sand, coarse aggregates (brick aggregates) and water was maintained the same for all specimens. Only the crack depth was changed by placing the greased steel plate, at the required depths in the specimen. Six or four test specimens were cast at a time. After keeping specimens in the room temperature for 24 hours, the wooden shutter and the steel plate were removed from the specimens and they were placed inside a water tank, which containing sea water for 28 days. Sea water was collected from directly Potenga sea beach of Chittagong. All beam specimens were tested by following ASTM C 1421 – 99 specifications. Four -point bending load was applied up to failure during test of the specimens.

Table 1: Specimen geometry and crack depth of laboratory fracture toughness test

Batch No.	Specimens No.	Crack Depth	Other dimensions of the specimens
01	06	30% of beam depth	L = 0.8064 m, B = 0.152 m, W = 0.2032 m
02	06	35% of beam depth	L = 0.8064 m, B = 0.152 m, W = 0.2032 m
Plain concrete specimens with variable widths			
01	04	45% of beam depth	L = 0.8064 m, B = 0.076 m, W = 0.2032 m
02	04	45% of beam depth	L = 0.8064 m, B = 0.101 m, W = 0.2032 m
03	04	45% of beam depth	L = 0.8064 m, B = 0.127 m, W = 0.2032 m
Uncrack Plain concrete specimens made with Brick aggregates			
01	06	Uncrack	L = 0.8064 m, B = 0.152 m, W = 0.2032 m

2.2 Testing Procedure

After curing the test specimens for 28 days in sea water, they were removed from the water tank and kept in a dry place for 24 hours to evaporate the moisture from their external surfaces. Loading positions and supporting positions of the speci-

men were clearly marked and were made smooth and even, using a metal hand grinder and sand paper. Swiveling supports (in one vertical plane, perpendicular to the length) were provided at a distance 12.5 mm (0.5 inch) from both ends of the beam. Four-point loading positions were fixed at one-fourth of span length from both supports. This loading was chosen for obtaining pure bending at the middle-half portion of the beam where crack was present. Load was applied on the beam monotonically without any jerk and it was increased continuously at a rate of 10kN/min until the test specimen failed. Failure load was recorded from a digital load meter. A dial gauge with a sensitivity of 0.01 mm was used for measuring the load point deflection. Displacement controlled load was applied on the specimen. Load was recorded at each 5 division increments of the dial gauge up to failure load. All specimens were tested under simply supported conditions. The complete setup of test specimen for fracture toughness test is shown in Figure 1.

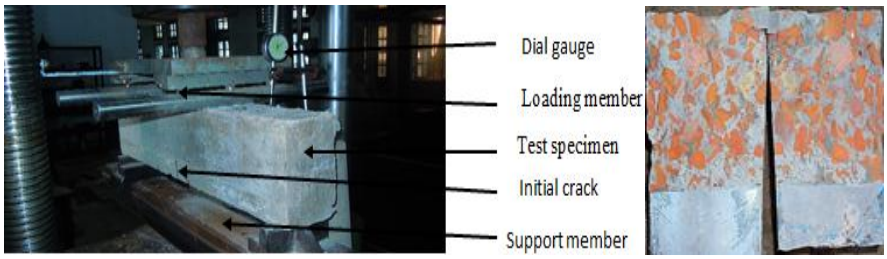

Figure 1: Experimental setup and tested specimen of beam

3 RESULTS AND DISCUSSIONS

The results obtained from different tests are given in Tables 2 and 3. Table 2 shows the values of different properties of materials used in this study. Table 3 shows the crack depth and peak load for each test beam and the corresponding computed fracture toughness. From this table it is seen that the magnitude of the maximum load varies with the depth of crack. Figure 2 illustrated typical load-deflection plots up to peak load for specimens made with brick aggregates with various a/W ratios, where a/W is the ratio between depth of crack and height of beam. Figure 2 also shows the load-deflection plot for uncrack beam made with brick aggregates. The load-deflection plot for beam made with brick aggregates of various width but same a/W=0.45 are shown in Figure 3.From all the load-deflection curves it is seen that material behaves almost linearly at the beginning of the applied load and becomes nonlinear near the peak load. A part of this non-linearity could be attributed to the coalescence of tensile micro-cracks (development of fracture process zone) before the subsequent crack extension. The remaining part is due to the nonlinear compression behavior near maximum loads. It was found that when the load reached its maximum value, the test specimen

began to lose its resistance very fast, which could not be plotted properly. For this reason, only the load deflection plots up to peak load have been showed in this study. The peak load was then used to determine the fracture toughness. The peak load was then used to determine the fracture toughness. The ASTM E1290-08 Standard suggests the formula for fracture toughness is given below [15]:

$$K_{IC}=\frac{P(l_1-l_2)\sqrt{a}}{BW^2}x\frac{3}{2(1-a/w)^{\frac{3}{2}}}x\ [1.989-1.33\frac{a}{w}-\frac{\left\{3.49-0.68\frac{a}{w}+1.35\left(\frac{a}{w}\right)^2\right\}\frac{a}{w}\left(1-\frac{a}{w}\right)}{(1+a/w)^2}]$$

For $0\leq\frac{a}{w}\leq 0.6$, $\frac{l}{w}=4$

where, P = Load, l_1 = The center to center support length, l_2 = Loading span, B = Width of the beam, W = Depth of the beam, a = Crack depth.

Table 2: Different test results of cement, sand, aggregate and plain concrete

Name of test	Test results
F.M. (Fineness Modulus) of sand	2.48
Initial and final setting time of Portland cement	1 hr. 5min. and 1 hr 55 min.
Slump value	68 mm
7 days compressive strength of cement mortar	25.5 MPa (3700 psi)
28 days compressive strength of cement mortar	33.8MPa (4900psi)
7 days tensile strength of cement mortar	2.15 MPa (310 psi)
28 days tensile strength of cement mortar	3.30 MPa (480 psi)
28 days cylinder compressive strength of cement concrete with brick aggregates	19.0 MPa (2750 psi)
Aggregate crushing value of brick aggregate	38.33%

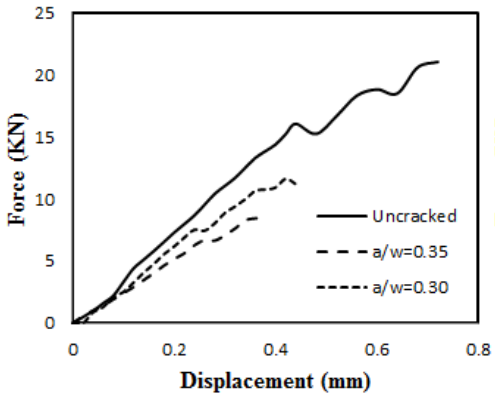

Figure 2: load-deflection plots of beam beam32x6x8 for various a/W ratios

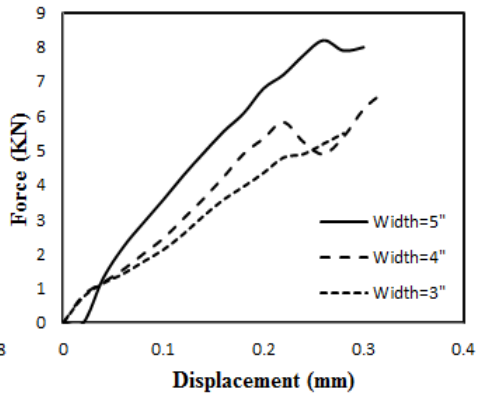

Figure 3: load-deflection plots for 32x8 but various width (a/W=.45)

Table 3: Fracture toughness of plain concrete specimens made with industry-burnt brick aggregates in marine environment.

Specimen no.	Beam dimension(inch)	Crack depth	Load (KN)	Fracture toughness K_{IC}(MPa√(m))
Fracture toughness for various a/W ratios				
1	32x6x8	35%	8.80	0.483
2			8.70	0.478
3			9.50	0.522
4			9.60	0.527
5			9.10	0.500
6			8.10	0.445
7	32x6x8	30%	13.5	0.654
8			11.2	0.543
9			11.9	0.576
10			10.9	0.528
11			12.5	0.606
12			12.1	0.586
Fracture toughness for various width of beam with same a/W ratio				
13	32x5x8	45%	8.00	0.687
14			7.80	0.670
15			7.70	0.662
16			7.80	0.670
17	32x4x8	45%	6.70	0.724
18			7.10	0.767
19			6.50	0.702
20			6.80	0.735
21	32x3x8	45%	5.50	0.790
22			5.40	0.775
23			5.30	0.761
24			5.50	0.790

4 CONCLUSIONS

The fracture toughness values in marine environment obtained from the experimental study were lies between 0.445 and 0.790.The value of Fracture toughness in marine environment was depending on the crack depth and the beam width. It was found that the values of failure load and fracture toughness were decreased with the increase of crack depth. On the other hand, when specimen width (having constant crack depth) reduced from the standard ASTM width, fracture toughness increased gradually but the failure loads were in decreasing order. It was seen that, some beams were failed with aggregate failure, some beams were failed with bond failure and also some beams were failed with both aggregate and bond failure.

REFERENCES

[1] D. Broek1989. The practical use of fracture mechanics, Kluwer Academic Publishers, Dordrecht and Boston.

[2] H. K. Hilsdorfand and W. Brameshuber, 1991. Code-type formulation of fracture mechanics concepts for concrete, International Journal of Fracture; 51, 61-72.

[3] J. M. C. Kishen, 2005. Recent developments in safety assessment of concrete gravity dams, Current Science; 89(4), 650-656.

[4] S. P. Shah and C. Ouyang, 1992. Measurement and modeling of fracture processes in concrete in Materials Science of Concrete, Vol.III, edited by J. Scalny, American Ceramic Society, Westerville, OH, 243-270.

[5] F. H. Wittmann and I. M. Gheorghita, 1985. Fracture toughness of concrete determined on large specimens, Materials and Structures; 18, 93-95.

[6] S. E. Swartz, K. K.Hu and C. M. J. Huang, 1982. Stress intensity factor for plain concrete in bending-prenotched versus precracked beams, Experimental Mechanics, 412-417.

[7] A. M. Neville, 1975. Properties of Concrete', Pitman Publishing Limited, London, pp. 167 – 178.

[8] A. M. Neville and J. J. Brooks, 1993. Concrete Technology', Longman Group UK Limited, pp. 147 – 175.

[9] R. N. Swamy, 1991. The Alkali – Silica Reaction in the Concrete, 1st edition, CRC Press, pp. 2 – 47.

[10] M. F. Bela, 1989. Properties of Seawater, U.S. Dept. of the Interior, Office of Saline Water, pp. 766 – 771.

[11] J. Prascal, D. K. Jain &A. K. Ahuja, 2006. Factors Influencing the Sulphate Resistance of Cement, Concrete and Mortar. Asian Journal of Civil Engineering (Building and Housing), 7(3), 259-268.

[12] M. Bryant, 1964. Effects of Seawater on Concrete. Miscellaneous paper no 6-690, U.S. Army Engineers, Corps of Engineers, Vicks berg, Mississippi.

[13] S. k. Lee, D. V. Reddy, W. H. Hartt and M. Arockiasamy, ASCE Library.

[14] I. Bar-on, G.D. Quinn, J. Salem and M.J. Jenkins, 2001. Development of ASTM C 1421-99 Stand. Test Methods of Determination of Fracture Toughness, Fatigue and Fracture Mechanics, 32nd volume, pp. 315-335.

[15] ASTM E1290: Standard Test Method for Crack-Tip Opening Displacement (CTOD) Fracture Toughness Measurement.

CICM 2015
First International Conference on
Advances in Civil Infrastructure and Construction Materials
MIST, Dhaka, Bangladesh, 14–15 December 2015

FINITE ELEMENT SIMULATION OF ULTIMATE AXIAL CAPACITY OF ECCENTRICALLY LOADED STEEL ANGLES

Iftesham BASHAR[1] and Khan M. Amanat[2]

[1, 2] Department of Civil Engineering, University of Information Technology and Sciences, Dhaka, Bangladesh
Email: [1]snow_himi@yahoo.com, [2]amanat@ce.buet.ac.bd

Abstract. *Generally, lattice towers are analyzed and designed assuming that each member is a two-force member. But, in practical cases, the behavior of angles used in these structures are different to some extent from that of other commonly used steel shapes in that these are unsymmetrical sections and are usually attached to other members at one leg only. The resulting eccentricity introduces end moment which complicates the buckling behavior of angle members. In this paper, a previously conducted experimental study of steel angles as a part of a truss is simulated. A numerical modeling based on finite element techniques is conducted to properly understand the complex load carrying behavior of single angles. Account is taken of member eccentricity, local deformation as well as material and geometric non-linearity. Results are then compared with the experimental records. Results show that Finite Element Analysis can simulate the practical test conditions satisfactorily and the results closely match with experimental records.*

Keywords: Steel Angles, Eccentricity, Finite element (FE) modeling, Nonlinearity, Load-deflection behavior.

1 INTRODUCTION

The performance of steel angles is of great interest in the field of electrical transmission tower design. In such structures, the angles are subjected to both tension and compression. Although single-angle compression members, attached by one leg, to the other connecting members appear to be simple structural elements, they are amongst the most complex of structural elements to analyze and design. This is due to the end eccentricities and the fact that the principal axes of the angle do not coincide with the axis of the structure.

Bathon and Mueller [1] tested a wide range of eccentrically loaded angles using a ball joint to model end conditions unrestrained against rotation. The measured ultimate strengths were compared with the American design code. Experiments were carried out by Adluri and Madugula [2] on single angles of different cross sectional dimensions and of different slenderness ratios. All the test specimens including those prone to local buckling failed in flexural buckling before exhibiting some local failure. Finally several column curves were developed to verify the test results, which showed that the generated column curves were very close to test results. Testing of crossed diagonal angles in a 3D truss by Elgaaly*et al.* [3] showed that different failure modes could occur, combining local, overall and torsional effects, but that residual stress had a relatively insignificant effect on the maximum loads. Liu and Hui [4] investigated the response of steel single angles subjected to axial eccentric loading by means of finite element method. The results showed that for major axis bending, a critical eccentricity exists, below which reduction in ultimate load capacity is marginal. On the contrary, for minor axis bending, the reduction in ultimate capacity due to increase of eccentricity is more significant.

It can be observed from the above-mentioned researches that most of the works related to the investigation of single steel angles are experiment based. Later some work has been performed by means of finite element method, but these may not be enough to give a proper correlation between results of the experiments and that found by means of finite element method. Thus the aim of this paper is to investigate ultimate capacity of eccentrically loaded steel angles as part of a latticed truss by means of numerical finite element analysis. Three dimensional finite element studies have been carried out to simulate previously conducted experimental works by the researchers. Comparison of compressive load capacity of the single angles obtained by finite element analysis and the experimental results has been made.

2 EXPERIMENT OF ELGAALY et al. (1991)

In 1991, Elgaaly *et al.* [3] conducted tests on 50 non-slender single steel angles as part of a latticed truss. Of the specimens, 25 were double bolted and the rest 22

were single bolted at their ends. Table 1 lists the angle sections by groups depending on difference in cross-sectional dimensions, slenderness ratios (*l/r*) and end conditions. Figure 1 illustrates the test setup of Elgaaly *et al.* [3].The truss was designed so that the target angle would fail first without introducing significant deformations in the remainder of the truss.

Table 1: Properties of test specimens

Group	Size	*L / r*	End Conditions	Test Nos.
1	1¾ × 1¾ × ⅛	98	double bolt	1, 2, 3, 4, 5
2	1¾ × 1¾ × 3/16	99	double bolt	6, 7, 8, 33, 34
3	2 × 2 × ⅛	85	double bolt	9, 10, 11, 12, 13
4	2 × 2 × 3/16	86	double bolt	20, 21, 22, 43, 44
5	2½ × 2½ × 3/16	87	double bolt	18, 19, 50, 51, 52
6	1¾ × 1¾ × ⅛	92	single bolt	53, 54, 55, 56, 57
7	1¾ × 1¾ × 3/16	93	single bolt	23, 24, 35, 36, 37
8	2 × 2 × ⅛	80	single bolt	26, 27, 28, 38, 39
9	2 × 2 × 3/16	81	single bolt	29, 31, 40, 41, 42
10	2½ × 2½ × 3/16	65	single bolt	45, 46, 47, 48, 49

3 COMPUTATIONAL MODELING

3.1 Finite Element Modeling of the Truss System

Figure 2 shows a general configuration of a part of the three dimensional finite element model of the truss structure. The model consists of a target angle as was in the test of Elgaaly *et al.* [3]. For the analysis, the entire truss frame has been modeled using finite element package ANSYS. Angle specimens are discretized into a mesh of elements using general-purpose 4-node shell elements.

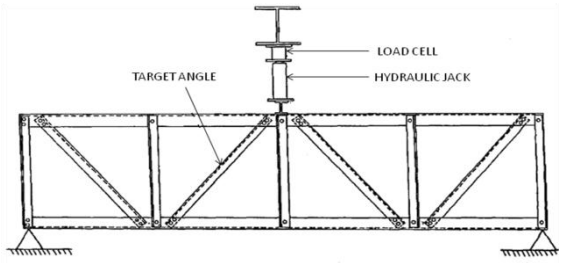

Figure 1: General 2-D sketch of test set-up of Elgaaly *et al.* (1991)

3.1.1 Meshing of the Angles

Each of the single angle members is divided along its width. Individual division is rectangular. In the finite element model of the present study, the target angle is discretized into finer mesh sizes (figure 2) considering the cross sectional

dimensions of the target angle rather than the dimensions of other angle members. The meshing of the remaining truss members has been done in such a manner so that the overall mesh size for each member remains uniform and the aspect ratio of the elements is reasonable.

3.1.2 Material Properties

The materials for the elements have been taken as bilinear kinematic hardening. In this model, it is assumed that the total stress range is equal to twice the yield stress, which is recommended for general small-strain use for materials that obey Von Mises yield criteria (which includes most metals). The Poisson's ratio is taken as 0.25. The modulus of elasticity of the angle members has been assumed 200 kN/mm^2 (the modulus of elasticity of steel).

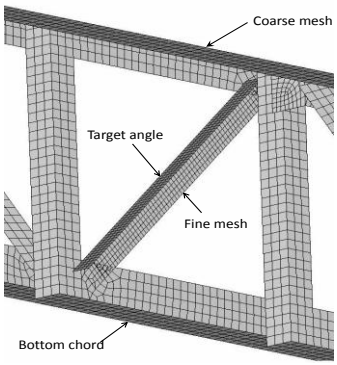

Figure 2: Close-up view of junction of a double bolted target angle with bottom chord

3.2 Boundary Conditions

In case of the bottom horizontal truss member, the leftmost node is kept restrained in X and Y-directions (The truss is in the X-Y plane). And the corresponding rightmost node is kept restrained in Y and Z- directions. The junction nodes of the leftmost and rightmost vertical angles with bottom horizontal angle are restrained in Y-direction only. Rest of the nodes is kept restrained in Z-direction only to prevent out-of-plane instability of the truss.

3.3 Loads

The load has been applied on the middle vertical angle member at its junction nodes with the top chord to allow the whole structure systematically deform. In

the present analysis, the load is applied slightly greater than the Euler Load of the corresponding target angle member for each case. Then the load has been augmented and then subdivided equally into the junction nodes to be applied on the truss structure (figure 3).

4 RESULTS AND DISCUSSIONS

4.1 Deformation Characteristics of the Target Angle

The load-deflection relationship has been signed out as the best characterization of the load carrying behavior of single steel angles subjected to eccentric axial loads. During present analysis of the truss, a load was imposed on the structure sub diving it on each of the junction nodes of the middle vertical angle with the top chord (figure 3).

Due to the nodal loads, each time target angle has undergone an axial compressive force along with some axial shortening, which is the axial displacement (Δ_a) of target angle (shown in figure 3) and at the same time, some

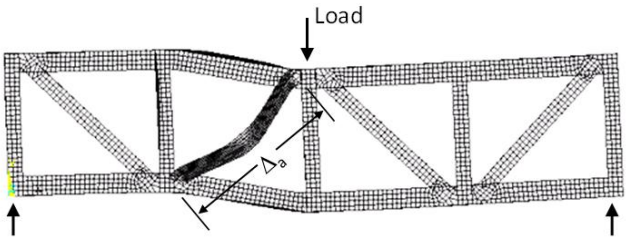

Figure 3: Deflection pattern at the final stage of buckling (front view)

lateral displacement (Δ_l) occurs (as shown in figure 6).At different stages of applying load, corresponding axial forces and the lateral displacements (Δ_l) have been obtained.

Typical axial load (P) versus lateral displacement (Δ_l) curves obtained for different angle sections from non-linear finite element analysis are shown in figures 4 (for single bolted angles) and figure 5 (for double bolted angles), where response is observed to be linear until failure.

As observed, all the load-deflection graphs show the same trend. Once the peak load is reached, it eventually diminishes with further increase of lateral deflection. The peak load is the indicator which shows that from this point

buckling of the target angle initiates. The deformation by considering the specimen of test-53 of Elgaaly *et al.* [3]. The specimen is single bolted and has width-thickness ratio is equal to 13.15 with slenderness ratio of 92.0 (the highest ratio of all the groups of single bolted target angles). From finite element analysis the obtained failure load is 47.42 kN whereas compressive load carrying capacity from the test of Elgaaly*et al.* [3] is 48.04 kN.

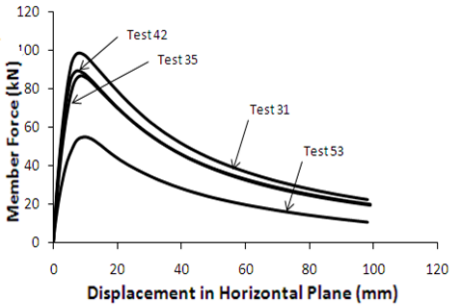

Figure 4: Typical axial force vs lateral displacement (in horizontal plane) graph for single bolted angles

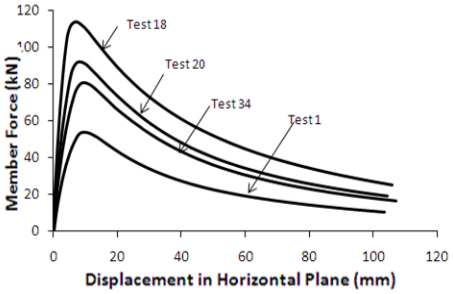

Figure 5: Typical axial force vs lateral displacement (in horizontal plane) graph for double bolted angles

In the initial stage, when the load reaches the pick, no significant deformation is observed initially. But gradually when the load tends to decrease and reaches a small but considerable percentage of the peak load value, some extent of deformation occurs. In this stage, the deflection initiates with the bending of the connected leg of the target angle. The rest of the truss members remain in the position where they were initially. When the load value eventually diminishes and comes to the final diminishing point, the deflection is associated with the bending of the connected leg along with the twisting of the unconnected leg of the target angle. Additionally the unconnected leg of the top horizontal member also faces twisting. The lower middle half portion of the target angle faces severe bending stress specially the lowermost connected region of the target angle (Figures 3 and 6).

The middle vertical angle and the corresponding junction (the load application zone) shift downwards from their original position. The deflected shapes of the target angle can be easily realized from figure 6.As expected, all samples failed due to bending of the connected leg of the target angle. The failure mode was global flexural torsional (FT) mode without local buckling of the angle leg which is similar to the failure mode of specimen 24 as described by Elgaaly *et al.* [3].

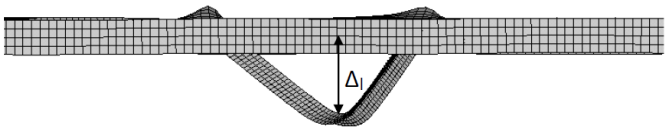

Figure 6: Deflection pattern at the final stage of buckling (top view (closeup))

4.2 Comparison of Finite Element Model with Experiment

Elgaaly *et al.* [3] described the member force vs displacement graphs of 2 single bolted (test 42 and test 26) and 2 double bolted (test 34 and test 9) target angles. The same specimens are analyzed by means of finite element method. It has been observed from the comparative figures that results from test of Elgaaly *et al.* [3] and from present analysis are relatively close for all the specimens except for specimen of test 26 (the reason may be the higher *w/t* ratio of the specimen, which is 13.88 as mentioned by Elgaaly). Here comparative results for test 34 and test 42 have been represented graphically in figures7 and8 respectively. The observed deviations, though not significant between both present analysis and test results of Elgaaly*et al.* [3] may be due to the fact that during modeling the truss system, bolted connection is simply replaced by modeling the connecting portions of target angle with the other angles as the integral parts of the truss just like modeling of the component angle members of the truss. So in the finite element model considered here, no stress concentration has occurred. So, some minor differences occur for some of the angles.

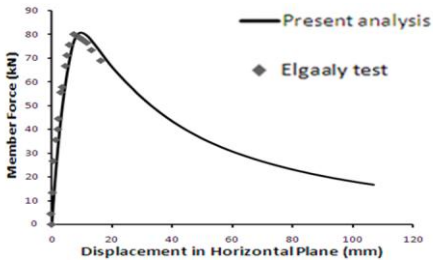

Figure 7: Load-deflection graph of angle size L 45.57×45.57×5.00, double bolted (test 34)

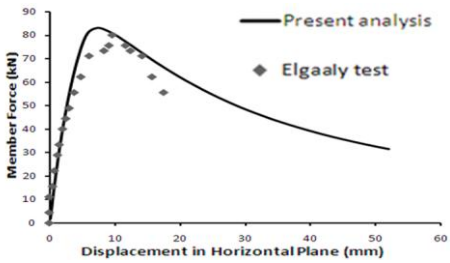

Figure 8: Load-deflection graph of angle size L 50.75×50.75×4.83, single bolted (test 42)

Overall, finite element analysis gives more logical results for double bolted angles than for single bolted specimens as the prevailing methodology of modeling the truss frame in finite element is more compatible to the restraint conditions of double bolted conditions (more fixity in double bolted than single

bolted connections). Different distinguished failure loads have been found for both single bolted and double bolted specimens. For the ease of discussion, 8 specimens (4 single bolted and 4 double bolted) are chosen by the authors as the representative of 47 specimens to describe the salient features of the buckling analysis of the target angles (shown in figures4 and 5with test numbers according to the test of Elgaaly *et al.* [3]). The geometric properties as well as loading conditions etc of the reference specimens are listed in the table 2(a) and table 2(b).

Table 2: Properties of reference specimens (a) single bolted (b) double bolted

(a)

test no.	width, w (mm)	thickness, t (mm)	w/t	slenderness ratio, l/r	yield stress, F_Y (kN/mm^2)
42	50.75	4.83	10.52	81	317.9
35	44.93	5.13	8.76	93	339.9
31	50.39	5.08	9.92	81	339.2
53	44.42	3.38	13.15	92	353

(b)

test no.	width, w (mm)	thickness, t (mm)	w/t	slenderness ratio, l/r	yield stress, F_Y (kN/mm^2)
18	63.17	5.05	12.50	67	315.2
20	50.6	5.08	9.96	86	326.9
34	45.57	5	9.11	99	342.8
1	43.97	3.53	12.45	98	344.1

From the illustration of figures4 and 5, different peak loads for the reference specimens have been observed for single bolted as well as double bolted angles. Figure 9 delineates the failure loads (peak loads) for the reference specimens of single bolted and double bolted angles. Both the demonstrations of figure 9 show that the results obtained from present analysis are very close to those found from the tests of Elgaaly *et al*. [3].

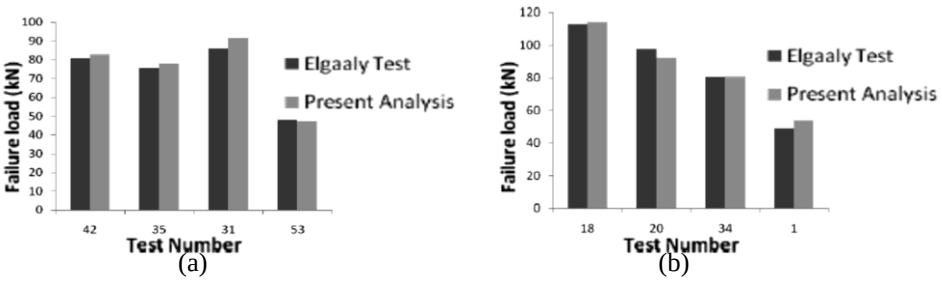

Figure 9: Comparison of Failure Loads of angles: (a) single-bolted and (b) double-bolted

5 CONCLUSIONS

The study originated with the aim to validate, through numerical simulation, the eccentric compressive load carrying capacity of a single steel angle (designated as target angle; either single bolted or double bolted) as part of a three-dimensional truss tested by Elgaaly *et al*. [3].The results of present study are in well agreement with those obtained from the tests. Therefore, FE analysis may be a good alternative to experiments of single angle structures and can be used for routine design of steel angles which will be helpful to find out better solutions for engineers.

REFERENCES

[1] Bathon, L., Mueller, W. H., and Kempner, L., 1993. Ultimate load capacity of single steel angles. *Journal of Structural Engineering, ASCE,* **119 (1),** Jan.,pp 279-300.

[2] Adluri, S. M. R., and Madugula, M. K. S., 1996. Development of column curve forsteel angles. *Journal of Structural. Engineering, ASCE,* **122 (3),** March, pp 309-317.

[3] Elgaaly, M., Dagher, H., and Davids, W., 1991. Behavior of single angle compression members. *Journal of Structural Engineering, ASCE,***117 (12),** Dec., pp3720-3741,

[4] Liu, Y., and Hui, L., 2010.Behaviour of steel single angles subjected to eccentric axial loads. *Canadian. Journal of. Civil Engineering*, **37 (6),** pp 887-896.

CICM 2015
First International Conference on
Advances in Civil Infrastructure and Construction Materials
MIST, Dhaka, Bangladesh, 14–15 December 2015

SMA-BASED LEAD RUBBER BEARINGS FOR SEISMIC CONTROL OF HIGHWAY BRIDGES

F. Hedayati Dezfuli[1] **and M. Shahria Alam**[2]

[1, 2] School of Engineering, The University of British Columbia, Kelowna,Canada.
Email: [1]farshad.hedayati@alumni.ubc.ca and [2]shahria.alam@ubc.ca

Abstract. *Smart elastomeric isolators incorporated with SMA wires are new generation passive earthquake protective devices with improved performance compared to conventional rubber bearings. SMA wires with unique flag-shaped hysteresis and superelastic behavior can enhance the re-centering capability and energy dissipation capacity of elastomeric isolators. This study aims to prove that SMA-based lead rubber bearings (SMA-LRB) can reliably control the seismic response of highway bridges under different loading conditions and reduce the failure probability of such structures at different damage states. In order to achieve this goal, the seismic vulnerability of a multi-span continuous steel-girder highway bridge, whichis isolated by SMA-LRB, is assessed and compared with a case where LRB is implemented as isolation system. Results reveal that equipping LRB with SMA wires decreases the possibility of occurring damage in isolation devices at all limit states and also reduce the failure probability of the bridge structure at collapse damage state. It means that in the most destructive loading conditions, SMA-LRB is more effective in making the highway bridge less vulnerable.*

Keywords: Seismic fragility assessment, Shape memory alloy, Lead rubber bearing, Smart elastomeric isolator, Steel-girder highway bridge.

1 INTRODUCTION

The performance of highway bridge systems subjected to earthquakes over 40 years (Loma Prieta 1989, and Chi-Chi 1999, Chile 2010, Tohoku 2011) has revealed that these structures are highly vulnerable to seismic events [1]. In such a situation, it is highly crucial to protect bridges against earthquakes and investigate their functionality under different ground excitations.

Among different types of passive earthquake protective mechanisms, elastomeric isolators (EIs) or rubber bearings are one of the most well-known systems that are used in bridge applications. They can effectively isolate the structure by providing flexibility and dissipating the earthquake's energy. Although lead rubber bearings (LRBs) are extensively used in several applications, they have some weaknesses such as limited shear strain capacity, un-recovered residual deformation, and instability due to a large deformation [2,3]. Using shape memory alloy (SMA) in the form of wire [2,4,5] is a solution to partially overcome the aforementioned limitations. Using SMA as a supplementary component is due to its unique characteristics such as a flag-shaped hysteretic response (high re-centering capability), a good superelastic effect (up to 13.5% re-coverable strain) [6] and a suitable fatigue property [7]. Hedayati Dezfuli and Alam[4] showed that incorporating SMA wires into the natural rubber bearings leads to improvements in the re-centering capability and the energy dissipation capacity.

In the seismic risk assessment of bridges, fragility curves are developed to determine the probabilities that a structural demand (structural response) exceed the structural capacity defined at a damage state. Analytical approach is mostly used in order to develop fragility curves [8, 9, 10]. Traditionally, bridge piers were considered as the primary component to be an indicative of the overall fragility of the structure [11, 12]. However, Nielson and DesRoches[13] showed that this is not an appropriate assumption for all types of bridges and could lead to significant errors in estimating the fragility functions of the whole system. Here, an important point is that for bridges with multi-column bents, major vulnerable bridge components should be considered to minimize errors and maximize the accuracy of the estimation of system fragilities.

This study evaluates the seismic vulnerability of a steel-girder highway bridge isolated by smart lead rubber bearings in which SMA wires are wrapped around the LRB in a double cross arrangement. A three-span continuous steel-girder bridge is considered where LRBs are used to isolate the bridge and ferrous-based SMA wires are employed as supplementary components. 3D finite element (FE) models are generated in SeismoStruct [14]. Incremental dynamic analyses (IDA) are carried out in order to estimate the seismic fragility functions of major vulnerable components (bridge pier and rubber bearing).

2 SEISMIC VULNERABILITY ASSESSMENT

Fragility theory investigates probability levels at which the seismic demand of a structure, D, is equal to or greater than the capacity of the structure, C. This statement is subject to a condition defined as a specified intensity measure (IM) indicating the level of seismic loading.

A probabilistic seismic demand model (PSDM), which shows a probability distribution for the demand, is developed to correlate the engineering demand parameters, EDPs, (e.g. pier displacement ductility and bearing deformation) with the intensity measure (e.g. peak ground acceleration). To develop PSDM, the scaling approach [10, 15] is used. A two-parameter lognormal probability distribution is assumed to represent the EDP.

Capacities of bridge components can also be defined with lognormal distributions. Therefore, the fragility equation can be written as [8]:

$$P[D \geq C \mid IM] = \Phi\left[\frac{\ln(S_d / S_c)}{\sqrt{\beta_{D|IM}^2 + \beta_c^2}}\right] \qquad (1)$$

in which Φ is the cumulative distribution function of the standard normal distribution, S_d and S_c are the median estimates of the demand and the capacity, respectively, and $\beta_{D|IM}$ and β_c are logarithmic standard deviations of the demand, and the capacity, respectively.

Limit states or structural capacities for a bridge component should provide a qualitative representation for that component. The limit states are classified to slight, moderate, extensive, and collapse [16]. Here, bridge piers and EIs are assumed as the main vulnerable components of the highway bridge because they often show nonlinear behaviour under strong ground motions. The quantitative measure of limit state for the piers is displacement ductility, μ_d, and for the isolation bearings is the shear strain, γ. Based on the available literature, the range of EDPs considered for each component is specified at each limit state level according to Table 1.

Table 1: Limit states of bridge pier and elastomeric bearing.

Bridge Comp.	EDP	Limit States				Reference
		Slight	Moderate	Extensive	Collapse	
Pier	Displacement Ductility	μ_d> 1.00	μ_d> 1.20	μ_d> 1.76	μ_d> 4.76	[8]
EI	Shear Strain	γ> 100%	γ> 150%	γ> 200%	γ> 250%	[15]

The system fragility is determined using the upper bound in the first order reliability theory (equation (2)) which provides a conservative estimation.

$$P[F_{system}] = 1 - \prod_{i=1}^{n} \left(1 - P[F_{comp,i}]\right) \quad (2)$$

P[F_s] and P[$F_{comp\ i}$] are the probabilities of failure for the system and *i*th bridge component, respectively, and Π is the product operator.

Among different intensity measures, peak ground acceleration (PGA)is selected in this study. 25 far-field earthquake records having different longitudinal and transverse components are collected from PEER strong motion database[17] to develop the fragility curves. Since the bridge simulated in this research is located in the province of British Columbia (western Canada), it is assumed that the ratio of PGA to PGV is between 0.8 and 1.2 [18].

As shown in Figure 1, the chosen structure is an irregular bridge (i.e. piers with different heights) consisting of two multi-column bents with a skew angle of 20 degrees. The columns are made of concrete reinforced with steel rebars. Considering two types of rubber bearing (LRB and SMA-LRB), two cases are explored; the bridge isolated by LRBs and the bridge isolated by SMA-LRBs.

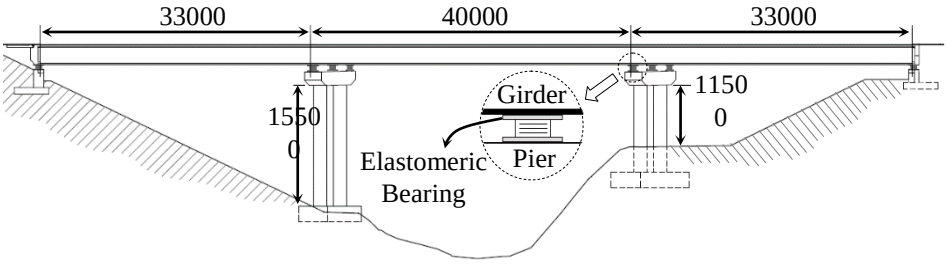

Figure 1: Three-span continuous steel-girder bridge.

A 3D finite element (FE) model is generated in SeismoStruct [14]. It should be noted that the effect of abutment on the seismic vulnerability is not considered. Moreover, it is assumed that the bridge piers are supported on a rigid foundation.

Based on the arrangement of SMA wires previously proposed by Hedayati Dezfuli and Alam [4], two wires are wrapped around the LRB in a double cross configuration. Both rubber bearings have same plan area of 350 mm by 350 mm with identical thicknesses of rubber layers (70 mm). The behavior of rubber bearings is simulated using the bilinear kinematic model. Actual hysteretic responses of LRB and SMA-LRB are plotted in Figure 2 along with responses of the idealized models.

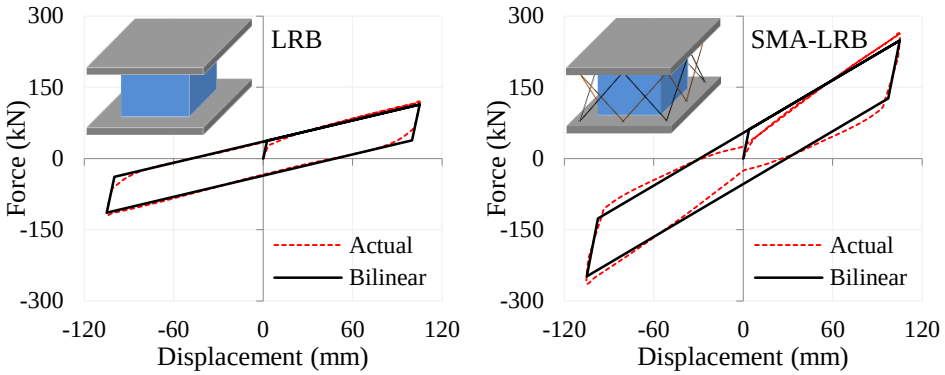

Figure 2: Actual and idealized shear hysteretic responses of LRB and SMA-LRB.

3 RESULTS AND DISCUSSIONS

3.1 Fragility of Components

Displacement ductility is defined as a ratio of the ultimate displacement to the yield displacement. Shear strain is defined as a ratio of the lateral displacement to the total thickness of rubber layers. Figure 3 demonstrates the fragility curves of bridge pier and rubber bearing when LRB and SMA-LRB are used as different isolation systems.

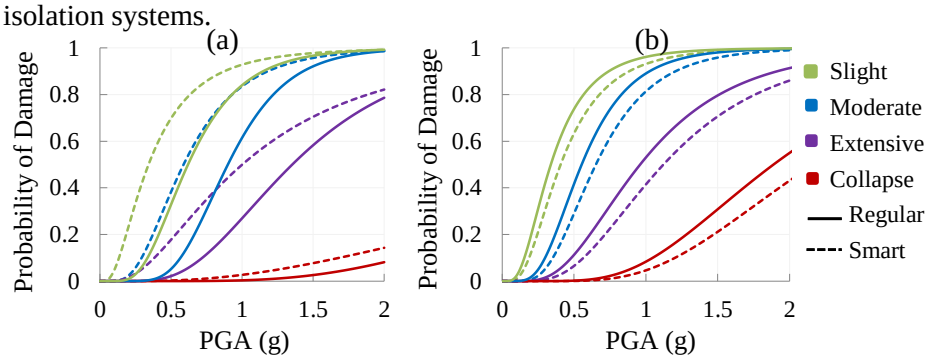

Figure 3: Fragility curves of (a) bridge pier and (b) rubber bearing for regular (LRB) and smart (SMA-LRB) isolation systems.

Comparing fragility curves of the bridge pier isolated by LRB and SMA-LRB depicts that using SMA wires in LRB increases the probability of damage of the pier as a result of stiffening the system which causes a higher seismic force demand. For example, if the bridge is excited by an earthquake with a PGA of 1.0g, the probabilities of occurring a moderate damage are 62% and 84% in the pier isolated by LRB and SMA-LRB, respectively. Both stiffness and energy dissipation capacity have contributions to the vulnerability of the pier. At high values of PGA (between 1.0g and 2.0g), the effective stiffness of SMA-LRB is

considerably higher than that of LRB. The fragility of pier increases by increasing the stiffness of rubber bearings and decreases by increasing the energy dissipation of isolation systems. In the case of using SMA-LRB, the influence of effective stiffness of elastomeric isolators is more than that of the energy dissipation capacity and as a result, the fragility of pier increases.

When SMA wires are incorporated into LRB, the vulnerability of elastomeric isolation system decreases. In fact, SMA wires with a high re-centring capability and a flag-shaped hysteresis stiffen the rubber bearing and improve the dynamic stability of the device by restricting it from over displacement.

Comparing the fragilities of bridge components reveals that in most cases, the pier is more vulnerable than the elastomeric bearing.

3.2 Fragility of Bridge

When LRB is replaced with SMA-LRB, the bridge structure becomes more fragile at slight, moderate and extensive limit states. The reason is that although using SMA wires in LRB can reduce the possibility of damage in isolation systems, it increases the fragility of the bridge pier in a way that the damage probability of the whole system increases. However, at the collapse level, using SMA-LRB instead of LRB is in support of the seismic response of system. It is because the fragility reduction in the rubber bearing outweighs the fragility increase in the pier and as a result, the seismic vulnerability of the whole structure decreases.

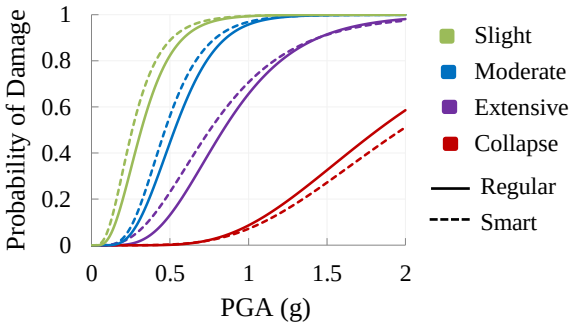

Figure 4: Fragility curves of the bridge system isolated by LRB and SMA-LRB

4 CONCLUSIONS AND RECOMMENDATIONS

Seismic fragility of a three-span continuous steel-girder bridge, with unequal pier heights and a skew angle of 20 degrees, was assessed in this study. Two cases were studied by implementing two different types of isolation systems; lead rubber bearing (LRB) and SMA wire-based LRB (SMA-LRB). The bridge pier and the isolation system were considered as major vulnerable componenets in developing fragility functions of the system. Each bridge model was subjected to 25 earthquake records having different longitudinal and transverse components,

with PGA values ranging from 0 to 0.6g. To establsih fragility functions, incremental dynamic analyses were carried out. Based on the reults, the following conclusions can be drawn.

- SMA wire can increase the stiffness of the system and as a result, the ductility demand in the bridge pier decreases for PGA values lower than 2.0g. In this range of PGA, the bridge pier becomes more vulnerable when LRB is replaced with SMA-LRB.
- SMA wires, with a high re-centering capability due to a flag-shaped hysteresis, stiffen the elastomeric isolation system and improve the dynamic stability of the device by restricting it from over displacement. As a result, these supplementary components could reduce the vulnerability of conventional natural rubber bearings.
- Using SMA-LRB instead of LRB makes the bridge structure less vulnerable at extreme damage states (collapse). It is because SMA-LRB makes the isolated bridge stiffer in comparison with the LRB. SMA-LRB is more effective in reducing the failure probability (fragility) of the bridge at the collapse damage level. It shows that this smart isolator performs more efficiently when the bridge system is subjected to large amplitude displacements.

In this study, some assumptions were made in order to simplify the process of developing fragility functions of a steel-girder highway bridge. Therefore, in order to make the fragility responses more accurate and improve the level of prediction, several factors including the effect of abutments and foundations, uncertainties in the geometry and material properties, and earthquake records with high PGA values should be taken into account in future works. Since far-field ground motions were considered in this study, fragility of bridges should also be estimated under near-field earthquakes.

REFERENCES

[1] Basoz, N., Kiremidjian, A. S., King, S. A., and Law, K. H., (1999). "Statistical analysis of bridge damage data from the 1994 Northridge, CA, earthquake." *Earthq Spectra*, 15, 25-53.

[2] Choi, E, Nam, T. H., and Cho, B. S. (2005). "A new concept of isolation bearings for highway steel bridges using shape memory alloys." Can J Civil Eng, 32 957–67.

[3] Bhuiyan, A. R., and Alam, M. S. (2012a). "Seismic Fragility Assessment of a multi-span continuous highway bridges isolated by shape memory alloy restrainer and lead rubber bearing." 15th World Council of Civil Engineers (WCEE), Lisboa.

[4] Hedayati-Dezfuli, F., and Alam, M. S. (2013). "Shape memory alloy wire-based smart natural rubber bearing." Smar Mat St, 22 045013 doi:10.1088/0964-1726/22/4/045013.

[5] Hedayati-Dezfuli, F., and Alam, M. S. (2014). "Performance-based assessment and design of FRP-based high damping rubber bearing incorporated with shape memory alloy wires." EngStruct, 61:166-183.
[6] Tanaka, Y., Himuro, Y., Kainuma, R., Sutou, Y., Omori, T., and Ishida, K. (2010). "Ferrous polycrystalline shape-memory alloy showing huge superelasticity." Science, 327, 1488-90.
[7] Alam, M. S., Youssef, M. A., and Nehdi, M. (2007). "Utilizing shape memory alloys to enhance the performance and safety of civil infrastructure: a review." Can J Civil Eng, 34 1075-86.
[8] Hwang, H., Liu, J. B., and Chiu Y. H. (2001). "Seismic fragility analysis of highway bridges." MAEC report: project MAEC RR-4. Urbana: Mid-America Earthquake Center.
[9] Nielson, B. G., and DesRoches, R. (2007a). "Seismic fragility curves for typical highway bridge classes in the Central and Southeastern United States." Earthq Spectra, 23:615-633.
[10] Alam, M. S., Bhuiyan, A. R., and Billah, A. H. M. M. (2012). "Seismic fragility assessment of SMA-bar restrained multi-span continuous highway bridge isolated with laminated rubber bearing in medium to strong seismic risk zones." Bull EarthqEng, 10(6), 1885-1909.
[11] Hwang, H., Jernigan, J. B., and Lin, Y. W. (2000). "Evaluation of seismic damage to Memphis bridges and highway systems." J Bridge Eng-ASCE, 5, 322-30.
[12] Mackie, K. R., and Stojadinovic, B. (2001). "Probabilistic Seismic Demand Model for California Bridges." J Bridge Eng-ASCE, 6(6), 468-480.
[13] Nielson, B. G., and DesRoches, R. (2004). "Improved Methodology for Generation of Analytical Fragility Curves for Highway Bridges." 9th ASCE Specialty Conference on Probabilistic Mechanics and Structural Reliability, Albuquerque, NM. ASCE.
[14] SeismoStruct 2014. SeismoStruct software v6.5. Available from www.seismsoft.com
[15] Zhang, J., and Huo, Y. (2009). "Evaluating effectiveness and optimum design of isolation devices for highway bridges using the fragility function method." EngStruct, 31:1648-1660.
[16] FEMA. 2003. HAZUS-MH MR1: Technical Manual, Vol. Earthquake Model. Federal Emergency Management Agency, Washington DC.
[17] PEER Strong Motion Database, http://peer.berkeley.edu/smcat/search.html
[18] Naumoski, N., Tso, W. K., and Heidebrecht, A. C. (1988). "A selection of representative strong motion earthquake records having different A/V ratios." EERG Report 88-01, Earthquake Engineering Research Group, Dept. of Civil Eng., McMaster University, Hamilton, ON, Canada.

CICM 2015
First International Conference on
Advances in Civil Infrastructure and Construction Materials
MIST, Dhaka, Bangladesh, 14–15 December 2015

NUMERICAL ANALYSIS OF A REINFORCED CONCRETE SLAB-COLUMN CONNECTION SUBJECTED TO LATERAL & VERTICAL SEISMIC LOADING

Mostafiz Emtiaz[1], A. S. M. Alauddin Al Azad[2] and H. M. SHAHIN[3],

[1, 2, 3] Department of Civil and Environmental Engineering, Islamic University of Technology, Gazipur, Dhaka.
Email: [1]mostafiz.emtiaz@gmail.com, [2]sajal105@iut-dhaka.edu, [3]shahin@iut-dhaka.edu

Abstract. *Reinforced concrete flat slabs are widely used because of its economical nature. Flat slab structures show significant vulnerability under lateral and vertical seismic loading as punching shear failure may occur in the joints of slab and column. In this research, finite element analyses have been carried out to predict how much seismic loading a flat slab-column connection can endure. The vulnerability of the flat slab-column connection is checked through the analyses. The finite element analyses have been conducted with ABAQUS software because of its wide material modeling capability and customization property. Elasto-plastic CDP model is used a material modelling for the reinforced concrete. It is found that thickness of the slab, reinforcement ratio, usage of bent bars, high strength materials are the important factors in punching shear failure in the slab-column connection.*

Keywords: Finite element analysis, ABAQUS, Punching shear failure, Seismic loading, Stress analysis.

1 INTRODUCTION

Recently many experimental works has been done on reinforced concrete structures subjected to seismic loading. Strengthening of both modern and aging infrastructures is essential because of recent earthquake activities. In this paper we want to focus on a reinforced concrete slab-column connection subjected to lateral seismic loading at the top and vertical seismic loading at the bottom of the column.

Many experiments have been performed to understand the behavior of the connection of a building. Performing experiment for a flat slab-column connection subjected to seismic loading requires more time and money. Such an experiment was performed by Robertson & Johnson [1] to determine the punching shear failure for a slab-column connection. In that experiment, six specimens were used. And for each specimen experimental setup was prepared and the specimens were subjected to lateral loading. In this research, we have analyzed the specimen one and applied both vertical and horizontal seismic loading.

2 FINITE ELEMENT ANALYSIS

2.1 Material Modeling

2.1.1. Concrete Damage plasticity Model

In the research of Genikomsou et al (2014) [2] it is said that, the concrete damage plasticity model is a continuum, plasticity-based, damage model, which assumes two main failure mechanisms: the tensile cracking and the compressive crushing. The model uses the yield function proposed by Lubliner et al. (1989) [3] and modification by Lee and Fenvas (1998) [4].

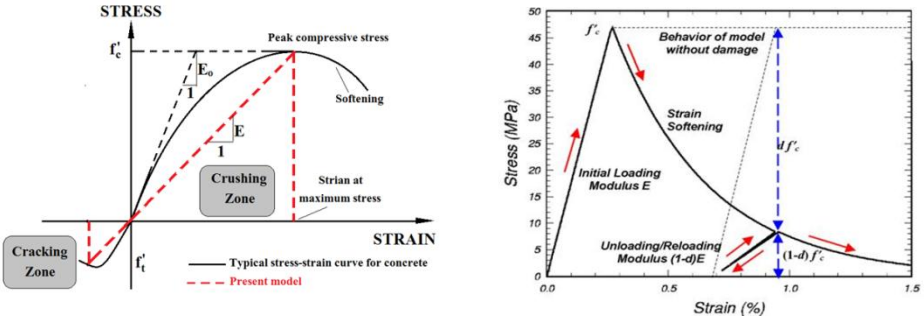

Figure 1: CDP Model for compression & tension.

2.1.2. Linear Elastic Plastic Model

The material returns to its original shape when the loads are removed. Strain in these materials is small and stress is proportional to strain.

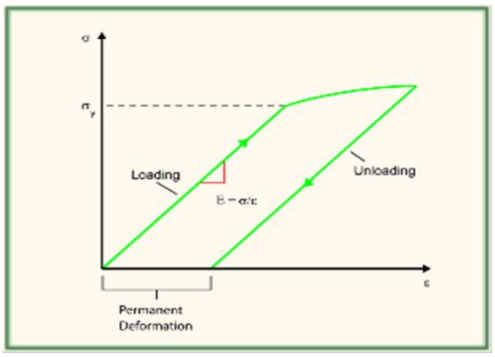

Figure 2: Linear elastic plastic model

3 SPECIMEN MODELING

3.1 Slab-Column Joint Modeling

An interior slab-column connection has been created using the co-ordinate system where the whole connection acted as the host element for the reinforcements. Concrete damage plasticity type model has been used here. Slab is placed with the thickness of 114mm and slab size is placed as 2743mm*3048mm. And the column size is placed as 254mm*254mm. And the height of the column is placed as 1524mm.

3.2 Reinforcement Modeling

Reinforcement of both slab and column has acted as the embedded element. The bottom slab reinforcements are placed at #10@356mm, #10@203mm, #10@152mm, #10@256mm & #10@356mm along the width of the slab and #10@356mm, #10@203mm, #10@152mm, #10@256mm & #10@356mm along the length of the slab.

The top slab reinforcements are extended to one third of the slab. The top slab reinforcements are placed at #10@152mm along the width of the slab and #10@152mm, #10@127mm, #10@127mm & #10@152mm along the length of the slab. Four rebar are used in column and no tie bars are used. #20 reinforcement is used as the column reinforcement.

3.3 Property Definition

3.3.1. Material property for slab & Column concrete

Table 1: Property for slab & column concrete

Density (kg/mm^3)	Young Modulus (MPa)	Poison's Ratio	Dilation Angle	Eccentricity	$\frac{FB_o}{FC_o}$	K	Viscosity Parameter	Yield Strength (Compressive)	Yield Strength (Tensile)	Fracture Energy (N/mm)
2.4E-6	34400	0.23	38	0.1	1.16	.67	8.5E-5	44	2.2	0.09

3.3.2. Material properties for reinforcement

Rebar's density is 7.75E-6 kg/mm^3 And Young modulus 210000 MPa. Poison ratio was taken 0.3. T3D2 element has been used. Truss elements are rods that can carry only tensile or compressive loads. They have no resistance to bending; therefore it can be modeled as a truss**.**

3.4 Meshing

Every part was individually meshed for finite element analysis. Mesh size 10mm is used in the host element and 10mm is used in the embedded element. T3D2 elements are used. Total number of element is 12,656. Total number of node is 16,846. Total number of variables in the model is 50,538.

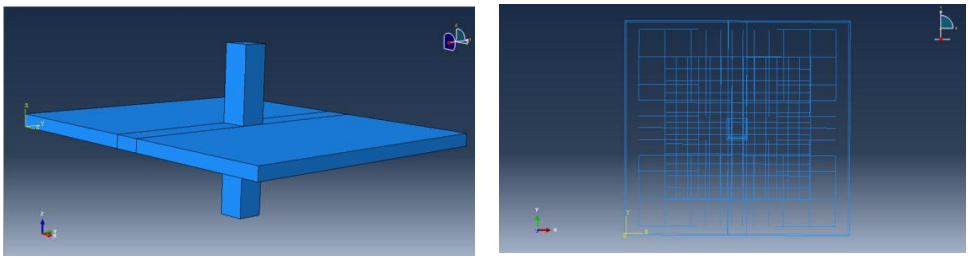

Figure 3: Modeling of the slab-column joint & reinforcement

4 RESULUTS AND DISCUSSIONS

4.1 Stress Distribution Analysis for Different Loading Cases

For the loading case 1 punching shear occurs at the critical perimeter according to ACI code where the top of the column is subjected to 1000 Hz of seismic loading.. The critical perimeter is located at a distance of d/2 from the face of the column. The maximum shear stress at critical perimeter is necessary to determine whether punching shear failure will occur or not. Stress distribution analysis has been done for various cases to find out the maximum stress at critical perimeter.

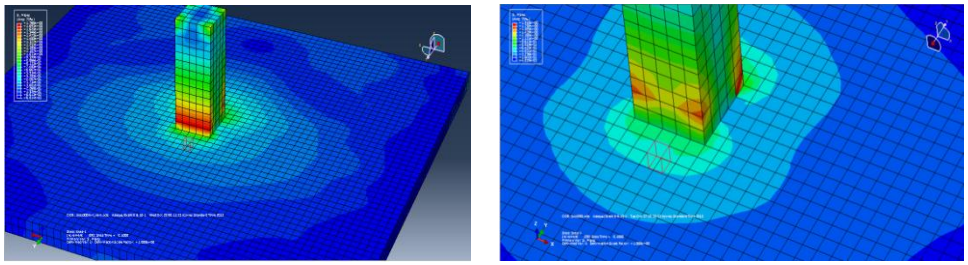

Figure 4: Contour plot of the slab column connection & Element at the critical parameter for stress distribution

4.2 Von Mises and Tresca Stress Distribution

For the loading case 1 it is considered that the top of the column is subjected to 1000 Hz of seismic loading in the horizontal direction. Von mises & Tresca stress distribution analysis is done for an element situated in critical parameter of the flat slab. For the loading case 2 it is considered that the top of the column is subjected to 2000 Hz of seismic loading in the horizontal direction. Von Mises & Tresca stress distribution analysis is done for an element situated in critical parameter of the flat slab. For the loading case 3 it is considered that the top of the column is subjected to 1000 Hz of seismic loading in horizontal loading & 1000 Hz of vertical Loading at the bottom of the column in vertical direction. Von mises & tresca stress distribution analysis is done for an element situated in critical parameter of the flat slab.

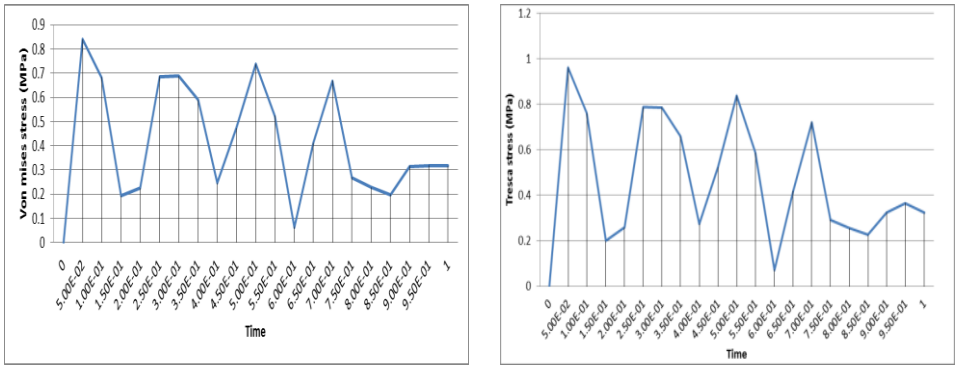

Figure 5: Maximum stress distribution curve for case-1

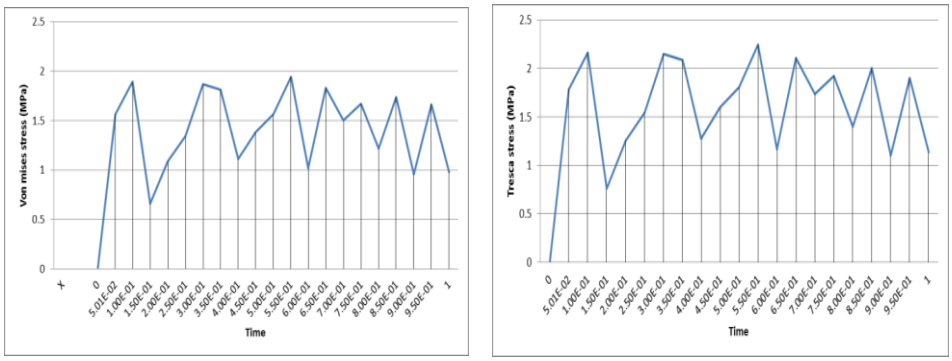

Figure 6: Maximum stress distribution curve for case-2

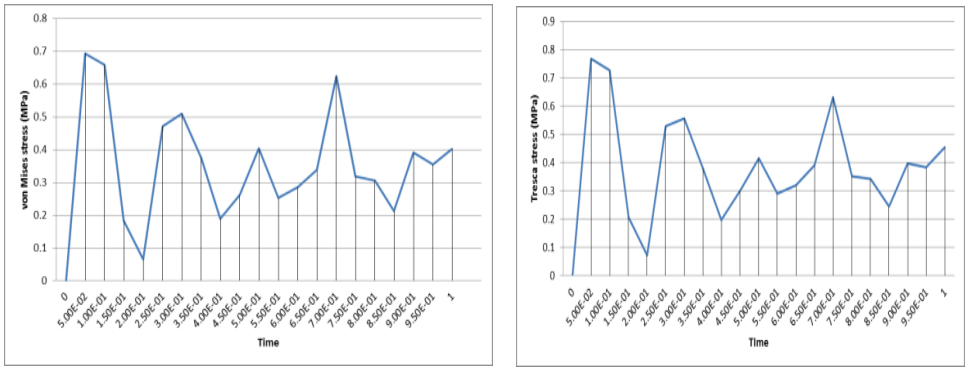

Figure 7: Maximum stress distribution curve for case-3

For the loading case 3 it is considered that the top of the column is subjected to 2000 Hz of seismic loading in horizontal loading & 2000 Hz of vertical Loading at the bottom of the column in vertical direction. Von Mises stress distribution analysis is done for an element situated in critical parameter of the flat slab.

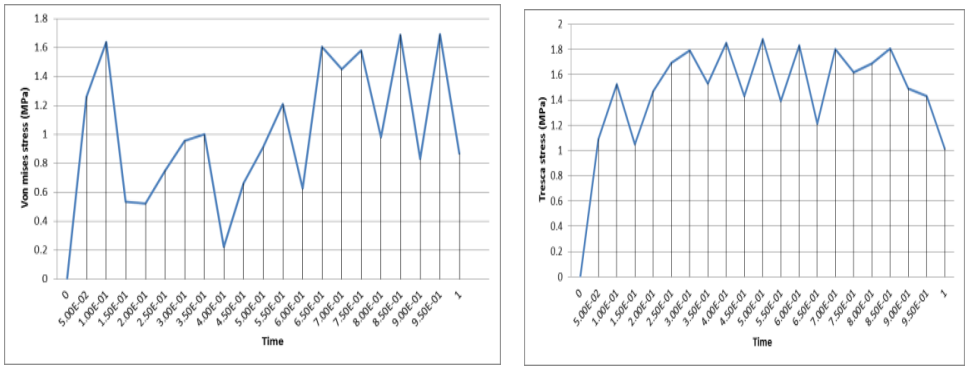

Figure 8: Maximum stress distribution curve for case-4

4.3 Comparison with ACI code

A value of 1.0 for the shear ratio would indicate that the connection is on the verge of punching shear failure according to the ACI Building Code.

The concrete shear stress is limited to the smallest of three concrete stress equations given in ACI 318 section 11.12.2.1.

$$v_c = \frac{1}{3}\sqrt{f_c} \qquad (1)$$

Shear ratio is the ratio of ultimate shear stress for the critical perimeter & concrete shear stress. If the ratio is 1 or greater than 1 then punching shear failure occurs. [8]

5 RESULTS AND DISCUSSIONS

The results of the analyses have been summarized in Table 1.

As from ACI building code it has been established that if shear ratio $\frac{v_u}{v_c} \geq 1$ then punching shear failure will occur. From the tabulated chart it is seen that punching shear failure occurred for a slab-column connection subjected to 2000 Hz of cyclic loading laterally at the top of the column and combination of 2000 Hz of cyclic loading at the top of the column laterally and 2000 Hz of cyclic loading vertically at the end of the column.

Table 2: Example of the construction of one table.

Different cases	Stress Distribution	Ultimate stress (v_u) (N/mm^2)	Concrete stress (v_c) (N/mm^2)	Shear Ratio $\frac{v_u}{v_c}$	Chance of occurring Punching shear failure
Case-1	Von-Mises	0.88	1.81	0.49	Crack may develop & Punching shear failure is not imminent
	Tresca	0.97	1.81	0.56	Crack may develop & punching shear failure is not imminent
Case-2	Von-Mises	1.97	1.81	1.09	punching shear failure
	Tresca	2.2	1.81	1.21	Punching shear failure
Case-3	Von-Mises	0.69	1.81	.38	Punching shear failure is not imminent
	Tresca	0.78	1.81	.94	Punching shear failure is not imminent
Case-4	Von-Mises	1.7	1.81	1.09	Punching shear failure
	Tresca	1.8	1.81	1.011	Punching shear failure

6 CONCLUSIONS

In this model Von Mises stress and Tresca stress distribution has been checked at the slab-column connection. It has been observed that it is possible to determine the behavior of a slab-column connection subjected to seismic loading. To minimize the effects of seismic loading the following should be taken into consideration –

- Increase the thickness of the slab,
- Increase the reinforcement ratio,
- Usage of bent bars,
- Usage of high strength materials.

REFERENCES

[1] Robertson and Johnson,(2004), "NON-DUCTILE SLAB-COLUMN CONNECTIONS SUBJECTED TO CYCLIC LATERAL LOADING", *13th World conference on Earthquake Engineering, Vancouver, B.C., Canada, Paper No-143*

[2] Genikoumsou & Polak(2014), Finite Element Analysis of a Reinforced Concrete Slab - Column Connection using ABAQUS, *Structures Congress 2014 © ASCE 2014*.

[3] Lee, J., and Fenves, G. L. (1998). "Plastic-Damage Model for Cyclic Loading of Concrete Structures." *Journal of Engineering Mechanics*, 124(8), 892-900.

[4] Lubliner, J., Oliver, J., Oller, S., and Onate, E. (1988). "A plastic-damage model for concrete." *International Journal Solids Structures*, 25(3), 299-326.

[5] Roylance (2001), "Finite Element Analysis", Department of material science and engineering, Massachusetts Institute of Technology, Cambridge, MA 02139

[6] ABAQUS (version 6.10), June 2010 "ABAQUS" user's manual.

[7] ACI. "Building Code Requirements for Structural Concrete (318-99) and Commentary (318R-99)." *American Concrete Institute Committee* 318, ACI, Farmington Hills, Michigan, 1999.

CICM 2015
First International Conference on
Advances in Civil Infrastructure and Construction Materials
MIST, Dhaka, Bangladesh, 14–15 December 2015

A PARAMETRIC STUDY ON THE BUCKLING AND POST-BUCKLING RESPONSE OF X100 UOE PIPES UNDER AXIAL COMPRESSION, BENDING MOMENT AND INTERNAL PRESSURE

Syeda N. Sharmin[1], Sabiha Sharmin[2], Celal Cakiroglu[3] and Kamrul Islam[4]

[1, 2, 4] Department of Civil Engineering, Military Institute of Science and Technology, Dhaka, Bangladesh. Email: [1]syedanusrat_27@yahoo.com

[3] Department of Civil and Environmental Engineering, University of Alberta, Edmonton, Canada. Email: cakirogl@ualberta.ca

Abstract. *Resistance due to the high operating pressure and deformability under different environmental effects, high strength steel (HSS) pipeline has the greater preference to transmit the natural gas or oil. The use of HSS pipe is increasing for its weight and cost reduction benefit. The UOE forming processes are commonly used for manufacturing pipes, where plastic deformation of pipe material is induced, generally results in initial geometric imperfections during manufacturing process. This study includes material anisotropy and geometric imperfection concurrently. It investigates the buckling and post buckling response of HSS pipes under different load combination. The geometric imperfections due to different Diameter/thickness ratios are incorporated in the finite element models consist of material anisotropy. This parametric study is conducted to investigate the influence of the internal pressure, wall thickness, pipeline diameter and axial compression on the local buckling response. The peak moment increased with decreasing pressure and for larger diameter to thickness ratio it secured higher value. The directional sensitivity of buckling has also been observed from the finite element models.*

Keywords: High strength pipelines, Geometric imperfection, Critical buckling strain, Local buckling

1 INTRODUCTION

In recent competitive era of sustainability, the use of natural resources in a steady level is a burning issue. The demand of exploitation and extraction of natural resources (like- gas, oil etc.) is increasing in a higher rate in different regions throughout the world. The price of fossil fuel has increased with the increase in their demand. At these consequences, the exploration of energy reserves in the sub-Arctic regions of North America has become an economically beneficial option. Accordingly, this industry has now an influential contribution to the Canadian economy. These industries generally account for exploration, extraction and transportation of oil and gas. For this buried pipelines are cheap and efficient form of transportation from the source to the point of consumption.

Due to the harsh geo-environmental conditions in the sub-Arctic regions, buried pipelines have to pass through regions of discontinuous permafrost. They are subjected to differential settlements, local buckling due to seasonal cyclic freeze-thaw phenomenon. The differential settlements impose bending stresses on pipe segments in addition to the stresses induced by internal and external pressure and differential temperature. These induced stresses are often responsible for pipeline failure. In current years, the use of high strength steel (HSS) pipes has increased due to its cost reduction benefits [1]. Manufacturers are able to produce grades as high as X80, X100, X120 which have Specified Minimum Yield Strength (SMYS) of 80 ksi, 100 ksi, and 120 ksi respectively. The use of higher steel grades has lighter pipe segments with higher diameter to thickness ratio as compared to normal grade steel pipes. The high strength large diameter pipes are generally manufactured by the UOE forming process. UOE is a cold forming process, where thin steel plates are first deformed into a U shape (U-forming), mechanically pressed in to an O shape (O-forming), and finally, expanded (E) into a cylindrical pipe segment. It has been found previously that the UOE forming process leaves the pipes with material, as well as geometric imperfections [2].

HSS pipes show anisotropic behavior in plastic range, while normal strength pipes show isotropic behavior in both elastic and plastic range [3, 4]. The specimens taken from longitudinal direction show different stress strain response compared to those taken from the circumferential direction. The yield stress in the circumferential direction is higher than that in the longitudinal direction. The circumferential stress strain curve shows a distinct yield point, while the longitudinal stress strain curve has a more round shape and generally lies below the circumferential stress strain curve. It was demonstrated that anisotropic behavior of HSS pipes can be modeled using a yield surface translation in the stress space [5]. During the expansion stage in the manufacturing process, the yield center moves in the stress space in the direction of increasing stress, i.e., the circumferential direction. Upon unloading and reloading, the yield point is expected to be higher than the original plate material in the circumferential direction, and lower in the longitudinal direction. Combined isotropic / nonlinear kinematic hardening mod-

el showing the plastic anisotropy of HSS pipes accurately were successfully introduced [5]. Virgin material curve from the available experimental stress strain data were approximated and the material parameters for the back-stress evolution laws were calibrated through optimization. To develop material model into Finite Element Analysis (FEA), software- like ABAQUS was used. The variation of wall thickness of pipe has larger effect on buckling than that of variation in radius [2]. Previously the moment rotation relations in case of wall thickness variation, radius variation in pressurized and unpressurized condition have already been showed.

The purpose of the current study is to develop finite element (FE) models of HSS pipelines using an advanced nonlinear material model like *Chaboche* model to investigate the upheaval buckling and local buckling response under the combinations of various loads. The developed FE models include both material and geometric nonlinearities. Results obtained from the FE analyses are compared against the available test results to fine tune the models.

2 HSS PIPES AND UOE FORMATION

In UOE developing process, a steel plate is first bent into a U shape, and then a press is created to convert the U shape into an O shape. After that plate is welded in the along longitudinal direction, and expanded in the circumferential direction. This process (expansion) induces 2% circumferential plastic strain. When a UOE formed HSS pipe is loaded in the circumferential direction, its yield point will be higher than the original plate material. When loaded in the longitudinal direction, its yield point will be lower than that of the original plate material. This is a result of strain hardening and Bauschinger effect, typically exhibited by elastic-plastic material subjected to cyclic loading.

3 DEVELOPMENT OF NUMERICAL MODEL

The objective of this study is to investigate the upheaval buckling and local buckling response under the combinations of internal pressure, bending moment and axial compression. In order to achieve the highlighted objective, a finite element (FE) model has been developed which considers all possible nonlinearity effects. The ABAQUS (ABAQUS 6.13.1) program has been chosen for this analytical work, as it possesses features essential for simulating post-buckling response of line pipe. In this program, finite element method (FEM) allows to model discontinuities, such as cracks, along an arbitrary, solution-dependent path during an analysis. This method has been also extended to support the application of distributed pressure loads to the cracked element surfaces, which makes the analysis more realistic. Its element library includes a certain element type which is capable of accounting for large displacement, large rotation, and initial imperfections [12]. The numerical development of a pipe segment includes appropriate selection of element type, element mesh generation and optimization, proper boundary

and loading conditions, material properties, and solution scheme. There is also significant improvement in the run time performance.

3.1 Element Selection

The element development formulation was based on finite-membrane-strain formulation. For the development of the present numerical model, 4-noded quadrilateral doubly curved general purpose shell elements were used with reduced integration. Each node of these shell elements has translational and three rotational degrees of freedom.

3.2 Geometrical Parameters

In recent years, the use of high strength steel (HSS) pipes has increased due to its cost reduction benefits [1]. Manufacturers are able to produce grades as high as X80, X100, X120 which have Specified Minimum Yield Strength (SMYS) of 80 ksi, 100 ksi, 120 ksi respectively. Kainat et al. (2013) used X100 with wall thickness 14.275 mm & outer dia 1067 mm whereas Nupane et al.(2012) worked on X100 pipe of 762 mm OD and 12.7 mm wall thickness. Arman et al.(2011) used for his research NPS16 (X60) ,NPS20 (X65) and also referred the experimental work of Das et al.(2002) on NPS12. Ali Fathi et al.(2012) used X80, X100,X120 grades to continue his research. From these studies the following geometrical specifications is chosen for current numerical model shown in Table 1.

Table 1: Geometric Properties of Element

Steel Grade	**X100**	
Nominal Outside Diameter (O.D.) *(mm)*	762	610
Nominal Wall Thickness, t(*mm*)	12.7	15.1
Length *(mm)*	2613	2613
Diameter/thickness ratio	60	40.4
Length/Diameter ratio	3.4	4.3

3.3 Material Modeling

The material model is assigned to a 3D cylindrical shell representing pipe of 762 mm and 610 mm OD, along with the initial conditions simulating the expansion process. The cylinder is then loaded in the longitudinal and circumferential directions by applying axial compression and internal pressure separately. Two material models are studied here. One is for Fredrik-Armstrong model, another is Chaboche model. The material models are assigned to a pipe of different OD and

wall thickness. The moment-rotation responses of the pipes are then observed. The moment-rotation curves from FEA results are shown in Figure 1 and 2.

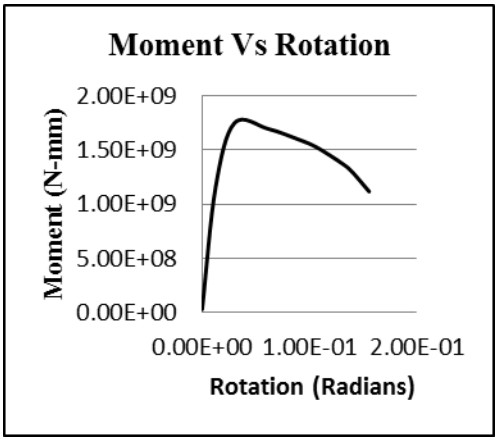

Figure 1: Pressurized condition

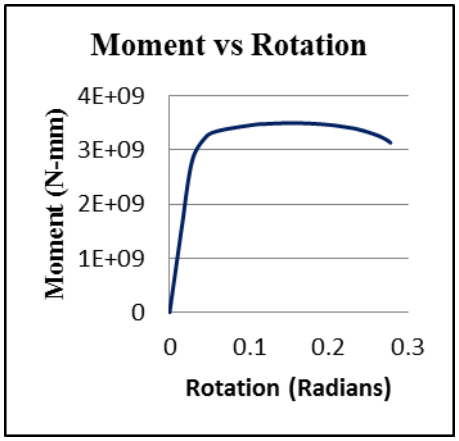

Figure 2: Unpressurized condition

3.3.1 Kinematic Hardening Laws

Kinematic hardening laws like- Armstrong-Frederick law and Chaboche law which could be calibrated using uniaxial tension test data in both longitudinal and circumferential direction were used here. The Armstrong-Frederick law contains two material parameters expressed as C and ɣ which can sufficiently describe the backstress evolution. The Chaboche law is considered as the extension to the Armstrong-Frederick law and holds sets of material parameters C and ɣ.

In this work sets of data for two existing pipes were used and those sets could accurately predict the behavior of the pipe specimens in the longitudinal direction.

4 RESULTS

18 different pipe models are developed to observe the effects of geometric imperfections using different material models. The length of the pipe is taken 2613 mm. S4R shell elements are used for the pipe model. Mesh size is selected as 40 mm by 40 mm. The pipe is fixed at one end, and a concentrated rotation is applied at the other end. Pipes are analyzed for unpressurized and pressurized conditions. For pressurized condition, a uniform internal pressure is applied that corresponds to a Hoop stress of 80% of SMYS. Riks method is applied to solve the non-linear buckling analysis due to applied rotation at one end.

From the moment-rotation curve for each case, the peak moment and the corresponding end rotation are observed, which signify the onset of buckling due to

pure bending (figure-1 and figure-2). The typical buckling shapes for pipes with and without internal pressure are shown in Figure 3 and Figure 4.

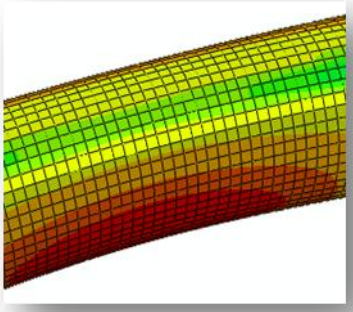

Figure 3: Typical Buckling mode for unpressurized pipe

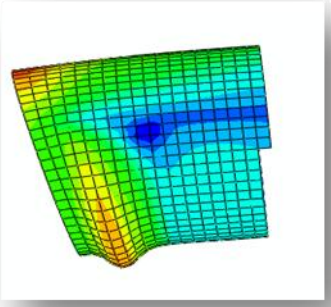

Figure 4: Typical Buckling mode for pressurized pipe

4.1 Effects of Geometric Imperfection on Moment-Rotation Relationship

Different pipe models are developed to observe the effects of geometric imperfections using different material models. The length of the pipe is taken 2613 mm. S4R shell elements are used for the pipe model. Mesh size is selected as 40 mm by 40 mm. The pipe is fixed at one end, and a concentrated rotation is applied at the other end. Pipes are analyzed for unpressurized and pressurized conditions.

Two material models are studied for comparison. One is for Fredrik-Armstrong model, as discussed previously, another is Chaboche model. The material models are assigned to a pipe of different OD and wall thickness. Therefore, the different responses obtained from these pipes are solely due to the effect of different material models. The moment-rotation responses for different materials are shown in figure 5 and figure 6.

5 DISCUSSION

From the moment rotation responses pertaining to different material and geometric models, it is observed that, the mode of buckling is different for pressurized and unpressurized pipes. Unpressurized pipes have higher peak moment and end rotation values for all cases compared to pressurized pipes. Unpressurized pipes buckle inward at mid length, while pressurized pipes buckle with outward protuberance at the end where rotation is applied. These modes are termed diamond mode and bulge mode respectively, and are typical to unpressurized and pressurized pipe buckling.

The pipe wall thickness variation models suggest that the behavior of the pipe is sensitive to the direction of the applied rotation/moment. For unpressurized condition, the peak moment and end rotation values are reduced by 2.83% and

8.23% respectively from the constant radius model. For pressurized condition, the reductions are 3.304% in peak-moment and 4.46% in end rotation.

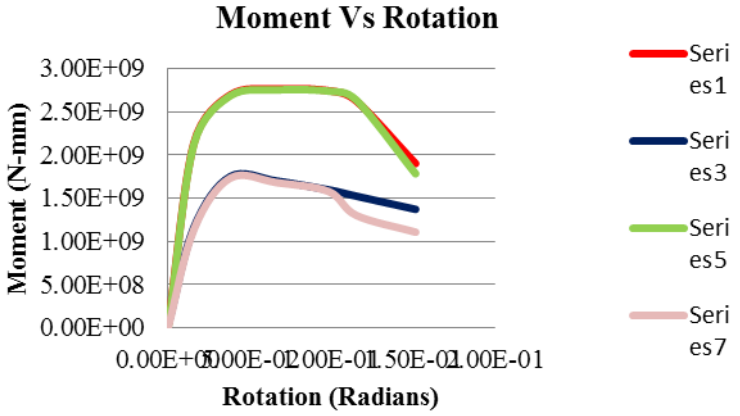

Figure 5: Moment-rotation response for pressurized pipe

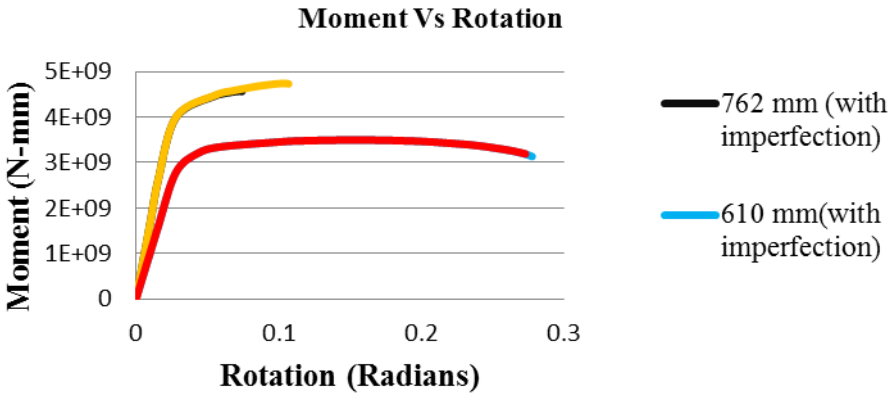

Figure 6: Moment-rotation response for unpressurized pipe

6 CONCLUSIONS

This study successfully showed the effects of geometric imperfections on the buckling response of X100 UOE pipes. From the analysis results, it is concluded that, geometric imperfections are bigger issues in X100 UOE pipes.

This study was limited to X100 pipes with two different OD and thickness. Further analysis on different pipe sizes can be carried out to capture the full picture regarding the effects of imperfection. This study was limited to modeling

anisotropic model. The development of ovalization due to pipe bends and their corresponding effects were beyond the scope of this study.

REFERENCES

[1] Hillenbrand, H-G., Kalwa, C., 2002. High Strength Line Pipe for Project Cost Reduction, World Pipelines, Vol 2, No 1, 1-9.

[2] Kainat,M., Adeeb,S., Cheng,R., Ferguso,J., Martens,M.,2013,Effects of Material Anisotropy and Geometric Imperfections on the Buckling Response of X100 UOE Pipes – A Finite Element Study, Proc. of CSCE 2013, Edmonton, Alberta, Canada, May 29-June1.

[3] Adeeb,S., Zhou, J., Horsley, D., 2006, Investigating the effect of UOE forming processes on the buckling of line pipes using finite element modeling. Proc. of IPC 2006, Calgary, Alberta, Canada, Sept 25-29.

[4] Fatemi, A., Kenny, S., Sen, M., Zhou, J., Taheri, F., Paulin, M.,2008, Investigations on the Local Buckling Response of High Strength Linepipe, Proc. of IPC 2008, Calgary,Alberta, Canada, Sept 29-Oct3, 2008.

[5] Neupane,S.,Adeeb,S., Cheng,R., Ferguso,J., Martens,M.,2012, Modeling the deformation response of high strength steel pipelines-part I: Material charaterization to model the plastic Anisotropy, Transaction of the ASME, Journal of Applied Mechanics, September 2012.

[6] Neupane,S.,Adeeb,S., Cheng,R., Ferguso,J., Martens,M.,2012, Modeling the deformation response of high strength steel pipelines-part II: effect of material characterization on the deformation response of pipes, Transaction of the ASME, Journal of Applied Mechanics, September 2012.

[7] Das, S., Cheng, J.J.R., and Murray, D.W. 2002. Fracture in wrinkled line pipe under monotonic loading. In Proceedings of the 4th International Pipeline Conference, Sep 30-Oct 3 2002, Vol. B, pp. 1613-1618.

[8] Fathi, A., Cheng, R., Adeeb, S., Zhou, J., Critical Buckling strain in high strength steel pipes using isotropic kinematic hardening, Proc. of IPC 2010,Calgary, Alberta, Canada,Sept27- Oct 1,2010.

[9] Fathi,A., Cheng,R., Effect of cross-sectional strain distribution on the critical buckling strain of energy pipelines, Proc.of ISOPE 2011, Maui, Hawaii, USA, June 19-24, 2011.

[10] Fathi,A., Cheng,R., A parametric study on buckling response of high strength steel pipes with anisotropic material properties , Proc. of IPC 2012 September 24-28, 2012, Calgary, Alberta, Canada.

[11] Fathi A., Cheng J.J.R, Adeeb S., 2010, "Effects of Material Anisotropy on the Buckling Behaviour of High Strength Steel Pipelines", Proceedings of USNCTAM2010,16th US National Congress of Theoretical and Applied Mechanics, June 27 - July 2, 2010, State College, Pennsylvania, USA.

[12] Dorey, A., Murray, D.W., and Cheng, J.J.R, 2006, "Critical Buckling Strain Equations for Energy Pipelines – A Parametric Study", Journal of Offshore Mechanics and Arctic Engineering, 128(3), pp. 248-255.

[13] Fatemi, A., Kenny, S., Sen, M., Zhou, J., Taheri, F., Paulin, M., Parameters affecting the buckling and post-buckling behaviour of high strength pipelines, Proc. of ASME 2009 28th International Conference on Ocean, Offshore and Arctic Engineering, May 31 - June 5, 2009, Honolulu, Hawaii, USA.

[14] Tsuru, E., Agata, J., Nagata, Y., Shirakami, S., Shinohara, Y., Forming and buckling simulation on high-strength UOE pipe with plastic anisotropy, Nippon Steel Technical Report No. 102 January 2013.

CICM 2015
First International Conference on
Advances in Civil Infrastructure and Construction Materials
MIST, Dhaka, Bangladesh, 14–15 December 2015

PARAMETRIC STUDY ON THE MULTI-BODY HYDRODYNAMICS INTERACTION OF LEVEL ICE AND A SEMI-SUBMERSIBLE

A. AHMED[1] and M. A. Hannan[1]

[1, 2] Department of Civil Engineering, National University of Singapore, Singapore.
Email: [1]ceeaziza@nus.edu.sg and[2]ceemah@nus.edu.sg

Abstract. *Floaters in the Arctic region constantly interact with level ice. Thus, hydrodynamic analysis of the isolated floater without accounting for the effect of the level ice is incomplete. This study aims to identify the most important parameters affecting the multi-body hydrodynamic behavior of level ice and a single floater. A standard semi-submersible represents the floater and a range of geometric variations of the level ice strives to simulate the varying nature of the ice environment encountered by the floaters in the Arctic. The findings from this study points towards the major focus areas for subsequent detailed studies. Additionally, this study makes some initial recommendations on the need and means of accounting for level ice in the hydrodynamic analysis of floaters in the Arctic.*

Keywords: Arctic environment, Level ice, Multi-body hydrodynamics, parametric study, Semi-submersible.

1 INTRODUCTION

Large reserves of oil and gas along with melting ice makes the Arctic, the next frontier in the hydrocarbon based energy race. The potential for renewable energy such as wind and wave energy also remains lucrative. To harvest such energy from the deeper region of the Arctic, floating oil and gas platform is the most suitable choice. Such platforms will most likely be able to disconnect in the event of large icebergs or very large multi-year ice floes. However, they will still have to encounter and withstand first year level ice of varying sizes. Such large ice floes will interfere with the hydrodynamic response of the floater. Squire *et al.* [1] studied the ocean wave scattering due to large ice floe. They studied how waves (particularly in the Antarctic) influence the large-scale dynamics, rheology, and thermodynamics of the ice cover. Next, Chwang [2] investigated the subject of interaction hydrodynamics between two floating bodies or between a floating body and an offshore structure. They briefly reviewed the mathematical model based on the energy principle. This model assumes the kinetic energies of an ice floe and the associated added mass to be constant before the impact and converted entirely into work done in crushing the ice floe. Chwang [2] advanced the energy principle by developing general formulation for the hydrodynamic interaction between two bodies with or without rotation based on the Lagrange equations of motion. However, their focus was on the iceberg structure interaction and associated additional added mass resulting from the one associated with the iceberg, another associated with the offshore structure, and the third one associated with the two-body interaction. Such studies point towards the importance of accounting for the presence of large ice floes on the overall hydrodynamic behavior of the floater. However, until now, there is a lack of readily useable values regarding the impact of large level ice sheets on the hydrodynamic response of a floating platform. Foschi*et al.* [3] attempts to provide wave-Iceberg load combination factor to be directly used by practicing engineers.

Current research thus attempts to identify the most important parameters in the multi-body hydrodynamics behavior between a level ice sheet and a semi-submersible. The methodology section defines parameters associated with the selected ice floe and the semi-submersible as well as the range of parameters studied. Subsequent section presents the findings from the investigation and makes recommendations for further research. Final section summarizes the findings and concludes the paper.

2 METHODOLOGY

The work selects a semi-submersible platform as a representative of a floater in the arctic region. The hydrodynamic study assumes the semi-submersible in operating condition where pontoons remain fully submerged in water and only semi columns cross the free surface. Table 1 lists the major dimensions of the platform.

The table also presents the dimensions of the ice floe. A 100 m length x 100 m width and 1 m thick level ice represents a realistic scenario potentially faced by a floater in the Arctic. The linear viscous damping of 9% for the floater bases on the standard practices for such semi-submersibles. The ice floe uses the linear viscous damping of 4%for this study, this vale bases on preliminary study of the individual ice floe hydrodynamics behavior. However, this damping value remains an open research parameter, which warrants further investigations. This paper employs the boundary element based software package 'Hydrostar' to perform the hydrodynamic analysis. Hydrostar [4] is the hydrodynamic software developed in Bureau Veritas since 1991 that provides a complete solution of first order problem of wave diffraction and radiation and the QTF of second order low-frequency wave loads for floating body with or without forward speed in deep water and in finite water depth. This software uses first and second order potential theory of free surface flow to solve the diffraction and radiation computation. Potential theory assumes the fluid as ideal, which implies that the fluid is inviscid and incompressible, hence making it irrotational. Current study varies two parameters, namely, ice floe distance (5, 10, 20 and 40 m) and ice floe orientation (0 and 45 degree), which results in total 8 cases in addition to the standalone semi-submersible case. Table 2 lists the case names along with the varied parameters. Figure 1 shows the panel model of the semi developed in Hydrostar.

Table 1: Particulars of the semi-submersible and level ice

Parameters	Units	Value
Platform pontoon length	M	75
Platform width	M	52
Platform draft	M	12.2
Platform weight	Tonne	17422
Linear viscous damping	%	9
Level Ice length	M	100
Level Ice width	M	100
Level Ice draft	M	0.907
Level ice weight	Tonne	3460
Linear viscous damping	%	4

Table 2: Parameters of studied cases

Ice floe orientation	Ice floe distance			
	5	10	20	40
0	Case 1	Case 2	Case 3	Case 4
45	Case 5	Case 6	Case 7	case 8

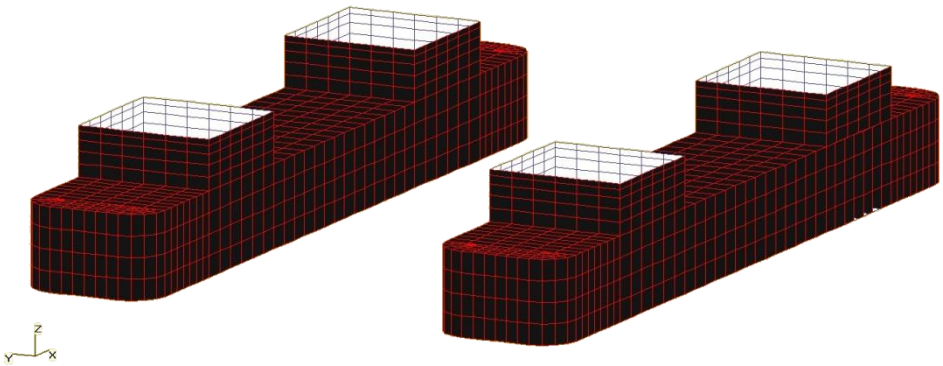

Figure 1: Panel model of the studied semi-submersible simulated in Hydrostar

3 RESULTS AND DISCUSSIONS

This section presents the finding from the parametric study. Figure 2 and 3 present the surge and sway Response Amplitude Operator (RAO) of the floater respectively. These figures also compare these responses with and without the presence of level ice at 10 m distance while the wave direction changes from zero to ninety degrees. The findings from these two figures emphasize the effect of the ice floe on the hydrodynamics response of the floater. The wave direction also becomes significant in the peak values observed in these RAOs.

Table 3 summarizes the findings from all nine cases. It assembles the maximum peak value observed in the RAOs in Surge, Sway, Heave, Roll, Pitch and Yaw directions along with the corresponding frequencies. However, this table only lists the values for a selected wave direction of 60^{o}. The time-periods associated with the highest peak values do not change significantly due to the presence of a large ice floe. Figure 4 plots the variations of maximum peak value with respect to the ice floe distance from the floater. It also compares the effect of ice floe orientation.

Figure 4 accentuates the effect of these parameters on the RAOs by displaying the ratios of the highest peak values against standalone semi-submersible response. The smaller ratios in the surge direction indicate that the ice floe deflects the wave energy into two main components. The component along the surge direction deflects parallel to the floater thus leaving the floater unaffected. In this direction, the level ice sheet demonstrates advantageous shielding effect. On the other hand, the level ice deflects another component of the wave energy along the orthogonal direction, thus amplifying the response of the floater along the sway direction. Similar worsening phenomenon remains visible along the pitch behavior too.

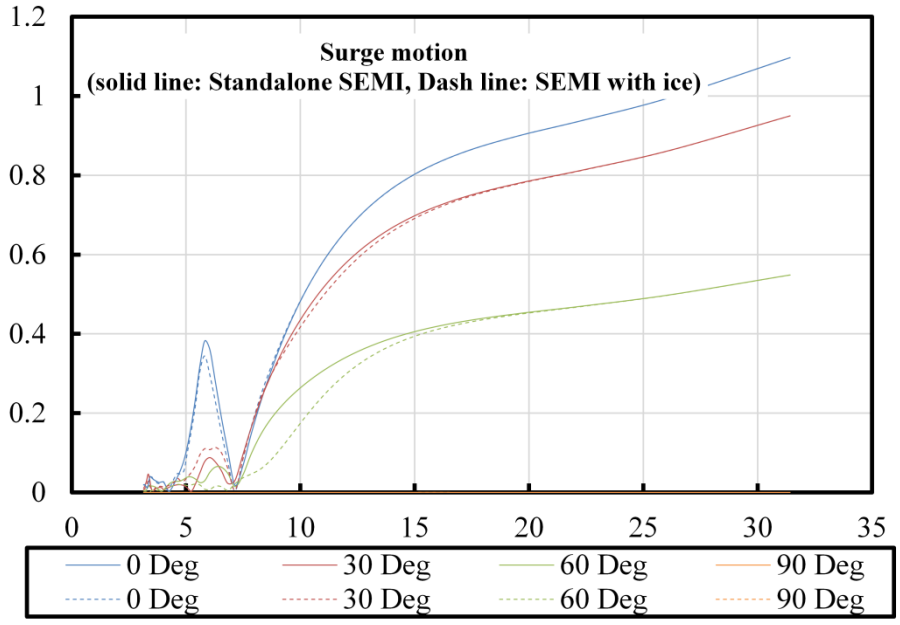

Figure 2: Comparison of surge Rao for the semi-submersible with and without the level ice at 10 m distance

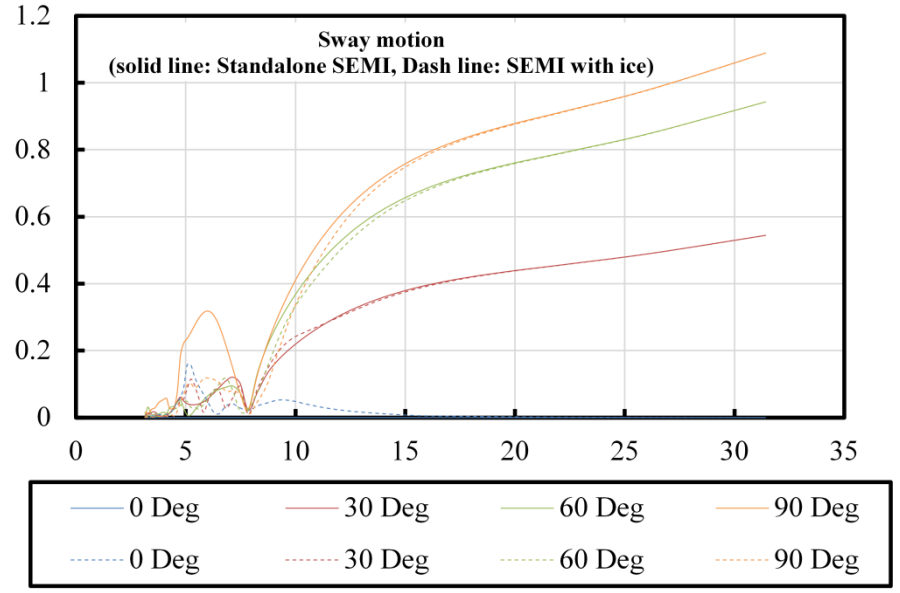

Figure 3: Comparison of sway Rao for the semi-submersible with and without the level ice at 10 m distance

Based on this initial parametric study, current paper identifies following focus areas for further studies,

1. Wave direction
2. Distance between ice floe and the floater
3. Orientation of the ice floe
4. Sway and pitch of the floater

In addition, there are few more parameters, which will benefit the development of a readily useable set of data for practicing engineers planning to simulate the hydrodynamic behavior of a floater in the Arctic.

1. Ice floe dimensions
2. Number of ice floes
2. Relative motion between ice floe and the floater

Table 3: Peak values and associated time-periods at 60^o wave direction

	Surge		Sway		Heave	
	Highest peak	Period	Highest peak	Period	Highest peak	Period
Case 0	0.064	6.3	0.094	7.1	1.825	15.7
Case 1	0.022	7.1	0.125	6.6	1.758	15.7
Case 2	0.022	7.1	0.117	6.8	1.802	15.7
Case 3	0.026	5.1	0.094	6.3	1.808	15.7
Case 4	0.040	5.1	0.134	6.6	1.807	15.7
Case 5	0.034	5.1	0.086	6.8	1.783	15.7
Case 6	0.036	5.1	0.081	6.6	1.795	15.7
Case 7	0.039	5.1	0.087	6.6	1.801	15.7
Case 8	0.045	5.1	0.076	5.1	1.803	15.7
	Roll		Pitch		Yaw	
	Highest peak	Period	Highest peak	Period	Highest peak	Period
Case 0	1.046	8.3	0.470	9.8	0.405	6.0
Case 1	0.805	9.2	0.353	12.1	0.180	5.8
Case 2	0.791	9.8	0.362	12.1	0.167	5.8
Case 3	0.780	9.8	0.373	12.1	0.191	5.8
Case 4	1.067	8.3	0.391	11.2	0.213	5.6
Case 5	0.790	7.5	0.421	10.5	0.165	6.6
Case 6	0.766	7.9	0.424	10.5	0.171	6.6
Case 7	0.941	8.3	0.430	10.5	0.185	6.3
Case 8	0.958	8.7	0.437	10.5	0.233	6.0

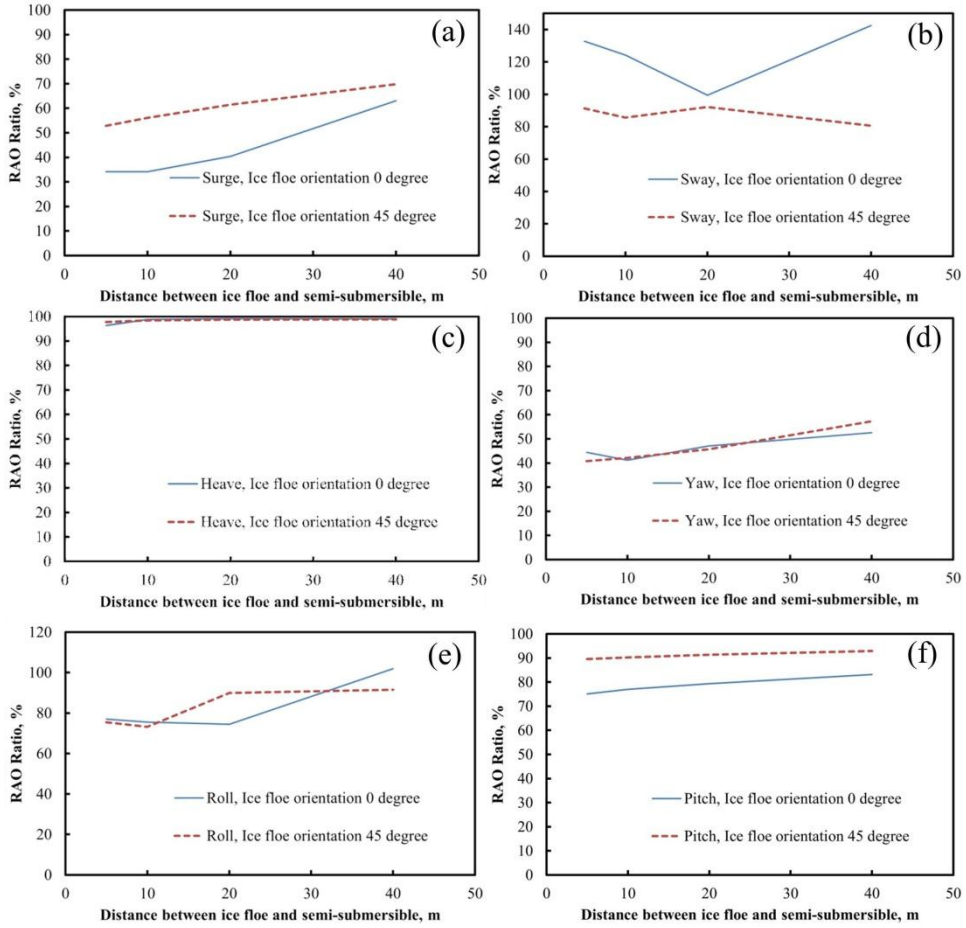

Figure 4: Comparison of max peak value of Rao against the distance and orientation of ice floe for the vessel motion component of (a) surge (b) sway (c) heave (d) roll (e) pitch (f) yaw

4 CONCLUSIONS

This paper presents a multi-body hydrodynamic study of level ice sheet and a semi-submersible. Current investigation focuses on the effect of distance between the level ice and the floater and the orientation of the ice floe. In total nine cases, examine the influence a 100 m x 100 m ice floe has on a 75 m x 52 m semi-submersible in terms of its six motion raos. Current investigation aims to narrow down the major focus areas while accounting for level ice in the hydrodynamic analysis of floaters in the Arctic for further study. The above study supports the following conclusions:

- The impact of a near field ice floe on the hydrodynamic rao of the floater is very significant; it can diminish the RAOs in some direction while enhancing the RAOs in other directions.
- The most important parameters are wave direction, ice floe distance, ice floe orientation. The most enhanced responses were the Sway and pitch.
- Future studies must include investigates the effect of ice floe dimension, a multiple number of ice floes and the relative motion between the ice floe and the floater.
- The complete parametric study coupled with a reliability-based analysis of the finding will provide the practicing engineers with useful factors to account for the effect of level ice interaction in hydrodynamic behavior of the floater without necessitating detailed multi-body hydrodynamics study.

REFERENCES

[1] V.A. Squire, J. P. Dugan, P. Wadhams, P. J. Rottier, A. K. Liu, 1995. Of Ocean waves and sea ice. *Annu. Rev. Fluid Mech* 1995, 27:115-68

[2] A.T. Chwang,2003.Interaction Hydrodynamics of two Bodies, Thirteenth (2003) International Offshore and Polar Engineering Conference, Honolulu, USA.

[3] R.Foschi, M. isaacson, N. Allyn, I. Saudy, 1998.Assessment of the Wave-Iceberg Load Combination Factor, *International Journal of Offshore and Polar Engineering*, Vol 8, No 1.

[4] Hydrostar, http://www.veristar.com/

CICM 2015
First International Conference on
Advances in Civil Infrastructure and Construction Materials
MIST, Dhaka, Bangladesh, 14–15 December 2015

SEVERE WAVE INDUCED CHARACTERISTICS OF DEEP WATER COUPLED FLOATING SPAR PLATFORM

Mahmudur R. SOEB[1], **A. B. M. Saiful Islam**[2], **Mohd Z. B. Jumaat**[3] **and Md. N. Huda**[4]

[1, 2, 3, 4] Department of Civil Engineering, University of Malaya, Kuala Lumpur, Malaysia.
Email: [1]soeb_buet@yahoo.com, [2]abm.saiful@gmail.com, [3]zamin@um.edu.my
and[4]nazmulhuda.128@gmail.com

Abstract. *Due to the cost effectiveness and productiveness in deep water investigation, floating structures are of great interest during a few decades. Spar platform has been seen as a latest and productive alternative amongst the floating platform categories. Exact conduct of completely coupled activity in deeper water is yet an extraordinary issue to be forecasted at real ocean environment. Nonlinear finite element (NFE) analysis for completely coupled 3D model of floating spar platform structure is an affluent appliance to conjecture the responses, where primary assemblage of Spar platform and mooring lines are considered in a joined compact coupled system. Thusly, the purpose of this paper is to examine the wave induced characteristics of newly modelled moored Spar platform under regular sea environment. The numerical simulation and motion investigations are completed with the commercial finite element (FE) package ABAQUS/AQUA. This moored Spar model is further precise to hold continuity of the structure and boundary conditions, loadings taking all the nonlinearities. Considering the coupling impacts of the platform and its mooring system, hydrodynamic examinations of a moored Spar has been done in time domain. Hydrodynamic properties are legitimately characterized. The wave induced effects have been evaluated and discussed here to investigate their interaction with the floating spar platform.*

Keywords: Spar platform, Deep-water, Coupled, Severe wave, Time domain.

1 INTRODUCTION

Oil and gas are the most widely used forms of energy that the world has ever known. The petroleum industry's expansion into the seas and oceans of the world has become unavoidable. Fixed and other platforms are costly and sometime not efficient at deep sea exploration. Floating structures [1] are now using for the production of oil and gas in various places of the world. Spar platform is the latest and advanced complaint offshore floating structure in deep and ultra-deep water. There are many spar platforms that have already been placed worldwide and they are very efficient and successful in deep water oil and gas [2]. The consequence of mooring lines on spar platform becomes more significant with development of water depth. Many researchers have done their investigation on coupled analysis between a floater and its mooring line [3-5]. Coupled dynamic analysis was developed by Ran and Kim [6] to assess wave loads on tethered Spar. Quasi-static approach (SMACOS) and coupled dynamic approach (COUPLE) was used by Chen et al. [7] to disclose coupling effects between floating spar and its mooring lines, where numerical program CABLE3D used to calculate dynamic of moorings. Differential equation was also established to calculate coupled effect on spar and its mooring lines [8]. Nonlinear coupled response analysis have been addressed for Spar [9, 10] and TLP [11] type floating structures. Ran et al. [5] studied coupled dynamic response of floating moored spar in haphazard waves, investigated both in time and frequency domain.

The objective of this study is to analyze a fully coupled spar platform subjected to severe wave forces under regular wave loading. This coupled spar mooring integrated system can be used to perform damping effects analysis of mooring lines and to obtain the coupled responses.

2 METHODOLOGY

2.1 Model of floating spar platform

In this study a floating spar platform is selected which is consist of three major part and they are spar hull, mooring line and sea bed. The properties of the spar mooring system and hydrodynamic characteristics are given in Table 1. The spar hull is modelled as rigid beam and it is connected at fair lead position and seabed by mooring lines. The spar platform has been connected to the mooring lines by means of six springs (Three for translational as surge, sway, heave and three for rotational as roll, pitch and yaw).Seabed is modelled such as the mooring lines will not penetrate the seabed. The contact is modelled as surface to surface and frictionless. The integrated spar hull and mooring line (Figure 1) have been modelled in finite element code ABAQUS [12].

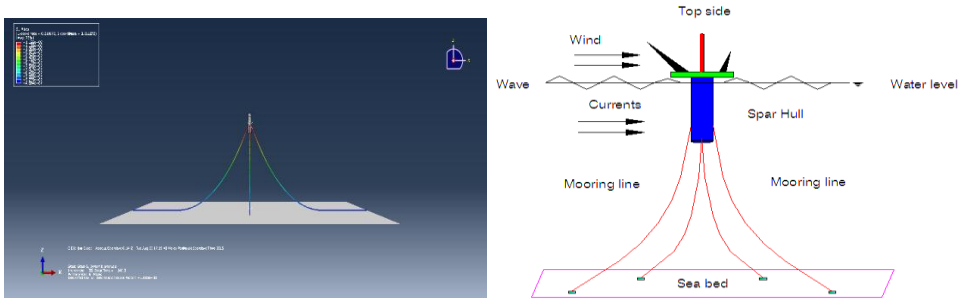

Figure1: Model of spar hull and sketch with mooring lines

The analysis of spar platform is possible using finite element method where considering actual bodily coupling between the rigid floating spar hull and mooring line. The ABAQUS/AQUA[12]module is efficient of simulating the hydrodynamic loading because of severe wave.

Table 1:Properties of Spar Model [3]

	Main particular	Properties	Hydrodynamic Coefficient
Spar	Length	213.044 m	Drag coefficient: 0.6 Inertia coefficient: 2.0 Added mass coefficient: 1.0
	Diameter	40.54 m	
	Draft	198.12 m	
	Mass	2.592×10^8 kg	
	Centre of gravity	92.14	
Mooring lines	No. of moorings	4	Drag coefficient: 1.0 Inertia coefficient: 2.2 Added mass coefficient: 1.2
	Length	2000 m	
	Mass	1100 Kg/m	
	Pre-tension	1.625E7 N	

All non-linearities are properly considered because of variable submergence, added mass, damping, contact of mooring line and seabed, and forces on the structure in analysis to show the damping effects of mooring lines and the importance of coupling effects. In addition, the participation of mooring lines in the overall response of the structure when wave forces act on the entire structure was well described. Alterable boundary conditions due to sea bed point were also properly assimilated.

2.2 Mathematical Formulation

The model involves solution of Airy wave theory which represents the water particle kinematics to know the drag and inertia. The static coupled problem is solved using Newton's method. Equation of motion has been used over an iterative time-domain mathematical interaction to obtain responses in time histories.

This equation (1) is given here for Spar hull and mooring line combination where this combination is equilibrium among inertia, damping, restoring and exciting forces.

$$[\mathrm{M}]\{\ddot{\mathrm{X}}\} + [\mathrm{C}]\{\dot{\mathrm{X}}\} + [\mathrm{K}]\{\mathrm{X}\} = \{\mathrm{F(t)}\} \tag{1}$$

Where,

$[\mathrm{M}] = [\mathrm{M}]^{\text{structural component}} + [\mathrm{M}]^{\text{Added mass}}$

$[\mathrm{C}] = [\mathrm{C}]^{\text{structural damping}} + [\mathrm{C}]^{\text{Hydrodynamic damping}}$

$[\mathrm{K}] = [\mathrm{K}]^{\text{Elastic}} + [\mathrm{K}]^{\text{Geomatric}}$

$\{\mathrm{X}\}$ = 6 DOF structural displacements at each node

Here, $\{\mathrm{F(t)}\}$ is representing the total force on a spar-mooring system, $\{\dot{\mathrm{X}}\}$ is velocity vector and $\{\ddot{\mathrm{X}}\}$ is acceleration vector. Total mass [M]is concentrated on the CG of Spar hull. Due to the seawater at surrounding of that spar hull there will be arise added mass. There are two parts of stiffness matrix [K], one is elastic stiffness matrix and another one is geometrical stiffness matrix. Other side, Damping [C] is considered as structural and hydrodynamic damping. Maximum damping here is happened because of hydrodynamic effects.

The motion equation (2) for the moored sparis as bellow:

$$\begin{aligned}[\mathrm{M_s} + \mathrm{M}(\infty)]\ddot{\mathrm{X}}(t) + \int_{-\infty}^{\mathrm{t}} \mathrm{C}(t-\tau)\dot{\mathrm{X}}(t)d\tau + \mathrm{b}^{WD}(t)\dot{\mathrm{X}}(t) + \mathrm{KX}(t) \\ = \mathrm{F}_w^{(1)} + \mathrm{F}_w^{(2)} + \mathrm{F}_{HSn} + \mathrm{F}_e + \mathrm{F}_M\end{aligned} \tag{2}$$

The steady forces functioning on the rigid hull, comprising the inertia and drag force through Morison equation including added mass. The force on mooring line F_M is captured in the coupled action in consistent manner. Where, $\mathrm{F_{Hsn}}$= nonlinear restoring forces, Fw = wave exciting force, Ms= 6x6 mass matrix, $\mathrm{M}(\infty)$ = added mass matrix and K = Hydrostatic Stiffness matrix.

3 RESULTS AND DISCUSSION

For assessing the response characteristics under severe environments, unidirectional regular wave models of the selected sea state has been used to compute the incident wave kinematics following the appropriate wave theories and Morison's equation. The sea state is critical as both the wave height (11.15 m) and wave

period (10.69 second) are severe mentioned as sea state S5 [13]. The responses in terms of surge, heave, pitch and mooring line tension are evaluated. Following sections discuss the time histories of structural responses.

3.1 Surge motion of spar at platform level

The wave induced time series of surge response due to severe sea environment at the deck level of the floating spar platform have been evaluated here. The peak of surge response at deck level for severe sea environment ranges from +14.90 m to -9.63 m and it is predominantly periodic as shown in (Figure 2). Pitch motion occurs simultaneously with surge. Surge response needs large amount of energy input due to large inertia. Nevertheless, pitching motion occur concurrently when surge gets excited. The surge motion at the platform level is controlled by the pitching motion of the spar with trivial excitation of surge mode. It happens because of the coupling of surge and pitch. Influence of non-linearity is not very strong on spar hull surge response.

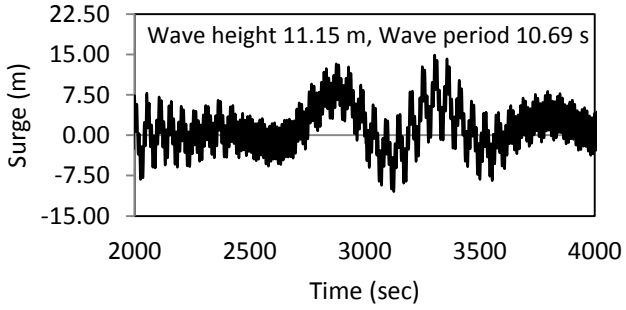

Figure 2: Surge at regular wave at platform level

3.2 Heave motion of spar at Platform level

Mooring Tension and other operations are influenced by spar hull heave responses. The heave motions under regular wave for severe sea environment are shown in (Figure 3). The heave response maximum peak touches to 0.52 m in case of wave loading for severe sea environment case. At 2200 sec the maximum peak occurs and after that the heave response decrease gradually for severe sea environment case. Additionally the downward translation of the Spar hull stretches to negative crest of 0.54 m. The time history again experiences a large peak at 3330 sec wave loading. The heave response fluctuates showing large average values after 2000 sec than earlier. After 3750 sec steady state is attained.

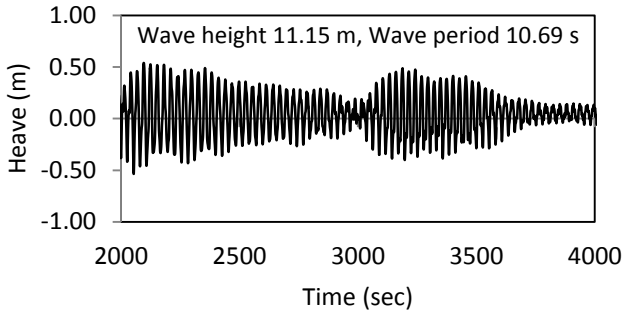

Figure 3: Heave at regular wave

3.3 Pitch motion of spar at platform level

The rotation behaviors of spar hull subjected to sea wave are illustrated in (Figure 4). The history output of pitch responses shows regular fluctuations initiating for zero up to peak of ± 0.06 rad. Theses peaks of two cases occur at different time station. The steady state is observed at around 3750 sec of wave loading. Significant value of pitch response leads to a momentous surge at deck level. It is coupled with the surge of rigid hull which otherwise is of small magnitude but gets enhanced due to pitch input. This is why the surge time series shows maximum peak at pitch frequency. Since the surge response is directly related to the pitch responses, the responses are regular in fashion. This pitching motion occurring with surge gets excited easily. Effect of non-linearity alters the pitch motion response.

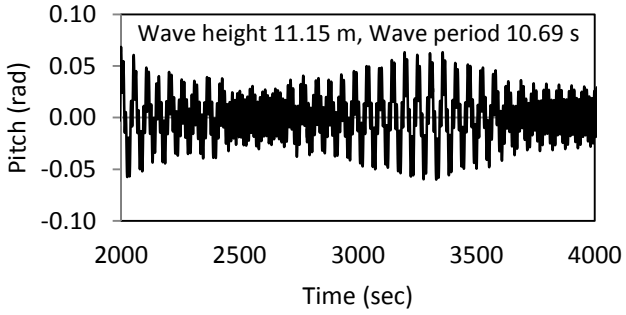

Figure 4: Pitch at regular wave

3.4 Top tension in mooring line

Critical responses of mooring lines play an important role in the coupled dynamic analysis of the Spar Platform. The regular wave loads simultaneously act on the hull and mooring lines. The designed pretension in each mooring line of the pre-

sent problem is 1.625E7 N as mentioned earlier. Mooring line shows the regular behavior of tension under severe sea environment (Figure 5). Surge response also causes increase in tension. Mooring line positioned in the direction of wave propagation experiences maximum top tension to support surge in the forward direction. For mooring tension at regular wave periodic behavior is governed. The top tension is quite regular in nature in longer time. It is also noted that for severe sea environment the magnitudes of regular peaks are close the maximum value 1.72E+07 N. Nevertheless atypical peaks show around 1.70E+07 N tensions in mooring line which is also larger than the usual values. Fluctuations of the time series remind that precise considerations are required for stable structure.

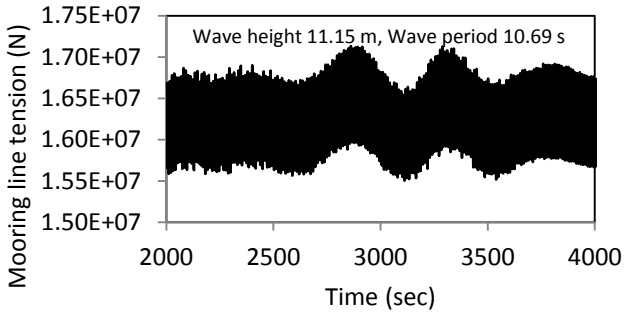

Figure 5: Top tension in mooring line at regular wave.

4 CONCLUSION

- Presented coupled analysis approach for Spar platform includes computational savings to forecast responses maintaining acceptable accuracy rather than the difficult experimental work.
- The coupled deep water Spar model maintains the structural regularity and captures the coupling of Spar-mooring and seabed-mooring interaction. It is expected to greatly promote operations in deep sea exploration.
- Rigid body resonant motions influence the dynamic motion responses of Spar and the responses are periodic in nature.

ACKNOWLEDGEMENT

The authors gratefully acknowledge University of Malaya (UM) and the Fundamental Research Grant Scheme (FRGS), FP004-2014B Ministry of Education, Kuala Lumpur, Malaysia for supporting this research work.

REFERENCES

[1] A. J. Hillis and C. Courtney, "Structural health monitoring of fixed offshore structures using the bicoherence function of ambient vibration measurements," *Journal of Sound and Vibration*, vol. 330, pp. 1141-1152, 2011.

[2] A. Agarwal and A. Jain, "Nonlinear coupled dynamic response of offshore Spar platforms under regular sea waves," *Ocean engineering*, vol. 30, pp. 517-551, 2003.

[3] X. Chen, J. Zhang, and W. Ma, "On dynamic coupling effects between a spar and its mooring lines," *Ocean Engineering*, vol. 28, pp. 863-887, 2001.

[4] M. Kim, Z. Ran, and W. Zheng, "Hull/mooring coupled dynamic analysis of a truss spar in time domain," *International Journal of Offshore and Polar Engineering*, vol. 11, 2001.

[5] Z. Ran, M. Kim, and W. Zheng, "Coupled dynamic analysis of a moored spar in random waves and currents (time-domain versus frequency-domain analysis)," *Journal of Offshore Mechanics and Arctic Engineering*, vol. 121, pp. 194-200, 1999.

[6] Z. Ran and M. Kim, "Nonlinear coupled responses of a tethered spar platform in waves," *International Journal of Offshore and Polar Engineering*, vol. 7, 1997.

[7] X. Chen, J. Zhang, and W. Ma, "Coupled time-domain analysis of the response of a spar and its mooring system," in *The Ninth International Offshore and Polar Engineering Conference*, 1999.

[8] L. Liu, B. Zhou, and Y. Tang, "Study on the nonlinear dynamical behavior of deepsea Spar platform by numerical simulation and model experiment," *Journal of Vibration and Control*, p. 1077546312472917, 2013.

[9] A. B. M. S. Islam, M. Jameel, S. Ahmad, and M. Z. Jumaat, "Nonlinear response of coupled integrated spar platform under severe sea states," in *ASME 2012 31st International Conference on Ocean, Offshore and Arctic Engineering*, Rio de Janeiro, Brazil, 2012, pp. 559-567.

[10] M. Jameel, S. Ahmad, A. B. M. S. Islam, and M. Z. Jumaat, "Nonlinear dynamic analysis of coupled spar platform," *Journal of Civil*

Engineering and Management, vol. 19, pp. 476-491, 2013/08/01 2013.

[11] C. K. Yang and M. Kim, "Transient effects of tendon disconnection of a TLP by hull–tendon–riser coupled dynamic analysis," *Ocean Engineering*, vol. 37, pp. 667-677, 2010.

[12] Hibbitt, Karlsson, and Sorensen, *ABAQUS/standard user's Manual* vol. 1: Hibbitt, Karlsson & Sorensen, 2001.

[13] A. B. M. S. Islam, M. Jameel, S. Ahmad, M. Z. Jumaat, and V. J. Kurian, "Structural behaviour of fully coupled spar–mooring system under extreme wave loading," *Journal of Civil Engineering and Management*, vol. 19, pp. S69-S77, 2013/12/19 2013.

CICM 2015
First International Conference on
Advances in Civil Infrastructure and Construction Materials
MIST, Dhaka, Bangladesh, 14–15 December 2015

NUMERICAL STUDY OF SIDE BY SIDE FLOATING AND SUBMERGED FIXED STRUCTURES IN SEA WAVES

M. A. HANNAN[1] **and W. Bai**[2]

[1, 2] Department of Civil and Environmental Engineering, National University of Singapore, Singapore.
Email: [1]ceemah@nus.edu.sg

Abstract. *With the increase of human activities in offshore areas in order to colonize the ocean mostly for space, food and energy; the study of multiple side by side structures in waves is becoming increasingly important. This study focuses on a multi-body wave interactions problem where a fully submerged cylindrical body coupled with a nearby floating barge is numerically simulated using fully nonlinear approach. The main purpose of this study is to provide a deep insight into the influence of the floating barge on the submerged body, from which a possible shielding effect can be identified. Extensive parametric studies are performed to understand the hydrodynamic characteristics of individual structures under various environmental conditions. Comparative conclusions are drawn to summaries the key findings.*

Keywords: Numerical analysis, Floating barge, Submerged structures, Wave interactions, Shielding effect.

1 INTRODUCTION

Mankind nowadays are constantly exploring the offshore regions with greater interests and undertaking challenging activities there. Most of these activities include complex interactions between multiple structures either floating, or submerged or a combination of floating and submerged bodies. As a result, researchers in these areas have also performed a lot of studies to understand the interactions between multiple floating bodies. For example, studies in [1-5] and many more papers discussed about the hydrodynamics of multiple floating bodies and both analytical and experimental as well as numerical analysis are being covered by these studies.

The study of submerged bodies has also received considerable attraction for many years and several papers have been dedicated to the analytical and experimental study of the hydrodynamic response of such submerged structures. Among some recent studies, Chaplin [6] and Conde *et al.* [7] performed some experimental studies to investigate the behavior of submerged cylinder under waves. Besides, Koo *et al.* [8] and Guerber *et al.* [9] developed two dimensional fully nonlinear potential flow model to study the wave interactions with submerged cylinder as well. Hannan *et al.* [10] and Bai *et al.* [11] on the other hand, developed three dimensional fully nonlinear time domain model to study the wave radiation of submerged bodies and wave interaction with submerged structures, respectively.

However, the wave interaction with coupled floating and nearby submerged structures has not been studied extensively yet. Although, several new offshore applications have such kind of coupled floating and submerged bodies, for example, submerged wave energy converter and nearby floating harnessing devices, floating oil storage and nearby submerged breakwater etc. The present study thus aims at studying coupled floating and submerged structures under wave action.

2 MATHEMATICAL FORMULATION AND NUMERICAL IMPLEMENTATION

In the numerical model of present study, the higher-order boundary element method is used to solve the mixed boundary value problem based on an Eulerian description at each time step. The 4th order Runge-Kutta scheme is adopted to update the free water surface boundary conditions expressed in a Lagrangian formulation. To demonstrate the three dimensional wave structures interaction problem, two right-handed Cartesian coordinate systems are defined (Figure 1). One is a space fixed coordinate system *Oxyz* having the *Oxy* plane on the mean free surface and the origin *O* usually at the centre of the numerical tank. In this case, the *z* axis is positive upwards. The other is a body fixed coordinate system with its origin placed at the center of mass of the body. Based on the potential flow theory, the wave–body interaction problem can be formulated in terms of a

velocity potential ϕ(x, y, z, t), which satisfies Laplace's equation within the fluid domain Ω,

$$\nabla^2\phi = 0$$

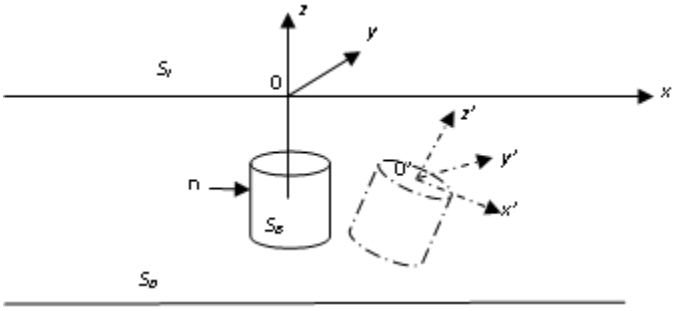

Figure 1: Sketch of problem definition

This is also subject to various boundary conditions on all surfaces S of the fluid domain.

More details of the formulation and numerical implementation of this problem can be found in Hannan and Bai [12]. A rectangular wave tank model as described in [12] is applied to study the various scenarios presented here. A floating barge and a fully submerged truncated vertical cylinder nearby are placed inside the three-dimensional wave tank. Both the barge and submerged cylinder are considered fixed with respect to the global coordinate system. Figure 2 shows the top view of the three cases investigated in this study.

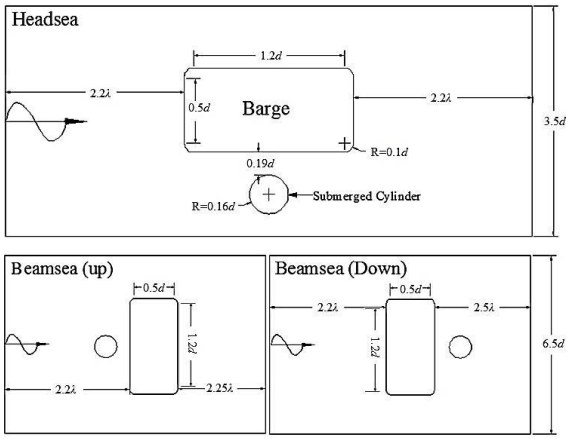

Figure 2: Different numerical model setups with corresponding particulars

In addition to three configurations provided above, some other simple cases (for example, only a submerged cylinder, only a barge in head sea and only a barge in beam sea)are also simulated and output results are compared among all the cases where applicable. The influence of variation of wave maker amplitude and frequency on the hydrodynamic behavior of the coupled floating barge and submerged cylinder system is studied in this analysis. The following section summarizes some of the key findings.

3 RESULTS AND DISCUSSIONS

As mentioned before, several models are developed by considering various scenarios in order to understand this coupled system from different point of view. These are:

a) Single submerged cylinder under wave action (without barge)
b) Single floating barge in head sea (without cylinder)
c) Single floating barge in beam sea (without cylinder)
d) Barge in head sea with submerged cylinder beside it
e) Barge in beam sea with submerged cylinder at upstream side
f) Barge in beam sea with submerged cylinder at downstream side

For all the above cases, the dynamic horizontal and vertical wave forces on floating barge and submerged cylinder, run-ups around the barge and wave elevations at various locations are calculated under various amplitudes and frequencies of the wave maker.

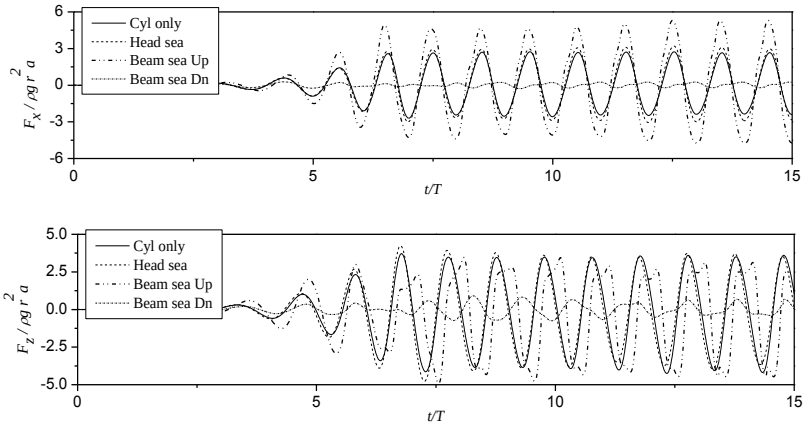

Figure 3: Wave forces on submerged cylinder under various circumstances, (a = 0.02, ω= 2.0). (a) Horizontal dynamic force. (b) Vertical dynamic force.

Among these results, Figure 3 shows the variation of horizontal and vertical dynamic forces acting on the cylinder with respect to time for different scenarios.

The wave maker motion amplitude in this case is a = 0.02. The forces obtained from the head sea scenario seem to be identical with the single cylinder case with a slightly higher crest and trough values at some points. On the other hand, horizontal forces in case of beam sea upstream condition are significantly larger compared to the above two situations and the vertical dynamic forces in this case though generate quite similar amplitudes with head sea and single cylinder case, yet shows significant amount of nonlinearity in the response. This increase in amplitudes and nonlinearity happens due to the presence of floating barge on the downstream side of the submerged cylinder even though the cylinder is situated below the draft level of the barge. The noticeable decrease in force values in case of beam sea downstream analysis is also occurred because of the floating barge. However, this time the cylinder is under the shed of the barge and thus not receiving most of the wave energy.

Comprehensive Fast Fourier Transform (FFT) analyses of the barge and cylinder forces under various situations are also performed to understand the pattern of nonlinearity involved in these cases with the variation of wave maker amplitudes and frequencies. The FFT comparison results for forces acting on the submerged cylinder are plotted in Figures4 and 5, respectively. The notion 'no barge' in these plots represents the scenario of a single submerged cylinder in domain without any barge floating beside it.

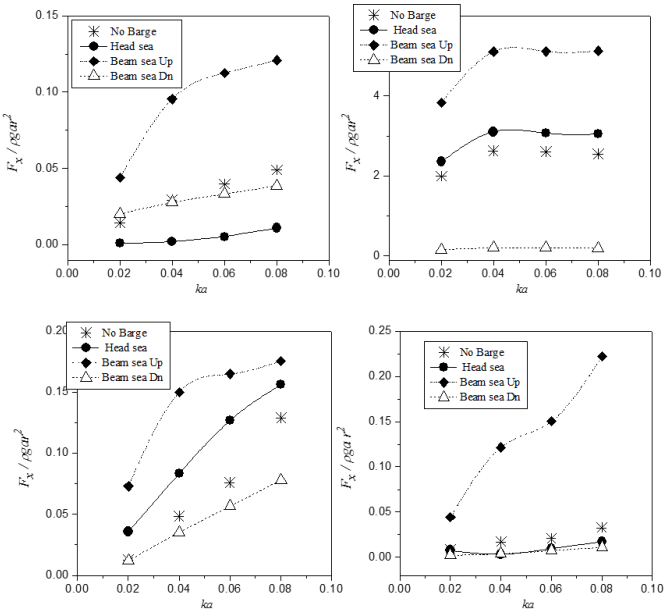

Figure 4: Horizontal force components acting on submerged cylinder (ω= 2.0). (a) Drift force. (b) 1st harmonic. (c) 2nd harmonic. (d) 3rd harmonic.

These two figures clearly reveal that both the surge and heave forces are significantly affected by the presence of barge in beam sea upstream situation. Force components on submerged cylinder in head sea configuration. However, this seems to be not much affected by the floating barge especially the vertical force components. Moreover, the beam sea downstream scenario produces the least responses for both the first order components and also for the mean of vertical force. Most of the forces acting on the downstream cylinder seem to be of 2nd order and the decreases in mean and 1st order components in this case can be attributed to the location of the barge in beam sea position before the cylinder. It is also noticeable from these two figures that 3rd harmonic of both the horizontal and vertical dynamic forces are very small for all the scenarios except for the beam sea upstream condition.

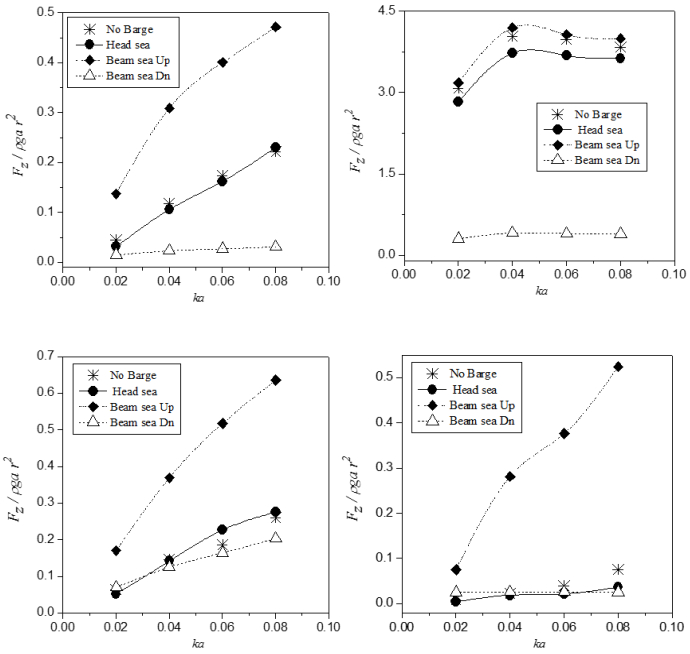

Figure 5: Vertical force components acting on submerged cylinder (ω= 2.0). (a) Drift force. (b) 1st harmonic. (c) 2nd harmonic. (d) 3rd harmonic.

Similar investigations are performed for forces acting on the floating barge. Besides, the influence of change of wave maker motion frequencies is also studied, although not presented in this paper due to space limitation.

Figure 6 provides snapshots of the free surface profiles captured at various time instant along the simulation period after a fully developed state is reached. The waves here are propagating from the left end of the tank and the damping layer is situated at the far right end side. As can be seen, presence of submerged

cylinder near the barge in head sea creates noticeable disturbance on free surface compared to the other side of the barge.

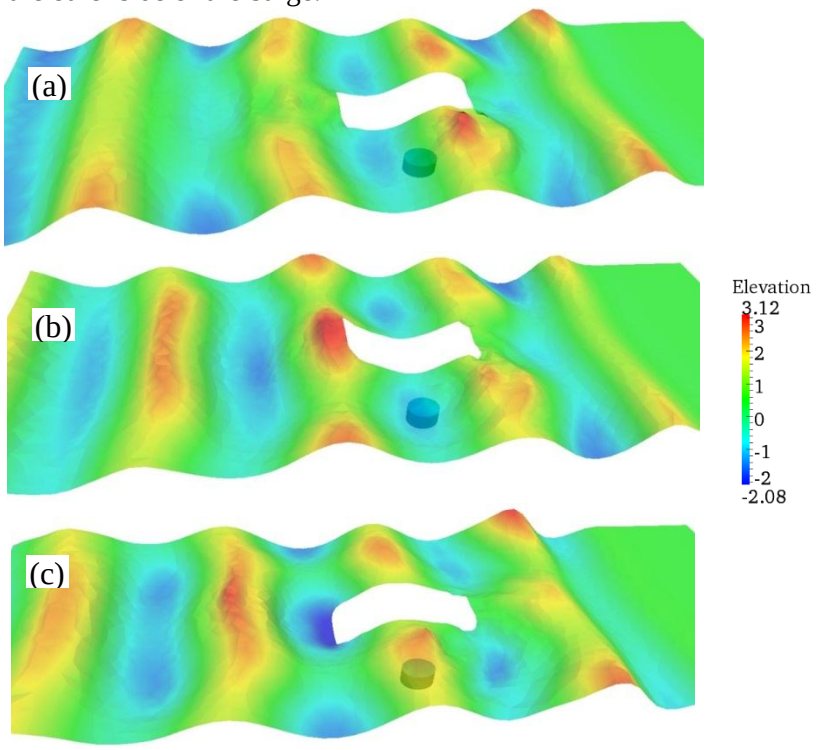

Figure 6: Free surface wave elevation at various time instants: Head sea (a = 0.02, ω = 2.0); (a) t =9.0T. (b) t =9.25T. (c) t =9.75T.

4 CONCLUSIONS

The three-dimensional fully nonlinear wave interaction with coupled floating barge and submerged cylinder system is investigated in this paper, where both the barge and cylinder are considered fixed in space.

- Detailed studies are performed to understand the hydrodynamics of the proposed coupled system. It is found that both the frequency and amplitude of wave maker motion significantly influence the coupled hydrodynamic behavior of floating barge and submerged cylinder system.
- For a fully submerged cylinder located near a barge in head sea, it is found that with the variation of wave maker amplitude the submerged cylinder significantly affects the surge force acting on the barge. A noticeable increase in drag force and higher order components are observed in such case, compared to a single barge in head sea situation.

REFERENCES

[1] M. Ohkusu, 1976. Ship Motions in Vicinity of Structure. *BOSS'76*.

[2] G.V. Oortmerssen, 1981. Hydrodynamic Aspects of Multi-body Systems. *International Symposium on Hydrodynamics in Ocean Engineering*, pp725-743.

[3] J. Newman, 2001. Wave effects on Multi Bodies. *Hydrodynamics in Ship and Ocean Engineering*, **3(26)**.

[4] Y. Choi, & S. Hong, 2002. An analysis of Hydrodynamics Interaction of Floating Multi-Body Using Higher-Order Boundary Element Method. *The Twelfth International Offshore and Polar Engineering Conference, 26-31 May, Kitakyushu, Japan*, pp. 303-308.

[5] S.Y. Hong, J.H. Kim, H.J. Kim&Y.R. Choi, 2002. Experimental Study on Behavior of Tandem and Side-by-side Moored Vessels. *The Twelfth International Offshore and Polar Engineering Conference, 26-31 May, Kitakyushu, Japan*,pp. 841-847.

[6] J.R. Chaplin, 2001. Nonlinear wave interactions with a submerged horizontal cylinder. *In proc 11th international offshore and polar engineering conference, Stavanger, ISOPE*,pp 272-279.

[7] J.M.P. Conde, E. Didier, M.F.P Lope and L.M.C. Gato, 2009. Nonlinear wave diffraction by submerged horizontal circular cylinder. *International Journal of Offshore and Polar Engineering*,**19**, pp. 198-205.

[8] W.C. Koo, M.H. Kimand A. Tavassoli, 2004. Fully nonlinear wave-body interactions with fully submerged dual cylinders. *International Journal of Offshore and Polar Engineering*, **14**, pp. 210-217.

[9] E. Guerber, M. Benoit, S.T. Grilli and C. Buvat, 2010. Modeling of fully nonlinear wave interactions with moving submerged structures. *In 20th International Offshore and Polar Engineering Conference,Beijing, China*,pp 529-536.

[10] M.A. Hannan, W. Bai and K.K. Ang, 2014. Modeling of fully nonlinear wave radiation by submerged moving structures using higher order boundary element method,*J of Marine Science and Application*,**13(1)**.pp 1-10.

[11] W. Bai, M.A. Hannan and K.K. Ang, 2014. Numerical simulation of fully nonlinear wave interaction with submerged structures: fixed or subjected to constrained motion,*Journal of Fluids and Structures*,**49**, pp 534-553.

[12] M. A. Hannan and W. Bai, 2015. Nonlinear hydrodynamic responses of submerged moving payload in vicinity of a crane barge in waves, *Marine Structures*, **41**, pp 154-179.

CICM 2015
First International Conference on
Advances in Civil Infrastructure and Construction Materials
MIST, Dhaka, Bangladesh, 14–15 December 2015

PERFORMANCE BASED SEISMIC DESIGN OF A TEN STOREY RCC COMMERCIAL BUILDING USING NONLINEAR PUSHOVER ANALYSIS

Jaher WASIM[1]

[1] Mantissa Design and Consultant, Dhaka, Bangladesh.
Email: wasim@jaherwasim.com

Abstract. *Performance-based design using nonlinear pushover analysis, which generally involves monotonous and intensive computational effort, is an elastic design methodology done on the probable performance of the building under input ground motions. In this Study, a ten storey commercial building is designed using ETABS and the performance based seismic design is performed by pushover analysis technique using ETABS 2015, a product of Computers and Structures International. An extensive study is conducted to investigate the effect of different parameters on the performance point. The parameters include the effect of input ground motions on the performance point, changing percentage of reinforcement in columns, size of columns and beams individually. The results of analysis are compared in terms of base shear and storey displacements.*

Keywords: Performance based design, Pushover analysis, Elastic response spectrum, Future trends

1 INTRODUCTION

Amongst the natural disaster the earthquake have the potential for a devastating damages. The basic concept of Performance-based seismic design (PBSD) is to provide engineers with the capability to design buildings that have a predictable and reliable performance in earthquake. Performance based design is an elastic design methodology which requires rigorous nonlinear analysis. Pushover analysis which is an iterative method under constant gravity loads and monotonically increasing lateral forces until a target displacement is reached is generally carried out to understand real behavior of structure during strong ground acceleration. The major outcome of pushover analysis is the capacity curve which shows the base shear vs. roof displacement.

2 LITERATURE REVIEW

Performance based design has been practiced since early in the twentieth century. The International Code Council (ICC) [1] in the United States had a performance code available for voluntary adoption since 2001 (ICC, 2001). In 1989, the FEMA-funded project was launched to develop formal engineering guidelines for retrofit of existing buildings began [2], it was recommended that the rules and guidelines be sufficiently flexible to accommodate a much wider variety of local or even building-specific seismic risk reduction policies than has been traditional for new building construction. The performance levels were generalized with descriptions of overall damage states with titles of Operational, Immediate Occupancy, Life Safety, and Collapse Prevention. Over the 10-year period after publication of FEMA 273 [3], its procedures were reviewed and refined and eventually published in 2006 as an American Society of Civil Engineers (ASCE) national standard - Seismic Rehabilitation of Existing Buildings, ASCE 41. It is considered to represent the first generation of performance-based seismic design procedures.

3 CASE STUDY

A 3-D model of ten story concrete commercial building shown in Fig.1 has been created using finite element package ETABS 2015 [4] to undertake the nonlinear analysis. The structure has designed according to the BNBC 2015[5](Bangladesh National Building Code). From soil report it has found the structure will be built in medium dense sandy soil (SC Type, SPT: 15 -50) in zone 4 (very severe seismic intensity zone) of Bangladesh Seismic map. For this zone PGA value is 0.36g. This building is 30m x 20m in plan and 3.5mm x 10 floors in elevation. There are 4 bays in the X direction and 3 bays in the Y direction.

Beams and columns are modeled as nonlinear frame elements with lumped plasticity at the start and the end of each element. ETABS 2015 provides default-hinge properties and recommends PMM hinges for columns and M3 hinges for beams as described in FEMA-356.

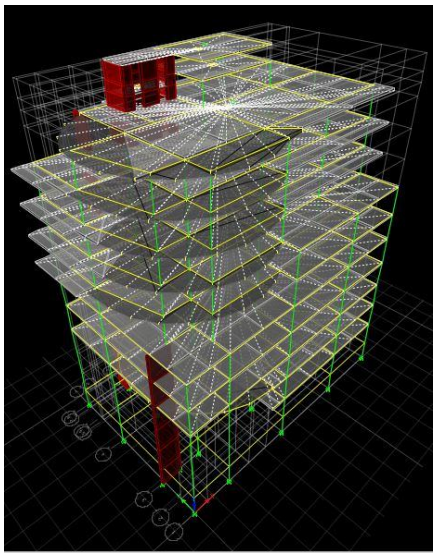

Figure 1: 3D Model of the Concrete Structures

4 PUSHOVER ANALYSIS

In the push over analysis method, earthquake load is applied on the model in an incremental basis. As the loads are increased, the building undergoes yielding at a few locations. Every time such yielding takes place, the structural properties are modified approximately to reflect the yielding. The analysis is continued till the structure collapses, or the building reaches certain level of lateral displacement. The material nonlinearities are assigned as hinges; M3 flexural hinges for beams and PMM flexural hinges for columns. Then each lateral load pattern is applied.

5 PERFORMANCE BASED DESIGN

Performance-based seismic design explicitly evaluates how a building is likely to perform; given the potential hazard it is likely to experience, considering uncertainties inherent in the quantification of potential hazard and uncertainties in assessment of the actual building response. As graphically presented in Fig. 2, the nonlinear static analysis procedure requires determination of three primary elements: capacity, demand and performance. The capacity spectrum can be obtained through the pushover analysis, which is generally produced based on the first mode response of the structure assuming that the fundamental mode of vi-

bration is the predominant response of the structure. This pushover capacity curve approximates how a structure behaves beyond the elastic limit under seismic loadings. The demand spectrum curve is normally estimated by reducing the standard elastic 5% damped design spectrum by the spectral reduction method. The intersection of the pushover capacity and demand spectrum curves defines the "performance point" as shown in Fig. 2.

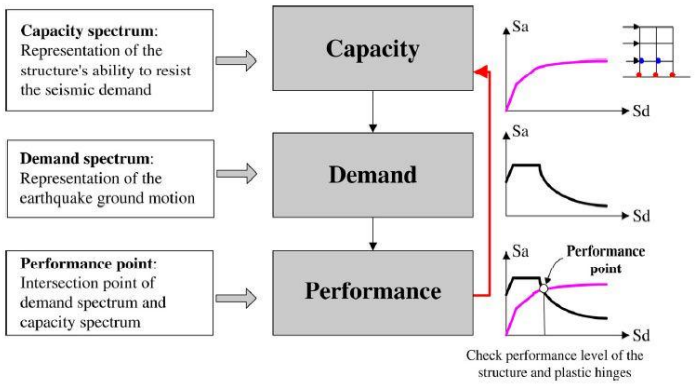

Figure 2: Nonlinear Analysis Procedure

At the performance point, the resulting responses of the building should then be checked using certain acceptability criteria. When the responses of a structure do not meet the targeted performance level, the structure needs to be resized the design process repeated until a solution for the desired performance level is reached. In general, the determination of the satisfactory performance response that fulfills both system level response and element level response requires a highly iterative trial-and-error design procedure even the aid of today's engineering computer software. The performance target can be a specified limit on and response parameter such as stress, strains, displacements, accelerations, etc. Usually drift levels are associated with specific damage categories. Some of the subjected performance levels can group in equivalent categories as listed in Table 1. [3]

Table 1: Definition of performance level according to FEMA

Performance level	Performance description	Story drift
Fully operational	Continuous service, negligible damage	<0.2 %
Operational	Safe for occupancy, light damage, repairs for Non-essential operation	<0.5 %

Life safety	Moderate damage, life safety protection, repair may be possible but impractical	<1.5 %
Near collapse	Severe damage, collapse prevented, falling Non-structural elements	<2.5 %
Collapse		>2.5 %

6 SIMULATION AND RESULTS

To illustrate the PBD procedure for finding the performance point, a ten storey concrete frame of a commercial building as shown in Fig.1 is taken as an example. The frame is designed according to BNBC 2015 using ETABS. Structural details and natural frequencies of the concrete frame are given in Table 2 and 3 respectively. The pushover analysis is performed on the RC building and redesigning by changing the main reinforcement of various frame elements and again analyzing. For parametric studies, a total of 13 cases as per Table 4, for a particular ten storey building frame located in Zone-4 have been analyzed, changing reinforcement and sizes of different structural elements, i.e. beams and columns, in different combinations as well as at different storey levels. Roof displacement, ductility demand, performance point and effect of change in beam and column size have been illustrated in the Table 5, 6, 7 and 8, respectively.

Table: 2 Structural Details as per ETABS

S. No.	Structural Element's	Dimension (m)		Reinforcement area (mm^2)	
		Breadth	Depth		
1	C1 Column Up to Ground Floor	0.813	0.813	10862	
2	C1 Column Ground Floor to 5^{th} Floor	0.762	0.762	10862	
3	C1 Column 6^{th} to Roof	0.762	0.762	7250	
4	C2 Column Up to Ground Floor	0.559	0.661	7150	
5	C2 Column Ground Floor to 5^{th} Floor	0.508	0.609	7150	
6	C2 Column 6^{th} to Roof	0.508	0.609	6050	
				Top	Bottom
7	Grade Beam	0.310	0.534	1650	1375
8	Floor Beam	0.310	0.610	2525	2031

Table 3: Natural frequency and time periods

Mode shape	Period (sec)	Frequency (cycle/sec)
1	1.272	0.786
2	0.462	2.164
3	0.257	3.891

Table 4: Various cases for parametric studies

Serial No	case	Description of case	Serial No	case	Description of case
1	A	Basic Structure	9	H	10% decrease in column size
2	B	10% increase in column reinforcement	10	I	20% decrease in column size
3	C	20% increase in column reinforcement	11	J	10% increase in beam size
4	D	10% decrease in column reinforcement	12	K	20% increase in beam size
6	E	20% decrease in column reinforcement	13	L	10% decrease in beam size
7	F	10% increase in column size	14	M	20% decrease in beam size
8	G	20% increase in column size			

Table 5: Roof displacement for elastic and inelastic response spectra for different Performance level

Serial no	Performance Level	Roof Displacement for PGA 0.36g (mm)	
		Elastic	Inelastic
1	Operational	63.11	57.39
2	Immediate Occupancy	144.23	133.1
3	Life Safety	212.67	208.31
4	Collapse Prevention	372.72	309.11
5	Complete Collapse	∞	∞

Table 6: Ductility demand for elastic and inelastic response spectra for different Performance level

Serial no	Performance Level	Ductility Demand for PGA 0.36g (mm)	
		Elastic	Inelastic
1	Operational	1	1
2	Immediate Occupancy	3.45	3.01
3	Life Safety	11.23	10.61
4	Collapse Prevention	14.22	13.59
5	Complete Collapse	∞	∞

Table 7: Performance point

	Performance point for PGA 0.36g	
	Elastic	Inelastic
Base Shear (KN)	6821	2593
Roof Displacement	198.34	35.33

Table 8: Effect of change in beam and column size and reinforcement

Serial No	Case	% change in roof displacement	% change in base shear
1	A	-	-
2	B	3.45	-4.72
3	C	7.45	-17.34
4	D	-1.76	-4.42
5	E	-6.87	15.29
6	F	2.63	-3.19
7	G	4.34	-20.22
8	H	-2.34	7.25
9	I	-6.66	12.11
10	J	1.21	-3.92
11	K	1.45	-4.99
12	L	-0.98	2.34
13	M	-1.62	3.31

7 CONCLUSION

Based on the present study, the following conclusions can be drawn:

- Since frequencies are varied, higher modes are neglected for pushover analysis
- As the response changes from elastic to inelastic, roof displacements and ductility demands decrease for different PGA level.
- The performance point obtained satisfies the acceptance criteria for immediate occupancy and life safety limit states for various intensities of earthquake.
- The increase in reinforcement of columns results in nominal change in base shear and displacement.
- As the beam and column section size increases, the roof displacement decreases whereas base shear increases.
- As the size decreases, the roof displacement increases whereas base shear decreases.

REFERENCES

[1] ICC, 2001, "International Performance Code for Buildings and Facilities", International Code Council, Whittier, California.

[2] [2]ATC (1996) Seismic Evaluation and Retrofit of Concrete Building (volume 1), Report (ATC-40), Applied Technology Council, California, USA.

[3] FEMA 356, 273.(2002) Pre-standard and Commentary for the Seismic Rehabilitation of Buildings, Federal Emergency ManagementAgency, Washington D.C., USA.

[4] Computer and Structures Inc., ETABS Nonlinear Version 15, California, USA.

[5] BNBC (2015) Bangladesh National Building Code, Housing and Building Research Institute, Mirpur, Dhaka, Bangladesh.

CICM 2015
First International Conference on
Advances in Civil Infrastructure and Construction Materials
MIST, Dhaka, Bangladesh, 14–15 December 2015

EFFECT OF WIND LOADS ON LATERAL DEFLECTION AND DRIFT BEHAVIOR OF VARIOUS BUILDING CODES ON STRUCTURES

M. MAHMOOD[1], S. Bhowmik[2] and A. B. Emon[3]

[1, 2, 3] Bangladesh University of Engineering and Technology, Dhaka, Bangladesh.
Email: [1]mukseet.mahmood@gmail.com, [2]sharmilyb@gmail.com
and[3]a.001.bashar@gmail.com

Abstract. *Lateral drift or lateral deflection is the difference in deflection between two adjacent stories. Without proper consideration during the design process, these deficiencies can have adverse effects on structural elements, non structural elements and adjacent structures. Of all forms of lateral loads, wind load is the most important one for structures with higher natural time period. This paper aims at calculating top lateral deflections of different structures applying different wind loads calculated from different building codes. Finite element analysis (ETABS) was performed for determining the deflection. The paper intends to discuss the difference of lateral deflections and highest lateral drifts associated with different building codes as BNBC 1993, BNBC 2015, International building code 2009 (USA) and National building code of India 2005. This paper outlines the graphical comparisons between the deflections and drifts calculated by wind loads from different building codes at different stories.*

Keywords: Lateral drift, Building codes, Wind load, Finite element analysis, Graphical comparison.

1 INTRODUCTION

Wind load is one of the most important factors to be considered for building safety as deflection and lateral drift created by wind forces can significantly affect the structure. Depending on terrain or exposure type, wind load varies from place to place. Wind damage prediction is an issue because all existing structures are not windstorm-resistant. Unfortunately, the important issues of wind damage prediction and mitigation have not kept pace with the level of recognition of the wind hazard .Wind is a phenomenon of great complexity because of the many flow situations arising from the interaction of wind with structures. Wind is composed of a multitude of eddies of varying sizes and rotational characteristics carried along in a general stream of air moving relative to the earth's surface. These eddies give wind its gusty or turbulent character. The gustiness of strong winds in the lower levels of the atmosphere largely arises from interaction with surface features. The average wind speed over a time period of the order of ten minutes or more tends to increase with height, while the gustiness tends to decrease with height[1].In this paper, wind forces acting on buildings having a plan area of 100ft x 80ft and storey varying from 5 to 50 were calculated using Bangladesh National Building Code (BNBC) 1993, National Building Code of India (NBI) 2005, International Building Code (IBC) 2009 and Bangladesh National Building Code (BNBC) 2015. Comparison was made among the deflections and lateral drifts obtained from different codes using ETABS software. Detailed calculation and comparison are describeed in this paper. The highest drift on a 50 storied building and the storey that carried the highest lateral drift is also discussed in this research.

2 REVIEW OF THE CALCULATION OF WIND LOADS BY DIFFERENT BUILDING CODES

Wind load varies to places due to difference in building codes. Wind load is mainly a factored wind speed which varies to different stories and different plans. The basic wind velocity is converted to the design reference wind velocity for a particular site by introducing the influence of local environment, directionality, mean recurrence interval, and significance factors associated with the planned structure. Wind load calculation mainly depends on the factors and specifications in different building codes.

The calculation process and the factors of Bangladesh National Building Code (BNBC) 1993, National Building Code of India (NBI) 2005, International Building Code (IBC) 2009 and Bangladesh National Building Code (BNBC) 2015 are described below in a table.

Table 1: Calculation of wind forces in different codes

BNBC 1993	NBI 2005	IBC 2009	BNBC 2015
q_z= Cc CI Cz Vb^2	$V_z = V_b k_1 k_2 k_3$	q_z= .000613$k_z k_{zt} k_d$ V^2I	q_z= .000613$k_z k_{zt} k_d$ V^2I
q_z = sustained wind pressure at height z, kN/m^2	V_z = design wind speed at any height z in m/s	k_d = wind directionality factor	k_d = wind directionality factor
C_I = structure importance coefficient	V_b = basic wind speed in m/s	k_z = velocity pressure exposure coefficient	k_z = velocity pressure exposure coefficient
C_c= velocity to pressure conversion =47.2 x 10-6	k_1 = probability factor	k_{zt}= topographic factor	k_{zt}= topographic factor
C_z = combined height and exposure coefficient	k_2 = terrain height and structure size factor	V = basic wind speed in m/s	V = basic wind speed in m/s
V_b = basic wind speed in km/h	k_3 = topography factor	I = importance factor	I = importance factor
P_z = CGCpqz	$p_z = 0.6\ V_z^2$	q_z = velocity pressure evaluated at height z above ground in N/m^2	q_z = velocity pressure evaluated at height z above ground in N/m^2
P_z= design wind pressure at height z,kN/m^2	p_z = design wind pressure in N/m^2 at height z	F = $q_z G C_f A_s$ (kN)	F = $q_z G C_f A_s$ (kN)
C_G = gust coefficient	$F = (C_{pe} - C_{pi})\ A\ p_d$	F = design wind force	F = design wind force
C_p = pressure coefficient	C_{pe}= external pressure coefficient;	G = gust effect factor	G = gust effect factor
$F_z = P_z$ x A	C_{pi}= internal pressure coefficient;	C_f = net force coefficient	C_f = net force coefficient
F_z = Design wind force	A= surface area of structural element in m	A_s = the gross area of the solid freestanding wall, in m^2	A_s = the gross area of the solid freestanding wall, in m^2
A = Effective area	p_d= design wind pressure in N/m^2		

3 METHODOLOGY

For this analysis, a residential building of 100ft x 80ft plan area and height varying from 5 storey to 50 storey was taken. Comparison was made between Bang-

ladesh National Building Code (BNBC) 1993, National Building Code of India (NBI) 2005, International Building Code (IBC) 2009 and BNBC 2015 on places of Bangladesh, USA and India having similar wind speed and terrain category.

Basic features of allthese codes are presented in table 1. In BNBC-93, calculation of design wind pressure is a two-step process. In the first step, the sustained wind pressure was calculated on the basis of importance of structure, height and exposure condition and basic wind speed, which in turn depends on the region the structure is located in. The exposure of the structure to wind forces is a function of terrain type, vegetation and built up environment in the surrounding. The sustained wind pressure was then converted to design wind pressure by multiplication with the gust coefficient and pressure coefficient for the structure. Pressure coefficient considers the direction of wind relative to the structure and roof slope. Finally force acting on each storey was calculated from wind pressure acting on effective area of each floor.

In NBI-2005, the design wind speed at various heights was determined first on the basis of risk level, terrain roughness, height and size of structure and local topography. The terrain factor refers to exposure category. In addition another factor describes the local topography e.g. hills, valleys, cliffs, ridges etc. In the second step, design wind speed was converted to pressure by a simple conversion factor. Force was calculated by taking account of the pressure difference between opposite faces of roof, walls and cladding.

There is no difference in the basic procedure of determining wind force in IBC 2009 and BNBC 2015. Velocity pressure was determined on wind directionality factor, topographic factor, velocity pressure exposure coefficient and structural importance coefficient. Design wind force was determined on the basis of velocity pressure evaluated at different heights, gust-effect factor, force coefficients and projected area normal to the wind.

The lateral drift was calculated by applying the wind forces of different building codes to every 50 storied building. And from the model the highest lateral drift and the storey where the highest drift effecting is calculated. The basic components of the places that were taken for the wind load calculation is given in Table 2.

Table 2: Basic components of places

BNBC 1993	NBI 2005	IBC 2009	BNBC 2015
Comilla city in Bangladesh	Agartala in India	Groton in Connecticut	Comilla city in Bangladesh
V_b=196kmph (54.4 m/s)	V_b=198kmph (55 m/s)	V=193kmph (53.6 m/s)	V_b=221kmph (61.4 m/s)
Exposure B.	Terrain category 2	Exposure C	Exposure B.

A finite element method based software ETABS 9.7was used as the computer analysis program. Here, different multi-storied structures were modeled in ETABS software and the top deflection in lateral direction and the top lateral drift of the structure was computed. In this case, the top deflection of 5, 10, 15,20,25,30,35,40,45 and 50 storied buildings were calculated. The top lateral deflection and the lateral drift was plotted in the graph and compared among the codes. The specific properties of the structures are shown in Table 3. No wall is considered in design. The design consists of just beam, column, and slab. It was considered 3 panels in X direction and 2 panels in Y direction.

Table 3: Specific properties of the structure

Properties	Value
Compressive strength of concrete	4 ksi
Yield strength of steel	60 ksi
Shear strength of steel	60 ksi
Panel dimension in X direction	100 ft
Panel dimension in Y direction	80 ft
Storey height	10 ft
Slab thickness	12 inch
Beam dimension	18inch×12inch
Column dimension	18inch×18inch

4 RESULT AND DISCUSSION

From the analysis results, it was obtained that deflection of the buildings gradually increases with storey height. Highest deflecttion was obtained from BNBC 1993 and lowest from NBI 2005 though basic wind speed was higher for india. The reason for such difference in deflection was due to the difference in procedure of calculation and difference in coefficients stated in codes.

Following figure shows the changes of deflection with the varying storey height.

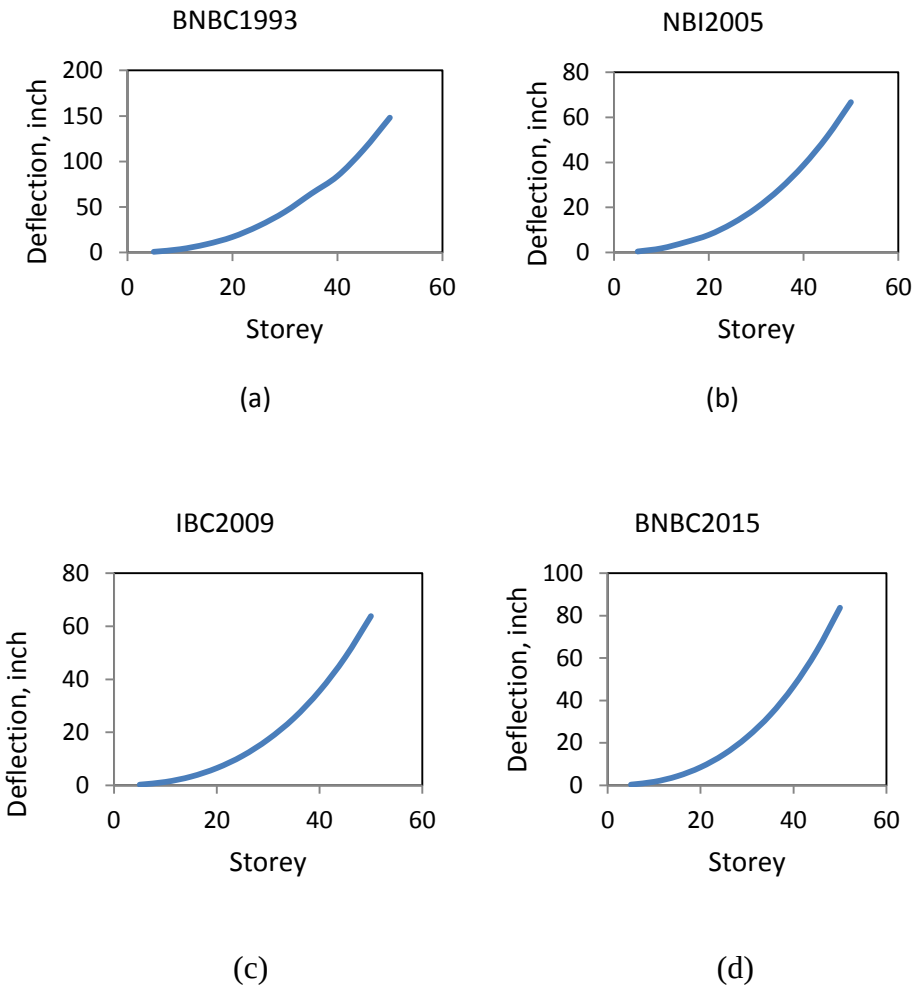

Figure 1: (a) deflection vs storey height(BNBC 1993) (b) deflection vs storey height(NBI2005) (c) deflection vs storey height(IBC2009) (d) deflection vs storey height(BNBC 2015)

The deflection among different building codes varies due to mainly the factors and the calculation process described in the building codes. The wind speed was considered almost same in all the wind load calculation but the wind load varied and thus the deflection also varied in all the calculations. A combined graph is provided to observe the difference in deflections due to the changes in wind loads.

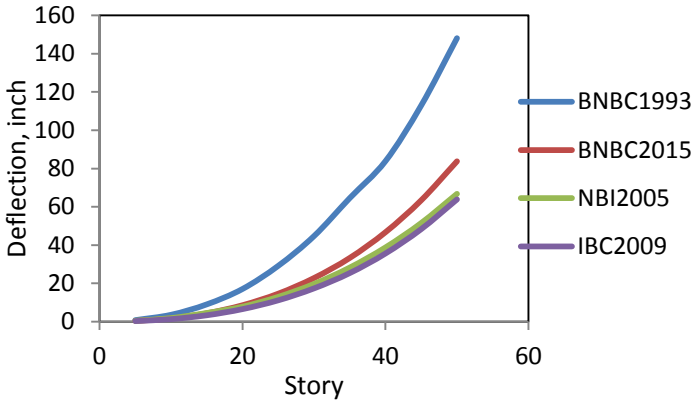

Figure 2: deflection vs storey in BNBC1993, BNBC2015, NBI2005 and IBC2009.

A change of lateral drifts was also seen in the analysis with building codes. It was observed that the highest drift was seen in the 3rd storey of the calculation by BNBN1993, BNBC2015 and IBC2009 but highest drift was observed on 2nd storey in NBC2005. The variation of the highest drift on a 50 storey building is also provided in the following table and the difference is acute.

Table 4: Lateral drifts calculation on 50 storied building

Building code	BNBC1993	BNBC2015	NBC2005	IBC2009
Highest drift on storey	3rd	3rd	2nd	3rd
Drift	0.038948	0.021154	0.017168	0.016121

5 CONCLUSION

This study mainly focuses on the difference of the deflection and lateral drifts calculated by four different building codes. Each building codes have own specification and thus the deflection varies to different building codes. In this study the place of calculation was chosen by which their almost similar wind speed. So, the wind force which mainly causes the top lateral deflection and drift varies to the factors provided by the building codes.

REFERENCES

[1] P. Mendis, T. Ngo, N. Haritos, A. Hira,B. Samali, J. Cheung,2007.Wind Loading on Tall Buildings,EJSE Special Issue: Loading on Structures

[2] Bangladesh National Building Code (BNBC) 1993

[3] National Building Code of India (NBI) 2005

[4] International Building Code (IBC) 2009

[5] Bangladesh National Building Code (BNBC) 2015

CICM 2015
First International Conference on
Advances in Civil Infrastructure and Construction Materials
MIST, Dhaka, Bangladesh, 14–15 December 2015

SEISMIC PERFORMANCE INVESTIGATION OF BASE ISOLATION SYSTEM FOR TYPICAL RESIDENTIAL BUILDING IN BANGLADESH

S. Tasnim[1], K. A. Farzana[2], K. S. Ahmed[3] and Aziz Ahmed[4]

[1, 2, 3] Military Institute of Science and Technology, Dhaka, Bangladesh.
Email: [1]asfaratasnim@yahoo.com,[2]afiasashi@yahoo.com,[3]sakil0104@gmail.com

[4]National University of Singapore, Singapore. Email: asif.nih@gmail.com

Abstract. *Base isolation system for building structure is a popular technique to release extensive energy by allowing displacement and hence to protect structures from earthquake excitation. This paper aims to investigate the performance of a base isolated building against seismic hazard compare to typical fixed base building using ETABS 2015. Commonly used isolator like rubber bearing and friction pendulum bearing are used at the base of the building. Parametric studies are conducted to study linear time history analysis and to investigate the performance of different type of isolator. In the parametric study, comparisons are made among fixed base, rubber and friction pendulum isolated based structure on the basis of base shear, story drift, displacement, acceleration and time period. Finally nonlinear static pushover analysis has also been conducted as per FEMA-440. It is observed from the study that a base isolation system in building significantly reduces base shear with the increment of displacement and time period compared to fix based building significantly.*

Keywords: Base isolation, Rubber isolator, Friction pendulum system, Linear time history analysis.

1 INTRODUCTION

Earthquake hazard is one of the most devastating influences on civilization that takes millions of life, demolishes the infrastructures and also changes the geography of the earth surface within just few seconds. Bangladesh being close to the Indian and Eurasian plate, it is likely to experience frequent earthquake due to collision of the north ward movement of Indian plate with respect to Eurasian plate. Seismic isolation is a process of increasing the earthquake resistance property of the building structure and reducing the probability of damage [1-2]

In recent years the concept of seismic isolation process has developed as the alternative to the conventional seismic strengthening process. The principles of base isolation were evolved by Skinner, Robinson and McVerry in 1993 and later extended by Naiem and Kelly in 1999.This base isolation technique grabs the attention of researchers, professors and engineers and day by day it is becoming a promising sector for improving the present concept of the building structure design in view of earthquake resisting structures.

Base isolation system works on a principle which tends to modify the response of a building so that the ground can move below the building without transmitting motions into structures. In isolated structures displacements are often large and efforts are made to releases the earthquake energy. It lengthens the natural period of vibration of the structure so that the responses are greatly reduced. Moreover isolator system is installed so that the building can move horizontally to ground and the displacement is limited up-to 100 mm to 1m. Base isolation does not make a building earthquake proof but enhances the earthquake resistance [2]. There are four types of base isolator generally used in building structures:

1) Lead Rubber Bearing (LRB).
2) Laminated Rubber (Elastomeric) Bearing.
3) High Damping Rubber (HDR) Bearing.
4) Friction Pendulum (FPS) System Bearing

In this paper a low to medium rise building (12 storey) building is modeled considering actual condition using ETABS-2015. Typical rubber isolator and friction pendulum are used to investigate their performance against seismic load. In order to figure out the improvement of isolation system, Non-linear Time History Analysis is conducted in both fixed based and base isolated conditions of the building.

2 MODELING OF STRUCTURE

In this paper, a12 storey reinforced concrete (RC) building located at Gazipur, Bangladesh which is nearly 30 km away from Dhaka city is taken for

investigation. The building is modeled using FE package ETABS 2013 and parameters are considered as per Bangladesh National Building Code (BNBC 2014). In order to investigate the performances of base isolators, in this study, rubber isolator and friction pendulum system are used. Typical rubber isolator and FPS system are discussed below.

2.1Lead Rubber Bearing (LRB):

A lead-rubber bearing is formed of a lead plug force-fitted into a pre-formed hole in an elastomer Bearing. The lead core provides rigidity under service loads and dissipates energy under high later loads. The rubber cover protects the steel from environmental effect. Lead yields at higher loads and thus lateral stiffness is reduced. For these properties the lead-rubber bearing is the most common type of isolator used.

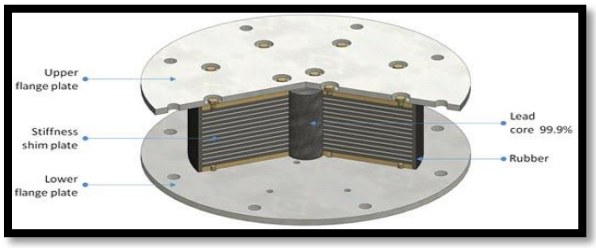

Figure 1: Lead rubber bearing

2.2Friction Pendulum (FPS) System Bearing:

In friction pendulum, bearing the sliding surface is spherical in shape. It gives resistance to service load by coefficient of friction. After overcoming the friction coefficient the slider moves and for the spherical shape a lateral movement is accompanied with vertical movement. This isolator allows the displaced structure to return to its original position.

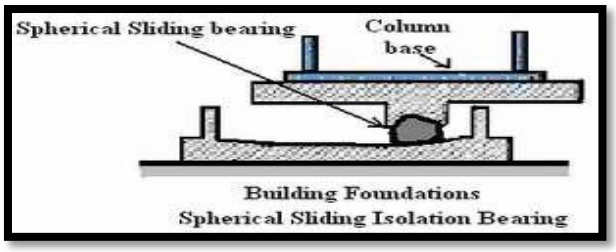

Figure 2: Friction pendulum sliding bearing

The dimensions of structural members are presented in Table 1

Table 1: Building Details

Name of structural member	Specification
Typical Beams	12 inch ×20 inch
Grade beam	14 inch × 24 inch
Columns	Varies (12” × 16” to 16”×20”)
Slab thickness	6.5 inch
Thickness of periphery wall	10 inch
Height of typical floor	10 feet
Height of parapet wall	3 feet
Compressive strength of concrete	4000psi for all
Grade of steel	50ksi
Dead load	PW(60psf),FF(30psf), periphey wall(400 plf)
Live load	story(40psf), roof ((30psf)

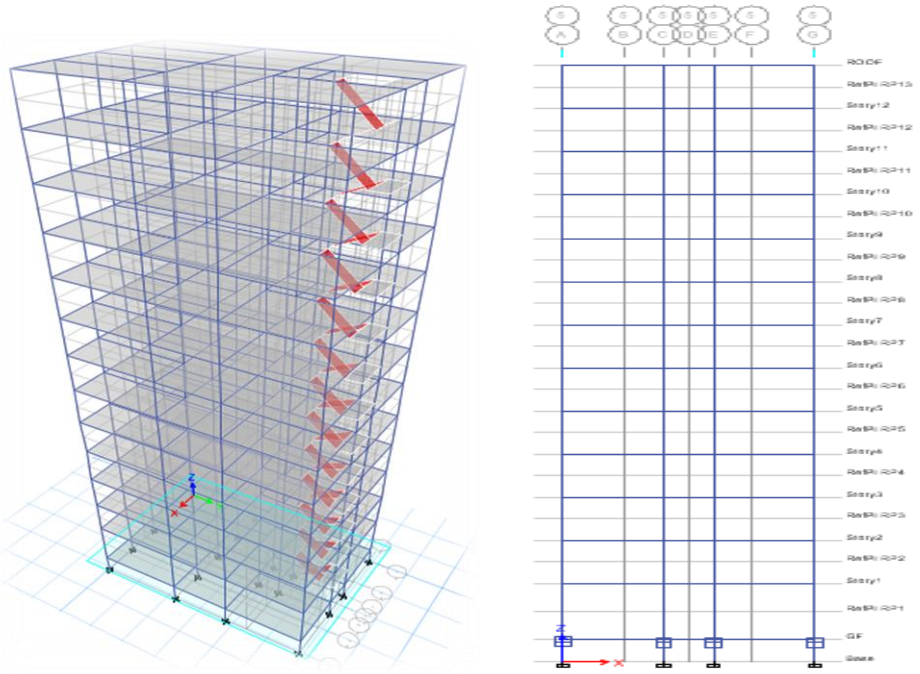

Figure 3: (a) 3D model and (b) elevation of 12 Storey RC building

3 ANALYSIS& RESULT

In this study, a series of Finite element analyses is conducted under different condition to evaluate the seismic behavior of structures in earthquake motion. The seismic analyses of the buildings are carried out both in the longitudinal and

the transverse directions. The parameters selected to define the rubber and friction pendulum isolators in the ETABS 2015 model are as follows:

Table 2: Properties of isolators

PROPERTIES OF ISOLATOR	RUBBER ISOLATOR	FRICTION PENDULUM
Linear Effective Stiffness UI (KN/m)	45000	1000
Linear Effective Stiffness U2 And U3(KN/m)	60000	250000
Non -linear Effective Stiffness U2 And U3(KN/m)	1500000	500000
Yield Strength (KN)	80	40
Post Yield Stiffness	0.1	-
Effective Damping	0.05	0.05
Rate Parameter	-	40
Net Pendulum Radius	-	2.23
Friction Co-Efficient Fast	-	0.05
Friction Co-Efficient Slow	-	0.03

3.1Comparative study of structural performance parameters:

Maximum storey displacement in X direction at different storey level for different base condition is presented in Figure 4. It can be shown from the figure that rubber isolated building displacement which increases up-to a maximum of 39.76% and in friction pendulum isolated building it increases up-to 55% than fixed based building with respect to earthquake in X direction.

Figure 5 shows displacement curve of earthquake in Y direction. Where rubber isolated building shows increment in displacement up-to 8.74% and in friction pendulum it increases up-to 25.52% than fixed based building.

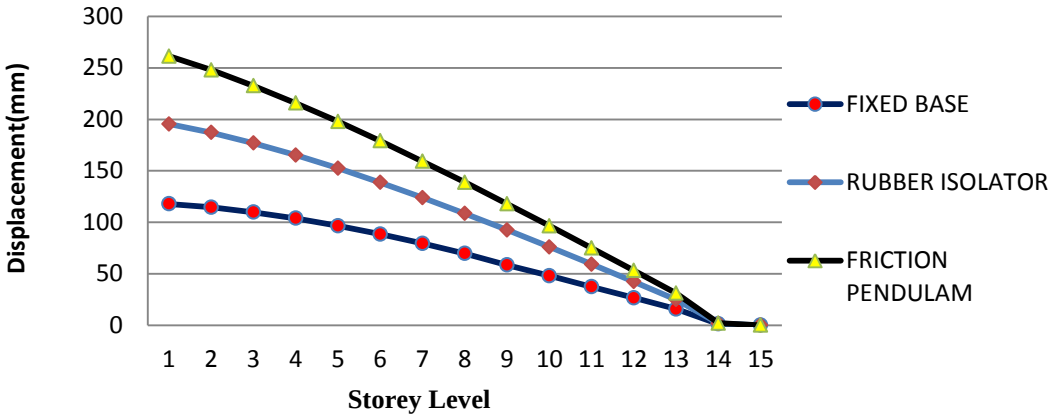

Figure4: Displacement in X direction

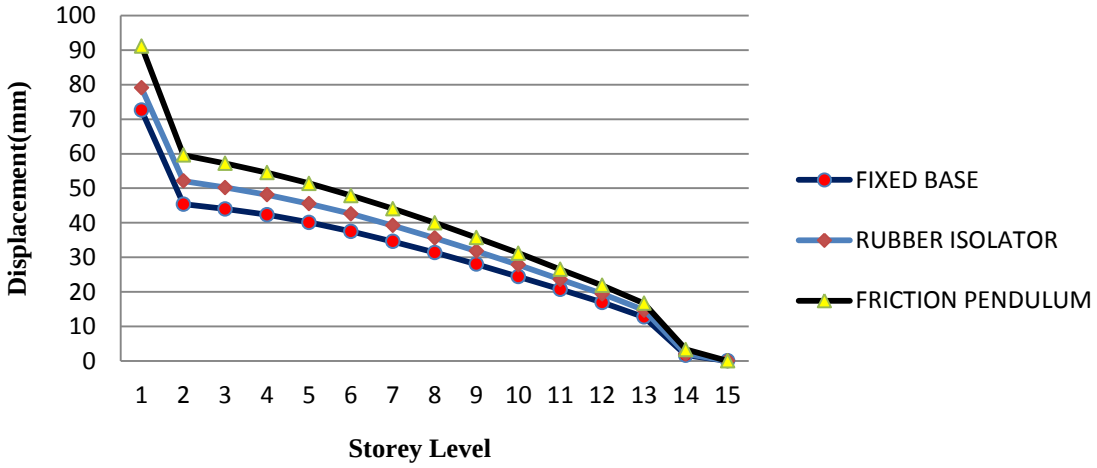

Figure5: Displacement in Y direction

Figure 6illustrates rubber isolated building story drift which increases up-to 60% and in friction pendulum isolated building it increases up-to 99.8% in story-1 than normal fixed based building with respect to earthquake in X direction.

Figure 7 shows displacement curve of earthquake in Y direction. Where rubber isolated building shows increment in story drift in story-1 up-to 14% and in friction pendulum it increases up-to 20.19% than fixed based building.

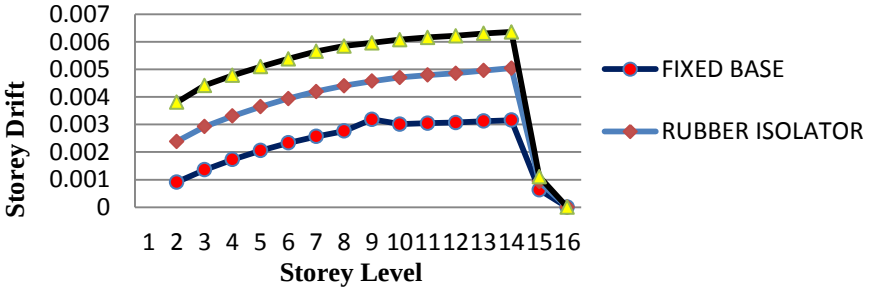

Figure 6: Storey drift in X direction

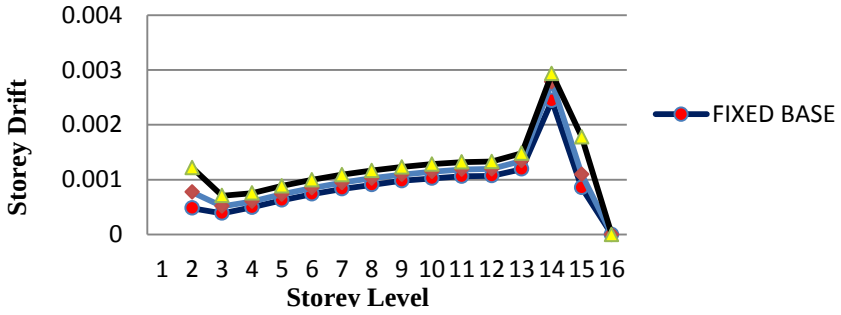

Figure 7: Storey drift in Y direction

3.2Time History Analysis:

Time history analysis is commonly used to observe performance of a structure at various well known ground motions. Non linear time history analysis is conducted in this paper to investigate resistance of the model 12Storey building under various real earthquake motions. The earthquake motion are used for this analysis are Corralit-1, Lacc Nor-1 (Northridge earthquake) and Holistic. Criteria of BNBC 2014 are fulfilled for setting up the maximum capable earthquake level [3].

3.2.1*Comparativestudy of structural parameter from time history analysis:*

In this section, effectiveness of base isolation is conducted by making comparison between fixed base structures and isolated structures which is done by rubber isolator and friction pendulum system. The results shows resistance against earthquake increases after using isolation system. Base shear reduces 17% after using rubber isolator bearing and around 22 % after using friction pendulum system. the base shear reduces dramatically. Displacement increases 5% after using rubber isolator bearing and around 6 % after using friction pendulum system. There is a significant increment observed in the result. But acceleration reduction is comparatively less than other parameter after using both isolator . The results also shows friction pendulum system is more effective than rubber elastomeric bearing.

Table3: Comparison results of structural parmeters of test model under three difeerent earthquake

Structural Parameters	Earthquake	Fixed Base	Rubber Isolator	Reduction or Increment (%)	Friction Pendulum	Reduction or Increment (%)
BASE SHEAR (KN)	CORRALIT	3032.21	2504.81	17	2392.37	21.10
	HOLISTIC	3654.31	3393.03	7.15	3381.27	7.47
	LACC NOR	2567.62	2529.25	0.1	2310.35	10.2
DISPLACEMENT (mm)	CORRALIT	39.03	39.86	2.08	40.72	4.15
	HOLISTIC	45.127	47.52	1.00	47.98	1.74
	LACC NOR	43.46	43.9	5.04	44..227	5.95
ACCELERATION (mm/s2)	CORRALIT	37774.79	3632.47	3.77	3599.28	4.65
	HOLISTIC	2488	2485.15	.1	2452.52	1.43
	LACC NOR	1909.13	1856.99	2.73	1843.47	3.44

3.2.2*Comparative Study of Base Shear at Different Earthquake:*

Figure 8 illustrates significant reduction of base after incorporating base isolation system. Behavior of base isolation system is distinctive for different earthquake. For Corralit earthquake Base shear reduced maximum 17% for rubber isolator and for friction pedulum system this percentage of reduction increases into around 22%. But for other earthquake motion like Lacc Nor this percenage is

lower than that of Corralit and Holistic earthquake motion, almost near to the fixed base structure for rubber isolation process. Using friction pendulum system as seismic isolation system base shear reduced almost 11 % at the same earthquake motion (Lacc Nor earthquake motion).

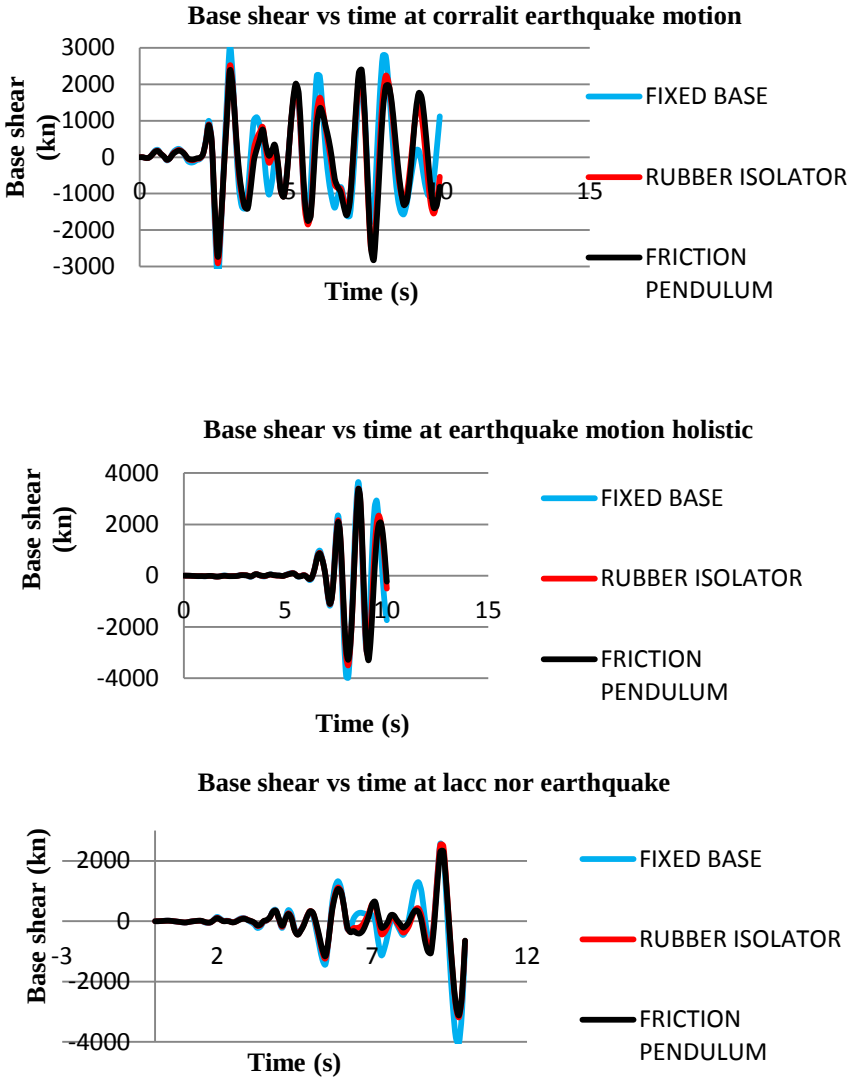

Figure 8: Comparison of base shear at different earthquake motion between base isolated and fixed base structure.

3.2.3*Comparative Study of Aceleration at Different Earthquake:*

Figure 9 represents significant reduction of accelration after incorporating base isolation system. Acceration reduced maximum 4 % for rubber isolator and for friction pedulum system this percentage of reduction increases into 5 %. But for holistic earthquake motion acceleration of rubber isolated structure almost near to the fixed base structure. Using friction pendulum system as seismic isolation process acceleration reduced a little around 1.5 % at the same earthquake motion.

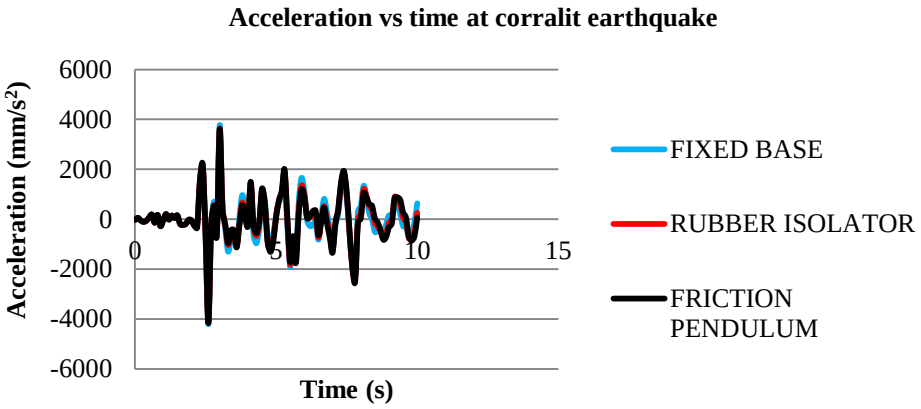

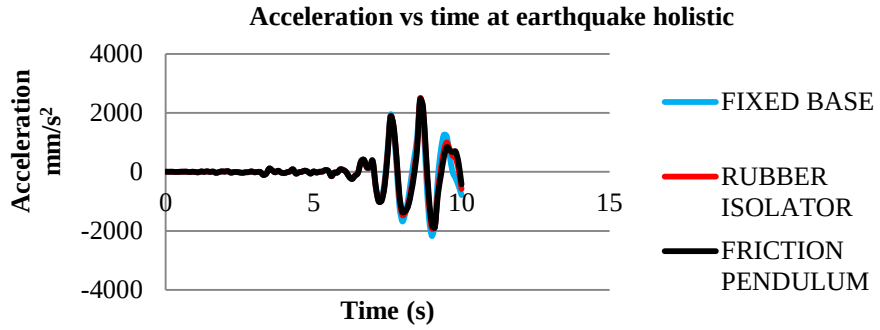

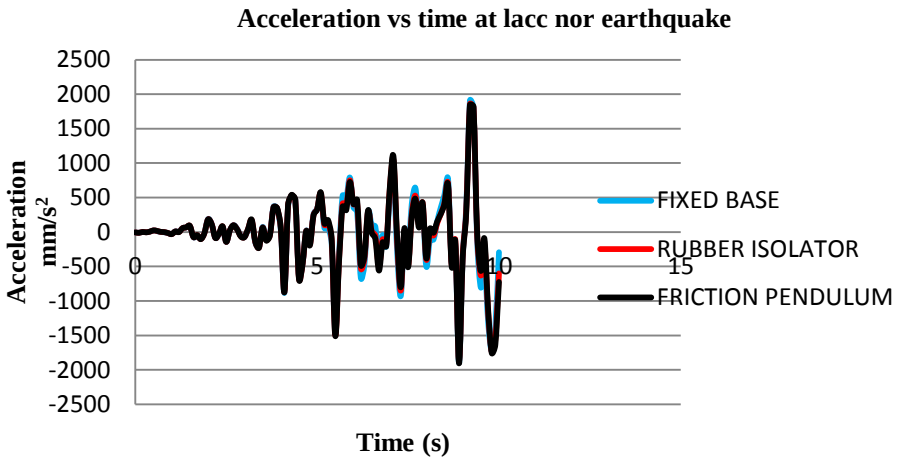

Figure 9: Comparison of acceleration at different earthquake motion between base isolated and fixed base structure.

3.2.4*Comparative Study of Displacement at Different Earthquake:*

Figure 10 represents significant increment of displacement after incorporating base isolation system. Displacement increased maximum 5% for rubber isolator and for friction pedulum system this percentage of reduction increases upto 6 % (Holistic earthquake motion).

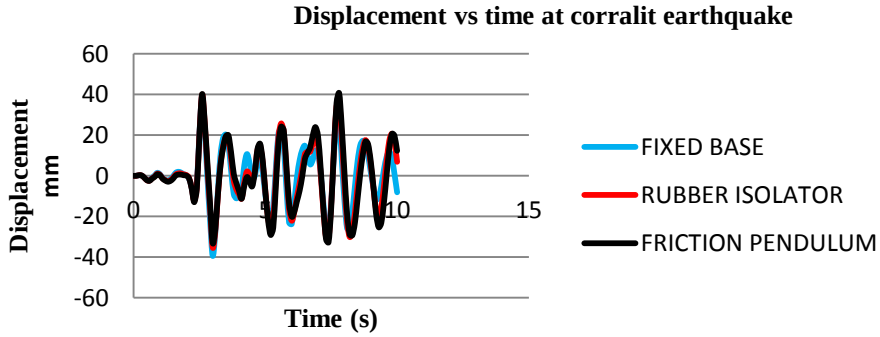

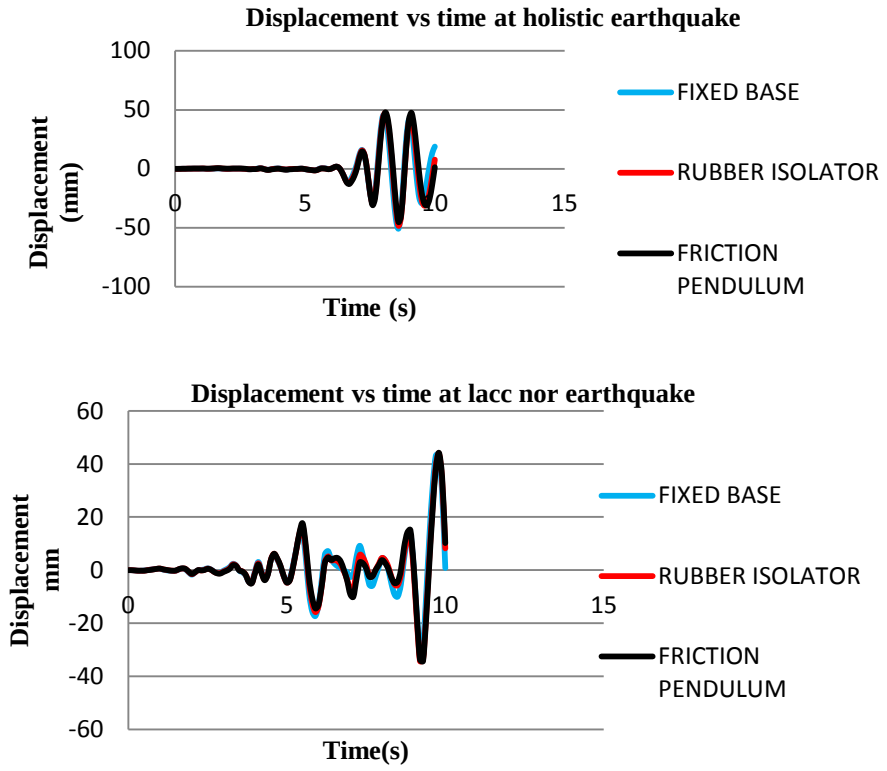

Figure 10: Comparison of displacement at different earthquake motion between base isolated and fixed base structure.

4. CONCLUSION:

- Base isolation technique is one of the most effective way to protect structure from adverse effect of earthquake.
- Friction pedulum is more effective and suitable for multistorey building as highest amount of base shear and acceration rudeced and displacement increases at every earthquake motion.
- For Corralit earthquake base shear reduced maximum 17% for rubber isolator and for friction pedulum system this percentage of reduction increases into around 21.1%. Acceleration reduced 3.77 % for rubber isolator and for friction pendulum system this percentage isaround 4.65%. Increment of displacement in rubber isolated structure is 2.08% and for friction pendulum system the increment value is 4.15%.

- For Holistic earthquake base shear reduced maximum 7.15 % for rubber isolator and for friction pedulum system this percentage of reduction increases into around 7.47%. Acceleration reduced .1 % for rubber isolator and for friction pendulum system this percentage is 1.43% . Increment of displacement in rubber isolated structure is 5.04%and for friction pendulum system5.95%.
- For Lacc Nor earthquake base shear reduced maximum .1% for rubber isolator and for friction pedulum system this percentage of reduction increases into around 10.2%. Acceleration reduced 2.73 % for rubber isolator and for friction pendulum system this percentage is 3.44%. Increment of displacement in rubber isolated structure is 1%and for friction pendulum system 1.74%.

REFERENCES:

[1] Dr.Tahmid.AL-Hussaini.2014.*Seismic Hazard and Risk Assessment for Bangladesh.* National Seminar on Engineers Role in Ensuring Safety.

[2] Trevor E Kelly, S.E.2001.*BASE ISOLATION OF STRUCTURES.* Design guidelines.

[3] Gomase O.P, Bakre S.V.2011.Performance of Non-Linear Elastomeric Base-Isolated building structure. International Journal of Civil and Structural Engineering.Volume 2, No 1. ISSN 0976 – 4399.

[4] HosseinMonfared, AyoubShirvani, Sunny Nwaubani.2013.*An investigation into the seismic base isolation from practical perspective.*International Journal of Civil and Structural Engineering.Volume 3, No 3.ISSN 0976 – 4399.

[5] SHIRULE.P. A, JAGTAP. L. P, SONAWANE. K. R,PATIL .T.D, JADWANIR.N and SONAR. S.K.2012.*Time History Analysis of Base Isolated Multi-Storyed Building.*ISSN 0974-5904, Volume 05, No. 04.P.P. 809-816.

[6] Vinodkumar Parma, G.S.Hiremath.2015.*Effect of Base Isolation in Inultistoried RC Irregular Building Using Time History Analysis.*International Journal of Research in Engineering and Technology (IJERT).pISSN: 2321-7308.Volume: 04

[7] Kubilay Kaptan.2013.*Seismic base isolation and energy* absorbing *devices.* European Scientific Journal.vol.9, No.18 ISSN: 1857 – 7881.

[8] TUN MYINT AUNG,TIN TIN WIN andNYAN.MY1NT KYAW.*Analysis and Design of Reinforced Concrete Structures with Spring Base Isolation.*

[9] Ganga Warrier A, Balamonica K, Sathish Kumar K, Dhanalakshmi.*Study on laminated rubber bearing base isolators for seismic protection of structures*. International Journal of Research in Engineering and Technology (IJRET).pISSN: 2321-7308.

[10] Dr. HadiNasirGhadhban AL-Maliki.2013.*Analytical Behavior of Multi-Storied Building with Base Isolation Subjected to Earthquake Loading.*Journal of Engineering and Development Vol. 17, No.2. ISSN 1813- 7822.

[11] EvanyNithya S., Dr. Rajesh Prasanna P.2012. *Moment Resisting Frame with Rubber Base Isolation for Development of Earthquake Resisting Structures.*International Journal of Modern Engineering Research (IJMER).Vol.2, Issue.4.pp-2431-2433.ISSN: 2249-6645.

[12] S.Keerthana, K. Sathish Kumar, K. Balamonica, D.S.Jagannathan.2014. *Seismic Response Control Using Base Isolation Strategy.*International Journal of Emerging Technology and Advanced Engineering.Volume 4, Special Issue 4.ISSN 2250-2459.

[13] FILIPE RIBEIRO DE FIGUEIREDO.*Design of base isolation systems in buildings.*

[14] A. B. M. Saiful Islam, Mohammed Jameel and Mohd Zamin Jummat.2011.*Study on optimal isolation system and dynamic structural responses in multi-storey buildings*.International Journal of the Physical Sciences Vol. 6(9), pp. 2219-2228. ISSN 1992 – 1950.

[15] Mr. Gururaj B. Katti and Dr. Basavraj S. Balapgol. 2014.*Seismic Analysis of Multistoried RCC Buildings Due to Mass Irregularity By Time History Analysis.*International Journal of Engineering Research & Technology (IJERT).ISSN: 2278-0181 .Vol. 3.

[17] Ashish R. Akhare, TejasR.Wankhade. 2014. *Seismic Performance of RC Structure Using Different Base Isolator*. International Journal of Engineering sciences ResearchTechnology (IJERT).ISSN: 2277-9655.

CICM 2015
First International Conference on
Advances in Civil Infrastructure and Construction Materials
MIST, Dhaka, Bangladesh, 14–15 December 2015

SEISMIC PERFORMANCE OF TYPICAL MASS DAMPERS

T. TABASSUM[1], N. Chowdhury[2], K. S. Ahmed[3] and Aziz Ahmed[4]

[1, 2, 3] Department of Civil Engineering, Military Institute of Science and Technology, Dhaka, Bangladesh.
Email: [1]tanzilalita99@yahoo.com, [2]nilufarchowdhury356@gmail.com and [3]sakil0104@gmail.com

[4] Department of Civil and Environmental Engineering, National University of Singapore, Singapore
Email: asif.nih@gmail.com

Abstract. *Seismic vulnerability of building structures has become a burning issue over the years particularly for South Asian countries like Bangladesh. The situation is even more critical for garments building of the country due to poor planning, design and construction. This research paper investigates how such type existing building structures behave against potential earthquake. This study primarily focuses on the effectiveness of different type dampers against different well known earthquake motion. A series of finite element model has been constructed to investigate the influence of different parameters of damper using ETABS 2015. The study has been further extended for different time history analysis to observe actual spectral response. Linear as well as nonlinear time-history analyses of the structure indicate that application of damper increases top story displacement, maximum joint acceleration, base reaction and energy dissipation by hysteresis loop for different earthquake for typical frame structures.*

Keywords: Earthquake, Mass damper, Finite element analysis, Static pushover analysis, Linear time history.

1 INTRODUCTION

Recent natural hazards like Earthquakes damage extensive number of buildings structures and other man-made structures. Existing research and experimental studies show that enforcing earthquake resistant regulations and their implementation in building constructions is the critical safeguard against earthquake-induced damage. Regarding the existing structures, it is necessary to evaluate and strengthen them based on evaluation criteria before an earthquake. Earthquake damage depends on many parameters including duration, frequency, intensity, geological condition, content of ground motion and quality of construction etc.

One of the major reasons to collapses building structure is non-adoption of seismic engineering practices and lack of seismic resistant features. The seismic performance of a building can be improved by installing energy absorbing device, which may be active and passive in nature. Damper for building structure is a well-known arrangement that deadens, restrains, or depresses violent shocks from earthquake and is designed to absorb significant amount of the forces from vibrations. There are many types of dampers like tuned mass damper, viscous damper, friction damper etc. [1-6].

Time history analysis Using Finite Element software like ETABS has already been established technique to observe the actual behavior of building structures against previous earthquake. In this regard nonlinear time history analysis are of paramount importance for seismic analysis to investigate the performance of such type of dampers.

The main objective of this research paper is to investigate the performance of mass damper under different previous earthquake for typical garments building at Dhaka City. A series of time history analysis is conducted to observe the actual behavior of eleven-story building frame structure. In addition, results are comparing in terms of base shear, joint acceleration and joint displacement for the structure with and without damper considering S_Monica, Altadena and Corralit earthquake motion.

2 FINITE ELEMENT MODEL

Using Finite Element software of ETABS 2015, the study of the installing damper in11 story 2D frame building having geometry of 8 bays in X direction and 6 bays in Y direction is an important factor for the analysis. The model of this building has been executed from an existing garment building design. There are many research works reported on various dampers aspect like linear and nonlinear static and linear and nonlinear dynamic analysis of buildings frame.

Following material properties and geometry have been considered:-

1) Compressive strength of concrete- 4000 psi
2) Yield strength of steel – 50 grade
3) The typical story height
    i) Floor to Floor height is 10 ft
    ii) GF and 1st floor height is 14 ft
4) Loads-
    a) Dead Loads: 75 psi
    b) Live Loads: 60 psi
5) Types of dampers-
    a) Exponential Damper
    b) Bilinear Damper
    c) Friction Spring Damper

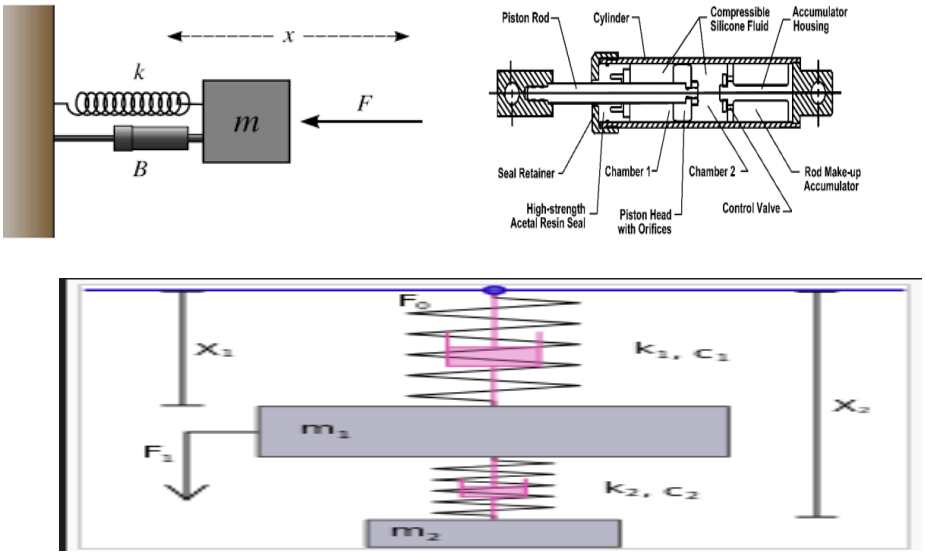

Figure 1: Typical figures of damper

In this research paper the dampers are provided on the top three floors for seismic analysis. A comparison of structure in EQ of different mass percentages and various time history analyses with and without mass dampers has been carried out.

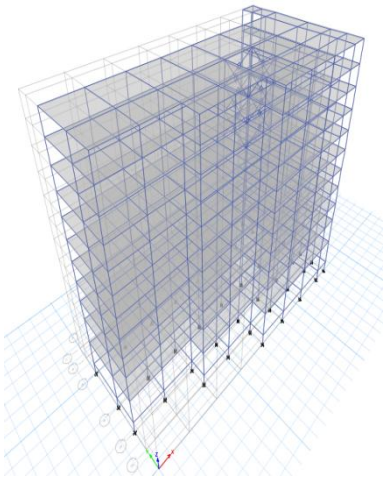

Figure 2: 3d view of eleven floor building model

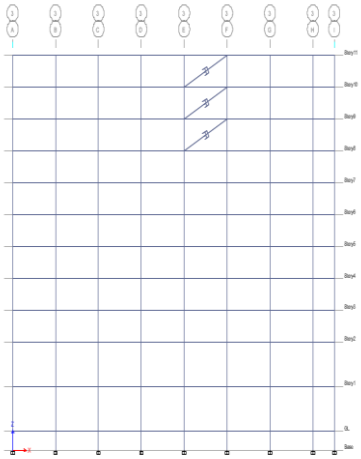

Figure 3: Elevation of model

Table 1: Damper properties

Damper	Linear Properties		Non- Linear Properties					
	Stiffness (Kip/in)	Effective Damping (kip-s/in)	Stiffness (Kip/in)	Damping Coefficient (kip-s/in)	Damping Exponent	Initial Damping Coefficient (kip-s/in)	Yielded Damping Coefficient (kip-s/in)	Linear Force Limit
Exponential	66.67	102	100	127	1	-	-	-
Bilinear	1333	455	2000	-	-	568.4	0	0.001
			Initial (Nonslipping) Stiffness (Kip/in)	Slipping Stiffness (Loading) (kip/in)	Slipping Stiffness (Unloading) (kip/in)	Precompression Displacement (in)	Stop Displacement	Active Direction
Friction Spring	1333	455	2000	1500	1000	-.05	0	Both

The established resultants are in modal time period, moment and shear values of frames, base shear, joint acceleration, maximum joint displacement and energy dissipation.

3. RESULT AND DISCUSSION

This exploration investigation seismic evaluation of the 11 story concrete building frame structure with different percentage of mass damper and time history analysis results were tabulated in the form of modal period, moment and shear value of building frames, base shear or force and base acceleration top story displacement observed that there is significant variation in results based on the different earthquake motions.

3.1 Mode Numbers with Period

With the installment of dampers in the frame it is noted that for different mode numbers and shapes, the time period is accelerated. In this regard, exponential dampers works more effectively and bilinear damper along with friction spring damper works more or less same. As the mass of the building is increased, the time period also increased according to the equation

$$T=(2\times\pi\times\sqrt{m})\div(\sqrt{k}) \qquad (1)$$

Here, m= mass of damper and k= stiffness of damper

Table 2 represents the first 6 modes of the increment of time period for different mode shapes. The increment of building time period varies between four to ten percentages.

Table 2: Increment of building time period

Mode Number/ Shape	Time Period (sec) Without Damper	Time Period (sec) With Exponential Damper	Percent Increased
1	1.389	1.635	18
2	1.285	1.552	21
3	0.219	1.288	5
4	0.428	0.461	8
5	0.396	0.434	10
6	0.376	0.392	4

3.2 Moment and Shear Value

Moment and shear value of analyzed building frames are drastically reduced if dampers are provided on the involved frames. Herefor elevation 34FF frames and load cases EQY and WINDY are only investigated. Table 3 illuminates the percentages of the maximum reduction of shear and moment values for the 34FF frame. It explores that maximum 74 percent of moment and shear values are reduced.

Table 3: Moment and shear value reduction

Kind of Response of Structure	Without Damper	Bilinear Damper	Percent Reduction %	Friction Dampers	Percent Reduction %
Moment Values (kip-ft) for EQY	282.8	100.04	65	93.77	69
Moment Values (kip-ft) for WINDY	271.73	73.18	73	70.54	74
Shear Values (kip) for EQY	38.52	19.510	49	18.56	52
Shear Values (kip) for WINDY	37.118	14.439	61	14.046	74

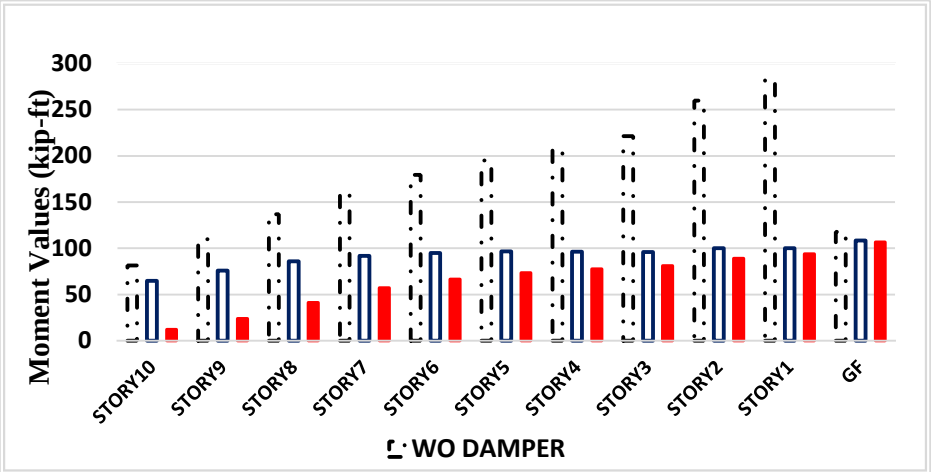

Figure 4: Moment values diagram for EQY

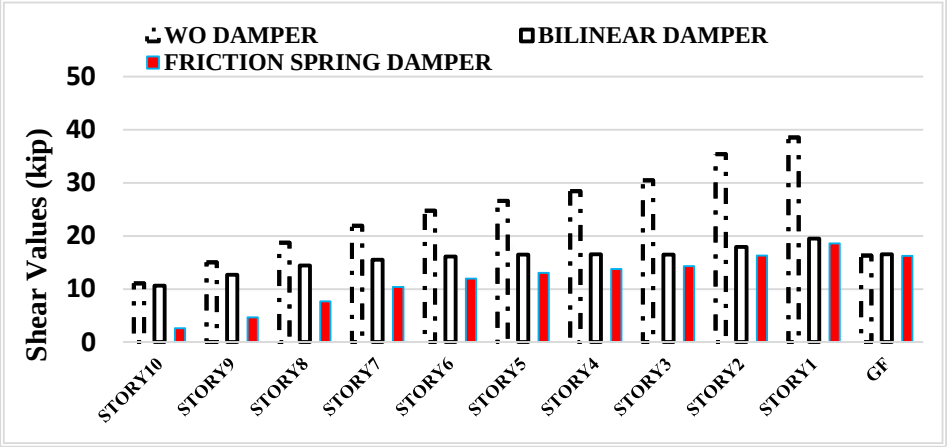

Figure 5: Shear values for EQY

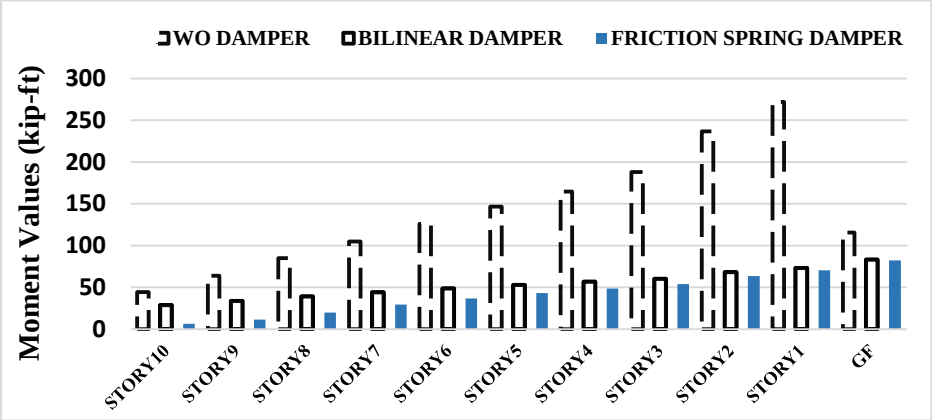

Figure 6: Moment values for WINDY

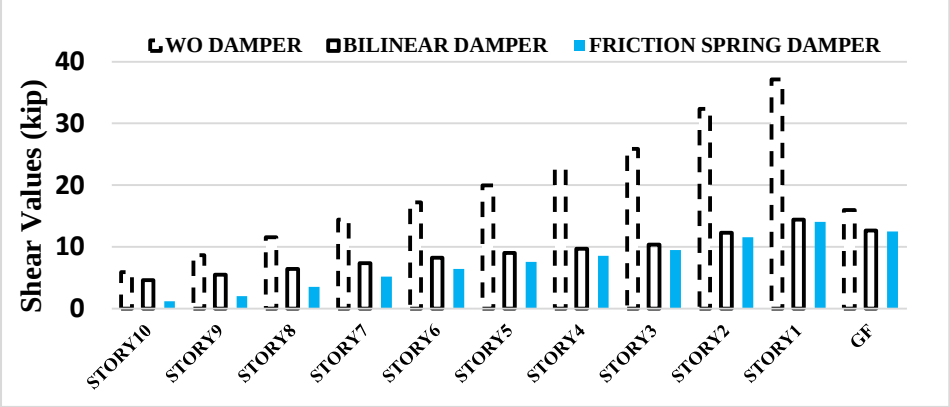

Figure 7: Shear values for WINDY

Figure four to seven explicit that by installing mass dampers in frame structures the moment and shear value decreases to a required level. Thus the amount of reinforcement can be reduced and the frames will be safer for their performance. It may be observed that the values drop down drastically for the floors near to the ground.

3.3 Percent Mass Damper Analysis

Mass percentages of dampers are determined from the total building weight and mass. Here varying building mass ratios of 0.5%, 1%, 2%, 3% and 5% were applied. Figure 8 and 9 executes that by increasing the mass percentages of dampers the story displacement of the building against EQ motion in both direction increases than without damper frame structure.

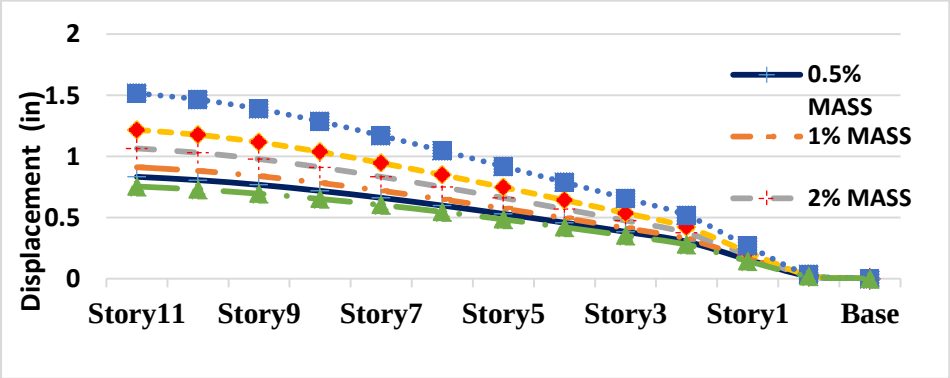

Figure 8: Displacement of stories for EQX

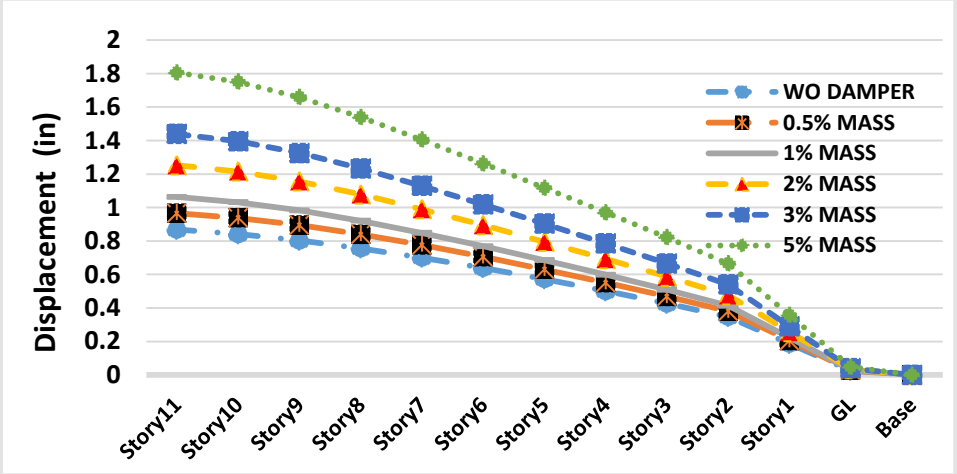

Figure 9: Displacement of stories for EQY

3.4. Time History Analysis of Building Frame

ETABS is a structural design and analysis programming software uses finite element method technique. With the help of ETABS 2015 eleven- story building frame has been analyzed for seismic performance without damper and with damper for linear and nonlinear time history analysis.

3.4.1 *Maximum Base Shear or Force*

The maximum values of base reaction of 11 floor frame while damper is provided on the top three floor for EQ S_Monica, EQ Altadena , EQ Corralit are specified in Table 4. It is noticeable that maximum base shear increase effectively for different earth-quake load case when dampers are provided compared to usual frame (Without damper). But for EQ Altadena it drastically reduces when Bilinear Damper is provided.
It is perceived that the base forces are maximum and almost same for Exponential Damper and Friction Spring Damper and a small amount less for Bilinear Damper than the other two. Moreover it is peak for EQ S_Monica then EQ Corralte and then EQ Altadena for Exponential Damper.

Table 4: Base shear

Load Cases	WO Damper(kip)	Base Reaction With Damper (Kip)		
		Exponential Damper	Bilinear Damper	Friction Spring Damper
EQ S_Monica2	774.069	1438.9	1275.3	1402.3
EQ Altadena	1536.8	1707.2	1022	1561.2
EQ Corralit	1143.3	1275.2	1294.1	1281.4

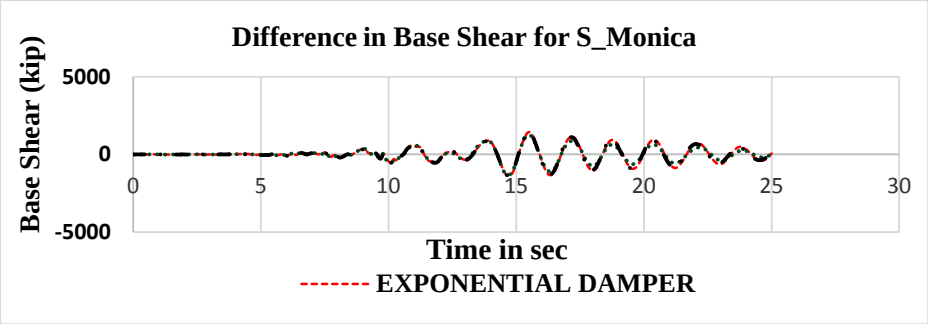

Figure 10: Base shear for different dampers

Figure 10 and 11 articulates that by installation of mass dampers the base shear upsurges fo regarding EQ Altadena only.r exponential damper and friction spring damper but drops down for bilinear damper.

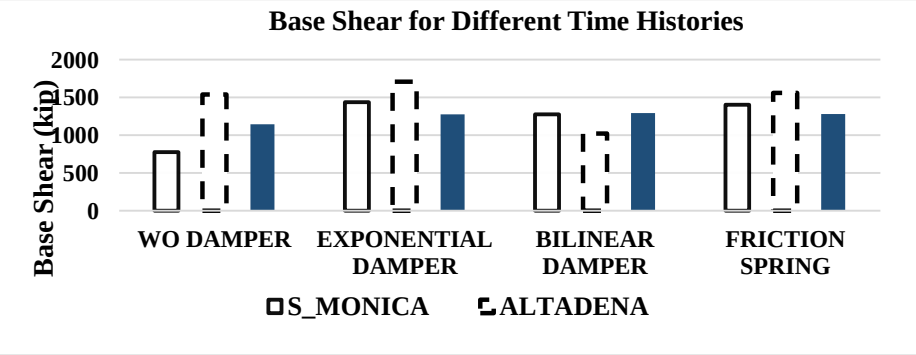

Figure 11: Bar chart for base shear for different dampers and time histories

3.4.2 *Maximum Joint Acceleration*

The maximum values of joint acceleration of 11 floor frame are found when damper is provided on top three floors for EQ S_Monica, EQ Altadena, and EQ Corralit load. Table 6 comply with the increment of top floor joint (number 2) acceleration for different earth-quake load case when dampers are provided in the building compared to without damper frame. For EQ S_Monica and EQ Corralit joint acceleration increases from the normal frame while providing damper but the opposite occurs for EQ Altadena.

Table 5: Joint acceleration

Load Cases	Joint Acceleration Without Damper (in/sec^2)	Joint Acceleration With Damper (in/sec^2)		
		Exponential Damper	Bilinear Damper	Friction Spring Damper
EQ S_Monica	47.3	58.42	61.44	53.53
EQ Altadena	151.79	132.28	110.35	130.51
EQ Corralit	55.968	65.55	73.43	64.81

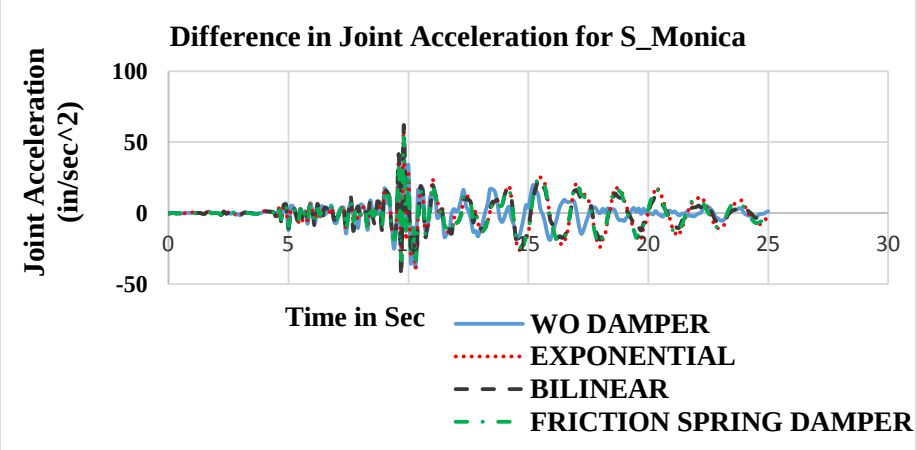

Figure 12: Joint acceleration for different damper

Figure 12 and 13 extracts that by installation of mass dampers the joint acceleration escalatesfor EQ S_Monica and Corralit. Interestingly the joint acceleration decreases for all three dampers in EQ Altadena.

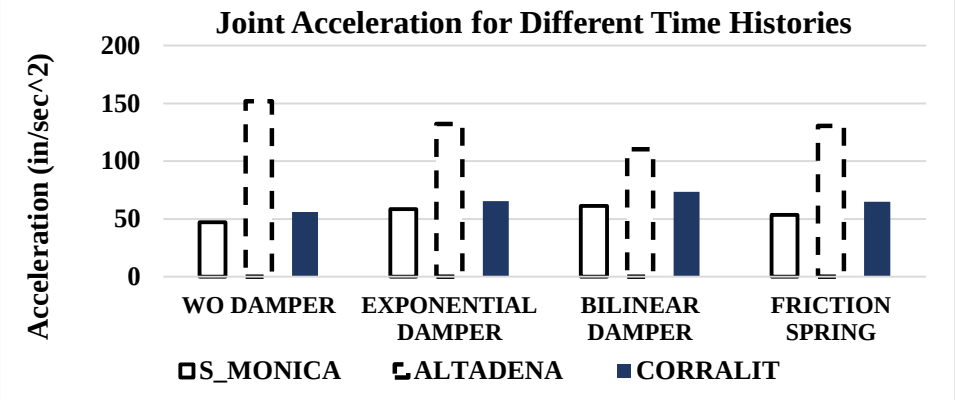

Figure 13: Bar chart for joint acceleration for different dampers and time histories

3.4.3 *Maximum Joint Displacement*

Table 6 perceives the upsurge of top floor joint (number 2) displacement for different earth-quake load case when dampers are provided in the building compared to without damper frame.

Table 6: Joint Displacement

Load Cases	Joint Displacement Without Damper (in)	Joint Displacement With Damper (in)		
		Exponential Damper	Bilinear Damper	Friction Spring Damper
EQ S_Monica2	.808	1.713	1.64	1.63
EQ Altadena	1.37	1.88	1.91	1.83
EQ Corralit	1.05	1.44	1.34	1.45

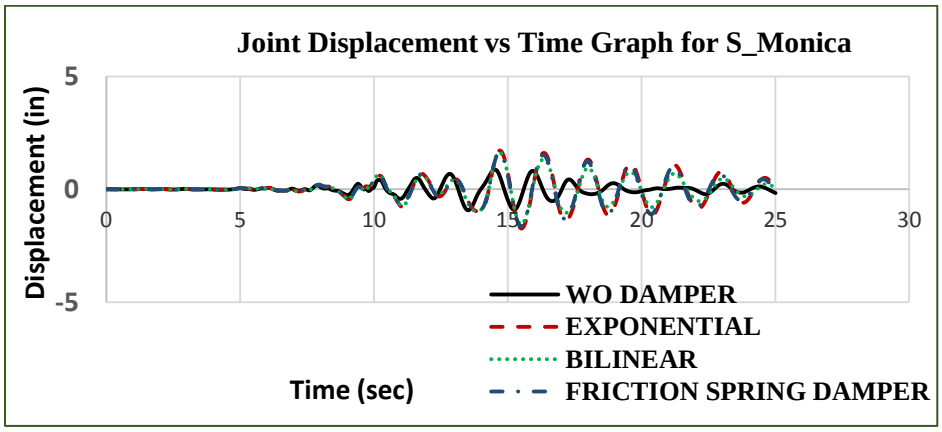

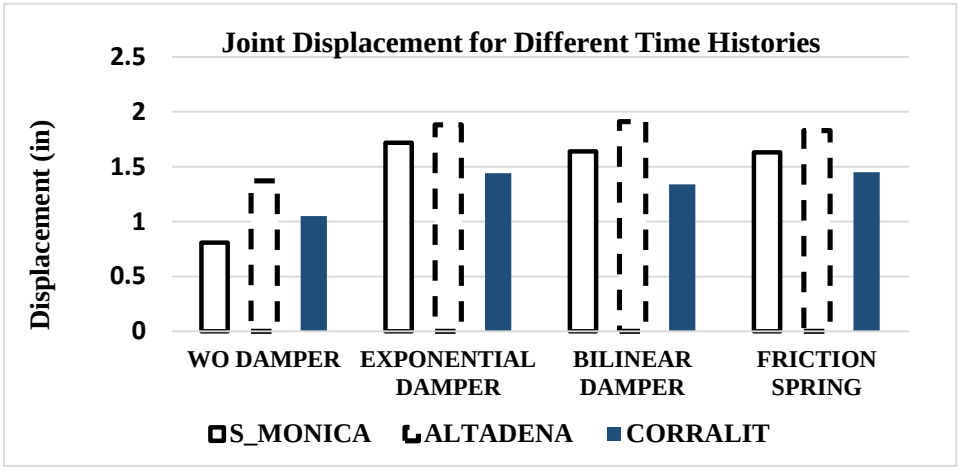

Figure 15: Bar chart for joint acceleration for different dampers and time histories

Figure 14 and 15showsthatmass dampers increase the joint displacement and the value is maximum for exponential damper for all three earthquake motions.

3.5 Hysteresis Loop

The hysteresis loop is the result of dynamic hysteresis as related to the dynamic nature of loading. The area of the hysteresis loop is proportional the energy that is dissipated by the dampers [10]. Nonlinear property of damper is well studied by the hysteresis loop. Figure 21 shows the hysteresis loop of only one damper for the EQ S_Monica for Exponential as well as Bilinear dampers at the largest

time period T=25 sec. The more is the hysteresis in the stress-strain curve, the greater is the energy dissipation, and hence the higher is the damping ability.

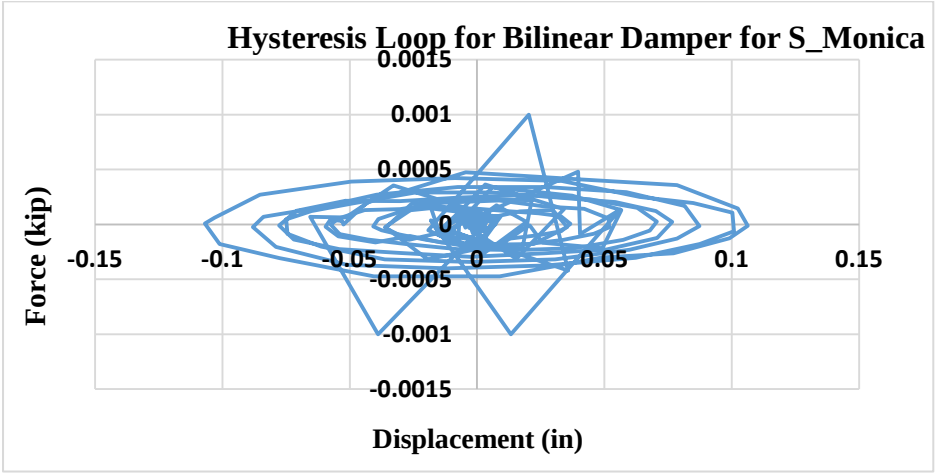

Figure 16: Hysteresis loop for bilinear damper

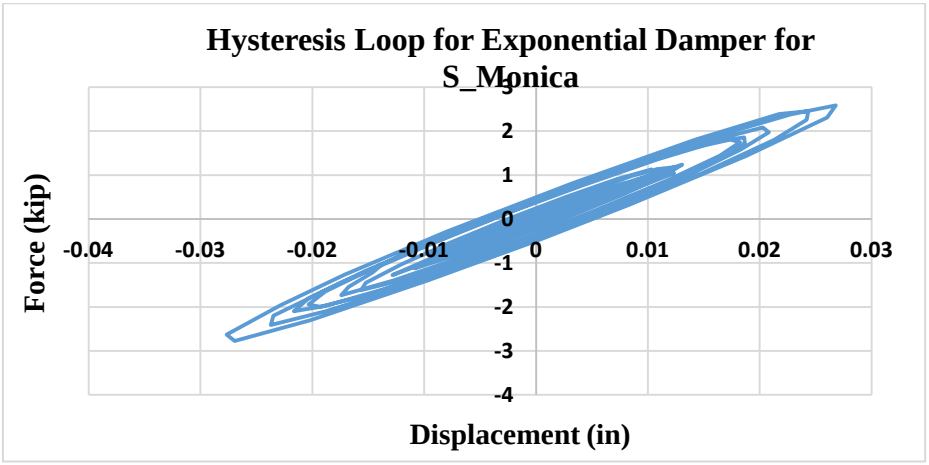

Figure 17: Hysteresis loop for exponential damper

In this force displacement curve, Figure 16 and 17 it is perceived that bilinear damper dissipates more energy than exponential damper as its loop area is more.

4. CONCLUSION

1. Seismic performance of building can be improved by providing energy dissipating device (damper) as the modal time period is increased.
2. The frames are safer when damper is provided in the structure as moment and shear values are drastically reduced.
3. According to the area covered by hysteresis loop, for EQ S_Monica Bilinear damper and Exponential damper dispels more energy.
4. Damper works effectively for high rise as well as slender buildings.
5. The story displacements are increased with the increment the percent of mass dampers for both EQ and time history load thus the building becomes more ductile.
6. With the deployment of dampers in the structure the base acceleration is decreased for some EQ motion thus the inertia forces are reduced.

REFERENCES

[1] Thakur V.M., Pachpor P.D., January 2012, International Journal of Engineering Research and Applications (IJERA) ISSN: 2248-9622 www.ijera.com Vol. 2, Issue 1, Jan-Feb. 2012, pp. 319-326.

[2] E. D. Wolff, E C. Ipek, M. C. Constantinou and M. Tapan, 2014. *Effect of viscous damping devices on the response of seismically isolated structures*, Published online in Wiley Online Library (wileyonlinelibrary.com). DOI:10.1002/eqe.24643.

[3] Waseem Khan, Dr. SaleemAkhtar, AslamHussain, April 2014, *Non- linear time history analysis of tall structure for seismic load using damper*, International Journal of Scientific and Research Publications, Volume 4, Issue 4.

[4] RupaPurasinghe, *Seismic Evaluation And Retrofit Of A Moment Frame Building With Viscous Dampers*, Professor of Civil Engineering, California State University at Los Angeles, California.

[5]QasimShaukat Khan, AsadUllahQasi, and Muhammad Ilyas, July 2013, *Improved Seismic Response of RC Frame Structures by Using Fluid Viscous Dampers*, Pak. J. Engg. & Appl. Sci. Vol. 13, (p. 8-18).

[6] https://en.wikipedia.org/wiki/Damper

[7] A.B.M. Saiful Islam, Mohammed Jameel, Md. AlhazUddin, MohdZaminJumaat, 2012, *Competent Building Elevation for Incorporating Base*

Isolation in Aseismic Structure, International Conference on Advances Science and Contemporary Engineering 2012 (ICASCE 2012)

[8] G.S. Balakrishna, Jini Jacob, *Seismic Analysis Of Building Using Two Types Of Passive Energy Dissipation Devices***,** IOSR Journal of Mechanical and Civil Engineering (IOSR-JMCE), PP 13-19.

[9] I. L!opez, J.M. Busturia, H. Nijmeijer, October 2003, *Energy dissipation of a friction damper*, Journal of Sound and Vibration 278 (2004) 539–561.

[10]*Mechanical_vibrations*_5th-edition_S-S Rao

CICM 2015
First International Conference on
Advances in Civil Infrastructure and Construction Materials
MIST, Dhaka, Bangladesh, 14–15 December 2015

EFFECT OF INCREASE OF BEAM STIFFNESS ON DRIFT IN TALL BUILDING FRAMES

Farhana KABIR[1], Md. Kamruzzaman[2]

[1, 2] Department of Civil Engineering, Rajshahi University of Engineering and Technology, Rajshahi, Bangladesh
Email: [1]farhanakabir97@yahoo.com and[2]kzaman@ruet.ac.bd

Abstract. *Recently there has been a considerable increase in the number of tall buildings in urban areas. The effect of lateral loads are attaining increasing importance in designing tall buildings as lateral loads cause large top deflection to tall buildings. The problem of providing adequate strength and stability against lateral loads is the main challenge in designing tall structures. Buildings having small numbers of storey are less affected by the lateral loads. As the height of the building increases; the effect of lateral loads increases. So the design of tall buildings requires necessary consideration for minimizing the top deflection or drift. This paper aims to find out the effect of floor beams which contribute more to drift. Later, the study attempts to minimize the obtained drifts to allowable limits by increasing the stiffness of concern floor beams. ETABS is used for analysis of tall buildings. Increasing the stiffness of floor beams results reduction of top deflection to about 28% and it also reduces inter storey drift significantly.*

Keywords: Drift, ETABS, Lateral loads, Tall buildings.

1 INTRODUCTION

Tall and slender buildings are strongly wind sensitive and wind forces are applied to the exposed surfaces of the building, whereas seismic forces are inertial (body forces), which result from the distortion of the ground and the inertial resistance of the building. The behavior of the tall building frame has been studied in the last few decades in attempt to develop a rational approach to minimize the drift of the tall building frames without changing the stiffness of column. It is worth mentioning that if the stiffness of beam is taken into account in the analysis and design of tall building frames, the resulting tall frame may be significantly different. Thus to bring the drift down to allowable limits cross sectional dimension of beams and columns may have to be increased.

2 DISPLACEMENT PARTICIPATION FACTOR AND DRIFT

For the analysis of tall building frames, deformation arising from flexural, axial and shear distortion occurring within the beams, columns and beam-column joints can be computed by Displacement Participation Factor (DPF) approach. DPF is a numeric value which represents the contribution of a structural member to the displacement occurring at a specific point and in a specific direction. For example, if it is known that the lateral displacement at the roof of a 40-storey tube is 500mm, and the DPF for a column at the base of the structure is calculated to be 2.5mm, that member is responsible for 2.5/500 or 0.5% of the total drift. The sum of the DPF for all the members of the structure is equal to the displacement at the specified location. Drift index is the ratio of the maximum deflection at the top of building to the total height of the building. Sound engineering judgment is required when deciding on the drift index to be imposed. Design drift index limits that have been used in different countries range from 0.001 to 0.005. Through this method, not only it is possible to determine the deflections resulting from loads of any type, causing any kind of strains in a structure, but it is also possible to compute deflections resulting from temperature changes, errors in fabrication, or shrinkage of the structural material (Sazzad and Kamruzzaman, 2002).

3 ANALYSIS PARAMETERS & BUILDING MODEL

To analyze the buildings certain parameters are used as mentioned by the BNBC, 2006. Wind and seismic analysis also have different parameters. For the study, building frames having 3 bays and Uniformly Distributed Load (UDL) is considered for 10, 15, 20, 25, 30, 35 and 40 storey buildings. The other analysis parameters are mentioned as in Table 1 and Table 2.

Table 1: General Parameters Used in the Analysis

No of Storey	Beam for i=1	Beam for i=2	Beam for i=3	Column Size	Slab Thick. (in)	Dead Load (psf)	Live Load (psf)
10	12"x12"	12"x15"	12"x18"	12"x12"	6	45	40
15	12"x15"	12"x18"	12"x24"	18"x18"	6	45	40
20	15"x15"	15"x18"	15"x20"	20"x20"	6	45	40
25	18"x18"	20"x20"	20"x24"	24"x24"	6	45	40
30	20"x20"	20"x24"	24"x24"	24"x24"	8	45	40
35	20"x24"	24"x24"	24"x30"	36"x36"	8	45	40
40	20"x24"	24"x24"	24"x30"	36"x36"	8	45	40

Table 2: Parameters for Wind and Earthquake Loading

Wind load		Earthquake load	
Parameters	Code	Parameters	Code
Windward co-efficient	0.8	Ct	0.035
Leeward co-efficient	0.5	Numerical co-efficient, Raw	8
Importance factor	1	Zone co-efficient	0.075
Wind speed	97 mph	Site co-efficient	1.2
-	-	importance factor	1

4 RESULTS AND DISCUSSION

Drift problem is one of the most serious issues in tall building design, relating to the dynamic characteristics of the building during earthquakes and strong winds. In this paper, the variation in drift or top deflection is found by analysis in ETABS. After the analysis the floors are identified which contributes more to drift. Then the stiffness (i.e moment of inertia) of the beams of those floors is increased by 2 to 3 times. The obtained drift values are compared to code and some significant results are found. This procedure is repeated to 10 to 40 storey building. Figure 1shows the variation of top deflection due to wind load on a 30 storey building by increasing the stiffness of the beam to 2 and 3 times. It is evident for that (Fig. 1), top deflection reduces to about 28% by increasing the floor beam stiffness by three times.

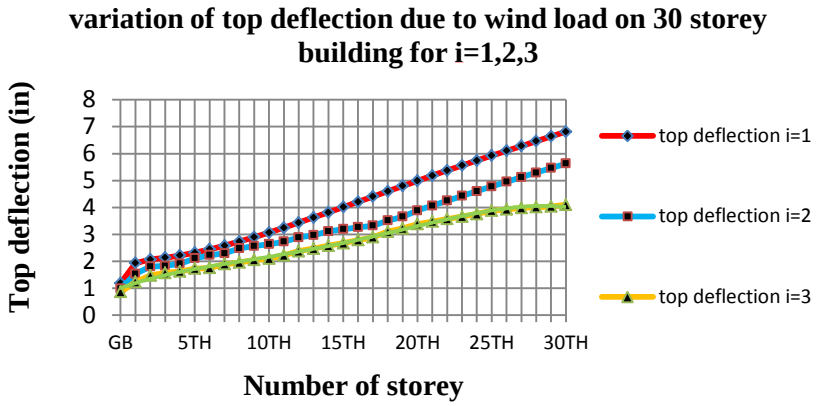

Figure 1: Wind Induced Inter Storey Drift Reduction on a 30-Storey Frame at I, 2I and 3I.

Following Fig. 2 and Fig. 3 depicts the minimization of Inter Storey Drift (ISD) due to wind load for 30 and 35 storey building respectively by increasing the stiffness of floor beams by 2 to 3 times.

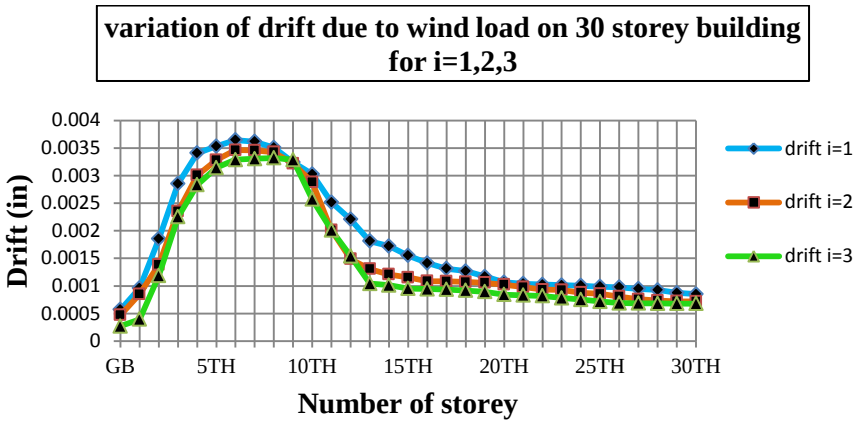

Fig. 2 Wind Induced Inter Storey Drift Reduction on a 30-Storey Frame at I, 2I and 3I.

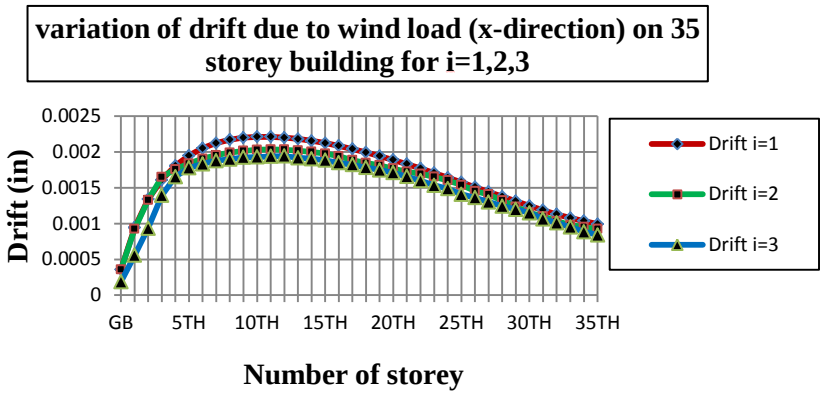

Fig. 3 Wind Induced Inter Storey Drift Reduction on a 35-Storey Frame at I, 2I and 3I.

Next Fig. 4 shows the variation of top deflection due to seismic load for 30 storey building by increasing the stiffness of beam by 2 and 3 times. About 19% top deflection can be reduced if the stiffness of floor beams is increased by threetimes (Fig. 4).

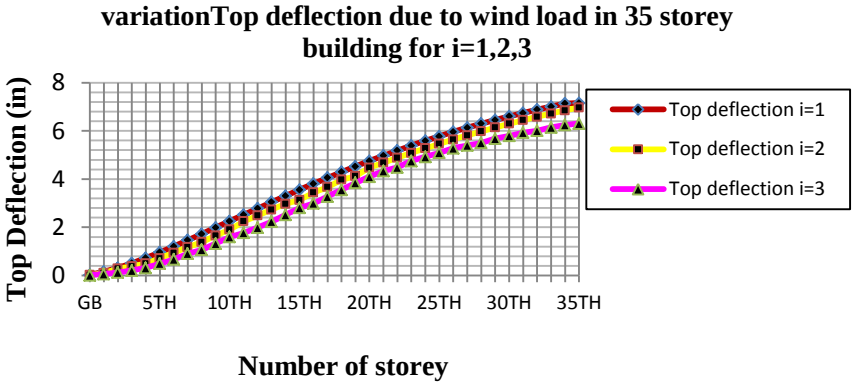

Fig. 4 Seismic Load Induced Drift Reduction on a 30-Storey Frame at I, 2I and 3I.

By increasing stiffness of floor beams to 2 and 3 times; top deflection can be reduced to about 24% for wind load. From the analysis of the buildings it is clear that the reduction in top deflection is considerable upto 30-storey building for wind load only. After that there seems to be no significant changes by increasing the floor beam stiffness (Fig. 5).

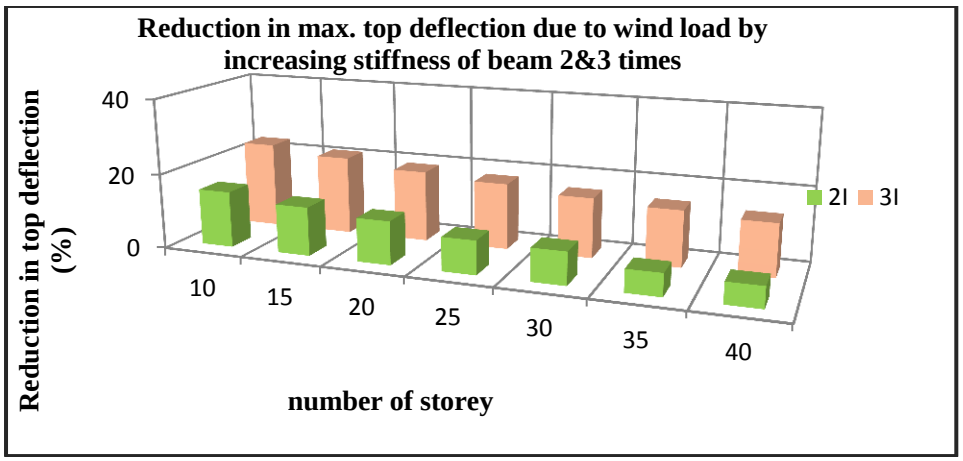

Figure 5 :Seismic load induced drift reduction on a 30 storey frame at I,2I, 3I

By increasing stiffness of floor beams to 2 and 3 times; top deflection can be reducedto about 22% for seismic load. From the analysis of the buildings it is clear that the reduction in top deflection is considerable up to 30-storey building for earthquake load only. After that there seems to be no significant changes by increasing the floor beam stiffness (Fig. 6).

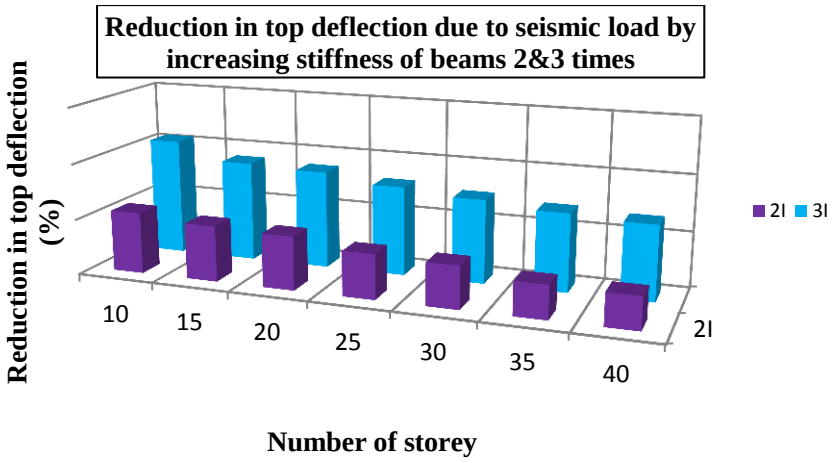

Fig. 6 Drift Reduction for Seismic Load on 10 to 40-Storey Frame at 2I & 3I

5 CONCLUSION

The result of the analysis can be summarized as follows –

1. Effect of increase in beam stiffness to certain floor beams is significant.
2. The intermediate floors contribute maximum ISD than the topfloor.

Table 3: Location of Floors Contributing Max. ISD

Storey	Floors Contributing Max. ISD due to Wind Load	Floors Contributing Max. ISD due to Seismic Load
10	2nd – 3rd	2nd – 4th
15	2nd – 4th	3rd – 4th
20	3th – 8rd	4th – 9th
25	4th – 8th	4th – 8th
30	4th – 8th	5th – 8th
35	5th – 9th	5th – 9th
40	6th – 10th	5th – 11th

3. For wind load, maximum 28% top deflection can be achieved by increasing stiffness up to 3 times at 2^{nd} to 10^{th} floors. For earthquake load, maximum 19% top deflection can be achieved by increasing stiffness up to 3 times at 3^{rd} to 9^{th} floor.
4. For wind load; max. ISD appears at 2^{nd} to 10^{th}storey. For earthquake load; maximum ISD appears at 3^{rd} to 9^{th} storey.

REFERENCES

1. M. M. Sazzad, and M. Kamruzzaman (2002), Characterization and Drift Minimization of Tall Building Frames, Journal of Civil Engineering, The Institute of Engineers (IEB),Vol. CE 30.

CICM 2015
First International Conference on
Advances in Civil Infrastructure and Construction Materials
MIST, Dhaka, Bangladesh, 14–15 December 2015

FINITE ELEMENT ANALYSIS OF AIRFIELD FLEXIBLE PAVEMENT

Tahmida H. Shimu[1], Mohd. M. RAHMAN[2], Md. N. Hossain[3], Nusrat J. Nilu[4], Khondaker S. Ahmed[5]

[1, 2, 3, 4, 5] Department of Civil Engineering, Military Institute of Science and Technology, Dhaka, Bangladesh.
E-mail: [1]tahmida@ce.mist.ac.bd and[2]mehedi1341@gmail.com

Abstract.*In recent days, finite element analysis is widely introduced to minimize the limitations associated with empirical methods in order to assess pavement performance (Stress, Strain, and Displacement) in an efficient manner. This research mainly focuses on the application of finite element method (FEM) to evaluate mechanical behaviors and pavement performance of an airfield pavement under a standardized aircraft loading. For this purpose, a 2-Dimensional, 3-layered aircraft pavement is modeled using finite element software ABAQUS 6.13. The layers are modeled as linear elastic layers which represent an asphalt surface, an aggregate base and a granular subgrade. Dimensions and material properties of these layers are taken from FAARFIELD, a software to design airport pavement. The aircraft wheel load is modeled as a uniform pressure load on the asphalt surface for simplicity. The objective of this study is to evaluate airfield pavement performance under simplified simulation environment in ABAQUS to serve as a preliminary basis of stress-strain analysis of pavement under aircraft loading.*

Keywords: Finite element analysis**,** Airfield flexible pavement, FAARFIELD, Dynamic loading.

1 INTRODUCTION

Transportation system is referred to as one of the most essential infrastructures that influence the overall development of a country. The design of airfield flexible pavement almost resembles to traditional empirical design methods of highway pavement and from generation to generation it is modified to handle vulnerable situations. Airports are invincible part of air transportation system. Most of the airports in our country are mainly flexible pavement comprising with asphalt layer at top followed by base, sub-base (optional), and sub-grade [2]. This pavement experiences not only domestic aircraft landing but also international. The expansion and maintenance of international airports are quite difficult due to financial constraints and land scarcity. As a result it generates a pressure on existing airport and ultimately affects both national and international communication [1-5]. To cater critical cases of existing pavement, an attempt has been taken in this research for predicting pavement performance. Both 2-D and 3-D modeling of airfield pavement can be used to evaluate pavement performance [2].

Based on existing literature, direct/analytical solutions of design approaches become convoluted due to some complexities of the system such as heavy aircraft loading, complex tire configuration, and dynamic implicit nature and direction of loading and acceleration-deceleration phenomenon [5-6]. This is why recent studies have approached numerical solutions by using finite element technique to study the pavement responses on an airfield.

In this study, a 2-D three layered pavement is modeled using finite element package Abaqus to investigate the structural performance in terms stress distribution in different layers of airfield flexible pavement. Since such problem can be idealized as plane stress problem, 2-D model is expected to extract results close to 3-D approximation considering all other challenges. Material properties are taken from FAARFIELD with an arbitrary aircraft combination. In addition, a brief study of convergence for different seed control is also conducted and finally meshing the most vital part is successively done by trial and error process with a view to achieve higher degree of accuracy.

2 METHODOLOGY

This study focuses on evaluating structural responses of airfield pavement in 2-D model using finite element software ABAQUS. A convenient approach has been taken to establish a standard wheel configuration, wheel pressure, contact area to use on this software for evaluating stress-strain characteristics of flexible pavement. Stress-strain analysis is used to predict distresses in pavement and different failure condition.

Basically, ABAQUS is a finite element software widely used for stress analysis. In this software, modeling of structural systems can be executed through ac-

commodating multifarious facilities such as boundary condition in both vertical and horizontal directions, loading as pressure or velocity and direction, surface condition, fine meshing, different material properties (linear elastic, elasto-plastic, hypo-elastic etc.) under a computer simulated environment [2]. Finally, using the finite element technique the software generates various output variables as requested such as plots of stress distribution and deflection along the modeled systems. The study of convergence of stress and deflection can also be done in this software by changing the mesh size control and comparing the variation in stress-deflection contour plots.

2.1 Dimensioning and Material Properties Considered

Considering four layered flexible pavement –HMA surface course, aggregate base course, crushed aggregate sub-base course and granular subgrade course, thickness of different layers are extracted from FAARFIELD for an arbitrary aircraft combination (Table-1). Arbitrary values are considered as inputs for annual departures of aircrafts. For these thicknesses, a 3-layered 2-D pavement is modeled in ABAQUS as a standard/explicit model. To simulate an infinite subgrade layer in the bottom, this layer is ignored in the model and is replaced with a fixed support. A constant slope of 45º is considered on both sides at each layer.

Assuming that all materials behave linearly within the elastic limit, moduli of elasticity of different layers are also taken from FAARFIELD for the above mentioned combination of aircraft loading (Figure 1). A constant poison's ratio of 0.35 is considered for all the layers as suggested in FAARFIELD. Densities of these layers are taken from Advisory Circular of FAA [7] for a typical airfield pavement (Table 2).

Table 1: Aircraft combination for which thickness of different layers are extracted from FAARFIELD

No.	Name	Gross Wt. lbs	Annual Departures
1	A320-100	150,796	360
2	B737-800	174,700	600
3	B757-300	273,500	800
4	B787-8 (Preliminary)	486,000	600
5	B707-320C	336,000	1,300
6	B737-900	174,700	300
7	A310-200	315,041	1,000
8	MD83	161,000	800

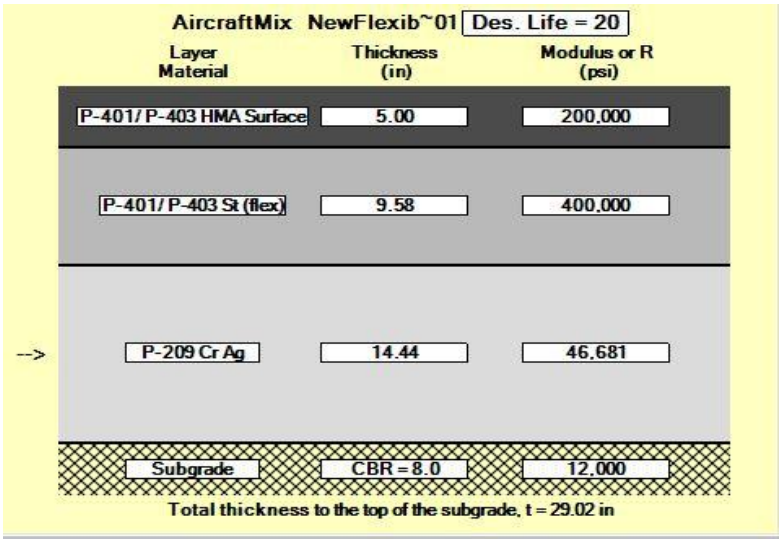

Figure 1: Structure of flexible pavement

Table 2: Material properties of different pavement layers

Layer No.	Type	Poison's Ratio	Density (pci)
1	P-401/ P-403 HMA Surface	0.35	0.069444
2	P-401/ P-403 St (flex) (Stabilized base coarse)	0.35	0.070602
3	P-209 Cr Ag (Sub base)	0.35	0.072338

2.2 Boundary and Surface to Surface Interaction Modeling

Boundary conditions are considered as displacement or rotational. The boundaries on both sides of the model are restricted to move along X axis and free to move along Y axis (U1=0) and at the bottom fixed support is considered (U1=U2=UR3=0) to simulate an infinite subgrade. Surface to surface interaction is taken as Tie and internal friction among them is neglected.

2.3 Loading

In this study, a uniform pressure load is applied at the top of asphalt surface. The loading value is obtained from FAARFIELD by considering the following parameters of Boeing 707-320C aircraft which is taken as the design aircraft for this study (Table-3).

Table 3: Loading parameters

Parameters	Values considered
Aircraft Model	B 707-320C
Gross Takeoff weight	336000 lbs
Tire Contact width	14 in
Wheel load	39900 lbs
Load given by FAARFIELD	2850 lb/in.

2.4 Element type and meshing

Fine meshing is done all through the section to obtain approximate results. Finer local seeds are considered with a direction towards load and a biased ratio of 5 (>1) where load is applied to accommodate for the higher stress and nodal displacements at that region. Meshing details used in this study are given in Table 4.

Table 4: Meshing details.

Mesh Control	Quad-Dominated		
Element Type	Standard-Linear-Plane Stress		
Number of seeds control (Edge)	Layer No.	Top	Bottom
	1	160	50
	2	50	55
	3	55	60

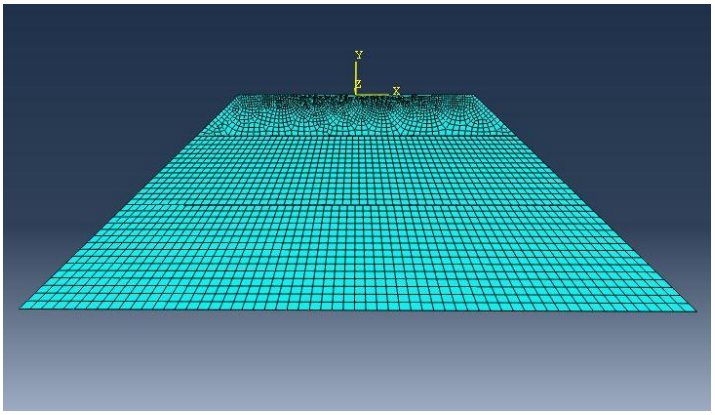

Figure 2: Element meshing with bias ratio

3 RESULTS AND INTERPRETATION

Finite element modeling provides stress in both directions. On the basis of element type, meshing, boundary condition and surface modeling, large variations in results are obtained. Stresses found in this study are shown in Figure 3.In this case due to vertical static load, tensile strain in horizontal direction and compressive strain in vertical direction prevail. Deflection plot found from analysis is given in Figure 4.

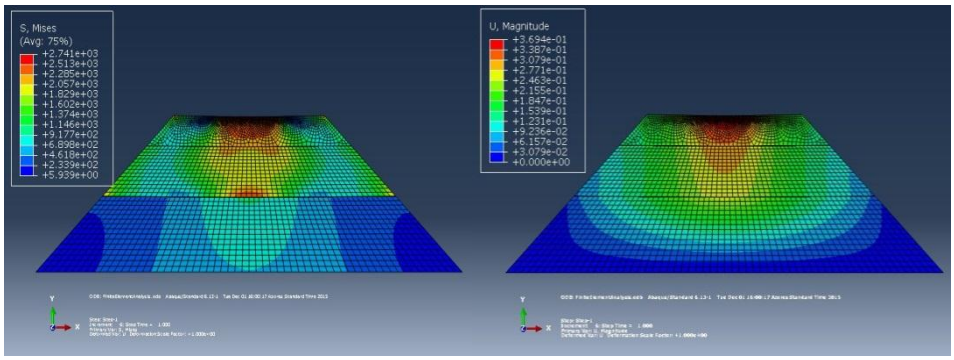

Figure 3 : von-Mises stress contour plotFigure 4: Maximum deflection plot

Stress at the top layer of asphalt surface course is found maximum where the load is applied as expected but there also generates a maximum stress zone at contact surface of base and subbase course. A uniform pressure bulb is seen in the stress contour plot as well as in deflection plot. Deflection gradually decreases with the depth of pavement layer. Maximum and minimum stress and deflection at different layers are shown in Table 5.

Table 5 : Maximum and minimum stress and deflection at different layers

Layer	Maximum Stress (psi)	Minimum stress (psi)	Layer	Maximum Deflection (inch)	Minimum Deflection (inch)
1st	2.741E+03	2.339E+02	1st	3.694E-01	1.231E-01
2nd	2.513E+03	6.898E+02	2nd	3.079E-01	6.157E-02
3rd	1.146E+03	2.339E+02	3rd	2.771E-01	3.079E-02

A convergence study is done with varying element number at top layer. From this study, it is found that stress increases with an ascending order along with

increasing number of element (Figure 4) and around at 300 no. of elements, the convergence is established and the stress value becomes saturated.

Table 6: Summary of convergence study

Element No at Top Edge	Maximum Stress, Psi
160	2.741E+03
200	2.781E+03
240	2.937E+03
280	3.289E+03
320	3.363E+03

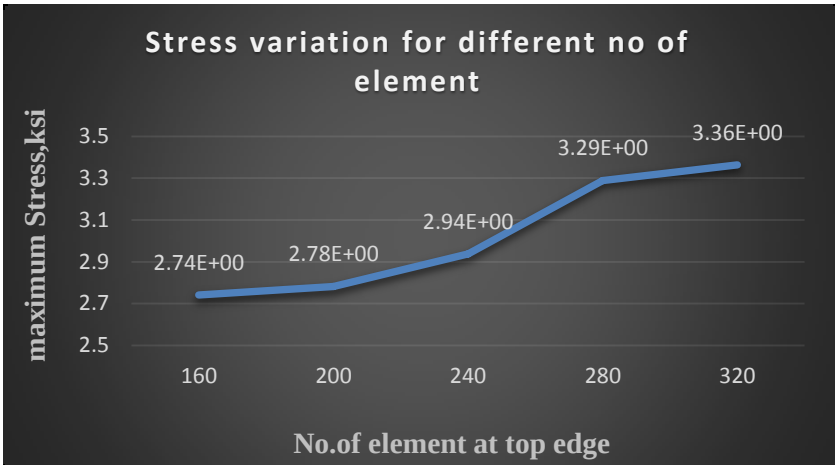

Figure5: Stress variation for different no of element

4 CONCLUSION

To draw an overview of this study, a typical airfield pavement was initially designed using FAARFIELD from where thicknesses of different layers and material properties are obtained against an arbitrary aircraft combination. Basing upon these parameters, a finite element model of airfield pavement was established in ABAQUS. From stress analysis, maximum values of von misses stress were found to be 2.741E+03, 2.513E+03 and 1.146E+03 psi, respectively at top, middle and bottom layer contact surfaces. These stress values found from this analysis can be further used to draw allowable stress or limit stress for mechanistic or empirical pavement design procedures. In addition, from the convergence check, a saturation condition was found at a number of element or mesh controls of 300 seeds at top edge. This parameter can be used to optimize the stress-strain analy-

sis of airfield pavement in further studies. A typical airfield pavement is of dynamic implicit nature as the pavement layers represent anisotropic characteristics. The wheel loading is also of nonlinear nature to apprise for acceleration/deceleration phenomenon of aircrafts. In this study, nonlinearity is assimilated only in geometry but the layers are modeled as linear elastic with standard/explicit system. A uniform and static pressure load which is equilibrium to that of a design aircraft loading is considered to represent wheel load.

For further research, a 3D dynamic implicit model along with standard tire imprint area can be carried out. Also, dynamic acceleration or velocity type load to apprise for the true representation of aircraft landing and takeoff can be considered. Thus, a complete finite element study on airfield pavement design approach can produce an economic design procedure for airport runways.

REFERENCES

[1] Bhalla, B.,Vankar, A. A., and Zala, L.B., "Runway Pavement Design of a proposed Airport with the use of FAARFIELD Software", *International Journal of Science and Modern Engineering (IJISME) ISSN: 2319-6386, Volume-1, Issue-6, May 2013.*

[2] Rahman, M.T., Mahamud ,K., and Ahsan, S., "Stress Strain characteristics of flexible pavement using Finite Element Analysis", *International Journal of Civil and Structural Engineering, ISSN 0976 – 4399,Volume 2, No 1, 2011.*

[3] Leonardi, G., "Finite Element Analysis of Airfield Flexible Pavement," *Science Letter Volume 3, University of Reggio Calabria, Italy.*

[4] Sukumaran, B., "Three Dimensional Finite Element Modeling Of Flexible Pavements," *Federal Aviation Administration (FAA) Worldwide Airport Technology Transfer Conference, USA (2004).*

[5] Zdiri, M., Abriak, N., Neji, J., and Ouezdou, M. B., "Modelling of the Stresses and Strains Distribution in an RCC Pavement Using the Computer Code Abaqus", *Electronic Journal of Structural Engineering, 9 (2009).*

[6] Wardle, L. J., and Rodway, B., "Recent Developments In Flexible Aircraft Pavement Design Using The Layered Elastic Method," *Third Int. Conf. on Road and Airfield Pavement Technology, Beijing, April 1998.*

[7] Advisory Circular, U.S Department of Transportation, Federal Aviation Administration, AC No -150/5320-6E, (2009).

CICM 2015
First International Conference on
Advances in Civil Infrastructure and Construction Materials
MIST, Dhaka, Bangladesh, 14–15December 2015

EFFECT OF MOISTURE CONTENT ON THE CBR PUNCTURE RESISTANCE OF JUTE GEOTEXTILE

Maruf HASAN[1], **Debojit Sarker**[2] **and Sarwar J. M. Yasin**[3]

[1, 2, 3] Bangladesh University of Engineering and Technology, Dhaka, Bangladesh.
Email: [1]hasan.maruf008@gmail.com, [2]debojitmom@gmail.com and
[3]sjmyasin@ce.buet.ac.bd

Abstract. *Jute geotextile has turned into a promising material for various Civil Engineering use. Utilization of jute geotextile as an alternative to synthetic geotextile is expanding by a great extent in present days because of its accessibility, availability and effectiveness in the countries like Bangladesh and India. Use of Jute geotextile instead of synthetic geotextile is cost effective. The adequacy of Jute Geotextile depends on several properties of jute sample. The fundamental properties are- Tensile Strength, Durability, Puncture, and Resistance and so on. Strength of Geotextiles is usually referred to as Grab Tensile strength and wide width Strip Tensile Strength. The objective of this paper is to observe the variation in Grab and Wide Width Strip Tensile Strength and Elongation of Jute Geotextile with the change in moisture content of the sample. Three types of Jute Geotextiles to be specific- Untreated, Bitumen Treated and Latex Treated specimens were tested. It is observed that Moisture content has an extraordinary impact on the tensile strength and elongation properties of the Jute Geotextiles. Both the Grab tensile strength and wide width strip tensile strength are decreased with the increase in Moisture Content. The CBR load is likewise reduced with the increase in Moisture Content. The rate of decrease is increased with the increase in Moisture Content.*

Keywords: Geotextile, Types of Geotextile, Moisture content, CBR Puncture Resistance.

1 INTRODUCTION

Geotextiles were the first to use in erosion control applications and were intended to be an alternative to granular soil filters. Thus, the original and still sometimes used term for geotextiles is 'filter fabrics'. The work originating in the late 1950s using geotextiles behind precast concrete erosion control blocks, beneath large stone riprap, and in other erosion control situations (Barrett, 1966). In the late 1960s, Rhone-Poulenc Textiles in France began working with nonwoven needle-punched fabrics for quite different applications (Koerner, 1997). Emphasis was given on reinforcing unpaved roads, beneath railroad ballast, within embankments and earth dams. The primary function in many of these applications was that of separation and/or reinforcement. The Dutch and the English can be given credit for early work in the use of geotextiles. ICI Fibers was a major influence in the use of nonwoven, heat-bonded fabrics in a wide variety of uses. Mirafi, Inc. imported the first nonwoven used in the U.S. from ICI Fibers in the late 1970s (Koerner, 1997).

In view of these developments, jute, a natural fiber has come up to supplement and/or replace synthetics, has been receiving increasing attention from the industry. The past success of jute is due largely to its environment friendly characteristics. Jute fiber is comparable or superior to synthetic fiber in physical and chemical characteristics. Jute is biodegradable and its products can be easily disposed without causing environmental hazards. The use of jute as a geotextile will help to; at least partially solves the two biggest environmental problems we are facing today: deforestation and soil erosion.

A joint project was taken by India and Bangladesh named as "Development and Application of Potentially Important Jute Geotextiles" in September, 2009. The main objective of the project was to research on the usage and advancement of the jute as a geosynthetics fiber and to make the people understand about the usefulness of Jute Geotextiles (JGT).

2 OBJECTIVES

The paper aims to present the following objectives:

- Values of CBR puncture resistance of various Jute Geotextile samples.
- The variation of puncture resistance with the change of moisture content.
- Test results on untreated, bitumen treated and latex treated JGT.

3 DEFINITION AND ADVANTAGES OF JUTE GEOTEXTILE

Jute produced in Bangladesh was once known as the 'Golden fiber' accounting for 80% of total world export. In course of time with the advent of synthetic material however, Jute lost that primary position and had to go for diversification. Jute Geo-textile is one of those effects of diversified approaches. Jute Geo-textile is capable of being used as the most reliable base material for protection of

slopes of embankments, roads and rivers. The flood affected roads and river embankments in our country are subjected to constant erosions all the year round because of the absence of any reliable protection measures. An in depth research carried out in this field has shown that Jute Geo-textile if properly treated with appropriate chemicals can successfully protect the roads and embankments against erosions and can also guarantee a desired durability. (Khan, A.J., et. al. 2009, 2014)Major functions of jute geotextile are depicted in Figure 1.

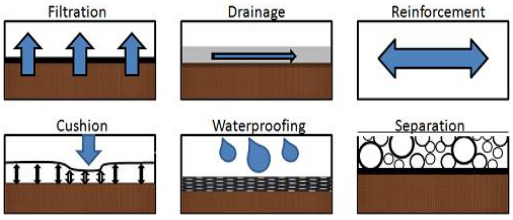

Figure 1: Major functions of Jute Geotextile.

Advantages of Jute Geotextile are: Abundant Availability, Superior drape ability, Greater Moisture Retention Capacity, Lower Costs compared to Synthetic Geo-textiles, Ease of Installation, Bio-degradable Properties, A renewable source of energy as natural biomass, Jute Geotextile is environmental friendly.

4 THE CBR PUNCTURE RESISTANCE OF JUTE GEOTEXTILE

The definition of puncture resistance which is used in this thesis is: resistance to the intrusion of aggregate, soil or other material into the geotextile which would cause perforation of the geotextile. A perforation is considered to be a hole; tear origin the geotextile. The resistance of geotextiles to puncturing stresses is an important element of geo-textile strength. Many geotextile functions rely on the geotextile remaining intact - referred to as continuity by Giroud (1987). He points out that, as granular materials are made up of discrete particles, they can be dispersed but, due to their structure, geotextiles cannot be dispersed. This is important as any punctures or tears will lead to a loss of continuity which can allow the undesirable dispersion of soil particles. Investigations of puncture resistance have been reported by many authors, some of whom have derived, either theoretically or empirically, expressions for the puncture resistance of geotextiles, usually as a function of the applied pressure (usually tire pressure or surcharge) and aggregate size. Other factors include variables such as subgrade bearing stress, aggregate shape (sphericity), initial void diameter and thickness of aggregate layer. Unlike synthetic geotextile, puncture resistance of jute geotextile may be affected by moisture content. This has been studied through a series of lab test (Hasan, 2015).

5 EXPERIMENTAL SETUP OF CBR PUNCTURE RESISTANCE TEST

5.1 Apparatus

- Testing Machine: with a constant rate of load
- Mould: a probe having inner dia 6.5" and outer dia 8.6" is used where the sample was set
- Test Specimens: specimen size: 280mm x 275mm

Total 45 specimens of 3 types JGT were tested. Universal Testing Machine and Mould preparation is presented in Figure 2.

Figure 2: Universal Testing Machine and Mould.

5.2 Summary of Test Method

A 1m width of JGT was procured. A line was drawn at 280mm distance from the edge of the fabric along the length of the specimen and draws 1 line from the edge at a distance 275mm along the width of the specimen. Then a specimen of 250mm*275mm was cut. Four holes is cut at the four corner of the specimen to set in probe by screw. The specimen was set in the mould by four screws. The mould is placed in the universal testing machine. A continuously increasing load is applied longitudinally to the specimen and the test is carried to rupture. Values for the breaking load are obtained from machine scale or dial reading. Obtained values of all specimens will represent the values of puncture resistance of the entire jute fabric.

6 DISCUSSION ON TEST RESULTS

6.1 Test Results

The values of puncture resistance test are presented in tabular form for each of Untreated, Bitumen treated and Latex treated Jute geotextiles.

6.2 CBR Puncture Test Results

CBR puncture resistance values were calculated from the CBR puncture test for each type of Jutes. Three types of JGT samples are tested. They are untreated JGT, bitumen treated and latex treated JGT. For each type of JGT, total 15 samples are tested at various moisture content such as 15%, 30%, 35%, 40% and air dry condition. The test results are presented in tabular form.

6.2.1 Untreated JGT

CBR puncture for untreated jute geotextile samples are given in Table 1.

Table 1: CBR puncture resistance for untreated JGT.

Moisture Content	Air-dry WT(gm.)	Load(N)	Average Load(N)	Avg. airdry WT(gm.)
40%	46	3332	2973	46
	47	2666		
	45	2921		
35%	40	2254	2627	44
	45	2999		
	45	2627		
30%	41	2568	2738	42
	43	2666		
	42	2980		
15%	44	2960	2927	44
	46	2882		
	43	2940		

Graphs of CBR puncture load vs. Moisture Content is presented in Figure 3.

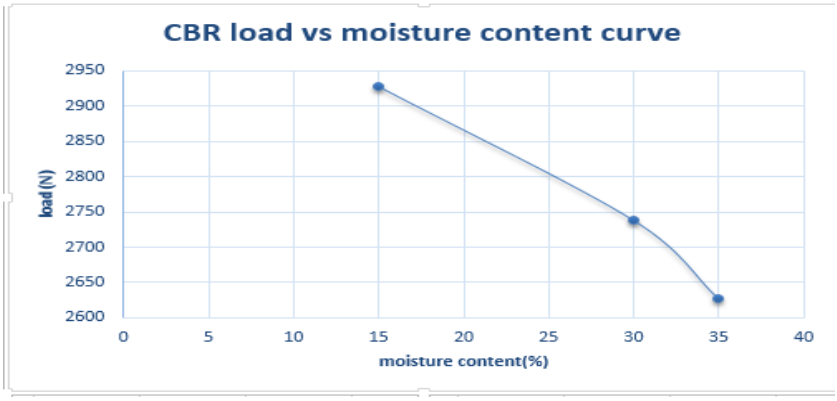

Figure 3: CBR puncture resistance variation with moisture content for untreated JGT.

6.2.2 Bitumen Treated Jute Geotextiles

Weights are measured of all bitumen treated JGT samples. All test results are measured in same units and is represented in tabular form.
CBR puncture for bitumen treated jute geotextile samples are given in Table 2.

Table 2: CBR puncture resistance for bitumen treated JGT

Moisture content	Air dry weight(gm.)	load(N)	Avg. load(N)	Avg. air-dry wt.(gm.)
40%	62	79	72	61
	51	40		
	68	98		
35%	63	216	183	62
	61	177		
	60	157		
30%	64	196	196	64
	63	216		
	61	177		
15%	74	334	272	70
	72	255		
	66	226		

Graphs of CBR puncture load vs. Moisture Content is drawn from the tabular data which is presented in Figure 4. Best fit curve is obtained from the graph. It can be observed that CBR load is decreasing with increase in moisture content.

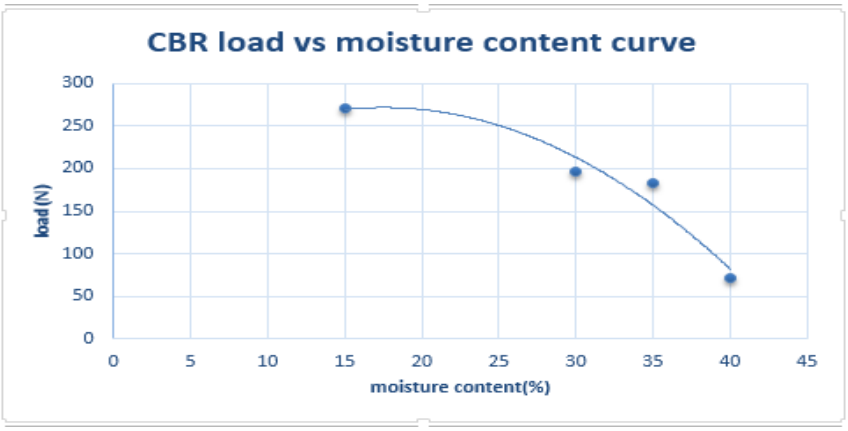

Figure 4: CBR puncture resistance variation with moisture content for bitumen treated JGT.

6.2.3 Latex Treated Jute Geotextiles

CBR puncture for latex treated jute geotextile samples are given in Table 3.

Table 3: CBR puncture resistance for latex treated JGT

Moisture content	Weight (gm.)	Load (N)	Avg. load(N)	Avg. wt.(gm.)
40%	42	2372	2424	42
	41	2470		
	41	2431		
35%	44	2431	2614	45
	45	2646		
	44	2764		
30%	47	2882	2702	46
	45	2568		
	46	2656		
15%	51	2764	2901	51
	51	3019		
	49	2921		

Graphs of CBR puncture load vs. Moisture Content is presented in Figure 5.

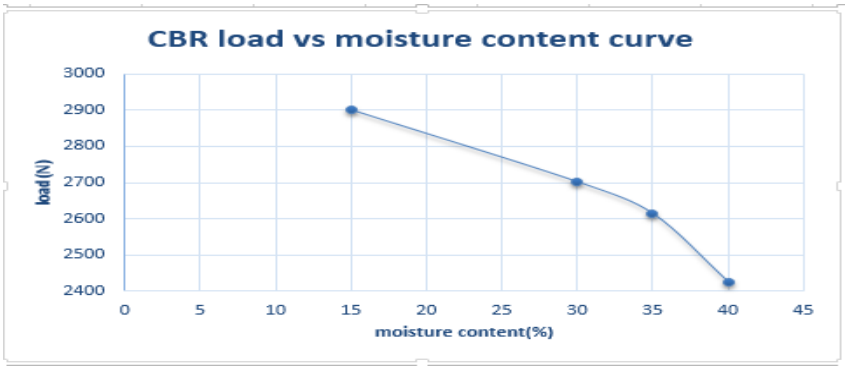

Figure 5: CBR puncture resistance variation with moisture content for latex treated JGT.

7 CONCLUSIONS

- CBR puncture resistance of Jute Geotextiles decreases with the increase in moisture content for untreated JGT as well as bitumen treated and latex treated JGT.

- Rate of decrease of CBR resistance increases with the increase in moisture content for all of three types JGT.
- CBR resistance of Latex Treated Jute Geotextiles is higher than other two types.
- CBR resistance of untreated and latex JGT nearly same
- For untreated JGT CBR puncture resistance decrease by 13.55% for change of moisture content from air dry condition to 35%. The reduction of Bitumen Treated and Latex Treated JGT for same change of moisture content are 45% & 11.1% respectively
- Latex treated JGT is best for field use among three types of JGT on the basis of CBR resistance
- Considering both CBR resistance and cost, Untreated JGT is best for field use.

Test was done only for CBR resistance. Other parameters like durability, tensile strength are not considered in this research. So Untreated JGT may not be the best for field use considering all conditions. Conclusion made here only on the basis of CBR resistance properties.

ACKNOWLEDGEMENTS

This research was partially supported by MD. Rafiqul Islam and Bidyut Narayan Sarker. We thank our colleagues from Bangladesh University of Engineering and Technology (BUET), who provided insight and expertise that greatly assisted the research.

REFERENCES

[1] Abdullah, A.B.M., (1999). "A hand book on Synthetic geotextiles Particularly Natural Synthetic geotextiles from Jute and other Vegetable Fibres", Bangladesh Jute Research Institute, Dhaka.

[2] Hasan, M., (2015). "Effect of Moisture Content on CBR Puncture Resistance of Jute Geotextile." UG Thesis, Bangladesh University of Engineering and Technology, Dhaka.

[3] Islam, M.S., Khan, A.J., Siddique, A., Kabir., R., Nasrin, S., (2014). "CONTROL OF EROSION OF HILL SLOPE TOP SOIL USING GEOJUTE AND VEGETATION." National Seminar on Jute Geo-textiles, Dhaka.

[4] Islam, M.S., Khan, A.J., Siddique, A., Kabir., R., Nasrin, S., (2014). "Performance evaluation of river bank protection using jute geotextiles."National Seminar on Jute Geo-textiles, Organized by Jute Diversification Promotion Centre(JDPC), Dhaka, Bangladesh.

[5] Khan, A.J., Huq, F., Hossain, S.Z., (2014), "Application of Jute Geotextiles for Rural Road Pavement Construction." Geoshaghai Conference on Ground Improvement and Geosysthetics GSP (ASCE), pp. 370-379.
[6] Khan, A.J. (2014) "Laboratory Assessment of Soil-Jute Geotextile Interaction Behavior." Electronic Journal of Geotechnical Engineering, 9, pp. 3949-3962.
[7] Khan, A.J. "Technical assessment of Jute Geotextiles for Civil Engineering application", Professor, Department of Civil Engineering, BUET, Dhaka.
[8] Khan, A.J., Rahman, M.M., (2009), "Road Subgrade Reinforcement Using Jute Geotextiles." Proc. of Bangladesh Geotechnical Conference, pp. 196-206.
[9] Maisano P.A.(1995) " Puncture resistance of Jute Geotextile for civil engineering and evaluation of the G-rating classification system"
[10] Mohy, M. A. (2005), Evaluation of properties of JGT and its assessment for short term and long term civil engineering applications. MSc thesis, Department of Civil Engineering, BUET, Dhaka.
[11] Prodhan, Z.H., (1994), "*Integrated Jute Geotextile Reinforced Earth Structures Design"*, Lead Paper presented on Regional Seminar on New Application of Jute, Jointly organized by IJO, UNIDO and ICS.
[12] Prodhan, Z.H., (2001), "Adaptive Research of Jute Geotextile in the Field of Civil Engineering Particularly in the Rural Roads for Pilot Scale Application", Project Paper on slope protection work at Pakulla-Lauhati road in Delduar Upazilla under Tangail district.
[13] Project "Development and application of potentially important jute geotextiles (CFC/IJSG/21)" website: http://www.jutegeotech.com
[14] Rahman, M.M., Khan, A.J., (2009), "RAINDROP EROSION CONTROL WITH GEOJUTE AND VEGETATION." Proc. of Bangladesh Geotechnical Conference, pp. 207-216.
[15] Rao, J.P., Viswanadham, B.V.S. & Yadav, (1994) O.P., "*Jute Based Geetextiles &Their Evaluation for Civil Engineering Applications",* Fifth International Conference on Geotextiles, Geomembrane and Related Products, Singapore, 5-9 September 1994, pp. 853-856.
[16] U.S. Departments of the Army and the Air force (1995), "*Engineering Use of Geotextiles"*, Technical Manual, Army TM 5-818-8 & Air Force Afjman 32-1030.
[17] Wikipedia: http://en.wikipedia.org/wiki/Geotextile Accessed on Feb-2015.
[18] Yamauchi, T. (1992). "*Historical Review of Geotextiles for Reinforcement of Earth Works in Asia*", Proc. of the International Symposium on Earth Reinforcement Practice, Fukuoka, Kyushu, Special & Keynote Lectures, pp. 1-15.

CICM 2015
First International Conference on
Advances in Civil Infrastructure and Construction Materials
MIST, Dhaka, Bangladesh, 14–15 December 2015

EFFECT OF MOISTURE CONTENT ON THE THIXOTROPIC STRENGTH RECOVERY OF DHAKA SOIL

Azmayeen R. SHAHRIAR[1]

[1]Bangladesh University of Engineering and Technology, Dhaka, Bangladesh.
Email: azmayeenrshahriar@gmail.com

Abstract. *Thixotropic phenomenon can cause significant strength increase over the range of water content of interest to the geotechnical engineers. An embankment constructed of a thixotropic soil would show less settlement than anticipated as a result of the beneficial structural change with time. This strength change is a function of several factors. The present study examines the thixotropic strength increase at moisture content ranging from 0.8LL to 1.2LL. The samples were collected from different locations of Dhaka city and remolded in the laboratory. Cone penetration tests were performed at specific time intervals to determine the shear strength of the soils. The results indicate that the shear strength gain rate decreases with the increase of water content within the test range. It was also found that soils with low 'activity' has higher strength gain tendency. The findings from the test serve as a preliminary guide to understand the influence of time factor on the strength recovery. It also suggests incorporating strict control on the time between sample preparation and testing.*

Keywords: Thixotropic strength recovery, Settlement, Moisture content, Liquid limit (LL), Shear strength, Activity.

1 INTRODUCTION

When a soil is disturbed upon remolding it loses a part of its initial strength. But as the time passes, it re-gains a part of its initial strength through structural rearrangement at constant volume and water content. This process is called "thixotropic hardening". In nature the varieties within soils of any particular area is significant. These natural varieties of soils hardly fulfil the simplifying assumption necessary to enable any mathematical analysis. As a result of this variety theoretical thixotropic strength change equations are not available to permit direct consideration of thixotropic effects into design problems. But it is imperative to know this time dependent, reversible process under constant composition, and moisture content for the efficient use of material.

There are mainly two time dependent physical processes on clay. One is 'thixotropy' and the other is 'aging in secondary compression' [1]. The term 'thixotropy' was first introduced in 1927 by A.F. Peterfi and used by H. Freundlich to describe the well- known phenomenon of isothermal, reversible, gel-sol transformation in colloidal suspensions. Essentially the gel-sol change is the change in consistency of colloidal suspensions; upon agitation gels lose their consistency and viscosity; after allowing the agitated suspension to rest, gels regain their original consistency. The temporary loss in consistency is caused but breakdown in the structure of the thixotropic matter [2, 3]

Thixotropic effects in remolded natural clays have been studied by O. Moretto and A.W. Skempton and R.D. Northey. These investigations aimed at determining the extent to which thixotropic hardening could contribute to the sensitivity of clays. Skempton and Northey defined thixotropy as the result of gradual rearrangement of the particles under the action of bonding forces into positions of increasing mechanical stability [4].

H. B. Seed and C. K. Chan have shown that compacted clays may also exhibit appreciable thixotropic strength gain with time [5]. These studies along with the studied of P. G. H. Boswell and conclusions reached by H. R. Kruyt suggest that thixotropy may be of general occurrence in the majority of clay water system [5].

Since thixotropic effects may result in strength increase of up to 100% or more after remolding, even in compacted soils, and thus could be of significance from an engineering point of view. So the factors responsible for the thixotropic strength increase should be zoomed at more details to get deep inside into the further understanding of soil structure and shear strength behavior.

At present the term thixotropy implies slightly different things to different investigators. The rheologist or colloid chemist is concerned with dilute suspensions and gel setting times of a few minutes to few days [6]. On the other hand, the engineer is concerned with the strength increase after remolding or compaction at water contents generally less than the liquid limit and measured in

weeks, months, or even years. Here in this paper the strength increase in one week time will be measured which would be used as a base to determine the thixotropic strength recovery.

2 MATERIALS AND METHODS

2.1 Remolding of the Sample

The samples were collected from three locations of Dhaka city named BUET, Pallabi and Rupnagar. Key index properties of these soils are given in Table 1. However to examine the thixotropic effects on clay, samples were remolded at moisture contents in multiples of the liquid limit i.e. within the range 0.75LL to 1.25LL. Four samples were prepared within this range to get the deep insight of effect of moisture content. The moisture content level was carefully controlled through checking this just before test program.

For the mixing purpose, a plastic bucket with a capacity of 0.0222 m^3 was taken. Then the soil and water are mixed approximately for 1 day. After mixing the soil thoroughly with water, the soil sample was poured in a plastic mold of 20cm × 12cm × 4.5 cm size for the thixotropic hardening to take place. The mold along with the sample is shown in Figure 1. The soil- water mixture was poured in three layers and tapped after pouring each layer, to eliminate the possibility of entrapping any air void in the sample. The soil bed was 45 mm thick and each layer was around 15 mm deep. Following the same procedure samples at other moisture contents were also prepared.

2.2 Cone Penetration Test

The fall cone test was conducted as per BS 1377, but the plotting and calculation portions were omitted which is generally done in liquid limit tests.

Table 1: Origin and index properties of the soils included in the paper

Soil Name	Origin	Liquid Limit %	Plastic Limit %	Plasticity Index %	Linear Shrinkage %	Clay Fraction %	Activity
S-1	BUET, Palashi	42	21	21	14	24	0.875
S-2	Pallabi, Mirpur	37	18	19	12	21	0.905
S-3	Rupnagar, Mirpur	39	17	22	15	27	0.815

The cone apparatus weighs 80 gram and has an apex angle of 30°. The prepared remolded sample is kept under the cone in such a way that the apex of the cone just touches the soil surface. To check the accuracy of the work a light source was used. When the image of the cone and the cone meet, it indicates that the cone has touched the surface. After that the cone was allowed to fall freely for 5 seconds. And the cone penetration depths were noted. Test was conducted for 7 days. Data were collected after 0, 0.1, 0.3, 0.6, 0.8, 1, 2, 4, 24, 48, 72, 96, 120, 144, 168 hours of sample preparation. To maintain same moisture content throughout the test program, the molds along with the sample were preserved in desiccator.

Figure 1: Remolded soil bed

From literature study it is quite evident that undrained shear strength of the clay sample can be related indirectly to the cone penetration depth [7]. Hansbo(1957), through static analysis, gave such a relation for clayey material. But Koumoto (1989) obtained improved agreement between theory and experiment by introducing dynamic analysis. The equation could be formulated as follows-

$$S_u = K\frac{W_c}{h^2} \tag{1}$$

Where, S_u = undrained shear strength in kN/m^2, W_c = Weight of the cone in kN, h = cone penetration in meter, K = Fall cone factor

Here it should be noted that this equation is applicable for low strain rates only. In the last equation K is calibration factor which is obtained as 1.0097-1.9716 for a standard cone with an apex angle of 30^0 and mass of 80 gm. This fall cone factor K can be obtained based on Koumoto and Houlsby method as-

$$K = \frac{3\xi}{\pi N_{ch} \tan^2(\Theta/2)} \tag{2}$$

Here ξ can be computed based on the shear strain rate during the fall cone tests as 0.74 for cone with apex angle of 30^0. N_{ch} is a bearing capacity factor which takes into consideration the effect of heaving around the cone while penetrating during the shear strength calculation. For smooth cone with apex angle 30°, the value of N_{ch} is 4.992. So, the calibration factor K may be obtained

as 1.9716 for standard cone with apex angle 30^0 and with smooth surface, and this value would be 1.0097 for the same cone with rough surface.

In this analysis the value of *K* would be taken 1.9716, as smooth cone with apex angle of 30° and a mass of 80 gram would be used in the experiment program.

3 RESULTS AND DISCUSSIONS

Figure 2 shows the depth of penetration vs. elapsed time at different water contents. Clearly, the relationship is non- linear. Sample with moisture content of 1.22LL showed the highest initial penetration. However all the samples showed almost similar rate of penetration in the first 8 hours. This is quite general that the soil sample would stiffen as time passes. But this hardening process is quite significant at lower moisture contents. The slope of the curve increases sharply at low moisture contents. The penetration depths of the sample at highest moisture content reach almost a horizontal plateau after 24 hour period.

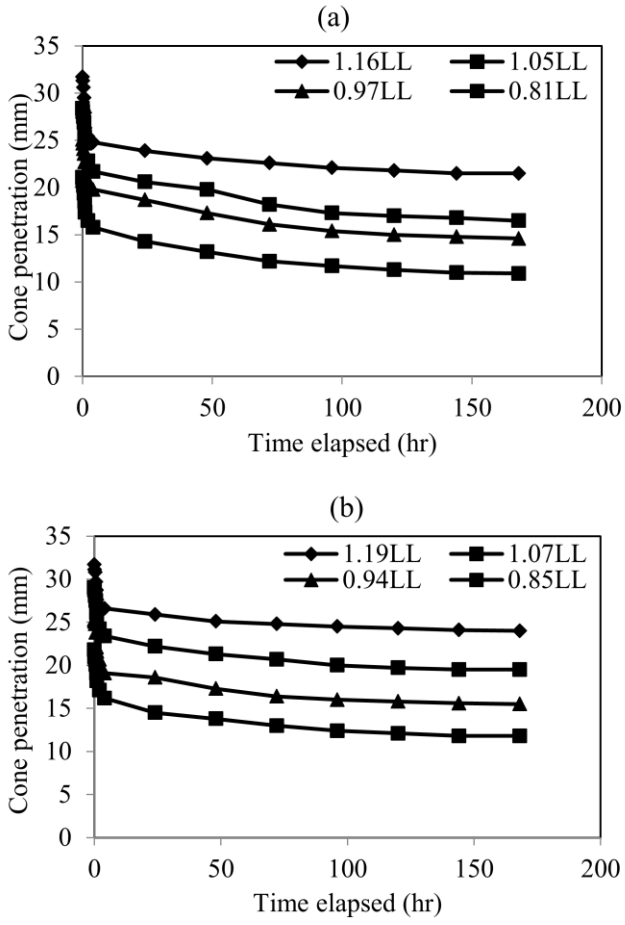

Figure 2: Variation in cone penetration depth during the thixotropic hardening process, (a) S-1 (b) S-2

Figure 3 represents the increase in shear strength as calculated from the previous formulae, with time at different moisture contents. It is clearly evident from the figure that the curves corresponding to 0.79LL, 0.81LL, and 0.85LL depart significantly from the

curves at other moisture contents. Samples with high moisture contents underwent negligible strength increase after four days, whereas the strength increase is significant at low moisture contents. The shear strength increases as much as 330% at moisture content of 0.79LL. The slope of the curves at 1.22LL, 1.19LL, and 1.16LL are very gentle.

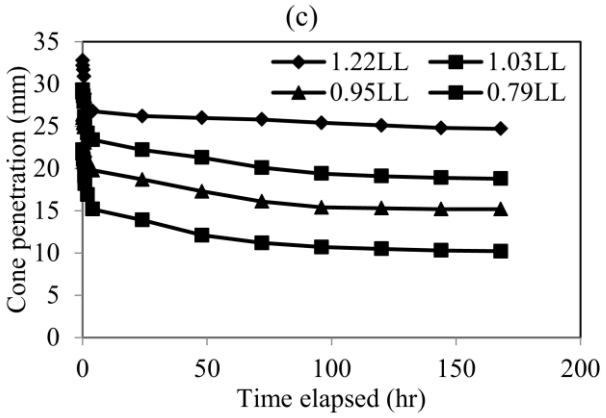

Figure 4 (cont.): Variation in cone penetration depth during the thixotropic hardening process, (c) S-3.

These two observations indicate that initial moisture content less than the liquid limit is imperative for thixotropic hardening to take place. At moisture content beyond the liquid limit, the soil- water matrix would be too liquefied. This situation can be viewed from the energy- distance principle. In dilute soil-water mixture the distance between the clay particles is such that an energy barrier prevents the particles to flocculate, on the other hand an additional energy of repulsion is introduced by additionally applied shearing strains while remolding. So finally the situation is such that the time provided to the soil

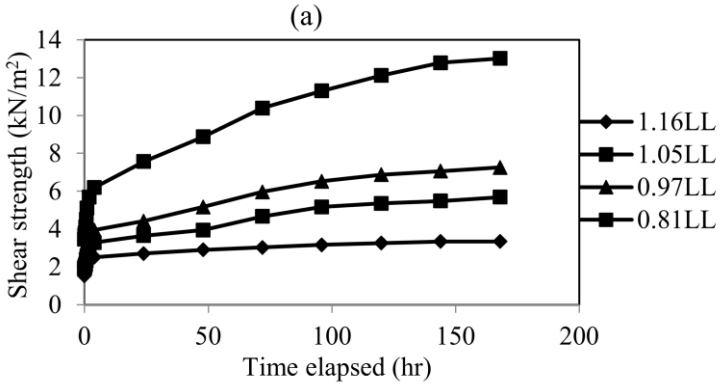

Figure 3: Variation in shear strength as obtained during the thixotropic hardening process, (a) S-1.

sample for hardening could not contribute to the thixotropic strength increase.

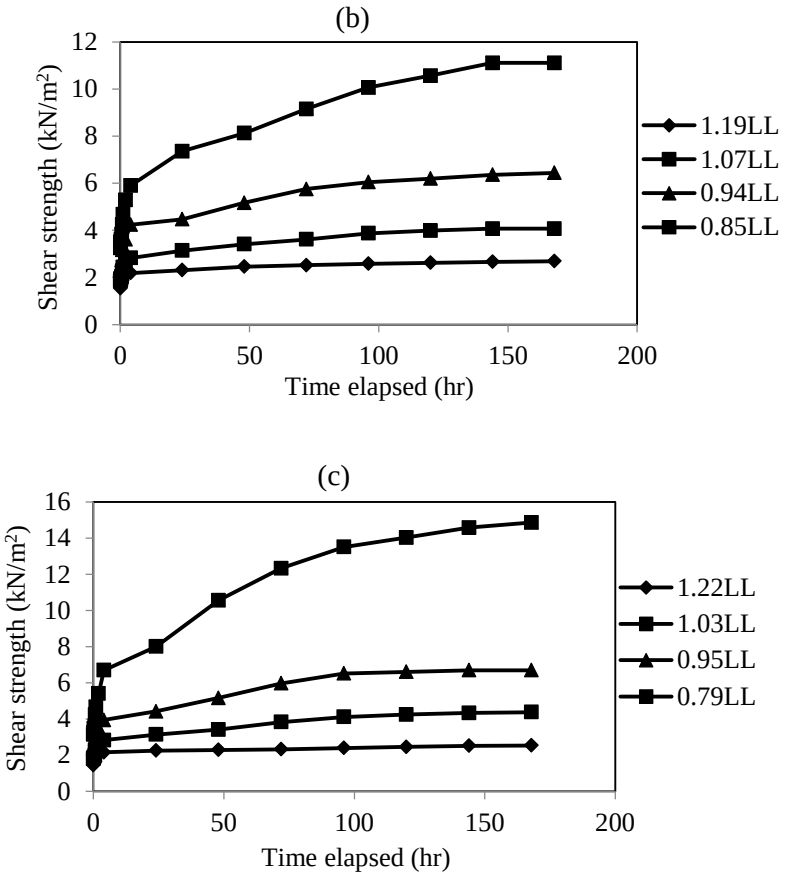

Figure 5 (cont.): Variation in shear strength as obtained during the thixotropic hardening process, (b) S-2 (c) S-3.

4 CONCLUSIONS

The basic conclusions can be arranged in the following way-

(a) The thixotropic strength gain rate increases as the moisture content decreases for all the three types of soils.

(b) Initial moisture content less than liquid limit is necessary for significant thixotropic hardening to occur.

(c) At higher moisture contents the soil- water matrix becomes too liquefied to flocculate.

(d) After six days, the strength vs. time curve becomes almost horizontal indicating no significant strength gain after six days' rest period. This data

might be useful in incorporating a minimum of seven days' rest period between sample preparations and testing to consider the thixotropic effects. It is to note that the test was conducted on the Dhaka soil only, so similar test could be performed on the soils collected from other locations of the country to warrant such rest period.

(e) Soil having the least activity has the highest strength gain tendency. It indicates that lower activity is required to get better advantage from thixotropic strength increase.

ACKNOWLEDGEMENT

The study was solely conducted under the Department of Civil Engineering of Bangladesh University of Engineering and Technology (BUET).

REFERENCES

[1] G.J. Meijer, 2012. Reconstitution of Sensitive Clays. M.Sc. Thesis, Delft University of Technology, Netherlands.

[2] James K. Mitchell and Kenichi Soga. *Fundamentals of Soil Behavior*, 3rd Edition, John Wiley & Sons, inc., 2005.

[3] Edward William Brand and Rolf Peter Brenner. Soft Clay Engineering, *Developments in Geotechnical Engineering*, Volume 20, pp. 1-779, Elsevier Scientific Publishing Company, 1981.

[4] A. W. Skempton and R. D. Northey. The Sensitivity of Clays, *Geotechnique*, Volume 3, No. 1, March 1952, pp. 40-51.

[5] James K. Mitchell. Fundamental Aspects of Thixotropy in Soils. *Journal of the Soil Mechanics and Foundation Division, Proceedings of the American Society of Civil Engineers*, Volume 86, No. 3, May/June 1960, pp. 19-52.

[6] Howard A. Barnes. Thixotropy- a review. *Journal of Non- Newtonian Fluid Mechanics*, Volume 70, No. 1-2, May 1997, pp. 1-33.

[7] T. Koumoto and G. T. Houlsby. Theory and Practice of Fall Cone Test. *Geotechnique*, Volume 51, No. 8, September, 2001, pp. 701-702.

CICM 2015
First International Conference on
Advances in Civil Infrastructure and Construction Materials
MIST, Dhaka, Bangladesh, 14–15 December 2015

SCREW PLATE LOAD TEST AND SPT IN THE ESTIMATION OF ALLOWABLE BEARING CAPACITY

Sarah, T. NOOR[1], **Shamsul Islam**[2] **and Bodrul Haider**[3]

[1, 3]University of Asia Pacific, Dhaka, Bangladesh.
[1]Email: sarah@uap-bd.edu

[2]ProSoil Foundation Consultant, Dhaka, Bangladesh.
Email: prosoil_9@hotmail.com

Abstract. *In-situ determination of pressure-settlement curve is attempted in order to avoid dependency to empirical and semi-empirical correlations. In this respect, ordinary plate load test that provides the pressure settlement behavior is often carried out at the ground level or at the foundation level. When expected depth of foundation is far below the ground level, screw plsate load test (SPLT) becomes the only suitable field test. SPLT can be performed in depth using a plate of helical shape that is screwed into the ground to a depth of test, without disturbing them. On the other hand, standard penetration test provides a means for indirect estimation of the bearing capacity and compressibility of soil under vertical load. This paper presents the results and analysis of the field tests (screw plate load test and SPT) and the laboratory tests of a site, proposed for a structure built on raft foundation. The significance of SPLT over SPT results are discussed, while emphasizing allowable bearing capacity.*

Keywords: Screw plate load test, Plate load test, SPT, Allowable bearing capacity.

1 INTRODUCTION

In a geotechnical site exploration program, field tests (plate load test, screw plate load test, standard penetration test, cone penetration test, pressure-meter test, vane shear test, etc.) are often preferred than laboratory tests. Though laboratory tests can be better controlled (in terms of stress level and stress path) than field tests, these test results are greatly influenced by the disturbances associated with sampling. Among all the field tests, ordinary plate load test (PLT) and screw plate load test (SPLT) provide pressure settlement curve and eliminate the use of correlations in settlement calculation. However, when the test level is far below the ground level, soils may be disturbed during field tests due to stress changes. In planning field test methods, some points should be given special considerations: significance of test results, extent of result interpretation, source of disturbance/stress release/stress concentrations associated with testing, loading direction, etc. In this regard, SPLT has added advantages over PLT [1-6].On the other hand, SPT is the most common soil exploration technique all over the world, as several correlationsbetween different soil parameters and SPT N-values are available in the literature.

This study presents the analysis of results of SPT and SPLT and laboratory tests carried out at a test site in Dhaka. The significance of SPLT was examined by comparing the allowable bearing capacity predicted from SPT N values.

2 STANDARD PENETRATION TEST (SPT) RESULTS

In SPT, the boreholes were made by the percussion drilling method.In SPT testing, the rope-and-pulley (R-P) method was used. The arrangement consists of a hollow cylindrical mass sliding over a steel rod, operated by lifting the mass with a rope over a cat head. At the instant the mass reached the required height (760 mm), the mass is released automatically driving the split spoon into the soil.

About 20 locations, borings were drilled vertically through soil approximately up to the depths of 34.5 m in Bh1, Bh2 and Bh4, 36 m in Bh3, 45m in Bh17 and Bh18, and 30 m in rest of the boreholes except BH5, BH15 and BH20.Boring was terminated due to rubbish at the depths of 3.5 m, 7.5 m and 12.5 m in BH5, BH15 and BH20, respectively. Layer of rubbish construction materials, varying 3 to 6 m in thickness, was found near the ground level in BH3, BH4, BH9, BH10, BH17, BH18 and BH19. InBH19. Moreover, rubbish materials were unusually found from 15 to 16.5 m below EGL.

Field SPT N values were corrected for all the standard SPT corrections to obtain N_{55}. Boreholes are grouped into three categories and summarized in Table 1 by consideringN_{55} at depths 12 m or greater. Table 2 presents the lowest SPT N-values for each group and also the smallest the largest ones at each depth from the $N_{55(lowest)}$ values of three groups. It can be noted that Group-1, where N_{55} is

mostly found 17 or more at depths of 13.5 m below EGL, shows better quality soil profiles than other two groups. Instead, N_{55} mainly varies from 14 to 17(13.5 m to 30 m), and from 10 to 18 (in 18 m to 27 m) in Group-2 and Group-3, respectively. Minimum and maximum $N_{55(lowest)}$ values are found about 13 and 20, respectively,

Table 1 Summarized SPT test results

Group	Boreholes	No. of observations(From 12 m to 30 m below EGL)		
		N_{55}<15	N_{55} = 15-20	N_{55}>20
G-1	BH-2, BH-6, BH-7, BH-8, BH-10 BH-11, BH-12, BH-14, BH-18, BH-19	<2	≤3	9-11
G-2	BH-9, BH-13, BH-16, BH-17	≤2	4-6	5-7
G-3	BH-1, BH-3, BH-4	3-5	≤2	6-9

Table 2 Group wise $N_{55(lowest)}$, minimum $N_{55(lowest)}$and maximum $N_{55(lowest)}$ at different depths from 12 m to 30 m

Depth	$N_{55(lowest)}$				
m	Group-1	Group-2	Group-3	Min. $N_{55(lowest)}$	Max. $N_{55(lowest)}$
12	8	1	10	1	10
13.5	21	10	12	10	21
15	20	15	20	15	20
16.5	13	15	20	13	20
18	18	17	10	10	18
19.5	20	17	18	17	20
21	18	16	14	14	18
22.5	17	15	13	13	17
24	23	14	13	13	23
25.5	14	13	13	13	14
27	25	19	14	14	25
28.5	26	21	26	21	26
30	13	19	28	13	28

3 LABORATORY TESTS AND VISUAL INSPECTION

Samples of soft clay to very stiff clay and sand layers were collected during SPT from the split-spoon sampler at different locations of all boreholes, and visually inspected before storing for laboratory testing. Most of the samples show their

liquid limits (LL) and plastic limits (PL) varying between 44% and 47% and between 18% and 24%, respectively. As exceptions due to large variations from the range, LL is found as low as 26.7% at 22.5 m depth in BH16 and 30.5%at 16.5 m depth in BH19. Moreover, PL is found less than 10%, in BH7, BH8, BH9, BH12 and BH16 at depths of 28.5 m, 27 m, 16 m, 25.5 m and 22.5 m, respectively. In Table 3,LL and PL of soils having the same SPT N-values within a group are comparedat adepthof 13.5 m, 16.5m, 18 m and 21/22.5 m.

Table 3: Atterberg's limits and N-values at different depths

Depth (m)	Group	BH-ID	N- Values	LL (%)	PL (%)
13.5	G-2	BH-9	17	43	20.1
		BH-16		47.2	16
		BH-17	25	47	21.5
16.5	G-2	BH-16	17	46.2	18.7
		BH-17		47.2	16.9
18	G-1	BH-7	20	46	25.3
		BH-8	22	47.4	23.6
	G-2	BH-9	17	46.9	23.6
		BH-16		47.4	13.6
		BH-17		49.6	27.2
21/22.5	G-2	BH-9	19	32.9	20.8
		BH-16		26	9.4
	G-3	BH-1	12	44.9	18.5
		BH-3		40.2	22.4

Organic soil (OL) was found in BH7 (from 7.5 to 10.5 m), BH8 (from 3 to 13.5 m), BH19 (from 4.5 to 6 m and 9 to 13.5 m), BH10 (from 7.5 to 12 m), BH16 (from 3 to 6 m) and BH19 (from 6 to 7.5 m).

Micaceous clay with sand (CL) was found at different depths in BH1 (28.5-31.5 m), BH3 (24-34.5m), BH7 (12-15 m), BH8 (21-24m and 27-28.5), BH9 (13.5-15m and 18-24m) andBH9 (22.5-24m, 25-27.5 and 30-30.45m), while micaceous sand (SM) was found inBH11 (28.5-30m), BH14 (15-16.5m, 24-28.5m and 30-30.45), BH16 (15-16.5m, 19.5-25.5m and 27-30m), BH18 (39-42.5m) and BH19 (18-25.5m and 27-30m). At 13.5 m depth, PL in BH 16 differs from BH9 and BH17, as the soils of BH9 and BH17 were of similar (stiff to very stiff, CL) and the that of BH16 was medium stiff to stiff, though all the three boreholes gave the same SPT N values. The samples from BH9, BH16 and BH17, obtained at a depth of 18 m, were further compared, and noted that PLof soil in BH16 is smaller than those of other two boreholes. This might be due to the fact that the soil of BH16 is present between two micaceous sand layers. Again, the

soils from BH9 and BH16at 21-22.5 m depth were compared. Both the soil samples, have mica contents and have low LL as compared to other soil samples in all the boreholes. The soil from BH16 is micaceous sand and shows significantly low plastic limit, while that from BH9 is micaceous clay showing no significant influence of mica content on its plastic limit.

4 SCREW PLATE LOAD TEST

Screw plate load testcan be conducted at any depth below the ground level using a plate of helical shape that is screwed into the ground to a depth of test, without any disturbance. The helical plate is 200 mm in diameter and has an equivalent area 315 square centimeters, and connected to the surface with a system of rods coaxial that allow plunging. synchronize the pitch of the propeller with the speed of rotation of the system of plunging.

Figure 1: Photographs of SPLT setup: Overall arrangement (left) and dial gauges for measuring settlements (right)

First the helical plate is lowered to the base of a pre-drilled hole of 254 mm diameter (approximately) and then advanced about 300 mm (1.5 diameters) below the bottom of the hole by rotation. In order to eliminate the disturbance in the soil below the test depth during the advance of the screw plate, its advance was controlled by maintaining its downward movement in each revolution equal to its pitch. An H-shaped frame of suitable size is placed with some small girders and some square plates of 122.5 kg onto four brick columns to bear the reaction of the hydraulic jack and is firmly anchored by means of two threaded rods. A hydraulic jack is set between the bottom of the load cell and the top of the vertial rods for the application of the load. The load of 0.05 tons on the internal rods is applied by a hydraulic jack and is accurately measured by a load cell connected to a digital datalogger. The overall arrangements of SPLT at the test site are

given in Figure 1. Two dial gauges were used to account for any differential settlements, as shown in Figure 1(right).

A seating load of 100kg is applied first, which is released after 15 minutes. The load is then applied in increments.The settlement is recorded from two dial gauges (sensitivity 0.01 mm) for 20 mins under each load. The settlement was found to cease, giving a deformation rate less than 0.05 mm/min, in 20 mins after application of each load. The screw plate was loaded by a 0.5 ton load increment upto a maximum load of 4 tons, and then unloaded by 1 ton. Settlement was recorded during loading and unloading paths.

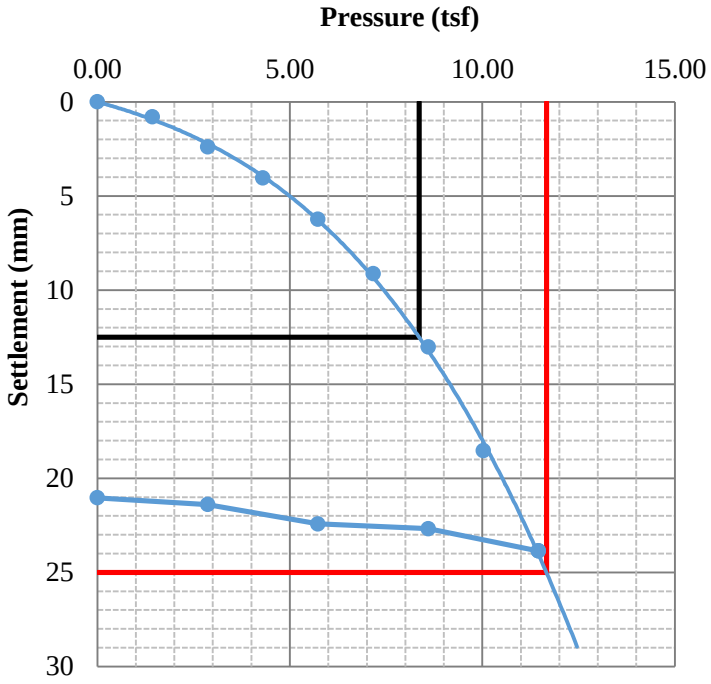

Figure 2: Pressure versus settlement curve from screw plate load test (Test location 1)

Two screw plate load tests were carried out at the proposed test site (Bashundhara, RA, Dhaka) at a depth of 13.5 m. BH12, BH17 and BH16 were the three closest boreholes for the location of SPLT-1, while BH2, BH13, BH15 and BH17 were for SPLT 2. Both the test locations are in between Group-1 and Group-2 boreholes. Figures 2 and 3 present the pressure settlement curves from both the SPLTs.

From the figures, uultimate bearing capacity was found 11.664 tsf and 10.4 tsf at test locations 1 and 2, respectively, for 25 mm settlement. By applying a factor of safety (FS) of 3, at test location 1 and test location 2, the allowable

bearing capacity is found 3.89 tsf and 3.47 tsf, respectively, and modulus of subgrade reaction is found 0.67 tsf/mm and 0.54 tsf/mm, respectively.

5 ALLOWABLE BEARING CAPACITY BASED ON FIELD TESTS

Allowable bearing pressures (q_a) are calculated for large footing width, based on N_{55} values using the design chart given by Bowles (1997), modified from the one by Meyerhof.The value of depth factor (K_d) was taken 1.33. While estimating q_a based on SPT N values, four different N-values: average of minimum $N_{55(lowest)}$and average of maximum $N_{55(lowest)}$ from the depth of 13.5 m to 30 m, and smallest and largest $N_{55(lowest)}$ at 13.5 m depth. These values of q_a are compared with the q_a from the SPLT tests conducted at a depth of 13.5 m in the test site, as given in Table 4.

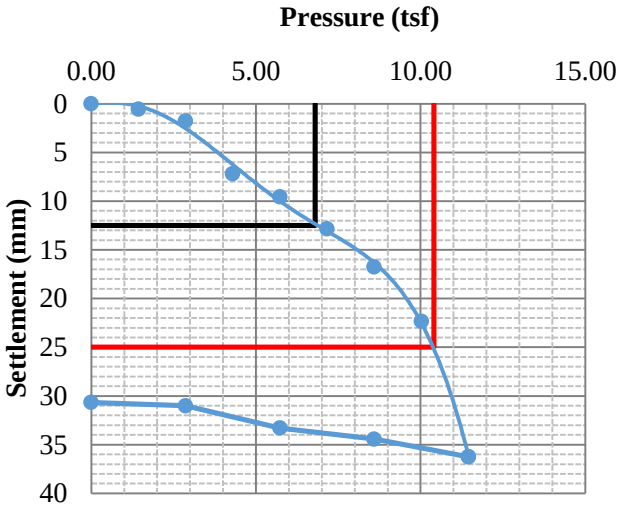

Figure 3: Pressure versus settlement curve from screw plate load test (Test location 2)

Table 4: Comparison of allowable bearing pressures for 25 mm settlement

Design Chart: Bowles (1997)			Field Test: SPLT		
Case #	N_{55}	q_a (kPa)	Test #	q_a (tsf)	q_a (kPa)
Avg. of min. $N_{(lowest)}$	13	239	1	3.89	372
Avg. of max. $N_{(lowest)}$	20	359			
Smallest N_{55} at 13.5 m	10	186	2	3.47	332
Largest N_{55} at 13.5 m	24	432			

Both the SPLTs gave values of q_a much closer to the one estimated from design chart by Bowles [7] based on theaverage of max. $N_{(lowest}$).

6 CONCLUSIONS

SPLT is found as a practical and convenient means for estimating settlement and allowable bearing capacity, when poor soil condition (due to the presence of organic matter and mica) up to a significant depth (13.5 m in present study) below the ground level and soil layers beneath the expected depth of foundation are mainly clays and/or silts.

In this study, allowable bearing capacities (q_a) from SPLTs are found much closer to the one corresponding to the average of max. $N_{55(lowest)}$, estimated from design chart by Bowles based on N_{55} value. According to SPLT results, design might be more conservative, if design is based on the lowest N_{55} value and average of max. $N_{55(lowest)}$.

REFERENCES

[1] W.A. Marr,2003. *A history of progress : selected U.S. papers in geotechnical engineering Vol. 1*. Reston, Va, American Society of Civil Engineers.

[2] G.E. Blight, 2013. *Unsaturated Soil Mechanics in Geotechnical Practice*. CRC Press, p437.

[3] B.B.K. Huat, A. Prasad, A. Asadi, S. Kazemian, 2014. *Geotechnics of Organic Soils and Peat*. CRC press, p41.

[4] Y.S. Lee, W.K. Hwang, Y. Choi, T.H. Kim, 2009. Development and Calibration of Screw Plate Load Tests. *19th International Offshore and Polar Engineering Conference*.

[5] T.H. Kim, G.C. Kang, W.K. Hwang, 2014. Developing a Small Size Screw Plate Load Test. *Marine Georesources and Geotechnology*, **32 (3)**, pp 222-238.

[6] R.K. Rowe, 2001. *Geotechnical and geoenvironmental engineering handbook*. New York, Springer Science & Business Media.

[7] J. H. Bowles, 1997. *Foundation Analysis and Design, Fifth Edition*, McGraw-Hill, p265.

CICM 2015
First International Conference on
Advances in Civil Infrastructure and Construction Materials
MIST, Dhaka, Bangladesh, 14–15 December 2015

FACTOR OF SAFETY OF SINGLE PILE IN COLLAPSIBLE SOIL DURING INUNDATION: NEGATIVE SKIN FRICTION

Sarah T. NOOR[1] **and Krishnandu Barma**[2]

[1, 2] University of Asia Pacific, Dhaka, Bangladesh.
Email: [1]sarah@uap-bd.edu and [2]utpol_ce@yahoo.com

Abstract. *Collapsible soils experience significant volume decrease due to the increase of soil moisture content, without increase in the in-situ stress level. Compacted soil that has little moisture (less than optimum moisture content) and low density may also behave like collapsible soil. Natural deposits of these soils are found in large parts of North and South America, Eastern Europe, China, Central Asia, Northern and Southern Africa, Russia, Egyptian western dessert, and the continuous deposit from North China to South-East England. For heavy structures, pile is considered perhaps the only alternative available type of foundation. In collapsible soil region, inundation affects the capacity and performance of both the shallow and the deep foundations, supporting structures in collapsible, adversely. In this paper, the factor of safety (FS) of single pile during inundation of collapsible soil was formulated including the maximum pile capacity available during inundation. Reduced pile capacity and development of drag load during inundation were given consideration in the calculation of true factor of safety during inundation. Therefore, a procedure of numerical modelling is developed to predict ultimate capacity and positive skin frictional resistance of single pile during inundation of collapsible soil, using the software PLAXIS (2D).*

Keywords: Numerical modeling, PLAXIS, Drag load, Factor of safety, Collapsible soil, Negative skin friction

1 INTRODUCTION

Collapsible soils experience significant volume decrease due to the increase of soil moisture content, without increase in the in-situ stress level. Pile foundations driven to an existing bearing stratum underlying the collapsible soil layer is often considered the only feasible type of foundation, in case of heavy loads and deep strata of collapsible soil, or any load (light or heavy) and a thin bed of collapsible soil at a depth [1].The presence of collapsible soil layer may also negatively affect the capacity and performance of these piles during the lifespan of the structure. To date, several cases of piles, supporting structures built in collapsible soil and experiencing sudden reduction in their bearing capacity and further excessive pile settlement immediately after inundation of collapsible soils, are reported in the literature [2]. When the soil around a pile settles faster than the pile, the skin friction developed on the pile surface acts downward and is called negative skin friction [1-4]. In order to ensure safety of the structure, total allowable load on pile should include expected drag load in design. However, performance of pile foundations in collapsible soil during inundation have been addressed little to none, in the literature. This paper has formulated a method of determining minimum and true factor of safety of pile in collapsible soil during inundation. Numerical model has been developed to investigate the factor of safety of single pile. Different parameters were varied to investigate their effects on the factor of safety of pile.

2 NEGATIVE SKIN FRICTION AND FACTOR OF SAFETY

Skin friction may act downward direction on the surface of a pile segment, when the soil in contact with that part of the pile settles faster than the pile, as shown in Figure 1. Due to immediate soil volume reduction (soil collapse) resulting from the inundation of a layer of collapsible soil (around the pile), the negative skin friction develops on the pile surface and accordingly, exerts drag load on the pile, in addition to the load on the pile head.

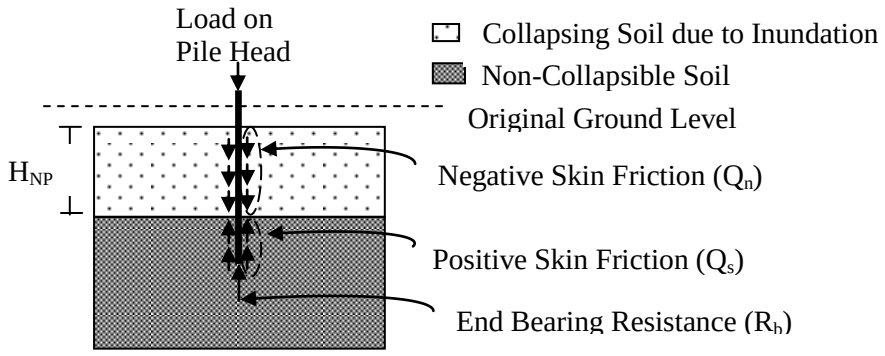

Figure 1: Load transfer mechanism: Pile in collapsible soil during inundation

When negative skin friction develops on the pile surface, the pile suffers from reduction in factor of safety from two different aspects: (a) reduction in ultimate pile load (capacity), and (b) increase in pile load. Ultimate pile capacity (i.e., a sum of positive skin frictional resistance and end resistance) decreases, because positive skin friction cannot develop on the pile surface through the full pile length. Instead, load on pile increases due to drag load, resulting from the development of negative skin friction.

3 NUMERICAL MODEL DEVELOPMENT AND VALIDATION

In this study, an axisymmetric finite element model is developed to simulate a single-axially loaded-vertical pile. The centerline of the axisymmetric geometry model coincides with the axis of the vertical pile. The outer vertical boundary is placed at 50 times the pile diameter. The horizontal boundary is placed at least at 0.7 L below the pile tip. The geometry model consists of soil and pile clusters.

Boundary condition of the geometry model is defined according to the rules of standard fixities. Fixities are applied to geometry lines by defining their prescribed displacements equal zero. Higher order triangular element, having 15 nodes (as shown in Figure 3.2), is chosen for both the soil and the pile clusters. The numerical integration involves twelve stress points (Gauss Points).Five-nodes line elements (termed as interface element in PLAXIS) are used along the pile-soil interface to capture a realistic interaction behavior between the pile surface and the soil during loading phase, to reduce the mesh dependency, and also to account for the relative pile-soil movement. Interface elements connect the elements of the soil clusters to those of the pile clusters. Figure 2 presents the axi-symmetric model, which was meshed of 'Medium' global coarseness' with interface elements and mesh refinement around the pile.

Pile is assumed to behave elastically. The pile cluster is modeled as non-porous material with Linear-Elastic (isotropic) constitutive relation, requiring only two input parameters: Young's modulus (Ep) and Poisson's ratio (υp). Soil behavior is defined by Mohr-Coulomb (MC) constitutive law, which simulates the soil behavior based on soil parameters known in most of practical situations. The MC soil model operates with five material parameters; including two plastic parameters (i.e., angle of internal friction (φ), cohesion (c) and angle of dilatancy (ψ)). Any unsaturated soil clusters (of sandy or clayey type either), above the groundwater table are modeled as drained type of materials. On the other hand, saturated soil clusters are modeled as drained and undrained types of materials for sandy and clayey soils, respectively. The behavior of the pile-soil interface is also defined by the MC Model.

The developed model was used for two different purposes/cases for each set of pile, soil and inundation conditions. Firstly, the model was used to estimate ultimate pile capacity (P_u) and positive skin frictional resistance (Q_s), and then end bearing resistance (R_b) accordingly, for 'before inundation' (without negative

skin friction) condition. The model is further used to estimate maximum positive skin frictional resistance (Q_s'), when negative skin friction developed on the part of the pile shaft existing above the neutral plane, called 'during inundation' condition. The sum of Q_s' and R_b provides the ultimate pile capacity (P'_u) during inundation. It can be noted that Q_s' will be smaller than Q_s.

For investigating each case, three calculation phases were defined through staged construction. For both the cases, first two calculation phases (initial phase and pile installation) were defined in the same manner. In the Initial Phase, the initial soil effective stresses and pore water pressures were generated from the input of coefficient of earth pressure at rest (K_0) and the given general phreatic level, respectively. In Phase I, bored pile was installed by changing the material dataset, which had 'Soil' property (in Initial phase), of the pile clusters with the 'Pile' property dataset.

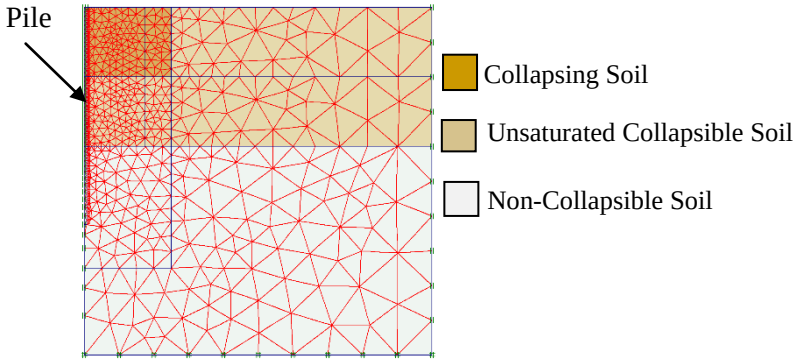

Figure2: Generated mesh of the axi-symmetric model

While modeling 'before inundation' condition, phase II was defined by applying a 'point load' on the pile head. On the other hand, while modeling 'during inundation' condition, phase II was defined by applying the point load at the centre of the pile cross-section at the bottom of the collapsing soil subjected to inundation. Further, mobilization of any skin friction in the pile interface (above neutral plane), which is in contact with the collapsing soil experiencing volume decrease, is restricted by adjusting the 'Interface' material set. For that part of the pile interface, the cohesion (c) and the angle of shearing resistance (φ) of the 'Interface' material set were set 1 kPa and 0°, respectively. For rest of the part of interface, the c and φ values of interface element were given input of 75% of the respective values of the surrounding soil.

The model gave good agreements with the results from the full scale pile test reported by Grigoryan [2], as given in Table 1.

Table 1: Frictional and base resistances under inundation

Load at Pile Head (kN)	Drag Load (kN)	Skin Frictional Resistance (kN)		Base Resistance (kN)	
		Experimental (Grigoryan 1997)	FEM	Experimental (Grigoryan 1997)	FEM
0	548	650	606	235	248

4 RESULTS AND ANALYSIS

Factor of safety (FS) of single pile in collapsible soil has been studied using the model developed in this paper. It can be noted that FS of pile varies with the magnitude of drag load, applied load on pile head and the pile's ultimate capacity. In this paper, FS has been studied in two different ways giving two values of FS (FS˝ and FS´) for a given set of pile, soil and inundation conditions. While calculating FS´, the magnitude of drag load and the maximum allowable load (obtained by applying FS of 3 on ultimate pile capacity (P_u) for 'before inundation' condition) were considered but reduction in ultimate pile capacity was not taken into consideration. Instead, while calculating FS˝, all the three factors (the magnitude of drag load, maximum allowable load on pile head and the pile's reduced ultimate capacity) were considered. For calculating FS, the value of drag load was obtained from the models developed by Noor et al [1].The schematic diagram of the case studied in this paper is shown in Figure 3. The variations of parameters, considered in the present investigation, are listed in Table 2. Dilatancy angle was considered zero, which is calculated as (φ-30°) in PLAXIS.

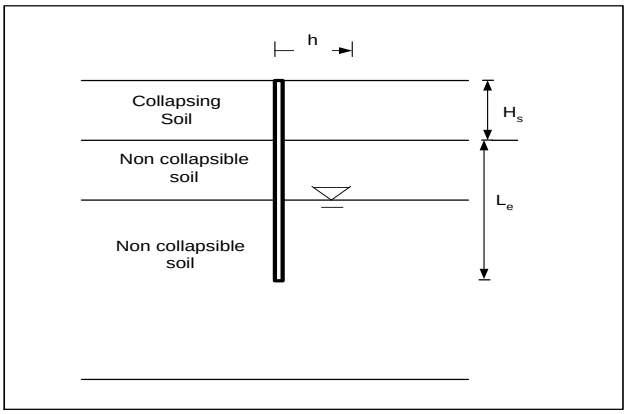

Figure 3: Schematic diagram of the case studied

Table 2: List of parameter variations

Parameters	Symbol	Unit	Value / Range
Pile length	L	m	12 and 25
Pile diameter	d_p	m	0.25 -1
Depth of collapsing soil	H_s	m	4 and 7
Radius of wetting	h	m	3
Collapse potential	C_p	%	7.5 and 12.5
Cohesion	c	kPa	15
Angle of internal friction	φ	° (degree)	30

For a given set of soil and inundation conditions and pile length, both the factors of safety (F.S′ and F.S′′) is found to vary with the ratio of depth of collapsing soil to pile diameter (H_s/d_p), shown in Figures 4-6. In all cases, the difference between F.S′ and F.S′′ is found significant, and the true factor of safety (F.S′′) approaches a critical value when the H_s/d_p ratio is high. Though each of the piles was designed with a factor of safety 3 under 'before inundation' condition in collapsible soil region, the pile acts with a factor of safety (FS′′) less than 3 for 'during inundation' condition. Due to inundation of collapsible soil surrounding a given length of short pile, FS is severely affected and may approach a value of 1 or even less (Figures 4 and 5), if H_s/d_p ratio is high.

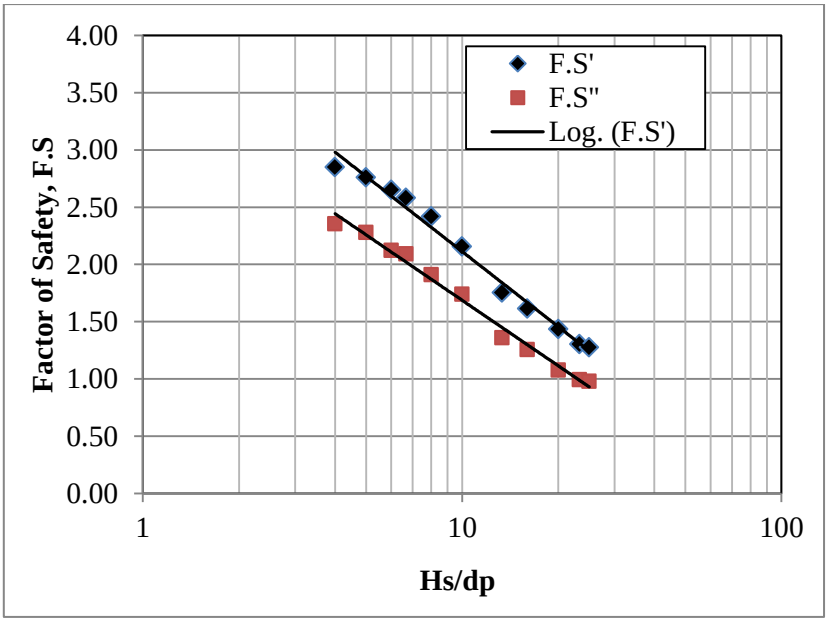

Figure 4: Factor of safety vs H_s/d_p when L = 12 m, H_s = 4 m, h = 3 m and C_p = 7.5 %

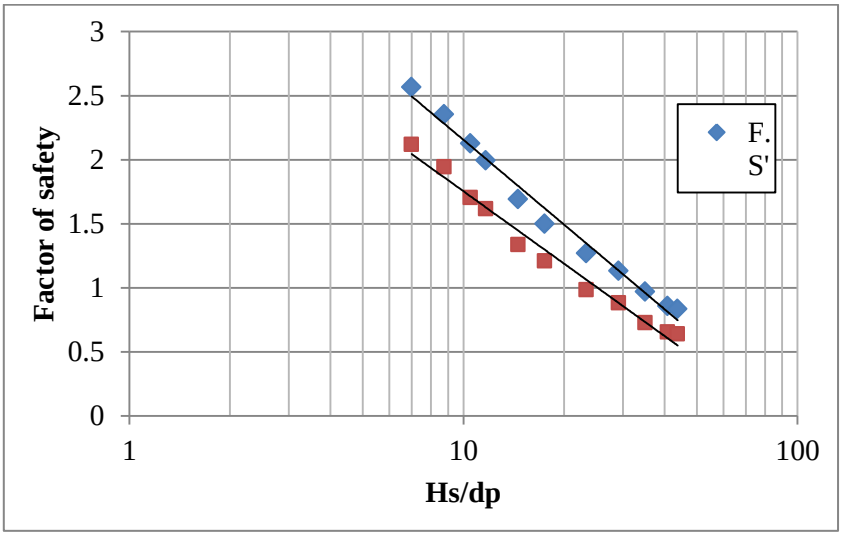

Figure 5: Factor of safety vs H_s/d_p, when L = 12 m, H_s = 7 m, h = 3 m and C_p = 7.5%

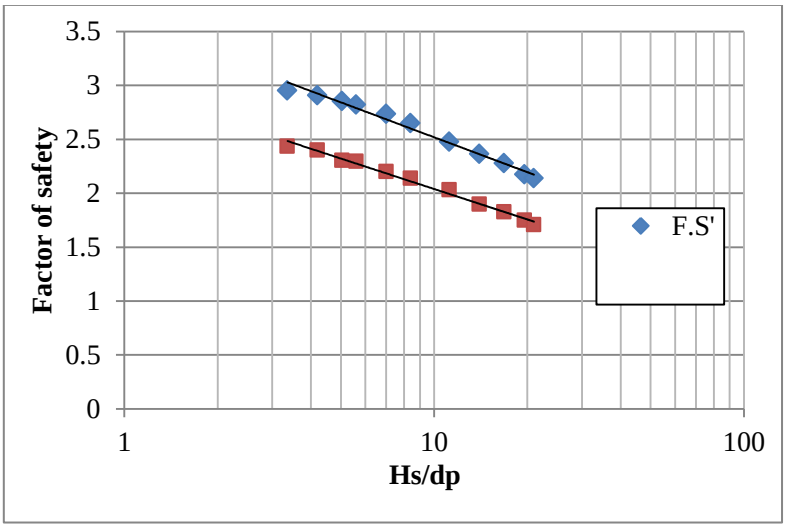

Figure 6: Factor of safety vs H_s/d_p, when L = 25 m, H_s = 7 m, h = 3 m and C_p = 12.5%

Reduction of FS´´ is related to increase in H_s/d_p ratio. Figure 4 and Figure 5 are compared to demonstrate that reduction due to increase in H_s is more severe than that due to the reduction in d_p.

In many instances of long pile, the minimum factor of safety was found greater than 1.5. This also implies that the conditions of short piles are more vulnerable than long piles during inundation of collapsible soil surrounding the pile. By comparing Figure 5 and Figure 6, it can be noted that minimum factor of safety for a 25 m long pile may not fall below 1, even under more critical collapse phenomena (C_p equal 12.5%) than the one (C_p equal 7.5%) experienced by the short pile.

5 CONCLUSIONS

This paper presents numerical models that allow determination of minimum factor of safety of pile in collapsible soil during inundation. Factor of safety of pile is found to decrease significantly, if negative skin friction develops on a part of the pile shaft. In order to ensure safety of the structure, total allowable load on pile should include expected drag load in design. Minimum factor of safety can be determined by considering magnitude of drag load, reduced ultimate pile capacity and maximum allowable load on pile and it should be maintained above 1. Based on the numerical results, short pile of 12 m length is found more vulnerable than long piles during inundation of collapsible soil surrounding the pile. Instead, FS of long pile may be maintained above 1.5, even under more critical collapse phenomena than the one experienced by the short pile causing failure.

REFERENCES

[1] S.T. Noor, A.M. Hanna, I. Mashhour, 2013. Numerical modeling of piles in collapsible soil subjected to inundation. *International Journal of Geomechanics*, ASCE, **13(5)**, pp 514-526.

[2] A.A. Grigoryan, 1997. *Pile Foundations for Buildings and Structures in Collapsible Soil.* A.A. Balkema Publishers, Brookfield, USA.

[3] C.J. Lee, M.D. Bolton, A. Al-Tabba A, 2002. Numerical modeling of group effects on the distribution of dragloads in pile foundations. *Geotechnique,* **52(5)**, pp 325-335.

[4] B.H. Fellenius, T.C. Siegel, 2008. Pile Drag Load and Downdrag in a Liquefaction Event. *ASCE Journal of Geotechnical and Geoenvironmental Engineering*, **134(9)**, pp 1412-1416.

CICM 2015
First International Conference on
Advances in Civil Infrastructure and Construction Materials
MIST, Dhaka, Bangladesh, 14–15 December 2015

EFFECT OF SALT WATER IN SAND, LIME AND FLY ASH MIXTURE

M. E. KARIM[1], **M. J. Alam**[2] **and M. S. Hoque**[3]

[1, 2, 3] Bangladesh University of Engineering and Technology, Dhaka, Bangladesh
Email: [1] emdadul.buet@gmail.com, [2] jahangir.buet@gmail.com, [3] shoque@ce.buet.ac.bd

Abstract. *Ensuring sustainable development of coastal areas require improvement of road embankment infrastructure. Being a byproduct of industry, fly ash may be considered as environment friendly and low cost material for this purpose. However, scarcity of fresh water in coastal areas may compel to use saline water. To investigate the effects of sodium chloride content of mixing water on fly ash and lime mixed compacted sand, a series of the Unconfined Compression tests have been conducted on 50 mm diameter specimens with 100mm height. Lime content was varied over a range of 1-5% of dry sand weight and fly ash contents were 9%, 15% and 30% of dry sand weight. Besides 0%, 4% and 8% of sodium chloride were mixed with tap water, which were used for preparing specimens at 10% moisture content by compaction method. The specimens were cured for 7, 15, 30 and 60 days by spraying method. Experiment results show that, the unconfined compression strength of fly ash and lime mixed compacted sand increases with the increase in sodium chloride content. However, the long term effect of using saline water in fly ash and lime mixed compacted sand should be investigated, which is out of scope of this study.*

Keywords: Unconfined compressive strength, Lime, Fly ash, Salt.

1 INTRODUCTION

Fly ash is largely used as a construction material and soil improvement. Enormous amount of fly ash is produced daily from the coal based power plant and other industrial units. A 500 MW thermal power plant releases 200 MT SO_2, 70 MT NO_2 and 500 MT fly ash approximately every day [1]. Bangladesh and India had inked a deal on April 20, 2013 to set up the 1,320 MW coal-fired power plants by 2021. Nearly 1320 MT of fly ash will be produced per day and cover huge areas for its disposal. Disposal of fly ash could be an environmental concern. Fly ash is a pozzolanic material. Soil, fly ash and lime react with each other forming bonds and cohesion [2; 3].

Several studies were conducted on lime and fly ash for soil improvement [4; 5; 6] and for durable and economic concrete, namely: (i) utilization of lime and fly ash increases the shear strength of soil [4; 5; 6], (ii) effect of moisture content [4] (iii) curing temperature accelerates the strength [5; 7] and (iv) quantity of lime and fly ash influences the strength [6]. Although, several previous studies were conducted on concrete under the effect of salt water, very little work is done to verify the behavior of soil towards soil improvement under the effect of salt content in water. The effect of salt content in concrete had mixed findings on the concrete strength. Some studies concluded that concrete strength increased with increase in salt content in water [8; 9; 10], while others concluded that concrete strength decreased with the increase of salt content in water [11]. The studies also witnessed an increase in the 28 days concrete strength without any effect on long term strength of concrete with salt water content [12].

Due to the presence of extreme salinity in the Bangladeshi geological conditions along the 2.85 million hectares coastal area [13] consisting of 19 districts with 35 million people [14], crop cultivation is not practiced. Further, frequent road damages and embankment collapses due to incessant rain and flood, presses the need to study the effect saline water on the use of lime and fly ash used for soil improvement in the coastal areas.

2 MATERIAL

Sand sample from Mawa and Padma river bank, lime from local market and fly ash from a local cement company were collected in the present study. Since, the properties of fly ash vary between the various sources [15; 16; 6] due to the calcium content, same source was considered in the present study. Further, locally available low calcium content fly ash is selected for the geotechnical purpose in the present study based on the recommendations [17; 15; 18], as high Calcium content increases the self-hardening value of fly ash [6]. Since, the fly ash sample contained no calcium content based on the Energy Dispersive X-ray (EDX) test results; it is classified under class F.

The grain size analysis of sand is shown in Figure 1. The Scanning Electron Microscopic (SEM) view of sand and fly ash are exhibited in Figure 2. The shape of

sand and fly ash particles are sub-angular and spherical respectively. The specific gravity of sand, lime and fly ash is 2.67, 2.57 and 2.18 respectively. The sand is fine sand.

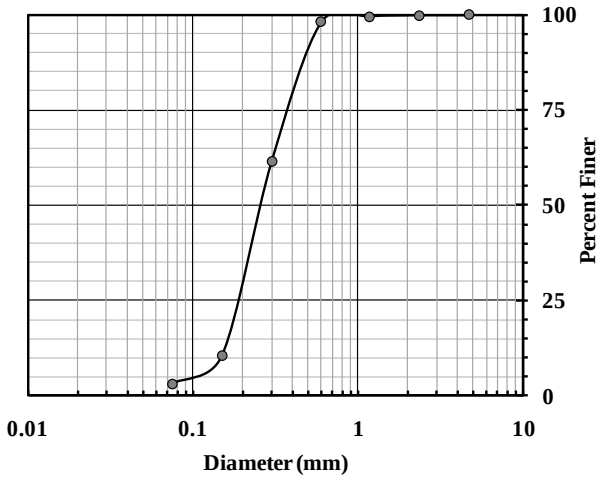

Figure 1: Grain size analysis of studied sand.

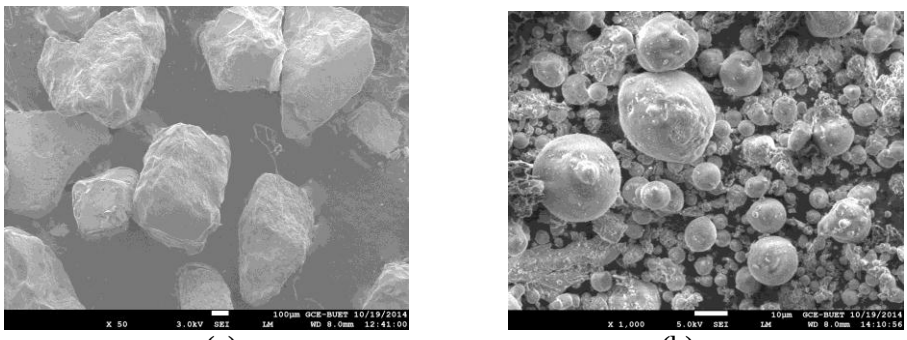

(a) (b)

Figure 2: Electron Microscopic view of (a) Sand and (b) fly ash particles.

3 EXPERIMENTAL PROGRAM

Lime content of 1%, 2%, 3% and 5% of dry sand weight and fly ash content of 9%, 15% and 30% of dry sand weight is used in the lime-fly ash treated sand. Sodium chloride (NaCl) is found predominant in sea water [20] with an average salt content of 3-5% [19]. To investigate the effect of this sodium chloride presence in the sea water, three NaCl solution are prepared with the fresh water using

0%, 4% and 8% (0g/L, 40g/L and 80g/L) NaCl concentration as the test specimens at 10% moisture content by wet compaction method. The dry density was maintained at 1.283, 1.467 and 1.558 g/cm3. Required amount of compaction was provided manually to meet the target density and controlled by trial and error method. Each specimen measuring 50mm in diameter and 100mm in height is prepared within a duration of 30 minutes.. The prepared specimen is preserved in 76 mm inner diameter hollow pipe in the curing box. 50 mm diameter specimen was kept in 76 mm hollow pipe so that it can get more surface area for curing to ensure lime, fly ash and salt water reaction in whole specimen.

A wet geotextile containing same NaCl solution was placed above reserved hollow pipes and a polythene sheet was used with the lid. Lid locks were used so that the moisture content does not decrease rapidly (refer Figure 3). Curing was done by spraying same NaCl solution 3 or 4 times in a week. 3 or 4 time spraying was found favorable to maintain high moisture content in the specimens. Temperature accelerates the reaction of sand-lime-fly ash mixture. With high curing temperature it is possible to get higher strength within a short time than that of low temperature and long time curing [21]. The temperature in the boxes was around 25°C to 28°C. The specimens were cured for 7, 15, 30 and 60 days.

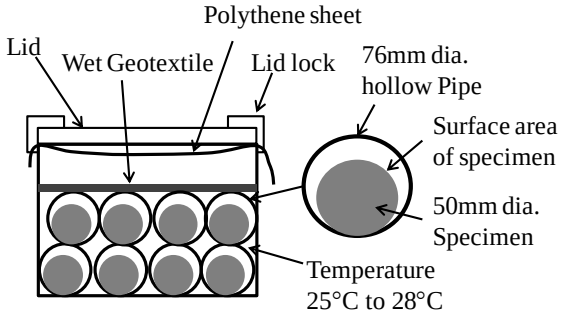

Figure 3: Specimens in the curing box.

3.1 Unconfined Compression Test

After curing, each specimen was submerged for 24 hours in the prepared NaCl solution to get better saturation ratio. This ensures the saturation ratio around 0.89 [22]. The Unconfined Compression test was conducted on submerged specimen at an axial strain rate of 1.2 % per minute (see Figure 4). Here the unconfined compressive strength (q_u) is peak value of the yield stress. Shear failure was monitored in all the specimens as shown in Figure 4.

Figure 4: Submerged specimen for Unconfined Compression test.

4 RESULTS AND DISCUSSION

4.1 Effect of lime and Fly ash

Lime is alkaline. Strong alkaline pH impels the silica and alumina of fly ash (glassy portion) and soil to dissolve which react with lime and form calcium silicate hydrate (C-S-H) and calcium aluminate hydrate (C-A-H) [23].

$$Si(OH)_5^- + Ca^{2+} \rightarrow Ca \cdot SiO_2 \cdot 2H_2O + H^+$$

Similar reaction occurs in sand-lime mixture and the result is interpreted based on the earlier studies (24; 21). Figure 5 shows the unconfined compressive strength (q_u) data of two constant dry densities (1.283 and 1.467 g/cm^3) containing equal amount of fly ash (30%) and salt (0%) but different percent (1, 2, 3 and 5 %) of lime content.

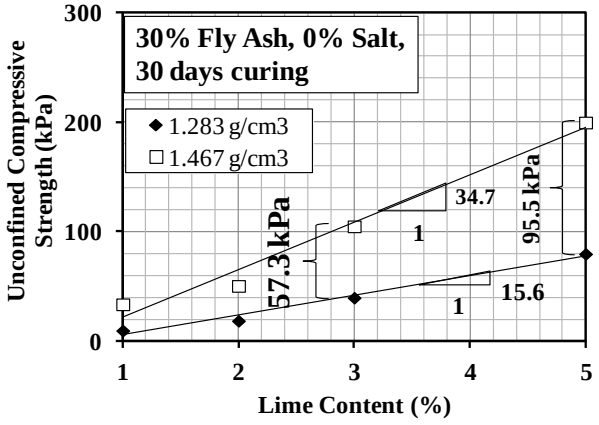

Figure 5: Effect of lime content on lime, fly ash and sand mixtures.

It can be observed that q_u is the function of lime content and dry density. With increase in lime content, q_u increases for both dry densities at constant fly ash content. Here 30% fly ash was used. At 1 % lime content the fly ash was not fully consumed by lime, at 2, 3 and 5% lime content more fly ash was consumed, and consequently the q_u increased. This consumption reduces the P^H value with time. Figure 6 traces the P^H value verses curing time graph. With long time reaction the p^H value decreases. The SEM micrograph of lime and fly ash is shown in Figure 7. Here the needle shaped ettringite crystals [25] formation is found. At higher dry density, q_u is greater. It could be a reason that at higher density the lime and fly ash get closer and accelerate the pozzolonic reaction therefore the strength increases with the increase in density. In Figure 8, the q_u increases with increase in fly ash content.

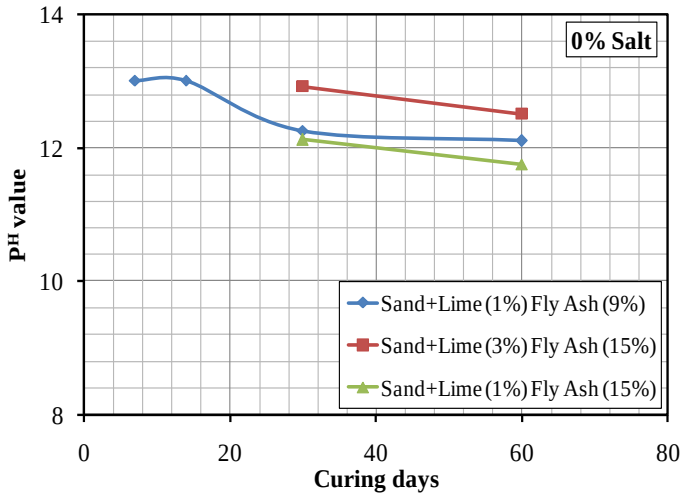

Figure 6: P^H value verses curing days.

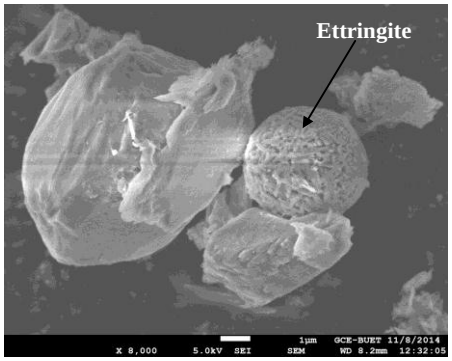

Figure 7: Scanning electron microscopic view of lime and fly ash after curing.

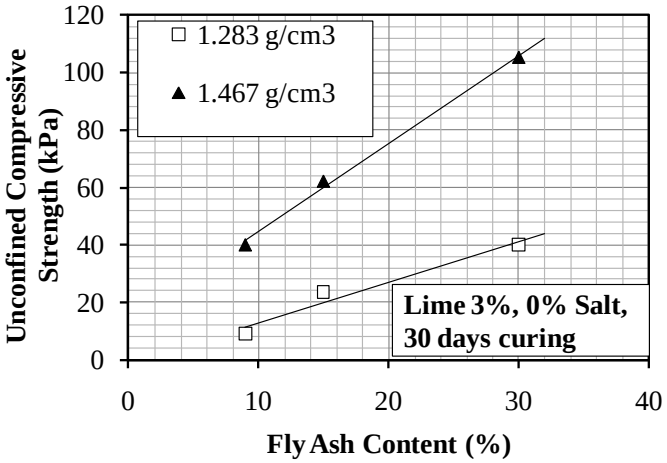

Figure 8: Effect of fly content on lime, fly ash and sand mixtures.

4.2 Effect of Salt

Three specimens were prepared using 0%, 4% and 8% salt content and cured under the same salt water solution for 30 days to investigate the effect of salt content in water on fly ash treated sample with sand and 10% fly ash (no lime). Figure 9 shows unconfined compressive strength of 10% fly ash treated sand vs. salt content of mixing water. No significant effect of salt content was observed.

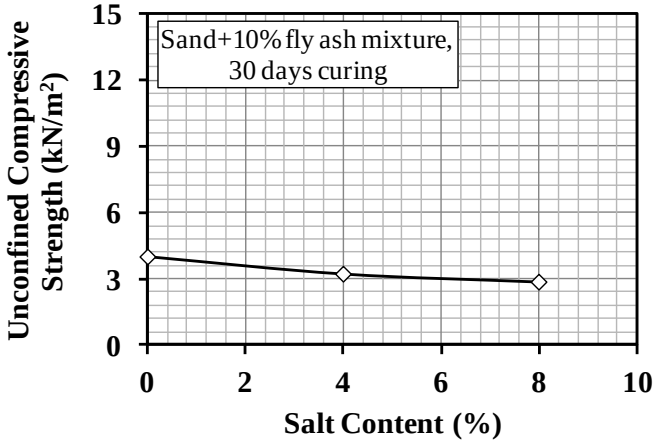

Figure 9: Effect of salt content on fly ash.

Similarly, lime-fly ash treated sand specimens were prepared using 3% lime and 9, 15, and 30% fly ash with 0, 4 and 8% salt content as mixing water solution. The specimens were cured for 30 days. Unconfined compression test results for

different percentages of fly ash content and salt content are shown in Figure 10. It is clearly seen that unconfined compressive strength increased with an increase of salt content of mixing water and fly ash content.

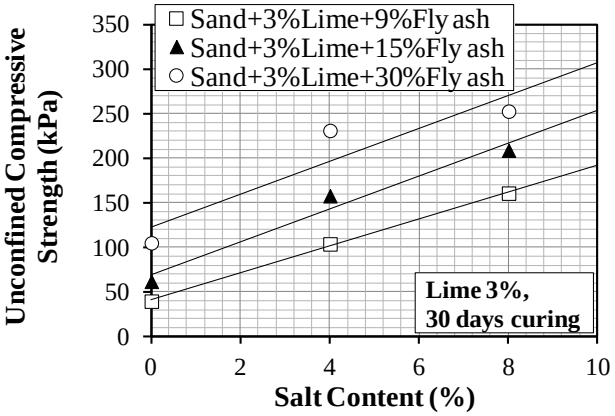

Figure 10: Effect of salt content on sand, lime and fly ash mixtures.

4.2.1 Porosity and b-value correction for best fit curve

In lime-fly ash treated sand, the porosity is considered as a function of sand, lime and fly ash content as proposed by Consoli et al., [22] and shown in Equation 1.

$$\eta = 100 - \left\{ 100 \left[\left(\frac{\left(\frac{\gamma_d V_S}{1+\left(\frac{L}{100}\right)} \right)\left(\frac{S}{100}\right)}{G_{S_S}} \right) + \left(\frac{\left(\frac{\gamma_d V_S}{1+\left(\frac{L}{100}\right)} \right)\left(\frac{FA}{100}\right)}{G_{S_{FA}}} \right) + \left(\frac{\left(\frac{\gamma_d V_S}{1+\left(\frac{L}{100}\right)} \right)\left(\frac{L}{100}\right)}{G_{S_L}} \right) \right] \right\} / V_S \quad \ldots\ldots\ldots\ldots\ldots (1)$$

where, η = porosity of specimen, FA = fly ash content, L = lime content, γ_d = dry density specimen of Vs = volume of specimen, G_{S_S} , $G_{S_{FA}}$, G_{S_L} , specific gravity of sand, fly ash and lime respectively. Using this equation Consoli, et al. [26] proposed η/L_{iv} ratio [L_{iv}, volumetric lime content] later Consoli, et al., [22] used an exponent for L_{iv} and proposed $\eta/L_{iv}^{0.12}$ to best fit, which is more reliable [22]. Figure 11 shows unconfined compressive strength verses $\eta/L_{iv}^{0.12}$ for all lime-fly ash treated sand of 30 days age specimens. The unconfined compressive strength increases with the reduction of $\eta/L_{iv}^{0.12}$. At higher density (lower $\eta/L_{iv}^{0.12}$) the salt effect is as significant as that of low density (higher $\eta/L_{iv}^{0.12}$).

In Figure 11, the best fitted curves of 0, 4 and 8% salt content specimens were tried to bring closer by multiplying the q_u of each specimens. Therefore by back calculation the b-value was determined. The *b*-value correction is shown in Figure 12. Here eq. 2 and 3 are for 4% and 8% salt content respectively. By multiplying the q_u with *b*-value all trend curves come closer. The *b*-values were used to normalize all the trend curves which finally fall in a single trend curve (see Figure 13). This curve can be used in determining the unconfined compressive strength of lime-fly ash treated sand at different percent of salt contents in mixing water.

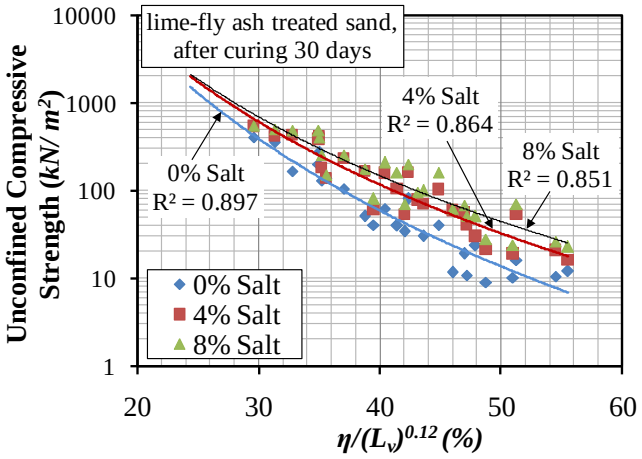

Figure 11: Unconfined compressive strength verses $\eta/L_{iv}^{0.12}$ graph.

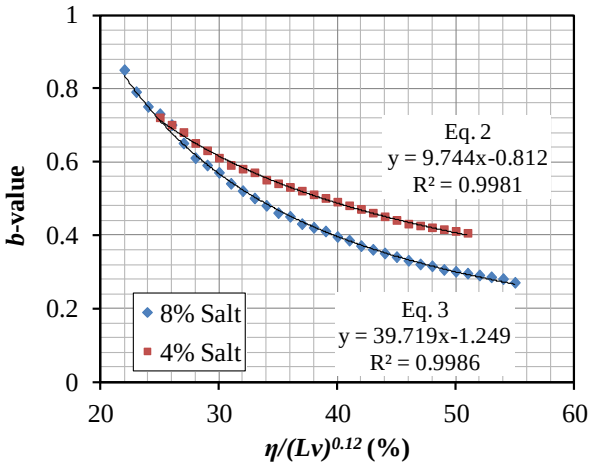

Figure 12: b-value graph.

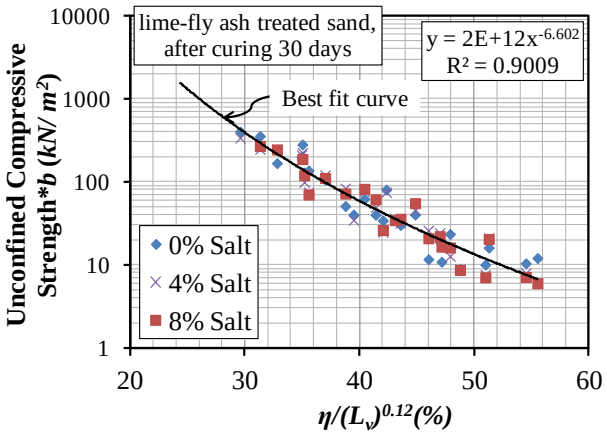

Figure 13: Best fit normalized curve of unconfined compressive strength for different porosities, lime content and salt contents

5 CONCLUSION

A series of unconfined compression tests was conducted on specimens containing different percentages of lime and fly ash mixed with sand. 0, 4 and 8% percent salt (*NaCl*) solution were used for preparing and curing the test specimens. The present study provided the following outcome:

1) With an increase in lime content, the unconfined compressive strength increased.

2) Salt content of water increases compressive strength of lime-fly ash treated sand.

3) Compressive strength of lime-fly ash treated sand increases with the increase in fly ash.

4) For fine sand, a correlation among unconfined compressive strength, porosity, volumetric lime content and salt content in water was developed.

ACKNOWLEDGEMENTS

Writers wish to express their gratitude to “Introduction of Quality Test Protocols for Road and Market Rehabilitation” under Coastal Climate Resilient Infrastructure Project (CCRIP) (Package No: CCRIP-S-05(C), LGED, GOB) for their financial support.

REFERENCES

[1] Akinkurolere, O. O., Jiang, C., & Shobola, O. M. (2007). The influence of salt water on the compressive strength of concrete. Journal of Engineering Applied Science, 2 (2), pp.412-415.

[2] Bell, F. G. (1993). An Examination of the Use of Lime and Pulverized Fly Ash to Stabilize Clay Materials. Environment and engineering geoscience, xxx (4), pp.469-479.

[3] Consoli, N. C., Johann, A. D., Gauer, E. A., Santos, V. R., Moretto, R. L., & Corte, M. B. (2012). Key parameters for tensile and compressive strength of silt–lime mixtures. Géotechnique Letters, 2 (3), pp.81-85.

[4] Consoli, N. C., Prietto, P. D., Carraro, J. A., & Heineck, K. S. (2001). Behavior of Compacted soil-fly ash-carbide lime mixtures. Journal of Geotechnical and Geoenvironmental Engineering, 127 (9), pp.774-782.

[5] Consoli, N. C., Rocha, C. G., & Silvani, C. (2014). Effect of curing temperature on the strength of sand, coal fly ash, and lime blends.

[6] Consoli, N. C., Rosa, A. D., & Saldanha, B. R. (2011). Variables Governing Strength of Compacted Soil–Fly Ash–Lime Mixtures. Journal of Materials in Civil Engineering, 23 (4), pp.432–440.

[7] Das, S. K., & Yudhbir. (2005). Geotechnical Characterization of Some Indian Fly Ashes. Journal of Materials in Civil Engineering, 17 (5), pp. 544-552.

[8] Emmanuel, A. O., Oladipo, F. A., & E, O. O. (2012). Investigation of Salinity Effect of Compression Strength of Reinforced Concree. Journal of Sustainable Development, 5 (6), pp.74-82.

[9] Fraay, A. L., Bijen, J. M., & Haan, Y. M. (1989). The reaction of fly ash in concrete a critical examination. Cement and Concrete Research, 19 (2), pp.235-246.

[10] Haque, S. A. (2006). Salinity problems and crop production in coastal regions of Bangladesh. Pakistan Journal of Botany, 38 (5), pp.1359-1365.

[11] Mahmuduzzaman, M., Ahmed, Z. U., Nuruzzaman, A. K., & Ahmed, F. R. (2014). Causes of Salinity Intrusion in Coastal Belt of Bangladesh. International Journal of Plant Research, 4 (4A), pp.8-13.

[12] Mbadikea, E. M., & Elinwab, A. U. (2011). Effect of salt water in the production of concrete. Nigerian Journal of Technology, 30 (2).

[13] Mohammed, T. U., Hidenori, H., & Toru, Y. Performance of seawater-mixed concrete in the tidal environment. Cement and Concrete Research , 34 (4), pp.593–601.

[14] Olutoge, F. A., & Amusan, G. M. (2014). The Effect of Sea Water on Compressive Strength of Concrete. International Journal of Engineering and Science Invention, 3 (7), pp.23-31.

[15] Porbaha, A., Pradhan, T. B., & Yamane, N. (2000). Time effect on shear strength and permeability of fly ash. Journal of Energy Engineering, 126 (1), pp.15–31.

[16] Rao, S. M., & Asha, K. (2012). Activation of Fly Ash-Lime Reactions: Kinetic Approach. Journal of Materials in Civil Engineering, 24 (8), pp.1110-1117.

[17] Rao, S. M., & Asha, K. (2013). Role of Fly Ash Pozzolanic Reactions in Controlling Fluoride Release from Phosphogypsum. Journal of Materials in Civil Engineering, 25 (8), pp.999–1005.

[18] Raymond, S. (1961). Pulverized fuel ash as embankment material. Proc. Inst. Civ. Eng., (pp. 515-536).

[19] Senapati, M. R. (2011). Fly ash from thermal power plants – waste management and overview. CURRENT SCIENCE, 100 (12), pp791-1794.

[20] Sudhakar, M. R., & Asha, K. (2012). Activation of Fly Ash–Lime Reactions: Kinetic Approach. Journal of Materials in Civil Engineering, 24 (8), pp.1110–1117. .

[21] Thompson, M. R. (1972). Deep plow lime stabilization for pavement construction. Journal f Teansformation Engineering, 98 (te2), pp.311-323.

[22] Tiwari, P., Chandak, R., & Yadav, R. K. (2014). Effect of Salt Water on Compressive Strength of Concrete. Int. Journal of Engineering Research and Applications , 4 (4), pp.38-42.

[23] Tiwari, P., Chandak, R., & Yadav, R. K. (2014). Effect Of Salt Water On Compressive Strength of Concrete. Int. Journal of Engineering Research and Applications, 4 (4), pp.38-42 .

[24] Urhan, S. (1987). Alkali silica and pozzolanic reactions in concrete. Part 1: Interpretation of published results and a hypothesis concerning the mechanism. Cement and Concrete Research, 17 (1), pp.141-152.

[25] Wegian, F. M. (2010). Effect of seawater for mixing and curing on structural concrete. The IES Journal Part A: Civil & Structural Engineering, 3 (4), pp.235–243.

[26] Winter, M. G., & Clarke, B. G. (2002). Improved use of pulverized fuel ash as general fill. Proc. Inst. Civ. Eng. Geotech. Eng., 155(2), pp. 1331-2341.

[27] Yudhbir, & Honjo, Y. (1991). Application of geotechnical engineering of environmental control. Proc. 9th Asian Regional Conf. on Soil Mechanics and Foundation Engineering, (pp. 431-469). Bangkok.

CICM 2015
First International Conference on
Advances in Civil Infrastructure and Construction Materials
MIST, Dhaka, Bangladesh, 14–15 December 2015

BEHAVIOR OF PADMA SAND-SILT MIXTURES UNDER CYCLIC AND STATIC LOADING

Mohammad E. KARIM[1] **and Md. J. Alam**[2]

[1, 2] Bangladesh University of Engineering and Technology, Dhaka, Bangladesh
Email: [1]emdadul.buet@gmail.com and [2] jahangir.buet@gmail.com

Abstract. *Cyclic and static triaxial tests have been conducted on clean sand, pure nonplastic silt and sand-silt mixtures (10-90% nonplastic silt content) at different relative densities with effective confining pressure 100 kPa. Main objective was to identify the Limiting Fines Content (LFC) and Equivalent Granular Steady State Line (EG-SSL) of Padma Sand-silt mixtures. The specimens of 71 mm diameter and 142 mm height were prepared by moist tamping method. With increasing percentage of silt content the Cyclic Shear Strength (CSS) and Static Shear Strength (SSS) decrease till Limiting Fines Content (LFC = 30% silt content, (calculated)), after LFC for further increment of silt content till pure silt the CSS and SSS remain near about constant. Thus calculated LFC was verified by experimental results. The concept of equivalent granular void ratio was found to be more appropriate to explain the behavior of sand–silt mixtures than that of relative density and global void ratio.*

Keywords: Cyclic stress ratio, Static shear strength, *LFC*, *EG-SSL*, Nonplastic silt.

1 INTRODUCTION

The behavior of sand and nonplastic silt mixture under cyclic and static loading has been discussed broadly in geotechnical literature. Nevertheless the conclusions are still conflicting. In some laboratory studies it is concluded that the presence of nonplastic silts decreases the liquefaction potential/static strength [1, 2, 3, 4, 5, 6, 7, 8, 9], some studies indicate that silts increases the liquefaction potential [10, 11] and some studies specify that the resistance initially decreases as the silt content increases thereafter increases as the silt content continues to increase [12, 13]. Recently some researcher proposed equivalent granular void ratio concept to explain the behavior of sand-silt mixtures [14, 15].

This paper focused on the behavior of sand and nonplastic silt mixtures under isotropically consolidated undrained static and cyclic loading. In undrained static test, soil specimens (each sand-silt mixtures) have been formed by moist tamping method. Also permeability test by falling head method have been conducted to verify the behavior.

2 EXPERIMENTAL PROGRAM

2.1 Tested Material and Sample Separation

Sand and silt were used in this study collected from sand bars of Padma River, Mawa, Munshiganj, Bangladesh, near proposed Padma Bridge site. The grain size analysis graph is shown in Figure 1. The shape of the sand and silt is near about similar angular (from scanning electron microscopic test). It was tried to determine the Plastic Limit (*PL*) of silt and observed that the silt sample is nonplastic. Index property of sand and silt, namely, specific gravity, maximum and minimum void ratio, liquid limit, plastic limit are given in Table 1.

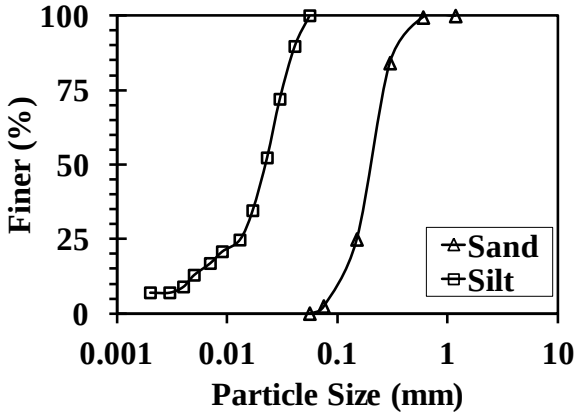

Figure 1: Grain size distribution of Sand and Silt used in this study.

2.2 Limiting Fines Content

When small amount of fines (silt) are mixed with sand, silt particles occupy the voids created by the sand particles. If the silt content is increased, the sand particles start to separate from each other. The percent of fines just necessary to separate sand particles from each other is called Limiting Fines Content (*LFC*). After the *LFC* the silt particles dominate the whole soil structure. The LFC is calculated using the following expression [16]:

$$LFC = \frac{W_{fines}}{W_{sand} + W_{fines}} = \frac{G_f e_s}{G_f e_s + G_s \left(1 + e_f\right)} \qquad (1)$$

Where, W_{fines} is the weight of fines and W_{sand} is the weight of sand in a sand–silt mixture. Similarly, G_f, G_s, e_f and e_s stand for specific gravity of silt and sand, maximum index void ratio of silt and sand respectively.

Table 1: Test conditions.

Soil Type	Sand	Silt
USCS classification symbol	SP	ML
Mean particle diameter D_{50} (mm)	0.2	0.02
Uniformity coefficient (C_u)	2.22	5.82
Coefficient of gradation (C_z)	1.17	2.15
Specific gradation (G_s)	2.69	2.72
Liquid limit (%)	N/A	38
Plastic limit (%)	N/A	N/A
Plasticity index	N/A	NP*
e_{max}	1.165	1.72
e_{min}	0.504	0.462

*NP: nonplastic

2.3 Cyclic Test and Static Test

All static triaxial tests were carried on 71 mm diameter and 142 mm height specimen. Samples were prepared adding the sand with nonplastic silt of 0 to 100% (percent by dry weight). In order to proper mixing, first of all dry clean sand and pure silt of required amount was put inside a five litre gallon and then the lid fitted; thereafter it was shaken 2 minutes. The specimens were prepared by moist tamping method [17] and saturated with sufficient back pressure till the skempton's b value reached 0.95. Subsequently the specimen was isotropically consolidated at 100 kpa effective confining pressure (for all tests). The values of relative densities presented in this paper are the values before consolidation. The duration of consolidation was 1 hour for sand and 3 hours for silt. After consolidation the

shearing/cyclic phase starts. The cyclic triaxial tests were stress controlled at frequency 1 Hz. The static triaxial tests were undrained strain controlled, at rate of 0.05% axial strain per minute.

Initial liquefaction (excess pore water pressure becomes equal to the initial effective stress, σ_{3c}') or a deformation of 6% double amplitude axial strain at 15th cycle was the criterion used in this study to define the cyclic resistance ratio (*CRR*). A minimum of three cyclic tests were carried out at different cyclic stress ratios to determine *CRR*. Once the *CRR* was determined, the cyclic shear strength (*CSS*) was calculated using eq. 2 as given below.

$$\sigma_c = 2 \times \sigma_{3c}' \times CRR \qquad (2)$$

Where, σ_c = Cyclic Shear Strength (kPa), σ_{3c}' = effective confining pressure (kPa), *CRR* = Cyclic Resistance Ratio.

Undrained Static Shear Strength (SSS) was determined from the plot of deviator stress verses axial strain graph. In a particular test the undrained shear stress (τ) of a specimen is the half of deviator stress ($q=(\sigma_1-\sigma_3)$) (eq. 3).

$$\tau = q/2 \qquad (3)$$

Here the peak deviator stress within 15% axial strain is the deviator strength. *SSS* is the half of deviator strength (ASTM D4767-11).

3 TEST RESULT AND DISCUSSION

In Figure 2, the cyclic and static triaxial test result of sand-silt mixtures prepared by moist tamping method are shown respectively. Here the undrained *SSS* and *CSS* verses silt content graph is exhibited. For both cyclic and static tests the *CSS* [18] and *SSS* respectively are decreasing with increasing silt content till *LFC* thereafter those become near about constant till pure silt.

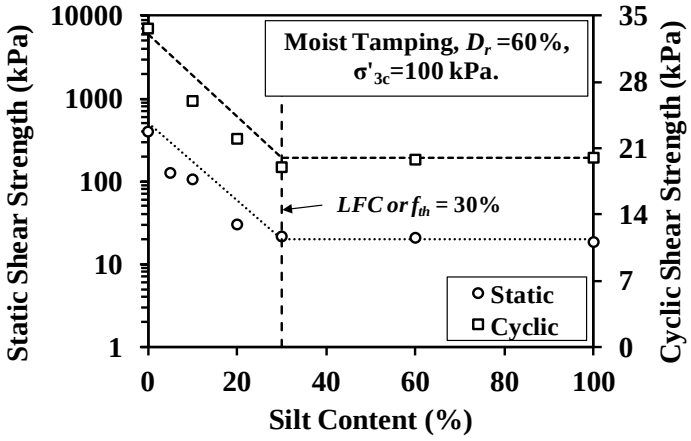

Figure 2: Shear Strength verses silt content graph.

The permeability test results of sand-silt mixtures for are shown in Figure. 3. Here the permeability is decreasing with increase in nonplastic silt content till *LFC* thereafter it is near about constant till pure silt. It means that for increase in silt content at constant relative density (D_r=*60%*) the void among the sand particles are filled with fine nonplastic silt particles. Hence the permeability is decreasing. For decreasing permeability at cyclic or static undrained loading, the excess pore water pressure develops rapidly so the *CSS* and *SSS* are decreasing (see Figure. 2). After *LFC* silt particles dominates the soil structure (sand-silt mixtures). The inner voids among the silt particles (in sand-silt mixtures) remain same (because the permeability after *LFC* remain same) with increasing silt content for this reason the *CSS* and *SSS* remain same with increasing silt content after *LFC*.

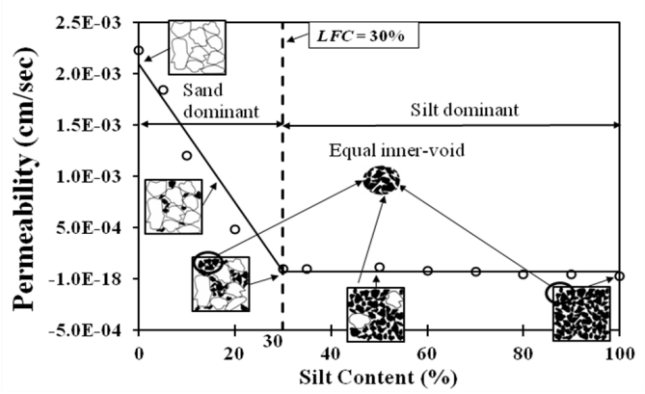

Figure 3: Grain size distribution of Sand and Silt used in this study.

4 EQUIVALENT VOID RATIO CALCULATION

Relative density is a problematic parameter for sand with fines, which might be the main reason of conflicting outcome as discussed above. The equivalent granular void ration (*e**) may be a more consistent parameter [19, 15]. So, to determine the equivalent granular void ratio the following equations are used:

For intergranular void ratio, $(e_c)_{eq} = \dfrac{e+(1-b)f_c}{1-(1-b)f_c}$ (4)

Where e = void ratio, b = portion of fines that contribute to active intergrain contacts, f_c = fines content, Rahamman et al. (2008) [19] proposed a semi-empirical equation expressed as,

$$b = [1-\exp(-0.3\frac{(f_c/f_{th})}{k})]x(r\frac{f_c}{f_{th}})^r \qquad (5)\ (0\langle b\langle 1)$$

Where, $r = (D_{10}/d_{50})^{-1} = d_{50}/D_{10}, k = \left(1 - r^{0.25}\right)$

To determine the f_{th}, Rahman et al. (2008) [19] proposed the following equation:

$$f_{th} = 40\left(\frac{1}{1+e^{\alpha-\beta x}} + \frac{1}{x}\right) \qquad (6)$$

Where $X=D_{10}/d_{50}$, α=0.50, β=0.13.
Using the equation (6), the F_{th} in this study was found 30%.

4.1 Equivalent granular steady state line

The *e – log(p')* graph of sand-silt mixtures is shown in Figure 4(a). It shows that the Steady State Line (*SSL*) of sand-silt mixtures go down ward with increasing in silt content, which was also observed by Murthy et al. (2007) [23]. A number of researchers have demonstrated that irrespective of silt, the SS data points in *e* - log(p')* (see Figure. 4(b)) space may be described by a single trend [21, 15]. This single relationship is referred to as "equivalent granular steady state" (*EG-SSL*) (shown in Figure. 4(b)). Here the *EG-SSL* is independent of fines. The *EG-SSL* obtained from the prediction approach can be used to predict undrained behaviour such as flow, non-flow or limiting flow behavior under Critical State Soil Mechanics (*CSSM*) framework [22]. $\psi^*(0)>0$, (ψ^* = Equivalent Granular State Pa-rameter = $e^*-e^*_{ss}$) shows flow-type behaviour; $\psi^*(0)<0$, shows non-flow behavior; and at $\psi^*(0)\approx 0$, shows limited flow behavior [15] (Rahman et al, 2014). Therefore, equivalent granular steady line concept was found to be valid from the data of this study.

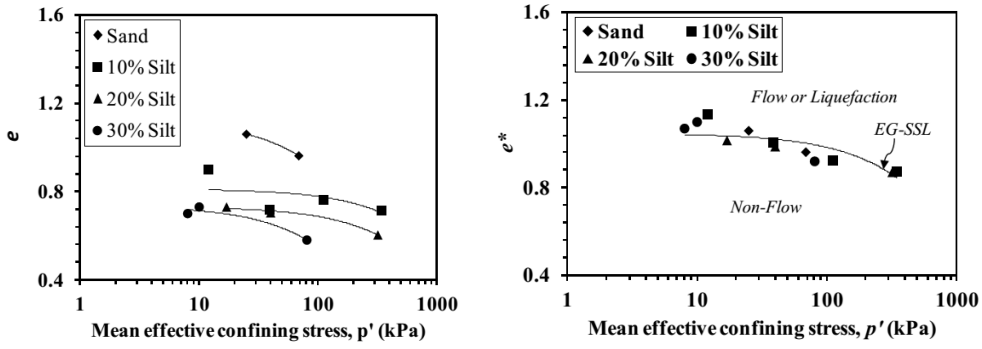

(a) (b)

Figure 4: (a) Steady State Line (*SSL*) with increase in fines content and (b) Equivalent Granular Steady State Line (*EG-SSL*) of studied sand and silt.

5 EFFECT OF MICA MINERAL IN SILT

To justify the effect of mica mineral in silt, 1 g of mica (passing through 75 μm sieve) was added with 1000g silt. After mixing of silt and extra 1 g mica (0.1% mica, by weight), a specimen of 73 percent relative density was tested at 100 kPa isotropic effective pressures. The test result is shown in Figure 10, where the silt with 0.1% mica specimen has lost 34 percent of deviator stresses. That means mica flings the silt to lose the undrained shear strength.

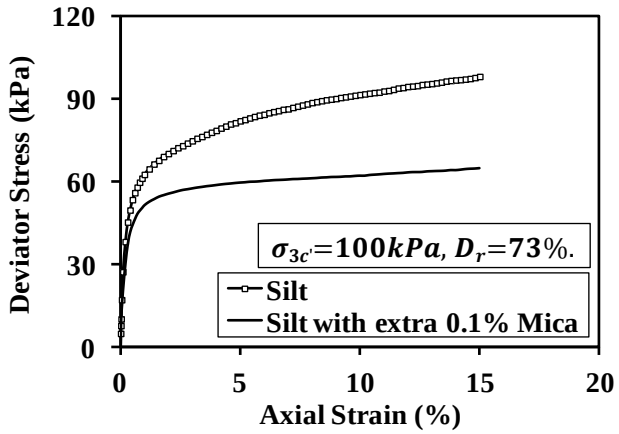

Figure 5: Effect of mica in silt.

6 CONCLUSIONS

- The *CRR* and *SSS* decrease with increasing nonplastic silt content till 30% silt content later it remains near about constant till pure silt. Here the calculated *LFC* is 30%, verified by experimental results.
- After *LFC* the inner voids among the silt particles remain same with increasing silt content because silt content dominates the soil structure after *LFC*. For this reason the *CSS* and *SSS* remain same with increasing silt content after *LFC*.
- The concept of equivalent granular void ratio was found to be more appropriate to explain the behavior of sand-silt mixtures than the relative density and global void ratio.
- Mica content decreases the shear strength of silt.

ACKNOWLEDGEMENTS

The research work has done under the M.Sc. project work. Financial support for this research work by Bangladesh University of Engineering and Technology is gratefully acknowledged.

REFERENCES

[1] Tokimatsu, K., and Yoshimi, Y. (1983). "Empirical Correlation of Soil Liquefaction Based on SPT N-Value and Fines Content." Soils and Foundations 23(4), pp 57-74.

[2] Seed, H. B., Idriss, I. M., and Arango, I. (1983). "Evaluation of Liquefaction Potential Using Field Performance Data." Journal of Geotechnical Engineering (ASCE) 109(3), pp 458-482.

[3] Robertson, P. K., and Campanella, R. G., (1985). "Liquefaction potential of sands using the CPT." Journal of Geotechnical Engineering (ASCE) 111(3), pp 384-403.

[4] Pitman, T. D., Robertson, P. K., and Sego, D. C., (1994). "Influence of Fines on the Collapse of Losse Sands." Canadian Geotechnical Journal, 31(5), pp 728-739.

[5] Yammamuro, J. A., and Kelly, M. C. (2001). "Monotonic and Cyclic Liquefaction of Very Loose Sands With High Silt Content." Journal of Geotechnical and Geoenvironment Engineering 127(4), pp 314-324.

[6] Belkhatir, M., Hanifi, M., Ahmed, A., Noureddine, D., and Tom, S. (2011): "Undrained Shear Strength of Sand-silt Mixture: Effect of Intergranular Void Ratio and Other Parameters." KSCE Journal of Civil Engineering (Springer) 15(8), pp 1335-1342.

[7] Arab, A., and Belkhatir, M. (2012): "Fines Content and Cyclic Preloading Effect on Liquefaction Potential of Silty Sand: A Laboratory Study." Acta Polytechnica Hungarica 9(4), pp 47-64.

[8] Belkhatir, M., Schanz, T., and Arab, A. (2013): "Effect of Fines Content and Void Ratio on the Saturated Hydraulic Conductivity and Undrained Shear Strength of Sand–silt Mixtures." Environ Earth Sci (Springer) 70(6), 2469-2479.

[9] Yin, Z., Zhao, J., and Hicher, P. (2013). "A Micromechanics-Based Model for Sand-Silt Mixtures." International Journal of Solids and Structures (Elsevier) 51(6), pp 1350–1363.

[10] Troncoso, J. H., and Verdugo, R. (1985). "Silt Content and Dynamic Behavior of Tailing Sands." In Proceedings of the 11th International Conference on Soil Mechanics and Foundation Engineering. San Francisco, Calif., 1985. pp 1311-1314.

[11] Sladen, J. A., D'Hollander, R. D., and Krahn, J., Mitchell, D. E. (1985): "Back Analysis of the Nerlerk Berm Liquefaction Slides." Canadian Geotechnical Journal, 22(4), pp 579-588.

[12] Chang, N. Y., and Kaufman, L. P. (1982). "Liquefaction Potential of Clean and Silty Sands." Seattle, USA: Proceedings of the 3rd International Earthquake Microzonation, 1982. pp 1017-1032.

[13] Singh, S., (1996): "Liquefaction characteristics of silts." Geotechnical & Geological Engineering, (Springer) 14(1), pp 1-19.

[14] Rahman, M. M., S. R. Lo and M. A. L. Baki. (2011): “Equivalent granular state parameter and undrained behavior of sand–fines mixtures.” Acta Geotechnica (2011) 6: pp 183–194.
[15] Rahman, M. M., M. A. L. Baki, and S. R. Lo. (2014): “Prediction of Undrained Monotonic and Cyclic Liquefaction Behavior of Sand with Fines Based on the Equivalent Granular State Parameter.” International Journal of Geomechanics, ASCE, 14(2), pp 254–266.
[16] Hazirbaba, K. (2005). Pore pressure generation characteristics of sands and silty sands: a strain approach. Dissertation presented for PhD program to the faculty of Graduate School at the University of Texas at Austin.
[17] Ladd, R. S. 1978. Preparing test specimens using under compaction, Geotechnical Testing Journal, 1, (1), pp 16–23.
[18] Karim, M. E. and Alam, M. J. (2014): "Effect of non-plastic silt content on the liquefaction behavior of sand–silt mixture." Soil Dynamics and Earthquake Engineering, 65, 142–150.
[19] Rahman, M. M., Lo, S. R., and Gnanendran, C. T., (2008) "On Equivalent Granular Void Ratio and Steady State Behaviour of Loose Sand with Fines." Can. Geotech. J. 45: pp 1439-1456.
[20] Murthy, T. G., Loukidis, D., Carraro, J. A., Prezzi, M., and Salgado, R. (2007). "Undrained monotonic response of clean and silty sands." Ge´otechnique, 57(3): pp 273-288.
[21] Thevanayagam, Sabanayagam. (2000) "Liquefaction Potential and Undrained Fragility of Silty Soils." 12WCEE 2000 Conference proceding, New York, pp 1-8.
[22] Rahman, M. M., Sik-Cheung Robert Lo, and Misko Cubrinovski. (2010), "On Equivalent Granular Void Ratio and Behaviour of Loose Sand." Canadian Geotechnical Journal, 45(10): pp 1439-1456.

CICM 2015
First International Conference on
Advances in Civil Infrastructure and Construction Materials
MIST, Dhaka, Bangladesh, 14–15 December 2015

DEVELOPMENT OF CORRELATION BETWEEN SOAKED AND UNSOAKED CBR OF LEAN CLAY

N. HOSSAIN[1], **S. S. Ahmed**[2], **A. J. Khan**[3] **and M. S. Islam**[4]

[1, 2, 3] Department of Civil Engineering, Bangladesh University of Engineering and Technology, Dhaka, Bangladesh
Email: [1]nusaeirhossain@rocketmail.com, [2]shahriar.0904027@gmail.com,
[3]jabbar@ce.buet.ac.bd, [4]msharifulbd@gmail.com

Abstract. *The load bearing capacity of subgrade soil supporting different pavement systems is of great importance to the integrity of the pavement. Soaked CBR is used as a design parameter for pavement design. However, derivation of CBR values for pavement design involves soaking soil sample for four days, which is time consuming. For this study, soil samples were collected from sub-grade of an existing flexible pavement of Savar Cantonment Area. The soil samples are identified as Lean Clay and CBR test is performed both in soaked and unsoaked conditions .The test results of sample soil has led to the formulation of an empirical equation relating unsoaked and soaked CBR for a varying range of dry density. This equation can be used to predict soaked CBR from available unsoaked CBR test data within the specified range of dry density where the sub-grade consists of Lean Clay.*

Keywords: California bearing ratio, Soaked CBR, Unsoaked CBR, Sub-grade, Lean clay.

1 INTRODUCTION

Roads and highways are in the center of economic activities in countries where land based communication is dominant. The construction, operation and maintenance of the roadways play vital role in the economy. To get uninterrupted and sustainable service from the roadways, the first requirement is to construct the roads in such a way that these are able to withstand heavy traffic loads and weathering effects during the expected service life. The strength of soil on which the roads will be constructed is the basis of pavement design. So, predicting the strength of soil is of vital importance. California Bearing Ratio (CBR) test is developed to predict the strength of soil with reasonable accuracy under different site conditions, which helps to determine the required sub-grade thickness for the construction of a road. This study is focused on two types of Laboratory CBR tests and the mathematical correlation between them. The present practice is to simulate the worst possible field condition for sub-grade soil in the laboratory by submerging the sample soil under water for four days and determine its strength. The samples are collected from different chainages along the centerline of a proposed road, the number of which is significantly large and takes a very long time to determine the strength. This affects the overall condition of the road construction project negatively. To overcome the negative effects of the elongated time requirement, it can be proposed that the strength of a particular type of sub-grade soil at worst field condition can be predicted by developing an empirical relationship between standard laboratory strength of soil in unsoaked condition and four days soaked condition.

2 EXISTING STUDIES FOR PREDICTING SOAKED CBR

None but Sathawara and Patel [1] experimented on CL type soil and established a correlation between 4-day soaked CBR and unsoaked CBR for the dry density achieved under different Proctor compaction efforts and developed the following equation to relate unsoaked CBR with 4-Day soaked CBR:

$$Y=0.936X^{0.819},\ [R^2=0.828] \quad (1)$$

Where, 'Y' stands for 4-day soaked CBR and 'X' stands for unsoaked CBR value.

3 METHODOLOGY AND RESULTS

The soil sample was collected from the sub-grade of a flexible pavement in Savar Cantonment, Dhaka. Then the investigation was carried out in following order:

- Atterberg Limits Test [2]
- Grain Size Analysis
- Proctor Compaction Test
- Soaked and Unsoaked CBR Test [4]

The soil sample is identified according to Unified Soil Classification System [3] and BNBC guideline [5] as Lean Clay with group symbol is CL.

Table 1: Percentage of Sand, Silt and Clay

Chainage	Liquid limit (LL)	Plastic Limit (PL)	Plasticity Index (PI)	Sand (%)	Silt (%)	Clay (%)
300m	38	14	24	4	50	46
600m	40	14	26	3	51	47
800m	38	13	25	6	50	44
1100m	39	18	21	3	68	29

Proctor compaction test with different compactive efforts was performed to determine optimum moisture contents for subsequent soaked and unsoaked CBR tests. The energy used in compaction test is presented in Table 2 and the results of Proctor compaction test is presented in Table 3.

Table 2: Energy used for Proctor Compaction

Compaction Method	Energy (lb-ft/ft^3)
½ of standard	6,435
Standard	12,375
Intermediate	33,750
Modified	56,250

Table 3: Optimum Moisture Content from Proctor Compaction

Chainage	Maximum Dry Density (kN/m^3)	Optimum Moisture Content (%)
300m	18.51	13.43
600m	18.97	13.66
800m	18.71	13.59
1100m	18.35	12.50

Optimum moisture contents determined from Proctor compaction test were used as reference moisture content to perform both soaked and unsoaked CBR tests. The compactive energies used for CBR test were slightly less than that for Proctor compaction test. The purpose of using reduced energy is to ensure that approximately 95% of maximum dry density is achieved in CBR test to properly resemble the field condition, where achieving a dry density equal to the maximum dry density is impractical from economic point of view. The summery of soaked and Unsoaked CBR test results are listed in Table 4 and Table 5.

Table 4: Soaked CBR Results

Chainage	Target Moisture Content (%)	Obtained Moisture Content (%)	Achieved Dry Density (kN/m^3)	Soaked CBR value
300m	13.43	13.37	13.37	1.62
		13.12	14.13	1.90
		13.43	16.08	2.57
		13.80	17.56	3.62
600m	13.66	13.57	14.10	1.43
		13.50	15.83	2.09
		13.48	17.02	2.85
		13.50	18.31	3.42
800m	13.59	13.57	13.65	1.43
		13.50	14.83	1.90
		13.48	17.02	2.66
		13.50	18.09	3.62
1100m	12.50	12.24	14.80	6.66
		12.65	15.41	8.37
		12.45	17.03	10.15
		12.37	17.52	11.03

Table 5: Unsoaked CBR Results

Chainage	Target Moisture Content (%)	Obtained Mois-ture Content (%)	Achieved Dry Density (kN/m^3)	Unsoaked CBR value
300m	13.43	13.42	14.82	2.79
		13.35	16.58	3.57
		13.41	17.68	4.74
		13.32	18.40	5.13
600m	13.66	13.56	14.23	2.01
		14.49	16.36	3.18
		13.54	17.45	4.35
		13.18	18.50	4.93
800m	13.59	13.53	14.10	2.11
		13.56	15.83	4.15
		12.06	17.02	4.93
		13.60	18.31	5.71
1100m	12.50	12.95	15.14	8.99
		12.11	16.45	12.93
		12.29	17.63	14.93
		12.72	18.82	20.12

To relate CBR value with dry density, power based regression equations were developed in following format:

$$Y=AX^{B} \quad (2)$$

Where, Y = CBR value
X = Dry Density in kN/m^3
A, B = Constants

The range of dry density was selected based on the observed maximum and minimum dry densities in CBR tests at different compactive energies. The obtained results are presented in Table 6.

Table 6: Unsoaked and Soaked CBR from Experimental regression equations

	Chainage 300 m		Chainage 600 m		Chainage 800 m		Chainage 1100 m	
Dry Density (kN/m^3)	un-soaked CBR	Soaked CBR	un-soaked CBR	Soaked CBR	un-soaked CBR	Soaked CBR	un-soaked CBR	Soaked CBR
	2.16	1.68	1.94	1.47	2.08	1.35	2.76	1.6
14.0	2.40	1.86	2.21	1.66	2.36	1.52	3.49	2.7
14.5	2.66	2.06	2.50	1.87	2.65	1.69	4.3	3.68
15.0	2.94	2.27	2.82	2.10	2.98	1.88	5.19	4.55
15.5	3.23	2.49	3.16	2.35	3.33	2.09	6.17	5.31
16.0	3.55	2.72	3.54	2.62	3.71	2.30	7.23	5.96
16.5	3.88	2.97	3.94	2.91	4.12	2.53	8.38	6.49
17.0	4.23	3.24	4.38	3.23	4.56	2.78	9.6	6.91
17.5	4.61	3.52	4.85	3.56	5.03	3.05	10.91	7.23
18.0	5.00	3.81	5.36	3.92	5.54	3.33	12.31	7.43
18.5	5.41	4.12	5.90	4.31	6.08	3.62	13.79	7.52

Using the above mentioned data, a power based equation was developed to relate unsoaked CBR with soaked CBR. With this equation, soaked CBR value can be predicted from the unsoaked CBR value for CL type soil. The equation is as following:

$$Y=0.7561X^{0.9578},\ [R^2=0.9404] \quad (3)$$

Where, Y = Soaked CBR Value
X = Unsoaked CBR Value

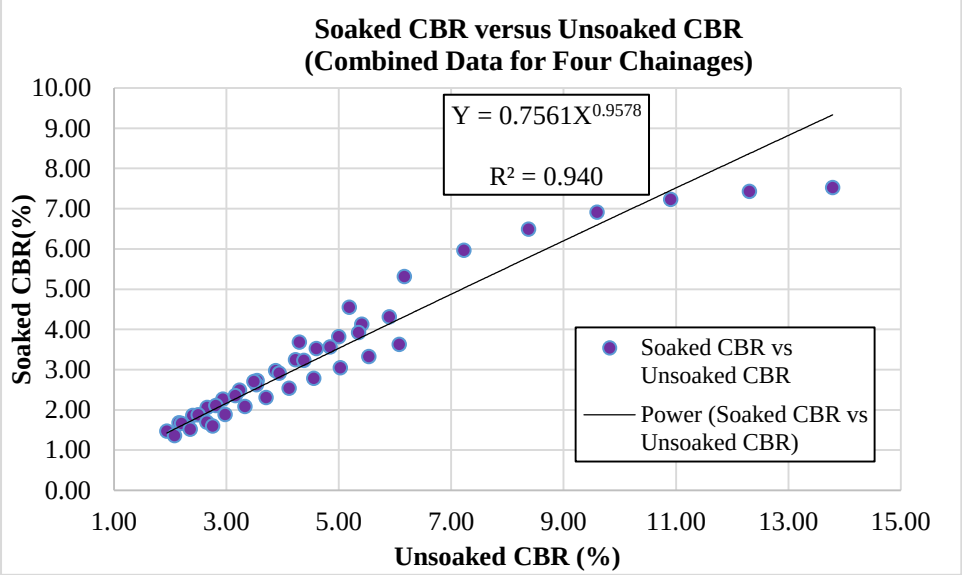

Figure 1: Soaked CBR versus Unsoaked CBR

The variation between predicted soaked CBR values using this model and the model suggested by Sathawara and Patel [1] is graphically represented in the following figure:

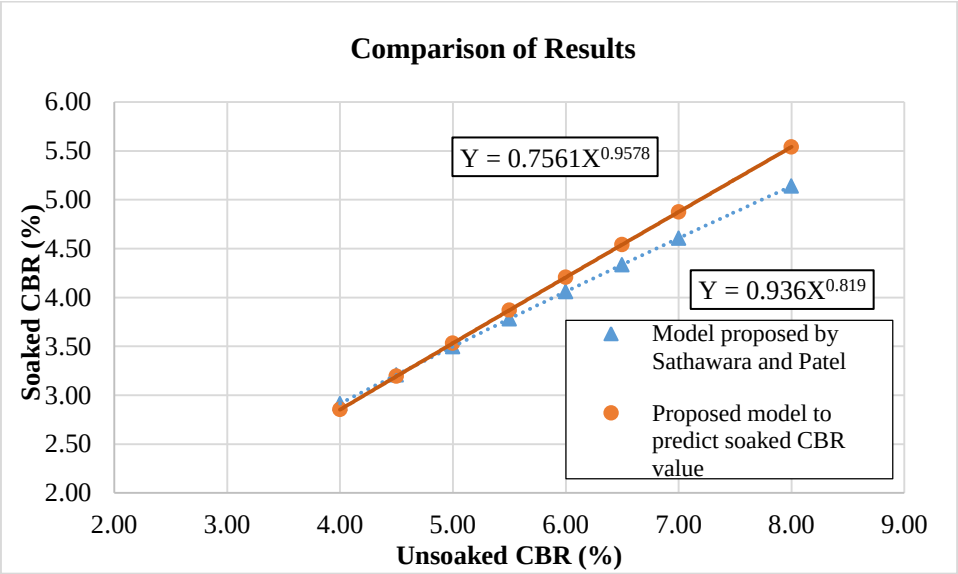

Figure 2: Comparison of Soaked CBR between proposed model and Sathawara and Patel [1]

4 CONCLUSIONS

Soaked CBR of the soil is an important parameter in designing a pavement. Thereby a quick and correct measure of soaked CBR value plays a vital part. In this study efforts have been made to develop a correlation between soaked CBR and unsoaked CBR for lean clay. The findings of the investigation are as follows:

- A regression equation has been developed to relate soaked CBR with unsoaked CBR for lean clay based on the laboratory test results. The equation is as follows:

$$Y=0.7561X^{0.9578},\ [R^2=0.9404]$$

Where, Y = Soaked CBR Value
X = Unsoaked CBR Value

- Comparison has been made with similar equation developed by Sathawara and Patel [1] and the results from this investigation closely resemble their findings.

Additional number of soil samples can be tested for further refinement of developed model. The same procedure of the investigation can be used for other types of soils to develop a correlation of soaked and unsoaked CBR values which can be used in the practical works with great convenience.

REFERENCES

[1] Sathawara J.K. and Patel A.K, 2013. Comparison between Soaked and Unsoakd CBR. *International Journal of Advanced Engineering Research and Studies*, **2 (1)**, pp 132—135.

[2] ASTM D 4318, 2004. *Standard Test Methods for Liquid Limit, Plastic Limit and Plasticity Index of Soils,* ASTM International, West Conshohocken, PA.

[3] ASTM D 2487, 2004. *Standard Practice for Classification of Soils for Engineering Purposes (Unified Soil Classification System),* ASTM International, West
Conshohocken, PA.

[4] ASTM D 1883, 2004. *Standard Test Method for CBR (California Bearing Ratio) of Laboratory-Compacted Soils*, ASTM International, West Conshohocken, PA.

[5] BNBC - Bangladesh National Building Code, 1993, Housing and Building Research Institute.

CICM 2015
First International Conference on
Advances in Civil Infrastructure and Construction Materials
MIST, Dhaka, Bangladesh, 14–15 December 2015

DEVELOPMENT OF EMPIRICAL CORRELATION BETWEEN DYNAMIC CONE RESISTANCE AND RELATIVE DENSITY OF SAND

Rowshon JADID[1], Ishika N. Chowdhury[2] and Md. F. Alam[3]

[1, 2, 3] Bangladesh University of Engineering and Technology, Dhaka, Bangladesh
Email: [1]rowshonjadid@yahoo.com, [2]ishika_nc@yahoo.com and
[3]ferdous@ce.buet.ac.bd

Abstract. *The Dynamic Probing Light (DPL) is a portable dynamic cone penetration test which is usually used for in situ measurement of resistance of cohesionless soil. An effort has been taken to establish a relationship between relative density and dynamic cone resistance of cohesionless soil measured from DPL test. This relationship is important since the Sand Cone Method, a common test used for quality control of sand fill in Bangladesh, cannot be applied at deeper locations or, in saturated sand to determine field density of soil. A series of tests was carried out in the field at different depth level to determine the field density of soil using Sand Cone Method. DPL test was performed then to determine the soil resistance at the adjacent location and depth where Sand Cone Method was applied. Field test results are compared with those from empirical approaches suggested by different researchers and codes in order to adopt a suitable approach. Based on field test results a new empirical correlation was suggested which can be used for similar soil where Sand Cone Method is not suitable.*

Keywords: Dynamic probing light, Sand cone method, Relative density, Cohesionless soil, Dynamic cone resistance.

1 INTRODUCTION

In Bangladesh, many construction works require well compacted sand fill to avoid foundation failure, excessive settlement and liquefaction in case of earthquake or any other vibration. To ensure the quality of compacted sand fill, relative density or density index[1]is the most appropriate index. Relative Density is defined as the state of compactness of a soil with respect to its loosest and densest states. It is also used to indicate the strength characteristics of cohesionless soil. To determine the relative density of sand fill, some of the in situ tests such as dynamic probing, sand cone method etc. have been adopted. Sand Cone Method (ASTM D 1556-90, 2006) is commonly used in Bangladesh to determine the quality of sand bed near the top surface of fill. However, Sand Cone Method cannot be applied at deeper locations or, in saturated sand to determine field density of soil [1]. To address this issue, Dynamic Probing Light (DPL) (DINEN ISO 22476-2:2012-03)can be a feasible alternative test which is used for in situ measurement of resistance of cohesionless soil. However, an appropriate relationship between relative density and dynamic cone resistance of cohesionless soil measured from DPL test should be established to utilize its benefits.
Since the resistance of cohesionless soil mainly depends on relative density, correlation between relative density and dynamic cone resistance was established and available in the literature (Alam et al., 2014; Radaszewski and Wierzbicki, 2011; EN ISO 22476, 2012). The proposed correlations are briefly presented in Table 1 which are applicable for clean sand only [1, 2, 3].

The main objective of this paper is to establish an empirical correlation between density index and penetration resistance obtained from DPL for greater amount of fines (8-17%) present in sands. Therefore, a series of tests was carried out in the field at different depth level to determine the field density of soil using Sand Cone Method. DPL test was performed then to determine the soil resistance at the adjacent location and depth level where Sand Cone Method was applied. Field test results are compared with those from empirical approaches suggested by different researchers and codes in order to adopt a suitable approach.

2 SAND COMPACTION TESTS

2.1 Sand-Cone Method (ASTM D1556)

The sand cone device consists of plastic jar with a metal cone attached at its top (Figure 1). The jar is filled with uniform dry Ottawa sand. The combined weight of the jar, the cone, and the sand filling the jar is determined. In the field, a small hole is excavated in the area where the soil has been compacted. After excavation of the hole, the cone with the sand–filled jar attached to it is inverted and placed over the hole (as shown in Figure 1). Sand is allowed to flow out of the jar to fill

[1] The terms-'Relative Density' and 'Density Index' will be used synonymously in this paper.

the hole and the cone. Then the combined weight of the jar, the cone, and the remaining sand is determined. The volume of the excavated hole is obtained from the weight of Ottawa sand filling that hole. Some soil sample is collected from the hole to measure the in situ water content which is used to determine the field dry density of soil.

Table 1: Correlation between soil resistance parameters and density index of soil

1	$D_r(\%) = 104.3312\, e^{\frac{-P_{index}\sqrt{D_{50}}}{18.1307}} - 1.4769$	Alam et.al. (2014)
2	$I_D = 0.429 \log N_{10} + 0.071$	Radaszewski and Wierzbicki (2011)
3	$I_D = 0.15 + 0.260 \log N_{10}$(above groundwater) $I_D = 0.21 + 0.23 \log N_{10}$(below groundwater)	EN ISO 22476-2:2012-03

Where,

D_r (%)= Relative Density = $\left(\frac{\gamma_d - \gamma_{min}}{\gamma_{max} - \gamma_{min}}\right).\left(\frac{\gamma_{max}}{\gamma_d}\right).100$

γ_d = Field dry density of sand deposit

γ_{max} = Maximum index density

γ_{min} = Minimum index density

I_D= Density Index = $\frac{D_r}{100}$

N_{10} =Number of blows per 10 cm of penetration

P_{index}=Penetration rate of cone in mm/blow

2.2 Dynamic Probing Light (DPL) (DINEN ISO 22476-2:2012-03)

Typical arrangement of Dynamic Probing Light is shown in Figure 2. First, the arrangement for dynamic probing light test is kept upright position with ground surface at the desired location where density index is to be determined. To drive a pointed probe (cone) attached at the tip of the extension rod (Figure 2), a hammer of mass 10 kg and a height of fall 50 cm are used. The hammer strikes on anvil which is rigidly attached to extension rods. Penetration of cone was recorded for every blow of hammer. The penetration resistance of soil is usually defined by two parameters, N_{10} and P_{index}. N_{10} is the number of blows per 10 cm of penetration of dynamic cone and P_{index} is the penetration rate of cone in mm/blow. After proper calibration, the results of dynamic probing can be used to get an indication of engineering properties, e.g. relative density, compressibility, shear strength, consistency etc. Specification of DPL used in the research is shown in Figure 2. DPL can be used up to 8m depth.

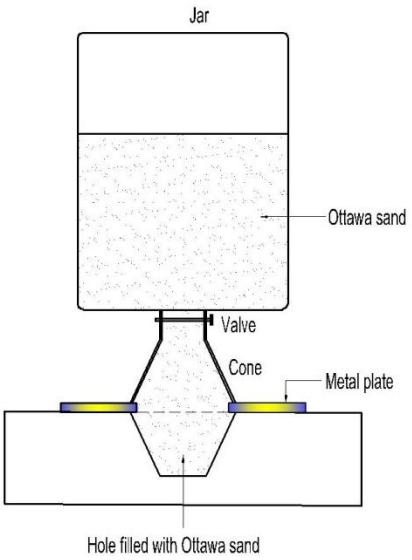

Figure 1: Field density determination using sand cone method [4]

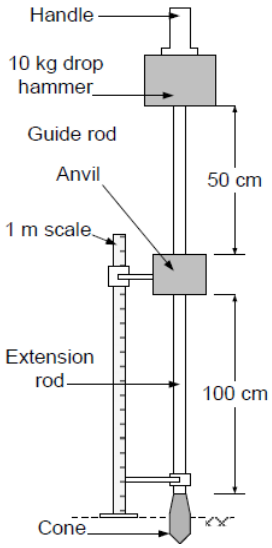

Figure 2: Schematic diagram showing arrangement for test with Dynamic Probing Light (DPL) [1]

3 MATERIAL AND METHODOLOGY

The Sand Cone Method and Dynamic Probing Light tests were done at 10 locations of the site at Gonokbari, Savar, Dhaka. The Sand Cone test and DPL test was performed at adjacent points of at least 2 feet distance apart. The depth of Sand Cone test was selected within the mid depth range of DPL test. Soil sample was collected from each of the 10 locations to perform some other necessary laboratory tests e.g., grain size analysis (ASTM D422), maximum and minimum index density (ASTM D4253 & D4254) and modified proctor test (ASTM D1557). A typical grain size distribution graph of the soil from test spot no. 9 is shown in the Figure 3. Some other index properties of the sand used in this study are summarized in Table 2. The field density obtained from Sand Cone Method was used to determine the relative density of soil at each test location. Then Penetration resistance was measured from DPL test. A typical graph of number of blows vs. cone penetration of DPL is illustrated in Figure 4 for test spot no 2, where the procedure of determining N_{10} and P_{index} is also shown. This data was used to develop a correlation between penetration resistance and relative density of soil.

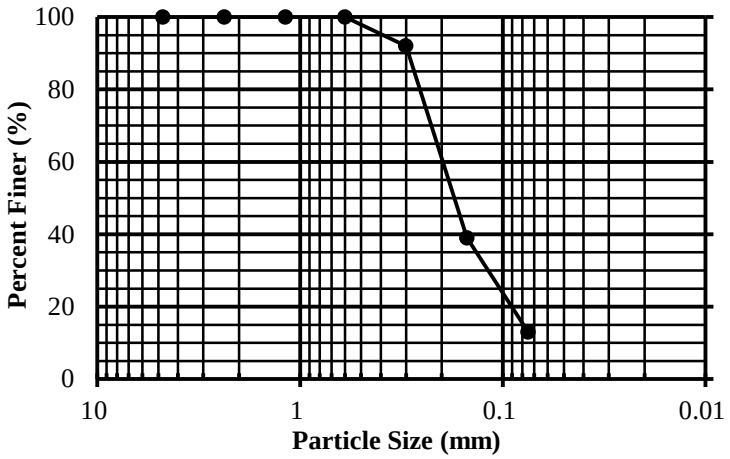

Figure 3: A typical Grain size distribution graph of sands used in the study

Table 2: Index Properties of sands used in the study

Property	**Characteristic value**
Fineness modulus	0.67-0.79
Fines,% (passing #200 sieve)	8-17%
Maximum Index density, γ_{dmax} (kN/m^3)	17.4
Minimum Index density, γ_{dmin} (kN/m^3)	11.6

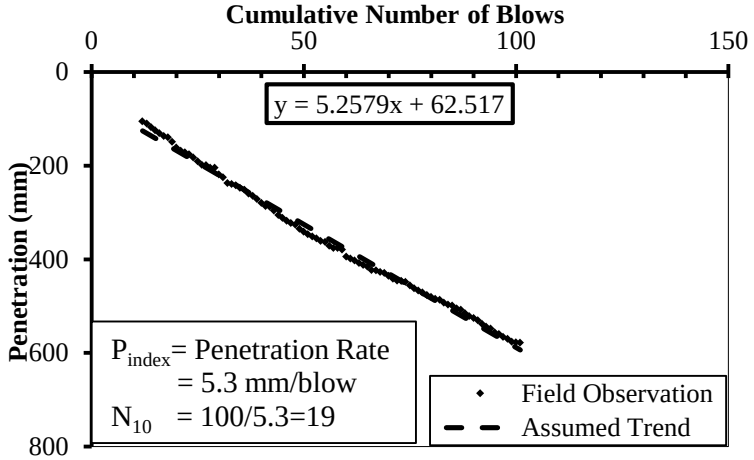

Figure 4: Typical plot of number of blows vs. cone penetration for sand used in the study.

4 RESULTS AND DISCUSSIONS

The test results obtained from Sand Cone Method and DPL tests are summarized in Table 3.Figure 5 represents the variation of density index obtained from sand cone method with logarithm of penetration resistance parameter, $N_{10.}$ Density index increases with the increase of N_{10} as expected. Based on Figure 5, the following empirical equation was proposed to predict density index when penetration resistance parameter (N_{10}) is known from DPL test.

$$I_d = 0.409 \log N_{10} + 0.203 \quad (4)$$

For comparison, density index of soil was calculated from penetration resistance parameters obtained from DPL tests using different empirical approaches (Table 1) and presented with in situ density index from Sand Cone Method in Figure 6.Density index of soil by Radaszewski and Wierzbicki's (2011)empirical equation shows close agreement with in situ test results. Whereas empirical equation of EN ISO 22476predicts lower density index than the in situ test results and equation of Alam et al. (2014) overestimates the density index.

Table 3: Summary of test results

Test Spot No	Depth of Penetration from EGL (mm)	Fines (%)	I_d* (%)	N_{10}	P_{index} mm/blow
1	0 to 544.7	13	0.80	17	6.04
2	300 to 878.4	8	0.68	19	5.26
3	450 to 1047.9	17	0.70	20	4.90
4	450 to 704.5	8	0.79	25	4.05
5	450 to 652.4	13	0.82	31	3.26
6	600 to 936.2	12	0.83	42	2.38
7	600 to 979.2	13	0.83	46	2.18
8	700 to 969.8	12	0.86	53	1.89
9	450 to 782.1	13	0.87	55	1.82
10	625 to 1000.1	17	1.09	61	1.63

* Obtained from Sand Cone Method

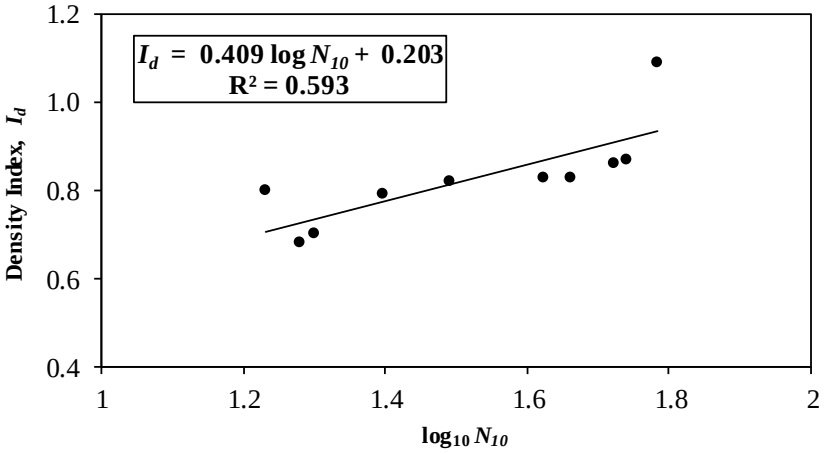

Figure 5: Variation of density index with logarithm of N_{10}

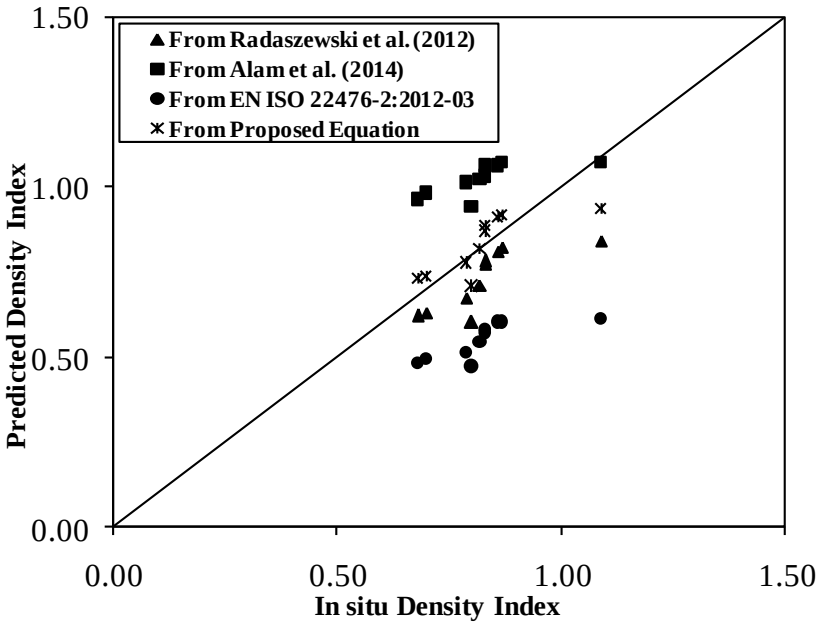

Figure 6: Comparison of density index from different empirical approaches and from sand cone method

5 CONCLUSIONS

Based on field test results, the following conclusions are made:

i. An empirical equation is proposed between Density Index and penetration resistance parameter $N_{10}$from DPL test, which is applicable for sand with greater fine contents (8-17%).
ii. The authors found that Radaszewski and Wierzbicki's (2011) empirical equation showed close agreement with the test results.
iii. Resistance of sand increases with density index.

ACKNOWLEDGEMENTS

The writers would like to thank Professor Dr. Md. Jahangir Alam (BUET) for his useful comments and suggestions.

REFERENCES

[1] O.C. Zienkiewicz, R.C. Taylor, 1989. *The finite element method, Vol. I, 4th Edition*. McGraw Hill, p198.

[2] J.T. Oden, T. Belytschko, I. Babuska, T.J.R. Hughes, 2003. Research directions in computational mechanics. *Computer Methods in Applied Mechanics and Engineering*, **192 (4)**, pp 913-922.

[3] J.H. Argyris, M. Papadrakakis, L. Karapitta, 2000. Elastoplastic analysis of shells with the triangular element TRIC. M. Papadrakakis, A. Samartin, E. Oñate eds. *4th International Colloquium on Computation of Shell and Spatial Structures (IASS-IACM 2000),* Chania, Crete, Greece, June 4-7, pp 110-118.

[4] M.J. Alam, M.S. Hossain, A.K. Azad, 2014. Development of correlation between dynamic cone resistance and relative density of sand. *Journal of Civil Engineering (IEB),* **42 (1),** pp. 63-76.

[5] R. Radaszewski, J. Wierzbicki, 2011. On the applicability of in situ soil probings to geological analyses. *Geologos,***17(1)**, pp. 5-16.

[6] DIN EN ISO 22476-2:2012-03. *Geotechnical Investigation and Testing – Field Testing–Part 2:* Dynamic Probing. DIN Deutsches Institute for Normung e. V., Berlin, BeuthBerlagGmbh, 10722 Berlin, Germany.

[7] B.M. Das, 2014. *Principles of Geotechnical Engineering, Eighth Edition,* PWS, pp. 173-174.

[8] ASTM D1556. *Standard Test Method for Density and Unit Weight of Soil in Place by Sand-Cone Method.*

CICM 2015
First International Conference on
Advances in Civil Infrastructures and Construction Materials
MIST, Dhaka, Bangladesh, 14-15 December 2015

SEISMIC SLOPE STABILITY ANALYSIS OF HOMOGENOUS CLAY SOIL

Md. S. SAKIB[1] and Md. K. Islam[2]

[1, 2] Department of Civil Engineering, Bangladesh University of Engineering and Technology, Dhaka, Bangladesh
Email: 1sakib.saadman@gmail.com and [2]raja4bd@gmail.com

Abstract. *An extensive numerical analysis is carried out on the slope stability of earthen embankments subjected to different seismic loading using the computer program XSTABL. The program calculates the factor of safety by simplified Bishop's method, based on two dimensional limiting equilibrium analyses. The embankment cross section is assumed to be homogenous and isotropic, which is a quite common practice in our country. The height of the slope of the embankment is considered 4m, 8m and 12m with a slope angle of 15°, 30°, 45° and 60°. Constant water table has been at height of crest, mid height and at toe. The un-drained shear strength parameter c has been considered 5kPa to 30kPa with 5kPa interval. Pseudo-static limiting equilibrium analysis is performed to study the effect of ground motion generated by earthquakes on the embankments. The cases of 0.15g and 0.25g peak ground acceleration are considered. Finally, a relation has been established between the stability of slope height, slope angle, cohesion intercept and seismic coefficients. These relations can be used to establish design charts for future embankment construction.*

Keywords: Homogeneous clay, Un-drained shear strength, Bishop's method, seismic loading, Pseudo-static analysis

1 INTRODUCTION

Bangladesh is situated in a high seismic region. Several earthquake heavy magnitudes have visited Bangladesh in recent past with epicenters within Bangladesh or close to Indo-Bangladesh border. Most of these earthquake occurred in the month of June to August, which is time of monsoon. As a result, earthquake may cause significant failures and movement of natural slopes, embankments and earth dames with high water table and can cause flood.

In Bangladesh, mostly available soils are clay in nature with high plasticity. So, it is hoped that, this simple analysis of seismic slope stability by homogenous clay soil might be helpful for rapid assessment of slope stability for flood control embankments in Bangladesh.

2 INPUT DATA

This section is divided into the following parts:

2.1 Embankment Geometry

The height of the embankment is detected by maximum flood level and wave height. Height considered here are 4m, 8m and 12m. A minimum freeboard of 0.6m is desired in Bangladesh condition[1], but in this study, extreme cases have been considered (e.g. water table at toe, at mid point and at crest). Considering the possible critical embankment slopes in Bangladesh, slope angles are taken as 15°, 30°, 45° and 60°.

2.2 Soil Parameters

The embankment is assumed to be homogenous, isotropic and without any drainage filters. As the embankment material is cohesive, only values of shear strength parameter c (cohesion intercept) are considered and they are 5kPa to 30kPa with a 5kPa interval. The moist and saturated unit weights of soil are taken as 18kN/m³ and 20kN/m³ respectively.

2.3 Seismic Cases Considered

According to the seismic zoning map of Bangladesh[2], it has been found that zone 2 and zone 3 have peak ground acceleration of 0.15g and 0.25g respectively. So, the horizontal coefficients have been considered 0, 0.15 and 0.25. As the vertical coefficient has been less significant on the factor of safety [3]since it reduces both the driving force and resisting force.

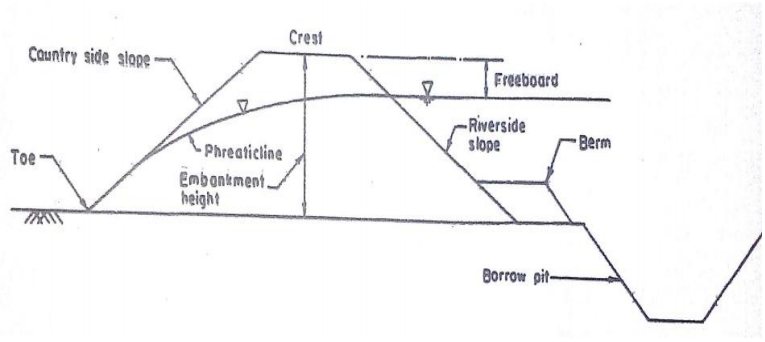

Figure 1: Schematic diagram of earthen embankment

3 METHODOLOGY

The two dimensional limiting equilibrium slope stability program XSTABL was used to conduct the numerical study. Soil parameters are provided in the soil parameter section. Each type of soil is described by moist unit weight, saturated unit weight, Mohr-Coulomb cohesion intercept and water surface index. The water table was chosen in the water surface index. The co-ordinates of water table were provided in the software.

The circular surface search was chosen for Bishop's simplified method[4]of stability analysis. 20 failure surfaces were generated from 10 initiation point for each section analysis. The range of initiation and termination point was also provided.

The use of coefficients allowed for a Pseudo-static representation [5]of earthquake effects within the limiting equilibrium model. Specified horizontal coefficients were used to scale the horizontal components of earthquake force relative to the weight of sliding mass.

4 RESULT

The following section shows the result of the analysis in tabular form:

Table 1: Factor of safety for K_h=0 condition (for slope angle 60° and 45°)

C	Factor of Safety																	
	Slope angle	.577H:1V(tan60°)									1H:1V(tan45°)								
	Height	H=4m			H=8m			H=12m			H=4m			H=8m			H=12m		
	Free Board	4m	2m	0m	8m	4m	0m	12m	6m	0m	4m	2m	0m	8m	4m	0m	12m	6m	0m
5		0.734	0.777	1.016	0.561	0.59	0.723	0.405	0.43	0.546	0.901	0.934	1.233	0.647	0.662	0.833	0.548	0.565	0.694
10		1.124	1.215	1.685	0.769	0.796	1.036	0.591	0.617	0.786	1.337	1.456	2.011	0.887	0.945	1.245	0.731	0.761	0.976
15		1.508	1.665	2.356	0.947	1.004	1.352	0.722	0.762	1.006	1.777	1.981	2.796	1.12	1.229	1.662	0.89	0.959	1.261
20		1.894	2.095	3.023	1.126	1.212	1.671	0.846	0.907	1.227	2.221	2.509	3.585	1.355	1.496	2.048	1.051	1.157	1.547
25		2.28	2.536	3.661	1.307	1.422	1.991	0.971	1.053	1.45	2.666	3.039	4.377	1.591	1.724	2.408	1.213	1.32	1.785
30		2.666	2.977	4.301	1.488	1.632	2.312	1.097	1.198	1.673	3.113	3.57	5.116	1.817	1.973	2.769	1.375	1.48	2.025

Table 2: Factor of safety for K_h=0 condition (for slope angle 30° and 15°)

C	Factor of Safety																	
	Slope angle	1.732H:1V(tan30°)									3.73H:1V(tan15°)								
	Height	H=4m			H=8m			H=12m			H=4m			H=8m			H=12m		
	Free Board	4m	2m	0m	8m	4m	0m	12m	6m	0m	4m	2m	0m	8m	4m	0m	12m	6m	0m
5		1.152	1.173	1.552	0.873	0.915	1.157	0.761	0.768	0.949	1.67	1.88	2.452	1.339	1.347	1.728	1.216	1.217	1.524
10		1.643	1.76	2.422	1.121	1.217	1.584	0.988	1.018	1.298	2.145	2.463	3.281	1.632	1.725	2.279	1.418	1.481	1.934
15		2.135	2.329	3.274	1.371	1.509	2.002	1.151	1.22	1.585	2.616	3.032	4.111	1.893	2.052	2.745	1.613	1.722	2.275
20		2.579	2.857	4.07	1.622	1.8	2.422	1.313	1.421	1.873	3.087	3.601	4.941	2.144	2.376	3.211	1.795	1.944	2.595
25		2.994	3.386	4.842	1.874	2.085	2.83	1.476	1.614	2.161	3.557	4.17	5.766	2.383	2.699	3.671	1.964	2.159	2.899
30		3.408	3.916	5.575	2.123	2.361	3.228	1.639	1.799	2.438	4.027	4.739	6.552	2.621	3.023	4.091	2.127	2.375	3.199

Table 3: Factor of safety for K_h=0.15 condition (for slope angle 60° and 45°)

C	Factor of Safety																	
	Slope angle	.577H:1V(tan60°)									1H:1V(tan45°)								
	Height	H=4m			H=8m			H=12m			H=4m			H=8m			H=12m		
	Free Board	4m	2m	0m	8m	4m	0m	12m	6m	0m	4m	2m	0m	8m	4m	0m	12m	6m	0m
5		0.602	0.608	0.708	0.446	0.457	0.498	0.39	0.515	0.662	0.733	0.721	0.857	0.538	0.552	0.623	0.432	0.423	0.464
10		0.926	0.968	1.16	0.63	0.626	0.729	0.555	0.773	1.051	1.099	1.137	1.161	0.786	0.782	0.845	0.602	0.592	0.692
15		1.251	1.302	1.347	0.781	0.797	0.964	0.722	1.036	1.363	1.269	1.302	1.348	0.953	0.967	1.069	0.738	0.753	0.89
20		1.406	1.451	1.51	0.934	0.968	1.201	0.891	1.277	1.531	1.406	1.451	1.512	1.121	1.141	1.254	0.876	0.889	1.04
25		1.541	1.595	1.665	1.087	1.141	1.38	1.06	1.418	1.698	1.542	1.596	1.667	1.241	1.293	1.389	1.014	1.014	1.176
30		1.677	1.738	1.819	1.241	1.314	1.515	1.23	1.551	1.864	1.677	1.74	1.822	1.347	1.413	1.524	1.125	1.139	1.298

Table 4: Factor of safety for K_h=0.15 condition (for slope angle 30° and 15°)

C	Factor of Safety																	
	Slope angle	1.732H:1V(tan30°)									3.73H:1V(tan15°)							
	Height	H=4m			H=8m			H=12m			H=4m			H=8m			H=12m	
	Free Board	4m	2m	0m	8m	4m	0m	12m	6m	0m	4m	2m	0m	8m	4m	0m	12m	6m	0m
5		0.856	0.811	0.928	0.658	0.63	0.691	0.576	0.53	0.581	0.925	0.92	0.958	0.777	0.73	0.765	0.712	0.656	0.682
10		1.116	1.134	1.167	0.846	0.838	0.917	0.717	0.695	0.757	1.117	1.138	1.178	0.925	0.915	0.96	0.826	0.798	0.854
15		1.268	1.298	1.344	1.007	1.022	1.106	0.84	0.822	0.912	1.274	1.306	1.358	1.047	1.057	1.117	0.933	0.922	0.998
20		1.407	1.453	1.516	1.137	1.177	1.262	0.952	0.949	1.063	1.418	1.467	1.531	1.166	1.187	1.267	1.03	1.04	1.141
25		1.543	1.598	1.671	1.249	1.305	1.407	1.054	1.076	1.207	1.557	1.615	1.689	1.269	1.305	1.4	1.126	1.154	1.269
30		1.68	1.743	1.827	1.358	1.428	1.546	1.147	1.193	1.34	1.696	1.763	1.847	1.371	1.421	1.529	1.221	1.268	1.392

Table 5: Factor of safety for K_h=0.25 condition (for slope angle 60° and 45°)

C	Factor of Safety																	
	Slope angle	.577H:1V(tan60°)									1H:1V(tan45°)							
	Height	H=4m			H=8m			H=12m			H=4m			H=8m			H=12m	
	Free Board	4m	2m	0m	8m	4m	0m	12m	6m	0m	4m	2m	0m	8m	4m	0m	12m	6m	0m
5		0.53	0.528	0.577	0.368	0.389	0.389	0.3	0.297	0.312	0.649	0.621	0.625	0.473	0.473	0.466	0.374	0.355	0.366
10		0.775	0.77	0.761	0.559	0.543	0.599	0.435	0.42	0.454	0.774	0.769	0.762	0.67	0.64	0.638	0.527	0.509	0.549
15		0.873	0.879	0.885	0.695	0.695	0.764	0.532	0.529	0.597	0.873	0.879	0.886	0.762	0.763	0.768	0.659	0.653	0.66
20		0.966	0.976	0.989	0.834	0.848	0.863	0.63	0.638	0.74	0.966	0.976	0.99	0.843	0.852	0.874	0.747	0.752	0.772
25		1.059	1.072	1.09	0.919	0.936	0.961	0.728	0.748	0.86	1.059	1.072	1.091	0.92	0.939	0.968	0.819	0.829	0.868
30		1.152	1.168	1.191	0.995	1.017	1.054	0.827	0.858	0.949	1.152	1.169	1.192	0.997	1.021	1.06	0.89	0.907	0.955

Table 6: Factor of safety for K_h=0.25 condition (for slope angle 30° and 15°)

C	Factor of Safety																	
	Slope angle	1.732H:1V(tan30°)									3.73H:1V(tan15°)							
	Height	H=4m			H=8m			H=12m			H=4m			H=8m			H=12m	
	Free Board	4m	2m	0m	8m	4m	0m	12m	6m	0m	4m	2m	0m	8m	4m	0m	12m	6m	0m
5		0.652	0.64	0.627	0.543	0.512	0.518	0.485	0.431	0.434	0.651	0.641	0.632	0.585	0.547	0.539	0.547	0.494	0.49
10		0.77	0.766	0.767	0.672	0.664	0.661	0.598	0.56	0.564	0.769	0.767	0.773	0.686	0.663	0.666	0.631	0.6	0.615
15		0.872	0.876	0.882	0.763	0.766	0.782	0.682	0.663	0.678	0.875	0.88	0.891	0.777	0.76	0.772	0.713	0.694	0.72
20		0.966	0.976	0.992	0.846	0.856	0.883	0.761	0.758	0.791	0.969	0.981	1	0.858	0.853	0.876	0.792	0.785	0.819
25		1.059	1.073	1.093	0.926	0.945	0.98	0.835	0.845	0.895	1.064	1.08	1.102	0.934	0.936	0.968	0.864	0.866	0.908
30		1.152	1.17	1.195	1.004	1.03	1.072	0.909	0.932	0.989	1.159	1.178	1.205	1.009	1.017	1.054	0.934	0.946	0.997

Some sample graphs are plotted from the above data:

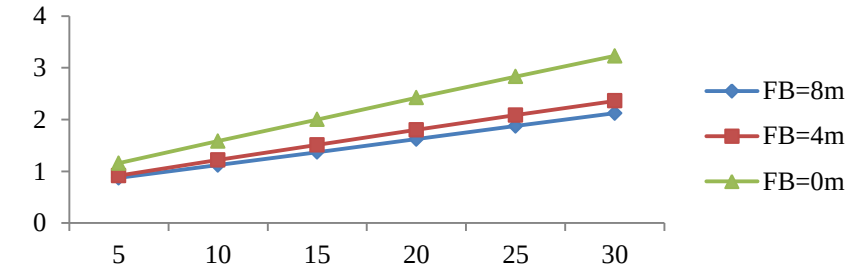

Figure 2: Factor of safety vs cohesion of clay (K_h=0, slop angle 30°, slope height 8m)

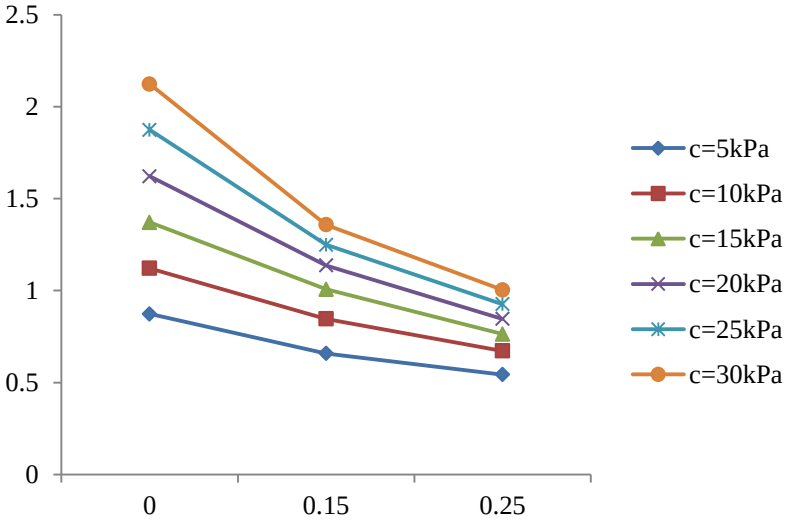

Figure 3: Factor of safety vs earthquake coefficient K_h (slope angle 30°, slope height 8m, Freeboard 8m)

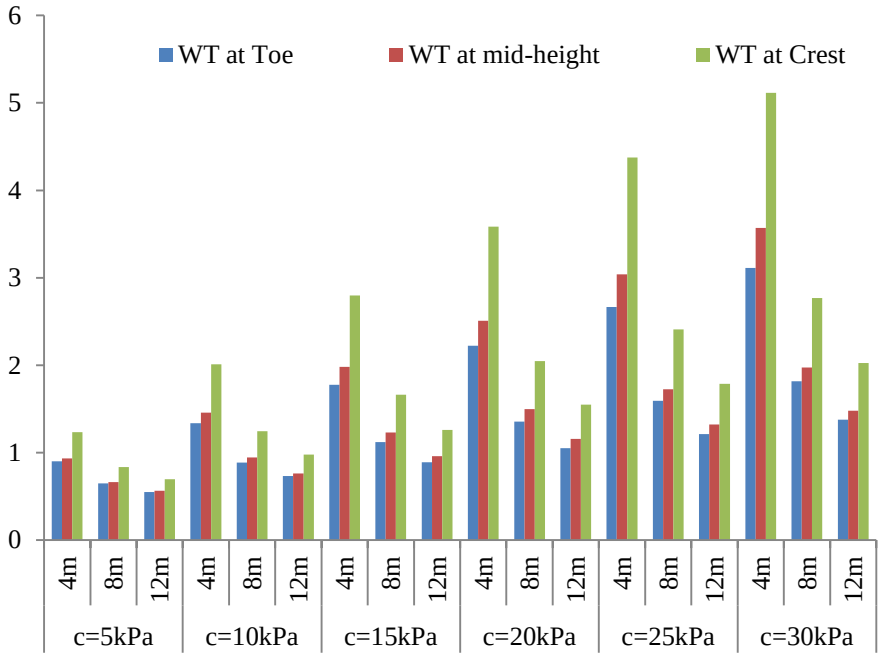

Figure 4: Factor of Safety vs slope Height (K_h=0, slope angle= 45°)

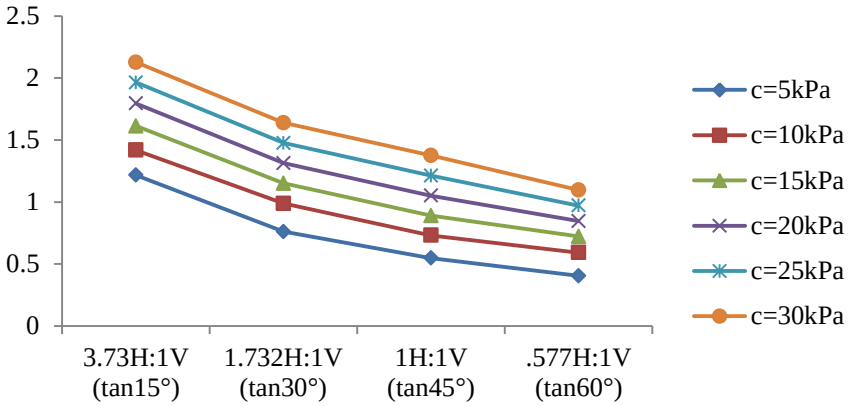

Figure 5: Factor of safety vs slope angle (K_h=0.00, H=12m, Freeboard=12m)

5 DISCUSSIONS

5.1 Effect of Soil Parameters

In this analysis, only the cohesion parameter has been changed frequently but the moist and saturated unit weight remained constant in all analysis. From Figure 1, it is found that, the factor of safety increases with the increment of cohesion. But with the increase of value of earthquake coefficient (e.g. k_h =0.15 or 0.25), the factor of safety does not change significantly with the change of freeboard for the same cohesive soil.

5.2 Effect of Horizontal Earthquake Coefficients

As the numerical study was conducted on three seismic conditions (e.g. K_h=0, 0.15 and 0.25), the results has been plotted against the K_h value in Figure 2. It is found that the factor of safety reduces with the increment of K_h value.

5.3 Effect of Slope angle

Figure 3 shows the change of factor of safety against the change of slope angle. In all cases of no earthquake condition and in most cases of earthquake loading, the factor of safety decreases with the increase of slope angle. This is because the increase in slope angle, α increases the driving force, hence reduces the factor of safety. But in cases of high seismic coefficients, the factor of safety does not fluctuate much with the change of slope angle.

5.4 Effect of Slope Height

The effect of slope height on stability of the embankment has been shown in Figure 4. It is found that the factor of safety is reducing with the increase of slope height. The steep height of slope increases the length of the failure surface resulting in increase of resisting force. But the weight of the sliding block also increases which increases the driving force. Ultimately, the factor of safety reduces with height.

6 CONCLUSSIONS

The main conclusions of this study may be summarized as follows:

- The factor of safety reduces with the slope height. So, too high slope construction should be prohibited.
- If all parameters remain same, the factor of safety reduces 2 to 3 times for high embankments during earthquakes.
- In many cases, it has been found that the stability reduces in an incredible manner in flatten slopes during earthquakes. So, adequate

control should be undertaken also in construction of a flatten embankment.

- In this study, the stability of embankment increased with the rise of water table. Though in practical cases, this phenomenon never occurs. This is because the un-drained shear strength of clay soil was considered.

REFERENCES

[1] Islam, M.Z., 1991. Failure of flood embankments: Case studies of some selected projects in Bangladesh, Final Report, BUET, p27

[2] Ali, M.H., Choudhury J.R., 1994. *Seismic zoning of Bangladesh*, paper presented at the international seminar on recent developments in earthquake disaster mitigation, IEB, Dhaka, p33

[3] Kramer, S.L. 1996. *Geotechnical earthquake engineering, 1st edition*, Pearson publications, p436-437

[4] Bishop, A.W., 1955. The use of the slip circle in the stability of slopes, vol.-1,p7-17

[5] Kramer, S.L. 1996. *Geotechnical earthquake engineering, 1st edition*, Pearson publications p434-437

CICM 2015
First International Conference on
Advances in Civil Infrastructure and Construction Materials
MIST, Dhaka, Bangladesh, 14–15 December 2015

DETERMINATION OF LIQUID AND PLASTIC LIMIT OF SOIL USING ELECTRICAL RESISTIVITY

O. F. MURAD[1], **Z. Chik**[2], **K. A. M. Nayan**[3] **and S. M. Mitu**[4]

[1, 2, 3] Universiti Kebangsaan Malaysia, Malaysia.
Email: [1]murad5353@yahoo.com, [2]irzamri@gmail.com, [3]kamn56@gmail.com

[4] Housing and Building Research Institute, Dhaka, Bangladesh
Email: sadiamitu89@gmail.com

Abstract. *Conventional methods for determining the moisture content, liquid limit and plastic limit of soil are tedious, time consuming and expensive in nature. But these properties have vital effects on the foundation of any type of structure. Among all geophysical methods, soil electrical resistivity measurement is one of the convenient one. In this study samples were collected from four locations at Universiti Kebangsaan Malaysia (UKM) to conduct sieve analysis, liquid and plastic limit test using Cone penetration and Rolling Thread test. Soil electric resistivity has non-linear inversely proportional relationship with water content. From the transition point of steep and gentle gradient plastic limits and from the transition point of gentle gradient and saturation line, liquid limits of soil are determined. Predicted liquid limits and plastic limits of soil were compared with the values obtained from conventional tests. The difference between the liquid limit and plastic limit predicted from the resistivity method were found to be 3.30% - 15.53% and 6.47% - 17.97% in comparison to the conventional method [1].*

Keywords: Soil electrical resistivity, Percentages of water, Liquid limit, Plastic limit.

1 INTRODUCTION

Soil investigation is very important for the construction of foundations for any structure. During the preparation of soil for any type of foundation, a certain level of compaction is required. On the other hand liquid and plastic limit test is one of the most commonly used tests of soil. As so many mechanical properties such as cohesion, penetration resistance etc are involved with the consistency limit of soil, these are very important content of soil investigation report [2]. The conventional methods for measuring the liquid limit and plastic limit of soil are expensive, time consuming and tedious in nature [3]. For reducing these types of obstacles, geophysical methods can be better alternatives. But these methods are not properly established yet. Among all geophysical methods electrical resistivity is a fast, overall cheap and comparatively less time consuming method. Also it is an effective tool for acquiring subsurface properties without soil disturbance.

2 BACKGROUND OF THE STUDY

Abu-Hassanein and Benson studied liquid limit and plasticity index of soil. It was shown that, fine soil with high liquid limit has lower electrical resistivity. Also some exceptions were found when higher percentages of coarse-size particles were involved in the analysis [4].

In 2012, a new technique was developed by Chik and Islam for the determination of plastic limit of soil from the correlation between soil resistivity and moisture content of soil [5]. Almost similar results were observed between the plastic limit values of conventional method and proposed technique. After one year, similar type of study was conducted by Osman, Siddiqui and Behan. In that study silty sand and poured sand was considered for both laboratory and field test [6]. Recently a study was performed by Abu zeid, Hassan and Abu Bakr, where soil samples were mixed with various ratios of Bentonite. Then the plastic limit and electrical resistivity of the soil samples was measured to study about the relationships between soil resistivity and plastic limit of soil mixed with various ratios of Bentonite.

3 METHODOLOGY

The soil sample for laboratory tests was collected from a four different locations of University Kebangsaan Malaysia (UKM), Malaysia. The gradation of these soil samples was illustrated as grain size distribution graph (Figure 1).

According to BS 1377, soil sample was sieved through 425 μm (No. 40) to obtained 250 gm of soil to produce homogeneous soil paste in a porcelain bowl. Soil paste was poured into the cup using a spatula. The excess amount of soil was striked off to make a smooth flat surface level with the rim of the cup. After that the cup was placed centrally under the cone as shown in the **Error! Reference source not found.**.

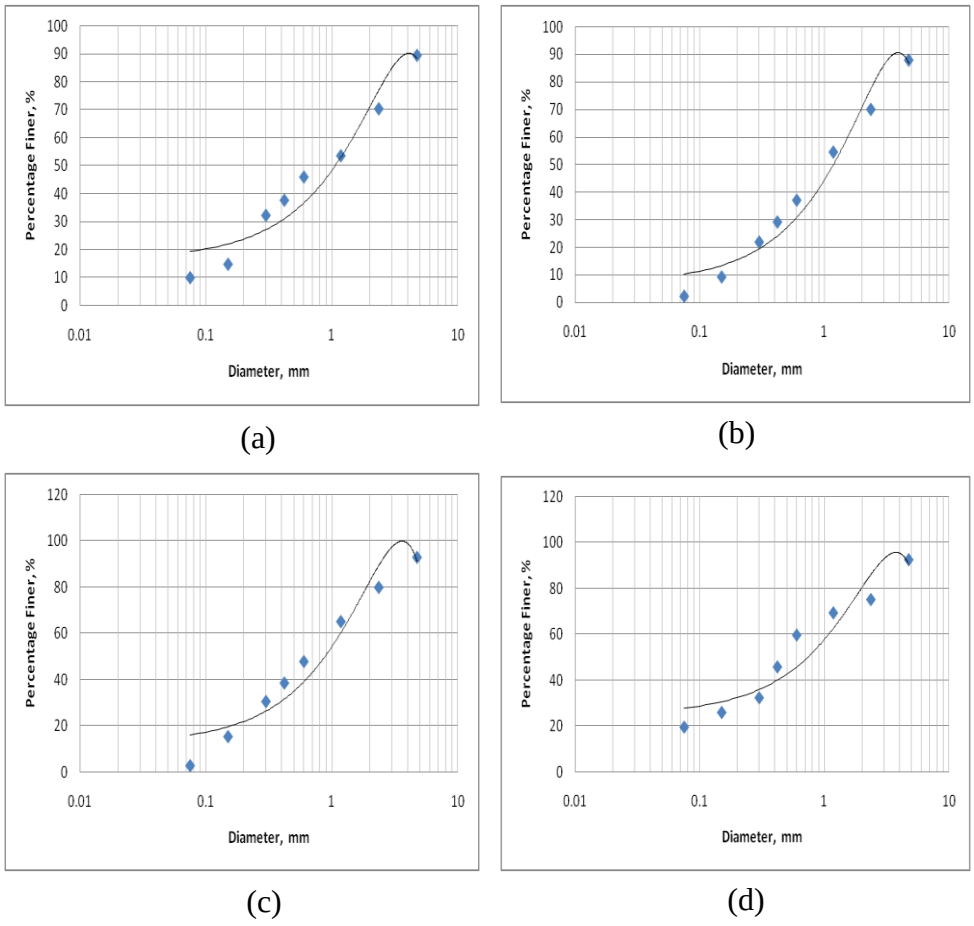

Figure 1: Sieve analysis of different type and gradation of soil

The penetration of the cone penetrometer was measured and recorded from the dial gauge. The soil paste was extracted from the cup and poured into a circular plastic box of 9 cm in radius was used for measuring soil electric resistance using four probe FLUKE 8846A precision multi-meter as shown in the **Error! Reference source not found.**.

During the measurement of soil electrical resistivity, the distance between the probes was 1 cm from each other. Total procedures were repeated for the soil sample mixed with increasing amount of water. Water was added with soil samples in such a way that the range of penetration values remain between 16 mm and 26 mm.

Figure 2: Measurement of soil liquid limit using cone penetrometer

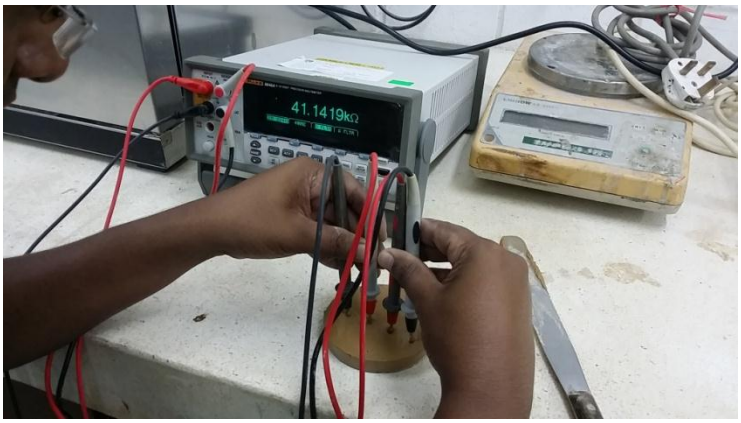

Figure 3: Measurement of soil electrical resistance in circular plastic box

For determination of plastic limit of soil 20gm soil passed through No. 40 (425 µm) sieve. Water was mixed with soil sample in the porcelain bowl. About 8 gm was taken in the glass plate for rolling. Then the mass of soil was rolled with a sufficient pressure to form threads of uniform diameter. The rolling rate of soil mass was approximately 80-90 strokes per minute. Rolling was continued until

the diameter of the thread reaches 3.2 ± 0.5 mm. Sometimes thread breaks into shorter segments before reaching 3.2 mm diameter.

Finally the crumbled threads of soil were kept in a container and covered with plastic to preserve the moisture. This procedure was continued until 10 gm of soil sample was accumulated. Then soil sample was weighted and inserted into the oven for drying.

The rest of the dry soil sample (sieved through 425 µm or No. 40 sieve) was mixed with the exact water content of corresponding to plastic limit. Then it was poured in the similar sized circular plastic box that was used in liquid limit test. Finally four probe FLUKE 8846A precision multi-meter was used to measure soil resistivity. The distance between the probes was 1 cm from each other. For measuring precise resistivity value, an average of 5 trials was considered.

4 RESULT AND DISCUSSION

From the graphs of electrical resistivity vs. moisture content of soil (Figure 4) it can be observed that, soil resistivity decreases rapidly with increasing moisture content of soil. In this stage, soil particles get saturated by moisture content. So the conductivity of soil increases dramatically with the increase of small amount of moisture content.

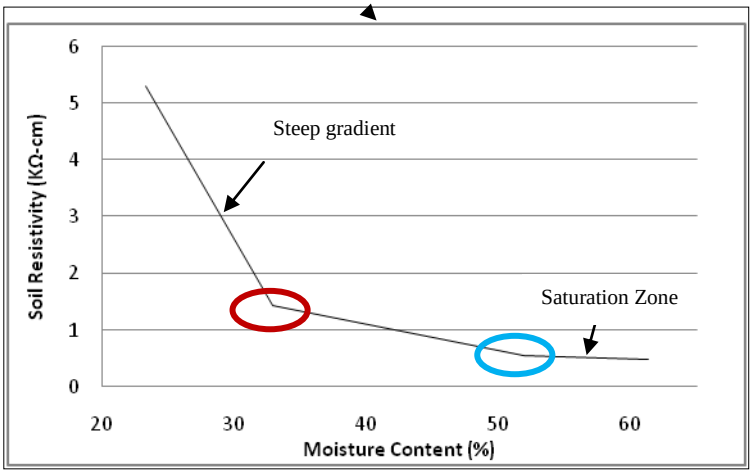

Figure **Error! No text of specified style in document.**: Common trend line of the graph of moisture content vs. soil electrical resistivity to predict liquid and plastic limit of soil

After a certain level of water contents, the soil resistivity decreases gently with increasing of water contents in soil sample. The moisture content at transition point of steep and gentle gradient can be considered as plastic limit of soil. At final stage, the soil resistivity almost achieves the state of saturation. In this

stage soil resistivity does not change considerable amount with the change of moisture content. The moisture content at transition point from gentle slope to saturation state indicates liquid limit of soil.

The predicted liquid limits and plastic limits of all four samples are shown in graphs (Figure 5) between soil resistivity and moisture content.

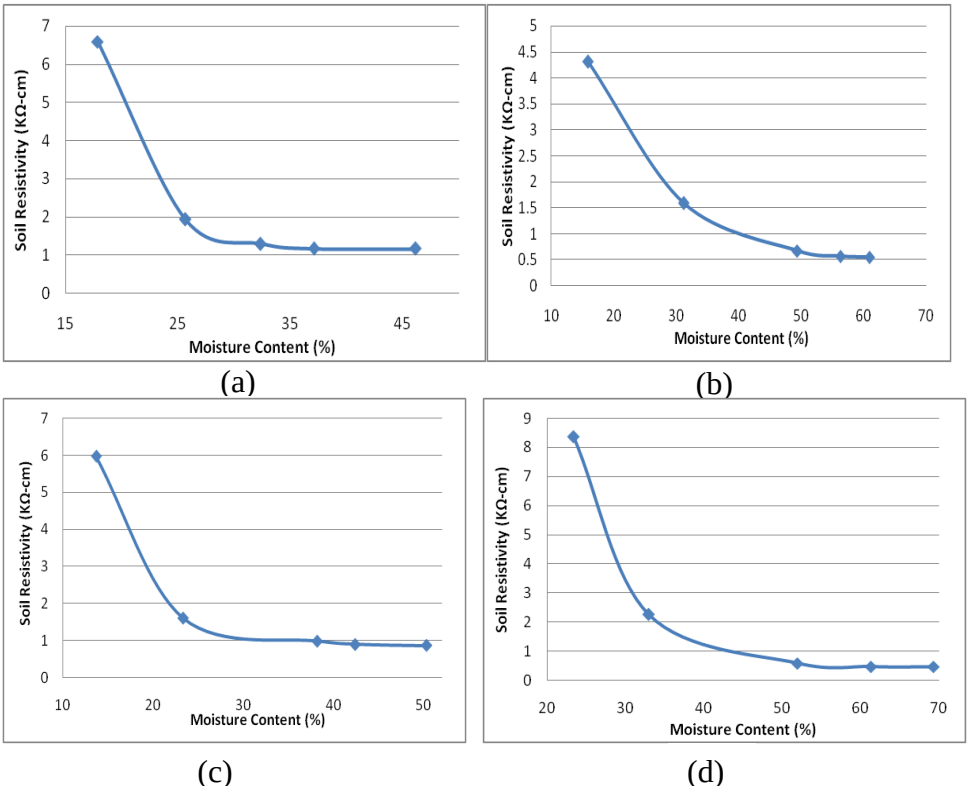

Figure 5: Graph of soil electrical resistivity vs. moisture content of soil for predicting liquid and plastic limit of soil

It was observed that liquid limits and plastic limits of soil, obtained from conventional tests and the relationship between soil resistivity and moisture content are quiet similar with each other. Both predicted liquid and plastic limits are higher than the liquid and plastic limits of soil obtained from the conventional tests. Maximum errors of liquid and plastic limits between the predicted and actual values are 15.53 % and 17.97 % respectively.

Table 1: Liquid limit and plastic limit of soil from laboratory test and resistivity vs. moisture content graphs

Sample	Actual (from laboratory tests)		Predicted (from the graphs between soil resistivity and moisture content)		Percentage error between actual and predicted value	
	Liquid Limit (%)	Plastic Limit (%)	Liquid Limit (%)	Plastic Limit (%)	Liquid Limit (%)	Plastic Limit (%)
Well graded sand	38.1	25.2	41.9	27.9	9.97	10.71
Poorly graded sand	36.4	21.7	37.6	25.6	3.30	17.97
Well graded gravel with sand	33.8	20.1	35.0	21.4	3.55	6.47
Poorly graded gravel with silt	43.8	28.2	50.6	31.3	15.53	10.99

5 CONCLUSION

Among all other geophysical methods, electrical resistivity measurement is more convenient. Because less mechanical works involve in this method. From the trend of soil electrical resistivity vs. moisture content graph liquid limit and plastic limit is calculated and compared with the laboratory test results. Minimum 3.30% and maximum 17.97% error is found between the predicted liquid and plastic limits from the trend of soil electrical resistivity vs. moisture content graph and measured values in the laboratory. Sometime it is difficult to obtain the accurate soil electrical resistance because of the contact issues between soil particles and electrical probes. For this reason higher percentage of error in predicted and measured values was obtained.

ACKNOWLEDGEMENTS

The authors wish to thank all the laboratory assistants of Geotechnical Engineering laboratory (UKM). This work was supported in part by a grant from ERGS/1/2012/TK03/UKM/01/3 and GUP- 2012-031.

REFERENCES

[1] S. Xuezheng, Y. Dengsheng, X. Tingyan, and J. Breburda, "Ssoil erodibility factor K as studied using field plots in subtropical China," *ACTA Pedol. Sin.*, pp. 399–404, 1997.

[2] A. Sridharan, A. S. Rao, and P. V Sivapullaiah, "Swelling Pressure of Clays," *ASTM Geotech. Test. J.*, vol. 1986, no. 9, pp. 24–33, 1986.

[3] F. I. Siddiqui and S. Osman, "Integrating Geo-Electrical and Geotechnical Data for Soil Characterization," *Int. J. Appl. Phys. Math.*, vol. 2, no. 2, pp. 104–106, 2012.

[4] Z. S. Abu-Hassanein, C. H. Benson, and L. R. Blotz, "Electrical resistivity of compacted clays," *J. Geotech. Eng.*, vol. 122, no. 5, pp. 397–406, 1996.

[5] Z. Chik, S. M. T. Islam, H. Sanusi, and M. M. Mustafa, "Expert Idea on Liquid Limit and Plastic Limit Estimation with Soil Resistivity Profile," *Online J. Sci. Technol.*, vol. 2, no. 4, 2012.

[6] S. B. S. Osman, F. I. Siddiqui, and M. Y. Behan, "Relationship of Plasticity Index of Soil with Laboratory and Field Electrical Resistivity Values," *Appl. Mech. Mater.*, vol. 353, pp. 719–724, 2013.

CICM 2015
First International Conference on
Advances in Civil Infrastructure and Construction Materials
MIST, Dhaka, Bangladesh, 14–15 December 2015

PERFORMANCE ANALYSIS OF DRIVEN AND BORED RCC PILES IN RECLAIMED LAND OF DHAKA CITY: A CASE STUDY

Mohiuddin AHMED[1], S. B. Anwar[2], M. I. Chowdhury[3] and S.T. Tabassum[4]

[1, 2, 3, 4] Department of Civil Engineering, Military Institute of Science and Technology
Dhaka, Bangladesh
E-mail: [1]mohi971@yahoo.com, [2]sumaiyaanika91@gmail.com,
[3]mazed_6638@yahoo.com and [4]tahsin1234.tt@gmai.com

Abstract. *This study endeavors to highlight the performance of both bored and driven RCC pile in a reclaimed land of Dhaka city having weak soil of soft to medium consistency (SPT 2 to 11). The study site was selected in Mirpur Defense Officers' Housing Scheme (M DOHS); plot no: 833; where bored pile was adopted. Capacity calculations of bored and driven pile by various methods have shown that driven pile achieves greater strength at comparatively shorter length with lesser geometric configuration than that of bored pile. The reduction in time (80%), labor and materials (40%) provide substantial cost savings (30%-40%). Users' unawareness regarding this fact leads to the traditional adoption of bored RCC pile which is not always rational in terms of strength, economy and time as well. The finding of this study thus reveals an economic solution to the general foundation system of this area. The study is primarily based on static analysis for simplification. The result can safely be utilized in the soils identical to selected site and help economizing foundation design to a greater extent.*

Keywords: Bored Piles, Driven Piles, Reclaimed Land, M DOHS, SPT

1 INTRODUCTION

Dhaka city is gradually expanding on reclaimed sites due to rapid urbanization and scarcity of original land areas. Almost all reclaimed lands of the city are underlined by dredged fill of silty sand which is vulnerable to long term consolidation[1]. Soils of reclaimed sites are basically soft to medium consistency in nature and necessitate deep foundation. In Dhaka city bored pile is a commonly adopted deep foundation system. The choice of driven pile as deep foundation system is seldom noticed in construction practices. Traditionally used bored pile has a number of limitations that leaves very narrow scope to the users and designers to optimize the cost vis-à-vis maintaining standard safety and quality.

On the other hand, driven piles, in particular, have been a preferred foundation system because of their relative ease of installation, low cost and a better control of quality (QC) performance. They are easily adaptable to variable site conditions thus eliminates uncertainty due to site variability mainly in reclaimed lands.

For reclaimed land of Dhaka city such as Mirpur DOHS no significant performance study between bored and driven pile has been reported in the recent past. Ahmed et. al [2] studied the dynamic stiffness of laterally loaded Pile foundation in M DOHS Soil, Ariful et. al [3] studied the ultimate load capacity of axially loaded vertical piles from 20 full scale load test at different parts of Bangladesh, Amin et. al [4] studied the Performance of bored cast-in-situ RCC piles in Bangladesh. None of them primarily focuses on driven piles reliability, strength and economy over bored pile.

2 DEVELOPMENT OF CASE STUDY

Rapid urbanization of Dhaka city is progressing towards north by indiscriminate filling of low-lying areas mostly by dredged fills where deep foundation remains a better choice to the foundation designers. Mirpur DOHS is a classic example of reclaimed land filled with silty sand underlined by predominant clay layer. Here commonly adopted deep foundation type is RCC bored piles. This site (Figure-1) is an appropriate place to study the comparative cases of deep foundation alternative, i.e., bored and driven. A short bored pile survey at few plots of M DOHS as presented in Table-1 shows that about 36 to 47 piles are available in a typical 268 sqm (4 Katha) plot where maximum seven storied RCC building was constructed. The length of the pile varies from 65ft to 85ft with a diameter of 20” (500mm).

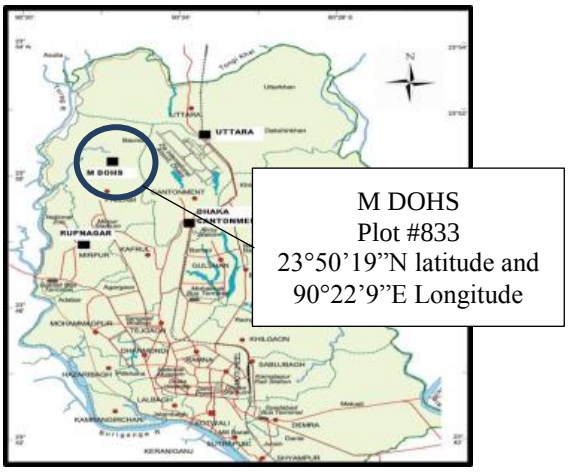

Figure 1: Location of study area, Mirpur DOHS

Table-1: Survey of bored piles (RCC, dia=20") at few plots in M DOHS

Serial	Plot No.	Area (Square Meters)	Number of piles used (20" / 500mm Dia)	Length (ft) of single pile
1	833	268	44	85
2	1059	268	42	75
3	828	268	36	70
4	847	268	37	85
5	764A	268	47	65
6	766A	536	86	75
7	567	536	86	75
8	554	536	65	65

2.1 Methodology

This study was systematically planned under the broad heads illustrated by the Figure-2. After site selection (plot no: 833, MDOHS, marked by coordinate points in Figure-1) comprehensive soil characterization was done through field and laboratory tests. Field investigations were performed in the form of SPT following standard test method ASTM D1586. Wash boring technique was used for SPT. Disturbed and undisturbed samples were collected from borehole and SPT N-values were recorded at a depth of every 1.5m interval. The boring was conducted up to 30m depth in respect to Existing Ground Level (EGL). Collected soil samples were then tested in the MIST laboratory. Few locally conducted SPT results were also collected from some of the plots shown in the Table-1 after proper verification including random laboratory tests of collected soil samples from there.

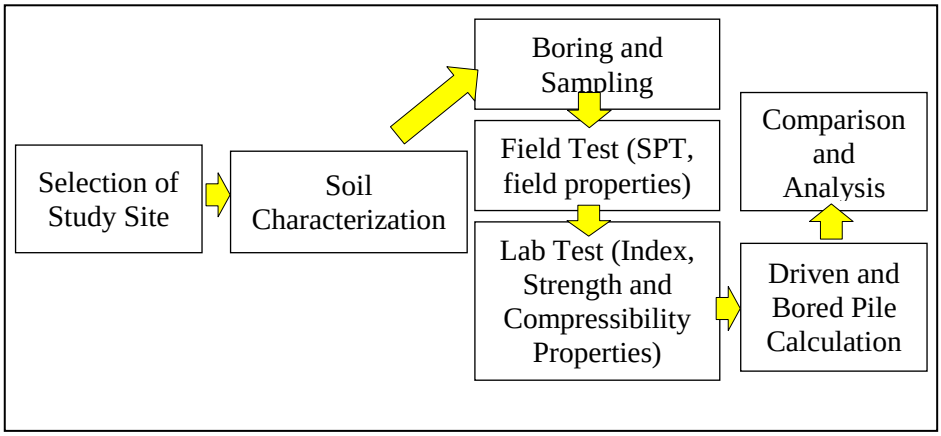

Figure 2:

2.2 Field and Laboratory Tests

The result of subsoil investigation report by borelog data including field SPT N values with few photographs are shown in Figure-3. There are seven variable soil layers (L) marked chronologically from L1 to L7 in Figure-3.

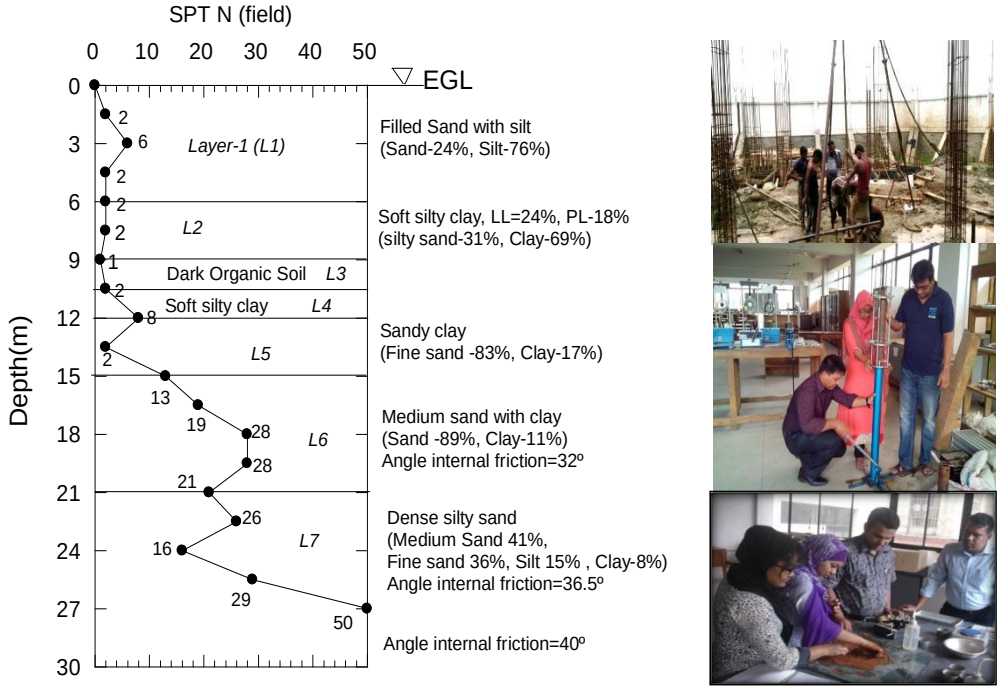

Figure-3: Borelog data and subsoil investigation result summary with few field and laboratory working photographs.

Up to 9m depth (L2) soil is basically a filled deposit dominated by silty clay. L3 contains organic matters. From L6 (clayey sand) greater penetration resistance begins and provides higher bearing capacity for foundation. Beyond 27m depth the soil exhibits higher SPT (N>=50). Laboratory tests of collected sample from each layer have been conducted for design calculation of both bored and driven pile. Basic laboratory tests include grain size analysis, Atterberg limit, specific gravity, direct shear and unconfined compression test etc. Test results are used to calculate the skin friction and end bearing of bored piles. For driven pile mainly SPT N value are employed for capacity calculation.

3 RESULT AND DISCUSSION

3.1 Calculation

For axial capacity calculation of both bored and driven pile, properties of soil and piles are summarized in Table-2.For calculation of axial capacity of bored pile commonly used Reese and Wright (1977) and Modified Beta methods have been used. On the other hand axial capacity of driven pile has been calculated by only Meyerhof's equation as this equation is generally found in close agreement with the field capacity observed in few cases in the nearby locations of selected site. Basic equations of all used bearing capacity calculation methods with names are presented in Table-3. Standard support reaction for a common unit of 2200sft five storied building has been considered. Axial capacity requirement of a 20" (500mm) diameter single pile for foundation is roughly considered as 70 ton based on a general data obtained from various sites of M DOHS area.

Table 2: RCC Pile and Soil Property

RCC Pile Property	Soil Property
Design Axial Load=833kN /m^2	GWT = EGL
Concrete's compressive strength, f_c' = 1800 psi	Wc =23% (Avg), Gs= 2.62 to 2.64
Rebar yield strength, f_y= 60 ksi	Dry Density =1.4 to 1.52g/cc
(1) Bored Pile	Wet Density = 1.85 to 1.98g/cc
Length, L = 90 ft	LL=24%, PL= 18% (L1,L2 & L4)
Diameter, D=20″(circular dimension)	$\Phi = 32^0$, 36.5^0& 40^0(L6, L7 and below)
(2) Driven Pile	S_u = 0.0625 N, (tsf)
Square dimension (12"x12"),	
Driven method : Pressure system	

Table 3: Formula used for calculation

Bored Pile Formula	Driven Pile Formula
Ultimate Capacity, $Q_{ult}=Q_s$ (side shear) + Q_b(end bearing)	Using Meyerhof's Equations
Where, Qs= π $\sum_{i=1}^{n}$ fsi LiDi	Structural Capacity, 0.30 f'$_c$ A_c
f_{si} = unit side shear for the i_{th}soil layer, Li is the thickness of (or length of shaft in) the i_{th} soil layer	Skin Friction in Sand, 2 N α A_s
Di is the diameter of the shaft in the i_{th} soil layer.	Skin Friction in Clay, 10 N α A_s
In Sand	End Bearing in Sand, 400 N A_b
Reese and Wright (1977)	End Bearing in Clay, 140 N A_b
f_s = N / 34, for N ≤53	Where,
f_s=(N-53)/450 +1.6,for 53 < N ≤100	A_c is Section Area, Friction Area is
Q_b = 2/3 N for N ≤ 60	A_s, End Area is A_b,
Q_b = 40 for N > 60	Minimum f'c = 2500 psi (17.2 MPa)
Modified Beta Method	
f_s= $\beta\sigma_v'$ < 2.0 tsf, for 0.25 ≤ β ≤ 1.2	
where,β =1.5- 0.135 $z^{0.5}$ for N > 15	
β = N/15 (1.5 - 0.135 $z^{0.5}$) for N ≤ 15	
Also by Reese and O'Neill (1988)	
Q_b = 0.6 N for N ≤ 75	
Q_b = 45 for N > 75	
In Clay	
side shear, f_s= α S_u(Alpha method) (values of α are obtained from BNBC 2012(draft) article 3.10.4.7.1)	
Q_b = N_c S_u ≤40 tsf	
N_c = 6 [1 + 0.2(Z/D)] ≤ 9 for S_u> 0.25 tsf	
N_c = 4 [1 + 0.2(Z/D)] ≤ 9 for S_u< 0.25 tsf	
(AASHTO, 1998)	

3.2 Result

Using data of Table-2with Figure-3 and adopting the formulas presented in Table-3the axial capacity of both driven and bored pilewere calculated and a comparison is presented below in Table 4.

Table 4: Axial capacity comparison of both bored and driven pile

Bored Pile Axial Capacity	Driven Pile Axial Capacity
For 90ft embedment length and 20" diameter RCC pile Q_{ult}= Q_s *(side shear)* + Q_b*(end bearing)=170+59*=229 ton [Reese and Wright (1977)] Q_{ult}= *159+53*=212 ton [Modified Beta] Adopted Capacity (ultimate) = 200 ton	To achieve 200ton capacity using a 12"x12" RCC precast pile length required = 60ft

3.3 Discussion

From Table-4 it is clear that in place of a 20" RCC pile of 90ft, only a 12"x12" size of driven pile of 60ft length is sufficient against anticipated axial capacity. A 30ft savings in length provides economy in labor, time, material and efforts as well. A quantity surveying reveals that currently per running feet material cost of bored pile is 967taka whereas that of driven pile is 892taka, hence 30% cost saving is achieved by only adopting a nontraditional mode of deep foundation of the area. Few more savings are quantified through different aspects as shown below in Table-5:

Table 5: Comparison between bored and driven pile in M DOHS Plots

Serial	Subject	Bored Pile	Driven Pile	Savings
1.	Required Pile length to support intended length	90ft	60ft	30%
2.	Material Cost for 60ft length as per current market rate	50,035 Tk	27,674 Tk	44.7%
3.	Driving/Boring time per day	1 to 2	10 to 15	80%

3.4 Comparison

Basing on above discussion a comparative analysis of pile system (as shown in Table-1) of the study area shows that for a plot of 268sqm (4Katha) approximately 40 bored piles are needed. According to the soil profile presented in the soil test report of corresponding plot it is observed that about 25 numbers of driven piles are sufficient to substitute those 40 piles. Hence approximately 38% of pile saving (in number) is achieved only by selecting driven pile system

instead of bored pile. The situation is almost similar for a 536 sqm (8Katha) plot too.

Table 6: Comparison between bored and driven pile in M DOHS Plots

Plot in sqm	No. of Bored Pile used	No. Driven pile required	No. Of pile Saving	Remark
268	40	25	38%	Pile number Saving 35~ 40 %
536	65	40	39%	

Table 7: Comparison between length of bored and driven pile in M DOHS Plots

Plot in sqm	Length of bored pile used (20" RCC pile)	Driven Pile length required to replace a bored pile (12"x12")	Length saving
268	80	60	20%
536	75	60	15%

From above tables 6 and 7 it is quite evident that almost 20% to 40% savings can be achieved by only selecting a different method of deep foundation design instead of traditionally used bored pile. Unfortunately most foundation designers are unaware about this important fact in this area. Lack of authenticated subsoil investigation report coupled with noninvolvement of foundation designer in building's design phase is a widely known cause of this problem. This study is thus an eye opener for the designer of this area.

4 CONCLUSION

Consistency of Mirpur soil is mostly medium to stiff which is suitable for deep foundation. Widely used deep foundation in Mirpur soil is bored pile. Current study shows that driven pile is more suitable than bored pile in terms of economy, strength, time saving and safety as well. Geotechnical considerations of foundation design in Mirpur soils are mostly ignored by common design engineers. Therefore, the choice of deep foundation remains within traditional concept of bored pile only. Driven pile system may increase the construction efficiency in terms time and economy. The performance of driven pile is found superior in all aspects where medium to stiff consistency soils are available. For soil of soft to medium consistency, driven pile is suggested in Mirpur DOHS soil subjected to site accessibility and technical support. Awareness should be raised amongst users and designers of Mirpur DOHS in selecting suitable pile

foundation type. It is to be noted that current study is based on static analysis only. Considerations for group efficiency with dynamic loading cases are ignored for simplicity.

ACKNOWLEDGEMENT

Authors acknowledge the contribution rendered by Grihayan Ltd and Fast Ground Engineering in obtaining the site information and in sample collection from the site.

REFERENCES

[1] Ahamed, S. 2005.*Soil characteristics and liquefaction potential of selected reclaimed areas of Dhaka city*, M.Sc. Engg.Thesis, Department of Civil Engineering, Bangladesh University of Engineering and Technology, Dhaka, Bangladesh.

[2] Mohiuddin Ahmed, Mohammad Shariful Islam and Raquib Ahsan, 2012, *Dynamic Stiffness of Laterally Loaded Pile Foundation in Dhaka Soil*, Electronic Journal of Geotechnical Engineering, Vol-17[2012], Bund,P

[3] Ariful Hasnat1, A. R. M. Farid Uddin, Emtazul Haque, Partha Saha, and Md. Wadud Rahman,2012, *Ultimate load capacity of axially loaded vertical piles from full scale load test results interpretations-applied to 20 case histories*,Proceedings of the 1st International Conference on Civil Engineering for Sustainable Development (ICCESD-2012), 23~24 March 2012, KUET, Khulna, Bangladesh (ISBN: 978-984-33-4247-8).

[4] Md. Nurul Amin, Sabina Shahnaz and Sonia Shahnaj, 1998, *Performance of bored cast-in-situ RCC piles in Bangladesh*, Proceedings: Fourth International Conference on Case Histories in Geotechnical Engineering, St. Louis, Missouri, March 9-12, 1998.

CICM 2015
First International Conference on
Advances in Civil Infrastructure and Construction Materials
MIST, Dhaka, Bangladesh, 14–15 December 2015

GEOTUBES FOR TEMPORARY EROSION CONTROL AND LAND RESTORATION OF SHORELINE ALONG THE COX'S BAZAR-TEKNAF MARINE DRIVE ROAD

Mohammad R. KARIM[1] and Anika Tahsin[2]

[1]Defence Services Command and Staff College
Dhaka, Bangladesh
Email: majrezakarim@gmail.com,

[2]Center for Environmental and Geographic Information Services (CEGIS)
Dhaka, Bangladesh
Email: atahsin@cegis.com

Abstract. *Driving along Cox's Bazar Teknaf Marine Drive Road along the beach is one of prime attractions to the tourist in Cox's Bazar beach. However, more than 20% of this beach along the road is suffering from severe problem of erosion. During 2009-2010, tropical storms caused severe beach erosion along the road; specially, in area Himchari of Cox's Bazaar. This erosion caused many segments of the road in danger, threatened the Army Project Camp of Himchari and narrowed down the beach at several points. To prevent such damages, shore parallel geotextile tubes (geotubes) were installed. Geotubes were placed at the embankments of the roads coupled with T -head groynes into the sea to restore the sands. The scope of this paper is to present the effectiveness of geotubes as beach erosion control measures based on the case study of Himchari beach. It will also evaluate the success of T-head groynes layout of geotubes for beach restoration. Satellite images and ground observation data has been used for analyzing the result. Moreover, few faults have been identified regarding the application of geotubes which severely damaged them and necessary guidelines have been put forward for future application.*

Keywords: Geotubes, Erosion control, Beach restoration.

1 INTRODUCTION

With more than 100 km of sand, Cox's Bazar has the world's longest uninterrupted natural beach. Cox's Bazar-Teknaf Marine Drive, an 80-km long road along the sandy beach was built to enable the tourists of home and abroad to enjoy the beauty of this spectacular beach. The Marine-drive road project is an exclusive development project in the communication sector of the coastal area of Bangladesh (Figure 1). This project possesses significant importance in the socio-economic development as well as political and environmental implication of the country. Since the construction of the road, the beach has been facing acute problems of erosion with beach sand get washed off from the shore by waves and more than 20% of this beach along the road is affected by this erosion problem. During 2009-2010, tropical storms caused severe beach erosion along the road; specially, in Himchari area of Cox's Bazar. The erosion also affected the Army camp situated near beach at Himchari and its adjacent areas during subsequent storms and gradual shoreline retreat. To prevent such damage, shore-parallel geotextile tubes (geotubes) were installed. However, very shortly it was observed that these geotubes got punctured/ failed due to wave action, human interference and were no longer effective to protect the beach from erosion. Afterwards geotubes were laid in form of T-head groynes with the existing shore parallel geotubes in two vulnerable portions of the project near Himchari to protect the road and restore the beach sand. This paper attempts to evaluate the effectiveness of geotubes as beach erosion control measures based on the case study of Himchari beach. It will also assess the success of T- head groynes of geotubes for beach restoration.

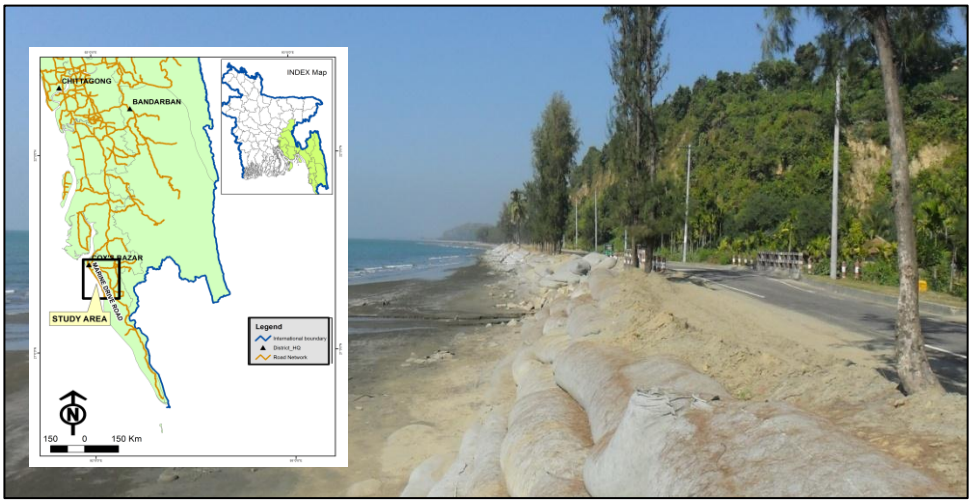

Figure 1: Cox's Bazar Teknaf Marine Drive Road.

2 LITERATURE REVIEW

The Beach erosion is the removal of beach or dune sediments either by wave action, tidal currents, wave currents, drainage or high winds. This phenomenon is observed for all the sandy beaches all over the world. Continuous beach erosion washes away beautiful beaches and also endangers the infrastructure built near those. Continuous erosion and failure of structures near beaches creates lots of environmental and economic problems by affecting the aquatic life and human beings.

There are numerous ways in which beach erosion can be controlled. Pilarczyk [1] reported that coastal structures like seawalls, dikes, revetments provide direct protection to the beaches whereas groynes and offshore breakwaters provide indirect method of shore protection. It was further reported that geo-synthetic family products like geotubes, geocontainers, geocurtains and other patented systems like reef balls, aqua reef (Hirose et al., [2]), prefabricated units, beach drainage, etc. have also been tried to contain the beach erosion due to their simplicity in placement and construction, cost effectiveness and for being environment friendly.

Koerner [3] reported that geotextile tubes can provide better protection for beach erosion. Geotextile tubes with diameters of up to 3m, made up of woven or knitted high strength fabric have been effectively used to control both inland and oceanfront erosion. Length of geotubes is decided based on ease in handling/placing and sand filling. The main tubes are generally flanked by tubes of smaller diameters on upstream side which help in resisting lateral pressure. Also, it is required to provide cover to geotubes to protect them from degradation/damage.

Shin et al. [4] had conducted pilot scale field tests to study the performance of geotubes made up from woven geotextile filled by hydraulically pumping dredged silty clay material into it. Based on this study, it was concluded that geotubes are feasible construction materials for use in coastal engineering projects.
James et al. [5] found that the geotube projects are effective for short-term erosion control. They are significant engineering structures that change the geomorphic and sedimentary environments of the beach/dune system. Continued maintenance and beach nourishment projects are required to maintain the geotubes and to mitigate adverse effects on public beaches.

3 BACKGROUND AND STUDY AREA

In 2009-2010, storms and tidal surge caused severe beach and dune erosion along the road. This erosion placed many portion of the road in danger of being undermined or damaged during subsequent storms and gradual shoreline retreat (Figure-2). As a temporary measure geotube and geobags had been laid along the road at different vulnerable points where the sea line reached upto the road

shoulder. Geotubes were laid on the road embankments to control erosion. However, it was observed that these geotubes got punctured due to repeated wave action and had to be replaced after every thrust of the high tidal surge.

Figure 2: Road affected by tidal surge.

In January 2011, two critical points at Himchari were selected where shore parallel geotubes with T-head groynes were laid with the aim to see the sustainability of geotubes as well as restoring capacity of beach sands by T-head groynes (Figure-3).

Himchari is located on 8 km south of Kolatali point of Cox's Bazar. It is one of the most attractive tourist spots of Cox's Bazar where tourist can enjoy combination of the sea and the waterfall. It is also exciting because the road to Himchari runs by the lovely green hills on one side and open blue sea on the other side. The Army Project camp and Battu Miar Khamar of Himchari are situated on the 7.5 km point and 8.5 km point of this road respectively. During the period of 2009 to 2010, beaches were severely erodedin these two points. The shore line in both the points came upto the border line of the road which earlier was 100-200 m away from Himchari Army Camp and 300 – 500 m away from Battu Miar Khamar.

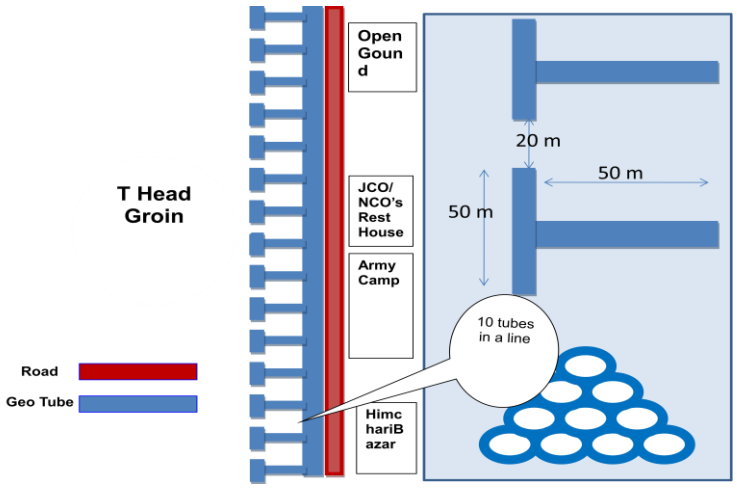

Figure 3: T-head groynes layout in front of Himchari Army camp.

4 METHODOLOGY

4.1 Geotube Application Procedure

To help prevent damage of the road, shore-parallel geotubes were laid on the beachside embankments of the road. The geotubes are sediment (sand) filled sleeves of geotextile fabric having an oval cross section of approximately 4m in perimeter. These geotubes were filled with the sand using pumps. They rest on a fabric scour apron that has sediment-filled anchor tube. Geotubes were placed at the toe of the embankment in a trench parallel to the road and subsequently placed on the sides of the embankments. Project designs called for sand and natural beach vegetation to cover them. However, it was not possible to cover the geotubes at all places as it demanded huge volume of earthwork and in few places where earth cover were given could not be retained due to wave action.
Again, Geotubes were used to design a series of T-head groynes to help stabilize the beach. The T-head acts as a breakwater dissipating wave energy that otherwise would start to erode the beach sand while the perpendicular section acts like a jetty and catches the sand, creating a restoration of the beach. The perpendicular section of the groynes extended 50m into the sea with 50m section parallel to the shoreline forming the "T". The gap between the flanges of successive groynes had been kept 20m to facilitate water to go out of the trap.

4.2 Evaluation Criteria

Field measurements include beach and dune topography, shoreline positions, geotubes exposure and damage condition assessment. From these measurements, the effects of the geotubes on the beaches were evaluated by sorting out their ability to slow erosion and prevent beach damages. Satellite images gave a pictorial overview of the beach condition including the extent and sand accumulation area of the beach.

4.2.1 Beach profiles

Beach profiles can detect short-term changes in morphology, sediment volume, and shoreline position. In this study, ground-surveyed topographic transects were conducted at 16 locations between 6.5 km to 8.0 km point and 11 locations between 8.5 to 9.5 km point at an interval of 200m for both the cases. Surveys were conducted twice during January 2011and January 2015 respectively. The beach profiles were oriented perpendicular to the road line during high and low tides.

4.2.2 Geotube Condition Surveys

Systematic ground observations and photographs of the geotubes were observed to assess the conditions, determine nature of damage of the tubes and find out the causes of damage.

4.2.3 Satellite Images

Time-series satellite images and historical Google maps have been used to observe the changes in both locations for last few years.

5 FINDINGS

5.1 Beach Width

Figure 4 shows profiles that compare the change of beach widths between the period of January 2011 and January 2015. The beach widths were taken both during the high and low tide situations. High water mark was considered for measurement at high tides from the reference line i.e. road shoulder line.

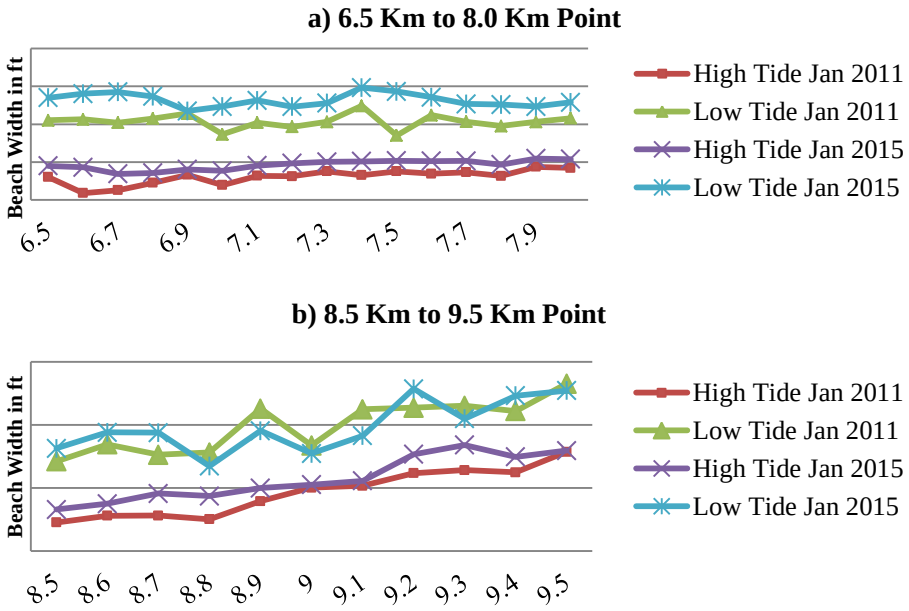

Figure 4: Change of beach width between the year January 2011 and January 2015.

Both the result and ground observations indicate that the road has been protected as well some accretion has occurred in beach due to the placement of geotubes (Figure 4). Moreover, it is found that from 6.5 km to 8.0 km point, an average 31 ft beach width has been increased with a standard deviation of 11.83 during high tide and 57 ft beach width has been increased with standard deviation of 22.86 during low tide. Again from 8.5 km to 9.5 km point average 21 ft beach has been increased with standard deviation of 13.02 during high tide and 1.2ft beach width has been decreased with standard deviation of 27.67 during low tide.

5.2 Geotube Condition Surveys

Many geotubes were found burst, damaged and worn out (Figure 5) .Geotubes placed under sand and covered by other geotubes found mostly in good conditions. Uncovered geotubes, subjected to direct wave action were found torn and burst. Again the geotubes placed near the shoulder of the road which rarely came in contact with water rather exposed to direct sunlight, were also found worn out.

Figure 5: Damaged and burst geotubes.

These geotubes were filled with the sea sands manually and using pumps. Various foreign particles like small stone, dried piece of weed, pieces of seashell, small debris were found with the filled sand. When sea wave hits the geotubes, due to the pressure on sharp edges of these materials geotextile get torn and make small holes in tubes. Again, beach crabs also create holes in the geotubes. These holes were increased in consecutive wave action and led to geotube burst. As a result, sand filled inside the geotubes come out leading to failure of those geotubes. In addition, geotubes which were exposed to ultraviolet light handled to the failure of geotubes.

5.3 Analysis of Satellite Images

Figure 6: Satellite and Google map images of the study area in various years.

From the satellite images taken at 2003, 2010, 2011, 2014 and Google images of 2009, 2012, 2014, 2015, it is found that T-head groynes geotubes are well stable and sands are accumulated inside the groynes areas (Figure 6). Thereby shoreline has been shifted further from the road line. Thus, a large area of sand has been reclaimed during last 2-3 years on the southern portion of the Himchari beach which was lost during the surge of 2009-10.

6 CONCLUSIONS

According to the observation and field survey, it was found that shore parallel geotubes coupled with T-head groynes became very effective to control erosion and beach sand restoration in Himchari area of Cox's Bazar. Sand, instead of disappearing with each storm event, is accumulating naturally between the T-head groynes, and the beach is beginning to once again build up. However, geotubes tend to fail when exposed to ultraviolet light and came under direct wave attack. Thereby it is necessary to carefully fill the tubes with fine sands free of dried seashell, weeds, stones etc and cover the geotubes with earth or vegetation to make them useful as more effective erosion control measures.

REFERENCES

[1] Pilarczyk, K.W. (2005). Coastal stabilization and alternative solutions in international perspective. Arabian Coast 2005 Key Note address, 1-26.

[2] Hirose, N., Watanuki, A. and Saito, M. (2002). New type units for artificial reef development of ecofriendly artificial reefs and the effectiveness thereof. PIANC Congress, Sydney.

[3] Koerner, R. M. (2000). Emerging and future developments of selected geosynthetic applications. Journal of Geotechnical and Geoenvironmental Engineering, 126(4), 293-306.

[4] Shin, E. C., Ahn, K.S., Oh, Y.I. and Das, BM. (2002).Construction and monitoring of geotubes. Proceedings of The Twelfth International Offshore and Polar Engineering Conference, Kitakyushu, Japan, May 26–31, 2002.

[5] James C. G., Hepner, Waldinger, R., Andrews, J.R., Smyth, R. C., Gutierrez, R. (2003). Geotubes for temporary erosion control and stormsurge protection along the gulf of mexico shoreline of Texas. Proceedings of the 13th Biennial Coastal Zone Conference Baltimore, MD July 13–17, 2003.

CICM 2015
First International Conference on
Advances in Civil Infrastructure and Construction Materials
MIST, Dhaka, Bangladesh, 14–15 December 2015

EFFECT OF CLIMATE CHANGE ON ROAD MAINTENANCE IN BANGLADESH

Moahammed R. Islam[1], S. M. Muniruzzaman[2], Md. K. A. MASUD[3], S. S. Morshed[4]

[1, 2, 3, 4] Department of Civil Engineering, Military Institute of Science and Technology, Dhaka, Bangladesh
E-mail: [1]ce_russel@ yahoo.com, [2]shah2713@gmail.com,
[3]masud_999@yahoo.com, [4]sadatmorshed@gmail.com

Abstract. *Bangladesh is one of the worst climate vulnerable countries in the world. According to scientists it is predicted that temperature and precipitation will increase 1-3% and 20% respectively by 2050 in Bangladesh. Increased temperature and precipitation will deteriorate flexible pavement in an accelerated rate. The study has developed a methodology by mechanistic-empirical method to find out the effect of moisture and temperature on the pavement. It has also provided solutions to minimize the effects. The study has found that damage done by a standard axle load during saturation period of 30 days is almost 2.5 times than that of dry condition. However, during 30 days of saturation if the axle is overloaded by 6 ton, damage is 30 times than that of a standard axle at dry condition. The study has also found that damage done by an axle load for temperature rise will increase significantly for roads in Bangladesh. The study has suggested imposing axle load restriction to minimize the effect for pavement saturation .It has suggested using improved material to fight against temperature rise. The outcome of study will help to guide road engineers of Bangladesh to prepare in advance to combat with the climate change effect.*

Keywords: Climate change, mechanistic-empirical method, pavement saturation, axle load restriction.

1 INTRODUCTION

The climate change adaptation becomes more critical development issues for Bangladesh. According to scientists, it is predicted that temperature will increase 1-3% and precipitation 20% by 2050 in Bangladesh [1]. Moreover Bangladesh is a flood prone country. Flood water causes enormous damage to the road infrastructure of the country.

Increase in pavement temperature will affect the functioning of the asphalt layer and will reduce the pavement life. Moreover, due to increase in precipitation and flooding pavement will remain in saturated condition for longer time. Saturated layers of the pavement cannot bear the wheel load of the vehicle. So, pavement life will reduce for both the cases and road maintenance cost will be increased.

However, it is important to quantify the pavement damage done by the temperature and moisture. If quantification of the damage can be done it will be possible to show the significance of the problem. Since road infrastructure is the main mode of transport of goods and passengers in Bangladesh, it should be safe against adverse climate change effect. Moreover, a developing country like Bangladesh has a limited budget allocation for road construction and maintenance. So, road design, materials selection, and traffic loading should be such that life road construction and maintenance become economic and durable.

The study has attempted to quantify the effect of temperature and moisture for a road in coastal region and for a typical national highway respectively with consideration of vehicle overloading. In Bangladesh, vehicle overloading is common as mentioned in the road master plan [2].To predict the life of the flexible pavement due to changes in temperature and moisture, the study has adopted mechanistic-empirical (M-E) approach. In this study mechanistic analysis was done with a software GAMES (General Analysis on Multi-layered Elastic system). GAMES provide strain values at critical location of the pavement. Pavement life is then predicted by using empirical model of Asphalt Institute as cited in [3] with the critical strain values. Finally it has suggested probable solutions to fight against the effects.

2 METHODOLOGY

The main objective of the study is to investigate how the pavement is affected due to rise in temperature and precipitation. For this purpose an M-E analysis was done with GAMES to determine horizontal tensile strain at the bottom of surface layer and vertical compressive strains at top of subgrade layer of flexible pavement as shown in the figure 1. By utilizing the strain at critical location, damage by an axle load for a single pass was determined from empirical equation of predicting pavement life.

The traffic loading has been considered as a prime factor simulating the pavement behaviors. This includes axle loads, configuration of axles, tire contact

area. Resilient modulus is a basic input for the mechanistic analysis. It was found that resilient modulus of asphalt layer varies with increase in temperature and pavement saturation. Additionally, all the layers are adversely affected by saturation condition of the pavement layers. Such behaviors of the pavement layers were utilized in predicting the responses due to temperature and moisture.

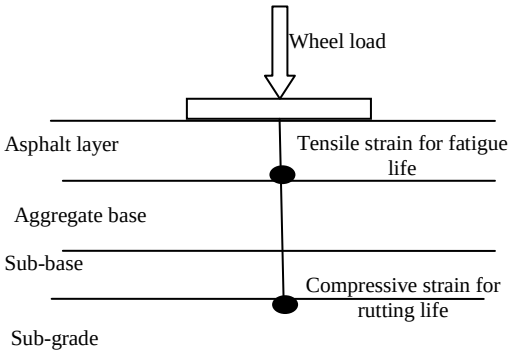

Figure 1: Critical location of strain values for analysis.

3 RESEARCH APPROACH

In this analysis single wheel loading conditions were considered for each of the two pavements. Standard single axle load for Bangladesh is 80 kN. However, to simulate overloading effect axle load of 100 kN, 120 kN, and 140 kN consecutively were also considered.

3.1 Pavement Analysis

After getting the strain values for critical location of the pavement layers, life was predicted by Asphalt Institute model as cited in [3].

$$N_{f1}=0.0796\,\epsilon_t^{-3.291}\,E_1^{-0.854} \quad (1)$$

$$N_{f2}=1.365E_1^{-09}\,\epsilon_v^{-4.477} \quad (2)$$

Where, N_{f1}= allowable number of load repetition to prevent fatigue cracking, N_{f2}= allowable number of load repetition to prevent rutting cracking, ϵ_t= tensile strain at the bottom of Asphalt layer, ϵ_v= compressive strain at the top of subgrade layer, E_1= elastic modulus of asphalt layer.

Moreover, the damage (D_i) caused by each application of axle load is given by:

$$D_i = 1/N_i \quad (3)$$

Where N_i is the minimum number of load repetitions required to cause either fatigue or rutting failure.

4 TEMPERATURE EFFECT ON PAVEMENT

For predicting temperature effect by M-E analysis it is required to know change of resilient modulus due to increase in temperature. It was found that resilient modulus of asphalt layer decreases with rise in temperature [4] as shown in figure 2. The input values for finding temperature effect on pavement are shown in table 1. It was found that rutting failure governs for the analysis for M-E. Damage done by the different single axle loads was normalized by the standard axle damage. It was found that with the rise in pavement temperature, damage done by a single pass of axle load also increases as shown in figure 3. However, it was found that when temperature effect was combined with overloading damage was severe.

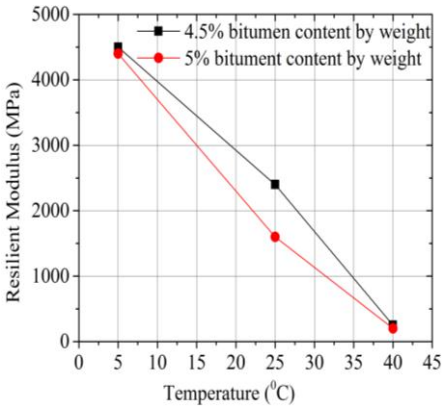

Figure 2: Relationship between resilient modulus and temperature. [4]

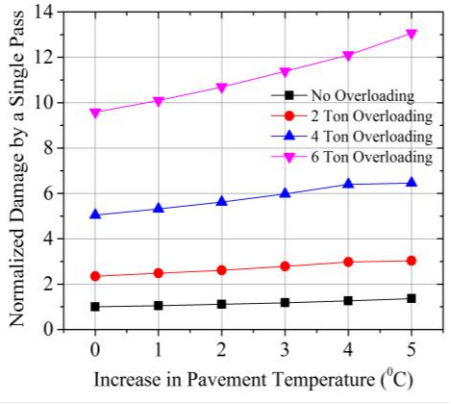

Figure 3: Normalized damage for temperature for different loading conditions.

Table 1: Input value for temperature effect

Layer	Layer thickness(cm)	CBR	M_r (MPa)	Poisson's ratio	M_r reduction
HMA	5.2	-	1379	0.35	121 Mpa
Base	20	80	862	0.4	with the
Sub-base	20	30	104	0.4	increase of
ISG	20	7	72	0.45	1℃
Sub grade	200	5	52	0.45	

4.1 Remedy For Temperature Effect: Improved Materials

In Bangladesh, for road construction 80/100 penetration grade is used. However, it is not suitable for high temperature as its viscosity is low at high temperature. Polymer modified asphalt is very popular for making temperature resistant asphalt pavement. The study leaves it for future investigation to find out cost effective and temperature resistant polymer modified asphalt for Bangladesh.

5 MOISTURE EFFECT ON PAVEMENT

It was found that marshal stability value decreases and flow value increases with the increase of inundation period [5].Marshal stability -flow ratio was found to decrease approximately 57% after 30 days of inundation as shown in figure 4. Moreover, stability-flow ratio was found to be proportional with resilient modulus of asphalt concrete [6]. So, to simulate moisture effect on pavement by M-E method, resilient modulus of asphalt layer was modified according to such correlation. Figure 5 shows 14 to 37 percent decrease of sub-grade CBR values is possible for 45 days flooding depending on the condition of compaction [5]. CBR value for subgrade is linearly correlated with the resilient modulus [7]. So, resilient modulus of the subgrade modulus was also decreased with inundation period. Additionally, resilient modulus for base and sub-base layer was assumed to be decreased with same proportion of subgrade value.

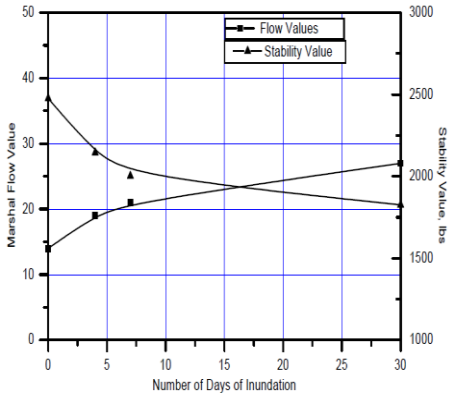

Figure 4: Effect of inundation on CBR of subgrade [5]

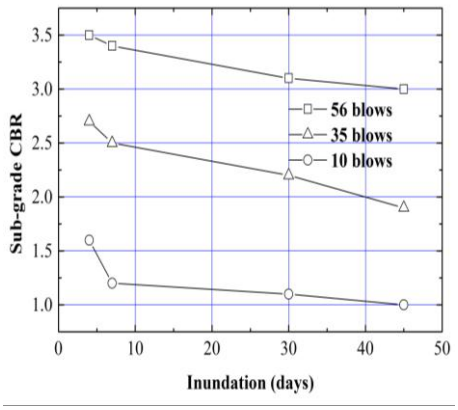

Figure 5: Effect of inundation on flow and stability of bituminous surface layer [5]

For finding the effect of moisture on pavement input values as shown in the Table 2 were used for the GAMES analysis. From the analysis it was found that rutting failure governs. It was found that moisture causes significant damage on

the pavement. From the Figure 6, it was found that for a standard loading damage after saturation period of 30 days is of 2.5 times than that of dry condition.

However, for overloading with 6 ton , saturation damage is 4 times than that of dry condition and overloading as found from the Figure 6. Here in Figure 6, all damage values were normalized by that of a standard axle at dry codition. For quantifying additional the damage done by the saturation, difference of damage between saturated and dry condition was calculated as shown in Figure 7.

Table 2: Input values for GAMES analysis to simulate moisture effect

Layer	Layer thick-ness(cm)	CBR	Mr (Mpa)	Poisson's ratio	Mr (MPa) After 30 days of saturation
HMA	12.5	-	1379	0.3	784
Base	15	80%	883	0.35	752
Sub-base	18	25%	124	0.35	105
ISG	20	8%	83	.4	70
Sub grade	200	5%	52	.45	40

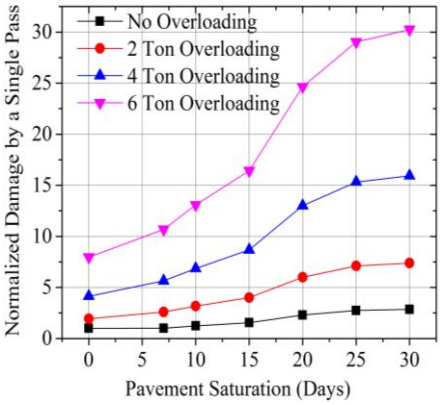

Figure 6: Damage for different saturation period with different loading conditions

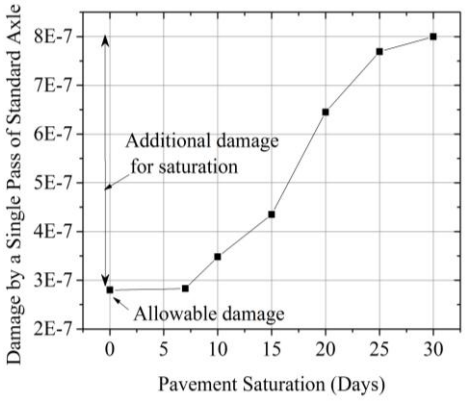

Figure 7: Quantifying additional damage for saturation effect for a standard axle load (80 kN)

5.1 Remedy For Moisture Effect: Axle Load Restriction

Since pavement layers were weakened for saturation, damage done by a standard axle load was greater than that of dry conditiont as shown in Figure 7. If it is desired to keep the damage as equal to the damage during dry condition, the load responsible for additional damage should be reduced from the standard axle. From the Figure 8, it is possible to determine the amount of load causing the

additional damage for different saturation condition for a standard axle laoding. Since oveloading always causes damage greater than the dry condition, overloading should be controlled totally.

It was found that if 18% load is reduced from the standard axle during the 20 days of saturation as shown in figure 9, damage done by the restricted axle load would be the same as that of a standard axle during dry condition.

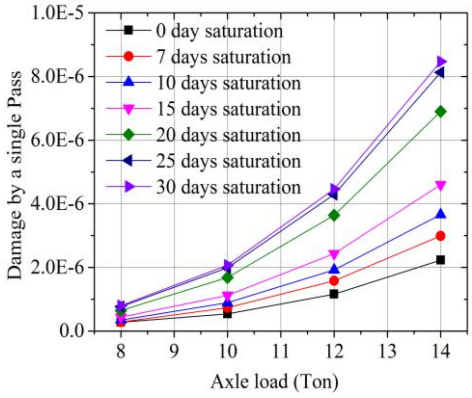

Figure 8: Load damage relationship for different saturation periods.

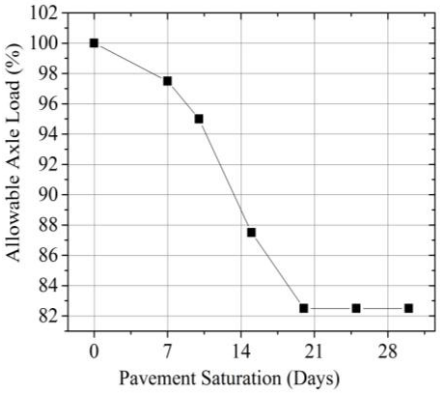

Figure 9: Allowable axle load for different saturation period.

6 CONCLUSION

The study has attempted to simulate the effect of climate change on road maintenance of Bangladesh. It has developed a methodology for finding the effect of temperature and moisture by M-E method. It has also proposed a methodology to impose axle load restriction on pavement to minimize the moisture effect. From the study the following conclusions are listed:

- From the study it was found that damage done by a standard axle load during 30 days of saturation is 2.5 times than that of dry condition.
- However, damage done by an axle with 6 ton of overloading for saturation of 30 days is 4 times than that of dry condition done by the same overloading. Moreover, damage done by the same overloaded axle after 30 days of saturation is 30 times than that of a standard axle at dry condtion.
- Reduction of the standard axle load will be necessary to minimize the effect. From the observed relationship between load and damage after M-E analysis, it is possible to find out the amount of load causing the additional damage for saturation. For a sturation period of 20 days, 18% of the standard axle load should be reduced to minimize the effect of pavement saturation.

- Moreover, overloading should be totally restricted during pavement saturation period.
- Temperature in combination with the overloading will cause significant damage to the pavement. The damage by a single axle with 6 ton overloading and with temperature increase of 5^0C would be 13 times than that of a standard axle load without increase in temperature.
- For minimizing the effect for temperature, it is suggested to use polymer modified asphalt with ability to resist high temperature effect. Further detailed study is necessary for this purpose.

REFERENCES

[1] The World Bank, 2011. The Cost of Adapting to Extreme Weather Events in a Changing Climate, Bangladesh Development Series, Paper No. 2, executive summary, pp. xiii.

[2] Ministry of Communication, Bangladesh, 2007. Road Master Plan, Roads and Highways Department, Vol. 1

[3] Huang, Y.H., 2004. Pavement Analysis and Design, 2nd edition, Pearson Education, Inc.

[4] S.A Tabatabie, H. Ziari and M. Khalili, 2008. Modeling temperature and resilient modulus of asphalt pavements for tropic zones of Iran, Asian Journal of Scientific Research, 1(6):579-588, ISBN1992-1454, pp 579-588.

[5] Alam, M. J. B. and Zakaria M. 2002. Design and Construction of Roads in Flood Affected Areas, Engineering Concerns of Floods a1998 Perspective. Directorate of Advisory, Extension and Research Services, BUET, Dhaka, Bangladesh, pp91-99.

[6] Ahmad H. Al-Zassar, Abdul Aziz M. Al Shehab,Aref Al Zaabi, 2003. Using Marshall test to assess asphalt-concrete modulus for mixes used in Kuwait, Kuwait J. Sci. Eng. 30(2), pp169-182

[7] Mamlouk, M.S., 2006. Design of Flexible Pavements, The Handbook of Highway Engineering edited by Fwa, T.F, Boca Raton, T& F groups, ch.8, pp. 8.22-24.

[8] Ministry of Communication, "Technical specifications," Bangladesh Roads and Highways Department, Vol. 7, 2011.

CICM 2015
First International Conference on
Advances in Civil Infrastructure and Construction Materials
MIST, Dhaka, Bangladesh, 14–15 December 2015

EXPLORING THE INTERFACE BOND CONDITION AND ITS EFFECTS ON PREMATURE FAILURE OF AN OVERLAY WORK: CASE STUDY ON NATIONAL HIGHWAY-5, BANGLADESH

ASADUZZAMAN[1] and Moahammed R. Islam[2]

[1] Ministry of Road Transport and Bridge Division
Email: sceazer131@gmail.com

[2] Department of Civil Engineering, Military Institute of Science and Technology, Dhaka, Bangladesh
Email: ce_russel@yahoo.com

Abstract. *The study has identified interface bond failure to be the reason for premature failure of an overlay work that is observed on N_5. Moreover, it has come out with remedial measures to counter that failure. Based on field investigation, it has found that surface of the old asphalt concrete layer was cracked and it was too smooth to create interlayer bonding with new asphalt overlay. It is assumed that clay particles with the entrapped water from the underlying WBM layer came up to the interface of new and old surface through the cracks due to pumping action generated by wheel loading. Thus, the clay layer has further destroyed the interface bonding between the newly constructed asphalt overlay with the old one. The new asphalt overlay without interface bond failed to bear the wheel loads consequently early cracks developed in the top. Rainwater penetrated through the cracks of the new surface and further helped to cause the premature failure of the new overlay work. To verify the field observation, the pavement is analysed by general analysis of multi-layered elastic system (GAMES) software. Different interface condition ranges from full bond to full slip can be applied in GAMES software. Analysis results indicate that overloading and interface bond condition can reduce pavement life to 10% within three to four months. The study suggests that interface bonding failure of overlay work can be solved by converting lower asphalt layer into granular base layer. These measures will surely increase pavement life.*

Keywords: Interface bond, Pavement cracks, Pumping action, Premature failure of overlay work, Multilayered elastic system software.

1 INTRODUCTION

National Highways (NHs) (N_1 to N_8, total length of 4780 km) are regarded as the lifelines of Bangladesh economy. The surface condition of NHs has to be maintained at a certain level for enhancing national economic growth. Roads and Highways Department (RHD) maintains those NHs through annual Periodic Maintenance Programs (PMP). Generally, PMP recommends 50-80 mm bituminous overlay (BO) or double bituminous surface treatment (DBST) with a consideration of surface condition [1]. If the surface condition is not good, BO is suggested otherwise DBST is preferred.

According to Highway Development and Management-4 (HDM-4) report, design life of BO work is five years [1]. But, previous failure history gives impression that bituminous overlay work's life in RHD would not be more than 3 years. After three years, pavement demands another BO work.

National highway-5 (N_5) connects the northern part of Bangladesh to capital Dhaka with a length of 500 km. Gaibandha Road Division maintains and manages 33 km of N_5. This portion was re-constructed in 1992-93 under Road Rehabilitation and Maintenance Project (RRMP). Before this reconstruction, this part was made of herring bone and RCC slab. After the reconstruction, PMP Overlay work program was taken on that portion in 2007-2008 as major cracks were appeared on the surface. Similarly, 50 mm PMP overlay work was done in 2013-2014 on the same portion.

2 PROBLEM STATEMENT

PMP overlay working N_5 (Gaibandha portion) was completed on 20April 2014. Three months after the construction that means in July 2014, cracks were appeared on the surfaces in some locations. After one year, in rainy season June 2015, different types of distress such as crack, slippage failure, heaving and hump widely appeared on the surface as shown in Figures 1 and 2. By observing the failures trends, it can be assumed that pavement life sustained only three months. Actually, the pavement was supposed to sustain up to expected design period (5 years). But, pavement life was reduced to almost zero by one year that means pavement surviving life was 20% of actual design period (5 years).

3 DAMAGE INVESTIGATION

An investigation was conducted on failure portion by RHD engineers. During excavation, it seemed that the top bituminous 100mm layer (work done on 2007-2008 and 2013-2104) was softer than the bottom bituminous 100mm layer. It was also observed that top and bottom bituminous layers were not bonded sufficiently. There was a clear separation between top and bottom layers as shown in Figure 3. A thin clay layer was created on opposite face of top bituminous layer as shown in Figure 4. This thin clay layer made opposite face smooth and friction-

less as shown in Figure 4. In some locations, bottom bituminous layer showed cracked surface as shown in Figure 5. Further investigation was conducted on macadam base layer which was brick macadam (WBM). The WBM looked wetted. The size of brick particle was changed and turned into finer particles as shown in Figure 6.

Figure 1: Cracks and Slippage failure

Figure 2: Heave and hump on the surface

Figure 3: Separation of top and bottom layers

Figure 4: Thin clay layer opposite of top layers

Figure 5: Bottom layer with cracks surface

Figure 6: Damp and wet WBM

4 DAMAGE HYPOTHESIS

In flexible pavement, general concept is that stiffness of layers will decrease with the increase of depth. During excavation in N_5, it was observed that the top surface of bottom asphalt layer was smooth and having no angular surface texture, which is necessary to create strong interfacial bond between two asphalt layers. It was also found that the bottom asphalt layer was stiffer than the top layers. Bottom asphalt layer behaves like a semi-rigid layer. Therefore, poor bond interface might have occurred between two asphalt layers. When traffic moves on pavement, the top asphalt layer tends to be slipped over the bottom asphalt layer. More tensile strain develops at the bottom of the top asphalt layers and results in minor crack on the top surface. Water infiltrates into this cracked surface and moves laterally along the interface between top and bottom layers as shown in Figure 7. This interfacial water deactivates the tack coat's bonding function; thereby interface bond failure occurs. Finally, more crack, slippage and heaving failures are observed on the surface.

Bottom bituminous layer was cracked as shown in Figure 5. Water infiltrated through this layer and reached to WBM layer. WBM which has finer particles could not drain out water properly and behaves like a clay layer. Therefore, water confines into WBM layer. Even though weather was dry (investigation period), the top of WBM looked dampish. The entrapped water comes out to the bottom of top layer by capillarity action. This water created a thin clay layer at the bottom of top asphalt layer as shown in figure 8. This thin clay layer deactivates tack coat's function and creates a frictionless interface condition and results in interfacial bond failure between top and bottom layers. Interface bond failure

redistributes the stress & strain pattern of pavement. Finally, cracks were developed on surface and made sudden pavement life reduction.

Overloading is frequently observed in NHs in Bangladesh. Permissible standard axle loading is 8.16 ton. According to Bangladesh Road Master plan (2007), 2-3 tones overloading is very common in Bangladesh [2]. So, overloading and interface bond failure may be the coupling factor for drastic life reduction of N_5.

Figure 7: Water moves laterally along the interface

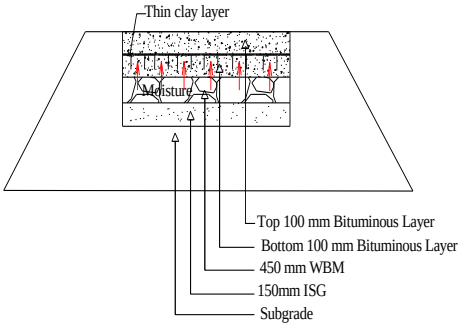

Figure 8: Thin clay layer at the interface

5 PAVEMENT ANALYSIS

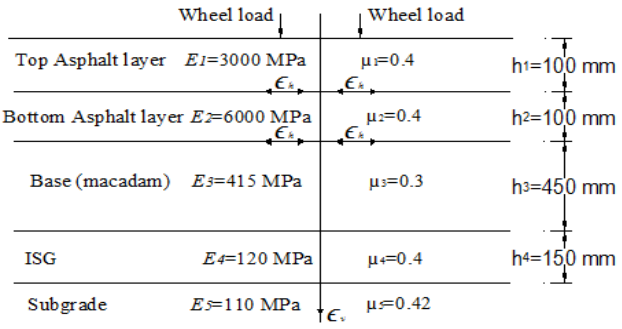

Figure 9: Pavement structure model

Pavement was analyzed by General Analysis of Multi-layered Elastic System (GAMES) software. In GAMES, five interlayer's pavement configuration model was used as shown in Figure 9. Standard axel load of 80kN was used in this model. Fatigue and rutting model coefficients based on Asphalt Institute were used for pavement life calculations which are given below:

$$N_{f1}=0.0796\,\epsilon t^{-3.291} E_1^{-0.854} \quad (1)$$

$$\text{and } N_{f2}= 1.365 E_1^{-09} \epsilon_v^{-4.477} \quad (2)$$

Where, Nf1= allowable number of load repetition to prevent fatigue cracking, Nf2= allowable number of load repetition to prevent rutting cracking, ϵt= tensile strain at the bottom of **A**sphalt layer, ϵv= compressive strain at the top of sub-grade layer, E1= elastic modulus of asphalt layer.

6 RESULT AND DISCUSSION

6.1 Interface bond failure and pavement life

Pavement was analyzed by GAMES to compute horizontal and vertical strain. Horizontal strains are presented on figure 10 with full bond and full slip conditions. Figure 10 indicates that interface condition significantly affects horizontal strain. If all layers of pavement are fully bonded, horizontal strain range is relatively in compressive zone. But for full slip condition, it is tensile dominated. When interfaces bonding condition are poor, cracks are likely to initiate at the bottom of top asphalt layer and maximum tensile strain may occur at the bottom of top asphalt layer. However, in full bond condition, maximum tensile strain occurs at the bottom of bottom asphalt layer. As fatigue and rutting lives are calculated from strains, interface bonding condition greatly affects pavement life. Figure 11 shows that fatigue and rutting lives are longer for full bonded condition than full slip condition. When top and bottom asphalt layers are de-bonded, fatigue and rutting lives are around 10% and 30% of full bond condition; fatigue lives are shorter than rutting. Fatigue failures occur earlier than rutting that was observed in N_5.

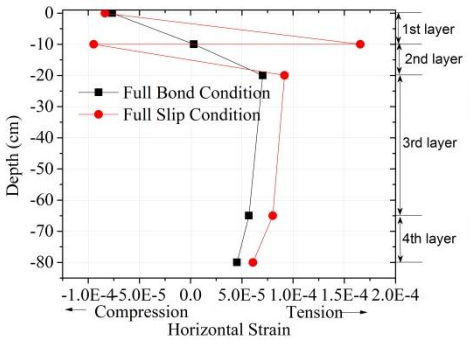

Figure 10: Horizontal Strain Distribution.

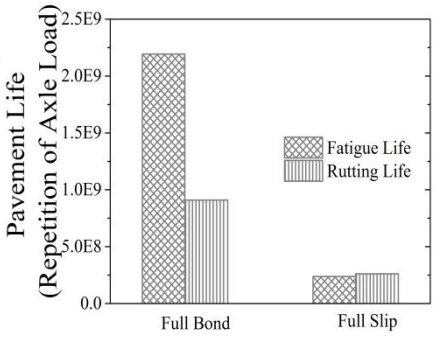

Figure 11: Pavement Life.

6.2 Overloading and interface bond condition on pavement life

The pavement was further analyzed by the coupling of overloading and changing interface bonding condition from full bond to full slip. Figure 12&13 indicate

that the interface bond condition between top and bottom layers is dominant factors for pavement deterioration. At standard axle loading (0 ton), fatigue and rutting life drastically reduces to 10% and 28% respectively. At 2 ton over loading with interface bond failure, it further reduces to 5% and 10% and reaches to zero at 10 tones of overloading. These reduction patterns indicate that pavement life can mostly be affected by bond condition at standard axle loading of 80Kn. If overloading with interface bond failure occurs in pavement, its life reduces to zero immediate after the construction.

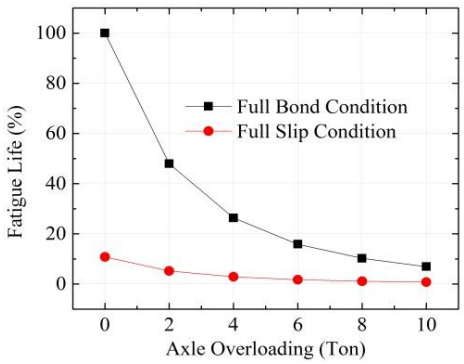

Figure 13: Overloading effect on fatigue life due to change in interface bonding condition.

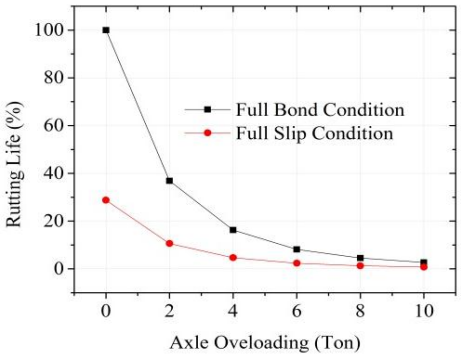

Figure 14: Overloading effect on rutting life due to change in interface bonding condition.

7 PROPOSED MEASURES

Bangladesh's road infrastructure faces severe fund crisis for maintenance works. Due to insufficient fund, the study emphasizes on economic and environmental friendly solution that could be applicable in Bangladesh road maintenance and management practices.

7.1 Long Term Measures

Old asphalt layer should be scarified and the particles should be separated from lumps and then reused these materials as base materials. However, the base should comply with the technical specification of RHD [3]. Finally, bituminous overlay should be placed over the base. Before placing bituminous layer, prime coat is applied to make bond between granular base and asphalt layer. In this measure, one asphalt layer is provided therefore there is no chance of interfacial bond failure between the asphalt layers. However, this measure is expensive and

time consuming process. If recycling technology is adopted in RHD technical specification, this measure could be effective and eco-friendly.

7.2 Short Term Measures

Short term maintenance strategy is important during the rainy season. During rainy season, the top asphalt layers were scarified and removed from the bed and refilled the scarified portion by asphalt materials as shown in figure 14. But, this process was not sustained in the rainy season. Later, top asphalt (100mm thick) layer was removed; brick flat soling and herring bone works applied over the bottom asphalt layer as shown in Figure 15. This works still remains in N_5 pavement which proves successful short term maintenance techniques in N_5.

Figure 14: Top layer removed and re-filled by new asphalt materials

Figure 15: Brick soling and herring bone in N5

8 CONCLUSION

The following findings can be concluded from the study:

- Due to absence of proper interlocking between old and new asphalt layers, poor bond occurred in interfacial position. As a result, early cracks generated in the new surface. A thin clay layer occurred in the interface generated by infiltrating water and pumping action further deteriorates the pavement. Therefore, full slip condition developed in the interface and resulted in early pavement failure.
- Interface bond failure can reduce pavement life by 90% at standard axle loading.
- Pavement life reduces to 5% and zero at 2-3 tones and 10 tons of overloading respectively.

- Further research is needed to find out the effect of layer rigidity on pavement life.

REFERENCES

[1] Roads and Highways Department, Bangladesh: Maintenance and Rehabilitation Needs Report, HDM Circle, 2012.

[2] Ministry of Communication, Bangladesh: Road Master Plan, Roads and Highways Department, Vol. 1, 2007.

[3] Ministry of Communication, "Technical specifications," Bangladesh Roads and Highways Department, Vol. 7, 2011.

CICM 2015
First International Conference on
Advances in Civil Infrastructure and Construction Materials
MIST, Dhaka, Bangladesh, 14–15 December 2015

LABORATORY CALIBRATION OF TIME DOMAIN REFLECTOMETRY (TDR) MEASUREMENTS TO DETERMINE WATER CONTENT AND DENSITY OF UNBOUND GRANULAR PAVEMENTS

M. H. BHUYAN[1], A. Scheuermann[2], D. Bodin[3] and R. Becker[4]

[1, 2] School of Civil Engineering, The University of Queensland,
Brisbane, Australia. Email: [1]h.bhuyan@uq.edu.au, [2]a.scheuermann@uq.edu.au

[3] ARRB Group, Melbourne, Australia.
Email: didier.bodin@arrb.com.au

[4] Rhine-Waal University of Applied Sciences, Germany
Email: rolf.becker@hsrw.eu

Abstract. *Soil water content and dry density of unbound granular pavements are important properties for compaction control which can exert a great influence on pavement performance. Conventional TDR uses probe sensors which provide pointwise readings of moisture content and density. However, proposed TDR method applies long insulated flat ribbon cable as sensors of length up to 6 meter providing spatially distributed information on electric parameters of soil. This paper introduces a new calibration function based on TDR measurements using flat ribbon cable embedded in the soil. TDR signals are analyzed in the laboratory for soil samples of both constant moisture content with different density and different moisture content at constant density. Calibration functions can be used to measure changes in moisture content and density in real pavement for long term pavement performance, like, managing rutting of roads and a flood event.*

Keywords: Moisture content; dry density; laboratory calibration; STDR; unbound granular pavement.

1 INTRODUCTION

Moisture content and density are the most influencing factors of unbound granular materials (UGM) for estimating road performance. Every year in Australia, roads are damaged by heavy vehicles when moisture content of the unsaturated zone has reached a critical value because of heavy rainfall as well as frequent flooding. When the moisture content changes, change in density might be accelerated under cyclic loading. Surface deformation and rutting are correlated with the moisture content and density variation of road materials.

TDR is a remote sensing electrical measurement technique that has been used for many years for various purposes [1]. It was used in telecommunication and computer network for localizing damages in long coaxial cables. Nowadays, it is widely used in civil and agricultural engineering for monitoring soil moisture, localized deformation of rock and soil and monitoring structural deformation as well.

The investigations of Topp et al. [2] formed the basis for the application of TDR for moisture measurement of soil. He developed an equation for deriving moisture content from permittivity measurements which is independent of soil type and density. Other researchers found that the relationship presented by Topp et al. [2] did not work well for organic and clayey soils [3]. Baran [4], Ekblad [5] and Jiang an Tayabshi [6] developed permittivity-moisture content relationships specially for crushed rock aggregates used for pavements.

Non-insulated metallic three rod probe are normally used as transmission lines (Figure 1) for conventional TDR applications. These kinds of probes provide point-wise moisture content measurements as a mean value along the length of the rod. Drnevich et al. [7] developed straight line soil specific relationship to calculate moisture content and density. However, in this relationship, additional parameter, name electrical conductivity, needs to be calibrated to obtain density. Moreover, rod probe sensors have limitation of length (maximum 30 cm).

To avoid the limitation of pointwise measurements and sensor length, Scheuermann et al. [8] proposed insulated flexible flat ribbon cable (FRC) as longer transmission line and successfully used it to observe changes in the moisture content distribution with in a levee model.

Time Domain Reflectometry in combination with FRC will be used in this research for determining moisture content and density of road materials. Spatial time domain reflectometry (STDR) involves the inversion of electrical parameters of TDR pulse which gives water content and density profile along insulated flat ribbon cable.

In this research, Laboratory calibrations are conducted aiming at developing calibration functions for measuring moisture content and density. The developed soil specific calibration functions are used to monitor in-situ moisture content and density variation of real roads.

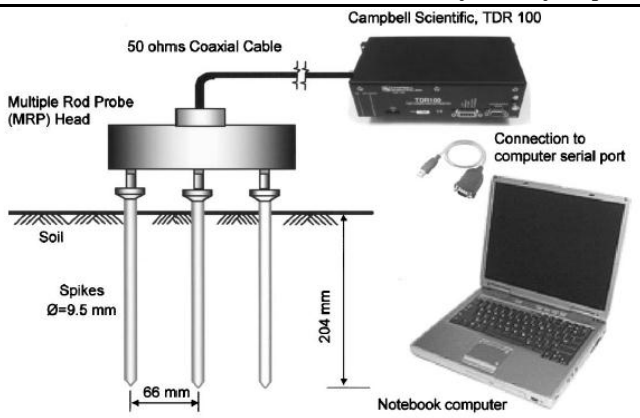

Figure 1: TDR arrangements with three rod probe [7]

2 RIBOB CABLE SENSOR DEVELOPMENTS

Flexible ribbon cable coupled with co-axial cable (Figure 2) can be installed easily during construction. It can be used with lengths of up to 40 m, if mean water contents are to be measured and 6 m, if the aim is to measure a profile [9]. In the capacitance model shown in Figure 3, C1 considers the influence from the permittivity of the surrounding soil; C2 takes into account the influence of the insulation between conductor and C3 between the conductors.

Figure 2: Flat ribbon cable with copper wire and polyethylene insulation connected with co-axial cable (left) and complete two ends ribbon cable sensor (right).

3 TRAVEL TIME DETERMINATION

A typical TDR pulse measured for water is shown in Figure 4. Initial inflection point (A) represents the point at which the pulse enters the sensor and the final inflection point (B) indicates the point at which the pulse passes the sensor. Using tangent method, the time difference between the two inflection points can be obtained. The travel time varies with the variation of electrical properties of the soil surrounding the sensor.

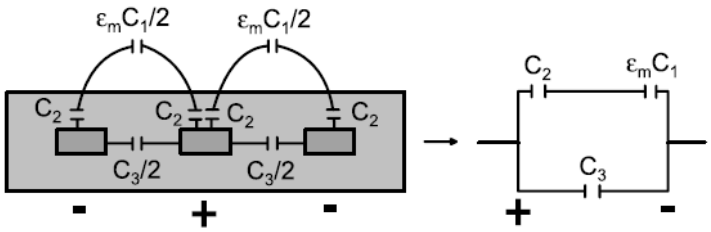

Figure 3: Capacitance model of the flat ribbon cable (Scheuermann et al. 2009) [8]

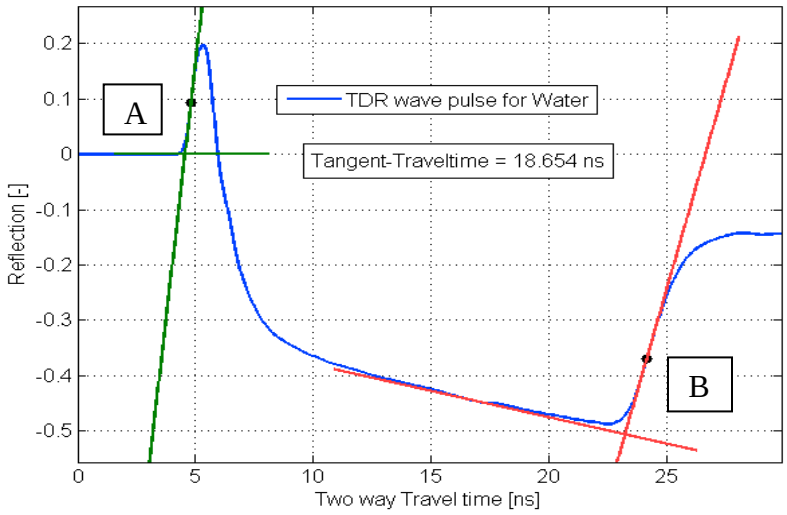

Figure 4: Tangent method to obtain travel time from reflected TDR pulse

4 PERMITTIVITY CALCULATION

The dielectric permittivity indicates how easily a material can become polarized by imposition of an electric field on an insulator. Since the permittivity of water is high compared to soil and air, dielectric permittivity indicates the amount of moisture in the soil. Mean capacitance, $C(\varepsilon_m)$ is a function of individual capacitance and permittivity. It is calculated using equation 1 where wave velocity, v is known and impedance, L=7.56*10^{-7} is constant.

$$v = \frac{\text{length of ribbon cable}}{\text{one way travel time}} = \frac{1}{\sqrt{L * C(\varepsilon_m)}} \qquad (1)$$

Permittivity, ε_m from equation 2 can be obtained where capacitances C1 = 3.4*10^{-12}, C2 = 23*10^{-12}, C3 = 4.8*10^{-12} are constant for fixed geometry of sensor.

$$C(\varepsilon_m) = \frac{\varepsilon_m * C1 * C2}{\varepsilon_m * C1 + C2} + C3 \quad (2)$$

5 LABORATORY CALIBRATION

Typical road base material was collected from Queensland Department of Transport and Main Roads (DTMR). A calibration box of 55 cm x 15 cm x 16 cm made of PVC sheets for soil specific calibration. The soil sample is compacted in three layers with the FRC sensors placed in between.

Soil sample of different moisture contents with constant density has been prepared. Volumetric water content is obtained from laboratory calibration data using the following Equation 3.

$$\theta = a_0 + a_1\varepsilon_m + a_2\varepsilon_m^2 + a_3\varepsilon_m^3 \quad (3)$$

Where a_0 to a_3 are calibration constants, θ is the Volumetric Water Content (VWC) and ε_m is the permittivity. Finally, permittivity-VWC relationship has been obtained for FRC sensor which is presented in Figure 6 with other established models. Permittivity-VWC is suited perfectly with the Baran (1994) and Ekblad (2007) models which were developed particularly for coarse materials.

Figure 5: Placement of FRC sensor between soil layers in the calibration box

6 DENSITY MEASUREMENT

With the same laboratory setup mentioned in section 5, road base material of 85% to 100% maximum dry density (mdd) has been prepared and TDR wave pulse was obtained. It is observed that with increasing density, the voltage drop (figure 7) of the reflected TDR pulse between the ends of the sensor increases. It needs to be mentioned here that travel time increases with increasing moisture content of the soil sample but is not very much influenced by the density. The following empirical equation 4 is proposed for measuring density.

$$\text{Dry density, } \rho_d \text{ (kg/m}^3\text{)} = 10^4 * \text{LN(TT)} * V \quad (4)$$

Where, TT is the two way travel time of TDR pulse in nS, V is the voltage drop.

To evaluate this empirical equation, a second set of experiments have been done with different densities. The density has been calculated using equation 4 and compared with test data (Figure 8). The calculated and measured densities are scattered around 1-1 line and fall within the range of 4% boundary line.

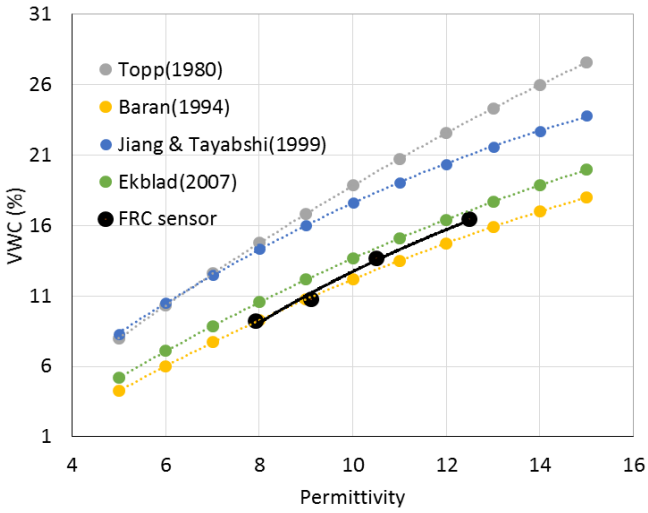

Figure 6: Permittivity measurement using FRC sensor

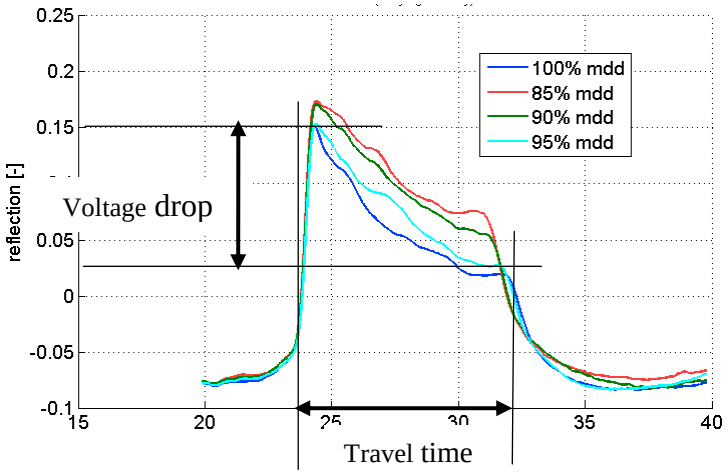

Figure 7: TDR pulse showing Voltage drop (V) and travel time

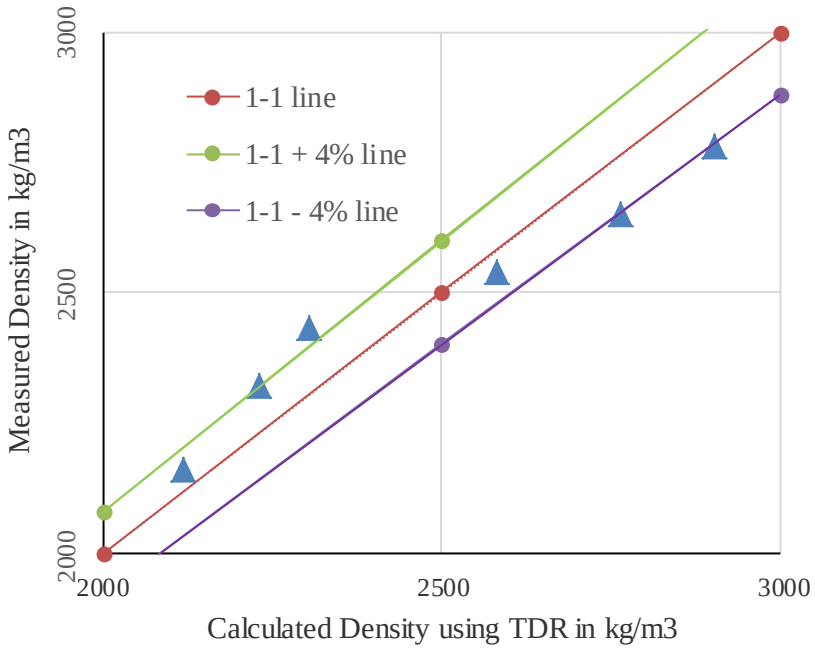

Figure 8: Comparison of measured and calculated density

7 CONCLUSION

The most significant state variable influencing the functionality of unbound granular pavement is the moisture content. When the moisture content changes, change in density might be accelerated under cyclic loading. This paper describes the determination of in situ moisture content and density using TDR along flat ribbon cable sensor. The permittivity-VWC relationship corresponds very well with the well-known Baran (1994) [4] and Ekblad (2007) [5] models. Moreover, calculated density with TDR matches well with the results from laboratory.

This non-destructive method of measuring moisture content and density can be used in real pavements for providing data which can be used to optimize management of roads. As a consequence, roads can me managed in case of critical moisture content as flood or flash flood events.

The Aim in future is to determine profile of moisture and density using Spatial TDR.

ACKNOWLEDGEMENTS

This research is funded by a Queensland Science Fellowship awarded by Dr Alexander Scheuermann. The first author acknowledges The University of Queensland for providing fund for his scholarship.

REFERENCES

[1] Andrew, J.R., 1994. Time Domain Reflectometry. Proceedings of the symposium on TDR in environmental, infrastructure and mining applications, Evaston, Illinois, U.S. Bureau of Mines, SP 19-94, NTIS PB95-105789, PP 4-13.

[2] Topp, G. C., Davis, J. L., and Annan, A. P., 1980. Electromagnetic determination of soil water content measurements in coaxial transmission lines. Water Resources Research, 16, 574–582.

[3] Dasberg, S.; Hopmans., 1992. J.W. Time domain reflectometry calibration for uniformly wetted sandy and clayey soils. Soil Science Society of America Journal, v.49, p.293-297.

[4] Baran E., 1994. Use of TDR for monitoring moisture changes in crushed rock pavements. Symposium and Workshop on TDR in Environmental, Infrastructure, and Mining Applications, Northwestern University, Illinois, USA.

[5] Ekblad J., 2007. Thesis Paper http:// www.divaportal.org/smash/ get/ diva2:11827/ FULLTEXT01.pdf

[6] Drnevich, V. P., Ashamawy, A. K., and Sallam, A. M., 2005. Time Domain Reflectometry for Water Content and Density of Soils: Study of Soil-Dependent Calibration Constants. Can. Geotech. J., Vol. 42, pp. 1053–1065.

[7] Jiang YJ & Tayabji SD, 1999. Analysis of Time Domain Reflectometry Data from LTPP Seasonal Monitoring Program Test Sections. Final Report, FHWA-RD-99-115, Federal Highway Administration, McLean, VA.

[8] Scheuermann, A., Hu¨bner, C., Schlaeger, S., Wagner, N., Becker, R., and Bieberstein, A., 2009. Spatial TDR and its Application for the Measurement of Water Content Distributions along Flat Ribbon Cables in a Full-Scale Levee Model. Water Resour. Res., Vol. 45, pp. W00D24.

[9] Stacheder, M., C. Huebner, S. Schlaeger, and A. Brandelik. (2005). "Combined TDR and low frequency permittivity measurements for continuous snow wetness and snow density determination." Electromagnetic Aquametry, edited by K. Kupfer, pp. 367– 382, Springer, Berlin.

CICM 2015
First International Conference on
Advances in Civil Infrastructure and Construction Materials
MIST, Dhaka, Bangladesh, 14–15 December 2015

APPLICATION OF SEISMIC REFRACTION METHOD TO INVESTIGATE SOIL STRUCURE OF DHAKA CITY

A. KHAIR[1], B. S. P. Biswas[2] and M. A. Ansary[3]

[1, 2, 3] Bangladesh University of Engineering and Technology,
Dhaka, Bangladesh
Email: [1]akhairce08@gmail.com, [2]pushpendue.biswas@gmail.com,
[3]ansary@ce.buet.ac.bd

Abstract. *This paper discussed the seismic refraction survey conducted to investigate subsurface structure of different locations of Dhaka city. In this study, one energy source and 24 geophones were used for the survey. The investigated depths depend on spread length and energy source. The depth is proportional to impulse energy and spread length. It has been observed that 2 to 3 meter geophone spacing and 140lb weight with a fall height of 5 to 10 feet is suitable in our mechanism. For enhancing the result more energy is required as energy source. Currently we are trying to develop a mechanical system to enhance the energy. From the collected data time – distance curves for each shot points were drawn, the velocities of the underlying layers for each point were obtained and the depths to the refractor layer were computed. The results obtained provide an overview of the lateral and vertical variation in the lithological changes of the subsurface earth materials together with the shear-wave velocity in the surveyed area.*

Keywords: Impulse energy, Seismic refraction, Shear wave velocity, Subsurface structure.

1 INTRODUCTION

Seismic refraction is a commonly used geophysical technique to determine depth-to bedrock, competence of bedrock, depth to the water table, or depth to other seismic velocity boundaries. This method involves the analysis of the travel times of arrivals that travelled roughly parallel to the upper surface of a layer during their transmission through the subsurface. [1]Seismic refraction measurements are applicable in mapping subsurface conditions for various uses including geological, geotechnical, hydrological, environmental, mineral and archaeological investigations.

2 STUDY BACKGROUND

The seismic refraction survey has application in a variety of geological exploration problems, where information on the depth and strength of subsurface materials is required. These surveys provide subsurface information over large areas at relatively low cost; locate critical areas for more detailed testing by drilling and can readily eliminate less favorable alternative sites. Seismic surveys can also reduce the number of boreholes required to test a particular site and improve correlation between boreholes.

2.1 Advantages / Disadvantages

- Difficulty of interpretation in areas morphologically rough or with many underground pipes
- Open spaces is needed for cables and electrodes array, the electrodes must be planted into the ground (can also be applied in paved areas or asphalt, drilling holes).
- Good vertical and lateral stratigraphic resolution.
- For best accuracy, a calibration reference stratigraphy is needed.
- Very useful for discrimination of metal, clay / sand and aquifers

2.2 Fundamental Theory

The refraction method consists of measuring (at known points along the surface of the ground) the travel times of compressional waves generated by an impulsive energy source [4]. The energy source is usually a small explosive charge and the energy is detected, amplified, and recorded by special equipment designed for this purpose. The instant of the explosion, or "zero-time," is recorded on the record of arriving pulses. The raw data, therefore, consists of travel times and distances, and this time-distance information is then manipulated to convert it into the format of velocity variations with depth. The interpretation of this raw data will be developed as we go along. The process is schematically illustrated in Fig. 1.

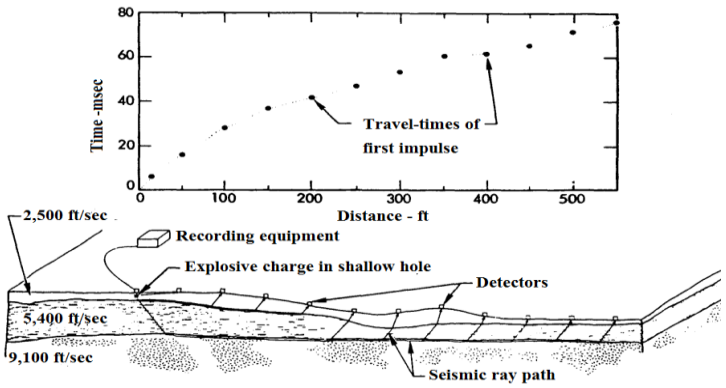

Figure 1: Schematic of seismic refraction survey

The fundamental law that describes the refraction of light rays is Snell's Law (see Fig. 2), and this, together with the phenomenon of "critical incidence," is the physical foundation of seismic refraction surveys.

A small explosive charge is detonated in a shallow hole at A and the energy is detected by a set of detectors laid out in a straight line along the surface. The arrival times of the impulses are plotted against the corresponding shot-to-detector distances as shown in Fig. 3. The first few arrival times are those of direct arrivals through the first layer, and the slope of the line through these points, $\Delta T/\Delta X$, is simply the reciprocal of the velocity of that layer; i.e., V_1/V_2. The energy that arrives at the detectors beyond the critical distance will plot along a line with a slope of V_1/V_2

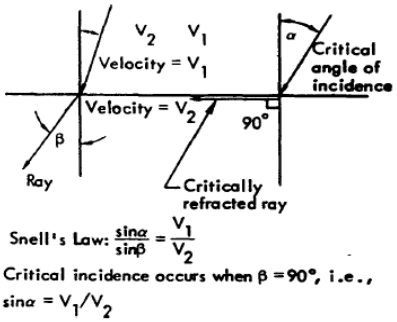

Figure 2: Snell's law and refraction of ray transmitted across boundary between two media with different velocities.

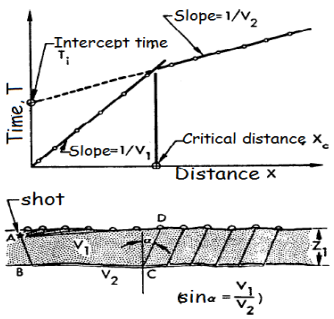

Figure 3: Simple two-layer case with plane, parallel boundaries and corresponding time-distance curve.

The rock types are classified by knowing the seismic velocity transmitted to the soil. The verities of seismic velocity of different layers indicated different types of soil [5]. There is an approximate range to classify rocks depends on seismic velocities.

Table 1: Approximate seismic velocities for rocks

Rock type	V_p(km/sec)	Rock type	V_p(km/sec)
Unconsolidated sediment		sandstone	2.0-5.0
Clay	1.0-2.5	Others	
Sand, dry	0.2-1.0	Air	0.3
Sand, saturated	1.5-2.0	Natural gas	0.43
Sedimentary Rocks		Ice	3.4
Limestone	3.9-6.2	Water	1.4-1.5
Salt	4.6	Oil	1.3-1.4

3 METHODOLOGY

3.1 Study Area Selection

The different locations of Dhaka city are selected as the study area. The locations are selected upon some criteria such as free open space, less noisy area, dominating soil characteristics of that region, land use characteristics etc. The map and table below show the location of the study area.

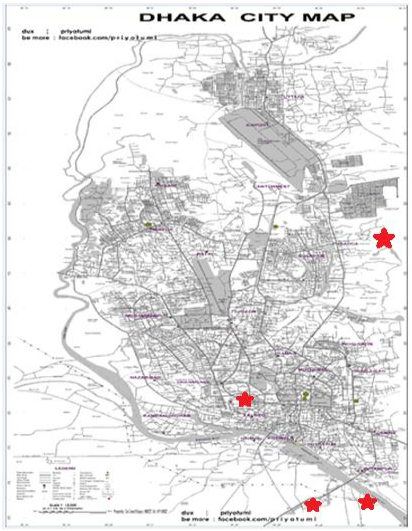

Fig 4: Location of study points in Dhaka city

Table 2: List of the study points of Dhaka city

Sl. no	Date	Points of Study Area	Location		City
			Latitude	Longitude	
01	14/11/2014	Garden ,Civil Building, BUET	23° 43' 19" N	90° 23' 48" E	Dhaka
02	13/11/2014	Vatara, Gulshan	23° 47' 39" N	90° 26' 40" E	Dhaka
03	14/11/2014	Bashaundhara River View, Keranigong	23° 39' 45" N	90° 26' 25" E	Dhaka
04	14/11/2014	New Jail, Keranigong	23° 39' 07" N	90° 23' 03" E	Dhaka

3.2 Data Collections and Results Analysis

The data of the different locations were collected using different combination of seismic impulse source and different spacing of geophones. Some specific software based on conventional method was needed to process seismic refraction.

3.2.1 Seismic refraction result analysis for soil at BUET

The geophone spread and impulse source is shown in Fig. 5 and Fig. 6 respectively during seismic refraction test at BUET. Five shot points were selected during this test named as middle shot, 1st offset shot, 1st end shot, last end shots and last offset shot and the positions of two offset shots 23 m away from 1st and last geophone, which is half of the total spread length 46m as shown in Fig. 7.

Figure 5: Spread of geophones during refraction test at BUET

Figure 6: Using 140lb hammer as impulse source

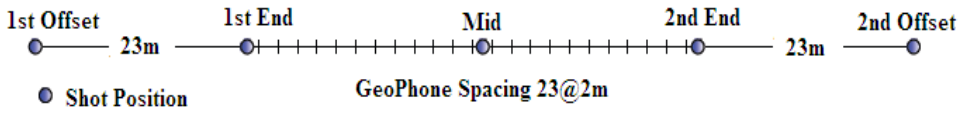

Figure 7: Layout of shots position during seismic refraction test at BUET

The soil profile of the seismic refraction test is shown in Fig. 8. It shows that the investigation depth of soil profile is about 30m. The seismic velocity ranges is about to 150m/s to 350m/s which range indicates the sub soil is dry sand according to Table 1.

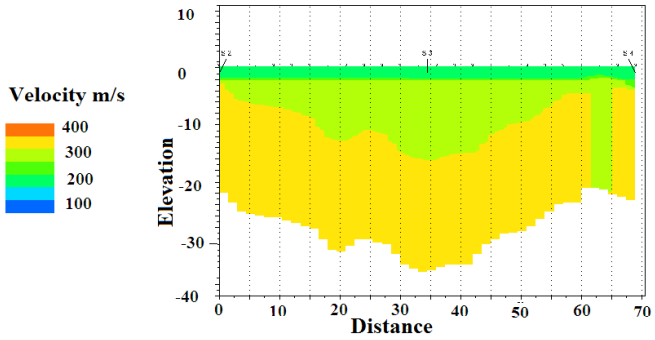

Figure 8: Soil profile at BUET playground using seismic refraction

3.2.2 Seismic refraction result for soil at Vatara

The soil profile of the seismic refraction test is shown in Fig. 9. It shows that the investigation depth of soil profile is about 30m. The seismic velocity range is about to 150m/s to 290m/s which range indicates the sub soil is dry sand.

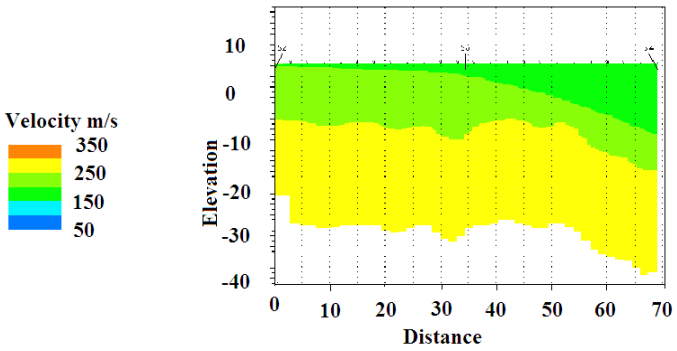

Figure 9: Soil profile at Vatara using seismic refraction

3.2.3 Seismic refraction result for soil at Bashundhara River View:

The soil profile of the seismic refraction test is shown in Fig. 10. It shows that the investigation depth of soil profile is about 35m. The velocity range is about to 50m/s to 250m/s which range indicates the sub soil is dry sand.

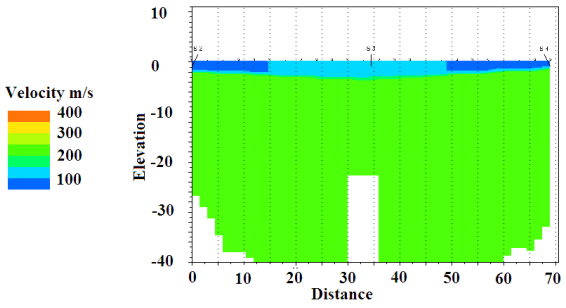

Figure 10: Soil profile of Bashundhara river view

3.2.4 Seismic refraction result for soil at Outside of New jail

The soil profile of the seismic refraction test is shown in Fig. 11. It shows that the investigation depth of soil profile is about 18 m. The velocity range is about to 150 m/s to 280 m/s which range indicates the sub soil is dry sand.

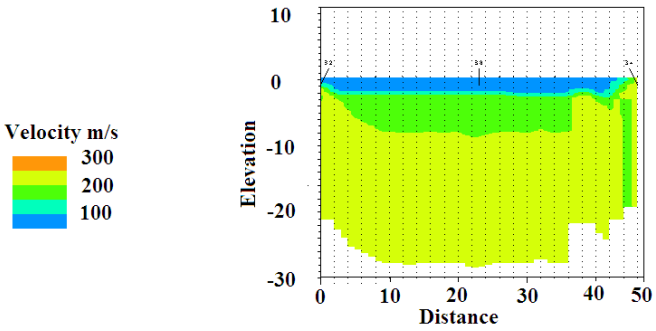

Figure 11: Soil profile beside new jail using seismic refraction

4 CONCLUSION

The interpretation of the results shows that all areas having consisted of two layers with approximate velocity 100 to 500 m/s underlie the study area. Table 1 indicates approximate ranges for velocities of different types of soil. The upper layer of surveyed areas consists of sand and sandy clay. The result of the investigation is therefore recommended as a useful guide for civil engineering planning and development of the area.

5 LIMITATIONS

A hidden layer, or blind layer, is one that is undetectable by refraction surveying [2]. A layer may simply not give rise to first arrivals, that is, rays traveling to

deeper levels may arrive before those critically refracted at the top of the layer in question (see Fig. 12). This may result from the thickness of the layer or from the closeness of its velocity to that of the overlying layer. A more insidious type of hidden layer problem is associated with a low velocity layer, as illustrated in Fig. 13. Rays cannot be critically refracted at the top of such a layer and the layer will, therefore, not give rise to head waves. Hence, a low velocity layer cannot be detected by refraction surveying.

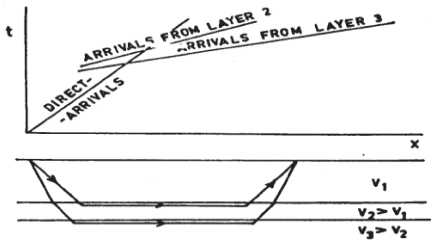

Figure 12: Hidden layer problem in seismic refraction

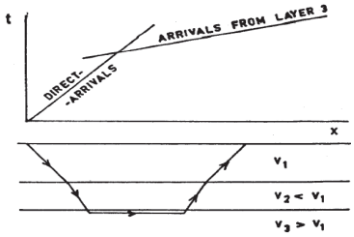

Figure 13: Blind zone problem in seismic refraction

Due to lack of available impulse sources the seismic refraction test is difficult in maximum places. Also we have no sufficient financial help to buy such type of high cost impulse sources. Hence here in Bangladesh seismic refraction test is not workable yet to investigate subsoil characteristics.

REFERENCES

[1] Alhassan, D. U., Dangana, L.M., Salako, K.A., Jonah, S.A. and Ofor, seismic refraction investigation of the subsurface structure at the southern part of niger state college of education, Bayero Journal of Pure and Applied Sciences, 3(2): 56 – 61

[2] Geological exploration by geophysical method (seismic refraction) —code of practice, burau of indian standard, is 15681:2006 , pp.8-15

[3] Keller G.R, Sinno Y.A, and Sbar M.L (1981). Seismic refraction in West and central Arizona, journal of Geophysical Research, New York, U.S.A, Vol. 86 ,No. 36, PP5023

[4] Redpath B. B., A book of "Seismic refraction exploration for Engineering site investigations" Explosive Excavation Research Laboratory Livermore, California, May 1973

[5] www.geo2X.com

CICM 2015
First International Conference on
Advances in Civil Infrastructure and Construction Materials
MIST, Dhaka, Bangladesh, 14–15 December 2015

PARAMETRIC STUDY OF GEOTEXTILE REINFORCED EARTH RETAINING WALL

Md. S. ISLAM[1] **and Md. J. Alam**[2]

[1, 2] Department of Civil Engineering, Bangladesh University of Engineering Technology, Dhaka, Bangladesh
Email: [1]shafik.buet@gmail.com and [2]jahangir.buet@gmail.com

Abstract. *Generally, the analysis of geotextile reinforced earth walls is performed using the simplified classical analysis or empirical methods which include a lot of assumptions and strenuous calculations. In this paper, the effect of various soil parameters on the required base length of reinforcement, load eccentricity and miscellaneous factor of safety is studied by using the MSEW (3.0) software. Base length of reinforcement decreases with the increase in angle of internal friction of reinforced soil. As a result, Factor of safety against overturning, sliding and bearing capacity decreases with the increase in angle of internal friction of reinforced soil. Factor of safety against bearing capacity and sliding increased with the increase in cohesion of reinforced soil. The results of this study will help to evaluate different soil profiles for designing reinforced soil walls and eventually understand the behavior of the geotextile reinforced soil wall.*

Keywords: Geotextile, Reinforced earth walls, Angle of internal friction, Unit weight, Cohesion, Factor of safety

1 INTRODUCTION

An earth retaining wall is a basic civil engineering structure which is comprised of a wall along with sufficient support of reinforcement. The technique of reinforced soil has been widely used in the hilly or steep slope areas especially in construction of retaining walls and levee foundations. A wide range of reinforcement elements of different materials is produced and developed for use in such structures. Geotextiles, nowadays have become the most convenient type of reinforcement used for supporting retaining wall as well as stabilizing loose soil or strengthening any soil mass beneath the structure. Soils have good resistance against compression, but are weak in tension. Numerous efforts are performed to overcome the weakness of the soil. Geotextiles are compatible with the soil in deformability. Also, they are resistant to corrosion and acid attacks.

Many investigators have studied the reinforced soil walls. Among them, Abi-oghli [1] performed a parametric study to study the reinforced earth walls with finite element method using PLAXIS software and found relationships of angle of internal friction, cohesion and stiffness of reinforcements with the deformation of facing and displacement of the wall. Siddiquee and Alam [2] performed a parametric study on the behavior of anchored earth wall. They observed that deformation of wall decreases with increasing stiffness of reinforcement and after certain value of stiffness it has no effect on deformation. On the other hand, anchor force increases with increasing stiffness of reinforcement and after a certain limit, it has no effect on anchor force. Wong et al. [3] studied failure modes of the geotextile reinforced earth wall. Their observed failure modes are block sliding and slope failure. Other potential modes of failure are rupture of the reinforcements, bearing capacity and overall stability.

2 METHODOLOGY

In this paper, the soil-geotextile interrelationship in the design of geotextile reinforced soil walls is studied by MSEW (3.0) software. Geometry of model wall is shown in Figure 1. Certain soil parameters are selected based upon their effect over some other internal and external geotextile design parameters. The soil parameters are the angle of internal friction of reinforced soil, unit weight of reinforced soil and cohesion of foundation soil. The output parameters are the required base length of geotextile reinforcement, the load eccentricity, the factor of safety against bearing capacity, factor of safety against sliding, factor of safety against overturning and overall factor of safety against the tensile strength of geotextile. The value of the soil parameters is varied within some practicable range and their commensurate effect upon other output parameters is observed by MSEW (3.0).

3 RESULTS AND DISCUSSION

Here, the results of the parametric study are presented. At first, the wall model is presented in Figure 1 which is comprised of a back slope, strip load, embedment and predefined soil profile. And then the effect of the angle of internal friction of reinforced soil, unit weight of reinforced soil and cohesion of foundation soil to the output parameters is presented.

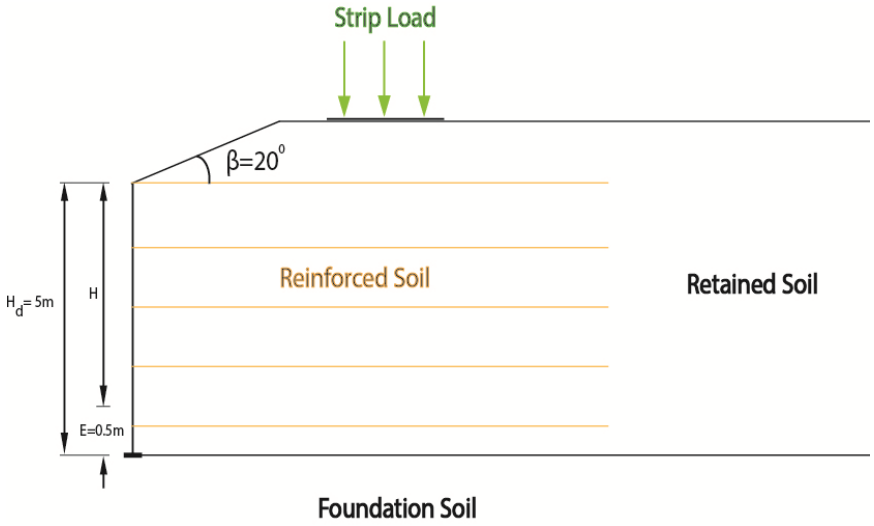

Figure 1: Geometry of the model reinforced soil wall.

3.1 Effect of Angle of Internal Friction of Reinforced Soil

The angle of internal friction (ϕ) of reinforced soil was varied keeping other parameters unchanged. Values of unchanged parameters are shown in Table 1. Figure 2 shows the effect of angle of internal friction of reinforced soil to the required base length of geotextile reinforcement, the load eccentricity, the factor of safety against bearing capacity, factor of safety against sliding, factor of safety against overturning and the overall factor of safety against tensile strength of geotextile respectively.

The effect of angle of internal friction of reinforced soil varies for different parameters. The load eccentricity and the overall factor of safety against geotextile strength increases nonuniformly with the increase in angle of internal friction of reinforced soil. The base length of reinforcement, factor of safety against bearing capacity and factor of safety against overturning reduces with the increase in angle of internal friction of reinforced soil.

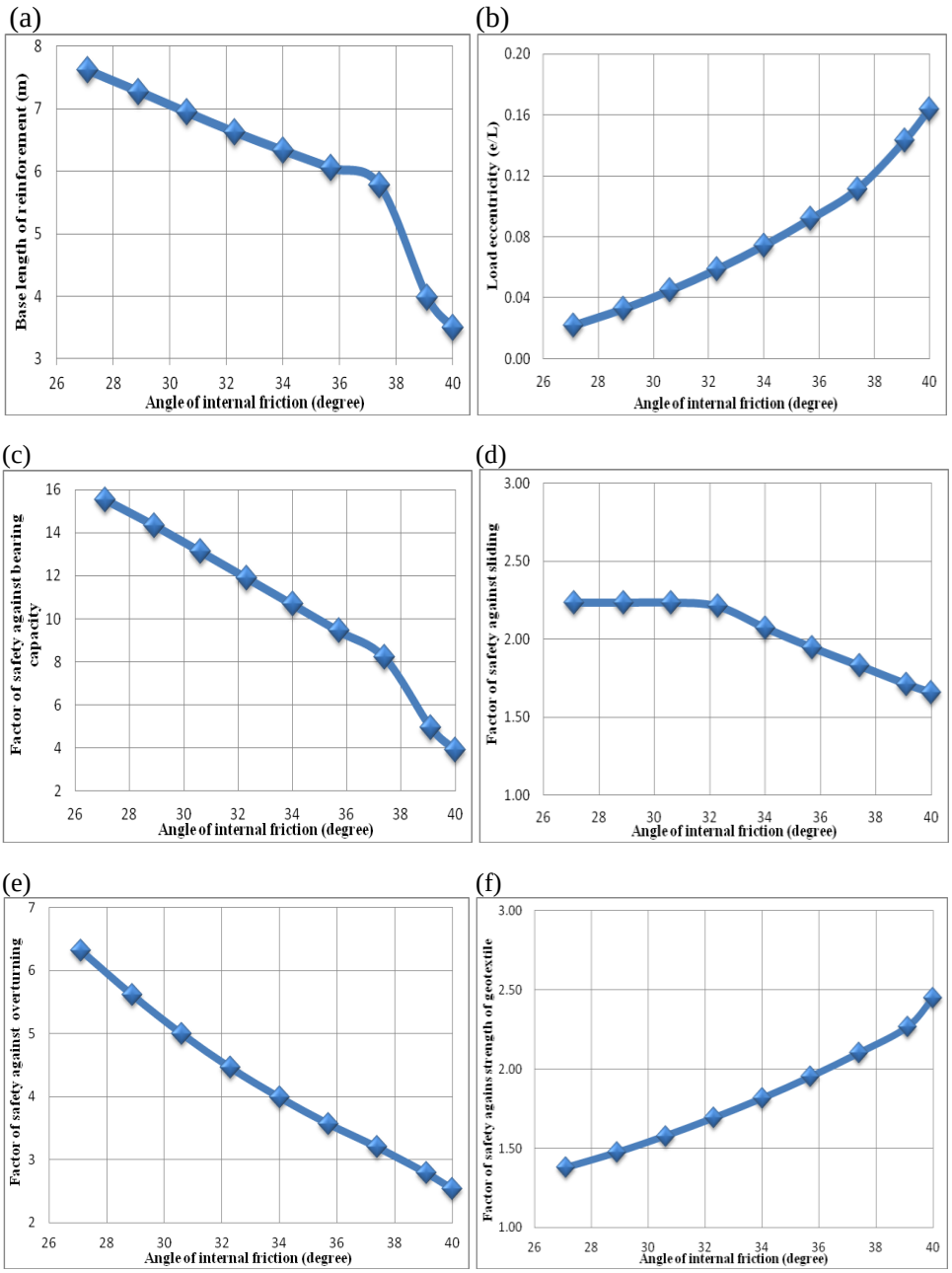

Figure 2: Effect of angle of internal friction of reinforced soil to (a) required base length of geotextile reinforcement, (b) load eccentricity, (c) factor of safety against bearing capacity, (d) factor of safety against sliding, (e) factor of safety against overturning and (f) overall factor of safety against tensile strength of geotextile.

With the increase of angle of internal friction, the required base length of reinforcement decreases which is the cause of decreasing the factor of safety against bearing capacity and overturning [4]. The factor of safety against sliding remains constant or is reduced by a little amount with the increase in angle of internal friction.

3.2 Effect of Unit Weight of Reinforced Soil

The unit weight (γ) of reinforced soil is varied. Figure 3 shows the effect of unit weight of reinforced soil to the required base length of geotextile reinforcement, the load eccentricity, the factor of safety against bearing capacity, factor of safety against sliding, factor of safety against overturning and the overall factor of safety against tensile strength of geotextile respectively. The load eccentricity and the factor of safety against sliding increases with unit weight of reinforced soil although the slope of later one is very negligible. The base length of reinforcement, factor of safety against bearing capacity, factor of safety against overturning and overall factor of safety against tensile strength of geotextile reduces with increase in unit weight of reinforced soil with nonuniform slope.

3.3 Effect of Cohesion of Foundation Soil

The cohesion (C) of foundation soil was varied. Figure 4 shows the effect of unit weight of reinforced soil to the factor of safety against bearing capacity and factor of safety against sliding respectively. The factor of safety against bearing capacity and sliding increases with the increase in cohesion of foundation soil. The later one has a very negligible slope.

Table 1: Unchanged and changed soil parameters.

Parameter changed	Parameter unchanged	Parameter unchanged
ϕ^*	γ = 20 kN/m^3	C = 0 kN/m^3
γ^*	C = 0 kN/m^3	$\phi = 34^0$
C*	γ = 20 kN/m^3	$\phi = 34^0$

* ϕ – Drained angle of internal friction of reinforced soil,
γ - Unit weight of reinforced soil,
C – Drained cohesion of foundation soil

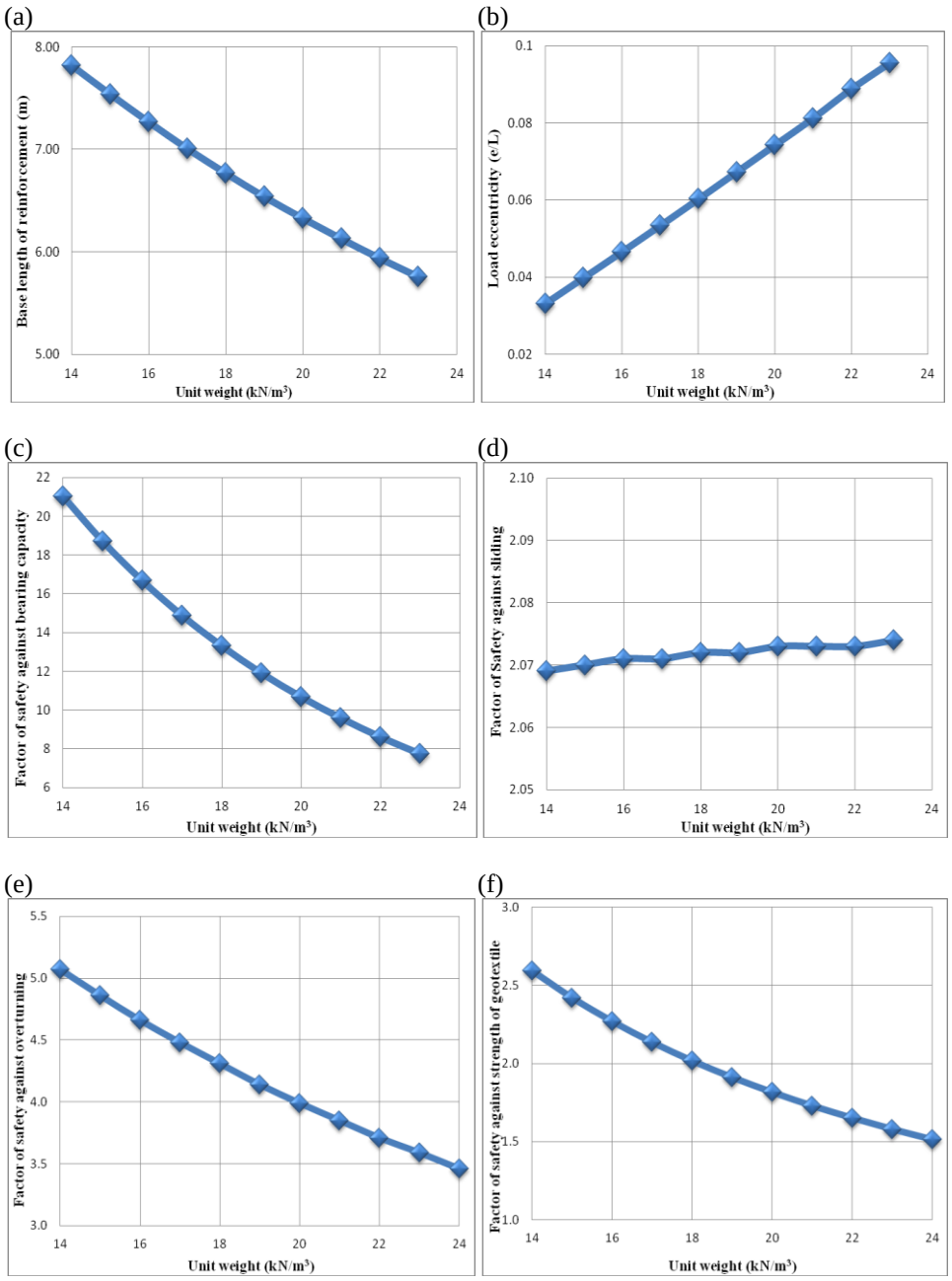

Figure 3: Effect of unit weight of reinforced soil to (a) required base length of geotextile reinforcement, (b) load eccentricity, (c) factor of safety against bearing capacity, (d) factor of safety against sliding, (e) factor of safety against overturning and (f) overall factor of safety against tensile strength of geotextile.

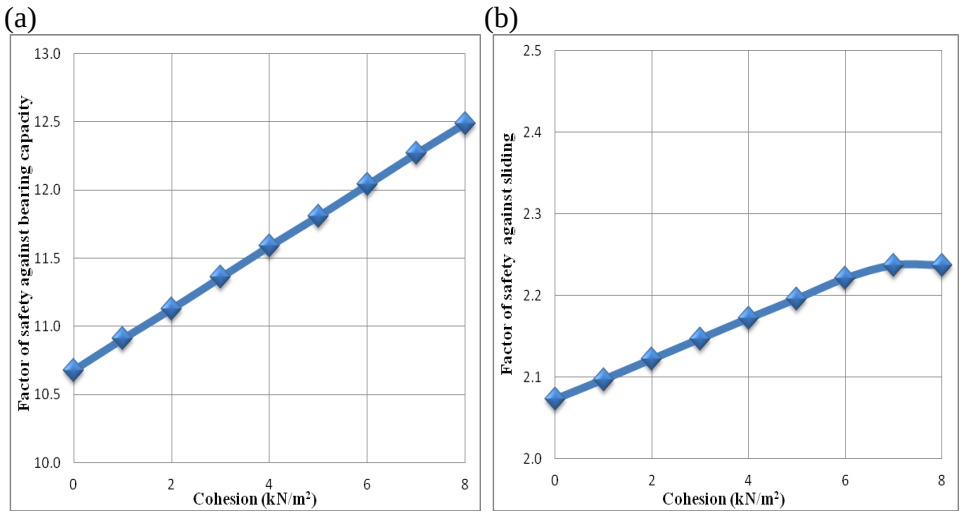

Figure 4: Effect of cohesion of foundation soil to (a) factor of safety against bearing capacity and (b) factor of safety against sliding.

4 CONCLUSIONS

In this paper, the effect of various soil parameters on the factor of safety is studied by using the MSEW (3.0) software. Base length of reinforcement decreases with the increase in angle of internal friction of reinforced soil. As a result, factor of safety against overturning, sliding and bearing capacity decreases with the increase in angle of internal friction of reinforced soil. Similar results were found for unit weight of reinforced soil. Factor of safety against bearing capacity and sliding increased with the increase in cohesion of foundation soil. The results of this study will help to understand the behavior of the geotextile reinforced soil wall and will assist to prepare a design manual for any kind of soil profile.

REFERENCES

[1] Abioghli, Hadi, "Parametric Study of Reinforced Soil Walls with the Finite Element Method", Australian Journal of Basic and Applied Sciences, 5 (10): 940-944, 2011 ISSN 1991-8178

[2] Siddiquee M. S. A and Alam M. J. (2005). "Effect Of Stiffness Of Reinforcing Tendon On The Behavior Of Anchored Earth Wall Supporting Soft Backfill", Proceedings of the Eastern Asia Society for Transportation Studies, Vol. 5, pp. 829 – 844.

[3] Wong K. S., Broms B. B. and Chandrasekaran B. (1994). "Failure modes at model tests of a geotextile reinforced wall", Geotextiles and Geomembranes, Volume 13, Issues 6–7, pp. 475-493.

[4] Koerner, Robert M., Designing with Geosynthetics, 4th edition, 2nd Chapter, pp 181-202

CICM 2015
First International Conference on
Advances in Civil Infrastructure and Construction Materials
MIST, Dhaka, Bangladesh, 14–15December 2015

FACTORS AFFECTING TRANSACTION COSTS IN BRUNEI CONSTRUTION

M. Motiar RAHMAN[1] **and Noor Hadijah**[2]

[1, 2] InstitutTeknologi Brunei, Gadong, Brunei Darussalam
Email: [1]motiar.rahman@itb.edu.bn and [2]hadijah.hadi@itb.edu.bn

Abstract. *The price to the contractor for constructing a project becomes cost to the client. In addition to such production cost, there are also transaction costs (TCs) to clients, e.g. costs of preparing bidding documents, drawing up a contract, selecting a contractor, administering the contract and dealing with any deviations from contract conditions. Examples of TCs incurred by contractors include preparing the bids, cost of bid bonds, cost of any risks, cost of delayed payments and cost of unsuccessful bids. Such TCs may vary from project to project, but are presumably included in contractors' bid price in the form of overheads and profits. However, they are frequently seen to be ignored, or not given proper attention to. Moreover, there is a perceived lack of established information on exactly what factors contribute to TCs in Brunei construction industry and their degree of impact on TCs. With such background, the present paper summarizes the interim outcomes from an ongoing study, and focused on responses from clients and consultants. A set of factors have been identified that affect TCs. Some of these factors are identified as more critical than some other factors. Next step will be to focus on collecting responses from contractors, before identifying a set of strategies for minimizing TCs in Brunei Construction.*

Keywords: Brunei, Clients, Construction, Consultants, Transaction costs.

1 INTRODUCTION

Transaction Cost Economics (TCE) considers the transaction as the basic unit of analysis in the study of economic organization, and any problem that can be posed directly or indirectly as a contracting problem is usefully investigated in TCE terms [1].A transaction occurs when a good or service is transferred across a technologically separable interface. The main contention is that, in addition to the cost of production, there are also transaction costs (TCs) between the parties [2]. TCs include the cost of "effort to identify, explicate and mitigate contractual hazards' [3].

For TCE analysis, the organization of construction projects is considered as 'organization' [2, 4]. It is implied in relevant literature that cost of production may be what it actually takes, so the focus is to reduce TCs. TCs in construction include: the costs originating from setting objectives, integrating contributions, making the various managerial decisions and controlling the contributors[5]. All these are aimed at achieving client's objectives. It is therefore important for clients to determine, before entering into contracts, their requirements and objectives, characteristics of proposed transaction(s); and the factors that cause transactional difficulties [6].

Examples of TCs relating to client include: the costs of preparing a bidding document, selecting a contractor, administering the contract and dealing with any deviations from contract conditions. Examples of TCs by contractors include preparing the bids, estimating, cost of bid bonds, cost of delayed payments and cost of unsuccessful bids. These costs may vary from project to project, and depend on the project management efficiency, uncertainty in the transaction (i.e. construction project) environment, and nature/behavior of the client [7]. Whether low or high, such costs are presumably included in contractors' bid price in the form of overheads and profits, on which clients can guess from any locally available construction cost data. However, it was revealed in a recently held seminar by the Ministry of Development, Brunei that contractors' bids to public contracts are alarmingly higher than the available construction cost hand book [8]. This indicated the existence of unknown/hidden TCs that contractors suffer. Present research project was therefore undertaken to investigate the underlying issues and to suggest relevant remedial measures, aiming at minimizing TCs in Brunei construction industry in particular and in construction in general.

2 RESARCH METHODOLOGY

The overall research project was designed with literature review, two questionnaire surveys and one interview based survey. Present paper summarizes interim outcomes of the study, on the basis of ongoing first questionnaire survey.

The objectives of this paper are to identify and prioritize the factors that affect TCs in construction. Data was collected from clients and consultants using a

questionnaire, which was designed to meet the above objectives, pilot-tested by three industry experts, and improved based on the opinions obtained from the experts. Among three, Section 1of the questionnaire included an 'introduction' clarifying the concept of TC and solicited opinions of the respondents. Section 2 was designed to collect information of the respondents. Section 3requested information on 59 factors arranged in four groups that potentially affect TC: factors relating to (1) client, (2) contractors, (3) project management, and (4) project environment, as shown in tables 2–5. They were sourced from [7, 9], adjusted to suit local situations and refined to meet the opinions obtained from experts during the pilot test. Additional spaces were also provided, at the bottom of each group, requesting respondents to add any additional factors, if they think suitable, and to assess the same. Moreover, blank space was also given at the end of the questionnaire to allow respondents to provide any comments on minimizing TC in general.

Public Works Department (PWD) of the government of Brunei Darussalam assisted in distributing the questionnaire and collecting the responses from to its officers and enlisted consultants. As such,57 responsive responses were received, with an average total work experience of 9.6 years, and average experience in construction of 8.9, as shown in table 1. This may relate to the quality of the data, as they are considered to reflect the experiential knowledge of the respondents. During the time of the survey, respondents were working on an array of positions, and with various kinds of managerial (e.g. project manager, assistant project manager, quantity surveyor, site supervision, and contract manager) and engineering type of responsibilities (e.g. structural designer/ engineer, architects, architectural designer, and quantity surveyor).

Table 1: Summary of respondents' profile

Description of information	Client	Consultant	Total
Number of responsive Responses	30	27	57
Average Total work Experience (years)	9.1	10.1	9.6
Minimum work experience (years)	1.0	1.0	1.0
Maximum work experience (years)	30.0	33.0	33.0
Average experience in construction (years)	8.0	9.8	8.9
Minimum experience in construction (years)	1.0	1.0	1.0
Maximum experience in construction (years)	26.0	30.0	30.0

Respondents were asked to score the listed 59 factors in section three, in terms of their frequency of occurrence and importance/impact on TC if they occur, on a scale from 1 to 5: 1 being the 'least frequent/important' and 5 being the 'most frequent/important'. All such responses received were then converted in to 'frequency index' (FI) and 'importance index" (II) [10] as:

Frequency (or Importance) Index (FI or II)

$$= (5n_5 + 4n_4 + 3n_3 + 2n_2 + n_1) / \{5(n_5 + n_4 + n_3 + n_2 + n_1)\} \quad (1)$$

where, n_1 the number of respondents who scored 1,
n_2 the number of respondents who scored 2,
n_3 the number of respondents who scored 3,
n_4 the number of respondents who scored 4, and
n_5 the number of respondents who scored 5.

The above two indices were then converted in to an overall index called "Severity Index" (SI), by multiplying FI and II. The SI was then used to rank the overall implication of each factor on TCs.

$$\text{Severity Index (SI)} = \text{FI} \times \text{II} \quad (2)$$

As used in this study, FI and II $\geq$ 0.8 was considered 'most frequent / important', between 0.80-.60 'more frequent/important', between 0.6-0.4 'frequent / important', between 0.4-0.2 'less frequent/important', and $\leq$ 0.2 'least frequent / important' or negligible. For SI $\geq$ 0.64 most critical, between 0.64 - 0.36 more critical, between 0.16-0.36 critical, and $\leq$0.16 less critical.

3 SUMMARY OF OUTCOMES

3.1 Factors Relating to Clients

Table 2 summarizes the criticality of the factors relating to 'clients'. Two factors are seen to be 'most critical': decision making and 'payment on time'.

Table 2: Comparing criticality of factors relating to clients

Factors Relating to Client	Severity Index	Rank
Decision making	0.654	1
Payment on time to contractors & suppliers	0.641	2
Relationships with other parties: contractors, suppliers, etc.	0.607	3
Organizational efficiency	0.597	4
Change orders (e.g. due to design/scope change)	0.541	5
Experience in similar type projects	0.514	6
In-house project management (e.g. as by PWD)	0.456	7

This is very important in the sense that the respondents are clients and their representatives, who are appreciating the impacts of their acts, reflecting and agreeing to the alleged perception of the contractors on slow decision making

and delayed payments to contractors / suppliers by clients. Other factors are seen to be of 'more critical' as their SI vary from 0.607 to 0.456. Such factors include 'change orders', reflecting the local situation of changes made to designs after contract award for construction.

3.2 Factors Relating to Contractors

Table 3 shows criticality of the factors relating to 'contractors'. Among 20 factors used in this group, nine factors are seen to be 'most critical' (if SI is rounded off to two digits after decimal), with 11 factors as 'more critical'. The lowest SI of 0.417 implies a general criticality of all factors on TC.

Table 3: Comparing criticality of factors relating to contractors

Factors Relating to Contractors	SI	Rank
Availability of resources: Labor, tech. staff, equipment, materials	0.714	1
Qualification of the contractor	0.713	2
Productivity of the construction team	0.707	3
Site management and supervision	0.706	4
Workmanship, degree of rework, etc.	0.687	5
Relationship with client	0.660	6
Payment on time from the client	0.639	7
Availability of subcontractors / specialty contractors	0.637	8
Reputation in the industry	0.635	9
Tender validity period	0.610	10
Experience in similar type projects	0.582	11
Relationships with subcontractors and suppliers	0.567	12
Profit margin	0.547	13
Office Overheads, e.g. administrative & management costs	0.534	14
Bidding behavior: high, suspicious, cheating, etc.	0.533	15
Relationships with previous clients that shaped 'present' behavior	0.527	16
Approach to claims / disputes	0.488	17
Rate / Chance of winning a bid	0.477	18
Material substitution	0.433	19
Special requirements, e.g. duration/amount of bid bond, etc.	0.417	20

Availability of resource (rank 1, SI = 0.714) reflects the local situation, as Brunei has to rely on importing construction materials to run her construction

industry, except for ordinary cement and MS bar, which are the only major materials produced locally. Another significant outcome is 'payment on time from the client' (rank 7)is 'most critical' to TCs, as there is alleged perception in the industry about not paying on time. Such realization is therefore expected to improve 'on time payments' to contractors, as clients and their representatives can influence payment to contractors.

3.3 Factors Relating to Project Management(PM)

Table 4 summarizes eight factors relating to project management arranged according to their ranks. It is seen that 'leadership' (SI = 0.795) tops the table and 'conflict management' lies at the bottom. Among eight, six factors are 'most critical' and the remaining two are 'more critical'. The lowest SI of 0.598 is high enough to indicate higher degrees of criticality of all factors, importance of PM to TCs &project delivery.

Table 4: Comparing criticality of factors relating to project management

Factors Relating to Project Management	Severity Index	Rank
Leadership	0.795	1
Quality of decision making	0.765	2
Quality of communication	0.761	3
Technical competency	0.716	4
Relationships with the construction / project team	0.711	5
Experience of Project Management Team	0.686	6
Education/skill of Project Management Team	0.624	7
Conflict management	0.598	8

3.4 Factors Relating to Project Environment

Table 5 presents the severity indices of 24 factors relating to project environment. 'Payment terms and conditions' is seen to top the list, indicating the need for serious attention, as 'payment' is consistently seen as 'most critical' factor. The remaining 18 factors are 'more critical'. Corporate income tax is seen as the least critical (SI = 0.372) in this group of factors, for its low rate, as government encourages business.

4 CONCLUDING OBSERVATIONS

The paper attempted to identify factors affecting Transaction Costs (TCs) in Brunei construction. All the 59 factors are seen as either 'most critical' or 'more critical' to TCs. The top three factors in project management (PM) group are also the

top three factors within the entire sample, indicating the higher criticality of PM to TCs. A few individual factors were surfaced out to be 'most critical': payments to contractors, H&S, quality and completeness of design at tender stage, and decision making by clients. Arguably, these factors need attention for performance improvement in construction. The survey is being extended to contractors. The next step will be to identify a set of strategies on how to overcome identified issues, e.g. those are surfaced out in this paper.

Table 5: Comparing criticality of factors relating to project environment

Factors Relating to Project Environment	Severity Index	Rank
Payment terms & conditions: progress payment, retention, etc.	0.754	1
Health and safety requirements	0.732	2
Quality of Design	0.656	3
Completeness of design at tender stage	0.642	4
Pre-contract activities: EIA, feasibility, design, tendering, etc.	0.641	5
Project duration: reasonableness, i.e. tight, adequate, etc.	0.635	6
Site conditions / constraints	0.632	7
Project delivery / contract method used	0.618	8
Integration of design and construction	0.603	9
Approach to risk allocation: risk avoiding or embracing, etc.	0.601	10
Competition required between bidders	0.573	11
Nature / Type of the project itself, e.g. buildings, roads, etc.	0.570	12
Project complexity	0.552	13
Bonding requirement	0.525	14
Environmental and/or sustainability requirements	0.522	15
Incentive / disincentive clauses	0.492	16
Novelty / uniqueness of design	0.452	17
Project uncertainty	0.447	18
Project auctioning and multiple layer of subcontracting	0.437	19
Import duties & taxes on materials & construction equipment	0.404	20
Third party influence on project preparation & construction	0.403	21
Range of 'non–construction' items included in the project	0.384	22
Money Exchange rate and fluctuation of price	0.373	23
Corporate income tax (e.g. for contractors & consultants)	0.372	24

ACKNOWLEDGEMENTS

ITB funding No. ITB/GSR/1/2014(3) for this study is gratefully acknowledged.

REFERENCES

[1] Williamson, O. E. (1987). *The Economic Institutions of Capitalism*. The Free Press, New York.

[2] Winch, G. (1989). "The construction firm and the construction project: a transaction cost approach." *Construction Management and Economics*, **7**, 331–45.

[3] Williamson, O. E. (1996). *The Mechanisms of Governance*. The Free Press, New York.

[4] Rahman, M.M. & Kumaraswamy, M.M. (2004). "Contracting relationship trend & transitions". *J. of Management in Engineering*, 20 (4), 147-161.

[5] Walker, D. H. T., Hampson, K. and Peters, R. (2000). Project alliancing and project partnering – what's the difference? – partner selection on the Australian National Museum project: a case study. In *Proceedings of the CIB W92 Conference*, Chile, pp. 641–55.

[6] Rahman, M. M. and Kumaraswamy, M. M. (2002). "Joint risk management through transactionally efficient relational contracting". Construction Management and Economics, 20, 45-54.

[7] Li, H. M., Arditi, D. and Wang, Z. (2013). "Factors that affect transactions costs in construction projects". Journal of Construction Management andEngineering , 1339(1), 60-68.

[8] Shafie, M. (2014). Brunei Darussalam construction cost handbook: interpretation of cost trends. Seminar arranged by Ministry of Development, Brunei.

[9] Rahman, M.M. (2003). *Revitalising construction project procurement through joint risk management*. PhD thesis, University of Hong Kong.

[10] Lim, E.C. and Alum, J. (1995). "Construction productivity: issues encountered by contractors in Singapore", *International Journal of Project Management*, 13(1), 51-58.

CICM 2015
First International Conference on
Advances in Civil Infrastructure and Construction Materials
MIST, Dhaka, Bangladesh, 14–15 December 2015

ONE DIMENSIONAL GROUND RESPONSE ANALYSES FOR SOIL IN DHAKA AND KHULNA REGION

Naveel ISLAM[1], Md. J. Alam[2] and A. S. M. Fahad Hossain[3]

[1, 2] Department of Civil Engineering, Bangladesh University of Engineering and Technology, Dhaka, Bangladesh.
E-mail: [1]naveel896@gmail.com, [2]mjahangiralam@ce.buet.ac.bd

[3]Department of Civil Engineering, Ahsanullah University of Science and Technology, Dhaka, Bangladesh. Email: [3]fahadrubel@gmail.com.

Abstract. *Ground response analyses are used to predict ground surface motions for development of design response spectra, to evaluate dynamic stresses and strains, for evaluation of liquefaction hazards and to determine the earthquake induced forces that can lead to instability of earth and earth retaining structures. The study was based on One–Dimensional ground response analysis by the use of program SHAKE 2000 where local site conditions was used for assessing the potential amplification of earthquake ground motions with respect to different characteristic parameters. A definite earthquake motion from the earthquake record database of the program was taken as the input motion. Maximum Shear Modulus was determined using SPT Test results. Damping of 5% was considered for all the locations. Research was based on 6 Sites (4 in Dhaka & 2 in Khulna). Characteristic graphs for the locations were compared to provide decisions about their change with respect to type of soil layers, depth, time and frequency relating with the input object ground motion. It was found that, the peak ground acceleration was high in soft soil areas indicating site amplification in soft soil. Maximum amplification ratio about 12 was found in Mouja –Tootpara, Khulna region for a frequency of 2 Hz.*

Keywords: Response Analyses, Earthquake, Amplification, Shear Modulus, Damping, Amplification Ratio

1 INTRODUCTION

The influence of local soil conditions on the nature of earthquake damage has been recognized for many years. Since 1920's, seismologists and more recently, geotechnical engineers have worked towards the development of quantitative methods for predicting the influence of local soil conditions on strong ground motions. The problem of ground response analysis had become one of determining the response of the soil deposit to the motion of bedrock immediately beneath it. Despite the fact that seismic waves may travel through tens of kilometers of rock and often less than 100 m of soil, the soil plays a very important role in determining the characteristics of the ground surface motions [1].

The study related to the one dimensional ground response analysis performed for site amplification was not much of importance maybe due to the lack of experienced research works or efficient instruments and programs at early days. Until significant earthquakes such as those that have affected Mexico City (1985), San Francisco (1989), Los Angeles (1995) and Ahmadabad (2001), Off West Coast of Northern Sumatra (2004), Near the East Coast of Honshu, Japan (2011); it has become apparent that the amplification produced by such earthquakes may result in severe damage to buildings, transportation corridors and other lifeline infrastructures. Thus site amplification has been identified as one of the important factors that controls damage in urban areas from large and moderate earthquakes.

It has been evident from the past earthquake events that has taken place all over the world that the amplification of ground motion is highly dependent on the local geological, topography and geotechnical conditions. Past studies, such as by Ansary et al [2], Ashford et al [3], Ranjan [4] and Abe et al [5] have demonstrated the role played by the surface geology in altering the observed seismic motion.Most of the methods are based on the assumption that the main response in a soil deposit is caused by the upward propagation of shear waves from the underlying rock formation. As a method of assessment, the one dimensional analysis by the program SHAKE 2000 [6] was followed for the local soil conditions at several locations to know about the amplification effects on the structures made at that locations based on the soil testing information for a particular damping and a generalized earthquake data. Background studies were conducted for the research works on one dimensional amplification analysis on various types of soil layers. Bore log data were collected based on SPT test result for some of the actual available recent soil test data.

In this study, the ground response analysis by the program SHAKE 2000 was done on the six study locations (Mirpur DOHS (North) and Mirpur DOHS (South), Bashundhara Residential Area, Mouja – Baniakhamarin Khulna Sadar, Mouja – Tootpara in Khulna and Gulshan -2 area in Dhaka) where the soil testing data of a particular site in that location was used to determine the characteristics of response analysis parameters. The objectives of the studies were to assess the potential amplification of earthquake ground motions and to determine

certain dominating response analyzed parameters in each of the study locations for computing the effects of local soil conditions on account of earthquake ground motions.

2 INPUT PARAMETERS

The program SHAKE 2000 models the nonlinear variation of the soil Shear Modulus and Damping as a function of shear strain. The in-situ soils were simplified to match the present soil types within the program. The soil types present on the actual bore log data are made to match the default soil profiles present within the program to get the Shear Modulus and Damping values based on the soil type at various strata. The Maximum Shear Modulus for sandy soil and clayey soil are determined following equations (1) and (2) in Table 1.0 (the simplified formulae which considers the SPT value only).

Table 1.0: Equations for Maximum Shear Modulus

Soil Type	Formulae	Variables	Unit	References	Equations
Sand	$G_{max} = 325N_{60}^{0.68}$	N_{60}= SPT value corrected to 60% of the free fall hammer energy	Kip/ft^2	[7]	(1)
Clay	$G_{max} = 2000S_u$ $S_u = 6\,Nf$	S_u= Undrained Shear Strength, N_f= Field SPT Value	KN/m^2	[8,9]	(2)

The equation for G_{max} in equation (1) depends on the value of N_{60}. Here, the subscript 60 denotes the free fall hammer energy in percentages. Kovacs [10] initially suggested that 55% be adopted as the efficiency at which most drill rig systems operated at the time that empirical correlations were made. Seed [11] suggested instead, 60% be used since it is associated with the safety hammer, the most commonly used SPT hammer in the United States hence Bowles [12] recommended to be 70%. It was also recommended in [13] to use 60% as the standard energy ratio because of greatly minimizing field data corrections since it is associated with the safety hammer as a commonly used SPT hammer in United States. The adoption of this standard energy requires the SPT N values obtained using any hammer to be corrected. The correction is done in accordance with the equation (3) [13]

$$N_{60} = N_f \times (ER_f / 60) \qquad (3)$$

Where, N_f denotes the field SPT Value and ER_f denotes the rod energy ratio for hammer used in the investigation (measured). For the calculation as per equa-

tion (1) ER_f of 60% was assumed as the rod energy ratio and the hammer type in the site locations was unknown. Thus from equation (3) putting $ER_f = 60$ we get,

$$N_{60} = N_f \tag{4}$$

The shear wave velocity at the bottom of the bedrock was considered to be of 700 m/s for the soil profiles. Due to unavailability of an earthquake source that influenced a significant amplification in the cities of Bangladesh; an earthquake source with a magnitude of 7.3 and a radius of 166 km was considered for the analysis for knowing the change in the characteristic curves in the soil profiles.5% damping was taken for the analysis. The earthquake at Southeastern, Alaska, and 1979 - M: 7.3 R: 166 km - N279E Component - Yakutat Station was taken as the input motion for the soil profiles as shown in Figure 1.0. The soil profiles of the study areas are shown in Figure 2.0.

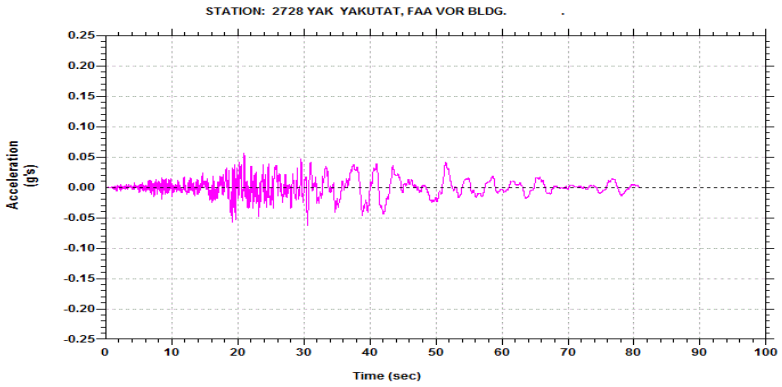

Figure 1.0: Acceleration Time History Recorded at Yakukat Station for South Eastern Alaskan Earthquake, 1979 from the earthquake record database of SHAKE 2000.

3 OUTCOMES OF ANALYSES

The results of analyses are obtained by the program SHAKE 2000 in the form of characteristic curves. The curve induces the following important defining parameters based on which relative discussions on response analysis over the soil profile are provided.

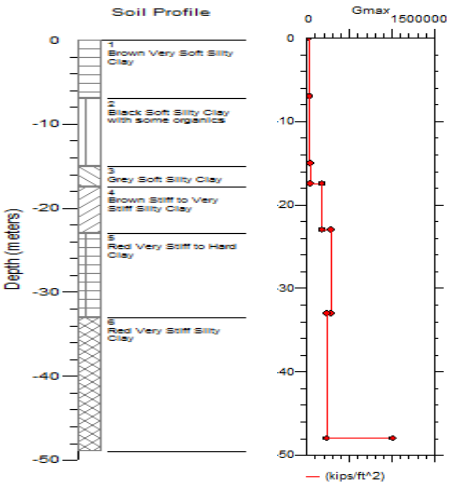

a) Bashundhara R/A, Dhaka

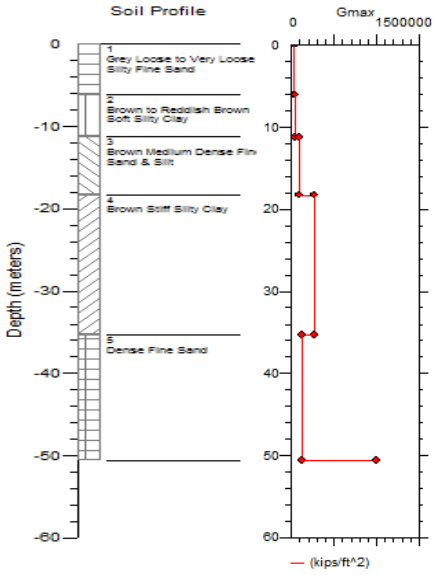

b) DOHS (North), Mirpur, Dhaka

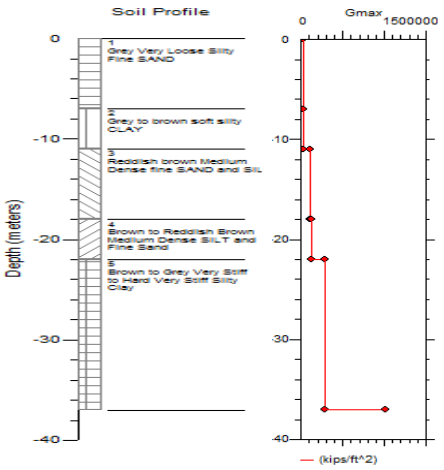

c) DOHS (South), Mirpur,Dhaka

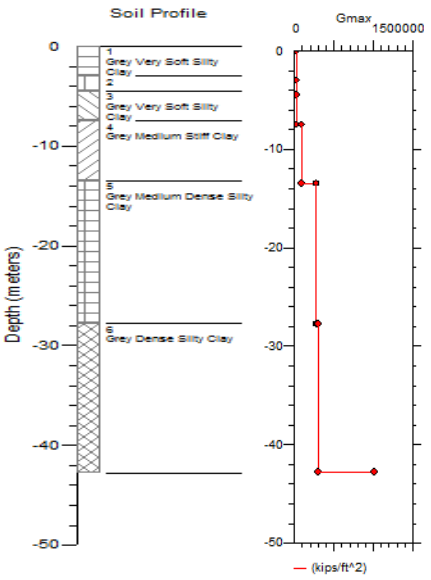

d) Mouja Tootpara, Khulna

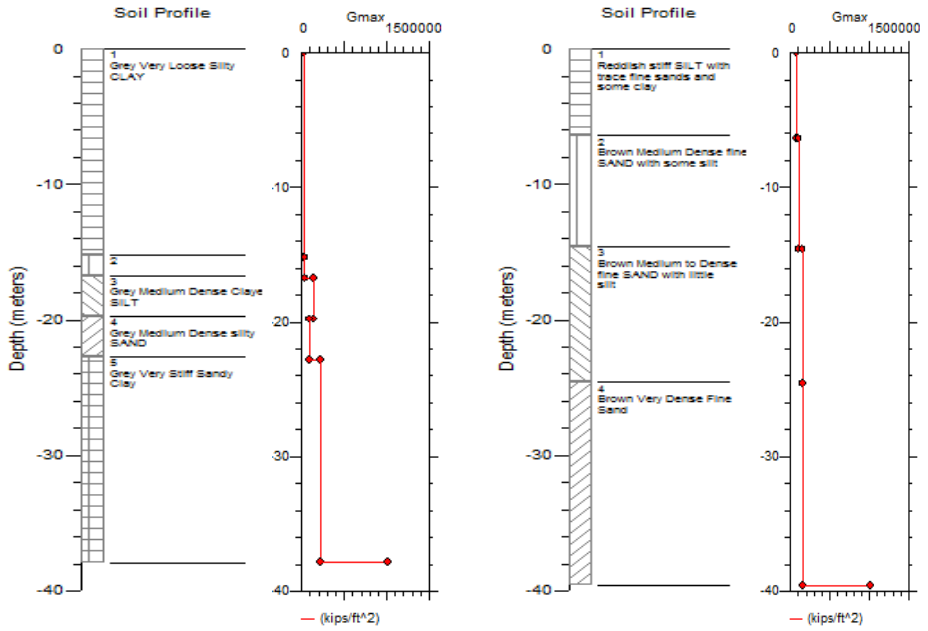

e) Mouja Baniakhamar, Khulna Sadar f) Gulshan-2, Dhaka

Figure 2: Soil Profile for the study locations.

3.1 Peak Acceleration

Peak (Ground) Acceleration signifies the maximum acceleration experienced at the surface or on the corresponding soil layer. The United States Geological Survey (USGS) developed an Instrumental Intensity scale (IIS) [14] which maps peak ground acceleration and peak ground velocity on an intensity scale similar to the felt Mercalli scale. These values are used to create shake maps by seismologists around the world. Figure 3.0 shows the relative change of peak acceleration with depth where each of the curves represent the soil profiles at the particular locations. In all the places there were significant amplification at the top surface soil but the highest peak acceleration was observed in Bashundhara Residential Area about 0.19g indicating maximum amplification in the soft clay layer as shown in Figure 2.0 (a), at the top surface and comparing with the IIS scale [14] it was found that the perceived shaking is very strong and there is moderate damage potential in that region. The least among the observations was obtained in Gulshan -2 areas where the SPT blow counts were higher in the top surface as in Figure 2.0 (f) than the other locations. Among the two observed soil profiles of Khulna region (Mouja – Tootpara and Mouja-Baniakhamar) though

having the same top soil layer as in Figure 2.0 (d) & (e), the peak acceleration was higher in Mouja Tootpara. That could be because of the existence of black organic clay layer underneath the Grey Soft silty clay layer as in Figure 2.0 (d). Most of the observed PGA lies within the region of 0.1 to 0.2 where the perceived shaking is from strong to very strong and the potential damage is from light to moderate. For Dhaka city expected intensity of earthquake is around VIII (Modified Mercalli Intensity Scale) [14] which may be assumed to correspond to a peak ground acceleration (PGA) in a range of 0.2g to 0.25g. According to current seismic zoning map of building code, for Dhaka city (Zone II) the PGA is around 0.15g on very firm soil, considering site effects it can be 0.20g or more [15]. This is similar to the analysis where the range of PGA was found to be 0.1g-0.2g as shown in Figure 3.0.

3.2 Shear Wave Velocity

Figure 4.0 shows the relative change of peak acceleration with depth where the curves represent the particular locations of the soil profiles. In case of DOHS (North), the shear wave velocity gradually increases from top to bottom, but a flat increase in slope occurs between brown to medium dense fine sand to brown stiff silty clay as shown in Figure 2.0 (b) from 175 m/s to 400 m/s and again a flat decrease in slope occurs from brown stiff silty clay to dense fine sand from 400 m/s to 190 m/s. For DOHS (South), the shear wave velocity increases with depth from 50 m/s to 400 m/s. In case of Bashundhara Residential Area, the shear wave velocity is almost equal over the first three clay layers but from third grey soft silty clay layer to red very stiff hard clay layer as shown in Figure 2.0 (a), a flat increase in slope occurs from 100 m/s to 410 m/s and a presence of less denser clay layer decreases shear wave velocity to 360 m/s. For Mouja- Baniakhamar, the shear wave velocity increase within the clay layers until there is a flat decrease in shear wave velocity from the grey medium dense clayey silt layer to grey medium dense silty sand layer as shown in Figure 2.0 (e). In Mouja – Tootpara, a decrease in shear wave velocity occurs from the top grey very soft silty clay layer to the black organic clay layer then a gradual increase is seen in the shear wave velocity to the bottom layer to 385 m/s as shown in Figure 2.0 (d). For, Gulshan -2, range of variation of shear wave velocity is low within the layers, maximum shear wave velocity occurs at the bottom layer which is about 230 m/s.

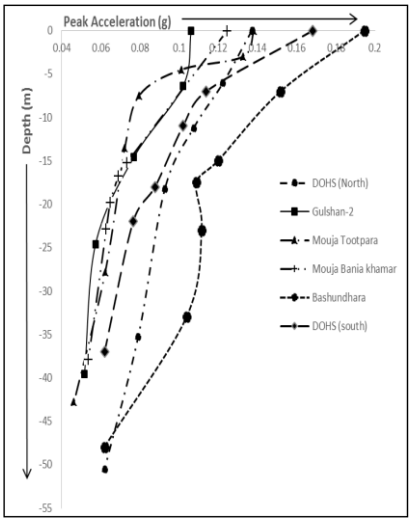

Figure 3.0 Variation of Peak Ground Acceleration with Depth in meters

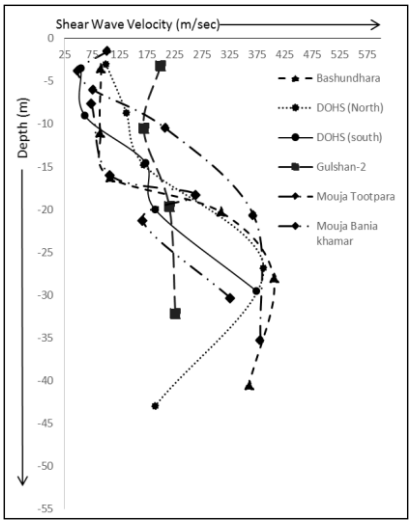

Figure 4.0 Variation of Shear Wave Velocity with Depth in meters

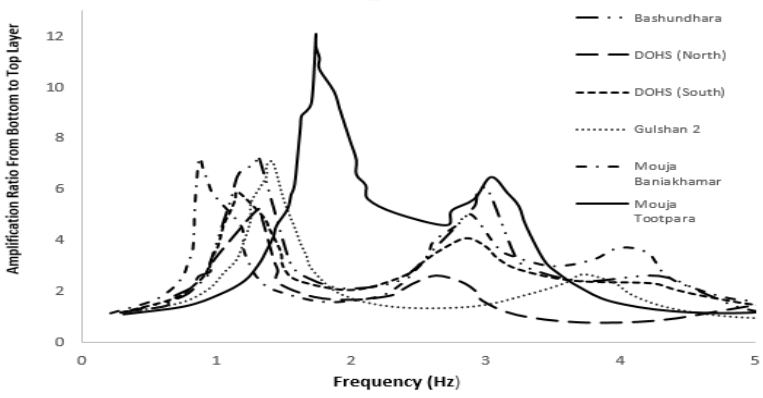

Figure 5.0: Showing Amplification Spectrum for different site locations

3.3 Amplification Spectrum

Figure 5.0 shows the variation of amplification spectrum (amplification ratio from bottom to the top layer) in the soil profiles for the different regions. In Bashundhara Residential Area, first order amplification ratio is high about 7.5 for 1.25 Hz and the second order ratio appears about 6 at 2.5 Hz. the range of variation is high from 1.5 to 7.5 Hz. On DOHS (North), first order peak amplification ratio is 5.5 for a frequency of 1.25 Hz, at a frequency of 2.5 Hz the second order

peak amplification ratio is 2.5. For DOHS (South) ,first order peak amplification ratio is 6 for 1.25 Hz, and the second order peak amplification ratio is 3.5 for 2.5 Hz. Whereas in case of Gulshan-2 area, the first order amplification ratio occurs at 7.0 for a frequency of 1.5 Hz and the second order peak ratio occurs at 2.0 Hz. In case of Mouja – Tootpara, the first order peak ratio appears at 12 for 2 Hz indicating maximum amplification with respect to the bottom layer and the variation of range is higher from 0.9 to 12. In case of Mouja –Baniakhamar, first order amplification ratio appears at 7.5 Hz for 1.25 Hz ,second order peak appears at 2.5 Hz and the third order peak appears at 4.5 Hz. All the curves where steady for a frequency higher than 5 Hz.

4 SUMMARY

From the six study location it can be summarized as, shear wave velocity is considerably low within the hard stratum of soil and with the densification of soil the shear wave velocity increased. Peak acceleration is highest at the top surface but relatively less in hard stratum compared to loose stratum. Among all the locations the highest acceleration occurs in Bashundhara Residential Area at 22 seconds and at 31 seconds about 0.19g for the input motion acceleration of 0.051g at 21 seconds. Maximum amplification ratio was at Mouja-Tootpara, Khulna Sadar among all the sites showing potentiality of higher amplification irrespective to the surface at the proximity with bedrock/input source. Based on the study, the range of peak ground acceleration as was defined in literature was seen to match with the analyses in this article as per SHAKE 2000. The analyses also indicate the inverse relation with peak ground acceleration and shear wave velocity. Where with depth the peak ground acceleration decreases but the shear wave velocity increases for the layers where the shear modulus is high. The amplification spectrum indicates the amplification from the bottom (proximity to bedrock/source) to the top surface (ground surface).

5 CONCLUSION

The study presents an attempt in performing one dimensional analysis by using the program SHAKE 2000 for assessing the potential amplification of a definite earthquake motion in different types of soil conditions in Bangladesh. For the case of simplicity, number of assumptions and simplified relations was used for the analysis. Although all the relations adopted in the analysis shows a certain consistency with the dataset, it is clear that more data are needed before a final decision from the response analyzed parameters can be drawn. Authors are determined for using more exact modulus equations based on micro tremor and down hole seismic measurements specifically for Dhaka and Khulna regions in their future studies. The results may also vary with the change in the earthquake intensity and with the attenuation relations used in the analysis for the program.

The study provides handful information about the characteristics of the motions likely to develop due to the soil formation underlying the site by defining the range of PGA for the study locations that is analogues to previous extensive studies in literature. Widespread studies are aimed to be conducted in future by the authors to present a generalized seismic zoning PGA map and shear wave velocity variations with depth for major cities of Bangladesh based on the analyses using SHAKE 2000 and depending on the availability of bore log data of the site locations. A number of other characteristic graphs can also be obtained from the program. The influence of those is targeted in the future publications.

REFERENCES

[1] S.L. Kramer, 1996.Geotechnical Earthquake Engineering. Prentice-Hall, Inc., Upper Saddle River, NJ

[2] M. A. Ansary, M. A. Noor and A. Rashid, 2004. Site Amplification Characteristics of Dhaka City. Journal of Civil Eng.(IEB), 32 (1) (2004) 1-16

[3] S. A. Ashford, W. Jakrapiyanun and P. Lukkunaprasit, 2005.Amplification of Earthquake Ground Motions in Bangkok. 12 WCEE 200, 1466.

[4] R. Ranjan, 2005.Seismic Response Analysis of Dehradun City, India Thesis submitted to the International Institute for Geo-information Science and Earth Observation, Dehradun, India

[5] K. Abe and H. Watanabe,1996.A Study on Amplification factors of earthquake motions observed at a granite site and relationships between their vertical and horizontal motions.11th World Conference on Earthquake Engineering, 1242.

[6] G. A. Ordonez 2011. SHAKE 2000 User's Manual per B. Schnabel, John Lysmer, H. Bolton Seed, University of California, Berkeley.

[7] T. Imai and K. Tonouchi, 1982.Correlation of N-value with s-wave velocity and shear modulus. Proceedings, 2nd European Symposium on Penetration Testing, Amsterdam, 57-72.

[8] H. B. Seedand I. M. Idriss, 1970.Soils Moduli and Damping Factors for Dynamic Response Analyses.Earthquake Engineering Research Center, UC. Berkeley, Report No EERC 70-10.

[9] W. D.Kovacs, L. A. Salomone and F. Y. Yokal, 1983.Comparison of Energy Measurements in the Standard Penetration Test Using the Cathead and Rope Method,National Bureau of Standards Report to the US Nuclear Regulatory Commission.

[10] H. B. Seed, K. Tokimastu, L. F. Harder and R. F. Chung, 1985.Influence of SPT Procedures in Soil Liquefaction Resistance Evaluations,Journal of Geotechnical Engineering, 111(12)

[11] J E. Bowles, 1996.Foundation Analysis and Design, The McGraw-Hill Companies, Inc. Fifth edition.

[12] M. S. Aggour and W. R. Radding, 2001. Standard Penetration Test (SPT) Corrections. Report submitted to Maryland State Highway and Corrections, Civil and Environmental Engineering, University of Maryland, College Park, Maryland.

[13] J A. Egan and R. M. Ebeling, 1985.Variation of Small Strain Shear Modulus with Undrained Shear Strength of Clays. Second International Conference on Soil Dynamics & Earthquake Engineering, Board The Liner Queen Elizabeth,UK 2

[14] U.S. Geological Survey, 2012.National Seismic Hazard Maps.

[15] Y.M. Wu, T.L. Teng, T.C. Shin and N.C. Hsiao, 2003.Relationship between Peak Ground Acc., Peak Ground Velocity and Intensity in Taiwan. Bulletin of the Seismology Society of America, 93(1), 386–396.

CICM 2015
First International Conference on
Advances in Civil Infrastructure and Construction Materials
MIST, Dhaka, Bangladesh, 14–15 December 2015

CORRELATION BETWEEN INSITU CONCRETE STRENGTH AND UPV FOR BRICK SAMPLES

Anan D. BRISTI[1], A. Fahim[2] and Mehedi A. Ansary[2]

[1] Military Institute of Science and Technology, Dhaka, Bangladesh
Email: ananabristi@gmail.com

[2] Department of Civil Engineering, Bangladesh University of Engineering and Technology, Dhaka, Bangladesh. Email: ansary@ce.buet.ac.bd

Abstract. *The ultrasonic pulse velocity (UPV) method considers indirect way to determine concrete strength in situ. Earlier researches conducted in finding the relation between concrete strength and UPV were generally limited to specimens prepared in the laboratory. Only a few of those relations were developed taking the concrete mix ratio into consideration. In the laboratory, good care in design and production of concrete are taken. On the other hand, many variations occur in the field concrete production. These variations should be considered before using strength-UPV relations developed in the laboratory to predict field concrete strength. In this study, a relationship is developed between concrete strength and UPV by using the data obtained from 2658 cores that are drilled from elements (column, beam, and slab) of 825 reinforced concrete structures having different ages of strength and unknown ratios of concrete mixtures. This relation is compared with previously laboratory developed relations. The reliability of previously developed relations is discussed to estimate in situ compressive strength of concrete. It is found that, in-situ concrete strength-UPV relations were less reliable and had very poor correlation with the compressive strength of concrete than the laboratory developed relations.*

Keywords: Ultrasounds, Nondestructive testing, Concrete, Core test.

1 INTRODUCTION

Concrete is the most widely used construction materials. As a result the quality of concrete is an important issue. The compressive strength is the most important property of concrete, as it is the main criteria to judge the quality of concrete, Aydin and Saribiyil 2010[6]. Direct determination of the compressive strength requires that concrete specimen must be loaded to failure. Therefore, it requires that the specimen to be taken according to standard and specified requirements, should be shipped and tested at laboratory. This procedure gives actual strength for under construction structures. But this procedure is time consuming and troublesome for existing structures. Because of these problems some of the techniques have been developed to measure other properties of concrete other than strength and relate them with the strength and, durability or any other properties, Qasrawi 2000[23].

The non-destructive test (NDT) methods can be employed for efficient time management of a large scale construction project.

2 EVALUATION OF CONCRETE STRENGTH BY DIFFERENT NDT

Various NDT that can be used for measuring concrete strength are shown in Figure 1.

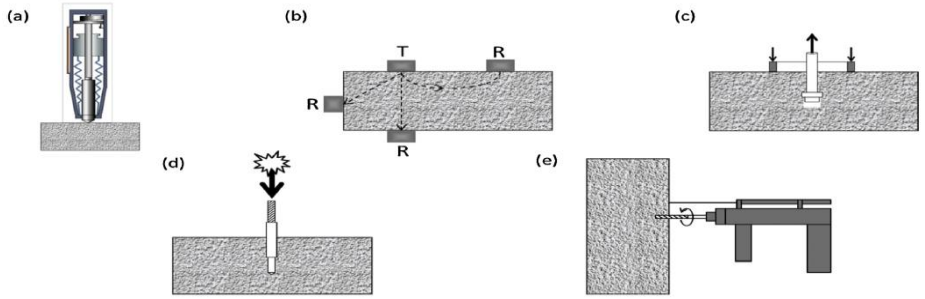

Figure 1: NDT techniques that have been or potentially can be used for in situ strength assessment of concrete: (a) rebound hammer; (b) Ultrasonic pulse velocity (UPV); (c) Pull-out-force; (d) Penetration Resistance ; (e) drilling resistance. Gunes 2015[13]

In the laboratory, access is generally available to opposite surfaces of a test specimen, and ultrasonic tests are commonly conducted using direct transmission. UPV test is prescribed in ASTM 2002[4] and BSI 1997[8].The principle of test is that the velocity of sound in a solid material V,is a function of the square root of the ratio of its modulus of elasticity E,to its density ρ,

$$V=f\,(g\,E/\rho)^{1/2} \qquad (1)$$

Where, g is the gravity acceleration. In the test, the traveling time of the pulses through concrete is recorded. Then, the velocity is calculated as:

$$V = L/T \quad (2)$$

Where V= pulse velocity (m/s), L= Length of sample (m), and T= effective time (s), which is the measured time minus the zero time correction. Based on experimental results, Tharmaratnam and Tan 1990[25] gave the relationship between the UPV in a concrete V and concrete compressive strength f_c as:

$$f_c = ae^{bV} \quad (3)$$

where a and b are parameters dependent upon the material properties, Turgut 2004[31].The ultrasonic pulse velocity results can be used to check uniformity of concrete, voids in concrete, the quality of concrete and concrete products by comparing results to a similar concrete, measure condition and deterioration of concrete, depth of surface crack, measure strength comparing with previous data Qasrawi 2000[23].

3 EXPERIMENTAL METHODOLOGY AND DISCUSSION

In this study the relations which are produced in the laboratory are compared with relations developed from the core test of existing reinforced concrete buildings. For this process starting from June 2013 to February 2015, 2568 cores are drilled from 825 reinforced concrete buildings. The age of the buildings varied from 5 yrs. to 40 yrs. Coarse aggregate and brick chips are two types of aggregates commonly used in Bangladesh.

Out of the total collected cores 1561 are of brick aggregate with mean strength of 21 MPa and standard deviation of 8.35 MPa. The diameter or core samples varied between 44 mm to 104 mm. Length of the sample were in the range of 69 to 206 mm. The unit weight of concrete cores varied between 300 to 21920 kg/m^3. Fig. 2 shows the distribution of the core test result of brick aggregate.

Number of core with coarse aggregates are 1095. They have a mean strength of 21 MPa and standard deviation is 8.33 MPa. The diameter varied between 44 to 112 mm. Length of the sample was in the range of 71 and 241 mm. The unit weight of concrete cores varied between 704 to 28037 kg/m^3.

Fig. 3 shows the correlation between strength and UPV for brick aggregate concrete. Figure 3(a) was drawn using all the cores of brick aggregate concrete after discarding. There were 1237 cores. The correlation equation was found to be $y = 917.26e^{0.0003x}$, where X= UPV in m/s and Y is strength in MPa. R^2 value for this equation was 0.17. This means that we could explain 17% of the variability for the data around the regression line and 83% remained without explanation. Fig. 3(b) was drawn using the cores taken from the slab made of brick aggregate concrete. It contained 147 cores .The correlation equation was found to be $y = 650.38e^{0.0004x}$, R^2 value for this equation was 0.26. It showed a slightly good rela-

tion than the correlation from all the cores. Fig. 3(c) shows correlation for cores taken from beams made of brick aggregate concrete. It contained total of 220 cores. Correlation equation was found to be $y = 938.14e^{0.0003x}$, R^2 value for this equation was 0.16. It is very close to the relation obtained from all cores. Fig. 3(d) shows correlation for cores taken from column made of brick aggregate concrete. It contained total of 873 cores. The correlation equation was found to be $y = 981.69e^{0.0003x}$, R^2 value for this equation was 0.16 which is similar to the relation obtained from beam element and close to relation obtained from all cores.

Fig. 4 showed comparison between previous studies of strength –UPV relation established in laboratory with the test results of core obtained from existing reinforced concrete structures, Qasrawi 2000[23] and Shariati et al. 2011[24], showed the highest degrees of correlation 0.95 and 0.92. Kheder 1999[16] showed the lowest value of 0.41. Among the cores obtained from existing reinforced concrete structures, cores obtained from the slab of brick aggregate concrete showed highest value of 0.26 and cores from the slab of stone aggregate concrete showed lowest value of 0.12. There was a huge variation among relations obtained in laboratory and relations obtained from existing structures. The previous studies derived good correlation between strength-UPV in the laboratory with a particular mix proportion. No clear evidence was provided about the effect of mix proportion on relation.

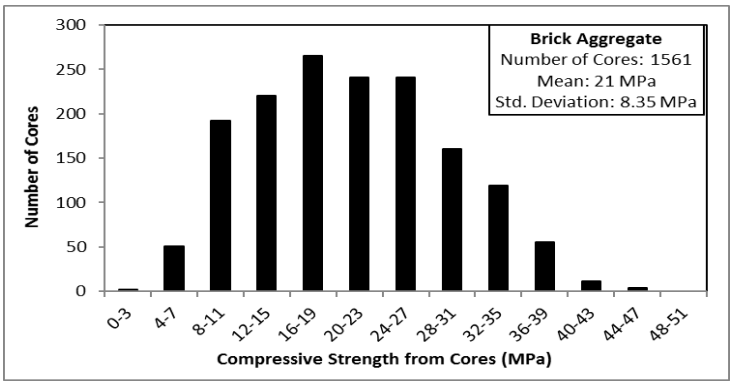

Figure 2: Core test result of brick aggregate

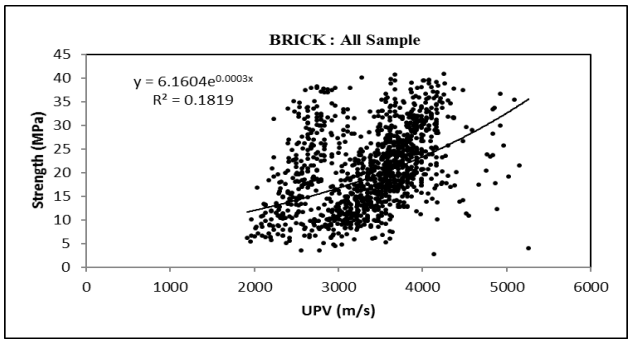

a) Strength-UPV relation for all cores of brick aggregate concrete

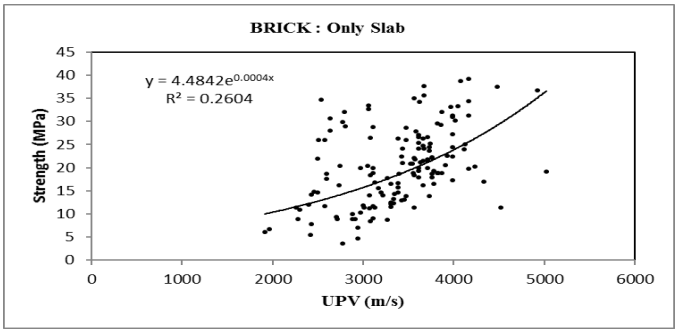

b) Strength-UPV relation for slab of brick aggregate concrete

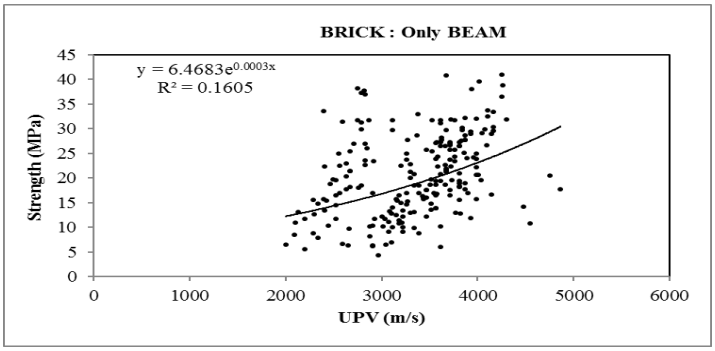

c) Strength-UPV relation for beam of brick aggregate concrete

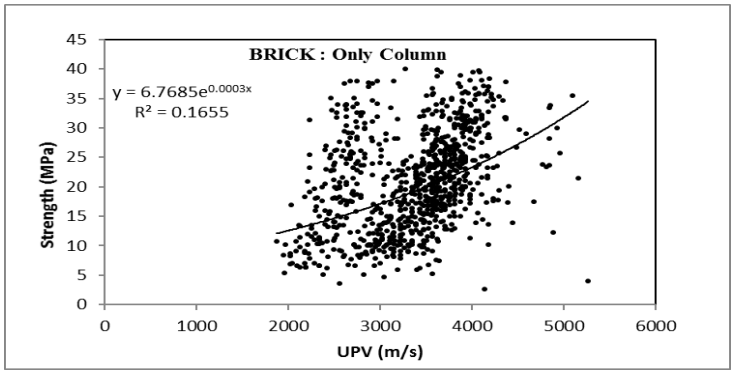

d) Strength-UPV relation for column of brick aggregate concrete

Figure 3: Strength-UPV relation for brick aggregate concrete

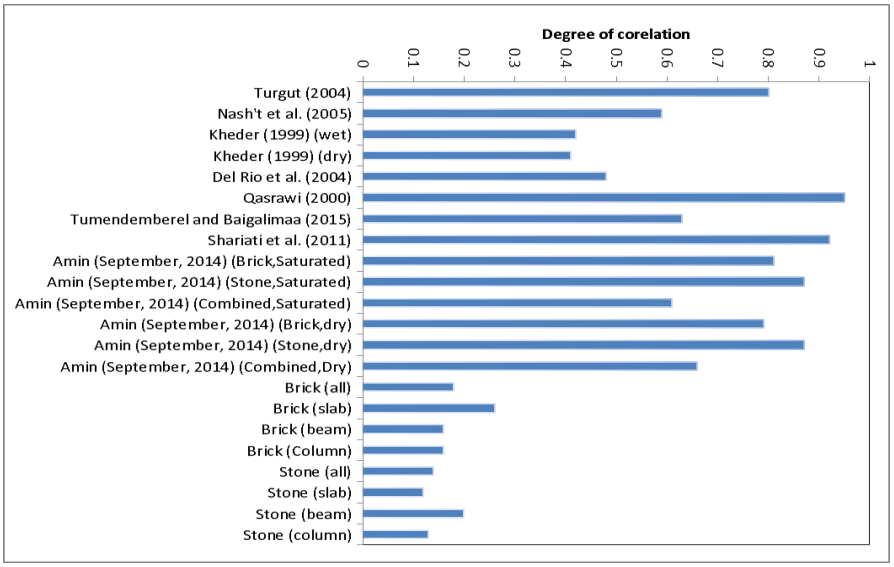

Figure 4: Comparison of correlation with previous studies

4 CONCLUSION

The UPV test has a strong potential to be developed into a very useful and relatively inexpensive in place test for assuring the quality of concrete placed in a structure. The main problem in realizing this potential is that the relationship between the compressive strength and UPV is uncertain and concrete is an inherently variable material. It is clear from the above study that in real field condition strength-UPV relations were less reliable and had very poor correlation with compressive strength of concrete than laboratory developed relations. The rela-

tion is influenced by number of factors stated above which would have to be taken in to account if a reasonable prediction of the compressive strength has to be made from pulse velocity measurements. Thus, the curve obtained from existing RC structures and laboratory specimens can be used only to measure approximate values of concrete strength. These methods can also be employed for the efficient planning of the construction works in huge infrastructure projects. It is necessary to know in-situ strength of concrete in order to determine the removal time of formwork, the stressing or releasing time for the wires in pre stressed members, the loading time for the system in post-tensional elements or the time for opening the structure to service safely. For economic and simplicity reasons, a two stage method of concrete strength verification can be introduced by a combination of destructive and nondestructive method. Among the various methods employed for the assessment of concrete strength in situ, the classical method is to involve compression tests on cylindrical specimens produced from cores drilled out of the structure. It should surely be recognized as having primary importance on account of reliability and accuracy of the result.

REFERENCES

[1] ACI (2013). "Code Requirements for Evaluation,Repair, and Rehabilitation of Concrete Buildings (ACI 562-13) and Commentary." ACI 562-13, American Concrete Institute, Farmington Hills, MI.

[2] ACI Committee 228 (2003). "In-Place Methods to Estimate Concrete Strength." ACI 228.1R-03, American Concrete Institute, Famington Hills, MI.

[3] Ariöz, Ö., Tuncan, A., Tuncan, M., Kavas, T., Ramyar, K., Kilinç, K., and Karasu, B. (2009). "Use of Combined Non-destructive Methods to Assess the Strength of Concrete in Structures." Afyon Kocatepe University Journal of Science, 147-154.

[4] ASTM (2002). "Standard Test Method for Pulse Velocity Through Concrete." ASTM C597 - 02, ASTM International, West Conshohocken, PA.

[5] ASTM (2008). "Standard Test Method for Rebound Number of Hardened Concrete." ASTM C805M-08, ASTM International, West Conshohocken, PA,.

[6] Aydin, F., and Saribiyil, M. (2010). "correlation between Schmidt Hammer and destructive compressions testing for concrete in existing buildings." Scientific Research and Essays, 5(13), 1644-1648.

[7] Breysse, D. (2012). Non-destructive Assessment of Concrete Structures: Reliability and Limits of Single and Combined Techniques: State-of-the-art Report of the RILEM Technical Committee 207-INR, Springer Science & Business Media.

[8] BSI (1986). "Testing concrete. Recommendations for surface hardness testing by rebound hammer." BS 1881-202 : 1986,, British Standards Institution, London, U.K.
[9] BSI (1997). "Recommendations for measurement of velocity of ultrasonic pulses in concrete." BS 1881-203:1986, British Standards Institution, London, U.K.
[10] Demirboğa, R., Türkmen, İ., and Karakoc, M. B. (2004). "Relationship between ultrasonic velocity and compressive strength for high-volume mineral-admixtured concrete." Cement and Concrete Research, 34(12), 2329-2336.
[11] Elvery, R., and Ibrahim, L. (1976). "Ultrasonic assessment of concrete strength at early ages." Magazine of Concrete Research, 28(97), 181-190.
[12] Gunes, O. (2015). "NDT techniques that have been or potentially can be used for in situ strength assessment of concrete." Elsevier, <http://www.sciencedirect.com/science/article/pii/S2214509514000321>
[13] Gunes, O. (2015). "Turkey's grand challenge: Disaster-proof building inventory within 20 years." Case Studies in Construction Materials, 2, 18-34.
[14] Jain, A., Kathuria, A., Kumar, A., Verma, Y., and Murari, K. (2013). "Combined Use of Non-Destructive Tests for Assessment of Strength of Concrete in Structure." Procedia Engineering, 54, 241-251.
[15] Karaesmen, E., Arioz, O., Armagan, C., Yaman, O., and Yildiz, D. "A study of the material aspect of the prestressed concrete technology." Proc., Fourth international conference on concrete technology in developing countries, Gazimagusa, Turkish Republic of Northern Cyprus, 7-8.
[16] Kheder, G. (1999). "A two stage procedure for assessment of in situ concrete strength using combined non-destructive testing." Materials and Structures, 32(6), 410-417.
[17] Leshchinsky, A. "Non-destructive methods instead of specimens and cores, quality control of concrete structures." Proc., Proceedings of the International Symposium held by RILEM, Belgium, E&FN Spon, UK, 377-386.
[18] Lin, Y., Lai, C.-P., and Yen, T. (2003). "Prediction of ultrasonic pulse velocity (UPV) in concrete." ACI Materials Journal, 100(1), 21-28.
[19] Mahure, N., Vijh, G., Sharma, P., Sivakumara, N., and Ratnam, M. (2011). "Correlation betweenpulse velocity and compressive strength of concrete." International Journal of Earth Sciences and Engineering, 04, 871-874.
[20] Malhotra, V. M. (1976). Testing hardened concrete: nondestructive methods, Iowa State Press.
[21] Nash't, I. H., A'bour, S. H., and Sadoon, A. A. (2005). "Finding an Unified Relationship between Crushing Strength of Concrete and Non-destructive Tests." 3rd MENDT - Middle East Nondestructive Testing Conference & Exhibition, www.ndt.net, Bahrain, Manama.

[22] Neville, A. M. (1995). Properties of concrete, Addison-Wesley Longman, U.k.

[23] Price, W. F., and Hynes, J. (1996). "In-situ strength testing of high strength concrete." Magazine of concrete research, 48(176), 189-197.

[24] Qasrawi, H. Y. (2000). "Concrete strength by combined nondestructive methods simply and reliably predicted." Cement and Concrete Research, 30(5), 739–746.

[25] Shariati, M., Sulog, N. H. R., H, M. M. A. K., Sharif, P., and Sinaei, H. (2011). "Assessing the strength of reinforced concrete structures through Ultrasonic Pulse Velocity and Schmidt Rebound Hammer tests." Scientific Research and Essays, 6(1), 213-220.

[26] Tharmaratnam, K., and Tan, B. (1990). "Attenuation of ultrasonic pulse in cement mortar." Cement and Concrete Research, 20(3), 335-345.

[27] Trtnik, G., Kavčič, F., and Turk, G. (2009). "Prediction of concrete strength using ultrasonic pulse velocity and artificial neural networks." Ultrasonics, 49(1), 53-60.

[28] TS (1978). "Beton yüzey sertliği yolu ile yaklaşık beton dayanımının tayini kuralı [Determination of compressive stength of Concrete Surface Hardness Method]." TS 3260, Turkish Standards Institute, Ankara, Turky

[29] TS (2010). "Basınç dayanımının yapılar ve öndökümlü beton bileşenlerde yerinde tayini [Assessment of in-situ compressive strength in structures and precast concrete components]." TS EN 13791, Turkish Standards Institute, Ankara, Turky.

[30] TS (2013). "Betonarme yapılara uygulanabilecek tahribatsız muayene (NDT) yöntemleri [Nondestructive testing methods applicable to Reinforced Concrete Structures]." TS 13543, Turkish Standards Institute, Ankara, Turky.

[31] Tumendemberel, B., and Baigalimaa, T. (2015). "Research into correlation betweenconcretes-trengthandUPVvalues."<http://www.ndt.net/article/ecndt2010/reports/1_14_29.pdf> (July 25, 2015).

[32] Turgut, P. (2004). "Research into the correlation between concrete strength andUPVvalues."NDT.net,<http://www.ndt.net/article/v09n12/turgut/turgut.htm> (May 5 , 2015).

[33] Yaman, I. O., Inci, G., Yesiller, N., and Aktan, H. M. (2001). "Ultrasonic Pulse Velocity in Concrete Using Direct and Indirect Transmission." ACI Materials Journal, 98(6), 450-457.

Yilmaz, I. (2009). "A new testing method for indirect determination of the unconfined compressive strength of rocks." International Journal of Rock Mechanics and Mining Sciences, 46(8), 1349-1357.

CICM 2015
First International Conference on
Advances in Civil Infrastructure and Construction Materials
MIST, Dhaka, Bangladesh, 14–15 December 2015

FOOD INSECURITY CAUSED BY HEAVY METAL DEPOSITION IN CHICKEN

R. SULTANA[1], B. N. Jahan[2], M. M. Islam[3] and M. Tauhid-Ur-Rahman[4]

[1, 2, 3, 4] Military Institute of Science and Technology, Dhaka, Bangladesh.
Email: [1]emasultana09@gmail.com, [2]nazia1151jahan@gmail.com,
[3]moonna56@gmail.com, [4]tauhid_cee@yahoo.com

Abstract. *The purpose of this study was to determine the source of toxic and hazardous elements and the levels of heavy metals (Cd and Cr) which intrude into chicken meat and eggs because of rapid industrialization. The concentration of toxic metals Cd and Cr were determined in chicken meats and eggs by using atomic absorption spectrophotomtery (AAS). The concentration of Cr was above the tolerance level in all the samples with the highest concentration recorded in brain of layer chicken at 10.5 mg/kg. Thigh and leg bone of broiler chicken contained the highest concentration of Cd; 2.53mg/kg. This observation shows that concentration of Cd and Cr in chicken are not within safe limits for consumption. The meat analyzed may have a serious health hazard to the consumers.*

Keywords: Heavy metal, Shaving dust, Poultry feed, Chicken meat, eggs.

1 INTRODUCTION

The insecurity related with the exposure to heavy metals present in food product has aroused widespread concern in human health. Developments in the food production and processing technology increases the chances of contamination of food with various environmental contaminants, especially heavy metals as well as toxic metals.

With expanding industrialization, more and more metals are entering into the environment. These metals stay permanently because they cannot be deteriorated in the environment. They enter into the food material and from there they ultimately make their passage into the tissue. Lead, cadmium, mercury and arsenic are among the main toxic metals which accumulate in food chains and have a cumulative effect. Although contamination of animal feed by heavy metals cannot be entirely avoided because of the prevalence of these metals in the environment, there is a clear need for such contamination to be minimized, with the aim of preventing both direct effects on animal health and indirect effects on human health.

The risk of heavy metal contamination in meat or flesh is of great concern for both food safety and human health because of the poisonous nature of these metals at relatively minute concentrations instances of heavy metal contamination in meat products during processing have been reported. In other cases, contaminated animal feed and rearing of livestock in proximity to polluted environment were reportedly accountable for heavy metal contamination in chicken meat.

2 STUDY AREA & SAMPLE COLLECTION:

2.1 Study Area

For the study Mirpur12, Mirpur 6, Mirpur 11, super markets in capital city Dhaka were selected for study purpose.

2.2 Sample Collection

Four types of chicken species were collected from the market of Mirpur 12 no. and duck sample was collected from the market of Mirpur 11, Eggs of local chicken, broiler chicken (white and brown) were collected from the market of Mirpur 12 The samples were collected in polyethylene bags and transported to the laboratory for analysis.

3 METHODOLOGY

3.1 Sample preparation:

The collected samples were cleaned with processed water to remove any contaminant particles. The samples were cut to small pieces using clean knife. Samples

were oven dried at 100ºC.After drying, the samples were ground into a fine powder by a ceramic pestle and mortar and stored till used for acid digestion. Acid mixture (10 mL, 70% high purity HNO_3 and 65% $HCLO_4$, 4:1 v/v) was added to the beaker carrying 5g dry sample. The mixture was then digested at 1000°C till the clear solution was achieved. After cooling, the samples were filtered using What man 042 filter paper.

The egg samples were boiled in distilled water and when boiling was completed albumen and yolk were separately oven-dried at 80 degree Celsius to remove all moisture. Every oven-dried albumen and yolk were examined and analyzed separately.

The samples were produced by using HNO_3 –$HclO_4$ acid digestion. Since the samples were of organic origin with a very high biologic content, HNO_3 –$HclO_4$ digestion was favored over the more common HNO_3 extraction for the determination of metals. This strong oxidizing digestion decomposes organics quickly and efficiently.

Finally determination of the heavy metals (Cd & Cr) in the filtrate was achieved by atomic absorption spectrophotometry (AAS).

3.2 Reagents and Solutions

The chemicals and reagents used for the sample analysis were of all scientific grades and distilled water was used in preparation and dilution of all the solutions. $HClO_4$ and HNO_3 were bought from E. Merk, Germany.

4 EXPERIMENTAL RESULTS AND ANALYSIS

The experimental results of Chicken and other sample are analyzed based on concentration of heavy metal present in different part of chicken in different species. The concentrations of Cd and Cr in thigh, thigh bone, leg, leg bone, breast, breast bone, wing, wing bone, liver, brain, heart and eggs of different chicken varieties are presented in Table 1, 2, 3 and Fig. 1, 2.

Table 1: Concentration (mg/kg) of Cd in chicken Samples

Species	Samples										
	Thigh	Thigh Bone	Leg	Leg Bone	Breast	Breast Bone	Wing	Wing Bone	Liver	Brain	Heart
Broiler	2.53	0.0718	0.0179	2.5	2.4	0.279	0.22	0.221	0.307	0.45	0.25
Layer	0.313	0.056	0.55	0.35	0.86	0.05	0.19	0.078	0.397	0.56	0.26
Local	0.235	0.035	0.473	0.026	1.39	0.024	0.057	0.27	0.249	0.43	0.35
Sonali	0.093	0.0026	0.25	0.005	0.132	0.014	0.21	0.004	0.25	0.35	0.3

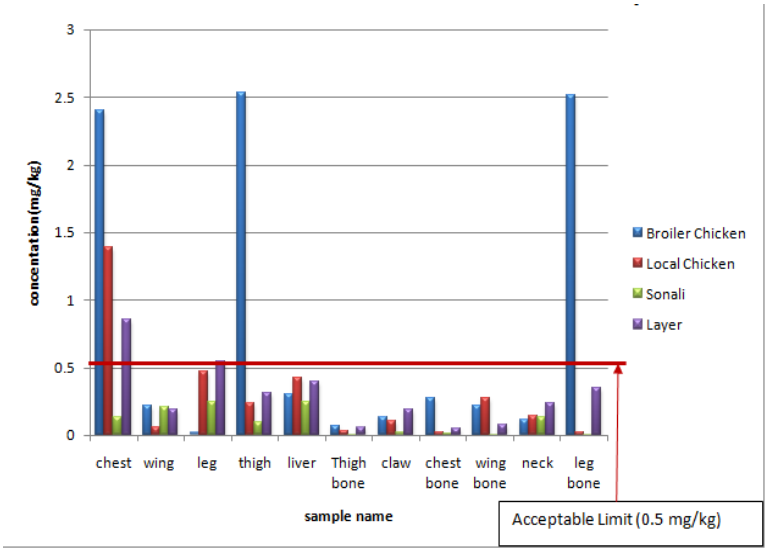

Figure 1: Graph showing concentration of Cd in Chicken

The concentrations of Cadmium (Cd) were observed in the thigh, thigh bone, leg, leg bone, breast, breast bone, wing, wing bone, liver, brain and heart Local and Sonali chicken are as presented in Table1 and Fig. 1. The highest concentration of Cd was found in the thigh of Broiler chicken (2.53 mg/kg) and the lowest level was observed in thigh bone of Sonali chicken (0.0026 mg/kg).Cd is poisonous to every system in human body. Since birth it is almost in human body.

Table 2: Concentration (mg/kg) of Cr in chicken samples

Species	Samples										
	Thigh	Thigh Bone	Leg	Leg Bone	Breast	Breast Bone	Wing	Wing Bone	Liver	Brain	Heart
Broiler	1.82	1.78	1.78	1.79	1.74	2.54	1.72	1.79	1.72	9.0	2.3
Layer	6.4	2.16	3.8	1.8	1.0	3.2	2.2	2.5	2.74	10.5	4.6
Local	0.564	0.568	0.546	0.55	0.56	0.46	0.56	0.613	0.56	4.45	0.35
Sonali	4.18	3.94	3.99	4.10	3.96	3.94	4.0	4.0	3.89	8.5	3.43

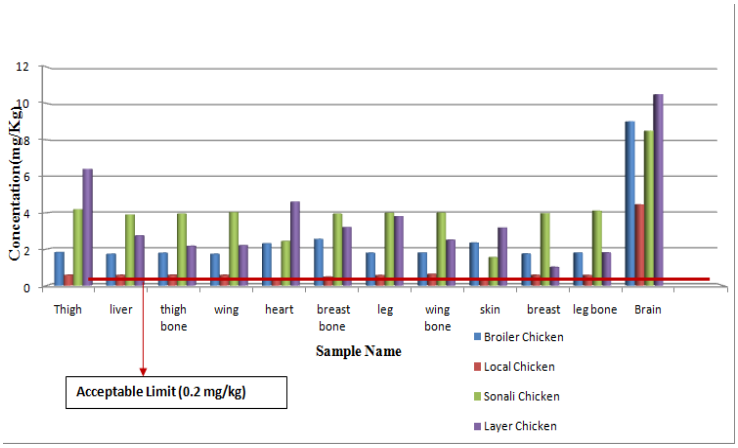

Figure 2: Graph showing concentration of Cr in chicken

But once absorbed, it starts to retain in body throughout life time. It has been stated by McLaughlin et al. (1999) that Cadmium accumulated in the kidney and liver over long period connects with a number of minerals mainly Zn, Fe and Cu. Cd can also be the reason of bone demineralization, either through direct bone damage or indirectly as a result of renal dysfunction[3].Cadmium concentration was determined in cattle in Poland by Aranha et al. (1994) and Roga-Franc et al. (1996) and found that it was above the maximum limit given by FAO/WHO,2000.From the observation of the results the concentration of Cd was found lower than the permissible limit given by FAO/WHO,2000,except thigh and leg bone of Broiler chicken.

Table 3: Concentration (mg/kg) of Cd & Cr in Chicken Eggs

Sample Name	Broiler Chick-en(Brown)		Broiler Chicken (White)		Local Chicken	
	Yolk	Albumen	Yolk	Albumen	Yolk	Albumen
Amount of Cd (mg/kg)	0.154	0.107	0.612	0.8	0.276	0.236
Amount of Cr (mg/kg)	1.84	4.77	3.66	11.8	4.7	4.84

Chromium (Cr) as observed in different parts of chicken showed the highest concentration of 10.5 mg/kg in brain of layer chicken and lowest concentration 0.35 mg/kg in the heart of local chicken. Cr is an important element which plays an important role in metabolic functions of human body but at the same time it is carcinogenic for organisms [9]. High concentration of Cr may cause harmful

health effects [2].The concentrations of chromium in all the samples of chicken studied were higher than the permissible limit of 0.20 mg/kg.

The results related to Cd and Cr levels in chicken egg are in accordance with the study carried out in the research which is represented in Table 3. Our measurements for Cd content in the eggs were lower than the standard limit except broiler chicken egg (white) samples However, recorded average concentration of Cr in eggs was greater than levels found in other local and international standards. These levels of heavy metals in chicken samples result from mainly contamination of the feed. As a result people that consume chicken meat are likely to be exposed to higher heavy metal levels. The facts given herein will be essential to set recommendations and standards for heavy metals in different varieties of chicken in Bangladesh.

5 CONCLUSION

- Among the heavy metals determined in the study, Cr displayed the largest number of samples that exceeded the tolerance level.
- Levels of Cd in chicken meat were also found to be beyond the tolerated limit. Maximum concentration of Cd was found in Broiler chicken.
- It was found from our research that among the four chicken species presence of heavy metal (Chromium) was found maximum in Layer Chicken as they consume poultry feed for a longer period (18 months) of time than other species.
- Concentration of chromium was minimum in local chicken compared to other species chicken. As layer chicken contains maximum heavy metal, so consumption of these chicken species should be minimized or avoided for human health betterment.
- The toxic elements are of particular concern as most of the detected concentrations in the samples exceeded the FAO/WHO, 2000 guideline value. Their consequence on the local population due to daily consumption of these contaminated chicken and chicken eggs is unknown and deserves further detailed study of feed used to feed these poultry chickens.

6 RECOMMENDATIONS FOR FUTURE STUDY

Due to limitation of time, equipment and other resource research was not done with more number of samples. It was not possible to investigate other chemical rather than Chromium and Cadmium present in collected samples. So enough scope is there for further studies on this topic. Some are given below:

- Chicken of certain age which is found in local market was used as a sample in our experiment. Chicken of different age can be collected from

poultry firm and presence of heavy metal in chicken flesh can be analyzed according to their age.

- Because of shortage of time we could not test the concentration of steroid and antibiotic in chicken, fish and duck sample. So this test can be done for further studies.
- Human bodies can be analyzed for deposition of Cd, Cr.
- We have determined only Chromium and Cadmium concentration. Further studies on Zn, Mn, and Pb determination in chicken sample can be carried out.
- Chicken sample can be analyzed according to different district of Bangladesh.

ACKNOWLEDGEMENTS

We would like to express our sincere gratitude to Mr. Kalam of the Department of Civil Engineering, MIST, Dhaka for his laboratory assistance.

REFERENCES

[1] Akan J.C., Abdu F.I., Irahman, O.A., Sodipo, Chiroma Y.A., 2010, Distribution of Heavy Metals in the Liver, Kidney and Meat of Beef, Mutton, Caprine and Chicken from Kasuwan Shanu Market in Maiduguri Metropolis, Borno State, *Research Journal of Applied Sciences, Engineering and Technology 2(8):pp 743-748.*

[2] ATSDR. 2004. Public health assessment guidance manual. Atlanta, GA: U.S. *Department of Health and Human Services, Public Health Service, Agency for Toxic Substances and Disease Registry*.

[3] Burger J. Heavy metals in avian egg shells: another excretion method. *Journal of Toxicology and Environmental Health 1994; 41: pp 207-220.*

[4] C. Hauber and H. P. Germann, Investigations on a possible formation and avoidance of chromate in leather, *World Leather, 13 (5), 2000, pp 38.*

[5] Elahi.S, Hossain. A; Islam.M, Kazi. M, Mamun. M and Rahman. M, 2009.Assessment of Tannery Based Chromium Eco-toxicity through Investigating Regional Bio-concentration in Commercially Produced Chicken Eggs and their Physical Properties. *Bangladesh J. Sci. Ind. Res. 44(1), pp 11-30.*

[6] Fakayode SO, Olu-Owolbi IB. Trace metal content and estimated daily human intake from chicken eggs in Ibadan, Nigeria. *Archives of Environmental Health 2003; 58:pp 245-251.*

[7] Golow A.A.,1993, Some heavy metals Accumulate more in the flesh of Thryonomisswinderianus (Lem), Grasscutter, than in Beef of Bos Species, Cow, *Bulletin of Environmental Contamination and Toxicology; 50:pp 823 –827.*

[8] Hasan. S, Mazumder. L and Rahman. M, 2013.Hexavalent Chromium in Tannery Solid Waste Based Poultry Feed in Bangladesh and Its Transfer to Food Chain. *IOSR Journal Of Environmental Science, Toxicology And Food Technology (IOSR-JESTFT)e-ISSN: 2319-2402,p-ISSN:2319-2399.Volume 3, Issue 4 (Mar. -Apr. 2013), pp 44-51*.

[9] Institute of Medicine,2002. Dietary Reference Intakes for Vitamin A, Vitamin K, Arsenic, Boron, Copper, Iodine, Manganese, Nickel, Silicon,Vandium and Zinc. *Institute of Medicine of the National Academies. The National Academy Press. Washington D.C. USA.*

[10] Kan CA, Meijer GAL. The risk of contamination of food with toxic substances present in animal feed. *Animal Feed Science and Technology 2007; 133(1/2): pp 84-108.*

[11] P. N. Sudha, 2010 "Are we eating chrome chicken?" *The Socioscan, 2(3&4), pp 69-71*.

[12] M. Mamun, M. A. I. Kazi, & S. F. Elahi, 2009. Assessment of tannery based chromium eco-toxicity through investigating regional bio-concentration in commercially produced chicken eggs and their physical properties. *Bangladesh J. Sci. Ind. Res., 44(1), pp 11-30.*

[13] M. Hossain, M.M. Monir, T. Rezwan, A.M. Haque, U.L. Kazi, M.S. Islam, and S.F. Elahi, Heavy metal concentration in tannery solid wastes used as poultry feed and the ecotoxicological consequences, *Bangladesh Journal of Science and Industrial Resources, 42(4), 2007, pp 397-416.*

[14] T. Mahmud, R. Rehman, S. Ali, J. Anwar, A. Abbas, M. Farooq, & A. Ali, 2011. Estimation of chromium (VI) in various body parts of local chicken. *J. Chem. Soc. Pak.,33(3), pp 339-342.*

CICM 2015
First International Conference on
Advances in Civil Infrastructure and Construction Materials
MIST, Dhaka, Bangladesh, 14–15 December 2015

A STUDY ON URBAN MOBILITY IN NORTHERN CITIES OF BANGLADESH

Riffat ISLAM[1] **and Md. Kamruzzaman**[2]

[1] Department of Civil Engineering, Rajshahi University of Engineering and Technology
Rajshahi, Bangladesh
Email: [1]riffat_sarzia@yahoo.com and [2]kzaman@ruet.ac.bd

Abstract. *The percentage of urban areas dedicated to streets and public spaces is a crucial feature of spatial planning of cities. By 2050 urban mobility will be one of the biggest confronts of cities around the globe. This study has been carried out to assess the ratio of public space allocated to the streets in some cities of Bangladesh. The length, width, area and number of street crossings have been counted for city core and its suburban area, as an indicator of the form and pattern of the street layout. In this exercise, the rest of the public space, like gardens and general public spaces for amenities, including sports, are not taken into account. The methodology of data collection has been through Google Earth and GIS software. For precise results, other more sophisticated software is essential. Nevertheless, even at these levels of precision, very interesting city patterns emerge. The findings of this study show that Bogra, Rangpur, Dinajpur are better cities having higher land allocation rate for street, including sufficient crossings. Nilphamari and Thakurgaon have lower land area for streets; tend to have lower connectivity and productivity. Rest of the cities has average land area for street and average number of street crossings.*

Keywords: Intersection, Street area, Street density, Urban mobility.

1 INTRODUCTION

Urban mobility often used to indicate a set of interrelated measures to satisfy the mobility needs of people and businesses, today and tomorrow; in city and their surrounding areas. Urban mobility can ensure accessibility to the transport system to all, improve safety and security, reduce pollution and can make the urban environment attractive. It is one of the toughest challenges that cities face today as existing mobility systems are close to breakdown (Little A., 2014). The question of how to enhance urban mobility while at the same time reducing congestion, accidents and pollution is a common challenge to all major cities in the world.

National guideline for urban mobility planning provides orientation to local authorities. In several countries, such as Brazil, France and India, the development of urban mobility plans has become an obligatory requirement for receiving national government funds for local transport projects (GIZ, 2014). Too often, transport infrastructure fails to keep up with the mobility needs of the growing urban population. Setting a city on a sustainable course regarding its land use and transport system requires a clear roadmap of urban mobility plan. A successful urban mobility plan can provide a feasible and powerful strategy to tackle urban mobility challenges.

The percentage of urban areas dedicated to streets and public spaces is a crucial feature of urban mobility. Cities that have adequate street and public spaces and greater connectivity are more livable and productive (UN-Habitat, 2013a). The significance of urban mobility plan in providing solution for urban transport system in Bangladesh holds in stark contrast with the very limited research on the topic. Lack of information on characteristics and scale of 'Urban Mobility' makes it difficult to formulate appropriate policies and this paper attempts to uncover these facts.

2 OBJECTIVE OF THE STUDY

Mobility flows have become a key concern of urbanization. Despite the increasing level of urban mobility worldwide, access to places, activities and services has become increasingly difficult (UN-Habitat, 2013b). Many of the world's cities face an unprecedented accessibility crisis, and are characterized by unsustainable mobility systems.

The aim of the study is to examine the state of urban mobility in some selected cities of Bangladesh. It attempts to explore the linkages between percentage of urban land allocated for street network and level of urban mobility. The study also intends to highlight the status of different mobility parameters of each cities and their interrelation on the mobility ranking of all cities. Finally, the study plans to compare the state of urban mobility among Bangladeshi cities with some international cities.

3 METHODOLOGY

Percentage land area for street, street density and number of intersection are the parameters under which mobility ranking of study cities are conducted to propose whether a city is highly, moderately or poorly accessible. The study used ortho-photos and GIS in determination of public space allocated to street in ten northern cities of Bangladesh. The number of street crossings also counted during the study. Images from 'Google Earth' were analyzed in AutoCAD first to find out the street length, street area and number of crossings.

Dinajpur, Bogra, Lalmonirhat, Pabna, Sirajganj, Rangpur, Nawabganj, Rajshahi, Nilphamri, Thakurgaon city are selected as study area. At the beginning, orthophotos of those cities are captured from Google Earth. Shape file of a particular city (under study) is collected and used in GIS software (Arc View) to convert it into KML file for projection on Google Earth. While considering a city under study, city core and suburb areas are considered for mobility analysis. City core is considered taking a particular radius around the buildup city centre. A greater study area has been considered ranging from city center to suburb to compare on the mentioned parameters. Using "Add Path" tool in Google Earth, street layout of all visible streets is drawn from Google Earth. The entire street network of study area including city core and suburb was exported to Auto CAD by converting the KML file to DXF file to work in AutoCAD platform. The map was drawn in proper scale. The entire area (city core and suburb) is divided into number of small blocks, using separate 'hatches', in Auto CAD. Street length is determined using '*tlen*' AutoLISP program. Land area and street area are computed for individual small blocks and the sum of all block determines total urban land area for street and the percentage of land allocated to street.

4 FIXATION OF STREETS IN CITY CORE AND SUBURBAN AREA

The city boundary is fixed by exporting the shape file of the corresponding city in Google Earth. For example, fixing of city core including suburb for Dinajpur city is shown in Fig. 1, 2 & 3 respectively.

Fig 1: Ortho Photo of Dinajpur from Google Earth

Fig 2: Suburb in Blue Color

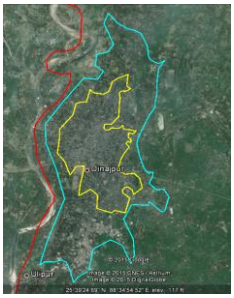

Fig 3: City Core in Yellow Color

Table 1 shows fixation of city core and suburb for Dinajpur city as an example:

Table 1: Fixation of City Core and Suburb Area (Dinajpur)

City Name	City core area (km^2)	Suburb area (km^2)	Remarks	
Dinajpur	5.35	15.97	City core is considered taking 1.0 km radius in 'X' direction & 2.0 km radius in 'Y' direction from the city center.	Suburb is considered taking 1.35 km radius in 'X' direction & 4.00 km in 'Y' direction from the city center.

5 COMPUTATION OF STREET LENGTH AND STREET AREA

Entire street layout is drawn in Google Earth (Fig 4). Length, width and land area of all streets and number of crossings are counted after the map is exported to AutoCAD (Fig 5) from Google Earth. Fig 6 shows street layout, hatched areas and street-intersections respectively for Dinajpur city.

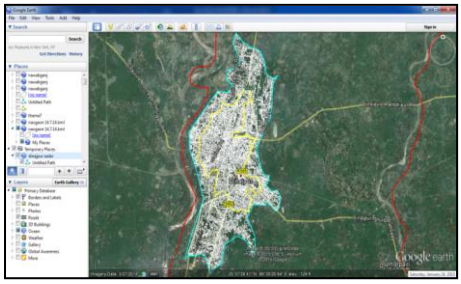

Fig 4: Entire Street Network of Dinajpur City is drawn in Google Earth.

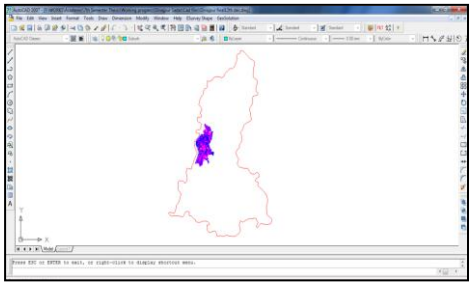

Fig 5: Complete Street Network of Dinajpur City is exported to AutoCAD for Analysis

Following the steps, street databases of all cities are prepared. For example street database for Dinajpur is presented in Table 2.

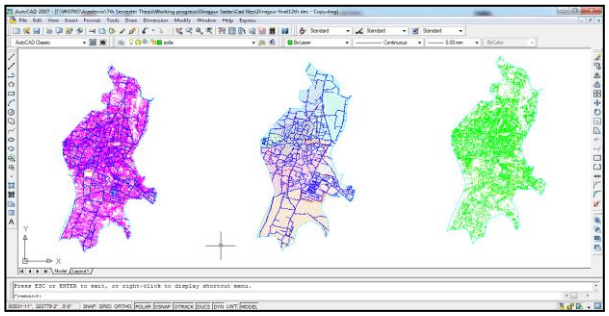

Fig 6: Street Network, Blocks and Marking of Crossings
for Dinajpur City using Auto CAD.

Table 2: Percentage of Land Allocation for Street & Street Density for Dinajpur

Region	Total Land Area (km²)	Total Street Area (km²)	Street Width (m)	Percentage of Street Area (%)	Total Streets Length (km)	Street Density (km/km²)	Total No. of Crossing	Intersection Density (Crossing/km²)
City core	4.07	0.34	3.64	8.35	93.45	22.96	767	188.45
City core & Suburb	15.81	0.93	3.26	5.88	285.41	18.05	1964	124.23

6 RESULTS & DISCUSSION

6.1 Mobility Gradation of Cities

Table 3 shows a very important disparity of land allocation rate for street network, varying from 8.91 to 18.75 percent. This disparity itself is a good entry point to describe the urban mobility consequences in cities in Bangladesh. The top five cities ranges between 16.35 and 18.75 percent of urban land allocated to the street and may be considered as cities having good mobility. Land allocation rate falls between 14.18 and 15.94 percent of some cities which are considered having average mobility. Finally, cities having land allocation rate between 8.91 and 9.03 percent, may be considered as cities having poor mobility. Table 4 shows above average, average and below average ranking of cities based on the criteria of street density. Fig 7 and Fig 8 are graphical representation of ranking of cities based on percentage of urban land for street and street density. In both cases, Dinajpur and Bogra city are top ranking cities having street density and

percentages of street area holds above average range. On the other hand, Nilphamari and Thakurgaon city has the lowest ranking having street density and percentages of street area having below average range. The remaining cities like Rajshahi (Boalia Thana), Sirajganj, Rangpur, Pabna, Nawabganj and Lalmonirhat has average accessibility and mobility.

Table 3: Ranking of Cities Based on Percentage of Urban Land for Street

Name of Cities	Area of City Core (km²)	Total Street Area (km²)	Percentage of Street Area (%)	Ranking Based on % of Street Area	Remarks
Bogra	4.16	0.78	18.75	1	
Rangpur	4.52	0.85	18.72	2	Above Average
Dinajpur	5.35	1.00	18.69	3	
Sirajganj	3.47	0.58	16.71	4	
Pabna	3.12	0.51	16.35	5	
Rajshahi (Boalia)	3.2	0.51	15.94	6	
Lalmonirhat	2.89	0.44	15.22	7	Average
Nawabganj	5.5	0.78	14.18	8	
Nilphamari	5.76	0.52	9.03	9	Below
Thakurgaon	18.4	1.64	8.91	10	Average

Table 4: Ranking of Cities Based on Street Density

Name of Cities	Area of City Core (km²)	Length of Street (km)	Street Density (km/km²)	Ranking Based on Street Density	Remarks
Dinajpur	5.35	309.4	57.83	1	Above Average
Bogra	4.16	238.58	57.35	2	
Lalmonirhat	2.89	146.38	50.65	3	
Pabna	3.12	153.84	49.31	4	
Sirajganj	3.47	164.15	47.31	5	
Rangpur	4.52	203.08	44.93	6	Average
Nawabganj	5.50	240.61	43.75	7	
Rajshahi (Boalia)	3.20	117.49	36.72	8	
Nilphamari	5.76	160.27	27.82	9	Below
Thakurgaon	18.4	406.02	22.07	10	Average

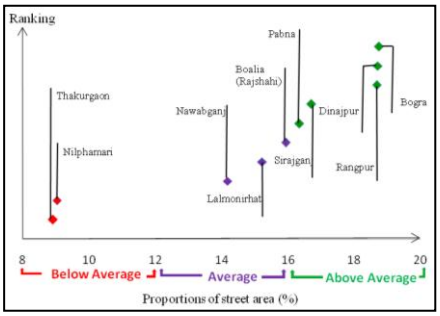

Fig 7: Ranking of Cities in Based on Percentage of Land for

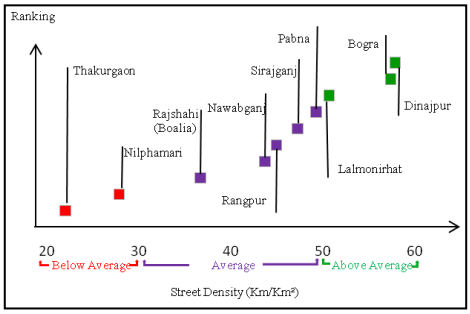

Fig 8: Ranking of Cities Based on Street Density

6.2 Relation between Percentages of Street Area and Intersection Density

Figure 9 establishes the inter-connection of the two variables studied above. The ranking of cities is provided for each variable and the linkage between the two variables. Ten cities have been chosen in order to have a wide variety of cities.

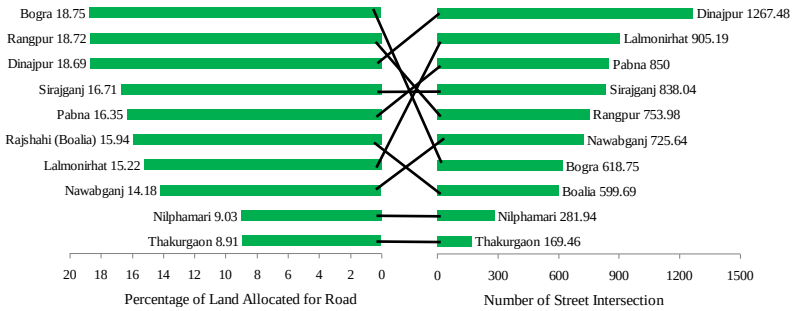

Fig 9: Inter-relation between Percentages of Street Area & Intersection Density

The central area of the city has been chosen, meaning areas of less than 5.0 km^2, in order to ensure the comparability of different cities. This provides for an interesting mixture of space and pattern which explains about the efficiency of the city. The result explores these factors in order to develop efficient tools of plotting for the matrix of the public space in the urban areas.

6.3 Frequency of Cities based on the Mobility Parameters

It is important to understand that the quantity of the public space is not related to the price of land. In general, the price of land is much higher in cities that have more public space. This should be an additional reason to ensure proper delinea-

tion of unbuilt space at the beginning of urbanization, when the price of land is cheaper. Figure 10 shows that there are about 5 cities having land area more 16% for street network and only 2 cities having lass than 12% land for street. Cities are more accessible and attractive if the street area and open space are more.

Figure 11 displays the number of street intersections per km^2 of urban area in selected cities as measured by the described methodology. Cities range from 1267 (Dinajpur) to 169 (Takurgaon) crossings per km^2. Cities having more crossing are considered walkable and appropriate in many cities, in order to generate street life and for moving goods and services productively and efficiently. Majority of cities of Bangladesh have good number of intersection.

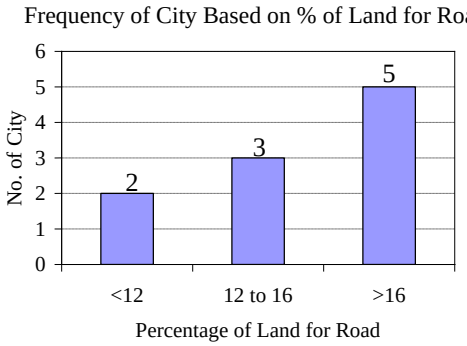

Fig 10: Frequency of Selected Cities having Different Percentage of Land for Street

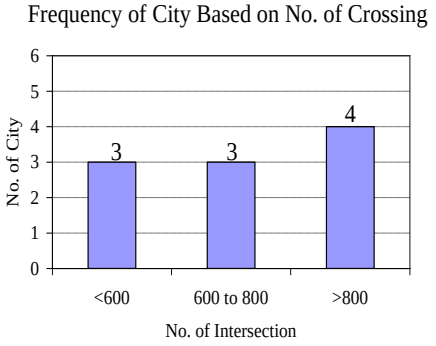

Fig 11: Frequency of Selected Cities having Different No. of Intersections

6.4 Comparison between International and Cities of Bangladesh

Fig 12 provides a clear representation of scale of urban mobility among various international cities and Northern cities of Bangladesh based on percentages of land area for street and number of crossing respectively. In general, international cities have more urban lands allocated for street and more intersections, which causes better mobility.

7 CONCLUSION

Ranking of cities according to the parameters gives a clear depiction of how mobility strengthens the accessibility of a high ranked city (Bogra) whereas weakens that of a low ranked city (Thakurgaon). These findings provides an entry point for addressing the issue of urban mobility, inefficiency or lack of urban planning and clearly suggest the high priority that cities in Bangladesh should put on early attention to planning when land is still inexpensive, in order to avoid future gridlocks and congestion.

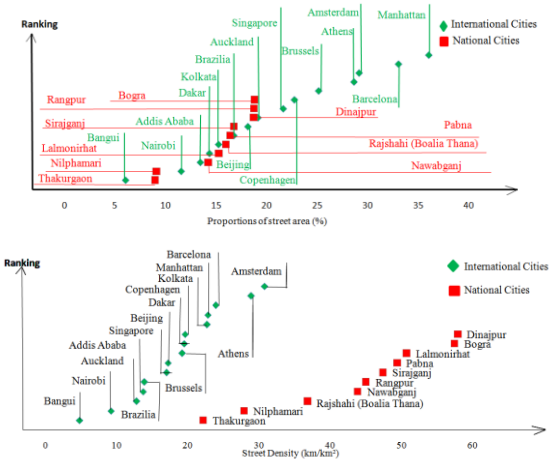

Fig 12: Ranking of 15 Different Cities of World and 10 Cities of Bangladesh in Relation to (Top) Percentage of Land Area for Street and (Bottom) Street Density.

REFERENCES

[1] Arthur D. Little (2014) 'The Future of Urban Mobility 2.0', UITP 2014 at (www.adl.com/FUM2.0)

[2] GIZ (2014) 'Urban Mobility Plans: National Approaches and Local Proactices', Sustainable Urban Transport Technical Document #13, Deutsche Gesellschaft für Internationale Zusammenarbeit (GIZ) GmbH. Available at: (http://www.eltis.org/sites/eltis/files/trainingmaterials/td13_ump_final.pdf).

[3] UN-Habitat (2013a) 'The relevance of street patterns and public space in urban areas', UN-Habitat Working Paper, April, Nairobi, http://www.unhabitat.org/pmss/listItemDetails.aspx?publicationID=3465

[4] UN-Habitat (2013b) 'Planning and Design for Sustainable Urban Mobility: Global Report on Human Settlement 2013', Earthscan, London.

CICM 2015
First International Conference on
Advances in Civil Infrastructure and Construction Materials
MIST, Dhaka, Bangladesh, 14–15 December 2015

MODELLING AND CALIBRATION OF FUNDAMENTAL DIAGRAM FOR MERGING MULTI-LANE TO SINGLE-LANE HETEROGENEOUS TRAFFIC FLOW SITUATION IN BANGLADESH

H. M. I. KAYS[1], M. A. H. Khan[2], M. Hadiuzzaman[3], S. M. Muniruzzaman[4], S. Hossain[5], N. Haque[6]

[1, 4] Department of Civil Engineering, Military Institute of Science and Technology, Dhaka, Bangladesh. Email: imran.kays@ce.mist.ac.bd, shah2713@gmail.com

[2] Works and Contract Section, Special Works Organization, Dhaka, Bangladesh Email: amir5266@gmail.com

[3, 5, 6] Department of Civil Engineering, Bangladesh University of Engineering and Technology, Dhaka, Bangladesh. Email: mhadiuzzaman@ce.buet.ac.bd, sanjana@ce.buet.ac.bd

Abstract. *In order to investigate the traffic flow characteristics, finding out fundamental diagram (FD) is one of the most important requirements. In fact, the FD (describing flow-density, speed-density or speed-flow relationship at a given location or section of the roadway) is a basic tool in understanding the behavior of traffic stream characteristics in macroscopic flow models. However, the structure of FD has not been investigated to model heterogeneous traffic condition. In this regard, two test sections having non-lane-based heterogeneous traffic composition were selected in Dhaka-Chittagong (N-1) Highway, Bangladesh. Moreover, considering the study objective, the test sites include a special geometric characteristic. Specifically, the test sections merge from two lanes to single lane in each direction. Three hour high-resolution traffic data was collected in these two sections in one direction (from Chittagong to Dhaka). Analyzing these data, the representative structures of FD along with the trends of the FD parameters were found out through calibration for representing the merging of heterogeneous non-lane-based traffic flow behaviour of highways.*

Keywords: Heterogeneous traffic, Fundamental diagram, Jam density, Multiple regression.

1 INTRODUCTION

The fundamental diagram (FD) is a speed-flow-density relationship that reflects the interrelation between these traffic flow parameters. It is of several equivalent forms: flow-density (occupancy), speed-density (occupancy), speed- flow with two foliations: upper limb and lower limb and sometime another point of capacity drop is found. It started from classical work of Greenshields [1], which provide a basic tool for traffic modelling. Traffic flow parameters can be estimated from gathered field data and empirical relationship in FD. The models within the fundamental diagram framework can be classified into two main classes. The first class is associated with Lighthill-Witham-Richard model (LWR) [2], where capacity of a roadway is denoted as the maximum flow in FD. An example of this model is Cell Transmission Model (CTM) by Daganzo [3]. The second class is associated with the classic General Motors (GM) model of Herman, Gazis, Rothery, Montroll and Potts [4] which states that at the beginning of critical density, there is instability of steady model state at the fundamental diagram. This instability is associated with a finite value of driver's reaction time. Examples of GM models can be Optimal Velocity (OV) model by Newell, Witham and Bando et al. [5], Payns's macroscopic model [6], Wiedemann's physiological traffic flow model [7], Nagel-Screckenberg Celular Automata (CA) model [8], Intelligent Driver Model (IDM) by Treiber et al. as well as huge other traffic flow models are found. Considering the number of state variables used to present traffic dynamics, macroscopic models are categorized into two major types: (1) 1^{st} order; and (2) 2^{nd} order. 1^{st} order traffic models contain a conservation equation: flow equals to the speed multiplied by density and a steady-state speed-density relation showing linear relationship of FD in Figure 1. 2nd order traffic models have an independent speed dynamics in addition to the 1^{st} order models hence showing non-linear relationship of FD in Fig 1.

In Bangladesh, where non-lane based heterogeneous traffic situation prevails, it is necessary to model FD for traffic operation and long-time traffic planning. Considering this, the primary objective of the paper is to model FD in context of Bangladesh and to investigate changes in shape and nature of FD in converging heterogeneous traffic flow situation in N-1 national highway.

This paper will present the data collection and analysing procedure in the test site. After that representative FD will be formed to represent the traffic flow parameters. Here R^2 and Root Mean Square Error (RMSE) value of the curve along with nature of traffic flow will be considered for FD validation.

The second part of the paper will give a comparative study of the best fitted FD for converging traffic flow situation. Here traffic from two-lane to traffic of single lane is considered for converging situation. The comparison will be based on fundamental traffic flow parameters.

Hence at the end of the paper, the shape and flow parameters will be found for non-lane based heterogeneous converging traffic in national highway of Bangladesh.

2 METHODOLOGY

2.1 Study Area

The test segment was chosen in Dhaka-Chittagong highway (N-3 Highway) Bangladesh, which links Dhaka and Chittagong, two major cities in Bangladesh. The location is shown in Fig 01. Traffic data was collected in two points, the two-lane highway point 01(23°35'56.76"N 90°37'10.84"E) was in the upstream and the single-lane highway point 02 (23°35'57.14"N 90°37'10.65"E) was in the downstream where merging traffic flow situation was found. The interval of these two point is .37 mile. The lane width was found 3.05m with 1.22m shoulder. Traffic distribution is found as: Truck 33%, Bus 20%, Car 17%, Pickup 13%, CNG Auto-rickshaw 10%. The two directional traffic is separated with raised divider in point 01 and with road marking in point 02. Lane discipline was absent in these points. As mild bend was present, data collection points are not visible.

Figure 1: Test location map (courtesy: Google Map) (left), Details of camera setting at point 01 (right) (Data Collected on 26 October 2015; 0900 to 1200Hr)

2.2 Data Collection and Processing

As FD will represent the fundamental parameter of highway, high resolution data is necessary for calibration. Under existing road condition, it was challenging to collect high accuracy data. Moreover loop detector is not recommended for the test site due to measurement error caused by non-lane-based movement of vehicles activating either both or neither of two adjacent detectors. Also traffic cam-

eras for vehicle detection are absent along the corridor. Under these circumstances, video cameras are installed at the two points of study site to provide traffic data for the research using image processing technique.

Two video cameras are installed in two locations along the mainline. Object detection algorithm has been developed based on Background Subtraction (BGS) for extracting high resolution data from video footage. The developed algorithm successfully detects non-lane-based movement of vehicles. It can also identify non-motorized traffic, dark car and shadow quiet accurately. The algorithm addresses some of the major problems faced in the BGS technique, like the camouflage effect, camera jitter, sudden illumination variation, low camera angle and elevation etc. video data and vehicle geometry are provided as input to the algorithm and it gives vehicle count and time mean speed at the test site. For measuring traffic flow, strip based counting method combining successive incremental differentiation is used. On the other hand, measuring speed, the algorithm segments the whole field of vision and detects the changes in centre of area of an object in each segment to find the corresponding pixel speed. Then calibrating the pixel distance with the field distance, instantaneous and time mean speeds are obtained, which can easily be converted to space mean speed. The developed algorithm has been proved to give highly accurate data with minimal Mean Absolute Error (MAE) of flow and speed measurements. The density of the traffic stream for the research is estimated from the measured flow and speed. Three hour data of 25th August 2015 was collected which covered both free flow region and congested region for calibrating FD. To ensure better quality of data camera height was maintained 25ft and 18ft for point 01 and point 02 respectively as shown in Figure 01 (right) to reduce object details detected. Camera angle of projection was also maintained less than 45^0 so as to cover approximately 150ft in the test site and to avoid perception problem.

3 CALIBRATION OF FUNDAMENTAL DIAGRAM

Different types of FD are proposed over year depending upon the traffic flow condition, roadway environment. To derive most appropriate FD for our test sites, more established models are tested and the field data are fitted to the representative equations with the help of Least Square Approach. In general, flow (q) is a concave function of density (ρ) in [0, ρ_j] (ρ_j is jam density) and also speed (v) is a function of density (ρ) generally showing decreasing trend.

To investigate the nature of FD of $v-\rho$ relationship of heterogeneous non-lane-based traffic situation oud field observed data are fitted in five different models, namely Greenshild's Linear Model, Edie's Logarithmic Model, Polynomial Model of two degree, three degree and Exponential Model shown in Figure 2 and Figure 3. The result found from these model fitting are tabulated in Table 1 and Table 2.

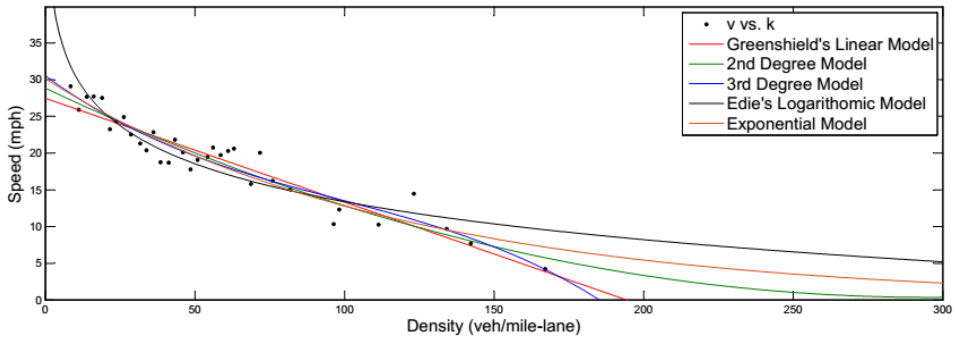

Figure 1: Five Different Model of FD for two lane highway.

Table 1: Results from different Model fitting for Two Lane Highway Data

Model	Equation	R2	RMSE
Greenshield's Linear model	$v = 0.1413k + 27.47$	0.8914	1.979
2nd degree model	$v = 0.000325k^2 - 0.1924k + 28.84$	0.9042	1.918
3rd degree model	$v = -6.625\times10^{-6}k^3 + 0.00195k^2 - 0.2992k + 30.53$	0.9118	1.871
Edie model (logarithm model)	$v = 47.71 - 7.45\log(k)$	0.855	2.322
Exponential Model	$v = 30.13e^{-0.0086k}$	0.8986	1.913

The first analysis is for test point 1, two lane highway. From Greenshild Model, it is found that R^2 and RMSE value are 0.8914 and 1.979 respectively with initial v_f is found 27.47 mph and ρ_j as 179 veh/mile-lane (vpml). Two degree model curve fitting shows more accurate relationship, R^2 and RMSE values are 0.9042 and 1.918 with v_f of 28.84 mph and ρ_j is not within limit. Three degree equation shows R^2 and RMSE value of 0.9118 and 1.871 with v_f of 30.53 mph and ρ_j as 175 vpml. Edie's Logarithmic Model shows unnatural behaviour of infinite initial speed and jam density out of the limit. Exponential Model have R^2 and RMSE value of 0.8986 and 1.913 respectively with v_f of 30 mph and ρ_j is found infinite without intercepting the axis.

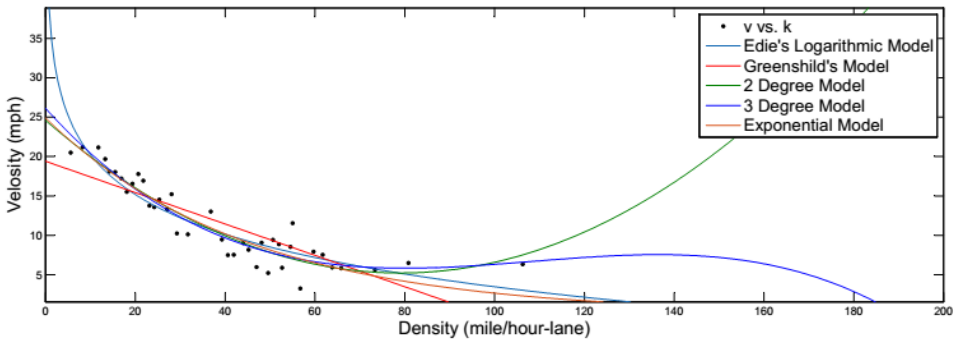

Figure 2: Five Different Model of FD for single lane highway.

Table 2: Results from different Model fitting for Single Lane Highway Data

Model	Equation	R^2	RMSE
Greenshields fundamental model	$v = -0.199k + 19.41$	0.7294	2.711
2nd degree model	$v = 0.0031k^2 - 0.4901k + 24.6$	0.8925	1.732
3rd degree model	$v = -1.923\times10^{-5}k^3 + 0.0062k^2 - 0.6303k + 26.14$	0.897	1.719
Edie model (logarithmic model)	$v = 37.72 - 7.481\log(k)$	0.87	2.003
Exponential Model	$v = 24.92e^{-0.0223k}$	0.8696	1.882

Another analysis is made for point 2 single lane highway. In this merging traffic condition five types of models fitted and hence the results are found. From Greenshild model fitting, R^2 and RMSE value are found as 0.7294 and 2.711 respectively with v_f of 19.41 mph and ρ_j of 88 vpml. For two degree model fitting, R^2 and RMSE value are found as 0.8925 and 1.732 respectively with v_f of 24.6 mph and ρ_j of 75.66 vpml as lowest point in the curve. Three degree model gives R^2 and RMSE value as 0.879 and 1.719 respectively with v_f 26.14 mph and ρ_j 186 vpml. Edie's logarithmic model also shows unnatural behaviour of infinite initial speed and ρ_j is found as 130vpml. Exponential Model shows R^2

and RMSE value are 0.8696 and 1.882 respectively with v_f of 25mph and ρ_j are found infinite without intersecting the axis.

4 RESULT

A comparison is made based on found results of R^2 and RMSE value is made in table 3.

Table 3: Comparison of R2 and RMSE value of different model

Model	Two Lane Highway		Single Lane Highway	
	R^2	RMSE	R^2	RMSE
Greenshield's Linear model	0.8914	1.979	0.7294	2.711
2nd degree model	0.9042	1.918	0.8925	1.732
3rd degree model	0.9118	1.871	0.897	1.719
Edie model (logarithm model)	0.855	2.322	0.87	2.003
Exponential Model	0.8986	1.913	0.8696	1.882

Considering the R^2 and RMSE value 3 degree model and exponential model are best suitable for both cases. Therefore, nature of curve and value of parameters are required to consider for investigation.

Exponential model for two lane and single lane highway are showed in Fig 3. The trend in both cases shows decreasing downward. Free flow speed value reduces from 30 mph to 20 mph for merging from two lanes to single lane. But jam density cannot be defined in both cases.

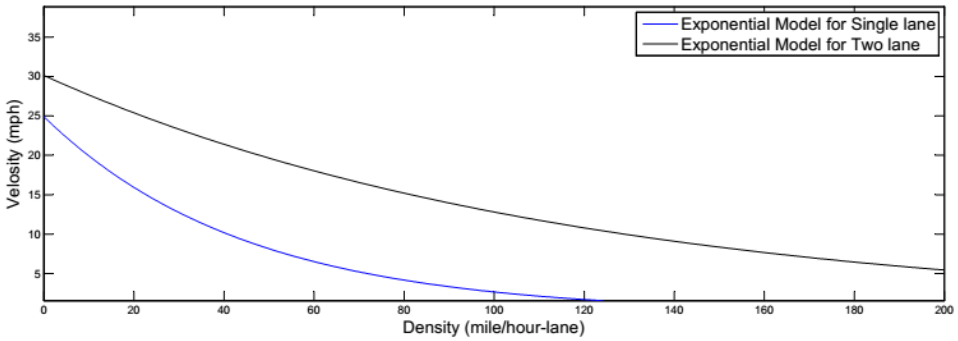

Figure 3: Comparison of Exponential model for point 1 and point 2.

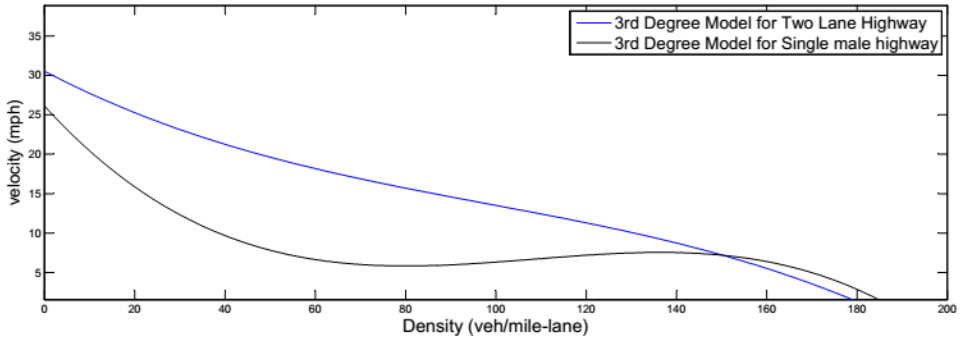

Figure 4: Comparison of Three Degree model for point 1 and point 2.

After calibration of three degree model for both two lane highway and single lane highway free flow speed is found 14.4% reduces in merging condition from two lane to single lane highway. Traffic density value depends on the length of vehicles, occupancy in that link and distance gaps between them. The model estimate Jam density of 175 vpml for two lane and 186 vpml for single lane highway. In these high density condition when density approaching jam density, this model estimate speed value higher for single lane highway segment than two lane highway segment. This behaviour is due to gap acceptance of vehicles in these section and presence of raised divider in two lane segment. Due to absence of raised divider and presence of road marking, when the density approaching jam density, some vehicle access roadway crossing the read marking. This is the main reason of estimation of increased velocity and higher density in interval of 100 vpml to 186 vpml for single lane highway. As density value is dynamic, change with variable, increased jam density value found in single lane highway won't disturb the model. Hence the 3 degree FD model we found after the investigation represents most reliable and realistic representation of the merging two lane to single lane traffic condition in N-1 highway of Bangladesh.

5 CONCLUSION AND FUTURE RESEARCH

A thorough and comprehensive literature review in introduction different fundamental diagram model is found but there is no specific fundamental diagram for non-lane-based heterogeneous traffic situation. So in this study we have collected field data with approximately 15% error and calibrate different fundamental diagram with these data. After very comprehensive analysing three degree FD model satisfy the limiting conditions and behaviour of the two test sites. Hence following remarks are found from the model.

(1) Free flow speed when density approaches to 0, is 14.4% higher for two lane highway.

(2) Initial slope of single lane highway is steeper than that of two lane highway which shows speed reduces drastically in single lane highway due to less headway distance.

(3) Roadway without raised divider shows higher jam density value because of driver behaviour.

This three degree model is useful in finding $v-\rho$ relationship in highways of Bangladesh which will be further used in car following model, lane changing model in heterogeneous, non-lane-based merging traffic condition. Further study on this area will be focused on modelling fundamental diagram for other roadway condition of different national highways of Bangladesh, so that we can model more generalised model to be used globally.

6 REFERENCES

[1] Greenshields, B. D., (1934). A study of traffic capacity, HRB Proceedings. 14, P448-481.

[2] Lighthill M. J. and Whitham G. B. (1955) on kinematic waves II. A theory of traffic flow on long crowded roads. Proc. Royal Society of London, Series A, 229, 317-345.

[3] Daganzo, C. F. (1994). The Cell Transmission Model: A Dynamic Representation of Highway Traffic Consistent With the Hydrodynamic Theory. Transportation Research -B, Vol. 28B, No. 4, pp. 269-287.

[4] Gazis D.C., Herman R., Potts B., (1959). Car-Following Theory of Steady-State Traffic Flow, Operation Research 9, pp. 499 – 505.

[5] Newell G. F. (1961). Nonlinear Effects in the Dynamics of Car Following. Operation Research 9, pp. 209 – 229.

[6] Bando M., Hasebe K., Nakayama A., Shibata A., Sugiyama Y.(1994). Structure stability of congestion in traffic dynamics, Japan Journal of Industrial and Applied Mathematics, Volume 11, Issue 2, pp 203-223.

[7] Payne H.J., (1971). Mathematical Models of Public System. Vol 1, Simulation Council, La Jolla.

[8] Rickerta M., Nagelb K., Schreckenbergc M., Latourd A., (1995). Two lane traffic simulations using cellular automata, Physica A: Statistical Mechanics and its Applications, Volume 231, Issue 4, 1 October 1996, Pages 534–550.

CICM 2015
First International Conference on
Advances in Civil Infrastructure and Construction Materials
MIST, Dhaka, Bangladesh, 14–15December 2015

IDENTIFICATION OF HAZARDOUS ROAD LOCATIONS AND BLACK SPOTS ON DHAKA-BARISAL NATIONAL HIGHWAY

Farzana RAHMAN[1], **Fayaz Uddin**[2], **Md. M. Rahman**[3], **Md. Ariful Islam**[4]**and Afzal Ahmed**[5]

[1, 2] Department of Civil Engineering, University of Asia Pacific, Dhaka, Bangladesh.
Email: [1]farzana-ce@uap-bd.edu, [2]fayazbd@yahoo.com

[5] Department of Civil Engineering, Military Institute of Science and Technology, Dhaka, Bangladesh.
Email: afzal.ahmed2008@gmail.com

Abstract. *Road traffic accidents and corresponding causality are the most concerning issue in the transportation sector of a developing country like Bangladesh where road crashes are remarkably high. According to police reported road traffic accident database, every year about 2800 or more accidents occur in Bangladesh. This research analyzes the various accident data from year 2007 to 2011 using Microcomputer Accident Analysis Package (MAAP5) software in route N8 (Dhaka – Mawa – Barisal –Patuakhali National Highway) in Bangladesh. This research reveals accident prone locations which are commonly termed as black spot and Hazardous Road location (HRL) on the route N8 followed by establishing maps by Geographic Information System (GIS). Head-on, rear-end, overturning, side-swipe and hit-pedestrian are the most dominant types of accidents. Analysis shows that maximum number of accidents occurred in fair weather in route N8. The result clearly indicates that buses contribute mostly in the accidents.*

Keywords: Accident, Dhaka-Barisal (N8) highway, Black spot, Hazardous road location, GIS, MAAP5.

1 INTRODUCTION

Road safety problem draws significant attention in a developing country like Bangladesh where road crashes are extremely high. Road traffic accidents and the corresponding deaths are the most concerning issue in the transportation sector of the world. According to WHO's global status report on road safety 2013, more than 1.24 million people die each year on the world's roads. Only 28 countries, covering 7% of the world's population, have comprehensive road safety laws on five key risk factors: drinking and driving, speeding, and failing to use motorcycle helmets, seat-belts and child restraints (WHO, 2013). It has been estimated that over 300,000 persons die and 10-15 million persons are injured every single year in road traffic accidents throughout the world. According to police reported road traffic accident database, every year about 2800 or more accidents occur in Bangladesh. But the actual estimated road fatalities are as high as 10,000-12,000 each year (Rabbi, 2013). Other sources estimated the fatalities as high as from 12,000 to 20,000 per year. Moreover, road accidents have been shown to cost around 1% of annual gross national product (GNP) resources of developing countries, which they can ill-afford to lose (Kalga and Silanda, 2002).Being a developing country the road safety situation in Bangladesh is very severe compared to international standards. Dhaka – Mawa – Barisal – Patuakhali national highway (N8) is one of the major routes where a lot of road accident took place. This study focuses particularly on accidents in the N8 route aiming to examine the distribution of accident by types with particular emphasis on identification of Hazardous Road Locations (HRL) and Black spot.

2 LITERATURE REVIEW

2.1 Accident Database and GIS History and Application in Transportation

Geographic information system (GIS) is a computer system for capturing, storing, querying, analyzing and displaying geographic data. Establishment of the geographic referencing scheme is the major contributor in making data more readily available. Since early stage of GIS, it is noticed that a vision of information technology outside the traditional transportation data analysis and even outside GIS was needed to implement this technology (Lewis, 1990). Another study Apparao et al. (2013) focused on identification of accident black spots for highway using GIS for some countries of weak economy. Road traffic accidents have been recognized as one of those adverse elements which contribute to the suffocation of economic growth in the developing countries, due to the high cost related to them, hence causing social and economic concern. So Traffic safety is an important key and integral role in sustainable transportation development areas.

2.2 Accident Data Analysis Using MAAP5 and GIS

Accident analysis of N1 National Highway was conducted by analyzing five years accident data from the year 2007 to 2011. The accident data was collected from the MAAP5 database of Accident Research Institute (ARI) of Bangladesh University of Engineering and Technology (BUET). The Hazardous Road Locations (HRL) and Blackspots were identified by analyzing total and fatal accident data on the highway. Accident data was analyzed at every 100 meter interval on the road. The locations which have three or more fatal accidents and/or five or more total accidents during the six year time period have been identified as HRL. (Alam M. and Ahsan H. M., 2013).Hauqe (2007) has analyzed a portion of N5 National Highway named Dhaka-Aricha highway by analyzing five years accident data from the year 1998 to 2004. The locations which have at least three accidents during the seven year time period have been identified as HRL.

3 ANALYSIS

The study involves crash data collection and analysis by using MAAP5 software to identify black spot or HRL using Geographic information system (GIS). GIS has been identified as an excellent storing and managing software for these types of data and possesses a better visualization system.

3.1 Data Collection

In Bangladesh there are many sources for collecting road accident data e.g. police records, hospitals, newspaper reporting etc. However the basic source of accident data is the Accident Report Forms (ARF), which is primarily filled up by police personnel. These ARF and MAAP5 soft copy are edited by Accident Research Institute (ARI), BUET. Accident data was analyzed for the period of 5 years from 2007-2011. Findings are organized by accident severity, accident categories, accident period, collision type, vehicle involvement in the accident, routes where accidents took place, pedestrian-casualties etc. Accident data was analyzed for the period of 5 years (2007-2011) for identifying black spot or HRL.

On any road network, it has been seen that accidents are not randomly distributed, but are clustered at certain locations. Accident data was analyzed at 100 meter interval on the N8 route. In a 100 meter segment of a highway if accident number is three or more in 5 year period then the location is termed as black spot. Similarly in a 1000m segment of a highway if accident number is four or more in 5 year period then the location is termed as hazardous road location (HRL). The procedure followed in identification of Blackspot or HRL on Dhaka-Barisal highway is divided into few steps. The steps are shown in figure 1:

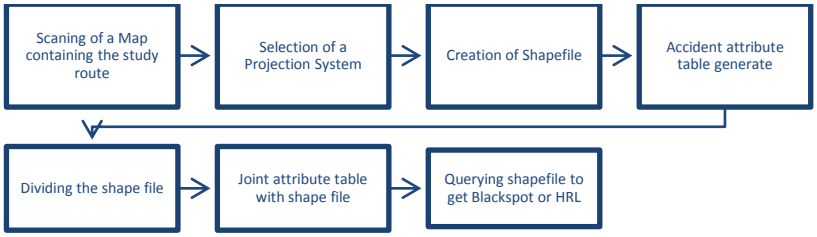

Figure 1: Steps Followed in GIS for Blackspot and HRL identification.

3.2 Data Analysis using MAAP5 Software

This section discusses the characteristics and striking features of overall road traffic accidents on national highways in Bangladesh. Accident data analysis was conducted for the period of 5 years from 2007-2011. The analysis involves the determination of accident and severity in the following two categories:

1. Accident of all route in Bangladesh
2. Accident of N8 route in Bangladesh (Dhaka – Mawa – Barisal -Patuakhali National Highway).

3.2.1 Accident of all routes in Bangladesh

The analysis involves the determination of accident and severity depending on several features.

Accident Severity: Analysis shows that accident in different routes of national highways in Bangladesh. Percentage of accident was 19%, 16%, 8%, 8%, 24%, 5%, 7%, 9% and 4% in route number N1 to N9 respectively. 80% of all accidents are fatal and 15% are grievous type. Fatality index is highest (1.59) in route N4.

Road Class: Figure 2 demonstrates accidents in different routes depending on road class. Result shows that 46% of total accident occurred in national highway which was the maximum. 18% of the total accident took place in city road, and 14% was in regional road.

Collision Type: Figure 3 shows that 42% of total accidents was vehicles hit pedestrians type, while head on collisions was about 23% of total accidents.

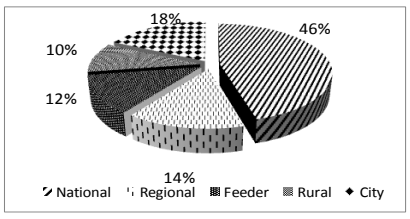

Figure 2: Accident in different road class

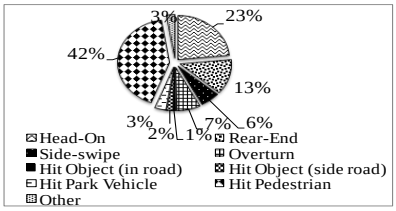

Figure 3: Distribution of accidents by collision type

Rear end collisions were 13% of the total accidents.

Pedestrians Accident: Figure 4 shows a comparison between total number of accidents and pedestrian accidents in different routes of Bangladesh. Figure 4 demonstrates clearly that in N3, N6, N7, N8 and N9 the difference between the total number of accident and the total pedestrian accident in the routes are comparatively less, which means that in these routes, pedestrian accident frequencies are higher. Therefore pedestrian safety is a major concern for those routes.

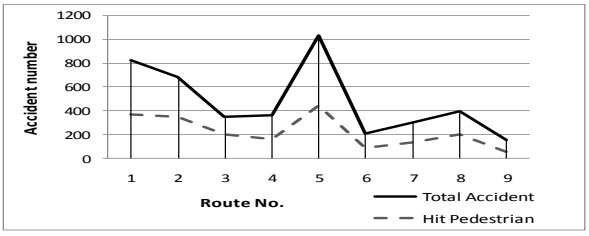

Figure 4: Comparative accidental number of hit pedestrian and total accident.

3.2.2 Accident in route N8 in Bangladesh

The analysis involves the determination of accident and severity features according to environmental characteristics, road related characteristics.

Environmental characteristics

Table 1: Distribution of accidents and casualties by year

Year	Accidents Number	Casualties Number	Casualty/Accident
2007	100	145	1.45
2008	110	178	1.62
2009	64	132	2.06
2010	41	87	2.12
2011	40	80	2
2012	43	73	1. 70
Total	398	695	1.75

Year: Table 1 illustrates yearly distribution of accident and corresponding causality. In 2007 casualties per accident rate was 1.45 and in 2010 the rate was the maximum (2.12). In 2012 casualties per accident was 1.70. Although accident frequency is decreasing but casualties per accident are increasing.

Time of Day and Lighting Condition: Figure 5 illustrates hourly distribution of accident in route N8. It is clear that accidents are more frequent between 9.00am-12.00pm. It is about 23% of total accident. In between 12.00pm -

3.00pm the accident frequency is also high. Figure 6 demonstrates that, most of the road accident and corresponding casualties occur in day light period. The frequency of accident in dusk is 12% of total accident in route N8. At night in darken condition 11% of total accident occurred. Point should be noted that at night traffic volume in route N8 is comparatively low.

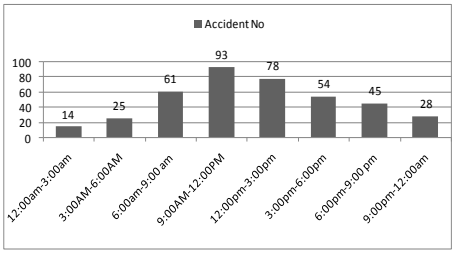

Figure 5: Accident distribution by time

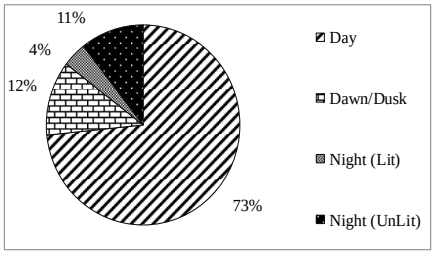

Figure 6: Accident distribution by lighting

Weather conditions: Table 2 shows the relationship of weather and vehicular contribution with accident rate. Analysis shows that maximum number (94%) of accidents occurred in fair weather in route N8. Bi-vehicular accident frequency represents the accident between two vehicles occurring in a particular weather. Bi-vehicular accident frequency is 57.15% in rainy weather. It is determined by the percentage of accidents occurring in contribution to two vehicle divided by the total number of accidents in that particular weather. At Fair weather bi-vehicular accident frequency is 35.2%. In fair weather chances of occurring accident between two vehicles are comparatively low than others.

Table 2: Distribution of accidents by weather

Weather	Accident Number				
	No. of Vehicles Contribution			Total	Bi-vehicular accident Frequency
	1	2	3		
Fair	242	132	1	375	35.2%
Rain	6	8	0	14	57.15%
Wind	0	1	0	1	100%
Fog	5	3	0	8	37.5%
Total	253	144	1	398	

Road related characteristics: Figure 7 shows the distribution of accident in different types of junction. 82% of total accidents occur in non-junction in route N8. In other types of junction and T junction the percentage of accidents are 9% and 5% respectively. Figure 8 shows the availability of divider in accident locations

of route N8. Result depicts that maximum accident occurs in the locations where no divider is present.

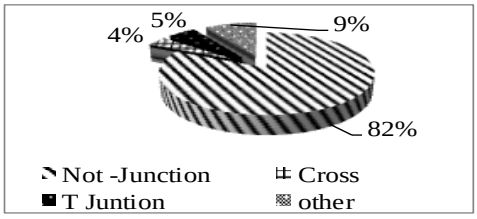

Figure 7:Accident distribution by type of junction

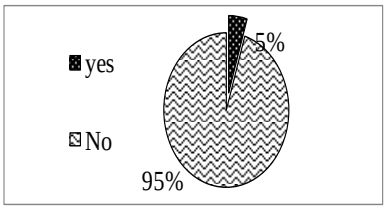

Figure 8:Accidents according to availability of road divider

3.3 Black-spot or HRL Identification

The study investigated a total length of 191 km of route N8. The highway under study encompasses varied geometrical and environmental condition. For accident analysis purpose the highway was divided into 1910 divisions where each section covered 100m length. The HRL and Blackspot location of this road on basis of accident data from year 2007 to 2011 is presented in Figure 9.

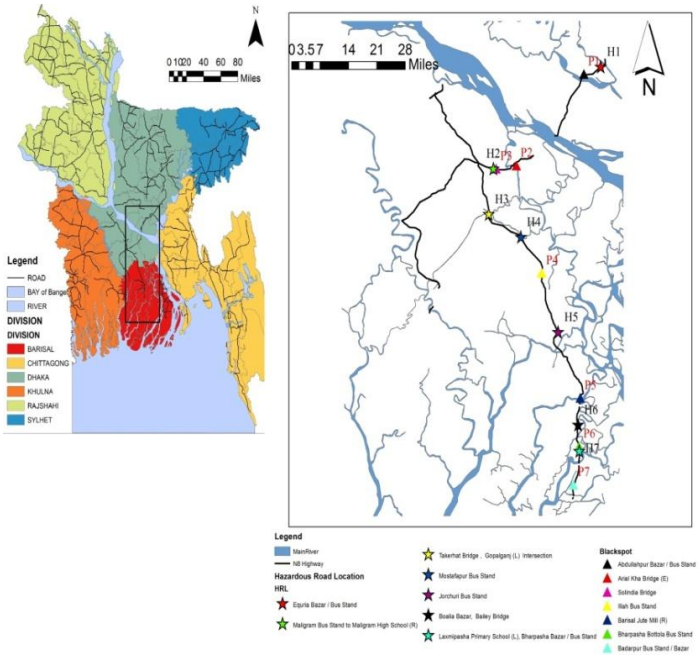

Figure 9: Blackspot and HRL on N8 highway (Map.1)

Table 3: Blackspot or HRL on Dhaka-Barisal highway (2007-2011)

Type *	km Post	Length (m)	Location	Total accident
H1	7 to 7.5	500	Equria Bazar / Bus Stand	5
P1	13.9 to 14	100	Abdullahpur Bazar / Bus Stand	4
P2	50.8 to 50.9	100	Arial Kha Bridge (E)	3
P3	57.6 to 57.7	100	Solindia Bridge	3
H2	59 to 59.7	700	Maligram Bus Stand, Maligram High School (R)	12
H3	184.5 to 185.3	800	Takerhat Bridge , Gopalganj (L) Intersection	5
H4	199.6 to 19.8	200	Mostafapur Bus Stand	6
P4	214.9 to 215	100	Illah Bus Stand	4
H5	236.8 to 237	200	Jorchuri Bus Stand	4
P5	266.2 to 267.3	100	Barisal Jute Mill (R)	3
H6	271.1 to 272.1	1000	Boalia Bazar, Bailey Bridge	4
P6	278.5 to 278.6	100	BharpashaBottola Bus Stand	3
H7	280.1 to 280.4	300	Laxmipasha Primary School (L), Bharpasha Bazar /Bus-stand	4
P7	289.6 to 289.7	100	Badarpur Bus Stand / Bazar	4

* P= Black spot and H=Hazardous Road Location

4 DISCUSSION

After conducting the detail study, it has been found that a total of 398 accidents have occurred on Dhaka – Barisal Highway during the five years duration from 2007-2011 and 311 accidents among the total are fatal. So, it is clearly visible that about 78% of the accidents are fatal which have caused severe casualty and loss to life as well as the economy of our country. About 9% of the total accidents occurred in this portion of Dhaka-Barisal highway. Most important feature in this route is pedestrian causality which account for 51% of total accident. So it has been clearly identified that accidents are concentrated on this portion of the Dhaka –Barisal Highway. This portion requires proper treatment and remedial measures to decrease the higher accident rates. Recently Padma Bridge Project has been started at Mawa-Jajira point beneath the route N8. So future expected average daily traffic (ADT) of N8 will be higher than other routes. So it is right time for analysis accident, establish engineering countermeasure and improve road safety for decreasing accidents for efficient operation in this route.

ACKNOWLEDGEMENTS

We would like to express profound gratitude and special acknowledgement to Dr. Tanweer Hasan, Professor, Department of Civil Engineering and Director of Accident Research Institute (ARI), BUET, for providing the crash data. Also we would like to express our sincere thanks to Shahnewaz Hasanat-E-Rabbi, Lecturer, ARI, BUET for providing support for crash data analysis.

REFERENCES

[1] Apparao. G, P. Mallikarjunareddy& Dr. SSSV GopalaRaju, 2013. "Identification of Accident Black Spots for National Highway Using GIS".

[2] Global Status Report on Road Safety (2013), World Health Organization (WHO).

[3] Hasanat-E-Rabbi, S., 2013. Modeling Critical Overturning Criteria for Single Vehicle Run-off-road Crashes for Bangladesh Context. M.Sc. thesis, Department of Civil Engineering, BUET, Dhaka, Bangladesh.

[4] Hoque M. S., Muniruzzaman S. M., Ahmed S. N. 2005. 'Performance Evaluation of Road Safety Measures: A Case Study of the Dhaka-Aricha Highway in Bangladesh",*Transport and Communications Bulletin* for Asia and the Pacific No. 74.

[5] Kalga, R.R. and Silanda, S.N. 2002. Accident rates Prediction on Arterial Roads of Durban, South Africa, *Indian Highways Journal.*

[6] Lewis, S.M. 1994. The Use of GIS in the federal highway Administration's office of Policy Development In*Proceeding, transportation Symposium.*

[7] Monisha A. and Hasib M. Ahsan. 2013. Identification and Characterization of Hazardous Road Locations on Dhaka-Chittagong National Highway.

[8] Road Safety Fact 2012, ARI, BUET, Bangladesh.

CICM 2015
First International Conference on
Advances in Civil Infrastructure and Construction Materials
MIST, Dhaka, Bangladesh, 14–15 December 2015

AN EXPERIMENTAL STUDY OF FLEXURE-SHEAR INTERACTION IN REINFORCED CONCRETE WALL SUBJECTED TO CYCLIC LOADING

Kashfia HUSSAIN

Structural Engineer, Acumen Consulting & Housing Ltd, Dhaka, Bangladesh.
Email: kashfia.hussain@gmail.com

Abstract. *Reinforced concrete structural walls are widely used for resisting lateral loads due to their high strength and stiffness. Structural walls are significantly deeper than typical beams or columns. In addition to significant strength, structural walls can dissipate an enormous energy if detailed appropriately the current study focuses on the typical design practice for reinforced concrete shear walls prevailing in low to moderate seismic regions. A reversed cyclic quasi-static loading test is conducted to assess the seismic performance of a large-scale flexure–shear dominated reinforced concrete shear wall specimen with an aspect ratio of 2. A strong coupling effect of flexure and shear responses is observed, even though the shear strength is about 1.5 times the shear corresponding to the nominal moment capacity of the specimen. The final mode of failure is concrete crushing and the buckling of vertical reinforcement in the boundary zones. An analytical comparison with existing code (ASCE-41-06) and fiber model is also conducted as a part of the verification of the experimental results. The analytical study showed that the negligence of flexure-shear interaction in the conventional fiber modeling can lead to overestimation of ductility, energy dissipation and unrealistic mode of failure.*

Keywords: Reinforced concrete wall, Cyclic load, Flexure-shear interaction, Aspect ratio, Deformation.

1. INTRODUCTION

The RC shear wall can be divided into three main categories depending upon their respective aspect ratio. Typically, A slender RC wall with an aspect ratio more than 3 is purely flexure-response dominated wall, whereas a low rise or short RC wall with an aspect ratio lower than 1.5 is purely shear response dominated. A large portion of RC shear walls constructed around the world are mid-rise with an aspect ratio ranging from 1.5 to 3. Figure 1.1 shows theoretically singular expected mode of failure of walls by comparing their flexure and shear capacities. Walls with high shear capacity as compared to the flexure capacity will be dominated by flexure mode of failure since the shear capacity is much higher than the flexure capacity and prevent the brittle shear failures. Shear walls with aspect ratios more than 3 fall in this category.

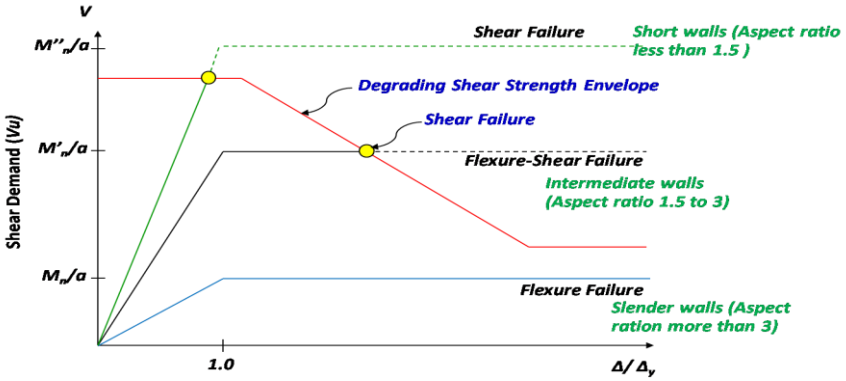

Figure 1: Mode of failure of Shear walls

Whereas walls with aspect ratio less than 1.5 will be dominated by shear mode of failure since the shear capacity is much smaller than the flexure capacity. Behavior of walls with aspect ratio in-between 1.5 to 3 is more complicated. Shear capacity and flexure capacity of such shear walls are very close to each other. Flexure failure causes the decreases in shear capacity of such walls therefore a flexure failure can be transformed into shear failure at later stages. This type of failure is commonly referred in literature as flexure-shear failure. Therefore for the flexure-shear dominated RC shear walls both non-linear flexure and non-linear shear responses are equally significant. Inclusion of axial load with flexure-shear interaction adds more complexity to predict the non-linear response of such flexure-shear dominated RC walls. For a better modeling technique the internal behavior of wall such as stress and strain in reinforcement and concrete, anchorage bond slip, flexure deformation, shear deformation etc should be observed experimentally.

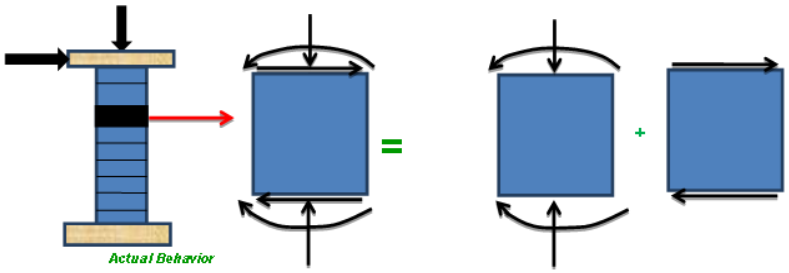

Figure 2: Coupling behavior of wall

And the best choice for investigating the coupling flexure-Intermediate wall (aspect ratio 1.5 to 3) will be shear behavior and also to investigate the seismic performance level of reinforced concrete walls.

2. EXPERIMENTAL PROGRAMME

2.1. Specimen description

Experimental programme include a large scale shear wall specimen with aspect ratio of 2. Fig.3 shows the dimensions of tested specimen. All dimensions are in mm. Table 1 shows the reinforcement detail of specimen.

Table 1 Material Properties

	Concrete	Reinforcement Horizontal		Vertical		Confinement	
Zone	fc′(Mpa)	ρ(%)	f_y(Mpa)	ρ(%)	f_y(Mpa	ρ(%)	f_y(Mpa)
Boundary	27	0.7	486	2.5	450	0.25	380
Web	27	0.35	486	0.6	486	-	-

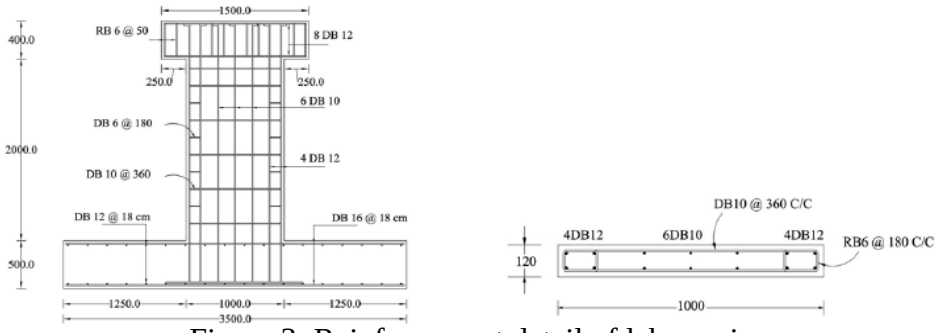

Figure 3: Reinforcement detail of lab specimen

2.2. Experimental Set up

The experimental set up was used to simulate gravity and lateral earthquake loads. An innovative gravity load frame is used to maintain a constant axial load throughout the test. The unique feature of this test frame is that the built-in rollers at the top of the frame enable the axial load to move along with the tip of the wall. The axial load that could follow the wall deformation simulates the real conditions of wall under earthquake loading. The constant axial load of 300kN (axial load ratio about 0.10) was applied to a specimen using a 600kN-jack. The axial load was monitored and kept constant throughout the test. The lateral load was applied using a 500kN-hydraulic actuator. The specimen was subjected to quasi-static loading history using a convenient target percent drift. The specimen was subjected to displacement-controlled to a percent drift of ±0.125, ±0.25, ±0.5, ±0.75, ±1.0, ±1.5, ±2.0, ±2.5, ±3.0 and etc. until the wall loss of its gravity load carrying capacity. Two cycles of loading were used with each drift ratio to ensure that the hysteretic behavior could be maintained.

2.3. Instrumentations

Strain gages were used to measure strain of reinforcement in web and boundary regions of specimen. Fig.4(a) shows the lay out strain gauges on longitudinal and horizontal reinforcement. A total of 42 strain gauges were used for the experimental data of strain in reinforcement.

To measure the components of lateral deformation linear variable deferential transducers (LVDTs) are used. Fig 4(b) presents the layout of LVDTs. Most of cracking is expected in plastic hinge zone of shear, which is considered as equal to length of wall (L_w=1000 mm) in this study. Fig.4(b). A total of 22 LVDTs are

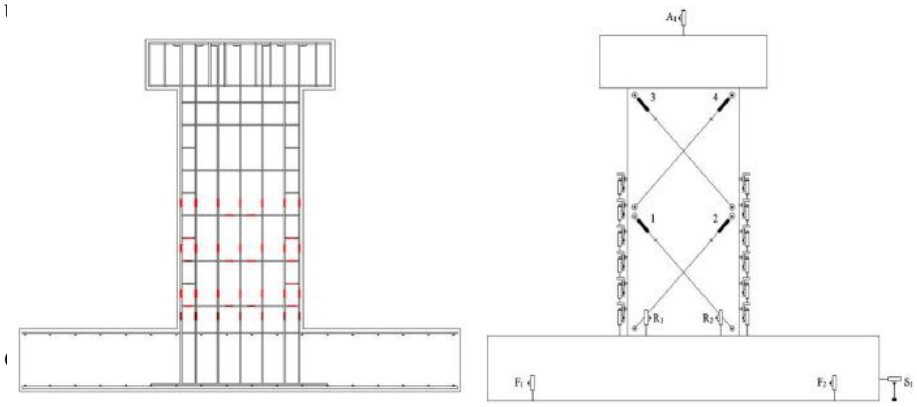

(a) (b)

Figure 4: (a) Strain gauges locations (b) LVDTs Layout

3. EXPERIMENTAL RESULTS

3.1. Damage propagation

The force-top drift relationship is shown in Fig6. The important damage stages are also shown on the Fig6. Fig5 presents the propagation of cracks. Initial cracking is observed at the first cycle of +0.25% drift. Initial cracks are almost horizontal, started from edges of wall and move towards the web. Similar cracking observed on the opposite face of wall at the first cycle of -0.25% drift. First yielding is observed at 0.5% drift with clear diagonal cracking extending from edges of wall and dipping in to web as shown in Fig5. At 0.5% drift the outer most longitudinal reinforcement in the boundary zone started yielding. At 0.75% drift cracks extended to higher levels along the height of wall. At the same 0.75% drift longitudinal reinforcement in the web of wall started yielding. At the 1% drift cracks became further widened and force- drift relationship became flatter. At 1.5% drift significant increase in diagonal crack width is observed which caused the yielding horizontal reinforcement. In the next cycle of 1.5% drift severe concrete crushing is observed in the boundary zone which resulted in the slight loss of lateral strength as shown in Fig6. The shear wall specimen able to sustain the same lateral strength at first cycle of 2% drift but longitudinal reinforcement exposed due to loss of concrete cover in the boundary zone, this caused the buckling of longitudinal reinforcement in the at 2% drift. In the second cycle of 2% drift sudden drop in the axial load is observed and the lateral strength dropped to 55% of peak lateral strength. Test is stopped at the stage to avoid the damage to instruments. After removing the lateral bracing frame clear photo of the shear wall specimen are taken as shown in Fig5. The buckling of longitudinal reinforcement in the boundary zone is clearly visible. No yielding in confinement reinforcement of boundary zone is observed. Over all shear wall specimen able to develop the yield moment effectively but showed very little ductility (i.e. Δ_{max}/Δ_y =2) due to crushing of boundary zone and buckling of longitudinal reinforcement in the boundary zone. High unsupported length (i.e. L/d =15 where L is unsupported length and d is the dia of longitudinal rebar) of longitudinal reinforcement in the boundary zone caused the buckling of the longitudinal reinforcement

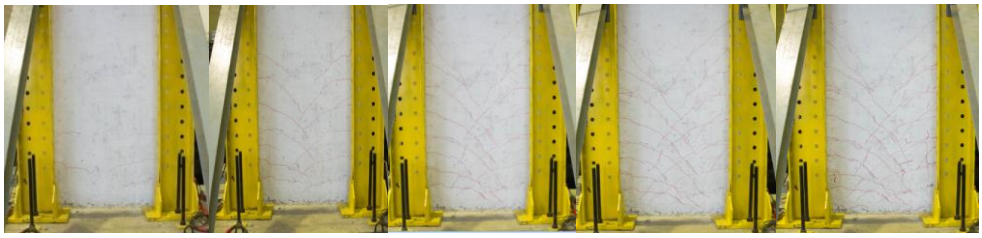

0.25% Drift 0.5% Drift 0.75% Drift 1% Drift 1.5%Drift

2% Drift 2% Drift after removing the lateral bracing frame

Figure 5: Propagation of damage

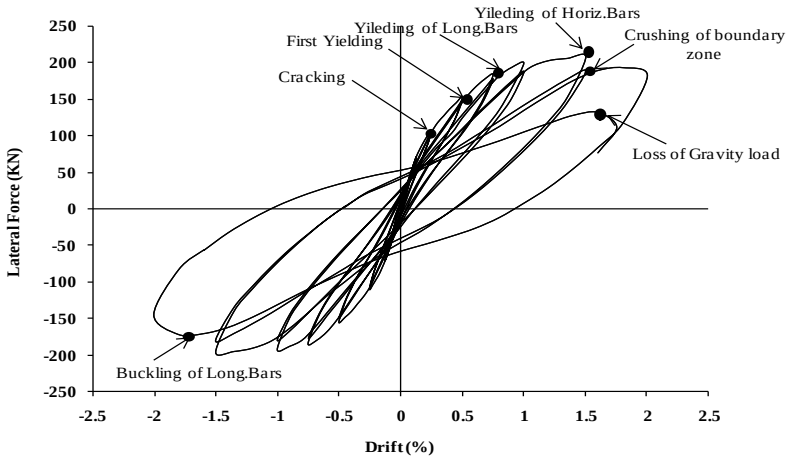

Figure 6: Lateral force –top drift relationship

3.2. Components of lateral deformation

For the calculation of flexure deformation, shear wall specimen divided into six sections along the plastic hinge area of wall (i.e. L_w=1000 mm) as shown in Fig4(b). By using this arrangement of LVDTs along the height of wall, the curvature of specific sections was obtained by following equation:

$$\emptyset_f = \frac{\Delta_1 - \Delta_2}{h_s L_w} \quad (1)$$

The flexure deformation (U_f) was the calculated by integrating the curvature of all section along the height of all.

The shear deformation is calculated using the LVDTs in the "X" configuration (Fig7(b)) as proposed by Thomsen by using following equation:

$$U_s' = \frac{\sqrt{D_1^2 - h^2} - \sqrt{D_2^2 - h^2}}{2} \quad (2)$$

The calculation of shear deformation in this way is influenced by flexure deformation (U_f), which resulted in over estimation of the shear deformation. As proposed by Massone(U_s') uncorrected shear deformation by "X" configuration can be corrected by using following equation:

$$U_s = U_s' + \left(\frac{1}{2} - \alpha\right) \emptyset . h \quad (3)$$

The centroid of the curvature distribution (α) is taken equal to 0.67 which is consistent with prior research (Thomsen [1]).,Rocking or Rigid body deformation of the shear wall specimen is calculated by using two LVDTs attached on the face of shear wall specimen (Fig4 (b)). The calculation procedure is explained in Fig7(c). Equation-4 is used to calculate the rigid body motion of shear wall specimen:

$$U_r = \left(\frac{\Delta_1 - \Delta_2}{L_w}\right) . H \quad (4)$$

Fig8 presents the results of flexure, shear and rigid body deformation of the shear wall specimen. Summation of all the deformation components is approximately equal to the total lateral deformation measure at the top of the shear wall specimen.Fig9 shows the percentage of each deformation components to the total lateral deformation at each drift. The flexure deformation has the highest contribution to the total lateral deformation (Approximately 60% of the total deformation at each drift). Shear deformation has the lowest but significant contribution to the lateral deformation, which cannot be ignored while modelling the dynamic response of such flexure-shear dominated shear walls. Furthermore, it is interesting to note that as the flexure yielding started at 0.75% drift, there is sudden increase in the shear deformation. As the flexure deformation went into the non-linear b behaviour, the shear deformation also went into the non-linear response.

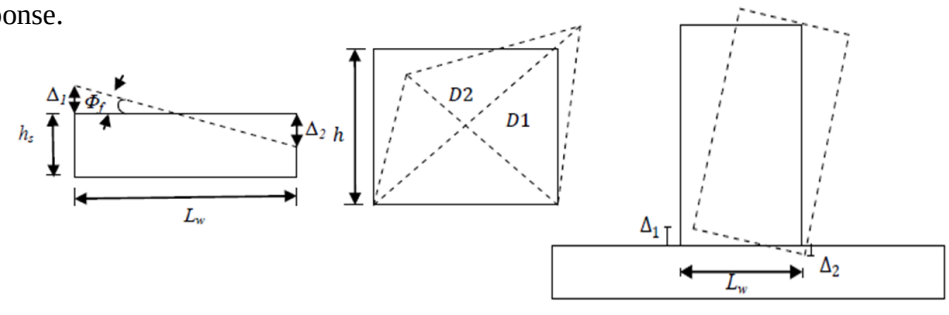

(a) (b) (c)

Figure 7: Calculation of lateral deformation

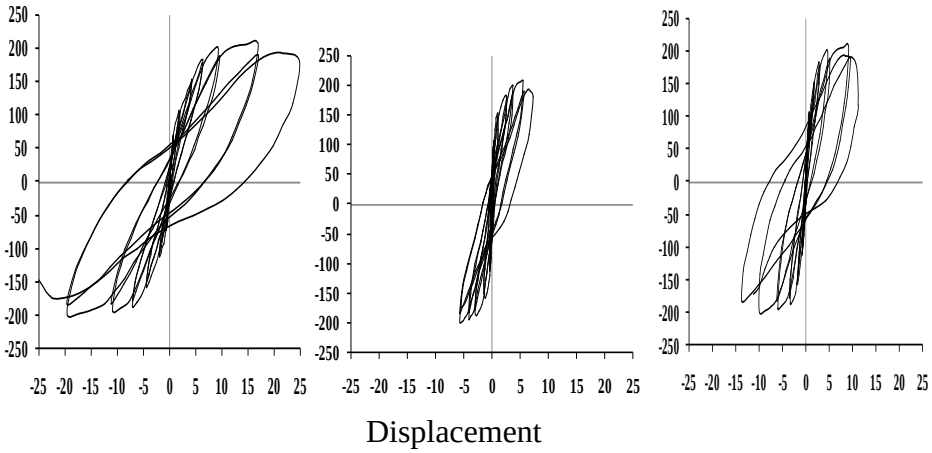

(a) (b) (c)

Figure 8: Components of lateral deformation (a) Flexure (b) Shear(c) Rigid body deformation

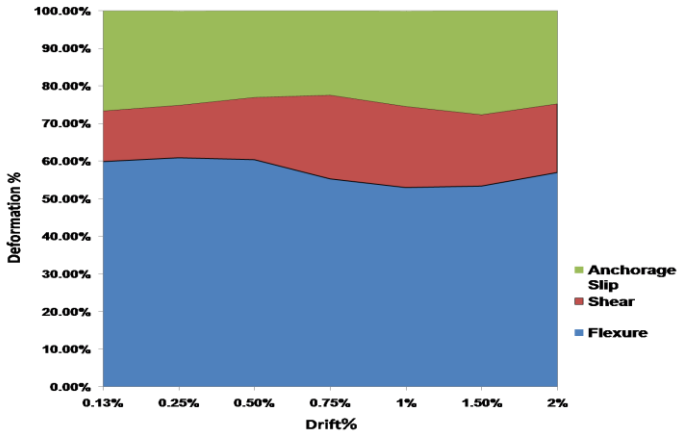

Figure 9: Components of lateral deformation in percentage

3.3. Strain and curvature distributions along the height

Fig10 presents the results of tensile strain in longitudinal reinforcement along the height of shear wall specimen at each peak drift. Only the results of longitudinal reinforcement in the boundary are presented here for sake of clarity. As can be seen at 0.75% drift strain in longitudinal reinforcement suddenly increases due to the yielding (yielding strain is $2.4x10^{-3}$). At 1.5% drift strain in longitudinal reinforcement started to reverse the sign (Fig10 right side). This is may be due to the residual strain after yielding of longitudinal reinforcement. It is important to note that strain beyond the height of 600mm is in elastic range to minor cracking

beyond that level. Most of the non-linearity is concentrated in the region upto 600mm which is equal to $0.6L_w$. The curvature distributions also present the same behaviour as shown in Fig11. The curvature values are very low beyond 600 mm of height due insignificant cracking beyond that height. ASCE-41-06 recommends a value of $0.5L_w$ for plastic hinge length of shear walls which seems reasonable.

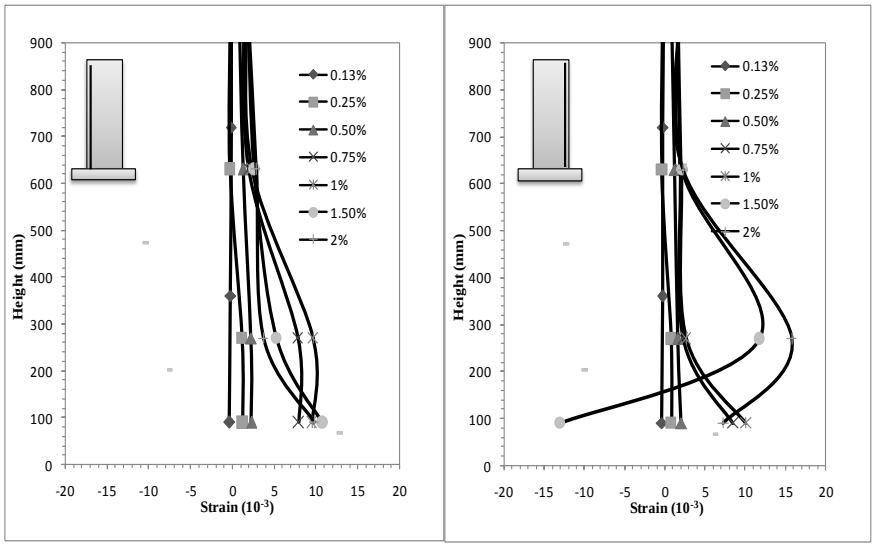

Figure 10: tensile strain in longitudinal reinforcement

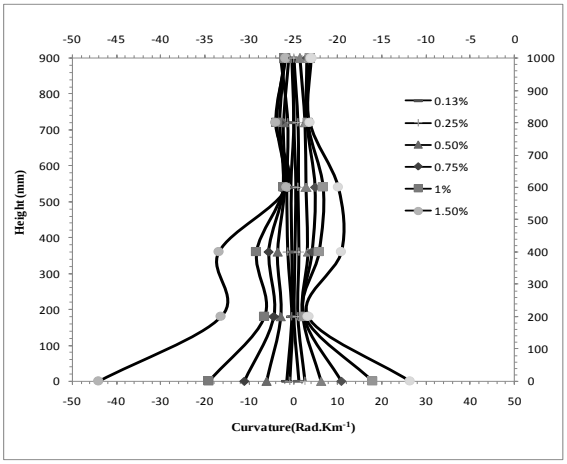

Figure 11: curvature distributions along wall height

3.4. Contribution of Concrete (Vc) and Steel (Vs) to Total lateral shear (Vn)

The total lateral shear force (Vn) is has been separated according to contribution of concrete (Vc) and steel (Vs) (Fig12) by using formula from ACI-318-11.At initial drift there is no contribution of load from steel. After 0.25% drift when the cracks have been seen in the wall surface, steels started taking load. Basically the equations of ACI-318-11 are only acceptable for linear behavior. At 1% drift all the lateral reinforcements are yielded and after this drift the behavior of the wall is purely nonlinear. So up to 1% drift the graph can be accepted.

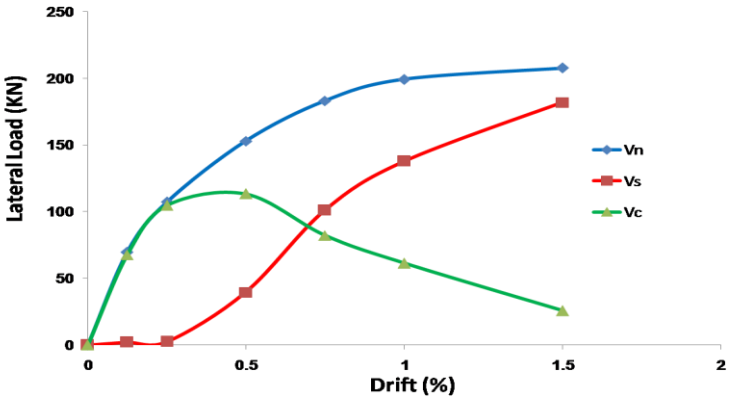

Figure 12: Contribution of Concrete (Vc) and Steel (Vs) to Total lateral shear (Vn)

4. ANALYTICAL STUDY

4.1. Moment Curvature

The idealized bilinear curve is also plotted according to ASEC-41-06 on the Fig13. The comparison of experimental results of moment-curvature backbone with the idealized backbone curve shows the poor prediction of initial stiffness as well as the yield curvature by ASEC-41-06. Moreover, due to diagonal cracking the stiffness of shear wall specimen decreases significantly, this cannot be considered by using simple equation of ASCE-41-06. This can lead to overestimation of elastic lateral strength of such flexure-shear dominated shear walls, which is particularly important for the design of such RC shear walls.

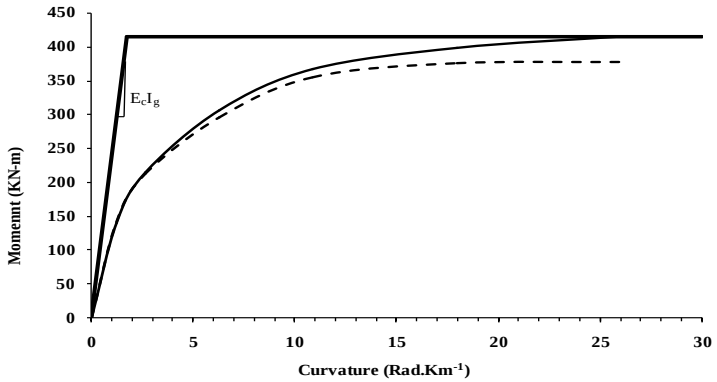

Figure 13: Moment Curvature

4.2. Conventional fiber model

Fig.14 presents the comparison of result of conventional fiber model with experimental results, in which the shear response is considered as elastic and uncoupled to the flexural response. The peak lateral force predicted by fiber model is reasonably close to the experimental values. Initial stiffness predicted is higher than the observed in the experiment, due to negligence of non-linear shear response. Due to the diagonal cracking initial stiffness is dropped in the experiment, which cannot be modeled by using the fiber model. The predicted hysteretic loops are much fatter and resemble to bilinear model. The fiber model failed to predict the pinching of the hysteric loops observed in the experimental results. Therefore the energy dissipation by fiber model is much higher than the experimental results. The decrease in the lateral strength due to boundary zone crushing is not predicted by fiber model. This overestimation of ductility can lead to unsafe retrofitting techniques of such non-ductile flexure-shear walls.

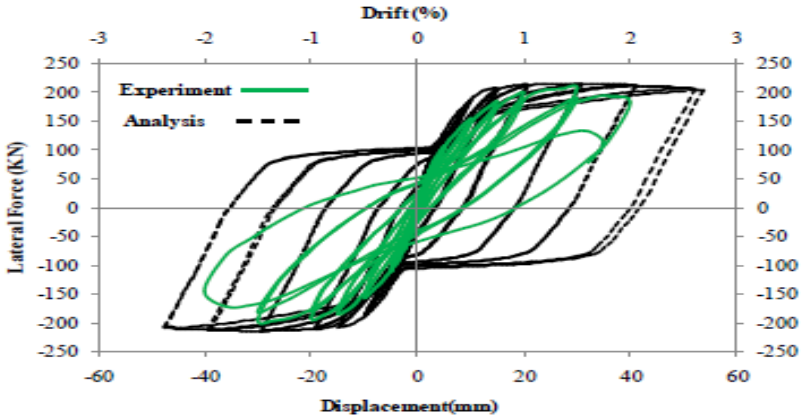

Figure 14: Analysis by Fiber model in Perform3D

5. CONCLUSIONS

Although relatively a large number of shear walls test have been conducted earlier but a very few tests have specified about the flexure and shear behavior individually. This paper contains a proper shear wall test with axial load and extensive instrumentation to get separated the lateral deformations. Detailed experimental results have been relived for the internal behavior of an Intermediate wall through this study. A strong coupling effect of flexure and shear responses has been observed for a RC wall with an aspect ratio 2. Results are compared with available analytical tools. Comparison with analytical study indicates that the negligence of coupling flexure and shear responses can lead to unreliable predictions of initial stiffness, ductility and energy dissipation capacity.

ACKNOWLAGEMENTS

The author would like also to express her solemn appreciation to her advisor, Dr. Pennung Warnitchai, for the supports, supervisions, forthcoming response, thought provoking discussions, and guidance during the writing of her thesis and his learning process in AIT.

REFERENCE

[1] American Concrete Institute ACI(2011). *"Building code requirements for structural concrete and commentary".*

[2] ACI 318-2011, Farmington Hills, MI ASCE/SEI (2006). *"Seismic Rehabilitation of Existing Buildings – ASCE Standard 41-06"*,

[3] American Society of Civil Engineers, Reston, Virginia PEER. (2005). PEER NGA Data Base. http://peer.berkeley.edu/nga/. Pacific Earthquake Engineering Research (PEER), University of California, Berkeley.

[4] Online reference, accessed in 2009 Orakcal, K., Massone, L. M. and Wallace, J. W. (2006). *Analytical Modeling of Reinforced Concrete Walls for Predicting Flexural and Coupled Shear-Flexural Responses*. PEER Report 2006/2007, Pacific Earthquake Engineering Research Center, University of California, Berkeley, October 2006, 213 pp.

[5] John W. Wallace (2012),‖ Behavior, Design, and Modeling of Structural Walls and Coupling Beams– Lessons from Recent Laboratory Tests and Earthquakes‖, *International Journal of Concrete Structures and Materials* Vol.**6**, No.1, pp.3~18, March 2012.

CICM 2015
First International Conference on
Advances in Civil Infrastructure and Construction Materials
MIST, Dhaka, Bangladesh, 14–15December 2015

BOND STRESS-SLIP BEHAVIOR BETWEEN CONCRETE AND STEEL REBAR VIA PULLOUT TEST: EXPERIMENTAL AND FINITE ELEMENT ANALYSIS

M. R. KABIR[1], M. M. Islam[2] and M. A. Chowdhury[3]

[1, 2, 3] Department of Civil Engineering, Ahsanullah University of Science and Technology, Dhaka, Bangladesh.
Email: [1]rashedulkabir777@gmail.com, [2]mashfiq7777@gmail.com and
[3]arman.chowdhury.ce@gmail.com

Abstract. *Composite behavior of reinforced concrete has always been an important part in the study of structural engineering. In general, the bond-slip behavior and ultimate pull-out strength for external loading are mostly covered by different researchers. In this study, the transfer of bond stress in concrete surrounding the reinforcing steel is thoroughly analyzed experimentally and on the Finite Element (FE) platform of ANSYS 11.0. Stress generated in the interface region between steel and concrete is observed from pull-out specimens made of brick and stone concretes with two different strengths and also for two steel grades. Total 8 numbers of pull-out specimens are prepared and tested. The pull-out resistance is found to increases significantly with the increase of concrete strength and also with the increase of yield strength of steel rebars for both brick and stone concrete specimens. There exists a good agreement between the experimental results and FE outcomes which are helpful for the construction industry of Bangladesh in selecting appropriate factor of safety in the design considerations.*

Keywords: Bond Stress-Slip Behavior, Pull-out Test, Finite Element (FE) Analysis, Brick concrete.

1 INTRODUCTION

The tensile stress from steel to concrete is transferred by interfacial interaction which can be termed as bond behavior. This mechanism is an important feature not only for characterizing crack pattern, but also for many other important issues related to structural concrete such as anchorage capacity, minimum development length and lap splice length of the bars [1, 3-7, 11]. When reinforcing bar is embedded in concrete and tested in tension pull out, concrete cracks due to the failure of chemical adhesion that has been formed during hardening of concrete [14]. Proper bonding between concrete and steel is crucial to ensure the composite action of reinforced concrete section. In case of plain bar, chemical adhesion and mechanical interlock contribute, whereas for deformed bar, the surface roughness and closely spaced ribs produce great interlocking with bearing against the key formed between concrete and ribs [10, 12]. A typical bond stress slips relationship as shown in Figure 1(a) & (b) gives an idea on how pull-out behavior of plain bar differs from deformed bar. Splitting type of failure does not allow much deformation of rebar and a common phenomenon in low strength concrete. In contrary, rebar embedded in high strength concrete undergoes large deformation and prone to pull-out failure. Now-a-days huge numbers of brick manufacturing industries are established around the major cities. Generally, clay burned bricks are very popular due to high cost and the lack of availability of stone aggregates. Bricks are also often broken manually or by using a brick crusher into coarse aggregate for concrete works. Stone chips and shingles are also used in construction [15]. Unfortunately, the deterioration of some concrete structures occurs within several years of construction due to the lack of knowledge on durability and bond behavior during the design, construction, and maintenance of civil infrastructures. Therefore, this study aims to investigate the bond behavior of deformed steel bar of different yield strength by employing two different types of coarse aggregate i.e. brick and stone aggregate in concrete.

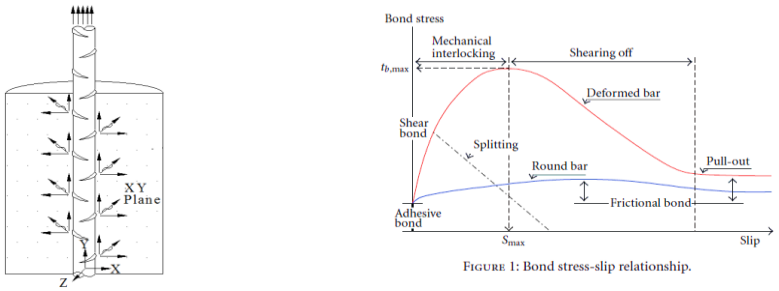

FIGURE 1: Bond stress-slip relationship.

Figure 1: (a) Shear stress distribution in the XY plane of concrete and (b) Bond stress-slip relationship (adopted from Hong and Park 2012 [13])

2 EXPERIMENTAL PLAN

To understand the bond stress slip behavior of pullout specimen, single pull out test is conducted using a 1000 kN capacity digital universal testing machine (UTM). Figure 2 (a), (b) & (c) shows the specimens casted for pullout test purpose.

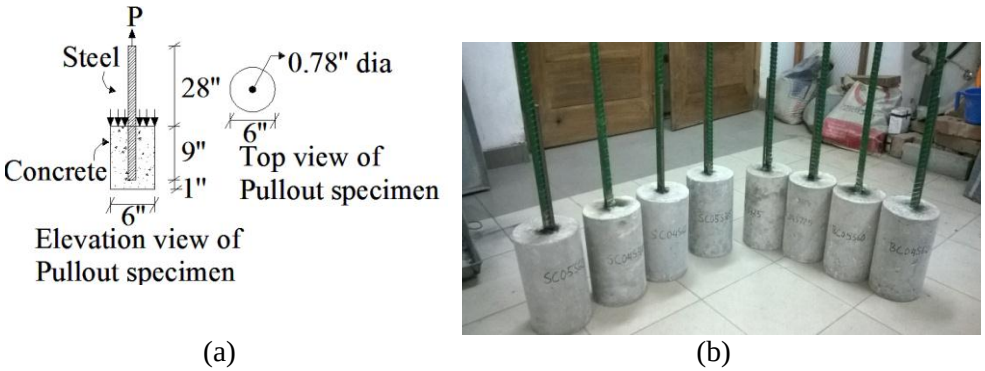

Figure 2: (a) Pullout specimen details, (b) All casted pullout specimens and (c) Details of steel rebar specimen

2.1 Material properties

2.1.1 Concrete

Two different types of aggregate, i.e. brick and stone aggregate are used to make the single pullout test specimens. The size of aggregate is maintained 25 mm passing and 19 mm retained and 19 mm passing & 12 mm retained with a ratio of 1:1. The average compressive strength ofa brick aggregate pullout specimen is 10.65 MPa. In case of stone aggregate specimen average compressive strength is 17.95 MPa. Average tensile strength of stone aggregate is 3.9 MPa and 2.78 MPa for brick aggregate specimen. The slump was kept within 110 mm which allowed good compaction without excessive bleeding. Concrete compressive strength was determined by 4 inches (101.6 mm) diameter and 6 inches (153 mm) height specimen. Tensile strength was determined by splitting cylinder test with the same

dimensional specimen. All compressive, tensile and split cylinder specimens was cured at room temperature for 28 days. Two different steel rebar of yield strength 60 ksi and 72.5 ksi is used to analyze the impact on bond behavior between steel and concrete. All specimen details are given in Table 1.

Table 1: Material properties

Coarse Aggregate Type	Brick				Stone			
w/c ratio	0.4		0.5		0.4		0.5	
Yield strength of steel*	60	72.5	60	72.5	60	72.5	60	72.5
Tensile Strength (MPa)	3.26	3.84	1.78	2.23	4.24	4.07	3.63	3.63
Compressive strength (MPa)	16.04	12.99	5.89	7.67	24.32	23.29	12.06	12.09
Bond strength (MPa)	6.19	8.16	4.28	6.91	8.33	11.06	8.76	7.17

* Yield strength of steel rebar is given in ksi

A total of sixteen (16) concrete cylindrical specimen and eight (8) pullout specimen were casted for determining the compressive, tensile and bond strength. These specimens'designationsare defined as shown in Figure 3

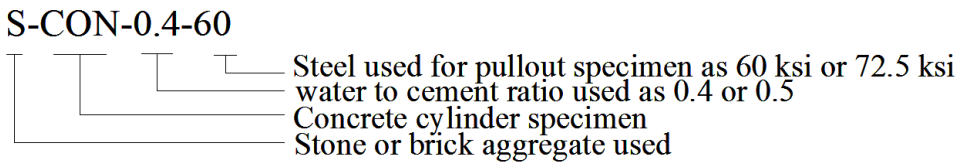

Figure 3: Concrete cylinder specimen designation

3 PULLOUT SPECIMEN FABRICATION

Bond of steel bar to the surrounding concrete influences the structural behavior of reinforced concrete structure and its primary component. That's why understanding the basic behavior between steel and concrete can be a key point to understand the ultimate load carrying capacity of structures and this is the prime factor worked behind this study. Despite numerous research has been conducted to evaluate the bond behavior between steel and concrete made of stone aggregate, a fewer research carried out by using brick aggregate. In context of Bangladesh, Brick aggregate (brick chips) is widely used in construction site for casting, which emphasize on experimental research on brick and steel bond behavior. To

evaluate the bond characteristics a number of key parameters are used as variable, i.e. aggregate type, steel grade and water to cement ratio. Total eight 8) specimens were casted and the specimen dimensions are given in Figure 2 (a) -(c). PVC pipes of 10" height and 6" diameter is used as molds for casting. A rectangular wooden frame was used during casting to keep the reinforcing bar in the center of the casting mold. Before casting molds were oiled thoroughly in inner surface and surface roughness was removed using a file. Embedded length of reinforcement was 9in. (12 d_b, d_b= bar diameter), sufficient to develop the required stress in steel at that section. Exposed parts of the reinforcements were painted before curing to prevent corrosion and contact with curing water.

4 EXPERIMENTAL SETUP

Single pullout test is done on 1000 kN capacity UTM machine. Pullout specimen was placed concentrically at the test base to avoid eccentric stress on concrete and steel joint. To ensure the vertical placement sufficient care was taken. Test setup is shown in Figure 4. Digital universal testing machine (UTM) of capacity 1000 kN is used to perform compressive, tensile and pullout test, of this experiment.

(a) (b)

Figure 4: Test setup (a) UTM machine and (b) Sample specimen is placed at UTM

This is a displacement controlled machine. Load and displacement values are measured from load cell of UTM. The splitting tensile strain was measured employing digital image correlation technique (DICT) using HD video footage of testing as also followed in [8] and [9]. In this experiment the displacement rate of 1 mm per minute was applied.

5 EXPERIMENTAL RESULTS

Figure 7 (a)-(h) shows that keeping the water cement ratio and aggregate type fixed, if the yield strength of steel is increases the ultimate bond stress will increase irrespective of both tensile and compressive strength of concrete. On the

other hand, when the aggregate type changes from brick to stone provided the yield strength and water cement ratio are fixed, the ultimate bond stress increases with the increase of tensile and compressive strength of concrete. Bond strength of brick aggregate reduced from 6.19 MPa to 4.28 MPa when water to cement ratio changed from 0.4 to 0.5 and steel yield strength is 60 ksi. When steel yield strength changed from 60 ksi to 72.5 ksi, bond strength reduced from 8.16 MPa to 6.91 MPa with water to cement ratio of 0.5. Although bond stress increases with the increasing steel yield strength, but relative slip for brick aggregate pullout specimen reduced from 1.25mm to 1 mm (Figure 7(a) & (b)). Similar results observed in stone aggregate concrete pullout specimen where for stone aggregate with a slip of 2.4 mm reduced to 1.25 mm. Stone aggregate shows a similar pattern with decreased bond strength from 11.06 MPa for water to cement ratio 0.4 to7.17 MPa for water to cement ratio 0.5. Stone aggregate shows overall good bond strength in comparison to brick aggregate. This might be due to more frictional resistance capacity, hardness and higher strength of stone aggregate. Inthe construction site of Bangladesh, extra amounts of water is added to cement to increase the workability of concrete [15] but these may lead to misinterpretation of bond strength as shown in Figure 7 (a) & (c) and Figure 7 (b) & (d).

6 FE MODELING OF PULLOUT SPECIMEN

In this work, simple pull-out specimens are modeled on the Finite Element (FE) framework of ANSYS 11.0. Eight models based on different material properties are prepared and analyzed with proper boundary condition. All the models are analyzed considering perfect bonding between reinforcing bar and surrounding concrete. Sufficient development length is provided to produce required stress in reinforcement. Development length is provided 9 inches (12 times of the diameter of rubberare used as per ACI 318-11, [2]. The concrete is modeled using SOLID65 eight-node brick element, which is capable of simulating the cracking in tension and crushing in compression behavior. In this study, reinforcement is modeled using SOLID45 element which has identical degrees of freedom to those for SOLID65. Perfect bonding between these two elements is ensured during modeling.In this study, embedded length of 12 times of the diameter, i.e. 9 inch of rubber is used as per [2]. While modeling, a cylinder length equals to the required embedded length and 6 inch diameter are considered. Extensive use of deformed bar in construction purpose has led us to consider perfect bonding between concrete and reinforcing steel bar. To resemble the experimental scenario, concentric steel bar of 20 mm diameter and 38 in (including 9 in embedded length) length is modeled (Figure 5 (a)). To obtain precise results in concrete vicinity of reinforcement, meshing was done much finer close to the reinforcement (Figure 5 (b) & 7(c)).

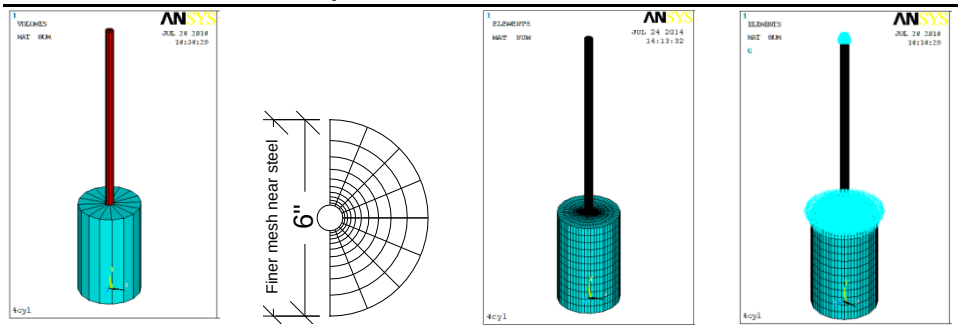

(a) (b) (c) (d)

Figure 5: FE model of Pull out specimen in ANSYS 11.0 (a) volume of concrete and steel rebar, (b) mesh across width (c) meshed volume, and (d) boundary condition

Slip at the interface between concrete and reinforcing steel is observed and corresponding stresses generated due to applied loading are also scrutinized (Figure 6(b) & 6(c)). Formation of crack in concrete due to divergent stress distribution in steel and surrounding concrete is also inspected from ANSYS program (Figure 6(d) & 6(e)). The displacement boundary condition is applied as load at top of the reinforcement (Figure 5 (d)). The boundary conditions are also applied to the concrete cylinder by restraining translation of nodes at the top surface of cylinder in three directions except the nodes adjacent and neighboring to the reinforcement. Displacement at the top of the reinforcement is given only in the positive Y direction (upward).

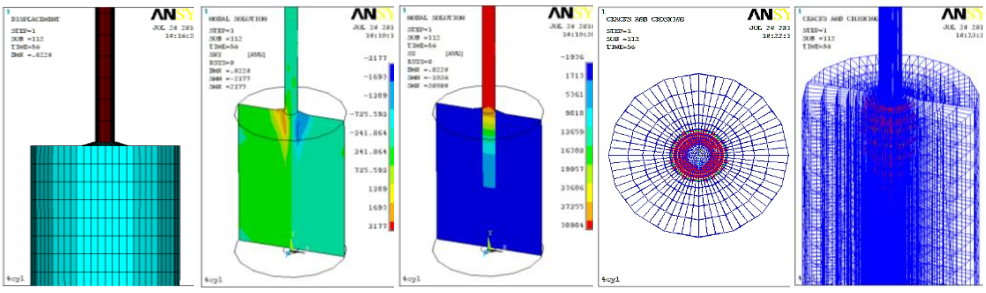

(a) (b) (c) (d) (e)

Figure 6: (a) deformed specimen, (b) stress distribution in XY plane, (c) Y direction stress distribution, (d) top view of cracks in pullout specimen, (e) crack formation zone in pullout specimen

7 COMPARISON OF EXPERIMENTAL AND FEM RESULT

The validation of FE analysis by ANSYS 11.0 of pullout specimen with the results gathered from the experimental measurements are shown in Figure 7 (a)-(h) which satisfactorily demonstrates the accuracy of the FE model of pullout specimen with both brick and stone aggregate. The bond stress is measured on the contact surface of concrete and steel. The FE results in most of the cases found to be more or less conservative with respect to the experimental outcomes which also ensure higher factor of safety as well as the reliability of the models. In all cases bond strength between stone aggregate concrete with steel is found higher than brick aggregate concrete which validates the experimental results. This indicates that the FE modeling of pullout specimens using the pertinent parameters gathered from experimental testing is validated and there remains a good agreement as well as it can be used in the future to predict the bond strength.

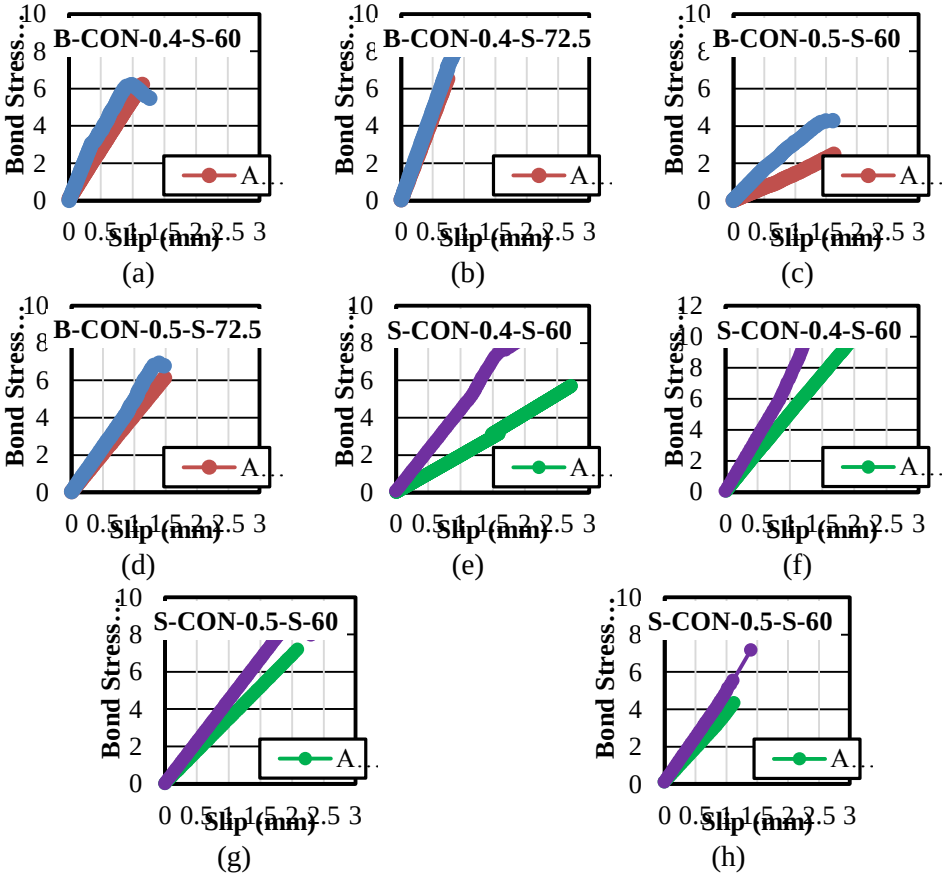

Figure 7: (a)-(h) Comparison of experimental to FEM results

8 CONCLUSIONS

The following conclusions can be said based on experimental and FEM results

- Stone aggregate shows much better performance than brick aggregate this may due to the better confinement effect on ribs of steel bars against slip.
- Within same aggregate, i.e. brick or stone aggregate, yield strength of steel rebar has a positive effect on increasing bond strength.
- Bond strength of brick aggregate increased by 32% when water to cement ratio is 0.4, increased by 44% when water to cement ratio is 0.5 and steel yield strength changed from 60 ksi to 72.5 ksi.
- Bond strength of stone aggregate increased by 33% when water to cement ratio is 0.4, decreased by 22% when water to cement ratio is 0.5 and steel yield strength changed from 60 ksi to 72.5 ksi.
- The Finite Element results compared with the experimental results and in most of the cases found to be more or less conservative with respect to the experimental outcomes which confirm the higher factor of safety as well as the reliability of the models.

This study has investigated two different aggregate performances with two different strength steel rebar which can be useful in understanding the difference in behavior between them and serve as a base for future research.

REFERENCES

[1] A. M. Diab, H.E. Elyamany, M.A. Hussein and H.M. Al Ashy, 2014."Bond behavior and assessment of design ultimate bond stress of normal and high strength concrete." Alexandria Engineering Journal 53.2 (2014): 355-371.

[2] ACI 318-11, (2011), Building Code Requirements for Structural Concrete and Commentry, An ACI Standard, Reported by ACI Committee 318, American Concrete Institute.

[3] ASTM C 900 – 06, Standard Test Method for Pullout Strength of Hardened Concrete, American Society for Testing and Materials, ASTM Committee C09. American Concrete Institute.

[4] ACI 228.1R-03, (2003), In-Place Methods to Estimate Concrete Strength, Reported by ACI Committee 228, American Concrete Institute, September- August.

[5] H. A. Al-Zuhairi and W. D. Al-Fatlawi, 2013. "Numerical prediction of bond slip behaviour in simple pull-out concrete specimens." Journal of Engineering 19.1 (2013): 72.

[6] L. Bouazaoui and A. Li, 2008. "Analysis of steel/concrete interfacial shear stress by means of pull out test." International Journal of Adhesion and Adhesives 28.3 (2008): 101-108.

[7] M. N. S. Hadi, 2008 "Bond of high strength concrete with high strength reinforcing steel." (2008): 143.

[8] M.M. Islam, M.S.I. Choudhury, M. Abdulla and A.F.M.S. Amin, 2011. "Confinement Effect of Fiber reinforced polymer wraps in circular and square concrete columns". 4th Annual Paper Meet and 1st Civil Engineering Congress, Civil Engineering Division, Institution of Engineers, Bangladesh (IEB), 22-24 December, 2011.

[9] M.M. Islam, M.S.I. Choudhury & A.F.M.S. Amin, 2015. "Dilation Effects in FRP-Confined Square Concrete Columns Using Stone, Brick, and Recycled Coarse Aggregates". Journal of Composites for Construction, 04015017.

[10] M. R. Kabir and M. M. Islam. 2014 "Bond stress behavior between concrete and steel rebar: Critical investigation of pull-out test via Finite Element Modeling." International Journal of Civil and Structural Engineering, Volume-5, No-1.

[11] Murcia-Delso, Juan, and P. Benson Shing, 2014. "Bond-Slip Model for Detailed Finite-Element Analysis of Reinforced Concrete Structures." Journal of Structural Engineering 141.4 (2014): 04014125.

[12] M.T.G. Barbosa and S.S. Filho, 2013. "Investigation of Bond Stress in Pull Out Specimens with High Strength Concrete". Global Journals Inc.

[13] S.Hong and S. K. Park, 2012 "Uniaxial bond stress-slip relationship of reinforcing bars in concrete." Advances in Materials Science and Engineering, 2012

[14] S. P. Tastani and S. J. Pantazopoulou, 2009 "Direct tension pullout bond test: Experimental results." Journal of Structural Engineering 136.6 (2009): 731-743.

CICM 2015
First International Conference on
Advances in Civil Infrastructure and Construction Materials
MIST, Dhaka, Bangladesh, 14–15 December 2015

SEISMIC PERFORMANCE OF CONCENTRICALLY-BRACED STEEL FRAMES

AKM G. Murtuz[1], M. R. KARIM[2], K. B. Jalal[3], R. J. Priti[4], K. Islam[5],

[1, 2 3, 4, 5] Department of Civil Engineering,
Military Institute of Science and Technology, Dhaka, Bangladesh
E-mail: [1]golam.murtuz.bd@gmail.com, [2]majrezakarim@gmail.com,
[3]nishi_vnsc@hotmail.com, [4]rifatjabin11@gmail.com, [5]kamrul1@ualberta.ca

Abstract. *Seismic vulnerability assessment of existing buildings is becoming a primary concern today due to the major threats that have been imposed by numerous earthquakes around the world in recent years. Recent earthquakes in the Asia-Pacific region have motivated researchers to concern themselves more with the development of a suitable and sustainable technique to minimize the seismic vulnerability of structures subjected to strong earthquakes through enhanced deformation capacity and ductility. This paper presents the improvements to seismic response of steel frames braced with the smart element using super-elastic (SE) shape memory alloy (SMA) and stainless steel. Three reference semi-rigid steel frames, one as conventional steel bracing, another with stainless steel bracing, and the other with smart bracing, are modeled and the seismic performance of the structure is investigated. In this study, a 2-D finite element (FE) analysis of the concentrically-braced steel (CBS) frames is carried out in order to assess the seismic performance of the CBS frame by exploiting the SE behavior of SMA and the high ductility of stainless steel. The nonlinearity of both geometric and material aspects are included in the established FE models. Numerical investigations on braced steel frames reveal that the uses of SMA bracing improves the performance of the steel frame compared to the stainless steel and conventional steel bracing approaches.*

Keywords: Seismic performance, Steel braced frame, Smart bracing and Stainless steel.

1 INTRODUCTION

Natural disasters such as earthquakes cause damage to civil engineering structures resulting in deaths, economic losses, and damage to infrastructure. Recent earthquakes in Nepal (2015), Japan (2011), New Zealand (2010, 2011), Mexico (2011), Indonesia (2010, 2011), China (2010), and Haiti (2010) have garnered the attention of researchers looking for a method by which to predict the severity of damages to infrastructure as a result of natural disasters [1]. Cities around the world contain vulnerable buildings under considerable seismic risk. Most of the steel buildings in North America were built almost 20 years ago using moment-resisting frames to resist lateral load during earthquakes. Earthquakes cause serious disruptions in a building's structural system due to the large lateral displacements of the beam-column connections. Lateral sway and seismic performance are prime considerations in designing multistoried steel frames, especially in zones of high wind and seismicity. Various mechanisms are found in the literature which control sway and improve the seismic performance of steel frames. At present, rigorous research is being conducted all over the world seeking to improve the performance of steel frames under high wind and seismicity conditions. One popular technique is the use of bracing elements. Properly oriented bracings can resist the sway of the frame, but the performance of braced steel frames is poor under the seismic loading condition due to the low ductility and energy dissipation capacity of steel-braced frames. Recent earthquakes have led researchers toward the design of a performance-based approach to improve resisting capacity during periods of high seismicity. In order to improve the seismic performance of a structure, numerous techniques have been widely used over the last few decades. The incorporation of innovative materials in bracing systems has been a widely accepted approach. In recent years, the structural engineering community has shifted its focus to the utilization of smart materials (i.e., super-elastic shape memory alloy) as a new component of structural systems to improve the performance of structures. Regular steel frames have been used in earthquake-vulnerable zones due to their ductile behavior, but brittle fractures of the beam-column connections and brace-to-column connections have led researchers to incorporate special metals and/or smart material as bracing elements. These innovative materials exhibit interesting characteristics which have made them useful in improving the performance of structures.

Stainless-steel (SS) is widely used due to its durability, corrosion resistance, fire resistance, weldability, low life-cycle cost, recyclability, and aesthetic appeal [2-3]. SS is a metallic alloy combined with iron groups, chromium, nickel and molybdenum [2-3]. Efficient use of SS in structural systems improves the performance and decreases life-cycle cost. Due to its heat and high corrosion

resistance capacities, SS has been used more recently in a number of bridges in North America and Europe, although it has increased the total costs of these projects. Previous studies have found that SS shows enhanced ductility, large plastic deformation under extreme loading conditions, and increased energy-absorbing capacity [4-6].

Shape memory alloys (SMAs) are a type of smart material that have the ability to undergo large plastic deformation under extreme loading conditions and return to their original shape upon the removal of the load. An SMA can recover a strain of about 10% without any permanent deformations. It is also highly resistant to corrosion. There are various SMA available like Ni-Ti SMAs (Nitinol), FeMnAlNi, FeNCATB etc. SMAs are unique materials. This unique and super-elastic (SE) characteristic of SMA makes it a potential candidate in regions with high seismic activity. However, the cost is much higher than the costs of SS and regular steels. Still, SMA as a bracing agent has emerged as a suitable candidate over other materials due to its large deformability during earthquakes and recoverable capability after the earthquake. SMAs have an excellent re-centering capacity and energy absorbing capacity which reduce the vulnerability of the structure. This characteristic of SMAs improves the seismic performance of the given structure. Researchers are using SMA as a base-isolation; as a passive energy dissipation device; for the retrofitting of structures; and as a bracing element [7-15].

Recently Asgarian and Moradi [12], Auricchio et al. [11], McCormick et al. [13] and Zhu and Zhang [14] performed numerical analyses to compare the seismic performance of the steel frames braced with either SMAs or conventional steel bracings and eventually found enhanced seismic force resistive capacity in the frames braced with SMAs.

The objective of the current study is to investigate the seismic performance of concentrically-braced steel (CBS) frames using the freely available FE software, SeismoStruct. Researchers have compared the seismic performance of steel frames braced with SS and regular steels [4-6], and a few researchers have performed analyses to compare SMA bracings to conventional steel bracings [11-14]. To the author's best knowledge, no such study has been conducted to compare the behavior of steel frames braced with either SMA or SS under earthquake loading for the purpose of investigating the seismic performance of structures.

2 DESIGN OF CBS FRAMES

In this study an interior frame of a 4-storey office building was considered. The 2-D frame consists of concentric bracing in a chevron configuration. Figure 1

depicts the elevation of the CBS frame used in this study. Several bracing configuration were found in literature. Among them, chevron bracing configuration is used in the current study.

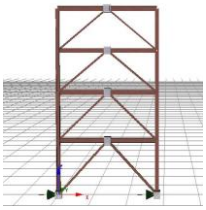

Figure 1: Elevation of four storied steel braced frame

The frame is proportioned in accordance with S16-09, which qualifies a ductility-related force modification factor, Rd= 2.0, and a strength-related force modification factor, Ro= 1.3. This chevron configuration is often dictated to provide adequate clearance for doors and other openings. The steel grade of W-shaped members is ASTM A992 with Fy= 345 MPa. The steel grade for braces is ASTM A500 Grade C square HSS with Fy= 345 MPa. Detailed member sizes are given in Table 1. The CBS frames with SMAs and SSs bracing have the same beam and column sections similar to conventional steel bracings.

Table.1. Four-Story CBS frame Model Information

Storey	Beam section	Column section	Bracing section
4	W360x39	W310x60	HSS127x127x6.4
3	W360x51	W310x60	HSS152x152x8.0
2	W360x51	W310x118	HSS152x152x9.5
1	W360x51	W310x118	HSS178x178x9.5

3 NUMERICAL MODELLING OF CBS FRAMES

3.1 Material Modelling

Accurate finite element modelling depends on the material modelling which is one the major challenges in any numerical analysis. Inappropriate material modelling will not be able to capture the exact behavior of the system even though the whole finite element modelling scheme is accurate. Therefore, to predict the exact behavior of the system accurate material modelling is the key. Special attention and effort were put in the present study to model the non-linear metallic elements accurately.

3.1.1 Conventional Steel Modelling

Commonly used material model for steel is bi-linear kinematic hardening model i.e. elastic, perfectly plastic. Stress-strain behavior of the conventional steel shows steep initial elastic response followed by a large strain-hardening. Hossain et. al. (2011) used bi-linear kinematic hardening material model for modelling the ordinary carbon steel [21]. In the current study bi-linear kinematic hardening material model available in SeismoStruct [26] is used for conventional steel modelling. Initial geometric imperfections and residual stresses highly affect the response of steel structures. But for simplicity of the numerical analysis geometric imperfections and residual stresses are ignored.

3.1.2 Stainless Steel Modelling

One of the most challenging tasks of the current study is to model the non-linear behavior of the stainless steel. Non-linear metallic materials like high strength steel, stainless steel and aluminum show abnormal behavior compare to conventional carbon steel [25]. Researchers have developed various modelling techniques to model those non-linear metallic elements. Rahman et. al. (2008) showed various material modelling approaches to model the behavior non-linear materials [22] using ANSYS. Neupane, S. (2010) showed how to model the high strength steel pipelines using ABAQUS [23]. All those studies mostly followed the Chaboche evolution law. However, Ashraf et. al. (2006) [24], Ashraf (2006) [3], Gardner and Ashraf (2006) [25], Sarno et. al. (2003, 2006, 2008) [4-6], Sarno and Elnashai (2003) [2] demonstrated the modelling of stainless steel using FE softwares. Sarno et. al. (2006, 2008) modelled the material based on modified Ramberg-Osgood (R-O) model. Gardner and Ashraf (2006) proposed a few form of the R-O model, and used the newly developed one to model the stainless steel. Modified R-O model proposed by Ashraf (2006) is used in the present study to model the stainless steel using SeismoStruct [26].

3.1.3 Shape Memory Alloy Modelling

In the present study SMA is incorporated as a bracing element. Therefore, one-dimensional model is perfect to fulfill the purpose of the material modelling. SE-SMA bracing is modeled according to the model of Auricchio et al. (1997) [15]. Recently various researchers used this material modelling approach to model SMAs [7,8,10, 12]. Fig. 2 depict the typical stress-strain diagram of the SE-SMA, and the 1-D super elastic model used in the SeismoStruct[26].

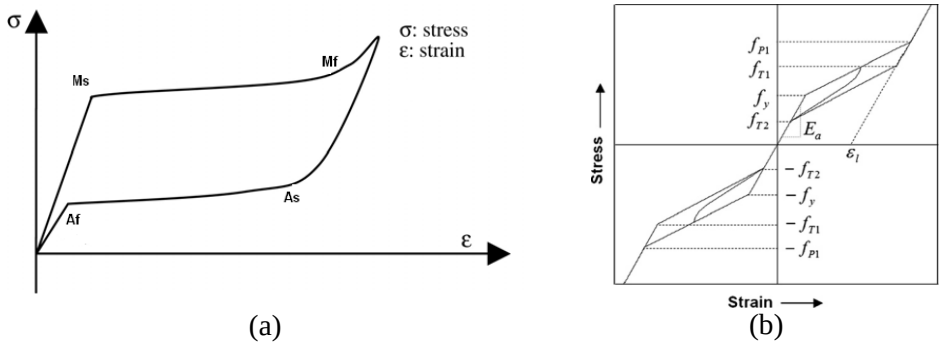

(a) (b)

Figure 2: (a) Typical Stress–strain relationship of the SMA, (b) 1-D super elastic model of SMA [26]

Table 2: shows the material properties used in the finite element analyses which have been adopted from Ashraf (2006), Asgarian and Moradi (2011), Billah and Shahria (2013)

Table.2. Material properties used in the finite element analysis [3, 12]

Materials	Mechanical property	Value
Steel	Modulus of elasticity (GPa)	200
	Yield strength (MPa)	345
	Strain hardening parameter (%)	0.5
SE SMA (FeMnAlNi)	Modulus of elasticity (GPa)	98.4
	Austenite-to-martensite starting stress (MPa)	320
	Austenite-to-martensite finishing stress (MPa)	442.5
	Martensite-to-austenite starting stress (MPa)	210
	Martensite-to-austenite finishing stress (MPa)	122
	Superelastic plateau strain length (%)	6.13
Stainless-steel	Modulus of elasticity (GPa)	206
	Yield stress (MPa)	314
	Ultimate stress (MPa)	659
	Ultimate strain	0.54
	Strain hardening parameter (%)	0.311
	Ramberg-Osgood parameter, n	6.8

4 SELECTION OF GROUND MOTION

Five ground motions recorded during Kobe, Loma Prieta, Erzincan, Northridge, C. Mendicino earthquake are used for this study. These earthquakes have been used in many research works internationally. Then a non-linear time-history

analyses are conducted in this study on the CBS frames under earthquake excitation. The spectral acceleration (5% damping) of the ground motion of the earthquakes are shown in Fig.3. According to the previous study, the seismic motion of the western part of the Canada have a PGA/PGV value around 1.0. Table 3 shows the details of the selected earthquake motions for the current study. But the PGA/PGV value for the current study is less than 1.07.

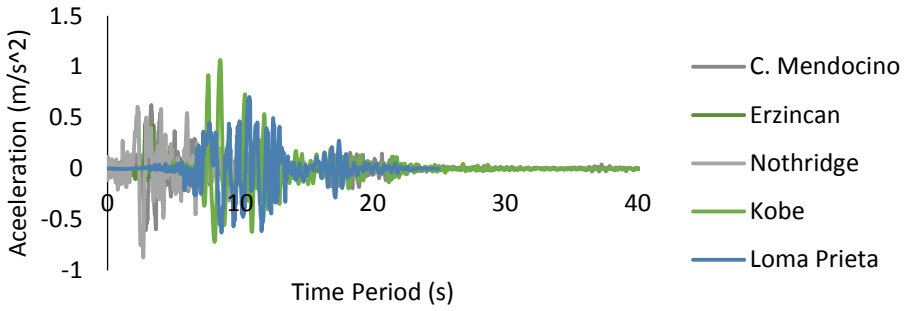

Fig.3. Spectral acceleration for the Kobe, Loma Prieta, Erzincan, Northridge, C. Mendicino earthquakes (damping = 5%)

Table. 3. Details of Earthquake ground motion records

EQ No	Earthquake			Recording Station	Epicentral	PGA max (g)	PGVmax (cm/s.)	PGV / PGA (sec)	Power Spectrum	Period
	M	Year	Name	Name						
3	7	1989	Loma Prieta	Los Gatos	3.5	0.70	170	0.246	0.226	0.63
7	7.1	1992	C. Mendocino	Petrolia	8.5	0.63	123.4	0.201	0.188	0.635
10	6.7	1992	Erzincan	Erzincan	2	0.45	57	0.13	0.224	1.781
13	6.7	1994	Nothridge	Rinaldi	7.5	0.87	171	0.2	0.173	1.28
17	6.9	1995	Kobe	JMA	3.4	1.07	157	0.15	0.273	0.836

5 RESULTS AND DISCUSSIONS

Dynamic time-history analyses and eigenvalue analyses are performed in the present study to investigate the seismic behavior, mode shapes, and to quantify the natural frequencies of the braced steel frames.

5.1 Eigen Value Analysis

Eigen value analyses are performed using SeismoStruct to investigate the mode shapes of three CBS frames, and their corresponding natural frequencies. Table 4 shows the values of few dynamic parameters obtained from the Eigen value analyses. There is a decrease in the natural frequencies of CBS frame braced with SMA compare to the conventional steel and the SS due to the lower modulus of elasticity of SMA.

Table.4. Natural frequencies and stiffness of the CBS frames

CSB Frame	Natural frequencies (Hz)			
	ω 1	ω 2	ω 3	ω 4
Conventional Steel	20.031	47.702	56.9199	69.189
Stainless Steel	20.805	51.3476	56.115	66.762
SMAs	16.598	41.966	50.290	55.367

5.2 Dynamic Time history Analysis

Five inelastic dynamic time-history analyses have been performed for each CBS frame using SeismoStruct software to compare the seismic performance under recorded ground motions.

5.2.1 Top Storey Drift Demand

Top storey drift demand is computed from the dynamic time history analyses under the two ground motion considered in the present study. Figure 4 depicts the roof drift demand for all types of frames under two different ground motions. CBS frame braced with SMA shows lower roof drift compare to the other two bracing elements. Conventional steel bracing and SS bracing experience more than 10% higher roof drift compare to the SMA braced frame. Conventional steel braced frame and SS braced frame experience almost similar roof drift.

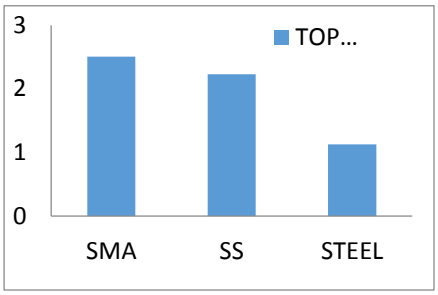

Figure 4: Roof drift demand for 4-storey CBS frame with three different bracing configurations

Figure 5 shows the displacement time history of roof drift under Kobe ground motion record. From this figure is clear that all three frames experience more than 50 mm roof displacement.

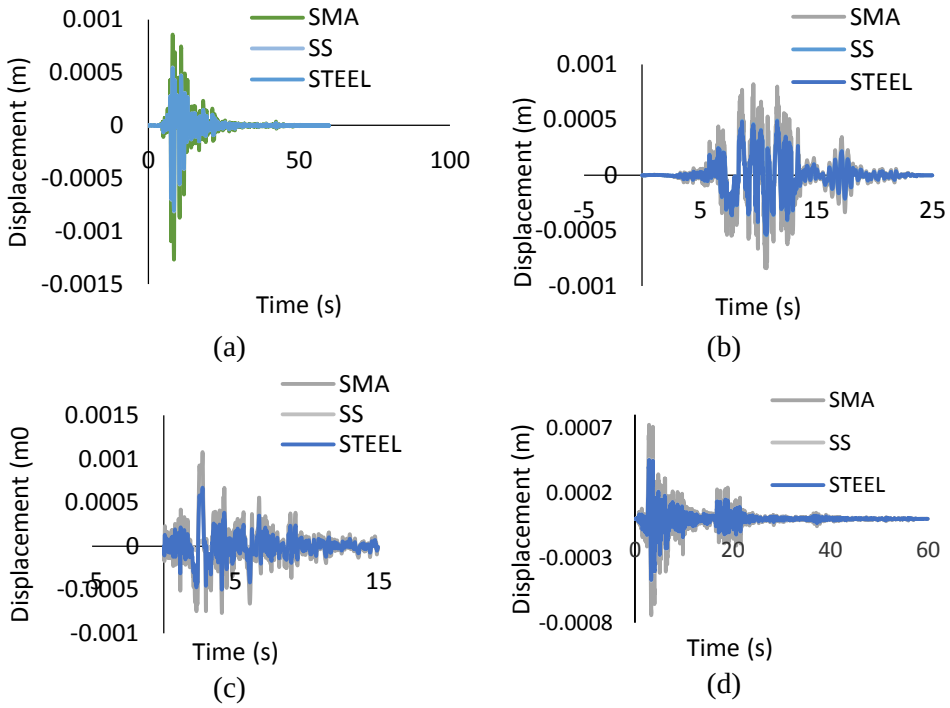

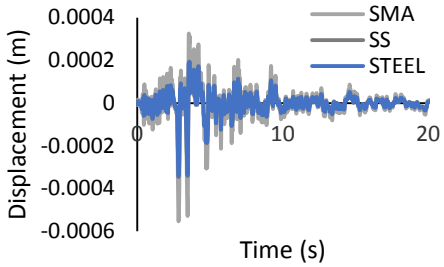

(e)

Figure 5: Roof top displacement time histories under five different earthquake.

5.2.2 Inter-storey Drift Demand

Inter-storey drift demand is computed the similar way like the top storey drift demand. All three frames experience lower inter-storey drift compare the NBCC code limit (2.5%) [27]. All frames experience highest drift at level 2, but in all cases SMA braced frame shows lower values due to its super elastic behavior.

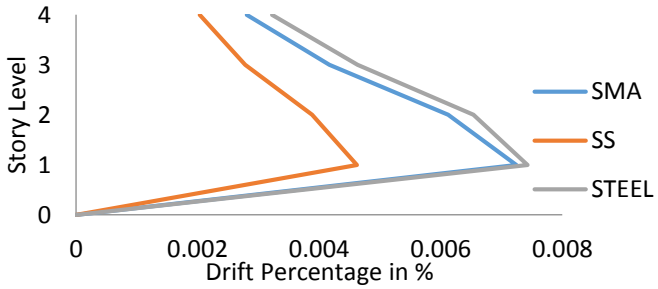

Figure 6: Inter-storey drift demand of 4 storey CBS frames for a typical ground motion data.

Figure 6 show the inter-storey drift demand under a typical seismic loading conditions. SMA braced frame shows better performance due to higher stiffness (Table 4).

5.2.3 Base Shear Demand

Base shear demand is defined as the maximum translational force (i.e. base shear) obtained for a given seismic loading. Figure 7 shows the base shear demand of the three different frames for the Kobe and Northridge earthquake

motions. CBS frame braced with SMA shows lower base shear demand compare to the conventional steel and the SS braced frames.

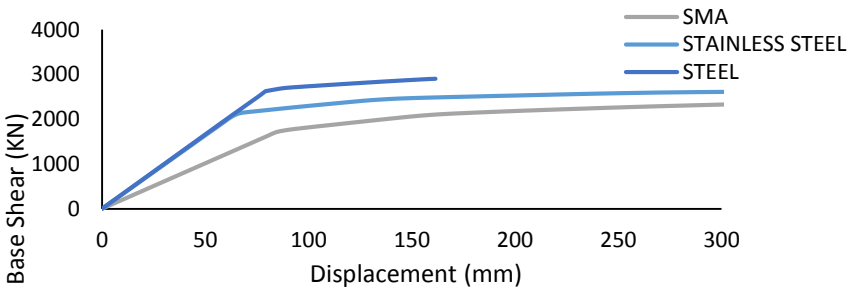

Figure 7 Base shear demand vs Displacement for 4-storey CBS frames.

5.2.4 Ductility

It can be easily observed that the global ductility value is higher for stainless steel and SMA as compared to the conventional steel bracings. Ductility increases by almost 112% for stainless steel bracings which can be attributed to the high ductility of the stainless steel materials.

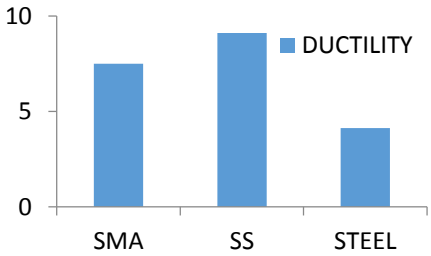

Figure 8: Ductility for 4-storey CBS frames.

6 CONCLUSION

This study performs a novel approach to decrease the seismic vulnerability of the CBS frames by incorporating non-linear metallic materials i.e., stainless steel and shape memory alloy as a bracing element. The main objective of the current study is to investigate the dynamic response of a four storey CBS frame incorporating three different types of materials as a bracing element. Firstly the frame is designed using NBCC2005 and S16-09 considering standard gravity

load and notional load. All models have been analyzed under 2 different past earthquake loading to investigate the different material response.

This study reveals that the use of SS bracing will not be advantageous in the low or moderate seismic zone. From the existing literature it was found that SS braced frames showed large plastic deformation, and enhanced energy absorbing capacity under high seismic loading. In the present study the yield strength of the conventional steel and the SS is almost similar. Therefore, incorporation of the SS bracing showed similar seismic performance compare to the conventional steel bracing. Moreover, in the current study only dynamic time history analyses were performed for two earthquake motions whose PGA/PGV ratio is less than 0.88. Therefore, none of the frames crossed their yield limit. Pushover analyses were not performed in the current study. This is one of the major limitations of this project. Without performing pushover analysis, capacity, ductility demand, and performance of the braced frames with SMA and SS under seismic loading conditions cannot be compared with conventional steel braced frame. Though little advantage was found using SMA bracing compare to the other two materials. SMA and SS bracings are advantageous in reducing large inelastic deformation. It was also found in the current literatures that after a large ground motion steel frames braced with SS undergo large plastic deformation which is not recoverable, and the frames experience permanent deformation. On the contrary, SMA braced frames recover their large inelastic deformation even after a strong earthquake due to its super elastic behavior to regain its original shape.
In the current study large inelastic deformation is not reached under any earthquake motions. Top roof displacement is within the NBCC 2005 specified allowable value. Residual drift is much lower compare to the other studies found in the literature. Therefore, the benefit of using SS bracing is almost minimal. However, the seismic performance of the frames are largely dependent on the seismological characteristics of the ground motions used in the study. As it is mentioned earlier that using the two earthquakes whose PGA/PGV value are less than 0.88, are not sufficient enough to compare the seismic performance. Most of the previous study used PGA/PGV ratio in between 0.9 and 1.3. This is another limitation of the current study.

Excessive residual stresses exist in the members after a structure experiences an earthquake which is the prime cause to adopt seismic retrofitting techniques of the existing structures. SMA is such an intelligent material that can overcome this large inelastic deformation due to its super-elastic behaviour compare to the SS and conventional steel. But the current design code has been established yet to incorporate those novel materials in real structures extensively. From this study it can be concluded that a hybrid bracing system (i.e., SMA-SS) might be a more appropriate solution which will exploit the unique behaviour of both materials

where SMA could be used in the plastic hinge region of the bracing, and SS in the rest of the region

REFERENCES

[1] http://earthquake.usgs.gov/earthquakes/eqinthenews/
[2] Di Sarno, L. and Elnashai, A.S. Special metals for seismic retrofitting of steel buildings. Progress in Structural Engineering and Materials 2003; 5: 60-76.
[3] Ashraf, M. Structural Stainless steel design: Resistance based on deformation capacity. PhD. Thesis, Department of Civil and Environmental Engineering, Imperial College London, UK 2006
[4] Di Sarno, L., Elnashai, A.S. and Nethercot, D.A. Seismic response of stainless steel braced frames. Journal of Constructional Steel Research 2008; 64: 914-925.
[5] Di Sarno, L., Elnashai, A.S. and Nethercot, D.A. Seismic performance assessment of stainless steel frames. Journal of Constructional Steel Research 2003; 59(10): 1289-1319.
[6] Di Sarno, L., Elnashai, A.S. and Nethercot, D.A. Seismic retrofitting of framed structures with stainless steel. Journal of Constructional Steel Research 2006; 62(1): 93-104.
[7] Nehdi, M., Alam, M.S. and Youssef, M.A. Development of a corrosion-free beam-column joint with adequate energy dissipation. Engineering Structures 2010; 32(9): 2518-2528.
[8] Alam, M.S., Nehdi, M., and Youssef, M.A. Seismic performance of concrete frame structures reinforced with super elastic shape memory alloys. Smart Structures and Systems 2009; 5(5):565-585.
[9] Alam, M.S., Youssef, M.A., Nehdi, M. Utilizing shape memory alloys to enhance the performance and safety of civil infrastructure: a review. Canadian Journal of Civil Engineering 2007; 34(9): 1075-1086.
[10] Alam, M.S., Moni, M., Tesfamariam, S. Seismic overstrength and ductility of concrete buildings reinforced with superelastic shape memory alloy rebar. Engineering Structures 2012; 34: 8-20.
[11] Auricchio, F., Fugazza, D. and DesRoches, R. Earthquake performance of steel frames with Nitinol braces. Journal of Earthquake Engineering 2006; 10(Sp. Issue 1):45-66.
[12] Asgarian, B. and Moradi, S. Seismic response of steel braced frames with shape memory alloy braces. Journal of Constructional Steel Research 2011; 67: 65-74.

[13] McCormick, J., DesRoches, R., Fugazza, D. and Auricchio, F. Seismic assessment of concentrically braced steel frames with shape memory alloy braces. Journal of Structural Engineering 2007; 133(6): 862-870.
[14] Zhu, S. and Zhang, Y. Seismic behaviour of self centering braced frame buildings with reusable hysteretic damping brace. Earthquake Engineering and Structural Dynamics 2007; 36: 1329-1346.
[15] Auricchio, F., Taylor, R.L. and Lubliner, J. Shape-memory alloys: macromodelling and numerical simulations of the superelastic behavior. Computer Methods in Applied Mechanics 1997; 146(3-4): 281-312.
[16] Annan, C.D., Youssef, M.A., and El-Naggar, M.H. Seismic over strength in braced frames of modular steel buildings. Journal of Earthquake Engineering 2008; 13(1): 1-21.
[17] Islam, K. Sway behaviour of rigid and semi-rigid steel frames. B.Sc. Thesis, Department of Civil Engineering, Bangladesh University of Engineering and Technology, Dhaka 1000, Bangladesh 2009.
[18] Auricchio, F. and Sacco,E. Super-elastic shape memory alloy beam model. Journal of Intelligent Material Systems and Structures 1997; 8(6): 489-501.
[19] Auricchio, F., Taylor,R.L.,and Lubliner, J. Shape memory alloys: macromodelling and numerical simulations of the superelastic behaviour. Computer Methods in Applied Mechanics 1997; 146(3-4): 281-312.
[20] Caicedo, J. M., Dyke, S., and Johnson, E. A. Natural excitation technique and eigen system realization algorithm for phase I of the IASC-ASCE benchmark problem-simulated data. Journal of Engineering Mechanics 2004; 130(1):49–60.
[21] Hossain, R., Ashraf, M., and Albermani, F. Numerical modeling of yielding shear panel device for passive energy dissipation. Thin-Walled Structures 2011; 49: 1032-1044.
[22] Rahman, S.M., Hassan, T., and Corona, E. Evaluation of cyclic plasticity models in ratcheting simulation of straight pipes under cyclic bending and steady internal pressure. International Journal of Plasticity 2008; 24:1756-1791
[23] Neupane, S. Material characterization of HSS pipes and its effect on the deformation response. M.Sc. Thesis, Department of Civil and Environmental Engineering, University of Alberta, Edmonton, Canada 2010.
[24] Ashraf, M., Gardner, L., and Nethercot, D.A. Finite element modeling of structural stainless steel cross-sections. Thin-Walled Structures 2006; 44: 1048-1062.
[25] Gardner, L., and Ashraf, M. Structural Design of non-linear metallic materials. Engineering Structures 2006; 28(6): 925-936
[26] SeismoSoft 2010. SeismoStruct - A computer program for static and dynamic nonlinear analysis of framed structured, V 5.2.2.
[27] NBCC 2005. National Building Code of Canada, Canadian Commission on Building and Fire Codes. National Research Council of Canada, Ottawa.